Radioactive Fallout from Nuclear Weapons Tests

AEC 5 SYMPOSIUM SERIES

U.S. ATOMIC ENERGY COMMISSION / Division of Technical Information

DISCLAIMER

Radioactive Fallout from Nuclear Weapons Tests

Proceedings of the Second Conference
Germantown, Maryland
November 3–6, 1964

Sponsored by the Fallout Studies Branch
Division of Biology and Medicine
U. S. Atomic Energy Commission

Alfred W. Klement, Jr.
Editor

November 1965

U.S. ATOMIC ENERGY COMMISSION / Division of Technical Information

Available as CONF-765 from
Clearinghouse for Federal Scientific and Technical Information
National Bureau of Standards, U. S. Department of Commerce
Springfield, Virginia 22151 $6.50

Library of Congress Catalog Card Number: 65-62945

Printed in the United States of America
USAEC Division of Technical Information Extension
Oak Ridge, Tennessee
November 1965

FOREWORD

In November 1961 the Division of Biology and Medicine held its first formal conference to review and discuss its research program in atmospheric radioactivity and fallout from nuclear weapons tests. Since new work had been accomplished and several more series of nuclear tests had been performed, a similar conference was held in the fall of 1964. The conference and this report of its proceedings are intended to highlight the recent major research findings in this area of the Division's program. It is hoped that the conference has assisted in the evaluation of fallout problems and that these proceedings will provide a useful reference to those having an interest in them.

I wish to express my appreciation to all who attended the conference and for their participation in the presentation of papers and subsequent discussions.

Charles L. Dunham, M.D.
Director, Division of Biology and Medicine
U. S. Atomic Energy Commission

PREFACE

The Second* Conference on Radioactive Fallout from Nuclear Weapons Tests, sponsored by the U. S. Atomic Energy Commission, was convened at the AEC headquarters, Germantown, Md., Nov. 3 to 6, 1964, under the auspices of the Division of Biology and Medicine. Papers were invited from among groups conducting research in the field supported at least in part under the research program† of the Fallout Studies Branch, Division of Biology and Medicine. There were two exceptions: Dr. Joseph B. Knox was asked to present studies of current interest related to local fallout from peaceful nuclear explosives (Operation Plowshare) detonations, and Dr. Howard A. Hawthorne was asked to present results from his studies, which have close relations to projects under the Fallout Studies Branch program. Many persons in the United States outside the program were invited to attend the conference and to participate in the discussions.

Much progress in understanding fallout mechanisms has been made by investigators throughout the world since the last such conference in 1961. Much new information that is useful in forming a sound basis for fallout prediction was presented. It can be concluded that a great deal of work has been and is being done toward elucidating fallout mechanisms from the source of nuclear debris to its contact with man. This is reflected by the greater sophistication of the studies and by

*The proceedings of the first conference, held at Germantown, Md., Nov. 15 to 17, 1961, have been published. [A. W. Klement, Jr. (Ed.), Radioactive Fallout from Nuclear Weapons Tests, USAEC Report TID-7632 (Bks. 1 and 2), February 1962.] Available from the Clearinghouse for Federal Scientific and Technical Information, National Bureau of Standards, U. S. Department of Commerce, Springfield, Va., 541 pp. (2 books), $5.75.

†The entire program, Atmospheric Radioactivity and Fallout Research, is described in USAEC Report TID-12616(Rev. 1), December 1962. Available from the Clearinghouse for Federal Scientific and Technical Information, National Bureau of Standards, U. S. Department of Commerce, Springfield, Va., 95 pp., $1.00.

the fact that, as more is learned about fallout, more specific and detailed studies are possible; improvements in equipment also have contributed. Several papers showed that studies conducted during atmospheric tests in 1961 and 1962 contributed greatly to our knowledge of fallout mechanisms. Of particular importance is the Springfield Program, a cooperative program with the Department of Defense, which permitted detailed studies of rainout as well as studies of mass transfer between the stratosphere and the troposphere. It has been clear for some time that the various mechanisms hypothesized cannot be described adequately by simple models. However, recent studies have provided information on certain fallout problems which permits better fallout predictions and assessments than was possible several years ago. For prediction methods of greater accuracy, applicable to all types of currently anticipated sources of atmospheric nuclear debris, further studies are necessary, including more information about the characteristics of the sources of fallout material. Other areas needing further detailed study were discussed.

Discussions are included in these proceedings. In some cases, the record was not adequate to permit transcription. For both the published papers and the discussions, authors and speakers had an opportunity to edit the manuscripts and transcripts. Since time for oral presentations of papers was limited, the published papers are considerably more detailed than the conference presentations.

An attempt has been made to formalize the style of the proceedings, which, in general, follows that of previous books in the AEC Symposium Series. Acknowledgment is due the Division of Technical Information Extension, Oak Ridge, Tennessee, for publishing assistance, particularly to Margaret L. Givens and Charles W. Carroll for their editorial help and to William E. Bost for his preparation of the index.

We wish to acknowledge with thanks assistance from many persons who helped in planning and conducting the conference. First are the session chairmen, who, although not responsible for the agenda, introduced the papers and conducted the discussions. Many administrative details were planned and executed by Robert C. Brothers, Chief, and other members of the Administrative Branch, Division of Biology and Medicine. R. W. Beadle, E. W. Bierly, W. F. Marlow, and J. E. Miller of the Fallout Studies Branch provided much assistance in preparing for and conducting the conference. Clara Mae Baker, Lydia Barchers, Georgetta Blasingame,

Leona von Bretzel, Earlene Easton, and Margaret Spangler handled many administrative details necessary for the smoothness of the conference. The Headquarters Services Division provided a number of services for which we are grateful; particular thanks are due Paul Barrett, projectionist.

Alfred W. Klement, Jr.
Acting Chief, Fallout Studies Branch
Division of Biology and Medicine
U. S. Atomic Energy Commission

CONTENTS

SESSION I

Physical, Chemical, and Radiological Characteristics of Atmospheric Radioactivity and Fallout

Edward C. Freiling, Chairman

NUCLEAR-DEBRIS FORMATION

EDWARD C. FREILING, GLENN R. CROCKER,
and CHARLES E. ADAMS
U. S. Naval Radiological Defense Laboratory, San Francisco, California

ABSTRACT

This paper describes the present program, recent progress, and future plans of the U. S. Naval Radiological Defense Laboratory (NRDL) in the field of nuclear-debris formation.

Two fallout-formation prediction systems have been programmed for computer calculation. The predictions represent great advancements over systems that do not account for fractionation, but much room remains for improvement. The greatest needs appear to be for the definition of particle-size distribution, the accounting for agglomeration effects, and the development of a kinetic approach. Preliminary steps in the development of a kinetic approach are described.

A by-product of the prediction system is the calculation of unfractionated radiological properties. As an example of this work, decay rates, dose rates, and spectra are given for the most important case of ^{238}U fission produced by a thermonuclear neutron spectrum.

Some results of correlating radiochemical data from fractionated samples of air-burst debris are discussed, but numerical results are reserved for a following paper* to facilitate comparison with correlations from other burst types.

Preliminary laboratory investigations of fission-product interaction with various substrate materials are described. These show large negative deviations from Raoult's law, particularly when the interaction is between a basic fission product and acidic substrate or an acidic fission product and basic substrate.

*See paper by Glenn R. Crocker, Francis K. Kawahara, and Edward C. Freiling, this volume.

Finally, the directions that we expect future efforts to take are indicated. These include a sensitivity analysis of our prediction system, extended fractionation correlations, model refinements, model extensions to new conditions, the retrieval of information from old debris, and laboratory studies of fallout formation under irreversible conditions.

INTRODUCTION

We have been asked to describe in this paper the project on studies of nuclear-debris formation that we are carrying out at NRDL for the Fallout Studies Branch, U. S. Atomic Energy Commission (AEC). This project is entitled "The Formation, Distribution and Characteristics of Nuclear Debris." However, if we were to limit this paper strictly to this part of our nuclear-debris program, we would present a very incomplete picture of our efforts. We have therefore chosen to preface this paper with a few remarks on what we are trying to do and for whom we are doing it. Figure 1 is a schematic presentation of the Physical Chemistry Branch, NRDL, fallout studies program at the present and in the recent past. Other, related work at NRDL is shown only where necessary. The various boxes are coded to identify sponsorship. Next to the AEC, the Defense Atomic Support Agency (DASA) sponsors most of our work. The focal point, the ultimate goal, is prediction capability. This is indicated by the box labeled "Model of Formation and Properties of Nuclear Debris." As input this box requires basic data from nuclear and physical chemistry, in addition to empirical relations such as scaling functions and fractionation correlations. The scaling functions come from laboratory experiments and the fractionation correlations from the analysis of nuclear debris. In addition to NRDL, data come from various sources.

This paper reports primarily, but not exclusively, on research completed or nearly completed in the four following subprojects of our work for the AEC:

1. Prediction of fractionation effects
2. Prediction of radiological properties
3. Fractionation correlations
4. Laboratory studies

Also included in each section is an indication of the future direction we visualize these studies will take.

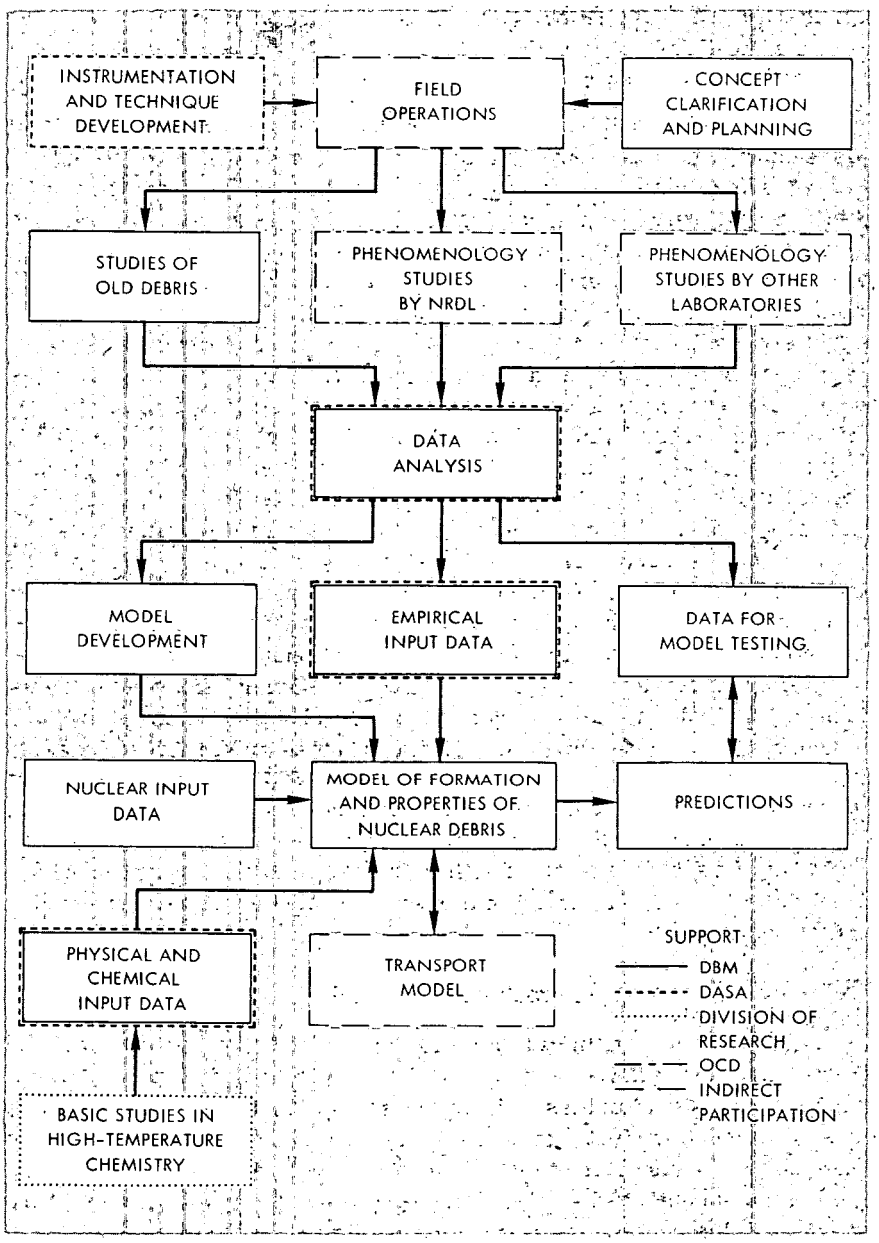

Fig. 1—Nuclear-debris study program.

PREDICTION OF FRACTIONATION EFFECTS

Clarification of Concepts

If the reader will permit a heterodox interpretation of the title of this subproject, it is appropriate to begin this discussion with the effect of fractionation on thought and communication—the semantic effect, if you will. With a realization of the existence and significance of fractionation, many terms previously used to describe and discuss fallout have become undefined and meaningless. Thus phrases like "bomb fraction," "fissions in the sample," and "kilotons per square mile" are no longer "OK terms." Moreover, as our understanding of fractionation has increased, deviation of fission-product abundances from those expected in instantaneous thermal-neutron fission of ^{235}U and of decay rates from the Way–Wigner $t^{-1.2}$ rule are no longer considered significant criteria or acceptable measures of fractionation effects. We have considered it an important part of our effort to suggest new definitions and, where possible, operational definitions for many of these terms. These are listed in the appendix to this paper. The essential features of some of these definitions are soundly grounded in the fundamental properties of the debris. Accidental features (e.g., the choice of standards for measuring fractionation) can be varied if sufficient justification appears for doing so. Other terms and definitions are merely matters of convenience, and these are appropriately indicated in the appendix. The adoption of these or similar definitions will be of great assistance, not only in promoting clear thinking and improving the signal-to-noise ratio when fractionation is discussed but also in planning analyses of those properties of nuclear debris affected by this phenomenon. Further background and justification for these definitions can be found in our set of reports with the series title "Fractionation."[1–4]

First Phase of Predicting Fractionation Effects

Early in the program we came to the conclusion that the prediction of fractionation effects could best be carried out in two concurrent phases.[5] The first of these phases consisted of rapidly assembling a prediction system that would give answers to urgent questions in as reasonable a manner as time allowed. The second phase consisted of a more fundamental long-range approach. The effects of interest are gross radiological effects (exposure-dose rate, exposure dose, decay rate, gamma spectra); radiochemical-composition effects (radionuclide partition between local and worldwide fallout, radionuclide ratios in particles of different size, type, and location, and relative biological availability); effects related to mass deposit (specific activity, mass–dose ratio); and various combinations of these (e.g., ^{131}I–dose ratio).

The first phase of this subprogram is virtually complete. We have available two models for prediction (a thermodynamic model and a radial-power-distribution model) and a means of modifying each semiempirically. The information flow in the system is shown schematically in Fig. 2.

Thermodynamic Equilibrium Model The thermodynamic equilibrium model developed by C. F. Miller has already been adequately described in detail in several publications[5–7] and applied with some success to the case of reactor excursions by C. E. Miller, Jr.[8] Essentially it consists of distributing the available radionuclides in the nuclear cloud among the particles present according to the predicted equilibrium distribution. The model takes 1400°C as the temperature below which particles are impenetrable to condensing nuclides. Unfortunately, adequate thermodynamic input data are not available to properly use and test the model in several critical cases (e.g., mass chains 89, 132, and 140 and their adjacent chains).

Radial-power-distribution Model The radial-power-distribution model[3] is an amplification of suggestions by R. D. Cadle, R. C. Tompkins, and P. W. Krey, namely, that refractorily behaving nuclides distribute themselves among particles according to the available volume whereas volatilely behaving nuclides distribute themselves according to the available surface. By assuming that a collection of spherical particles exists and that all mass chains are distributed according to some power of the radius, one finds that the model predicts logarithmic correlations of radionuclide ratios for monodisperse samples. This is a happy result because radionuclide ratios observed in fractionated nuclear debris can be correlated logarithmically, at least as well as they can linearly, and the correlation parameters then become useful for model predictions. If one further assumes a particle distribution such that the mass is distributed lognormally with particle diameter with modal diameter x_v and variance σ^2, one finds that all mass chains are distributed among the particles with variance σ^2 and modal diameters given by $x_v \exp [(b_i - 1)\sigma^2]$. Here b_i is a slope correlation parameter. This permits a great simplification in the calculations and makes hand calculation feasible, whereas, in the case of the thermodynamic equilibrium model, a computer is required. Although the thermodynamic equilibrium model is a more fundamental approach, the assumptions, simplifications, and approximations involved in its use, together with the state of the available input data, make the two approaches, at least for the present, of competitive reliability. The radial-power model has a great advantage in being presently applicable to air-, tower-, and surface-burst predictions.

The semiempirical aspect of the radial-power-distribution model consists of the way it utilizes empirical correlation parameters (ob-

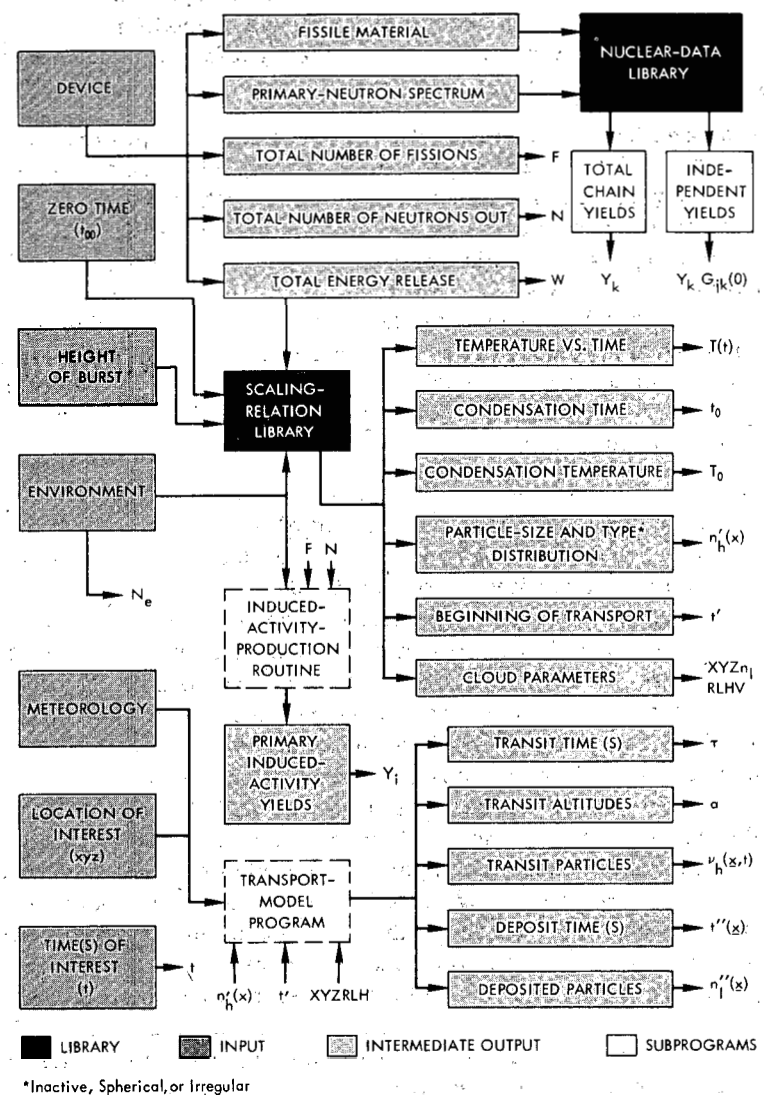

Fig. 2—Information flow in the present system for predicting fractionation effects.

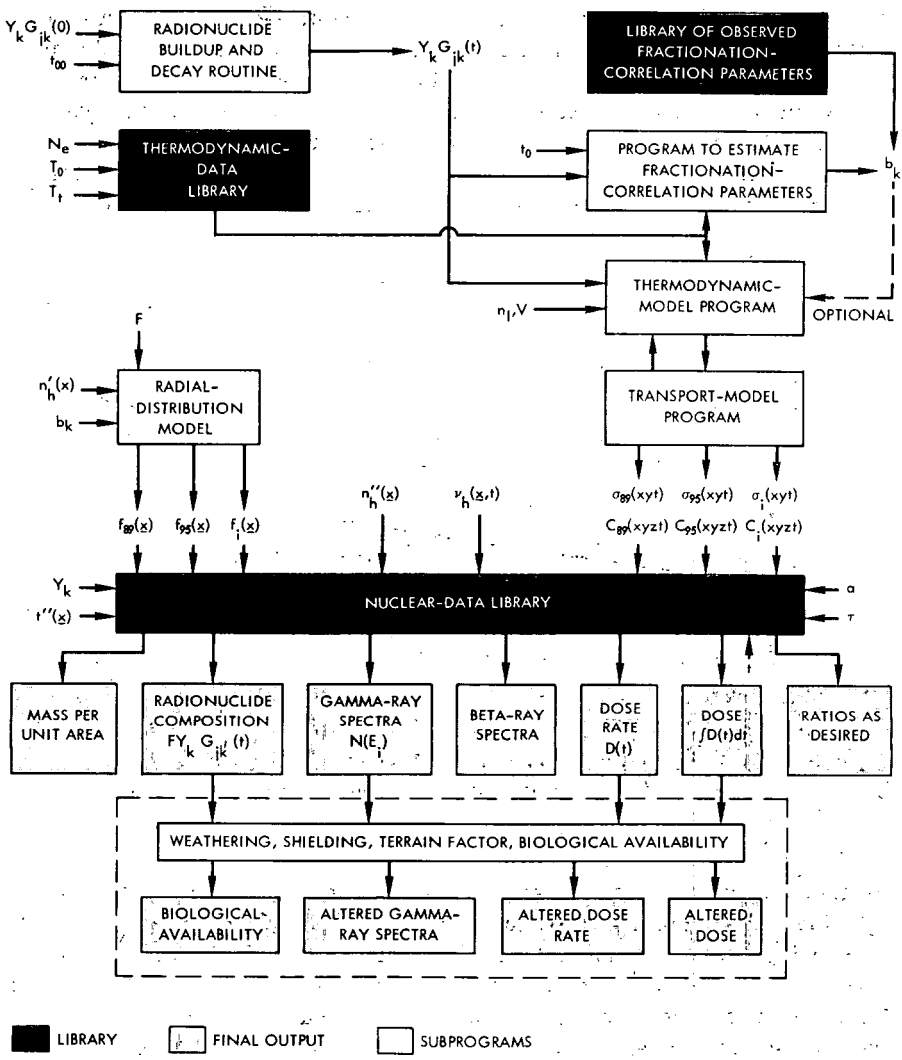
$Y_k G_{ik}(0)$
t_∞
RADIONUCLIDE BUILDUP AND DECAY ROUTINE
$Y_k G_{ik}(t)$
LIBRARY OF OBSERVED FRACTIONATION-CORRELATION PARAMETERS
N_e
T_0
T_t
THERMODYNAMIC-DATA LIBRARY
t_0
PROGRAM TO ESTIMATE FRACTIONATION-CORRELATION PARAMETERS
b_k
THERMODYNAMIC-MODEL PROGRAM
n_l, V
OPTIONAL
F
$n'_h(x)$
b_k
RADIAL-DISTRIBUTION MODEL
TRANSPORT-MODEL PROGRAM
$n''_h(x)$
$\nu_h(x,t)$
$f_{89}(x)$ $f_{95}(x)$ $f_i(x)$
$\sigma_{89}(xyt)$ $\sigma_{95}(xyt)$ $\sigma_i(xyt)$
$C_{89}(xyzt)$ $C_{95}(xyzt)$ $C_i(xyzt)$
Y_k
$t''(x)$
NUCLEAR-DATA LIBRARY
a
τ
MASS PER UNIT AREA
RADIONUCLIDE COMPOSITION $FY_k G_{ik'}(t)$
GAMMA-RAY SPECTRA $N(E_i)$
BETA-RAY SPECTRA
DOSE RATE $D(t)$
DOSE $\int D(t)dt$
RATIOS AS DESIRED
WEATHERING, SHIELDING, TERRAIN FACTOR, BIOLOGICAL AVAILABILITY
BIOLOGICAL AVAILABILITY
ALTERED GAMMA-RAY SPECTRA
ALTERED DOSE RATE
ALTERED DOSE
LIBRARY
FINAL OUTPUT
SUBPROGRAMS

tained from the radiochemical analysis of fractionated fallout samples) to predict fractionation effects.[4] When so used, with a lognormal particle-size distribution, mass-balance requirements are automatically fulfilled for each mass chain. The assumptions of spherical particles and radial power distribution guarantee logarithmic correlations for monodisperse samples, and mass-balance fulfillment can be expected for any overall particle-size distribution.

The thermodynamic equilibrium model can be utilized in a semiempirical manner by using it as originally described to calculate the

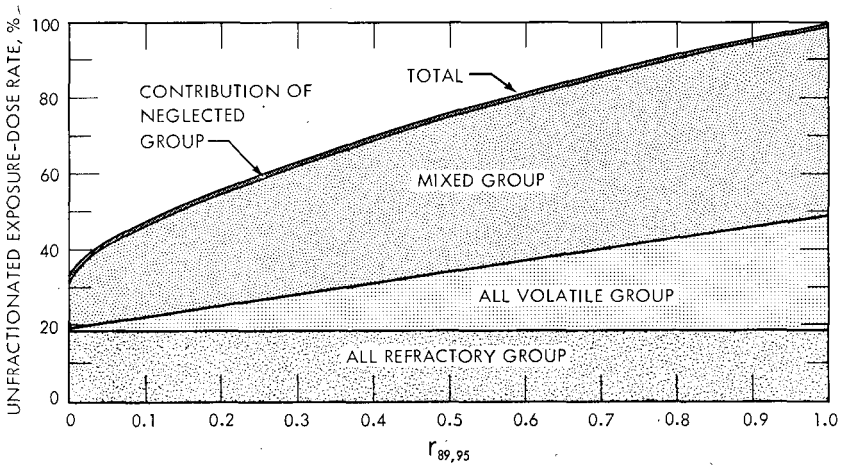

Fig. 3—Semiempirical model prediction of the effect of fractionation on the 1.12-hr dose rate for a burst in which solidification occurs in 6 sec.

degree of fractionation for each sample and then attaching to that sample the effect empirically expected for that degree of fractionation. It has not yet been demonstrated, however, that mass-balance requirements will then be fulfilled. The seriousness of this defect would be less for dose-rate estimates than for radionuclide partition and may not be serious in either case, compared to the magnitude of other uncertainties.

Figure 3 shows the percentage of unfractionated exposure-dose rate expected for different degrees of fractionation at 1.12 hr from a burst in which solidification occurred in 6 sec. According to Miller's estimates[7] this would correspond to a yield of 25 kt. The prediction indicates a maximum depletion of a factor of 5 in the dose rate from local fallout. We have data from the 1962 test series in Nevada which indicate that depletion may be much greater in actual situations. The observations require further substantiation and verification, however.

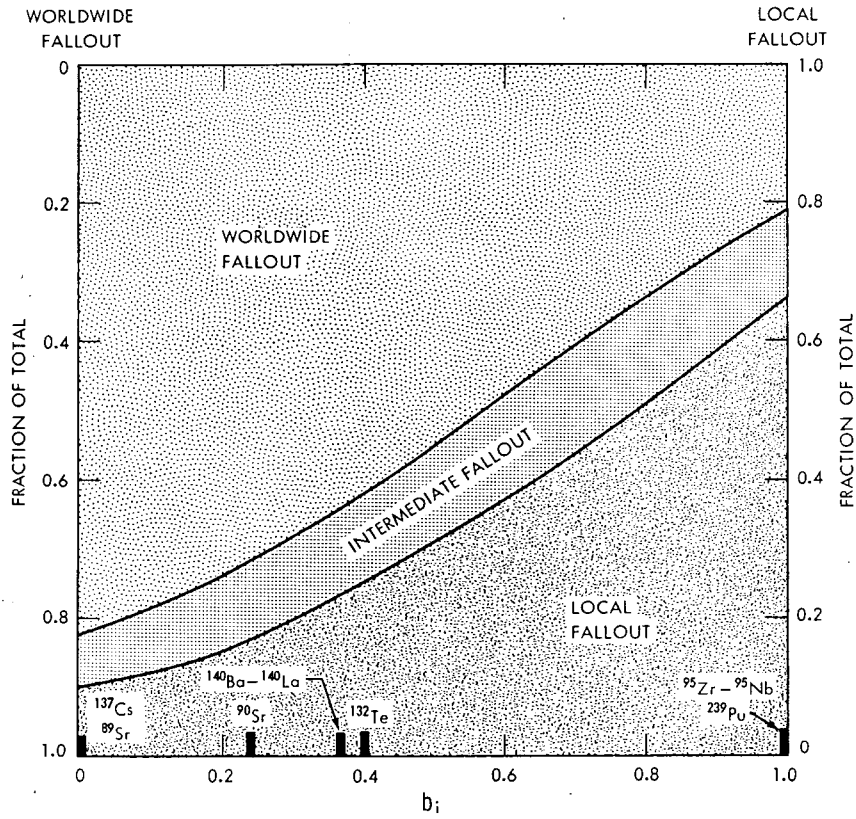

Fig. 4—Semiempirical model prediction of radionuclide partition in a land-surface burst.

In the case of volatile-chain enrichment under extreme conditions (base surge from an underwater burst or gas venting from a subsurface burst), the ratio of dose rate to the unfractionated dose rate calculated from the mass-95 chain may greatly exceed a factor of 10.

Another point of interest predicted by our model is that debris may adhere more closely to the Way–Wigner $t^{-1.2}$ decay rule if it is fractionated than if it is unfractionated; this is supported by unpublished observations on fallout from weapons tests.

Finally, the model has been used to predict the partition of various mass chains among local fallout (particles of 50 μ or greater in diameter), intermediate fallout (particles between 25 and 50 μ in diameter), and worldwide fallout (particles less than 25 μ in diameter). The predictions are shown in Fig. 4 and are compared in Table 1 with partitions inferred from fallout analysis.[9,10] The data from the high-yield coral-surface burst are of poor reliability and show only qualitative agreement. The data from the low-yield silicate-surface burst agree much better. The agreement is somewhat fortuitous, however, because the

Table 1 — COMPARISON OF RADIONUCLIDE PARTITIONS PREDICTED BY THE SEMIEMPIRICAL METHOD WITH OTHERS INFERRED FROM ANALYSIS OF NUCLEAR DEBRIS

Radionuclide	Predicted fractions			Fractions in 24-hr cloud of a high-yield, coral-surface burst	Fractions in a low-yield, silicate-surface burst		
	Local	Intermediate*	Worldwide		Local	Intermediate†	Worldwide
^{137}Cs	0.1	0.1	0.8	0.36 ± 0.36	0.00	0.22	0.78
^{89}Sr	0.1	0.1	0.8		0.02	0.24	0.74
^{90}Sr	0.15	0.1	0.75	0.11 ± 0.11	0.07	0.24	0.69
$^{140}Ba - ^{140}La$	0.25	0.1	0.65		0.20	0.26	0.54
^{132}Te	0.25	0.1	0.65		0.18	0.26	0.56
$^{95}Zr - ^{95}Nb$	0.65	0.1	0.25		0.72	0.19	0.09
^{99}Mo (coral)	0.65	0.1	0.25	0.02 ± 0.02	0.72	0.19	0.09

*Intermediate fraction taken as 25 to 50 μ in diameter.
†Intermediate fraction taken as 18 to about 90 μ in diameter.

particle-size distribution in the latter case differed considerably from that used in the model.

In summary, the present state of the art puts us in the position of the meteorologist who has to predict the weather even though he can't. We make the most reasonable attempt our knowledge permits and cross our fingers.

Second Phase of Predicting Fractionation Effects

We will now discuss the second, long-term phase of predicting fractionation effects, the phase concerned with piecewise refinement of weak links in the calculational chain. Figure 5 shows the fallout-formation processes that have to be taken into account in a fundamental approach. Our thinking on this is still the same as when we presented this diagram at the last conference.[5] Perhaps the weakest links are the definition of particle size and the absence of accounting for agglomeration effects, and next in importance is the transition from an equilibrium (thermodynamic) to a nonequilibrium (kinetic) approach. However, the definitive work being done by Russell on the first problem[10] and the need to properly plan our high-temperature experimental work has led us to attack the last problem first. Our efforts in this direction form the subject of this section of the report. One should not jump to the conclusion that the thermodynamic equilibrium treatment is inapplicable or that, even if it were, thermodynamic data are no longer required. As will be seen, each approach has its place in the overall development.

The plan of developing a kinetic model has been, first, to decide on a mechanism; second, to assemble useful, available theoretical and experimental results; and, third, to integrate these and fill in the missing steps to obtain the complete treatment. We are now in stage two. We are obviously not concerned so much at this point with developing a new theory of fallout formation as with the application of established theory.

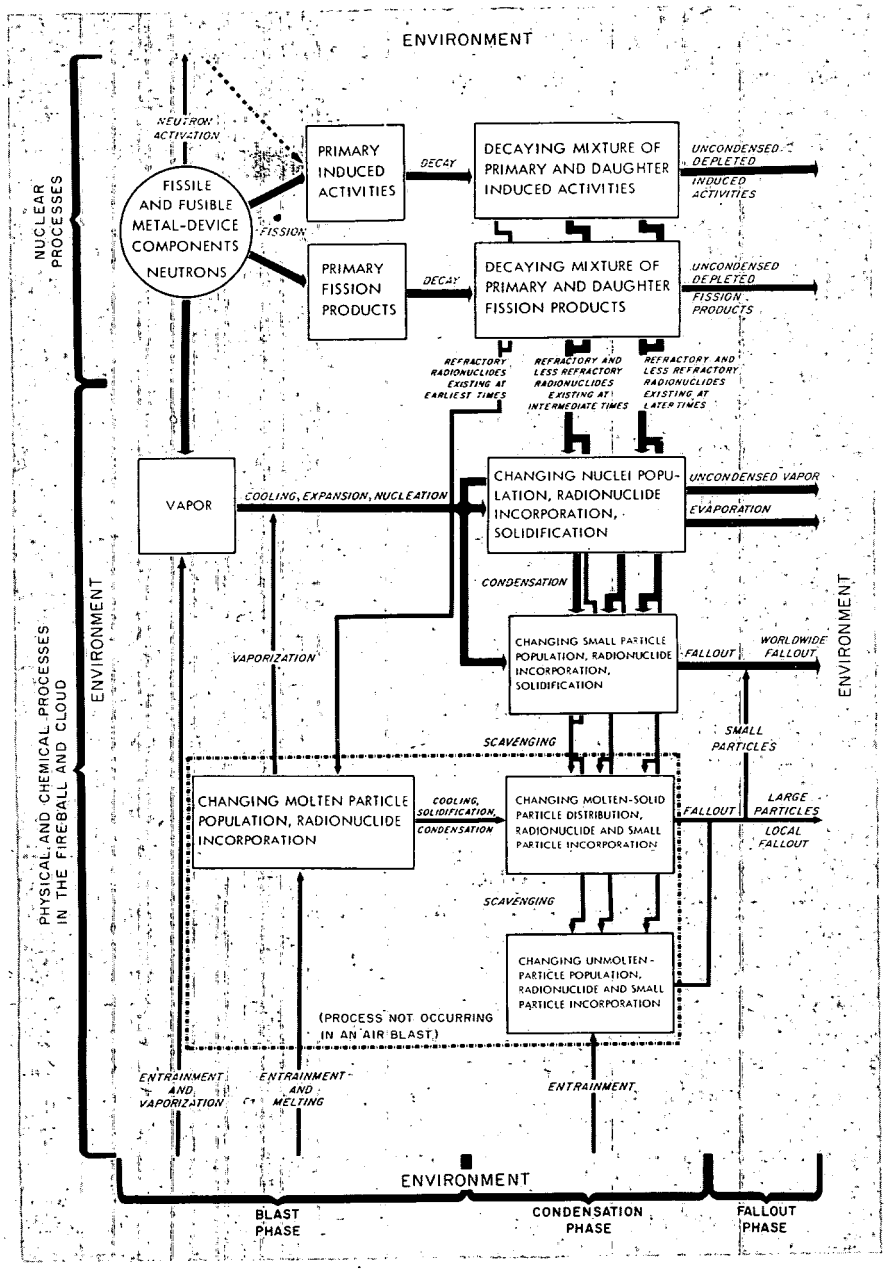

Fig. 5—Fallout-formation processes in air and surface bursts.

Mechanism With the help of Fig. 6, the mechanism can be described in the simple case from the viewpoint of a condensable molecule in the vapor phase. To be condensed, the molecule must first diffuse through the gas to the surface of a particle. Upon striking the surface the molecule can either rebound into the vapor or cling to the surface. After

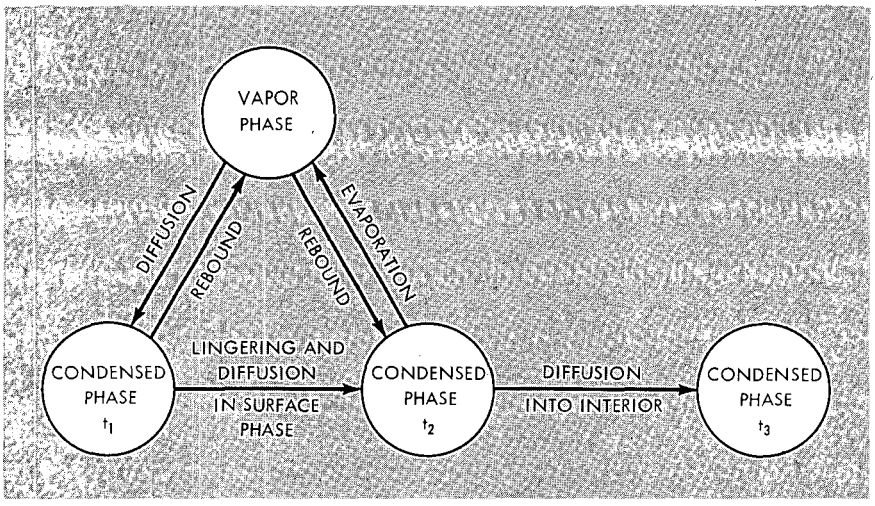

Fig. 6—Mechanism for kinetic approach to radionuclide incorporation by fallout particles.

clinging to the surface awhile, the molecule may reevaporate or diffuse into the bulk of the particle. If it reevaporates, it can easily be deflected back to the surface by the first collision with another vapor molecule. Inside the particle the molecule may diffuse back to the surface. In the actual case these processes will be occurring while the temperature is dropping. Simultaneous condensation of macroscopic quantities of evaporated carrier can occur at early stages. Particles can collide and stick. Various chemical reactions and changes of species can occur at different steps of the way. Radioactive transformations will proceed concurrently. Evaporation of volatile daughters of condensed nuclides may be important, and radiation effects may be considerable. A rigorous treatment would obviously be highly complex. However, we can visualize certain simplifications under various conditions.

Equilibrium Approximation One such simplification is the thermodynamic approach already described.[4,5] This will apply when the times for condensation and diffusion are short in comparison to the rates of radioactive decay and temperature decrease. This approximation will be

favored by small particles and rapidly diffusing molecules. Einstein's equation

$$t = \frac{\xi^2}{2D_{12}}$$

provides a helpful rule of thumb in this regard. This equation relates the time t required for the mean-square displacement $\overline{\xi^2}$ to the coefficient of interdiffusion D_{12}. To estimate the time required to approach a significant degree of equilibrium, we can calculate the time required for ξ to equal one-tenth of a particle diameter. The degree achieved in this time will be appreciable as shown in the section entitled "Particle Diffusion." Thus, for D_{12} equal to 5×10^{-7} cm^2/sec, a 100-μ-diameter particle would be well on the way to equilibrium in about a second. Interdiffusion coefficients for fission products in fused silicates are scarce. Figure 7 shows some cases that have been measured, together with some for elements that reasonably approximate fission products. Thus the curves for Rb^+ and Cs^+ in $Na_2O \cdot CaO \cdot 4SiO_2$ would probably be similar to, but below, that for Na^+, with Cs^+ being lowest. Similar relations would be expected among Sr^{2+}, Ba^{2+}, and Ca^{2+}.

To determine the validity of the thermodynamic equilibrium treatment under different conditions, one must compare the diffusion times with the cooling rate. The cooling rate is easily calculated by combining Hillendahl's equations,[15]

$$T(°K) = 7000\ W(kt)^{-0.07} \left(\frac{t}{t_{fmax}}\right)^{-0.34}$$

and

$$t_{fmax}(sec) = 0.037\ W(kt)^{0.49}$$

to eliminate t_{fmax} (the time of the final maximum) and differentiating the result. The cooling rate, in terms of either time or temperature, is then given by

$$\frac{-dT}{dt} = 776W^{0.10}\ t^{-1.34}$$

$$= 30W^{-0.29} \left(\frac{T}{1000}\right)^{3.94}$$

$$\cong 3 \times 10^{-11}\ W^{-0.3}\ T^4$$

The last equation was used to prepare Fig. 8, which shows cooling rate as a function of temperature for a wide range of total yields. We can now see what would happen during the 1-sec equilibration time referred

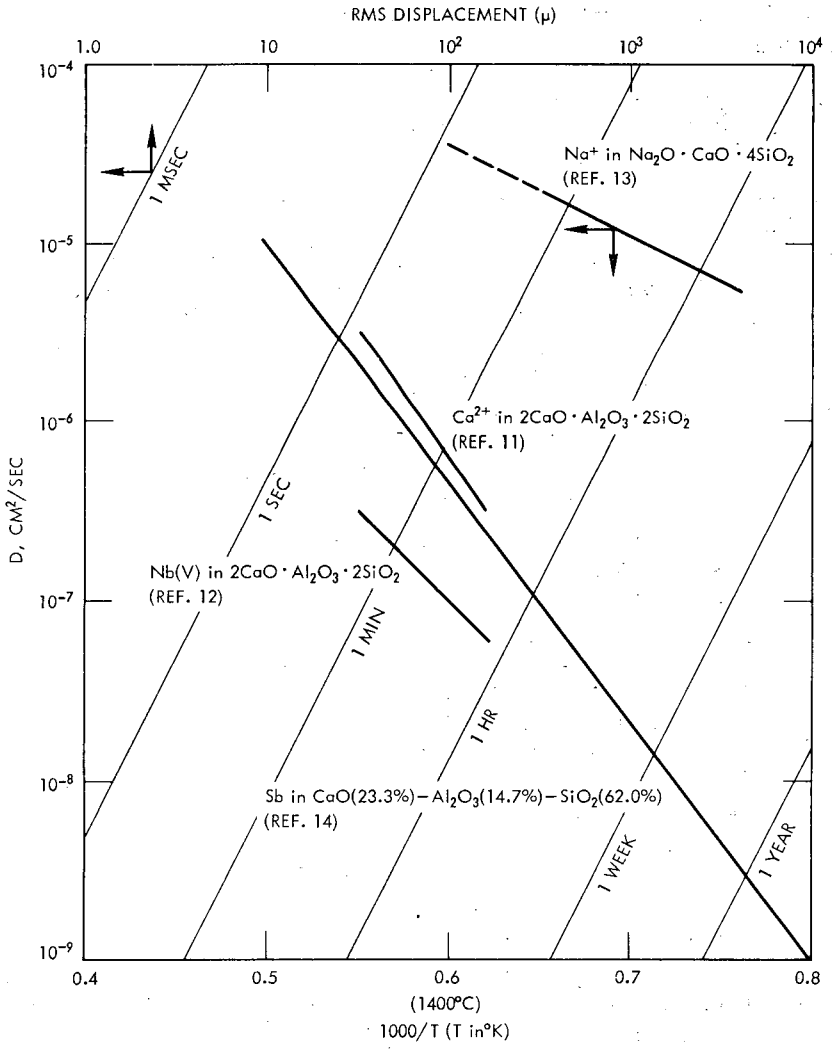

Fig. 7—Some experimental values of diffusion coefficients in molten silicates compared with the values necessary to achieve various root-mean-square displacements in given times.[11–14]

to previously under various conditions. At a temperature of 1400°C, a fireball from a 10-kt device would cool about 100°C in a second, and equilibration would never catch up to the falling temperature. For a 10-Mt burst (which is more in the high-yield range for which the treatment was originally designed), the temperature would fall only about 10°C, and the approximation is much more realistic, if still not entirely satisfactory. It should not be surprising, then, if the accuracy of

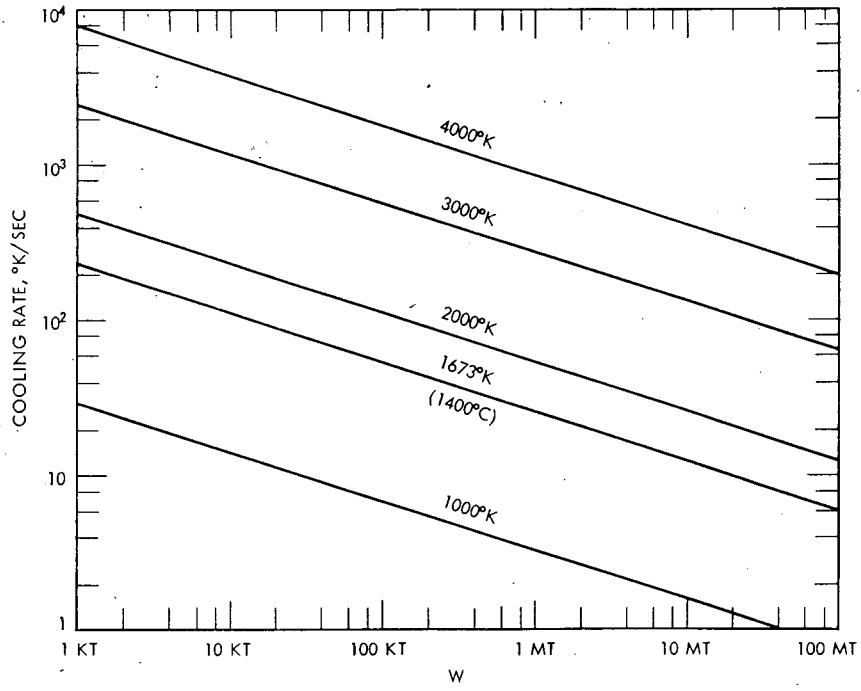

Fig. 8—Cooling rates as a function of temperature and total weapon yield.

predictions made with the thermodynamic equilibrium model is sensitive to yield.*

Examination of the previous figures clarifies the nature of another approximation used by the present system. The equilibrium treatment considers fallout formation to occur in two distinct stages. According to this approach, the particles during the first stage form an assembly of liquid drops, and condensing radionuclides distribute themselves among the particles in proportion to their volumes. At 1400°C the particles solidify, and further condensation results in surface distributions.

The diffusion data in Fig. 7 show no breaks, either in the neighborhood of 1400°C or anywhere else, for any of the silicates studied.

*Unfortunately, Hillendahl's equations are based on data which do not extend below 2000 degrees. Below 2000 degrees radiation becomes less important as a means of cooling than other processes, especially the engulfment of cold air. The cooling rates estimated here are therefore merely lower limits. Storebö[21] has attempted to account for the engulfment of cold air in air bursts. His cooling equations lead to cooling rates of the order of 10^3 degrees per second at 1400°C.

A sudden change in distribution type due to solidification therefore appears unlikely. What appears more likely is that under different conditions the mass-transfer reactions are controlled by resistance in either vapor, surface, or condensed phases. Thus, in the first stage of condensation, fission-product diffusion through the vapor phase and condensation on the surface may be negligibly fast, and diffusion through the particle would be the rate-controlling step. At lower temperatures the diffusion through the particle may be negligibly slow, not so much because of solidification as because of the small diffusion coefficients existing at low temperatures. Vapor diffusion and surface deposition may then be the only processes requiring consideration. The transition point (or region) in such an instance would be different for every fission-product species. The transition points would occur more abruptly, the faster the cooling rate. Equilibrium distributions and sharp transition points are therefore mutually contradictory simplifications. Sharp transitions would favor mass-transfer resistance at the surface.

Diffusion in the Vapor Phase Diffusion is usually treated by means of Fick's first law, according to which the net number of molecules of type 1 crossing a unit surface in unit time is given by a vector equation that we will write in the form

$$\underline{J}_1 = -D_{12} \nabla f_1 n_1$$

where D_{12} is the interdiffusion coefficient for type 1 molecules in gas molecules of type 2, n_1 is the number of type 1 molecules per unit volume, and f_1 is the thermodynamic activity coefficient. Fick's second law

$$\frac{\partial n_1}{\partial t} + \nabla \cdot \underline{J}_1 = 0$$

supplies the material-balance requirement. The activity coefficients are usually taken as unity. The interdiffusion coefficient D_{12} can be estimated from the Stefan–Maxwell equation

$$D_{12} = \frac{1}{\pi \sigma_{12}^2 (n_1 + n_2)} \left(\frac{2kT}{\pi \mu} \right)^{1/2}$$

where σ_{12} = the mean collision diameter $[\frac{1}{2} (\sigma_1 + \sigma_2)]$
μ = the reduced molecular mass $[m_1 m_2/(m_1 + m_2)]$
k = Boltzmann's constant
T = absolute temperature

From the equation it is seen that D_{12} is proportional to $T^{1/2}$, inversely proportional to the pressure, and independent of composition. By way of orientation, in air at 1 atm pressure and 0°C, D_{12} is 0.611 cm^2/sec

for H_2 and 0.138 cm^2/sec for CO_2. The application of the equation requires a knowledge of the molecular species of the diffusing substance. For cases of interest in fallout formation, this is usually unknown.

The case where diffusion through the gas is rate determining has been studied theoretically by Fuchs[17] and theoretically and experimentally by Lassen, Rau, and Weicksel.[18] These authors applied Fick's second law to the case of steady-state condensation on a spherical particle of radius R on the assumption that the law is still valid at a distance of one mean free path, λ, from the surface. They further assumed that the flux density on the surface is that expected for the concentration at the distance λ. They thus obtained the expression for the total flux at the surface

$$4\pi R^2 \left(\frac{kT}{2\pi m}\right)^{1/2} n_\infty \frac{R + \lambda}{hR^2 + R + \lambda}$$

where n_∞ is the concentration of diffusing atoms at a large distance from the sphere and h is $(kT/2\pi m)^{1/2}/D$. At 0°C and 1 atm pressure, λ is of the order of 0.1 μ. The equation predicts that, for values of $R \gg \lambda$ (i.e., $\sim 1\ \mu$), attachment is proportional to the first power of the diameter; whereas, for particles much smaller (0.01 μ), it is proportional to the second power. The effect was produced experimentally by Lassen and coworkers but has not been observed in fallout particles. This does not necessarily mean that transport of matter through the gas phase is never rate controlling. It may mean simply that turbulence, flow, depletion, and charge effects nullify the applicability of an approach based on field-free steady-state diffusion through the gas phase.

Collision with the Surface The number of type i molecules striking a unit area of surface per unit time is given by kinetic theory as

$$J_i = \frac{n_i \bar{v}_i}{4}$$

The mean velocity $\bar{v}_i$ is equal to $(8kT/\pi m_i)^{1/2}$; therefore

$$J_i = n_i \left(\frac{kT}{2\pi m_i}\right)^{1/2}$$

For O_2 and N_2 at room temperature, $\bar{v}_i$ is approximately equal to the speed of sound in air, 5×10^4 cm/sec.

Upon collision these molecules can either cling to the surface (condense) or rebound. The fraction that condenses is usually signified by α and called the condensation coefficient. It is frequently called the accommodation coefficient, but this term is best reserved to describe the fraction of possible heat exchange actually experienced by the molecule in bouncing off the surface. The condensation coefficient is

not well understood. When the condensed and vaporized species are identical, as in the case of condensing mercury, it is usually near unity. When there is a change in species, as in the cases of P_4 condensing on P_2 and of As_4O_6 condensing on As_2O_3, it can be extremely low. In these two cases[16] it is less than 10^{-7}. Apropos of the case of fallout, we have recently obtained evidence for low evaporation coefficients of alkali metals from fused oxides which indicates the likelihood of similarly low condensation coefficients.

When the condensation coefficient is incorporated into Fuchs' equation, one finds the condensation rate to be

$$\alpha S \frac{n_i v_i}{4} \frac{R + \lambda}{\alpha h R^2 + R + \lambda}$$

where S is the surface of the particle. If α is very small ($\alpha h R^2 \ll R + \lambda$), surface resistance to mass transfer predominates and the condensation rate is

$$\alpha S \frac{n_i v_i}{4}$$

It is instructive at this point to consider the case of a volume V of condensable molecules at concentration n_i exposed to S square centimeters of condensing surface. If there is no reevaporation and first-order kinetics can be assumed, the condensation rate is

$$-\dot{n}_i = \alpha J_i \frac{S}{V} = \alpha n_i \frac{\bar{v}_i S}{4V}$$

from which

$$n_i = n_i^0 \exp\left(-\frac{t}{t_v}\right)$$

where n_i^0 is the initial concentration and

$$t_v = \frac{4V}{\alpha \bar{v}_i S} = \frac{V}{\alpha S}\left(\frac{2\pi m_i}{kT}\right)^{1/2}$$

is the mean molecular residence time in the vapor phase.

If reevaporation can occur the rate equation of the previous paragraph must be modified. Again assuming first-order kinetics, this is most simply done in terms of the mean residence time on the surface t_s. Letting $(n_s)_i$ denote the number of molecules per square centimeter of surface, we can write

$$-\dot{n}_i V = (\dot{n}_s)_i S = \frac{n_i V}{t_v} - \frac{(n_s)_i S}{t_s}$$

At equilibrium (denoted by *) the net rate is zero and

$$\frac{n_i^* V}{t_v} = \frac{(n_s)_i^* S}{t_s}$$

Away from equilibrium the equation integrates to

$$\left[\frac{n_i V}{t_v} - \frac{(n_s)_i S}{t_s}\right] = \left[\frac{n_i^0 V}{t_v} - \frac{(n_s)_i^0 S}{t_s}\right] e^{-t/\tau}$$

where τ is the reduced molecular residence time $t_v t_s/(t_v + t_s)$. The first bracketed term is the departure from equilibrium at time t, the second is the initial departure from equilibrium, and $e^{-t/\tau}$ is the exponential decay factor. The quantity t_s is frequently called the lingering time or *die Verweilzeit*.

The temperature can be incorporated explicitly into the rate equation by means of the definition of t_v and Hückel's expression for t_s:

$$t_s = CT^{-1/2} e^{U_0/RT}$$

where U_0 is the molar heat of adsorption and C is a constant. This can be incorporated into the rate equation, combined with a suitable expression for temperature decay, and integrated.

Particle Diffusion The fundamental formulas for heat conduction are formally identical to those previously given for diffusion in the vapor phase. The former can be written in terms of a thermal flux $\underline{J}_T$, a thermal conductivity K, a temperature T, and a heat capacity per unit volume c:

$$\underline{J}_T = -K \nabla T$$

$$\frac{\partial T}{\partial t} + \nabla \cdot \underline{J}_T = 0$$

By making the substitutions

$$\underline{J}_T \rightarrow \underline{J}_1$$

$$K \rightarrow D_{12}$$

$$c \rightarrow 1/f_1$$

$$T \rightarrow n_1 f_1$$

the identity becomes apparent, with the result that solutions for heat flow can be easily adapted to the analogous cases for diffusion.

Carslaw and Jaeger[19] treat the case of a "radiating" solid sphere of radius R with initial temperature distribution f(r). Their solution is readily adaptable to the case of n^0 atoms of a fission product evenly distributed on the surface of a spherical particle and diffusing inward. We first write Carslaw and Jaeger's Eq. 9.4(9) in diffusion notation in the form

$$n = \frac{2}{Rr} \sum_{n=1}^{\infty} \exp(-D\,\alpha_n^2 t)\, C_n I_n \sin \alpha_n r$$

where $\alpha_n R$ is the n*th* root of the transcendental equation

$$\tan \alpha_n R = \alpha_n R$$

For the case of no radiation (no mass transfer), C_n reduces to

$$C_n = \frac{R^2\alpha_n^2 + 1}{R^2\alpha_n^2}$$

which, by the use of the transcendental restriction, can be written

$$C_n = \frac{1}{(\sin \alpha_n R)^2} = \frac{\alpha_n R}{\alpha_n R - \sin \alpha_n R \cos \alpha_n R}$$

These various forms of C_n have different limit properties, and for evaluation of C_1 by letting α_1 approach its value of zero, the last form must be used. Thus C_1 equals $^3/_2 R^2 \alpha_1^2$.

The integrals I_n have the general form

$$I_n = \int_0^R r' f(r') \sin \alpha_n r'\, dr'$$

For the case where n^0 atoms are deposited in a surface layer of thickness g,

$$I_n = \frac{n^0}{4\pi R^2 \alpha_n^2 g} [\sin \alpha_n(R-g) - \alpha_n(R-g) \cos \alpha_n(R-g)]$$

The equilibrium concentration at $t = \infty$ will be $n_f = 3n^0/4\pi R^3$. Writing I_n in terms of n_f and letting g approach zero,

$$I_n = \frac{n_f R^2}{3} \sin \alpha_n R$$

As α_1 becomes zero I_1 becomes $n_f\alpha_1 R^3/3$ and I_1C_1 equals $n_f R/2\alpha_1$. Further evaluation reveals the first-order term (which is the term that becomes important at long times) to be n_f. The solution can therefore be written in terms of the fractional departure from equilibrium:

$$\frac{n(r,t) - n_f}{n_f} = \frac{2R}{3r} \sum_{n=2}^{\infty} \exp(-D\alpha_n^2 t) \frac{\sin \alpha_n r}{\sin \alpha_n R}$$

This has the extreme radial values

$$\frac{n(0,t) - n_f}{n_f} = \frac{2}{3} \sum_{n=2}^{\infty} \exp(-D\alpha_n^2 t) \cos \alpha_n R$$

and

$$\frac{n(R,t) - n_f}{n_f} = \frac{2}{3} \sum_{n=2}^{\infty} \exp(-D\alpha_n^2 t)$$

Figure 9 shows how the fractional departure from equilibrium varies with the reduced radius ($\rho = r/R$) for various reduced times ($\theta = Dt/R^2$). The calculation was carried out to n = 6.

Since heat transfer in the particle will be fast in comparison with diffusion, the effect of changing temperature can be accounted for by replacing the exponent θ with

$$-\alpha_n^2 D_0 \int_0^t \exp(-Q/RT)\, dt$$

where Q is the activation energy for diffusion and T is the temperature as a function of time.

Rare-gas Behavior It is worth digressing briefly to consider the behavior of krypton and xenon, the rare-gas precursors prominent in the 89, 90, and 91 and the 137, 140, and 141 chains, respectively. These are not expected to be taken up significantly by fallout particles, but it is of interest to know by how much and by what processes. Gas solubility is conveniently and customarily expressed by a distribution coefficient called the Ostwald coefficient of solubility, β, which is insensitive to pressure at a given temperature:

$$\beta = \frac{v}{V}$$

Here v is the volume of gas dissolved in a volume V of solvent. The value of β for helium has recently been determined for glass melts by

Scholze, Mulfinger, and Franz.[20] Its solubility gives an indication of what can be expected for other noble gases. In the temperature range 1200 to 1480°C, these workers found a value of β ranging from 0.012 to 0.035. (For water at 0°C, β is 0.0094!) Solubility was favored by high

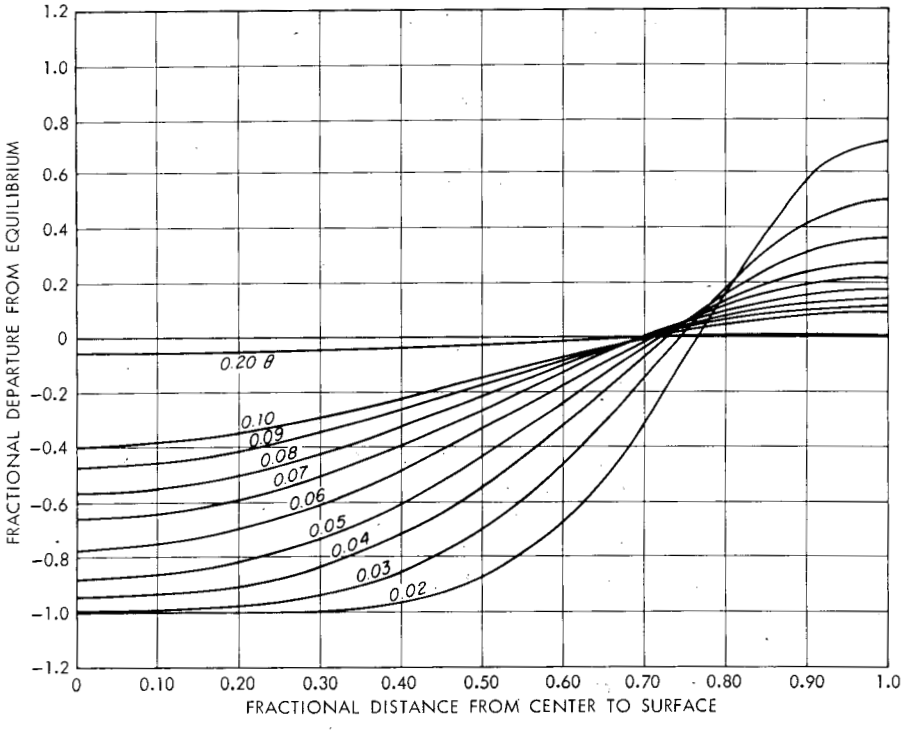

Fig. 9—Diffusion of n^0 atoms into a sphere. Fractional departure from equilibrium as a function of reduced radius for various reduced times.

silica content and high temperature. Obviously, solubility alone is not a great consideration.

Vesicularity (the presence of gaseous occlusions) is a commonly observed property of fallout particles. In the larger particles the fraction of the volume due to occlusions has been observed to vary from 5 to 44%. This would raise the effective value of β to 0.06 to 0.46. Thus, although the factor of 10^3 to 10^4 in the ratio of vapor volume to soil volume at the time of particle formation prevents solubility and occulsion of rare gases from being important, they appear to be on the borderline of significance and may require consideration in extreme cases.

Conclusions

Under certain conditions of nuclear-debris formation, the thermodynamic model is realistic, but under others a kinetic approach is necessary to treat the formation processes in a reasonable manner. The situation is too complex to say at this time what the gain will be in terms of accuracy in predicting fractionation effects. The kinetic approach involves the determination of mass-transfer coefficients for fission-product deposition on various substrate materials, and these in turn depend upon both equilibrium (distribution coefficients and heats of adsorption) and kinetic parameters (interdiffusion coefficients, lingering times) and the species of the fission products which exist under the formation conditions. However, a completely fundamental approach for each nuclide would place exhorbitant requirements on both input data and computer time. The semiempirical approach offers a reasonable compromise among the demands of economy, realism, and fundamental understanding.

Despite recent advances[10,21] questions of particle-size and type distribution and of agglomeration effects continue to be pressing.

PREDICTION OF RADIOLOGICAL PROPERTIES

The capability of predicting radiological properties constitutes a module of our prediction system worthy of individual attention. Although the primary purpose of this module is the prediction of radiological properties from fractionated debris, it is presently being used to harvest an important by-product: the radiological properties of unfractionated debris. This by-product is important primarily because it can be compared with laboratory and large-scale measurements of unfractionated debris carried out under carefully controlled conditions and presently under accumulation. This comparison, particularly in the cases of gamma-ray spectra and dose rate, will establish our confidence in the potential accuracy of such calculations. It is also of importance as a basis of comparison by which to evaluate the magnitude of fractionation effects.

The heart of this module is a computer program for calculating the abundances of fission-product nuclides. This program solves the Bateman equation for each nuclide at the time point requested, yielding an output list (on magnetic tape) of all nuclides, and the number of atoms of each present at the time point. For fission-product predictions fission is assumed to take place instantaneously. An optional calculation, used for reactor-contamination predictions, assumes fission to occur at a finite number of intervals, each of constant rate.

The program can be operated for 12 fission cases as follows:

1. Fission of ^{235}U by thermal neutrons
2. Fission of ^{235}U by fission-spectrum neutrons
3. Fission of ^{235}U by 14-Mev neutrons
4. Fission of ^{233}U by thermal neutrons
5. Fission of ^{233}U by fission-spectrum neutrons
6. Fission of ^{233}U by 14-Mev neutrons
7. Fission of ^{239}Pu by thermal neutrons
8. Fission of ^{239}Pu by fission-spectrum neutrons
9. Fission of ^{239}Pu by 14-Mev neutrons
10. Fission of ^{238}U by fission-spectrum neutrons
11. Fission of ^{238}U by 14-Mev neutrons
12. Thermonuclear fission of ^{238}U

The program will also calculate abundances for any desired combination of the above fission cases.

Supplementary computer routines will convert the abundance lists to activity lists and calculate gamma-photon emission rates and dose rates or ionization rates.

Since the calculations made by the computer are exact, the limitations on the predictions are imposed by the limitations on the input data supplied to the program. For this reason the input data used are discussed in some detail.

Input Data

The input data can best be discussed by dividing it into the following classes:

1. Chain and independent (i.e., primary) yields
2. Description of decay chains
3. Half-lives and branching fractions
4. Gamma-photon emission data
5. Gamma-energy conversion data

Chain- and Independent-yield Data* The values supplied for the amount of each nuclide produced by the fission process are taken from Reports USNRDL-TR-633 (Ref. 22) and USNRDL-TR-642 (Ref. 23). These val-

*Consider the average situation arising from the fission of 100 nuclei before beta-decay processes have begun. The number of atoms of a given nuclide formed under these conditions is called the primary, or independent, yield of that nuclide in percent. The total of independent yields for all nuclides of a given mass is called the primary chain yield for that mass in percent. If no members of the chain emit neutrons or are formed by neutron emission from neighboring chains, the observed chain yield is always equal to the primary chain yield.

ues were obtained by first constructing a mass chain-yield curve from literature values judged to be the most reliable and then distributing the chain yield among the chain members according to the method of Coryell.[24] The reliability of the values obtained in this way is difficult to estimate and probably varies from one fission case to another. The chain yields are known quite well for thermal-neutron fission of ^{235}U but are probably subject to some revision in all other cases. It is conceivable that such revisions might sometimes involve sizable factors.

The distribution of the chain yields among the members of the chain, charge distribution, is even more uncertain. Again, the values for thermal fission of ^{235}U are most reliable since they are supported by considerable experimental evidence. The experimental values for ^{235}U thermal fission are, in fact, the principal basis of the charge-distribution method. For the other fission cases, data to support the calculated distributions are sparse.

An important gap in the independent-yield information is the lack of knowledge concerning the partition of independent yields among isomeric states—usually the ground state and an excited state. When no experimental data are available, the computer program assumes that the independent yield of the nuclide is divided evenly among the isomers. This is not expected to be correct, and recent reports[25,26] of experimental studies along these lines indicate that it is not.

Description of Decay Chains The nuclides comprising a decay chain (mass chain) must be specified, including isomeric states, and the parent–daughter relations indicated. These are mostly well known, of course, but some uncertainties involving isomeric states still exist.

Half-lives and Branching Fractions The values for half-lives and branching fractions now in use are listed in Report USNRDL-TM-137.* An uncomfortable percentage of these (26% of the half-lives and 18% of the branching fractions) are estimates. Most of the half-life estimates are taken from Bolles and Ballou.[27] In addition, about 15% of the half-lives are not even estimated but are simply assigned an arbitrary value of 1 msec. These all pertain to early chain members of very low independent yields and very short half-lives. The 26% that were estimated involve values that range from a few seconds to a few minutes. Experience has shown that these estimates may be in error by as much as a factor of 100. The branching-fraction estimates were made mostly by assigning equal probability to two or more branching paths. No way is known to approximate these values more accurately.

*G. R. Crocker, R. C. Scheidt, and M. A. Connors, *Radionuclide Input Data for Fission-product Abundance Computations*, U. S. Naval Radiological Defense Laboratory Technical Memorandum (USNRDL-TM) No. 137, San Francisco, Aug. 6, 1963. USNRDL-TM's are not generally available for distribution.

Delayed-neutron emission has accounted for only seven cases—bromine in mass-chains 87, 88, 89, and 90 and iodine in chains 137, 138, and 139. The branching fractions for these decays are taken from the National Science Foundation–National Research Council Nuclear Data Sheets. A few other decays of this kind are supposed to occur among the fission products, but reliable data are not available.

It should be remembered that at least a few long-accepted half-life values may still be subject to rather drastic revision. A case in point is the 50-min state of ^{117}Cd reported as long ago as 1940. It now appears[26] that this half-life is closer to 3 hr. Serious revision of currently accepted experimental values for branching fractions is even more probable.

In view of the uncertainties so far discussed, it is very difficult to estimate a time point after fission at which one could begin to take the details of the computer abundance lists seriously. In view of the fact that several of the crudely estimated half-lives are as long as a few minutes, we are inclined to be skeptical of abundances listed for times earlier than 15 to 30 min. Even at these times, the pertinent input data for the chain involved should be carefully scrutinized before an abundance figure is accepted.

Gamma-photon Emission Data The program converts the abundance list to an activity list (by reference to the input half-lives). The activities are then considered one by one along with input gamma-photon emission data for the appropriate nuclide. These data specify by energy all gamma and X-ray photons emitted by the nuclide and provide the number of each emitted per disintegration. This permits calculation of photon-emission rates, which may be stored by energy increments and eventually output as gamma-emission spectra or which may be converted to dose-rate or ionization-rate contributions for storage and accumulation.

The gamma-photon emission data used in the program[28] have been listed in detail in USNRDL-R&L-143. This list contains all data of reasonable reliability currently available for fission-product nuclides. The data cover about 180 of a total of about 690 nuclides contained in the program. As might be expected, most of the nuclides for which gamma-emission data are not available have relatively short half-lives; many of them are very short indeed. In fact, data are available for all with half-lives greater than 10 hr, with the exception of about 25-year ^{121}Sn. (The amount of this nuclide produced in uranium and plutonium fission is exceedingly small.) For nuclides with shorter half-lives, the situation is summarized in Table 2. However, an inspection of the activity predictions indicates that the missing gamma-ray data for nuclides with half-lives greater than 10 min are not important since none of these nuclides ever contributes more than 1 or

Table 2—AVAILABILITY OF GAMMA-PHOTON EMISSION DATA FOR FISSION PRODUCTS WITH HALF-LIVES LESS THAN 10 HR

Half-life range	Total number of nuclides in program	Number for which gamma data are not available
0 to 1 min	311	296
1 to 5 min	106	32
5 to 10 min	19	3
10 to 30 min	66	7
30 to 60 min	19	2
1 to 10 hr	100	3

2% of the total activity. At times earlier than 10 min, the uncertainty in the abundances, previously discussed, compounds with the absence of gamma-photon data to make predictions uncertain.

A second consideration, insofar as gamma-radiation predictions are concerned, involves the reliability of the gamma data that are available. It is not possible to discuss this point generally since the data vary widely in this respect. For some of the nuclides, the literature provides extensive and detailed reports of gamma-emission studies, whereas for others only fragmentary data are available. X-ray photon abundances are particularly difficult to find in the literature, but fortunately these seem to have relatively minor effects on prediction of such properties as dose rates and ionization rates.

Gamma-energy Conversion Data To predict dose rates one must apply conversion factors to the photon-emission rates to convert them to roentgens per hour at some point in a well-defined geometric situation with respect to the emitter. For fallout predictions the situation usually chosen is a point 3 ft above a uniformly contaminated infinite plane. The conversion factors are a function of photon energy as well as of the geometry of the situation.

For the case of dose-rate calculation at a point 3 ft above an infinite plane, conversion factors were calculated according to the method of Gates and Eisenhauer[29] by using their tabulated "build-up" factors. The resulting conversion factors are a smooth function of energy which can be approximated for computer use by a simple polynomial. It should be remarked that Gates and Eisenhauer calculations do not extend below 0.2-Mev photon energies. Conversion factors below this point are obtained by linear extrapolation through the origin. A recent report[30] indicates that this extrapolation may be considerably in error. In the region from 0.2 to 5.0 Mev, the Gates and Eisenhauer calculations are generally considered reliable although there is very little experimental data to verify them.

Any other available conversion curve—applicable to different geometry, for example—can be substituted into the program rather

simply. Similarly, a response curve for an instrument can be substituted. We have calculated the response of the NRDL 4π ionization chamber,[31] by using the response curves of Report USNRDL-TR-155.

Results

A forthcoming USNRDL technical report will list the predicted radiological properties of unfractionated debris for seven important cases:

1. ^{235}U, thermal neutrons
2. ^{235}U, fission-spectrum neutrons
3. ^{235}U, high-energy neutrons
4. ^{233}U, fission-spectrum neutrons
5. ^{239}Pu, fission-spectrum neutrons
6. ^{238}U, fission-spectrum neutrons
7. ^{238}U, thermonuclear neutrons

Twenty-nine time points, ranging from 1 hr to 70 years, were requested from the computer. The output for 24 hr is analyzed to produce gamma-photon emission spectra from 0 to 4.0 Mev in 0.100-Mev increments. At each time point total disintegration rates and dose rates, together with individual nuclide contributions (when these amount to 1% or more of the total), are itemized. In addition, total ionization currents and individual nuclide contributions are listed for thermal neutron fission of ^{235}U. The output is far too voluminous to give more than a sample here. We will therefore restrict further discussion to the most important case, that of ^{238}U fission with a thermonuclear neutron spectrum.

The total activity in disintegrations per second is shown in Fig. 10. The individual activities have been plotted in Fig. 11 as relative values (percents of total activity) against time in the manner of Hunter and Ballou.

Two points are worth mentioning here about the effect of neutron energy on the activities after 1 hr. The nuclides ^{125}Sb and ^{127}Te, which do not appear for ^{235}U thermal fission, do appear in the present case. This is due to an increase in chain yield. Note that relative-activity curves for several nuclides in the hours and days ranges have been omitted from Fig. 11 in the interest of legibility.

The gamma-photon spectra at 6 hr, 7 days, and 270 days are shown in Fig. 12 as composite histograms. These show general order of magnitude agreement with Björnerstedt's predictions,[32] but a detailed reconciliation remains to be made.

Figure 13 shows the gross exposure-dose rate for gamma radiation at 3 ft above an infinite plane uniformly contaminated with 10^4 fissions/cm^2.

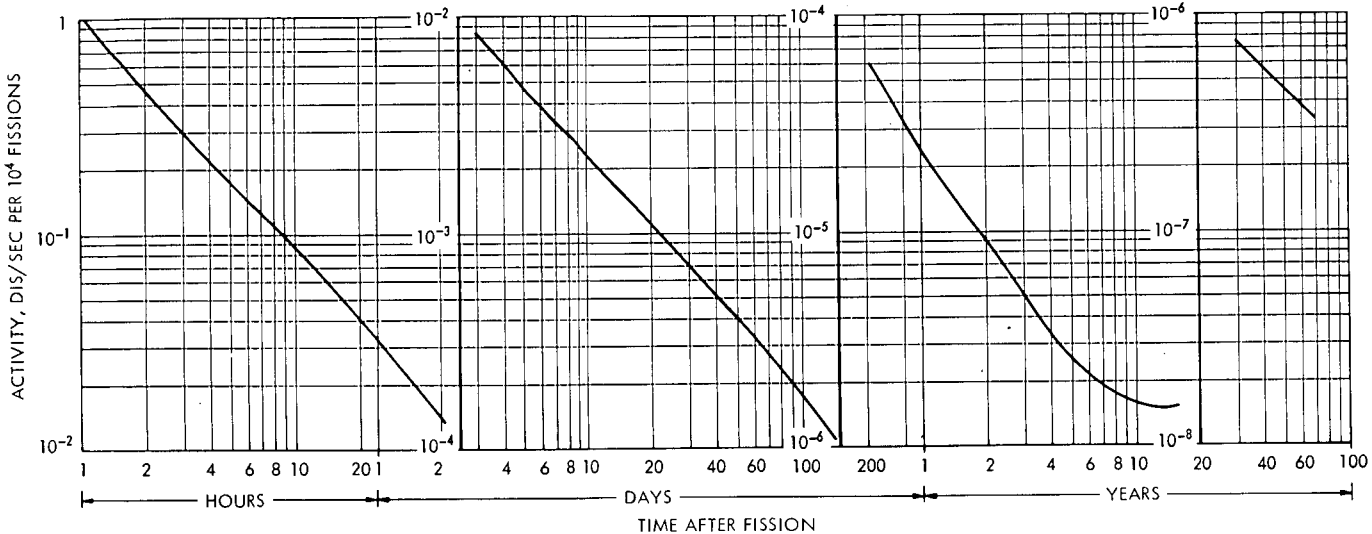

Fig. 10—Gross disintegration-rate decay of products of ^{238}U fission produced by a thermonuclear neutron spectrum.

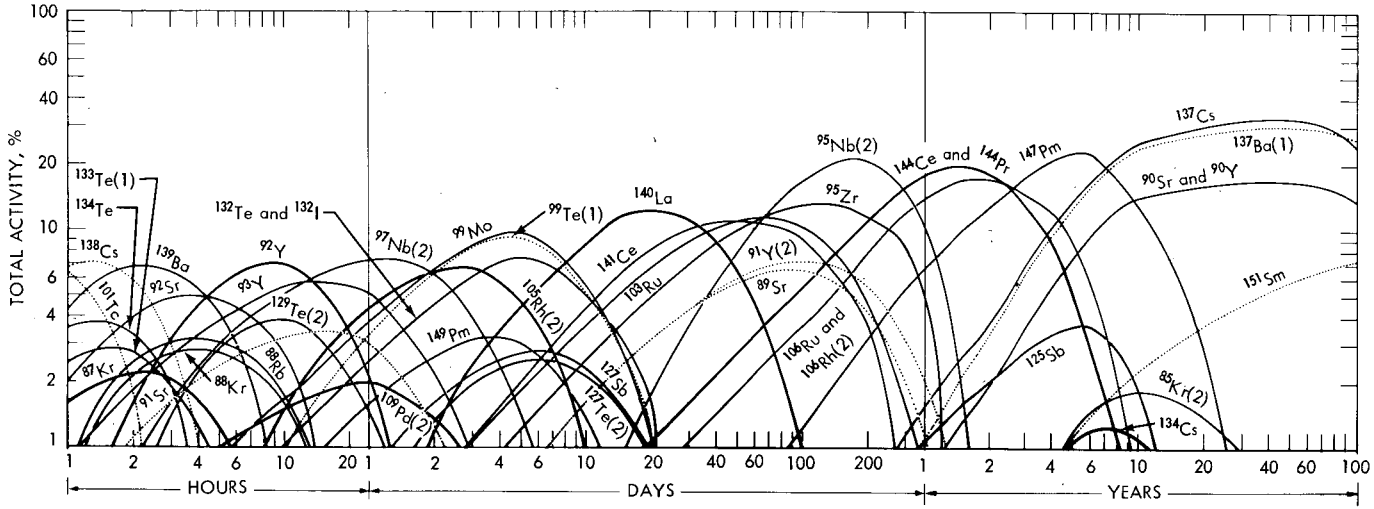

Fig. 11—Relative disintegration rates as a function of time for individual fission products in the case of ^{238}U fission produced by a thermonuclear neutron spectrum.

TEF 55 Conf 765

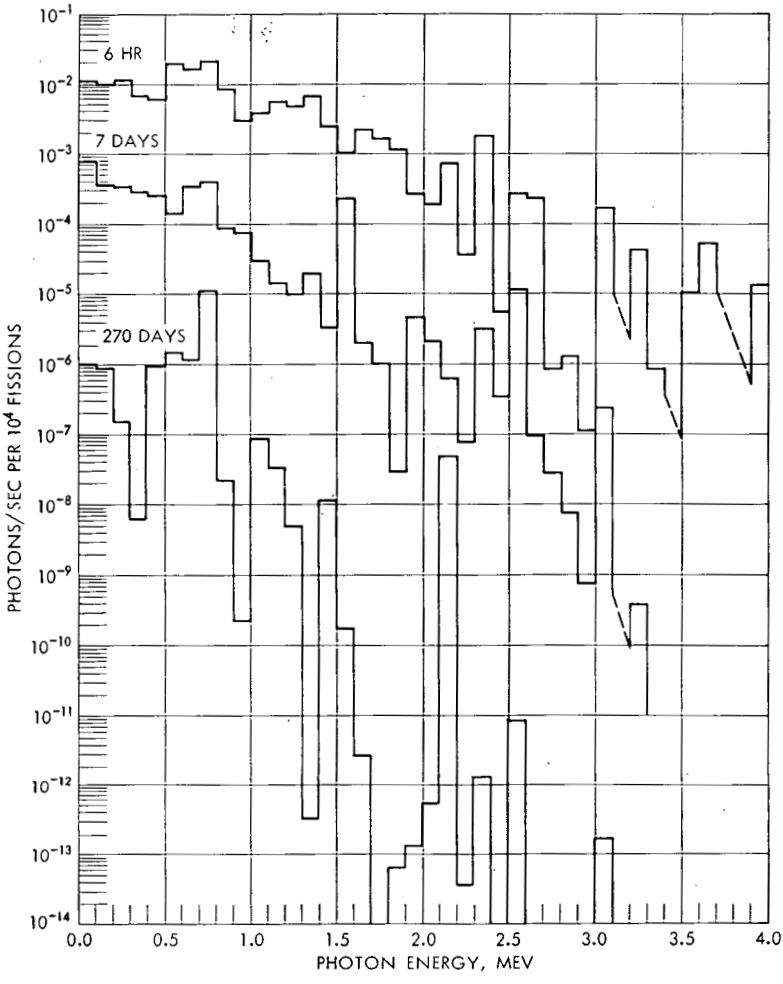

Fig. 12—Gamma-photon spectra from fission products at various times after ^{238}U fission produced by a thermonuclear neutron spectrum.

The relative contributions of the important gamma-emitting nuclides to the total dose-rate have been plotted vs. time in Fig. 14. It is interesting to note that from a few days onward much of the dose rate at any given time can be accounted for in terms of two or three nuclides and that volatilely behaving mass chains contribute prominently to the dose rate. The dose-rate contributions given here pertain, of course, to unfractionated debris. Since many of the hard emitters (e.g., cesium and iodine isotopes) are subject to fractionation, the relative dose-rate contributions will be greatly modified in the case of fractionated debris.

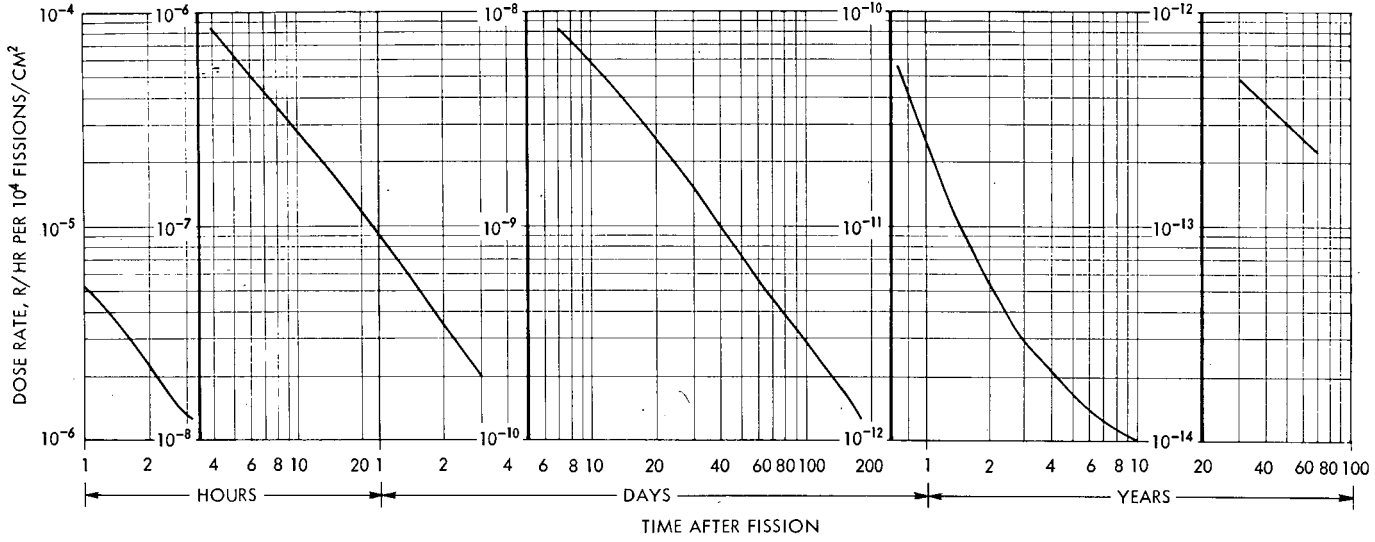

Fig. 13—Gross exposure-dose-rate decay for products of ^{238}U fission produced by a thermonuclear neutron spectrum.

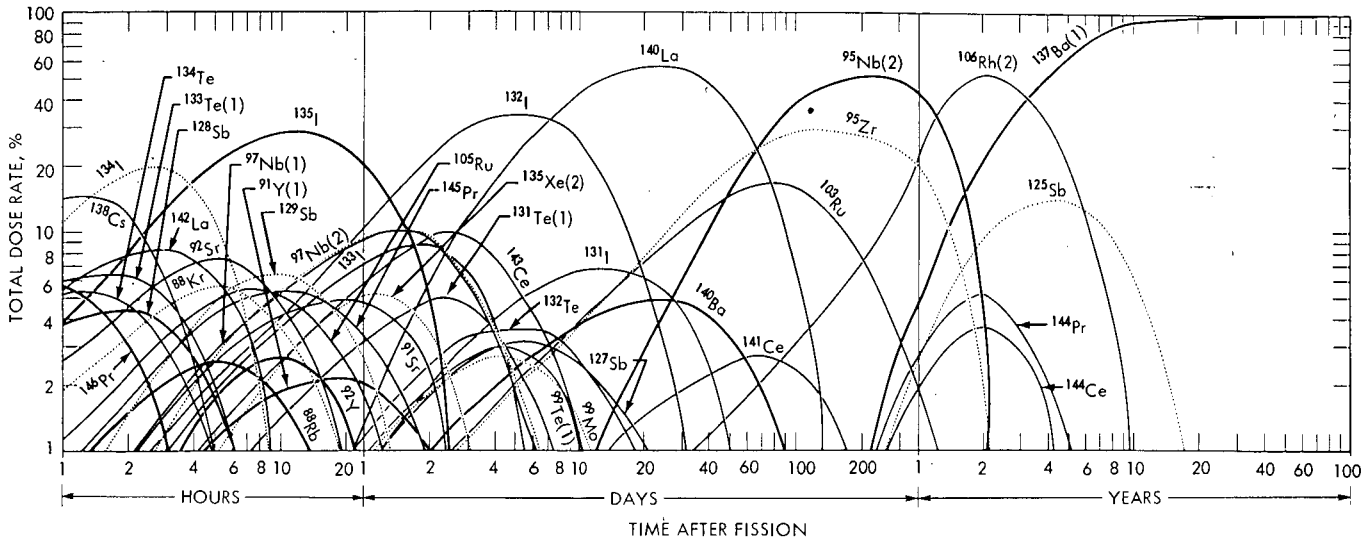

Fig. 14—Relative contributions to the exposure-dose rate as a function of time for individual fission products in the case of ^{238}U fission produced by a thermonuclear neutron spectrum.

FRACTIONATION CORRELATIONS

As previously explained, correlation parameters for fractionated radiochemical compositions provide useful and realistic input for the semiempirical prediction of fractionation effects. Moreover, the results of statistical analyses of fractionation data furnish insight into the overall fractionation process. We are presently completing the correlation of thousands of analytical results on fractionated debris from 15 air bursts covering a yield variation of over 300-fold. Details will appear in a forthcoming USNRDL technical report. For a more effective comparison of the correlation parameters for air bursts with those obtained from surface bursts, the air-burst data will be presented in a following paper.* Some observations on air-burst data of interest, however, are appropriately given here:

1. Although the majority of $r_{89,95}$ values observed fell in the range from 0.1 to 3.0, several shots showed a hundredfold variation, and the greatest was over 900-fold.
2. The preference for linear or logarithmic correlations was variable and depended upon the "goodness-of-fit" criteria.
3. There was little, if any, dependence of correlation parameters on device yield.
4. Tests are still in progress to determine whether the values of given nuclide ratios (as determined on different shots) are all from the same population.

Upon completion of air-burst data correlations, we plan to correlate data from underwater bursts and additional high-yield surface bursts. Another project under way in this area is the retrieval of information from old fallout samples. There are extant debris samples from most nuclear detonations. Many of these detonations were poorly documented with regard to fractionation data. In addition, some large gaps exist in our knowledge of fractionation phenomena (e.g., tower-burst fractionation, fractionation of soil-induced activities, and fractionation as a function of particle type). There remain in these samples both volatile and refractory fission products to use as standards (e.g., ^{137}Cs and ^{144}Ce). Thus the present moratorium on weapons testing offers an opportunity to recover much pertinent data, and this project has already yielded a few surprises.

LABORATORY STUDIES

Our laboratory studies to date have been concerned with the equilibrium properties of systems containing volatile oxides. These studies

*See paper by Glenn R. Crocker, Francis K. Kawahara, and Edward C. Freiling, this volume.

provide both direct input information for the thermodynamic model and knowledge of molten-soil chemistry which allows extension to many soil types. The information required by the model is the number of moles n_1^0 of volatile constituent in the vapor phase and the number of moles n_1 in the condensed phase at equilibrium. To make this ratio invariant to the relative quantities of each phase, it is customary and convenient to express the partition in terms of concentrations, e.g., the mole fractions in either phase ($N_1 = n_1/\Sigma n_i$), concentration in the gas phase ($c_1^0 = n_1^0/V$), or concentration in the condensed phase ($c_1 = n_1/M$). Here V refers to the volume of vapor and M to the mass of condensate. Partitions can then be expressed in terms of Henry's law:

$$\frac{c_1^0}{N_1} = \frac{k_1}{RT}$$

where k_1 is Henry's law constant, R is the molar gas constant, and T is the absolute temperature, or in various forms of a distribution coefficient, such as

$$\lambda_1 = c_1^0/c_1$$

$$\lambda_1' = c_1^0/N_1$$

$$\lambda_1'' = N_1^0/N_1$$

Henry's law expression is applicable only if the species of volatile material in the vapor state is known (monomer, dimer, degree of dissociation, degree of hydration, etc.), whereas λ_1 and λ_1' are applicable under all circumstances of present interest.

It is appropriate at this point to raise a number of questions about the sensitivity of the distribution coefficients to several environmental variables: How will they be affected by (1) various soil compositions, (2) the presence of volatile material in the soil, (3) the concentration level of the active species, (4) the presence of moisture, and (5) the temperature? We have not tried to answer all questions at once, only the first three. The studies have been concerned with the basic oxide, Rb_2O (precursor of strontium radionuclides), and the acidic oxide MoO_3 (precursor of ruthenium radionuclides). The results here include some obtained for the Division of Research, AEC.

Soil Composition

Soil compositions vary over wide ranges, but usually they are composed of a relatively small number of major constituents, both refractory (SiO_2, Al_2O_3, Fe_2O_3, FeO, MgO, and CaO) and volatile (Na_2O,

K_2O, and H_2O). Rather than treat various soil samples chosen at random, we have studied the effects of representative individual constituents and pairs of constituents and their contribution to the overall affinity for rubidium when present in a soil sample. This approach greatly reduces the number of measurements to be made but has some fundamental drawbacks.

One kind of measurement consisted in equilibrating constituents with vapor from a Rb_2O-TiO_2 source at 1272°C in a platinum isopiestic chamber. Under these conditions, c_1^0 was determined by transpiration measurements to be 1.1×10^{-5} mole/liter, assuming Rb_2O to be the vapor species. The actual species is unknown. Constituents studied were SiO_2, Al_2O_3, iron oxide,* and CaO. An attempt to include Na_2O and K_2O resulted in their complete replacement by Rb_2O; therefore Rb_2O played a double role. It represented both the fission-product species of interest and the displaced Na_2O and K_2O. The results are summarized schematically in Fig. 15. This diagram shows the N_i value of each constituent of a ternary equilibrium mixture. Neither MgO nor CaO (the principal constituent of molten debris from a coral-surface burst) shows any affinity for rubidium. The highest affinity is shown by Al_2O_3 (major constituents of air-burst debris). The pair SiO_2-MgO forms an almost ideal solution; i.e., it takes up Rb_2O in proportion to the SiO_2 concentration, the MgO acting as an inert diluent. On the other hand, CaO monopolizes SiO_2 and prevents it from taking up rubidium until its concentration drops to the value represented by the compound $2CaO \cdot SiO_2$. This compound behaves ideally with respect to SiO_2 at the remaining compositions. The system $SiO_2-Al_2O_3$ splits into two ideal portions at the composition $Rb_2O \cdot Al_2O_3 \cdot 2SiO_2$. The systems Al_2O_3-CaO and Fe_2O_3-CaO (important for tower bursts on coral surfaces) show no ideality.

For application of these data to actual soil samples, a sample of silicate soil (Ambrose clay loam) of known compositon was melted in the isopiestic apparatus and its uptake of Rb_2O measured. By means of the experimental data described above, it was estimated that the soil would take up about 52% by weight of Rb_2O. The measured uptake was 49%. A similar experiment was tried using a sample of the rockforming mineral orthoclase feldspar. The predicted uptake was 48%. The actual uptake was only 32 to 43% with some uncertainty in the experimental value, possibly because of failure to achieve equilibrium.

Results with MoO_3 vapor in the SiO_2-CaO system show the opposite behavior from Rb_2O. Here SiO_2 takes up no MoO_3 whereas 1 mole of

*Regardless of whether the initial form of iron oxide is FeO, Fe_2O_3, or Fe_3O_4, the species resulting from equilibration with air will be the same in each case.

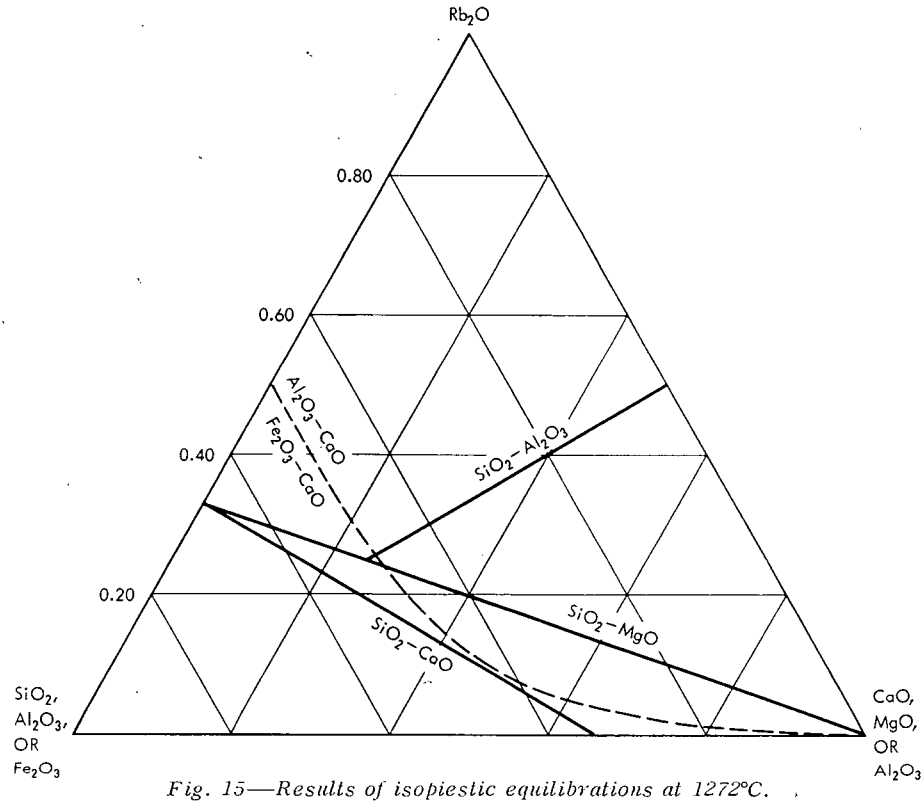

Fig. 15—Results of isopiestic equilibrations at 1272°C.

CaO takes up 1 mole of MoO_3. The curve shows a small, negative departure from ideality.

Effect of Moisture

The previously mentioned experiments were carried out under dry, if not anhydrous, conditions. A virtue of isopiestic results is their independence of the species present in the vapor state. The presence of a small amount of moisture will not, therefore, affect the relative Rb_2O uptake of these systems, but it could affect the equilibrium vapor concentration. Several oxides of interest form gaseous hydroxides in the presence of moisture. Glemser and Wendlandt[33] have recently reviewed information on gaseous hydroxides and present evidence for the stability of gaseous NaOH, KOH, RbOH, CsOH (precursor of $^{140}Ba-^{140}La$), $MoO_2(OH)_2$, and $TeO(OH)_2$ (precursor of iodine radionuclides). Future experiments will have to test the effect of water vapor on the distribution coefficients.

Effect of Fission-product Concentration and Volatile Soil Constituents

The concentration of a given fission product in the fireball is extremely small (of the order of 10^{-12} mole/liter). This very low concentration level affects its behavior in the vapor phase, its interaction with vaporized material, its species in the condensed phase, and, consequently, its distribution coefficient.

The effect of low concentrations on the vapor species can be viewed from both kinetic and thermodynamic viewpoints. Consider a fission product M that is formed initially as MO but whose normal species is M_2O. The formation of an M_2O molecule requires the collision of two MO molecules. At low MO concentrations such collisions will be comparatively rare with respect to collisions with macroscopic concentrations of vaporized soil or device constituents. Furthermore, kinetic activation energies and transition probabilities for reactions involving MO may be considerably different from those involving M_2O. Thermodynamically, we would say that the low concentrations would have the effect of impeding association to form polynuclear or polymeric compounds.

The fission-product species that wants to form a polynuclear molecule but is unable to find an identical species to pair up with may settle for a reasonable approximation. Thus it is very unlikely that two $^{90}RbOH$ molecules would pair up in a silicate-surface burst to form the dimer $(^{90}RbOH)_2$. It is much more likely that each would pair up with a NaOH molecule (formed from vaporized water and Na_2O soil constituents) to form the well-known $^{90}RbOH{\cdot}NaOH$. One can visualize many similar situations which are likely but which have never been investigated. The net reaction between such monomers and the refractory portion of the soil (indicated by R) can be written as $Na_2O{\cdot}R(c) + RbOH(v) \rightleftharpoons NaRbO{\cdot}R(c) + NaOH(v)$. Here (c) and (v) indicate condensed and volatile phases, respectively. The equilibrium constant for this reaction is expressed in terms of activities as

$$K = \frac{a^0_{NaOH}}{a^0_{RbOH}} \frac{a_{NaRbO{\cdot}R}}{a_{Na_2O{\cdot}R}}$$

Replacing vapor-phase activities by partial pressures and assuming equal activity coefficients for the condensed species,

$$K = \frac{(p_{NaOH}/N_{Na_2O{\cdot}R})}{(p_{RbOH}/N_{NaRbO{\cdot}R})}$$

According to this expression, K is essentially a selectivity coefficient, the quotient of two distribution coefficients. From a knowledge of K,

the variation in rubidium distribution with sodium content at any given temperature can be calculated, with appropriate corrections made for polymerization.

Considerations for the condensed phase are similar to those for the vapor phase. Lapple[34] has speculated on the existence of pure ^{90}SrO particles. The most favorable situation for producing these would be an air burst, where ^{90}Sr might be present in the condensed phase at the relatively high average concentration of 10^{-3} at.% of all atoms (e.g., a 20-kt air burst containing 1 ton of steel or aluminum). No such particles have ever been reported. All observations indicate that the fission products are highly dispersed on or throughout the substrate material.

Future Plans

The described considerations all indicate the approximations involved in judging the behavior of tracer components by the properties they exhibit at high concentrations. In our experiments the vapor concentration of rubidium was some millionfold greater than that in the fireball. On the other hand, the excess rubidium served to approximate the effect of macroscopic vapor concentrations of Na_2O and K_2O. Although the latter effect was overcompensated in the condensed phase, the data provide upper limits of the distribution coefficients, and in a number of instances these suffice. In the other instances the degree of approximation is probably not bad compared to other uncertainties with which the fallout-formation model maker is faced. The wisest course appears to consist in being aware of the difficulties, in making experiments as realistic as feasible, and in judging the adequacy of the results by comparison with observations on nuclear debris in the light of sensitivity analyses of the prediction scheme.

With improved measurement techniques we have constructed a furnace that consists of two zones at different temperatures. Whereas our previous isothermal–isopiestic technique relied solely on source dilution to limit the fission-product vapor concentration, our new biisothermal-isopiestic apparatus will permit attainment of lower vapor pressures by using a source that is cooler than the sample, besides providing higher temperatures in the sample zone. With this apparatus we expect to achieve more realistic conditions of concentation, temperature, moisture content, and soil volatility.

We are also developing a method of making dynamic studies at high temperatures. This method promises to permit the simultaneous investigation of many kinetic properties. If successful, this method will permit a degree of realism far surpassing any thus far achieved. The ultimate method would consist of temperature-programed inorganic gas chromatography with a polydisperse fluidized bed, with humidity-controlled air as a carrier gas, carried out in both the presence and the absence of high radiation fields.

ACKNOWLEDGMENTS

We are most grateful to Col. Irving J. Russell of the Air Force Weapons Laboratories and Dr. John Norman of General Atomic Division, General Dynamics Corporation, for permission to present their data prior to publication.

APPENDIX

TERMS AND DEFINITIONS

RADIONUCLIDE FRACTIONATION Any alteration of radionuclide composition occurring between the time of detonation and the time of radiochemical analysis which causes the debris sample to be nonrepresentative of the detonation products taken as a whole.

FRACTIONATED Two substances, either radionuclides or inert material, are fractionated with respect to each other in a sample of debris if they are not present in their representative ratio. The term is meaningless when applied to a single substance.

*POTENTIAL FRACTIONATION The existence of different compositions in various portions of a sample of debris when these portions are subject to separation by subsequent natural processes, e.g., the existence of particles of different size with different compositions in the same portion of a nuclear cloud or of a slurry in which different nuclides are distributed between liquid and solid phases in different proportions.

*NATURAL FRACTIONATION Fractionation produced by the processes occurring subsequent to detonation.

*PRIMARY FRACTIONATION IN AIR, TOWER, AND SURFACE BURSTS Actual fractionation produced by meteorological, gravitational, and centrifugal separation of potentially fractionated particles in a cloud.

*SECONDARY FRACTIONATION IN AIR, TOWER, AND SURFACE BURSTS Fractionation produced by interaction of the debris with radioactively inert environment (e.g., leaching with water or preferential small particle adsorption on surfaces).

*ARTIFACTITIOUS FRACTIONATION Fractionation resulting from human intervention (e.g., biased sampling, incomplete decontamination of collector surfaces, and faulty analytical techniques).

FRACTION OF CONSITITUENT OR EXTENSIVE PROPERTY IN A SAMPLE The ratio of the quantity of said constituent or property to the total amount produced by the device and measured at the same time when necessary (replaces the "bomb-fraction" concept).

*Asterisks indicate convenient, but not essential, terms.

EQUIVALENT FISSIONS The number of equivalent fissions present in a sample as determined by analysis for any constituent is the product of the total number of fissions produced by the device and the fraction of the total amount of constituent present (replaces the "fissions in the sample" concept).

FRACTIONATION COEFFICIENT OF TWO CONSTITUENTS IN A SAMPLE The ratio of their fractions or equivalent fissions.

*THE FRACTIONATION RATIO The ratio of fractions or equivalent fissions of ^{89}Sr to ^{95}Zr.

*DEGREE OF FRACTIONATION The Briggsian logarithm of the fractionation ratio.

*TERACALORIE 10^{12} calories (the kiloton equivalent of energy).

*TERACALORIE EQUIVALENT OF A NUCLIDE The ratio of quantity of nuclide produced in a detonation to the energy release in teracalories by fission.

TERACALORIE EQUIVALENT PER SQUARE MILE A unit of contamination surface density (replaces the "kilotons per square mile" concept).

REFERENCES

1. E. C. Freiling, *Fractionation. I. High Yield Surface Burst Correlations,* Report USNRDL-TR-385, U. S. Naval Radiological Defense Laboratory, Oct. 29, 1959; and *Science, 133:* 1991 (1961).
2. E. C. Freiling and S. C. Rainey, *Fractionation. II. On Defining the Surface Density of Contamination,* Report USNRDL-TR-631, U. S. Naval Radiological Defense Laboratory, Mar. 13, 1963.
3. E. C. Freiling, *Fractionation. III. Estimation of Degree of Fractionation and Radionuclide Partition for Nuclear Debris,* Report USNRDL-TR-680, U. S. Naval Radiological Defense Laboratory, Sept. 12, 1963; and *Science, 139:* 1058 (1963).
4. E. C. Freiling, M. A. Kay, and J. V. Sanderson, *Fractionation. IV. Illustrative Calculations of the Effect of Radionuclide Fractionation on Exposure Dose Rate from Local Fallout,* Report USNRDL-TR-715, U. S. Naval Radiological Defense Laboratory, Jan. 6, 1964.
5. E. C. Freiling, Fractionation in Surface Bursts, in *Radioactive Fallout from Nuclear Weapons Tests,* A. W. Klement, Jr. (Ed.), USAEC Report TID-7632, pp. 25-46, Feb. 1962.
6. C. F. Miller, *A Theory of Formation of Fallout from Land-surface Nuclear Detonations and Decay of the Fission Products,* Report USNRDL-TR-425, U. S. Naval Radiological Defense Laboratory, May 27, 1960.
7. C. F. Miller, *Fallout and Radiological Countermeasures,* Stanford Research Institute, Menlo Park, Calif., January 1963.
8. C. E. Miller, Jr., W. E. Browning, Jr., B. F. Roberts, and R. P. Shields, *Theory of Fission Product Fractionation in Reactor Fuel Experiments, Reactor Accidents and Weapons Fallout,* paper presented at the 148th National Meeting of the American Chemical Society, Chicago, Ill., Aug. 30 to Sept. 4, 1964.
9. S. L. Whitcher, L. R. Bunney, R. R. Soule, and R. da Roza, *Fallout Measurements by Aircraft and Rocket Sampling,* Operation Hardtack Report, WT-1625, U. S. Naval Radiological Defense Laboratory, Sept. 29, 1961. (Classified)

10. I. J. Russell, *A Radiochemical and Physical Investigation of a Low-yield Surface Burst,* Defense Atomic Support Agency, Project Officers Report, in preparation.
11. T. B. King and P. J. Koros, Diffusion in Liquid Silicates, in *Kinetics of High-Temperature Processes,* W. D. Kingery (Ed.), pp. 80-85, published jointly by Technology Press of Massachusetts Institute of Technology and John Wiley & Sons, Inc., New York, 1959.
12. V. I. Musikhin and O. A. Esin, Diffusion Coefficients in Molten Slags, in *Physical Chemistry of Molten Salts and Slags, Proceedings of the All-Union Conference, Nov. 22 to 25, 1960,* USAEC Report AEC-tr-5948, pp. 481-491.
13. V. I. Malkin and V. M. Mogutnov, Measurement of Coefficients of Autodiffusion of Sodium Ion in Three-component Silicate Melts, in *Physical Chemistry of Molten Salts and Slags, Proceedings of the All-Union Conference, Nov. 22-25, 1960,* USAEC Report AEC-tr-5948, pp. 492-501.
14. J. H. Norman, personal communication, 1964.
15. R. W. Hillendahl, *Characteristics of the Thermal Radiation from Nuclear Detonations,* Report USNRDL-TR-383, U. S. Naval Radiological Defense Laboratory, June 30, 1959. (Classified)
16. O. Knacke and I. N. Stranski, The Mechanism of Evaporation, in *Progress in Metal Physics,* Vol. 6, B. Chalmers and R. King (Eds.), p. 181, Pergamon Press, London, 1956.
17. N. Fuchs, Über die Verdampfungsgeschwindigkeit kleiner Tröpfchen in einer Gasatmosphäre, *Phys. Z. Sowjet, 6:* 224 (1934).
18. L. Lassen, G. Rau, and H. Weicksel, The Deposition of Radioactive Atoms on Monodisperse and Polydisperse Aerosols, *Z. Physik, 160:* 504-519 (1960); *161:* 339-345 (1961); and *163:* 363-376 (1961); see also USAEC Report UR-tr-647, University of Rochester, June 8, 1964.
19. H. S. Carslaw and J. C. Jaeger, *Conduction of Heat in Solids,* Clarendon Press, Oxford, 1959.
20. H. Scholze, H. Mulfinger, and H. Franz, Measurement of the Physical and Chemical Solubility of Gases in Glass Melts (He and H_2O), in *Advances in Glass Technology,* p.230, Plenum Press, New York, 1962.
21. P. B. Storebö, *On Particle Formation in Nuclear Bomb Debris,* Report F-446, Norwegian Defense Research Establishment, May 12, 1964.
22. L. E. Weaver, P. O. Strom, and P. A. Killeen, *Estimated Total Chain and Independent Fission Yield for Several Neutron-Induced Fission Processes,* Report USNRDL-TR-633, U. S. Naval Radiological Defense Laboratory, Mar. 5, 1963.
23. G. R. Crocker, *Estimates of Fission Product Yields of a Thermonuclear Explosion,* Report USNRDL-TR-642, U. S. Naval Radiological Defense Laboratory, Apr. 4, 1963.
24. C. D. Coryell, M. Kaplan, and R. D. Fink, Search for Correlations of Most Probable Nuclear Charge Z_p of Primary Fission Fragments with Composition and Excitation Energy, *Can. J. Chem., 39:* 646 (1961).
25. I. F. Croall and H. H. Willis, The Yields of the Isomers of Se-81 and Se-83 in the Thermal Neutron Fission of Pu-239, *J. Inorg. Nucl. Chem., 25:* 1213 (1963).
26. Massachusetts Institute of Technology, *Laboratory for Nuclear Science Progress Report,* USAEC Report NYO-10063, May 1, 1963.
27. R. C. Bolles and N. E. Ballou, *Calculated Activities and Abundances of U^{235} Fission Products,* Report USNRDL-456, U. S. Naval Radiological Defense Laboratory, Aug. 30, 1956.
28. G. R. Crocker and M. A. Connors, *Gamma Emission Data for the Calculation of Exposure-Dose Rates from Nuclear Debris,* Report USNRL-R&L-143, U. S. Naval Radiological Defense Laboratory, May 12, 1964.
29. L. D. Gates, Jr. and C. Eisenhauer, *Spectral Distribution of Gamma Rays Propagated in Air,* Report AFSWP-502A, Armed Forces Special Weapons Project, 1954.

30. D. A. Holme and K. Stewart, *The Gamma Dose-Rate above an Infinite Plane Source,* Report AWRE-E-6/63, United Kingdom Atomic Energy Authority, May 1963.
31. C. F. Miller, *Response Curves for USNRDL 4-pi Ionization Chamber,* Report USNRDL-TR-155, U. S. Naval Radiological Defense Laboratory, May 17, 1957.
32. R. Björnerstedt, Health Hazards from Fission Products and Fallout. II. Gamma Radiation from Nuclear Weapons Fallout, *Ark. Fysik, 16:* 293 (1959).
33. O. Glemser and H. G. Wendlandt, Gaseous Hydroxides, in *Advances in Inorganic Chemistry and Radiochemistry, Vol. 5,* H. J. Emeleus and A. G. Sharpe (Eds.), Academic Press Inc., New York, 1963.
34. C. E. Lapple, *Fallout Control,* Report SRIA-3, Stanford Research Institute, Aug. 1, 1958.

SMALL BOY SHOT FALLOUT RESEARCH PROGRAM

CARL F. MILLER and JAMES D. SARTOR
Stanford Research Institute, Menlo Park, California

ABSTRACT

In this paper the general outline of a field test program is presented along with the application of the outline to the design of the experimental program for the Small Boy shot. Also, a preliminary analysis and correlation of the data obtained on two of the projects is presented in a discussion and an evaluation of the intensity–activity ratio and the intensity–area integral per unit fission yield (i.e., the ratio of roentgens per hour at 1 hr per kiloton per square mile) for the fallout from the Small Boy shot.

INTRODUCTION

Over the past decade many significant advances in development and field testing of nuclear explosives have been made. In the field testing of nuclear weapons, explosion products, called fallout, received increasing attention as the testing proceeded. One of the major reasons for the increased attention to fallout was that, during this same period of time, better understanding and recognition of the radiological hazards to biological species from exposures to nuclear radiation were accomplished. In addition, studies of the application of nuclear explosives in possible future warfare showed that exposure of human beings and other living species to the nuclear radiations associated with fallout could result in many fatalities.

Field experimental programs designed to obtain information on fallout became increasingly complex as time progressed. The evolvement of experimental procedures in the field tended to reflect, at the time, both the understanding of the radiological hazards and the

technical parameters that influenced the character and magnitude of the hazards.

The fallout study program for the Small Boy shot, as part of the last series of aboveground field tests of nuclear weapons, was cooperatively organized and sponsored by the Office of Civil Defense (OCD), the Department of Defense (DOD), and the Atomic Energy Commission (AEC). The projects sponsored by OCD were under the operational control of the Defense Atomic Support Agency (DASA); those sponsored by AEC were under the operational control of their Civil Effects Test Organization (CETO).

WEAPON-TEST-FALLOUT STUDY PROGRAM

A general outline of the information and data requirements and the program objectives was prepared prior to the establishment of the experimental projects for the Small Boy shot field test. This outline was reviewed by various representatives of OCD, DASA, and AEC.

The outline, reflecting operational data requirements by the three agencies, included an overall design of field experimental programs for improving the data base on fallout. The data needs were divided into the following four subprograms or study areas:

1. Fallout formation
2. Distribution of fallout
3. Definition of radiological exposure environments
4. Alteration of exposure environments by radiological countermeasures

For each of the four study areas, a general list of the parameters for direct or indirect experimental evaluation was prepared. These are given in Tables 1 to 4. The first three study areas were organized to provide input data for fallout-model development and radiological-hazard evaluations needed by all three agencies. The fourth study area was designed somewhat more specifically for providing information for use in the evaluation of radiological-safety programs for AEC and in the design and evaluation of radiological-defense systems for OCD.

The main overall objective of the weapon-test-fallout study was to make experimental determinations and to obtain and report experimental data needed for describing and defining the parameters in each of the four study areas. The objective for the field-test program was limited to the taking and reporting of experimental data because each agency sponsored other research tasks for the correlation and evaluation of the observed data and because inclusion of data analysis in field-test reports previously had usually resulted in extended delays in report publication.

Table 1— FALLOUT-FORMATION PARAMETERS

Initial condition variables
- Composition of the device
- Composition and physical properties of the environmental materials at shot point

Geometric parameters
- Dimensions and location of the visible fireball and cloud as a function of time after detonation
- Dimensions of the apparent crater and crater lip
- Spatial distribution of radioactivity in the fireball and cloud volume as a function of time after detonation
- Spatial geometry of toroidal circulation of the rising fireball and cloud

Energy balance parameters
- Air overpressures and ground-shock energies
- Radiant energy emitted as a function of time after detonation
- Temperature of fireball gas as a function of time after detonation
- Material composition of fireball and influx, mixing, and ejection of gases and particles as a function of particle size and time after detonation
- Energetics (dynamics) of particle circulations in and about the rising fireball and cloud

Related resultant parameters
- Chemical composition of fallout particles
- Radiochemical composition of particles as a function of particle diameter, including specific activity of the particles
- Radioactivity and mass-distribution functions
- Solubility of radioelements as a function of particle size
- Shape, structure, and density of fallout particles and internal distributions of crystalline and glass phases and of the radioelements within the fallout particles

Table 2— FALLOUT-DISTRIBUTION PARAMETERS

Initial-condition variables
- Spatial distribution of radioactivity and mass of particles at the time of cloud stabilization and at the times when particles start free-gravity fall

Particle-fall-rate parameters
- Density distribution of fallout particles as a function of particle diameter, shape, and number or mass
- Atmospheric conditions (air density, viscosity, temperature, pressure, relative humidity, etc.) as a function of altitude over the fallout area
- Particle shape and drag factors
- Agglomeration effects (including incorporation of solid particles in raindrops)

Meteorological parameters
- Wind speeds and direction as a function of altitude and time over the whole fallout area
- Vertical air motions
- Effect of terrain features and diurnal heating and cooling on the air-flow patterns

Deposition dynamics
- Time of arrival of fallout particles at given locations on the ground or in the air as a function of particle size
- Duration of fallout deposition at given locations in the fallout area

(Table 2 continues on page 47)

Rate of accumulation of particles in terms of radioactivity and mass at given locations in the fallout area
Effect of rainfall on deposition rates and air concentration of particles

Area distribution of the fallout particles
Standard intensity contours (usual fallout pattern expressed in roentgens per hour at 1 hr at 3 ft above an open contaminated area)
Intensity–activity ratios (in roentgens per hour at 1 hr per kiloton per square mile at various locations in the fallout area
Intensity–area integral and fraction of the device in the fallout area
Fraction of the total radioactivity and mass of particles deposited on the earth's surface as a function of time after detonation
Surface-density contours (mass of particles deposited per unit area)
Gross fractionation numbers for the fallout deposited at given locations in the fallout area as a function of particle diameter

Table 3— RADIOLOGICAL-EXPOSURE-ENVIRONMENT PARAMETERS

Initial contamination of surfaces
Surface wind speeds and directions and relative humidity
Effect of large- and small-scale surface roughness features of terrain on the airflow over the surface
Shape, size, general orientation, and character of the surface
Impaction and retention efficiency of particles and surfaces as a function of the above parameters, particle diameter, and surface density of the deposit
Initial contamination factors for plants, animals, and humans
Inhalation of fallout particles during fallout deposition by animals and humans as a function of particle diameter, wind speed, and related factors

Natural redistribution of deposited fallout particles and radiation sources
Transfer of soluble radionuclides from the fallout particles to surfaces by dew and rain as a function of time, particle size, and amount of dew and/or rain
Effect of erosion by wind and rain of the deposited fallout particles from and onto surfaces on the ionization rate and particle surface density as a function of particle diameter, type of surface, wind speed, amount of rainfall, time period over which erosion occurs, and general terrain features
Movement of soluble radionuclides and particles in and over soils due to rainfall as a function of particle diameter, gross deposit surface density, soil type, number of rain showers, and amount of rainfall
Movement of soluble radionuclides and particles in streams and rivers as a function of particle size, deposit surface density, water flow rates, and other stream or river characteristics
Variation of retention efficiencies and contamination factors on meteorological parameters (wind, rainfall, relative humidity, etc.)
Inhalation of redistributed (wind-blown) particles
Movement of particles by people and vehicular traffic

External gamma-radiation-exposure parameters
Variation of air ionization rates with time after detonation at given locations in the fallout region (reference geometry: 3 ft above an open contaminated area)
Gross ionization-rate decay of the radioactivity carried by particles as a function of particle diameter
Attenuation of gamma rays by terrain-roughness features
Variation of the air ionization rate with altitude over given locations in the fallout area

(Table 3 continues on page 48)

Table 3— (Continued)

Response factors for radiation detecting instruments
Area radiation-contribution factors for discontinuous source geometries and variable source intensities
Skyshine-contribution factors as a function of surface roughness and source geometry

Contact radiation exposures
Beta dose and dose rates in air over contaminated surfaces as a function of distance from the surface
Absorbed beta dose to the tissue of contaminated plants, animals, and humans
Dependence of absorbed contact beta doses on meteorological factors, exposure times, and environmental factors (all biological species, including insects)

Internal radiation-exposure parameters
Biological availability of individual radionuclides as a function of particle size
Foliar absorption of radionuclides by edible plants or plant parts as a function of particle diameter
Uptake rate of radionuclides by edible plants grown on tilled and untilled soils as a function of particle diameter or location, plant growth rates, soil type, and climatic variables
Ingestion and assimilation rates of radionuclides by tissues of animals and radionuclide concentrations in animal tissues and food products from animals fed with contaminated plant parts and water obtained from different locations in the fallout area
Absorbed doses to plants, animals, and humans from ingestion of radionuclides (all intake paths)

Table 4— ALTERATION OF EXPOSURE ENVIRONMENTS BY RADIOLOGICAL COUNTERMEASURES

Attenuation of gamma-ray intensities
Shelter protection factors as a function of wall materials and thickness, radiation-source geometry, and compartment size, shape, and location in building
Attenuation by barriers as a function of barrier height and thickness and other geometric parameters, such as the distance from barrier or the dimensions of area enclosed by the barrier
Attenuation by burial of the fallout particles by covering them with soil or by plowing (i.e., mixing the fallout with soil to various depths) land areas

Decontamination
Effectiveness of the removal of fallout particles from contaminated surfaces as a function of the method and its procedural parameters, particle diameter of the fallout, surface density of the fallout, weathering, type of surface, and effort applied
Disposal of fallout particles removed by decontamination
Exposure dose to decontamination crews during decontamination operations as a function of the type of area that is cleaned, the operation schedule, and the methods of decontamination
Effectiveness of water purification methods in the removal of soluble radionuclides and fallout particles from exposed water sources
Effectiveness of food processing and treatment methods in the removal of soluble radionuclides from contaminated food products (i.e., milk decontamination, removal of particles from grains in threshing and milling, desorption of radionuclides from vegetables into water, etc.)

(Table 4 continues on page 49)

Table 4 — (Continued)

Exposure control methods
Reduction in exposure doses by scheduling of exposures for operations
Reduction in exposure doses by adjustment of living routines as a function of time after detonation and radiation intensity
Reduction in absorbed doses to animals and humans by storage and allocation of contaminated foodstuffs
Ingress of fallout particles into shelter spaces through openings and ventilation systems and effect on the exposure dose or on the shelter protection factor
Verification of shielding provided by specially designed shelter-entryway configurations
Proof tests of operational radiological-defense systems and overall effectiveness evaluations

The individual project titles, as parts of the field-test fallout program for the Small Boy shot, are listed in Table 5. The projects, with a few exceptions, were very successful in meeting their individual objectives. This general success was due, first, to the detailed development of the project experimental designs on the part of the project leaders and the efforts of all the project personnel in carrying out the work and, second, to the favorable winds that carried the fallout over the established station array. It should be noted that projects involving the design and testing of sampling equipment for possible use in future programs were included in the program.

Table 5 — PROJECT PARTICIPATION IN SMALL BOY SHOT FALLOUT PROGRAM

1.	Thermal measurements and fireball photography
2.	Meteorological measurements
3.	Radiological survey of the fallout area
4.	Aerial survey of the fallout area
5.	Fallout collection and gross sample analysis (onsite and offsite)
6.	Field ionization-rate measurements
7.	Long-range fallout collection and radiochemical analysis
8.	Physiochemical and radiochemical analysis of fallout samples
9.	Terrain shielding measurements and field spectra (onsite and offsite)
10.	Contamination of plants
11.	Ingestion of radionuclides in fallout by native animals
12.	Assimilation of radionuclides in fallout by humans
13.	Contamination of milk (unscheduled)
14.	Proof-test of a prototype rocket-mounted collector
15.	Test of a prototype fallout sampler
16.	Comparison of aerial-survey instruments

THEORY OF THE INTENSITY–ACTIVITY RATIO AND THE INTENSITY–AREA INTEGRAL

Known relations between the observed radiation rates and the radioactivity carried by fallout particles spread over real (open) terrain are required to evaluate radioactive-material balances and

the relative worldwide disposition of all the radionuclides produced in a nuclear detonation. The ratio of the roentgens per hour at 1 hr to kilotons per square mile, where the kilotons are taken as being a measure of the radioactivity carried by the fallout particles, is used in the integration of fallout-pattern contours to estimate the fraction of the device accounted for in the pattern. Other more detailed uses of the ratio include the effects of terrain roughness and radionuclide fractionation on gamma-radiation intensities. Some mathematical fallout models utilize this ratio in estimating standard intensities (i.e., the roentgens per hour at 1 hr values at 3 ft above a uniformly contaminated plane) in computing fallout patterns.

It is generally known that the intensity–activity ratio can be defined for the intensity as observed at a given location or, as an average, for a whole fallout area, where it is sometimes called the intensity–area integral per unit fission yield. It is convenient in data analyses to express the surface density of the radioactivity in fissions per square foot rather than in kilotons per square mile. Both representations of the surface density of radioactivity are independent of time after detonation. Since the relation between the number of fissions and the energy released in fission is about the same for most common fissile materials, namely, $(1.45 \pm 0.03) \times 10^{23}$ fissions per kiloton of fission yield, the two representations of the surface density of radioactivity are related by

$$A_f = 5.20 \times 10^{15} A_w \tag{1}$$

where A_f is in fissions per square foot and A_w is in kilotons per square mile.

The intensity–activity ratio for a given location in a fallout region is defined by

$$K_0 = \frac{I_s}{A_f} \tag{2}$$

where I_s is an observed or a measured value of the (standard) intensity in roentgens per hour at 1 hr at 3 ft above an extended open flat area uniformly covered with fallout particles carrying the appropriate amount of radionuclides to result in the surface density, A_f, in fissions per square foot or the equivalent surface density, A_w, in kilotons per square mile, as given by Eq. 1. The standard intensity, I_s, is usually determined from a measurement of the roentgens per hour at the location after all the fallout has been deposited and a decay correction of the observed intensity to the standard time of 1 hr after detonation has been made.

The value of K_0 has been computed for uniform depositions of unfractionated fission products on ideal smooth planes. However, the calculated values of K_0 from observed values of I_s over real terrain for a given value of A_f or A_w are lower than those computed for the ideal plane because of attenuation of the gamma-ray intensity by both small- and large-scale roughness of real terrain, nonidealized responses of radiac instruments used in measuring the intensity, and decreased contributions from the more volatile fission-product radionuclides whose relative concentrations in the fallout are decreased (i.e., the radioactive composition is altered or fractionated). The values of I_s, relative to those for the fission products, are increased by the production of induced radionuclides (usually through neutron capture) in both weapon components and nearby environmental materials. The representation of K_0, including consideration of the four factors discussed in this paragraph, is given by

$$K_0 = Dq(r_{fp}k_{fp} + r_i k_i) \qquad (3)$$

where D = instrument response factor for the assumed detector–radiation source geometry
q = terrain attenuation factor
k_{fp} = computed value of I_s/A_f for 3 ft above an ideal plane uniformly contaminated with unfractionated fission products
r_{fp} = gross fractionation number and is equal to the ratio of I_s for the fractionated mixture of radionuclides to the I_s for the unfractionated mixture
k_i = computed value of the I_s/A_f contributions from induced radionuclides for the same detector–source geometry as for k_{fp}
r_i = gross fractionation number for the induced radionuclides and is related to k_i in the same way that r_{fp} is related to k_{fp}

If it is accepted that the radionuclide composition varies with the size of the fallout particles, the major factors in Eq. 3 that are dependent on particle diameter are r_{fp} and r_i. In more precise treatments, D and q also depend on the radionuclide composition because both of these parameters are functions of gamma-ray energy, which, in turn, depends on the relative abundance of the radionuclides in the fallout.

The value of the intensity–area integral for a fallout pattern usually is determined by integration of the standard intensity contours from the highest intensity to a selected low-valued contour. The fractions of the radionuclides deposited outside the lowest contour are not included in the pattern summations. Also, the quantities that are buried

in the crater and crater lip would not be included in the pattern summations. The intensity–area integral is defined mathematically by

$$J_R = \int_R I_s \, da \tag{4}$$

$$= \int_R K_0 A_f \, da \tag{5}$$

where da is the incremental area, dx dy, and R is the region within the lowest I_s contour included in the integral. If $\bar{K}_0$ is designated as the weighted average value of the K_0's and C as the ratio of intensity area for the region R to the integral for the region enclosed by the contour of I_s equal to zero, then J_R can be represented by

$$J_R = C\bar{K}_0 BW \tag{6}$$

where W is the total weapon yield and B is the fraction of the total yield due to fission. If the $\bar{K}_0$ value for the unfractionated mixture of radionuclides produced in the detonation is designated as K_0^0 ($r_{fp} = 1$, $r_i = 1$), then the fraction of the device deposited in the region, R, is given by

$$F_D = \frac{J_R/BW}{K_0^0} \tag{7}$$

or

$$F_D = \frac{C\bar{K}_0}{K_0^0} \tag{8}$$

If $\bar{K}_0$ is written in the form of Eq. 3, then Eq. 8 becomes

$$F_D \approx \frac{C[\bar{r}_{fp}k_{fp} + \bar{r}_i k_i]}{[k_{fp} + k_i]} \tag{9}$$

In Eq. 9 the two bracketed terms refer to the intensities over an ideal smooth plane on the assumption that the product $D\bar{q}$ for $\bar{K}_0$ is equal to Dq for K_0^0.

The values of $C\bar{K}_0$ and F_D for a fallout pattern can be estimated from the intensity–area integral and the values of k_{fp}, k_i, D, and $\bar{q}$ or q. The value of C can be estimated if $\bar{K}_0$ is evaluated separately, and K_0 can be evaluated if the variation of K_0 with particle size and the fraction of the total radioactivity carried by particles of different sizes are known. With these two types of data, K_0 is calculated from

$$\overline{K}_0 = \sum_j f_j K_{0j} \tag{10}$$

where f_j is the fraction of the total activity carried by particles with a range in diameter designated by j and K_{0j} is the value of K_0 for the same particle-size groups. However, for a determination of the variation of K_0 with particle size, the variation of r_{fp} and r_i with particle size must be known, and approximate values of q or Dq must be determined.

The average value of r_{fp} (and of r_i) for the intensity summation can be calculated in the same way as $\overline{K}_0$ so that

$$\overline{r}_{fp} = \sum_j f_j r_j \tag{11}$$

where r_j is the r_{fp} value for the *jth* particle group.

TREATMENT OF THE DATA

Preliminary analyses and correlations of the radiochemical data and gross-sample-activity, sieved-sample-activity, decay-rate, and intensity measurements in the field on the fallout from the Small Boy shot have been made, leading to the evaluation of preceding parameters. Certain simplifying assumptions are made for portions of the analyses to facilitate the treatment of the data and the presentation of the computational results.

First, it is assumed that, in Eq. 3, the values of $r_i k_i$ are small compared with the values of r_{fp}, and K_0 is represented only by

$$K_0 = Dq r_{fp} k_{fp} \tag{12}$$

The values of K_0 were determined according to Eq. 2, in which the I_s value of each fallout-collecting station was derived from correlations between data from gamma intensity time recorders (GITR's) and activity measurements on the collected samples.[1,2] The values of A_f were derived from radiochemical analyses of the collected fallout samples, and the fission yield equivalent for each sample was based on the amount of ^{95}Zr found in each sample.[3]

The values of r_{fp} were determined by taking the ratio of the ion current per fission of a gross fallout sample, as measured in a calibrated 4π ion chamber[4] to the computed ion current per fission for an unfractionated fission-product mixture.[5] In the field project,[1] the radioactive content of all collected gross samples and all sieved

fractions of gross samples was measured either with the ion chamber or with a calibrated gamma scintillation counter. The activity of many samples was measured with both instruments. The measured ion currents in milliamperes and the photon pulse rates in counts per minute for each sample were decay-corrected to 100 hr after detonation.

If the measured ion current per ^{95}Zr fission at 100 hr from the ion chamber is designated as i(100) and the calculated ion current per fission for the unfractionated fission product at 100 hr after fission is designated as $i_0(100)$, then the gross fractionation number for the measured sample at 100 hr is

$$r_{fp}(100) = \frac{i(100)}{i_0(100)} \tag{13}$$

The definition of the r_{fp} by ratios of the ion currents from the ion chamber implies the assumption that i/i_0 is equal to I_s/I_s^0, where I_s^0 is the roentgens per hour for an unfractionated fission-product mixture. This assumption is fairly valid for most measurements on fission-product mixtures.[5] For correlation purposes, a fractionation number, r'_{fp}, is defined for the calibrated gamma-scintillation-counter measurements as

$$r'_{fp}(100) = \frac{i'(100)}{i'_0(100)} \tag{14}$$

where $i'(100)$ is the observed counting rate per ^{95}Zr fission at 100 hr after detonation for a sample of fallout and $i'_0(100)$ is the calculated counting rate per fission for the unfractionated fission-product mixture.

The r_{fp} of Eq. 12 is for the i ratios at 1 hr after detonation rather than at 100 hr. For evaluation of r_{fp} the i(100) values were decay-corrected to 1 hr after detonation (or after fission). The assumed decay-correction factors for i and i′ are represented by

$$i(1) = 250\ i(100) \tag{15}$$

and

$$i'(1) = 200\ i'(100) \tag{16}$$

The only available computed values of i_0 and i'_0 for the 4π ion chamber and the calibrated gamma scintillation counter, respectively, are those[5,6] for the products from thermal-neutron fission of ^{235}U. For this mixture $i_0(100)$ is 2.48×10^{-20} ma/fission and $i'_0(100)$ is 2.10×10^{-9} counts/min per fission. The two respective calculated decay-correction factors from 100 to 1 hr after fission are represented by

$$i_0(1) = 435\ i_0(100) \tag{17}$$

and

$$i_0'(1) = 246\ i_0'(100) \tag{18}$$

Thus

$$r_{fp} = 0.575\ \frac{i(100)}{i_0(100)} \tag{19}$$

and

$$r'_{fp} = 0.813\ \frac{i(100)}{i_0(100)} \tag{20}$$

Actually the decay factors for i and i′ should vary with r_{fp} or with the particle size of the fallout. Thus, for samples in which the degree of fractionation (^{235}U products) is small, the decay factor from 100 to 1 hr should approach 435. In this preliminary analysis, the previously assumed decay factors (Eqs. 15 to 18) were used for all samples; neither observed nor specially computed decay factors for all fallout samples were available for application in Eq. 19. The assumption that all samples had the same decay factor could result in an error of a factor of 2 in the r_{fp} value for some of the fallout samples.

The variation of i(100), $r_{fp}(100)$, and r_{fp} with particle size was investigated by using ion-chamber and radiochemical-analysis data[3] on sieved fractions of collected fallout samples. Two sets of the ion-chamber measurements were reported. In addition to the field measurements, which were corrected to absolute ion-current values, an uncorrected second set of measurements was reported by the radiochemical-analysis project.[3] These data were corrected to 100 hr after fission by using $(t/100)^{1.07}$ for computing the decay factors. The decay-corrected data were then correlated with the field measurements to obtain a correction factor for conversion of the data to absolute units. This was done by computing the ratio of the two measurements (corrected to 100 hr) on each sample. The median value of this correction factor was calculated to be 0.788, which is close to the value of 0.78 obtained in the past with a radium standard.[7] After application of this second correction factor to the second set of measurements, the geometric mean value of i(100) was calculated from the two sets of the ion-chamber measurements and the reported[3] fission-yield content of each sample. The i(100) values thus obtained are given in Table 6 and are plotted in Fig. 1 as a function of the midrange particle diameter, $\bar{d}$, for each sieve fraction. Subsieve analyses indicated the

Table 6—ION CURRENT PER FISSION FOR SIEVED FRACTIONS OF FALLOUT SAMPLES

[i(100) (10^{-20} ma at 100 hr per fission)]

Station	Midrange particle diameter, μ							
	22	66	132	264	530	1060	2120	>4000
100	3.88	3.30	0.950	1.02	0.676	0.844	1.32	
101	3.74	1.48	1.14	0.855	0.680		0.791	1.48
201	4.50	2.07	1.02	0.668	0.967	0.751	0.846	15.9*
203	0.271*	1.70	1.72	0.678	0.997	0.662	1.60	
305	3.96	1.78	1.10	1.04	0.983	0.784	0.741	1.08
403	3.90	2.34	0.782	1.02	0.693	1.04	4.62*	3.24*
505	4.42	2.39	0.669	1.00	0.768	16.8*	8.44*	4.28*
507	0.821*	1.37		1.01	0.656	0.726	19.7*	
603	3.52	1.72	0.610	0.462	0.682	35.9*	0.880	
707	5.49	1.86	1.06	1.00	0.615	10.3*		
813	3.56	0.942	1.25	0.810	3.90*	1.53	1.52	
Mean	4.06	1.82	0.989	0.848	0.759	0.871	1.05	1.26
Smoothed curve	4.06	1.82	1.10	0.78	0.76	0.87	1.05	1.26
$r_{fp}(100)$	1.64	0.734	0.444	0.315	0.306	0.351	0.424	0.508
r_{fp}	0.942	0.422	0.255	0.181	0.176	0.202	0.244	0.292

*Values not used in calculating mean values.

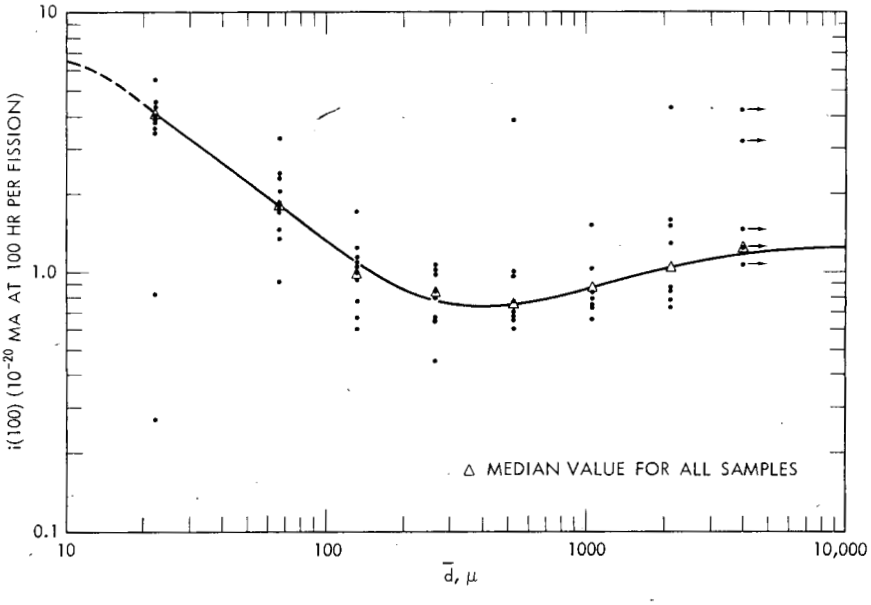

Fig. 1—Variation of i(100) with particle diameter.

presence of particles with diameters as small as 1 to 3 μ in all samples;[2] therefore the midrange diameter of the 0- to 44-μ fraction was taken as 22 μ.

The mean values of i(100) were computed for each particle-size fraction on the assumption that the average radionuclide composition carried by particles of a given size is the same everywhere and is independent of where the particles land. After correlation the two sets of ion-chamber data were generally in very good agreement; therefore most of the spread in the i(100) values for each particle size is due mainly to spread in the radiochemical results. The spread in the values is largest for the smallest and largest particle diameters where the analytical sample sizes were smallest. In the midrange of the curve, the minimum-to-maximum spread in i(100) is a factor of about 3.

The major significance of the data is in the variation of i(100) and therefore of $r_{fp}(100)$ and r_{fp} with particle size. From the average particle diameter of 22 μ up to an average particle diameter of about 400 μ, i(100) decreases by a factor of about 5.5. At 400 μ diameter, a minimum in the curve exists. A similar variation with particle size in the gross solubility of the radionuclides is observed.[3]

The K_0 values for the collecting-station locations in the fallout area from the Small Boy shot were calculated with adjusted and averaged A_f values; correlations of the variation in i'(100) and i(100) with the median particle size of the fallout particles at each station were used to make the adjustments in A_f. Initial correlations of i'(100) indicated a consistent difference in value depending on the time at which the samples were allocated for chemical analysis; the median value of the correlation factor for this difference was calculated to be 1.56. Since evidence for locating the cause of this difference is presently not available and since the calibrated gamma-scintillation-counter measurements were a highly unlikely source of error, the reported A_f values[3] for the samples with the higher values of i'(100) were increased by a factor of 1.25, and the A_f values for the remainder of the samples were decreased by a factor of 1.25. If the same type of correlation, including comparisons with the observed I_s values,[1] are applied to a third set of samples collected at offsite locations, the reported A_f values[2] are found to be more or less consistently high by a factor of 10.

The data for the fallout samples leading to the calculation of K_0 for each location are summarized in Table 7. Included are the activity median particle size, d_{50}; the ion-chamber measurements on the gross samples, I_1, I_2, and I; the values of $i_1(100)$, $i_2(100)$, and i'(100), as calculated from the initially adjusted values of A_f (given as A_1); the smoothed-curve values of i(100) and i'(100), as taken from the curves in Figs. 2 and 3; the recomputed values of A_f, where A_2 is $I_1/\bar{i}(100)$, A_3 is $I_2/\bar{i}(100)$, and A_4 is $I'/i'(100)$; the average value of A_f; I_s; and K_0.

Table 7—SUMMARY OF CALCULATIONS* OF A_f AND K_0 FOR THE SMALL BOY SHOT FALLOUT

Station–sample No.	d_{50}, μ	$I_1(100)$, ma/ft^2	$I_2(100)$, ma/ft^2	I′(100), counts/min per sq ft	$i_1(100)$, 10^{-20} ma fission	$i_2(100)$, 10^{-20} ma fission	i′(100), 10^{-9} counts/min fission	$\bar{I}$ (100), 10^{-20} ma fission	$\bar{I}'(100)$, 10^{-9} counts/min fission
100–1	640	212×10^{-8}	220×10^{-8}	2.22×10^{5}	0.763	0.791	0.802	0.836	0.785
100–2	640	220×10^{-8}	220×10^{-8}	2.37×10^{5}	1.048	1.048	1.130	0.836	0.785
101–1	1100		174×10^{-7}	1.30×10^{6}		1.193	0.890	0.880	0.893
101–6	1100		174×10^{-7}	1.29×10^{6}		0.650	0.482	0.880	0.893
103–9		131×10^{-11}			0.0570†			(1.0)	(0.93)
200–9	130	122×10^{-9}	143×10^{-9}	1.16×10^{4}	1.100	1.288	1.046	1.13	0.985
201–7	750		831×10^{-8}	7.95×10^{5}		0.950	0.908	0.842	0.835
201–10	750	113×10^{-7}	831×10^{-8}	7.92×10^{5}	0.876	0.645	0.614	0.842	0.835
202–9		827×10^{-12}			0.484			(0.843)	(0.84)
203–16	780	246×10^{-8}	258×10^{-8}		0.779	0.816		0.844	0.840
203–21	780	266×10^{-8}	258×10^{-8}	2.65×10^{5}	0.873	0.846	0.870	0.844	0.840
204–9		300×10^{-12}			0.848			(0.85)	(0.85)
207–9		451×10^{-12}			0.780			(0.90)	(0.91)
209–9		488×10^{-12}			0.175†			(0.95)	(0.92)
300–9		259×10^{-10}		2.53×10^{3}	1.006		0.984	(0.85)	(0.74)
303–9	530	746×10^{-8}	673×10^{-8}	8.34×10^{5}	10.10†	9.12†	11.28†	0.830	0.758
305–2	660		460×10^{-8}	3.34×10^{5}		0.788	0.572	0.837	0.800
305–4	660	452×10^{-8}	460×10^{-8}		0.820	0.834		0.837	0.800
305–9	660	456×10^{-8}	460×10^{-8}	5.31×10	0.818	0.825	0.954	0.837	0.800
309–16		167×10^{-11}			4.75†			(0.85)	(0.85)
311–9		341×10^{-12}			0.573			(0.90)	(0.91)
400–9		469×10^{-10}		3.41×10^{3}	0.635		0.462	(0.84)	0.74
401–9	380	473×10^{-8}	456×10^{-8}	5.48×10^{5}	0.663	0.639	0.768	0.852	0.744
403–2	340		629×10^{-8}	3.45×10^{5}		0.955	0.524	0.856	0.750
403–3	340		629×10^{-8}	5.43×10^{5}		1.182	1.022	0.856	0.750
403–4	340	697×10^{-8}	629×10^{-8}		0.817	0.737		0.856	0.750
405–9	310	192×10^{-8}	214×10^{-8}	1.23×10^{5}	0.725	0.808	0.465	0.868	0.760
407–9	310	158×10^{-10}	159×10^{-10}	1.20×10^{3}	0.963	0.969	0.731	0.868	0.760
413–9		596×10^{-12}			0.390†			(0.95)	(0.84)
501–9	250	406×10^{-10}	893×10^{-10}	4.70×10^{3}	0.708	1.556	0.820	0.896	0.792
502–9		379×10^{-12}			0.907			(0.88)	(0.78)
503–9	310	182×10^{-8}	182×10^{-8}	1.59×10^{5}	0.847	0.847	0.740	0.868	0.760
505–1	260		334×10^{-8}	2.99×10^{5}		0.994	0.890	0.890	0.780
505–6	260	345×10^{-8}	334×10^{-8}	3.42×10^{5}	0.876	0.849	0.869	0.890	0.780
507–4	180	890×10^{-9}	124×10^{-8}	1.53×10^{5}	0.940	1.310	1.616	0.990	0.870
507–5	180	128×10^{-8}	124×10^{-8}	1.53×10^{5}	1.202	1.164	1.437	0.990	0.870
509–9		286×10^{-9}	650×10^{-9}	2.98×10^{4}	1.173	2.665†	1.222	(1.0)	(0.88)
513–9		296×10^{-12}			0.304†			(1.1)	(0.95)
601–9		104×10^{-9}	188×10^{-9}	1.07×10^{4}	0.971	1.758	1.000	(1.1)	(0.95)
603–1	150	169×10^{-8}	173×10^{-8}	2.04×10^{5}	0.478†	0.489†	0.577	1.06	0.930
603–4	150		173×10^{-8}	2.01×10^{5}		0.112†	0.130†	1.06	0.930
605–9	160	177×10^{-8}	144×10^{-8}	1.64×10^{5}	1.106	0.900	1.025	1.03	0.905
607–9		128×10^{-9}		1.16×10^{4}	0.800		0.725	(1.0)	(0.88)
700–9		145×10^{-11}			0.900			(1.4)	(1.2)
701–9		176×10^{-11}			0.682			(1.3)	(1.1)
703–9		171×10^{-9}		1.75×10^{4}	0.768		0.785	(1.2)	(1.0)
704–9		131×10^{-11}			1.928			(1.1)	(0.95)
707–3	145	683×10^{-9}	767×10^{-9}	6.23×10^{4}	0.905	1.016	0.826	1.07	0.942
707–6	145		767×10^{-9}	7.44×10^{4}		1.056	1.023	1.07	0.942
813–10	90	914×10^{-10}	813×10^{-10}	9.61×10^{3}	1.057	0.910	1.112	1.42	1.17
814–4	88	850×10^{-10}	886×10^{-10}	7.88×10^{3}	0.265†	0.276†	0.246†	1.43	1.18
815–10	37		133×10^{-9}	8.86×10^{3}		3.03	2.02	2.73	1.94
816–16	40	961×10^{-10}	108×10^{-9}	8.65×10^{3}	2.29	2.57	2.06	2.57	1.85
18–9	(77)			9.28×10^{3}			1.232	1.58	1.27
18–10	(79)			9.60×10^{3}			1.207	1.55	1.25
18–11	(79)			1.11×10^{4}			1.115	1.55	1.25
18–12	(79)			1.43×10^{4}			1.560	1.55	1.25
27–1	(64)			2.91×10^{3}			38.75†	1.82	1.39
27–2	(64)			2.43×10^{3}			1.273	1.82	1.39
27–3	64.5			2.44×10^{3}			1.220	1.80	1.38
27–4	(64)			7.79×10^{2}			0.815	1.82	1.39
35–17	(43)			4.41×10^{2}			1.522	2.43	1.77
35–18	(43)			7.13×10^{2}			1.873	2.43	1.77
35–19	(42)			1.05×10^{3}			2.55	2.48	1.79
35–20	38			1.10×10^{3}			1.280	2.70	1.90
56–11	(23)			7.69×10^{2}			3.37	3.90	2.67
56–12	(21)			7.88×10^{2}			3.97	4.20	2.87
56–14	(20)			3.47×10^{2}			1.753	4.36	2.97

*Values in parentheses are estimated. †Values not used in the analyses.

Notes: (1) I_1 is the ion-chamber measurements by the radiochemical project corrected to 100 hr and to absolute units by a factor of 0.788.

Table 7—(Continued)

A_1, fission/sq ft	A_2, fission/sq ft	A_3, fission/sq ft	A_4, fission/sq ft	$\bar{A}_f$, fission/sq ft	I_s, r/hr at 1 hr	K_0, 10^{-13} r/hr at 1 hr / fission/sq ft	K_0, r/hr at 1 hr / kt/sq mile
2.78×10^{14}	2.54×10^{14}	2.63×10^{14}	2.83×10^{14}	2.70×10^{14}	26.0	0.963	501
2.10×10^{14}	2.63×10^{14}	2.63×10^{14}	3.02×10^{14}	2.60×10^{14}	26.0	1.00	520
1.46×10^{15}		1.98×10^{15}	1.46×10^{15}	1.63×10^{15}	206	1.26	657
2.68×10^{15}		1.98×10^{15}	1.44×10^{15}	2.03×10^{15}	206	1.01	528
2.30×10^{12}	1.31×10^{11}			1.31×10^{11}	0.015	1.14	595
1.11×10^{13}	1.08×10^{13}	1.26×10^{13}	1.18×10^{13}	1.16×10^{13}	1.69	1.46	758
8.76×10^{14}		9.88×10^{14}	9.52×10^{14}	9.39×10^{14}	98.4	1.05	545
1.29×10^{15}	1.34×10^{15}	9.88×10^{14}	9.48×10^{14}	1.14×10^{15}	98.4	0.862	449
1.71×10^{11}	9.81×10^{10}			9.81×10^{10}	0.010	1.02	530
3.16×10^{14}	2.92×10^{14}	3.06×10^{14}		3.05×10^{14}	30.5	1.00	520
3.05×10^{14}	3.15×10^{14}	3.06×10^{14}	3.15×10^{14}	3.10×10^{14}	30.5	0.985	512
3.54×10^{10}	3.53×10^{10}			3.54×10^{10}	0.0035	0.990	515
5.79×10^{10}	5.01×10^{10}			5.01×10^{10}	0.0052	1.04	540
2.79×10^{11}	5.13×10^{10}			5.13×10^{10}	0.0057	1.11	578
2.57×10^{12}	3.05×10^{12}		3.42×10^{12}	3.01×10^{12}	0.30	0.998	519
7.39×10^{13}	8.99×10^{14}	8.11×10^{14}	1.10×10^{15}	8.55×10^{14}	79.7	0.932	485
5.84×10^{14}		5.50×10^{14}	4.18×10^{14}	5.17×10^{14}	54.4	1.05	547
5.52×10^{14}	5.41×10^{14}	5.50×10^{14}		5.46×10^{14}	54.4	0.995	518
5.58×10^{14}	5.45×10^{14}	5.50×10^{14}	6.64×10^{14}	5.79×10^{14}	54.4	0.940	489
3.52×10^{10}	1.96×10^{11}			1.96×10^{11}	0.020	1.02	531
5.95×10^{10}	3.79×10^{10}			3.79×10^{10}	0.0040	1.06	549
7.39×10^{12}	5.58×10^{12}		4.61×10^{12}	5.09×10^{12}	0.54	1.06	551
7.14×10^{14}	5.55×10^{14}	5.35×10^{14}	7.37×10^{14}	6.35×10^{14}	53.9	0.848	441
6.59×10^{14}		7.35×10^{14}	4.60×10^{14}	6.18×10^{14}	74.5	1.20	627
5.32×10^{14}		7.35×10^{14}	7.24×10^{14}	6.64×10^{14}	74.5	1.12	584
8.54×10^{14}	8.14×10^{14}	7.35×10^{14}		8.01×10^{14}	74.5	0.930	483
2.65×10^{14}	2.22×10^{14}	2.47×10^{14}	1.62×10^{14}	2.24×10^{14}	25.4	1.13	590
1.64×10^{12}	1.82×10^{12}	1.83×10^{12}	1.58×10^{12}	1.72×10^{12}	0.18	1.05	545
1.53×10^{11}	6.18×10^{10}			6.18×10^{10}	0.0070	1.13	589
5.74×10^{12}	4.53×10^{12}	9.96×10^{12}	5.93×10^{12}	5.40×10^{12}	0.57	1.06	549
4.18×10^{10}	4.31×10^{10}			4.24×10^{10}	0.0044	1.04	540
2.15×10^{14}	2.10×10^{14}	2.10×10^{14}	2.09×10^{14}	2.11×10^{14}	21.5	1.02	530
3.36×10^{14}		3.76×10^{14}	3.83×10^{14}	3.65×10^{14}	39.6	1.08	565
3.94×10^{14}	3.88×10^{14}	3.76×10^{14}	4.38×10^{14}	3.86×10^{14}	39.6	1.03	533
9.48×10^{13}	8.99×10^{13}	1.25×10^{14}	1.76×10^{14}	1.22×10^{14}	14.7	1.20	626
1.065×10^{14}	1.29×10^{14}	1.25×10^{14}	1.76×10^{14}	1.34×10^{14}	14.7	1.10	570
2.44×10^{13}	2.86×10^{13}	6.50×10^{13}	3.39×10^{13}	2.90×10^{14}	3.4	1.17	610
9.74×10^{10}	2.69×10^{10}			2.69×10^{10}	0.0034	1.26	657
1.07×10^{13}	9.46×10^{12}	1.71×10^{13}	1.13×10^{13}	1.05×10^{13}	1.4	1.33	693
3.54×10^{14}	1.60×10^{14}	1.63×10^{14}	2.19×10^{14}	1.81×10^{14}	20.4	1.13	586
1.55×10^{15}		1.63×10^{14}	2.16×10^{14}	1.90×10^{14}	20.4	1.07	559
1.60×10^{14}	1.72×10^{14}	1.40×10^{14}	1.81×10^{14}	1.63×10^{14}	17.0	1.04	542
1.60×10^{13}	1.28×10^{13}		1.32×10^{13}	1.41×10^{13}	1.5	1.06	553
1.61×10^{11}	1.04×10^{11}			1.32×10^{11}	0.017	1.29	670
2.58×10^{11}	1.35×10^{11}			1.96×10^{11}	0.020	1.02	530
2.23×10^{13}	1.42×10^{13}		1.75×10^{13}	1.82×10^{13}	2.0	1.10	571
6.80×10^{10}	1.19×10^{11}			1.19×10^{11}	0.015	1.26	655
7.55×10^{13}	6.38×10^{13}	7.17×10^{13}	6.61×10^{13}	6.93×10^{13}	9.08	1.31	682
7.28×10^{13}		7.17×10^{13}	7.90×10^{13}	7.45×10^{13}	9.08	1.22	634
8.65×10^{12}	6.44×10^{12}	5.72×10^{12}	8.21×10^{12}	7.25×10^{12}	1.58	2.18	1133
3.21×10^{13}	5.95×10^{12}	6.20×10^{12}	6.68×10^{12}	6.28×10^{12}	1.32	2.10	1094
4.39×10^{12}		4.87×10^{12}	4.57×10^{12}	4.61×10^{12}	1.18	2.56	1330
4.20×10^{12}	3.74×10^{12}	4.20×10^{12}	4.68×10^{12}	4.20×10^{12}	1.17	2.79	1450
7.54×10^{12}			7.56×10^{12}	7.55×10^{12}	1.17	1.55	805
7.95×10^{12}			7.42×10^{12}	7.42×10^{12}	1.18	1.59	830
9.96×10^{12}			8.88×10^{12}	8.88×10^{12}	1.32	1.49	775
9.17×10^{12}			1.14×10^{13}	1.14×10^{13}	1.58	1.39	725
7.52×10^{10}			2.09×10^{12}	2.09×10^{12}	0.28	1.34	697
1.91×10^{12}			1.75×10^{12}	1.75×10^{12}	0.47	2.68	1395
2.00×10^{12}			1.77×10^{12}	1.77×10^{12}	0.27	1.52	793
9.68×10^{11}			5.60×10^{11}	5.60×10^{11}	0.15	2.68	1390
2.90×10^{11}			2.49×10^{11}	2.49×10^{11}	0.12	4.82	2510
3.81×10^{11}			4.03×10^{11}	4.03×10^{11}	0.18	4.47	2320
4.12×10^{11}			5.87×10^{11}	5.87×10^{11}	0.27	4.60	2390
8.60×10^{11}			5.82×10^{11}	5.82×10^{11}	0.26	4.47	2320
2.28×10^{11}			2.88×10^{11}	2.88×10^{11}	0.074	2.57	1335
1.98×10^{11}			2.75×10^{11}	2.75×10^{11}	0.16	5.72	3020
1.98×10^{11}			1.17×10^{11}	1.58×10^{11}	0.087	5.50	2860

Notes: (2) I_2 is the ion-chamber measurements by the field project (average for each station). (3) I′ is the calibrated gamma-scintillation-counter measurements by the field project. (4) i and i′ are values read from the curves in Figs. 2 and 3, respectively.

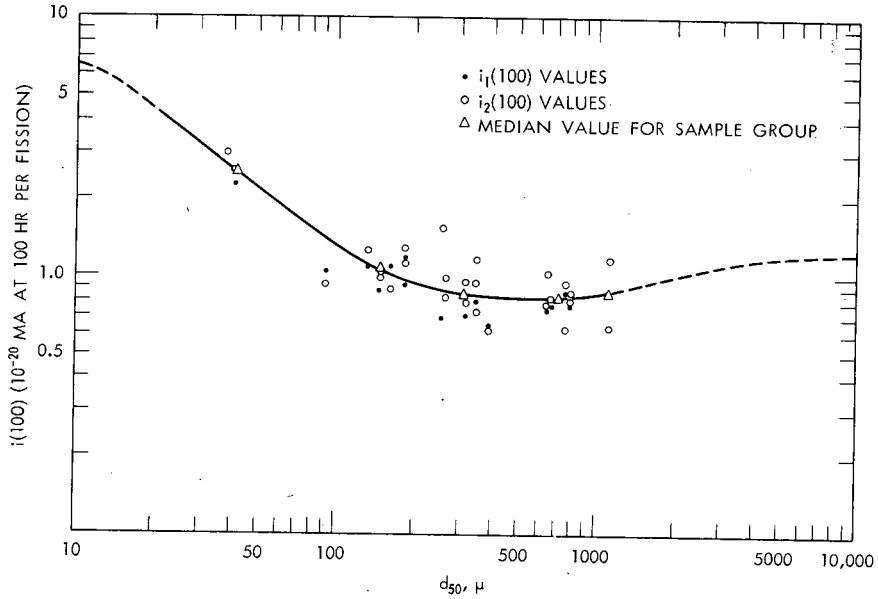

Fig. 2—Variation of i(100) with d_{50} for gross fallout samples.

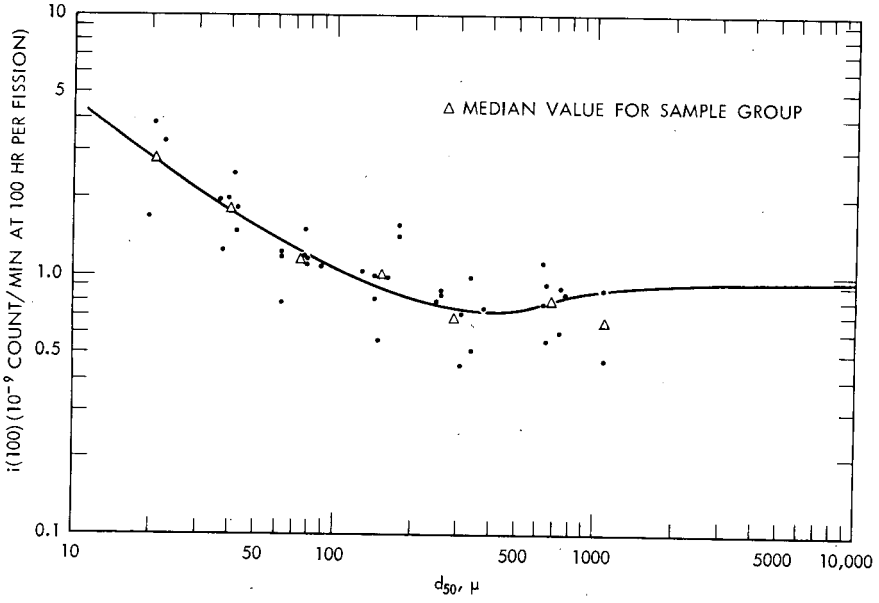

Fig. 3—Variation of i'(100) with d_{50} for gross fallout samples.

The computed values of K_0 are plotted as a function of d_{50} in Fig. 4. It may be noted that the curves of i(100), i'(100), and K_0 given as a function of d_{50} in Figs. 2, 3, and 4 are very similar to the curve for i(100) plotted as a function of $\bar{d}$ in Fig. 1.

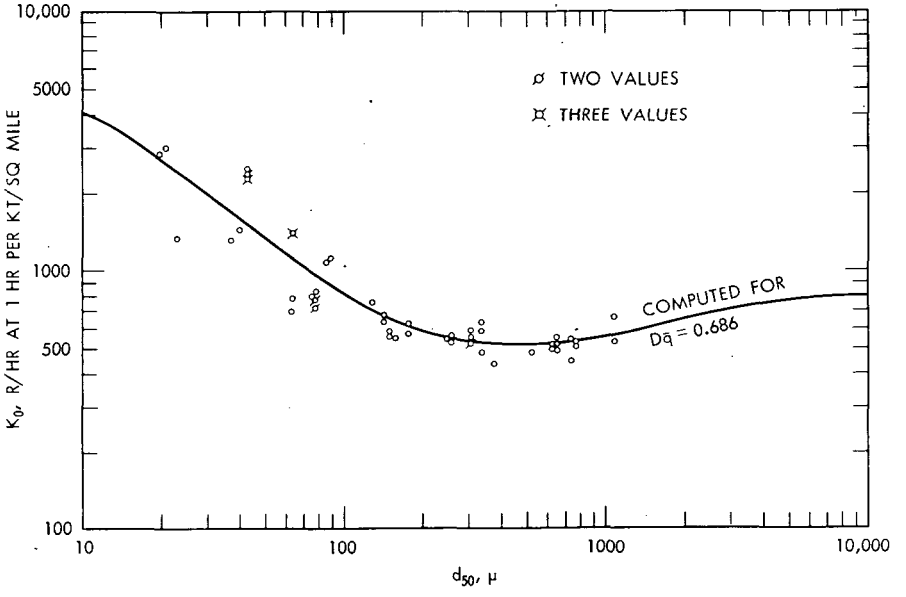

Fig. 4—Variation of K_0 with d_{50} for fallout-collecting stations.

The high values of K_0 for the stations in the 35- and 56-numbered series (Table 7) suggest that the I_s values are overestimated by correction of the monitoring data[1] to 1 hr with the $t^{-1.2}$ function. The adjustment of the two apparently different sets of reported A_f values[2] to a midvalue rather than correction of one of the two sets of data to be consistent with the other may have resulted in K_0 values that are either low or high by 25%. Further investigation of the reported data[3] together with theoretical analyses may suggest what corrections are appropriate.

The Dq terms of Eq. 12 can be evaluated using an appropriate value of k_{fp}. The selection of a value here is limited to the k_{fp} value for the fission products from the thermal-neutron fission of ^{235}U because the i(100) and r_{fp} values, as deduced from the ion-chamber measurements, are based on the response of the ion-chamber to the ^{235}U products. The calculated value[8] of k_{fp} is 3950 r/hr at 1 hr per kiloton per square mile. The Dq of Eq. 12 is given by

$$Dq = \frac{K_0}{3950\ r_{fp}} \qquad (21)$$

The values of $r_{fp}(100)$, $r'_{fp}(100)$, r_{fp}, r'_{fp}, K_0, and Dq for each station are summarized in Table 8. The value of K_0 in Table 8 for stations having more than one estimated value of K_0 in Table 7 is a median value. The terrain about the stations generally increased in roughness[1] proceeding from station 100 to station 707; however, this general increase in roughness is not reflected in a corresponding general decrease in Dq values for these stations. At the stations of the 800 series, the terrain was fairly smooth and flat at stations 813 and 814 and somewhat rougher at stations 815 and 816. The terrain features at the remainder of the stations were varied. At the stations in series 100 through 800, the GITR's were calibrated to have a response factor, D, near unity; thus for these stations the computed value of Dq is practically equal to q. For the other stations the response factor for the instruments and monitor has not been reported, but it is assumed to be about 0.7. Therefore, where the computed value of Dq is in excess of 0.7, either the I_s value is too large or the A_f value is too small (i.e., the r_{fp} value is too small).

Table 8—SUMMARY OF CALCULATED r_{fp}, r'_{fp}, K_0, AND Dq VALUES* FOR THE SMALL BOY SHOT FALLOUT-COLLECTING STATIONS

Station and sample No.	$r_{fp}(100)$	$r'_{fp}(100)$	r_{fp}	r'_{fp}	K_0, r/hr at 1 hr / kt/sq mile	Dq
100	0.338	0.369	0.194	0.304	511	0.667
101	0.355	0.425	0.204	0.346	589	0.731
103	(0.403)	(0.443)	(0.232)	(0.361)	595	0.650
200	0.456	0.469	0.262	0.382	758	0.724
201	0.340	0.398	0.195	0.324	494	0.642
202	(0.340)	(0.400)	(0.196)	(0.326)	530	0.685
203	0.341	0.400	0.196	0.326	515	0.666
204	(0.343)	(0.405)	(0.197)	(0.330)	515	0.663
207	(0.363)	(0.433)	(0.209)	(0.353)	540	0.678
209	(0.383)	(0.438)	(0.220)	(0.357)	578	0.665
300	(0.343)	(0.352)	(0.197)	(0.287)	519	0.691
303	0.335	0.361	0.192	0.294	485	0.640
305	0.338	0.381	0.195	0.310	518	0.673
309	(0.343)	(0.405)	(0.197)	(0.330)	531	0.684
311	(0.363)	(0.433)	(0.209)	(0.353)	549	0.665
400	(0.339)	(0.352)	(0.195)	(0.287)	551	0.717
401	0.344	0.354	0.198	0.289	441	0.564
403	0.346	0.357	0.199	0.291	561	0.715
405	0.350	0.362	0.202	0.295	590	0.741
407	0.350	0.362	0.202	0.295	545	0.684
409	(0.383)	(0.400)	(0.220)	(0.326)	589	0.678
501	0.362	0.378	0.208	0.308	549	0.669
502	(0.355)	(0.372)	(0.204)	(0.303)	540	0.671
503	0.350	0.362	0.202	0.295	530	0.665

(Table 8 continues on page 63)

Table 8—(Continued)

Station and sample No.	$r_{fp}(100)$	$r'_{fp}(100)$	r_{fp}	r'_{fp}	K_0, r/hr at 1 hr / kt/sq mile	Dq
505	0.359	0.372	0.206	0.303	549	0.674
507	0.399	0.415	0.230	0.338	598	0.659
509	(0.403)	(0.419)	(0.232)	(0.342)	610	0.666
513	(0.444)	(0.452)	(0.255)	(0.369)	657	0.654
601	(0.444)	(0.452)	(0.255)	(0.369)	693	0.688
603	0.428	0.443	0.246	0.361	572	0.590
605	0.415	0.431	0.239	0.351	542	0.575
607	(0.403)	(0.419)	(0.232)	(0.342)	553	0.605
700	(0.565)	(0.571)	(0.325)	(0.466)	670	0.523
701	(0.524)	(0.524)	(0.302)	(0.427)	530	0.445
703	(0.484)	(0.476)	(0.278)	(0.388)	571	0.522
704	(0.444)	(0.462)	(0.255)	(0.369)	655	0.644
707	0.431	0.449	0.248	0.366	658	0.673
813	0.573	0.557	0.330	0.454	1,133	0.870
814	0.576	0.562	0.332	0.458	1,094	0.836
815	1.100	0.924	0.633	0.753	1,330	0.533
816	1.037	0.880	0.596	0.718	1,450	0.617
18–9	0.638	0.605	0.367	0.482	805	0.556
18–10	0.625	0.595	0.360	0.485	830	0.585
18–11	0.625	0.595	0.360	0.484	775	0.546
18–12	0.625	0.595	0.360	0.485	725	0.511
27–1	0.735	0.662	0.422	0.540	697	0.418
27–2	0.735	0.662	0.422	0.540	1,395	0.838
27–3	0.726	0.657	0.418	0.535	793	0.482
27–4	0.735	0.662	0.422	0.540	1,390	0.835
35–17	0.980	0.843	0.564	0.687	2,510	1.128
35–18	0.980	0.843	0.564	0.687	2,320	1.043
35–19	1.000	0.852	0.575	0.695	2,390	1.053
35–20	1.090	0.905	0.626	0.737	2,320	0.939
56–11	1.573	1.272	0.905	1.037	1,335	0.374
56–12	1.695	1.367	0.975	1.113	3,020	0.785
56–14	1.760	1.414	1.012	1.152	2,860	0.717

*Values in parentheses are derived from estimated d_{50} values for the station.

The mean value of Dq for all the stations in the 100 to 700 series, for which d_{50} is given, is 0.686 ± 0.025. With this value of Dq, Eq. 12 becomes

$$K_0 = 2710\, r_{fp} \qquad (22)$$

Thus K_0^0 for all the indicated stations is 2710 (i.e., K_0 with $r_{fp} = 1$).

The f_j values for the Small Boy shot fallout pattern were computed by constructing fallout patterns for a given range in particle size and evaluating the intensity–area integral for each pattern. The fraction of

I_s at each station contributed by each particle-size group was calculated from activity measurements on sieved fractions of the fallout samples. The constructed fallout patterns for several of the particle-size ranges and for the total fallout pattern are shown in Figs. 5 to 8. The activity–size distribution derived from this analysis is shown in Fig. 9. The median particle diameter for the distribution is 210 μ. The derived distribution is not lognormal.

The f_j values from which the distribution was determined are summarized in Table 9; also given in the table are the $f_j r_j$ and $f_j K_{0j}$ values leading to the estimates of $\bar{r}_{fp}$ and $\bar{K}_0$ for the whole fallout pattern. The sum of the intensity–area integrals, J_R, of the fallout patterns for the different particle groups is 580 r/hr at 1 hr per square mile; the value of J_R for the pattern of the gross I_s contours is 640 r/hr at 1 hr per square mile, about 11% larger. The yield of the Small Boy shot has not been reported, except that the yield was small.[9] With the use of the intensity–area integral for the I_s contours and the yield, the value of J_R/BW for the pattern thus could be estimated. With a $\bar{K}_0$ value of 1070 r/hr at 1 hr per kiloton per square mile, the value of C could be estimated; and the fraction of device, F_D, accounted for within the constructed fallout pattern of Fig. 8 could similarly be estimated.

The fallout patterns constructed for the various particle-size fractions do not include contributions from the regions of high I_s values near ground zero nor from the large area of low-level fallout that was deposited in northern Utah. These contributions are not included in the analysis because fallout samples for determining the distribution of radioactivity among the fallout particles deposited in these regions were not available for analysis. For the total fallout pattern, including the contributions to I_s from these areas, a J_R value of 1460 r/hr per square mile is obtained; this value is a factor of about 2.3 larger than that calculated for the fallout pattern constructed from the I_s values at the stations for which particle-size data are available.

The fraction of the device, F_D, accounted for within the larger fallout pattern, would therefore be 2.3 times that for the smaller pattern mentioned earlier. The ratio of the contributions to the intensity–area integral for the high-intensity region to the low-intensity region, as determined from integrals, is about 3 to 1. If an average r_j value of 0.29 is assumed for the fallout in the high-intensity region and an average r_j value of 1.5 for the low-intensity region, a value of $\bar{K}_0$ can be estimated for the larger pattern from the data of Table 9. Allocation of appropriate fractions of the intensity–area integral to the three areas gives a weighted average value for $\bar{K}_0$ of 1400 r/hr at 1 hr per kiloton per square mile; the corresponding

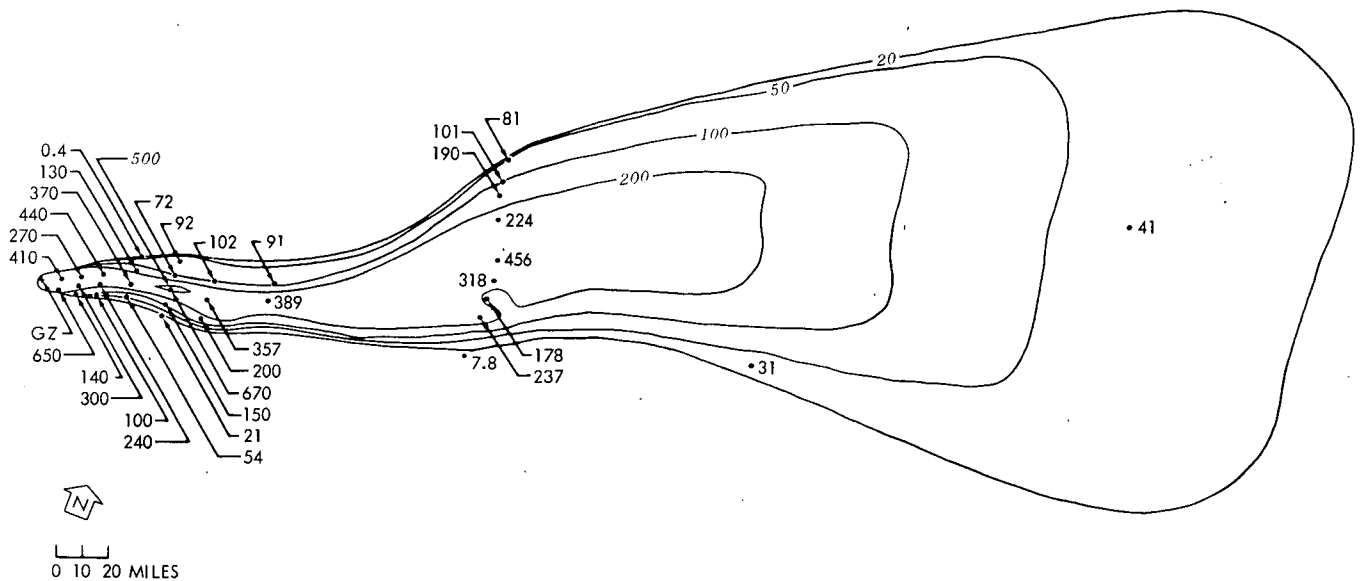

Fig. 5—Isointensity contours for 20- to 50-μ particle diameters in milliroentgens per hour at 1 hr.

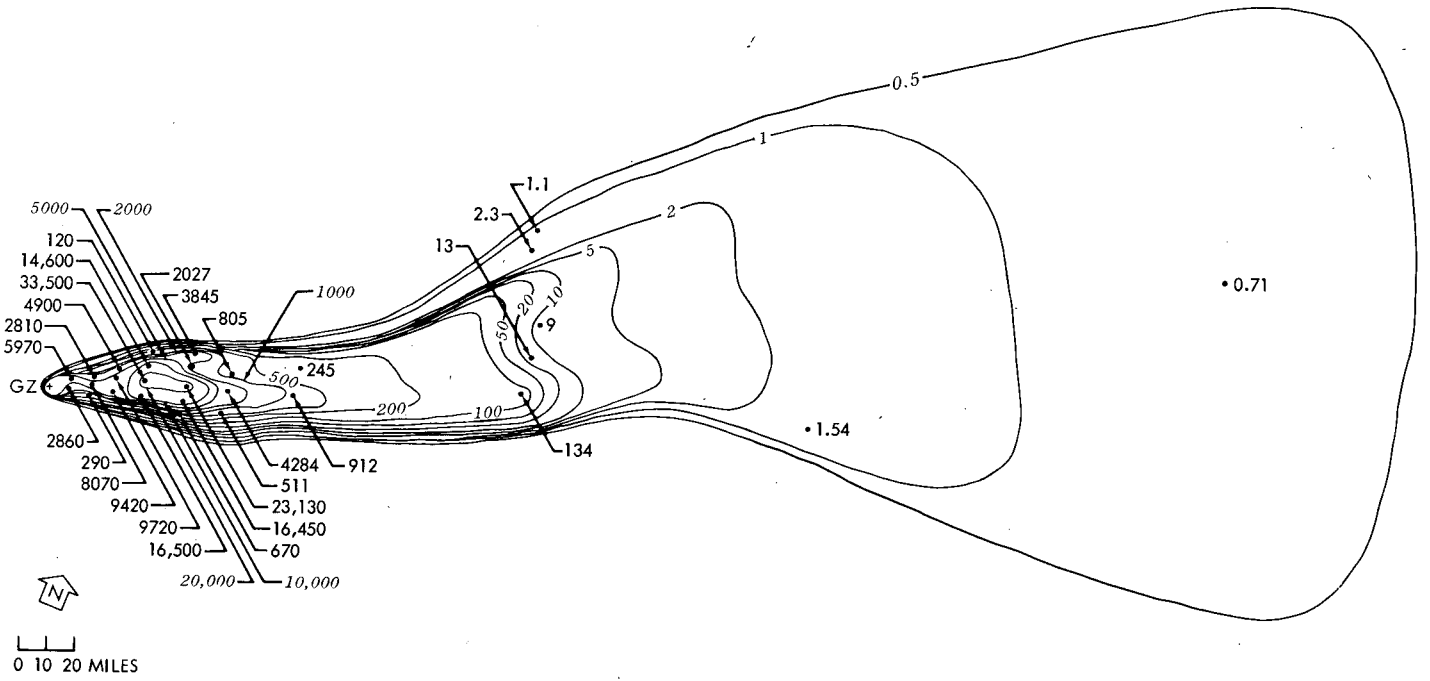

Fig. 6—Isointensity contours for 200- to 350-μ particle diameters in milliroentgens per hour at 1 hr.

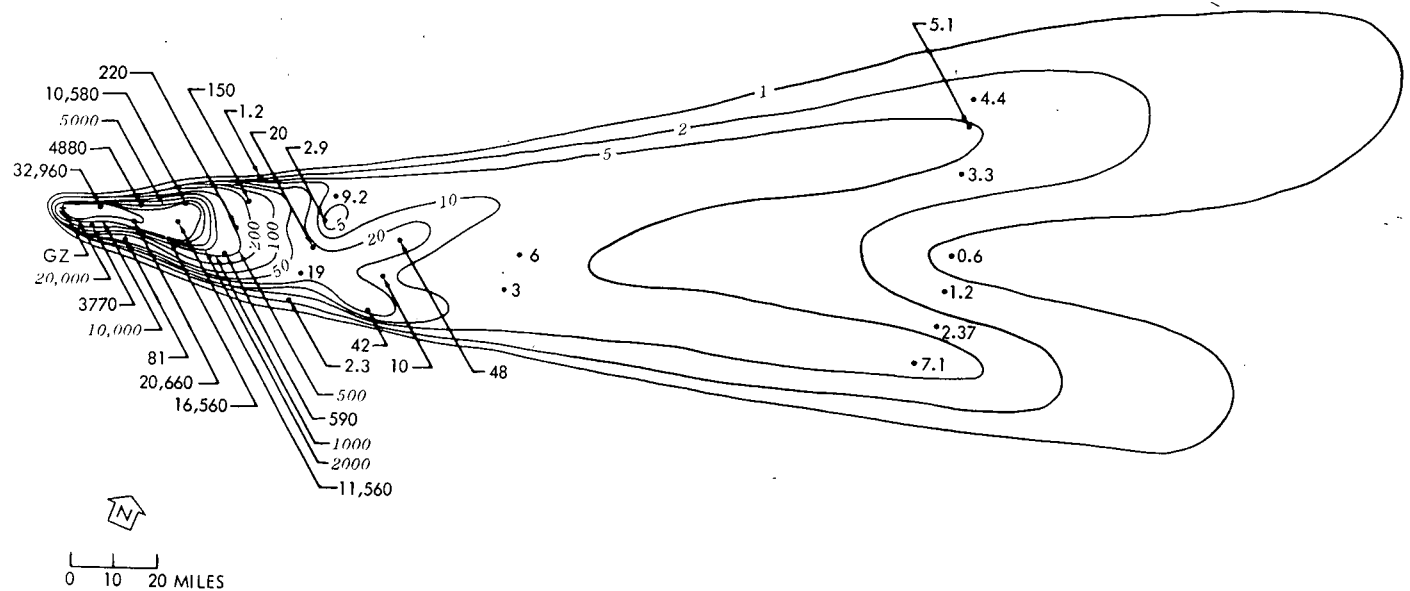

Fig. 7—Isointensity contours for 750- to 1000-μ particle diameters in milliroentgens per hour at 1 hr.

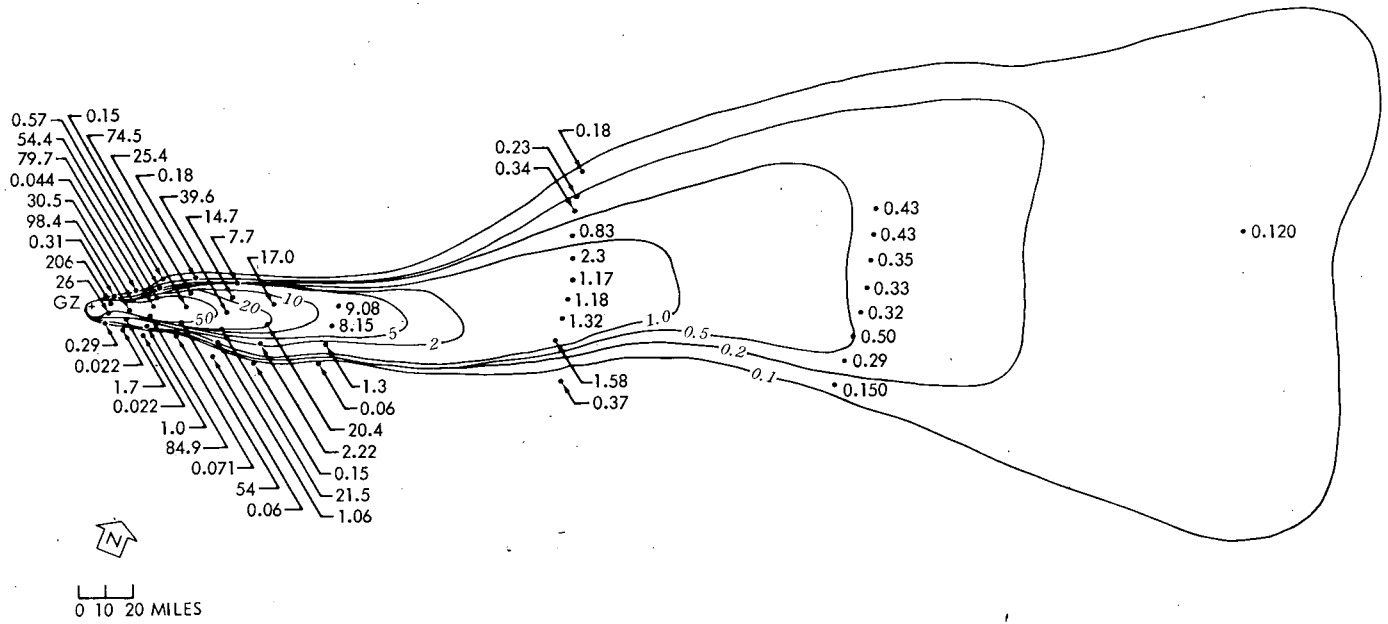

Fig. 8—Total fallout isointensity contours in roentgens per hour at 1 hr.

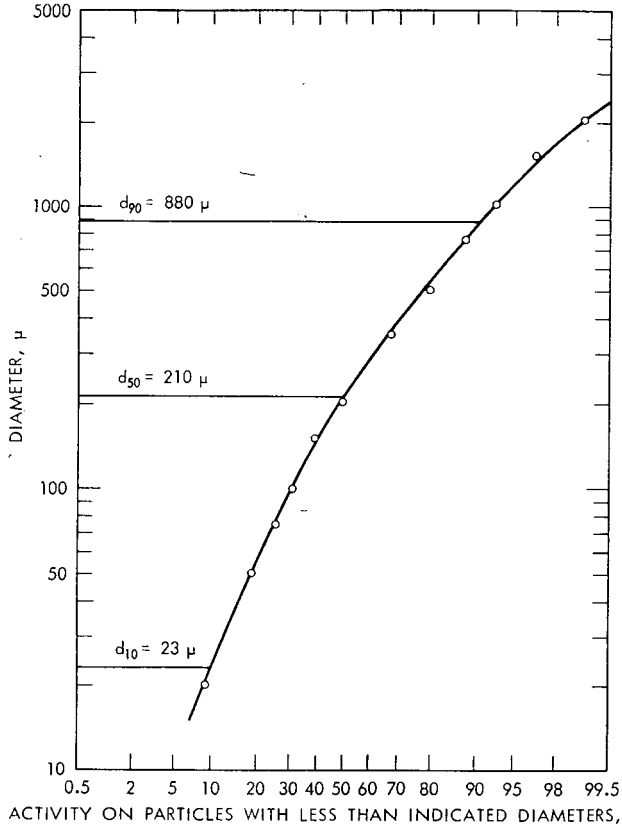

Fig. 9—Gross size vs. activity—area integrals for particles of different sizes.

Table 9—SUMMARY OF THE f_j VALUES FOR THE SMALL BOY SHOT FALLOUT AND THE CALCULATIONS FOR $\overline{r}_{fp}$ AND $\overline{K}_0$

Δd, μ	$\overline{d}$, μ	r_j	K_{0j}, r/hr at 1 hr / kt/sq mile	f_j	$f_j r_j$	$f_j K_{0j}$, r/hr at 1 hr / kt/sq mile
0 to 20	10	1.51	4090	0.091	0.137	372
20 to 50	35	0.665	1800	0.093	0.062	167
50 to 75	62.5	0.429	1160	0.075	0.032	87
75 to 100	87.5	0.334	905	0.049	0.016	44
100 to 150	125	0.269	729	0.076	0.020	55
150 to 200	175	0.232	629	0.108	0.025	68
200 to 350	275	0.204	553	0.182	0.037	101
350 to 500	425	0.195	529	0.122	0.024	64
500 to 750	625	0.194	526	0.082	0.016	43
750 to 1000	875	0.198	537	0.053	0.011	28
1000 to 1500	1250	0.210	570	0.040	0.008	23
1500 to 2000	1750	0.230	623	0.021	0.005	13
>2000		0.292	791	0.0095	0.003	7
				Sum	0.396	1072

Notes: (1) $r_{fp} = \Sigma f_j r_j = 0.396$. (2) $\overline{K}_0 = \Sigma f_j K_{0j} = 1072$ r/hr at 1 hr per kiloton per square mile.

value of C for the larger fallout pattern could then be calculated if the yield were known.

A commonly used value of K_0^0 in Eq. 7 for estimating the fraction of a device in the fallout pattern, especially when experimental values of $D\overline{q}$ are not directly available, is 2000 r/hr at 1 hr per kiloton per square mile. If this value is used with the J_R value, 1460 r/hr at 1 hr per square mile, for the Small Boy fallout pattern, the estimated value of F_D could be compared to that obtained through use of the radiochemical analysis of the fallout material and the methods outlined in this report.

COMMENTS AND CONCLUSIONS

The computed r_{fp} values appear to be somewhat low, especially for the median particle diameters between about 200 and 800 μ. Further examination of the radiochemical data with respect to the fractionation of individual nuclides and to the fission yield of ^{95}Zr, as a measure of the number of fissions, could provide further information on the r_{fp} values. The major factors in determining the r_{fp} values, if the data from ion-chamber measurements are accepted as being by far the most accurate, are the fission content of the samples and the decay factors from 100 to 1 hr after detonation for the ion-chamber data. The absolute value of i_0 for the unfractionated mixture of radionuclides from thermal-neutron fission of ^{235}U rather than for fission by fission neutrons would result in a relatively small error in the r_{fp} estimates. It should be expected that the decay factors for the samples would approach those for i_0 as the $r_{fp}(100)$ values approach unity, indicating a relatively unfractionated mixture of radionuclides.

The Dq values derived from the data are consistent with other previously derived values of q for the Nevada Test Site terrain.[8] These values generally would not be influenced by possible future changes in the r_{fp} values since any change in r_{fp} would result in an equivalent change in the values of the K_0.

The example analysis of some of the Small Boy shot data applicable to evaluation of the intensity–activity ratio shows that the ratio is not a constant for a given fallout pattern but varies over the pattern depending on the particle sizes in the deposited fallout. However, when gross activity–size distribution data are evaluated, an average value of the ratio can be derived for the fallout pattern. On the other hand, the average value of the intensity–activity ratio is not required for estimating the fraction of the device within a fallout pattern. A value for this ratio for the fallout deposited uniformly over an ideal plane, an average terrain attenuation factor, and an instrument response factor, however, are needed for estimating the fraction of device in the pattern.

Further detailed analyses of the available data are needed to verify or adjust the values of several of the parameters, as described in this preliminary analysis of the reported data, for more accurate evaluations of the intensity–activity ratios and the fraction of device accounted for within the fallout pattern.

REFERENCES

1. P. D. LaRiviere, Hong Lee, and K. H. Larson, Ionization Rate Measurements, Project 2.11, Operation Sun Beam Report POR-2217, April 1964. (Classified)
2. P. D. LaRiviere, J. D. Sartor, W. B. Lane, and K. H. Larson, Fallout Collection and Gross Sample Analysis, Project 2.9, Operation Sun Beam Report POR-2215, October 1964. (Classified).
3. E. C. Freiling, L. R. Bunney, and F. K. Kawahara, Physiochemical and Radiochemical Analysis, Project 2.10, Operation Sun Beam Report POR-2216, October 1964. (Classified)
4. C. F. Miller, Response Curves for USNRDL 4-pi Ionization Chamber, Report USNRDL-TR-155, U. S. Naval Radiological Defense Laboratory, May 1957.
5. C. F. Miller and P. Loeb, Ionization Rate and Photon Pulse Decay of Fission Products from the Slow-Neutron Fission of U-235, Report USNRDL-TR-247, U. S. Naval Radiological Defense Laboratory, August 1958.
6. P. D. LaRiviere, Response of a Low-Geometry Scintillation Counter to Fission and Other Products, Report USNRDL-TR-303, U. S. Naval Radiological Defense Laboratory, February 1959.
7. W. B. Lane, Stanford Research Institute, private communication, July 1964.
8. C. F. Miller, Fallout and Radiological Countermeasures, Vol. I, Stanford Research Institute, Project IMU-4021, January 1963.
9. Samuel Glasstone (Ed.), *The Effects of Nuclear Weapons*, Revised Edition, U. S. Government Printing Office, Washington, D. C., 1962.
10. L. Machta, Meteorological Processes in the Transport of Weapon Radioiodine, *Health Phys.*, *9*(12): 1123-1132 (1963).

RADIOCHEMICAL-DATA CORRELATIONS ON DEBRIS FROM SILICATE BURSTS

GLENN R. CROCKER, FRANCIS K. KAWAHARA, and EDWARD C. FREILING
U. S. Naval Radiological Defense Laboratory, San Francisco, California

ABSTRACT

Local-fallout samples collected in 1962 in the Johnie Boy, Small Boy, and Sedan shots were analyzed radiochemically for ^{89}Sr, ^{90}Sr, ^{91}Y, ^{95}Zr, ^{99}Mo, ^{103}Ru, ^{106}Ru, ^{131}I, ^{132}Te, ^{136}Cs, ^{137}Cs, ^{140}Ba, ^{141}Ce, ^{144}Ce, ^{239}Np, and ^{239}Pu. These results, as reported by the project officers, have been correlated by plotting the log of the ratio of equivalent fissions of each nuclide, i, to equivalent fissions of ^{95}Zr, $r_{i,95}$, against the log of the similar ratio for ^{89}Sr and ^{95}Zr, $r_{89,95}$. The data were fitted to straight lines by linear regression; and slopes, intercepts, coefficients of correlation, and confidence limits were determined. The slope of such a line for a nuclide i is an indication of the degree of fractionation of the nuclide relative to the fractionation of ^{89}Sr. For all cases observed in these Nevada shots, the same group of nuclides (^{89}Sr, ^{90}Sr, ^{91}Y, ^{103}Ru, ^{106}Ru, ^{131}I, ^{132}Te, ^{136}Cs, ^{140}Ba, ^{137}Cs, ^{141}Ce, and ^{239}Np) fractionated from ^{95}Zr. The nuclides ^{99}Mo, ^{144}Ce, and ^{239}Pu did not fractionate appreciably from ^{95}Zr. For the Sedan shot the slope of the ^{137}Cs plot is near 1.0, but, for the remaining fractionating nuclides, the slopes lie within a narrow intermediate range. For the Johnie Boy and Small Boy shots, for which the results are quite similar, these slopes show much wider variation. The results of the correlation have been compared with those from similar correlations for a coral-surface burst and some air bursts. Aside from the fact that ^{99}Mo fractionated from ^{95}Zr in the air bursts and that ^{239}Np did not fractionate from ^{95}Zr in the coral-surface burst, the results indicate that differences in the fractionation behavior of the nuclides are of degree rather than of kind. Correlation of radiochemical results with particle size indicates increasing degree of fractionation with increasing particle size.

INTRODUCTION

In the summer of 1962, the U. S. Naval Radiological Defense Laboratory (NRDL) collected fallout from three shots at the Nevada Test Site (NTS)—Johnie Boy, Small Boy, and Sedan. Radiochemical studies were made of the debris from these shots and were reported.[1–3] During the past several months, we have made log–log correlations of these radiochemical results and have attempted some interpretation of them.

Before the results are discussed, it seems appropriate to review the shot conditions since important differences existed among the three events. These differences undoubtedly had effects on the fractionation behavior of the fallout.

SHOT CONDITIONS

Small Boy was a low-yield shot fired from atop a 10-ft-high wooden tower above alluvial soil in Area 5 at NTS. NRDL collected many fallout* samples of debris at 43 stations within 8.7 miles of ground zero and took other samples on a line 15 miles from ground zero. Further samples were supplied by the University of California at Los Angeles sampling network at distances of 18, 27, 36, 52, and 70 miles. Four cloud samples were supplied by Los Alamos Scientific Laboratory. The discussion in this report is mainly restricted to samples from within 8.7 miles of ground zero and from the cloud samples. The number of samples used from each station varied, and many samples were subdivided by sieving into seven fractions that were analyzed individually. A total of about 187 samples is dealt with here, all of which were analyzed for ^{89}Sr, ^{90}Sr, ^{91}Y, and ^{95}Zr. In addition, about one-third of them were analyzed for ^{99}Mo, ^{103}Ru, ^{106}Ru, ^{136}Cs, ^{137}Cs, ^{140}Ba, ^{141}Ce, ^{144}Ce, ^{239}Np, and ^{239}Pu. Some of this last group of samples were also analyzed for ^{131}I and ^{132}Te. The numbers quoted do not include a fairly large number of radiochemical analyses on samples used for solubility studies.

NRDL's participation in the Johnie Boy and Sedan shots was on a rather limited basis. Johnie Boy was a low-yield burst 23 in. below the surface of basaltic material in Area 18 at NTS. Forty-four fallout samples from the area out to about $1\frac{1}{4}$ miles from ground zero and two cloud samples were studied radiochemically. All of these were analyzed for ^{89}Sr, ^{90}Sr, ^{91}Y, and ^{95}Zr, and about one-third of them were analyzed for the long list of nuclides previously given for the Small Boy samples.

*As distinguished from cloud and air-filter samples.

Sedan was the well-known 100-kt cratering shot for the Plowshare program. The device was buried 635 ft below the surface in alluvial material in Area 10. NRDL collected samples at stations within 1 to 3.6 miles of ground zero. Analyses were performed on about 50 samples for the short list of nuclides previously given, and about one-third of these were analyzed for the long list.

TREATMENT OF THE DATA

The radiochemical analytical work was contracted out to three commercial laboratories since NRDL does not have facilities for handling a large volume of samples for routine analysis. The contractors were selected on the basis of qualification tests, which were also intended to serve for interlaboratory calibration purposes. It required nearly a year for all the contractors to complete and report the analyses. The results were reported to NRDL as disintegrations per minute or equivalent ^{235}U thermal-neutron fissions at shot time. NRDL then converted the values to equivalent fissions of the device at shot time, using mass-chain yield values supplied by the weapons laboratories. At the same time the calibration factors derived from the qualification-test analyses were applied.

As a reference nuclide ^{95}Zr was chosen for fractionation studies. Some such choice seems unavoidable if fractionation is to be discussed. Zirconium-95 belongs to a class of nuclides (other members are ^{99}Mo, ^{144}Ce, and ^{147}Nd) that are generally present in debris in equal quantities when expressed as equivalent fissions. Strontium-89, on the other hand, shows wide variation when compared with any of these. The ratio of equivalent fissions of ^{89}Sr to equivalent fissions of ^{95}Zr is, in fact, a fairly good indicator of the degree to which a sample is fractionated. The ratio will be 1 for an unfractionated sample, less than 1 for a sample depleted in ^{89}Sr, and greater than 1 for a sample enriched in ^{89}Sr.

The behavior of other fractionating nuclides can be correlated with that of ^{89}Sr by log–log plotting. The log of the ratio, $r_{i,95}$, of equivalent fissions of nuclide i to equivalent fissions of ^{95}Zr is plotted against the log of the similar ratio for ^{89}Sr and ^{95}Zr. The data so treated can be fitted more or less satisfactorily to a straight line. The slope of the line is then an indication of the extent of fractionation of nuclide i.

RESULTS AND DISCUSSION

For the Johnie Boy and Small Boy shots, the local-fallout collections were sufficient to define the geographical extent of the close-in

fallout fairly well. The Small Boy field was the cigar-shaped downwind area typically associated with such shots. The Johnie Boy field was very, perhaps atypically, narrow with a very hot line down the center, which was visible on the ground as a darkened streak. The NRDL collection array at Sedan was not sufficiently widespread to define the limits of the close-in fallout field.

With each of these shots, one can associate a sort of average, or typical, value (or narrow range of values) for the ratio $r_{89,95}$ observed in gross samples. It is to be understood that this range of $r_{89,95}$ is much extended when cloud samples, sieve-fraction samples, and samples from the peripheral stations are considered. Nonetheless, the average value is useful for describing the overall degree of fractionation of the shot. For Johnie Boy a weighted average of this ratio for the hot-line stations is around 0.03, indicating very severe fractionation. For Small Boy the values for most stations are in the range 0.1 to 0.2, indicating more moderate fractionation. All Sedan samples were sieved, but the $r_{89,95}$ values for gross samples were reconstructed by properly weighting the values for the sieve fractions and were found to range from about 0.5 to 3.8. Values in this range would be anomalous for local fallout from a true surface burst, but they seem to be characteristic of cratering (buried) shots, venting underground explosions, and venting underwater bursts.

All of the Johnie Boy, Small Boy, and Sedan $r_{i,95}$ values have been log–log plotted against $r_{89,95}$. Figure 1 indicates how some of the data accommodate themselves to this treatment. These are the data on ^{140}Ba for the Johnie Boy shot, and they illustrate a particularly satisfactory fit. The slope, the y intercept at log x = 0 (x = 1), and the coefficient of correlation* have been determined by linear regression to be 0.61, 2.4, and 0.98, respectively. Not all of the data, by any means, fit a log–log plot so neatly. Figure 2 shows a much less satisfactory and more typical example. These data are part of the results for ^{90}Sr in the Small Boy shot. The coefficient of correlation here is only 0.684.

The data were originally fitted by lumping together data points from all three contracting laboratories. In the process of investigating a poor fit of ^{141}Ce data for Small Boy, we noticed that points from Laboratory A could be fitted fairly well, whereas those from Laboratory B were scattered so badly as to suggest that Laboratory B was experiencing difficulty with this analysis. Figure 3 shows these data. Investigation of the ^{103}Ru and ^{106}Ru data showed a similar situation, but it was reversed with respect to the two laboratories—Laboratory B points correlated notably better than did Laboratory A points.

*The square of the coefficient of correlation reflects that part of the variation in one set of measurements which can be explained by their dependence on the other.

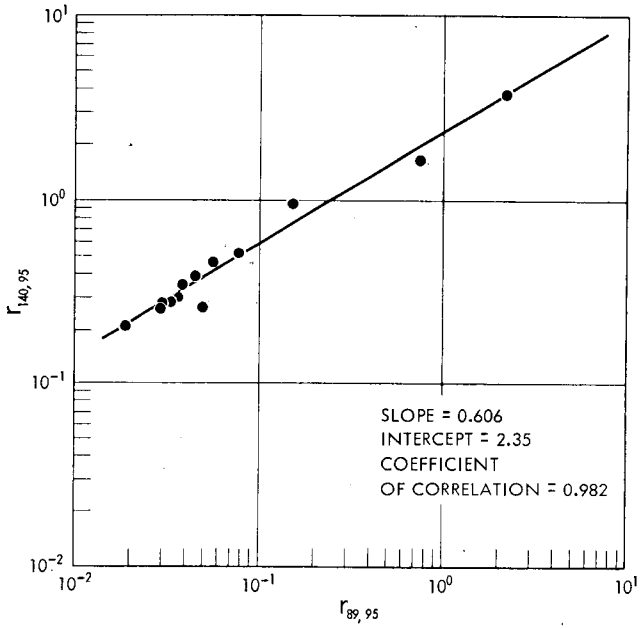

Fig. 1—Fractionation plot for ^{140}Ba in Johnie Boy.

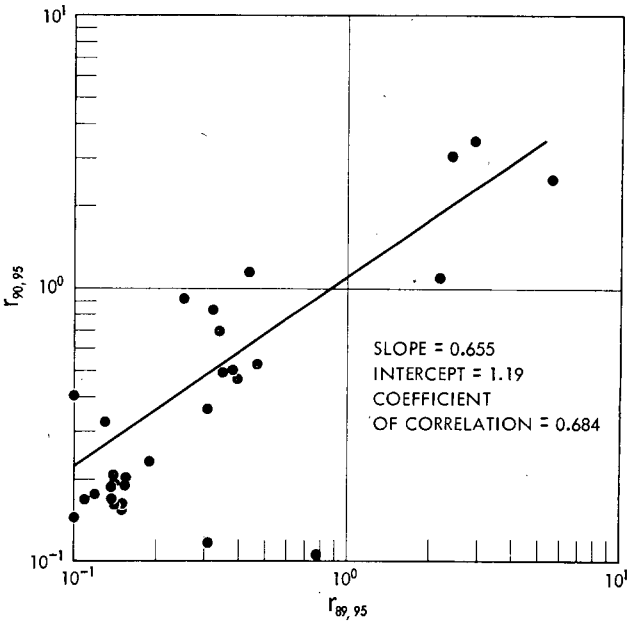

Fig. 2—Fractionation plot for ^{90}Sr in Small Boy.

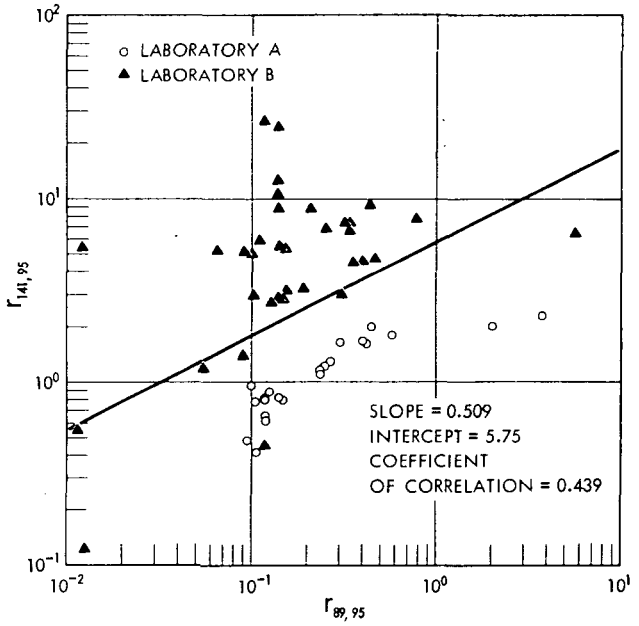

Fig. 3—Fractionation plot for ^{141}Ce in Small Boy.

All the data were reinvestigated by plotting and fitting the data points of each laboratory separately. Differences in the degree of correlation appeared which were sufficient to cast suspicion on part of the data for ^{132}Te, ^{136}Cs, and ^{137}Cs. Calibration differences among the laboratories also appeared to be obscuring the correlation in some instances. Figure 4 illustrates this effect. When the data from the three laboratories are treated separately, the three lines shown are obtained with a reasonable degree of confidence. Note that their slopes do not differ greatly. However, when the data are lumped together, the correlation is much less clear.

In spite of the difficulties involved in correlating the data, some facts emerge fairly clearly, as can be seen in Table 1. First, the same group of nuclides previously mentioned (^{89}Sr, ^{90}Sr, ^{91}Y, ^{103}Ru, ^{106}Ru, ^{131}I, ^{132}Te, ^{136}Cs, ^{137}Cs, ^{140}Ba, ^{141}Ce, and ^{239}Np) fractionated from ^{95}Zr in all three shots, whereas ^{99}Mo, ^{144}Ce, and ^{239}Pu did not. Second, ^{137}Cs appears to fractionate about as severely as ^{89}Sr. Beyond these basic points, the Sedan data display some differences from the data obtained in the other two shots. This is not surprising in view of the radical differences in the Sedan shot conditions. For Sedan the fractionating nuclides other than ^{137}Cs all showed a more or less intermediate degree of fractionation—the slopes of the log–log plots were between about 0.3 and 0.6—whereas, for Johnie Boy and Small Boy,

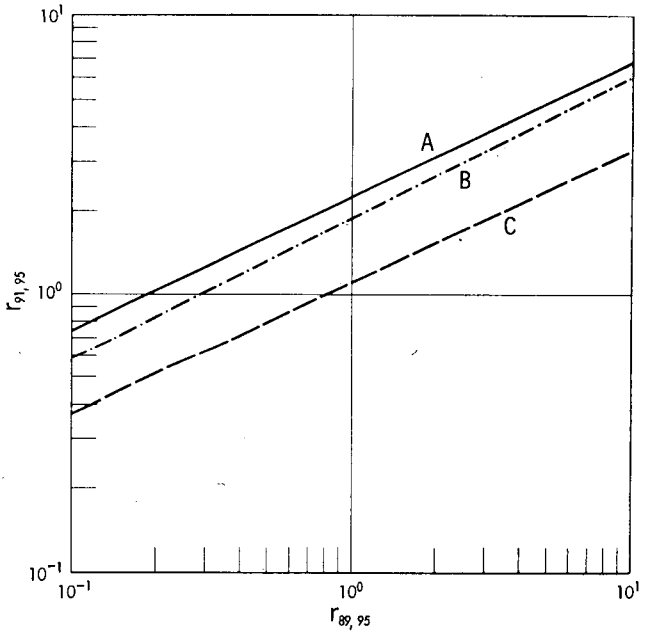

Fig. 4—Correlation lines for ^{91}Y in Small Boy from three different laboratories.

Table 1—SUMMARY OF SLOPES OF FRACTIONATION PLOTS

	Silicate-surface and subsurface bursts in 1962			High-yield coral-surface	
Nuclide	Sedan	Small Boy	Johnie Boy	burst	Air bursts
^{137}Cs	0.99	1.19	1.11	1.03	0.90
^{89}Sr	1.0	1.0	1.0	1.0	1.0
^{132}Te	0.43	0.90*	1.08*	0.60	
^{106}Ru	0.58*	0.89*			
^{131}I	0.56	0.84	1.10		
^{90}Sr	0.54	0.73	0.73	0.76	0.92
^{136}Cs	0.38*	0.65*	0.83*		
^{140}Ba	0.48	0.53	0.61	0.63	0.62
^{103}Ru	0.50*	0.52*			
^{91}Y	0.44	0.51	0.54		0.56
^{239}Np		0.48	0.48	−0.02	0.80
^{141}Ce	0.23*	0.43*	0.39*		0.40
^{239}Pu	0.04	0.07	0.18		
^{144}Ce	0.17	0.03	−0.003	0.08	0.18
^{99}Mo	0.04	0.04	−0.017	−0.10	0.30
^{95}Zr	0.0	0.0	0.0	0.0	0.0

*Certain reservations relative to these values are expressed in the text.

the range was considerably wider. The slope values obtained from the Johnie Boy and the Small Boy data are in quite good agreement with each other. The Sedan data are also given for purposes of comparison along with slopes from previous correlations on a high-yield coral-surface burst[4] and on some air bursts. A few interesting points with regard to the table may be mentioned. The nonfractionating behavior of ^{239}Np in the coral-surface burst is at variance with its behavior in the air bursts and the silicate bursts. On the other hand, ^{99}Mo fractionates in the air bursts but not in the other shots. There is an indication of possible slight fractionation of ^{144}Ce in Sedan and in the air bursts. In the silicate bursts ^{136}Cs fractionates less than ^{137}Cs. The fractionation of the latter is explainable on the basis of its rare-gas precursor, ^{137}Xe. Cesium-136, on the other hand, is shielded; i.e., it has no precursors. A possible explanation of its fractionation behavior lies in the basicity of the alkali-metal oxide or hydroxide relative to the silicate soil medium.

A reservation should be noted for the slope values reported for the 103-, 106-, and 132-mass chains for Johnie Boy and Small Boy. There is some indication in each of these cases that the data points belong to two different families and should not be fitted to the same straight line. The available data are unfortunately inadequate to resolve the question.

Aside from the ^{99}Mo and ^{239}Np anomalies just mentioned, insofar as the table permits one to judge, the differences in fractionation in the various kinds of bursts are of degree rather than kind.

Analysis on many samples separated into sieve fractions displays the trend of fractionation with particle size in a rough way. Figure 5 shows an example of these data from the Small Boy shot and also illustrates the variability of the ratios observed. The ratio of ^{89}Sr to ^{95}Zr has been plotted against the sieve-opening diameter. There is, of course, no really accurate way of plotting these data. For example, any point on the right side of the 1580-μ line corresponds to a sample that passed a No. 7 sieve (2800-μ openings) and was caught on a No. 12 sieve (1580-μ openings); presumably the sample may contain particles up to 2800 μ. The scattering of the points is thought to be due to the combined effects of heterogeneity and very small sample size. At least two kinds of active particles, smooth spheres and irregular particles, were discernible in these samples. Since many of the sieve fractions consisted of only a few particles, their compositions may not have been truly representative of their particle-size classes. If an average weighted according to sample masses is taken, one obtains the points of Fig. 5 through which a line has been drawn. The figure is quite representative of the behavior of fractionating nuclides in both Small Boy and Sedan. The sieve data on the Johnie Boy samples were too few to draw any conclusions relative to particle size.

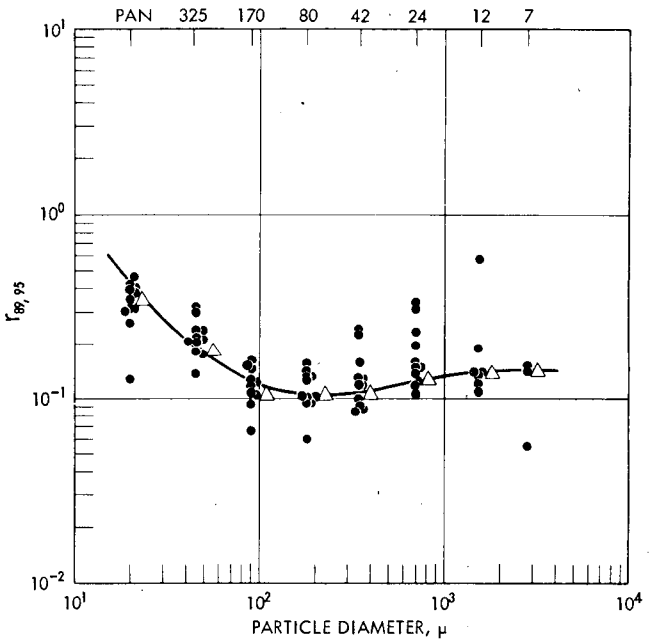

Fig. 5—Effect of particle size on fractionation ratio.

SUMMARY

Correlations indicate that the fractionation behavior of ^{89}Sr, ^{90}Sr, ^{91}Y, ^{137}Cs, ^{140}Ba, and ^{144}Ce relative to ^{95}Zr in silicate-surface bursts does not differ essentially from that observed in a coral-surface burst or in air bursts. Differences are noted for ^{99}Mo and ^{239}Np. For ^{103}Ru, ^{106}Ru, ^{131}I, ^{132}Te, ^{136}Cs, ^{141}Ce, and ^{239}Pu, some differences in degree of fractionation are indicated, and further study of these nuclides is recommended.

ACKNOWLEDGMENTS

In addition to the U. S. Atomic Energy Commission, the Defense Atomic Support Agency contributed generously to the support of this study. Some of the data were obtained from U. S. Air Force sources.

REFERENCES

1. D. E. Clark, F. K. Kawahara, and W. C. Cobbin, Fallout Sampling and Analysis: Radiation Dose Rate and Dose History at 16 Locations, Report POR-

2289, U. S. Naval Radiological Defense Laboratory, Oct. 24, 1963. (Classified)
2. E. C. Freiling, L. R. Bunney, and F. K. Kawahara, Physicochemical and Radiochemical Analysis, Report POR-2216, U. S. Naval Radiological Defense Laboratory, Oct. 28, 1964. (Classified)
3. W. B. Lane, Some Radiochemical and Physical Measurements of Debris from an Underground Explosion, USAEC Report PNE-229F, Jan. 7, 1964.
4. E. C. Freiling, Radionuclide Fractionation in Bomb Debris, *Science, 133* (3469): 1991–1998 (1961).

LONG-RANGE FALLOUT FROM SEDAN AND SMALL BOY SHOTS

PHILIP W. KREY and RALPH E. FRIED
Isotopes, Inc., Westwood, New Jersey

ABSTRACT

A sampling network was established across the United States to collect debris from the Sedan and Small Boy shots. Gross gamma assays, gamma-decay measurements, and gamma-spectrum and radiochemical analyses were performed on retrieved samples. Sedan, an underground burst, produced a cloud that was fairly homogeneous and highly fractionated. Small Boy, a surface burst, produced a heterogeneous cloud and even greater fractionation effects than Sedan. Molybdenum-99 in both shots behaved as a refractory material and did not represent an ideal tracer of fission-product debris.

OBJECTIVES

In the spring of 1962, Isotopes, Inc., undertook to collect, analyze, and characterize fallout from subsurface and surface bursts at intermediate- and long-range downwind distances from ground zero. The nuclear bursts studied were the Sedan and Small Boy shots in Operation Sun Beam. Sedan was approximately a 100-kt total yield with less than 30-kt fission; Small Boy was a low-yield surface burst.[1]

SAMPLING SITES

Three lines of sampling stations extending in a north–south direction were established across the country (Fig. 1). The most westerly line for the Sedan shot consisted of 12 stations situated about 15 miles apart at a distance of approximately 630 miles from ground zero. The

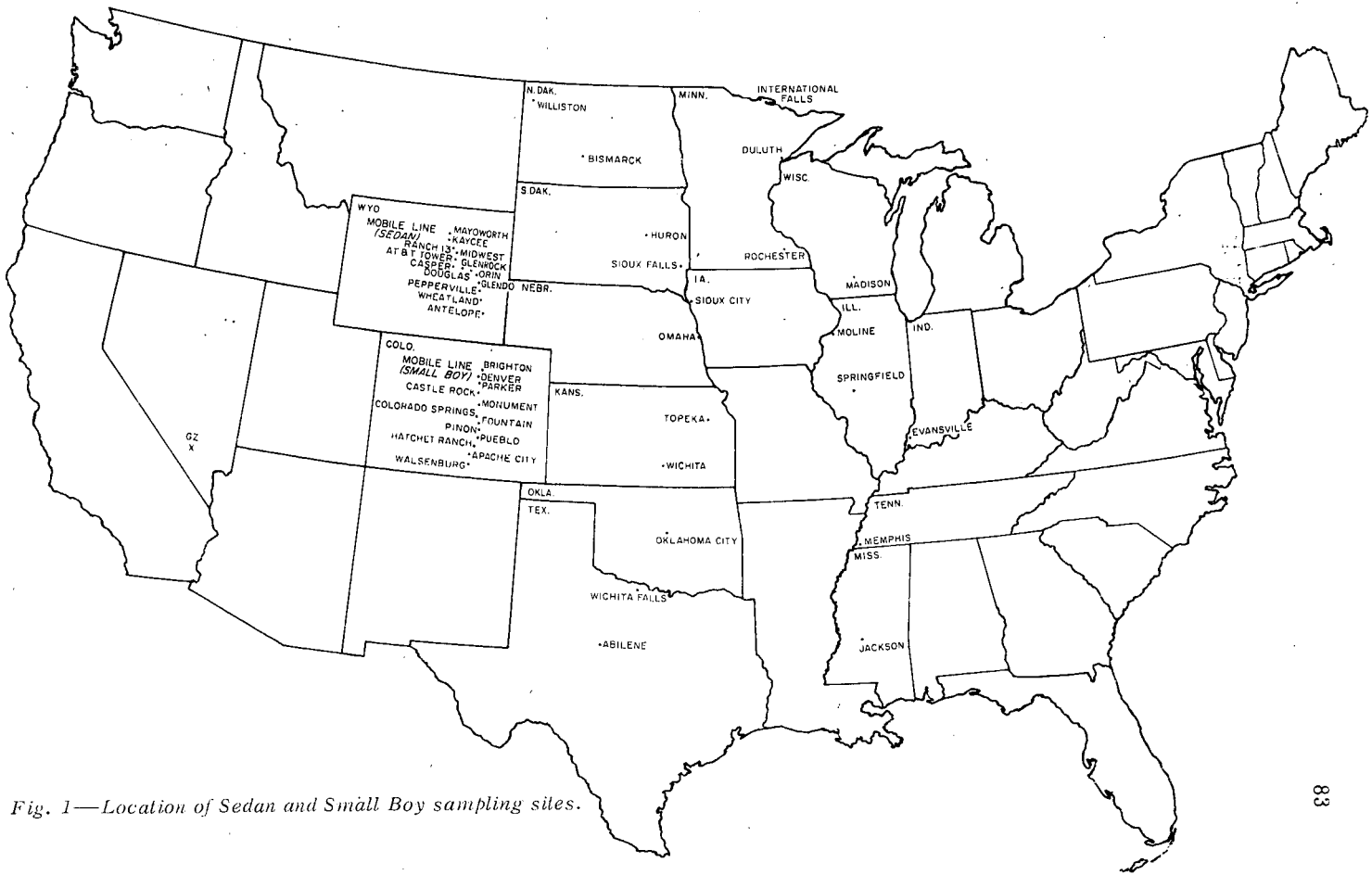

Fig. 1—Location of Sedan and Small Boy sampling sites.

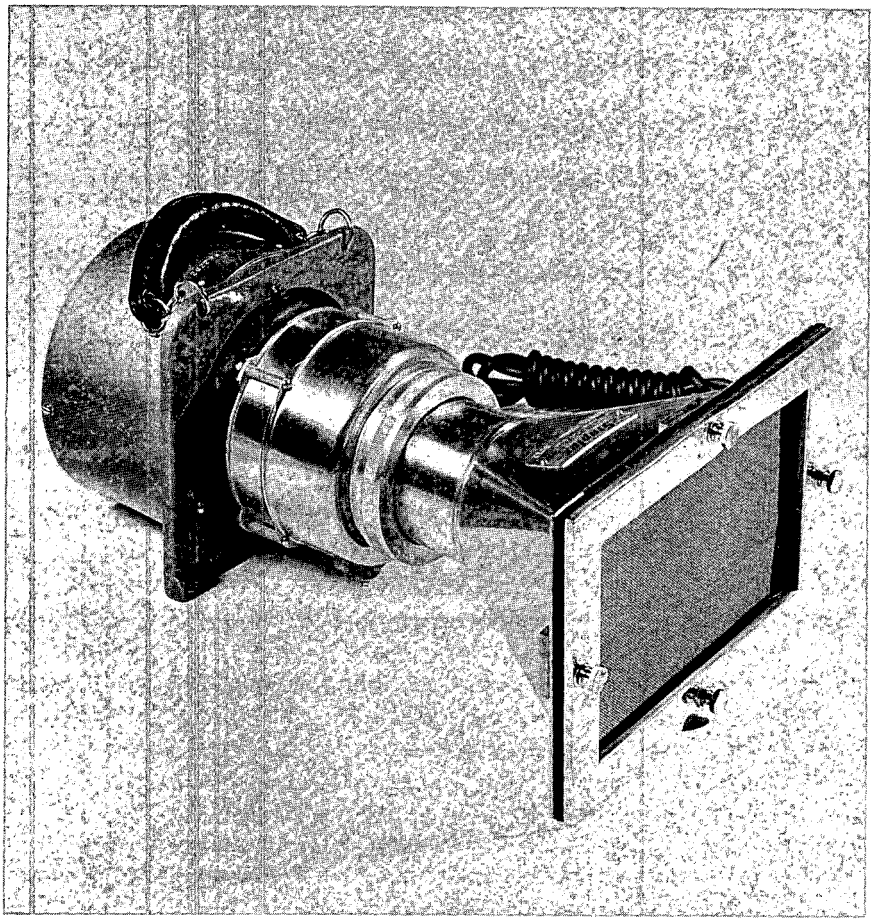

Fig. 2—Staplex high-volume air sampler.

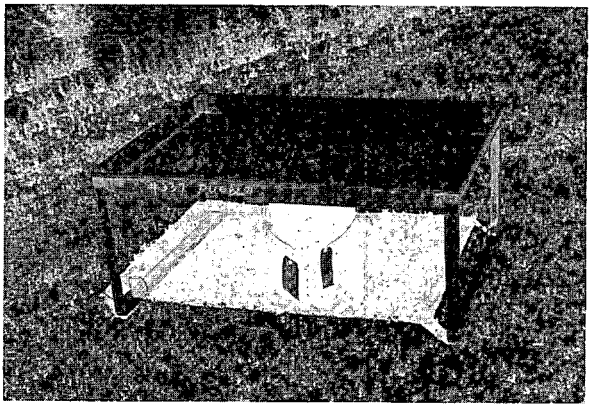

Fig. 3—Fallout collector.

length of this sampling line was 170 miles and extended northward from Antelope to Mayoworth, Wyo. Since the trajectory of the cloud from the explosion could not be predicted accurately enough to permit preshot installation of sampling sites, this line had to have the capability of being rapidly deployed after the shot when better meteorological data were available. Rapid deployment was accomplished by the sampling crew with a DC-3 aircraft and local commercial automobiles. Therefore this line of stations was called "the mobile line." The mobile line for the Small Boy shot extended from Walsenburg in southern Colorado to Brighton in the northern part of the state.

A second line of 11 stations, about 1000 miles from ground zero and approximately 1100 miles long, extended from Abilene, Tex., to Williston, N. Dak. A third line of nine stations, 1400 miles from ground zero and 1100 miles long, extended from Jackson, Miss., to International Falls, Minn. First-order U. S. Weather Bureau stations along these lines were used as sampling sites for both the Sedan and the Small Boy shots. Since these sites were not movable, they were referred to, respectively, as the first and second line of fixed stations.

INSTRUMENTATION

Each site on the mobile and the first fixed line was equipped with a Staplex high-volume air sampler and a fallout collector. The stations on the second fixed line were provided with only the air sampler. The air sampler is shown in Fig. 2 with an 8- by 10-in. filter holder. A TFA No. 41 ashless filter paper was used which is rated at a 95% collection efficiency for particles as small as 1 μ in diameter. The units were adjusted to a flow rate of about 50 cu ft/min at the start of the sampling period. The actual flow rate at subsequent times was read from a small rotameter affixed to the rear of the sampler. After the initial adjustment the flow rate was recorded every 6 hr for a total of five readings over a 24-hr period. The paper was replaced, and the cycle was repeated until three 24-hr samples were collected. The total volume sampled by each filter paper was determined by plotting these readings as a function of time and integrating the area under the curve.

The fallout collector consisted of a galvanized tray 42 in. long, 33 in. wide, and 3 in. deep (see Fig. 3). The surface of the collector was about 18 in. aboveground and sloped gently toward the center of the tray where a $^3/_4$-in. hole drained into a 5-gal polyethylene-lined drum beneath the collector. The capacity of the drum was equivalent to 0.83 in. of rain falling on the collecting surface. The active area of the fallout collector was coated with a thin layer of white petroleum jelly to present a tacky surface. Theoretically, the tacky surface would

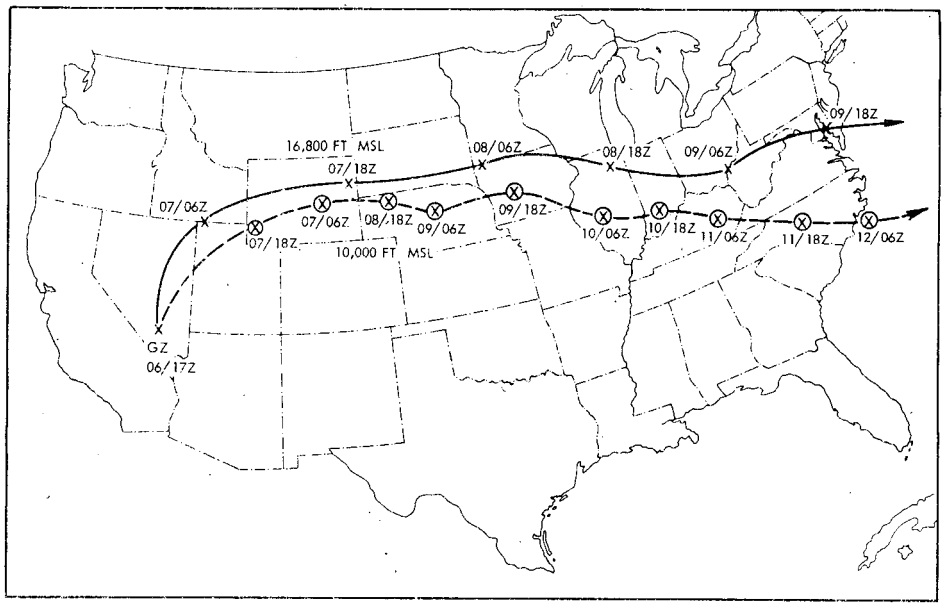

Fig. 4—Meteorological trajectories for Sedan. [*Date(July)/time (GCT).*]

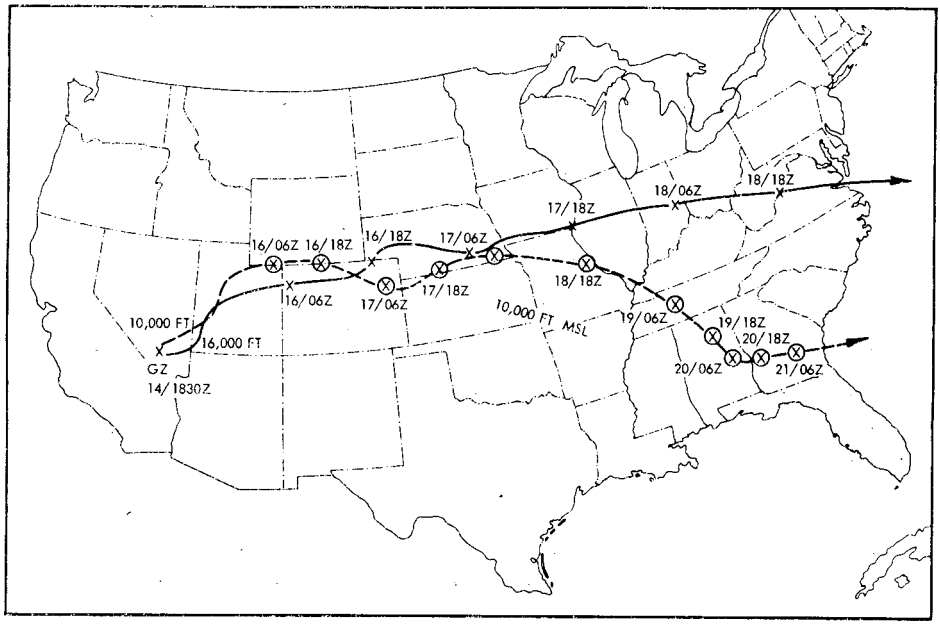

Fig. 5—Meteorological trajectories for Small Boy. [*Date(July)/time (GCT).*]

minimize redispersion by the wind of the debris which had already been collected. Each collector was exposed for a 72-hr sampling period.

After postshot notification from the Nevada Test Site as to the expected arrival of the clouds at each of the three sampling lines, sampling was begun about 12 hr before the estimated arrival time. These time estimates were based upon the latest meteorological and survey data available. Figure 4 shows the Weather Bureau's trajectory of the Sedan cloud. There was a wind sheer of the original cloud at 10,000 and 16,800 ft; the higher level of the cloud traveled slightly north of the lower level and at a faster velocity. Both levels of the cloud were intercepted by the mobile line. For the Small Boy shot (see Fig. 5), a wind sheer occurred at 10,000 and 16,000 ft with the 16,000-ft level traveling at a faster velocity than the 10,000-ft level. The two levels crossed at the northern end of the mobile line although the higher level arrived at the stations about 12 hr before the lower level.

MEASUREMENTS

All samples collected from both shots were radioassayed on a 3- by 3-in. NaI(Tl) crystal in conjunction with a 400-channel pulse-height analyzer. The fallout collectors were scrubbed with chloroform and a rubber squeegee to remove all debris from the collection surfaces. The resultant mixtures were evaporated to dryness in 500-ml nickel crucibles and ashed over a Meeker burner. Any rain or other contents of the 5-gal drum associated with each collector was combined with the material in the crucible. The mixture in the crucible was finally evaporated to dryness and assayed on the 3- by 3-in. crystal.

The total gamma spectrum of each sample, including preshot background samples, was obtained by these measurements. The integration of the activity beneath the spectrum after subtraction of detector background represented the total gamma activity of each sample. Selected filter papers were dry-ashed at 440°C, refluxed in nitric and hydrofluoric acids, and dissolved in nitric acid. Specific fallout-collector residues were fused with sodium carbonate and dissolved. These solutions were then analyzed radiochemically for a number of radionuclides. In the interest of brevity, only the results from the mobile lines are discussed in this paper. Although debris from the shots was recognizable at the fixed stations, it was much less pronounced, and measurements of it were greatly complicated by background levels.

RESULTS

Gamma-decay Measurements

The gross gamma-decay rate of a Sedan air-filter sample is plotted as individual points in Fig. 6. The decay rate of similar Small Boy debris is normalized to these points and drawn as the solid and

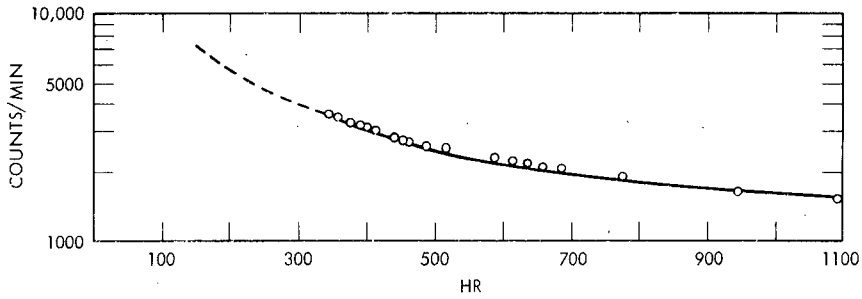

Fig. 6—Gross gamma decay of Sedan and Small Boy air-filter samples. (July 6, 1962.)

dashed line in Fig. 6. It is clear that the gross gamma-decay rates of the samples from both events are identical during the period of measurement. Plotted on log paper, the data follow the expression

$$A = A_1 t^{-0.89}$$

where A is the activity at time t after fission and A_1 is the activity at unit time after fission.

The exponent of the time is greater than the −1.2 usually employed. It is interesting that the debris from two such widely different events decay at exactly the same rate.

Gross Gamma Analyses

The plot of the gross gamma activity vs. site location (from north to south) for the Sedan mobile line is given in Fig. 7. The activity for each postshot sample was corrected to 1000 hr on D + 1 by using an extrapolation of the Sedan gross gamma-decay curve (Fig. 6). The background levels reflected in Fig. 7 are the activity of a preshot air-filter sample assayed on D + 7 and the activity of a preshot fallout collector assayed on D + 10. Since the background samples were not followed for decay, it is impossible to correct the data to a previous time. The background may constitute a major part of the activity in the first day of air sampling, but it is of little consequence in sub-

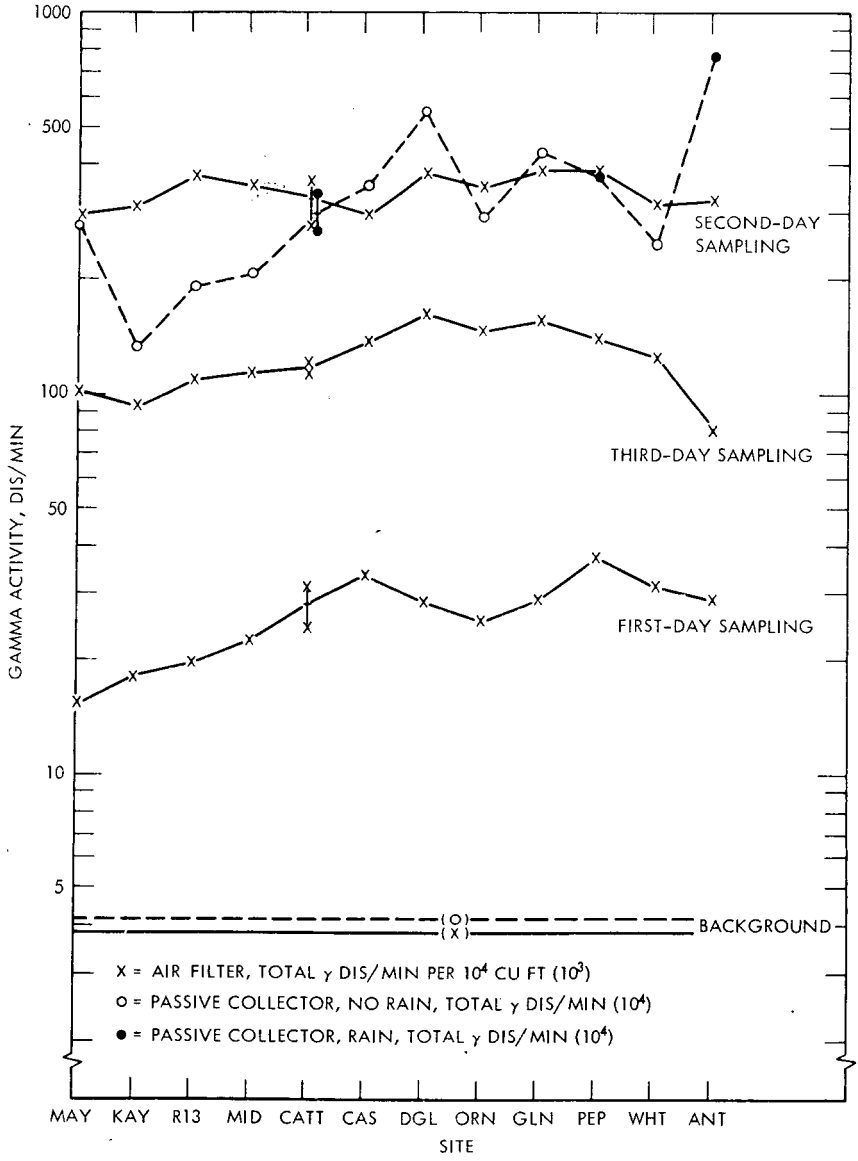

Fig. 7—Sedan total gamma activities (mobile line sites; see Fig. 1 for meaning of abbreviations).

sequent days. With this restriction in mind, Fig. 7 reveals the collection of fresh activity at all sites on the first day of sampling with higher concentrations in the southern half of the line. The activity on the second day is diffused throughout the arc with concentrations again generally higher in the southern sector. Prominent peaks are observed for the 72-hr fallout-collector samples at Douglas and Antelope; significantly, both these samples contained a large rainfall

component. Activities on the third day of sampling are lower by a factor of 2 or 3 than those on the previous day; the distribution of concentrations approximates that of the first day of sampling.

The total gamma activities of the Small Boy mobile-line stations (north to south) corrected to 1130 hr on D + 1 but uncorrected for background contribution are shown in Fig. 8. The preshot air filter was counted on D + 4, whereas the background fallout collector was assayed on D + 9. The background could have amounted to about one-half the total activities in the postshot samples, particularly in the southerly stations. However, the presence of fresh debris is clear and the relations between samples should not be seriously hampered. Figure 8 shows a maximum in total gamma activity at the northern extremity of the line for the fallout-collector samples and for each of the three days of air sampling. It is evident that the mobile line was situated too far south to provide for a central interception of the cloud. Furthermore the increase in activity concentrations on consecutive days along the southern sector of the line indicates that sampling in that sector was discontinued too early.

Gamma-spectrum Analyses

The gamma-spectrum analyses did not uncover any pronounced effects except for the presence of induced ^{181}W in the Sedan fallout. Particular attention was given to identifying ^{24}Na in the Sedan underground-burst debris, but none could be found. The spectra permitted easy identification of fresh debris, and they verified the conclusions drawn from the gross gamma considerations. A comparison of the spectra from the two shots is given in Fig. 9. The spectra of two air-filter samples collected at about the same time after each shot and assayed at about the same elapsed time after each detonation are normalized to the 1.60-Mev photopeak of ^{140}La. Weaker energy emitters, possibly associated with ^{132}Te, ^{132}I, ^{131}I, ^{99}Mo, ^{103}Ru, and ^{106}Ru, are in slightly greater abundance relative to ^{140}La in the Small Boy debris than in the Sedan material. However, as was observed, these differences did not bring about any marked variations in the rate of gamma decay of the debris from each shot.

Sedan Radiochemical Analyses

It was found that the measured pre-Sedan shot levels of ^{90}Sr, ^{91}Y, ^{95}Zr, ^{106}Ru, and ^{144}Ce at the mobile line which resulted mainly from stratospheric fallout represented a large fraction of the total activities of these nuclides collected in post-Sedan samples. It is likely that the background levels vary significantly from day to day depending upon local meteorological conditions. Therefore, the background levels determined for a period of time at one location on the sampling line

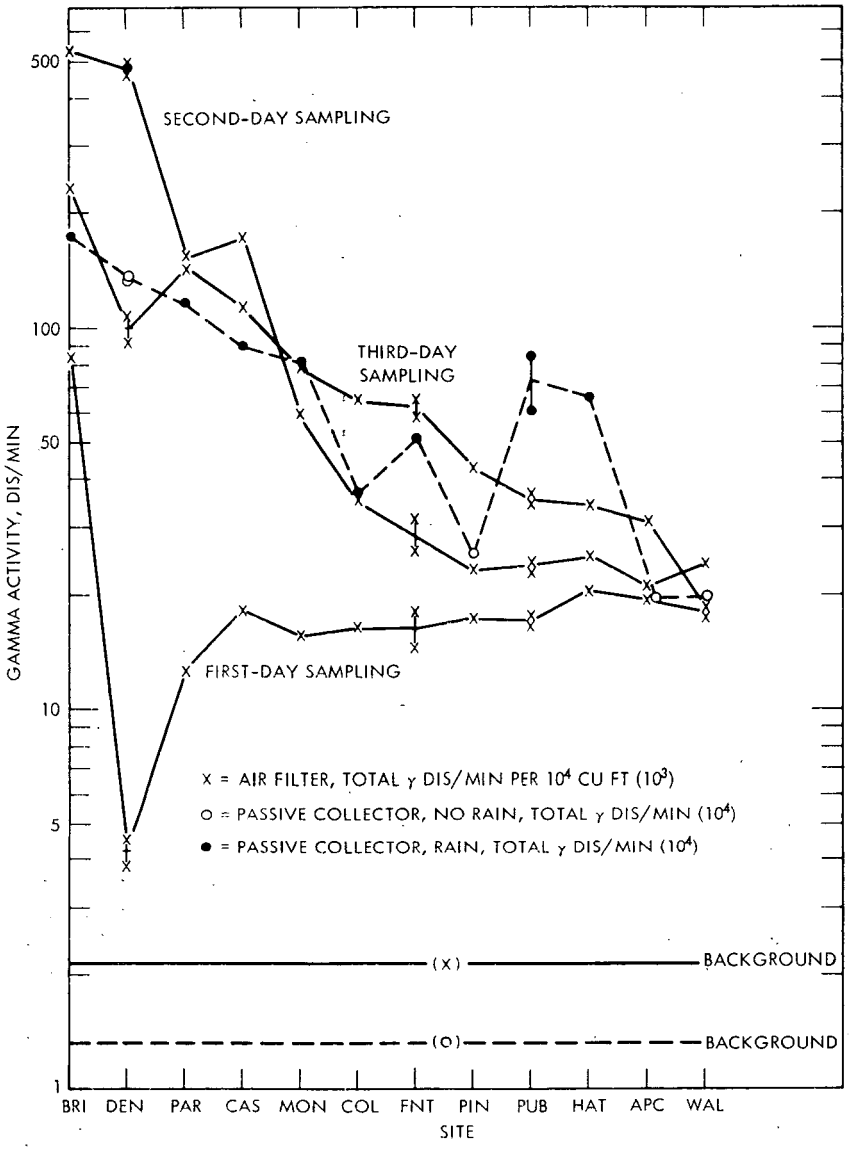

Fig. 8—Small Boy total gamma activities (mobile line sites; see Fig. 1 for meaning of abbreviations).

may not be directly applicable to another location on the same line at another time. Consequently, interpretations involving these radionuclides must be made with this reservation in mind.

The disintegrations per minute ratios of the various fission products to ^{99}Mo corrected to shot time are given in Table 1 for the air-filter samples collected from D + 2 to D + 3. These values are

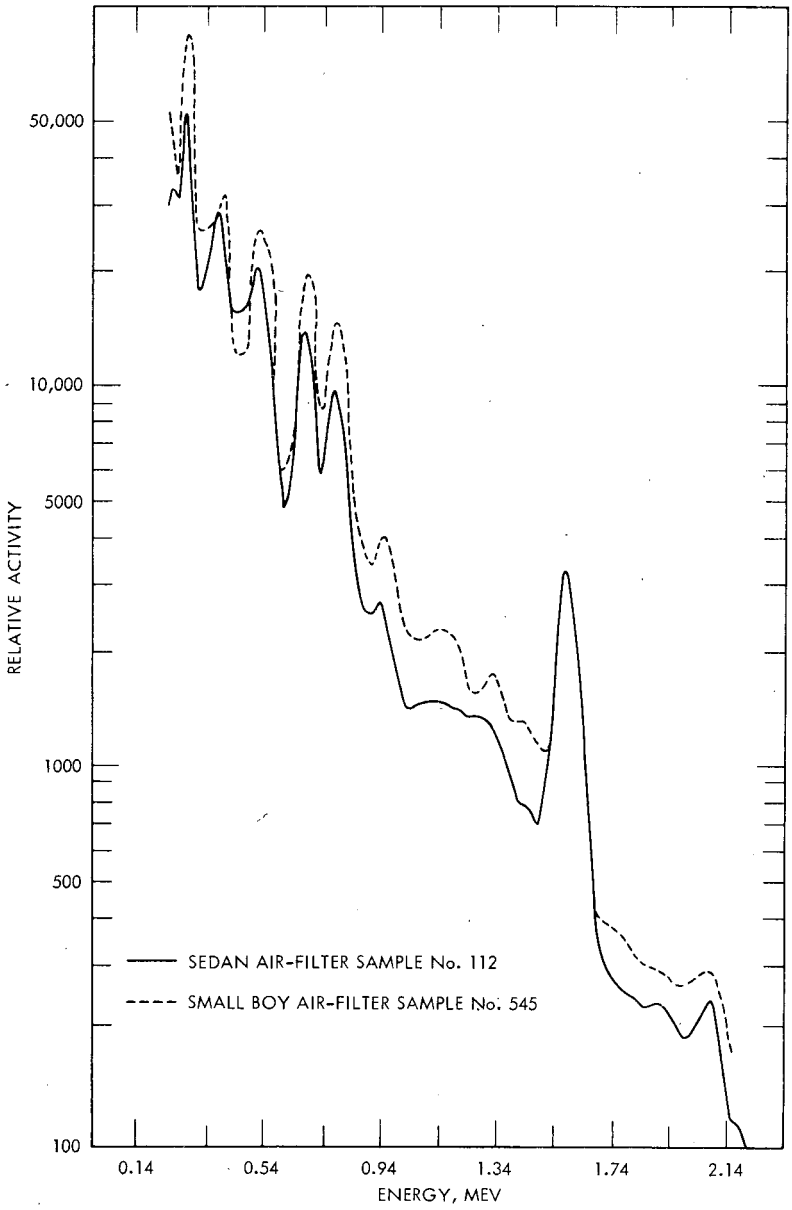

Fig. 9—Comparison of Sedan and Small Boy gamma spectra.

Table 1—DISINTEGRATIONS PER MINUTE RATIOS TO ^{99}Mo AT SHOT TIME FOR SEDAN AIR-FILTER SAMPLES ADJUSTED FOR BACKGROUND

Source and sample No.	^{89}Sr	^{90}Sr (10^{-3})	^{95}Zr (10^{-2})	^{91}Y (10^{-1})	^{103}Ru (10^{-1})	^{106}Ru (10^{-2})	^{137}Cs (10^{-2})	^{140}Ba	^{141}Ce (10^{-2})	^{144}Ce (10^{-2})
Kaycee, 107	2.54	7.25	0	2.16	5.50	14.0	4.58	2.39	0	1.9
Midwest, 167	2.24	4.31	0	1.52	2.60	4.08	2.48	1.92	11.0	0
Casper ATT, 142	2.99	7.00	0	2.10	2.28	4.05	3.97	3.98	0	0
Casper ATT, 157	3.39	9.59	0	3.12	2.77	4.7	5.26	4.06	0	0
Casper, 117	3.60	6.06	0	2.60	2.81	2.92	4.66	3.45	0	15.7
Orin, 112	2.19	8.93	0	2.30	2.38	6.74	4.92	2.15	0	0
Pepperville, 173	4.32	8.49	2.60	2.57	2.81	0.67	6.06	3.94	0	0
Average	3.04	7.38	~0	2.34	3.01	5.31	4.56	3.13	~0	~0
Katcoff, thermal ^{235}U	0.0434	0.258	4.4	~0.43	0.34	0.047	0.0257	0.227	~8.3	~0.98
Dolan, 14-Mev ^{238}U	0.0248	0.144	3.49	0.287	0.545	0.356	0.0268	0.170	6.27	0.559

adjusted for the preshot background levels. The theoretical ratios for the thermal fission of ^{235}U by Katcoff[2] and the 14-Mev neutron fission of ^{238}U by Dolan[3] are listed in Table 1 for reference. Presumably the production ratios for the Sedan shot would be closer to Dolan's figures. There are no obvious trends in the data with collection site which suggests that the two levels in the cloud were not fractionated with respect to each other. The zeros in Table 1 represent the situation where no measurable activity was found or where the measured activity was less than the background activity. Comparing the average ratios with Dolan's values shows a deficiency of ^{95}Zr, ^{141}Ce, and ^{144}Ce with respect to ^{99}Mo in the airborne particulate matter of the Sedan debris. The radionuclides ^{89}Sr, ^{90}Sr, ^{91}Y, ^{137}Cs, and ^{140}Ba have rare gaseous or volatile precursors. Because of their volatile precursors, all of these nuclides show a surplus to ^{99}Mo compared to Dolan's production values. Ruthenium has volatile oxides, and both ^{103}Ru and ^{106}Ru reflect an overabundance with respect to ^{99}Mo. However, it is likely that the 103 and 106 mass chains would be present as their respective niobium or molybdenum precursors during the time of radioactive-particle formation.

The disintegrations per minute ratios to ^{99}Mo at shot time adjusted for background levels are given in Table 2 for the fallout-collector samples. As for the air-filter samples, there is no observable trend with collection site. The ^{95}Zr behaves as a refractory exhibiting a deficiency in the fallout, whereas the ^{89}Sr, ^{90}Sr, ^{91}Y, ^{103}Ru, ^{106}Ru, ^{137}Cs, and ^{140}Ba show a surplus. Contrary to the air-filter samples, ^{141}Ce and ^{144}Ce also show a surplus with respect to ^{99}Mo although there are several zeros for these nuclides in Table 2. These zeros may be the

Table 2—DISINTEGRATIONS PER MINUTE RATIOS TO ^{99}Mo AT SHOT TIME FOR SEDAN FALLOUT COLLECTORS ADJUSTED FOR BACKGROUND

Source and sample No.	^{89}Sr (10^{-1})	^{90}Sr (10^{-3})	^{95}Zr (10^{-2})	^{91}Y (10^{-2})	^{103}Ru (10^{-2})	^{106}Ru (10^{-2})	^{137}Cs (10^{-3})	^{140}Ba (10^{-1})	^{141}Ce (10^{-2})	^{144}Ce (10^{-2})
Mayworth, 62	4.08	1.34	0	8.05	18.7	5.01	3.83	4.80	9.76	2.34
Ranch 13, 74	4.70	1.62	Lost	3.64	17.0	3.69	7.29	7.78	12.3	0
Midwest, 100	5.80	1.97	0	8.14	5.49	0	12.8	6.76	61.4	9.38
Casper ATT, 64	6.46	2.57	Lost	8.93	1.94	0.87	16.1	10.0	4.42	0.701
Casper ATT, 75	7.05	2.54	Lost	9.45	3.30	1.8	16.4	10.9	6.09	0.35
Casper, 66	5.89	2.37	0	7.34	14.6	2.20	9.89	7.85	19.8	0.542
Orin, 72	4.98	1.51	16.6	6.74	8.38	2.20	8.89	7.24	0	0
Pepperville, 68	7.22	3.70	0	12.4	9.18	1.0	13.9	10.5	22.3	3.92
Antelope, 71	3.54	1.16	Lost	4.21	0.875	0	6.52	4.84	3.47	0
Average	5.22	2.09	~0	7.66	8.83	1.86	10.6	7.85	15.5	1.91
Katcoff, thermal ^{235}U	0.434	0.258	4.4	~4.3	3.4	0.047	0.257	2.27	~8.3	0.98
Dolan, 14-Mev ^{238}U	0.248	0.144	3.49	2.87	5.45	0.356	0.268	1.70	6.27	0.559

result of the uncertainty in the background values subtracted. A plausible explanation for all the measured fission products except ^{95}Zr showing a surplus to ^{99}Mo is that ^{99}Mo is not a good reference nuclide and is itself deficient in the fallout-collector debris. This is not unreasonable because ^{99}Mo would most probably be present as refractory ^{99}Y or ^{99}Zr at the time of radioactive-particle formation in the Sedan cloud.

If we define an F value, a fractionation index, as the observed disintegrations per minute ratio to ^{99}Mo divided by Dolan's production ratio to ^{99}Mo, the F value will indicate the intensity of the fractionation that occurred at the Sedan event. A value of unity would indicate no fractionation. Table 3 gives the F values for the average of the air-

Table 3—MOLYBDENUM-99 F VALUES FOR AVERAGE SEDAN DATA

Nuclide	Air-filter sample	Fallout-collector sample
^{89}Sr	122	21
^{90}Sr	51	14
^{91}Y	8.2	2.7
^{103}Ru	5.5	1.6
^{106}Ru	15	5.2
^{137}Cs	178	40
^{140}Ba	18	4.6
^{141}Ce		2.5
^{144}Ce		3.4

filter and fallout-collector samples. The F values in excess of 100 for ^{89}Sr and ^{137}Cs for the air-filter samples reflect extreme departure from ideal behavior. Although the values are not as large for the fallout-collector samples, they still represent strong fractionation for most nuclides.

The relation of the air-filter samples to the fallout-collector samples can be described by dividing the ratios to ^{99}Mo in the one type of sample by the same ratio in the other (see Table 4). This calculation

Table 4—SEDAN ^{99}Mo RATIOS OF AIR-FILTER SAMPLES VS. THOSE OF FALLOUT-COLLECTOR SAMPLES

^{89}Sr	^{90}Sr	^{91}Y	^{103}Ru	^{106}Ru	^{137}Cs	^{140}Ba	^{141}Ce	^{144}Ce
5.8	3.5	3.0	3.4	2.8	4.3	4.0	0	0

assumes that ^{99}Mo behaves as an ideal tracer of the fission products and does not fractionate with respect to particle size. The values greater than unity in Table 4 reflect a preferential association of the volatile nuclides with the smaller particles collected in the air-filter samples as compared to the larger particles of the fallout-collector samples. The opposite is true for ^{141}Ce and ^{144}Ce which exhibit a preference for the larger particles of the fallout-collector samples.

Small Boy Radiochemical Analyses

The disintegrations per minute ratios to ^{99}Mo for the Small Boy air filters adjusted for background levels are reported in Table 5. All

Table 5—DISINTEGRATIONS PER MINUTE RATIOS TO ^{99}Mo AT SHOT TIME FOR SMALL BOY AIR-FILTER SAMPLES ADJUSTED FOR BACKGROUND

Source and sample No.	^{89}Sr (10^{-1})	^{90}Sr (10^{-3})	^{95}Zr (10^{-2})	^{91}Y (10^{-2})	^{103}Ru (10^{-1})	^{106}Ru (10^{-2})	^{137}Cs (10^{-3})	^{140}Ba (10^{-1})	^{141}Ce (10^{-2})	^{144}Ce (10^{-2})
Brighton, 545	1.33	2.14	4.95	7.02	0.921	2.27	3.91	6.91	0	3.93
Denver, 518	1.15	2.26	5.17	6.53	2.49	3.22	3.61	6.35	10.4	2.90
Denver, 562	1.16	1.96	4.80	7.27	Lost	Lost	3.34	6.20	8.42	2.91
Parker, 547	1.40	3.06	7.46	8.63	1.72	3.01	6.28	4.96	0	1.2
Castle Rock, 553	0.936	4.28	8.74	6.52	0	1.3	6.49	4.60	0	5.55
Monument, 554*	1.60	6.12	17.3	0.2	0.44	0	7.14	4.62	0	11.1
Colorado Springs, 753*	1.75	5.1	15.2	9.48	3.47	6.96	10.4	3.98	0	5.1
Average	1.33	3.56	9.09	6.52	1.51	2.79	5.88	5.37	~0	4.67
Katcoff, thermal ^{235}U	0.434	0.258	4.4	~4.3	0.34	0.047	0.257	2.27	~8.3	~0.98
Dolan, 14-Mev ^{238}U	0.248	0.144	3.49	2.87	0.545	0.356	0.268	1.70	6.27	0.559

*These samples collected from D + 3 to D + 4, all others were collected from D + 2 to D + 3.

samples were collected from D + 2 to D + 3, except for the last two in the table which were collected from D + 3 to D + 4. Some of the ratios exhibit trends with geographical location; ^{90}Sr, ^{95}Zr, and ^{137}Cs increase with southerly direction, whereas ^{140}Ba appears to decrease slightly in that direction. All the nuclides except ^{141}Ce show a surplus compared to either of the reference production ratios. This behavior is particularly surprising for refractory nuclides like ^{95}Zr and ^{144}Ce. As in the case of the Sedan fallout-collector samples, the pattern suggests that ^{99}Mo is behaving as a refractory material.

Table 6 gives the disintegrations per minute ratios to ^{99}Mo of the fallout-collector samples from Small Boy adjusted for background

Table 6— DISINTEGRATIONS PER MINUTE RATIOS TO ^{99}Mo AT SHOT TIME FOR SMALL BOY FALLOUT-COLLECTOR SAMPLES ADJUSTED FOR BACKGROUND

Source and sample No.	^{89}Sr (10^{-2})	^{90}Sr (10^{-2})	^{95}Zr (10^{-1})	^{91}Y (10^{-1})	^{103}Ru (10^{-2})	^{106}Ru (10^{-2})	^{137}Cs (10^{-2})	^{140}Ba (10^{-1})	^{141}Ce (10^{-1})	^{144}Ce (10^{-1})
Brighton, 344	4.22	0.512	1.00	0.664	9.26	4.13	0.758	3.02	1.78	2.18
Denver, 343	4.62	0.153	2.51	0.742	0	0.511	0.460	1.57	1.22	0.791
Denver, 345	6.09	0.258	3.51	0.865	0	0.23	0.436	1.95	1.54	0.626
Parker, 342	7.97	0.877	1.80	1.63	6.99	12.9	1.57	6.52	4.53	1.87
Castle Rock, 341	22.5	3.02	5.48	3.98	4.36	0.13	2.14	8.48	3.91	5.20
Monument, 340	99.8	18.4	24.5	18.3	90.8	67.1	18.4	5.66	4.94	5.30
Colorado Springs, 339	30.1	4.33	2.8	6.10	57.8	5.38	6.13	5.78	0	9.22
Pinon, 338	14.5	1.85	15.8	5.76	18.1	2.7	1.82	5.50	7.94	8.19
Average	24.0	3.7	7.2	4.8	23.0	12.0	4.0	4.8	3.2	4.2
Katcoff, thermal ^{235}U	4.34	0.0258	0.44	~0.43	3.4	0.047	0.0257	2.27	~0.83	~0.098
Dolan, 14-Mev ^{238}U	2.48	0.0144	0.349	0.287	5.45	0.356	0.0268	1.70	0.627	0.0559

contribution. Severe dependence upon sampling location is clearly evident from these data. All the ratios either peak around Monument, Colo., or increase with southerly collection. In the comparison of the average values with Dolan's ratios, all nuclides show a marked surplus with respect to ^{99}Mo. This observation supports the previous conclusion that ^{99}Mo behaves as a refractory material. A possible explanation of the wide variations displayed in Table 6 is derived from the cloud sheer. Because of its more southerly swing near the sampling line, the lower 10,000-ft level might have contributed more debris to the southern stations than to the northern ones. This concept and the data in Table 6 describe the Small Boy cloud as a heterogeneous mixture.

The F values to ^{99}Mo for the average ratios given in Tables 5 and 6 are presented in Table 7. Average ratios for the fallout-collector samples are not very meaningful because of the large range in the data, but the F values give some indication of the magnitude of the

Table 7—MOLYBDENUM-99 F VALUES FOR AVERAGE SMALL BOY DATA

Nuclide	Air-filter sample	Fallout-collector sample
^{89}Sr	5.4	9.7
^{90}Sr	25	260
^{95}Zr	2.6	21
^{91}Y	2.3	17
^{103}Ru	2.8	4.2
^{106}Ru	7.8	34
^{137}Cs	22	150
^{140}Ba	3.2	2.8
^{141}Ce	0	5.1
^{144}Ce	8.4	750

fractionation in Small Boy. A comparison of Tables 3 and 7 shows that the air-filter samples are less fractionated in Small Boy than they are in Sedan. The opposite is true for the fallout-collector samples; that is, they are more fractionated in Small Boy than they are in Sedan. This is a surprising observation.

CONCLUSIONS

This program has proved the feasibility of collecting offsite samples at long downwind distances from nuclear detonations. Debris from Sedan depicts the cloud from an underground burst to be fairly homogeneous and highly fractionated. Small Boy, a surface burst, gave a heterogeneous cloud and even greater fractionation effects than Sedan. Molybdenum-99 in both shots behaved as a refractory material and did not represent an ideal tracer of fission-product debris.

REFERENCES

1. U. S. Weather Bureau, Announced Nuclear Detonations 1945–1962, in Fallout Program Quarterly Summary Report for September 1, 1963 through December 1, 1963, USAEC Report HASL-142, Health and Safety Laboratory, pp. 218-242, Jan. 1, 1964.
2. S. Katcoff, Fission-Product Yields from Neutron-Induced Fission, *Nucleonics*, *18*(11): 200-208 (November 1960).
3. P. J. Dolan, Calculated Abundances and Activities of the Products of High Energy Fission of Uranium-238, Report DASA-525, Defense Atomic Support Agency, May 1959.

PHYSICAL CHARACTERISTICS OF SINGLE PARTICLES FROM HIGH-YIELD AIR BURSTS

P. BENSON, C. E. GLEIT, and L. LEVENTHAL
Tracerlab, A Division of Laboratory for Electronics, Inc.,
Richmond, California

ABSTRACT

Particles, isolated from high-altitude nuclear explosions, were separated and their physical parameters determined. The particles varied in color from colorless to black. They were generally spherical, and some had satellites that were a result of collisions of small particles with larger particles before complete solidification had occurred. Particles with diameters greater than 2 μ were isolated.

The beta radioactivity of the particles was measured at 25 days and was found to be related to the diameter expressed in the following way: $A = aD^b$, where b showed values of 3.06 ± 0.08, 3.22 ± 0.16, and 3.01 ± 0.30 for the three shots studied. Since the standard deviations were due to variations in activities of the particles and not in experimental errors, it was concluded that the activity was directly proportional to the particle volume. The standard deviations were found to be unrelated to particle size and color, but the value of a was found to be a function of the weapon yield. The value of b, however, was not related to weapon yield.

Individual particles were allowed to decay to determine the decay rate of the fission-product mixtures. On the average, the particles followed the relation $A = kt^{-1.10}$. Values of the decay slopes varied from 0.7 to 1.4. The distributions of the decay slopes of the individual particles from the average was found to be Gaussian. The deviations were not a function of particle size or color; they are explained as being a result of the widely different radionuclide content of the particles.

PHYSICAL CHARACTERISTICS

The fireball of a nuclear explosion contains material from two sources, the weapon itself and the explosion environment. In studies of the physical phenomena occurring during cloud cooling and of the precipitation of the vaporized materials and radioactivities in the form of a particulate aerosol prior to the Operation Dominic I test series, the processes have been hard to resolve because of incomplete vaporization of the environmental materials and the incorporation of new materials into the fireball as it rose. During the Operation Dominic I test series, however, it was possible to study high-altitude nuclear explosions in which the material incorporated into the fireball was only that of the weapon itself plus its ballistic casing. This relatively small amount of material was completely vaporized by the heat of the nuclear explosion.

As the fireball expands and cools, the vaporized materials condense in the form of small droplets that solidify, forming the small particles which we are examining in the investigation reported here. Figure 1 shows photomicrographs of particles isolated from high-yield air bursts from the Operation Dominic I series. These particles show the spherical-shape characteristic of solidified droplets. When viewed under the optical microscope, these particles show great differences in color, varying from colorless to black. This may be due to variation in matrix-element composition or to surface effects.

The radioactive part of the nuclear debris consists of fission products, radionuclides produced by neutron reactions with the matrix materials, and the unreacted fissile material of the nuclear device. The majority of the radionuclides are incorporated into the particles, with the fission products contributing the dominant part of the radioactivities. The composition of the fission-product mixtures varies with fission mode and time after fission. Table 1 shows the composition of an unfractionated ^{235}U fission-product mixture 25 days after the time of fission.

Figure 2 shows the activities of the isolated particles plotted as a function of particle diameter. The analysis of particle samples, 2 μ in diameter or larger, shows that the beta activity increases as the cube of the particle diameter. Three shots were analyzed in this study, and a least-squares fit of the logarithm of the activity vs. the logarithm of the particle diameter of the form $\log A = b \log D + a$ gave values of b of 3.06 ± 0.08, 3.22 ± 0.16, and 3.01 ± 0.30. The standard deviations observed are due to variations in the activities of the various particles and not to experimental errors in the measurement of these activities.

The cubic relation of beta activity to size is used to describe one of the important physical properties of particles, the activity per unit

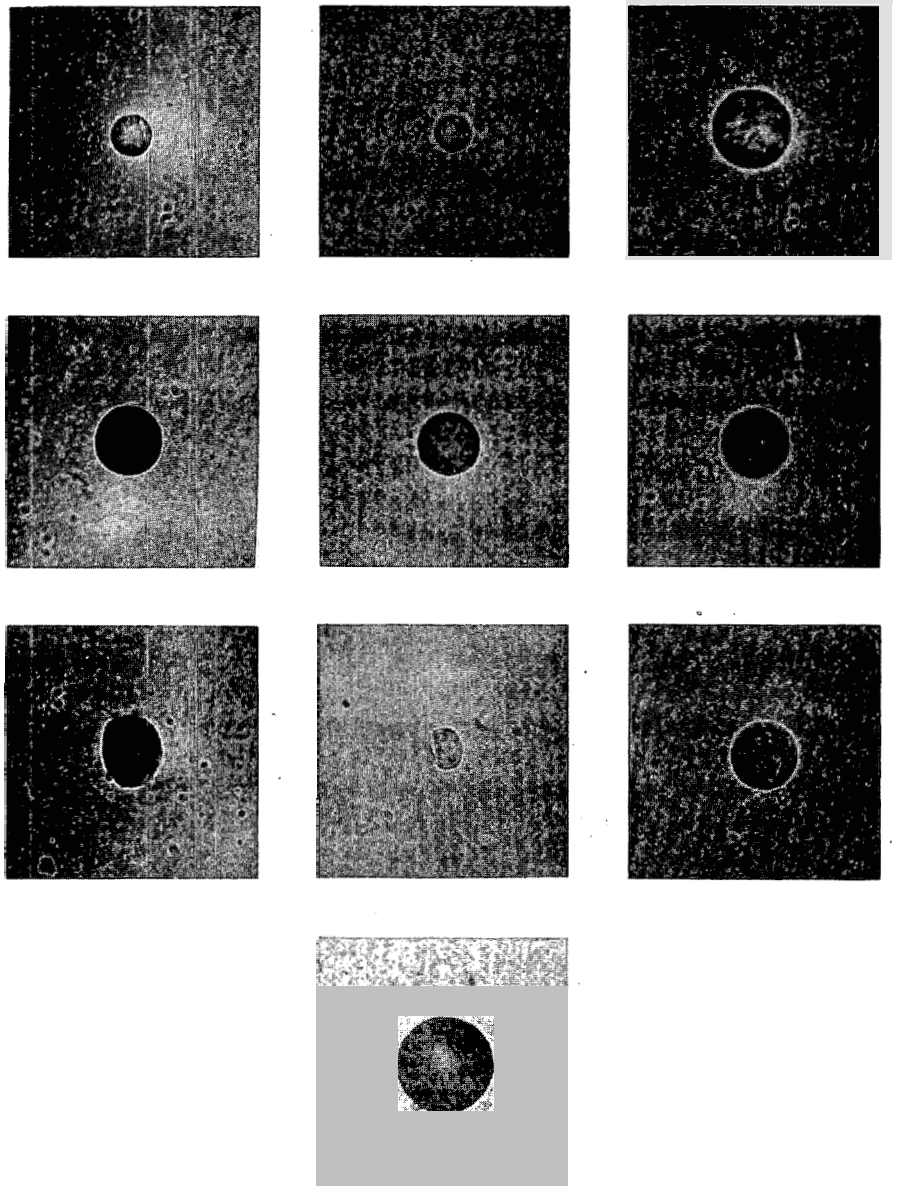

Fig. 1—Photomicrographs of particles.

Table 1 — THE RADIONUCLIDE CONTENT OF AN UNFRACTIONATED ^{235}U FISSION-PRODUCT MIXTURE AT 25 DAYS

Radionuclide	Activity, %	Radionuclide	Activity, %
^{89}Sr	5.4	^{131}I	1.7
$^{90}Sr-^{90}Y$	0.05	^{133}Xe	4.75
^{91}Y	6.4	^{137}Cs	0.05
^{95}Zr	6.5	^{140}Ba	8.1
^{95}Nb	2.8	^{140}La	9.2
$^{99}Mo-^{99}Tc$	0.3	^{141}Ce	9.1
^{103}Ru	3.8	^{144}Ce	1.5
^{106}Ru	0.08	^{143}Pr	25.6
^{129m}Te	1.4	^{147}Nd	12.5
$^{132}Te-^{132}I$	0.5	^{147}Pm	0.2

particle volume. Figure 3 shows the activity per unit particle volume as a function of particle diameter for two shots. As is to be expected, the activities per unit particle volume tend to fall at a common average for each of the three shots studied, depending on the fission yield of the nuclear device. For each case, however, there are particles that vary considerably from the norm. This variation appears not to be related to particle color, and on a fractional basis it appears to be as large in large particles as it is in small particles.

The beta-energy spectrum, of course, varies as a function of time as the composition of the fission-product mixture changes. Figure 4 shows aluminum absorption measurements on a particle sample at different times. Close to zero time the absorption curve approaches a straight line on semilog plots, but as time passes the absorption curve shows a shape of a low-energy component plus a high-energy component. When the sample has decayed 200 days, the major high-energy component is due to ^{144}Pr, the daughter of ^{144}Ce.

In the discussions so far, the similarities between particles have been noted. Striking dissimilarities become apparent, however, after decay. Figure 5 shows the beta decay of ^{235}U and ^{239}Pu fission-product mixtures as measured with a methane-end-window proportional counter. Although it is readily apparent that the rate of decay of these fission-product mixtures varies with time, a relation of $A = kt^{-1.2}$ is a close approximation of the decay from 3 to 4000 days.

The decay of isolated particles was followed and the data during the period 3 to 200 days were chosen to determine the decay rate by a least-squares curve fit. Figure 6 shows plots of the number of particles vs. the decay slope of those particles. As analytical aids the standard deviation of the decay slope, the standard error of the estimate, the variance in each variable, and the difference between each experimental value and the unfractionated fission-product mixtures, derived

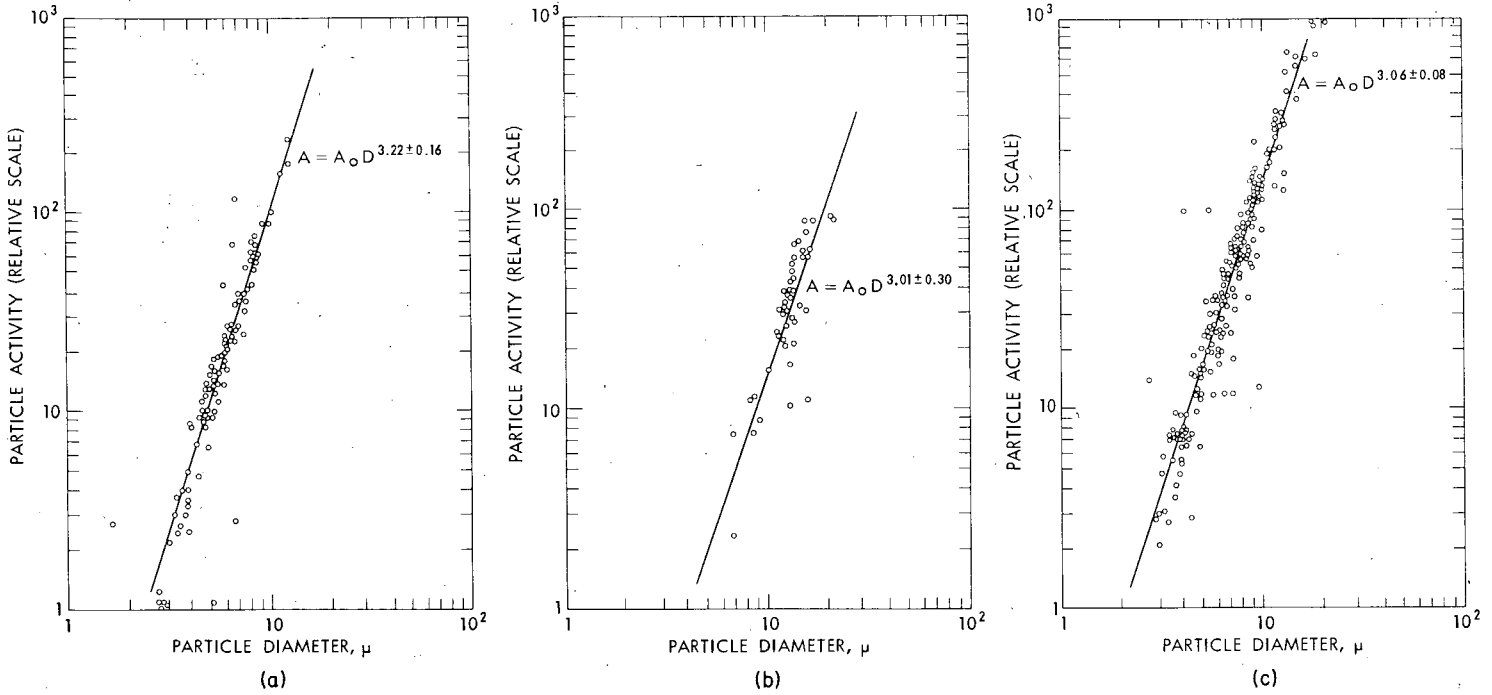

Fig. 2—Total beta activity as a function of particle diameter.

TCT BALANCE 46 KILL ALL LETTERING Card 765

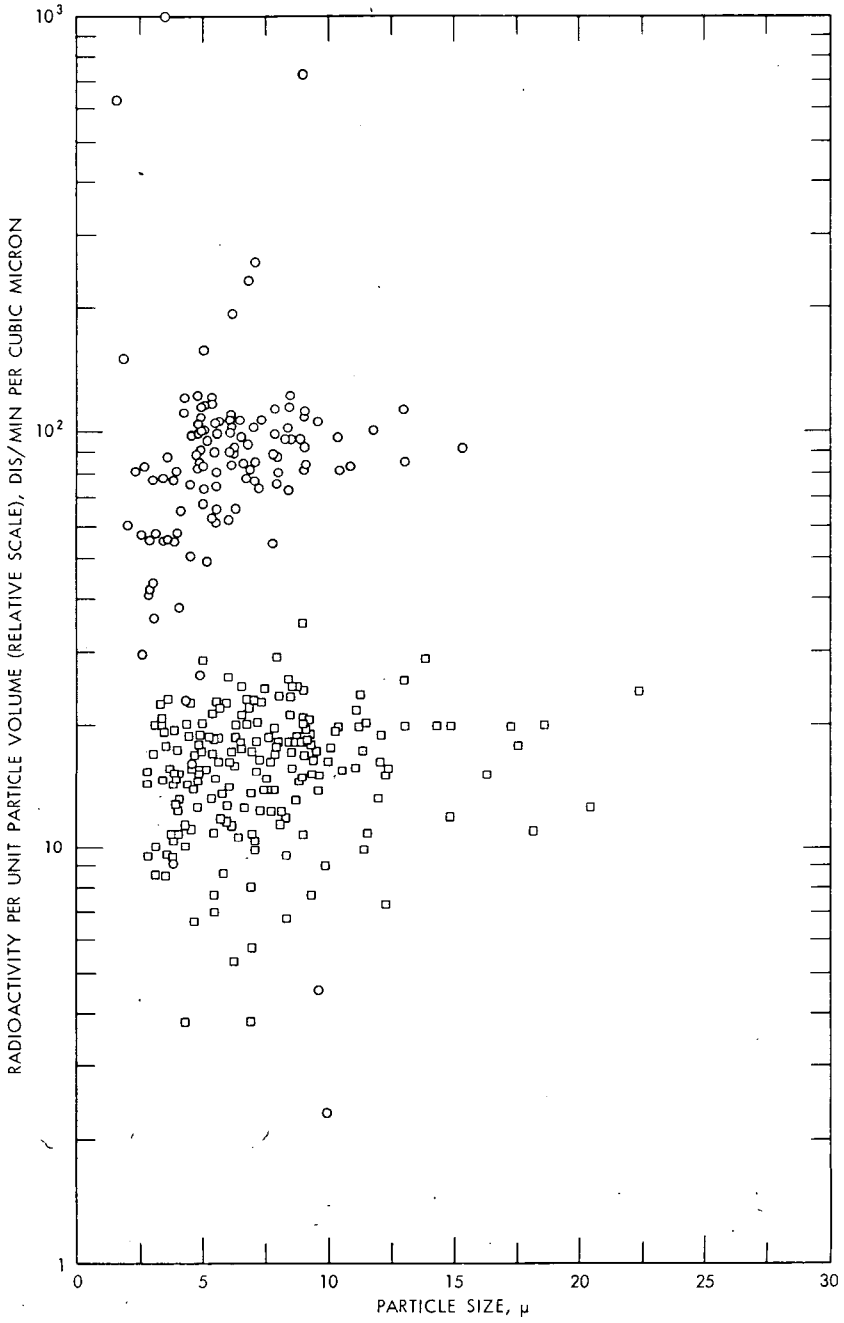

Fig. 3—Radioactivity per unit particle volume for two shots as a function of particle size.

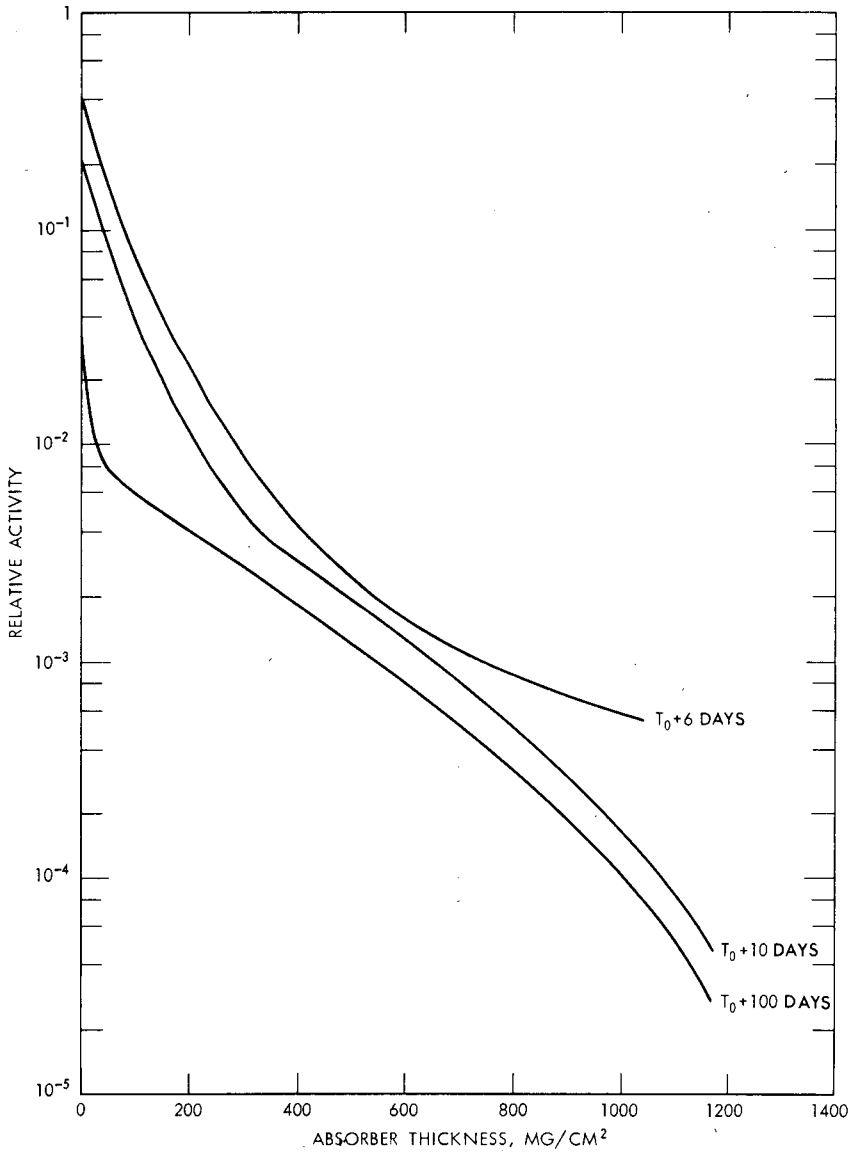

Fig. 4—Aluminum absorption measurements as a function of time.

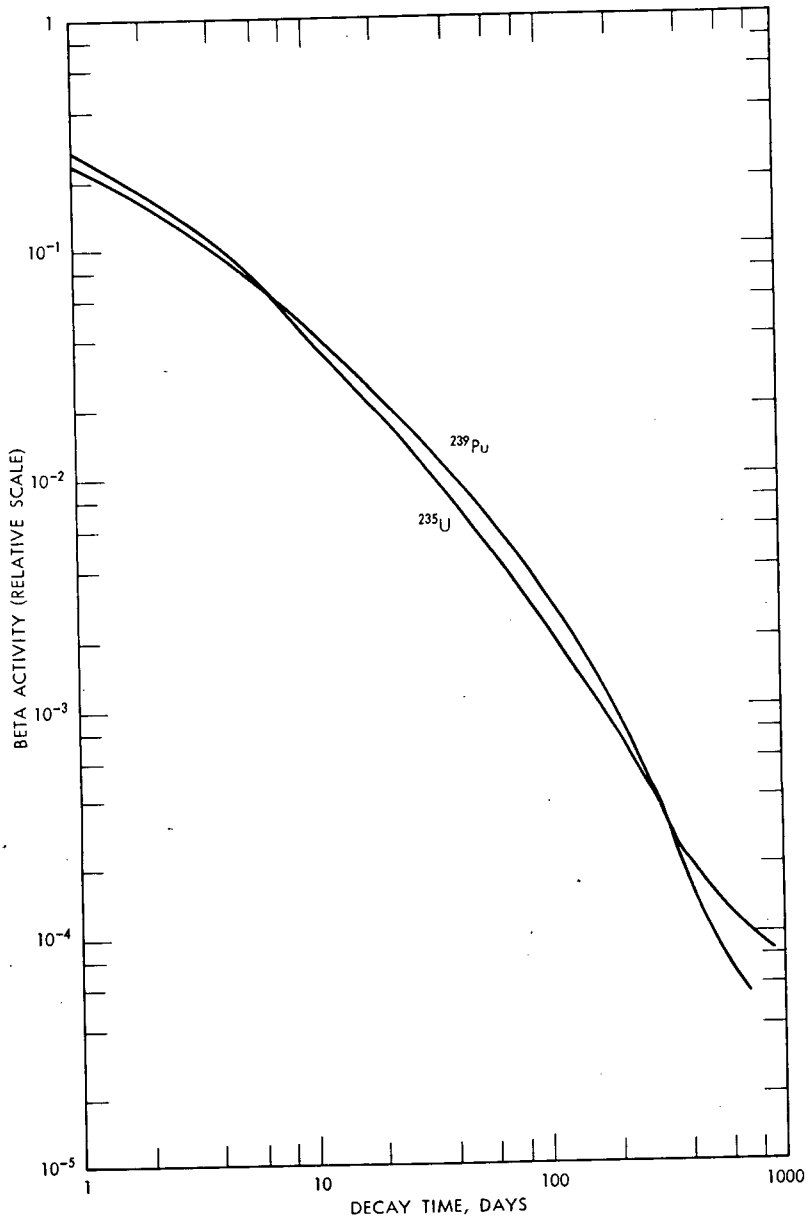

Fig. 5—Beta-activity decay of unfractionated ^{235}U and ^{239}Pu fission-product mixtures.

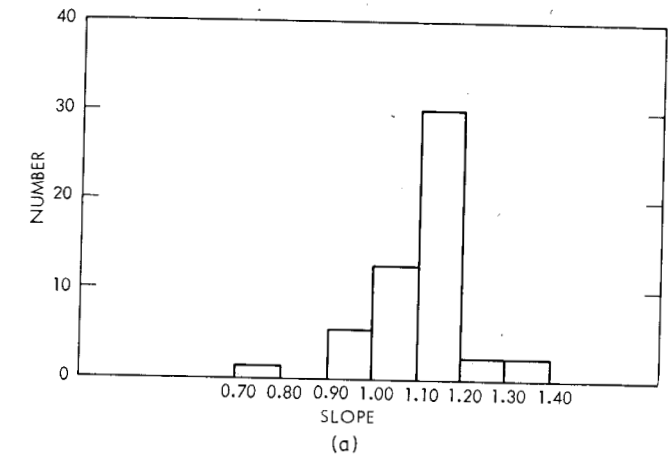

(a)

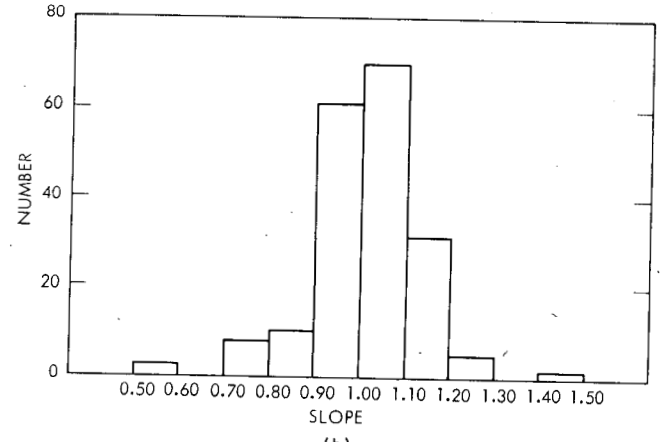

(b)

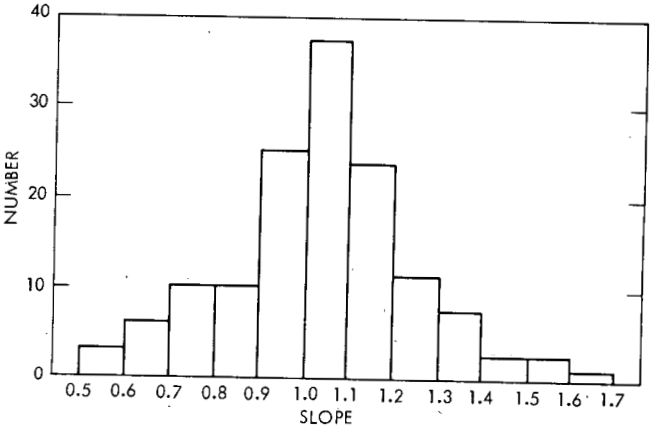

(c)

Fig. 6—The number of particles observed with various decay slopes.

from the straight-line approximation, were calculated. For over 90% of the decay curves, the standard error in the exponent was less than ± 3%. The excellence of the curve fit was further demonstrated by the magnitude of the correlation coefficient, which exceeded 0.99 for over 90% of the decay curves.

Values of the decay constant were 0.7 to 1.4, with an average value for all shots of 1.10. These variations were found among particles of approximately the same size from each shot. There was no correlation between the decay slope and the particle size or the color. A statistical analysis of the variance indicates that a negligible variation can be associated with experimental errors or statistical fluctuations, and it is concluded that the wide variations in the beta-decay rates result from widely varying fractionation patterns among the particles. These distributions appear to be Gaussian and independent of weapon yield.

The physical characteristics of single particles can yield information concerning the radiochemical content. Although single-particle beta and gamma decay curves, the beta-energy spectrum (as well as the gamma-energy spectrum), and the activity per unit particle volume can give valuable information from the health-hazard point of view, the radionuclide concentrations as a function of particle size are of prime importance for an understanding of the fractionation process. In any laboratory program dealing with single-particle analysis, it is desirable to provide simple test procedures to select those particles which will yield particles exhibiting the interesting radionuclide compositions. A correlation of the radionuclide compositions with the physical parameters of the particles will provide a field test-particle selection procedure. The radiochemical composition of these particles was also investigated, and the program concerned will be reported in the next paper.*

*P. Benson, C. E. Gleit, and L. Leventhal, this volume.

RADIOCHEMICAL FRACTIONATION CHARACTERISTICS OF SINGLE PARTICLES FROM HIGH-YIELD AIR BURSTS

P. BENSON, C. E. GLEIT, and L. LEVENTHAL
Tracerlab, A Division of Laboratory for Electronics, Inc.,
Richmond, California

ABSTRACT

The radiochemical fractionation characteristics from two Operation Dominic high-yield air bursts were studied. Particles measuring from 2.5 to 20.0 μ were isolated from filter-paper matrices by autoradiographic registration and confirmed by optical microscopy. After physical measurements radiochemical and/or gamma-spectroscopy studies were performed on individual and aggregates of particles. Of particular interest was the distribution of volatile and refractory nuclides for each particle size. The nuclides radiochemically analyzed were ^{99}Mo, ^{89}Sr, ^{90}Sr, ^{95}Zr, ^{129m}Te, ^{132}Te, ^{137}Cs, ^{140}Ba, ^{141}Ce, ^{144}Ce, ^{147}Nd, ^{237}U, and ^{239}Np. Gamma-spectra analysis was used to determine the ^{95}Zr and ^{140}Ba concentrations in 334 particles. A computer technique for resolving these nuclides and ^{99}Mo, ^{103}Ru, ^{131}I, ^{132}Te, ^{137}Cs, ^{141}Ce, ^{144}Ce, ^{147}Nd, and ^{239}Np was developed.

The particles were found to be extremely fractionated. A logarithmic fractionation correlation plot for ^{140}Ba was determined which compared within the limits of error with data plotted by Freiling for high-yield water bursts. The logarithms of ^{95}Zr and ^{140}Ba activities were plotted as functions of the particle diameters for the two shots. The slopes for the regression plot for ^{95}Zr were 3.41 ± 0.18 and 3.09 ± 0.37. These values imply a cubic relation. The slopes for the regression plot for ^{140}Ba were 2.63 ± 0.24 and 2.32 ± 0.50, somewhat between a square and a cubic relation. These results point toward condensation of the refractory nuclides initially with subsequent precipitation of the volatiles on the particles at later times.

These experiments have proved that important radiochemical fractionation information can be obtained from single particles. Both the limitations and the advantages of this technique have been delineated.

INTRODUCTION

The 1961 Dominic test series presented the first opportunity to study radionuclide fractionation in single particles from high-yield air bursts. In these air bursts the condensation matrices were dependent only on the weapon composition. Masses of contaminating materials such as tower, water, and salt, which would present indeterminable factors, were not present. The radionuclide distributions in selected particles obtained from several tests in this series were analyzed radiochemically and by gamma spectrometry. Of particular interest was the distribution of volatile and refractory nuclides for each particle size. The nuclides radiochemically analyzed were ^{99}Mo, ^{89}Sr, ^{90}Sr, ^{95}Zr, ^{129m}Te, ^{132}Te, ^{137}Cs, ^{140}Ba, ^{141}Ce, ^{144}Ce, ^{147}Nd, ^{237}U, and ^{239}Np. It soon became apparent that the radiochemical method was too time consuming, and as an alternative a nondestructive gamma-spectrometric technique, which also yielded the required data on radionuclide behavior, was employed. A computer technique was developed for resolving the spectra, and 334 of the particles were examined by this method. Analysis of the radionuclide concentrations in individual particles so far has been confined to the determination of correlations between the data and the particle diameters.

PROCEDURE

The radioactive particles were located by autoradiography and isolated from the filter-paper matrix. After particle size and other physical parameters were measured, the particles were subjected to sequential radiochemical analysis (see Fig. 1). Particles ranged in size from 4 to 20 μ and contained between 10^8 and 10^{10} fissions based on ^{99}Mo analysis. Aggregates of particles representing groups 4 to 5 μ and 4.5 to 9 μ were similarly analyzed to determine radionuclides that were in too low abundance to be measured in single particles. A complete study was made on integral papers. The nuclides were assayed by standard counting techniques, and the results were converted to R* values for fission products or atoms for induced radionuclides.

*An R value is defined as the ratio of the ratio (r) of calculated fissions in isotope (i) to fissions as calculated from ^{99}Mo to a similar ratio (r) determined from thermal-neutron fission of ^{235}U; i.e., $(r_{i,99})x/(r_{i,99})th$.

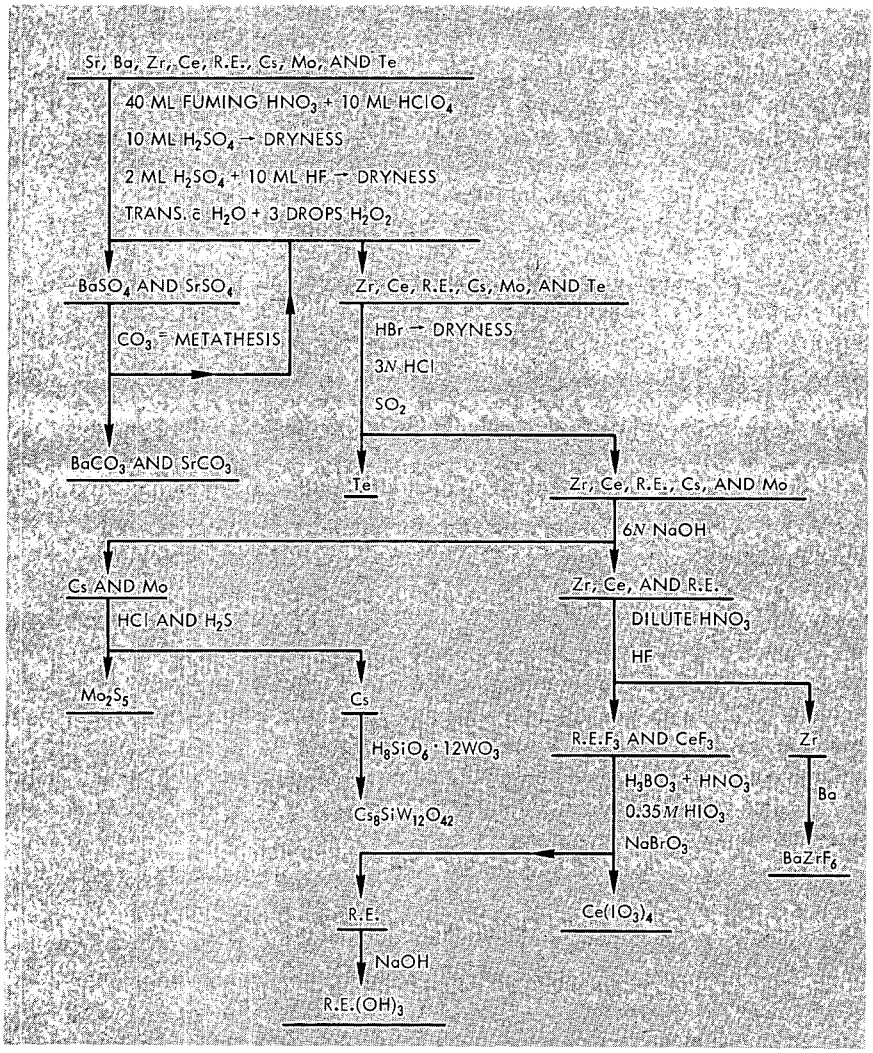

Fig. 1—Sequential separation of particle radionuclides.

Gamma spectra of individual particles were obtained with a 3- by 3-in. NaI detector and a 400-channel pulse-height analyzer. The particles were analyzed as early as two days after the shot and thereafter once every two particle half-lives.

In general, six spectra per particle were obtained over a two-year period. Particles studied ranged in size from 2.5 to 25 μ and contained 10^8 to 10^{11} ^{95}Zr fissions. The gamma spectra were normalized prior to gamma-spectra stripping by a computer program written in FORTRAN for the IBM-7094. This program has a capability for the determination of ^{95}Zr, ^{99}Mo, ^{137}Cs, ^{141}Ce, ^{144}Ce, ^{140}Ba, and ^{239}Np, as well as for others, and is based on the method proposed by Carnahan.[1] The isotopes men-

tioned represent the predominant peaks in the spectra obtained. Figure 2 indicates a typical gamma-spectrometer scan observed over a two-year period. The background radiation is the lowest line. The peaks of interest are singled out on the figure.

RADIOCHEMICAL STUDIES

Calculations of the counting-rate yield at zero time for a particle representing 10^8 fissions indicated that measurable activities would be obtained for the nuclides of interest if *no* fractionation is assumed (see Table 1). However, fractionation effects in single particles caused wide

Table 1— THEORETICAL RADIOCHEMICAL SENSITIVITY FOR A PARTICLE OF 10^8 FISSIONS

(Basis: Counting Rate at Zero Time for 100% Chemical Yield)

Nuclide	Counts/min	Remarks
^{89}Sr	23	R = 1
^{90}Sr	0.1	R = 1
^{95}Zr	10	R = 1
^{97}Zr	1000	110 abs, R = 1
^{99}Mo	562	R = 1
^{111}Ag	0.5	R = 1
^{115}Cd	2	R = 1
^{103}Ru	2	Zero abs, R = 1
^{106}Ru	0.2	Zero abs, R = 1
^{136}Cs	0.05	R = 1
^{137}Cs	0.09	R = 1
^{140}Ba	94	R = 1
^{141}Ce	24	Zero abs, R = 1
^{144}Ce	7.4	Zero abs, R = 1
^{91}Y	25	R = 1
^{156}Eu	0.06	74 abs, R = 1
^{147}Nd	40	R = 1
^{7}Be	0.004	N/f* = 100×10^{-5}
^{24}Na	44	N/f = 100×10^{-5}
^{64}Cu	200	N/f = 1000×10^{-5}
^{67}Cu	0.06	N/f = 1×10^{-5}
^{187}W	0.23	N/f = 1×10^{-5}
^{203}Pb	0.015	N/f = 1×10^{-5}
^{231}Th	900	N/f = 100×10^{-5}
^{237}U	690	N/f = 0.3
^{239}Np	2880	N/f = 0.3
^{240}U	2880	N/f = 0.1
^{238}Pu	0.00005	N/f = 10×10^{-5}
$^{239}Pu/J$†	0.0009	N/f = 0.5

*N = atoms, f = fissions.
†J = [atoms ^{239}Pu/atoms ^{240}Pu/(atoms ^{239}Pu/atoms ^{240}Pu) + 3.7].

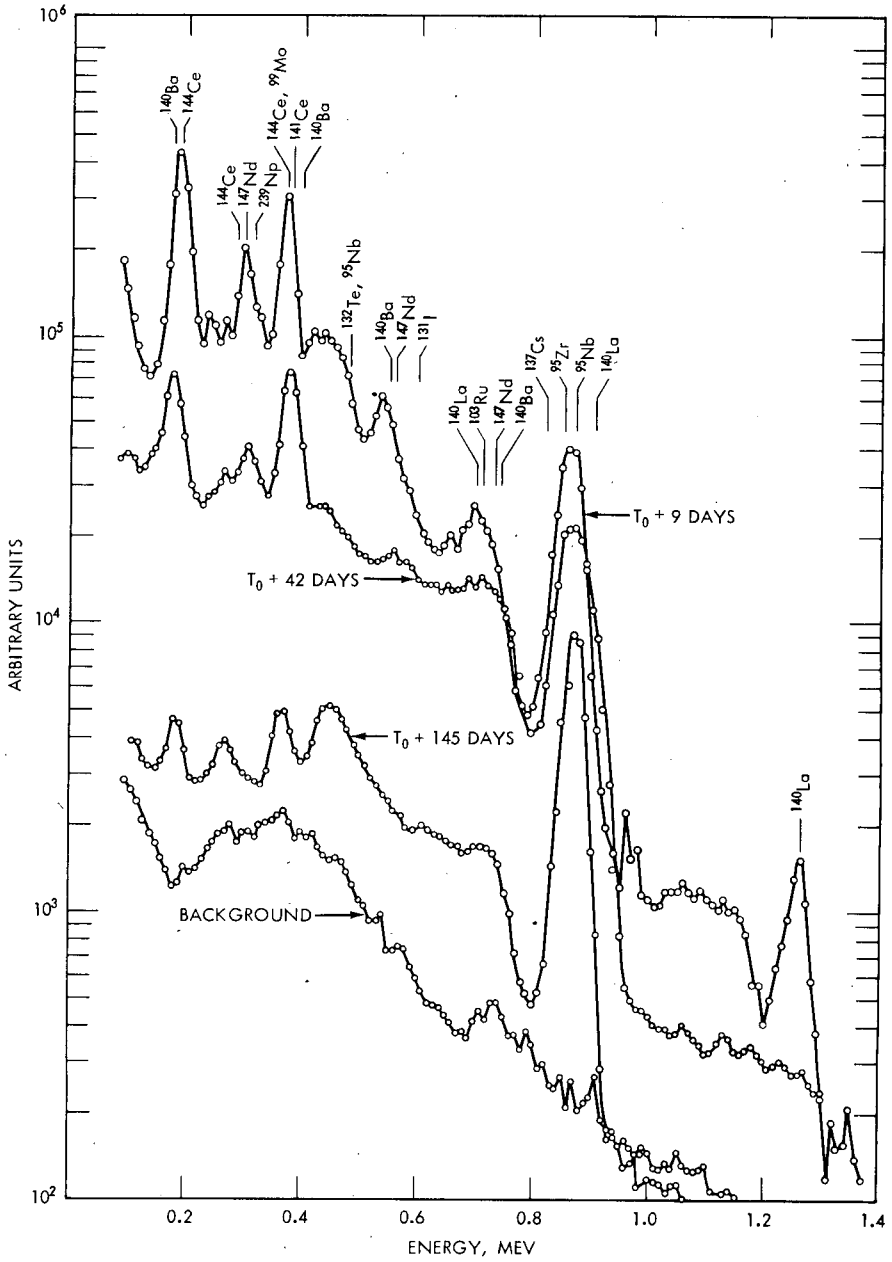

Fig. 2—Particle gamma spectrum.

variations from predicted values. Particles ranging in size from 5 to 20 μ were analyzed from each of two shots. Two sets of selected aggregate particles between 4 to 9 μ were also analyzed.[2]

A logarithmic fractionation correlation plot of $r_{140,89}$ vs. $r_{95,89}$* incorporating filter-paper aggregate particles and individual particle data from both shots fitted linearly (see Fig. 3). Freiling[3] has plotted $r_{140,89}$

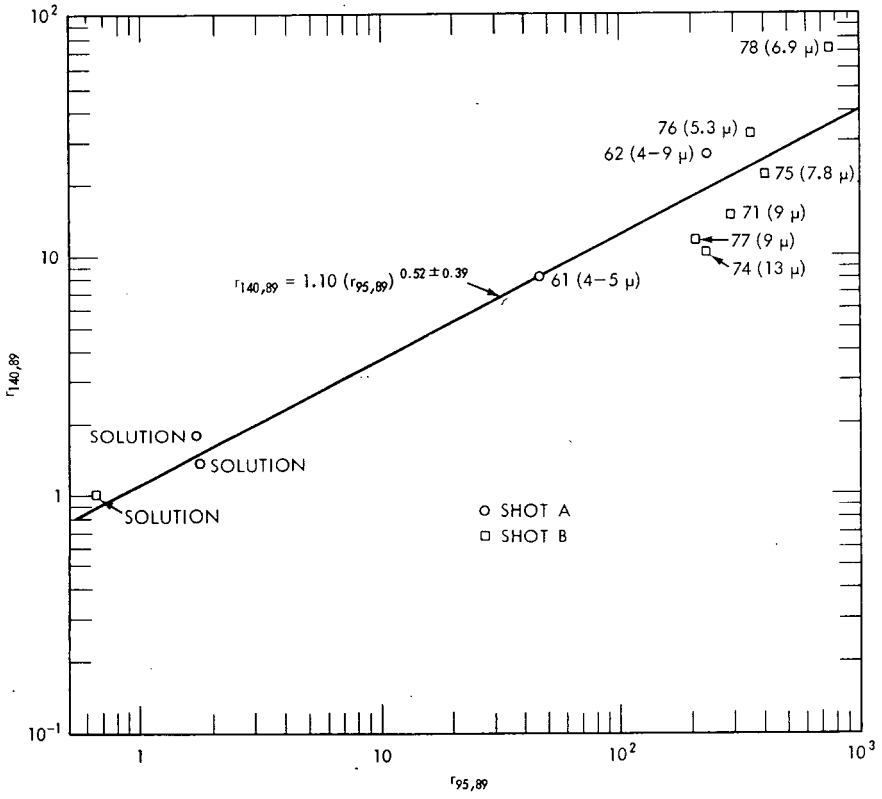

Fig. 3—Logarithmic fractionation correlation for ^{140}Ba.

data for megaton-range coral-surface bursts and three types of water bursts. Within the limits of error, the slope and intercept of the regression line of Fig. 3 are comparable with those of Freiling's plot.

The single particles are severely fractionated with respect to the total sample. It is interesting to note that for these particles the fractionation plot had to be extended another decade to include the particle r-value ratios.

---

*$r_{i,89}$ is defined as the ratio of calculated isotope (i) fissions to calculated ^{89}Sr fissions, f_i/f_{95}, where f equals fissions.

Table 2— PRINCIPAL GAMMA RAYS OF THE MAJOR FISSION PRODUCTS FOR A PARTICLE OF 10^8 FISSIONS

(Basis: Gammas Per Minute at Zero Time)

Radionuclide	Energy, Mev	Dis/min	Gammas/min
$^{95}Zr-^{95}Nb$	0.717	47.0	47.0
	0.745	8.6	8.5
	0.235		0.17
$^{99}Mo-^{99m}Te$	0.780	1050.0	210.0
	0.740		146.0
	0.180		10.5
	0.041		105.0
	0.141	930.0	930.0
$^{103}Ru-^{103m}Rh$	0.498	38.0	36.0
	0.040		38.0
^{131}I	0.364	170.0	138.0
$^{132}Te-^{132}I$	0.231	670.0	670.0
	1.40		76.0
	0.96		130.0
	0.777		490.0
	0.673		670.0
	0.528		170.0
$^{137}Cs-^{137m}Ba$		0.29	
	0.661		0.270
$^{140}Ba-^{140}La$	0.54	230.0	70.0
	0.30		23.0
	0.16		23.0
	0.03		230.0
	1.60		220.0
	0.815		67.0
	0.49		91.0
^{141}Ce	0.145	89.0	60.0
^{143}Ce	0.660	2100.0	325.0
	0.356		260.0
	0.289		1285.0
	0.126		260.0
$^{144}Ce-^{144}Pr$	0.134	10.0	10.0
	0.081		10.0
	0.034		10.0
	1.480		0.20
	0.695		0.41
^{147}Nd	0.532	100.0	25.0
	0.318		1.50
	0.092		60.0

Similar graphs were prepared for ^{144}Ce and ^{237}U. The plot of the particle data for ^{144}Ce also had to be extended a decade higher. The uranium activity per particle was too low to get accurate data, and a linear fractionation plot could not be developed from these data.

Analyses were made for ^{90}Sr, ^{136}Cs, ^{132}Te, ^{143}Ce, and ^{239}Np, but they were not detected in the samples. Satisfactory values were obtained for ^{129m}Te, ^{141}Ce, and ^{147}Nd.

GAMMA-RAY SPECTRA

The individual radionuclides that are susceptible to gamma-spectra analysis in particles were determined. Limits of detection were obtained for the radionuclides of interest by assuming 10^8 thermal-neutron fissions. This was done by correction of the estimated gamma rays per minute for the efficiency of the 3- by 3-in. NaI crystal at a particular energy. Further selection was made by determining if interfering gamma energies were present that produced unresolvable spectra in the region of interest. Of the heavy elements, ^{239}Np was the only nuclide high enough in yield for analysis. However, because of its short half-life, no attempt was made to resolve this nuclide. The induced activities were too low for spectral analysis. Among the fission products listed in Table 2, ^{99}Mo also was too low for spectral analysis. The radionuclides ^{103}Ru, ^{131}I, and ^{137}Cs were not detected, but ^{95}Zr and ^{140}Ba were resolved. Also ^{132}Te, ^{141}Ce, ^{144}Ce, and ^{147}Nd can be resolved.

The ^{140}Ba and ^{95}Zr fissions for two high-yield shots have been calculated[4] from gamma spectra obtained from 21 particles from shot A and 45 particles from shot B. Peak resolution was confirmed by decay of the respective peaks. Three of the particles were sacrificed after gamma stripping and were radiochemically analyzed for ^{140}Ba and ^{95}Zr. Agreement between physical and radiochemical measurements was ± 5%.

The logarithm of ^{140}Ba fissions was plotted as a function of the logarithm of the particle diameter (Figs. 4 and 5), and a linear regression calculation was performed. The slopes of the regression line obtained for the shots A and B data were 2.63 ± 0.24 and 2.32 ± 0.50, respectively. The hypotheses that the populate slopes are square or cubic (equal 2.0 or 3.0) were tested. Because of the scatter of the points about the regression line, both hypotheses could not be rejected except for the hypothesis that the shot A slope was two, which was rejected at the 95% confidence interval. The intermediate value may be explained as due to the decaying of volatile precursors before particle condensation. The slopes obtained for the regression plots for ^{95}Zr (Figs. 6 and 7) for shots A and B were 3.41 ± 0.18 and 3.09 ± 0.37. For this nuclide a cubic relation appears to hold. An explanation for the large value for ^{95}Zr for shot A is not apparent. Spectra stripping of additional particles may reduce this value.

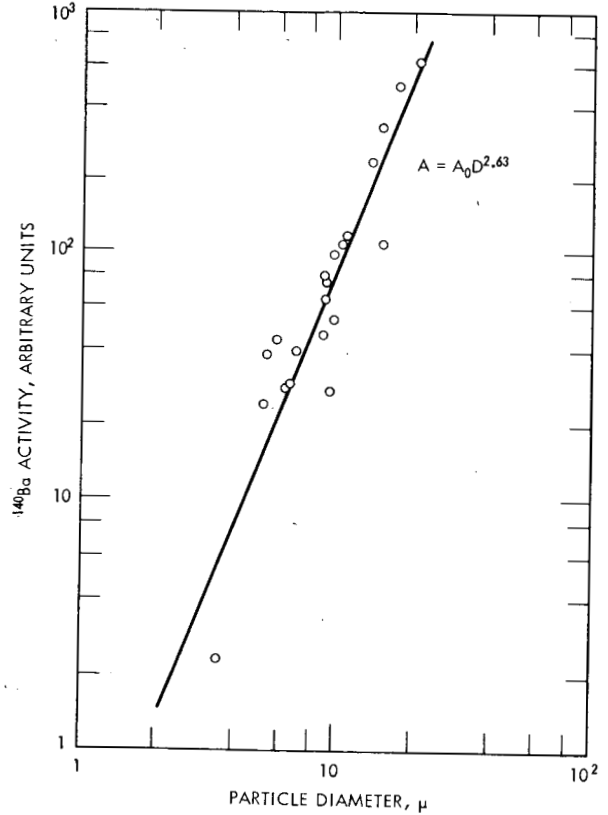

Fig. 4—Barium-140 activity as a function of particle diameter for shot A.

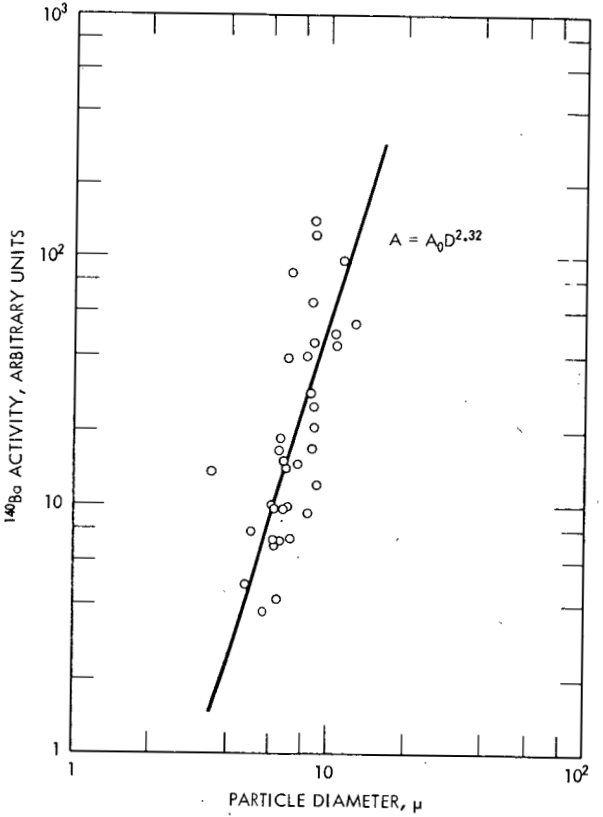

Fig. 5—Barium-140 activity as a function of particle diameter for shot B.

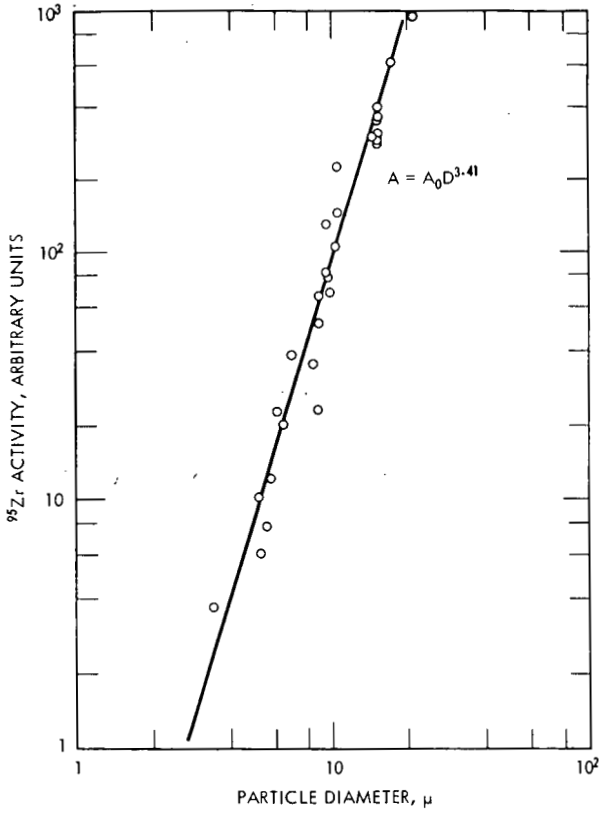

Fig. 6—Zirconium-95 activity as a function of particle diameter for shot A.

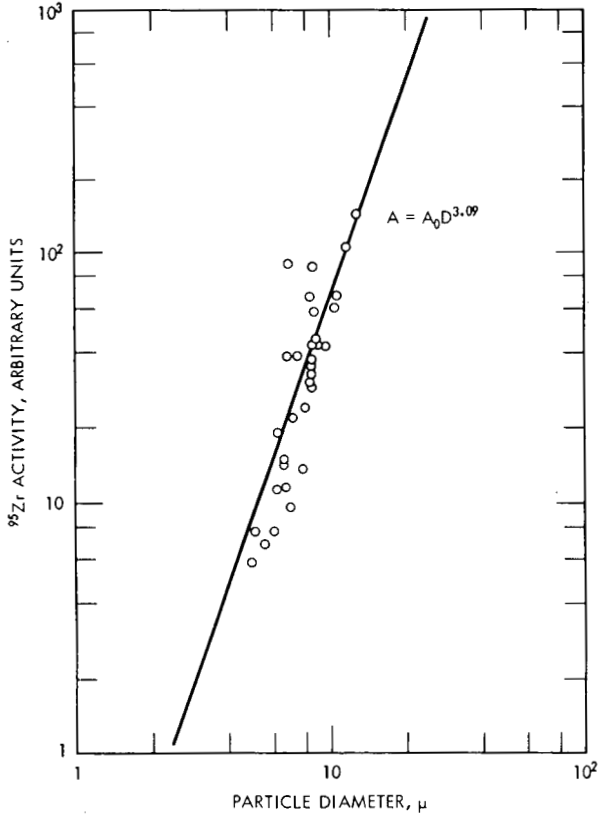

Fig. 7—Zirconium-95 activity as a function of particle diameter for shot B.

Although the surface relation between ^{140}Ba activity and particle size cannot be demonstrated on the basis of these data, the variance in the activity per unit area is quite obvious. One would expect this in nuclear-explosion clouds in which the particles form rather quickly and the volatile constituents precipitate on the particle surfaces much later. This hypothesis appears to be confirmed if one considers the ^{95}Zr as representative of a refractory nuclide. The cubic relation then would indicate that the ^{95}Zr is condensed initially and is distributed as a function of the volume of the particle. In effect, regularity is observed through approximately a hundredfold change in volume.

Another interesting observation that stems from a comparison of the shots A and B plots is that the intercept of the ^{140}Ba regression line of the nuclides of a particular particle size is a function of the yield to mass ratio.

CONCLUSIONS

The feasibility of isolating and analyzing individual particles by radiochemical and gamma-spectrometric techniques has been demonstrated.

Particles under 10 μ and as low as 10^8 fissions have yielded accurate values for the important volatile and refractory fission products. Heavy-element analysis is borderline for ^{237}U and ^{239}Np and is dependent on analysis at early times. Unless an induced activity is present in abnormally large amounts, the analyses of these radionuclides in single particles are not feasible.

Gamma spectrometry is a satisfactory technique for the resolution of nuclides in large numbers of individual particles and may be used to obtain ^{140}Ba and ^{95}Zr values to $\pm 5\%$.

Logarithm fractionation plots of particles from high-yield air tests have been found to correlate well with $r_{140,89}$ and $r_{95,89}$ values from a coral-surface burst and three types of water bursts.

Barium-140 fissions have been found to correlate with between a square and a cubic relation to particle diameter. Zirconium-95 fissions have demonstrated a cubic relation to particle diameter.

REFERENCES

1. C. L. Carnahan, A Method for the Analysis of Complex Peaks Occurring in Gamma Ray Pulse Height Distributions, Report USNRDL-TR-572, U. S. Naval Radiological Defense Laboratory, July 1962.
2. Tracerlab, A Division of Laboratory for Electronics, Inc., The Analysis of Particulate Debris from Pacific Air Shots, Final Report, Dec. 16, 1964.
3. E. C. Freiling, Radionuclide Fractionation in Bomb Debris, *Science 133:* 1991 (1961).
4. P. A. Benson, Sixth Quarterly Progress Report to USAEC, Tracerlab, A Division of Laboratory for Electronics, Inc., Apr. 1, 1964. (Classified)

DISTRIBUTION OF AIRBORNE RADIOACTIVITY WITH PARTICLE SIZE

LUTHER B. LOCKHART, JR., ROBERT L. PATTERSON, JR.,
and ALLEN W. SAUNDERS, JR.
U. S. Naval Research Laboratory, Washington, D. C.

ABSTRACT

Particle-size resolution of radioactive particles has been obtained by use of a filter-pack technique wherein atmospheric air containing radioactive aerosol particles successively transits a series of filters of increasing retentivity for small particles. From the relative amounts of radioactivity collected on the various filters and a knowledge of the retentivity characteristics of the filters as a function of particle size, information can be obtained on the size distribution of the radioactive particles.

Following the termination of atmospheric testing of nuclear devices in December 1962, fission-product radioactivity was observed to become associated with particles of smaller average size. Within a matter of months, however, this trend ended, but large short-term differences continue to be observed. Radiochemical analysis of material collected by three-filter packs during 1963 and 1964 showed no gross evidence of isotopic fractionation with size; however, some differences in composition were noted between the largest and the smallest size fractions.

It is concluded that nuclear debris from a stratospheric source becomes associated with the relatively large nonradioactive aerosols characteristic of the tropospheric air by the time the debris arrives at ground level. The resulting particles have an average size between 0.3 and 1.0 μ in diameter (assuming spherical particles of 1.8 g/cm^3 density) and a rather restricted particle-size distribution.

INTRODUCTION

All nuclear explosions produce a wide spectrum of particles of various sizes, but the conditions under which an explosion is carried out markedly affect the shape of the distribution curve. Fractionation of the various nuclides relative to one another can occur during the cooling and condensation phases immediately following the detonation with the result that ratios of nuclides may be expected to vary with particle size.

The use of a series of filters of different retentivities arranged in a pack so that the same air parcel passes through them in succession has been under consideration for a number of years as a possible means for determining the relation of radioactivity to particle size. A few measurements made at close-in sites during the Operation Greenhouse tests[1] indicated that size discrimination could be obtained by this method and, furthermore, that fractionation of nuclides with particle size occurred to a measurable extent in fresh nuclear debris. More recently, measurements made of the retentivity of filters to fission products and to the short-lived natural radioactive aerosols have shown gross differences in the behavior of the two types of radioactive particles as well as day-to-day differences in filter retentivity.[2,3] It was obvious that a pack of filters of different retention characteristics could effect at least a partial separation of radioactive particles into different size groupings.

As a consequence of the preceding findings, a program was initiated to study the feasibility of the filter-pack technique for particle-size determinations, to make measurements of the temporal changes in the particle size of fission debris following cessation of the nuclear-test programs, and to determine the extent of fractionation of fission-product radionuclides in relation to particle size.

EXPERIMENTS

Collections of Gross Beta Activity

Routine collections of gross fission-product radioactivity in the air at ground level have been made since the end of 1962 through use of three different filter media arranged in a three-filter or a four-filter pack, as shown in Fig. 1. Filters 4 in. in diameter were employed; the pumping rate was about 18.5 cu ft/min. Since filter efficiency is a function of air velocity through the filter, positive displacement blowers have been used to give more reproducible and constant flow rates. The air flow was calibrated against a 55 cu ft/min Fischer and Porter Flowrater and a working graph of pressure vs. flow used for routine flow determinations.

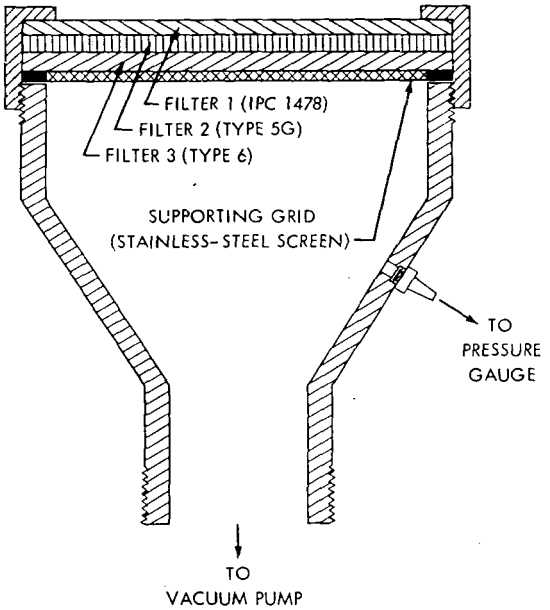

Fig. 1—Schematic of a filter holder with a three-filter pack.

The initial, and poorest, filter (or, in the case of four-filter packs, the first two filters) was IPC 1478 paper, the next filter was type 5G cellulose–glass fiber paper, and the final filter was type 6, a so-called "absolute filter" of cellulose–asbestos paper. The calculated relation of particle size to the distribution of particles among filters in a four-filter pack under standard operating conditions of 280 to 290 linear feet per minute (145 cm/sec) is shown in Fig. 2. This information is based on the measured filter retentivity toward monodisperse H_2SO_4 aerosol particles (spherical particles of 1.8 g/cm^3 density) over a size range of 0.3 to 1.2 μ in diameter; values below 0.3 μ have been inferred from retentivity measurements of the extremely small natural radioactive aerosols containing RaB + C (^{214}Pb + ^{214}Bi) activity.

Determinations of the distribution of gross fission-product beta activity among the filters in a pack were made by counting the filters in sequence on the same counter unit after allowing a minimum of seven days for decay of natural radioactivity (10.6-hr ThB). Sufficiently long counting times were employed to give good statistical accuracy. So that collections of reasonable size could be obtained, the collection periods were generally of two to four days duration.

In a few cases collections of RaB + C activity were made to obtain information on the size distribution of this natural radioactivity, which is known to become rapidly attached to the extremely small nonradio-

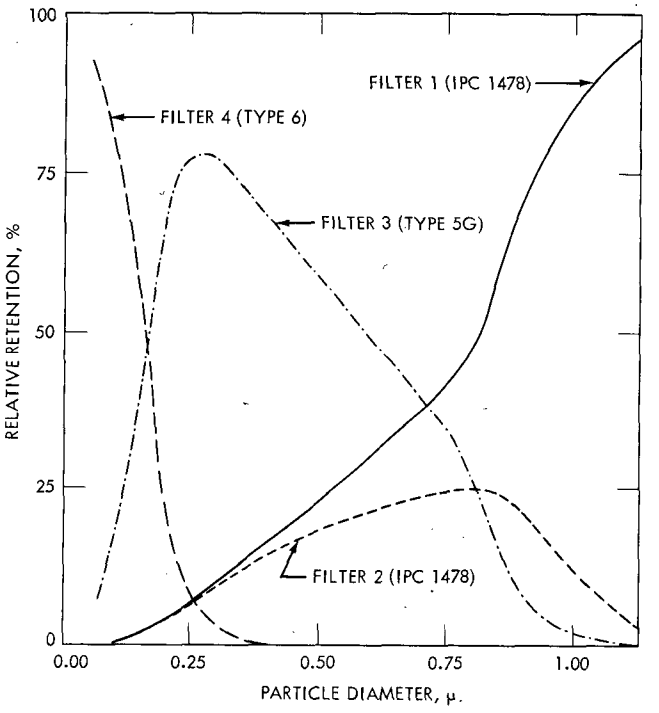

Fig. 2—Effect of size on the distribution of particles among filters in a four-filter pack (air velocity, 145 cm/sec).

active component of the atmospheric dust.[4] For these determinations 30-min collections were made, and the filters were counted immediately and simultaneously for 45 min on intercalibrated beta-counting units. Corrections were made where needed for the small quantities of longer lived activities that were also collected.

Collections for Radiochemical Analyses

Since the start of 1963, radiochemical analyses have been performed on large collections of long-lived components of the airborne radioactivity through use of a three-filter pack employing 13- by 17-in. pieces of the filter media previously described. Sampling was done over a one- to three-week period at the rate of about 152 cu ft/min (4.34×10^4 m^3 per week) at an average face velocity of 120 linear feet per minute (61 cm/sec). Little change in flow with time occurred over collection periods as long as three weeks. The calculated distribution of particles of various sizes among the three filters is shown in Fig. 3. Generally, greater penetration of the larger particles occurs in this pack than in that used for gross beta measurements because of the

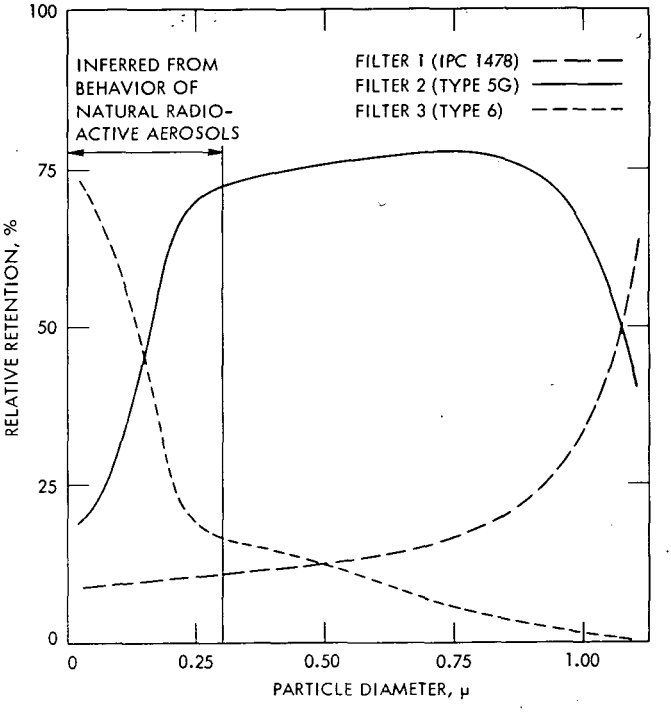

Fig. 3—Effect of size on the distribution of particles among filters in a three-filter pack (air velocity, 61 cm/sec).

lower air velocity with consequent lessening of the effects of particle capture through impaction on the filter fibers.

Radiochemical analyses were performed by previously described techniques[5] for ^{89}Sr, $^{90}Sr-^{90}Y$, ^{91}Y, ^{137}Cs, $^{144}Ce-^{144}Pr$, ^{147}Pm, and ^{210}Pb; radioactivity determinations were made by beta counting on equipment that had been standardized against similar mounts containing known quantities of standardized radionuclides. Routinely, corresponding nuclides from each of the filters in a pack were counted sequentially on the same unit to minimize uncertainties in counter performance or calibration.

RESULTS

Measurements of Gross Fission-product Beta Activity

A rough idea of the changes occurring in the contribution of the larger particles to the total fission-product radioactivity in the air at ground level since termination of atmospheric nuclear testing is shown

in Fig. 4, where the percentage of the total activity retained by the top (poorest) filter in a series of identical filter packs under the same conditions of flow is plotted against the sampling date. This graph demonstrates that initially there is a general decrease in particle size as tropospheric debris is deposited and also that large, short-term

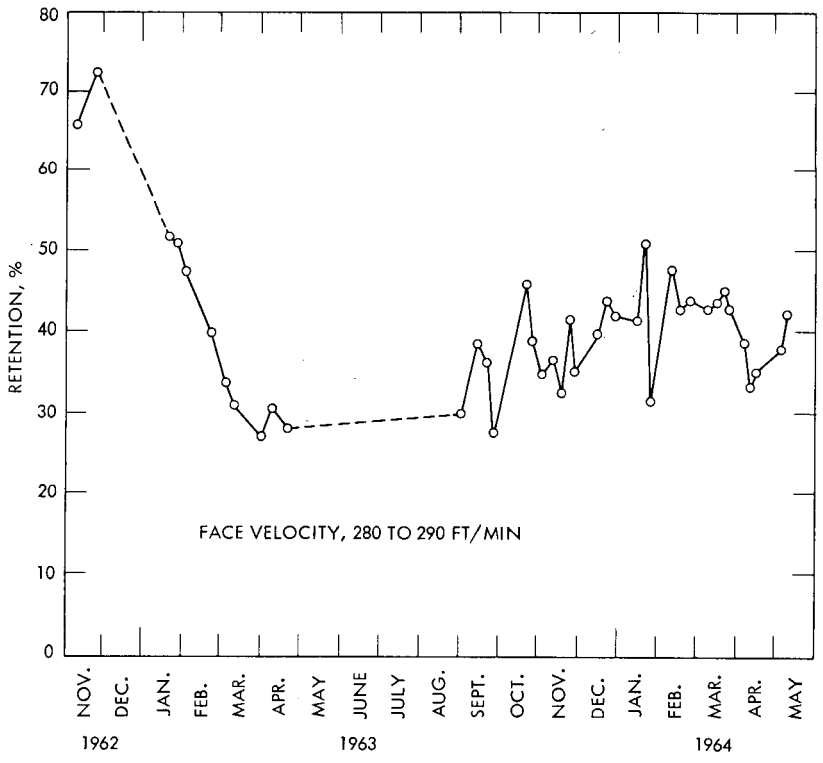

Fig. 4—Temporal changes in the retention of gross fission-product radioactivity by IPC 1478 filters.

variations in particle size occur even when the sole source of fission-product radioactivity is located within the stratosphere. Meteorological phenomena must therefore influence the size distribution of atmospheric radioactivity as well as the concentration of radioactivity in the lower atmosphere.

The variations shown in Fig. 4 are real; they have been verified both by duplicate collections and by others made at the same time but at different flow rates.

Attempts have been made to obtain a more quantitative representation of the size distribution of the particulate radioactivity by a mathematical analysis of the radioactivity data.[2] Some preliminary re-

sults from three-filter packs have been obtained by solution of three simultaneous linear equations of the form

$$A_1 = 0.86\ x_1 + 0.12\ x_2 + 0.00\ x_3$$

$$A_2 = 0.14\ x_1 + 0.80\ x_2 + 0.20\ x_3$$

$$A_3 = 0.00\ x_1 + 0.08\ x_2 + 0.80\ x_3$$

where A_1, A_2, and A_3 are the measured activity distributions on the three filters; x_1, x_2, and x_3 are the relative amounts of activity in three size groupings; and the coefficients of these terms represent the theoretical distribution of particles of these sizes among the filters. Analyses of data from several collections of different types are shown in Table 1. The large, but not unexpected, differences between the

Table 1 — APPROXIMATE PARTICLE-SIZE DISTRIBUTIONS DETERMINED FROM THE RELATIVE RADIOACTIVITY OF FILTERS IN A THREE-FILTER SYSTEM

Collection dates	Collection data: Filter	Order	Relative activity, %	Distribution: Particle size, μ	Activity, %
Fission products (Beta)					
Nov. 23 to 26, 1962 (76 hr)	IPC 1478	1	72.62 ± 0.21*	1.0	82.2
	Type 5G	2	24.64 ± 0.08	0.3	16.0
	Type 6	3	2.74 ± 0.05	0.05	1.8
	(Total activity, 981.1 counts/min)				
Jan. 25 to 28, 1963 (75 hr)	IPC 1478	1	51.82 ± 0.17	1.0	53.7
	Type 5G	2	45.03 ± 0.18	0.3	47.1
	Type 6	3	3.15 ± 0.03	0.05	−0.77
	(Total activity, 1314.8 counts/min)				
Natural activity (RaB + C)					
Oct. 19, 1962 (30 min)	IPC 1478	1	7.0 ± 0.4	1.0	0.25
	Type 5G	2	53.9 ± 0.7	0.3	56.5
	Type 6	3	39.1 ± 0.6	0.05	43.2
	(Total activity, 457.0 counts/min)				

*Standard deviation, σ, based on counting statistics.

sizes of the aerosol particles with which fission-product and natural radioactivity (RaB + C) are associated are clearly evident. These analyses also showed that the coefficients that had been derived from filter calibrations with H_2SO_4 (or DOP) smokes were not entirely satisfactory, as demonstrated by the negative value obtained in one case, and hinted that greater difficulties would be encountered in the solution of four-filter collections. These suspicions were justified.

The Applied Mathematics Staff at the U. S. Naval Research Laboratory (NRL) has devised a scheme which would give better values for

the coefficient matrix of the terms in the system of four simultaneous linear equations. The criteria used were that the filter retentivities or coefficients derived be reasonably close to the filter calibration data and, in addition, permit real solutions to some 40-odd filter collections. A tentative solution has been formulated as follows, where the terms correspond to those of the previous set of equations:

$$A_1 = 95.00\ x_1 + 30.00\ x_2 + 10.00\ x_3 + 2.00\ x_4$$

$$A_2 = 4.75\ x_1 + 21.00\ x_2 + 9.00\ x_3 + 1.96\ x_4$$

$$A_3 = 0.25\ x_1 + 48.80\ x_2 + 77.80\ x_3 + 38.00\ x_4$$

$$A_4 = 0.00\ x_1 + 0.20\ x_2 + 3.20\ x_3 + 58.04\ x_4$$

Particle-size distributions derived for some of the four-filter collections are shown in Table 2. The sizes listed are really particle-

Table 2— PARTICLE-SIZE DISTRIBUTIONS DETERMINED FROM SOME FOUR-FILTER-PACK COLLECTIONS OF RADIOACTIVE FISSION PRODUCTS

Collection dates	Total activity, counts/min	Activity on initial filter, %	Activity contribution of various size groups, %				Weather	
			1.1 μ	0.6 μ	0.3 μ	0.15 μ	Cloud cover, %	Rainfall, in.
1963								
Jan. 18 to 21	679.9	51.3 ± 0.5*	45.3	16.0	34.2	4.5	100	0.42
Mar. 1 to 4	1423.9	33.6 ± 0.2	25.4	11.6	58.4	4.5	50	0.04
Apr. 19 to 22	3098.8	27.8 ± 0.1	21.1	2.7	67.2	9.0	40	Trace
Oct. 18 to 21	380.3	46.0 ± 0.3	34.8	31.9	33.1	0.2	30	0.0
Oct. 25 to 28	173.7	38.7 ± 0.4	25.8	35.2	36.0	3.0	80	Trace
Nov. 1 to 4	143.9	34.8 ± 0.4	17.8	49.6	29.3	3.2	50	0.71
1964								
Mar. 20 to 23	274.2	45.4 ± 0.4	30.1	50.1	18.0	1.8	80	1.05
Mar. 24 to 27	311.3	42.6 ± 0.3	32.4	26.2	39.0	2.4	60	0.01
Apr. 3 to 7	456.6	39.0 ± 0.2	24.1	43.4	30.6	1.9	80	0.76
Apr. 7 to 10	273.0	33.3 ± 0.3	18.4	38.5	42.3	0.8	60	0.64

*Standard deviation, σ, based on counting statistics.

size distributions of unknown form centered about the indicated particle size. If it can be assumed that the equations adequately define the filter system under the operating conditions given in the table or that the filters and their calibration can be accepted as a standard, measurements made at other times and perhaps under other conditions can be interpreted in terms of the standards. Moreover, simultaneous pack collections, wherein one pack is a duplicate run of the standard that serves to characterize the radioactivity distribution during that particular sampling period, can be employed to define the filtration characteristics of an unknown filter.

The size distributions shown in Table 2, calculated from the four-equation set, again demonstrate that there have been large random changes in size distribution with time, as well as a progressive decrease in size which occurred immediately after cessation of atmo-

spheric testing (January through April 1963). It is apparent, too, that the fission debris, even from a stratospheric source, is associated with particles in the 0.3- to 1.1-μ range on arrival at ground level. This strongly suggests that the assumed small fission-product conglomerates existing in the stratosphere coalesce with or become attached to the larger nonradioactive tropospheric aerosols during slow migration of the aerosols to ground level. Thus meteorological phenomena that affect the size distribution of normal atmospheric dusts should have a corresponding effect on the fission-product conglomerate seen at ground level. Although as yet no attempt has been made to correlate the particle-size distribution with weather, the data for March and April 1964 suggest a progressive decrease in the size of the radioactive aerosol particles during a prolonged rainy period.

A comparison of the size distribution of radon daughter products (RaB + C) with the extremes in the fission-product distributions observed through use of this method is shown in Table 3. It is obvious that

Table 3—COMPARISON OF THE SIZE DISTRIBUTION OF RaB + C ACTIVITY WITH THE OBSERVED EXTREMES FOR FISSION PRODUCTS

Collection dates	Total activity, counts/min	Activity on initial filter, %	Activity contribution of various size groups, %				Weather	
			1.1 μ	0.6 μ	0.3 μ	0.15 μ	Cloud cover, %	Rainfall, in.
			RaB + C					
Mar. 15, 1963 (0810–0840)	136.4	9.0 ± 1.2*	4.8	0.5	30.0	64.7	0	0.0
Mar. 27, 1963 (0815–0845)	270.5	9.9 ± 0.5	3.6	6.8	33.2	56.4	100	0.0
Mar. 18, 1964 (0830–0900)	151.8	13.1 ± 0.6	5.3	16.4	20.1	58.2	0	0.0
			Fission products					
Apr. 19 to 22, 1963	3098.8	27.8 ± 0.1	21.1	2.7	67.2	9.0	30	Trace
Oct. 4 to 7, 1963	467.8	26.3 ± 0.2	13.1	27.0	56.8	3.1	10	0.0
July 23 to 27, 1964	41.6	59.6 ± 1.4	46.6	51.0	0.1	2.3	70	Trace

*Standard deviation, σ, based on counting statistics.

RaB + C activity is associated primarily with particles smaller than 0.3 μ in diameter. The smallest observed fission-product distribution peaked near 0.3 μ, whereas the largest distribution peaked between 0.6 and 1.1 μ. In most cases the contribution of fission products to the <0.3-μ grouping was about 2 to 3% of the total, although on one occasion (Apr. 19 to 22, 1963) 9% of the fission-product radioactivity fell into this grouping.

Radiochemical Results

Radiochemical analyses for some long-lived fission products and for ^{210}Pb (RaD) have been carried out on seven three-filter collections[6] made during 1963. Similar analyses are being performed on one combined month-long collection during each quarter of 1964.

Table 4 — RESULTS OF RADIOCHEMICAL ANALYSES OF FILTER-PACK COLLECTIONS MADE AT NRL

Collection dates, 1963	Volume sample, m^3	Filter	Order	Activity distribution on filters, %							Selected activity ratios			
				^{89}Sr	^{90}Sr	^{91}Y	^{137}Cs	^{144}Ce	^{147}Pm	^{210}Pb	$\frac{^{89}Sr}{^{90}Sr}$	$\frac{^{89}Sr}{^{91}Y}$	$\frac{^{144}Ce}{^{90}Sr}$	$\frac{^{137}Cs}{^{90}Sr}$
February 15 to 21	3.72×10^4	IPC 1478	1	16.3	18.7	21.3	14.3	29.4	22.0	10.9	22.1	0.70	37.7	1.10
		Type 5G	2	75.0	74.2	71.9	77.3	64.6	71.2	74.4	25.7	0.95	20.9	1.50
		Type 6	3	8.7	7.1	6.8	8.4	6.0	6.8	14.7	31.2	1.16	20.5	1.71
Total activity, dis/min,* and average ratios				9.28×10^4	3.65×10^3	1.02×10^5	5.25×10^3	8.78×10^4	1.49×10^4	8.17×10^2	25.4	0.91	24.0	1.44
May 3 to 10	4.34×10^4	IPC 1478	1	13.1	13.3	13.9	10.3	17.3	17.0	14.8	7.8	0.68	25.8	1.11
		Type 5G	2	74.2	75.2	74.1	80.7	70.5	72.2	67.2	7.9	0.73	18.7	1.55
		Type 6	3	12.7	11.5	12.0	9.0	12.2	10.8	18.0	8.9	0.77	21.3	1.14
Total activity, dis/min,* and average ratios				8.63×10^4	1.08×10^4	1.19×10^5	1.56×10^4	2.16×10^5	3.27×10^4	1.10×10^3	8.0	0.73	20.0	1.45
July 19 to August 9	1.30×10^5	IPC 1478	1	23.2	23.9	23.6	20.7	22.0	22.0	24.7	3.4	0.74	19.6	1.25
		Type 5G	2	64.1	63.7	64.8	69.2	66.8	67.7	62.2	3.5	0.75	22.3	1.57
		Type 6	3	12.7	12.4	11.6	10.1	11.2	10.3	13.1	3.6	0.83	19.2	1.18
Total activity, dis/min,* and average ratios				7.42×10^4	2.13×10^4	9.85×10^4	3.08×10^4	4.52×10^5	1.09×10^5	7.93×10^2	3.5	0.75	21.3	1.45
August 10 to 17	4.34×10^4	IPC 1478	1	10.2	14.0	12.4	15.1	16.5	11.6	10.9	2.4	0.61	19.3	1.31
		Type 5G	2	73.5	72.4	75.3	77.2	69.7	75.8	69.0	3.4	0.72	15.8	1.30
		Type 6	3	16.3	13.6	12.3	7.7	13.8	12.6	20.1	4.1	0.98	16.8	0.69
Total activity, dis/min,* and average ratios				2.90×10^4	8.62×10^3	3.92×10^4	1.05×10^4	1.42×10^5	3.26×10^4	7.07×10^2	3.4	0.74	16.4	1.22
August 17 to September 6	1.24×10^5	IPC 1478	1	21.6	21.6	21.9	34.0	23.8	23.6	18.7	2.2	0.64	18.4	1.22
		Type 5G	2	68.2	69.6	68.6	58.4	59.4	64.7	65.9	2.1	0.65	14.3	0.65
		Type 6	3	10.2	8.8	9.5	7.6	16.8	11.7	15.4	2.5	0.70	31.9	0.67
Total activity, dis/min,* and average ratios				3.07×10^4	1.41×10^4	4.71×10^4	1.09×10^4	2.36×10^5	4.95×10^4	1.97×10^3	2.2	0.65	16.7	0.77
September 6 to 13	4.34×10^4	IPC 1478	1	14.3	17.5	15.3	16.7	16.3	15.2	14.2	2.0	0.75	17.2	1.02
		Type 5G	2	76.5	73.4	75.4	72.5	74.9	75.7	67.7	2.6	0.81	18.8	1.06
		Type 6	3	9.2	9.1	9.3	10.8	8.8	9.1	18.1	2.5	0.79	17.6	1.26
Total activity, dis/min,* and average ratios				9.23×10^3	3.76×10^3	1.16×10^4	4.03×10^3	6.92×10^4	1.68×10^4	1.27×10^2	2.5	0.80	18.4	1.07
October 24 to November 8	9.30×10^4	IPC 1478	1	14.0	24.1	23.4	22.0	23.7	23.0	16.5	0.8	0.52	15.4	1.49
		Type 5G	2	77.1	68.2	70.0	70.7	68.8	69.2	61.1	1.6	0.95	15.8	1.69
		Type 6	3	8.9	7.7	6.6	7.3	7.5	7.8	22.4	1.7	1.16	15.2	1.55
Total activity, dis/min,* and average ratios				6.16×10^3	4.23×10^3	7.14×10^3	6.90×10^3	6.62×10^4	2.00×10^4	1.37×10^3	1.5	0.86	15.7	1.63

*Activity corrected for decay to midpoint of collection period.

The activity levels existing in the air at the time the various collections for radiochemical analysis were made are shown in Fig. 5. Both the monthly average air concentrations of fission products reported by the Radiation Surveillance Network, U. S. Public Health Service, for Washington, D. C., and the results of various short-term collections made at NRL are depicted. The wide scatter in the values of the short-term collections demonstrates the extreme dependence of the ground-level activity concentrations on meteorological processes bringing upper tropospheric air down to ground level and on those cleansing the air of particulate matter. As in previous years a strong spring maximum in the concentrations of airborne fission products resulting from the winter–spring subsidence of stratospheric air was observed during 1963.

The results of the radiochemical analyses of the seven collections made during 1963 are presented in Table 4. The wide variation in the distribution of radioactivity among the filters of packs collected at different times during all seasons of the year demonstrates that local meteorological conditions are of more significance than purely seasonal effects as a causative mechanism. Indeed, the greatest variation observed among the samples occurred during consecutive collection periods in August 1963.

As indicated in Fig. 3, the particle-size ranges represented by the activity on the three filters are roughly as follows: filter 1 (IPC 1478) contains the bulk of the activity associated with particles around 1.0 μ in diameter and some contribution from smaller particles; filter 2 contains particles in the range 0.3 to 1.0 μ; and filter 3 contains the remainder, primarily in the size range below 0.3 μ. Over a wide range of particle sizes, approximately 75% of the activity should appear on the middle filter of the pack; consequently, nuclide ratios measured here should reflect the average of the collection rather than specific fractionation effects. The data in Table 4 substantiate this conclusion.

The most likely evidence for nuclide fractionation would show up in nuclide ratio differences between particles retained by the initial and the final filters where the largest and the smallest particles, respectively, would be concentrated. The ratios of activity of each nuclide relative to ^{90}Sr as a reference on the top filter to the same activity ratio on the final filter, $(X/^{90}Sr)_{IPC}/(X/^{90}Sr)_{type\ 6}$, are listed in Table 5. It should be noted that any inadequacies in counter standardization are eliminated by this method of presentation; therefore the results should be as reliable as counter stability and counting statistics allow. For the radioactivity determinations the standard deviation, σ, based on counting, has been kept below $\pm 1\%$, except in the case of ^{89}Sr, where its lower activity and the necessity of obtaining it by difference has led to larger errors.

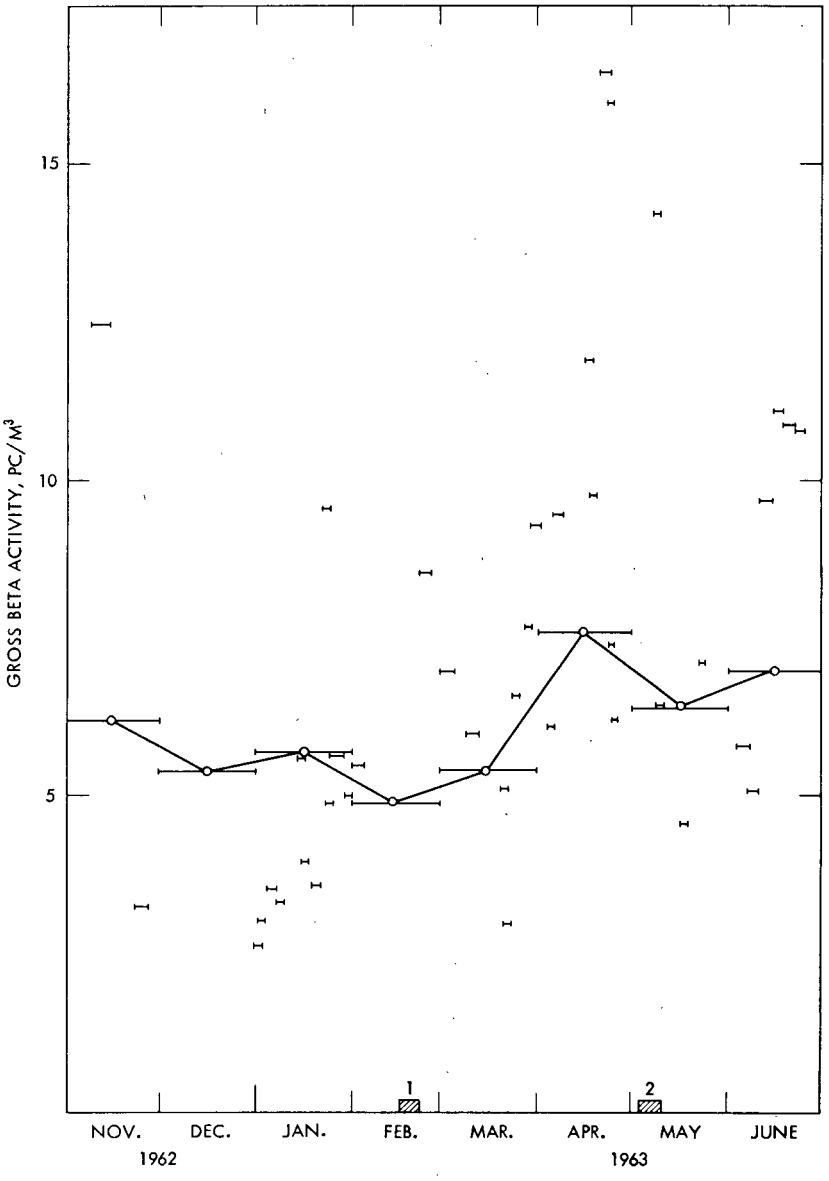

Fig. 5—Concentration of fission-product beta activity in the ground-level air at Washington, D. C., during 1963.

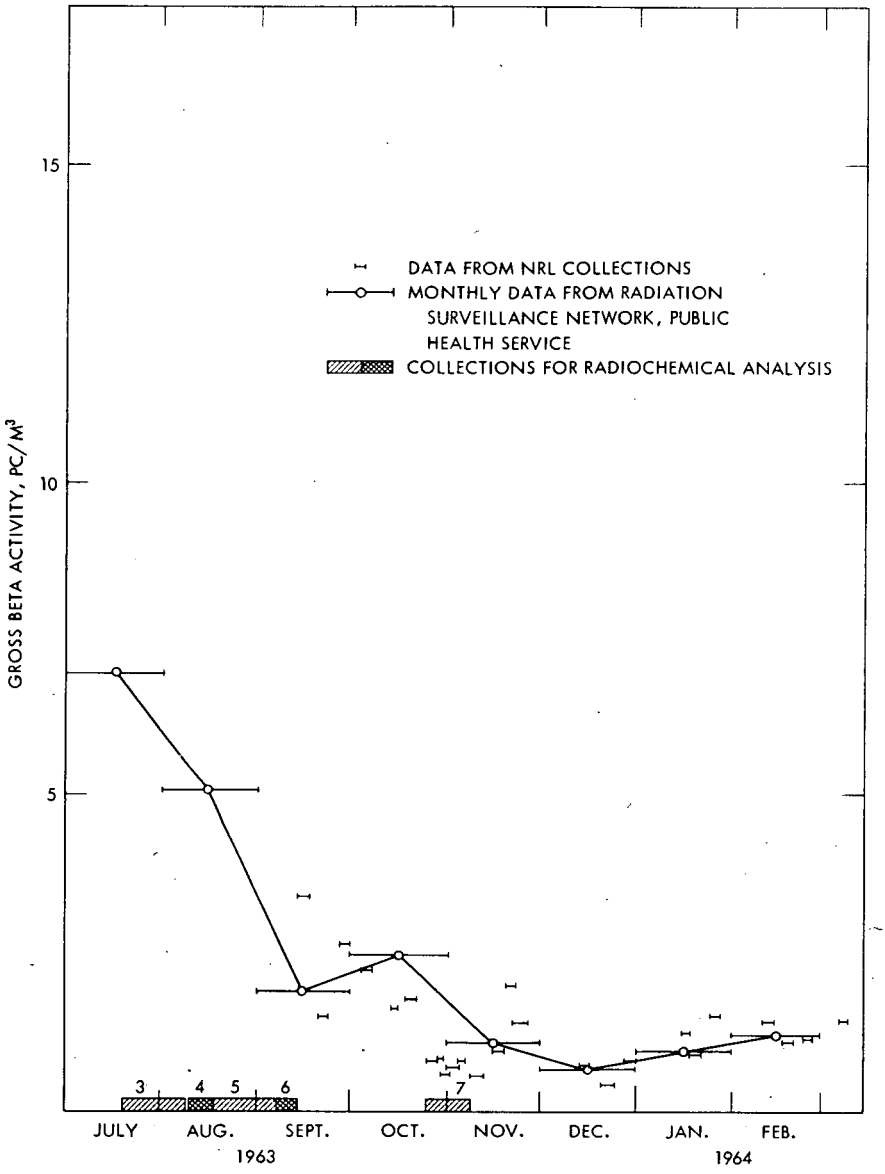
15
10
5
GROSS BETA ACTIVITY, PC/M³
DATA FROM NRL COLLECTIONS
MONTHLY DATA FROM RADIATION SURVEILLANCE NETWORK, PUBLIC HEALTH SERVICE
COLLECTIONS FOR RADIOCHEMICAL ANALYSIS
3
4
5
6
7
JULY
AUG.
SEPT.
OCT.
NOV.
DEC.
JAN.
FEB.
1963
1964

A comparison of the overall distribution of the various radionuclides among the filters of a given collection discloses surprisingly little evidence of fractionation; however, the comparison of the nuclide ratios of the extremes in the particle-size ranges shown in Table 5 gives definite indications of fractionation. With ^{90}Sr as a reference, it

Table 5—COMPARISON OF ACTIVITY RATIOS RELATIVE TO ^{90}Sr FOR THE LARGEST AND THE SMALLEST PARTICLE-SIZE FRACTIONS

Collection dates, 1963	Ratio of activity ratios to ^{90}Sr for initial filter vs. final filter					
	^{89}Sr	^{91}Y	^{137}Cs	^{144}Ce	^{147}Pm	^{210}Pb
February 15 to 21	0.71	1.19	0.65	1.85	1.23	0.28
May 3 to 10	0.89	1.01	0.99	1.23	1.36	0.71
July 19 to August 9	0.95	1.05	1.06	1.02	1.11	0.97
August 10 to 17	0.61	0.99	1.89	1.17	0.89	0.53
August 17 to September 6	0.86	0.94	1.83	0.58	0.82	0.49
September 6 to 13	0.81	0.85	0.80	0.96	0.87	0.41
October 24 to November 8	0.50	1.13	0.96	1.01	0.94	0.23
Average	0.76	1.02	1.17	1.12	1.03	0.52
Standard deviation of the mean	±0.06	±0.04	±0.19	±0.15	±0.08	±0.10
Standard deviation of a single ratio	±0.16	±0.11	±0.50	±0.39	±0.21	±0.25

may be noted that ^{89}Sr and ^{210}Pb are consistently depleted in the largest particles. The nuclides ^{137}Cs, ^{144}Ce, and ^{147}Pm are rather variable in their distribution, and ^{91}Y appears to be fractionated least. There was no apparent relation between the extent or direction of fractionation and the existence of gaseous or volatile precursors in the decay chains of the nuclides. For example, there appeared to be no preferential association of ^{91}Y, ^{144}Ce, and ^{147}Pm with the larger particles, as might be inferred from their lack of volatile ancestors. The observed association of ^{210}Pb with smaller particles is to be expected on the basis of its shorter average lifetime in the atmosphere since it is continually being reintroduced through decay of the 3.8-day ^{222}Rn primarily in the lower levels of the troposphere.

CONCLUSIONS

The results obtained in these studies of the distribution of radioactivity among filters in a pack indicate that the fission-product conglomerate encountered at ground level some months after a series of nuclear detonations has the bulk of its radioactivity associated with

particles between 0.3 and 1.1 μ in diameter with only minor components of very small (<0.3 μ) particles. On the other hand, the short-lived natural radon daughter products (RaB + C) are associated with much smaller particles with the major part of the activity attached to aerosol particles of less than 0.3 μ in diameter. The longer-lived natural radioisotope ^{210}Pb, because of its longer average residence time in the atmosphere, behaves more like the fission products.

The size distribution of the fission products found at ground level is quite unlike that expected for the stratospheric source from which these fission debris are derived. The long residence time of this material in the stratosphere precludes the presence there of any considerable quantity of larger particles; it might be supposed that the particle-size range would be similar to that found by Junge and Manson for nonradioactive stratospheric aerosols.[7] Indeed, it would appear likely that the smaller particles from nuclear explosions would soon become attached to the inactive aerosols and would partake in the growth processes involving those aerosols.

The filter-pack technique shows considerable promise as a means of obtaining information on the size distribution of aerosols. Its utility is not limited to the study of radioactive aerosols but is applicable to the sizing of any kind of airborne particulate matter for which suitable analytical methods are available. The techniques of radioactivity measurement, chemical and activation analyses, etc., may be equally suitable provided the filters employed have sufficiently low backgrounds of interfering substances.

REFERENCES

1. U. S. Naval Research Laboratory, Final Report; Greenhouse, Project B-29 and Project B-28, Report NRL-3963, Mar. 3, 1952. (Classified)
2. L. B. Lockhart, Jr., and R. L. Patterson, Jr., Filter Pack Technique for Classifying Radioactive Aerosols by Particle Size. Part 1. Preliminary Report and Evaluation, Report NRL-5970, U. S. Naval Research Laboratory, Aug. 16, 1963.
3. L. B. Lockhart, Jr., R. L. Patterson, Jr., and W. L. Anderson, Characteristics of Air Filter Media Used for Monitoring Airborne Radioactivity, Report NRL-6054, U. S. Naval Research Laboratory, Mar. 20, 1964.
4. M. H. Wilkening, Natural Radioactivity as a Tracer in the Sorting of Aerosols According to Mobility, *Rev. Sci. Instr., 23:* 13 (1952).
5. R. A. Baus, P. R. Gustafson, R. L. Patterson, Jr., and A. W. Saunders, Jr., Procedure for the Sequential Radiochemical Analysis of Strontium, Yttrium, Cesium, Cerium, and Bismuth in Air-filter Collections, Report NRL-Memo-758, U. S. Naval Research Laboratory, November 1957.
6. L. B. Lockhart, Jr., R. L. Patterson, Jr., and A. W. Saunders, Jr., Filter Pack Technique for Classifying Radioactive Aerosols by Particle Size. Part 2. Isotopic Fractionation with Particle Size, Report NRL-6164, U. S. Naval Research Laboratory, October 1964.
7. C. E. Junge and J. E. Manson, Stratospheric Aerosol Studies, *J. Geophys. Res., 66:* 2163-2182 (1961).

PARTICLE SIZE DISTRIBUTION OF STRATOSPHERIC AEROSOLS AT 110,000 FT

PETER LOYSEN
Health and Safety Laboratory, U. S. Atomic Energy Commission, New York, N. Y.

ABSTRACT

Aerosol samples collected directly on electron-microscope specimen grids were used to determine the size of stratospheric particles at an altitude of about 110,000 ft. The samples, which were obtained as part of balloon flight tests of an experimental electrostatic-precipitator sampler during the period from October 1961 through June 1963, were photomicrographed and counted for determination of size distributions. The median particle diameters determined from these tests were in the range 0.002 to 0.13 μ.

Prior to these tests information about the size of stratospheric aerosols was available only for altitudes below 100,000 ft. Since particle size information is important in determining the performance requirements of stratospheric air-sampling equipment that may be used at altitudes up to 150,000 ft, it is needed in both the design and the testing of such equipment. The Health and Safety Laboratory (HASL) is continuing its stratospheric-particle studies with the objective of obtaining information about size distributions over the complete range of balloon-sampling altitudes from 60,000 to 150,000 ft.

INTRODUCTION

The need for stratospheric particle size data is evident. In addition to being a basic requirement for data as input to weapons-debris transport and fallout predictions, particle size determines the performance requirements of stratospheric air-sampling devices to an

important degree. Thus, for HASL to fulfill its responsibilities in the development and evaluation of high-altitude balloon-sampling equipment, particle-size data are necessary in both the design and the laboratory testing of such devices.

In December 1963 HASL prepared a technical memorandum describing some preliminary determinations in 1961 and 1962 of the size distributions of stratospheric aerosols collected at an altitude of about 110,000 ft. In 1963 additional samples were collected with an electrostatic precipitator on two balloon flights, during which the sampling system operated with complete reliability. This paper summarizes the results of all the measurements performed so far.

Samples of particulate material collected directly on electron-microscope grids were photomicrographed and counted for size-distribution determinations. Because the samples were collected in conjunction with balloon flight tests of an experimental electrostatic precipitator designed for another purpose, certain qualifications must be taken into account in interpreting the results. However, in the absence of other data for this altitude, the information is presented here for its use by investigators. Prior to these tests information about the sizes of stratospheric aerosols was available*[1,2] only for altitudes below 100,000 ft.

METHOD OF COLLECTION

Balloon flights to determine the feasibility of an electrostatic-precipitator sampler designed by Del Electronics Corporation were conducted in Minneapolis, Minn., and San Angelo, Tex., during the period from October 1961 to June 1963. The sampler was designed to collect stratospheric aerosols in the region of 70,000 to 135,000 ft for radiochemical analyses. It consisted of a 6-in.-diameter 4-ft-long aluminum cylinder with an axial corona wire. Air was drawn through the cylinder by a battery-operated axial-vane fan at a rate of either 100 or 200 ambient cubic feet per minute.[3] The basic components of the sampler are shown in Fig. 1. Collection was made on an aluminum-foil liner coated with a colloidal graphite suspension on the inner surface of the cylinder. The total collection-surface area was 6 sq ft.

A ½-in. strip along the liner in the direction of air flow was not coated so that, prior to each flight, carbon-coated electron-microscope specimen grids could be mounted at intervals along the liner. This was done as an adjunct to the main purpose of the flight tests in the hope that a sufficient number of particles would be collected for study. How-

*See paper by P. J. Drevinsky and J. Pecci, this volume.

ever, the sampler was not specifically designed with such collection as an objective.

In the first five tests, the electron-microscope grids were taped to the clean aluminum surface. In the last two tests, the uncoated strip was eliminated, and the grids were attached with a small amount of the colloidal graphite suspension. The number of grids mounted in the

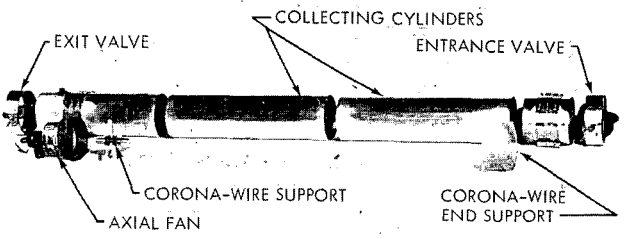

Fig. 1—Components of Del Electronics Corporation electrostatic-precipitator sampler.

sampler ranged from 8 in the first test to as many as 25 in subsequent tests. Precoated grids were obtained from a commercial source.

Before the grids were mounted, they were spot-checked for cleanliness in an electron microscope and were found to be clean. However, in recent, more thorough examinations of new carbon-coated grids obtained from the same source, particles have been detected. This finding raised a question regarding differentiation between stratospheric particles and background contamination on the grids. Radioautographs of sections of the uncoated aluminum strips on which the grids were mounted definitely established the fact that radioactive particles were collected. Figure 2 is a typical radioautograph on nuclear-track emulsion showing the presence of both alpha and beta radioactivity. The approximate concentration of these particles as determined from the radioautographs is 10^4 particles per cubic foot. The concentration of all particles as determined from the photomicrographs is also about 10^4 particles per cubic foot. Therefore it appears that the particles that were counted were both stratospheric and radioactive.

After the grids were mounted on the aluminum liner, the ends of the electrostatic precipitator were covered and sealed with polyethylene bags until launch time. The precipitator was equipped with butterfly valves at each end to prevent the entry of air from the time that the balloon was launched until the sampling altitude was reached. The valves did not provide an airtight seal, however. At the end of the 3- to 4-hr sampling period at a fixed altitude, the butterfly valves were closed, and the sampling unit was released from the balloon to return

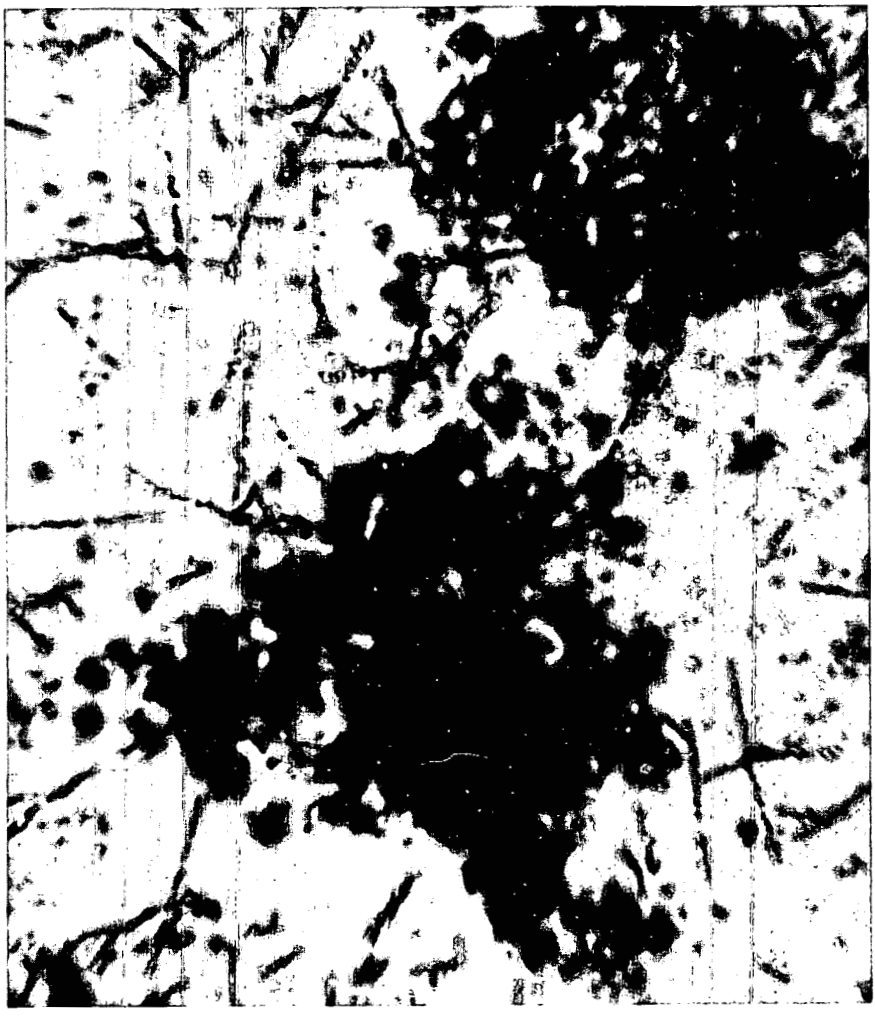

Fig. 2—Radioautograph of aluminum-foil liner. Flight 2572.

to earth by parachute. Upon recovery the precipitator was again capped at both ends with polyethylene bags and then returned to the launch site, where the precipitator was dismantled and the sections containing the liner, along with the electron-microscope grids, were removed and sent to HASL.

Although the procedures described minimized contamination of the samples with nonstratospheric particles, the absence of extraneous material on the electron-microscope grids cannot be taken as a certainty.

Several balloon flights were made during which particle size samples were collected. The sampler used in the last three flights of the series embodied improvements based on experience in the earlier flights; therefore measurements of samples from these last flights were used for most of the data reported here. The flight series is identified in Table 1. The relatively few measurements from flights 2556, 2562, 2569, and 2572 were consolidated.

Table 1—FLIGHT TEST DESIGNATION

Flight No.	Date	Location	Altitude, ft
2556	August 1961	Minneapolis, Minn.	106,000
2562	September 1961	Minneapolis, Minn.	115,000
2569	October 1961	Minneapolis, Minn.	109,000
2572	October 1961	Minneapolis, Minn.	109,000
2611	October 1962	Minneapolis, Minn.	108,000
T-781-A	May 1963	San Angelo, Tex.	106,000
T-796-A	June 1963	San Angelo, Tex.	106,000

METHOD OF COUNTING AND SIZING PARTICLES

The grids were examined at HASL in an electron microscope. Approximately 150 fields were photographed at magnifications ranging from 300× to 190,000×, depending on the size of the particles. Photographic enlargements were made from the film plates, generally to an 8- by 10-in. size. This resulted in overall magnifications of 1200× to 764,000×. In all cases particles were sized by equal-area techniques by using either a series of transparent overlays or a Zeiss automatic particle counter. Size groups were established in a geometric progression, and particles were classified in each group.

RESULTS

The size-distribution results for the seven tests are presented in Table 2, and graphical representations are given in Figs. 3 to 6. Photomicrographs of several types of particles collected by the sampler are included as Figs. 7 to 14. Upon examination of the figures, the median diameters can be estimated to range from 0.002 to 0.13 μ as shown in Table 3.

The differences in median size among the four test groups may be explained by the fact that a large number of particles in some size ranges were counted from a single or a few photographs. This caused the distribution to be biased. Correlation of the differences in the size distributions with the occurrence of weapons tests, the radioactivity

Table 2—SIZE-DISTRIBUTION RESULTS

Particle diameter, μ	Number of particles			
	Flights 2556, 2562, 2569, and 2572	Flight 2611	Flight T-781-A	Flight T-796-A
< 0.0008	*	*	*	*
0.0009 to 0.0016	354	*	*	9
0.0017 to 0.0032	58	32	*	10
0.0033 to 0.0064	205	257	5	2
0.0065 to 0.0128	32	1998	7	4521
0.0129 to 0.0256	46	139	51	2205
0.0257 to 0.0512	9	366	1173	140
0.0513 to 0.102	4	62	455	171
0.103 to 0.205	2	17	1376	76
0.206 to 0.409	0	27	716	70
0.410 to 0.819	0	28	188	46
0.820 to 1.64	0	15	23	16
1.65 to 3.28	0	7	2	35
3.29 to 6.75	0	1	1	2
6.76 to 13.5	0	1	0	0
13.6 to 27.0	0	1	0	0
Totals	710	2951	3997	7303

*The lack of data is the result of either an absence of particles in the size group or microscope resolution limitations or both.

concentrations, the time of year, and the sampler performance was not significant. However, changes produced by the weapons tests of 1961 and 1962 could have given rise to the observed variations in the particle size distributions.

Further examination of the size-distribution results reveals differences in the lower cutoff points among the test groups. These differences may be the result of different minimum sizes in the stratosphere at the time of collection, of variation in the resolution obtained with the electron microscope, and of different particle-charging probabilities.* These probabilities, which are related to ion densities and particle residence times in the sampler, may have been affected by the use of different flow rates and precipitator corona currents in the tests.

Because of the limitations in the collection of particles by the experimental sampler, in the evaluation of contamination, and in the subsequent size determinations (which are reflected in the wide range of median sizes reported), the results should be used only as indications of the true size distributions. Similarly, the calculated particle concentration of 10^4 particles per cubic foot (3.5×10^{-1} particle per cubic centimeter) should be regarded qualitatively.

*See paper by B. Y. H. Liu and K. T. Whitby, this volume.

DISTRIBUTION OF PARTICLES LESS THAN STATED SIZE

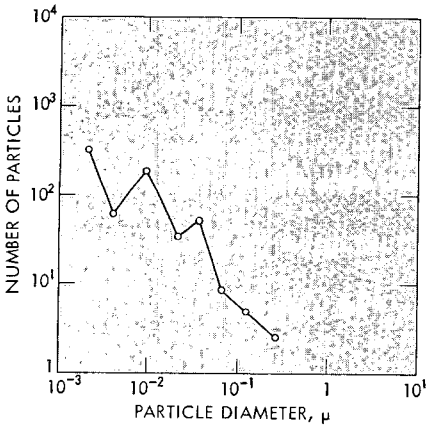

Fig. 3—Flights 2556, 2562, 2569, and 2572, August to October 1961, Minneapolis, Minn.

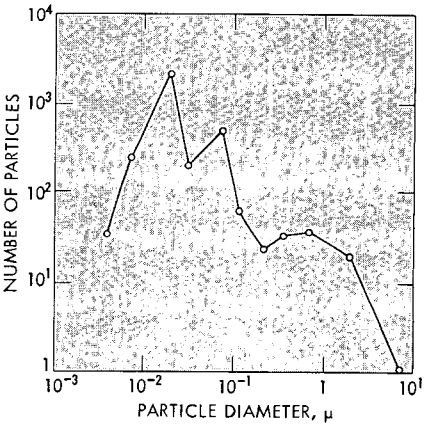

Fig. 4—Flight 2611, October 1962, Minneapolis, Minn.

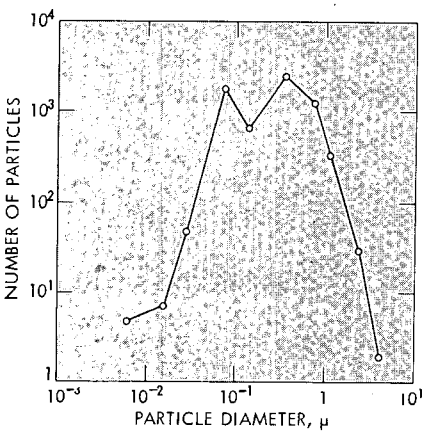

Fig. 5—Flight T-781-A, May 1963, San Angelo, Tex.

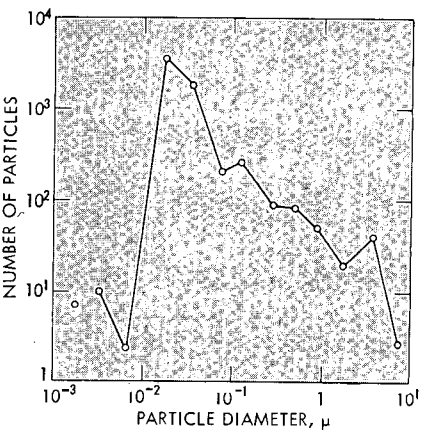

Fig. 6—Flight T-796-A, June 1963, San Angelo, Tex.

PHOTOMICROGRAPHS OF STRATOSPHERIC PARTICLES

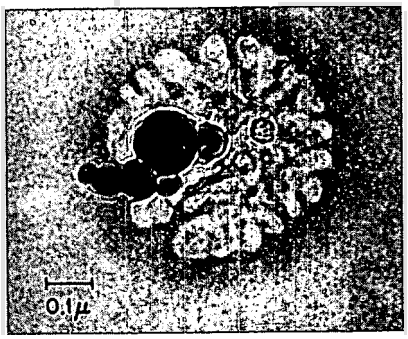

Fig. 7—Flight T-796-A.

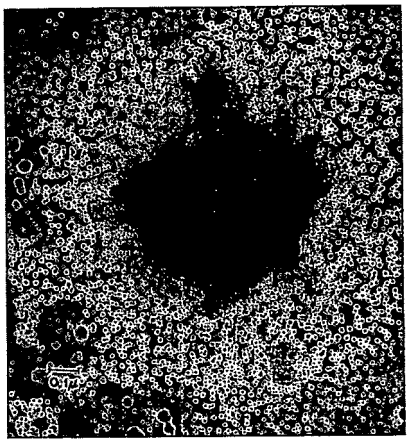

Fig. 8—Flight T-796-A.

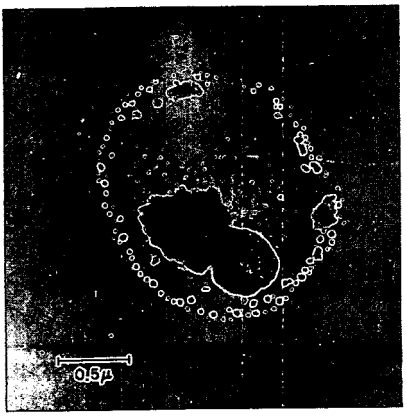

Fig. 9—Flight T-796-A.

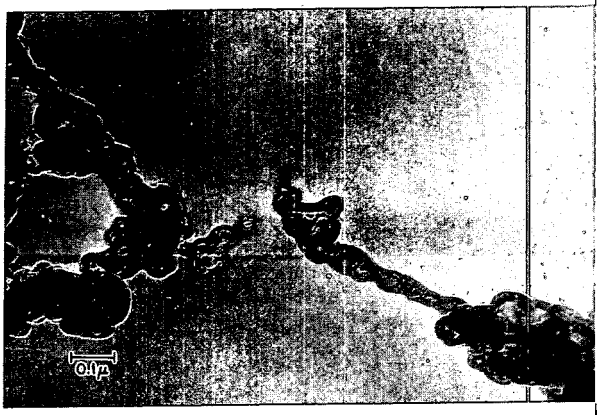

Fig. 10—Flight T-781-A.

PHOTOMICROGRAPHS OF STRATOSPHERIC PARTICLES

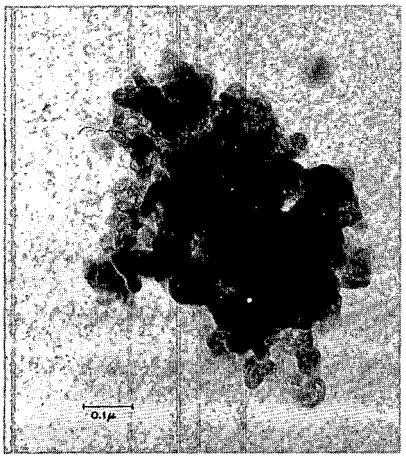

Fig. 11—Flight 2611.

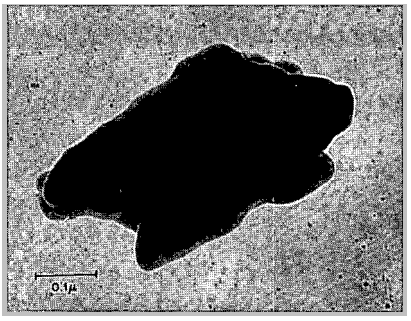

Fig. 12—Flight 2611.

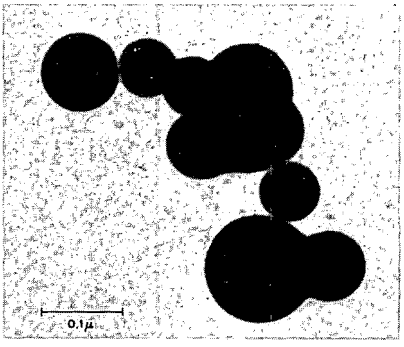

Fig. 13—Flight 2556.

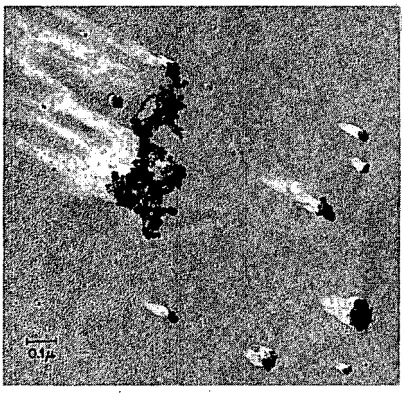

Fig. 14—Flight T-781-A.

Table 3—MEDIAN PARTICLE SIZE

Flight No.	Estimated particle diameter, μ
2556, 2562, 2569, and 2572	0.002
2611	0.008
T-781-A	0.13
T-796-A	0.008

HASL is continuing its efforts in stratospheric particle studies to verify the findings reported here and to obtain information about particle size distributions at other balloon-sampling altitudes. A compact, lightweight electrostatic precipitator is now being developed for the specific purpose of collecting samples for making the appropriate measurements. The design of this sampler will eliminate the causes of uncertainties in the quality of samples, particularly with respect to sample contamination by nonstratospheric particles.

REFERENCES

1. C. E. Junge and J. E. Manson, Stratospheric Aerosol Studies, *J. Geophys. Research, 66*(7): 2163-2182 (1961).
2. J. P. Friend (Ed.), The High Altitude Sampling Program, Report DASA-1300, Vol. 5, Supplementary HASP Studies, Isotopes, Inc., Aug. 31, 1961.
3. M. Lippmann (Comp.), Stratospheric Monitoring Program, Summary Progress Report, February 1961–April 1962, USAEC Report NYO-9675, Del Electronics Corporation, Sept. 10, 1962.

CHEMICAL STATE OF TRITIUM IN THE ATMOSPHERE AND SOURCES OF TRITIATED METHANE

A. HAINES and B. MUSGRAVE
University of Arkansas, Fayetteville, Arkansas

ABSTRACT

The T/H ratios in atmospheric hydrogen and methane are discussed in relation to some of the available information on the amounts of tritium released by the nuclear industry. The increase in the T/H ratio in atmospheric hydrogen prior to 1952 can be attributed to this source. From the rate of tritium release, an estimate of the production of tritiated methane can be made. Such an estimate gives reasonable agreement with the observed T/H values.

INTRODUCTION

The presence of tritium (^{3}H or T) in at least three different chemical forms in the atmosphere is well known. A number of studies have been made which have resulted in a reasonably good understanding of the general nature of this distribution. Lack of detailed information about the sources of the tritium, however, has prevented a complete explanation of the variations with time of the T/H ratio in hydrogen and methane.

The data[1–7] for T/H ratios in northern- and southern-hemisphere methane and northern-hemisphere hydrogen from 1948 to 1955 are shown in Fig. 1. Bishop and Taylor[8] have suggested that the T/H ratio in hydrogen was increasing exponentially prior to the 1952 Operation Ivy nuclear test series and is continuing to increase in this manner. More recently Bainbridge et al.[1] have proposed that the natural level was high and that no increase occurred prior to 1954; however, the

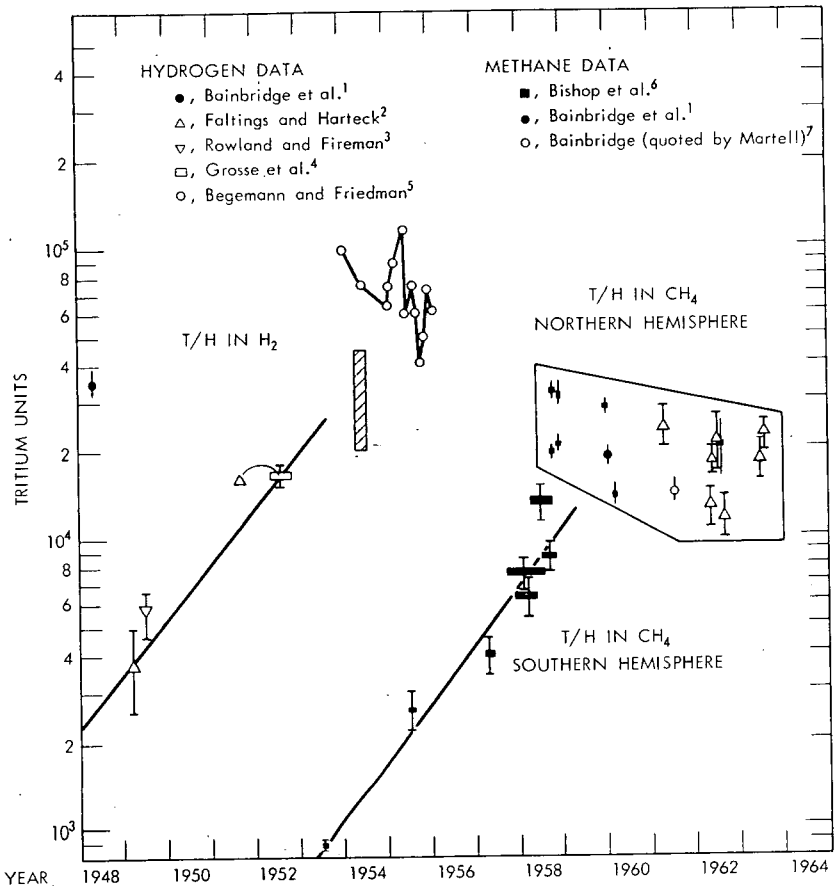

Fig. 1—Tritium concentration in hydrogen and methane.

data of Rowland and Fireman[3] and Grosse et al.[4] tend to support the idea of an increase. Since the report of Bishop et al.[6] that there is a significant tritium level in methane in the atmosphere, a variety of proposals concerning the mechanism of the incorporation of tritium into methane have been advanced. Some of the proposals are based on the assumption that the tritium becomes incorporated in the methane during a nuclear explosion or by reactions occurring in the atmosphere under ordinary conditions. Martell[7] has discussed the various proposals and offered a mechanism based on the incorporation of HT into methane through radical reactions initiated by energy released by electric discharges, such as lightning, etc.

The rate of the T/H increase in southern-hemisphere methane is consistent with a source in the northern troposphere which does not inject all the tritium at a single time.[9]

Recent results of Begemann[9] show that the T/H ratio in the northern-hemisphere methane has been essentially constant from 1958 to 1963; during this time the tritium content of atmospheric hydrogen increased by a factor of 2 to 4. This observation makes it seem most probable that the tritiated methane was of synthetic origin and not due to the incorporation of HT into methane in the atmosphere.

A final determination of the source of tritium in methane may not be possible; it will be apparent, however, that there are sufficient sources in the nuclear industry to account for the increase in the T/H ratio in atmospheric hydrogen prior to 1952 and that these same sources were releasing tritiated methane during this period. Although the methane and the HT may be from a common or a similar source, there is no particular significance to be given to an apparent exponential T/H increase in methane or hydrogen in the northern hemisphere.

CAUSE OF THE T/H INCREASE IN ATMOSPHERIC HYDROGEN PRIOR TO 1952

Fairly detailed information is available from the tritium production techniques employed at Los Alamos Scientific Laboratory.[10] The system involved a thermal-diffusion column that included seven mass-spectrometer leaks for controlling the feed and for withdrawing tritium from the column. The combined leak total was about 10 ml of tritium per day, mostly as T_2. The depleted tritium was reprocessed, with the depleted fraction from the second cycle being exhausted into the atmosphere. At the minimum estimated rate of operation of the system, the reprocessing released another 10 ml of tritium per day. It is stated that the final stripped product was "vented with safety." It can be assumed that the vacuum systems connected to the mass spectrometers and those used for final sample storage were vented in a like manner.

The rate of tritium release estimated for this thermal-diffusion column fits the increase in the T/H ratio reported for hydrogen between 1949 and 1952. Examining this rate of release from a different approach, we can estimate the minimum amount of tritium that eventually must have been released by the time of the 1954 Operation Castle test series. For the production system to release the amount of tritium that was estimated to have been released by the Ivy and Castle tests, the minimum amount released should have been 9 to 12 g. This corresponds to a T/H ratio of approximately 0.2 to 0.3×10^5 tritium units (T.U.) as of 1954. The amount released may have been as high as 22 g; this would give a T/H ratio of 0.5×10^5 T.U. for the 1954 level. The values measured[5] were in the range of 0.4 to 1.2×10^5 T.U. for 1954 and 1955. The highest of these values was from a sample taken before the Castle test series.

If one assumes that sources other than those in the United States were releasing tritium during the period 1950 to 1955, the release curve should turn upward. When similar release rates are assumed for such other tritium-producing laboratories, a value of 0.4 to 1.5×10^5 T.U. is obtained for a total of two or three of these laboratories. The tritium released in the early tests then is superimposed on a level that already has been made fairly high by 1953.

Unknown factors in the estimation of the amount of tritium released from all sources are the starting dates for the releases and the period of time over which they occurred. Also unknown is the relative rate of release from the laboratories outside the United States. The significance of accidental releases of large amounts of tritium cannot be determined. Robinson et al.[10] refer to "accidents releasing appreciable quantities of gaseous tritium." However, a given size release would have a greater significance for the T/H levels observed in hydrogen prior to 1953 than would the same amount if released at the present time. These uncertainties are probably no greater than the rather large errors in the present estimation.

The quoted value of 15 kg of tritium released during the Ivy and Castle tests is based on an estimated value for a rate of release per megaton of nuclear energy.[7] These release-rate values must depend, in a manner not well defined, on the composition of the nuclear devices exploded. It is entirely possible that the tritium level in 1953 and 1954 was due to releases by the production systems only.

At this point at least three different conclusions are possible: (1) the Ivy and Castle tests did not release significant amounts of "unburnt" tritium as HT, (2) the total tritium released in these series was actually much less than the estimated 15 kg (operating at maximum capacity, the thermal-diffusion column at Los Alamos could have produced 15 kg in the 5.5 years considered between 1949 and 1954); and (3) perhaps the production systems and the bomb test each might have released approximately equal amounts of HT.

SOURCES OF ATMOSPHERIC TRITIATED METHANE

In their description of the tritium-production system, Robinson et al.[10] show a mass-spectrum curve for the impurities observed in tritium handled in a system containing stopcocks and vacuum grease. These impurities include OH^+, H_2O^+, OT^+, T_2O^+, and CT_4^+. The statement "at somewhat lower isotopic purity a CHT_3 ion of mass 22 appears, etc." is made. An all-metal system that employed Kel-F seals was constructed to avoid these impurities. Although this did eliminate the problem of labeled hydrocarbons appearing in the tritium-production system, it did not eliminate the release of tritium-labeled molecules, particularly methane, into the atmosphere.

From the available data several requirements appear necessary for a source of tritiated methane: (1) a source in the northern troposphere, (2) a continuous injection over some period of time, and (3) an injection that has probably ceased or a rate of injection that is not large compared to the present total. It is clear that release of tritium by production laboratories would mostly have occurred in the northern hemisphere and that these production systems would have continuously injected tritium during the time of production. The rate of release of tritium from this source would have decreased when sufficient tritium was stored. Continued release of tritium and tritiated methane will occur each time the large amounts of tritium in storage are processed to recover the accumulated ^3He.

Helium-3 is recovered by condensing tritium onto charcoal and pumping off the ^3He. Charcoal adsorbs about 20 ml of hydrogen per gram at a vapor pressure of 1.3×10^{-3} atm. This is equivalent to 1 curie per liter of vacuum-line volume; therefore a significant amount of tritium may be pumped away during any processing of the stored material.

The fact that organic molecules exposed to tritium gas undergo exchange because of the ionization effects of the tritium betas was first reported[11] in 1956. Since then numerous studies that have extended this observation indicate that an important product in the self-labeling of any organic molecule containing a methyl group with tritium is tritiated methane. The preparation system at Los Alamos must have included mechanical pumping as a primary stage. Therefore all the tritium released was passed through hot pump oil on the way to the atmosphere. Under conditions of steady operation, the mechanical-pump oil would be saturated with T_2.

If oil diffusion pumps were used as boosters, additional exposure of hot organic molecules would have occurred. Unfortunately, there are no applicable data available to allow reasonable estimates of the rate of methane production from such sources. Wilzbach[12] reports incorporation of up to 1% of tritium gas per day when it is exposed to solid materials. The incorporation of T_2 dissolved in hot organic oils should occur at a rate sufficient to produce the observed tritiated-methane activity.

The rate of exchange of most gases between the northern and southern hemispheres[13] is about 0.5 per year. Although the data are not accurate enough to allow precise calculation, an estimate of the T/H ratio in methane can be made for dates earlier than those measured. For a rate as high as 0.5 per year, the T/H ratios in northern-hemisphere methane may be estimated as 2 to 4×10^3 in 1953. Methane is present[6] in the atmosphere at about 1 ppm; therefore the total tritium in methane in 1953 would have been of the order of 0.1 g. This is

less than 1% of the maximum amount of tritium estimated to have been released.

The production and release of methane in a system using oil diffusion pumps should also have produced other tritium-containing hydrocarbons such as ethane and propane. It is possible that a significant number of the molecules would contain more than one tritium atom. Continuing release of labeled molecules will void any attempt to estimate the number of atoms per molecule on the basis of an apparent mean lifetime for tritiated methane in the atmosphere.[9]

REFERENCES

1. A. E. Bainbridge, H. E. Suess, and I. Friedman, Isotopic Composition of Atmospheric Hydrogen and Methane, *Nature, 192:* 648-649 (1961).
2. V. Faltings and P. Harteck, Der Tritiumgehalt der Atmosphare, *Z. Naturforsch., 5a:* 438 (1950); see also V. Faltings and P. Harteck, The Helium-3 Problem of the Atmosphere, *Nature, 166:* 1109 (1950).
3. F. S. Rowland and E. L. Fireman, An Additional Measurement of the Tritium Content of Atmospheric Hydrogen in 1949, *J. Geophys. Res., 66:* 4321 (1961).
4. A. V. Grosse, A. D. Kirschenbaum, J. L. Kulp, and W. S. Broecker, The Natural Tritium Content of Atmospheric Hydrogen, *Phys. Rev., 93:* 250 (1954).
5. F. Begemann and I. Friedman, Tritium and Deuterium Content of Atmospheric Hydrogen, *Z. Naturforsch., 14a:* 1024-1031 (1959).
6. K. F. Bishop, H. J. Delafield, A. E. Eggleton, C. O. Peabody, and B. T. Taylor, The Tritium Content of Atmospheric Methane on Tritium in the Physical and Biological Sciences, Report STI/PUB/39, Vol. 1, pp. 55-63, International Atomic Energy Agency, 1962.
7. A. E. Martell, On the Inventory of Artificial Tritium and Its Occurrence in Atmospheric Methane, *J. Geophys. Res., 68:* 3759-3769 (1963).
8. K. F. Bishop and B. T. Taylor, Growth of the Tritium Content of Atmospheric Molecular Hydrogen, *Nature, 185:* 26-27 (1960).
9. F. Begemann, Tritium Determinations in Atmospheric Gases and Meteorites, Final Report, Report AF 61(052)-465, Max-Planck-Institut für Chemie, November 1963.
10. E. S. Robinson, A. C. Briesmeister, B. B. McInteer, and R. M. Potter, Separation of Tritium from Hydrogen by Thermal Diffusion, in Radioisotopes in Physical Sciences and Industry, Report STI/PUB/20, Vol. II, pp. 431-438, International Atomic Energy Agency, 1962.
11. R. Wolfgang, T. Pratt, and F. S. Rowland, Production of Labeled Organic Material with Accelerated Tritium, *J. Am. Chem. Soc., 78:* 5132 (1956).
12. K. E. Wilzbach, Tritium-labeling by Exposure of Organic Compounds to Tritium Gas, *J. Am. Chem. Soc., 79:* 1013 (1957).
13. C. E. Junge, Note on the Exchange Rate Between the Northern and Southern Hemispheres, *Tellus, 14:* 242 (1962).

PARTICLE ANALYSIS PROGRAM AT LAWRENCE RADIATION LABORATORY

ROBERT E. HEFT and JAMES S. KAHN
Lawrence Radiation Laboratory, Livermore, California

ABSTRACT

A program has been established for determining the distribution of individual radionuclides in particulate radioactive material. Particulate samples collected at their point of origin and selected on the basis of the degree to which they represent the true particle population are separated into groups and analyzed on a totality basis. The overall analytical program is described, and an example is given of the initial information produced in a particle-group separation performed on a filter sample from the Sedan shot.

INTRODUCTION

The Particle Analysis Program at the Lawrence Radiation Laboratory (LRL) is concerned with characterizing particulate radioactive material as a function of sedimentation rate. Particulate samples collected at their sources are separated in the laboratory into fractions corresponding to discrete sedimentation-rate intervals. Each fraction is then subjected to chemical, physical, and radioisotopic analyses to provide a complete inventory, according to particle class, of each radionuclide studied. In addition, chemical composition, size distribution, density, and crystallographic character of the particles are determined for each fraction. The data provided by this program are directly applicable to three main problem areas: fallout, particle formation, and biological availability.

Fallout

A necessary input to meteorological models of the fallout process is the distribution of the particulate material in terms of sedimentation rate, i.e., what fraction can be treated as a stable aerosol and what fractions will be deposited by sedimentation at various rates. Total beta radiation, total gamma radiation, total mass, and individual radionuclides may each be distributed differently in terms of sedimentation rate. The analytical program is designed to provide information from which the various distribution functions can be determined. If the samples from which the distribution functions are determined are representative of the true particle population, then the distribution functions can be used to deduce the absolute amount of individual radionuclides introduced into the various atmospheric reservoirs.

Particle Formation

The size, the composition, and the radionuclide distributions of particles produced by a specific nuclear shot depends upon the energy output of the shot, the mass and the chemical composition of the vaporized material, and the environment in which the shot occurs. Intercomparison of the distribution functions obtained from a series of shots occurring in similar environments can in principle be used to arrive at relations between parameters of the distribution functions and those of energy, mass, and composition of the nuclear shot. Such relations would permit the prediction of particle characteristics for specific combinations of energy, mass, and composition. The manner in which the distribution of individual radionuclides varies from element to element for a particular shot and from shot to shot as condensation conditions change should provide a valuable insight into the thermodynamics of the condensation process.

Biological Availability

In general, each radionuclide will be distributed uniquely among the particle classes, with the volatile elements tending to be concentrated in the finer particles and the more refractory elements being concentrated in the coarser particles. Biological availability of a particular radionuclide may be assessed if both its distribution among the particle groups and the chemical composition of the particles are known. The data provided by the analytical program include a spectrum of radionuclides ranging from extremely volatile to extremely refractory species.

Although the program at LRL is intended ultimately to include all forms of man-made particulate radioactivity, the initial work has been

solely with particulate radioactive debris resulting from nuclear detonations. Two reasons for selecting this problem area are that (1) such debris represents an important fraction of the total burden and (2) samples suitable for particle analysis are available. These samples are residual parts of aerial filter papers containing radioactive debris from the initial cloud from a number of nuclear-device tests. Radiochemical-analysis data on counterparts of the existing filters provide guidance concerning the representativeness of the sample; i.e., if the most volatile and most refractory radionuclides are present in the correct relative abundance, then the sample may be considered to be representative of the true particle population.

EXPERIMENTAL PROCEDURE

The overall experimental procedure can be described in terms of three main divisions: sample processing, particle separation, and analysis.

Sample Processing

The sample as received consists of a few square inches of IPC 1478 cellulose-fiber filter in which the particles are entrapped. The experimental objective is to recover the particles from the filter without altering them in any way. The method used is the so-called "low-temperature ashing method," in which oxygen gas at low pressure is passed through a radiofrequency field and over the filter sample. Under these conditions a gradual oxidation of the cellulose occurs, during which the temperature of the sample is kept below 100°C. Particles released during the oxidation of the cellulose are electrostatically attracted to the wall of the glass vial in which the ashing is conducted. Recovery is monitored by gamma counting the sample vial before and after ashing and is essentially 100%. Comparison of the gamma spectra before and after ashing indicates no change. For a permanent gamma-spectral reference, a disk is cut from the original filter sample and mounted for counting in the same configuration as the final particle samples. The remainder of the filter is ashed in a weighed vial, and the ash weight is determined.

Particle Separation

The particle-separation procedure must provide a series of particle samples in which the particles are divided into groups according to their sedimentation rates. This may be accomplished by sedimentation in a liquid medium. Large particles may be separated into

sedimentation-rate groups by gravitational settling. Small particles require centrifugation. In practice, particle samples fall into one of two classes: those in which many milligrams of particulate material are present, most particles being greater than 1 μ in size, and those in which less than a milligram of material is present, with the particles being smaller than a few microns in size. Clean separations require that the particle volume be kept low relative to the fluid volume (less than 0.5%) and that a density gradient be maintained in the sedimentation fluid. For gravitational settling the particle sample is added to the top of a 30-cm-long, 1-in.-diameter glass column (see Fig. 1). The density gradient is maintained by cooling the system from the bottom. The top of the column is sealed, and samples are collected at the base of the column. The collecting vessel is changed periodically to obtain about ten equal-mass particle fractions. During the changing process, the liquid column is held by a 16-mesh wire screen sealed across the bottom of the glass column. Each fraction is filtered through a weighed Millipore filter, weighed, and mounted for counting. Following a sedimentation period of about one day, the column is drained in sections, and the particles remaining in each section are treated as individual particle fractions. For centrifugal separation, centrifuge tubes of the type shown in Fig. 2 are used. A density gradient is established by mixing fluids of unequal density. Centrifugation speeds and times are selected to provide 10 to 12 particle fractions of approximately equal activity. Again, the column charge is maintained by a 16-mesh screen at the base of the centrifuge column. A small aliquot of each particle fraction is used to prepare a microscope slide. The remaining solution is filtered through a weighed Millipore filter with pore diameters of 0.01 μ and the filter is mounted for counting. A flow diagram of the analysis is shown in Fig. 3.

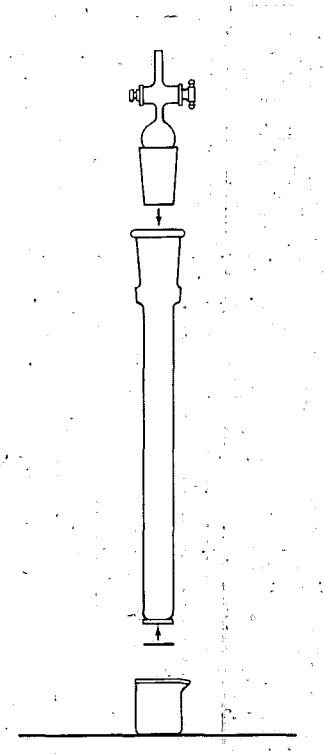

Fig. 1—Gravitational sedimentation column.

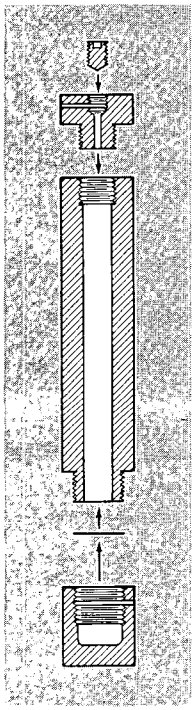

Fig. 2—Centrifugal sedimentation tube.

The original ashed filter sample is divided into five portions. One of these is mounted directly on a Millipore filter as a postashing control sample, and the remaining four are used to prepare sets of particle-fraction samples by sedimentation. The number of sedimentation runs per original sample is dictated partly by the variety of subsequent analysis requirements and partly by the need to know how the sedimentation-rate distribution varies with the density of the sedimentation fluid. Briefly, the particle-separation experimental procedure is as follows:

1. The weighed, ashed particle sample is suspended in a known volume of isobutyl alcohol. The volume used is determined by the requirement that the particle volume should not exceed 0.5% of the isobutyl alcohol volume.

2. Three 25% aliquots of the suspension are taken for sedimentation and mounted filter-sample preparation. One 5% aliquot is taken for sedimentation preparation of a set of particle samples sus-

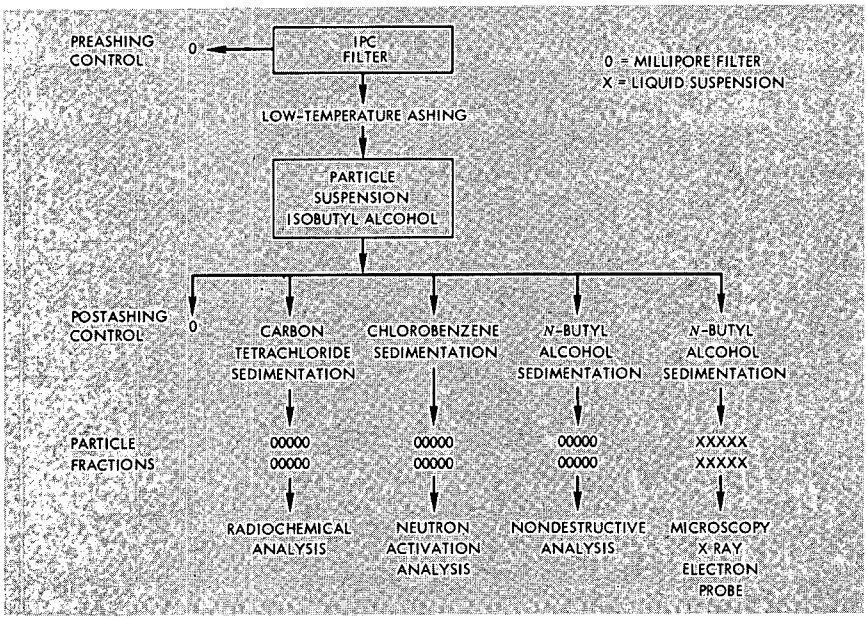

Fig. 3—Analysis flow diagram.

pended in liquid. One 5% aliquot is mounted as a control sample. During the aliquoting process, the suspension is vigorously mixed by air that bubbles through the suspension.

3. Suitable sedimentation fluids are used. These fluids are moderately viscose, have densities that exceed the density of isobutyl alcohol but are less than 2 g/cm^3, and have no solvent effect on the particles. *n*-Butyl alcohol, chlorobenzene, and carbon tetrachloride have been used.

Analysis

The four sets of particle samples produced by the sedimentation are required for four separate analytical programs. Set 1 is reserved for permanent reference and is used for nondestructive analysis, principally gamma spectrometry and X-ray fluorescence. Set 2 is committed to radiochemical analysis for those isotopic species whose half-lives and abundances combine to make them of interest but which cannot be determined by instrumental analysis. Set 3 is committed to neutron-activation analysis, first to short-term activation and gamma-spectral analysis and ultimately to long-term activation and chemical separation. Set 4 consists of particle samples suspended in an organic medium and is allocated for optical and electron-microscopic examination and to X-ray diffraction and electron-microprobe analysis.

Existing LRL analytical facilities are used when possible. Analyses such as those in sets 1 and 3, which constitute a continuing heavy workload, are made using analytical facilities provided especially for particle work.

PROGRAM STATUS

Since its inception in April 1964, the Particle Analysis Program has been engaged in procedural development in connection with the particle-separation problem and with equipment procurement in connection with the analysis problem. The ashing and sedimentation procedures previously described were developed and tested with aerial filter samples collected at other than the source. The first application of these procedures to a prime sample was in October. A portion of an aerial filter sample taken at zero + 8 min in the particulate cloud resulting from the Sedan shot was ashed and separated into sedimentation-rate fractions by using gravitational sedimentation in *n*-butyl alcohol. The distribution of mass and gross gamma activity among the particle fractions is given in Table 1. These data in themselves are insufficient to permit the calculation of the atmospheric sedimentation rate of the particle groups. They are presented only

Table 1—DISTRIBUTION OF MASS AND GROSS GAMMA ACTIVITY AMONG THE PARTICLE FRACTIONS

Particle sample	Distance fallen,* cm	Time removed,† min	Weight, mg	Cumulative weight, mg	Cumulative weight fraction, mg	Gamma activity, counts/min	Cumulative activity, counts/min	Cumulative activity fraction, counts/min
1	31.7	16.5	13.46	13.46	0.208	1736	1736	0.196
2	31.7	31.5	10.98	24.44	0.378	1386	3122	0.353
3	31.7	46.9	8.57	33.01	0.510	1105	4227	0.478
4	31.7	61.2	5.23	38.24	0.591	763	4990	0.565
5	31.7	91.5	6.73	44.97	0.695	888	5878	0.665
6	31.7	125	5.23	50.20	0.776	804	6682	0.756
7	31.7	191	4.48	54.68	0.846	710	7392	0.837
8	31.7	252	1.91	56.59	0.875	324	7716	0.873
9	31.7	310	0.81	57.40	0.888	174	7890	0.893
10	31.7	436	1.51	58.91	0.911	259	8149	0.922
11	31.7	1339	2.21	61.12	0.945	367	8516	0.964
12	15.2	1339	1.50	62.62	0.968	149	8665	0.981
13	4.8	1344	1.08	63.70	0.985	95	8760	0.992
14	<4.8	1349	0.97	64.67	1.000	75	8835	1.000

*Particles introduced onto 30.7-cm column of *n*-butyl alcohol in a 2-cm layer of isobutyl alcohol. Range for distance traveled is 30.7 to 32.7 cm. The values in this column correspond to the midpoint of the range.

†Sedimentation-rate calculations should include the column-temperature gradient: base, 4.5°C; 8 cm, 5.6°C; 16 cm, 11°C; and 32 cm, 20°C.

because they may be of some general interest. The additional information required will derive from sedimentation runs in media of different density than the *n*-butyl alcohol and on particle size measurements on the individual fractions. Although these analyses are in process, the data from them are not available at the time of this writing.

Further analyses of the Sedan particle samples to obtain distribution data on individual isotopes must await the installation and calibration of low-background high-resolution gamma–gamma and beta–gamma coincidence counting systems. The final pieces of the equipment are now being installed at the laboratory. It is expected that, by the time the counting systems are operational, a steady input of particle fractions prepared from filter samples covering a variety of events from previous years can be maintained. A substantial amount of useful data should be produced.

SIZE AND VERTICAL DISTRIBUTIONS OF STRATOSPHERIC RADIOACTIVE AEROSOLS

P. J. DREVINSKY and J. PECCI
U. S. Air Force Cambridge Research Laboratories, Bedford, Massachusetts

ABSTRACT

Four balloon flights were made over Minneapolis, Minn. (45°N 93°W), during 1962 and 1963 to collect radioactive aerosols for the determination of size and vertical distributions over the altitude range of 9 to 30 km. The sampler consisted of a two-stage impactor followed by a polystyrene microfiber filter for collecting the smallest particles. This sampler had been designed to collect particles of about 0.15 μ in radius and larger on the first stage and particles between about 0.02 and 0.15 μ in radius on the second stage on the basis of a particle density of 2 g/cm^3. With the use of four samplers during each flight, four-point profiles were obtained by collecting samples over altitude intervals of 9 to 15, 15 to 21, 21 to 27, and 27 to 30 km. All samples were measured for total beta radioactivity, ^{90}Sr, and ^{144}Ce. For the 1963 samples ^{95}Zr was also determined. With few exceptions most of the activity is carried by particles of about 0.02 to 0.15 μ in radius and shows a peak concentration at altitudes between 15 and 21 km. Limited data for total gamma activity, ^{54}Mn, and ^{140}Ba were also obtained.

INTRODUCTION

The particle size distribution of artificial radioactivity in the stratosphere is important because of its influence in causing variations in atmospheric concentrations of nuclear debris with respect to time and location and because of its role in the calibration of sampling sys-

tems for the measurement of absolute concentrations of atmospheric radioactivity. Previous impactor–filter studies have provided some results on the total beta-activity distribution[1,2] and limited data on the ^{90}Sr and ^{144}Ce distributions[2] as a function of particle size. Balloon flights were made in 1960 over Minneapolis, Minn. (45°N 93°W), and in 1961 over Hyderabad, India (17°N 79°E), and stratospheric aerosols were collected over specific altitude intervals up to about 30 km. At least 60% of the total beta activity was found to be associated with particles of 0.02 to 0.15 μ in radius up to about 27 km, and at least 60% was found on particles smaller than 0.02 μ in radius in the altitude range of 27 to 30 km. From a number of constant-level balloon flights, with each balloon having a pair of filter samplers with one operating at a different velocity from the other, and a few flights with a two-stage cascade impactor[1] at altitudes ranging from 18 to 27 km during 1959, mean particle sizes of radioactive debris were calculated on the basis of total beta activity and found to be roughly in the range of 0.02 to 0.05 μ in radius. There were, however, large variations from this range, and these values should be regarded as tentative.

Our report presents the results of the four balloon flights conducted over Minneapolis, Minn., during 1962 and 1963 for the collection of radioactive particulates specifically for the determination of size and vertical distributions of selected individual fission products over the altitude range of 9 to 30 km. This study is a continuation of the impactor–filter studies initiated earlier, which are described by Drevinsky and Martell.[2] All samples were analyzed for total beta activity, ^{90}Sr, and ^{144}Ce. The 1963 samples were also analyzed for total gamma activity, ^{54}Mn, and ^{95}Zr. Some data were obtained for ^{140}Ba in 1962 samples. Individual radionuclide concentrations and activity ratios are reported. A discussion is given of the significance of our findings with respect to the question of chemical fractionation of measured fission products in stratospheric aerosols that were collected from several days to about 240 days after a megaton-range atmospheric nuclear test. Further analysis of our data is in progress.

EXPERIMENTAL TECHNIQUES

Sampling

The balloon-borne sampling system consisted of four large-volume impactor–filter samplers, which had been designed and calibrated in cooperation with General Mills, Inc. (GMI).*[3] The system

*Now Atmospheric and Aerosol Physics Research Section, Applied Science Division, Litton Systems, Inc., St. Paul, Minn.

is designed to collect air at a flow rate of 0.7 m^3/min ambient (capacity of 28 m^3 ambient volume per sample). It is basically a scaled-up version of the impactor air sampler used by Chagnon and Junge[4,5] in studies of particle sizes of natural aerosols.

Figure 1 shows an exploded view of one impactor–filter sampler with its cylindrical housing of stainless steel. A manifold connects the

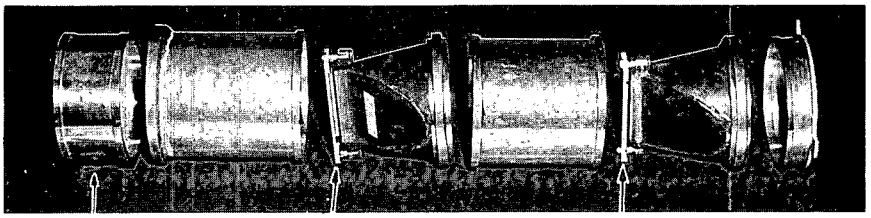

Fig. 1—Exploded view of a single impactor–filter sampler.

pumping system to four of these samplers, which are individually programed to operate successively over the altitude intervals of 9 to 15, 15 to 21, 21 to 27, and 27 to 30 km. A single balloon flight, therefore, provides a four-point vertical profile. The balloon ascent rate was about 0.15 km/min, and flights were concluded with a float at maximum altitude for about 30 min. Over each altitude interval, the operating sampler is designed to collect particles larger than 0.15 μ in radius on stage 1, particles in the range of 0.02 μ to 0.15 μ in radius on stage 2, and the smallest particles on either a 25-cm-diameter (9 to 15-km altitude interval) or a 15-cm-diameter (all other altitude intervals) polystyrene backup filter. At these particle cutoff sizes, the collection efficiency is 50% on the bases of a particle density of 2 g/cm^3 and the design flow rate. The impactor jets were individually designed and calibrated with homogeneous aerosols at midaltitude for each sampling interval. Jet dimensions were increased on samplers operating at higher altitudes to compensate for the decrease in air density, according to theoretical considerations, so that constant cutoffs could be maintained regardless of altitude. The collection surfaces on stages 1 and 2 consist of a 3.8- by 11.8- by 0.3-cm glass slide covered with pressure-sensitive cellophane tape which is coated with a thin film of high-vacuum silicone grease.

Radiochemical Analyses

Samples from stages 1 and 2 were removed from the slides by stripping off the tape, which was then mounted on Lucite semicylinders

for total beta measurement on miniature thin-wall Geiger counters whose backgrounds were about 0.2 count/min with 20-cm-steel and anticoincidence shielding.[6] Filters were measured for total beta activity on a larger Geiger counter of identical design with identical shielding with a background of about 6 counts/min. All total beta counting rates were normalized by multiplying by factors of 3.44 (miniature counter and 3.09 (large counter) to correct for geometry (G). Beta-absorption differences between the two counters were considered to be negligibly small. For total gamma measurements (0.1 to 1.0 Mev), card-mounted stages 1 and 2 samples and pelletized filters (2.5 cm in diameter by 1.3 cm in height) were placed on an 8- by 8-cm NaI(Tl) crystal located within 10 cm of lead shielding. The distance between the crystal surface and the card-mounted samples was about 0.6 cm. Filter counting rates were normalized to those of stages 1 and 2 samples by an increase of 40% to correct for geometry differences. Samples were then dissolved from the tape and the filter by digestion with aqua regia in the presence of appropriate carriers. Individual radionuclides were separated and purified by standard radiochemical procedures. All beta-activity measurements for the determination of ^{90}Sr, ^{95}Zr, ^{140}Ba, and ^{144}Ce were made on miniature Geiger counters by using the Libby thick-solid-sample technique,[7] and radionuclides were identified by either beta-particle absorption in aluminum or by decay. Corrections for counter background, geometry, self-absorption, and external absorption were made in converting counts per minute into disintegrations per minute. For ^{54}Mn measurements the 0.84-Mev gamma ray was counted, and all gamma-counting data were recorded on a multichannel analyzer. Individual radionuclide concentrations in units of disintegrations per minute per cubic meter [S.T.P. (0°C and 760 mm Hg)] were obtained by using volume data provided by GMI.

RESULTS AND GENERAL DISCUSSION

Sampling data for the impactor–filter collections for the four balloon flights are given in Table 1. Although there are slight variations, the sampling-altitude intervals will be considered to be 9 to 15, 15 to 21, 21 to 27, and 27 to 30 km, and the particle cutoff sizes will be considered to be 0.15 and 0.02 μ in radius for stages 1 and 2, respectively.

Table 2 lists our sampling dates relative to announced atmospheric nuclear tests whose fission yields were at least about 1 Mt. Time intervals between the last reported test of at least this size and our sampling dates are 132, 145, and 236 days for collections of March 1962, May 1963, and August 1963, respectively. In each of these cases,

Table 1—SAMPLING DATA FOR IMPACTOR–FILTER COLLECTIONS

Flight No.	Date	Sampling altitude interval, km	Tropopause height, km	Volume, m³		Radius* of particle cutoff size (stage 1), μ
				Ambient	S.T.P.	
2576	Mar. 16, 1962	9.1 to 14.4	10.7	25.4	6.20	0.16
		14.4 to 21.3		20.4	1.98	0.18
		21.3 to 27.4		28.2	0.954	0.12
		27.4 to 29.8		22.7	0.351	0.12
2606	Sept. 25, 1962	9.1 to 15.2	10.5	23.4	5.55	0.16
		15.2 to 21.3		22.3	2.14	0.18
		21.3 to 27.4		23.2	0.793	0.12
		27.4 to 29.6		43.1	0.646	0.12
2617	May 16, 1963	9.1 to 15.2	12.1	24.4	5.72	0.16
		15.2 to 21.3		22.6	2.21	0.20
		21.3 to 27.4		32.3	1.18	0.12
		27.4 to 29.6		31.4	0.464	0.12
2627	Aug. 15, 1963	8.4 to 15.2	11.8	14.6	3.37	0.16
		15.2 to 22.5		14.9	1.33	0.20
		22.5 to 27.9		19.8	0.700	0.12
		27.9 to 30.0		56.4	0.844	0.14

*The sampler consists of a two-stage impactor with backup filter. The radius of the particle cutoff size for stage 2 for all flights was 0.02 μ. Cutoff sizes are based on a 50% collection efficiency and a particle density of 2 g/cm³ at midaltitude for the sampling interval.

Table 2—IMPACTOR–FILTER COLLECTION DATES RELATIVE TO ANNOUNCED NUCLEAR TESTS*

Collection date	Date of most recent nuclear test	Approximate age of fresh-debris component (Δt), days
Mar. 16, 1962	Nov. 4, 1961†	132
Sept. 25, 1962	Within test series‡	Fresh
May 16, 1963	Dec. 25, 1962†	145
Aug. 15, 1963	Dec. 25, 1962†	236

*Only announced atmospheric nuclear tests[8] with fission yields greater than about 1 Mt have been considered.
†Conducted by U.S.S.R. at Novaya Zemlya (75°N 55°E).
‡The U.S.S.R. conducted about six tests in the megaton range in September 1962 prior to the collection date. Most recent test date for the U. S. Pacific tests (2°N 157°W) prior to the collection date was July 11, 1962.

the test preceding our collection was conducted by the U.S.S.R. Our collection of September 1962 is expected to contain primarily a mixture of fresh nuclear debris from the U. S. Operation Dominic series and the U.S.S.R. 1962 series. We have assumed that there is a negligibly small contribution of radioactivity to our samples from Plowshare cratering experiments and surface detonations at the Nevada Test Site during 1962.

Data for total beta and total gamma activity on the counting date and for individual radionuclide concentrations on the flight date for 1962 and 1963 collections are presented in Tables 3 and 4, respectively.

Table 3—RADIOACTIVITY DATA FOR 1962 IMPACTOR–FILTER COLLECTIONS

Sampling-altitude interval, km	Fraction	Concentration on flight date, dis/min per cubic meter (S.T.P.)			Total beta* concentration on counting date, counts/min × G/m³ (S.T.P.)
		^{144}Ce	^{90}Sr	^{140}Ba	
		Mar. 16, 1962			
9.1–14.4	Stage 1	10.3 ± 0.2	1.53 ± 0.75	<0.3	88.6 ± 0.4
	Stage 2	247 ± 3	9.59 ± 0.49	0.959 ± 0.217	1706 ± 8
	Filter	29.8 ± 0.5	1.17 ± 0.22	<2.0	401 ± 2
	Total	287 ± 3	12.3 ± 0.9	2.1 ± 1.3	2196 ± 8
14.4–21.3	Stage 1	5.30 ± 0.76	3.78 ± 1.67	<1	82.5 ± 0.4
	Stage 2	1570 ± 10	42.0 ± 4.7	27.3 ± 1.5	12800 ± 100
	Filter	262 ± 2	6.47 ± 0.29	<5.0	1750 ± 10
	Total	1840 ± 10	52.3 ± 5.0	30.3 ± 4.5	14600 ± 100
21.3–27.4	Stage 1	1.63 ± 0.42	0.53 ± 0.30		12.0 ± 0.4
	Stage 2	181 ± 3	12.8 ± 4.1	3.8 ± 2.1	1770 ± 12
	Filter	45.0 ± 0.9	24.0 ± 4.6	<24	2610 ± 15
	Total	228 ± 3	37 ± 6		4390 ± 19
27.4–29.8	Stage 1	1.6 ± 1.2	<3		6.05 ± 0.43
	Stage 2	10.0 ± 1.2	<1		34.3 ± 1.1
	Filter	8.60 ± 1.2	2.1 ± 1.0		27.2 ± 1.8
	Total	20 ± 2	4.1 ± 3.0		67.6 ± 2.2
		Sept. 25, 1962			
9.1–15.2	Stage 1	8.82 ± 0.21	0.16 ± 0.11		374 ± 2
	Stage 2	66.7 ± 0.4	2.38 ± 0.25		536 ± 4
	Filter	2.50 ± 0.19	0.13 ± 0.06		17.4 ± 0.1
	Total	78.0 ± 0.5	2.7 ± 0.3		927 ± 4
15.2–21.3	Stage 1	18.5 ± 0.5	<0.4		732 ± 5
	Stage 2	406 ± 5	13.1 ± 3.2		3850 ± 21
	Filter	174 ± 2	4.41 ± 0.77		2530 ± 10
	Total	599 ± 5	17.5 ± 3.3		7110 ± 24
21.3–27.4	Stage 1	10.5 ± 1.3	<0.6		34.3 ± 1.2
	Stage 2	21.2 ± 1.3	3.40 ± 0.13		83.8 ± 1.5
	Filter	20.0 ± 1.7	1.7 ± 1.0		39.3 ± 0.3
	Total	51.7 ± 2.5	5.1 ± 1.0		157 ± 2
27.4–29.6	Stage 1	6.43 ± 2.07	1.5 ± 1.1		0.907 ± 0.193
	Stage 2	11.5 ± 1.9	<1		14.3 ± 0.6
	Filter	6.54 ± 1.53	<1		2.83 ± 0.61
	Total	24.5 ± 3.2	2.5 ± 2.1		18.0 ± 0.9

*Beta-counting interval for the Mar. 16, 1962, collection is Apr. 1 to 16, 1962, and for the Sept. 25, 1962, collection is Oct. 9 to 25, 1962.

The assigned errors represent one standard deviation, 1 σ, in the observed net counting rates as well as an estimate of the accuracy in resolving beta-particle absorption or decay curves. Whenever observed counting rates were close to detector background levels, gross counting rates were increased by 2 σ, and upper limits were calculated. The low concentrations and small sample volumes prevented extensive ^{140}Ba analyses and, in some fractions, ^{54}Mn determinations. It can be noted from the data that the general reliability of the values for individual radionuclides increases in the order ^{140}Ba, ^{90}Sr, ^{54}Mn, ^{144}Ce, and ^{95}Zr, which is approximately the order of increasing observed activity.

Table 4—RADIOACTIVITY DATA FOR 1963 IMPACTOR–FILTER COLLECTIONS

Sampling-altitude interval, km	Fraction	Concentration on flight date, dis/min per cubic meter (S.T.P.)				Concentration on counting date	
		^{144}Ce	^{90}Sr	^{95}Zr	^{54}Mn	Total beta,* counts/min × G/m³ (S.T.P.)	Total gamma,† counts/min × G/m³ (S.T.P.)
				May 16, 1963			
9.1–15.2	Stage 1	11.4 ± 0.3	0.461 ± 0.226	9.18 ± 0.56	0.922 ± 0.273	47.8 ± 0.9	7.94 ± 0.04
	Stage 2	290 ± 4	9.69 ± 0.81	139 ± 3	33.2 ± 11.6	1170 ± 9	154 ± 1
	Filter	23.0 ± 0.4	0.756 ± 0.107	27.6 ± 0.8	2.62 ± 0.51	55.1 ± 0.9	8.67 ± 0.04
	Total	324 ± 4	10.9 ± 0.9	176 ± 3	36.7 ± 11.6	1270 ± 9	171 ± 1
15.2–21.3	Stage 1	37.9 ± 1.3	0.922 ± 0.393	43.2 ± 2.1	2.39 ± 1.39	131 ± 2	20.6 ± 0.1
	Stage 2	1130 ± 20	33.9 ± 3.0	706 ± 14	95.4 ± 4.0	4750 ± 30	663 ± 1
	Filter	211 ± 2	5.58 ± 0.33	122 ± 4		559 ± 3	
	Total	1380 ± 20	40.4 ± 3.0	871 ± 15		5440 ± 30	
21.3–27.4	Stage 1	13.4 ± 0.9	0.30 ± 0.16	18.0 ± 2.3		36.7 ± 0.3	4.77 ± 0.03
	Stage 2	306 ± 5	9.97 ± 0.69	187 ± 5	17.5 ± 1.9	1340 ± 5	173 ± 1
	Filter	189 ± 8	4.38 ± 0.38	221 ± 9	8.99 ± 1.75	551 ± 3	111 ± 1
	Total	508 ± 10	15 ± 1	426 ± 11		1930 ± 6	289 ± 1
27.4–29.6	Stage 1	59.8 ± 6.1	< 0.5	10.8 ± 3.2	141 ± 7	9.21 ± 0.68	
	Stage 2	198 ± 16	6.97 ± 2.71	31.8 ± 3.9		336 ± 7	27.7 ± 0.3
	Filter	142 ± 8	3.44 ± 1.20	112 ± 4	< 7.4	197 ± 2	30.8 ± 1.2
	Total	400 ± 19	10.4 ± 3.0	155 ± 6		542 ± 7	
				Aug. 15, 1963			
8.4–15.2	Stage 1	3.41 ± 0.41	< 0.09	1.61 ± 0.18	0.60 ± 0.56	12.3 ± 0.2	6.15 ± 0.13
	Stage 2	100 ± 2	3.68 ± 0.26	19.6 ± 0.5	8.49 ± 0.69	280 ± 2	19.9 ± 2.6
	Filter	1.46 ± 0.36	0.170 ± 0.055	4.42 ± 0.26	1.87 ± 0.70	< 9	0.459 ± 0.182
	Total	105 ± 2	3.85 ± 0.27	25.6 ± 0.6	11 ± 1	297 ± 7	26.5 ± 2.6
15.2–22.5	Stage 1	22.0 ± 0.9	< 0.3	10.8 ± 0.5		87.6 ± 1.1	5.10 ± 0.39
	Stage 2	822 ± 12	29.9 ± 3.0	230 ± 6	49.1 ± 2.8	2810 ± 22	22.7 ± 0.1
	Filter	31.9 ± 1.0	0.747 ± 0.237	7.31 ± 0.44	10.2 ± 1.4	55.8 ± 0.8	7.75 ± 0.44
	Total	876 ± 12	30.6 ± 3.0	256 ± 6		2950 ± 22	35.6 ± 0.6
22.5–27.9	Stage 1	5.21 ± 2.00	0.57 ± 0.48	1.94 ± 0.87		15.2 ± 0.4	22.3 ± 0.6
	Stage 2	266 ± 5	8.69 ± 0.62	57.4 ± 2.3	52.9 ± 5.4	877 ± 6	60.8 ± 0.6
	Filter	504 ± 3	5.72 ± 1.22	47.0 ± 1.4	125 ± 5	236 ± 1	22.2 ± 1.0
	Total	775 ± 6	15 ± 1	106 ± 3		1130 ± 6	105 ± 1
27.9–30.0	Stage 1	2.85 ± 1.27	< 0.7	3.65 ± 0.99	17.2 ± 2.3	3.11 ± 0.19	13.3 ± 0.6
	Stage 2	88.8 ± 3.3	4.60 ± 0.94	15.3 ± 1.1		239 ± 1	6.81 ± 0.60
	Filter	29.0 ± 1.7	1.18 ± 0.45	12.4 ± 0.9		47.6 ± 1.4	9.29 ± 0.80
	Total	121 ± 4	5.78 ± 1.04	31.4 ± 1.7		290 ± 2	19.4 ± 1.2

*Beta-counting interval for the May 16, 1963, collection is June 10 to 26, 1963, and for the Aug. 15, 1963, collection is Sept. 16 to Oct. 2, 1963.
†Gamma-counting interval for the May 16, 1963, collection is June 13 to July 5, 1963, and for the Aug. 15, 1963, collection is Oct. 9 to 23, 1963.
‡Total gamma obtained was between 0.10 and 1.00 Mev.

Total beta and individual radionuclide concentrations on the counting date and the flight date, respectively, for the four flights are plotted as a function of altitude in Figs. 2 to 5. Data are plotted as the midpoint of each altitude band sampled. The vertical profiles of both total concentration and concentration within each size range and the activity–size distribution are remarkably similar for all cases. Thus several general observations can be made.

Total Beta Radioactivity

Let us first consider the sum of the total beta activity values found in each of the three size fractions at each given altitude interval. The vertical profiles are nearly identical for all flights with a peak concentration in the 15- to 21-km region followed by a sharp decrease with increasing altitude. This decrease is more pronounced in the samples of 1962 than in those of 1963. The predominance of beta activity in the 15- to 21-km altitude band corresponds well with the peak in the number distribution of the natural sulfate aerosol.[9]

In the 1963 collections the total beta-activity altitude and size distributions are quite similar to those for total gamma activity (0.1 to 1.0 Mev) except for the persistence of gamma activity in particles with $r > 0.15\ \mu$ at 21 to 30 km in August 1963. The need for sensitive low-level beta-counting techniques is demonstrated particularly by the Sept. 25, 1962, flight for which observed total beta-activity results for the largest particles varied over three orders of magnitude.

Size data show that most of the total beta activity is on particles with $r < 0.15\ \mu$. Within this range the highest percentage is associated with particles of radius 0.02 to 0.15 μ. In general, less than about 5% of the total beta activity for total sample was found on particles with $r > 0.15\ \mu$. The only exceptions to this are the 27- to 30-km altitude band for the March 1962 collection (about 9%) and the September 1962 collection that showed the influence of fresh debris by varying from 5 to 40% with decreasing altitude band in this particle size range. With few exceptions all flights gave vertical distributions of total beta activity for each of the size fractions that were similar to each other and to that for the total of the combined fractions. Relatively higher levels of total beta activity, however, do persist on particles with $r < 0.02\ \mu$ in the upper two sampling intervals for the 1963 collections. Particles with $r < 0.02\ \mu$ show a peak in beta activity at 21 to 27 km in the March 1962 and August 1963 collections. It should be noted that, even if one were to correct the total beta concentrations observed for the 9- to 15-km interval by assuming that all of the activity had been sampled above the tropopause, the peak in the 15- to 21-km interval would remain in all cases except for the largest particles in the March 1962 collection.

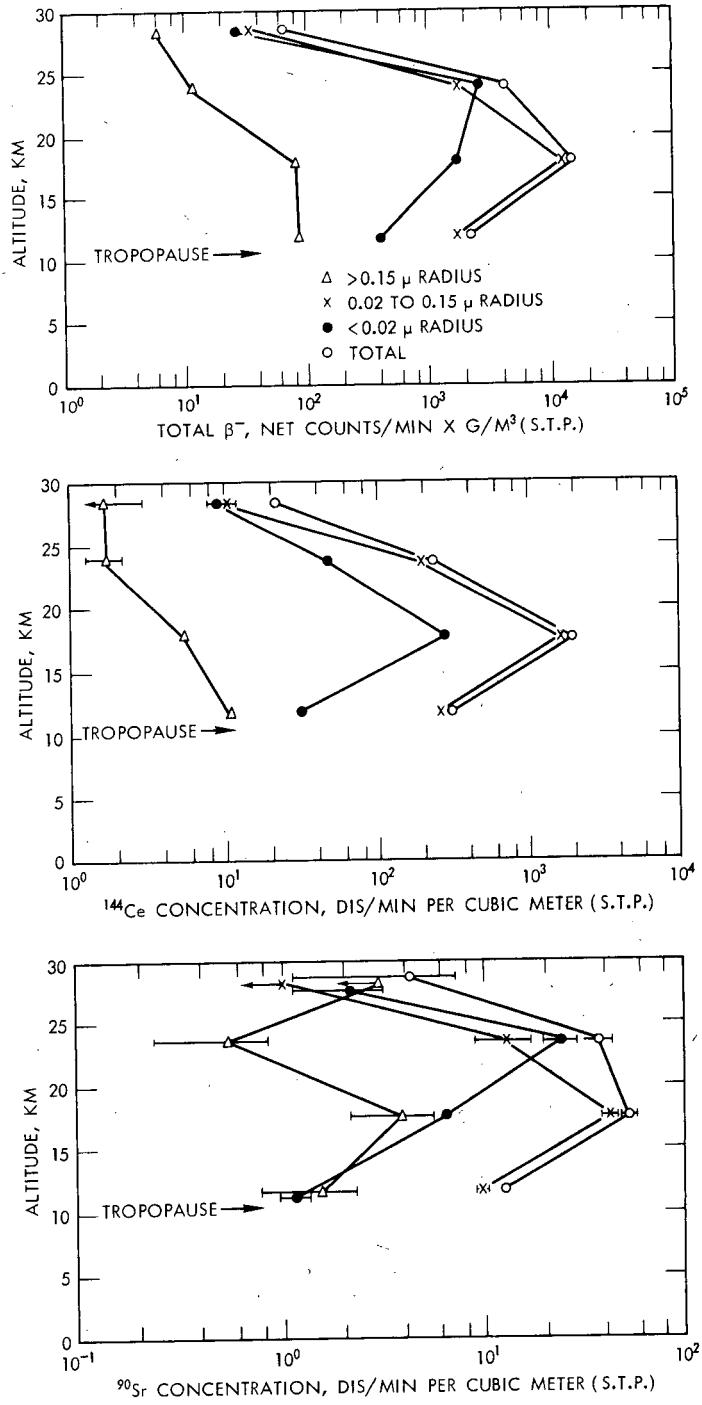

Fig. 2—Radioactivity data for impactor–filter collections over Minneapolis, Minn. (45°N 93°W), on Mar. 16, 1962.

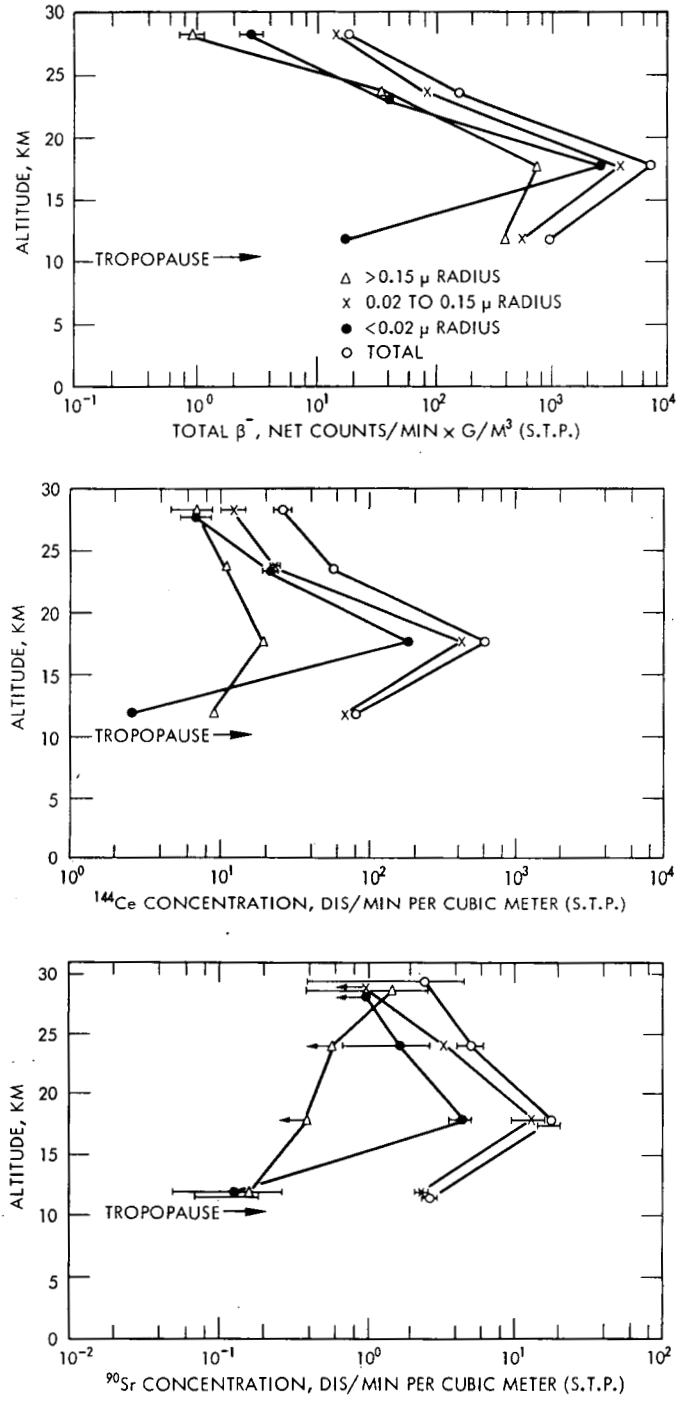

Fig. 3—Radioactivity data for impactor–filter collections over Minneapolis, Minn. (45°N 93°W), on Sept. 25, 1962.

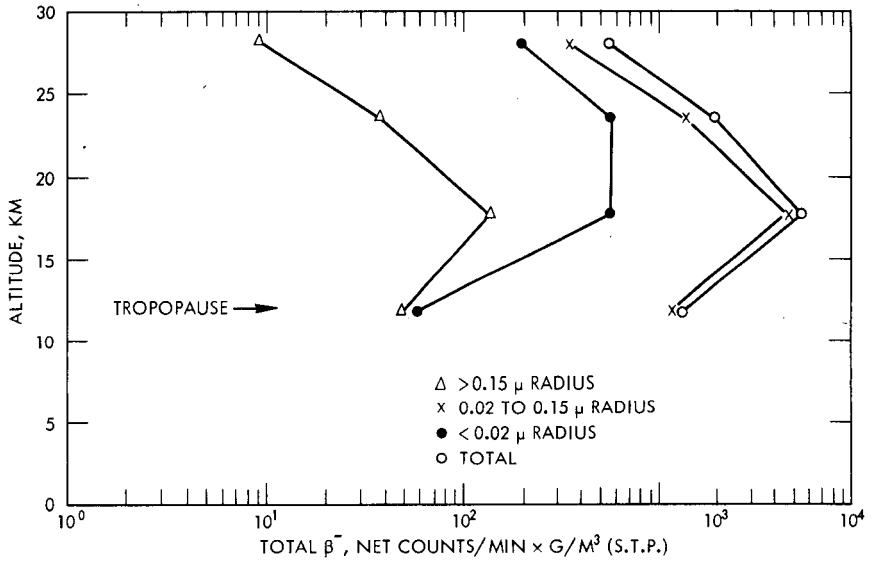

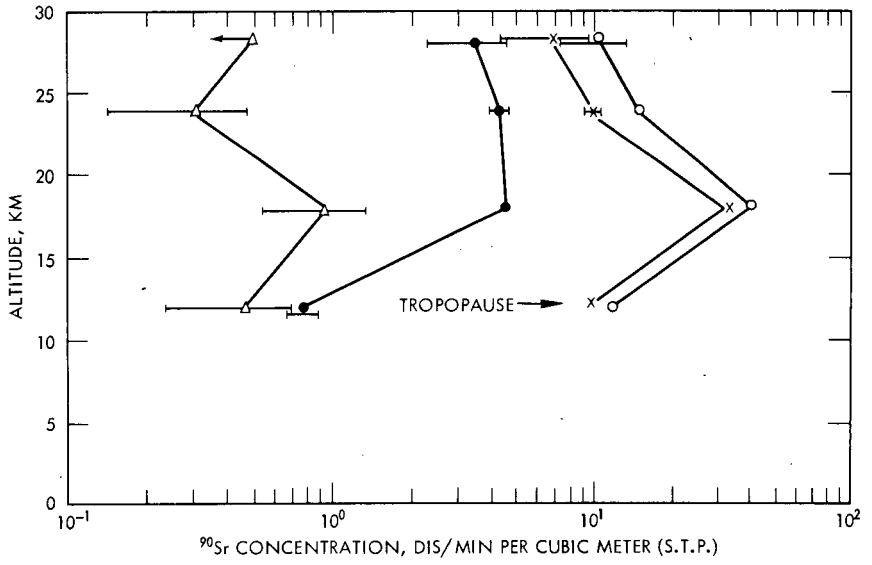

Fig. 4—Radioactivity data for impactor–filter collections over Minneapolis, Minn. (45°N 93°W), on May 16, 1963.

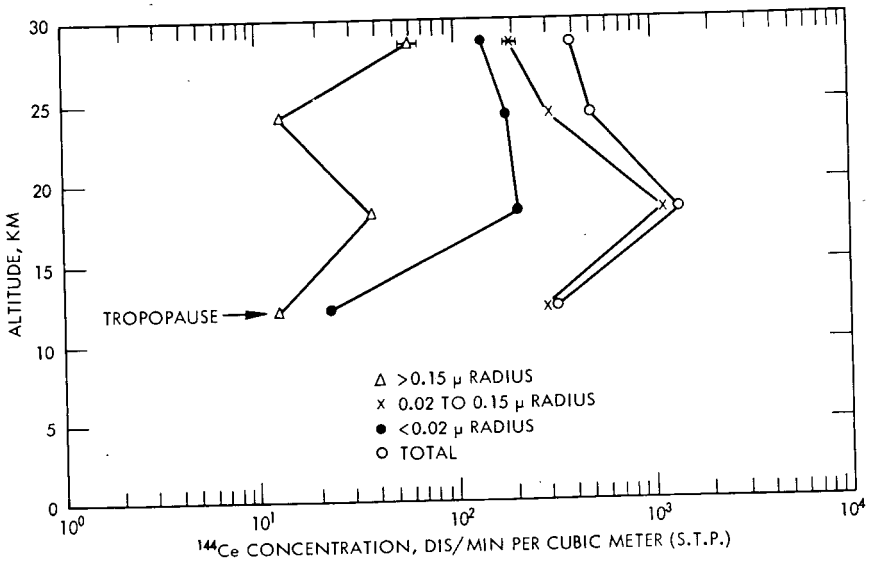

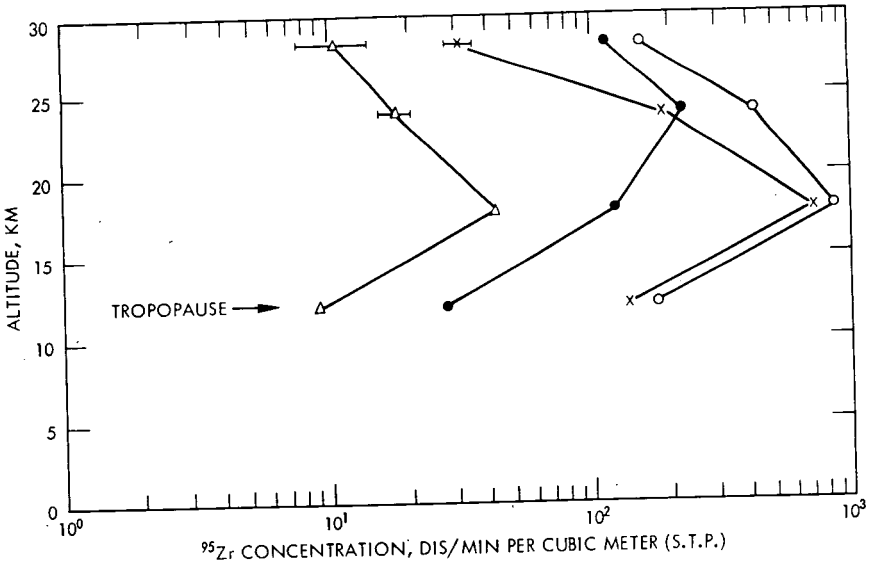

Fig. 4—(Continued)

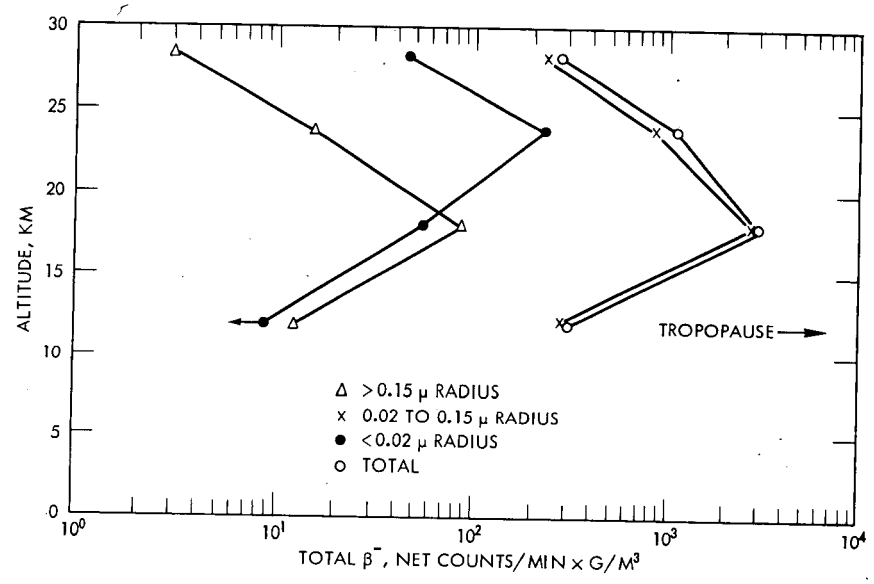

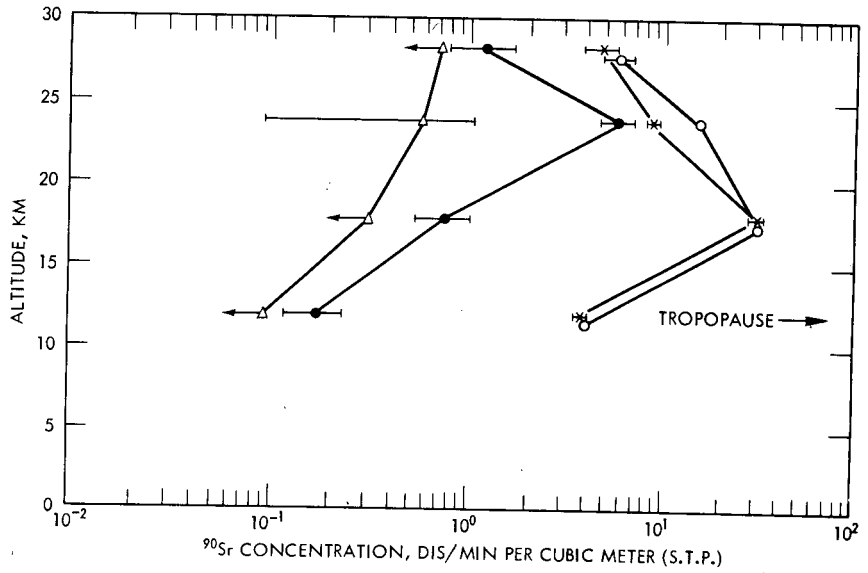

Fig. 5—Radioactivity data for impactor–filter collections over Minneapolis, Minn. (45°N 93°W), on Aug. 15, 1963.

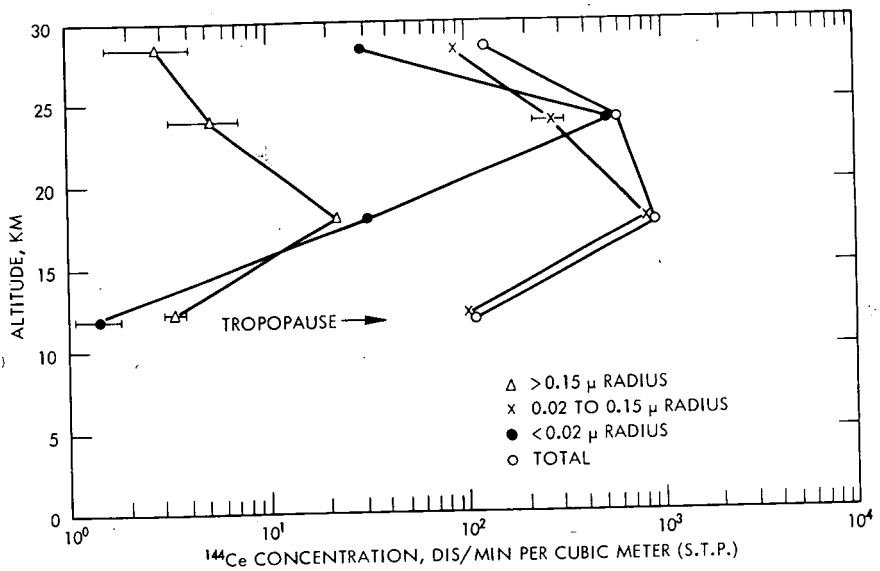

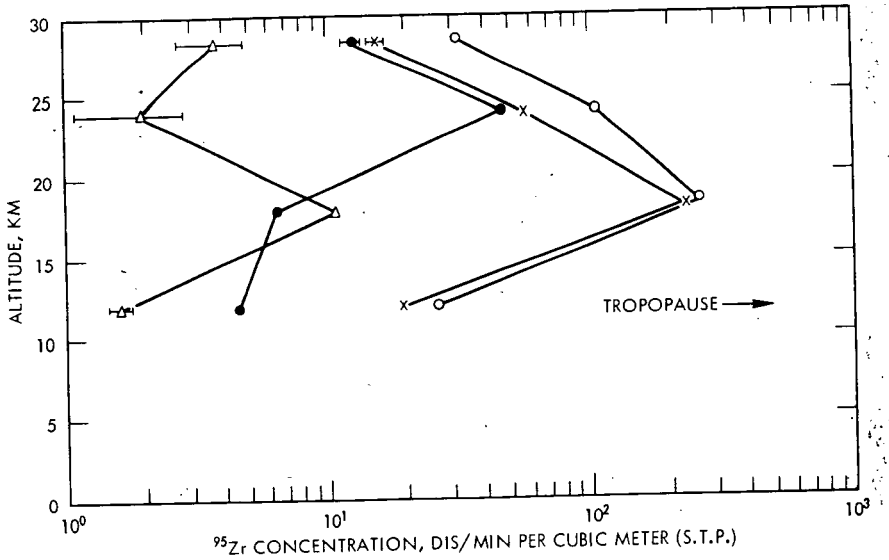

Fig. 5—(Continued)

It is of interest to compare these results with total beta-activity data from collections of June and October 1960 over Minneapolis with Δt of about 660 days. The vertical profiles[2] of total beta activity for total sample observed in 1960 showed a nearly constant concentration [about 60 net counts per minute time geometry factor per cubic meter (S.T.P.)] over the 16- to 30-km altitude region. This would be consistent with the concept of a more uniformly mixed lower stratosphere with respect to debris of this age. The concentration was higher by a factor of about 15 than that obtained for the 9- to 15-km altitude band. In general, most of the total beta activity in 1960 was on particles with $0.02\ \mu < r < 0.15\ \mu$ except for the 27- to 30-km altitude band within which most of the beta activity was associated with particles of $r < 0.02\ \mu$.

Individual Radionuclides

For each flight vertical profiles of both total concentration and concentration within each size range and the activity–size distribution for ^{144}Ce, ^{90}Sr, and ^{95}Zr are very similar to each other and to the total beta activity. There is little variation over all flights. There is a notable persistence of higher levels of radioactivity on particles with $r < 0.02\ \mu$ at 21 to 30 km in the 1963 collections; this could be because of the relatively greater influence at these levels of debris from higher altitude sources. On particles with $r < 0.02\ \mu$ at 21 to 30 km, there is a higher percentage of ^{144}Ce and ^{90}Sr in 1963 than in 1962. It should be especially noted that a large fraction of ^{95}Zr is found on the smallest of the particles in the May 1963 collection. The total concentrations of ^{144}Ce, ^{90}Sr, and ^{95}Zr which we observed at each altitude interval are in reasonably good agreement with those reported by Salter[10] for filter collections over San Angelo, Tex., during the same time periods in 1962 and 1963.

The limited data on ^{54}Mn show that most of this radionuclide is on particles with $0.02\ \mu < r < 0.15\ \mu$ with a peak concentration at 15 to 21 km in May 1963, but on particles with $r < 0.02\ \mu$ at the concentration peak of 21 to 27 km in August 1963. Data for ^{140}Ba concentrations are sparse, although most of the ^{140}Ba seems to be on particles with $0.02\ \mu < r < 0.15\ \mu$ at 15 to 21 km as shown by the March 1962 results.

It is clear that most of the ^{144}Ce and ^{90}Sr radioactivity has been found to be associated with the particle sizes $0.02\ \mu < r < 0.15\ \mu$ and $r < 0.02\ \mu$. In 13 out of 16 samplings within the altitude bands, the $^{144}Ce/^{90}Sr$ activity ratios in these two size ranges were identical within the estimated error limits, and there is little indication of chemical fractionation between these two nuclides in stratospheric nuclear debris whose age is predominantly several days to 240 days. Clearly, there is no evidence for such fractionation in the May 1963 collections.

Table 5 — RADIONUCLIDE RATIO DATA FOR 1962 IMPACTOR–FILTER COLLECTIONS

Sampling-altitude interval	Fraction	$^{144}Ce/^{90}Sr$	$^{140}Ba/^{90}Sr$	$^{140}Ba/^{144}Ce$
		Mar. 16, 1962		
9.1–14.4	Stage 1	6.74 ± 3.32	< 0.2	< 0.03
	Stage 2	25.7 ± 1.4	0.100 ± 0.023	0.00389 ± 0.00088
	Filter	25.3 ± 4.8	< 1.7	< 0.07
14.4–21.3	Stage 1	1.40 ± 0.65	< 0.3	< 0.2
	Stage 2	37.3 ± 4.2	0.650 ± 0.083	0.017 ± 0.001
	Filter	40.4 ± 1.8	< 0.78	< 0.019
21.3–27.4	Stage 1	3.1 ± 1.0		
	Stage 2	14.1 ± 4.5	0.30 ● 0.19	0.021 ± 0.011
	Filter	1.87 ± 0.36	< 1	< 0.5
27.4–29.8	Stage 1	> 0.6		
	Stage 2	> 8		
	Filter	4.2 ± 2.1		
		Sept. 25, 1962		
9.1–15.2	Stage 1	54 ± 34		
	Stage 2	28.0 ± 3.0		
	Filter	19 ± 9		
15.2–21.3	Stage 1	> 40		
	Stage 2	31.0 ± 7.7		
	Filter	39.4 ± 6.9		
21.3–27.4	Stage 1	> 20		
	Stage 2	6.24 ± 2.35		
	Filter	12 ± 7		
27.4–29.6	Stage 1	4.2 ± 3.4		
	Stage 2	> 9		
	Filter	> 5.2		

If one of the primary causes of chemical fractionation is the presence of gaseous precursors in fission-product decay chains, one might have expected fractionation between ^{144}Ce and ^{90}Sr. The mass-144 chain has no known gaseous precursors except for the extremely short-lived xenon, whereas the mass-90 chain includes 1.4-sec-bromine and 33-sec-krypton precursors. It appears, therefore, that the particle size distribution of ^{144}Ce and ^{90}Sr in debris of this age is independent of considerations of the gaseous nature of precursors.

ACTIVITY RATIOS

For the comparison of the size distributions of individual radionuclides within each given flight and over all flights, it is best to consider activity ratios. Direct insight concerning the possibility of chemical fractionation between specific radionuclides can be obtained. Tables 5 and 6 contain all activity-ratio data, corrected for radioactive decay to the flight date, obtained for the 1962 and 1963 impactor–filter

Table 6— RADIONUCLIDE RATIO DATA FOR 1963 IMPACTOR–FILTER COLLECTIONS

Sampling-altitude interval	Fraction	$^{144}Ce/^{90}Sr$	$^{95}Zr/^{90}Sr$	$^{54}Mn/^{90}Sr$	$^{144}Ce/^{54}Mn$	$^{95}Zr/^{54}Mn$	$^{95}Zr/^{144}Ce$
				May 16, 1963			
9.1–15.2	Stage 1	24.8 ± 12.3	19.9 ± 9.9	2.00 ± 1.15	12.4 ± 3.7	9.95 ± 3.02	0.805 ± 0.054
	Stage 2	30.0 ± 2.6	14.4 ± 1.5	3.42 ± 1.24	8.76 ± 3.08	4.20 ± 1.48	0.479 ± 0.012
	Filter	30.4 ± 4.4	36.5 ± 5.3	8.40 ± 0.84	8.76 ± 1.73	10.5 ± 2.1	1.20 ± 0.04
15.2–21.3	Stage 1	40.9 ± 17.9	46.9 ± 20.7	2.59 ± 1.89	15.8 ± 3.0	18.1 ± 10.6	1.14 ± 0.07
	Stage 2	33.1 ± 3.0	20.8 ± 1.9	2.82 ± 0.27	11.8 ± 0.5	7.40 ± 0.34	0.625 ± 0.017
	Filter	37.7 ± 2.2	21.9 ± 1.5				0.578 ± 0.020
21.3–27.4	Stage 1	45 ± 25	60 ± 34				1.34 ± 0.19
	Stage 2	30.8 ± 2.2	18.7 ± 1.4	1.76 ± 0.23	17.5 ± 2.0	10.7 ± 1.2	0.611 ± 0.019
	Filter	43.1 ± 4.3	50.3 ± 4.9	2.05 ± 0.44	21.0 ± 4.2	24.5 ± 4.9	1.17 ± 0.07
27.4–29.6	Stage 1	> 100	> 20	> 300	0.422 ± 0.049	0.0766 ± 0.0231	0.181 ± 0.057
	Stage 2	28.3 ± 11.2	4.55 ± 1.86				0.161 ± 0.023
	Filter	41.3 ± 14.8	32.7 ± 11.6	< 2.2	> 19	> 15	0.789 ± 0.053
				Aug. 15, 1963			
8.4–15.2	Stage 1	> 40	> 20	> 7	5.62 ± 5.28	2.6 ± 2.4	0.471 ± 0.079
	Stage 2	27.1 ± 2.0	5.31 ± 0.40	2.30 ± 0.25	11.8 ± 1.0	2.31 ± 0.20	0.195 ± 0.006
	Filter	8.60 ± 3.49	26.0 ± 8.6	11.0 ± 5.5	0.782 ± 0.351	2.37 ± 0.90	3.03 ± 0.76
15.2–22.5	Stage 1	> 70	> 30				0.490 ± 0.031
	Stage 2	27.5 ± 2.8	7.68 ± 0.80	1.64 ± 0.19	16.8 ± 1.0	4.68 ± 0.29	0.279 ± 0.007
	Filter	42.7 ± 13.7	9.79 ± 3.18	13.6 ± 4.7	3.14 ± 0.45	0.720 ± 0.110	0.229 ± 0.016
22.5–27.9	Stage 1	9.2 ± 8.6	3.4 ± 2.9				0.372 ± 0.221
	Stage 2	30.6 ± 0.2	6.61 ± 0.54	6.09 ± 0.76	5.02 ± 0.52	1.09 ± 0.12	0.217 ± 0.009
	Filter	88.1 ± 18.7	8.22 ± 1.77	21.8 ± 4.7	4.04 ± 0.17	0.376 ± 0.019	0.0932 ± 0.0027
27.9–30.0	Stage 1	> 4	> 5	> 30	0.166 ± 0.078	0.213 ± 0.065	1.28 ± 0.67
	Stage 2	19.3 ± 4.1	3.33 ± 0.73				0.172 ± 0.012
	Filter	24.5 ± 9.5	10.5 ± 4.1				0.425 ± 0.033

collections. The errors in these ratios are based on a 1 σ counting error and the estimated error in the decay-curve resolution as mentioned earlier. Data for ^{144}Ce, ^{90}Sr, and ^{95}Zr are the most complete and will be considered in detail. Figure 6 depicts $^{144}Ce/^{90}Sr$ activity ratios as a function of particle size and altitude as observed for the 1962 collections, and Figs. 7 and 8 show $^{144}Ce/^{90}Sr$, $^{95}Zr/^{90}Sr$, and $^{95}Zr/^{144}Ce$ activity ratios from the 1963 collections. It should be noted that the respective production ratios estimated from the data of Katcoff[11] are approximately 40, 220, and 4.8.

$^{144}Ce/^{90}Sr$ Activity Ratios

For the March 1962 collection (see Fig. 6), approximately 130 days after the most recent atmospheric nuclear test with a fission yield greater than about 1 Mt, there appears to be a wide variation in ^{144}Ce and ^{90}Sr distributions with particle size. Within the altitude bands at 9 to 15 and 15 to 21 km, however, the $^{144}Ce/^{90}Sr$ activity ratio is constant among particles with $0.02\ \mu < r < 0.15\ \mu$ and $r < 0.02\ \mu$. With the exception of a relatively high ^{90}Sr concentration in the 27- to 30-km altitude band, these two particle size ranges contained about 90% of the ^{144}Ce and ^{90}Sr activities observed in the March 1962 collections.

We find a more systematic pattern in the ^{144}Ce and ^{90}Sr distributions with particle size for the September 1962 collection (see Fig. 6), which was made during a period of nuclear testing. Although the errors in the $^{144}Ce/^{90}Sr$ activity ratios are admittedly large because of the low ^{90}Sr concentrations encountered, the observed variation in size distribution of ^{144}Ce and ^{90}Sr at each altitude band is never greater than about a factor of 2. One is tempted to conclude that, within the estimated accuracy of the observed ratios, there is no chemical fractionation between ^{144}Ce and ^{90}Sr in this collection. There is a slight tendency, however, toward enrichment of ^{144}Ce, relative to ^{90}Sr, in the largest particles in the 9- to 27-km altitude region. Also, the $^{144}Ce/^{90}Sr$ ratios in September are about a factor of 10 higher than those observed in March 1962. Both of these observations support the fact that relatively fresh debris was collected in September 1962. The decrease in $^{144}Ce/^{90}Sr$ activity ratios with increasing altitude is probably a result of the continuing influence of older debris at 21 to 30 km.

In Fig. 7 a most striking result is observed in the plot of $^{144}Ce/^{90}Sr$ activity ratios as a function of particle size and altitude for the May 1963 collection when Δt is equal to about 150 days. With the exception of only the largest size fraction at the highest altitude sampled, which showed a very low ^{90}Sr concentration, the ^{144}Ce and ^{90}Sr are distributed in an identical manner among the three particle size ranges. Less than 5% of the total ^{144}Ce and ^{90}Sr collected within each of the four altitude bands for this flight is found on particles with $r > 0.15\ \mu$. Also,

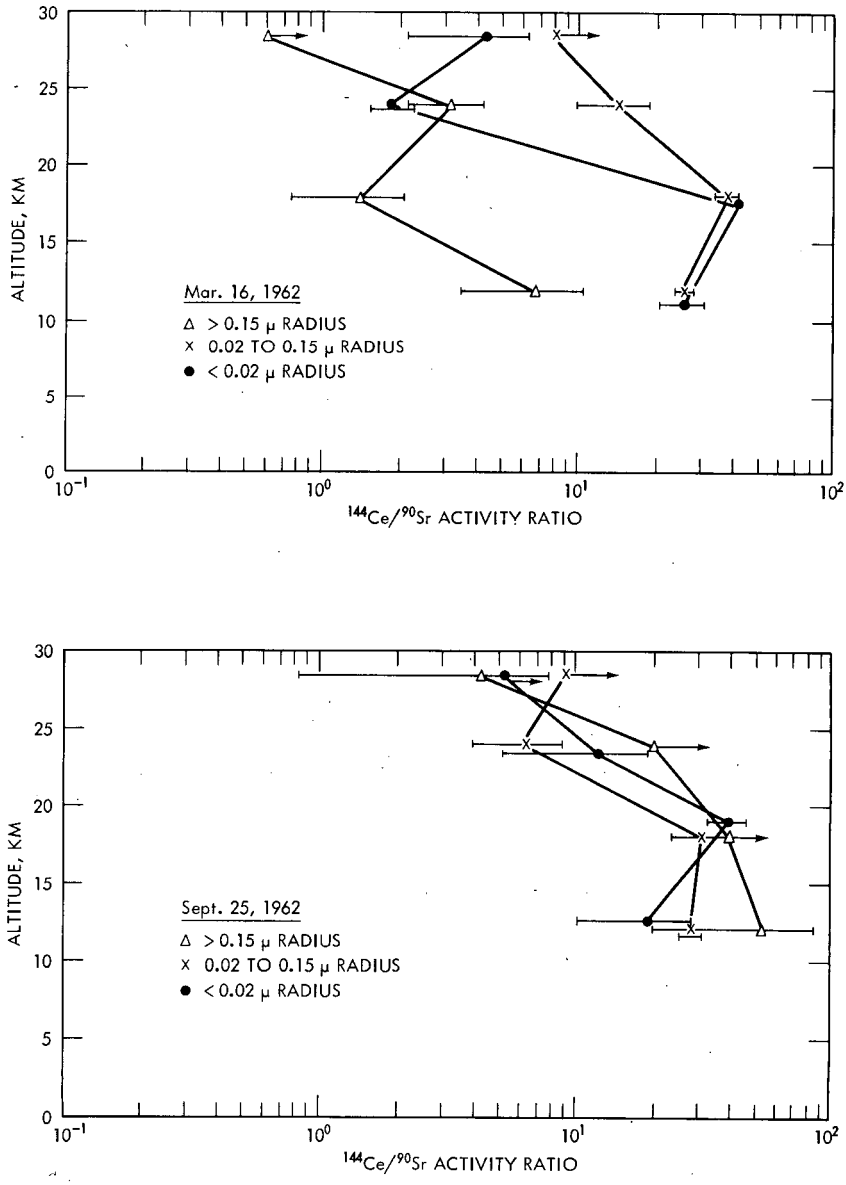

Fig. 6—$^{144}Ce/^{90}Sr$ activity ratios for impactor–filter collections over Minneapolis, Minn. (45°N 93°W), on Mar. 16 and Sept. 25, 1962.

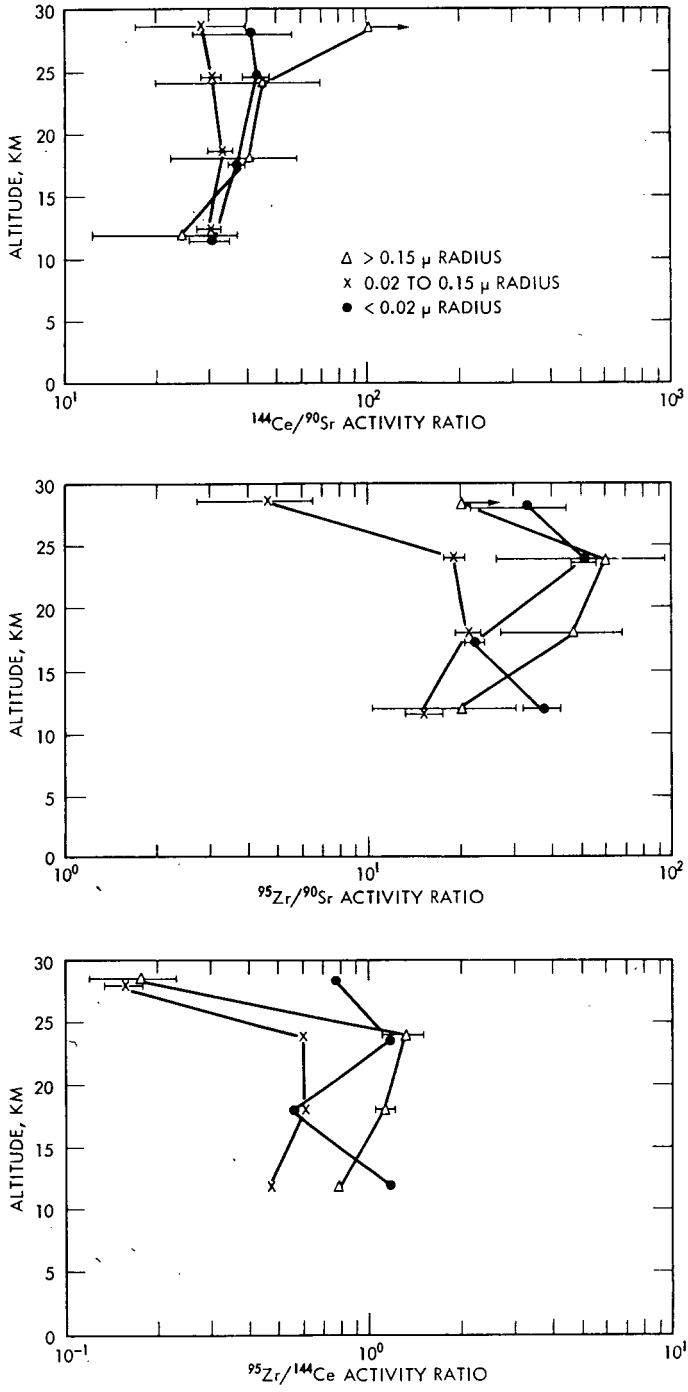

Fig. 7—Activity ratios for impactor–filter collections over Minneapolis, Minn. (45°N 93°W), on May 16, 1963.

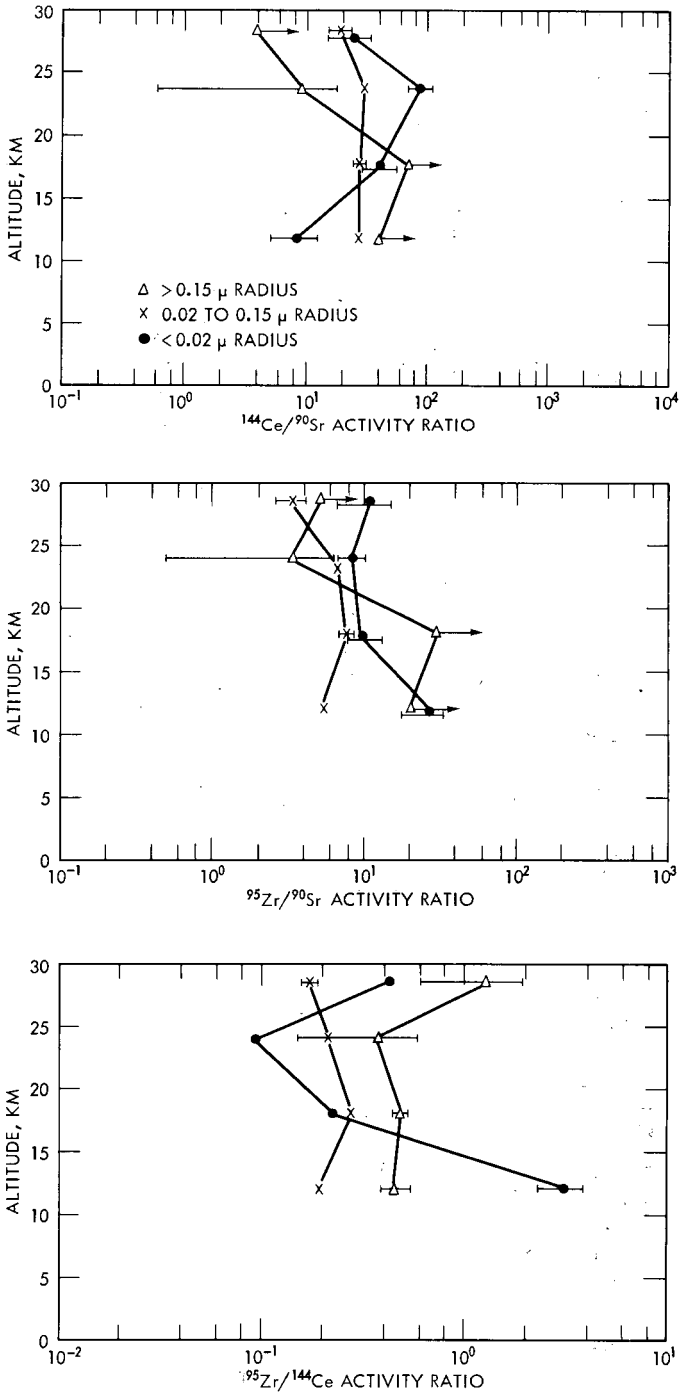

Fig. 8—Activity ratios for impactor–filter collections over Minneapolis, Minn. (45°N 93°W), on Aug. 15, 1963.

the activity ratio shows very little altitudinal variation, having an average value of about 35.

In Fig. 8 the $^{144}Ce/^{90}Sr$ activity-ratio data are plotted for the August 1963 collection when Δt is about 240 days. If one disregards the three ratios with upper limits and the abnormally high activity ratio for $r < 0.02\ \mu$ particles at 21 to 27 km, an average activity ratio of about 25 is obtained for this collection. When this value is corrected for radioactive decay to the May 1963 collection, the result is consistent with the average $^{144}Ce/^{90}Sr$ activity ratio observed for that collection. Again, less than 5% of the total ^{144}Ce and ^{90}Sr collected within each altitude band in August 1963 is on particles with $r > 0.15\ \mu$. It is concluded that these data also show that the two nuclides are unfractionated. The need for larger volume samples became apparent, particularly in this flight, because of the very low ^{90}Sr concentrations encountered.

$^{95}Zr/^{90}Sr$ Activity Ratios

In Figs. 7 and 8, $^{95}Zr/^{90}Sr$ activity ratios are plotted as a function of size and altitude for the May and August 1963 collections, respectively. The general pattern appears to be less systematic than that shown by the $^{144}Ce/^{90}Sr$ activity-ratio data with the possible exception of some of the August 1963 results. The ^{95}Zr and ^{90}Sr distributions among the particle size ranges $0.02\ \mu < r < 0.15\ \mu$ and $r < 0.02\ \mu$ appear to be identical in three of four cases for this collection. One can say little with respect to the question of chemical fractionation of ^{95}Zr relative to ^{90}Sr on the basis of $^{95}Zr/^{90}Sr$ activity ratios alone except that there are large fluctuations in the size distribution as a function of altitude. For example, see Fig. 7, which depicts the May 1963 data. If ^{144}Ce and ^{90}Sr are not fractionated in this collection, then the variable $^{95}Zr/^{90}Sr$ activity suggests the occurrence of fractionation between ^{95}Zr and ^{90}Sr. In Fig. 8 $^{144}Ce/^{90}Sr$ activity ratios for the three uppermost sampling intervals for August 1963 suggest an identical distribution of these nuclides between the size ranges $0.02\ \mu < r < 0.15\ \mu$ and $r < 0.02\ \mu$. The same result is obtained for ^{95}Zr and ^{90}Sr for this collection. As observed for ^{90}Sr, at least 90% of the ^{95}Zr is found on particles with $r < 0.15\ \mu$.

The most striking result derived from the May and August 1963 data for ^{95}Zr is that, for particles with $r < 0.15\ \mu$, the smaller particles ($r < 0.02\ \mu$) appear to be the more highly enriched in ^{95}Zr relative to ^{90}Sr. This is the case throughout the 9- to 30-km region for both flights. On an activity basis, this effect has its greatest influence on the 21- to 30-km altitude region within which these smallest particles carry from about 40 to 70% of the total ^{95}Zr and 20 to 40% of the total ^{90}Sr. Data for the 9- to 21-km altitude region show that only about 5 to 15% of the ^{95}Zr and ^{90}Sr is associated with the smallest particles.

The average $^{95}Zr/^{90}Sr$ activity ratios for $r < 0.02\ \mu$ particles over all altitudes in the May and August 1963 collections are about 35 and 14, respectively. The corresponding average $^{95}Zr/^{90}Sr$ activity ratios for $0.02\ \mu < r < 0.15\ \mu$ particles, excluding the 27- to 30-km collection of May 1963, are 18 and 6. The ratio in both particle size ranges has decreased in accord with the 65-day half-life of ^{95}Zr.

$^{95}Zr/^{144}Ce$ Activity Ratios

In Figs. 7 and 8, $^{95}Zr/^{144}Ce$ activity ratios are also plotted as a function of size and altitude for the collections of May and August 1963, respectively. One advantage of considering this ratio is that it is thought to be more accurate than those involving ^{90}Sr, whose sample concentrations were frequently very low and difficult to measure. Another advantage is that the ratio should be less sensitive to older debris than $^{144}Ce/^{90}Sr$ and $^{95}Zr/^{90}Sr$ activity ratios.

There is little similarity in the trends of the $^{95}Zr/^{144}Ce$ and $^{144}Ce/^{90}Sr$ activity ratios with size. Our data suggest that there is chemical fractionation between ^{95}Zr and ^{144}Ce although additional data would be helpful.

The smallest amount (about 10% or less) of the total ^{95}Zr and ^{144}Ce is carried by particles with $r > 0.15\ \mu$, and the largest amount is generally carried by particles with $0.02\ \mu < r < 0.15\ \mu$. It is notable that the altitudinal variations of $^{95}Zr/^{144}Ce$ activity ratios for these two size ranges are nearly identical. The same ratio for the smallest particles, however, is highly variable with altitude.

Activity Ratios Involving ^{54}Mn and ^{140}Ba

Since data for ^{54}Mn and ^{140}Ba were far less complete than for the ^{90}Sr, ^{95}Zr, and ^{144}Ce, the concentrations and the activity-ratio data are merely listed in Tables 3 to 6. As mentioned earlier, we can only say from the March 1962 collection that most of the ^{140}Ba appears to be carried on particles with $0.02\ \mu < r < 0.15\ \mu$ and that there seems to be a peak concentration in the 15- to 21-km band. The ^{54}Mn concentrations for the May and August 1963 collections also show this same general behavior although the largest particles in May seem to contain an unusually high amount.

A comparison of the three activity ratios involving ^{54}Mn (see Table 6) indicates that its size distribution is quite variable relative to ^{90}Sr, ^{95}Zr, and ^{144}Ce. There seems to be closer agreement in the May and August 1963 collections in the 9- to 27-km region between the $^{144}Ce/^{54}Mn$ activity ratio and particle size, however, and it is possible that these two nuclides have more similar distributions in debris of this age.

SUMMARY AND CONCLUSIONS

From this study altitude and size distributions have been obtained primarily for total beta activity and the fission products ^{90}Sr, ^{95}Zr, and ^{144}Ce. The 9- to 30-km altitude range over Minneapolis, Minn. (45°N 93°W), has been sampled with a balloon-borne inpactor–filter sampler that collected particles in three size ranges with radius, r, of approximately $r > 0.15\ \mu$, $0.02\ \mu < r < 0.15\ \mu$, and $r < 0.02\ \mu$. Collections were made on Mar. 16 and Sept. 25, 1962, and on May 16 and Aug. 15, 1963; these samplings contained primarily nuclear debris that was from several days to about 240 days old.

The altitude distributions of the total activity (beta activity, ^{90}Sr, ^{95}Zr, or ^{144}Ce) within each altitude interval sampled in all four flights show a peak concentration in the 15- to 21-km band. This is consistent with the broad maximum at 18 to 23 km in the number concentration of worldwide natural aerosols in the stratosphere and the peak in the number distribution of the natural sulfate aerosol.[9]

In the majority of cases at least 90% of the measured radioactivity was carried by particles with $r < 0.15\ \mu$. Within this general size range, most of the radioactivity was found on particles with $0.02\ \mu < r < 0.15\ \mu$, a range which is at the lower end of particle sizes observed for stratospheric natural aerosols.[9] The influence of relatively fresh debris was evidenced in the September 1962 results by the presence of a higher percentage of radioactivity on particles with $r > 0.15\ \mu$ compared to the March 1962 data. The general trends shown by the vertical profiles of total beta activity, ^{90}Sr, ^{95}Zr, and ^{144}Ce within each given size range are quite similar to each other and to the total radioactivity. In the May and August 1963 collections, a surprisingly large amount (about 50 to 70%) of the ^{95}Zr was found on particles with $r < 0.02\ \mu$ in the 21- to 30-km altitude region. These were the only collections which were analyzed for ^{95}Zr.

Our findings from activity-ratio data for the three particle size ranges studied may be summarized as follows: First, there is no chemical fractionation between ^{90}Sr and ^{144}Ce in debris of several days to 240 days old; i.e., the $^{144}Ce/^{90}Sr$ activity ratios are constant as a function of particle size range. Second, on the basis of the ^{95}Zr, ^{90}Sr, and ^{144}Ce results, it is impossible to make a conclusive statement about the possible occurrence of chemical fractionation of ^{95}Zr relative to ^{90}Sr and ^{144}Ce in debris of this age. The $^{95}Zr/^{90}Sr$ activity ratios in May 1963 are extremely variable with particle size range; but for August 1963 the size ranges that contain most of these nuclides exhibit constant ratios in the 15- to 30-km region. The $^{95}Zr/^{144}Ce$ activity ratios observed in both May and August fluctuate widely as a function of size range.

In this paper we have presented our basic data. Further study is necessary for a better understanding of the worldwide stratospheric radioactivity relation with particle size. A more detailed analysis of these data from the viewpoint of aerosol dynamics is required. A sampler that would provide larger volume collections with emphasis on obtaining increased resolution within the size range $r < 0.15\,\mu$ and operate reliably, especially at altitudes higher than 30 km, would contribute immeasurably to this study.

ACKNOWLEDGMENTS

We are grateful to Miss Anahid Thomasian for the radiochemical analysis of ^{54}Mn and J. V. Nikula for all gamma-activity measurements. Thanks are due to M. I. Kalkstein for helpful discussions.

REFERENCES

1. J. Baumstark, L. Graf, I. Hall, S. Jones, J. Nash, R. Olson, S. Stern, L. Torgeson, and W. Zeller, Upper Atmosphere Monitoring Program, Report No. 2039, General Mills, Inc., June 1, 1960; and R. C. Wood et al., Upper Atmosphere Monitoring Program, Report No. 2109, General Mills, Inc., Sept. 15, 1960.
2. P. J. Drevinsky and E. A. Martell, Preliminary Results on the Size and Vertical Distributions of Residual Nuclear Debris in the Stratosphere, in Radioactive Fallout from Nuclear Weapons Tests, A. W. Klement, Jr.(Ed.), USAEC Report TID-7632, pp. 170-187, February 1962.
3. H. W. Zeller, Balloon-borne Particulate Fractionator, Report No. 1922, Final Report, General Mills, Inc., Feb. 1, 1960.
4. M. I. Kalkstein, P. J. Drevinsky, E. A. Martell, C. W. Chagnon, J. E. Manson, and C. E. Junge, Natural Aerosols and Nuclear Debris Studies, Report AFCRC-TN-59-627, Air Force Cambridge Research Center, November 1959.
5. C. W. Chagnon and C. E. Junge, The Vertical Distribution of Sub-micron Particles in the Stratosphere, *J. Meteorol., 18*: 746-752 (1961).
6. E. A. Martell, The Chicago Sunshine Method, USAEC Report AECU-3262, Enrico Fermi Institute for Nuclear Studies, University of Chicago, May 1956.
7. W. F. Libby, Absolute Assay of Beta Radioactivity in Thick Solids, *Anal. Chem., 27*: 921-927 (1955); and Simple Absolute Measurement Technique for Beta Radioactivity, *Anal. Chem., 29*: 1566-1570 (1957).
8. U. S. Weather Bureau, Announced Nuclear Detonations 1945-1962, in Fallout Program, Quarterly Summary Report, USAEC Report HASL-142, pp. 218-239, Health and Safety Laboratory, Jan. 1, 1964.
9. C. E. Junge, C. W. Chagnon, and J. E. Manson, A World-wide Stratospheric Aerosol Layer, *Science, 133*: 1478-1479 (1961); and C. E. Junge and J. E. Manson, Stratospheric Aerosol Studies, *J. Geophys. Research, 66*: 2163-2182 (1961).
10. L. P. Salter, High Altitude Balloon Sampling Program, in Fallout Program, Quarterly Summary Report, USAEC Report HASL-140, pp. 166-214, Oct. 1, 1963, and USAEC Report HASL-144, pp. 184-219, Apr. 1, 1964, Health and Safety Laboratory.
11. S. Katcoff, Fission-product Yields from U, Th, and Pu, *Nucleonics, 16*(4): 78-85 (1958).

FALLOUT MEASUREMENTS BY TOTAL-ABSORPTION GAMMA-RAY SPECTROSCOPY

ROBERT S. FOOTE
Texas Instruments Incorporated, Dallas, Texas

ABSTRACT

The growth and the decay of gamma-ray-producing radionuclides in the field near Dallas, Tex., have been measured since Dec. 22, 1962. All data have been resolved to provide the effective surface amounts of the fission-produced radionuclides as well as the natural gamma-ray emitters. A discussion of the data-reduction procedure is included which shows the capability of the method to account for the entire field gamma-ray spectrum. Initial fallout measurements of fission debris from the 1964 test by Communist China are included.

METHODS AND MEASUREMENTS

Gamma-ray-producing radionuclides in the field near Dallas, Tex., have been determined and monitored by the use of gamma-ray spectroscopy since Dec. 22, 1962. The objectives of these measurements have been (1) to demonstrate the exactness and consistency with which gamma-ray spectral data can be resolved from field data, (2) to optimize data-handling techniques, and (3) to follow the change of nuclear fallout debris in the field.

A large, near-total gamma-ray-absorption NaI(Tl) crystal that is $11\frac{1}{2}$ in. in diameter and 4 in. thick and multichannel pulse-height-analysis equipment consisting of a 400-channel analyzer operating in the 200-channel mode have been used to measure the gamma-ray energy spectrum of the terrestrial gamma radiation. A 40-min multichannel pulse-height-analyzer live time was the counting-time period

for data accumulation. Each counting period was followed by data readout on punched paper tape and initiation of the subsequent counting period. All data were tape-to-card converted and supplied to a computer for reduction. The field-instrumentation enclosure with its detector pod is shown in Fig. 1. An example of the change in time of the

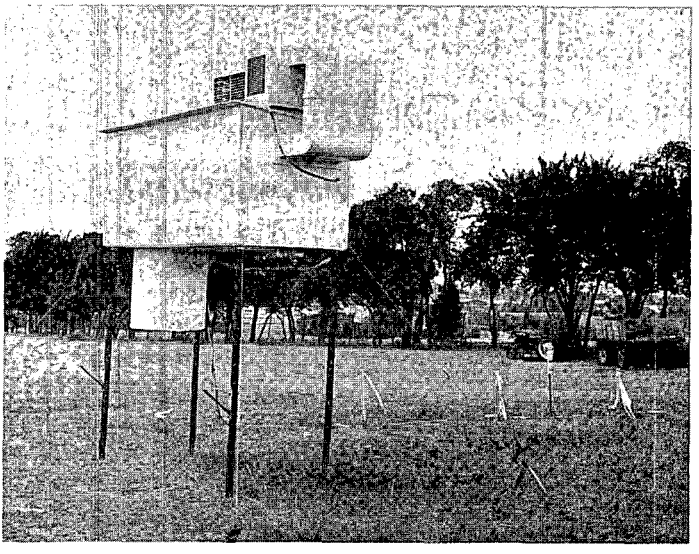

Fig. 1—Field instrumentation for total-absorption gamma-ray spectrometer.

field gamma-ray energy spectral shape caused from decay of surface nuclear fallout is given in Fig. 2.

Proper and adequate methods of data reduction must then be utilized to determine what radionuclides provide the gamma radiation of which the field spectrum is composed. The precise energy spectral calibration standard of each radionuclide composing the field gamma-ray spectrum must be determined. The optimum computer method for the determination of the amounts of each radionuclide must be resolved on the basis of the computer time requirement and results. Energy calibration of all spectral data is required. The radionuclides that create the most intense gamma-ray energy lines can initially be located. The selection of two energy lines such as the 2.615-Mev line from ^{208}Tl and a line of lesser energy, preferably of low energy, allows energy calibration to a high degree of accuracy and consistency.[1] There are many ways of locating the photopeak energy positions. Texas Instruments' method of locating is indicated in Fig. 3, where the sides of a near-Gaussian-shaped curve are matched by two straight lines; the

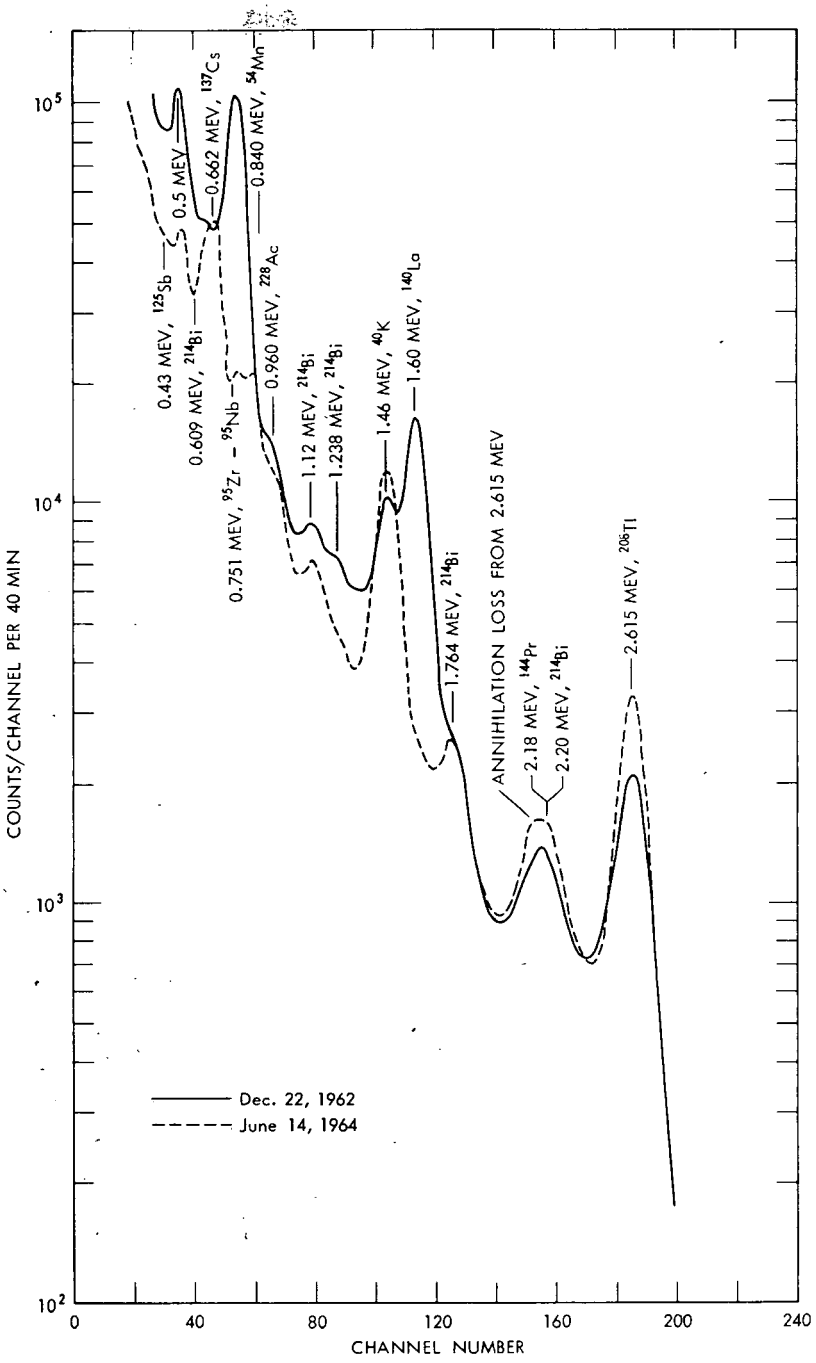

Fig. 2—Gamma-ray field spectra on Dec. 22, 1962, and June 14, 1964.

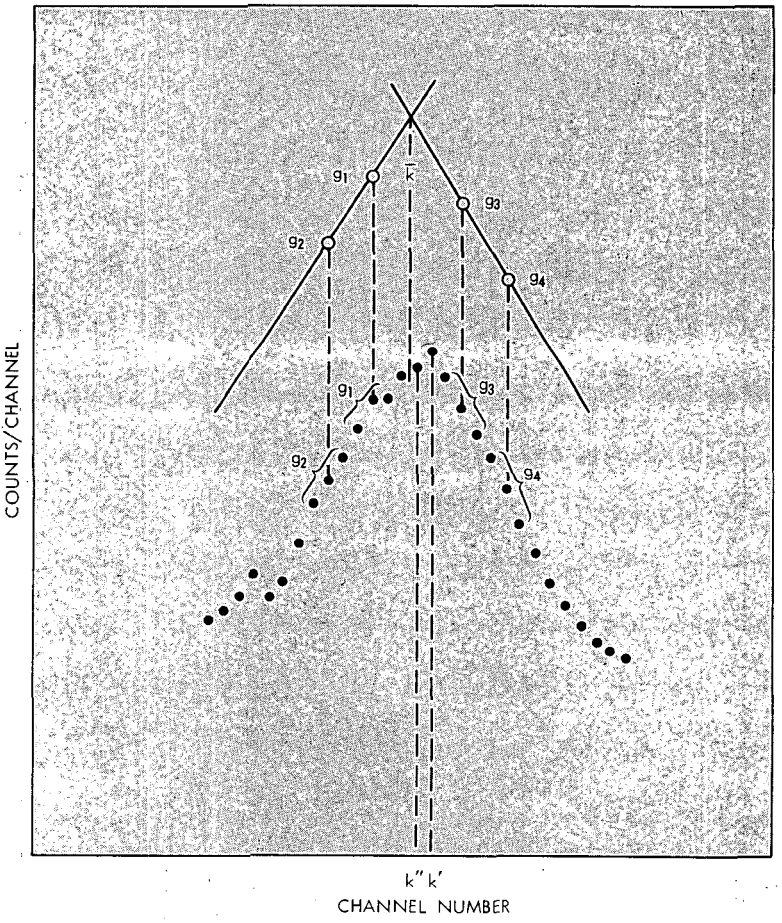

Fig. 3—Method of locating photopeak positions. k', maximum count channel; k", photopeak center, even-channel location; and $\bar{k}$, computed photopeak, center location.

solution for their intersection is assumed to be the peak location. This manner of peak locating has proved to require little computer time and is consistent to about ±0.2 channel at channel 185. The lower energy line selected has varied, depending upon the intensity of energy lines that might overlap others. The 0.751-Mev line from $^{95}Zr-^{95}Nb$ was used initially because of the superposition of the ^{140}La line at 1.60 Mev overlapping the ^{40}K line at 1.46 Mev.

After calibration using two photopeaks, the total spectrum is corrected, channel by channel, to be even-channel-corrected for precise energy calibration. If noncorrected field data were utilized, errors would result for ^{214}Bi, as shown in Fig. 4. This figure shows the loca-

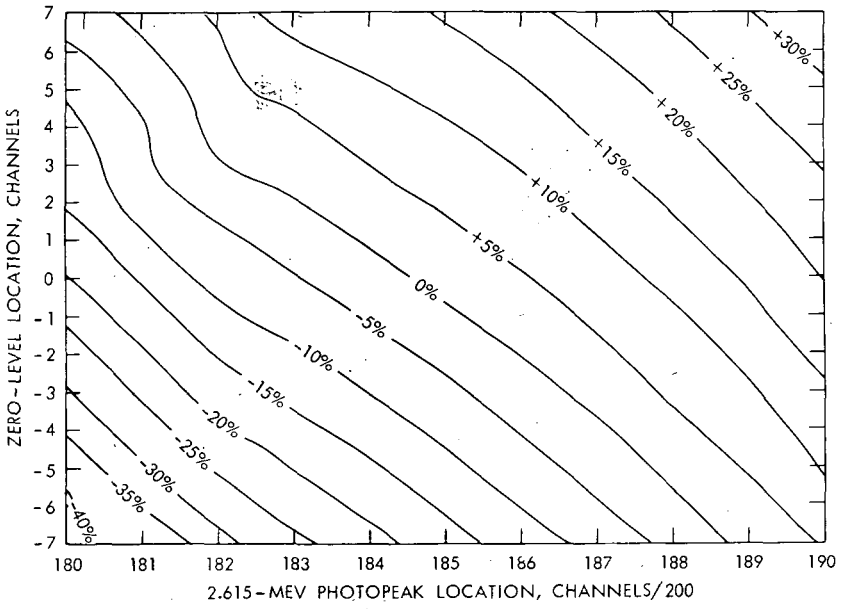

Fig. 4—Bismuth-214 matrix output error as a function of zero level and ^{208}Tl photopeak location.

tion of the ^{208}Tl peak at channel 184.5 and the zero-energy position at channel 0 for perfect calibration and the errors created by improper calibration of the average field spectrum for the matrix amounts of ^{214}Bi. Figure 5 shows the errors introduced in the ^{140}La amounts present in May 1963. The radionuclides initially detected to be present on Dec. 22, 1962, were ^{208}Tl, $^{144}Ce-^{144}Pr$, $^{140}Ba-^{140}La$, ^{40}K, $^{95}Zr-^{95}Nb$, ^{137}Cs, ^{54}Mn, ^{125}Sb, ^{131}I, and an unknown cluster providing lines of about 0.5 Mev. A recent study has attempted to determine the sources that create the energy line at 0.5 Mev.

Calibrations were obtained for each noncoincident gamma source in close geometry with the use of a large tank of sand contaminated with the desired radioactive source. For those sources providing the coincident gamma radiation, a solution containing the source was spread and watered into the ground over a large detector solid angle on the ground surface. With all input calibrations then known, the amounts of each input relative to the calibration amounts were determined by matrix-reduction techniques. These amounts were determined for each gamma-ray-producing radionuclide for each 40-min spectrum and plotted as a function of time in units of months. A typical period is shown in Fig. 6, which shows $^{95}Zr-^{95}Nb$ amounts.

Rainfall modulates the measured amounts of all inputs to a high degree. Figure 7 shows the measured amounts of ^{214}Bi found to be pres-

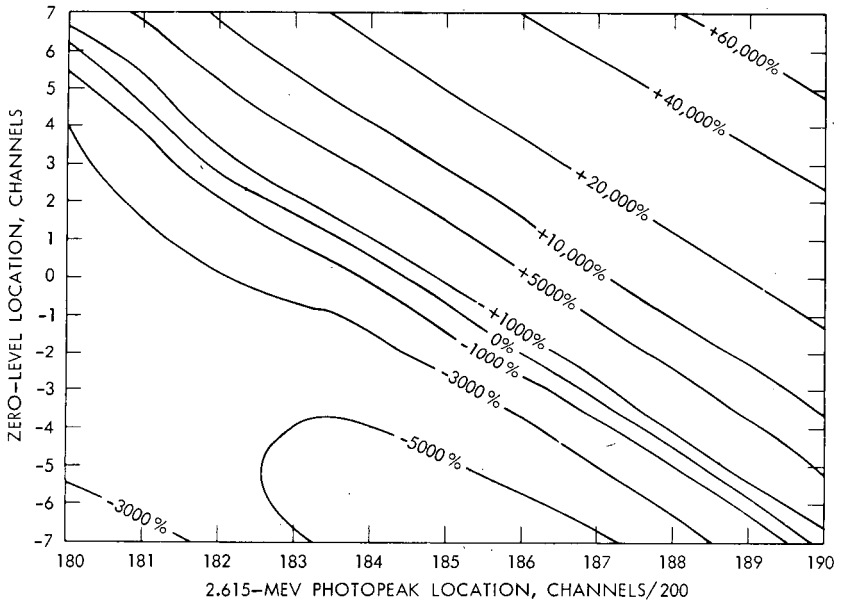

Fig. 5—Lanthanum-140 matrix output error as a function of zero level and ^{208}Tl photopeak location.

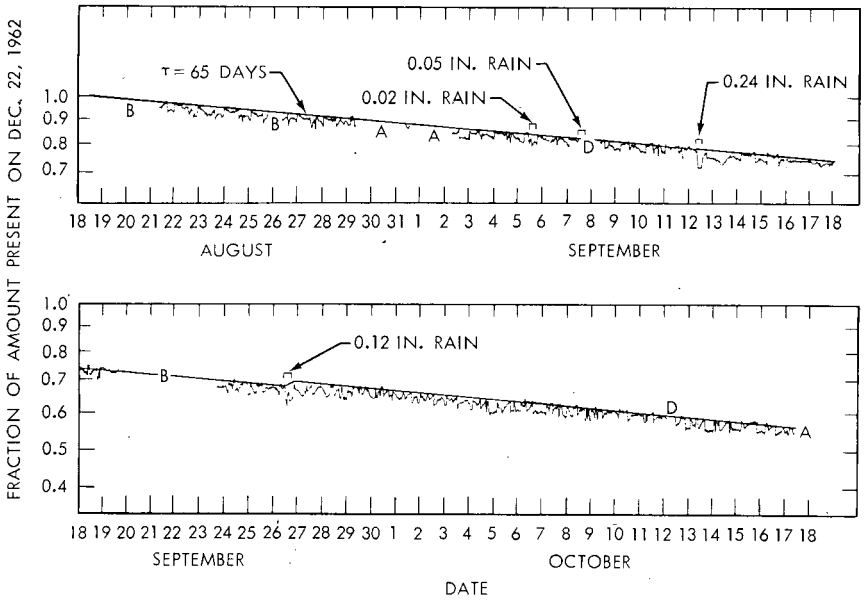

Fig. 6—Zirconium-95–niobium-95 effective surface amounts as a function of time, 1963.

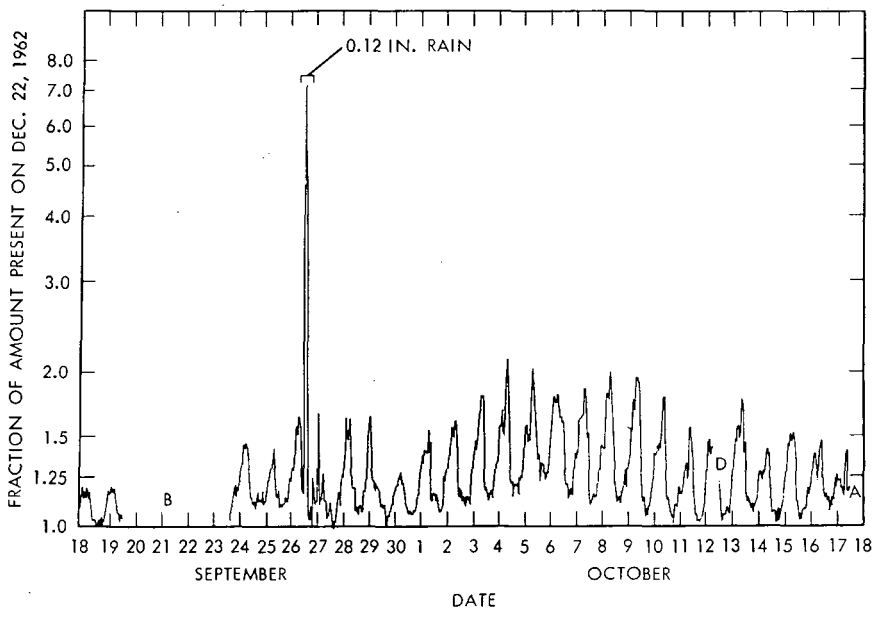

Fig. 7—Bismuth-214 effective surface amounts as a function of time, 1963.

ent in September and October 1963. The similar period for 1964 is shown in Fig. 8. The modulation of some of the measured radionuclides by an 8-in. snow cover in January 1964 is seen in Fig. 9. Initially, ^{125}Sb and ^{54}Mn were not observed to be in the gamma-ray spectrum, but as the amount of $^{95}Zr-^{95}Nb$ diminished, these nuclides were observed in the residual amounts left after the attempt to account for all the gamma spectrum. If it is assumed that all gamma-ray inputs have been accounted for and that proper calibrations for each source in the field geometry are available, then, by multiplication of each calibration spectrum by the amounts of each determined to exist and addition of all these amounts channel by channel, the original field spectrum should be obtained. How well the reduction technique accounted for the initial field spectrum is determined by subtracting the created spectrum from the original field spectrum. The residual spectrum should be zero. A residual spectrum for current data is shown in Fig. 10. The nuclides ^{208}Tl, ^{144}Pr, ^{214}Bi, ^{140}La, ^{40}K, ^{54}Mn, $^{95}Zr-^{95}Nb$, ^{137}Cs, ^{125}Sb, and ^{131}I, and the 0.5 Mev radiation have been accounted for. However, neither ^{140}La nor ^{131}I existed. The reduction should provide ^{140}La and ^{131}I to be zero if the accounting is proper. Near-zero residual spectral amounts remain when an 11 by 11 inverted matrix is used for reduction. If only the amounts of all gamma emitters creating energy lines, including the ^{137}Cs, are removed, the residue of Fig. 11 exists. Here the 0.43- and

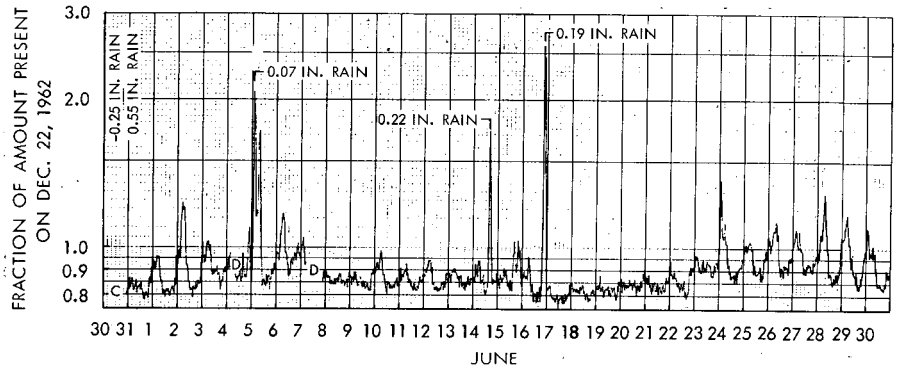

Fig. 8—Bismuth-214 effective surface amounts as a function of time, 1964.

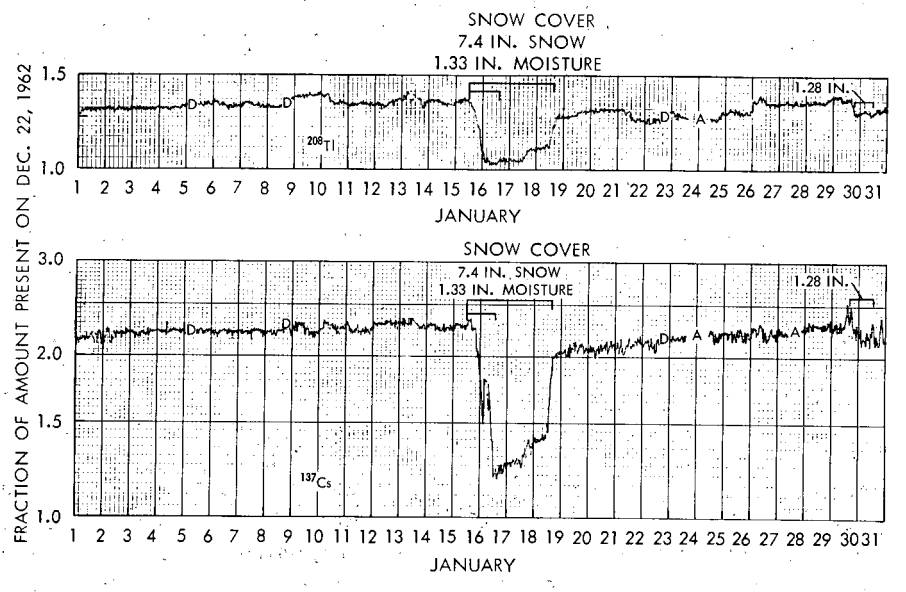

Fig. 9—Thallium-208 and cesium-137 effective surface amounts as a function of time, 1964.

0.60-Mev photopeaks of ^{125}Sb appear. The ^{125}Sb field calibration standard is shown in Fig. 12. The removal of ^{125}Sb amounts from the data of Fig. 9 leaves the photopeak at 0.51 Mev, as shown in Fig. 13. At this point it is difficult to determine the balance of inputs where ^{103}Ru, ^{106}Rh, and annihilation radiation may exist in large or small amounts. Figure 14 indicates the field spectral shapes for ^{103}Ru, ^{106}Rh, and annihilation radiation.

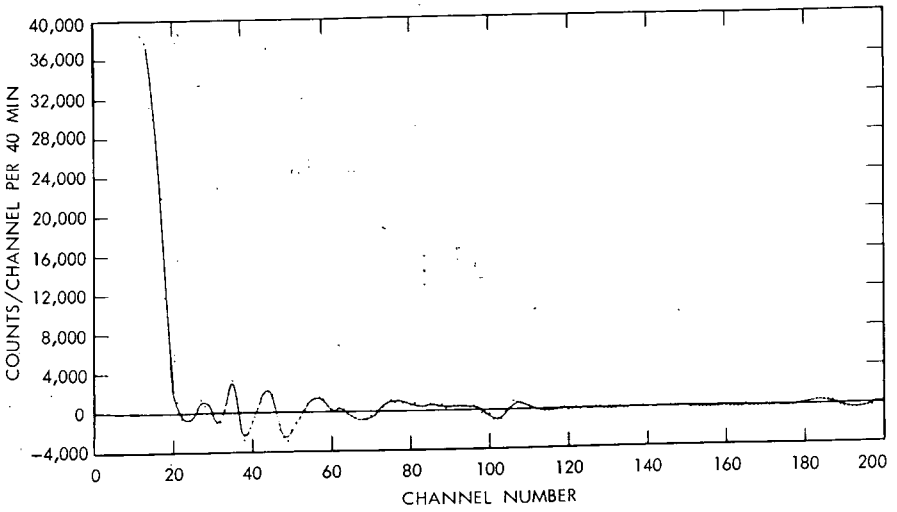

Fig. 10—Residual gamma-ray spectrum, June 28, 1964.

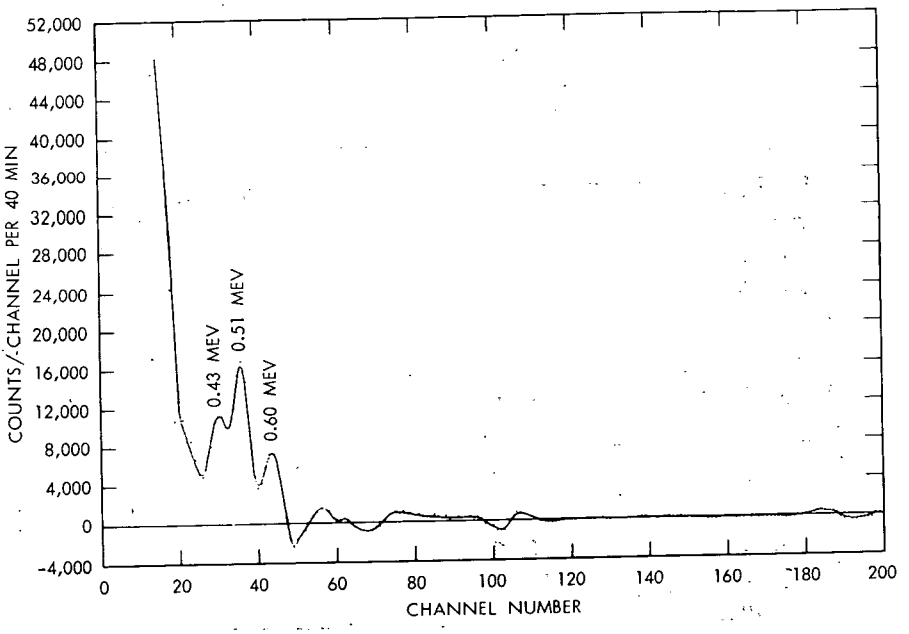

Fig. 11—Residual gamma-ray spectrum after removal of ^{208}Tl, ^{144}Pr, ^{214}Bi, ^{40}K, ^{54}Mn, $^{95}Zr-^{95}Nb$, and ^{137}Cs, June 28, 1964.

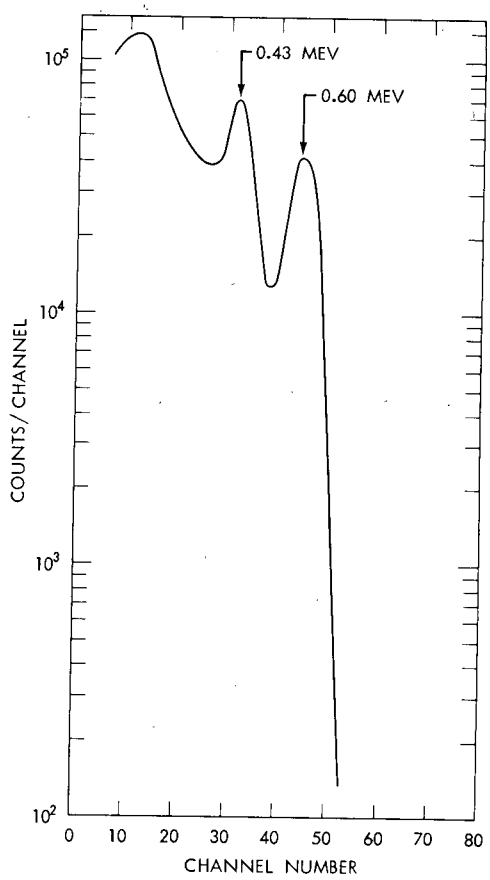

Fig. 12—Field gamma-ray calibration spectrum for ^{125}Sb.

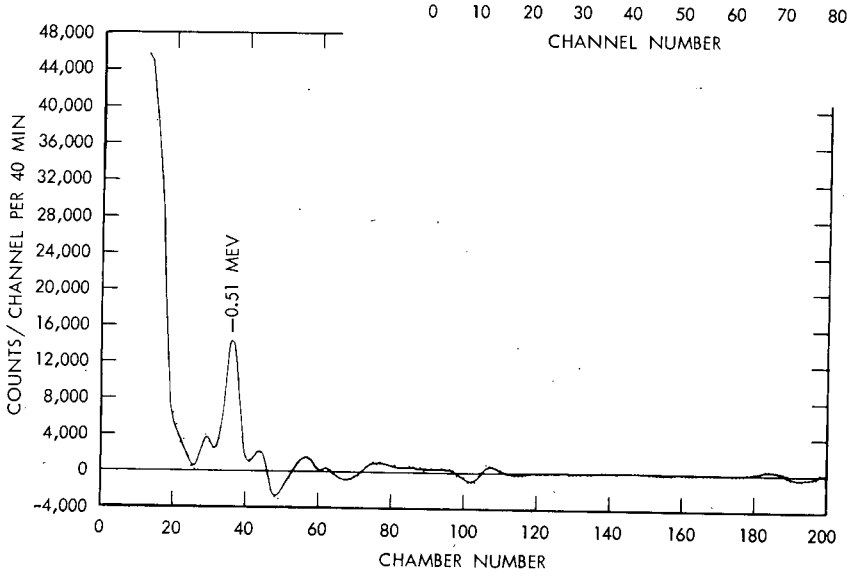

Fig. 13—Residual gamma-ray spectrum after removal of ^{208}Tl, ^{144}Pr, ^{214}Bi, ^{40}K, ^{54}Mn, $^{95}Zr-^{95}Nb$, ^{137}Cs, and ^{125}Sb, June 28, 1964.

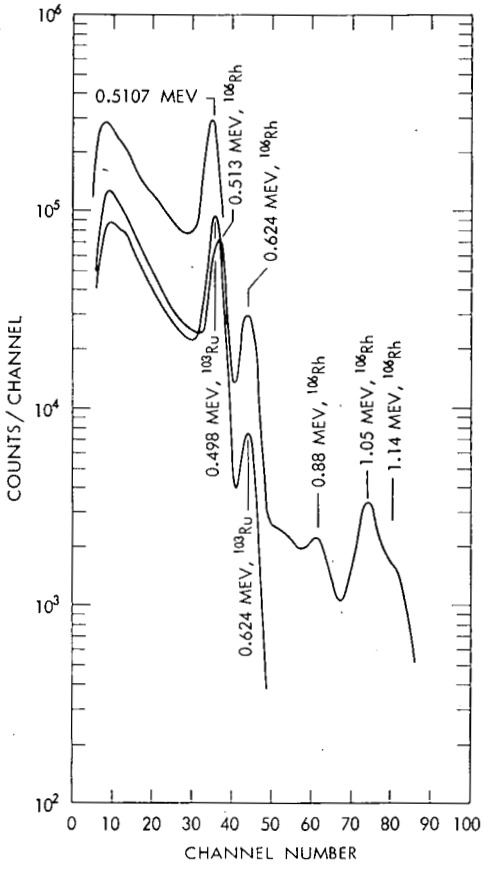

Fig. 14—Field gamma-ray spectra for annihilation radiation, ^{103}Ru, and ^{106}Rh.

The single spectrum per day results for each major fallout radiation contributor are shown in Figs. 15 to 19. Figure 15 shows the amounts of ^{144}Pr from December 1962 to July 1964. The decrease from decay and the increase from fallout are seen. Similarly, Fig. 16 shows ^{140}La and the capability of the method to resolve zero amounts. Figure 17 shows the ^{54}Mn amounts that built up to a maximum in March 1964. Figure 18 represents the $^{95}Zr-^{95}Nb$ amounts, and Fig. 19 represents the ^{137}Cs amounts. The gamma-ray energy at 0.662 Mev is sufficiently low that many factors cause the amounts measured to vary. Soil moisture is a large factor. The long half-life of ^{137}Cs allows time for the radionuclides to penetrate more deeply into the soils, and the effective source is one similar to ^{40}K, one of an infinite slab. Also, errors both in energy calibration for each spectrum and in the individual source calibrations can create errors, especially when there are very large amounts of the adjacent overlapping data from decay of $^{95}Zr-^{95}Nb$. The

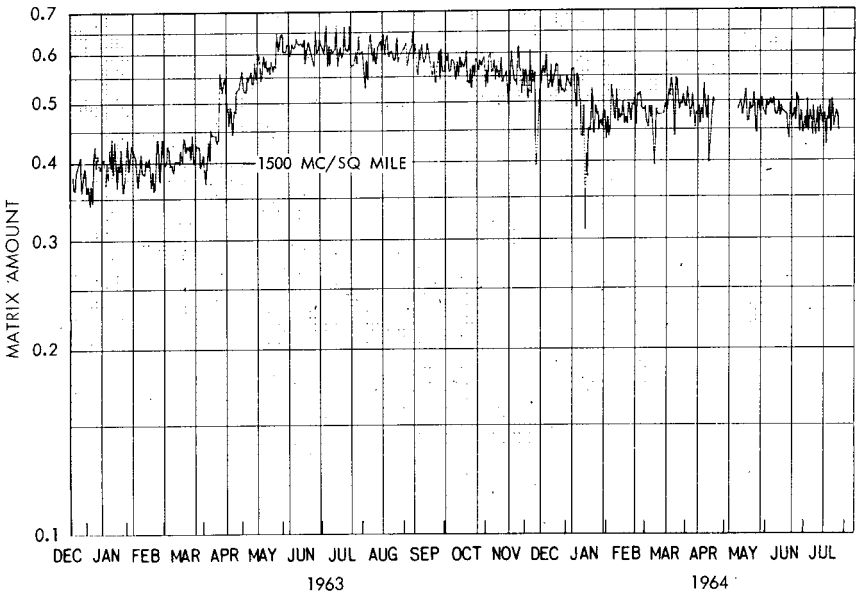

Fig. 15—Praseodymium-144 effective surface amounts as a function of time, 11 by 11 matrix reduction.

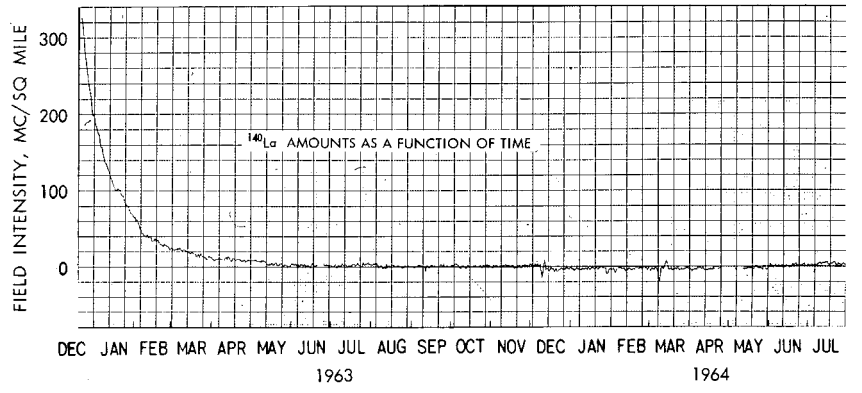

Fig. 16—Lanthanum-140 effective surface amounts as a function of time, 11 by 11 matrix reduction.

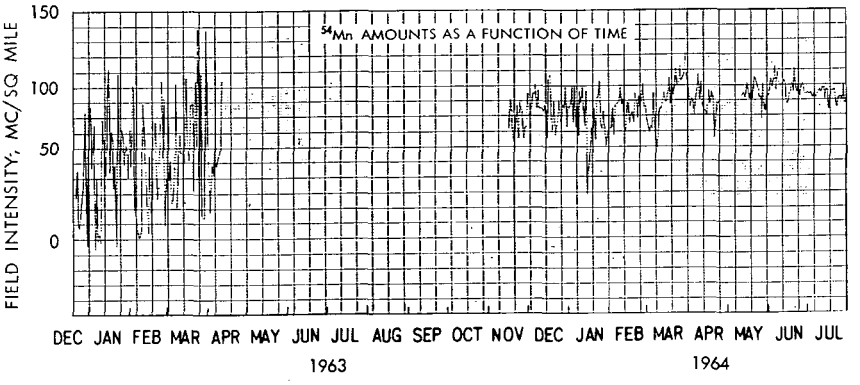

Fig. 17—Manganese-54 effective surface amounts as a function of time, 11 by 11 matrix reduction.

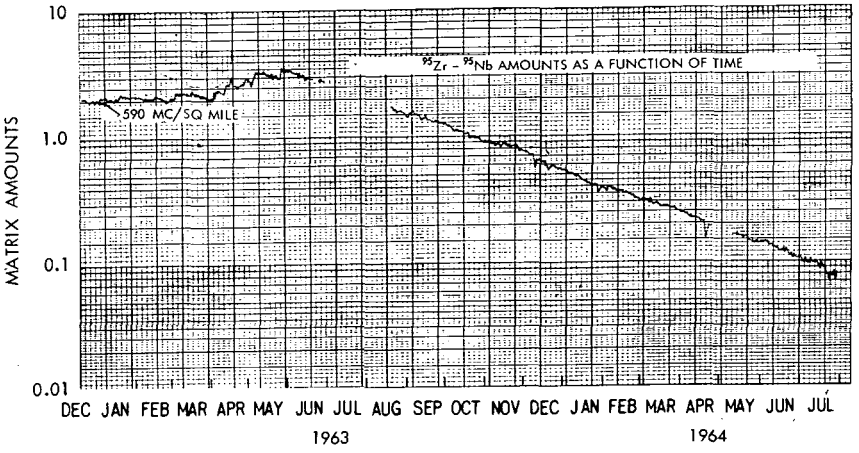

Fig. 18—Zirconium-95–Niobium-95 effective surface amounts as a function of time, 11 by 11 matrix reduction.

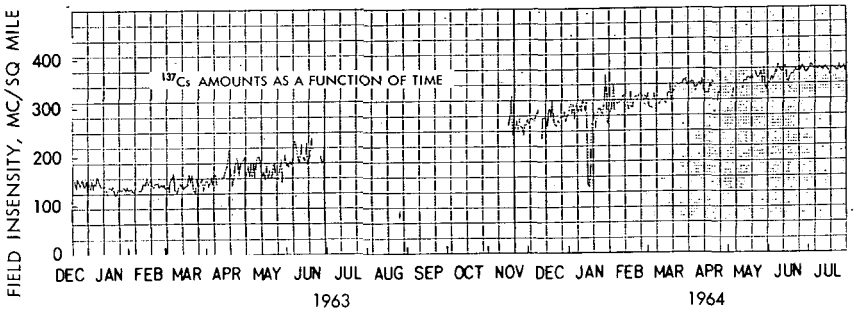

Fig. 19—Cesium-137 effective surface amounts as a function of time, 11 by 11 matrix reduction.

resultant fallout amounts of each material as a function of date are given in Table 1, where the amounts are in millicuries per square mile.

Table 1 — PERIODIC FALLOUT LEVELS, I, IN MILLICURIES PER SQUARE MILE DETERMINED BY USING AN 11 BY 11 MATRIX EXCEPT AS NOTED

Date	$I_{^{95}Zr}$, $I_{^{95}Nb}$ (τ = 65 days)	$I_{^{140}Ba}$, $I_{^{140}La}$ (τ = 12.8 days)	$I_{^{137}Cs}$ (τ = 30 years)	$I_{^{144}Ce}$, $I_{^{144}Pr}$ (τ = 285 days)	$I_{^{54}Mn}$ (τ = 314 days)	$I_{^{125}Sb}$ (τ = 2.0 years)
Dec. 22, 1962	590	325	152*	1500	61	344
June 30, 1963	855	0	182*	2380		
Jan. 1, 1964	168	0	280	2030	89	106
June 30, 1964	33	0	375	1750	97	150

*Determined by use of a 10 by 10 matrix.

Recent measurement of the rainfall atmospheric washout near Hattiesburg, Miss., shows fission debris from the Nov. 16, 1964, test by Communist China. About 157 mc/sq mile of $^{140}Ba-^{140}La$ and 30 mc/sq mile of $^{95}Zr-^{95}Nb$ washed out in the rains of Oct. 27 and 28, 1964. Also, there is an indication of dry fallout of $^{140}Ba-^{140}La$ prior to October 27 as seen in Fig. 20.

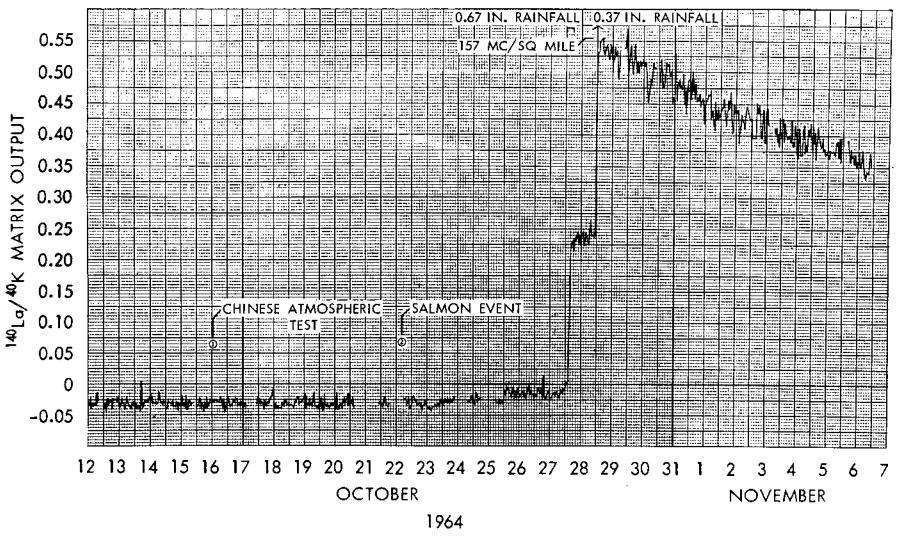

Fig. 20—Indication of $^{140}Ba-^{140}La$ fallout.

The replacement of the matrix-reduction method by the least-squares method is being evaluated. The improvement by use of the least-squares technique is insignificant if routine calculations are being made with known spectra, whereas the cost per spectrum is approximately four times greater than with the use of the matrix technique. If unknown inputs are involved, the least-squares technique is superior. Investigations and comparisons are being made by Bruce Foster using techniques similar to those of Trombka.[2] Current computer-reduction costs for the matrix technique are about $0.15 per spectrum.

It is felt that field gamma-ray measurements offer the most rapid method for the determination of the presence, the type, and the amount of radioactive fallout. The equipment is compact and portable, permitting transportation by aircraft or other vehicle to any location.

REFERENCES

1. R. S. Foote, Measurement of Radioactive Fall-Out by Field Total Absorption Gamma Ray Spectroscopy, Report No. 1, AEC Contract AT(40-1)-3147, Texas Instruments, Inc., Sept. 30, 1963.
2. J. I. Trombka, Least-Square Analysis of Gamma-Ray Pulse Height Spectra, Technical Report No. 32-373, Jet Propulsion Laboratory, California Institute of Technology, Dec. 15, 1962.

MEASUREMENTS OF AIRBORNE RADIONUCLIDES AND DETERMINATION OF THEIR PHYSICAL CHARACTERISTICS

R. W. PERKINS, C. W. THOMAS, and J. M. NIELSEN
Hanford Laboratories, General Electric Company, Richland, Washington

ABSTRACT

Newly developed counting techniques that employ multidimensional gamma-ray spectrometry have been employed for the direct measurement of a large group of radionuclides in fallout samples. These techniques have made it possible to study the distribution of many of the trace constituents of fallout and also to improve the precision for the measurement of the more abundant radionuclides. The concentrations of ^{7}Be, ^{22}Na, ^{54}Mn, ^{60}Co, ^{88}Y, $^{95}Zr-^{95}Nb$, ^{106}Ru, ^{124}Sb, ^{125}Sb, ^{134}Cs, ^{137}Cs, and ^{144}Ce can be measured directly. Their concentrations in air during the past $2\frac{3}{4}$ years are reported. The measured solubility of the fallout radionuclides is reported, and their deposition as dry fallout and as rainout in the area of Richland, Wash., is compared. The distribution and movement of the tracer radionuclides ^{88}Y and ^{124}Sb and of ^{239}Pu both in the stratosphere and in the troposphere are discussed. The cosmic-ray-produced radionuclides ^{38}Cl and ^{38}S are mentioned, and their application along with other cosmic-ray-produced radionuclides in atmospheric research is considered.

INTRODUCTION

The absolute and relative concentrations of the various airborne radionuclides are of interest both in measuring their distribution and deposition rates and in studying the physical and chemical processes

that occur in the atmosphere. Knowing the precise relative concentrations of a group of radionuclides is of particular value since this knowledge allows the relative deposition and circulation rates of each radionuclide to be followed. The accurate measurements of a large group of the airborne radionuclides in a sample require extremely sensitive and selective analytical techniques that are often prohibitive both in cost and time. Measurements of the physical and chemical states of airborne radionuclides require fractionation into the desired species and add to the required analytical sensitivity.

Studies of the type mentioned and others dealing with the characteristics and behavior of airborne radionuclides have become practical through our development of a highly sensitive and selective multidimensional gamma-ray spectrometer.[1] This instrument uses the cascade gamma-ray decay characteristics of each radionuclide for its identification and measurement and employs anticoincidence techniques for background and Compton suppression. The instrument permits an air-filter sample to be measured directly for ^{7}Be, ^{22}Na, ^{54}Mn, ^{60}Co, $^{95}Zr-^{95}Nb$, ^{88}Y, ^{106}Ru, ^{124}Sb, ^{134}Cs, ^{137}Cs, and ^{144}Ce. Measurements of these 12 radionuclides after physical- and chemical-fractionation procedures are also possible. The use of these advance techniques plus conventional means have been applied in tropospheric- and stratospheric-distribution studies and in physical- and chemical-characteristics determinations.

MULTIDIMENSIONAL SPECTROMETER

The multidimensional spectrometer is described in detail elsewhere,[1] but its basic operational characteristics and counting efficiency are covered here. The spectrometry system consists of a Nuclear Data 4096 channel analyzer used in a 64- by 64-channel grouping arrangement in conjunction with two anticoincidence shielded 4-in.-thick 6-in.-diameter NaI(Tl) detectors (see Fig. 1). One of these detectors has a 4-in. light pipe of pure sodium iodide which serves to shield the detector from gamma radiation originating in its phototube. The anticoincidence annulus is a $11\frac{1}{2}$ in.-diameter 12-in.-long NaI(Tl) crystal with a $6\frac{1}{2}$-in.-diameter center hole to accommodate the principal detectors. The analyzer is equipped with an Optikon photographic printer that permits a readout of the entire memory in about 4 min. A Tally Register Corporation paper-tape unit can be used as a readout for computer calculations. The sample to be measured is sandwiched between the two 6-in.-diameter detectors. The signals from the two detectors are fed to the two separate analog-to-digital converters of the analyzer for energy and coincidence analysis and from there to the memory storage unit. When a single photon interacts with one of the

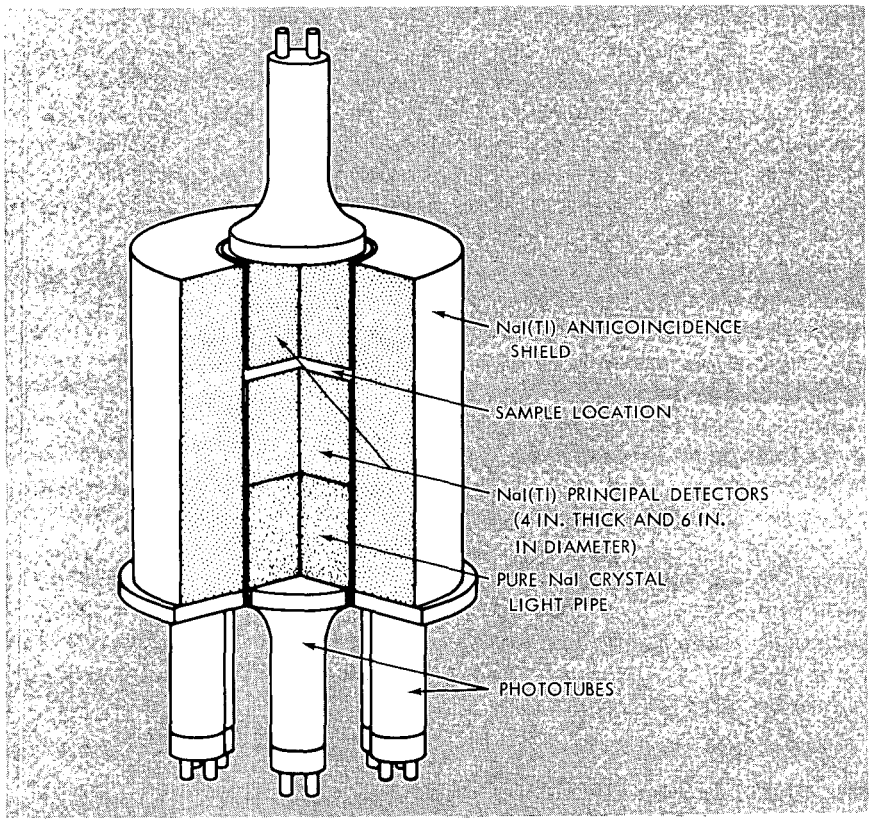

Fig. 1—Detection system for multidimensional gamma-ray spectrometer.

detectors, the event is stored on the corresponding X or Y axis of the memory. When two photons are emitted simultaneously, each interacting with a separate detector, the event is stored in an energy–energy plane at a point uniquely characteristic of the two energies. The spectra of ^{64}Cu and ^{60}Co illustrate (Figs. 2 and 3) the manner of storage. The normal spectra of these radionuclides as seen by one of the detectors are shown for comparison. With such a detection system, the unique decay characteristic of many radionuclides is readily resolvable. This permits a far greater sensitivity for detection and direct measurement of many minor radioactive constituents. In addition, a much lower background is obtained.

In Fig. 4 the background of a 4-in.-thick 6-in.-diameter single-crystal detector without a light pipe or anticoincidence shielding is compared with that of the two-crystal multidimensional detector system in which the two detectors are separated by a 1-in.-thick lead

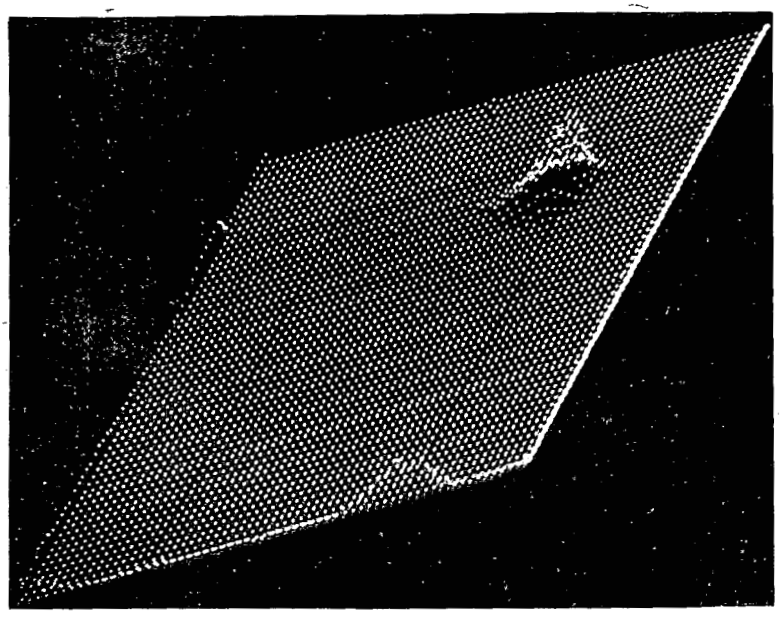

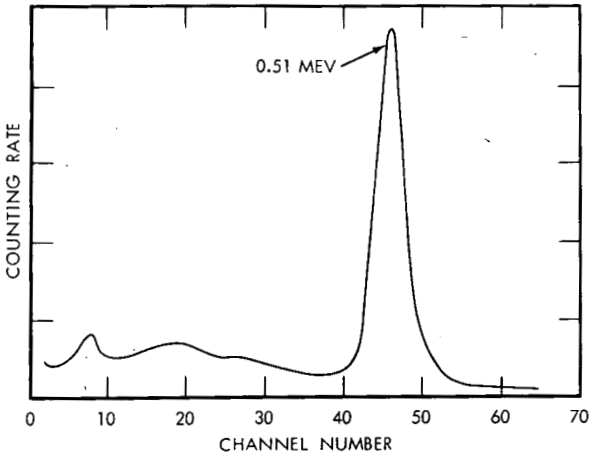

Fig. 2
Spectra for ^{64}Cu.

absorber. The background shown for the multidimensional detector system is for an energy diagonal from 0 to 3 Mev and therefore represents the case of 0- to 3-Mev absorption by each detector. These curves can also be used to compare the background that would be obtained with two crystals used in a summing arrangement with that shown for the two crystals in the multidimensional arrangement. In this case the background at a given energy on the top curve should be doubled and compared with a point of half that energy on the bottom

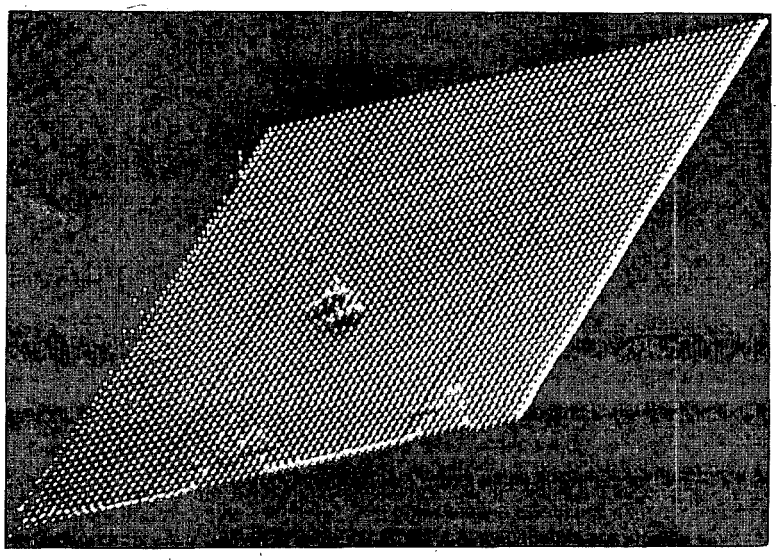

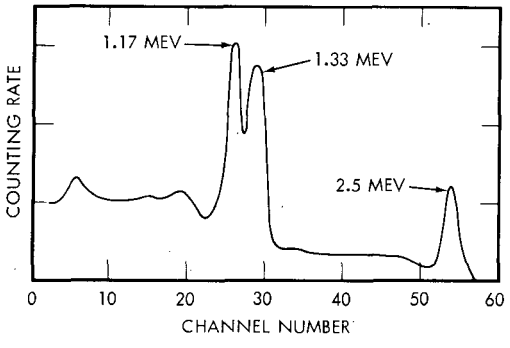

Fig. 3—Spectra for ^{60}Co.

curve. By either this method or the comparison shown in the figure, the background suppression with multidimensional analysis is three to five orders of magnitude lower.

The sensitivity for the measurement of a given radionuclide is dependent on the counting efficiency of the instrument used as well as on the background counting rate and the Compton interference from other radionuclides. In Fig. 5 the efficiency for total absorption by either crystal for gamma rays originating in the sample is plotted as curve 2E. The curve $2E^2$ gives the efficiency for two coincidence gamma rays to be totally absorbed, one each by the two detectors. This curve thus gives the probability that a coincidence event in the sample will be stored in a total absorption peak (either one of the two) in the energy–energy plane. Although the curve also is plotted for the

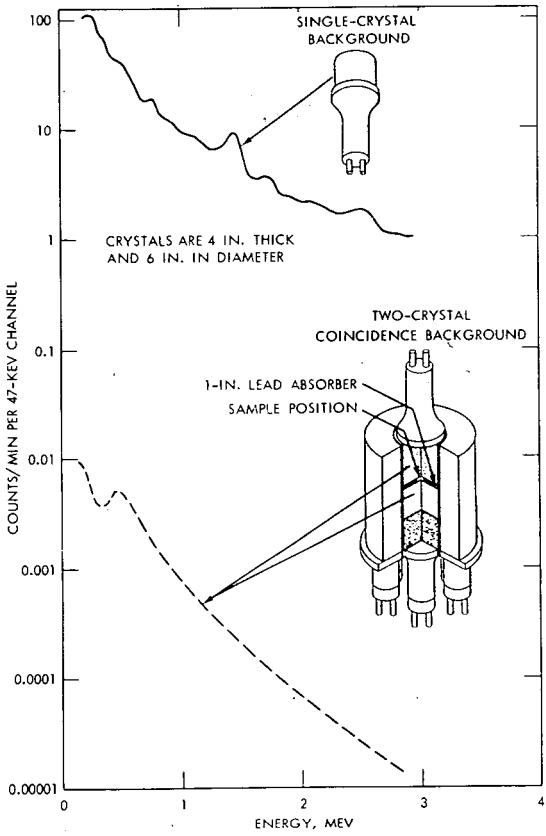

Fig. 4—Comparison of the background of a single-crystal detector with that of the two-crystal multidimensional detector system.

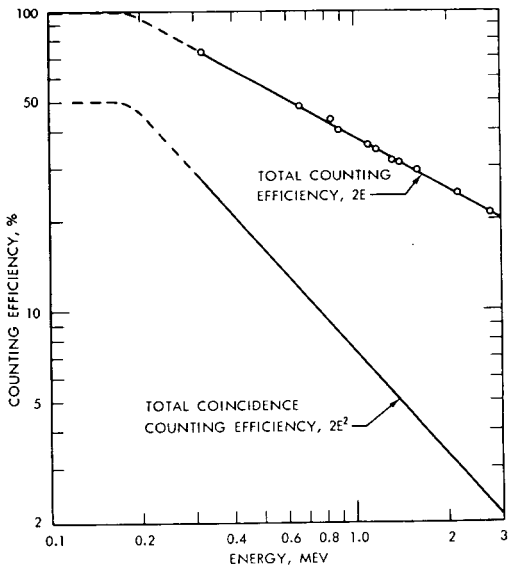

Fig. 5—Total counting efficiency and total coincidence counting efficiency of the two-crystal multidimensional detector system.

special case where the two gamma rays have equal energy, it also serves to illustrate the change in efficiency with energy.

It is evident that with this relatively high geometry system, coincidence counting rates can be measured with a reasonably high efficiency. This, together with the system's extremely low backgrounds and elimination of most of the Compton interference, makes the device an extremely sensitive and selective instrument.

EXPERIMENTAL RESULTS AND DISCUSSION OF MEASUREMENTS OF AIRBORNE RADIONUCLIDES NEAR GROUND LEVEL

Air sampling[2] near ground level was performed with a continuously operating vacuum pump that pulled air at 100 cu ft/min through a membrane filter of 5-μ pore size (AM-1, Gelman Instrument Company). These membrane filters have been shown to be essentially absolute for the collection of fallout radionuclides.[2] The filters are composited on a monthly or semimonthly basis, pressed into a standard geometry of $\frac{1}{2}$ in. thick by 1 in. in diameter, and counted on the multidimensional gamma-ray spectrometer. The air samples were obtained at a point 15 ft above the ground 6 miles north of Richland, Wash. The annual precipitation in this area is only about 8 in. and dry deposition accounts for a significant fraction of the fallout. In Fig. 6 the concentration in air of 13 radionuclides is recorded for the period January 1962 through September 1964. A tabulation of data is given in Table 1. All these radionuclides except ^{239}Pu were measured by the direct spectrometric analysis. With the exception of ^{239}Pu, which is a residue of the nuclear devices exploded, these radionuclides result from fission and neutron activation during atomic tests and from cosmic-ray interactions with nuclei in the atmosphere. The radionuclides ^{95}Zr–^{95}Nb, ^{106}Ru, ^{125}Sb, ^{137}Cs, and ^{144}Ce are fission products; presumably nuclear testing is their main source in the atmosphere. The radionuclides ^{54}Mn, ^{60}Co, ^{88}Y, ^{124}Sb, and ^{134}Cs are formed as neutron-activation products during nuclear testing; and ^{7}Be and ^{22}Na are produced continuously in the atmosphere by interactions of cosmic rays. The fallout rates of many of the fission products are measured at sampling locations the world over[3] and perhaps their main value here is to serve as a base line for comparing the concentrations of less abundant radionuclides in the atmosphere.

Sodium-22 was first reported to be present in the atmosphere by Marquez[4] in 1957, who found it in rainwater at Rio de Janeiro, Brazil, in a concentration of 0.017 dis/min per liter. It is produced naturally by cosmic-ray spallation of argon in the atmosphere and also results from the reaction ^{23}Na(n,2n)^{22}Na during tests of nuclear weapons. Its potential value as a tracer of atmospheric circulation has been recog-

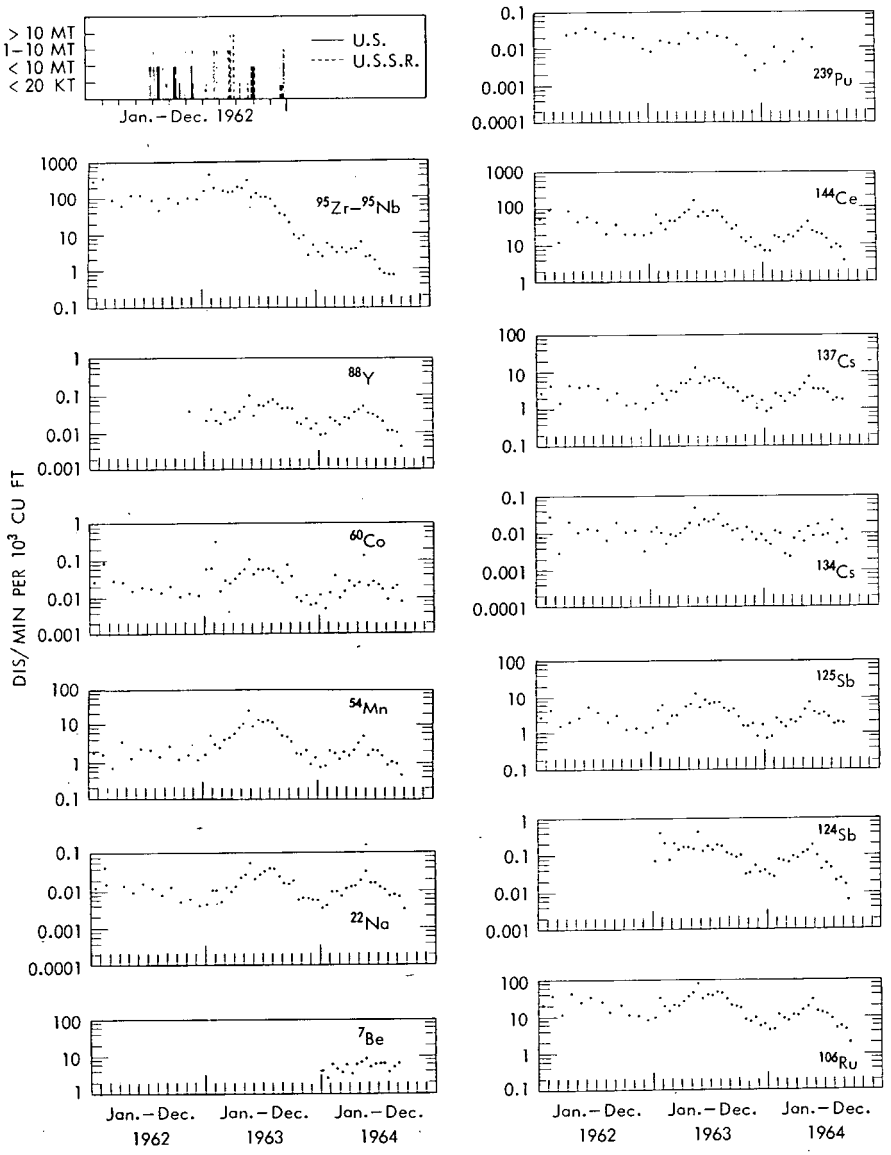

Fig. 6—Air concentrations of radionuclides at Richland, Wash., from January 1962 through September 1964. The uppermost left box indicates aboveground detonations in 1962; a clearer graph of these detonations can be seen in Fig. 14.

Table 1 —RADIONUCLIDE CONCENTRATIONS IN THE AIR AT RICHLAND, WASH., DURING 1962 TO 1964, DIS/MIN PER 10^6 CU FT (S.T.P.)

Date	^{7}Be	^{22}Na	^{54}Mn	^{60}Co	^{88}Y	^{95}Zr–^{95}Nb	^{106}Ru	^{124}Sb	^{125}Sb	^{134}Cs	^{137}Cs	^{144}Ce
1-62*		11.9	1,870	26.2		287,000	20,600		2,590	6.8	2,730	53,500
2-62*		41.6	1,690	83.3		349,000	36,600		4,220	24.7	4,260	90,300
3-62*		0.8	722	28.1		85,700	11,500		1,490	2.5	1,470	12,400
4-62		13.5	3,520	26.2		59,600	42,700		1,900	17.8	4,430	86,100
5-62		8.85	1,350	15.0		114,000	25,000		2,470	9.1	3,900	43,600
6-62		15.8	2,310	18.9		113,000	34,100		5,200	11.6	4,540	58,800
7-62		11.5	2,180	17.3		83,200	25,900		3,620	10.7	3,710	43,000
8-62		7.54	1,500	13.5		44,000	13,300		1,890	5.7	1,810	20,500
9-62		12.7	2,800	19.9		97,900	20,700		2,890	17.0	2,750	36,500
10-62		4.89	1,260	10.6		70,400	11,300		1,170	9.4	1,290	19,900
11-62		5.86	1,640	13.0	25.7	95,800	10,500		1,280	10.6	1,450	20,000
12-62		3.97	1,210	11.3		89,700	8,090		996	2.9	1,030	19,200
1-63A†		4.33	1,670	58.0	20.5	156,000	9,540	68	1,330	9.8	1,490	22,500
1-63B		10.8	5,070	61.9	40.2	436,000	32,200	399	4,340	21.5	4,410	69,800
2-63A		10.4	3,200	324	20.9	188,000	19,400	202	5,810	9.1	2,610	38,400
2-63B		4.96	2,320	15.0	17.0	105,000	14,200	74	1,700	4.7	1,730	27,300
3-63A		12.1	4,060	28.8	34.4	158,000	20,100	201	2,900	8.3	3,090	45,200
3-63B		9.36	4,620	24.8	22.6	142,000	19,600	135	2,920	7.5	2,960	45,700
4-63A		13.9	5,890	32.1	24.4	145,000	25,300	159	3,240	8.9	5,130	55,400
4-63B		22.7	8,310	44.1	32.5	175,000	33,200	159	5,350	12.0	5,080	73,100
5-63A		27.8	10,900	56.5	48.1	184,000	43,600	145	6,380	17.1	6,550	90,000
5-63B		55.0	25,700	107	99.1	307,000	77,700	422	12,300	43.2	13,400	162,000
6-63A		21.3	9,190	42.1	27.9	101,000	30,600	125	5,100	14.6	5,010	59,400
6-63B		27.8	13,500	58.6	53.4	134,000	39,100	167	8,420	20.8	7,390	78,000
7-63A		34.0	12,100	54.7	51.8	105,000	37,000	137	6,450	18.9	5,990	60,500

7-63B		39.5	13,500	59.9	67.0	106,000	45,200	185	6,890	20.7	6,910	86,000
8-63A		39.5	11,900	52.3	77.2	92,400	42,100	169	7,160	29.2	6,980	85,000
8-63B		24.7	8,050	35.6	57.8	56,900	29,200	110	4,820	13.5	5,030	56,200
9-63A		16.4	5,340	25.0	44.4	36,100	20,500	99	3,940	15.4	3,820	40,600
9-63B		15.2	4,890	77.2	45.7	33,100	18,800	84	4,540	10.3	3,890	27,700
10-63A		17.9	3,700	38.1	44.1	21,200	17,500	97	2,620	11.5	3,010	33,600
10-63B		5.80	1,850	10.1	18.2	9,690	8,220	30	1,480	5.8	1,620	16,500
11-63A		6.43	1,730	7.94	16.9	7,830	7,080	33	1,440	21.5	2,060	12,800
11-63B		6.17	2,190	11.4	23.4	9,240	9,260	52	1,620	8.9	2,170	16,300
12-63A		5.76	963	6.24	12.6	2,620	5,500	34	757	5.8	1,030	9,150
12-63B		5.62	1,490	6.88	17.5	5,130	6,040	38	1,580	8.1	1,700	9,810
1-64A	4,330	3.42	794	11.8	8.73	3,230	4,250	29	679	5.4	870	7,030
1-64B	2,620	4.01	866	4.83	9.31	2,450	4,440	26	854	4.3	1,020	7,080
2-64A	6,310	9.61	2,170	13.6	25.4	5,690	11,100	73	2,320	10.1	2,620	18,000
2-64B	4,760	9.48	1,840	38.9	20.0	4,460	8,810	67	1,780	8.5	2,140	16,300
3-64A	3,790	7.21	1,330	9.64	16.1	3,210	7,540	61	1,320	2.4	1,570	12,500
3-64B	5,980	11.6	1,970	14.7	25.3	4,360	11,000	88	2,070	13.2	2,640	18,800
4-64A	3,500	13.0	1,630	27.2	24.0	3,270	10,700	79	1,780	6.3	2,250	17,000
4-64B	6,080	14.0	2,190	20.2	34.3	3,940	14,800	109	2,450	9.3	3,260	23,700
5-64A	7,260	19.4	3,400	24.4	40.9	4,280	18,100	124	4,330	5.0	4,950	29,700
5-64B	8,720	34.2	5,130	136	52.3	6,260	28,800	179	7,050	13.1	7,480	42,800
6-64A	5,260	16.3	1,640	20.5	33.6	2,390	13,700	94	4,590	7.3	3,470	24,000
6-64B	6,260	16.6	2,190	26.4	30.4	2,470	12,800	40	3,080	15.1	3,380	21,300
7-64A	6,410	12.8	2,140	21.8	25.5	1,950	11,300	58	3,350	7.4	3,390	19,500
7-64B	6,400	10.6	1,640	16.1	20.3	1,090	8,590	43	2,590	8.2	2,700	15,000
8-64A	3,880	7.08	905	8.7	11.1	835	4,700	20	1,600	19.1	1,600	8,270
8-64B	5,160	7.69	1,100	16.8	11.0	749	5,320	23	1,760	4.6	1,880	10,200
9-64A	6,460	6.91	994	20.5	10.0	743	4,200	16.2	1,670	10.5	1,720	8,500
9-64B		3.08	471	7.4	4.2		2,010	5.9		5.7		3,910

*Only small samples were available and the ^{22}Na and ^{134}Cs values give only the order of magnitude.
†A and B signify approximately the first and second half of each month, respectively.

nized, and recently reported measurements for this purpose of air filters collected prior to the 1961 test series[5] have shown air concentrations ranging from 1 dis/min per 10^6 cu ft below the tropopause to 460 dis/min per 10^6 cu ft above the tropopause. Our measurements show concentrations ranging from 4 to 40 dis/min per 10^6 cu ft in the troposphere to 12,000 dis/min per 10^6 cu ft in the stratosphere. This suggests that a large amount of ^{22}Na was injected into the atmosphere during the 1961 and 1962 series of tests.

Cesium-134 appears to be produced in nuclear detonations mainly by an (n,γ) reaction on ^{133}Cs, but it is also produced directly by fission.[6] The ratio of ^{134}Cs to ^{137}Cs during the past 2½ years has not shown a pronounced drop; however, our biological studies[7] have shown that the ratio of these radionuclides in Alaskan caribou flesh dropped by a factor of 4 during the period from just prior to the 1961 test series through July 1963. This suggests that a major injection of ^{134}Cs into the atmosphere occurred prior to the last test series.

The radionuclides ^{60}Co and ^{54}Mn were reported to be present in the atmosphere in 1958 by Marquez et al.,[8] who found them in rainwater collected between June 1957 and March 1958. Their presence was attributed to thermonuclear testing. It was recently reported[3] that a number of activation products including ^{54}Mn, ^{55}Fe, and ^{124}Sb were produced in relatively high abundance in the high-yield detonations carried out by the Union of Soviet Socialist Republics (U.S.S.R.) at Novaya Zemlya in the fall of 1961 and that ^{88}Y and ^{124}Sb were produced in U.S.S.R. tests in late 1962. These tests appear to be the major source of the ^{54}Mn, ^{60}Co, ^{88}Y, and ^{124}Sb. The radionuclides ^{88}Y and ^{124}Sb were first observed in our studies during November 1962 and January 1963, respectively. Both ^{54}Mn and ^{60}Co showed a sharp rise during January and February 1963. This indicated an additional injection of these radionuclides.

Beryllium-7 is produced by cosmic-ray spallation reactions in the atmosphere; its presence was first reported in the atmosphere by Arnold and Al-Salih[9] in 1955, who chemically separated it from rainwater samples. Measurements of its concentration in the atmosphere at various altitudes and latitudes have since been reported.[5,10,11] Only recently have we begun to study the concentration of ^{7}Be in the atmosphere. It is interesting that, unlike other fallout radionuclides, ^{7}Be has not shown a large seasonal concentration change.

Plutonium-239 was separated chemically from air filters after gamma-ray spectrometric analysis. Its concentration change with time is somewhat similar to that of ^{137}Cs (see Fig. 6) but shows a larger increase during 1962.

The ratios of ^{239}Pu to ^{137}Cs as a function of time are given in Table 2; they show a relatively large peak with its maximum in October 1962. Alpha-particle-energy analysis of the plutonium separated

Table 2—RATIO OF ^{239}Pu TO ^{137}Cs IN GROUND-LEVEL AIR AT RICHLAND, WASH., FROM APRIL 1962 THROUGH JUNE 1964

Month	Ratio, $\times 10^3$		
	1962	1963	1964
January		5.5	4.3
February		6.2	4.0
March		4.6	3.2
April	5.8	2.6	3.5
May	7.6	3.9	3.6
June	8.2	3.7	3.0
July	8.2	4.5	
August	10.0	3.0	
September	8.9	5.2	
October	13.0	4.1	
November	9.0	3.0	
December	9.6	2.4	

from air filters has shown that the ratio of ^{238}Pu to ^{239}Pu is less than 0.02 at the present time.

It is both interesting and significant that the activation products ^{88}Y (105 days) and ^{124}Sb (60 days) reached concentrations this year (1964) which are comparable with those of last year, whereas the fission product $^{95}Zr-^{95}Nb$ (65 days) is lower by about a factor of 20. Also, the fission product ^{137}Cs (30 years) reached a concentration comparable with that of last year, and ^{106}Ru (1 year) and ^{144}Ce (285 days) reached a concentration about one-half that of last year. Since there have been no nuclear detonations aboveground[12] during 1963 and through September 1964, all of these radionuclides entered the atmosphere prior to 1963, and their reservoir in the atmosphere has decreased with their respective half-lives since that time. These concentrations point to an obviously different source of ^{88}Y and ^{124}Sb relative to most of the $^{95}Zr-^{95}Nb$ and the other fission products. In Fig. 7 the air concentrations of ^{88}Y and ^{124}Sb have been corrected for decay to the time of their probable injection into the atmosphere[3] and are compared with ^{137}Cs. The large increase in the fallout rates of ^{88}Y and ^{124}Sb relative to ^{137}Cs clearly points to a different origin.

AIR PROFILES OF RADIONUCLIDES

During the 1962 nuclear-weapons testing period, a few sampling flights were made. The flights were planned with the object of measuring air profiles under specific meteorological conditions. Air was drawn by a vacuum pump through a membrane filter of 5 μ pore size

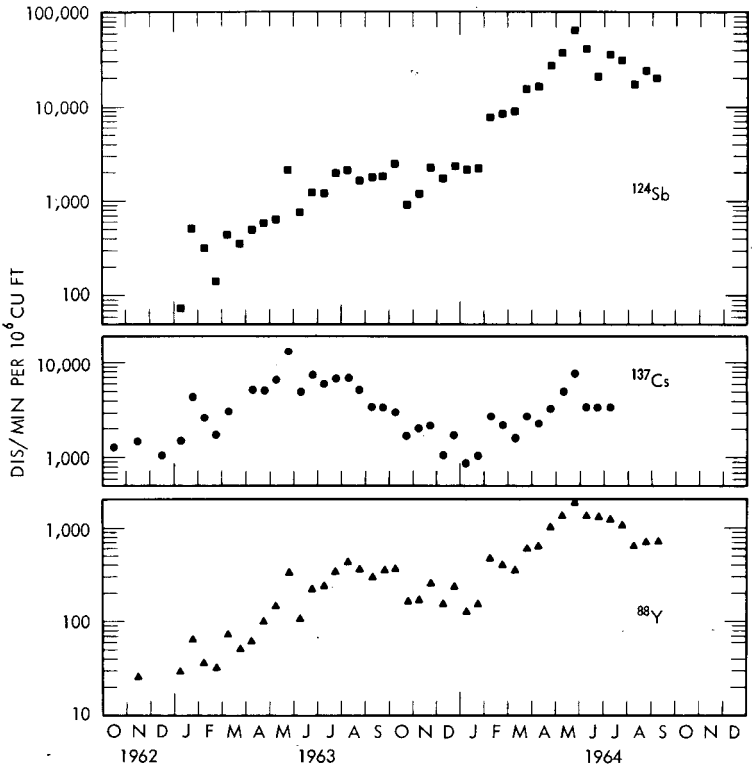

Fig. 7—Comparisons of the air concentration of ^{88}Y and ^{124}Sb with ^{137}Cs. Yttrium-88 and ^{124}Sb are corrected to the time of their probable injection, Nov. 15 and Dec. 31, 1962, respectively.

which was followed by an activated charcoal trap for collection of gaseous radioiodine. These flights were limited to 12,000 feet altitude because of the type of airplane used, but they served to show that significant variations in radionuclide concentrations did exist at these low altitudes. Figure 8 gives typical profiles of the concentrations of five radionuclides as a function of altitude showing comparatively high concentrations at 12,000 ft.

The availability of stratospheric air filters, which were furnished by Isotopes, Inc., Westwood, N. J., has made it possible to compare the air concentrations observed near ground level at our geographical position with those present in the stratosphere above. In Fig. 9 the ratios of the radionuclide concentrations for stratospheric air to those of ground-level air are compared for 12 radionuclides. These measurements were made on samples collected during January 1964. It is interesting that these ratios range from about 1500 to 3000 for all the radionuclides except ^{88}Y, ^{124}Sb, and ^{134}Cs. The high stratospheric con-

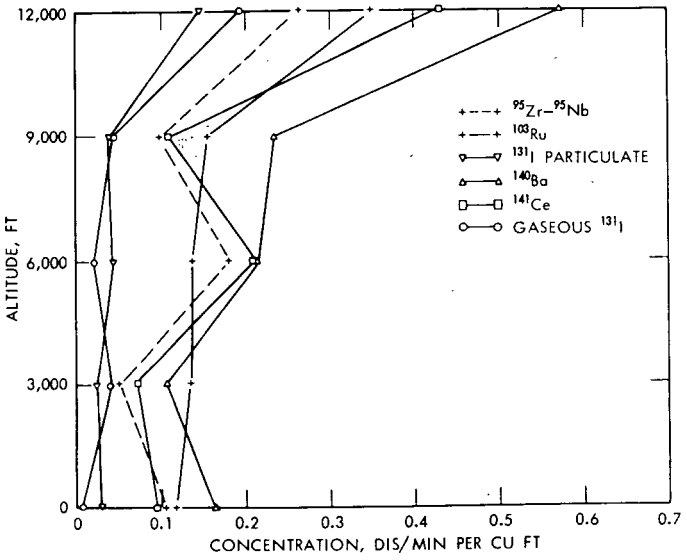

Fig. 8—Radionuclide concentration as a function of altitude (Nov. 13, 1962).

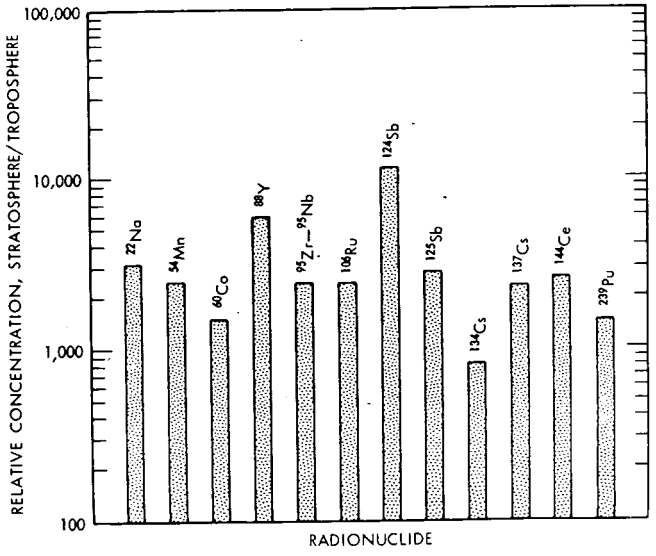

Fig. 9—Ratios of radionuclide concentrations in the stratosphere to those near ground level in the northwestern United States in January 1964. Stratospheric samples taken at 65,000 ft at 37 to 43°N and 110°W; trophospheric samples taken at 15 ft aboveground at 47°N and 119°W.

centrations of ^{88}Y and ^{124}Sb during January 1964 help explain the observed high fallout rates of these radionuclides during the summer of 1964 (see Fig. 7). The relatively low concentrations of ^{134}Cs in the stratosphere are in accord with the ^{134}Cs to ^{137}Cs ratio measurements on biological samples,[7] which show a large drop in this ratio since 1961 and indicate that a major injection of ^{134}Cs into the atmosphere occurred prior to the past test series.

Stratospheric samples were available which covered latitudes from about 26 to 70°N at longitudes of 97 to 146°W. This covers an area from southern Mexico to northern Alaska. These samples were collected between Jan. 8, 1964, and Feb. 18, 1964. In Fig. 10 the ratios

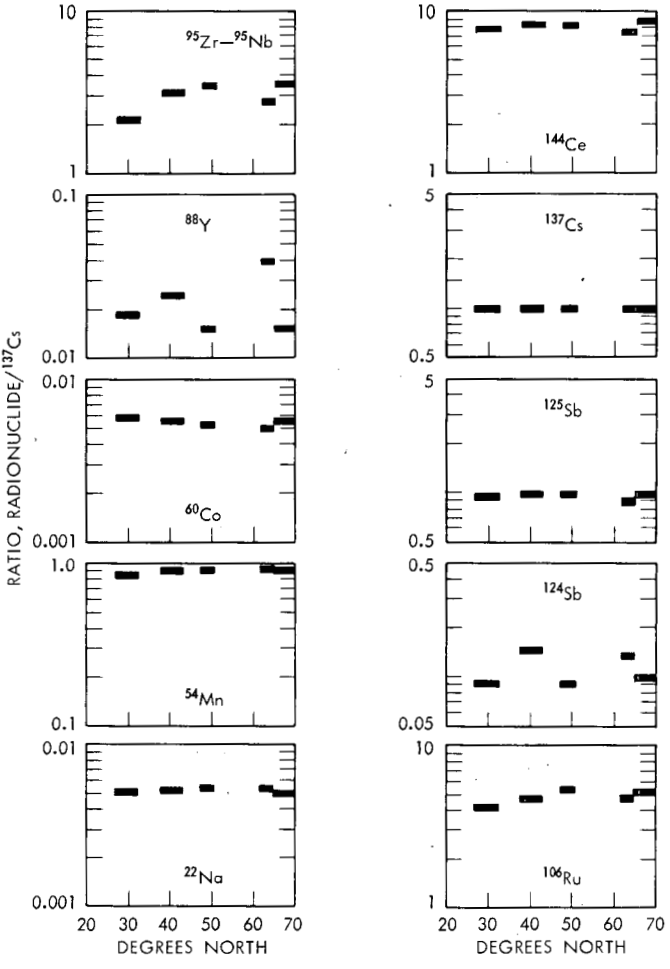

Fig. 10—Ratios of the concentrations of various airborne radionuclides to ^{137}Cs as a function of latitude (stratospheric samples).

of the various radionuclides in these samples to their ^{137}Cs content are plotted as a function of latitude. It is interesting that these ratios are essentially constant with changing latitude for all the radionuclides except ^{88}Y, ^{124}Sb, and ^{95}Zr. These three radionuclides have short half-lives compared with the others, and it might be expected that their concentration would decrease with decreasing latitude since the most recent high-yield nuclear shots were made at a high latitude. This is generally true for $^{95}Zr-^{95}Nb$ since it does decrease with decreasing latitude. However, both ^{88}Y and ^{124}Sb show peak concentrations at about 41 and 63°N, and a definite lack of mixing relative to ^{137}Cs.

DEPOSITION AND PROPERTIES OF AIRBORNE RADIONUCLIDES

It has been pointed out that a definite correlation exists between the air concentrations of radionuclides and the seasonal precipitation rate.[13] This correlation appears to exist at our sampling location in Richland, Wash., as shown in Fig. 11. Here the monthly precipitation rate shows the typical inverse relation to the ^{137}Cs content of the air.

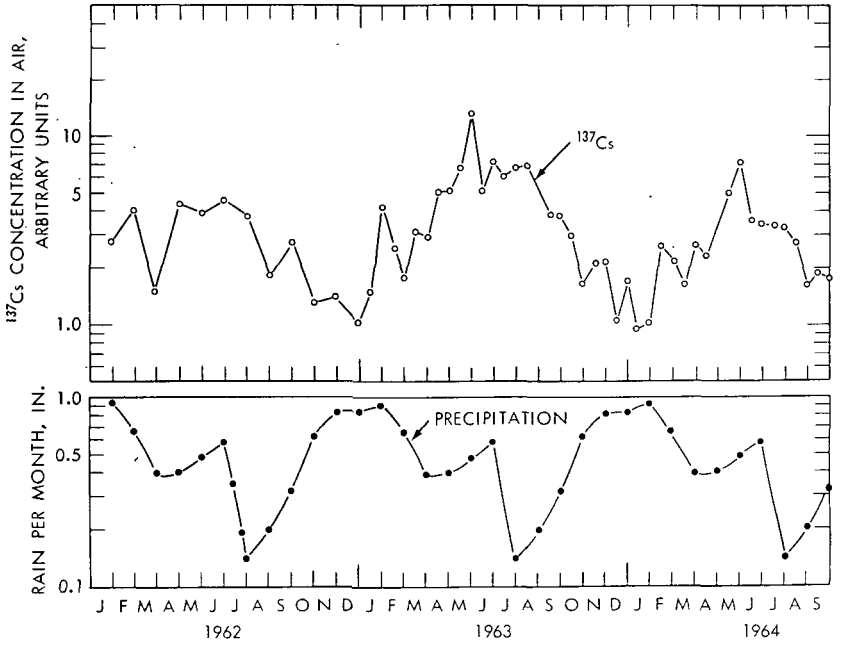

Fig. 11—Comparison of airborne ^{137}Cs concentration with annual precipitation.

However, the annual precipitation in this area is only about 8 in., and it seems unlikely that local precipitation has a marked effect on air concentrations. Precipitation is not the major mode of fallout deposition during the summer months at our geographical location. Figure 12 shows the fractions of the various airborne radionuclides that were

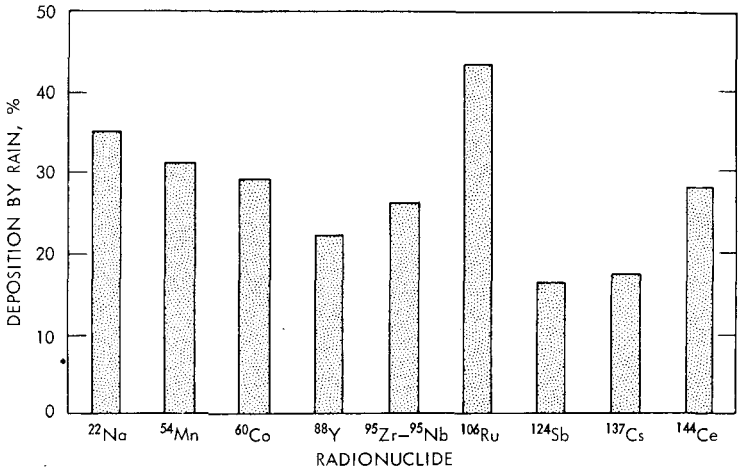

Fig. 12—Percent of radionuclide deposition due to rain from June 11 to Sept. 15, 1964.

carried down by rain during the summer of 1964. The total fallout, including both dry deposition and rain, was collected in plastic-lined trays containing about $\frac{1}{2}$ in. of water and with a surface area of about 80 sq ft. In addition, rain was collected separately in a 90 sq ft dry tray that was lined with a new coat of plastic daily to prevent accumulation of dry fallout in the tray before it rained. The fractions of various radionuclides that were carried down by rain ranged from 16% for ^{124}Sb to 43% for ^{106}Ru. The reason for this selectivity is not clear, but such selectivity does suggest that the various airborne radionuclides are attached to aerosols of different characteristics.

The water solubility of the fallout radionuclides is of interest in the estimation of their availability for uptake in the biosphere. The relative solubility of these radionuclides was determined by filtering both the water in which the dry fallout was collected and rainwater samples through a membrane filter of 0.3 μ pore size. The fractions of the various radionuclides that were found to be in solution by this method are shown in Fig. 13. A considerable variation exists in the solubility of the different radionuclides. The solubilities shown for the rain-carried radionuclides are probably more representative of the actual properties of the fallout since the rainwater was collected in a

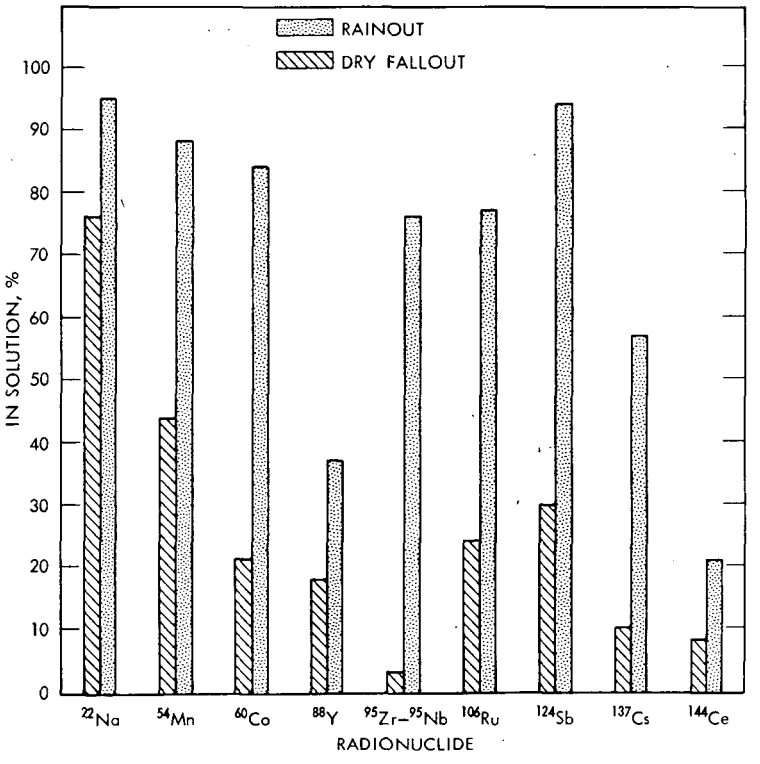

Fig. 13—Percent of radionuclide found in solution in fallout trays.

rather short period of time and was then filtered, whereas the dry fallout was collected over a period of several days in the water-filled trays prior to filtration. The rather high solubilities of these radionuclides facilitate studies of their oxidation states. Measurements designed to determine the radionuclide oxidation states and other chemical properties are presently being conducted.

PHYSICAL AND CHEMICAL CHARACTERISTICS OF ^{131}I IN FALLOUT

During the nuclear test series of 1962, measurements were made to determine both the physical and the chemical form of ^{131}I in fallout.[2] The physical form of ^{131}I whether gaseous or particulate was determined by filtering air through a filter of 5 μ pore size for particle removal and then passing it through an activated charcoal trap for removal of gaseous ^{131}I. The fraction of ^{131}I associated with particulate

material is compared with the total ^{131}I content of the air in Fig. 14. The fraction of airborne ^{131}I in the particulate form ranged from about 10 to 90%. The peak ^{131}I air concentration in October 1962 was accompanied by a definite peak in the fraction of particulate activity (~ 90%), whereas the peak ^{131}I air concentration in November 1962 was accompanied by a minimum of particulate ^{131}I (~ 12%). Presumably, these extreme differences in the fraction of particulate ^{131}I are due to the nature of the nuclear detonations responsible for these peaks in the ^{131}I activity. The nature of the gaseous ^{131}I in fallout was investigated by placing a 2-in.-thick silver-mesh (1 by 20-mil silver-plated copper mesh) bed in the air-sampling head between the filter and the charcoal.[2] Laboratory experiments had shown that for the flow velocities used this bed was 95 and 99% efficient for removal of I_2 and HI, respectively. It was observed that less than 10% of the gaseous ^{131}I was held by the silver mesh; therefore greater than 85 to 90% of the ^{131}I is in a form other than I_2 or HI and is presumably present as organic iodides.

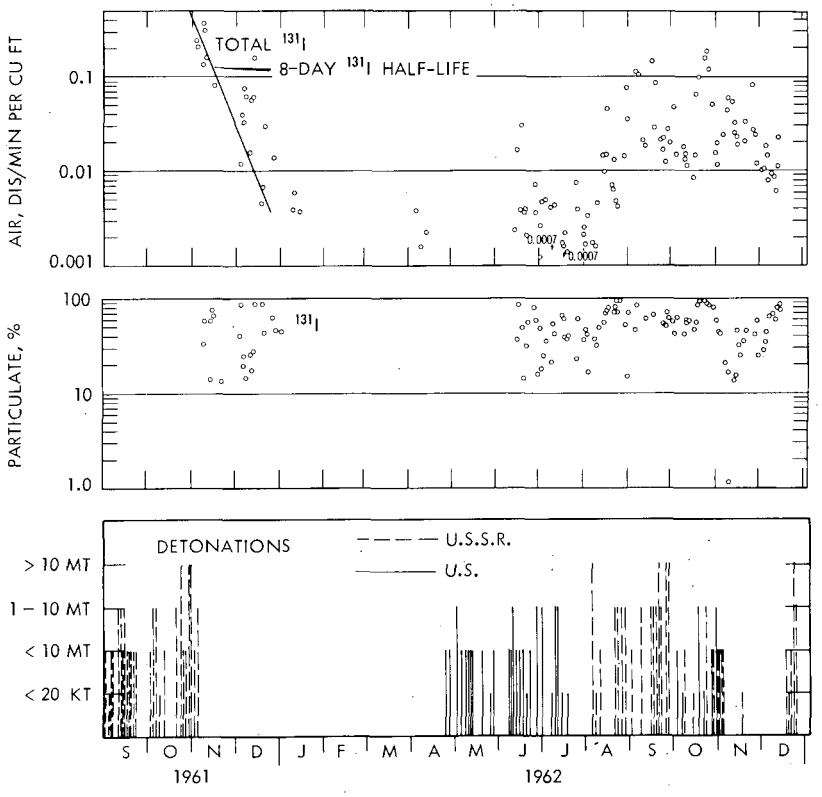

Fig. 14—Physical form and abundance of airborne ^{131}I.

The particulate material collected on membrane filters was chemically fractionated to determine the oxidation states of the associated ^{131}I. This involved addition of I^-, IO_3^-, and IO_4^- carriers, leaching with cold water at pH 12, and chemical fractionation. The experimental results are summarized in Table 3; they show that about two-

Table 3—CHEMICAL FORM OF ^{131}I COLLECTED ON MEMBRANE FILTERS

Date	^{131}I leached from filters, %	Fractionation of leached ^{131}I		
		$I_2 + I^-$, %	IO_3^-, %	IO_4^-, %
Oct. 24, 1962	44	~57	~38	<5
Oct. 25, 1962	42	~66	~29	<5

thirds of the ^{131}I was in the form of I_2 or I^-, about one-third was present as IO_3^-, and little or none was present as IO_4^-.

At the Hanford Atomic Products Operation at Richland, Wash., small amounts of ^{131}I are released continuously from the exhaust stacks of the chemical-separations plants. This source of ^{131}I permits a continuation of studies of the physical and chemical behavior of atmospheric radioiodine. Although the ^{131}I released from the separations-plant stacks is essentially gaseous, it has been found to be a complex mixture consisting of about one-half I_2 and HI, with the remainder consisting of several different organic iodide compounds.[14] The chemical species of these organic iodides are presently being investigated.

During a period of above normal ^{131}I emission from a separations-plant stack, air samples were collected at distances up to 25 miles to determine if rapid changes occurred as the material moved from its point of release. Sampling was performed from an airplane with the use of a vacuum pump that pulled air through a membrane filter of 5 μ pore size followed by a charcoal trap. Samples were collected at 200 to 500 ft by multiple penetrations of the stack plume at 1, 3, 5, 10, and 25 miles from the source. The fraction of ^{131}I in the gaseous state is shown in Table 4. It is interesting that there was very little change in physical form over the distances measured. The total sample activities collected at 25 miles on Sept. 4, 1963, and 10 miles on Sept. 3, 1963, were low, and the apparent change in physical form may not be significant. The major change occurred within the first mile.

SHORT-LIVED COSMIC-RAY-PRODUCED RADIONUCLIDES

In a consideration of methods of studying atmospheric phenomena including cloud physics, washout, and rainout, it becomes apparent that

Table 4— PHYSICAL FORM OF ^{131}I AT VARIOUS DISTANCES FROM THE SOURCE

Distance, miles	^{131}I present as a gas, %
Sept. 4, 1963	
0	> 99
1	73
3	90
5	92
10	92
25	96 ± 10*
Sept. 3, 1963	
0	> 99
1	82
3	82
5	81
10	58 ± 20*

*The plus and minus values are the standard deviations.

the use of short-lived natural tracers, which are produced by cosmic-ray spallation reactions, would be very useful. In investigations the natural presence in the atmosphere of cosmic-ray-produced ^{38}Cl (37.3 min) and ^{38}S (2.9 hr) was discovered. These radionuclides were found to be present in rainwater at concentrations that are readily measurable with the multidimensional analyzer. They are produced by cosmic-ray spallation reactions on atmospheric argon. The concentrations of ^{38}Cl and ^{38}S in six rains are recorded in Table 5 along with the concentrations of ^{39}Cl (55 min), which was measured simultaneously.

An additional spallation-produced radionuclide that is present in the atmosphere and can be readily measured in rainwater with the multidimensional spectrometer is ^{24}Na (15 hr). Its concentration in three rains is compared with that of ^{22}Na in Table 6.

Table 5— CONCENTRATIONS OF THE COSMIC-RAY-PRODUCED RADIONUCLIDES ^{38}Cl, ^{38}S, AND ^{39}Cl IN RAINWATER*

Date	Volume, liters	Collection time, min	Dis/min per liter		
			^{38}Cl	^{38}S	^{39}Cl
July 29, 1964	5.10	50	147 ± 15	13 ● 5	200 ± 17
July 30, 1964	6.64	15	~18	4 ± 2	~10
Aug. 1, 1964	3.5	50	9 ± 5	†	15 ± 3
Aug. 1, 1964	1.8	10	31 ± 12	†	28 ± 5
Aug. 12, 1964	2.2	5	42 ± 13	~7	62 ± 12
Aug. 18, 1964	10.0	40	55 ± 9	†	53 ± 3

*The plus or minus values are the standard deviations.
†Not measured.

Table 6—CONCENTRATIONS OF ^{22}Na AND ^{24}Na IN RAINWATER*

Date	Sample volume, liters	Dis/min per liter	
		^{24}Na	^{22}Na
June 15, 1964	60	0.70 ± 0.13	0.36 ± 0.03
June 17, 1964	6.64	2.22 ± 0.25	0.25 ± 0.04
June 18, 1964	14.32	0.59 ± 0.09	0.19 ± 0.02

*The plus or minus values are the standard deviations.

Measurements of radionuclides such as these during the course of a rain would provide useful information for calculating rainout and washout coefficients of the normal atmospheric aerosols.

BIOSPHERIC DISTRIBUTION OF ^{22}Na

Like ^{137}Cs, ^{22}Na distributes itself through the biosphere, and it can be measured in many biological materials by direct counting of the sample ash on the multidimensional analyzer. Measurements of its distribution through the food chain and its calculated concentration in man based on bioassay measurements are given in Table 7. These data point out the usefulness of ^{22}Na as a tracer of weapons-testing debris.

Table 7—DISTRIBUTION OF ^{22}Na IN FOODS, BIOASSAY SAMPLES, AND MAN

Sample	Location	Date obtained	^{22}Na, dis/min per liter
	Western United States		
Elk	Quinault, Wash.	May 1964	74.4
Bass	Columbia River	April 1964	8.3
Milk	Washington	March 1964	6.2
Wheat	Washington	August 1963	3.31
Beef	Local food store, Washington	May 1964	2.47
Beef	Local food store, Washington	March 1964	0.52
Corn	Oregon	April 1964	~0.04
Lettuce	California	March 1964	0.16
Carrots	California	April 1964	~0.07
Potatoes	Idaho	April 1964	0.68
Green beans	Oregon	April 1964	~0.20
Urine*	Washington		1.45
Man†	Washington	November 1963	39.5†

(Table 7 continues on page 220)

Table 7 — (Continued)

Sample	Location	Date obtained	^{22}Na, dis/min per liter
		Alaska	
Caribou meat	Near Kotzebue	July 1963	180
Caribou meat	Near Kotzebue	July 1963	89.1
Moose meat	Near Kotzebue	March 1964	58.7
Moose meat	Near Kotzebue	March 1964	80.6
Caribou meat	Near Kotzebue	Aug. 5, 1961	9.13
Caribou meat	Near Kotzebue	Oct. 9, 1961	23.0
Reindeer meat	Near Kotzebue	August 1963	15.6
Urine‡	Anaktuvuk Pass	January 1964	126
Man (Eskimo)†	Anaktuvuk Pass	January 1964	3427†

*Richland, Wash., composite from several individuals.

†These values are estimated whole-body burdens for ^{22}Na based on an 11-day biological half-life.

‡Composite from two Alaskan Eskimos.

REFERENCES

1. R. W. Perkins, Anticoincidence Shielded–Multidimensional Gamma Ray Spectrometry for Direct High Sensitivity Analysis of Radionuclide Mixtures, Paper No. SM 55/53, in *Symposium on Radiochemical Methods of Analysis*, Salzburg, Austria, October 18 to 23, 1964, to be published.
2. R. W. Perkins, Physical and Chemical Form of ^{131}I in Fallout, *Health Phys.*, *9:* 1113-1122 (1963).
3. E. P. Harvey, Jr., and W. R. Collins, Jr., Health and Safety Laboratory, Fallout Program Quarterly Summary Report for June 1, 1963, to September 1, 1963, USAEC Report HASL-140, Oct. 1, 1963; and Fallout Program Quarterly Summary Report for December 1, 1963, to March 1, 1964, USAEC Report HASL-144, Apr. 1, 1964.
4. L. Marquez, N. L. Costa, and I. G. Almeida, The Formation of ^{22}Na from Atmospheric Argon by Cosmic Rays, *Nuovo Cimento, 6*(6): 1292-1295 (1957). [Cited in *Nucl. Sci. Abstr., 12:* 6022 (1958).]
5. N. Bhandari and Rama, Atmospheric Circulation from Observations of Sodium-22 and Other Short-lived Natural Radioactivities, *J. Geophys. Res.*, *68:* 1959-1966 (1963).
6. H. E. Palmer and R. W. Perkins, Cesium-134 in Alaskan Eskimos and in Fallout, *Science, 142:* 66-67 (1963).
7. R. W. Perkins and J. M. Nielsen, Sodium-22 and Cesium-134 in Foods, People, and Air, to be published.
8. L. Marquez, N. L. de Costa, I. G. de Almeida, Centro Brasileiro de Pesquisas Fisicas, Cobalt-60 from Thermonuclear Tests in the Atmosphere, Report NP-7022, Notas de Fisica, Vol. IV, No. 6, May 22, 1958; and Radioisotopes from Fusion in Rain Water, Report NP-7023, Notas de Fisica, Vol. IV, No. 7, June 4, 1958.
9. J. R. Arnold and H. A. Al-Salih, Beryllium-7 Produced by Cosmic Rays, *Science, 121:* 451-453 (1955).
10. Rama and M. Honda, Natural Radioactivity in the Atmosphere, *J. Geophys. Res., 66:* 3227-3231 (1961).
11. A. K. Stebbins III, Second Special Report on High Altitude Sampling Program, Report DASA-539B, Defense Atomic Support Agency, Aug. 1, 1961; and J. P. Friend (Ed.), The High Altitude Sampling Program, Report DASA-1300, Isotopes, Inc., Aug. 31, 1961.
12. U. S. Public Health Service, Radiological Health Data, Vol. III, 1963, and Vol. IV, 1964.

13. T. Hvinden, A. Lillegraven, and O. Lillesaeter, Seasonal and Latitudinal Variations in Radioactive Fallout, Report F-412, Norwegian Defence Research Establishment, January 1961.
14. R. W. Perkins, Physical and Chemical Forms of ^{131}I from Fallout and Chemical Processing Plants, in Hanford Radiological Science Research and Development Annual Report for 1963, USAEC Report HW-81746, Hanford Atomic Products Operation, January 1964.

MEASUREMENTS OF THE PARTICLE SIZE DISTRIBUTION OF THE TROPOSPHERIC AEROSOL WITH A ROTATING-DISK SAMPLER

S. K. FRIEDLANDER* and RALPH E. PASCERI†
Johns Hopkins University, Baltimore, Maryland

ABSTRACT

Measurements were made of the particle size distribution of the aerosol at Baltimore, Md. Particles smaller than a few tenths of a micron in diameter were sampled by diffusion from room air to a rotating disk with an electron-microscope grid attached. The rotating disk provides a known convective field with a number of desirable characteristics. Particle size distributions were calculated from the distribution measured on the disk grid.

INTRODUCTION

As part of a study of the dynamics of the atmospheric aerosol, measurements have been made of the size distribution of the aerosol at Baltimore over the range between 70 A and 140 μ in diameter.[1] The experimental data are reported in terms of a size-distribution function, n(r), and the cumulative distribution function, N(r), defined as follows: The quantity n(r) dr is the number of particles per unit volume with radii between r and r + dr. Then N(r), the total number of particles per unit volume with radii greater than or equal to r, is given by

*Present address: W. M. Keck Engineering Laboratories, California Institute of Technology, Pasadena, Calif.
†Present address: Allegany Ballistics Laboratory, Cumberland, Md.

$$N(r) = \int_r^\infty n(r)\, dr \tag{1}$$

For this work it is convenient to divide the size spectrum into two regions: the upper end for particles larger than 0.2 μ in diameter and the lower end for those smaller than 0.2 μ in diameter. A simple new method was used to sample the lower end of the distribution. Particles were collected from room air by Brownian diffusion to an electron-microscope grid placed at the center of a 1-in. stainless-steel disk rotated about the axis normal to its face. The results of the rotating-disk study are reported in this paper.

THEORY

The theory of convective diffusion to a rotating disk has been worked out for the laminar flow regime by Levich[2] based on the velocity distribution derived from the theory of von Karman. This velocity distribution represents one of the few exact solutions of the Navier–Stokes equations of fluid motion. A striking result of the theory of the fluid motion is that the component of the velocity normal to the disk is a function only of distance from the disk surface and not of distance from the axis of rotation or angular position. As a result, Levich noted, there exists a solution to the equation of convective diffusion in which the concentration is a function only of distance from the disk surface. Moreover, the diffusion flux is uniform over the surface of the disk and is given by the following expression:

$$\frac{J}{C_\infty - C_0} = 0.62\, \nu^{-1/6} D^{2/3} \omega_0^{1/2} \tag{2}$$

where J = flux of matter, moles or particles/cm^2/sec
C_∞ = concentration at infinity
C_0 = concentration at disk surface
ν = kinematic viscosity
D = diffusion coefficient of the species with flux J
ω_0 = rotational speed of the disk

This expression is derived for the limiting-case Schmidt number = $\nu/D \to \infty$, but Eq. 2 is accurate[3] to within 7% of a more exact solution when ν/D is greater than 100. This limit corresponds to particles larger than about 0.0035 μ in radius under ordinary atmospheric conditions. The theory is also limited to the laminar flow regime, which has been found by experiment to exist below a Reynolds number, $\omega_0 R^2/\nu$, of 10^4 or 10^5, where R is the disk radius.

The theory has been checked experimentally by several investigators. Litt and Serad[4] rotated disks of various materials in water and

air. They measured the rates of dissolution of benzoic acid, cinnamic acid, and β-naphthol in water and the rate of evaporation of naphthalene in air. The experimental results agreed well with theory.

The rotating disk acts as a kind of centrifugal fan drawing in air from afar and hurling it out at its periphery. Continuity requires that the component of the fluid velocity normal to the disk be finite even at an infinite distance from the disk surface. The limiting value of this velocity component is $0.886\ (\omega_0 \nu)^{1/2}$; the limiting value is reached to a close approximation not far from the disk surface at a distance about equal to $5\ (\nu/\omega_0)^{1/2}$. For $\omega_0 = 2000$ rpm, the experimental condition, and $\nu = 0.150$ cm^2/sec for air, the limiting velocity of 5 cm/sec was attained at about 1.5 mm from the disk surface. With reasonable precautions against major drafts, velocities of this magnitude will be of controlling importance in the transfer process.

Olander[5] has considered the response of the transport rate to a rotating disk to a sudden concentration change at its surface. A step change of concentration at the surface is equivalent to a step change at the edge of the concentration boundary layer. For Schmidt numbers between 10^2 and 10^4, Olander found the mass transfer rate was within 5% of the new steady rate in the times $t = 8/\omega_0$ and $t = 30/\omega_0$, respectively. For the experimental ω_0 used in this study, the maximum time was about 0.25 sec.

Since the response time of the disk is so small, it may be considered to follow changes of concentration in the ambient atmosphere instantaneously. Hence, if a size-distribution function is determined for a sample run, it will have the time-averaged form

$$n(r) = \frac{\int_0^\tau n(r,t)\, dt}{\tau} \tag{3}$$

where τ is the sampling time.

Consistent with the theory of the diffusion battery, it is assumed that the disk is a perfect sink; i.e., $C_0 = 0$. Since a particle adhering to a rotating disk is subjected to centrifugal force, it is necessary to consider the magnitude of the force at the experimental rotation speeds. In this work, traversing in the electron microscope was limited to an inner circle of 0.03 cm in radius on the sampling grid. The acceleration on a particle situated on the circumference of this circle is about 2 G. Jordan[6] has presented calculations on the approximate forces required to dislodge small particles from surfaces and has shown that they are considerably greater than 2 G.

EXPERIMENTAL WORK

Sampling

The stainless-steel disk, 1 in. in diameter and $\frac{1}{4}$ in. thick, was connected to a Heller GT-21 stirrer with electronic speed control. The speed was checked with a stroboscope. The electron-microscope grid was centered on the disk face and attached to the surface with two pieces of scotch tape.

Two runs, 10 and 11, were made in the laboratory with the rotating disk at speeds of 2040 and 1980 rpm, respectively. The experiments were carried out consecutively (Sept. 11 to 13, 1963) with a brief interruption to replace the electron-microscope grid and to adjust the position of the rotating-disk assembly. The sampling times were approximately 13 and 25 hr for runs 10 and 11, respectively. In run 10 the disk face was positioned in a vertical plane, and in run 11 it was horizontal and faced the ceiling. The laboratory door was kept closed most of the time. A 20-in. window fan installed above the laboratory door was not operated during the sampling periods, but the fan opening permitted contact with the outside hallway. Since a draft was always present in the hallway, air exchange with the room was probable.

It should be possible to reduce the sampling time in a number of ways: (1) Since the deposition rate is directly proportional to the aerosol concentration, the sampling time would be reduced in direct proportion to an increase in concentration; (2) since the deposition rate is proportional to $\omega_0^{\frac{1}{2}}$, the speed can be increased above the 2000 rpm of these experiments with proper attention to mechanical problems and to the maintenance of a laminar flow regime; and (3) it would be possible to run over a shorter time by examining and photographing more fields. A limitation is imposed by the amount of background material present on the fresh grid.

Preparation of Electron-microscope Grids

The grids were made of 400-mesh copper screen with a diameter of $\frac{1}{8}$ in. and a thickness of approximately 0.001 in. They contained about 600 square openings, each having dimensions on each side of about 25 μ. The grid substrate was a carbon film prepared by evaporating carbon onto freshly cleaved mica. Details of the process are given in Pasceri's dissertation.[1] The films obtained were estimated to be between 100 and 200 A in thickness.

The carbon films were stripped from the mica by floating them onto the surface of demineralized, double-filtered (0.3-μ Millipore filters) water. Beneath the surface of the water, several grids were laid on a clean Monel screen. The screen was gently lifted from the

water to transfer the film to the grids. The carbon was caught on the grids as they passed through the water surface.

Grid Shadowing with Platinum

After being rotated in room air, the grid was carefully removed from the disk with sharp tweezers and placed in a petri dish to be shadowed with platinum. A blank grid, which was prepared along with the sample grid, was also set aside to be shadowed. The blank served as a check on the particulate contamination level in the substrate application process. The shadowing served two purposes: (1) It assured good visibility of particles not opaque to the electron beam, and (2) it provided a permanent impression of particles that might have been destroyed in the electron beam.

The shadowing technique was similar to that described by Hall.[7] The electron-microscope grids were placed in an evaporator pumped down to 0.05 μ Hg in about 30 min. Platinum evaporated from a wire wound about a tungsten support wire condensed on the grids. The effect of the size distribution of the deposited particles is not known. It would be of interest to vary the time of exposure of the grid to vacuum to see the effect on the measured distribution.

Electron-microscope Examination

Sample grids were examined with an RCA type EMU-3 electron microscope at various magnifications (18,200X to 5610X), depending on the particle size range under study and the abundance of these particles on the grid. Since the instrument had grid-position indicators, it was possible at each magnification to traverse a grid in a regular fashion. The magnification was determined before and after each set of traverses by photographing areas of a shadow-cast carbon-grating replica (28,000 lines per inch) with the magnification of the set taken as the mean of the two determinations. No micrographs were made of a region on which the substrate was broken.

The photographic plates exposed in the electron microscope were examined with a 10-power Bausch and Lomb eyepiece fitted with 0.1-mm grating. The apparent particle diameter measured in this way included a contribution from the thickness of the platinum cap. Based on careful experimental measurements with shadowed polystyrene spheres, a correction factor of 40 A was applied to the apparent diameter.

RESULTS

The flux, dJ, of particles in the range r, dr to the grid surface is

$$dJ = 0.62\, D^{2/3}\nu^{-1/6} n(r)\, dr \tag{4a}$$

$$= k_d n(r)\, dr \tag{4b}$$

where k_d, the deposition velocity, is defined by the preceding expression and $n(r)\,dr$ is the ambient concentration of particles in the range r to r + dr. The deposition flux may be expressed in terms of the cumulative distribution of particles measured on the electron micrographs, $\Sigma(r)$:

$$dJ = -\frac{d\,\Sigma(r)}{A\tau} \tag{5}$$

where A is the area examined on the grid and τ is the total sampling time of the rotating disk. Hence, from Eqs. 4b and 5,

$$n(r) = -\left[\frac{d\,\Sigma(r)}{dr}\right]\left(\frac{1}{k_d A\tau}\right) \tag{6}$$

where n(r) is the time-averaged distribution defined by Eq. 3.

The particle diffusion coefficient, D, can be estimated from the Stokes–Einstein expression

$$D = \frac{kT}{f} \tag{7}$$

where k is Boltzmann's constant and T is the absolute temperature. The coefficient of frictional resistance, f, can be calculated (assuming a spherical particle) by the expression

$$f = \frac{6\pi\mu r}{C} \tag{8}$$

where μ is the viscosity of the medium (air). The semiempirical correction factor recommended by Davies[8] is

$$C = 1 + \frac{\lambda}{r}\left(1.257 + 0.400e^{-1.10r/\lambda}\right) \tag{9}$$

when the mean free path of the air, λ, is given by

$$\lambda = 0.708\nu\left(\frac{\pi M}{RT}\right)^{1/2} \tag{10}$$

where M is the molecular weight, ν is the kinematic viscosity, and R is the gas constant.

Since each sample grid was examined at two magnifications, there are two $\Sigma(r)$ curves for each run, one covering the size range below about 0.02 μ and the other the range 0.015 to 0.08 μ. In principle, the two sets of $\Sigma(r)$ data can be combined to form one set by the application of a correction factor involving the areas examined at each magnification. This method was rejected since the uncertainties of low particle count around 0.015 μ for the smaller particle set and inaccurate sizing around 0.015 μ for the larger particle set would magnify the error in the overlap region. For these reasons, it was decided to seek an

algebraic expression for the $\Sigma(r)$ data of each range and then apply Eq. 6 to obtain $n(r)$ for each range. The two $\Sigma(r)$ curves could then be compared in the overlap region to ascertain the previously mentioned uncertainties.

The $\Sigma(r)$ data for runs 10 and 11 are shown in Figs. 1 to 4. For both runs the $\Sigma(r)$ data obtained at high magnification (smaller size

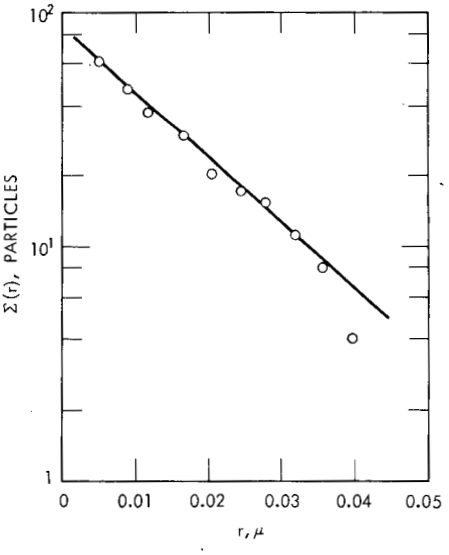

Fig. 1—Cumulative distribution data for run 10. In the very small particle size range, there is a linear relation between the log of the cumulative function and the radius.

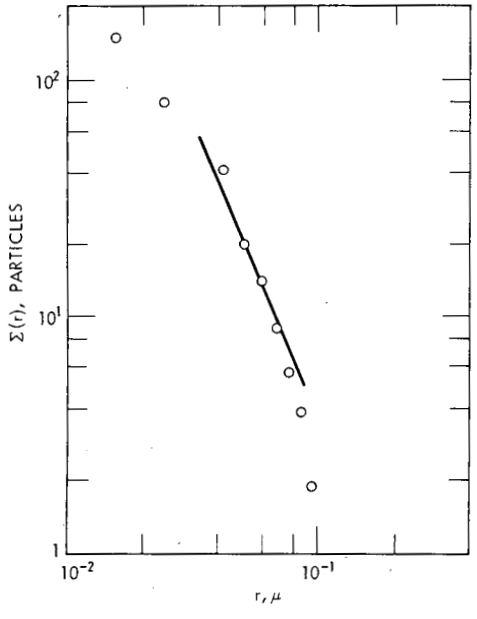

Fig. 2—Cumulative distribution data for run 11. In the small particle size range, there is a linear relation between the log of the cumulative function and the radius.

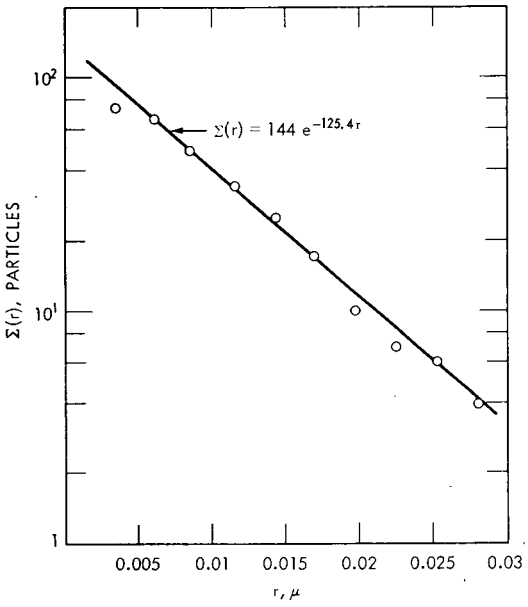

Fig. 3—Cumulative distribution data for run 10 showing the larger particle size range. A linear relation can be used to approximate the data over part of the range on a log–log plot.

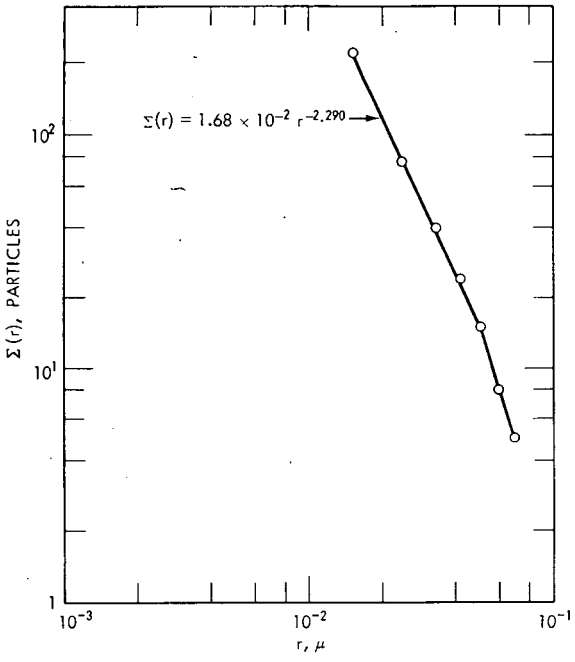

Fig. 4—Cumulative distribution data for run 11 showing the larger particle size range. A linear relation can be used to approximate the data over part of the range on a log–log plot.

range) fell on a straight line on semilog paper. At low magnifications (larger size range), the data followed a linear relation on log–log paper, at least through the most reliable data points. Analytical expressions for $\Sigma(r)$ were obtained from these figures. The expressions were differentiated and divided by $-k_d A\tau$ to yield $n(r)$. The deposition velocity k_d had an awkward form but was approximated by two simple expressions of the type $k_d \sim r^p$ for the two size ranges examined. The final expressions for $n(r)$ are given in Table 1.

Table 1 — FORMULAS FOR n(r) OF RUNS 10 AND 11

	Run 10	Run 11
High magnification	$3.98 \times 10^8\, e^{-63.3}\, r^{+1.29}$ $(0.0056 < r < 0.04\ \mu)$	$3.26 \times 10^9\, e^{-125.4}\, r^{+1.29}$ $(0.0035 < r < 0.019\ \mu)$
Low magnification	$3.31 \times 10^2\, r^{-2.28}$ $(0.04 < r < 0.08\ \mu)$	$5.22 \times 10^2\, r^{-2.047}$ $(0.019 < r < 0.05\ \mu)$

These curves are shown in Fig. 5 with the vertical bars representing the radius increments of the original electron-micrographic measurements.

The preshadowing contamination on the grids used for runs 10 and 11 was checked with blank grids. It was found that the particulate contamination level present before sampling was always less than 3% of the total particle count made at each magnification.

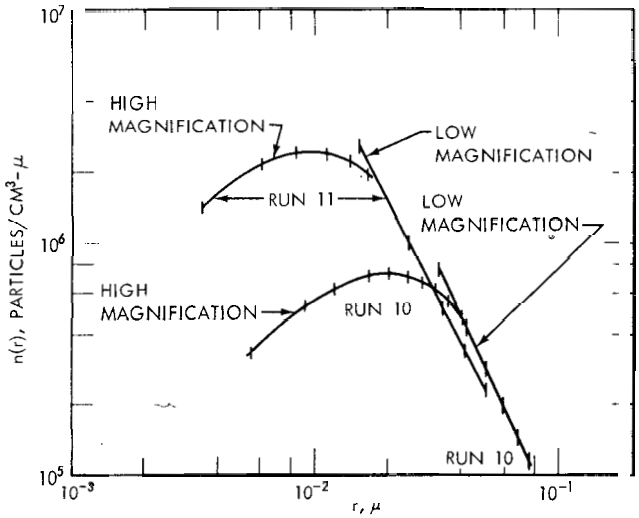

Fig. 5—Size distribution functions for runs 10 and 11. The number of particles in the range between r and r + dr is given by n(r) dr. The distribution peaks near radii of 0.02 and 0.01 μ.

DISCUSSION

The two consecutive time-averaged distributions differ about two-fold in magnitude in the range $r < 0.025\ \mu$ and also show a shift in the maximum with radius. In both runs the maximums are well defined although the behavior of the distribution function below $r = 0.005\ \mu$ is not known. For $r > 0.025\ \mu$, the distribution function shows little change with time. The very small particle end of the spectrum seems more susceptible to variation than the part above $r = 0.025\ \mu$. This variation may be the result of fluctuations in the strength of local sources of very finely dispersed matter. Such particles can diffuse rapidly from their point of introduction into the atmosphere. On the other hand, the possibility of an artifact in the sampling cannot be ruled out as an explanation of the variation between the two runs.

The results of the two runs are shown in Fig. 6, with the distribution functions calculated from data presented by Junge[9] and Cartwright[10] for the small particle range. Junge calculated his data points from ion-mobility measurements. The Zugspitze curve shows a maximum at about the same radius observed in this study. The original data of

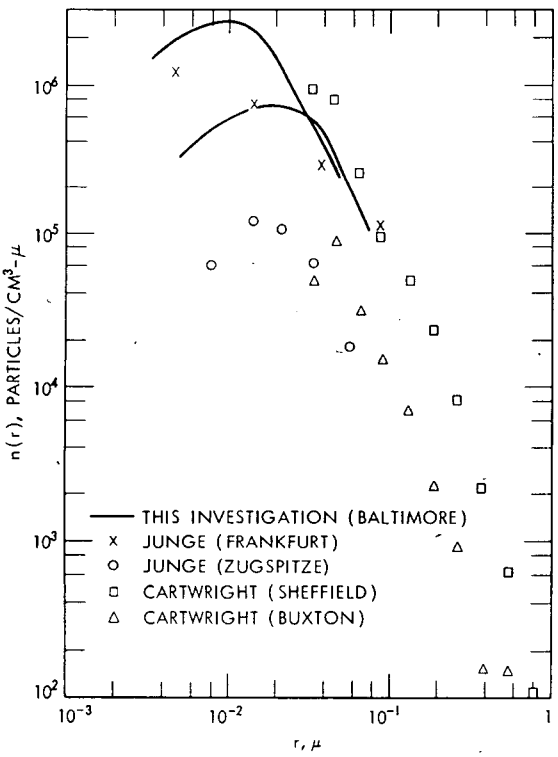

Fig. 6—Comparison of the particle size distribution data obtained in the small size range in this study with the results of other investigators. A considerable variation occurs in the shape of the distribution from place to place and time to time. This is in contrast with the behavior of the upper end of the distribution ($r > 0.02\ \mu$), which appears to be more stable.

Cartwright were obtained with a thermal precipitator. The shapes of the spectra obtained in this study and in those by Junge and Cartwright are similar above a radius of 0.04 μ. This is consistent with the theory of self-preserving size distributions proposed by Friedlander.[11,12,13] Below 0.04 μ the shape of the distribution is subject to variation with time and location. It should be noted that the distributions reported in this study are time-averaged over both one-half day and one day; Junge's data are the average of several determinations taken over short (a few minutes) consecutive intervals and Cartwright's distributions represent single determinations over equally short sampling times.

CONCLUSIONS

This new sampling method has a number of important advantages. It is very simple, and it provides a large surface over which deposition is uniform. The relation of the distribution of the deposited sample to the distribution in the gas is known from theory. Efficiency of removal increases as particle size decreases. The method should be easily adaptable to autoradiographic techniques.

REFERENCES

1. R. E. Pasceri, The Size Distribution of Atmospheric Aerosols, Ph. D. Dissertation, Johns Hopkins University, Baltimore, Md., 1964.
2. V. G. Levich, *Physicochemical Hydrodynamics*, pp. 65-72, Prentice-Hall, Inc., Englewood Cliffs, N. J., 1962.
3. E. M. Sparrow and J. L. Gregg, Heat Transfer from a Rotating Disk to Fluids of any Prandtl Number, *J. Heat Transfer, 81:* 249-251 (1959).
4. M. Litt and G. Serad, Chemical Reactions on a Rotating Disk, Part II—Experimental, to be published in *Chemical Engineering and Science.*
5. D. R. Olander, Unsteady-state Heat and Mass Transfer in the Rotating Disk System, *Intern. J. Heat Mass Transfer, 5:* 825-836 (1962).
6. D. W. Jordan, The Adhesion of Dust Particles, *Brit. J. Appl. Phys., 5* (Suppl. 3): S194-S197 (1954).
7. C. E. Hall, Measurement of Globular Protein Molecules by Electron Microscopy, *J. Biophys. Biochem. Cytol., 7:* 613-618 (1960).
8. C. N. Davies, Definitive Equations for the Fluid Resistance of Spheres, *Proc. Phys. Soc., 57:* 259-270 (1945).
9. C. Junge, The Size Distribution and Aging of Natural Aerosols as Determined from Electrical and Optical Data on the Atmosphere, *J. Meteorol., 12:* 13 (1955).
10. J. Cartwright, The Electron Microscopy of Airborne Dusts, *Brit. J. Appl. Phys., 5* (Suppl. 3): S109-S119 (1954).
11. S. K. Friedlander, On the Particle Size Spectrum of Atmospheric Aerosols, *J. Meteorol., 17:* 373 (1960).
12. S. K. Friedlander, Similarity Considerations for the Particle-Size Spectrum of a Coagulating, Sedimenting Aerosol, *J. Meteorol., 17:* 479 (1960).
13. D. L. Swift and S. K. Friedlander, The Coagulation of Hydrosols by Brownian Motion and Laminar Shear Flow, *J. Coll. Sci., 19:* 621 (1964).

DOSIMETRIC INVESTIGATIONS OF ENVIRONMENTAL GAMMA RADIATION FROM DEPOSITED FISSION PRODUCTS

WAYNE M. LOWDER, HAROLD L. BECK, and WILLIAM J. CONDON
Health and Safety Laboratory, U. S. Atomic Energy Commission, New York, New York

ABSTRACT

The presence of significant quantities of gamma-emitting fission products in the environment as a result of nuclear-weapons testing has made necessary the development of techniques for differentiating between the natural- and the fallout-gamma components of the total environmental radiation field. This has been achieved by the use in the field of a gamma-spectrometer system with a 5- by 3-in. NaI(Tl) detector. A combination of theoretical calculations and laboratory calibration experiments has enabled natural-gamma-radiation dose rates to be obtained from estimated total-absorption peak areas in the spectra or from the total counts in bands including these peaks. The peak method can be similarly applied to the main fallout-gamma emitters ($^{95}Zr-^{95}Nb$, ^{137}Cs, ^{106}Rh, and ^{103}Ru) to obtain their respective dose-rate contributions. The total fallout dose rate can be obtained from the difference between the total gamma dose rates and the natural-gamma contribution. It is estimated that the total dose rate can be measured to ± 0.5 μr/hr (standard deviation) and the individual components to $\pm 10\%$.

Over 300 gamma-energy spectra have been obtained at more than 200 different locations throughout the United States. Most of the inferred natural-gamma dose rates were in the range of 5 to 9 μr/hr. Open-field-fallout dose rates between July 1962 and September 1963 ranged between 2 and 6 μr/hr, except in areas having very little rain-

fall. By the end of 1963, dose rates in the eastern United States had declined to approximately 1 μr/hr, mainly from ^{137}Cs, and have since remained close to that value. No increased gamma radiation has been noted in New York from fallout from the 1964 Chinese test.

INTRODUCTION

Estimates of long-term human exposure to environmental radiation require detailed information on the properties of the various natural and man-made components of the environmental radiation field in areas of human habitation and activity. Since 1955 the Health and Safety Laboratory (HASL) has been conducting a study of the properties of the more penetrating components of the natural environmental radiation field, which include the cosmic radiation and gamma rays from radioisotopes in the ground and the lower atmosphere. Sensitive ionization chambers have been developed which provide accurate measurements of the total dose rate. The significant contribution in recent years from gamma-emitting fission products to the total dose rate has made necessary the development of supplementary techniques for differentiating between the natural and fallout components. Gamma-ray spectra obtained directly in the field with a large NaI(Tl) detector have been found to provide sufficient detail to allow reasonably precise and accurate estimates of the dose-rate contributions from the gamma rays of ^{40}K and the daughters of ^{238}U and ^{232}Th and also from those of the significant fallout-gamma emitters, in particular, ^{95}Zr–^{95}Nb, ^{106}Rh, and ^{137}Cs. The success of these techniques has made possible the continuation of our natural-radiation studies through periods of substantial fallout deposition besides providing information relevant to considerations of human exposure to fallout-gamma radiation.

Several hundred gamma spectra at over 200 different locations in the United States have been obtained over the past several years. These measurements were taken to obtain information on gamma-radiation fields in particular areas of interest, to study the applicability and validity of our spectrometric methods over a wide range of environmental radiation fields, and to evaluate the performance of our instrumentation under differing field conditions.

We shall briefly outline here the methods used to infer dose rates from these spectra, present some evidence to indicate the validity of these dose-rate estimates, and discuss some of the results of our various measurements. The complete data for all locations are being presented in a series of HASL reports.[1–3] In addition, we have published several review articles,[4–6] and a detailed report on our spectrometric techniques has recently been published.[7]

SPECTROMETRIC TECHNIQUES

Figure 1 shows a typical field measurement in progress. The site chosen is usually a large flat open space situated in or near a populated area. A 5- by 3-in. cylindrical NaI(Tl) detector is placed 1 m above-

Fig. 1—HASL pressurized ionization chamber and spectrometer set up for a typical measurement. Saratoga Springs, N. Y., 1963.

ground facing downward through a hole in a small wooden platform. A 50-ft coaxial cable connects the detector to a multichannel pulse-height analyzer mounted in the HASL vehicle. Readout is by both typewriter and paper-tape punch. Power is supplied by a 300-watt 12-volt d-c–115-volt a-c rotary inverter operating off the car battery. A 20-min live time for each reading has been found to provide sufficiently detailed spectra. A high-pressure ionization chamber is placed nearby. This chamber contains 8 liters of argon at 40 atm and is carefully calibrated against standard radium sources and known cosmic-ray fields.[8] A battery-operated vibrating reed electrometer is mounted directly on the chamber head, thus making the instrument completely self-contained.

Two typical gamma spectra are shown in Fig. 2. All field spectra obtained during 1962 and 1963 show the same four conspicuous total-

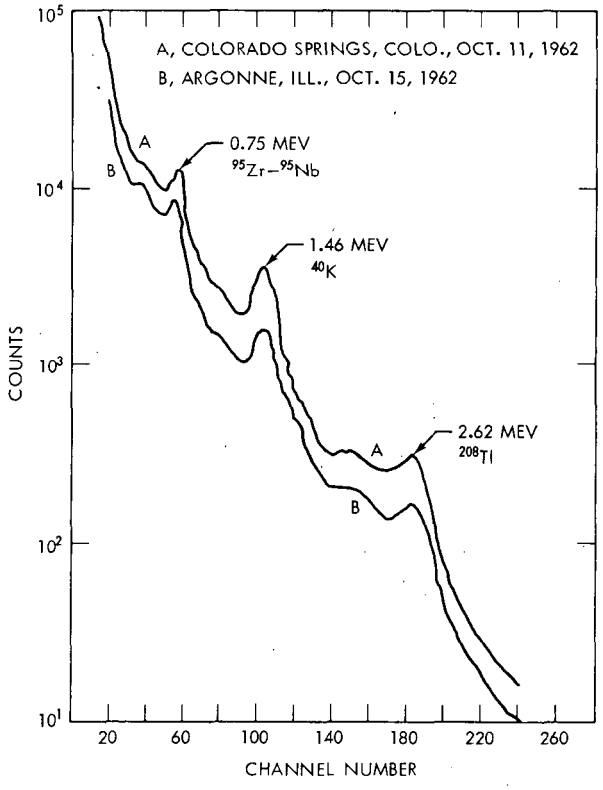

Fig. 2—Two typical field spectra obtained during late 1962. The cosmic, natural-gamma, and fallout-gamma levels are all somewhat higher at location A.

absorption peaks, at 0.5 Mev (^{140}Ba–^{140}La, ^{103}Ru, and ^{106}Rh), 0.75 Mev (^{95}Zr–^{95}Nb), 1.46 Mev (^{40}K), and 2.62 Mev (^{208}Tl), as well as other minor peaks, including the 1.76 Mev ^{214}Bi peak. By a determination of the area under these peaks or of the total number of counts in energy bands bracketing them, estimates can be made of the contribution from each emitter or series of emitters to the total dose rate in air at 1 m aboveground.

In the former method the area under each total-absorption peak is approximated by assuming a linear continuum under the peak on semi-log paper, fit to the values on each side. This area, although not necessarily identical to the true number of total-absorption counts, is assumed to be directly proportional to the incoming flux of primary photons. This has been satisfactorily checked in the laboratory for several energies and over a wide range of flux values. If a uniform source distribution in the soil for the naturally occurring radioisotopes and an exponential distribution for fallout emitters are assumed, the flux and

angular distribution of the primary photons and the total dose rate expected per unit source concentration can then be calculated for infinite-half-space geometry, using the best available decay schemes. The response of the detector in terms of estimated peak counts per unit flux is obtained in the laboratory as a function of angle by using standard monoenergetic gamma sources, and a simple calculation then provides a conversion factor from estimated peak counts to dose rate.[5–7]

The second method of obtaining component dose rates is to relate the total detector response in bands bracketing the three peaks characterizing the major natural emitters by means of three simultaneous equations. This is similar to the technique used in many laboratory spectrometric analyses except that, instead of determining the coefficients of these equations by calibration with standard sources, which is not practical for our case of an infinite-half-space geometry, we obtained them by applying regression analyses to a large number of spectra, using the dose-rate predictions from the absorption peak areas.[7] This band method is more amenable to routine data-analysis procedures and also provides more precise individual dose-rate determinations.

CALIBRATION VERIFICATION

The analysis of spectra by these methods provides the type of information shown in Table 1. The particular locations were chosen at random to demonstrate the consistency of our results over a wide range of natural, fallout, and cosmic dose rates. The consistency obtained is in fact the ultimate justification for our procedures. The column labeled "Spectrometer" is the total terrestrial gamma dose rate inferred from the spectra by dividing the total energy in the spectra between 0.15 and 3.4 Mev by an empirically determined conversion

Table 1 — REPRESENTATIVE SURVEY RESULTS

Town	Date	Dose rates, μr/hr							
		Total gamma		Natural gamma			Fallout gamma		Cosmic ray
		Ion chamber	Spectrometer	K	U	Th	1	2	
Memphis, Tenn.	Apr. 1963	11.8	11.2	1.8	1.7	2.7	5.0	5.3	3.5
Lake Charles, La.	Apr. 1963	8.4	8.6	0.7	0.9	1.9	5.2	5.0	3.4
Bonnydoon, Calif.	Oct. 1962	13.6	13.4	8.5	2.2	1.9	1.8	0.9	4.0
	Oct. 1962	12.3	12.7	7.7	2.5	1.5	1.2	1.0	4.0
Denver, Colo.	Oct. 1963	16.3	15.4	4.0	2.5	8.7	0.6	0.6	6.3
Clallam Bay, Wash.	Oct. 1962		5.3	1.0	1.3	0.4	2.8	2.6	3.6
North Conway, N. H.	Aug. 1962	13.2	12.7	3.8	1.1	5.0	2.9	2.8	3.6
	Sept. 1963		14.9	3.5	2.1	5.2	3.5	4.1	3.5
	May 1964	10.7	11.0	3.0	1.5	4.8		1.7	3.6

factor.[7] Note that this dose-rate estimate agrees closely with the pressure-chamber prediction in almost all cases. The column labeled "1" under the "Fallout gamma" heading gives the sums of the $^{95}Zr-^{95}Nb$, ^{106}Rh, and ^{137}Cs dose rates as estimated from the spectrum absorption peaks. The column labeled "2" gives the differences between the best value of the total gamma dose rate and the sum of the natural-gamma dose-rate components. The agreement of these two fallout estimates over this wide range of natural, fallout, and cosmic dose-rate levels is typical of almost all our data. These results imply that the fallout emitters considered in our analyses do contribute the bulk of the fallout dose rate and also indicate the general validity of our component dose-rate estimates. The North Conway, N. H., measurements show that our estimates are reproducible within the limits imposed by actual time variations in the natural-gamma-radiation field due to such causes as natural fallout, soil-moisture changes, and ^{222}Rn migration.

Further evidence of the accuracy of our natural-component dose-rate estimates is provided in Figs. 3 and 4. Figure 3 shows mean soil concentrations of ^{40}K obtained by spectrometric analysis of soil samples carried out at several laboratories plotted against the HASL dose-rate estimates. The curve is the theoretical conversion from percent potassium to dose rate, assuming uniform soil distribution. The soil concentrations are given in terms of percent of potassium per gram of dry soil, whereas our dose-rate estimates are for *in situ* material. Thus, since most soils contain some moisture, the points should be expected to fall slightly above the line on the average. Furthermore, since only one or two soil samples were taken at each site, these de-

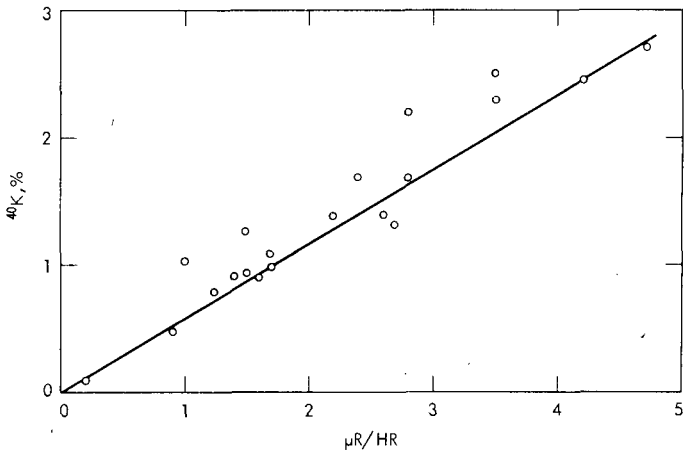

Fig. 3—Potassium soil content determined by soil-sample analysis vs. HASL ^{40}K dose-rate estimate. ——, the theoretical conversion from percent potassium to microroentgens per hour.

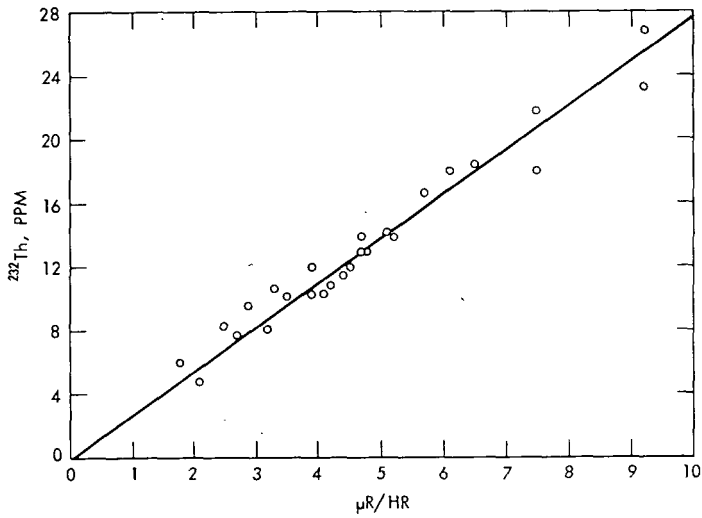

Fig. 4—Rice University in situ ^{232}*Th soil content vs. HASL energy-band* ^{232}*Th dose-rate determinations. ——, the theoretical conversion from* ^{232}*Th parts per million to microroentgens per hour.*

terminations of soil concentration may not necessarily be representative of the average concentration in the volume seen by the spectrometer. The scatter of points seen in Fig. 3 reflects this fact as well as the usual instrumental uncertainties.

Figure 4 shows soil concentrations of ^{232}Th plotted against the HASL ^{232}Th dose-rate estimates. The curve is again the theoretical conversion, assuming uniform soil distribution. These soil concentrations were obtained in the field by J. A. S. Adams of Rice University, using a portable scintillation spectrometer system.[9] Both these and the HASL measurements are *in situ*, and thus no systematic difference in slope is observed between the line and the points. The results shown in Figs. 3 and 4 indicate the high degree of reliability of our ^{40}K and ^{232}Th dose-rate estimates. Unfortunately, soil concentrations of ^{238}U derived by assuming radioactive equilibrium in the decay series, e.g., by soil analyses when such equilibrium is often closely approximated, are not directly comparable to our uranium-series dose-rate estimates due to the reduction in dose rate caused by ^{222}Rn emanation from the soil in the field situation. The available ^{238}U results do indicate, however, that our uranium-series dose-rate estimates are reasonable, although not as precise as those for ^{40}K and the thorium series.

SURVEY RESULTS

In Table 2 are listed the surveys undertaken by HASL teams during the past three years. The indicated gamma dose-rate ranges include 80 to 90% of the spectrometer readings for each survey. Most of the

Table 2—SUMMARY OF SURVEY RESULTS IN 1962 TO 1964

Survey area	Date	No. of locations	Gamma dose-rate range, μr/hr	
			Natural	Fallout
New York	Aug. 1963	35	5 to 7	3 to 4
South and west	Aug. 1964	9	5 to 7	0.5 to 1
North	Aug. 1963	19	4 to 8	3 to 5
New York City	May to Sept. 1962	3	5 to 10	3 to 5
	May to Sept. 1963	3	7	4 to 5
	Jan. to Sept. 1964	3	7	0.5 to 2
Vermont	July 1962	26	4 to 8	2 to 3
	Aug. 1963	6	4 to 8	4 to 5
New Hampshire	July 1962	39	6 to 15	2 to 3
	May 1963	5	6 to 8	3 to 5
	Sept. 1963	10	6 to 15	3 to 5
	May 1964	4	7 to 11	1 to 2
Southeastern United States*	Apr. 1963	8	3 to 7	4 to 7
South Carolina	Apr. 1963	6	3 to 10	4 to 7
North Carolina	Apr. 1963	2	15 to 19	2 to 4
Western United States				
Black Hills, S. Dak.	Oct. 1962	6	6 to 8	2 to 5
	Oct. 1962	4	6 to 8	3 to 4
Seattle, Wash.	Oct. 1962	3	4	2
Olympic Peninsula, Wash.	Oct. 1962	9	3 to 5	1 to 4
San Francisco, Calif.	Oct. 1962	6	4 to 8	1 to 2
	Oct. 1963	6	5 to 8	1
Nevada and Utah	Oct. 1962	6	5 to 9	1 to 4
	Oct. 1963	3	5 to 9	2 to 3
Denver and Colorado Springs, Colo.	Oct. 1962	9	9 to 14	2 to 3
	Oct. 1963	10	8 to 15	1 to 2
Central United States†	Oct. 1962	15	7 to 9	3 to 6
	Oct. 1963	11	7 to 9	2 to 4

*Includes locations in Texas (2), Louisiana (1), Arkansas (1), Alabama (2), Tennessee (1), and Georgia (1).

†Includes locations in Wisconsin (1), Minnesota (1), eastern South Dakota (4), Illinois (4), Kansas (3), and Missouri (2).

natural-gamma values fall between 5 and 9 μr/hr, with an average reading for all 210 locations of 7 μr/hr. Higher observed natural-gamma dose rates occurred in the Denver, Colo., and the Conway, N. H., areas, where average readings of 11 μr/hr were encountered. In both of these regions, high thorium contents in the soils were primarily responsible for the enhanced readings (e.g., see Table 1). In general, it has been observed that ^{40}K and the thorium series contribute roughly equally to the natural-gamma-radiation field and the uranium series a somewhat lesser amount, seldom amounting to more than 25% of the total. The unexpectedly low uranium-series dose rates at many locations are related to the removal of the parents of the gamma-emitting radioisotopes from the upper layers of the soil by the leaching of ^{238}U and ^{226}Ra and the emanation of free ^{222}Rn gas from the soil into the atmosphere.

The preceding discussion of natural-radiation measurements sets into proper perspective the significance of additional gamma radiation in the environment from man-made sources. In Table 2 it is note-

worthy that during the 1962 and 1963 surveys the fallout-gamma levels were a significant fraction of the total. Dose rates of 3 to 4 μr/hr seemed to be typical of the eastern United States during this period. The highest fallout levels were observed during the spring and summer of 1963, with dose rates of 4 to 6 μr/hr at a number of locations scattered throughout the eastern states. The 1964 measurements, limited to the northeastern states, all indicate greatly reduced fallout levels, averaging 1 μr/hr, with ^{137}Cs replacing ^{95}Zr–^{95}Nb as the main contributor.

These apparently rather significant changes in typical fallout-gamma-radiation fields during the past two years have been followed closely at three locations in Westchester County, N. Y., separated by distances of approximately 5 miles from one another. The measurements at these locations all show comparable variations with time, the fallout-gamma dose rates remaining roughly constant at 5 μr/hr from May to September 1963 and then declining with an apparent half-life slightly longer than that for the previously dominant ^{95}Zr–^{95}Nb. By the end of 1963, the levels were down to 1 μr/hr and have remained close to that value throughout 1964. It is interesting to note that these Westchester County measurements are in very close agreement with the dose-rate values calculated from detailed deposition data for the various fallout gamma emitters obtained at Westwood, N. J., approximately 15 miles to the west.[10]

The complete data for the Pelham, N. Y., location are given in Table 3. The agreement between the two fallout estimates is generally

Table 3—MEASUREMENTS AT PELHAM, N. Y.

	Gamma dose rates, μr/hr						
	K	U	Th	Total natural	Fallout 1	Fallout 2	Total
1963							
May 3	2.8	1.5	3.6	7.9	7.2	4.6	12.5
May 13	3.0	1.0	3.3	7.3	4.9	5.1	12.4
May 27	2.9	1.2	3.4	7.5	5.7	5.8	13.3
June 24	2.5	1.2	3.4	7.1	4.8	5.1	12.2
July 26							11.6
Aug. 6	2.5	1.6	2.9	7.0	6.5	5.1	12.1
Aug. 26	2.3	1.7	3.6	7.6	5.3	4.1	11.7
Sept. 12							11.3
Sept. 27							10.3
Oct. 29	2.3	1.2	3.4	6.9	2.3	2.4	9.3
Nov. 20	2.4	1.2	3.0	6.6	2.3	2.6	9.2
1964							
Jan. 22							7.8
Apr. 17	2.1	1.3	2.6	6.0	1.3	1.8	7.8
May 8	2.4	1.7	3.1	7.2	1.2	1.1	8.3
July 21	2.1	1.4	2.6	6.1	1.4	1.6	7.7
Aug. 12	2.7	1.2	3.2	7.1	1.1	1.1	8.2
Sept. 25	3.1	1.7	3.4	8.2	1.1	0.7	8.9
Oct. 21	2.1	1.4	2.8	6.3	0.9	1.2	7.5
Nov. 2	2.3	1.7	3.0	7.0	0.8	0.4	7.4
Nov. 27	2.1	1.4	2.8	6.3	1.0	1.0	7.3

close. The decline in late 1963 is quite striking. It should be noted that the differences in the various natural-gamma readings are at least partly real. For example, the low reading in April 1964 was obtained when the ground was quite wet. This would tend to reduce all components to some extent.

Rainfall can have a significant effect on both the total observed fallout dose rates and on how well they can be determined. This is exemplified by our October 1962 measurements on the Olympic Peninsula in the state of Washington, given in Table 4. Over a distance of 50

Table 4 — MEASUREMENTS ON THE OLYMPIC PENINSULA, WASHINGTON, OCTOBER 1 AND 2, 1962

Town	Mean annual rainfall, in.*	^{90}Sr, mc/sq mile†	Gamma dose rates, $\mu r/hr$						
			^{40}K	^{238}U	^{232}Th	$^{95}Zr-^{95}Nb$	Total Natural	Total Fallout 1‡	Total Fallout 2§
Sequim	14	42.0	1.2	0.9	1.2	0.6	3.3	0.8	0.7
Sequim	14		1.5	0.9	1.4	0.8	3.8	1.1	1.4
Port Angeles	24	65.3	1.6	0.9	1.0	1.1	3.5	1.4	1.7
Port Angeles	24		1.2	1.1	0.9	1.0	3.2	1.3	1.5
Joyce	54	84.1	1.7	1.2	0.8	1.8	3.7	2.4	1.8
Clallam Bay	81	133	1.0	1.3	0.4	2.2	2.7	2.8	2.6
Forks	118	153	1.7	2.2	1.3	2.6	5.2	3.4	2.7
Forks	118		1.5	1.7	1.2	2.5	4.4	3.7	2.8
Forks	118		1.1	1.1	0.9	2.3	3.1	3.4	2.8

*1960–1962 value.
†Oct. 1–2, 1962, soil determinations (L. T. Alexander).
‡From photopeak calibrations.
§From total terrestrial dose-rate measurements with natural component subtracted.

miles from east (Sequim) to west (Forks), the mean annual rainfall increases by a factor of nearly 10. This was strikingly illustrated for us at Forks by the soggy condition of the ground, the mist in which we made our measurements, and the two sudden downpours that nearly put a permanent end to our survey. The strong increase in the fallout-gamma levels with mean annual rainfall is clear from the table, as is the poorer agreement between our two methods for estimating these levels at Forks than at the other locations. The latter phenomenon can be explained as the effect of recent deposition of significant quantities of fission products, particularly $^{95}Zr-^{95}Nb$, forming a more nearly plane source than our theory assumes and thus resulting in an overestimate of the dose rate from the peak method. The presence of the short-lived $^{140}Ba-^{140}La$ peaks in our Forks spectra provides further evidence of recent deposition.

Our survey results taken as a whole indicate that, until late in 1963, $^{95}Zr-^{95}Nb$ contributed 60 to 80% of the observed fallout-gamma dose rate in the environment and that these dose rates were of the order of 50% of the natural levels at typical locations over open ground. By one year after the last nuclear weapons tests in December 1962, these levels had fallen to 10 to 20% of the average natural-gamma dose

rates; it is expected that this percentage will remain nearly constant for some time because of the important contribution from long-lived ^{137}Cs. Any consideration of the degree of exposure of the general population to external gamma radiation from fallout in the environment must take into account a number of factors that have not been discussed here, one of the most important of which is that open-field dose rates are certainly not typical of highly urbanized areas where structural shielding and the removal of the fission products from hard surfaces play important roles in reducing the exposure of large numbers of people. However, our observations during and shortly after the recent period of nuclear testing indicate that at such times the exposure of the general population to fallout-gamma radiation cannot be considered negligible in comparison with that from natural sources.

CONCLUSIONS

The techniques briefly described in this paper enable total environmental radiation dose rates to be measured to an accuracy of close to ±5% (standard deviation) in a typical situation and the individual components to an accuracy of approximately ± 10%. It seems quite probable that real changes of 0.5 μr/hr or less in the total radiation field would be unambiguously detected by both the high-pressure ionization chambers and the spectrometer and that the appearance of the field spectrum would be noticeably changed if the contributing gamma emitters had not been previously present in significant quantities. It follows then that such techniques are particularly applicable to any situation where the possibility of widespread low-level contamination of the environment by gamma-emitting radioisotopes is of concern and the rapid accumulation of information is of special value.

ACKNOWLEDGMENTS

We would like to acknowledge the assistance and encouragement of James E. McLaughlin, Director, Radiation Physics Division, in many phases of the work described herein, as well as the participation of a number of our colleagues, including Keran O'Brien, Robert Sanna, and Stephen Samson, in some of the survey work. Data on the radioactivity of soil samples were kindly furnished by L. T. Alexander, U. S. Department of Agriculture, J. A. S. Adams, Rice University, P. F. Gustafson, Argonne National Laboratory, and A. R. Smith and H. A. Wollenberg, Lawrence Radiation Laboratory.

REFERENCES

1. H. L. Beck, W. J. Condon, and W. M. Lowder, Environmental Radiation Measurements in the Southeastern, Central, and Western United States, 1962-1963, USAEC Report HASL-145, Health and Safety Laboratory, April 1964.
2. W. J. Condon, W. M. Lowder, and H. L. Beck, A Study of Population Exposure to Environmental Radiation in Northern New England, Health and Safety Laboratory, to be published.
3. W. M. Lowder, H. L. Beck, W. J. Condon, and A. Shambon, Environmental Radiation Survey in Selected Communities of New York State, Health and Safety Laboratory, to be published.
4. W. M. Lowder, A. Segall, and W. J. Condon, Environmental Radiation Survey in Northern New England, in *The Natural Radiation Environment*. J. A. S. Adams and W. M. Lowder (Eds.), Chap. 56, pp. 907-918, University of Chicago Press, Chicago, 1964.
5. W. M. Lowder, W. J. Condon, and H. L. Beck, Field Spectrometric Investigations of Environmental Radiation in the USA, in *The Natural Radiation Environment*, J. A. S. Adams and W. M. Lowder (Eds.), Chap. 35, pp. 597-616, University of Chicago Press, Chicago, 1964.
6. W. M. Lowder, H. L. Beck, and W. J. Condon, Spectrometric Determination of Dose Rates from Natural and Fall-out Gamma-Radiation in the United States, 1962-63, *Nature, 202:* 745 (1964).
7. H. L. Beck, W. J. Condon, and W. M. Lowder, Spectrometric Techniques for Measuring Environmental Gamma Radiation, USAEC Report HASL-150, Health and Safety Laboratory, October 1964.
8. W. J. Condon, W. M. Lowder, and H. L. Beck, Pressurized Ionization Chambers for Environmental Radiation Measurements, Health and Safety Laboratory, to be published.
9. J. A. S. Adams and G. E. Fryer, Portable γ-Ray Spectrometer for Field Determination of Thorium, Uranium, and Potassium, in *The Natural Radiation Environment*, J. A. S. Adams and W. M. Lowder (Eds.), Chap. 34, pp. 577-596, University of Chicago Press, Chicago, 1964.
10. H. L. Beck, to be published.

KREY: I would like to ask Mr. Crocker for a discussion of the situation for the Sedan shot. I recall that he indicated that ^{99}Mo did not appear to fractionate. Some of our data from that shot indicated that it did fractionate. The situation may well depend upon the distance from ground zero. I would like to hear if he has any comments on it.

CROCKER: I must not have made myself clear. Molybdenum-99 did not fractionate in our Sedan samples. It did show some fractionation in some air-burst correlations that Dr. Freiling has made.

KREY: I believe you performed some upwind and crosswind sampling. Did you find any variation of the fission products with respect to ^{99}Mo in the samples?

CROCKER: There was very little difference. I am speaking mainly of Small Boy which is the shot from which I had the most data and am in the best position to judge. There was very little upwind, downwind, or crosswind fractionation of gross samples in the field. A very few of the peripheral stations, those which collected very little activity near the edges of the deposition pattern, showed a slight indication that the fission products were a little more depleted in ^{95}Zr or a little more enriched in ^{89}Sr, but the effect was not very noticeable.

FREILING: I think you had something you wished to bring up about the ratio of dose rate to the number of fissions.

CROCKER: I don't believe Dr. Carl Miller is here. [He was unable to remain for the discussion.] I wanted to ask him about his calculation of roentgens per hour per kiloton per square mile. If anyone else has made such a calculation from field data, I would like to know the answers he obtained.

FREILING: Is there anyone here from Stanford Research Institute who can speak about their results? Has anyone else looked at the data from this point of view? [No response.]

CROCKER: It appeared to me from what Dr. Miller presented that the roentgens per hour were less than one expects. He presented his data so fast that I had difficulty in making sure, but it appeared to me that his value was too low. I also find the dose rate too low for the amount of fission products that were deposited on the ground, but I think the effect is much greater than Dr. Miller showed.

LOYSEN: I don't have any questions, but I would like to mention that Mr. Wood from Litton Systems, Inc., handed me a set of preliminary photographs just a short time ago which were taken from a high-volume impactor flight at approximately 120,000 ft last week. If there are people who are interested in seeing these, I would be happy to show them later on.

DREVINSKY: I would like to ask Mr. Nielsen for the estimate of accuracy for ^{7}Be measurements and ^{22}Na measurements with the use of his analyzer.

NIELSEN: For ^{22}Na, I can give you an example of our measurements: 0.36 ± 0.03; in other words, about 10%. Our accuracy was limited by the counting time chosen. If one wanted better accuracy, he would have to count longer.

HEFT: I would like to ask Dr. Drevinsky about the remark he made relative to the cerium/strontium ratios exhibiting no fractionation from altitude to altitude and from particle size to particle size. How did the observed ratios compare to expected values? Did they fractionate relative to the expected ratios? Was there no fractionation as a function of particle size?

DREVINSKY: We did not attempt to date the debris found in the size ranges studied by using activity ratios such as $^{144}Ce/^{90}Sr$ because of the uncertainties in assigning a particle size distribution to residual, long-lived activities such as ^{90}Sr. In the two particle size ranges with radii less than 0.15 μ, the $^{144}Ce/^{90}Sr$ activity ratios were close to the production ratio of 40 except for the 21- to 30-km interval in March and September 1962. My main point on the constancy of the $^{144}Ce/^{90}Sr$ activity ratio was that it did not vary with particle size in those size ranges that contained most of the activity. I did not mean to indicate that this ratio is invariant with altitude as well as with particle size for all flights as dramatically shown for the May 1963 flight. There are some differences. For example, the September 1962 data show a decrease in the ratio with increasing altitude. Presumably, this is an

effect of older debris, with ^{90}Sr concentrations becoming higher with increasing altitudes.

FREILING: In looking at Dr. Drevinsky's slides, I got the impression that, as the altitude decreased, there was more activity in the larger particles and less activity in the smaller particles. I am wondering whether the large particles you collected are large single particles or composites of smaller particles. Have you examined these with an electron microscope?

DREVINSKY: It is generally true that with decreasing altitude an increasingly higher percentage of activity was found to be carried by particles with $0.02\ \mu < r < 0.15\ \mu$ relative to those with $r < 0.02\ \mu$. [r is radius.] However, we have not studied our samples by optical techniques to determine their physical nature.

FREILING: If they were formed by agglomeration processes, there would be no reason to expect larger sizes to have a different radiochemical composition than the smaller particles.

Dr. Nielsen, do you have any comments?

NIELSEN: No, I might ask Dr. Lockhart a similar question, i.e., whether or not he has looked at the larger particles he collects to see if they are single particles.

LOCKHART: One nice thing about filter collection is that the investigator does not have to worry about single particles. He can treat them all as a group the same way that Dr. Drevinsky did. Therefore we have not looked at individual particles at all.

I have a question for Dr. Nielsen about the ^{88}Y and ^{124}Sb. We have seen no ^{124}Sb that stands out among the large quantity of ^{125}Sb. The ^{88}Y is very low, but it is detectable, having about the same activity as the small amount of gamma associated with the beta-emitting ^{91}Y. Do you have any idea how these isotopes of antimony and yttrium compare at ground level?

NIELSEN: The ^{125}Sb concentration according to our figures was about 5 dis/min, and the ^{124}Sb was about 0.1 dis/min per 1000 cu ft. It is less at the present time. Our latest figures show about 0.009 dis/min for ^{124}Sb and about 1 dis/min for ^{125}Sb.

The ^{88}Y concentration is presently about 0.005 dis/min. It has fallen off quite a bit. For about two years the concentration was about 0.03 dis/min per 1000 cu ft.

FREILING: I have a question for Mr. Benson. You mentioned the activity per unit volume of the particles was such that you would infer devices of greater mass producing these particles than was actually the case. Since some of these high-yield bursts engulf many cubic

kilometers of air, I was wondering whether or not the natural aerosol concentrations in these large volumes would be sufficient to add anything appreciable to the weight of the debris and tend to produce this effect.

BENSON: I don't think so. A high-energy thermonuclear device is a fairly heavy weapon, and, at these fairly high altitudes, the natural aerosol is small. The contribution of dust raised from the ground is insignificant. Therefore the total mass engulfed at high altitudes would be rather small.

I think the main reason, however, for this peculiarity lies in the fact that we are talking about large particles, in the neighborhood of 5 to 15 μ. With respect to the radiochemical analysis of these particles, one of the facts we did not bring out in the paper was that the volatile constituents had yields of less than the independent fission yield. Values of barium were found, for example, which were 0.003 of what they should have been in relation to what the zirconium was. This implies that at the temperatures at which particles of this type are formed (roughly the boiling point of aluminum oxide, which is rather high) elements like rubidium and barium are volatile. The first member of the ^{95}Zr fission chain is rubidium. I think the effect is caused by a volatilization of the early precursors within the fission-product chains. Although we think of the refractory fission products as being distributed evenly throughout the mass of the weapon, this does not appear to be true. When we are talking about large particles, the fission products are all potentially being reduced rather than being enriched or evenly distributed throughout the volatilized mass.

FOOTE: I would like to know the approximate cost of Dr. Nielsen's spectrometer.

NIELSEN: It cost us about $70,000. It can be obtained for less than $50,000 today.

BENSON: While we are talking about costs, I would like to ask Mr. Foote how he gets the $0.15 per analysis that he mentioned.

FOOTE: That is the total cost of readin and readout.

MILLER (C. E., Jr.): I would like to point out that we have in progress a program on the fractionation of fission products as part of the Nuclear Safety Program at Oak Ridge National Laboratory. It is sponsored by the AEC's Division of Reactor Development and Technology rather than the Division of Biology and Medicine and is, therefore, not being reported here. However, I do feel that the work is pertinent to the fallout program. We are interested in amounts of fission products contained in transported materials in a reactor accident and in any information we can extract concerning the mecha-

nisms of their release, transport, and deposition. We have developed a model which predicts fission-product fractionation and which gives satisfactory agreement with data from the in-pile experiments in which we have melted UO_2 fuel elements. The data are plotted in a manner identical to that of Dr. Freiling and his coworkers, with a straight line being obtained. Our theoretical analysis shows that the slope of the line is a simple function of the heats of vaporization of the fractionating species. The intercept of the line can be calculated from information on the total inventory of the material vaporized. We have performed this type of analysis for all our own in-pile experiments as well as for the experiments of other researchers in the field of nuclear safety. These include experiments on fission-product release by postirradiation annealing below the melting point of the fuel, by melting fuel under varying conditions, and by operating reactors. We also were able to predict the slopes in fair agreement with those measured by Dr. Freiling and reported in his published work on nuclear debris. Our theory is described in USAEC Report ORNL-3547, which is an Oak Ridge National Laboratory Nuclear Safety Semiannual Progress Report. We call the model the vapor-transpiration model because in our own experiments we feel that fractionation is actually taking place at the time that the fission products are vaporized from the fuel. Characteristics, such as particle size, of the subsequently condensed aerosol serve to spread out the released fission products so that they can be sampled at various locations in the experiment. Our theoretical analysis of Freiling's data treats fractionation as occurring during condensation of the debris from nuclear weapons.

FREILING: Thank you very much, Dr. Miller. It is gratifying to hear that the considerations of fallout are also applicable to reactor work, and we hope that they will also be applicable to the medium in between these two extremes, namely, destructs of NERVA reactors by one means or another and the resulting production of nuclear debris. I would like to think of and refer to nuclear debris instead of fallout to keep our thinking broad on this subject. [Editor's Note: In the AEC's Atmospheric Radioactivity and Fallout Research Program, the term "*radioactive* fallout" is defined to include any atmospheric radioactivity, irrespective of source. Hence, the specification for this conference that the papers presented be limited to fallout from tests of nuclear weapons.]

SESSION II

Long-term Particle Behavior

S. K. Friedlander, Chairman

THEORY OF SELF-PRESERVING SIZE DISTRIBUTIONS IN A COAGULATING DISPERSION

S. K. FRIEDLANDER
W. M. Keck Engineering Laboratories, California Institute of Technology, Pasadena, California

ABSTRACT

A reduced form of the particle-size-distribution function, designated "self-preserving," satisfies Smoluchowski's equation of coagulation by Brownian motion. Both theory and experiment indicate that the self-preserving form is approached by coagulating systems having a wide variety of initial distributions. This effect offers an explanation for the regularities observed in the size distribution of the atmospheric aerosol.

INTRODUCTION

The theory of self-preserving size distributions was proposed by Friedlander[1] to explain experimentally observed regularities in the particle size distribution of the atmospheric aerosol. The theory was developed and tested experimentally by Swift and Friedlander.[2] In this paper, abstracted in part from Ref. 2, an account of the theory is given for the case of Brownian diffusion.

BROWNIAN COAGULATION

The course of a coagulation process can be described by the time variation of the particle-size-distribution function. This function can be defined by using the radius, the area, or the volume as an independent

variable. Because of certain simplifications in the equations and the fact that the experimental distributions were in terms of particle volume, the volume will be used for this presentation. The continuous distribution function, n(v,t)* (where v is the particle volume in cubic centimeters and t is the time in seconds), is defined such that n(v,t) dv is the particle concentration in the volume range from v to v + dv. It follows that the total number of particles per cubic centimeter, N_∞, is defined by

$$N_\infty = \int_0^\infty n(v)\, dv \tag{1}$$

and the number of particles per cubic centimeter larger than a given volume, N_v, is defined by

$$N_v = \int_v^\infty n(v)\, dv \tag{2}$$

The total volume fraction of particles is given by

$$\phi = \int_0^\infty vn(v)\, dv \tag{3}$$

where ϕ is the phase volume ratio (volume of dispersed phase per unit volume of continuous phase). This fraction is constant in an experiment because no second-phase material is lost or gained. It is to be understood that n(v), N_∞, and N_v are all time-dependent functions, but this will not always be shown explicitly henceforth. The Brownian-motion collision frequency between particles of volumes v and $\tilde{v}$ is

$$b_{v,\tilde{v}} = \frac{2kT}{3\mu}\left(\frac{1}{v^{1/3}} + \frac{1}{\tilde{v}^{1/3}}\right)(v^{1/3} + \tilde{v}^{1/3})n(v)n(\tilde{v})\, dv\, d\tilde{v} \tag{4}$$

where k = Boltzmann's constant
T = temperature
μ = fluid viscosity

With the use of this expression for the collision frequency, an equation for the rate of change of the distribution function with time can be written as follows:

$$\frac{dn(v)}{dt} = \frac{kT}{3\mu}\int_0^v n(\tilde{v})n(v-\tilde{v})\left[\frac{1}{\tilde{v}^{1/3}} + \frac{1}{(v-\tilde{v})^{1/3}}\right][\tilde{v}^{1/3} + (v-\tilde{v})^{1/3}]\, d\tilde{v}$$
$$-\frac{2kT}{3\mu}n(v)\int_0^\infty n(\tilde{v})(\tilde{v}^{1/3} + v^{1/3})\left(\frac{1}{\tilde{v}^{1/3}} + \frac{1}{v^{1/3}}\right) d\tilde{v} \tag{5}$$

*Particles/cm^6.

This equation is similar in form to the one presented by Friedlander,[1] who used the radius as the independent variable.

Another relation between N_∞ and n(v) may be obtained by integrating Eq. 4 twice over all particle sizes to give twice the total number of collisions. Since each collision results in the loss of a particle, the number of collisions per second is the rate of change of N_∞:

$$\frac{dN_\infty}{dt} = -\frac{kT}{3\mu} \int_0^\infty \int_0^\infty n(v)n(\tilde{v})(v^{1/3} + \tilde{v}^{1/3}) \left(\frac{1}{v^{1/3}} + \frac{1}{\tilde{v}^{1/3}}\right) dv\, d\tilde{v} \tag{6}$$

Smoluchowski's decay law for uniform-size particles can be obtained from Eq. 6 by noting that, for $v = \tilde{v}$, $(v^{1/3} + \tilde{v}^{1/3})[(1/v^{1/3}) + (1/\tilde{v}^{1/3})] = 4$, and the equation reduces to

$$\frac{dN_\infty}{dt} = -\frac{4kT}{3\mu} \int_0^\infty \int_0^\infty n(v)n(\tilde{v})\, dv\, d\tilde{v} = -\frac{4kT}{3\mu} N_\infty^2 \tag{7}$$

SELF-PRESERVING SIZE DISTRIBUTION

In principle, the course of a coagulation process could be predicted theoretically by solving Eq. 5 by using a given initial distribution function n(v,0). Equation 5 is a nonlinear partial integro-differential equation, and an analytic solution is not known. However, it will be shown in this paper that it is possible to reduce Eq. 5 to a total differential equation by means of a similarity transformation. This is a mathematical device by which a particular grouping of the independent variables is chosen as a new independent variable. The transformation makes it possible to express the differential equation and the boundary conditions solely in terms of the new independent variable. Simultaneously it helps in the correlation of experimental data and gives physical insight into the problem.

The basic assumption for this theory is that the distribution function, n(v,t), can be expressed as

$$n(v,t) = g(t)\, \psi \left(\frac{v}{v^+}\right) \tag{8}$$

where g(t) and v^+ are functions of time. It is assumed that the size distribution function, ψ, does not change with time. Friedlander[1] pointed out that when an equation of this form was substituted into the coagulation–sedimentation equation, a total integro-differential equation was obtained. This showed that the assumed form represented a particular solution of the equation but perhaps not the only one.

Expressions for g(t) and $v^+(t)$ can be obtained by substituting Eq. 8 into Eqs. 1 and 3:

$$g(t) = \frac{N_\infty}{v^+}\left[\int_0^\infty \psi \, d\left(\frac{v}{v^+}\right)\right] \tag{9}$$

$$v^+(t) = \frac{\phi \int_0^\infty \psi \, d(v/v^+)}{N_\infty \int_0^\infty (v/v^+)\, \psi \, d(v/v^+)} \tag{10}$$

Substituting these expressions in Eq. 8 and noting that $\int_0^\infty \psi \, d(v/v^+)$ and $\int_0^\infty (v/v^+)\, \psi \, d(v/v^+)$ are dimensionless constants, one finds

$$n(v,t) = \frac{N_\infty^2}{\phi}\, \psi_1\left(\frac{vN_\infty}{\phi}\right) \tag{11}$$

The function ψ_1 differs from ψ. It is a dimensionless size-distribution function, and its argument

$$\frac{vN_\infty}{\phi} = \eta \tag{12}$$

is the ratio of the particle volume for a given size range to the average volume ϕ/N_∞. Substitution of Eq. 12 into Eqs. 1 and 3 shows that

$$\int_0^\infty \psi_1(\eta)\, d\eta = 1 \tag{13a}$$

and

$$\int_0^\infty \eta\psi_1(\eta)\, d\eta = 1 \tag{13b}$$

SELF-PRESERVING FORM AND SMOLUCHOWSKI KINETICS

The self-preserving form Eq. 11 must satisfy the equation for the rate of change of the distribution function with time. If the Smoluchowski expression, Eq. 5, is accepted as the proper kinetic equation, Eq. 11 can be substituted to give the following result:

$$\frac{1}{N_\infty^2}\frac{dN_\infty}{dt}\left[2\psi_1 + \eta\frac{d\psi_1}{d\eta}\right] = \frac{kT}{3\mu}\int_0^\eta \psi_1(\tilde\eta)\, \psi_1(\eta - \tilde\eta) \times [\tilde\eta^{1/3} + (\eta - \tilde\eta)^{1/3}]\left[\frac{1}{\tilde\eta^{1/3}} + \frac{1}{(\eta - \tilde\eta)^{1/3}}\right] d\tilde\eta - \frac{2kT}{3\mu} \times \psi_1(\eta)\int_0^\infty \psi_1(\tilde\eta)\,[\eta^{1/3} + \tilde\eta^{1/3}]\left[\frac{1}{\eta^{1/3}} + \frac{1}{\tilde\eta^{1/3}}\right] d\tilde\eta \tag{14}$$

The expression for $(1/N_\infty^2)(dN_\infty/dt)$ can be obtained by substituting Eq. 11 into Eq. 6, which gives, after some simplification,

$$\frac{1}{N_\infty^2}\frac{dN_\infty}{dt} = -\frac{kT}{3\mu}\left[2 + 2\int_0^\infty \eta^{-1/3}\,\psi_1(\eta)\,d\eta \int_0^\infty \tilde{\eta}^{1/3}\,\psi_1(\tilde{\eta})\,d\tilde{\eta}\right] \tag{15}$$

This expression substituted into Eq. 14 gives the final form

$$\left[1 + \int_0^\infty \eta^{-1/3}\,\psi_1(\eta)\,d\eta \int_0^\infty \tilde{\eta}^{1/3}\,\psi_1(\tilde{\eta})\,d\tilde{\eta}\right]\left[2\,\psi_1(\eta) + \eta\frac{d\psi_1}{d\eta}\right]$$

$$+\frac{1}{2}\int_0^\eta \psi_1(\tilde{\eta})\,\psi_1(\eta-\tilde{\eta})\,[\tilde{\eta}^{1/3} + (\eta-\tilde{\eta})^{1/3}]\left[\frac{1}{\tilde{\eta}^{1/3}} + \frac{1}{(\eta-\tilde{\eta})^{1/3}}\right]d\tilde{\eta}$$

$$-\psi_1(\eta)\int_0^\infty \psi_1(\tilde{\eta})\,[\eta^{1/3} + \tilde{\eta}^{1/3}]\left[\frac{1}{\eta^{1/3}} + \frac{1}{\tilde{\eta}^{1/3}}\right]d\tilde{\eta} = 0 \tag{16}$$

The partial integro-differential Eq. 5 has been transformed into an ordinary integro-differential equation by the substitution of Eq. 11. With the assumption that a solution exists, the new equation must be solved subject to the integral conditions shown in Eqs. 13a and 13b. The self-preserving form, Eq. 11, represents a particular solution to the kinetic equation for coagulation by Brownian motion. It can be shown that Eq. 11 is not the most general solution to the coagulation equation. Both computer calculations and experiments indicate that the self-preserving form is an asymptotic limit approached by the actual solution.

One can gain some understanding of the coagulation of a heterodisperse hydrosol without solving Eq. 16. For a monodisperse hydrosol whose coagulation is described by Smoluchowski's model, the coagulation rate is given by

$$\frac{dN_\infty}{dt} = -\frac{4kT}{3\mu}N_\infty^2$$

By rearrangement of Eq. 15, the rate of coagulation of a dispersion with a self-preserving size distribution can be expressed as

$$\frac{dN_\infty}{dt} = -\frac{kT}{3\mu}\left[2 + 2\int_0^\infty \eta^{-1/3}\,\psi_1(\eta)\,d\eta \int_0^\infty \tilde{\eta}^{1/3}\,\psi_1(\tilde{\eta})\,d\tilde{\eta}\right]N_\infty^2 \tag{17}$$

and, because the integrals are independent of time, the quantity

$$A_1 = [2 + 2\int_0^\infty \eta^{-1/3}\,\psi_1(\eta)\,d\eta \int_0^\infty \tilde{\eta}^{1/3}\,\psi_1(\tilde{\eta})\,d\tilde{\eta}] \tag{18}$$

can be substituted to give

$$\frac{dN_\infty}{dt} = -\frac{A_1 kT}{3\mu} N_\infty^2 \tag{19}$$

It has thus been shown that the kinetics of Brownian coagulation of heterodisperse hydrosols are second order if the self-preservation hypothesis holds throughout the coagulation process. For heterodisperse hydrosols the value of A_1 is greater than 4. This value can be determined from Eq. 18. Thus, if ψ_1 is known, the effect of heterogeneity on the rate of coagulation can be determined.

SIGNIFICANCE OF THEORY

The theory has been tested experimentally, and the results have been reported by Swift and Friedlander.[2] They found that the size distributions of coagulating hydrosols, initially unimodal, tend to preserve their shape when plotted in proper dimensionless form. If the distribution is self-preserving, it is completely determined by specifying ϕ and N_∞. This result should be useful in correlating and extrapolating experimental data and in calculating the average properties of disperse phases. When two heterodisperse hydrosols are mixed, the distribution tends to approach the same shape exhibited by an initially unimodal system. It appears that the self-preserving form is approached no matter what the initial distribution of the coagulating dispersion. Computer calculations by Hidy,[3] following the studies of Friedlander[1] and Swift and Friedlander,[2] have shown that a self-preserving form is indeed approached asymptotically for several arbitrarily chosen initial distributions. Hidy's calculations give the most accurate representation available for the form of the self-preserving distribution.

The theory developed in these papers offers an explanation for the regularities observed in the size distribution of the atmospheric aerosol. It is interesting to note that, if $N_v \sim 1/v$ as is often observed experimentally over part of the size distribution range of the atmospheric aerosol, the self-preserving form requires that

$$N_v = \frac{A_2 \phi}{v}$$

where A_2 is a universal dimensionless constant. Thus it is necessary to measure only ϕ to establish the size distribution of the suspension over the range where $N_v \sim 1/v$, provided A_2 is known. This constant has been calculated by Friedlander[4] and has a value of about 0.08.

REFERENCES

1. S. K. Friedlander, Theoretical Considerations for the Particle Size Spectrum of the Stratospheric Aerosol, *J. Meteorol., 18:* 753 (1961).
2. D. L. Swift and S. K. Friedlander, The Coagulation of Hydrosols by Brownian Motion and Laminar Shear Flow, *J. Colloid Sci., 19:* 621-647 (1964).
3. G. M. Hidy, On the Theory of the Coagulation of Non-Interacting Particles in Brownian Motion, to be published in *Journal of Colloid Science,* 1965.
4. S. K. Friedlander, The Similarity Theory of the Particle Size Distribution of the Atmospheric Aerosol, paper presented at First National Symposium on the Physical Chemistry of Aerosols, Prague, Czechoslovakia, 1962.

PARTICLE CHARGING AT LOW PRESSURES

BENJAMIN Y. H. LIU and KENNETH T. WHITBY
University of Minnesota, Minneapolis, Minnesota

ABSTRACT

The electric charge imparted to particles at reduced pressures has been measured for particles ranging from 0.02 to 2.0 μ and for pressures ranging from 0.01 to 1.0 atm with an improved particle-mobility analyzer of cylindrical geometry. The solid spherical particles of methylene blue dye are charged by positive ions in electric fields of various intensities. The measured particle charge is generally higher than the values predicted by White's equations, and the difference increases with decreasing pressure. Typically, the measured charge at 0.01 atm is 100% higher than the values predicted by the diffusion-charging equation and is slightly less than one order of magnitude higher than what the field-charging equation predicts.

INTRODUCTION

The electrical charging of small particles in the micron and submicron size range has been the subject of numerous theoretical and experimental studies. It is an important factor in the design of electrostatic precipitators, which are among the most effective devices for removing small airborne particulate matter. Electrostatic precipitators have been used extensively as air or gas filters and, more recently, as atmospheric dust samplers at both ground levels and high altitudes for radioactive-fallout studies.

Particle-charging experiments have been reported by Hewitt,[1] Penney and Lynch,[2] White,[3] Cochet,[4] Drozin and La Mer,[5] Langer,[6] and others, and considerable particle-charging data are now available for

charging at atmospheric pressure. However, no low-pressure charging data are available. The purpose of our present studies is to obtain experimental particle-charging data at the low pressures encountered in operating electrostatic-precipitator aerosol samplers at high altitudes.

Electrical particle-charging theories have been summarized in a recent book by White,[7] who also showed that the electrical charge imparted to particles can be calculated from the following two equations if certain simplifying assumptions regarding the particle-charging mechanism are made:

$$n_p = \left(1 + 2\,\frac{K-1}{K+2}\right)\frac{Ed_p^2}{4\,e}\,\frac{\pi\,NeZ_i t}{\pi\,NeZ_i t + 1} \tag{1}$$

$$n_p = \frac{d_p kT}{2\,e^2}\,\ln\left(1 + \frac{d_p \bar{c} Ne^2 t}{2\,kT}\right) \tag{2}$$

where n_p = number of elementary units of charge on particle, dimensionless
K = dielectric constant of particle, dimensionless
E = intensity of applied electric field, statvolts/cm
d_p = particle diameter, cm
e = elementary unit of charge = 4.803×10^{-3} esu
N = ion concentration, number of ions/cm^3
Z_i = electric mobility of ions, cm^2/sec-statvolt
t = charging time, sec
k = Boltzmann's constant
$\bar{c}$ = mean speed of ions, cm/sec
T = absolute temperature, °K

Equation 1 represents the so-called "field-charging process" in which the ions are assumed to be driven onto the particles along the electric-field lines. The effect of ion diffusion is neglected. Equation 2 is for the diffusion-charging process where it is assumed that the charging is due to the random thermal motion of the ions in the absence of an applied electric field. In both equations, the mean free path of the ions is assumed to be small compared to the diameter of the particles. These equations have been found to be reasonably accurate in predicting the particle charge if the experimental data are obtained under such conditions that the assumptions made in deriving these equations are nearly satisfied. However, in many charging processes where both the field and diffusion mechanisms of particle charging are of equal importance or where submicron particles are involved whose diameters are of the same order of magnitude as the mean free path of the ions, these equations are known to predict incorrect particle charges. Attempts to solve the particle-charging equations more rigorously by means of numerical methods and com-

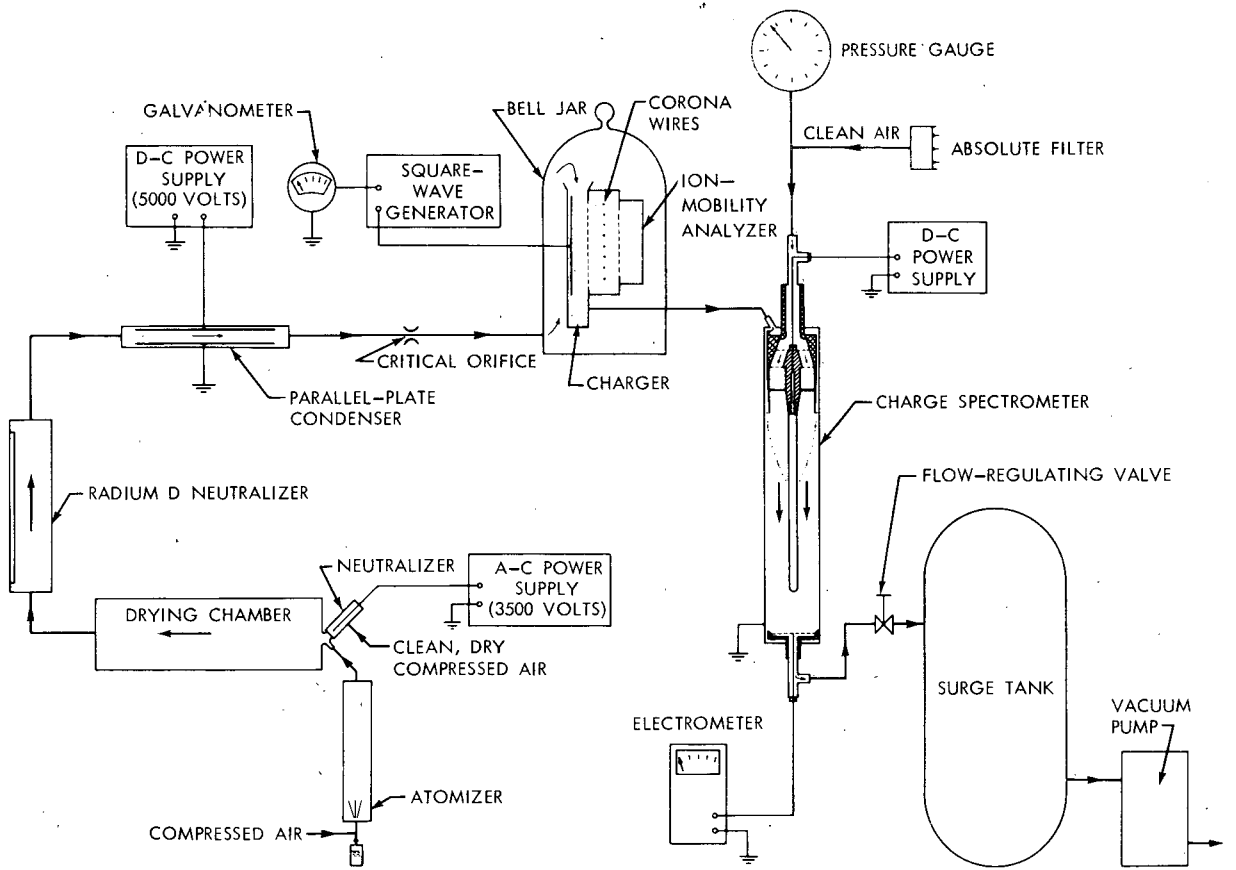

Fig. 1—Experimental system.

puter calculations[8] have been met only with limited success because of the complexity of the charging equations involved. It is hoped that the present study, in which the mean free path and the electric mobility of the ions are varied over a wide range of values because of the variation in pressure, will provide data that can be used as rather severe tests of any new charging theories.

EXPERIMENTAL APPROACH AND APPARATUS

Any experimental study of the physics of aerosols can be made, in principle at least, on a single particle or on a cloud of particles. The latter approach is generally preferred since the statistical nature of the processes generally involved would render the results of many single-particle measurements quite difficult, if not impossible, to interpret. Furthermore, for submicron particles of interest in the present study, single-particle measurements are quite difficult to make.

Figure 1 is a diagram of the experimental system used. More detailed diagrams of the particle charger, small ion-mobility analyzer, and particle-charge spectrometer are shown in Figs. 2 and 3. It should be noted that the charging and precipitation of the particles are carried out in two separate devices. This approach of separating the particle charger and the precipitator (the particle-charge spectrometer) has the advantage of permitting a more accurate determination of the particle charge than is possible when the charger and precipitator are combined as in the conventional electrostatic precipitator. It also permits the variables affecting the particle charge to be more precisely defined.

AEROSOL GENERATION AND NEUTRALIZATION

The aerosols used in these experiments were solid, spherical particles of dye obtained by atomizing solutions of the dye and drying the liquid droplets formed. Commercial-grade methylene blue dye was used in all the tests with the exception of two in which uranine was used. Uranine is somewhat hygroscopic and cannot be dried as readily as methylene blue. However, the fact that very minute quantities of uranine can be measured accurately by means of fluorescence techniques[9] has made it a desirable material to use when the mass of aerosol collected must be determined.

Aerosols produced by atomization processes have been found to carry a very substantial electrical charge. Since it is desirable that the aerosols be neutral initially, provision must be made to remove these initial electrical charges. The usual procedure of neutralizing an aerosol is to mix the aerosol stream with a mixture of ions of both plus and minus signs. A sonic-jet bipolar ion generator (described in

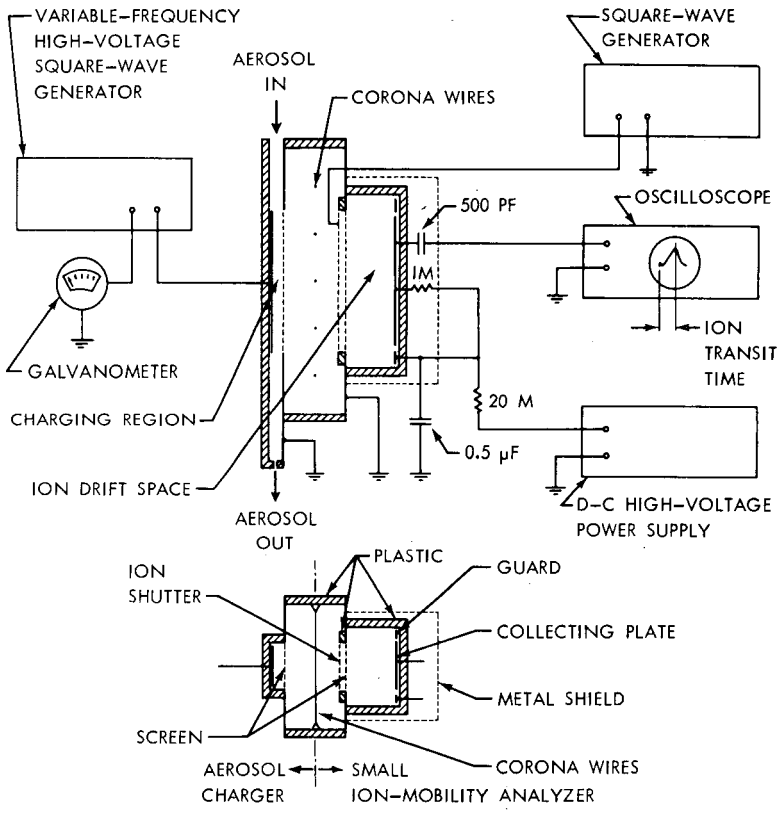

Fig. 2—Aerosol charger and small ion-mobility analyzer.

Ref. 10) and a radium D radioactive foil with an activity of 500 μc have both been used with success for producing the bipolar ions needed for charge neutralization. The radium D neutralizer was used when a very high aerosol concentration was needed and when it was undesirable to have the aerosol concentration reduced by the diluting air from the sonic-jet ion generator.

When aerosol carrying high electrical charges is mixed with small ions of both signs, the electrical charge on the aerosol is reduced. However, the electrical charge is not removed completely. If sufficient time is allowed for equilibrium to be established, the distribution of charge on the particles can be shown to be given by Boltzmann's distribution law:[11]

$$f(n) = \frac{\exp\left[-(ne)^2/d_p kT\right]}{\sum_{n=-\infty}^{\infty} \exp\left[-(ne)^2/d_p kT\right]} \qquad (3)$$

where f(n) is the fraction of particles carrying n units of charge (dimensionless). According to Eq. 3, 99.3% of all the particles of 0.01

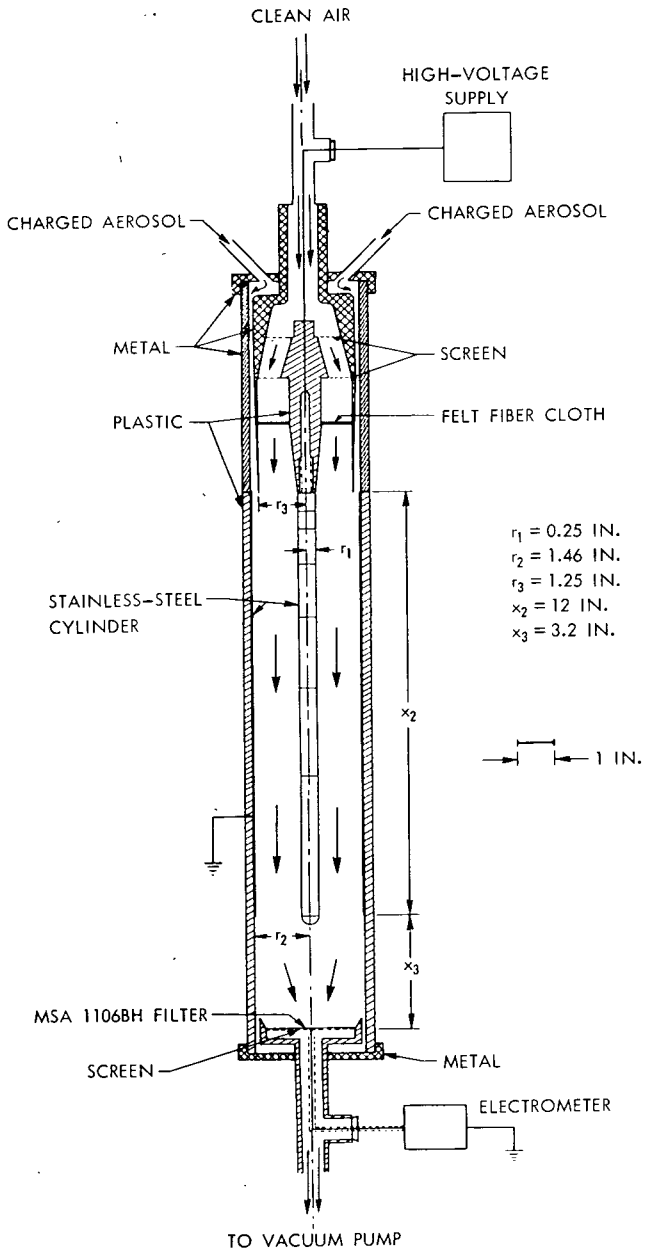

Fig. 3—Charge spectrometer.

μ in diameter will be uncharged under Boltzmann equilibrium. However, the fraction of particles which are neutral decreases steadily with increasing particle diameter. For instance, at 0.1 μ 42.4% of the particles are neutral, whereas at 1 μ only 13.3% are neutral. Therefore the aerosol stream was passed between the parallel-plate condenser as shown in Fig. 1 to ensure that all particles entering the particle charger were neutral or, at most, carried a negligible electrical charge. The voltage applied to the condenser plates was such that all singly charged particles smaller than approximately 0.5 μ were removed from the aerosol stream and that, for all practical purposes, the aerosols emerging from the parallel-plate condenser could be considered as neutral.

AEROSOL CHARGER AND SMALL ION-MOBILITY ANALYZER

The aerosol charger and small ion-mobility analyzer were combined into one unit as shown in Fig. 2 so that both could be operated under the same ambient conditions and with the same source of ions in both devices. This ensures that the mobility of ions measured by means of the mobility analyzer is actually that of the ions used in charging the particles. Since it is known[12] that the mobility of air ions is affected by impurities that may be present in the air and by the age of the ions and since it is impractical in these charging experiments to purify the air stream sufficiently to allow any control of ion mobility, it is essential that the ion mobility be measured under actual operating conditions.

The principle of operation of the aerosol charger is similar to that described by Hewitt.[1] The charging region through which aerosols flow is bounded on one side by a metal screen and on the other side by a metal plate. The high voltage applied to the metal plate was in the form of a 500 cycle/sec square wave. When the polarity of the voltage applied to the plate was opposite to that of the ions produced by the corona wires, the ions were drawn into the charging region to charge the particles. A square wave was used to prevent the precipitation of the aerosols in the charging region after they became charged. All data presented here were obtained with a positive voltage applied to the corona wires, and hence positive ions were used in charging the particles.

The mobility of small ions at various pressures is measured by measuring the transit time of the ions in flowing across a drift space under a known voltage-potential gradient. The mobility is then calculated from the equation

$$Z_i = \frac{x^2}{Vt} \tag{4}$$

where Z_i = mobility of ions, cm^2/statvolt-sec
x = width of drift space, cm
V = potential difference across drift space, statvolts
t = transit time of ions, sec

The operation of the small ion-mobility analyzer shown in Fig. 2 is briefly as follows: A square-wave voltage is applied to the ion shutter, which regulates the flow of ions into the drift space. The ion-collecting plate is maintained at a negative d-c potential (for positive ions), V, with respect to the screen, which is held at ground potential. The transit time of the ions in flowing across the drift space under the potential gradient, V/x, is measured from the pattern obtained on the oscilloscope. Figure 4a shows the transit time of the ions for various applied voltages plotted against 1/V, and a straight line is obtained for each pressure. The slopes of these straight lines are used to calculate the ion mobilities that are shown in Fig. 4b for positive ions at various pressures. The fact that the straight lines in Fig. 4a do not pass through the origin of the coordinate axes as required by Eq. 4 indicates that

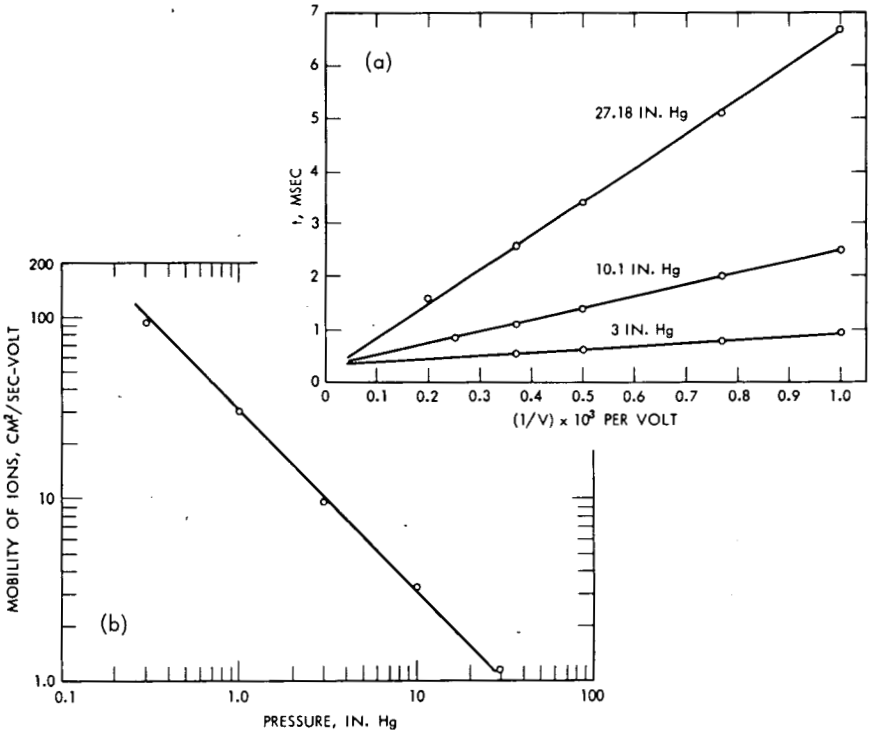

Fig. 4a—Transit time of positive ions for various applied voltages and at various pressures.
Fig. 4b—Mobility of positive ions.

there is a small difference between the measured transit time and the true transit time of the ions. The difference is apparently the result of such factors as the diffusion of ions and the space charge created by the ions.

MEASUREMENT OF PARTICLE CHARGE AND MOBILITY

The charge spectrometer shown in Fig. 3 was used to measure the electrical charge on particles. The stream of charged particles was brought into the charge spectrometer through the annulus opening near the circumference of the outer cylinder and flowed with the clean air brought in through the center as a laminar stream. A negative voltage (for positively charged particles) was applied to the center rod, and the radial electric field thus established between the center rod and the outer cylinder forced the charged particles to move toward the rod as they flowed down with the laminar air stream. Electron-microscope grids were placed at 1-in. intervals along the center rod to collect the particles. The electrical charge on a particle collected on individual grids was then calculated from the position of the grid and the operating conditions in the charger and the measured particle size. The laminar nature of the flow in the charge spectrometer was established by placing a filter in the filter holder and observing the pattern of dye deposits on the filter. When the flow was laminar and no voltage was applied to the center rod, a sharply defined ring was observed.

If a uniform velocity profile for the air stream in the charge spectrometer is assumed, the mobility of a particle easily can be shown to be related to the spectrometer dimensions on operating conditions by the following equation:

$$Z_p = \frac{q \ln (r_2/r_1)}{2 \pi x V} \frac{r_4^2 - r_1^2}{r_2^2 - r_1^2} \tag{5}$$

where Z_p = electrical mobility of particle, cm^2/statvolt-sec
q = total volumetric rate of flow, cm^3/sec
x = distance between point on rod where particle is collected and entrance, cm
V = voltage applied to center rod, statvolts
r_1, r_2, and r_3 = radii shown in Fig. 3
$r_4 = \frac{1}{2} (r_2 + r_3)$

For calculation of the charge on the particle, Stokes' law with Cunningham's correction must then be used:

$$n_p = \frac{3\pi \eta d_p Z_p}{C e} \tag{6}$$

where n_p is the number of elementary units of charge on particle, η is the viscosity of air, in poises, and C is Cunningham's correction to Stokes' law (dimensionless).[13]

The charge spectrometer was designed so that several independent procedures could be used to determine the particle charge. These procedures have been described in detail in Ref. 14. The present procedure of placing electron-microscope grids at intervals along the center rod of the charge spectrometer for particle collection and for charge measurement is the most direct and reliable procedure since it allows the particle size to be directly measured from electron micrographs. The procedure has the further advantage of permitting the determination of particle-charging data over a decade range of particle sizes from a single run by using a polydisperse aerosol. However, the procedure is tedious since a large number of particles must be sized from the electron micrographs to obtain a good statistical average. Sample electron micrographs are shown in Fig. 5. The magnification of the electron microscope was established directly each time the microscope was used by means of a carbon replica of a diffraction grating of 54,864 lines per inch. The nominal magnification of the electron microscope was not used.

EXPERIMENTAL RESULTS

The measured charge on particles of various sizes is presented in Figs. 6 to 8 for particles charged in an electric field of 240 volts/cm at 0.01 atm. The results were obtained from electron micrographs similar to those presented in Fig. 5.

Figure 6 shows the results of two tests in which different ion densities, N, and different charging times, t, were used. However, the product Nt was the same for the two tests. The close agreement between the results of these two tests indicates that the particle charge is primarily a function of the product Nt, if other conditions remain constant, and is independent of the individual values of N and t occurring in the product. This is to be expected from both Eqs. 1 and 2 and has been shown by Hewitt[1] to be true for charging at atmospheric pressure. Also included in Fig. 6 are two theoretical curves calculated from Eqs. 1 and 2 for conducting particles (i.e., $K = \infty$). The measured charge is seen to be much higher than the charges predicted by Eqs. 1 and 2.

Figures 7 and 8 show the effect of varying the Nt product on the particle charge and particle mobility. The increase in particle charge and particle mobility with increasing Nt shows that these particles can be charged to higher levels by using higher Nt values. The relations between the particle charge and the particle size in Fig. 7 are linear on the log–log plot. This indicates that these relations can be represented by an equation of the form

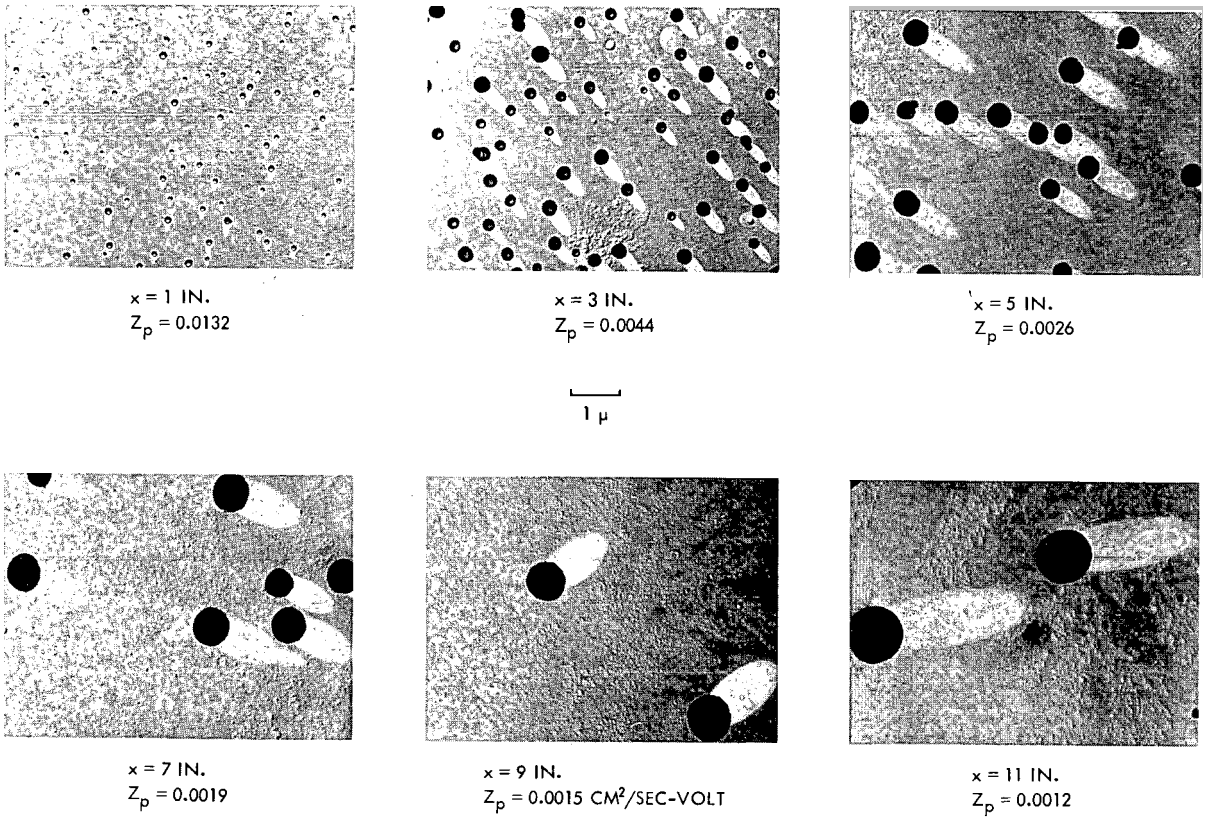

Fig. 5—Sample electron micrographs ($p = 0.1$ atm, $E = 240$ volts/cm, and $Nl = 6.85 \times 10^6$ ions/cm^3 per second).

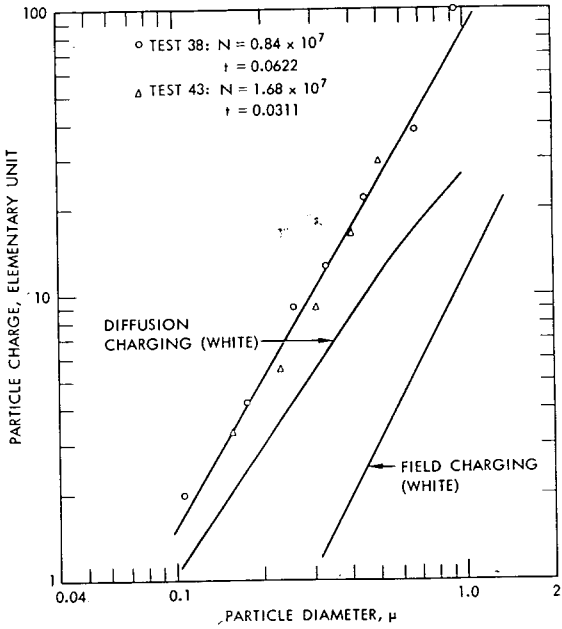

Fig. 6—Experimental particle charge for p = 0.01 atm and E = 240 volts/cm.

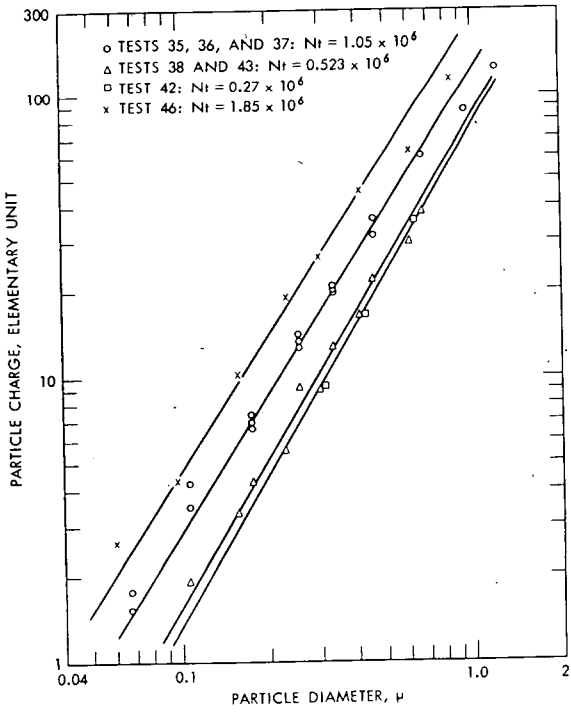

Fig. 7—Experimental particle charge for p = 0.01 atm and E = 240 volts/cm.

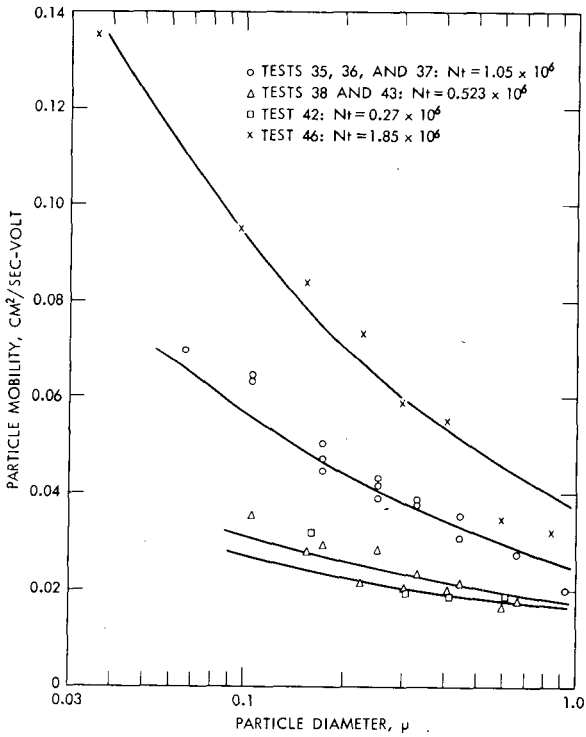

Fig. 8—Experimental particle mobility for p = 0.01 atm and E = 240 volts/cm.

$$n_p = ad_p^b \tag{7}$$

where a and b are constants. The exponent, b, for these tests ranges from approximately 1.60 to 1.75. If the field-charging process is the predominant mechanism of charging, then according to Eq. 1 the particle charge, n_p, should be a function of the square of the particle diameter (i.e., b = 2). If the diffusion-charging process is predominant, then, according to Eq. 1, b should be more nearly equal to 1.5 for particles charged under these conditions. The fact that the experimental value of b is nearly equal to the average of 1.5 and 2.0 indicates that both mechanisms are operating to some extent in the actual charging process, and a satisfactory particle-charging theory probably should take both mechanisms into account.

It is of interest to note that in Fig. 7 the horizontal intercepts of the four experimental lines represent diameters of particles carrying a unit charge. Since the minimum charge that any particle can carry is a unit charge, the data thus appear to indicate that particles smaller than those represented by the horizontal intercepts would be uncharged under these conditions. From the standpoint of operating an electrostatic precipitator as an aerosol sampler, it is important to determine

whether any of these small particles were charged and, if so, what fraction were charged.

To answer these questions two tests were performed in which uranine aerosols were used to measure the fraction collected on the center rod and the afterfilter. The operating conditions in the charger were identical to those used in obtaining the data shown in tests 35, 36, and 37 in Fig. 7, the electric-field intensity being 240 volts/cm and the Nt product 1.05×10^6 ions/cm^3 per second. The aerosols were produced by an atomizer–impactor (described in Ref. 9). The geometrical standard deviation of the particle size distribution was approximately 1.5. The mass median diameters of the aerosols used were 0.049 and 0.028 μ, respectively, both of which were smaller than the horizontal intercept of 0.052 μ as shown in Fig. 7. The charge spectrometer was operated with a sufficiently high voltage on the center rod so that all particles that were charged would be collected by the center rod. The mass of uranine collected on the center rod and on the afterfilter were determined separately in a fluorimeter. The fraction of particles that were charged was then calculated from these data. It was found that, under these charging conditions, 56% of the 0.049-μ particles were charged whereas only 24% of the 0.026-μ particles were charged.

A theoretical equation is derived in the appendix to this paper for calculating the fraction of particles that are charged. The experimental data obtained appear to agree well with the theoretical predictions. Figure 9 is a plot of the fraction, f, of particles that are charged as a

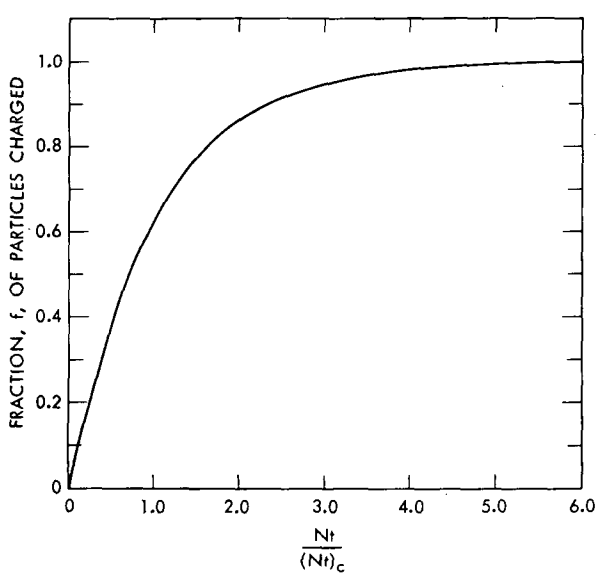

Fig. 9—Fraction of particles charged.

function of the ratio $Nt/(Nt)_c$, where $(Nt)_c$ is a characteristic Nt product depending upon particle size as shown in Fig. 10. In Fig. 10 the two experimental points shown are computed from the results of these two tests. The agreement is seen to be satisfactory.

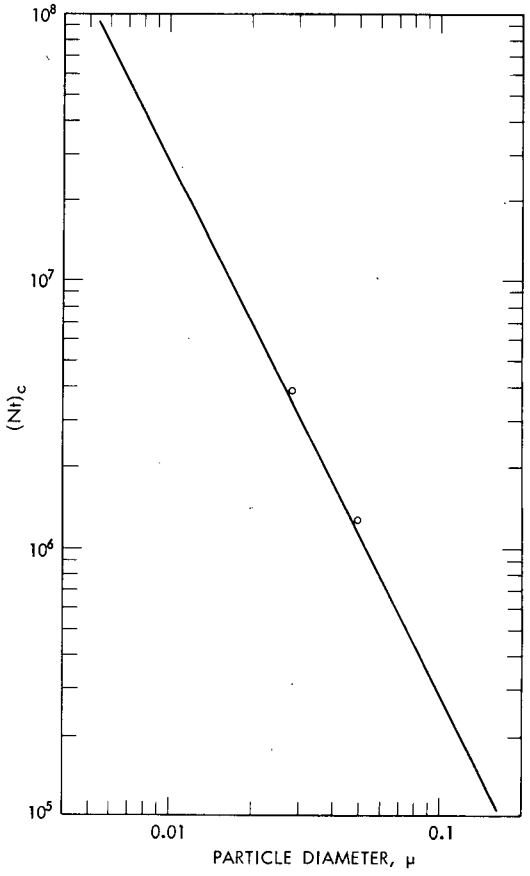

Fig. 10—Characteristic Nt as a function of particle size.

Similar particle charging data have been obtained at 0.1 atm with various applied electric-field intensities. The results are shown in Figs. 11 to 16. Some data were also obtained at atmospheric pressure, and these are presented in Figs. 17 and 18 for purposes of comparison. It should be noted that the mobility curve in Fig. 18 for atmospheric pressure shows a well-defined minimum at approximately 0.2 μ. This minimum mobility has not been observed in all low-pressure charging data obtained thus far. This is apparently due to the large variation in the Cunningham correction to the Stokes' law for particles of various sizes at such low pressures.

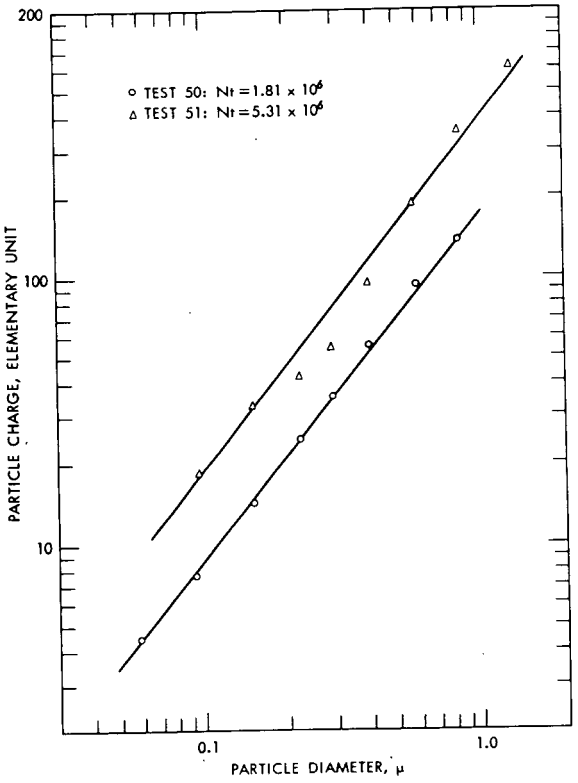

Fig. 11—Experimental particle charge for p = 0.1 atm and E = 2730 volts/cm.

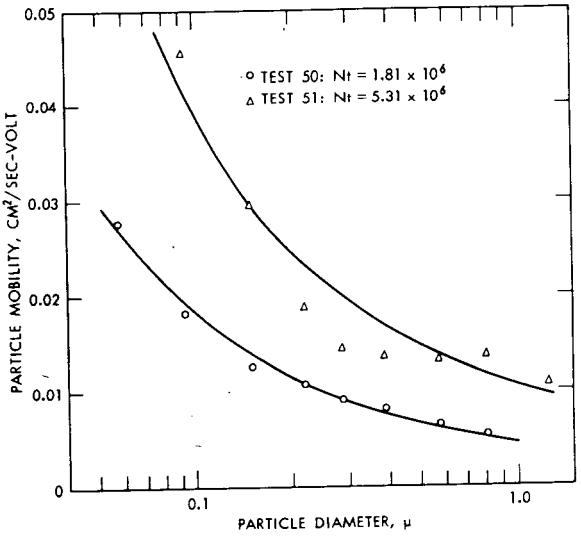

Fig. 12—Experimental particle mobility for p = 0.1 atm and E = 2730 volts/cm.

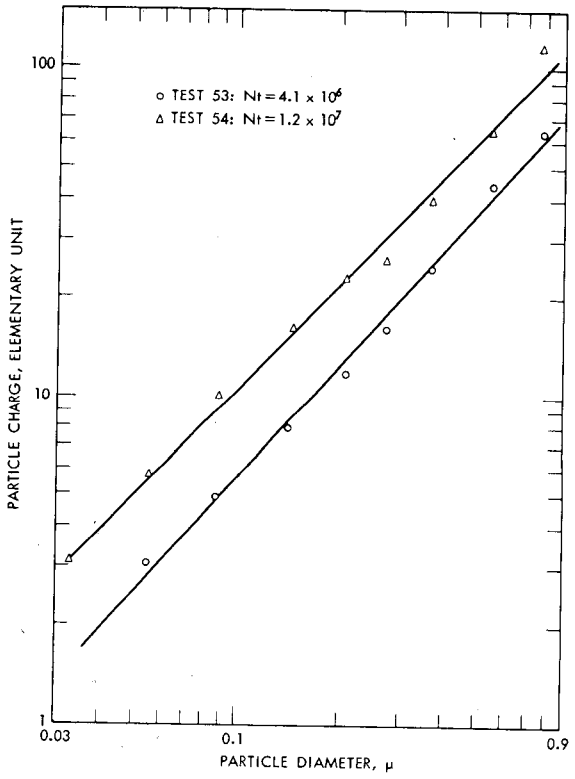

Fig. 13—Experimental particle charge for p = 0.1 atm and E = 800 volts/cm.

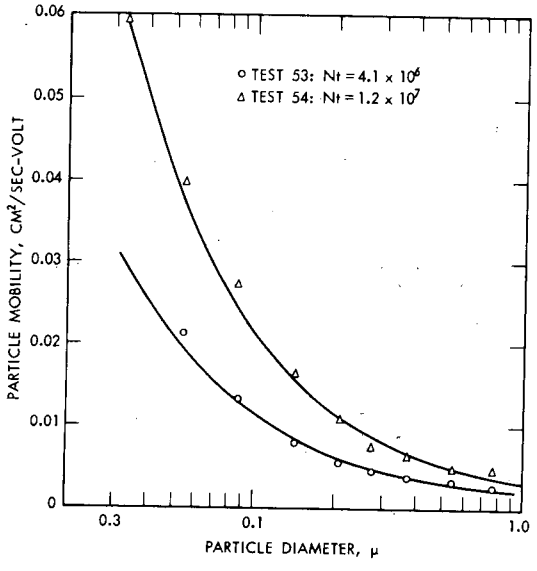

Fig. 14—Experimental particle mobility for p = 0.1 atm and E = 800 volts/cm.

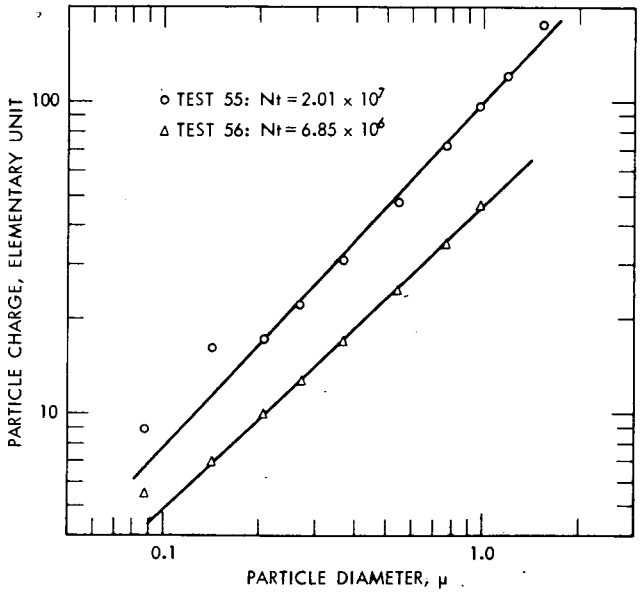

Fig. 15—Experimental particle charge for p = 0.1 atm and E = 240 volts/cm.

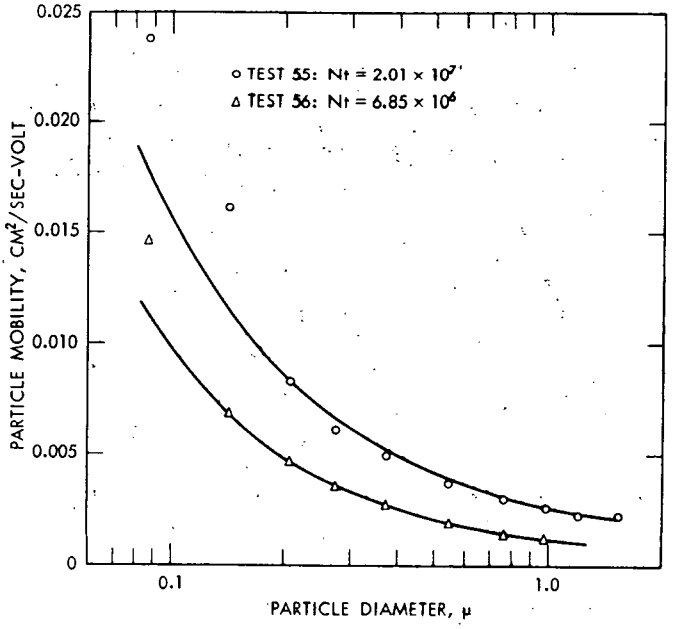

Fig. 16—Experimental particle mobility for p = 0.1 atm and E = 240 volts/cm.

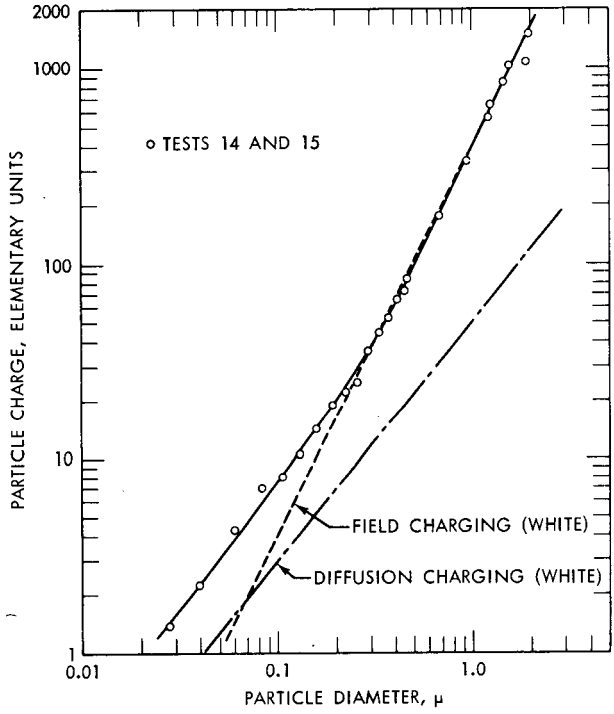

Fig. 17—Experimental particle charge for p = 0.95 atm and E = 9650 volts/cm.

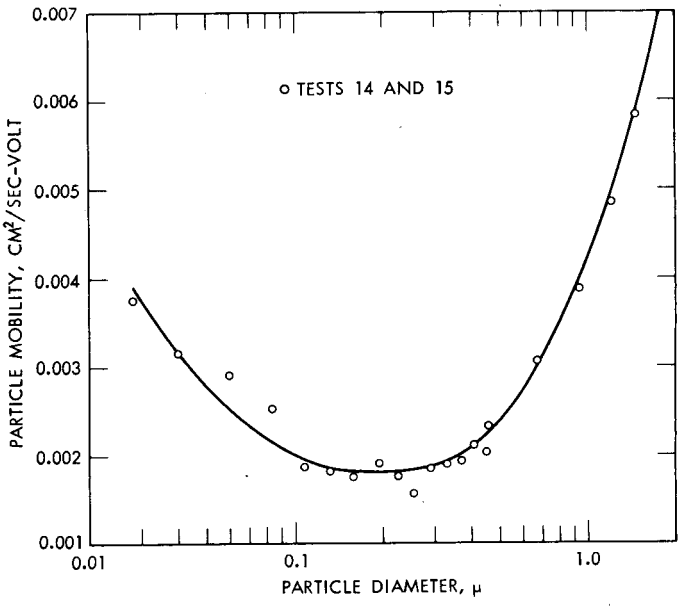

Fig. 18—Experimental particle mobility for p = 0.95 atm and E = 9650 volts/cm.

APPENDIX

DERIVATION OF EQUATIONS FOR CALCULATING FRACTION OF CHARGED PARTICLES

The number of ions striking a unit surface area in the time interval, dt, is, according to kinetic[15] theory, $\frac{1}{4} N\bar{c}\,dt$, where N is the ion density and $\bar{c}$ is the mean speed of the ions. If the diameter of a neutral particle is d_p, then the probability that this particle will be struck by an ion in the time interval dt and thus become charged is $\frac{1}{4} N\bar{c}\,\pi\,d_p^2\,dt$. If there are N_p such neutral particles at time, t, then the following number would be struck by ions during the time interval dt: $N_p\,\frac{1}{4} N\bar{c}\,\pi\,d_p^2\,dt$ Hence

$$dN_p = -N_p\,\tfrac{1}{4} N\bar{c}\,\pi\,d_p^2\,dt \tag{A.1}$$

This equation can be integrated with respect to time. With the initial condition that $N_p = N_{p0}$ at $t = 0$, the following equation is obtained:

$$N_p = N_{p0}\exp(-\tfrac{1}{4}\,\pi\,d_p^2\bar{c}Nt) \tag{A.2}$$

Since the number of particles that become charged is $N_{p0} - N_p$, the fraction, f, of particles that become charged in time from $t = 0$ to $t = t$ is

$$f = \frac{N_{p0} - N_p}{N_{p0}} = 1 - \exp(-\tfrac{1}{4}\,\pi\,d_p^2\bar{c}Nt) \tag{A.3}$$

If we define a characteristic product, $(Nt)_c$, as

$$(Nt)_c = \frac{4}{\pi\,d_p^2\bar{c}} \tag{A.4}$$

then

$$f = 1 - \exp\left[-Nt/(Nt)_c\right] \tag{A.5}$$

Equations A.5 and A.4 are plotted in Figs. 9 and 10, respectively.

REFERENCES

1. G. W. Hewitt, The Charging of Small Particles for Electrostatic Precipitation, *Trans. Am. Inst. Elec. Engrs.*, *76*II: 300 (1957).
2. G. W. Penney and R. D. Lynch, Measurements of Charge Imparted to Fine Particles by a Corona Discharge, *Trans. Am. Inst. Elec. Engrs.*, *76*I: 294-299 (1957).

3. H. J. White, Particle Charging in Electrostatic Precipitation, *Trans. Am. Inst. Elec. Engrs., 70*: 1186-1191 (1951).
4. R. Cochet, Lois de charge des Fines Particules (submicronique) Etudes Theoretiques—Controles Recents Spectre de Particles, in *Colloque International—La Physique des Forces Electrostatiques et Leurs Applications*, pp. 331-338, Centre National de la Recherche Scientifique, Paris, 1961.
5. V. G. Drozin and V. K. La Mer, The Determination of the Particle Size Distribution of Aerosols by Precipitation of Charged Particles, *J. Colloid Sci., 14*: 74-90 (1959).
6. G. Langer, Electrostatic Classification of Submicron Airborne Particles, Report No. 3187-5 to AEC, Armour Research Foundation, August 1961.
7. H. J. White, *Industrial Electrostatic Precipitation*, Addison-Wesley Publishing Co., Inc., Reading, Mass., 1962.
8. A. T. Murphy, F. T. Adler, and G. W. Penney, A Theoretical Analysis of the Effects of an Electric Field on the Charging of Fine Particles, *Trans. Am. Inst. Elec. Engrs., 78:* 318-325 (1959).
9. K. T. Whitby, D. A. Lundgren, and C. M. Peterson, Generation and Measurement of Homogeneous Fluorescent Aerosols, Preprint 27, presented at the Symposium on Particulates and Air Ions, 55th Annual Meeting of American Institute of Chemical Engineers, Chicago, Ill., Dec. 2–6, 1962.
10. K. T. Whitby, Generator for Producing High Concentrations of Small Ions, *Rev. Sci. Instr., 32*(12): 1351-1355 (1961).
11. K. T. Whitby and C. M. Peterson, The Electrical Neutralization and Particle Size Measurement of Dye Aerosols, presented at the American Chemical Society Meeting, Atlantic City, N. J., Sept. 13, 1962.
12. L. B. Loeb, *Basic Processes of Gaseous Electrons*, University of California Press, Berkeley, Calif., 1961.
13. N. A. Fuks, *The Mechanics of Aerosols* (English translation by E. Lachowicz, U. S. Army Chemical Warfare Laboratories, Spec. Publ. 4-12, Army Chemical Center, Md., 1958).
14. B. Y. H. Liu and K. T. Whitby, The Electrical Charging of Small Particles at Low Pressures, First Progress Report to AEC, Contract AT(11-1)-1248, University of Minnesota, October 1961.
15. E. H. Kennard, *Kinetic Theory of Gases*, McGraw-Hill Book Company, Inc., New York, 1938.

KINETICS OF WETTING IN WASHOUT OF DUST

T. G. OWE BERG, T. A. GAUKLER, and LAVON A. SQUIER
Aerojet-General Corporation, Downey, California

ABSTRACT

The rates of wetting of solids by water were measured under conditions simulating those in washout of dust by a water spray and of radioactive debris by rain. The solid was pressed against a water drop, and the event was followed by high-speed photography at 26,000 frames/sec. A voltage was applied between the solid and the water drop so as to simulate an electrostatic charge. The delay between contact and wetting depends upon the wettability of the solid and the voltage applied. Wetting is the formation of hydrogen bonds between H_2O molecules in the water drop and OH on the surface of the solid. This process requires the reorientation of bonds in the drop by an electric field operating on the dipole moment of the bond. Wetting in collision requires that wetting occur rapidly enough, i.e., before rebounce. In the case of mild steel, wetting is promoted by hydrogen in the steel and does not occur if hydrogen is not present.

INTRODUCTION

An important problem in industrial hygiene is how to get rid of harmful dust in the air. One approach to this problem that has been tried extensively in mines is to wash out the dust by a water spray. Recently, such washout has attracted attention as a natural process for deposition of radioactive debris, notably washout by rain.

A conceivable mechanism for such washout is the collision and coalescence between dust particles and spray drops or between debris

particles and raindrops. This process occurs in two steps: (1) collision and (2) coalescence or wetting during contact in collision. The last step has been studied. This paper summarizes the results of the study.

A similar phenomenon, namely, the coalescence of two liquid drops in contact with each other, was studied previously.[1] This investigation showed that there is a delay, t, between contact and coalescence and that the product of t and the voltage, V, across the drops is a constant. Accordingly, colliding drops do not coalesce but bounce apart unless they are electrically charged. Experiments with various liquids showed that

$$(\epsilon-1)^{1/2}\, tV = \text{constant} \tag{1}$$

(where ϵ is the dielectric constant) and that

$$M = (\epsilon-1)^{1/2} \tag{2}$$

is the induced dipole moment.

It follows from this result that all the intermolecular hydrogen bonds are engaged within each drop and that coalescence requires the reorientation of such bonds across the contact surface. This reorientation is a slow process and may be effected by an applied electric field.[2] The same conclusion should apply to the wetting of a solid particle in its collision with a water drop. Wetting is the formation of bonds between the liquid and the solid, notably, hydrogen bonds between H_2O molecules in the drop and OH groups in the solid.[3,4] Thus there are two conditions for the rapid wetting in collision: (1) the presence of OH groups in the solid and (2) the reorientation of hydrogen bonds in the H_2O molecules.

It was shown by Rayleigh[5] that colliding water drops bounce apart unless they are charged. This experiment was repeated by Boys.[6] More recently, McCulley *et al.*[7] showed that powder particles blown onto a stationary water drop bounce off if they are not wettable but are swallowed by the drop if they are. The particles must have been charged in this experiment.

EXPERIMENTAL TECHNIQUE

The experimental technique used was similar to that used in the preceding investigation with a pair of liquid drops.[1] Figure 1 shows the arrangement schematically as used previously. In this investigation, the movable drop was replaced by a solid. The drop was approximately 2 mm in diameter. The solid had the shape of a sphere or a flat sheet. Experiments were also conducted with pointed wires. However, the end of the wire formed a depression in the water drop, and it was not pos-

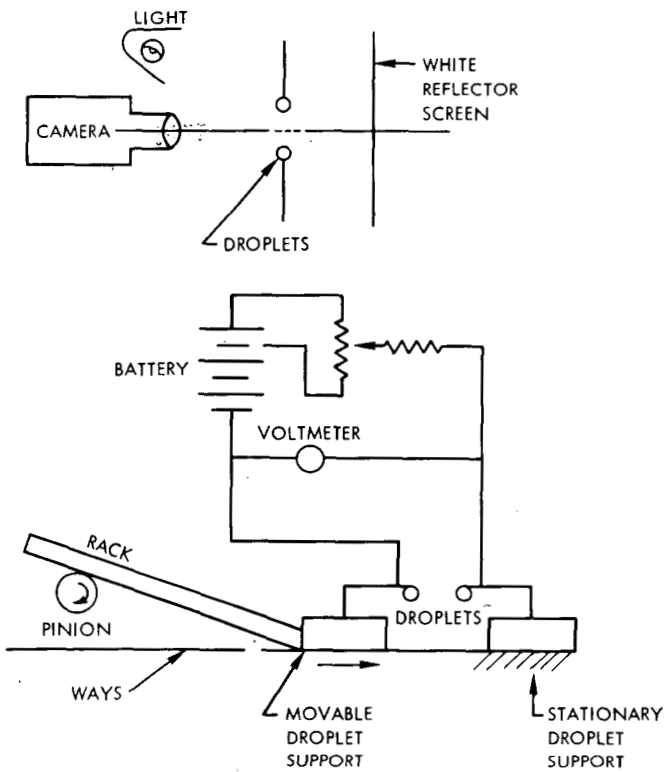

Fig. 1—Experimental setup for coalescence between two water drops.

sible to determine the actual instant of wetting because the wire end was hidden by the water.

The solid was pushed against the drop at a speed of 125 cm/sec. Photographs were taken of the event at 26,000 frames/sec. The total exposure time was approximately 10 msec. There was approximately 7 msec of useful exposure time (i.e., time after establishment of contact).

A typical sequence of frames is shown in Fig. 2. The phenomenon is very similar to that observed with a pair of liquid drops. One first sees a slight flattening of the drop and later a thin lens at the interface. This lens then spreads over the drop. The first appearance of the lens is taken as the indication of wetting or coalescence. The formation of a bond between the drop and the solid is thus indicated by a disturbance of the drop surface. The flattening of the drop is not very pronounced in the frames shown in Fig. 2. Other frames, taken in cases of no

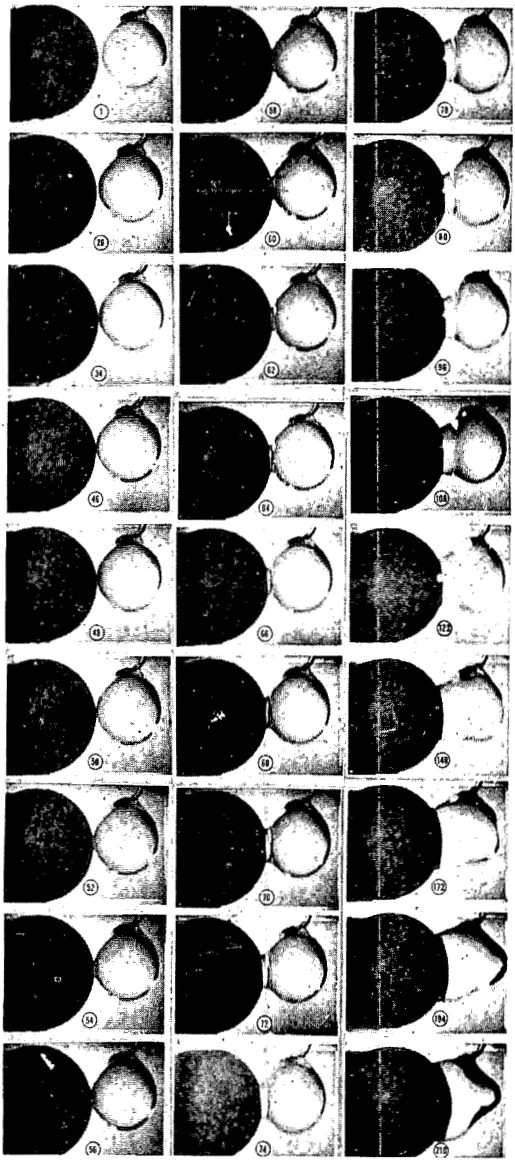

Fig. 2—Frames from a film showing a water drop and a steel bead under front illumination.

wetting in 7 msec, show the flattening to be quite pronounced. Contact was considered to be established when the projected contours touched in the picture.

The time interval between successive frames was approximately 40 μsec. The delay times measured were less than 1 msec, or less than 26 frames. Very short delay times, of the order of $\frac{1}{8}$ msec, gave only three or four frames. An error of one frame then causes an error of 25 to 30% in the delay time. In most determinations of these very

short times, the delay time measured is a little too long because the indication of contact may be too early and the indication of wetting is inherently too late.

A voltage was applied across the holders for the water drop and the solid by means of a battery and the circuit shown in Fig. 1. Most measurements were made at voltages below 50 volts. Higher voltages were tried occasionally, but the high field tended to deform the water drop by pulling out a cone. In all the cases studied, the optimum voltage with respect to the duration of the delay time was below 30 volts.

Much experimentation was devoted to the preparation of the surfaces of the solids. It was thought that surface oxide and other contaminants, e.g., dirt or grease from handling, might have decisive effects. It was found, however, that the surface state has a remarkably small influence. In one extreme case, two drops of water were used, each of which was covered with a thin but visible film of oil. The delay time did not differ markedly from that determined with clean drops. Glass beads were used in one series of experiments after various surface treatments (and lack of treatment), cleaning with HNO_3 or a grease solvent, and rinsing in water. There was no marked effect of these treatments upon the delay time. Nevertheless, the solids were handled with forceps, and attempts were made to avoid contaminating the materials.

The experiments were initially conducted in the ambient laboratory air, except for some experiments conducted at a controlled humidity in a glove box. The results were fairly reproducible. However, experiments with steel surfaces gave a very wide scatter of the data. This was first attributed to dust in the air issuing from another experiment. Thereafter the experiments with steel were conducted in filtered air in a glove box. However, this made no difference in the scatter and an extensive investigation was made. The results showed that the scatter was caused by varying contents of hydrogen in the steel. This phenomenon is of particular importance with respect to the experimental technique used, and mentioning it here may be useful to those attempting to reproduce our results.

RESULTS

Table 1 summarizes the results and gives at the same time a list of the materials used. The results are given in further detail in Figs. 4 to 17. For comparison, measurements were made with a pair of water drops. The data obtained at high voltages are presented in Fig. 3. These data give $tV^2 = 29$ at high voltages. For establishment of the value of tV at low voltages, numerous measurements were made at 4 volts, and the average value was taken. This gave $tV = 7.48$ at low voltages.

Table 1—SUMMARY OF EXPERIMENTAL RESULTS

Solid used	Dependence of delay time on voltage	For results
Borosilicate glass	t independent of V	Table 2
Copper	$tV^{1/2} = 1.27$, no polarity effect	Figs. 12 and 13
Copper with a drop of $12N$ HNO_3 solution	$tV = 6$, polarity effect not studied	Fig. 17
Magnesium	$tV = 5.33$, Mg^+, H_2O^- $tV = 9.50$, Mg^-, H_2O^+	Fig. 11
Steels	Dependence on treatment	Table 4 Figs. 14 to 16
NaCl saturated solution	$tV = 6.30$, $tV^2 = 58.3$, $NaCl^+$, H_2O^-	Figs. 7 and 8
	$tV = 7.80$, $tV^2 = 77.0$, $NaCl^-$, H_2O^+	Figs. 9 and 10
NaCl dry crystals, 3 and 45% relative humidity	$tV = 2.33$, $NaCl^+$, H_2O^-	Fig. 4
	$tV = 3.78$, $NaCl^-$, H_2O^+	Fig. 5
NaCl dry crystals, 60 to 65% relative humidity	$tV = 1.96$, $NaCl^-$, H_2O^+, no appreciable polarity effect	Fig. 6
NaCl dry crystals, 75% relative humidity	Erratic	Fig. 6

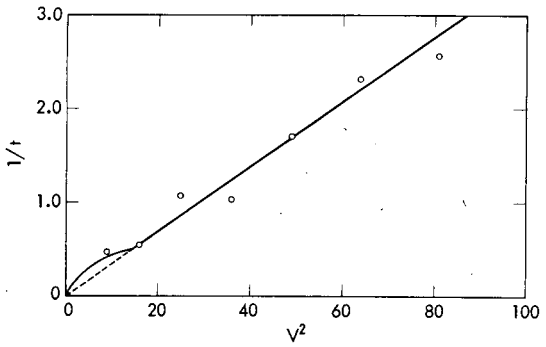

Fig. 3—Rate of coalescence vs. V^2 for a pair of water drops.

These results differ markedly from those obtained in the previous investigation,[1] $tV = 3.85$ and $tV^2 = 78.5$. At least part of this difference may be attributed to the temperature difference, the previous data being taken at a considerably higher temperature, but this phenomenon was not investigated. It is of little significance to the purpose at hand. The new data for the pair of water drops were obtained under the same conditions as the other data taken in this investigation, with which they should be compared.

A few comments are warranted concerning the special conditions for the experiments and the treatment of samples. The measurements

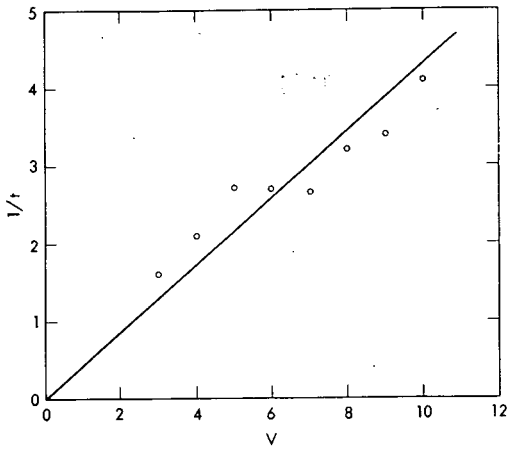

Fig. 4—Rate of coalescence vs. V for NaCl crystals at 40 to 55% relative humidity (crystal positive, water negative).

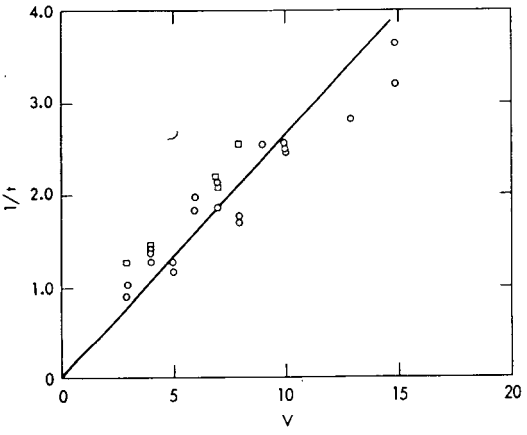

Fig. 5—Rate of coalescence vs. V for NaCl crystals at 3% (□) and 45% (○) relative humidity (crystal negative, water positive).

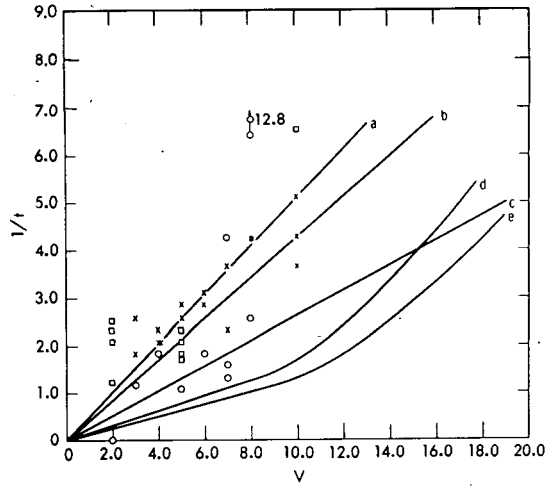

Fig. 6—Rate of wetting of NaCl crystals at 60 to 65% relative humidity (□, solid positive, water negative; ×, solid negative, water positive) and at 75% relative humidity (○, solid positive, water negative). The curves from Figs. 4, 5, and 7 to 10 are shown for comparison. The denotations are: a, 60 to 65% relative humidity; b, 3 and 45% relative humidity (solid positive); c, 3 and 45% relative humidity (solid negative); d, saturated NaCl solution (solution positive); e, saturated NaCl solution (solution negative).

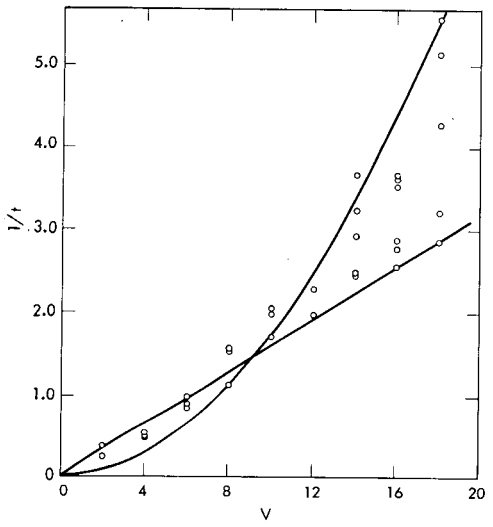

Fig. 7—Rate of coalescence vs. V in ambient air for saturated NaCl solution (solution positive, water negative).

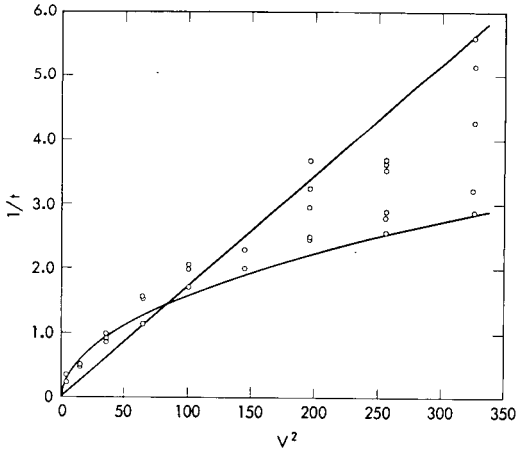

Fig. 8—Rate of coalescence vs. V^2 in ambient air for saturated NaCl solution (solution positive, water negative).

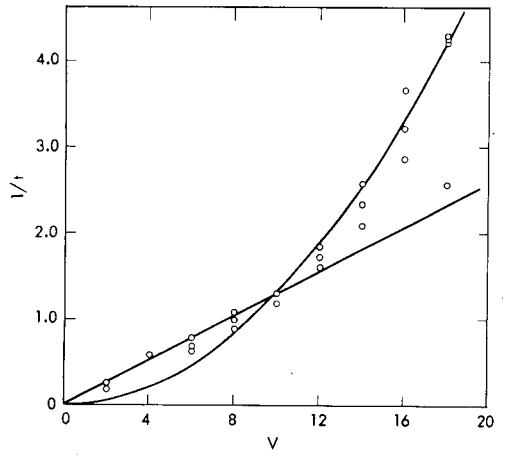

Fig. 9—Rate of coalescence vs. V in ambient air for saturated NaCl solution (solution negative, water positive).

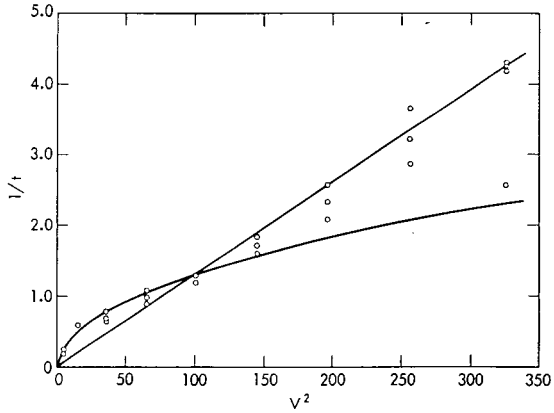

Fig. 10—Rate of coalescence vs. V^2 in ambient air for saturated NaCl solution (solution negative, water positive).

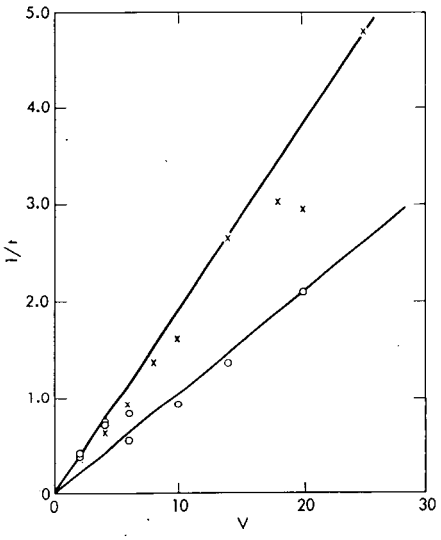

Fig. 11—Rate of coalescence vs. V in ambient air for magnesium (×, metal positive, water negative; ○, metal negative, water positive).

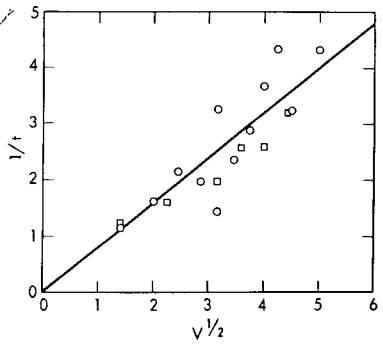

Fig. 12—Rate of coalescence vs. $V^{1/2}$ in ambient air for copper sheet (□) and copper-plated steel beads (○) (solid positive, water negative).

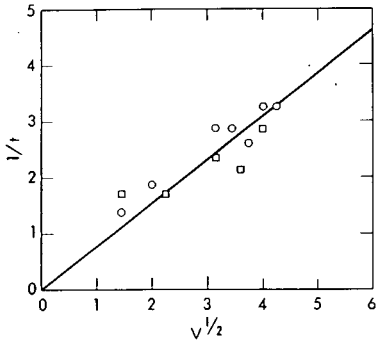

Fig. 13—Rate of coalescence vs. $V^{1/2}$ in ambient air for copper sheet (□) and copper-plated steel beads (○) (solid negative, water positive).

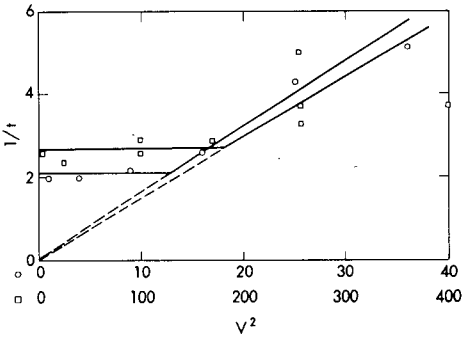

Fig. 14—Rate of wetting of steel B after pickling in 2N H_2SO_4 for 2 hr (○, steel positive, water drop negative; □, steel negative, water drop positive).

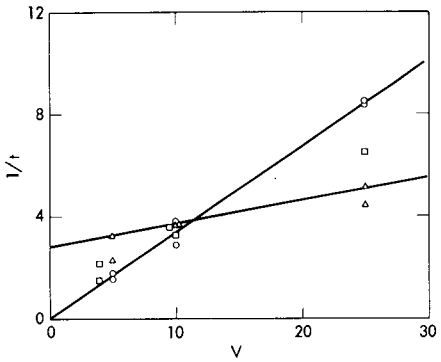

Fig. 15—Rate of wetting of steel C after pickling in 12N HNO_3 overnight [○, steel positive, water drop negative; □, steel negative, water positive; △ (treatment followed by tumbling steel in sand), steel positive, water drop negative].

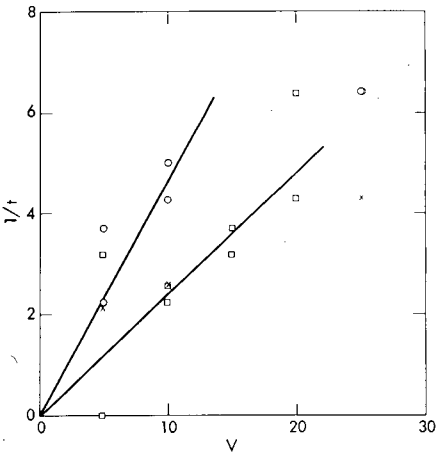

Fig. 16—Rate of wetting of steel B after pickling in 12N HNO_3 [×, steel positive, water negative (Nov. 6, 1963); ○, steel negative, water drop positive (Nov. 7, 1963); □, steel negative, water drop positive (Nov. 11, 1963)].

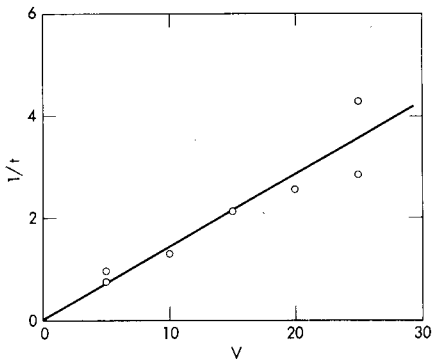

Fig. 17—Rate of wetting of sheet copper by 12N HNO_3.

were limited to voltages above 2 volts. At lower voltages there was a considerable scatter of the data, and apparently the voltage had only a small effect in this region. No complete explanation can be given, but it was suggested by Rayleigh[8] that uncharged water drops may coalesce in the presence of charged dust in the air. Preliminary results from other studies seem to confirm this explanation.[9]

It was thought that hygroscopic salts might be affected by the humidity of the air. This issue was studied extensively with NaCl crystals. These were cleaved out of large single crystals into pieces approximately 12 by 12 by 4 mm. They were mounted so as to present a corner, an edge, or a flat surface to the water drop. There were no differences in delay times for these different mountings. Two sets of data were obtained from experiments conducted in a glove box at 3 and 45% relative humidity. There was no difference between the two sets of data (Figs. 4 and 5). The relative humidity was then increased to 60% (Fig. 6). The data then scattered badly at high voltages. A similar phenomenon had previously been observed with aqueous solutions, which gave tV = constant at low voltages and tV^2 = constant at high voltages with data between these relations at intermediate voltages.[1] The scatter was taken as an indication that the NaCl crystal may behave as a saturated solution at this high humidity. This is suggested also by the observations of Orr *et al.*[10] Experiments with a drop of saturated NaCl solution and a water drop (Figs. 7 to 10) and with "dry" NaCl crystals at 75% relative humidity (Fig. 6) confirm this view.

The effect of the relative humidity of the air upon the rate of wetting of NaCl crystals is shown in Fig. 6, in which all the data are included. In the range 3 to 45% relative humidity, there is no humidity effect, but, at 60 to 65% relative humidity, the rate of wetting is noticeably higher. At 75% relative humidity, the crystals are dripping wet and are obviously covered by saturated NaCl solution. The rate of wetting scatters between the curve for the saturated NaCl solution and the values at 60 to 65% relative humidity. Thus the crystal is not uniformly covered by the saturated solution.

Experiments conducted with borosilicate-glass beads gave the results shown in Table 2. There is no trend in the data. However, the glass may not have been conducting enough to be affected by the ap-

Table 2—DELAYS OBSERVED AT VARIOUS VOLTAGES FOR BOROSILICATE-GLASS BEADS, MSEC

Treatment	Polarity	Applied voltage									
		2	4	6	8	10	12	14	16	18	20
None	+	0.84	1.29		1.71	1.34	1.24	1.48			
None	−	0.86	1.41	1.55	1.18	0.78	1.83	1.26	2.71	1.00	1.07
HNO_3	+	0.84	1.24	0.90	1.26	1.30	1.95	1.85	1.75		

plied voltage. The data should then be representative of an unknown and uncontrolled floating potential. Even so, the data show that the wetting of glass is a slow process.

The two processes involved in wetting, namely, the supply of a bond by the water drop and the formation of a bond with the solid surface, are particularly conveniently studied with metals. With a metal, there is no doubt about a sufficient conductivity for the application of the voltage to the surface.

Figure 11 shows the results obtained with a magnesium ribbon. At low voltages the rate is apparently independent of the polarity, but at high voltages the rate is almost twice as high for positive magnesium as for negative magnesium.

Figures 12 and 13 show the results obtained with sheet copper and copper-plated steel. The data for the two materials are not significantly different although, on the whole, the copper-plated steel gave higher rates than did the copper sheet. There is no appreciable polarity effect. This is the only case found so far that gives a constant product $tV^{1/2}$. It is noteworthy that the data scatter more in the case of copper than in the case of magnesium.

Experiments were conducted with various types of steel. The material used in the first experiments was copper-plated air-rifle pellets pickled in concentrated HNO_3 to remove copper, rinsed in distilled water, and dried. This material was not wetted within 7 msec at any voltage up to ± 25 volts. The material was then treated in the same way as before but, in addition, pickled in $2N\ H_2SO_4$ overnight. This treatment led to rapid wetting of the pellets; the rate was independent of the voltage.

There appeared to be two possible explanations for these observations. Either the surface becomes passivated by the HNO_3 or hydrogen dissolved in the steel is instrumental in the wetting process. Pickling in H_2SO_4 gives a high concentration of hydrogen in the steel; concentrated HNO_3 removes dissolved hydrogen from the steel.

The air-rifle pellets pickled in HNO_3 presented the first case of nonwetting encountered in the investigation. Since a change in treatment (pickling in $2N\ H_2SO_4$) caused rapid wetting, it is apparent that the state of the solid is essential to the wetting and that the rate of wetting is not determined by the phenomena in or on the water drop alone. The treatment with H_2SO_4 gave a rate of wetting that was independent of the voltage applied.

It was therefore decided to investigate the wetting of the steel with a view to the effect of the solid upon the rate of wetting. Of course, it is clear from a comparison of the data for the other solids used with those for a pair of water drops that the solid takes part in the rate-determining process, but it appeared that steel would be particularly well suited for the study of the effect.

Experiments were next conducted with ball-bearing steel. This material gave rapid wetting after pickling it in $12N$ HNO_3. Hence the passivation of the surface by the concentrated HNO_3 is not decisive to the wetting. It was then attempted to study the effect of dissolved hydrogen in the steel. To this end the two steels mentioned (steels A and B) and also stainless steel 440 (steel C) were given various pickling treatments and cleaned by tumbling them in silica sand. The analyses of the three steels are given in Table 3. The results obtained after various treatments are summarized in Table 4.

Table 3 — ANALYSES OF THREE STEELS

	Mild steel (A), %	Ball-bearing steel (B), %	Stainless steel 440 (C), %
Carbon	0.10	0.45	0.80
Manganese	0.10	0.30	1*
Silicon		0.25	1*
Chromium	0.20	1.3	17*
Nickel	0.10	0.40	
Molybdenum		0.01	0.75*

*Nominal analysis (steel was analyzed for carbon only).

Table 4 — TIME DELAYS FOR STEEL AFTER VARIOUS TREATMENTS, MSEC

Treatment	Mild steel (A)		Ball-bearing steel (B)		Stainless steel 440 (C)	
	+	−	+	−	+	−
Pickling in $2N$ H_2SO_4	0.2	0.3	0.5 $tV^2 = 6$	0.4 $tV^2 = 66$	No wetting	
Pickling in $2N$ HNO_3; for steel A followed by tumbling in sand	0.15 to 0.40 (erratic)	0.25 to 1.5			No wetting	
Pickling in $12N$ HNO_3 Tumbling in sand	No wetting		$tV = 3$ $\frac{1}{t} = 1.5 + 0.17\ V$ $\frac{1}{t} = 3.30 + 0.17\ V$	$tV = 3$	$tV = 3$ $\frac{1}{t} = 2.80 + 0.09\ V$	$tV = 3$

The results are discussed in detail later in this paper. Mild steel holds hydrogen in interstitial solid solution. The hydrogen moves rapidly within the metal. Its rate of exchange with the environment is determined by surface reactions. This subject has been studied in previous investigations.[11–13] High-carbon steels, particularly hardened ones, contain a hydrogen-rich carbide, known as ϵ carbide. This carbide[14] probably has the composition Fe_2HC. The hydrogen is comparatively strongly held in this carbide but is released in the transformation of ϵ carbide into cementite, Fe_3C. The ϵ carbide is known to be stabilized by chromium. Therefore steels B and C may be expected to

hold such bound hydrogen in their interiors but much less at their surfaces owing to transformation of the carbide at the surface. Pickling or abrasion of steels B and C removes the surface layers and exposes the hydrogen-bearing carbide. It makes little difference in this respect what acid is used.

Pickling of steel A in $2N$ H_2SO_4 or tumbling it in sand causes the steel to pick up hydrogen, either from the H_2SO_4 or from the water present. Pickling of steel A in $2N$ HNO_3 and $12N$ HNO_3 (for a sufficient time) removes the dissolved hydrogen partially and completely, respectively, for the pickling times used.

It follows from these arguments that steel A should give rapid wetting after pickling it in $2N$ H_2SO_4, somewhat less rapid wetting after tumbling it in sand, and slow wetting after pickling it in $2N$ or $12N$ HNO_3. It also follows that steels B and C should give comparatively rapid wetting after all these treatments. These expectations are partially verified by the data. However, steel C was not attacked by $2N$ H_2SO_4 or $2N$ HNO_3 and was not wetted in 7 msec after treatments with them.

It appears, therefore, that wetting is promoted by a reaction between hydrogen in the steel and water in the drop. The mechanism of this reaction is discussed later. However, if this concept holds true for steel, it may hold more generally; therefore any rapid reaction between a solid and water would cause rapid wetting. This concept does not include electrolytic decomposition of the water because no current can flow prior to wetting.[8]

Experiments were undertaken with sheet copper and drops of $12N$ HNO_3 to follow up this concept. Since these two materials react very rapidly, wetting by $12N$ HNO_3 was expected to be more rapid than wetting by pure water. The results of these measurements are presented in Fig. 17. They are quite different from those obtained with pure water, which are shown in Figs. 12 and 13. The product tV is constant for $12N$ HNO_3, whereas the product $tV^{1/2}$ is constant for water.

DISCUSSION

There are two conceivable ways for the formation of bonds between a metal and water, namely, with or without decomposition of the water. Without decomposition the water is held physically adsorbed; with decomposition the water is held chemically adsorbed, notably as OH. Decomposition of water on a metal surface may occur by two mechanisms:

$$H_2O_{ads} \rightarrow H_{abs} + OH_{ads} \qquad (3)$$

and

$$H_{abs} + H_2O_{ads} \rightarrow H_{2\,gas} + OH_{ads} \quad (4)$$

The first mechanism should be operative on hydrogen-replacing metals. The second mechanism should be operative on any metal containing dissolved hydrogen, whether the metal itself is hydrogen-replacing or noble.

There is an important difference between the two mechanisms. The reaction given as Eq. 3 requires that there be a free adsorption site next to that holding the H_2O; the reaction given as Eq. 4 does not.[11] Thus the rates of the two reactions are

$$\frac{d[OH]}{dt} = k_1 [H_2O] (1 - \Theta) \quad (5)$$

and

$$\frac{d[OH]}{dt} = k_2 [H_2O] \{H\} \quad (6)$$

In these formulas $[OH]$ and $[H_2O]$ denote surface coverages, $\{H\}$ denotes volume concentration of dissolved hydrogen, Θ denotes the total coverage, and k_1 and k_2 are constants. The total coverage may be given as

$$\Theta = [OH] + [H_2O] \quad (7)$$

The rate (Eq. 5) is zero when $\Theta = 1$.

When a water drop is pressed against a metal surface, one may assume $[H_2O]$ to be very large, close to unity. The first mechanism (Eq. 3) then contributes little to the formation of OH on the surface. However, in the transient state preceding this high coverage by H_2O, some OH_{ads} should be formed. Hence wetting may occur in this case by bonding between the water drop and the surface OH. Physically adsorbed H_2O apparently does not hold on strongly enough to metal to cause wetting of the metal. However, if the H_2O_{ads} is bonded to the water in the drop, the OH_{ads} should be also.

A steel that contains much hydrogen, e.g., steel A or steel B after pickling in $2N$ H_2SO_4, should be expected to be wetted by the second mechanism (Eq. 4). The fact that the rate of wetting is independent of the voltage applied shows that the reorientation of bonds at the surface of the water drop as caused by the applied field takes no part in the rate-determining step. The process is rapid. It is much more rapid at low voltages than in the case of a pair of water drops. It follows that the reorientation of the bonds is caused by the reaction itself; i.e., the H_2O_{ads} and OH_{ads} in the formula remain bonded to the H_2O in the drop. This should apply equally to the first mechanism (Eq. 3) in the transient state. Consequently the fact that no wetting of steel A occurs in

the absence of dissolved hydrogen, i.e., after pickling it in 12*N* HNO_3, shows that the rate (Eq. 5) is small at all values of Θ and therefore that the reaction does not occur within a period of 7 msec. The reaction of the second mechanism (Eq. 4) is found to occur within a period of 0.2 msec.

The data disclose the interesting fact that hydrogen is much more strongly hydrogen-replacing than is iron. This, of course, is well known. They also suggest that iron free of hydrogen may not be hydrogen-replacing at all with respect to water. This point is difficult to prove because as the period of observation is extended beyond 7 msec traces of hydrogen become increasingly important until it is very difficult to distinguish between the slow reaction of Eq. 3 and the slow ($\{H\}$ small) reaction of Eq. 4.

Equation 6 expresses the rate of wetting by the second mechanism (Eq. 4) because the OH_{ads} is bonded to the water in the drop. On the other hand, the reorientation rate, v, of bonds at the water surface is

$$v = k_3 V \tag{8}$$

When this rate is greater than the rate of Eq. 6, the formation of OH_{ads} contributes less to the wetting than does the mechanism of reorientation of bonds and bonding with already present OH_{ads}. Hence at high voltages the rate should depend upon V. We may expect

$$v = k_2 [H_2O] \{H\}, \text{ V small} \tag{9}$$

and

$$v = k_3 V, \text{ V large} \tag{10}$$

Such is not quite the case, however, because v is proportional to V^2 at high values of V. The same relation is shown in the results with saturated NaCl solutions in Figs. 7 to 10. Accordingly, the formula given as Eq. 8 does not hold any more when

$$k_3 V > k_2 [H_2O] \{H\} \tag{11}$$

In this region we have

$$v = k_4 V^2 \tag{12}$$

Hence, instead of Eqs. 7 and 8, we have

$$v = k_2 [H_2O] \{H\}, \text{ V small}$$

and

$$v = k_4 V^2, \text{ V large} \tag{13}$$

The data for steel pickled in $2N$ H_2SO_4 show very little scatter at low voltages. This indicates highly reproducible conditions.

Tumbling the steel in sand was studied with steel B. In two experiments (Table 4), the scatter was not extensive, but in two other experiments the data were widely scattered. The conditions are not highly reproducible with this treatment. The formulas given in Table 4 indicate that two processes are operative together and that the rate of wetting is the sum of the rates of Eqs. 9 and 10. These data are reproduced with steel C after pickling it in $12N$ HNO_3 followed by tumbling it in sand (Table 4 and Fig. 15).

The reaction given as Eq. 4 also occurs with hydrogen bound in carbide. It is, indeed, part of the mechanism for the transformation of the carbide into cementite or graphite.[15] The rate is much smaller than for dissolved hydrogen. Nevertheless, the exposure to the humid ambient air should completely transform the surface carbide and give a coverage of OH on the surface. Accordingly, wetting consists in the establishment of bonds between the H_2O in the drop and the OH already present in abundance on the surface. Rate determining should then be the reorientation of bonds at the drop surface, just as in the coalescence of a pair of water drops. This is indicated by the data. The product $tV = 3$ is the same for steels B and C and somewhat lower than one-half the value $tV = 7.5$ for a pair of drops

The results with copper and water show no polarity effect. The empirical rate formula is

$$v = k_5 Vt \tag{14}$$

so that $tV^{1/2}$ is constant. Since copper is a noble metal, it is surprising that it is wetted at all. Since it reacts rapidly with concentrated HNO_3, one would expect a much more rapid wetting by $12N$ HNO_3, especially at low voltages. The opposite is observed. This could conceivably be attributed to surface oxide or hydroxide, but the rate of wetting by $12N$ HNO_3 did not change when the oxide was wiped off with a piece of tissue soaked in $12N$ HNO_3. The rate of wetting of copper by $12N$ HNO_3 is smaller (about one-half) than that of steels B or C by water after pickling in $12N$ HNO_3, but it follows the same formula.[8]

A plausible, but somewhat speculative, mechanism for explaining Eq. 14 is that the copper surface is partially covered with partially hydrated oxide with very little OH in it and that wetting occurs when a reorientated hydrogen bond from the water drop coincides with an OH group within the contact area. Logic then requires that there be much

OH on the surface for Eq. 8 to be valid. This is well in keeping with the role of hydrogen in the wetting of steel as just discussed. By the same token, the HNO_3 should wet the oxide on the copper surface whether it contains OH or not. This appears reasonable since the oxide reacts rapidly with acids.

This reasoning should be equally applicable to all metals, including magnesium. Accordingly, the data for magnesium should indicate a surface layer of hydrated oxide, i.e., $Mg(OH)_2$, on the metal. It is noteworthy that the average value of tV for the two polarities is almost exactly equal to the value of tV = 7.5 for a pair of drops.

It is a remarkable fact that the coalescence with a saturated NaCl solution is slower than the wetting of a dry NaCl crystal. It should be borne in mind, however, that the coalescence requires the reorientation of hydrogen bonds in both drops, whereas the wetting requires that this process occur on one drop only. In the saturated NaCl solution, the sodium and chlorine are surrounded by water molecules,[16] and the NaCl solution should therefore not differ appreciably from pure water. This has been found to apply to HCl solutions.[1] The average value of the product tV for the two polarities does not differ appreciably from that for pure water. In the dry NaCl crystal, the sodium and chlorine atoms should be directly accessible to the water in the drop. However, such atoms exposed to the ambient air, even at very low relative humidities, may be expected to react with the water in the air and to form effectively NaOH and HCl at the surface. In particular there should be a surface coverage of OH. Hence, just as explained in the case of hydrogen-bearing carbide in steel, the rate-determining step in the wetting of dry NaCl crystals should be the reorientation of bonds in the water drop in the direction of the applied field. The value of tV for the negative crystal is approximately one-half that for two drops. This indicates that the reorientation of the hydrogen bond is such that H connects with OH at the surface. The low value of tV for the positive NaCl crystal should then indicate some accelerating effect of the surface upon the formation of bonds with OH in the water. The nature of this effect is not revealed by these experiments.

In the case of metallic magnesium, there is a similar polarity effect. The average value of tV for the two polarities is almost exactly equal to that for a pair of drops. Again, the polarity effect cannot be explained.

CONCLUSIONS

1. Wetting of a solid consists in the formation of hydrogen bonds between H_2O in the water and chemically bound OH on the solid. Physically adsorbed H_2O on the solid does not cause wetting.

2. Wetting is a rate process. Unless the rate is great enough, colliding solid particles and water drops bounce apart.

3. A solid salt that is hydrated so as to be effectively in the form of a saturated solution at the surface is wetted by the mechanism of coalescence and at the rate of coalescence of two water drops. Rate determining is then the reorientation of hydrogen bonds across the interface. This requires an orientating electric field; i.e., the colliding particles must be charged.

4. A solid that is covered by OH is more rapidly wetted than one that is covered by H_2O because the reorientation of bonds is required on the part of the water drop alone in the former case and on the part of both in the latter case. Again, the colliding particles must be charged.

5. In principle, a hydrogen-replacing metal may decompose liquid H_2O to form chemisorbed OH without breaking the bonds between the liquid H_2O and the chemisorbed OH. In this mechanism the orientation of bonds is automatically satisfied. Atomic hydrogen in solution in the metal is much more powerful in this mechanism than is the metal itself, namely, according to Eq. 4.

It appears that iron is not a hydrogen-replacing metal but decomposes water only by virtue of its dissolved hydrogen. As a consequence, iron free of hydrogen does not decompose water in the short period of contact in collision and therefore is not wetted by this mechanism.

6. Iron free of hydrogen, e.g., after pickling it in concentrated HNO_3, does not decompose water and therefore does not cover itself with chemisorbed OH even during prolonged exposure to the ambient air. Iron free of hydrogen is therefore not wetted by any mechanism in collision.

REFERENCES

1. T. G. Owe Berg, G. C. Fernish, and T. A. Gaukler, The Mechanism of Coalescence of Liquid Drops, *J. Atmospheric Sci., 20:* 153 (1963).
2. T. G. Owe Berg, Sur la Théorie de la Conductivité Électrique des Solutions Aqueuses d'Acides, *J. Chim. Phys., 50:* 247 (1953).
3. M. R. Basila, Hydrogen Bonding Interaction Between Adsorbate Molecules and Surface Hydroxyl Groups on Silica, *J. Chem. Phys., 35:* 1151 (1961).
4. T. G. Owe Berg, The Kinetics of Wetting of Solid Hydrocarbons, Special Report No. 0780-01(01) SP, Aerojet-General Corporation, September 1963.
5. Lord Rayleigh, The Influence of Electricity on Colliding Water Drops, *Proc. Roy. Soc., 28:* 406 (1879).
6. C. V. Boys, Soap Bubbles (3rd revised edition), Dover Publications, New York, 1959.
7. C. R. McCulley *et al.*, Scavenging Action of Rain on Airborne Particulate Matter, *Ind. Eng. Chem., 48:* 1512 (1956).
8. Lord Rayleigh, Further Observations upon Liquid Jets, *Proc. Roy. Soc., 34:* 130 (1882).
9. U. S. Army Signal Corps, Contract No. DA-36-039-AMC-03378-(E).
10. C. Orr, F. K. Hurd, and W. J. Corbett, Aerosol Size and Relative Humidity, *J. Colloid Sci., 13:* 472 (1958).

11. T. G. Owe Berg, Kinetics of Hydrogen Absorption, Desorption and Permeation of Metals, *Corrosion, 14:* 562 (1958).
12. T. G. Owe Berg, Kinetics of Absorption of Hydrogen from Water and Aqueous Solutions, *Corrosion, 16:* 198 t (1960).
13. T. G. Owe Berg, Heterogeneous Hydrogen Exchange Processes, Materials Research Report No. LB-30117, Douglas Aircraft Company, Inc., 1959.
14. Hydrogen in Carbide in Steel, *Am. Ceramic. Soc. Bull., 40:* 78 (1961).
15. T. G. Owe Berg, The Role of Hydrogen in Formation, Decomposition, and Transformation of ϵ-Carbide in Steel, Materials Research Report No. LB-30294, Douglas Aircraft Company, Inc., 1959.
16. T. G. Owe Berg, Liquid Structure of Aqueous Solutions of NaCl: Solubility, Vapor Pressure, and Conductivity, *Acta Chem. Scand., 8:* 1 (1954).

STRATOSPHERIC DISTRIBUTION OF NUCLEAR DEBRIS IN 1962, 1963, AND 1964

HERBERT W. FEELY and FERNANDO BAZAN
Isotopes, Inc., Westwood, New Jersey

ABSTRACT

An estimate may be made of the stratospheric distribution of nuclear debris by using a combination of data from the balloon sampling program and the WU-2 aircraft sampling program. The stratospheric ^{90}Sr distributions from January 1962 through May 1964 have been estimated, and from them the stratospheric burdens (ranging from 0.9 Mc before the 1961 U.S.S.R. tests to perhaps over 7 Mc by early 1963 and then falling to about 4.4 Mc in late 1963) have been calculated.

The observed vertical distributions of ^{90}Sr and of certain tracer nuclides, such as ^{54}Mn, indicate that little debris from the pre-1962 U.S.S.R. test series and even from events of very high yield had stabilized at altitudes above 70,000 ft in the polar stratosphere and that only a small fraction of the debris from the 1962 U.S.S.R. test series stabilized above that altitude.

Relatively little debris from either the 1961 U.S.S.R. tests or the 1962 United States tests reached the southern polar stratosphere during 1962. During 1963, however, large quantities of debris from the 1961 and 1962 test series did reach that region, as revealed by sampling in the vicinity of Australia. This debris appeared in the 80,000- to 90,000-ft layer at Mildura during June to August 1963 (the southern-hemisphere winter), and it was found by both balloon and WU-2 sampling in the region below 80,000 ft from September through November 1963 (the southern-hemisphere spring). The rate of southward

movement of the debris was probably controlled by seasonal changes in the coefficients of turbulent exchange within the tropical stratosphere.

INTRODUCTION

The moratorium on nuclear-weapons tests, which had begun in November 1958, was ended in September 1961 when the U.S.S.R. began a series of atmospheric tests of nuclear devices. After the end of the moratorium and before the 1963 treaty banning atmospheric weapons tests went into effect, there were three major series of tests which injected large amounts of nuclear debris into the stratosphere. These were test series conducted by the U.S.S.R. during September to November 1961 and August to December 1962 and by the United States during April to November 1962 (Operation Dominic I). Debris from these test series was sampled by the High Altitude Balloon Sampling Program.[1,2] The combination of data from this program with data from other programs of stratospheric sampling, such as Project Star Dust, sponsored by the Defense Atomic Support Agency,[3] permits the delineation of the stratospheric distribution of nuclear debris from these test series and a description of the changes that have occurred in that distribution during the past three years.

In this discussion we will pay special attention to information concerning the initial vertical distribution of debris injected into the stratosphere and information concerning the factors that influence the later movement of the debris within the stratosphere. We will note evidence that suggests that almost all debris injected into the polar stratosphere, even by weapons of very high yield, has tended to stabilize in the lower polar stratosphere, below 70,000 ft. We will also note evidence concerning the seasonal dependence of rates of transfer of debris from one region of the stratosphere to another. We have found no evidence that any organized circulation of the stratosphere exists which plays a major role in the movement of debris within the stratosphere. Therefore our discussion is based on the assumption that turbulent exchange plays the major role in the transfer of debris within the stratosphere, although organized circulation and particle settling probably also play less important roles.

CORRELATION OF BALLOON AND WU-2 DATA

Both the balloon and the WU-2 samplers have been calibrated. Nevertheless it is desirable that empirical data be used to substantiate the validity of their intercalibration. Since mid-1962 the collection of samples by the balloon program has been performed at altitudes of approximately 65,000, 80,000, 90,000, and 105,000 ft. As a result, during

the last few years there has been an overlapping of balloon and WU-2 aircraft sampling at altitudes between 65,000 and 70,000 ft. There has been no attempt to schedule routinely balloon and WU-2 flights; therefore it is unusual for flights of the two programs to sample the same region of the stratosphere on the same day. Nevertheless, if we compare results obtained from both programs at two locations regularly sampled by each, we should detect any systematic discrepancy due to sampler calibration or to analytical procedures.

The results of ^{90}Sr analyses of balloon and aircraft samples collected at 65,000 to 70,000 ft at about both 31°N and 34°S latitudes during January 1962 through May 1964 are plotted in Fig. 1. Over short intervals there appear to be systematic differences between results for the two programs, but these differences are not consistently in one direction. They may result from differences in sampling altitude and from the fact that the WU-2 samples are normally collected over a range of 5 to 20 degrees in latitude. When the data for the entire 29-month period are considered, the agreement between the results for the two programs is satisfactory.

We will assume that the calibrations of both the balloon sampler and the WU-2 samplers are accurate for all altitudes and that data from the balloon program and from the WU-2 aircraft are comparable. Therefore we will combine them to obtain an estimate of the stratospheric distribution of nuclear debris.[4]

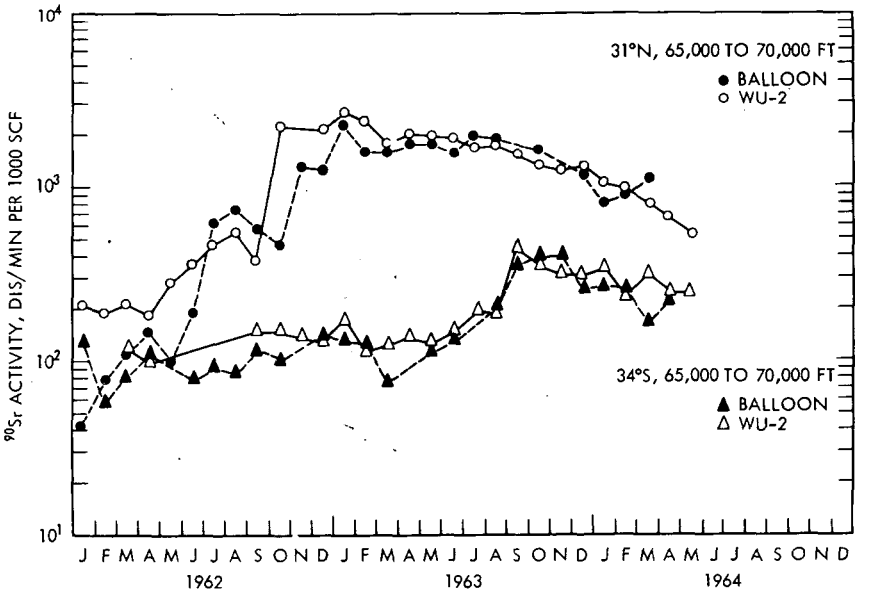

Fig. 1—Trends in ^{90}Sr activity.

CHANGES IN ^{90}Sr CONCENTRATIONS

The concentrations of nuclear debris in the stratosphere have changed repeatedly during the course of the last three years in all regions sampled. These changes have resulted from the injection of new nuclear debris into the stratosphere at various times during 1961 and 1962, from the dilution of the new debris, from the movement of debris from one region of the stratosphere to another, from radioactive decay, and from fallout of debris into the troposphere and thence to the ground.

In the northern hemisphere similar changes in concentration with time generally seemed to occur at all altitudes, though there were some differences between the trends at the higher and lower altitudes during 1962. This is evident from Fig. 2, in which are plotted the ^{90}Sr concentrations found in the vicinity of Goodfellow Air Force Base, San Angelo, Tex., by balloon sampling at 65,000 to 70,000 ft and at about 105,000 ft. In general, during 1962 the ^{90}Sr activities at 65,000 to 70,000 ft increased with time as debris first from the 1961 U.S.S.R. tests, then from the 1962 United States tests, and finally from the 1962 U.S.S.R. tests reached 31°N. At 105,000 ft, however, no significant change in ^{90}Sr concentrations was detected before early 1963. The fission-product ratios in the new debris that reached San Angelo at

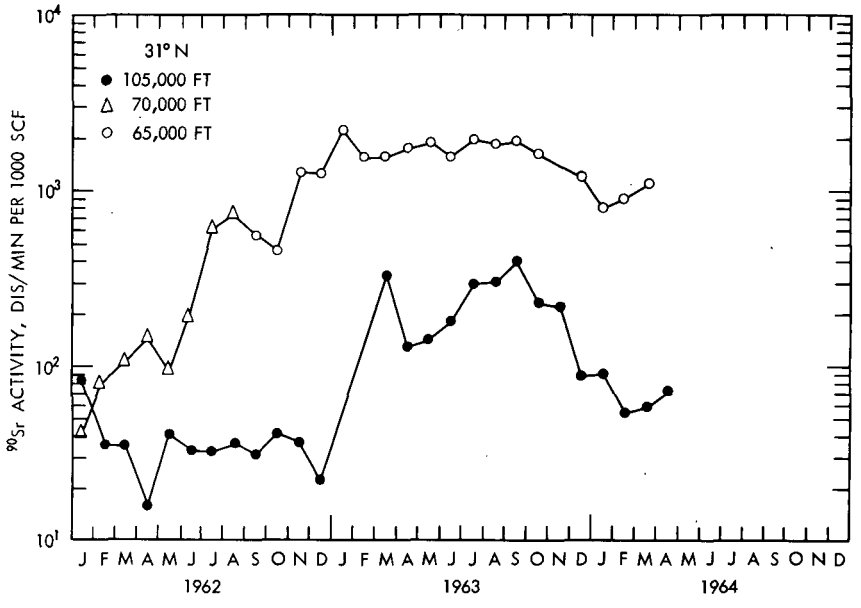

Fig. 2—Trends in ^{90}Sr activity.

high altitudes in early 1963 indicate that the main souce of debris was the 1962 test series. This observation is one of the several lines of evidence that has led us to the conclusion that almost all the debris from U.S.S.R. weapons tests, especially that from tests performed before 1962, was injected into the lower polar stratosphere and that virtually none stabilized at high altitudes.[5]

By early 1963 high concentrations of ^{90}Sr were found at all altitudes sampled at San Angelo, from 65,000 to 105,000 ft. At 105,000 ft the concentrations appeared to decrease sharply after April but then to rise again gradually during the second and third quarters of the year to about the same concentration as was found in April. Between September 1963 and February 1964, the concentrations at 105,000 ft decreased significantly, but during early 1964 they again slowly began to increase. At 65,000 to 70,000 ft, the ^{90}Sr concentrations remained fairly steady during the first three quarters of 1963 but then decreased during the last quarter of the year. During early 1964 the concentrations at 65,000 to 70,000 ft, like those at 105,000 ft, slowly began to increase again.

The changes in ^{90}Sr concentration observed at 65,000 to 70,000 ft at San Angelo during late 1963 and early 1964 might be attributed to a large-scale exchange of air between the northern polar and the tropical stratosphere during the autumn and winter seasons of the northern hemisphere. The result was a decrease in ^{90}Sr concentrations in the vicinity of 31°N as polar air, containing high concentrations, was diluted by tropical air, containing lower concentrations. With the breakdown of the winter night circulation in early 1964, the exchange of air between polar and tropical regions probably slowed drastically. As a result of turbulent exchange within the polar stratosphere, the southward migration of debris from the polar source region continued to bring additional ^{90}Sr to the vicinity of 31°N. However, the drastically reduced exchange rates between the polar and tropical regions which were in effect after the breakdown of the winter circulation resulted in an inhibition of the movement of this ^{90}Sr toward still lower latitudes, and concentration began to build up at 31°N.

The changes in ^{90}Sr concentration observed at about 105,000 ft at San Angelo during 1963 and early 1964 were more abrupt than those at 65,000 to 70,000 ft. These abrupt changes are attributable to the presence of large parcels of air containing low concentrations of nuclear debris at the higher altitudes which had not yet mixed with the parcels of air containing high concentrations. As a result it may have been mid-1963 before concentrations at 105,000 ft were fairly uniform throughout the northern polar stratosphere. When mixing between the polar air and the tropical air of very low concentration began in late 1963, the concentrations at 31°N dropped rapidly.

Before accepting the hypotheses given in the preceding paragraphs to explain the observations at San Angelo, it would be well to consider

the data from Mildura, Australia (34°S latitude), which are presented in Fig. 3. In this figure the ^{90}Sr concentrations measured in balloon samples collected at 65,000 to 70,000 ft and at about 105,000 ft are plotted.

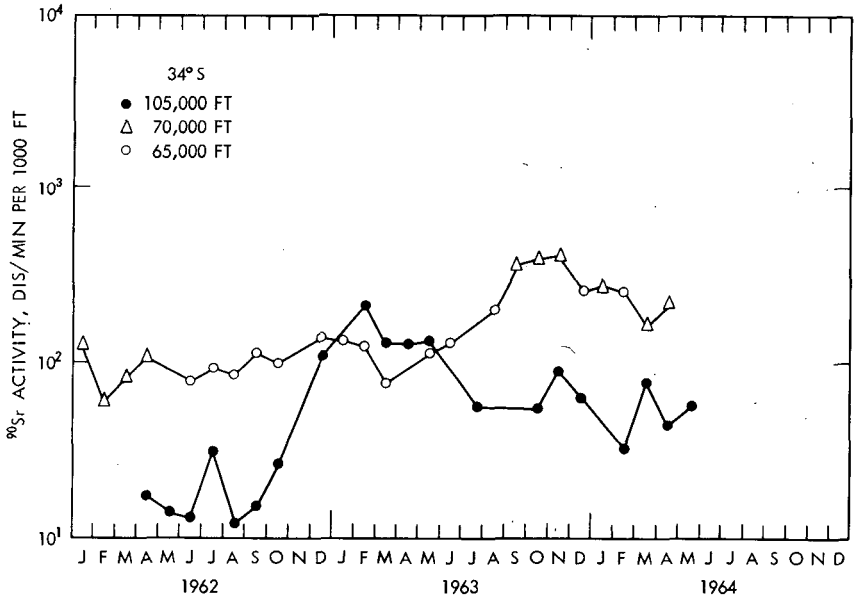

Fig. 3—Trends in ^{90}Sr activity.

At 65,000 to 70,000 ft, there was no great increase in the ^{90}Sr concentrations at Mildura until the second half of 1963, although new debris from the 1962 United States tests (indicated by the presence of short-lived fission products) reached Mildura by August 1962. Between June and August 1963, the ^{90}Sr concentration at 65,000 to 70,000 ft increased severalfold, only to decrease again after November 1963. Data from Project Star Dust, which will be discussed later, suggest that most of the rise in ^{90}Sr concentrations observed during late 1963 resulted from the southward movement of nuclear debris from the northern hemisphere. The subsequent drop in concentrations may have resulted from a decrease in exchange rates of air between the northern and the southern hemispheres because of a seasonal change in patterns of stratospheric circulation.

At 105,000 ft at Mildura, the ^{90}Sr concentration rose during late 1962. The debris that was appearing at Mildura at that time contained ^{109}Cd, as reported by Salter;[6] therefore some, and perhaps most, of the new debris may be attributed to the high-altitude Starfish Prime rocket

shot, which produced that tracer nuclide. By mid-1963 the ^{90}Sr and the ^{109}Cd concentrations had decreased substantially. Perhaps this decrease resulted from dilution of the debris as it mixed horizontally and vertically. At 90,000 ft at Mildura, relatively high concentrations of ^{90}Sr and ^{109}Cd were found by April 1963, and by mid-1963 they were found at still lower altitudes. Thus the debris from the Starfish Prime injection, and perhaps debris from other high-altitude injections, was moving downward through the stratosphere of the southern hemisphere during 1963, causing changes in the concentrations of ^{90}Sr found at various altitudes at Mildura. It is not possible to ascertain whether the effective source region was in the tropical stratosphere near the latitude of injection or whether this debris, like that from the Orange rocket shot in 1958, entered the lower stratosphere in the polar regions and subsequently spread equatorward.[7,8]

Additional information on the changes that occurred with time in the stratospheric concentrations of ^{90}Sr at altitudes below 70,000 ft may be found in data obtained by means of WU-2 aircraft sampling in Project Star Dust. Monthly mean values of ^{90}Sr concentrations found at 45,000, 55,000, and 65,000 ft in the northern polar stratosphere at 65°N are shown in Fig. 4. At all three altitudes there was a general increase in concentrations between early 1962 and late 1962 and a general decrease between early 1963 and mid-1964.

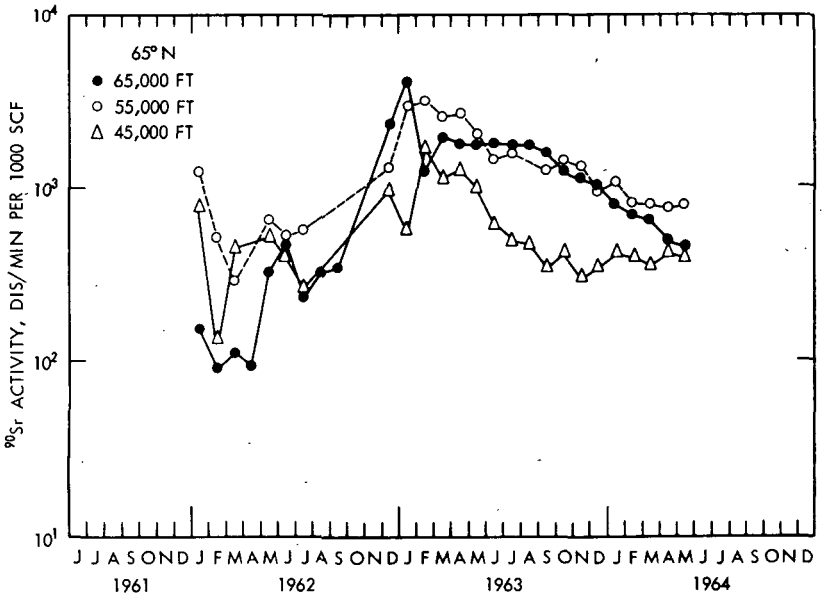

Fig. 4—Trends in ^{90}Sr activity.

Monthly mean ^{90}Sr concentrations at 65,000 ft at a series of latitudes are shown in Figs. 5 and 6. Maximums occurred in the concentration curve for 45°N (Fig. 5) in October 1961, with the first interception of fresh debris from the 1961 U.S.S.R. tests, and in early 1963, following the 1962 U.S.S.R. test series. At 65°N (Fig. 5) maximums occurred in the concentration curve in June 1962, with the delayed arrival in the Star Dust sampling corridor of debris from the high-yield 1961 U.S.S.R. events, and in January 1963, following the 1962 U.S.S.R. test series. At 10°N (Figs. 5 and 6) maximums occurred in the concentration curve in July 1962, with the interception of fresh debris from the 1962 United States Operation Dominic I tests and in mid-1963, probably as a result of equatorward (and upward) movement of debris from the lower northern polar stratosphere. Maximums occurred in the concentration curve for 10°S (Fig. 6) in September 1962, with the interception of fresh debris from Dominic I shots, and in September to November 1963, when debris moving southward from the northern hemisphere was sampled. This southward-moving debris was also sampled at 35°S in late 1963 (Fig. 6), and a maximum in the concentration curve was noted.

These data obtained by means of WU-2 aircraft sampling during Project Star Dust appear to be consistent with the conclusions reached above based on data obtained from balloon sampling.

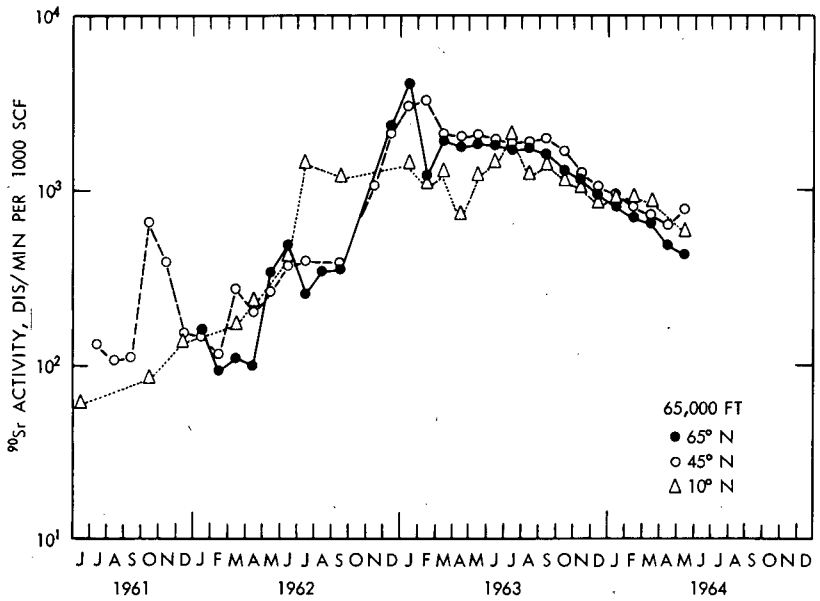

Fig. 5—Trends in ^{90}Sr activity.

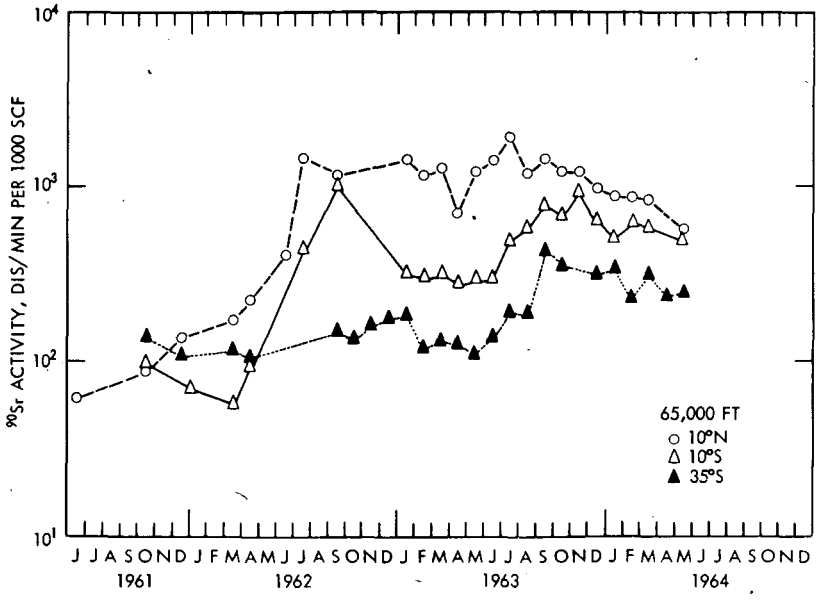

Fig. 6—Trends in ^{90}Sr activity.

VERTICAL DISTRIBUTION OF ^{90}Sr

The stratospheric residence time of nuclear debris should depend to a large extent on the height of injection of the debris into the stratosphere. It is especially desirable to obtain evidence on the height of stabilization of debris from the 1961 and 1962 test series because of the unusually high yields reported for several of the devices tested by the U.S.S.R.[9] We believe that the vertical profiles of activity calculated on the basis of the stratospheric sampling programs provide the information necessary to estimate these heights of stabilization.

The calculated vertical distributions of ^{90}Sr at three latitudes at a series of times during late 1961 to early 1964 are shown in Figs. 7 to 9. Data for samples collected at 65°N are shown in Fig. 7. During January 1962, following the 1961 U.S.S.R. test series, a strong maximum in the concentration profile was found at about 55,000 ft. At that time, however, only low concentrations of ^{54}Mn, ^{124}Sb, and other products of neutron activation, which are considered to be tracers for one or more of the high-yield devices tested[3] in October 1961, were present in the sampled region. By June 1962 debris containing high concentrations of these activation products was intercepted, generally at altitudes of 60,000 ft or higher, and the maximum in the concentration profile, although still at about 55,000 ft, was not as sharp as it had been

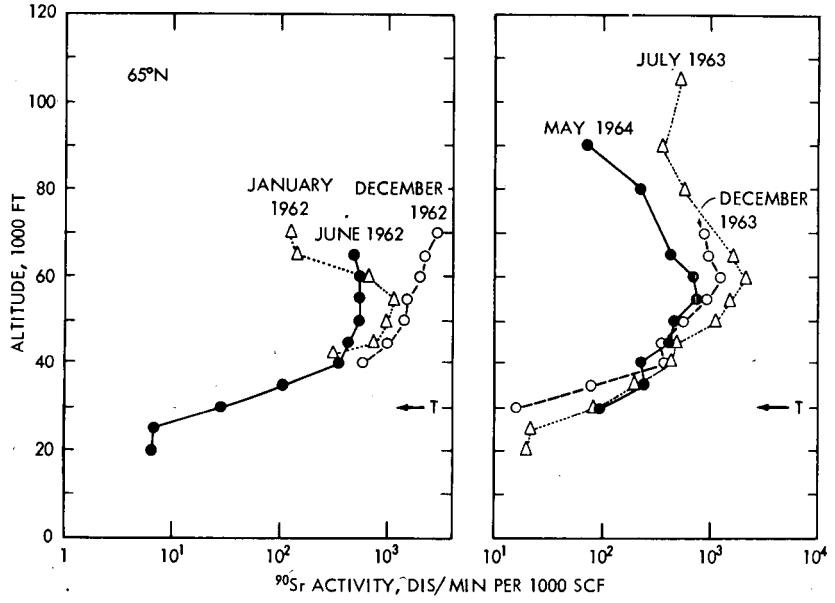

Fig. 7—Vertical profiles of ^{90}Sr activity.

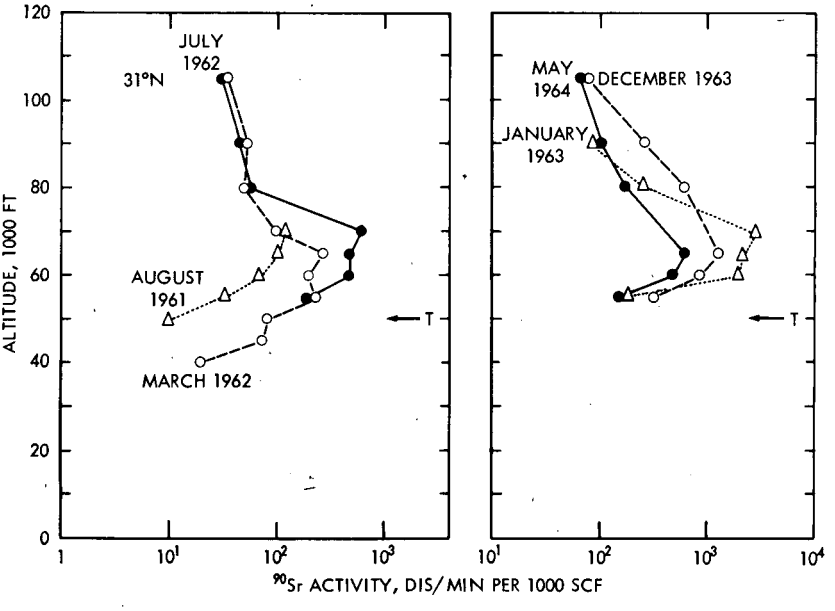

Fig. 8—Vertical profiles of ^{90}Sr activity.

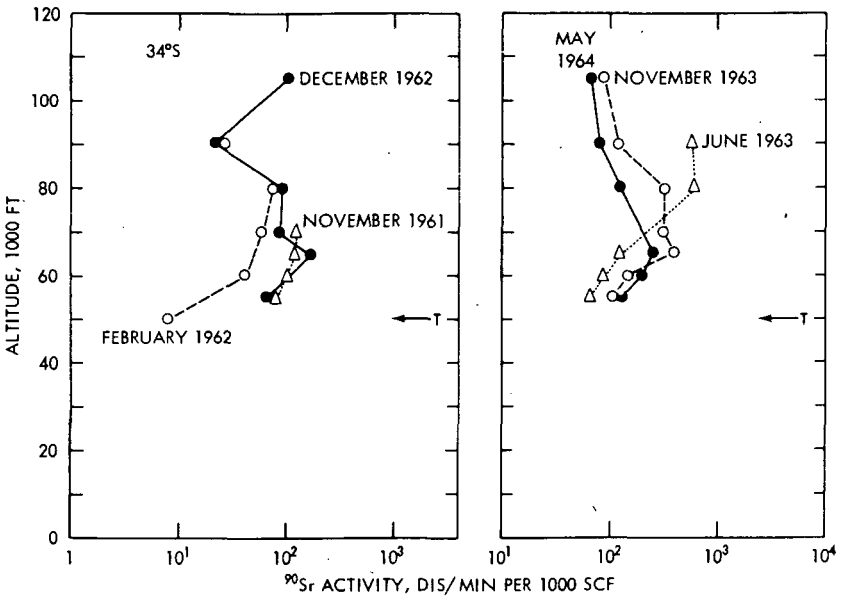

Fig. 9—Vertical profiles of ^{90}Sr activity.

in January 1962. The flattening of the maximum in the vertical profile was doubtless due to the vertical diffusion of the debris away from the maximum, as well as to the appearance of the new debris at the higher altitudes sampled. Some debris from Dominic I was found in the layer between 50,000 and 60,000 ft at 65°N during mid-1962 (as recognized by the presence of short-lived fission products such as ^{140}Ba), but it contributed only a small percentage of the total ^{90}Sr found there.

By December 1962, following all but the last few of the 1962 U.S.S.R. tests, the concentrations of ^{90}Sr found at 65°N were very high, generally exceeding 1000 dis/min per 1000 scf (1000 disintegrations per minute of ^{90}Sr per 1000 cu ft at 15°C and standard pressure). In December 1962 the highest concentrations were found at 70,000 ft, the highest altitude sampled. By July 1963 the maximum concentrations at 65°N were found at 60,000 ft, and balloon sampling indicated that the ^{90}Sr activities did generally tend to decrease with altitude above 70,000 ft. In December 1963 the maximum concentrations were still found at 60,000 ft, and concentrations at all altitudes sampled were lower than they had been in July 1963. Sampling in May 1964 revealed that concentrations had decreased further at all altitudes above 50,000 ft but that at some altitudes below 50,000 ft they had increased. Maximum concentrations were found at 55,000 ft.

More-extensive data on the vertical distribution of ^{90}Sr are available for 31°N, where balloon sampling is performed on a regular

monthly basis. These data are presented in Fig. 8. In August 1961, before the U.S.S.R. 1961 test series began, the highest activities were found at 70,000 ft, the highest altitude sampled. In March 1962 high ^{90}Sr activities were found in the layer between 55,000 and 65,000 ft. By July 1962 debris from the high-yield devices tested by the U.S.S.R. in October 1961 had reached 31°N, and quite high ^{90}Sr activities were found in the layer between 60,000 and 70,000 ft. Even at this time, however, no significant quantities of U.S.S.R. debris were found in the stratospheric layer between 80,000 and 105,000 ft.

The best explanation for this observation is that significant quantities of U.S.S.R. debris had not been injected into this high layer. It could be postulated that debris was injected into this layer in late 1961 but that subsidence or particle settling brought it down into the lower stratosphere by mid-1962. Either or both of these factors may have affected the debris during the first nine months following its injection, but neither the data for 65°N (Fig. 7) nor those for 31°N (Fig. 8) show effects in the lower stratosphere attributable to these factors. It seems unlikely, therefore, that they played more than a secondary role in the movement of the debris during the winter of 1961–1962. Sporadically during early 1962 debris from the high-yield October 1961 events was found in WU-2 samples collected in the northern polar stratosphere in the layer between 60,000 and 70,000 ft. When, after April 1962, this debris reached the Star Dust sampling corridor to stay, it was still in this same layer. This is consistent with the hypothesis that the failure of both the WU-2 and the balloon sampling to find it earlier had resulted from incomplete mixing of the debris in the zonal direction. Apparently a reasonably uniform zonal distribution of the debris had been achieved at the higher latitudes by May 1962 and at 31°N by July 1962.

Debris from the 1962 U.S.S.R. tests (including the late December 1962 tests[3]) was found at 31°N in the layer between 60,000 and 70,000 ft during January 1963 (Fig. 8). By December 1963 lower concentrations were found in this layer, but the concentrations in the layer between 65,000 and 105,000 ft had increased. Concentrations at all altitudes had decreased by May 1964.

Sampling in the southern hemisphere at 34°S (Fig. 9) revealed somewhat different vertical distributions of debris, but the similarities between the distributions at 31°N and 34°S are more striking than the differences when it is considered that all important injections of debris into the stratosphere have occurred in the northern hemisphere.

No detectable debris from the 1961 U.S.S.R. tests had reached 34°S by November 1961, and significant quantities had not reached that latitude by February 1962. By December 1962 debris from Dominic I had reached 34°S but not in sufficient quantity at most altitudes to raise the concentrations above those found there in November 1961. At 105,000 ft, however, most of the ^{90}Sr present was attributable to the United States

tests. The presence of high ^{109}Cd activities in the debris indicates that some, if not all, of the new ^{90}Sr had originated in the 1962 Dominic I rocket shots, particularly in the Starfish Prime shot, which produced the ^{109}Cd. By June 1963 the ^{90}Sr concentrations in the layer between 80,000 and 90,000 ft had increased and so had the ^{109}Cd concentrations. Some of the increase in ^{90}Sr in this layer can thus be attributed to the downward movement of rocket-injected debris, but some may also have been caused by southward movement of debris from low-altitude injections in the northern hemisphere. By November 1963 ^{90}Sr concentrations had increased in the layer between 55,000 and 70,000 ft, but they had decreased substantially in the layer between 80,000 and 105,000 ft. By May 1964 further increases in the concentration had occurred at 55,000 and 60,000 ft, but at all higher altitudes the concentrations had decreased.

Can we attribute to the Dominic I rocket shots all the new debris found at 105,000 ft in December 1962? The nuclide ratios in the debris are generally consistent with such a hypothesis.[5] Did this debris actually move downward in the southern polar stratosphere during 1963, leaving the higher altitude layers and reaching the 80,000- to 90,000-ft layer by June 1963 and the 60,000- to 80,000-ft layer by November 1963? The preliminary ^{109}Cd data reported by Salter[6] are consistent with this hypothesis. If these hypotheses are both correct, a mechanism for such movement must be found, and only particle settling appears to be feasible. Turbulent exchange would not produce movement opposite to the concentration gradient, and an organized circulation could not have moved air containing low ^{90}Sr concentrations into the upper region of the southern polar stratosphere because there was no stratospheric region from which such air could have been derived.

STRATOSPHERIC BURDEN OF ^{90}Sr

Using data from the balloon and the WU-2 sampling programs, we have estimated the distribution of ^{90}Sr in a meridional plane through the atmosphere. These estimated distributions should adequately represent the actual distribution in the sampling corridor used by both programs, though extrapolation and interpolation of data into unsampled regions have been necessary. During the past few years, however, it has become clear that the sampling corridor has not always been completely representative of the atmosphere as a whole. This has been true during periods of weapons testing and during the first four or five months following the termination of such tests. On the other hand, we have reason to believe that within six months following a test series the injected debris is rather uniformly distributed in the zonal direction within the region of the stratosphere (tropical or polar) into which it

was injected and that subsequent sampling along any meridian should give a representative cross section of the atmosphere. Thus, although we must remember the limitations on the accuracy of the distributions we measure and the stratospheric burdens of ^{90}Sr we calculate from them, our estimates of the burden should generally be accurate to within 25%.

The stratospheric distributions of ^{90}Sr calculated from a combination of balloon and WU-2 data are shown in Figs. 10 to 13. The distribution during January through April 1962 (Fig. 10) reveals the presence of fairly high ^{90}Sr concentrations in the layer between the tropopause and 70,000 ft in the northern hemisphere. The concentrations of ^{90}Sr in this layer which can be attributed to pre-1961 weapons tests were approximately equal to the total ^{90}Sr concentrations in the same region in the southern hemisphere. The remaining ^{90}Sr was produced by the 1961 Soviet tests. It is noteworthy that in spite of the very high yields of some of the devices tested during that series, the injected debris was contained almost completely in the lower stratosphere. Of course, as we have previously stated, representative concentrations of the debris from these high-yield weapons were not present in the sampling corridor at the time.

The distribution of ^{90}Sr during May to August 1962, presented in the lower half of Fig. 10, shows the effects in the northern polar stratosphere of the debris from the very high yield weapons and in the tropical stratosphere of the debris from the 1962 United States tests. The appearance of the debris from the high-yield weapons caused an increase in the concentrations of ^{90}Sr in the 60,000- to 100,000-ft layer in the polar stratosphere but not enough of an increase to change our opinion that comparatively little debris had been injected above 70,000 ft. The concentrations of ^{90}Sr indicated in the tropical stratosphere are actually quite uncertain. Sampling in the region below 70,000 ft was not intensive enough to ensure its representativeness during this period of weapons testing. The concentrations shown in the region above 70,000 ft are conjectural since debris from the United States tests had not yet reached either San Angelo or Mildura in quantity and no sampling was performed within the upper tropical stratosphere where this debris had been injected.

The ^{90}Sr distributions during September and October 1962 and November and December 1962 are shown in Fig. 11. Both of the indicated distributions are subject to relatively large errors because the 1962 U.S.S.R. tests were in progress during both intervals and even the debris from the earlier United States Dominic I series was apparently still not uniformly distributed in the zonal direction. The distributions indicated in the upper stratosphere, above 70,000 ft, and in the entire tropical stratosphere are quite uncertain.

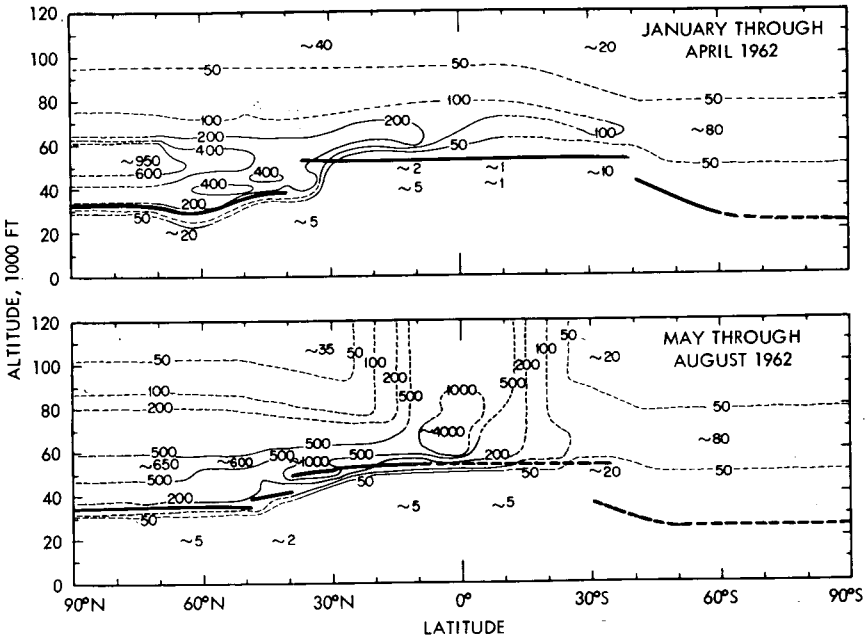

Fig. 10—Stratospheric distribution of ^{90}Sr (dis/min per 1000 scf).

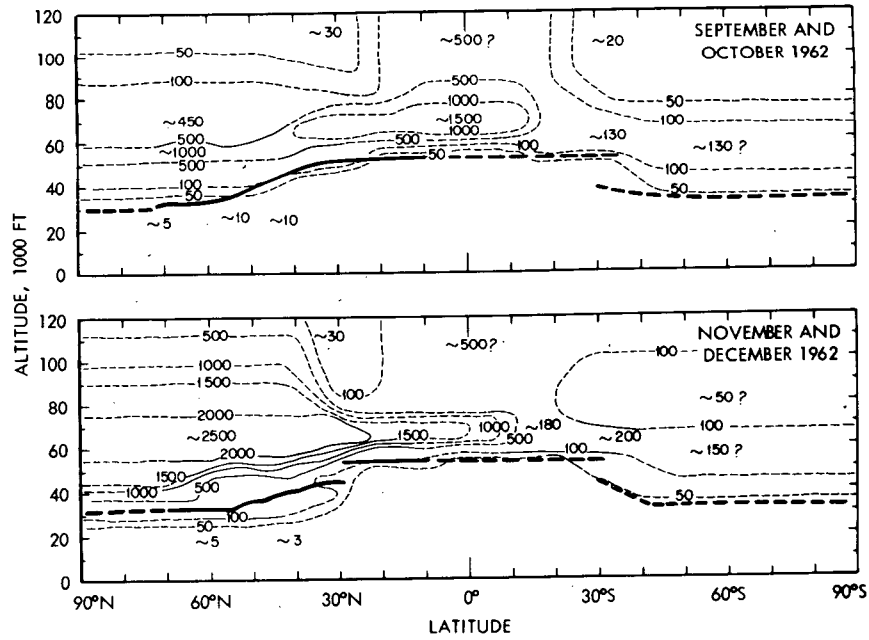

Fig. 11—Stratospheric distribution of ^{90}Sr (dis/min per 1000 scf).

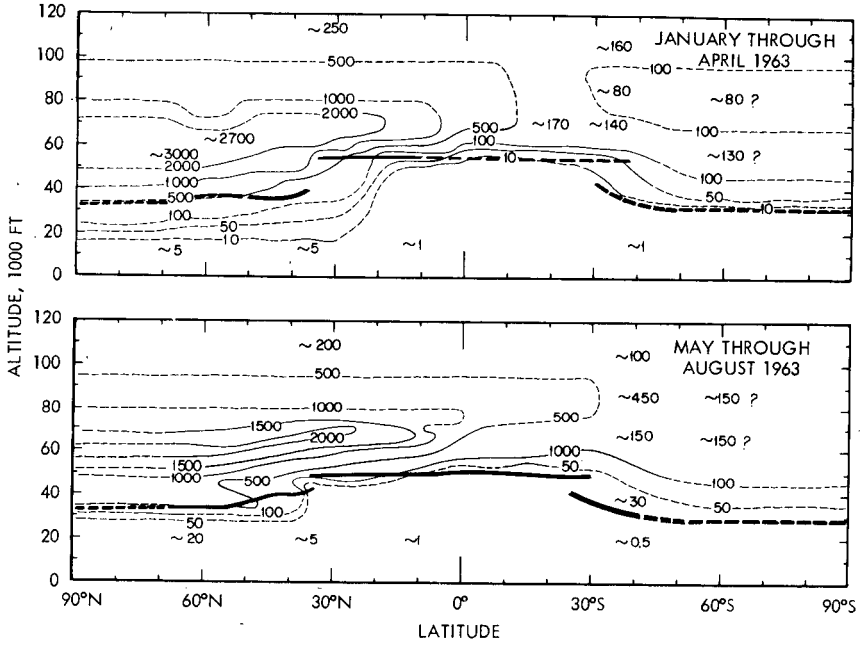

Fig. 12—Stratospheric distribution of ^{90}Sr (dis/min per 1000 scf).

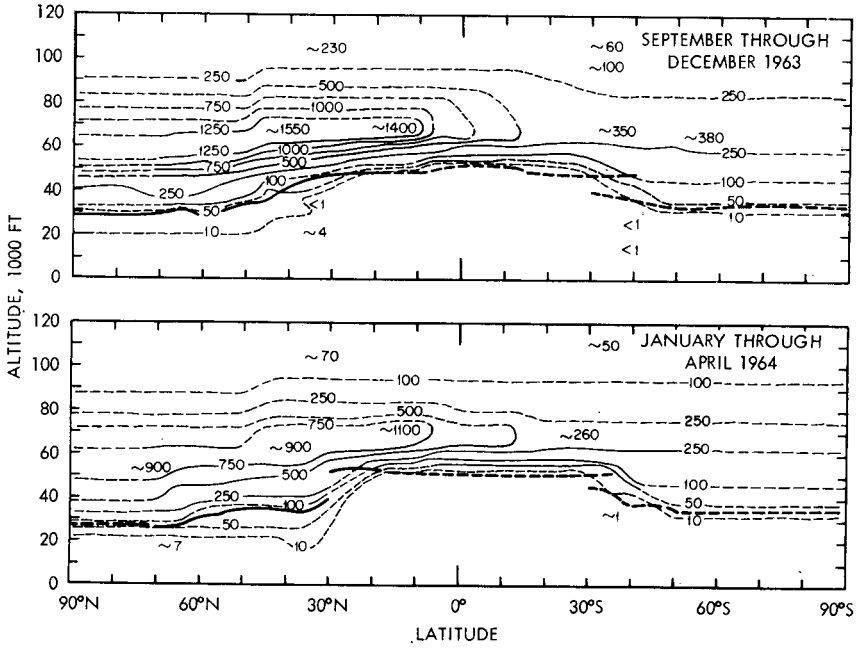

Fig. 13—Stratospheric distribution of ^{90}Sr (dis/min per 1000 scf).

The distributions of ^{90}Sr during January to April 1963 and May to August 1963, shown in Fig. 12, are based on more substantial data. The high concentrations of ^{90}Sr in the northern polar stratosphere resulted from the injection of debris into that region by the late 1962 U.S.S.R. test series, including the December 1962 tests. It is unlikely that the zonal distribution of the debris from these tests was uniform as yet. The subsequent rapid drop in concentrations of debris in this region suggests that the ^{90}Sr concentrations sampled during early 1963 were anomalously high. The somewhat lower concentrations found during May to August 1963 may have been more representative of the average values in the stratosphere. Since few data are available for the ^{90}Sr concentrations in much of the southern polar stratosphere during the first two-thirds of 1963 and since none are available for the upper tropical stratosphere, the distributions that are shown in these regions in Fig. 12 may be in error. These distributions are based on several assumptions. One is that the high concentrations of ^{90}Sr (greater than 100 dis/min per 1000 scf) found at 105,000 ft at Mildura during January to April 1963 were derived from high-altitude injections, such as Starfish Prime. Another assumption is that most of the ^{90}Sr found at 90,000 ft at Mildura during May to August 1963 had moved southward to 34°S from the tropical stratosphere.

The ^{90}Sr distributions during September to December 1963 and January to April 1964 (Fig. 13) show continuing decreases in the ^{90}Sr concentrations in most regions of the stratosphere. The decreases that occurred in the concentrations in the region above 90,000 ft between mid-1963 and early 1964, as we discussed previously, seem to be attributable only to settling of fallout particles from that region into the lower stratosphere. It may be noted that this same mechanism could be used to explain the changes in stratospheric concentrations that occurred during the 1958 to 1961 moratorium on weapons testing.

The horizontal profiles of ^{90}Sr at 65,000 ft which are plotted in Figs. 14 to 16 may aid in the visualization of the changes that have occurred in the ^{90}Sr distribution during 1962 to 1964. Between August 1961 and March 1962 (Fig. 14), the ^{90}Sr concentrations increased in the northern hemisphere as a result of the 1961 U.S.S.R. tests. By July 1962 the peak concentrations, attributable to the Dominic I tests, were found in the tropical stratosphere. The high concentrations of ^{90}Sr produced in the northern hemisphere by the 1962 U.S.S.R. tests resulted in the presence of a steep concentration gradient across the tropical stratosphere by January 1963. This gradient was still quite steep in July 1963 (Fig. 15), but it had decreased considerably by October 1963 as a result of the movement of debris from the northern into the southern hemisphere. The gradient was about the same in January 1964 (Fig. 16), but by May 1964 it appeared again to have become still more gentle, perhaps because of more debris entering the southern hemi-

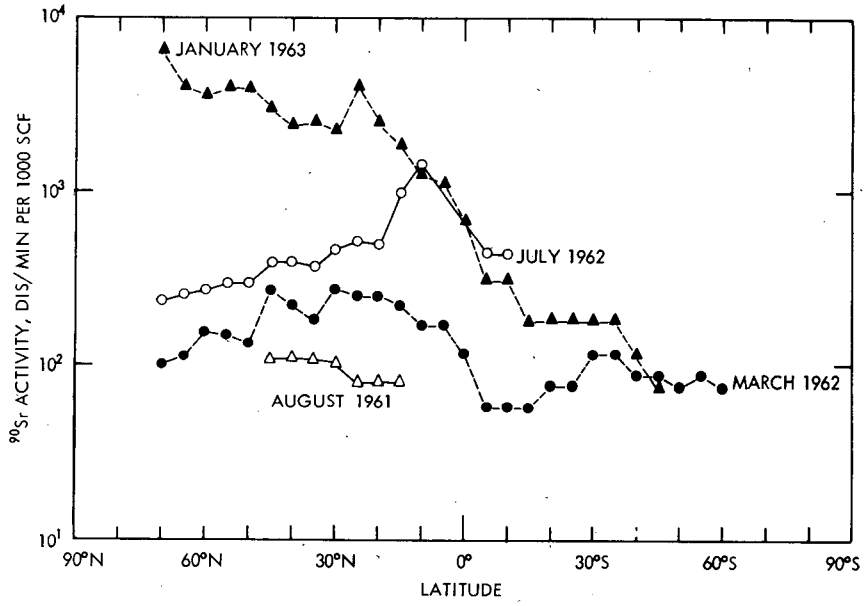

Fig. 14—Horizontal profiles of ^{90}Sr activity at 65,000 ft.

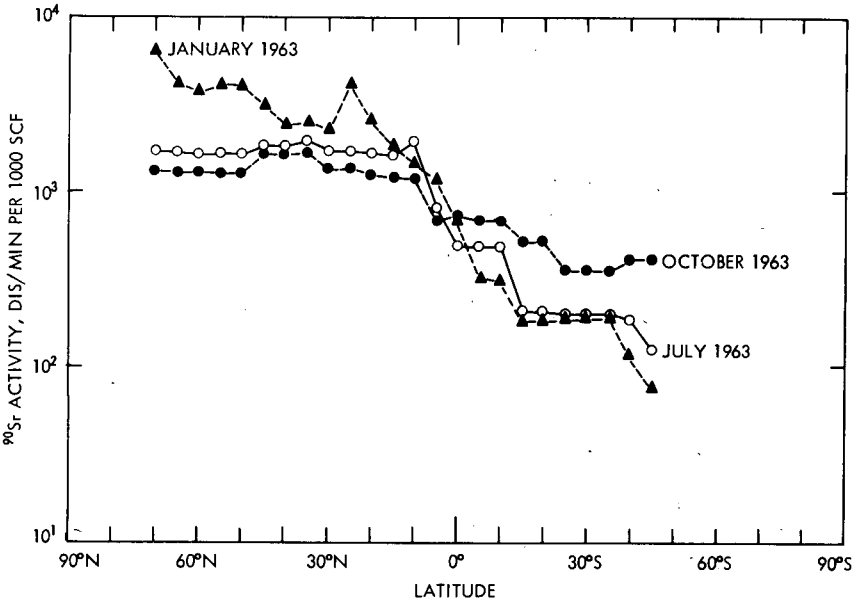

Fig. 15—Horizontal profiles of ^{90}Sr activity at 65,000 ft.

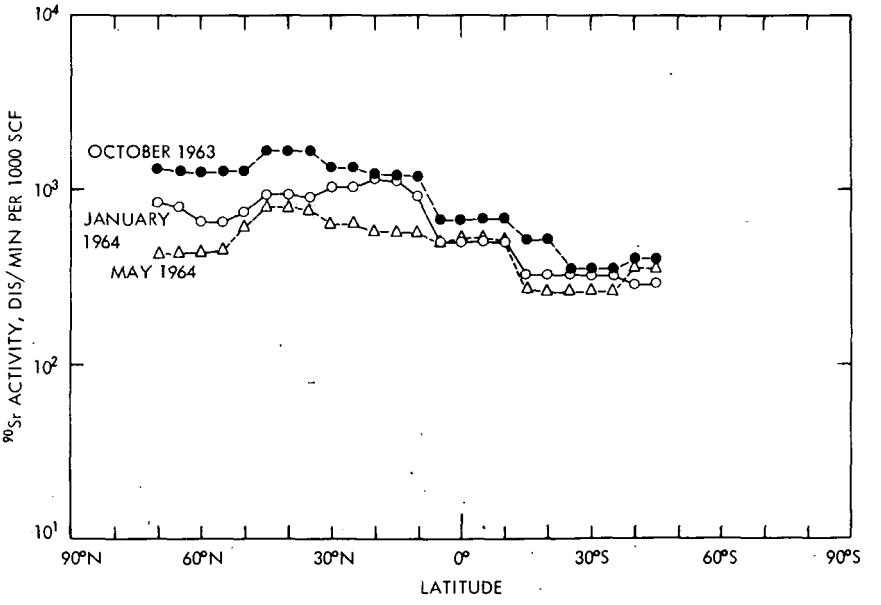

Fig. 16—Horizontal profiles of ^{90}Sr activity at 65,000 ft.

sphere during the winter season. The concentrations decreased at all latitudes between October 1963 and May 1964, no doubt as a result of fallout of nuclear debris to the troposphere.

With the use of the estimated distributions in the stratosphere, including some shown in Figs. 10 to 13, the stratospheric burdens of ^{90}Sr between mid-1961 and late 1963 have been calculated. The results are presented in Table 1. Before the renewal of weapons testing, the burden was about 0.9 Mc. By early 1962 it had reached about 2.0 Mc, and by early 1963 it had reached perhaps more than 7 Mc. During 1963 the burden decreased, however, reaching 4.4 Mc by late 1963.

Table 1—STRATOSPHERIC BURDENS OF ^{90}Sr

Time interval	Megacuries of ^{90}Sr		
	Northern hemisphere	Southern hemisphere	Total burden
June through September 1961	0.37 ± 0.13	~0.5	~0.9
October through December 1961	~1.6	0.47 ± 0.17	~2.1
January through April 1962	1.6 ± 0.3	0.4 ± 0.1	2.0 ± 0.3
May through August 1962	2.5 ± 0.5	~1.0	~3.5
September through October 1962	2.2 ± 0.7	1.0 ± 0.3	3.2 ± 0.8
November through December 1962	5.6 ± 1.9	0.8 ± 0.3	6.4 ± 1.9
January through April 1963	6.7 ± 1.7	0.7 ± 0.3	7.4 ± 1.7
May through August 1963	4.9 ± 1.5	0.9 ± 0.3	5.8 ± 1.5
September through December 1963	3.3 ± 0.6	1.1 ± 0.4	4.4 ± 0.7

OTHER COMPONENTS OF NUCLEAR DEBRIS

Nuclear debris contains many components besides ^{90}Sr, including other fission products and products of neutron activation. Results of measurements of a number of fission products and activation products in balloon and WU-2 samples have been discussed elsewhere[3–5] and will not be discussed here. We will mention, however, that many of these nuclides should be useful as tracers of atmospheric motions. Among those which have been so used are ^{124}Sb, ^{54}Mn, and other activation products that were produced in unusually large quantities by certain events in the 1961 and 1962 U.S.S.R. test series. Similarly, ^{109}Cd, produced by the Starfish Prime rocket shot, should serve, as did ^{102}Rh, produced by the 1958 Orange rocket shot (Operation Hardtack I), as a tracer for high-altitude injections.[6] The nuclides ^{88}Y and ^{22}Na may also serve as tracers for debris from the 1961 and 1962 test series or from particular events in those series.

In Figs. 17 to 19 we have reproduced data from a report on Star Dust[3] which show some vertical profiles of ^{90}Sr and of several activation products at 65°N to illustrate the information obtainable from measurements of tracer nuclides. During most of 1962 (Figs. 17 and 18), the highest concentrations of ^{54}Mn, ^{55}Fe, and ^{124}Sb were found in the layer between 60,000 and 70,000 ft. There were fairly constant ratios between activities of these nuclides in all samples in which they were abundant. This suggests that they had a common origin, perhaps in a single event during the 1961 U.S.S.R. test series. Since the maximum in the vertical profile of the activation products occurred at significantly higher altitudes than did the maximum in the ^{90}Sr profile,

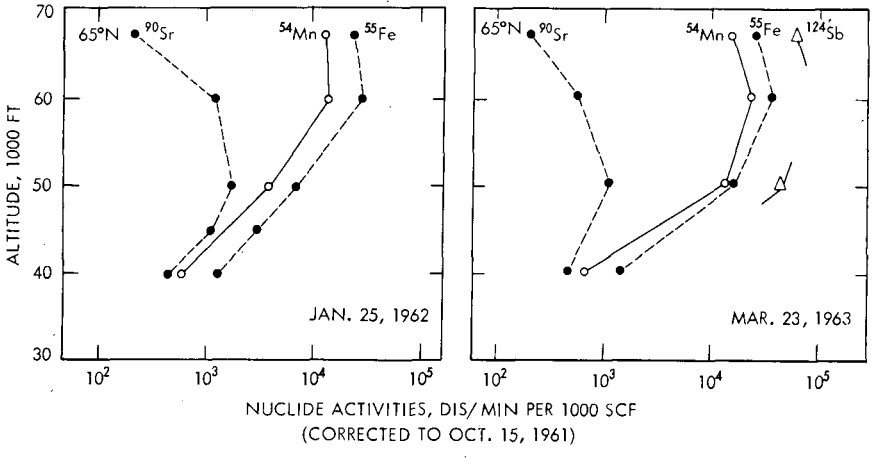

Fig. 17—Vertical distribution of activation products and ^{90}Sr.

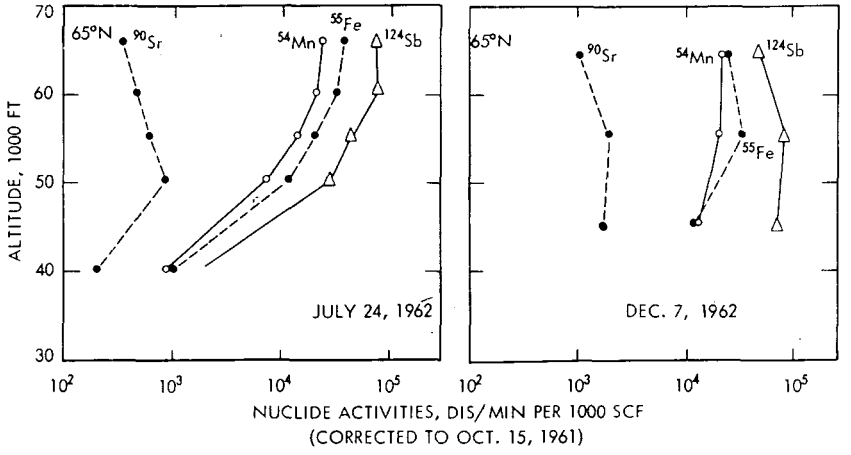

Fig. 18—Vertical distribution of activation products and ^{90}Sr.

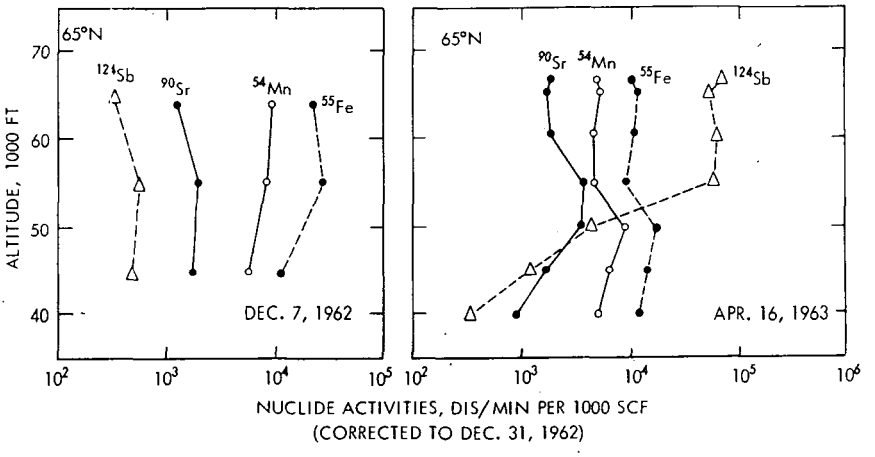

Fig. 19—Vertical distribution of activation products and ^{90}Sr.

it appears reasonable to attribute these nuclides to the high-yield October 1961 events. By December 1962 the vertical distribution of the activation products at 65°N was more uniform. There is evidence to indicate that this uniformity had been produced by additional injections of these nuclides into the lower polar stratosphere during the 1962 U.S.S.R. test series.[3] One or more events during the December 1962 test series[3] produced large quantities of ^{124}Sb which were injected into the polar stratosphere above 55,000 ft. The new vertical profile for this nuclide, found by sampling during 1963, is illustrated in Fig. 19. As a result of the 1962 injections, ^{54}Mn and ^{55}Fe could not be used after about September 1962 as unique tracers for the high-yield 1961 events,

but during 1963 ^{124}Sb was used as a unique tracer for certain December 1962 events.

SUMMARY

The distribution of ^{90}Sr and of other components of nuclear debris in the stratosphere may be determined with fair accuracy by using data from the balloon-sampling program and the Project Star Dust WU-2 aircraft sampling program. The distributions of ^{90}Sr observed during 1962 to 1964 provide information on the initial altitude of injection of debris from U.S.S.R. polar tests and on the seasonal nature of changes in the stratospheric distribution. Specifically, it would appear that little debris injected into the polar stratosphere, even by events of very high yield, stabilizes at altitudes above 70,000 ft. Movement of debris from the northern-hemisphere source regions into the southern hemisphere appears to occur preferentially during the autumn and winter seasons of the southern hemisphere. Measurements of other fission products and of a number of products of neutron activation should also be useful for studying atmospheric motions.

REFERENCES

1. L. P. Salter, High Altitude Balloon Sampling Program, in Fallout Program Quarterly Summary Report, USAEC Report HASL-140, pp. 166-214, Health and Safety Laboratory, Oct. 1, 1963.
2. L. P. Salter, High Altitude Balloon Sampling Program, in Fallout Program Quarterly Summary Report, USAEC Report HASL-149, pp. 54-99, Health and Safety Laboratory, Oct. 1, 1964.
3. H. W. Feely, B. Davidson, J. P. Friend, R. J. Lagomarsino, and M. W. M. Leo, Ninth Quarterly Report on Project Star Dust, Report DASA-1309, Defense Atomic Support Agency, Sept. 1, 1963.
4. H. W. Feely and F. Bazan, Second Interpretive Report on the High Altitude Balloon Sampling Program, USAEC Report NYO-10498, Isotopes, Inc., June 10, 1964.
5. F. Bazan and H. W. Feely, First Quarterly Report on the High Altitude Balloon Sampling Program, USAEC Report NYO-10496, Isotopes, Inc., Feb. 1, 1964.
6. L. P. Salter, Results of Measurements Made at HASL and Reported at a Conference Held at the New York Operations Office, AEC, on Dec. 6, 1963.
7. M. I. Kalkstein, Rhodium-102 High Altitude Tracer Experiment, *Science, 137:* 645-652 (1962).
8. J. P. Friend, H. W. Feely, P. W. Krey, J. Spar, and A. Walton, The High Altitude Sampling Program, Report DASA-1300, Defense Atomic Support Agency, Aug. 31, 1961.
9. U.S. Weather Bureau, Announced Nuclear Detonations, 1945–1962, in Fallout Program Quarterly Summary Report, USAEC Report HASL-142, pp. 218-242, Health and Safety Laboratory, November 1963.

FRIEDLANDER: I would like to begin by asking Dr. Owe Berg a question. Near the end of your discussion, you said that you would not expect drops to coalesce unless they were charged, that generally you expect rebound to occur. That seems like a sweeping statement. Can you amplify your remarks?

OWE BERG: It was shown by Lord Rayleigh in 1890 that such is the case. He used droplets produced by jets. Colliding drops coalesced when charged; otherwise they bounced.

FRIEDLANDER: There must be kinetic-energy considerations. If you just have a few drops located next to each other, presumably they will coalesce?

OWE BERG: The duration of the contact in elastic collision depends only slightly upon the impact velocity. The coalescence must occur during the period of contact; otherwise bouncing occurs. I am aware of experiments showing coalescence in all collisions, but the charges on the drops were not controlled in these experiments. It is very difficult to produce uncharged drops.

BOLIN: Dr. Friedlander, the rate with which the spectrum you obtain in your work will be approached depends, of course, upon the total number of particles per unit volume. Furthermore, you have assumed that no settling of the particles takes place; this is correct only if the distance traveled by the particles is short during the time required to approach the equilibrium spectrum that you derive. Can you estimate for which particle concentrations and sizes your theory is valid?

FRIEDLANDER: The theory we have worked out so far applies to nonsedimenting systems. We have checked it experimentally with an

oil and water emulsion that was essentially nonsedimenting. The problem becomes more complicated in sedimenting systems because another term is introduced into the Smoluchowski equation. We are examining this now. The time it takes to reach an asymptotic self-preserving form, as we call it, depends on the initial distribution. If there is an initial distribution that is near the self-preserving form, then within relatively short times this asymptotic limit is reached. If one begins with a system that differs greatly from the self-preserving form, it will take longer.

I think some answers will come out of calculations such as those recently done by Dr. George Hidy of the National Center for Atmospheric Research, who has put in various types of initial distributions and followed coagulation in a computer experiment. An appropriate characteristic time for an initially monodisperse system would be $3\mu/kTN_0$, where μ is the viscosity of the fluid, k is the Boltzmann constant, T is the temperature in °K, and N_0 is the total number of particles in the system. Hidy found, as I recall, that about three of these characteristic times were necessary for an initially monodisperse system to reach the self-preserving form. He also tried very unusual initial distributions and found that they took a longer characteristic time. So these are reasonable questions to ask and they are the same ones we are asking now, having worked out the initial formalism and checked the method experimentally with hydrosols.

STEVENSON: Would the formation of compounds such as sulfates from the oxidation of sulfur dioxide to sulfur trioxide add another term to the Smoluchowski equation, and have you also investigated this?

FRIEDLANDER: We have not investigated this. I think this effect probably could be accounted for in the Smoluchowski equation by adding a term for condensation. Again, one would have to look at the equations and see whether or not the so-called "self-preserving forms" still satisfy the modified equations.

FREUDENTHAL: I would like to ask Dr. Feely if he noticed seasonal differences in the horizontal stratospheric data?

FEELY: Yes, very much so. The movement of nuclear debris through the tropical stratosphere especially seems to be seasonally dependent. In both 1959 and 1963, we observed movement of debris from the northern tropical stratosphere into the southern polar stratosphere during the winter and the spring seasons of the southern hemisphere. I do not know what the cause is, but there does seem to be a seasonal dependence.

BENSON: I have a question for Dr. Feely. Generally, a half-residence time of about five years for ^{90}Sr in the stratosphere has been

assumed. During the U.S.S.R. tests in the far northern atmosphere, the fallout was considerably faster than what it would be based on this assumption. Could it be that this is due to the fact that the debris itself was injected at a fairly low, about 65,000-ft, altitude instead of at the higher altitudes of the shots that gave rise to this five-year half-residence time.

FEELY: I think the five-year half-residence time is an overestimate. For debris from all past tests — and I know that many others who have worked with fallout data would agree — the data indicate that a one-year half-residence time would be a better estimate. For debris from the 1959 U.S.S.R. tests, a half-residence time of much less than one year was indicated.

If there is a one-year half-residence time in 1963 to 1964, this would be in general agreement with past observations. The only debris that might approach a five-year half-residence time, I believe, would be debris from rocket shots such as the 1958 Orange shot. The ^{102}Rh data indicate a long residence time. Hopefully, measurements of the ^{109}Cd from the 1962 Starfish Prime shot will help us to estimate the residence time of the debris from it.

BENSON: I have another question that concerns the increase in the activity belt at 75,000 ft. It appeared from your slides that this belt was rather constant regardless of the height of the tropopause and the latitude at which the sample was taken. Is this true? Do you have any explanation for why the activity belt should be that high above the tropopause, in terms of equilibrium particle content, for example?

FEELY: We do find most of the debris from low-altitude bursts stabilizes within, say, 30,000 ft above the tropopause for very high yield shots. We don't have as much evidence on tropical nuclear bursts as we would like, because most of our conclusions are based on data from WU-2 aircraft sampling. Balloon sampling is not being performed in the equatorial area where injections have been made. I do think this belt increases with altitude toward the equator and decreases with altitude toward the poles, more or less subparalleling the tropopause and the isentropic surfaces. The belt is not exactly horizontal. [Editor's note: The AEC Balloon Sampling Program began high-altitude sampling at a tropical site in October 1964.]

FROM THE FLOOR: Dr. Whitby, what is the purpose of RaD [^{210}Pb] in your equipment, and what is the charge on the aerosol you use?

WHITBY: I am sorry that I did not mention in my condensed presentation here that the ions we use are positive. The complete paper has all of these details.

The charge on the aerosol which must be taken care of by the neutralization equipment results from the atomization of the dye solution. Most of the time this charge is a mixture of positively and negatively charged drops. In a few cases we observed a unipolar negative charge on water and alcohol solutions of dye. As the atomized droplets evaporate, the charge is conserved, and what was initially a low charge-to-mass ratio droplet becomes a high charge-to-mass ratio solid particle. In charging experiments, one must eliminate the initial charge on the droplet. This is the reason for the elaborate drying and neutralization equipment ahead of the charger. Neutralization is done in two steps. First, the evaporating droplets are mixed with bipolar ions generated by a sonic jet ionizer. After passing through the diffusion dryer, the solid particles are again exposed to bipolar ions generated by 500 μc of RaD. This brings the charge on the dry particles to near Boltzmann equilibrium. At this equilibrium the number of particles with positive and negative charges is equal. This is the same charge equilibrium that exists in the atmosphere on sufficiently aged particles. It is independent of concentration and depends only on size distribution.

We use positive ions in the charger because at low pressures the corona discharge generates a significant number of free electrons, as well as negative ions. These free electrons make a calculation of the charging conditions difficult.

FROM THE FLOOR: Concerning the fission products in the stratosphere, do you think they are charged positively or negatively depending upon whether or not they are beta emitters?

WHITBY: I do not know about the charge distribution of radioactive particles in the stratosphere, but I would suspect that they are near Boltzmann equilibrium because the charging rate of the particles due to radioactive decay would be much less than the frequency of collision with bipolar ions in the atmosphere. Thus they should reach Boltzmann equilibrium within a few hours.

WALLACE: Dr. Feely's observations show a rather marked decrease of ^{90}Sr concentrations with height above 70,000 ft. In view of the rather vigorous eddies that are known to exist at these levels, I wonder whether the upward mixing of radioactive debris by turbulence might play an important role in producing the observed concentration gradient.

FEELY: The highest altitude sampled was about 105,000 ft. The activity was decreasing at 70,000 and at 105,000 ft had decreased markedly. The movement upward of all of this debris would produce very substantial increases in the concentrations in the region above 100,000 ft, where there is relatively little air. If the debris is mixed

uniformly—I have not done a quantitative calculation on this point—I would judge that two or three times more debris disappears from the layer between 70,000 and 100,000 ft than could be accommodated in the region above 100,000 ft while still giving concentrations there that are lower than those observed at 100,000 ft, but this figure is a guess.

FROM THE FLOOR: Your illustrations showed values only for ^{90}Sr. Have you calculated the values for other nuclides?

FEELY: We also have calculated stratospheric burdens for ^{54}Mn ^{55}Fe, ^{124}Sb, and ^{102}Rh. I do not have all the data with me. We have measured ^{88}Y and artificial ^{22}Na and do intend to calculate burdens for them.

WHITBY: I would like to ask Dr. Owe Berg if he has done any experiments in his drop-coalescence work on the time that it takes the surface of a drop to reach the equilibrium state? There are some data that I have seen and heard about which indicate that very freshly formed drops always tend to coalesce. The thought occurs to me that perhaps the time required for the surface to reach equilibrium is affected by trace amounts of surface-active material that might be present in the drops. Perhaps this would explain the somewhat contradictory data from different investigators. Do you have any comment?

OWE BERG: To my knowledge, very little work has been done on the new surfaces of liquids. However, a great deal has been done on new surfaces of solids.

Concerning the effect of a new liquid surface upon the coalescence of drops, the experiments that you refer to have to be conducted under controlled conditions of charge on the drops to give information on the effect of the new surface. I don't think that it takes any time at all for the surface tension to become established. The equilibrium within the drop would be established very rapidly apart, of course, from the hydrodynamic vibrations of the drop.

On the other hand, the equilibrium between the water in the drop and the atmosphere around the drop may very well take some time, particularly at very, very low pressures. I would think, however, that at ordinary pressures in the ambient atmosphere the aging of the water surface would be fairly rapid.

SALTER: To clear up a point on the drop-off of the debris at 70,000 ft, I would like to point out that the ^{54}Mn concentrations in early 1962 at 60,000 and 90,000 ft at 31°N are about equal and at least an order of magnitude above those at 70,000 ft. This shows that, although the levels of 1961 debris do decrease at 70,000 ft, a second peak of material from this series is present at the higher altitudes sampled. The $^{54}Mn/^{90}Sr$ ratio for this new debris sampled at 90,000 ft is about 100 to 1.

SESSION IIIA

Local Atmospheric Transport

Alfred W. Klement, Jr., Chairman

PREDICTION OF FALLOUT FROM SUBSURFACE NUCLEAR DETONATIONS

JOSEPH B. KNOX
University of California, Lawrence Radiation Laboratory,
Livermore, California

ABSTRACT

A numerical simulation model has been developed for the prediction of fallout from subsurface nuclear detonations that produce craters through spall and the action of the cavity gas. The physical processes modeled are atmospheric transport, lateral eddy diffusion, and gravitational sedimentation of radioactive particulates. This cratering fallout model is normalized to the observed external gamma-dose-rate fields of the Sedan (100 kt) and the Danny Boy (0.43 kt) cratering shots conducted at the Nevada Test Site. Calculations of the fallout patterns for additional shots, used for testing the prediction capability of the cratering fallout model, indicate that the model gives estimates of the external gamma dose rate at H + 1 hr with a maximum error of a factor of 2 to 3 in the gamma dose rate vs. distance along the hot line of the pattern.

INTRODUCTION

During the past few years, a small but continuing effort has been expended in developing a model for predicting fallout from subsurface nuclear detonations. In this report the experience in predicting fallout from surface bursts that is transferable to the construction of a fallout model for subsurface detonation is summarized, the development of the fallout model for subsurface nuclear detonations (the cratering fallout model) is described, the predictive capability of the model is illustrated by means of independent test cases, and some of the problems asso-

ciated with the prediction of fallout from row-charge subsurface nuclear detonations are discussed. This paper is limited to research or development in which the investigator has been personally involved within the Plowshare Program of the Lawrence Radiation Laboratory.

CRATERING FALLOUT MODEL

Basis of Model Construction

For prediction of the area affected by radioactive fallout from a subsurface detonation of a nuclear explosive and of the gross external gamma dose rate in the surface-fallout pattern, knowledge of the following factors are needed:

1. The heights of the base, the top, and the radius of each radioactive cloud (i.e., the main cloud and the base surge) formed by the detonation at the time the clouds cease to rise in the atmosphere. This time is defined as the time of cloud stabilization. The cloud heights are prescribed in terms of height above surface zero.

2. The total yield of the explosive, W_T; the fission yield of the explosive, W_f; the depth of burial of the explosive, z; the fraction of the fission-product gamma emitters expected to appear in the fallout pattern beyond the estimated radius of direct ejecta, F_c; and the equivalent fission-yield gamma needed to simulate the gamma dose from induced activities.

3. The activity–particle size distribution in both the main cloud and the base surge and the fraction of F_c in each.

4. The terminal fall velocity of the fallout particles (in still air) as a function of particle size and height in the atmosphere.

5. The time and space prediction of the horizontal wind at the level of each cloud top along with the specification of the wind-shear tangential and normal to the wind for the layer through which particles fall. This knowledge is required because in a fallout calculation involving two clouds (main cloud and base surge), the calculation of the fallout pattern for each cloud is done separately. The total surface-fallout pattern of the shot is found by summing the patterns from the base surge and the main cloud.

6. The effect of horizontal eddy diffusion on the growth of the horizontal radius of the disks of radioactive particles as the disks fall earthward. The initial debris cloud is subdivided into disks of debris in the model as a function of initial height in the cloud and of particle size.

The preceding information (items 1 through 6) provides the simplest, but still adequate, basis for constructing a cratering fallout model. In addition to this information, it is assumed that the fission-

product radioactivity is unfractionated and that 1 kt of unfractionated fission products spread uniformly over 1 sq mile corresponds to an (H + 1)-hr dose rate of 3380 r/hr at a height of 3 ft above an infinite plane.[1] This normalization constant of 3380 r/hr is corrected for terrain shielding by a factor of 0.8.

Certain atmospheric processes or effects have been neglected in developing the cratering fallout model, just as these same effects were neglected in developing the land surface-burst fallout model:[2]

1. The effect of synoptic-scale vertical motions on the vertical displacement of the falling disk of particles.
2. The effect of the mean divergence of the horizontal wind on the radius of the disk of falling particles during descent.
3. The effect of vertical eddy diffusion.
4. The time from detonation to cloud stabilization.
5. The development of subsynoptic-scale wind systems.
6. Changes in time and space of the shear tangential and normal to the horizontal wind at cloud-top level.
7. The effect of water products of condensation on the size and fall rate of radioactive particles.

Fraction of Gamma Activity in the Close-in Pattern

For calculation of the close-in fallout pattern from a subsurface detonation, the fraction of the gamma activity produced by the fission yield and appearing in the close-in fallout pattern, F_c, must be known. Thus far, experimental data from the Sedan, the Teapot ESS, the Jangle U, the Neptune, the Jangle S, and other surface-burst shots have provided a basis for estimating F_c. The measured fallout patterns from these shots have been integrated[3] from the radius of direct throwout to the limit of the measured pattern. The results are shown in Table 1.

These F_c calculations were performed by assuming a normalization constant of 3380 r/hr per kiloton of fission yield per square mile at H + 1 hr and a terrain shielding factor of 0.8. The graphical presentation of F_c as a function of z/W is shown in Fig. 1. In construction of the experimental F_c curve, the following asymptotes were used: (1) an

Table 1—EXPERIMENTAL DATA

Shot	W, kt	z, ft	F_c	Medium
Sedan	100	635	~0.10	Alluvium
Teapot ESS	1.2	67	0.46	Alluvium
Jangle U	1.2	17	0.64	Alluvium
Neptune	0.115	100	0.005	Tuff
Jangle S	1.2	0	0.50	Alluvium
Danny Boy	0.43	109	0.04	Basalt
Blanca	19	835	0.0005	Tuff

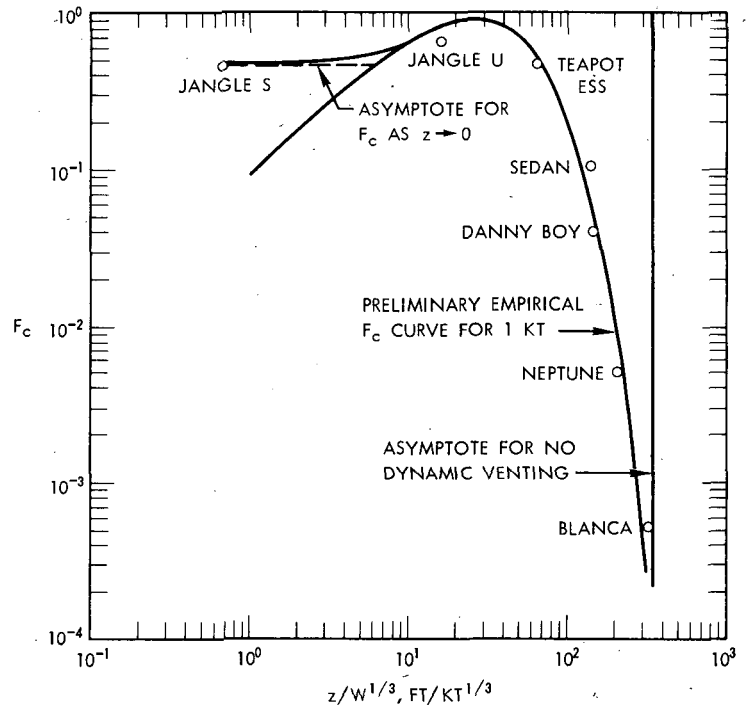

Fig. 1—Fraction of gamma activity appearing in the close-in fallout pattern.

asymptote of $F_c = 0.50$ for $z = 0$, suggested by the Jangle S data in Table 1 and supported by previous work,[4] and (2) an asymptote of no dynamic venting for $z/W^{1/3} = 330$ ft/kt$^{1/3}$, supported by experimental evidence[5] and by studies of containment physics.[6]

It should be noted that the value of F_c (estimated by pattern integration) for the Sedan shot departs considerably from the curve fitted to the whole sample of F_c data. This departure could arise because of an F_c yield dependency that is inadequately known at this time. In the absence of knowledge of such a dependency, F_c estimates made from the curve in Fig. 1 for high-yield cratering events (of the order of 100 kt and above) should be considered as uncertain by a factor of 2. It should be further stated that F_c estimates derived from Fig. 1 are made with the tacit assumption that the nuclear explosive is fully tamped and that no additives for fission-product gamma-radiation suppression have been placed around the explosive.

It should also be mentioned that the maximum value of F_c (0.75 at $z/W^{1/3} \approx 30$) occurs at very nearly the same value of $z/W^{1/3}$ as the maximum base-surge radius (crosswind) in a neutral atmosphere, reported

in Ref. 7. The author believes that this coincidence of maximums at $z/W^{1/3} \approx 30$ is physically consistent.

Cloud Geometries

The geometrical definition of the top, the base, and the radius of both the main cloud and the base surge at the time of cloud stabilization is shown in Fig. 2. In addition to the definitions given in Fig. 2, the

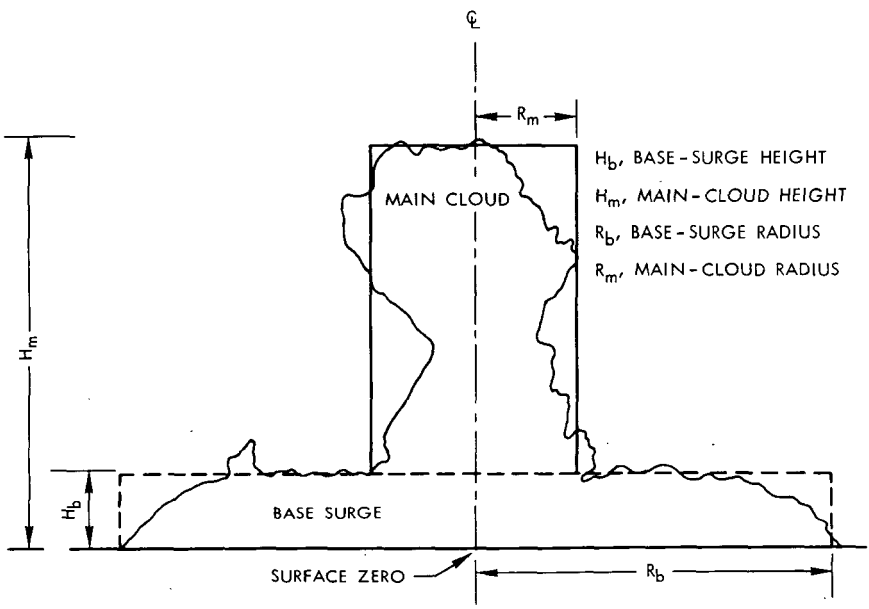

Fig. 2—Definition of cloud dimensions and symbols.

height of the base of the main cloud is defined as being equal to the height of the base-surge top, H_b, in the model.

Evidence suggests that the geometry of these two clouds at the time of stabilization is a function of the total explosive yield, the material in which the detonation occurs, the depth of burial of the explosive, and the meteorological conditions existing during the development of the clouds.[7] At present, the cloud-geometry parameters (R_b, H_b, R_m, and H_m) must be evaluated experimentally as functions of total yield and depth of burial. Reasonable samples of experimental data exist for alluvium and basalt materials. Examples from one of the most useful summaries of cloud-geometry data for alluvium[8] are shown in Figs. 3b to 3g. (Figure 3a is a computational aid to the acquisition of input to Figs. 3b to 3g. In these figures, z denotes depth of burial and D_a denotes the depth of apparent crater.) This summary utilizes all the known

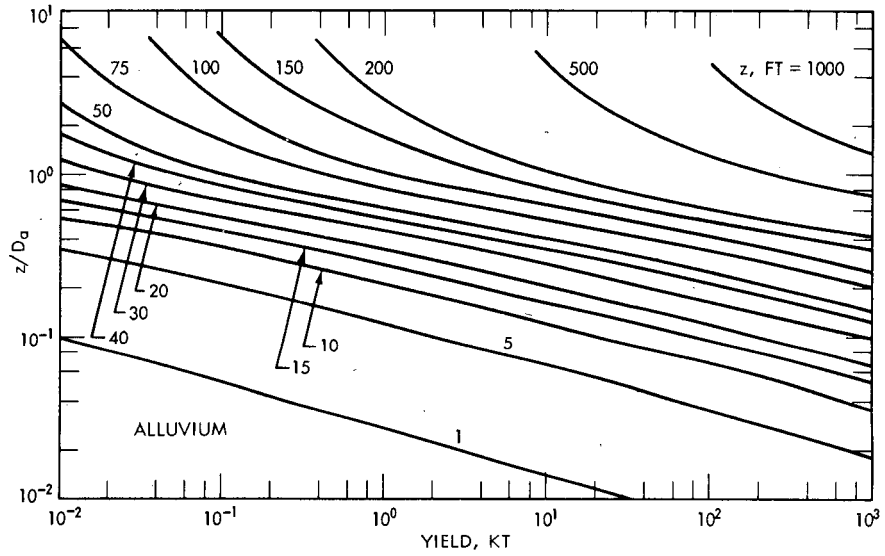

Fig. 3a—Computational aid to the acquisition of input data to the cloud-dimension graphs of Figs. 3b to 3g.

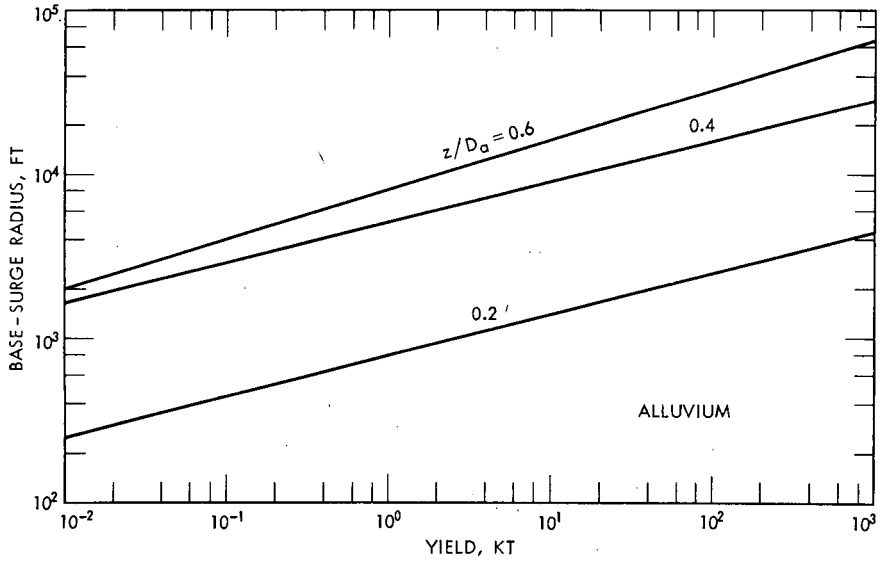

Fig. 3b—Base-surge radius as a function of the total yield and the parameter z/D_a.

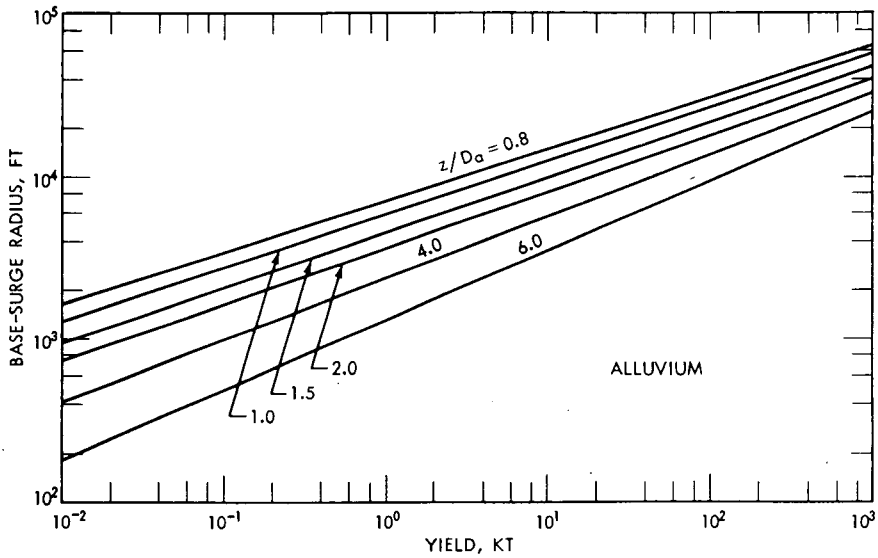

Fig. 3c —Base-surge radius as a function of the total yield and the parameter z/D_a.

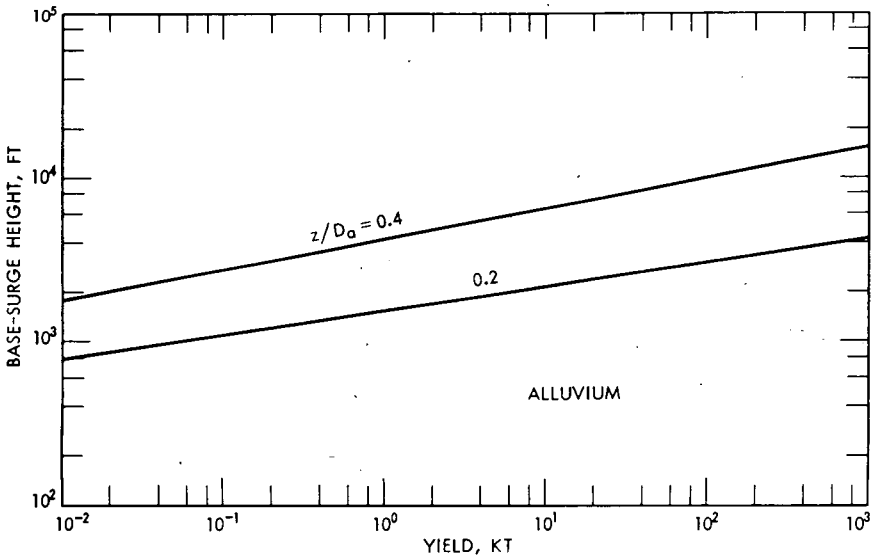

Fig. 3d —Base-surge height as a function of the total yield and the parameter z/D_a.

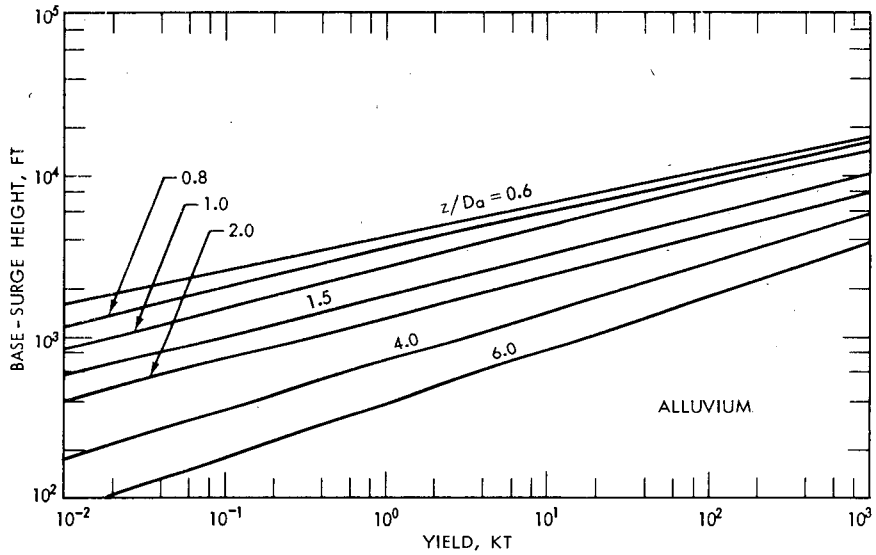

Fig. 3e—Base-surge height as a function of the total yield and the parameter z/D_a.

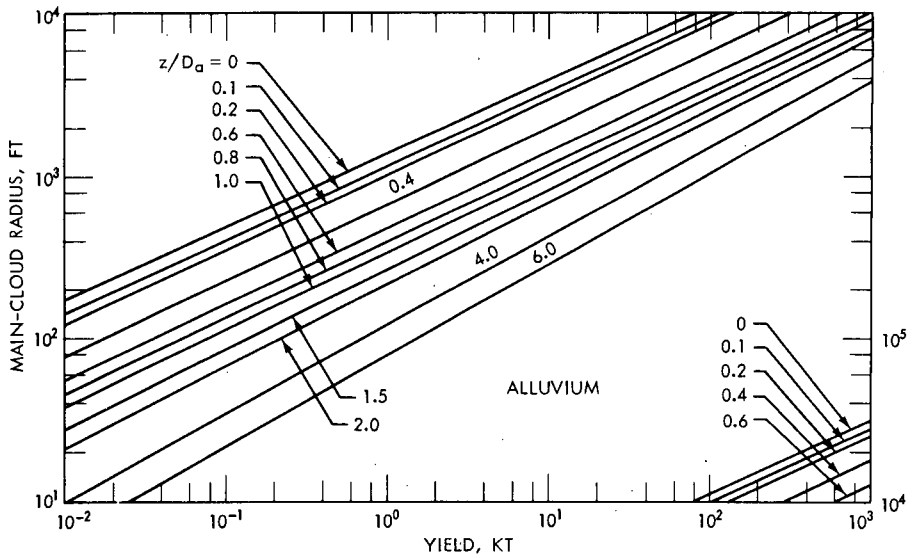

Fig. 3f—Main-cloud radius as a function of the total yield and the parameter z/D_a.

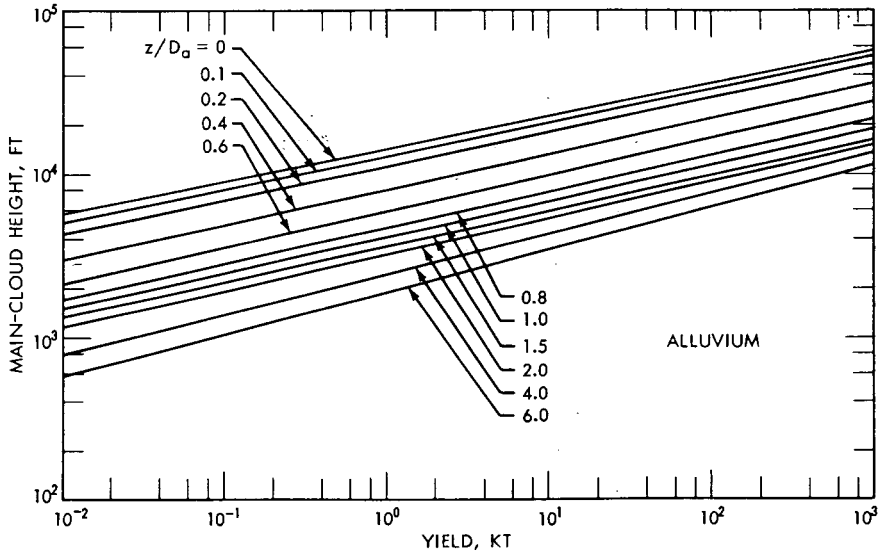

Fig. 3g—Main-cloud height as a function of the total yield and the parameter z/D_a.

cloud-geometry data from high-explosive and nuclear-explosive detonations conducted by the U. S. Atomic Energy Commission in alluvium and basalt. Implicit in the summary is the assumption that a high explosive and a nuclear explosive detonated in the same material at identical depths of burial and under similar meteorological conditions produce the same cloud geometries.

Activity–Particle Size Distributions

In a typical subsurface nuclear detonation in alluvium, two clouds are formed. The main cloud is composed mostly of vented cavity gas and particulates (originating from either condensation or injection and entrainment of soil). The base surge is composed of ejecta and suspended fine particulates. For a nuclear cratering shot in alluvium, it is assumed that 80% of the F_c gamma activity is in the main cloud and 20% is in the base surge. The 0.8 F_c main-cloud activity is assumed to be subdivided between two lognormal activity–particle size distributions. The first activity–particle size distribution contains the activity 0.8 $w_m(1)F_c$ and is characterized by the mean $\ln \bar{r}_m(1)$ and the standard deviation $\sigma_m(1)$. The second activity–particle size distribution contains the activity 0.2 $w_m(2)F_c$ and is characterized by the mean $\ln \bar{r}_m(2)$ and the standard deviation $\sigma_m(2)$. The activity of the first distribution is assumed to be homogeneously mixed through the whole main cloud, whereas that of the second distribution is assumed to be homoge-

neously mixed only in the lower fifth of the cloud. A similar prescription of activity–particle size is used for the base surge. Figure 4 summarizes the parameters governing the activity–particle size distributions in the two clouds at the time of cloud stabilization. These parameters governing the activity–particle size distributions in the

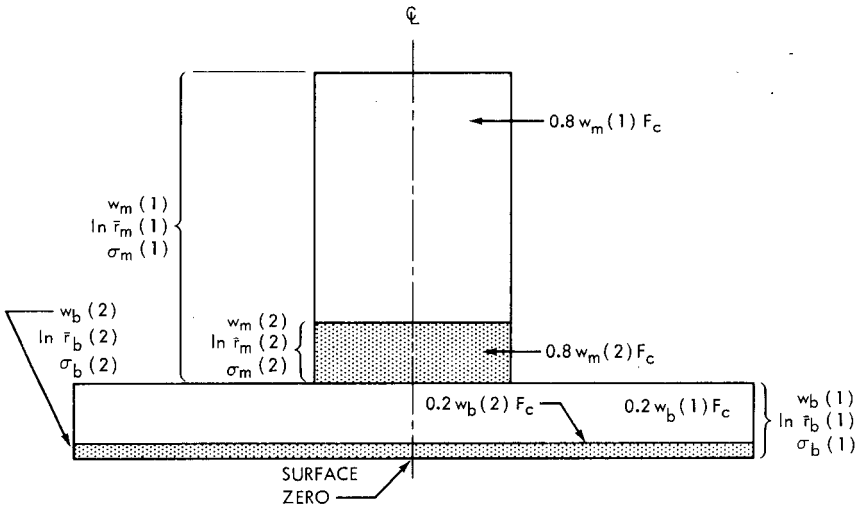

Fig. 4—Schematic drawing of an idealized cloud from a subsurface detonation showing spatial relations of the activity–particle size distribution assumed in the model.

cratering fallout model have been determined by mathematical experimentation with the model in the re-creation of the observed fallout patterns for the Sedan and the Danny Boy shots. Results of these calibration calculations will be discussed in a later section.

Terminal Fall Velocity of Fallout Particles

The vertical fall velocities of the fallout particles are modeled as the terminal fall velocities of smooth spheres of density 2.5 g/cm^3 in an International Civil Aeronautical Organization standard atmosphere as computed by McDonald[9] for both the Stokes'-law region and the aerodynamic region (wherein the Reynolds number exceeds 1). If some fallout particles are a cluster of small spheres attached to a large central particle, these complex particles are assumed to fall with the speed of the equivalent smooth spherical particle of the same mass. Experimental evidence has been obtained by Rapp and Sartor[10] to support this assumption.

Specification of the Horizontal Wind Field for the Model

The horizontal wind field that transports the debris-disk centroids during their fall to the earth's surface may be specified in two ways in the cratering fallout model:

1. Idealized Wind Hodograph. If H denotes height above surface zero, then the horizontal wind, $\underset{\sim}{v}_h$, at height H for a simple wind hodograph (see Fig. 5) is

$$\underset{\sim}{v}_h(H) = \underset{\sim}{v}_h(H_m)\frac{A(p)}{A(p_m)} - S(H_m - H)\underset{\sim}{n}$$

where $\underset{\sim}{v}_h(H_m)$ = steady-state wind at cloud-top level H_m (or it can be specified as a function of time and space in either wind component form or by means of a stream function)

$A(p)$ = wind-shear component tangential to the horizontal wind at cloud-top level and is evaluated from shot-time winds in a diagnostic fallout calculation or from preshot wind information for a predictive fallout calculation (it is held constant in time for the period of fallout deposition)

$A(p_m)$ = value of $A(p)$ at cloud-top level (normally it is set equal to 1)

S = wind-shear component normal to the horizontal wind at cloud-top level (it is evaluated from shot-time winds or preshot wind information, depending on the purpose of the fallout calculation, and is held constant in time)

$\underset{\sim}{n}$ = unit vector normal to $\underset{\sim}{v}_h(H_m)$ in a right-handed system

p = atmospheric pressure corresponding to H

2. Arbitrary Hodograph. The horizontal wind can be specified in wind-component form for as fine a vertical interval as desired or for which wind information exists.

Debris-disk Radius as a Function of Time

For estimation of the radius of a debris disk expanding by horizontal eddy diffusion during its fall to earth, it is proposed that the disk radius as a function of time $R_e(t)$ be represented by

$$R_e(t) = (R_{e,0} + 2Dt')^{1/2}$$

where t' is the distance traveled by the disk centroid divided by the mean horizontal wind speed in the layer through which the disk has settled, $R_{e,0}$ is the debris-disk radius at time of stabilization, and D is the horizontal eddy-diffusion coefficient.[2] The diffusion coefficient D is estimated as the Richardson's diffusion coefficient $0.2 \times \ell^{4/3}$, where

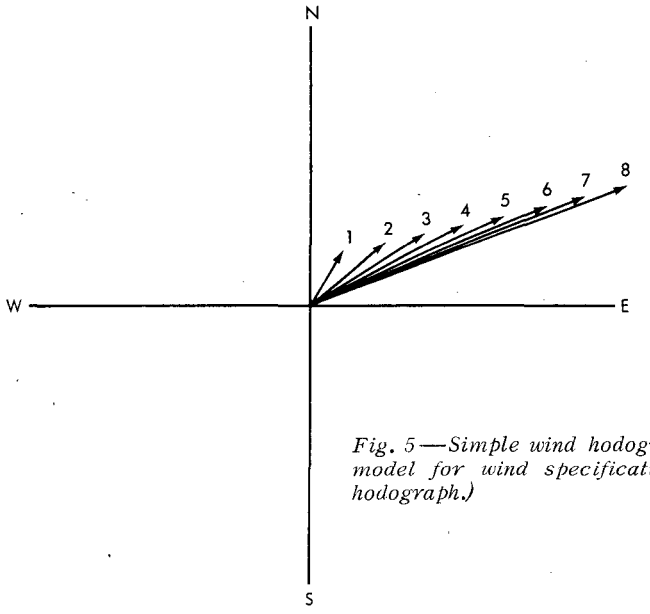

Fig. 5—Simple wind hodograph assumed in the model for wind specification. (Idealized wind hodograph.)

ℓ is the standard deviation of the position of the particles (in the disk) from the disk centroid. Since ℓ is poorly known in nuclear-debris clouds, it is usually set equal to $R_{e,0}$ or $2R_{e,0}$ if accelerated relative diffusion is to be approximated in the fallout model.

Physical Processes Simulated in the Model

The principal physical or meteorological processes simulated by the cratering fallout model are (1) the transport of the debris disks by the mean wind in the layer through which the disks are falling, (2) the relative advection of the debris disks by the horizontal wind field containing both a speed and a directional shear, and (3) the lateral eddy diffusion, which expands the disks falling earthward.

The first two processes are simulated by calculating the transport of the disk centroids by the ambient horizontal wind field during the disk's earthward fall until the disk centroid is on the ground surface by using either the idealized wind hodograph or the arbitrary hodograph for the horizontal wind specification. The result of this calculation is the position vector from surface zero to the predicted ground position of each disk centroid and the time of arrival at the ground surface of each disk. The lateral eddy-diffusion process is modeled by the expression for $R_e(t)$ which estimates the debris-disk radius at the time of arrival of the disk centroid on the ground surface.

The debris disks tracked earthward are defined as follows: In each cloud (main cloud and base surge), 11 disks of particle size r_I are defined at each isobaric surface p_p such that

$$\ln r_I = \ln r_L - \frac{I}{10}(\ln r_L - \ln r_s)$$

where I is equal to 0, 1, 2, ..., 10; r_L is the radius of the largest particle modeled in the cloud; and r_s is the radius of the smallest particle modeled in the cloud. The term p_p is equal to $p_B - [P/10(p_B - p_m)]$, where P is equal to 0, 1, 2, ..., 10; p_B is the pressure at the base of the cloud at the time of cloud stabilization; and p_m is the pressure at the top of the cloud at the time of cloud stabilization.

The (H + 1)-hr external gamma dose rate (for a height 3 ft above an infinite plane) is calculated by using the method of Batten, Iglehart, and Rapp[11] modified to account for the effect of normal shear and lateral eddy-diffusive disk growth.

The following quantities are calculated in the model and are output in the indicated modes:*

	Printout	Cathode-ray-tube display
Position of surface zero		x
(H + 1)-hr dose rate at the predicted ground position of each disk centroid for each cloud	x	
Predicted ground position of each disk centroid for each cloud	x	x
Envelope containing the area affected by the fallout from each cloud		x
Time of beginning and end of fallout deposition at each ground-position centroid for each cloud	x	
Isopleths of the (H + 1)-hr dose rate for any specified interval of dose rate (each contributing cloud and total pattern)		x
(H + 1)-hr dose rate as a function of distance along the hot line (each cloud and total pattern)		x

DIAGNOSTIC CALCULATION FOR SEDAN

For calibration of the cratering fallout model on the Sedan shot, the observed shot-time winds, the observed cloud geometry of the main cloud and the base surge, the estimated $F_c = 10\%$, and the appropriate fission yield were input to the model. A first guess of the 12 activity–particle size parameters, to be discussed later, was also input to the

*About 0.25 min of IBM 7094 computer time is required for the calculations for a two-cloud nuclear-cratering fallout problem, and 2.4 min of Livermore Advanced Research Computer time is required for the cathode-ray-tube displays indicated above.

model. The main cloud was assumed to contain 80% of F_c; the base surge, 20%. The parameters governing the activity–particle size distributions have been determined from the observed Sedan gross gamma fallout pattern by mathematical experimentation. The values of these parameters are as follows:

$$w_m(1) = w_b(1) = 0.9$$

$$w_m(2) = w_b(2) = 0.1$$

$$\ln \bar{r}_m(1) = \ln \bar{r}_b(1) = 2.9$$

$$\ln \bar{r}_m(2) = \ln \bar{r}_b(2) = 5.0$$

$$\sigma_m(1) = \sigma_b(1) = 0.69$$

$$\sigma_m(2) = \sigma_b(2) = 0.59$$

Figure 6 shows the calculated and the observed gamma dose rate* at H + 1 hr from fission products vs. distance along the hot line for the Sedan shot.

DIAGNOSTIC CALCULATION FOR DANNY BOY

The Danny Boy shot was a 0.42-kt nuclear cratering detonation emplaced at a depth of 109 ft in dry basalt. The observed gamma fallout pattern for Danny Boy has been published.[4] By mathematical experimentation with the cratering fallout model, the activity–particle size distribution parameters can be adjusted to duplicate the observed Danny Boy fallout pattern. In this shot no visible main cloud was observed.[4] Thus, in the diagnostic calculation with the cratering fallout model, it is assumed that 100% of the F_c gamma activity is in the base surge and that there is a preliminary value of 0.05 for F_c. The activity–particle size distribution parameters determined in this calculation are given below:

$$w_b(1) = 0.9$$

$$w_b(2) = 0.1$$

$$\ln \bar{r}_b(1) = 3.0$$

$$\ln \bar{r}_b(2) = 5.7$$

$$\sigma_b(1) = 0.69$$

$$\sigma_b(2) = 0.59$$

*The observed (H + 1)-hr gamma dose rate for fission products derived from the observed total gamma dose rate at H + 24 hr, assuming that 52% of the (H + 24)-hr gamma dose rate was from tungsten.[12]

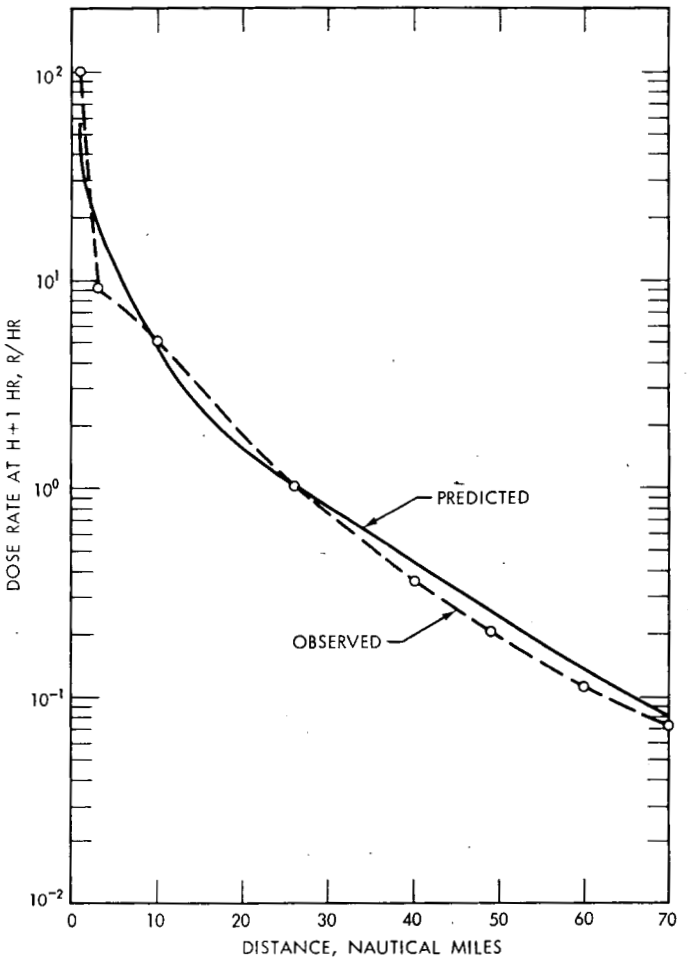

Fig. 6—The calculated and observed gamma dose rate at H + 1 hr as a function of distance along the hot line of the Sedan pattern (diagnostic calculation).

Figure 7 shows the calculated (H + 1)-hr dose rate vs. distance curve from the model, and the observed (H + 1)-hr dose rate vs. distance. As was previously mentioned, the value of F_c used in the cratering-fallout-model calculation was 0.05. If a value of 0.04 for F_c (as reported in Ref. 4) had been used, the agreement between the calculated (H + 1)-hr dose rate and the observed (H + 1)-hr dose rate vs. distance would have been better than shown in Fig. 7.

Recently effort has been expended to obtain machine capability of plotting the calculated (H + 1)-hr dose-rate patterns for an arbitrarily selected interval of dose rate. Figure 8 shows the machine-plotted dose-rate pattern for the Danny Boy diagnostic calculation. The computer-

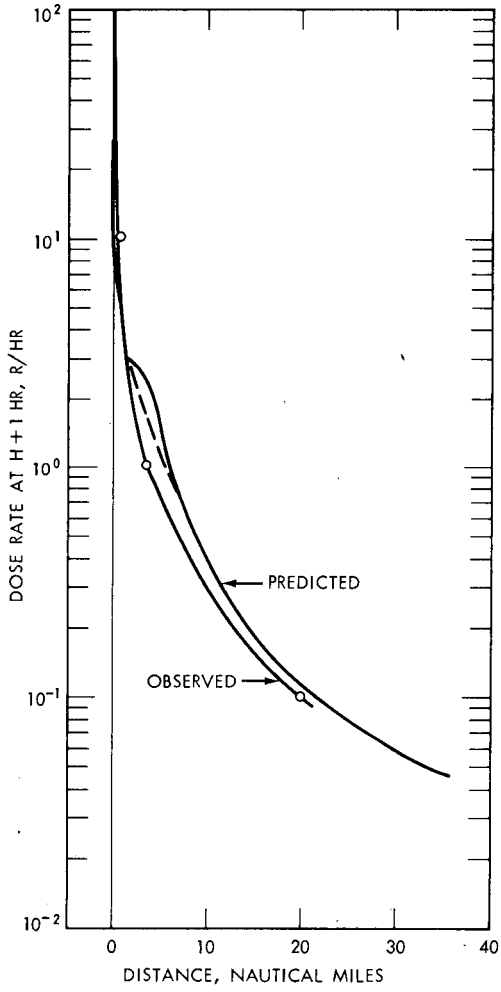

Fig. 7—The calculated and observed gamma dose rate at H + 1 hr as a function of distance along the hot line of the Danny Boy pattern (diagnostic calculation).

pattern breadth at 25 miles downwind is about 7 miles; the observed-pattern breadth at 25 miles downwind is 5.5 miles. It should be noted that the closure of the isodose-rate line of 10^{-4} r/hr at H + 1 hr in the plotted pattern is artificial and is the result of the logic used for the computer plotting rather than of the logic used for the cratering fallout model. All isodose-rate lines will apparently be closed at the downwind edge of the pattern if computed dose-rate information is insufficient for their appropriate extension downwind. The observed (H + 1)-hr gamma-dose-rate pattern for Danny Boy is shown in Fig. 9 for comparison with the computer-plotted pattern.

INDEPENDENT TESTS OF THE MODEL

An independent test calculation of the cratering fallout model (calibrated on Sedan) was performed by using data from the Teapot ESS

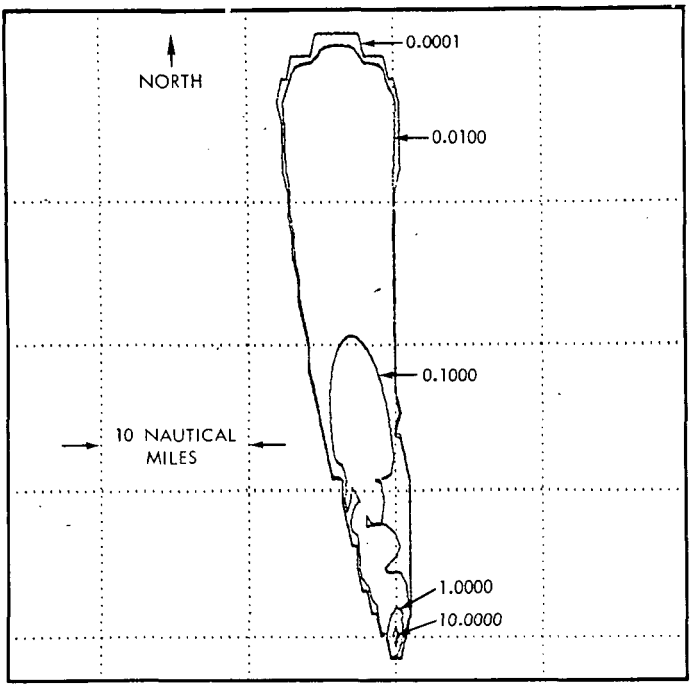

Fig. 8—The machine-plotted (H + 1)-hr gamma-dose-rate pattern for the Danny Boy shot (diagnostic calculation), roentgens per hour.

shot. The observed winds at shot time, the observed cloud geometry, the published fission yield of 1.2 kt, and a value of 0.85 (an early preliminary value) for F_c were input to the model. Figure 10 shows the calculated and the observed (H + 1)-hr gamma dose rate as a function of distance along the hot line of the pattern. A comparison of these two dose rate vs. distance curves shows that the largest error between calculation and observation is of the order of a factor of 2.5. An examination of the radiosonde observation near shot time at the Nevada Test Site indicates that the vertical temperature distribution of the layer through which the particles were falling was slightly superadiabatic. Under such conditions, it is possible that the vertical eddy diffusion on the day of the Teapot ESS shot was larger than average. If enhanced vertical eddy diffusion were operative, the dose rate would have been slightly less near ground zero and would have been enhanced downwind.

Other model confirmation tests have been performed. These include calculations with the surface-burst version of the model on the Apple II and the Zucchini shots[2] and on several other atmospheric shots for which the data are still classified. The results of these additional tests were satisfactory.

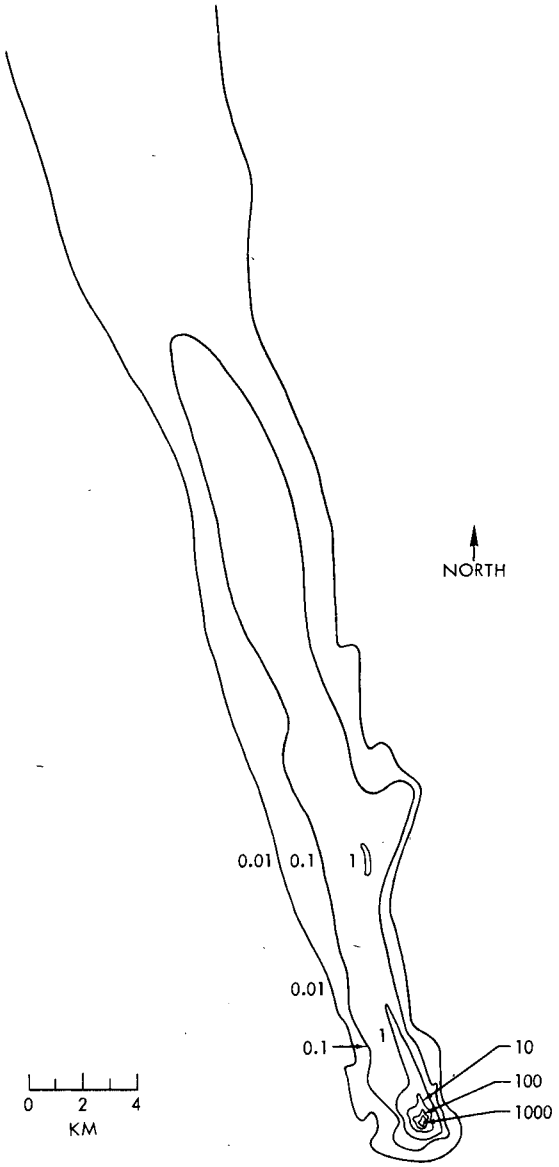

Fig. 9—Preliminary gamma-isodose-rate contours observed at H + 1 hr.[4] Readings in roentgens per hour minus H + 1 hr. Data taken from Nuclear Defense Laboratory ground surveys (close in); Edgerton, Germeshausen & Grier, Inc., aerial surveys (intermediate range); and U.S. Geological Survey aerial survey (long range).

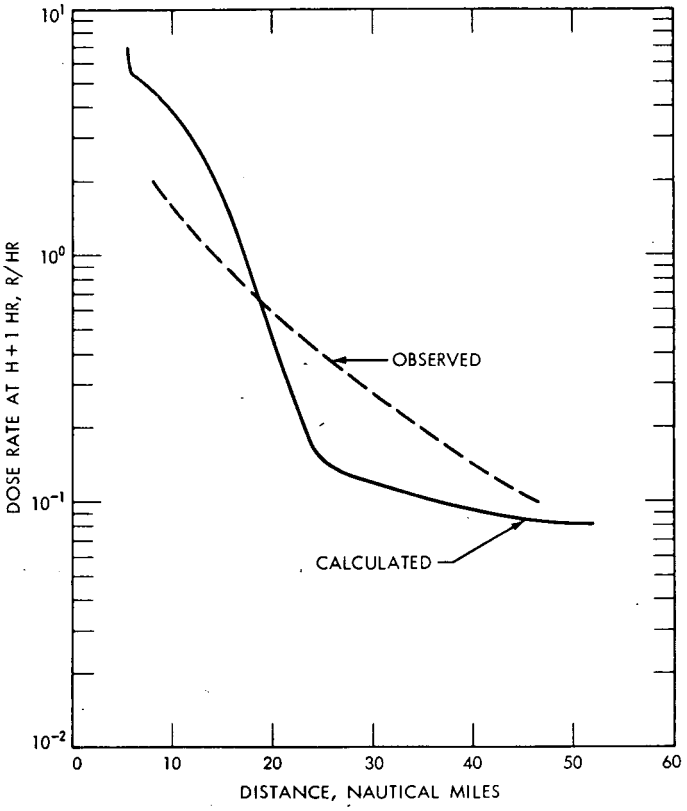

Fig. 10—The calculated and the observed gamma dose rates at H + 1 hr as a function of distance along the hot line of the pattern (predictive calculation) from the Teapot ESS shot.

PREDICTION OF FALLOUT FROM ROW-CHARGE SHOTS

In principle, the fallout pattern from a row of subsurface nuclear detonations may be estimated with the cratering fallout model, provided the model input parameters are adequately known for row-charge events. In the current state of knowledge, the cloud-geometry input parameters and the value of F_c appear to be the most difficult to specify. Study of time-lapse photography of the main-cloud and the base-surge evolution from past high-explosive row-charge tests give significant experimental information on the cloud-geometry parameters. For example, empirical methods of predicting crosswind radius and height of the base surges originating from high-explosive row-charge shots have been studied.[7] In this study it was shown that for five equal-weight charges, equally spaced and emplaced at the same depth of burial, the

resulting base surge has approximately the same radius as the base surge from a large single shot of the same total yield and emplaced at the same scaled depth. The base-surge height for a five-charge row shot is reasonably well approximated by scaling the height of the base surge for a single-charge event by the 0.2 power of the total yield of the row-charge shot.

A first approximation to the geometries of the individual main cloud may be obtained by treating each main cloud independently and estimating the top and the radius of each cloud from the work of Day.[8] Examination of the high-explosive row-charge documentary photographs of the Rowboat, the Dugout, and the Pre-Buggy shots indicates that such an approximation is reasonable. This approximation can, of course, be in error if main-cloud interactions occur. There is a need to evaluate the uncertainty in fallout prediction for multiple-charge shots in cases where cloud interactions lead to the injection of radioactivity at levels higher in the atmosphere than predicted.

Concerning the F_c for row-charge shots, preliminary experimental results for high-explosive single- and row-charge shots have been reported previously.[13] In this study, results of the measured vented fraction of ^{140}La tracer from single- and row-charge high-explosive shots were given. The experimental evidence suggests that the vented fraction from row-charge shots may be about twice that from single-charge shots. One of the most pressing needs for fallout prediction from row-charge shots is the establishment, through either experiment or theory, of the dependency of the F_c on yield, depth of burial, or charge spacing.

The development of computer aids for the row-charge fallout-prediction problem, however, can proceed independently of the solution of the two previously cited problems: (1) the specification of initial cloud geometry and (2) the specification of F_c. Therefore the capability of plotting fallout patterns for multicloud and/or multidetonation events has been developed. Figures 11 and 12 show, respectively, the (H + 1)-hr dose-rate patterns computed for 10 Danny Boy detonations on an east to west line with charge centers separated by 33.5 m and for 10 Danny Boy detonations on a north to south line with charge centers separated by 33.5 m. For the purpose of these calculations, each detonation is assumed to vent 5% (e.g., $F_c = 0.05$), each cloud is assumed to be the same as that for Danny Boy, and the input wind for each cloud fallout problem is assumed to be the same as the shot-time wind for Danny Boy. These two row-charge fallout patterns, although detectably different as determined from the printout, appear to be very similar. Calculational results suggest that the fallout pattern from a small-scale row-charge shot is not sensitive to the orientation of the wind to the alignment of the charges.

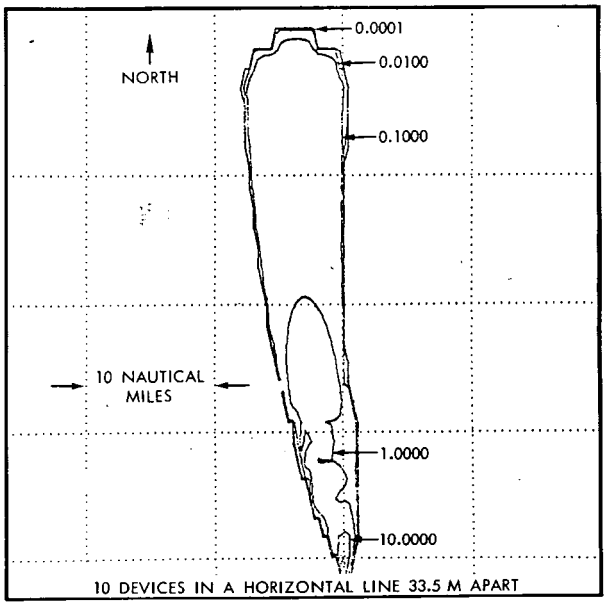

Fig. 11—The (H + 1)-hr gamma-dose-rate pattern computed for 10 Danny Boy detonations on an east to west line with charge centers separated by 33.5 m. Values are in roentgens per hour.

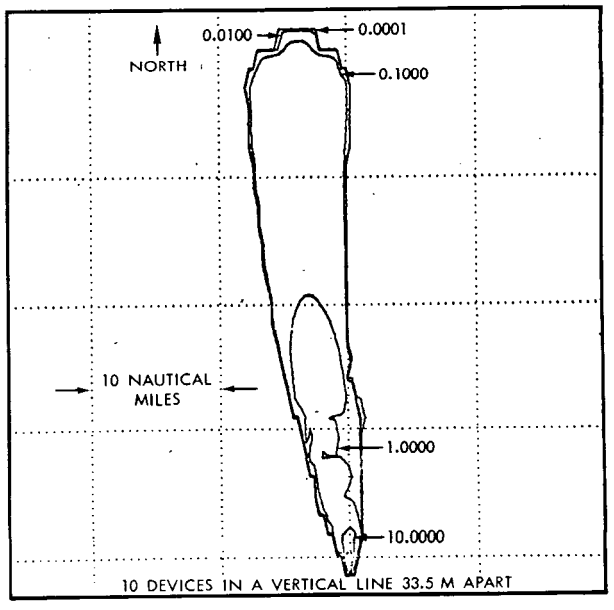

Fig. 12—The (H + 1)-hr gamma-dose-rate pattern computed for 10 Danny Boy detonations on a north to south line with charge centers separated by 33.5 m. Values are in roentgens per hour.

CONCLUSIONS

In conclusion, it may be stated that the cratering fallout model developed gives reasonable results for the prediction of the area of the pattern, the geometry of the dose-rate contours, and the (H + 1)-hr dose rate vs. distance along the hot line. The independent testing of the model should be extended to include more than the Teapot ESS case described and the several others cited.

Meteorological improvements in the cratering fallout model could well include the following items:

1. The prediction of synoptic-scale changes in the normal- and tangential-shear components.
2. A better understanding of the growth of the debris disks through horizontal eddy diffusion during their earthward fall.
3. The prediction of diurnal change of wind at low levels and close to ground zero.
4. The inclusion of the effects of topography on the evolution of the horizontal wind field.
5. The effect of terrain-induced circulations on fallout deposition.
6. A better solution to the cloud-rise problem for cratering detonations.

Before embarking on the development of these meteorological improvements in fallout predictions, however, one must consider potential improvements that may come from other areas. Areas of promise are cratering physics and filtration theory for the vented-fraction problem, special emplacement for control of vented fraction, and improvement of nuclear explosives.

ACKNOWLEDGMENTS

The author wishes to acknowledge the interest often expressed by Gary Higgins and the late A. Vay Shelton in the work herein reported, as well as programming support given by Mrs. Leota Barr and Roger Fulton.

REFERENCES

1. G. H. Higgins, Calculation of Radiation Fields from Fallout, USAEC Report UCID-4539, University of California Lawrence Radiation Laboratory, Jan. 25, 1963.
2. J. B. Knox, The Prediction of Wind and Fallout, USAEC Report UCID-4662, University of California Lawrence Radiation Laboratory, November 1962.
3. M. M. Williamson, private communication, 1964.
4. M. D. Nordyke and W. Wray, Cratering and Radioactivity Results from a Nuclear Cratering Detonation in Basalt, *J. Geophys. Res.*, *69*(4): 675-689 (1964).
5. G. H. Higgins, University of California Lawrence Radiation Laboratory, private communication, 1964.

6. J. B. Knox, University of California Lawrence Radiation Laboratory, unpublished data, 1963.
7. J. B. Knox and R. Rohrer, Project Pre-Buggy. Base Surge Analysis, USAEC Report PNE-304, University of California Lawrence Radiation Laboratory, Sept. 1, 1963.
8. W. Day, University of California Lawrence Radiation Laboratory, private communication, 1964.
9. J. D. McDonald, Rates of Descent of Fallout Particles from Thermonuclear Explosions, *J. Meteorol., 17:* 380-381 (1960).
10. R. R. Rapp and J. D. Sartor, Rate of Fall Through the Atmosphere of Irregularly Shaped Particles, Report RM-2006, RAND Corporation, Nov. 1, 1957.
11. E. S. Batten, D. L. Iglehart, and R. R. Rapp, Derivation of Two Simple Methods for the Computation of Radioactive Fallout, Report RM-2460, RAND Corporation, Feb. 18, 1960.
12. J. B. Knox, Status Report on Cratering Fallout Models, USAEC Report UCID-4663, University of California Lawrence Radiation Laboratory, Jan. 30, 1963.
13. E. Graves, W. R. Wray, and R. B. Pierce, Scope of Chemical Explosive Cratering Experiment, USAEC Report PNE-300, University of California Lawrence Radiation Laboratory, May 15, 1963.

SESSION IIIA
DISCUSSION

REED: Dr. Knox, when you talked about F_c decreasing in row charges, was that for special tests? Would it go up a factor of maybe 5 for rows of 15 or 20 charges?

KNOX: In fallout from row-charge detonations, F_c, the fraction of the gamma activity appearing in the close-in fallout pattern, is not well known. The paper I presented utilizes F_c data from USAEC Report PNE-300. This report describes the F_c experiments and measurements for tracer-loaded high-explosive sources detonated as single charges and as rows in alluvium (Pre-Buggy I). These measurements of F_c for row-charge shots and the corresponding measurements of F_c for single-charge shots indicate that F_c for a row charge does not exceed that for a single charge by more than a factor of 2. It is not thought that F_c is a linear function of the number of charges. However, a definite need exists to obtain better information on the vented fraction for row charges since the number of experiments contained in the Pre-Buggy Program is small.

SESSION IIIB

Global Atmospheric Transport

Elmar R. Reiter, Chairman

STRONTIUM-90 ON THE EARTH'S SURFACE. III

ROBERT J. LIST,* LESTER MACHTA,* LYLE T. ALEXANDER,† JAMES S. ALLEN,† MILTON W. MEYER,† V. T. VALASSIS,† and EDWARD P. HARDY, JR.‡

*Weather Bureau, U. S. Department of Commerce, Washington, D. C., †Soil Conservation Service, U. S. Department of Agriculture, Beltsville, Maryland, ‡Health and Safety Laboratory, New York Operations Office, U. S. Atomic Energy Commission, New York, New York.

ABSTRACT

A worldwide soil-sampling program was conducted in late 1963 and early 1964. This program was a continuation of earlier programs carried out in 1956, 1958, 1959, and 1960 to study the total deposition and distribution of ^{90}Sr over the surface of the earth. It is estimated on the basis of the data obtained that 7.6 Mc of ^{90}Sr were on the surface of the earth in late 1963. Some possible sources of error in this estimate are discussed.

INTRODUCTION

Since 1955 the U. S. Department of Agriculture has been conducting a soil-sampling program at the request of the U. S. Atomic Energy Commission to ascertain the worldwide distribution and total amount of ^{90}Sr fallout. Previous reported surveys[1,2] on a worldwide basis were conducted in 1956, 1958, 1959, and 1960. A fifth worldwide survey was conducted in late 1963 and early 1964; the results of this survey[3] are discussed here.

Samples have been collected from more than 100 sampling sites chosen to measure the total amount of ^{90}Sr fallout at particular locations. These sites are level or nearly so, have a complete vegetative cover, and are sufficiently permeable to absorb all the precipitation that falls on them. The sites receive no water from higher ground.

SAMPLE COLLECTION AND ANALYSIS

The samples were taken with two instruments: a "cookie cutter" that removes a 3.5-in.-diameter core to a depth of 2 in. and an orchard auger which cuts a hole the same diameter as the cookie cutter and removes the soil to the desired depth from a beginning depth of 2 in. The cookie cutter is used for the first 2 in. because the auger has a tendency to make a hole larger than its diameter as it cuts through a mat of grass and roots. In all cases, the error in the measurement of the sampled area was not greater than 1 or 2%.

The sample includes all the vegetation, both living and dead. The final aliquot for analysis includes the proper fraction of vegetation that segregates during sample preparation. Also, all rocks are crushed and included in the analyzed sample. The sample is usually a composite of 20 individual cores. The weight of the sample ranges from 20 or 30 lb for highly organic or peaty soils to as much as 100 lb for samples taken to a depth of 10 in. from dense soils.

After the soil was dried, crushed, and homogenized, aliquots of about 1 lb, identified only by number, were sent to the Health and Safety Laboratory (HASL) for analysis. Two aliquots were sent from each sample, but each member of the pair was sent in a different group to include a time-of-analysis variable. In addition, single blind aliquots of 41 of the soils were also analyzed at the Soil Survey Laboratory of the Soil Conservation Service at Beltsville, Md. The results of the comparison of the two analyses performed on each sample by HASL are shown in Fig. 1. An intercomparison of the HASL and the Soil Survey Laboratory results is shown in Fig. 2.

The extraction of the ^{90}Sr was accomplished by an HCl leach. However, there are unresolved differences between the results obtained by an HCl leach and by a more complete dissolution of the sample by fusion. The HCl leach values are about 5 to 10% lower than the fusion values. These differences are currently under intensive study, and it is hoped that they will be resolved in the near future. Until that time the reported soil data must be viewed as tentative.

Samples collected in the 1963 to 1964 survey were taken to a depth of 8 in. Previous studies[4] have shown (Fig. 3) that virtually all the ^{90}Sr is contained in the upper 8 in. of soil.

It is also possible to compare the fallout of ^{90}Sr in the period from 1960 to 1963, as indicated by the soil samples, with that collected by means of pots and ion-exchange columns in the monthly precipitation sampling network of HASL. At 15 sites the soil samples were taken within a few miles of the precipitation samples and at approximately the same elevation. A comparison of the soil increment with the total observed precipitation deposition over the same interval is shown in Fig. 4. The unlabeled points in the lower portion of the diagram repre-

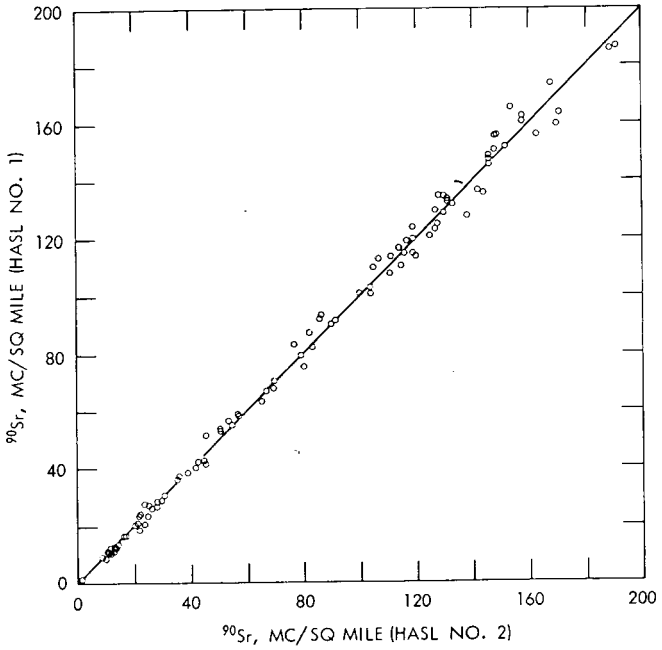

Fig. 1—Comparison of two separate determinations of ^{90}Sr in soil from the same sample by HASL.

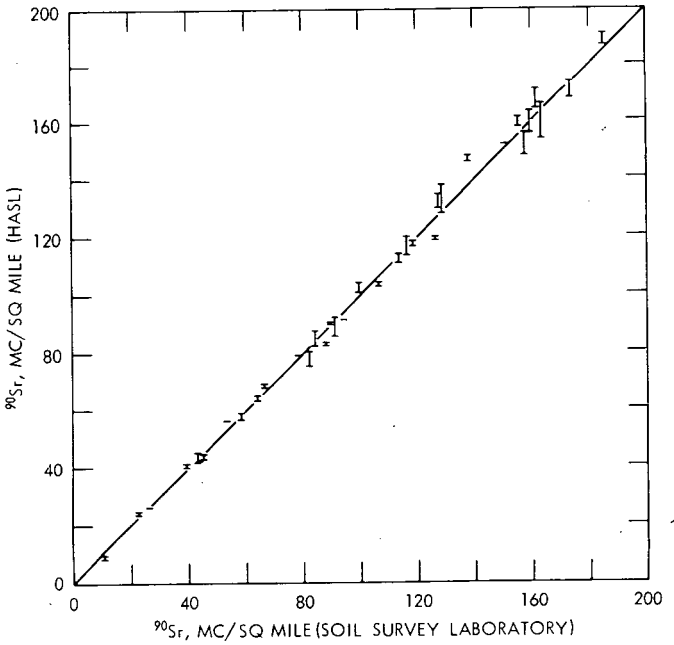

Fig. 2—Comparison of ^{90}Sr in soil as determined by the Health and Safety Laboratory and by the Soil Survey Laboratory.

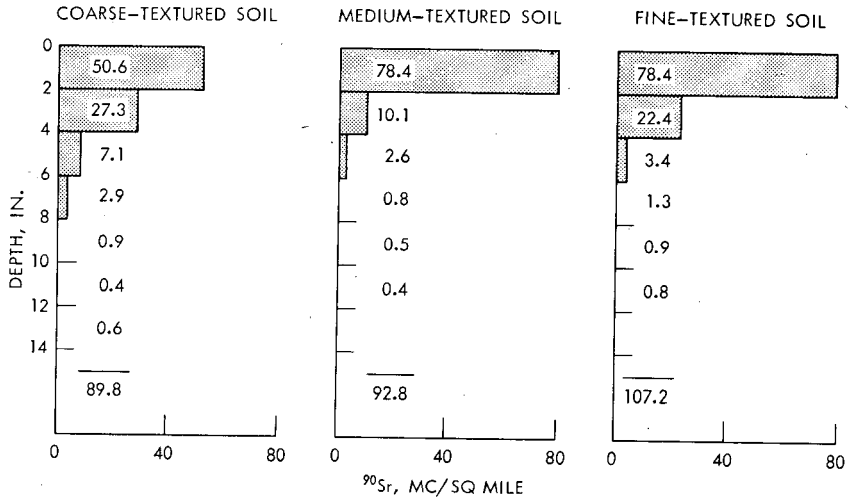

Fig. 3—Vertical distribution of ^{90}Sr in several typical soil types in early 1963.

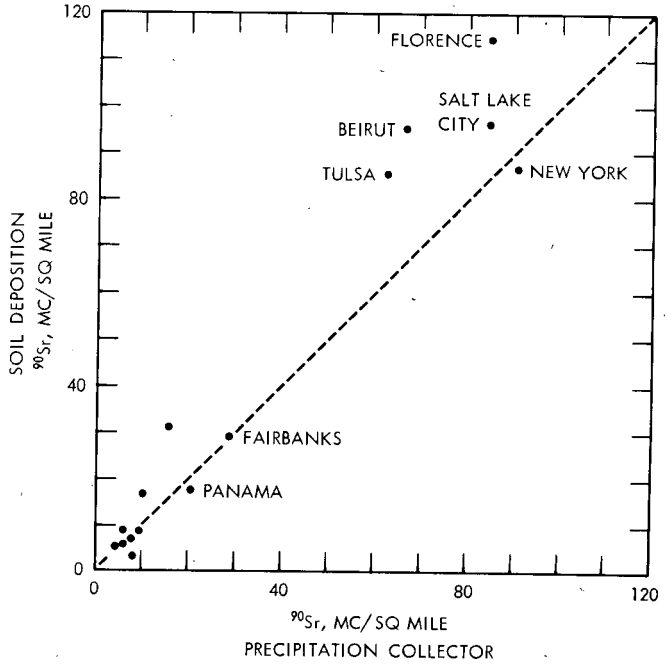

Fig. 4—Comparison of ^{90}Sr deposition in soils from 1960 to 1963 with ^{90}Sr deposited in nearby precipitation collectors during the same period.

sent southern-hemisphere sampling points. Sites in the northern hemisphere are labeled with the city name. The five sites with fallout of more than 60 mc/sq mile indicate that the soil values averaged about 10 to 15% greater than the deposition collected in the pots during the same period. These results are not surprising since dry fallout has been shown to be of about this order of magnitude and would be less efficiently sampled by the precipitation collectors. There is also evidence, especially during periods of high winds or snow, that precipitation collectors are not completely efficient in collecting all the precipitation falling on a given area.

GLOBAL DEPOSITION

The results of the 1963 and 1964 sampling are shown in Fig. 5. The isolines are drawn on the basis of the observed worldwide sampling data and mean precipitation patterns since precipitation is a principal mechanism for the deposition of ^{90}Sr on the surface of the earth. The individual data for the continental United States will be shown separately.

The latitudinal distribution is shown in Fig. 6. Sites in the United States are indicated by crosses. The solid curve indicates the mean latitudinal values as determined from Fig. 5. Since samples are collected principally in or near populated or agricultural areas, normally regions with adequate rainfall, there is a tendency for the individual points to lie above the mean curve. The mean latitudinal values reflect interpolation that includes regions of sparse rainfall. The total global fallout indicated by the 1963 to 1964 sampling is 7.6 Mc of ^{90}Sr with an estimated random uncertainty of less than ± 3 Mc. Table 1 shows the inventory of ^{90}Sr in late October 1963 and a comparison with the amount thought to be available for global fallout.

In addition to the random uncertainties, there are several possible sources of systematic uncertainties, most of which would tend to make the true deposition higher than that estimated from the data. Among these are percolation of the ^{90}Sr to greater depths in the soil; the

Table 1—INVENTORY OF ^{90}Sr IN OCTOBER 1963

	Megacuries*
Worldwide deposition	8
Estimated in atmosphere below 100,000 ft	5
Local fallout	2
Total	15
Estimated total production	19

*Corrected for decay.

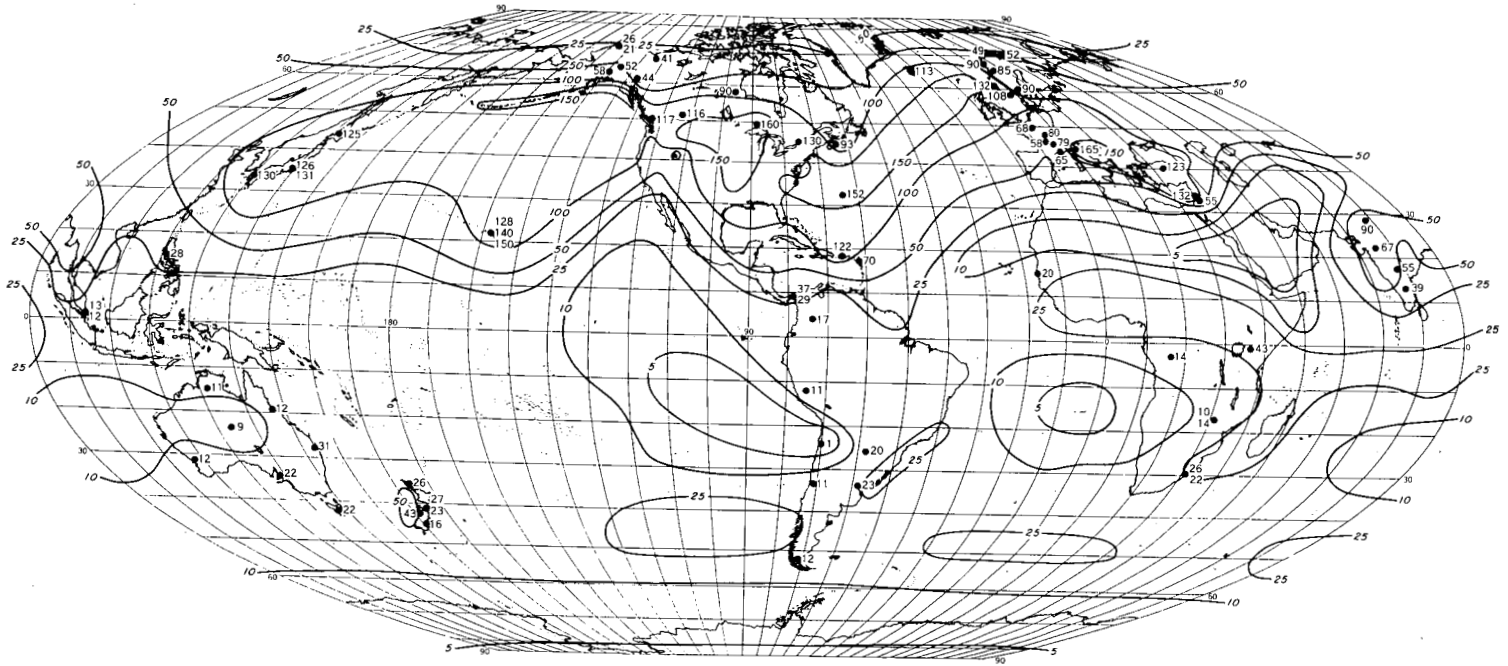

Fig. 5—Strontium-90 in soil determined from the 1963 and early 1964 survey, millicuries per square mile. Isolines are based on observed data and mean precipitation patterns.

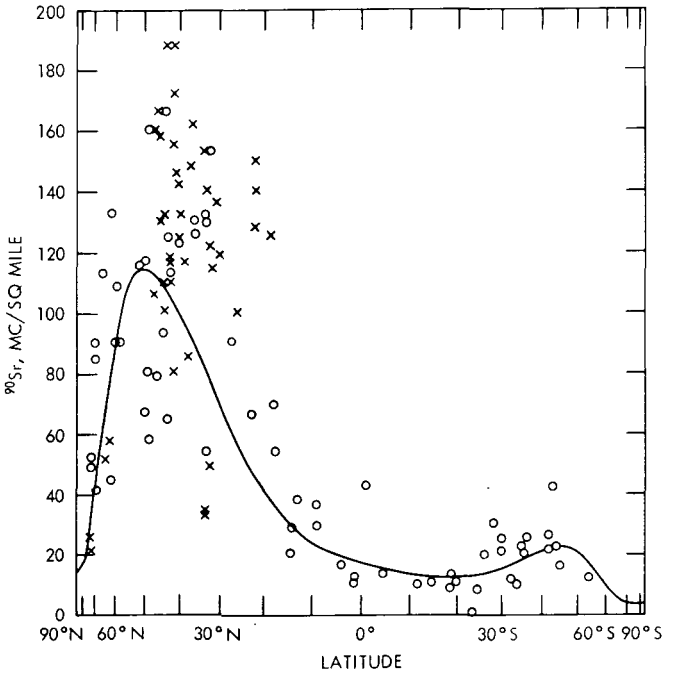

Fig. 6—Latitudinal distribution of ^{90}Sr in soil in 1963 and early 1964. (Crosses indicate samples collected in the United States.)

related error is believed to be small. There are unresolved differences between extraction of the ^{90}Sr from the soil sample by the HCl technique and by fusion; this could result in as much as a 10% underestimate of the total deposition. It has also been suggested that fallout over the oceans might be considerably higher than that over the land, but a comparison of soils from sites having a maritime exposure with soils from sites having a continental exposure indicated no systematic differences either in the total amount deposited or in the amount of ^{90}Sr deposited per inch of rainfall.

DEPOSITION IN THE CONTINENTAL UNITED STATES

The greatest density of soil-sampling sites is located in the continental United States and southern Canada, permitting a more detailed study of variability from site to site. The results of the 1963 to 1964 soil survey are shown in Fig. 7. As can be seen, the general pattern of deposition is influenced by the precipitation pattern; for example, the dry southwestern states have the lowest ^{90}Sr fallout. However, there are two obvious exceptions. One is the maximum found in the vicinity of the Great Salt Lake. The deposition at Salt Lake City,

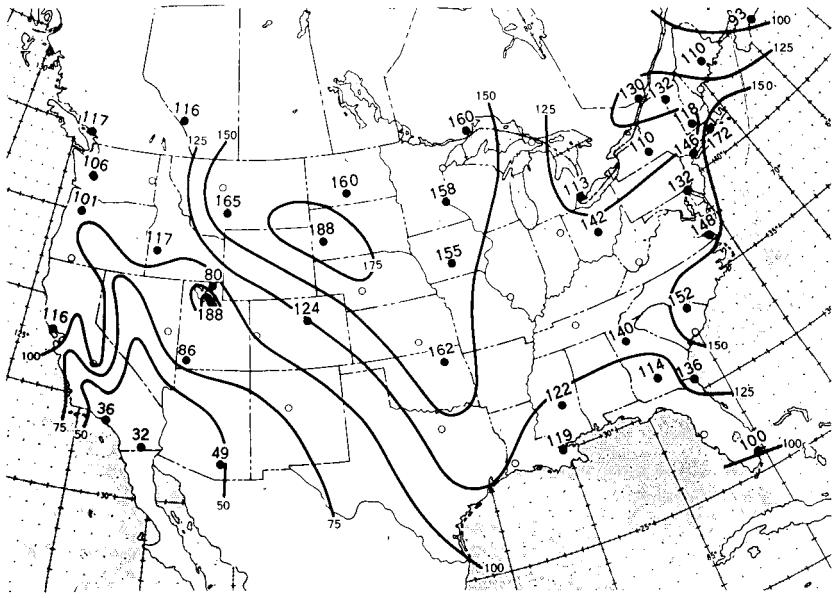

Fig. 7—Strontium-90 in soil in 1963 and early 1964 in the continental United States and southern Canada, millicuries per square mile.

on the western side of the Wasatch Mountains, is more than twice as great as that found at Logan, Utah, about 70 miles to the north but on the eastern slopes of the mountain range. The discrepancy between the values at Salt Lake City and at Logan suggested that a more complete investigation in the vicinity of the Great Salt Lake was in order. It was originally suggested that the very high deposition at Salt Lake City was somehow connected with its position relative to the Nevada Test Site. In 1962 additional samples on the east and west sides of the Wasatch Mountains were obtained.[5] The stations on the western, or lake, side of the mountains showed ^{90}Sr deposition values about twice those on the eastern side. Another sampling in 1963 in the southwestern corner of Utah and very much closer to the Nevada Test Site showed values comparable to those on the eastern side of the Wasatch Mountains. This led to the conclusion that the high values at Salt Lake City were related to the proximity to the Great Salt Lake or to surrounding salt deserts. Although no complete physical explanation of the phenomenon has been advanced, presumably it is related to the abundance of salt nuclei in the air. It is interesting to note that the total ^{90}Sr deposition reported for the HASL ion-exchange column at Salt Lake City for the 1960 to 1963 period compares very closely with the deposition occurring in Salt Lake City soils during the same period.

Another, much larger area of high ^{90}Sr deposition is in the central and northern Great Plains states. There have been several attempts

to explain this phenomenon, which occurs consistently in the soil data. It was evident in the earlier surveys and in the incremental depositions between 1960 and 1963. Among the explanations of the cause advanced have been the mean storm tracks over the United States, the effect of the Rockies in creating vertical motions, and the position of the jet stream. None of these explanations has been rigorously tested, due principally to lack of adequate data. It is interesting to note that the Public Health Service Radiation Surveillance Network data indicate that the ground-level air in the Great Plains states does not contain a higher concentration of gross beta activity than air in other sections in the country. The HASL precipitation collectors do indicate somewhat higher deposition per inch of rainfall, but the total deposition during the 1960 to 1963 period is lower than that in the soil increment. (Unfortunately, there are no directly comparable soil sites and precipitation collectors in this area.) Although the northeastern states receive about three times more (45 vs. 15 in.) annual rainfall than does, say, Rapid City, S. Dak., in the late spring months, the period of maximum deposition, the average rainfall at Rapid City is quite comparable to that in the northeastern states. There is a pronounced spring maximum of rainfall in the Great Plains states, whereas there is a relatively uniform distribution of precipitation throughout the year in the northeastern states. Recent studies have also shown that the precipitation in the Great Plains states occurs from clouds extending to much higher altitudes than those in the northeastern states.[6] Precipitation clouds extending about the tropopause are quite rare in New England, but they are a common phenomenon in the spring thunderstorms over the Great Plains. This may contribute to the high deposition rate although it cannot serve to explain all the difference. Another suggestion is that dry deposition is possibly more important over the Great Plains region. Surface winds over the Great Plains are, on the average, higher than over any other large region of the country. This may result in greater impaction of particles on growing vegetation.

CONCLUSION

The global soil survey provides useful information on the total deposition of ^{90}Sr on the surface of the earth and on the characteristics of its distribution. The observed distribution seems to correlate principally with latitude and precipitation amounts. Mechanisms responsible for deviations from the expected pattern are being studied.

REFERENCES

1. L. T. Alexander, R. H. Jordan, R. F. Dever, E. P. Hardy, Jr., G. H. Hamada, L. Machta, and R. J. List, Strontium-90 on the Earth's Surface, USAEC Report TID-6567, February 1961.

2. E. P. Hardy, Jr., R. J. List, L. Machta, L. T. Alexander, J. S. Allen, and M. W. Meyer, Strontium-90 on the Earth's Surface II, USAEC Report TID-17090, November 1962.
3. E. P. Hardy, Jr., and Joseph Rivera, in Fallout Program Quarterly Summary Report, USAEC Report HASL-149, pp. 29-42, Health and Safety Laboratory, Oct. 1, 1964.
4. E. P. Hardy, Jr., Vertical Penetration of ^{90}Sr in Three Soils Sampled in March 1963, in Fallout Program Quarterly Summary Report, USAEC Report HASL-138, pp. 249-250, Health and Safety Laboratory, July 1, 1963.
5. L. T. Alexander, J. S. Allen, and E. P. Hardy, Jr., Strontium-90 in Soils Collected in 1962, in Fallout Program Quarterly Summary Report, USAEC Report HASL-142, pp. 293-296, Health and Safety Laboratory, Jan. 1, 1964.
6. H. H. Hanks, Jr., M. J. Long, and R. G. Beebe, Tropopause Penetration by Cumulonimbus Clouds, Report AFCRL-64-111, Air Force Cambridge Research Laboratories, February 1964.

STATUS OF GLOBAL RADIOACTIVE-FALLOUT PREDICTIONS

LESTER MACHTA
U. S. Weather Bureau, Department of Commerce, Washington, D. C.

ABSTRACT

The atmosphere transports, dilutes, and removes radioactive contaminants. Contaminants added almost anywhere in the earth's atmosphere can be brought to man's environment or food. The details of individual trajectories and precipitation-scavenging areas play prominent roles for tropospheric sources, and the statistical behavior of the stratosphere controls the long-term transport and dilution of radioactive material at higher levels.

INTRODUCTION

The objective of this paper is to summarize certain aspects of predictions of man-made radioactive fallout. Included is a discussion of the fate of radioactive gases and particulates injected into both the troposphere and the stratosphere. However, a number of important items are entirely or largely omitted; among these are local fallout and close-in contamination, stratosphere–troposphere exchange, precipitation-scavenging mechanisms, special removal mechanisms such as might exist over the oceans, redeposition, and others.

TROPOSPHERIC FALLOUT

Predictions of the fate of radioactivity introduced into the troposphere fall in two categories. The first is a forecast of the generalized fallout made well in advance of an event in order to plan for or to ap-

preciate the consequences of a proposed or accidental release of radioactivity. The second category involves the forecast of fallout on a current basis, either just before or soon after an event.

Planning

Climatological winds and past fallout experience form the basis for estimating the distribution of fallout from tropospheric injections of particulate radioactivity.

Global-scale air motions are mainly zonal in nature. Superimposed on the zonal basic current are waves producing north to south motions. This general airflow should result in a global fallout pattern with highest deposition or air concentrations at about the latitude of the test site, generally decreasing with distance from the source. The middle part of Fig. 1 shows this expected pattern. It has been obtained by averaging the global gross deposition on gummed paper during the Operation Upshot-Knothole tests in Nevada in 1953 around each circle of latitude.[1]

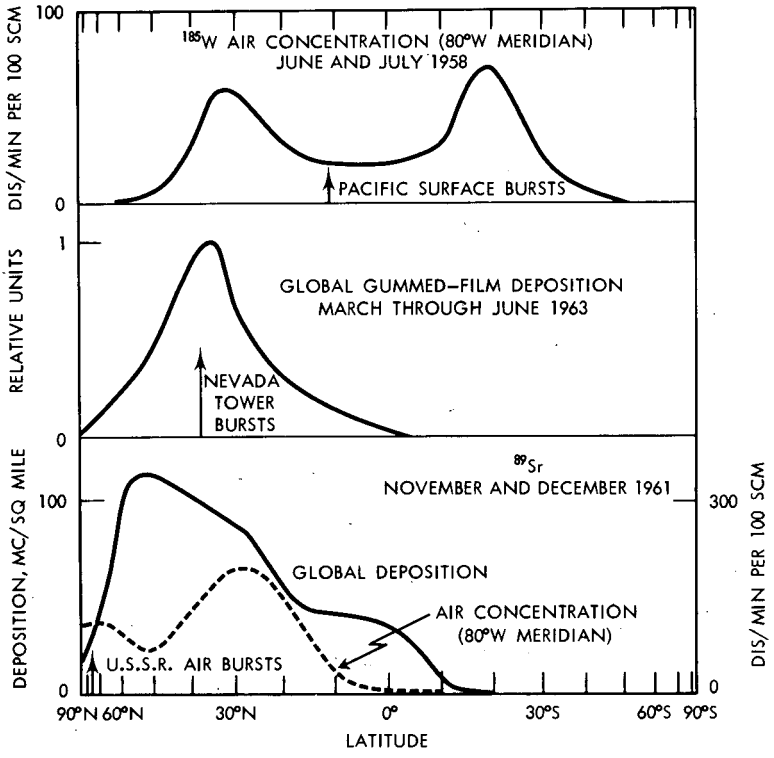

Fig. 1—Latitudinal variation of surface observations of tropospheric radioactivity as a function of injection point.

However, this simple picture may not always be found. The upper and lower parts of Fig. 1 illustrate two exceptions. In the upper part the ground-level ^{185}W air concentrations measured by the Naval Research Laboratory (NRL) along the 80th meridian are plotted schematically, with some liberties being taken with the observed data because of differences in station elevation.[2] The peak concentration is displaced to the subtropical latitudes of each hemisphere. Machta[3] has argued that bomb debris placed initially in the upper equatorial troposphere will be carried poleward by the return poleward circulation of the Hadley Cell to subtropical latitudes. The lower part of Fig. 1 shows fallout at stations of the Health and Safety Laboratory (HASL) pot and ion-exchange network and along the NRL 80°W meridian network during the U.S.S.R. 1961 nuclear test series. The peak deposited ^{89}Sr radioactivity occurs 20 to 30 degrees south of the source, and the air-concentration maximum is over 40 degrees south of the source. In part, this pattern may result from limited or poor sampling, especially near the pole. More likely it is real and results from meteorological processes. Material injected into the upper polar troposphere will mix downward along isentropic surfaces to lower levels in temperature latitudes in days or weeks. Thus debris is more readily available for precipitation scavenging and final mixing to the ground temperature latitudes than in polar latitudes for sources originally in the upper polar troposphere.

Current Forecasting

The specific trajectory, spread of debris, and precipitation-scavenging areas must be known to predict radioactive fallout after an atmospheric injection. It is believed that "true" trajectory predictions are useful to two days and that after-the-fact reconstructed trajectories are likely to be useful to perhaps five or ten days. Beyond these periods the average error may be too large for the results to contribute to the understanding of the fallout distribution.

The past operational forecasts by the Weather Bureau were based on subjectively predicted or reconstructed constant-level or constant-pressure trajectories. A swath rather than a line was used to incorporate both the diffusive spread and the uncertainties of meteorology. An example of this kind of an after-the-fact forecast is given in Fig. 2 along with ground-level verification over the United States and Canada. In this case, the 30,000-ft, or 300-mb, level was chosen because it was believed that most of the tropospheric fission products from the test lay near the tropopause. Rain areas through which the nuclear cloud might pass were also given with the forecast or reconstructed trajectories since it is in these regions where greater deposition should be expected.

The shaded areas delineate first arrival of the debris in ground-level air at the station shown by the dots. The verification shows a de-

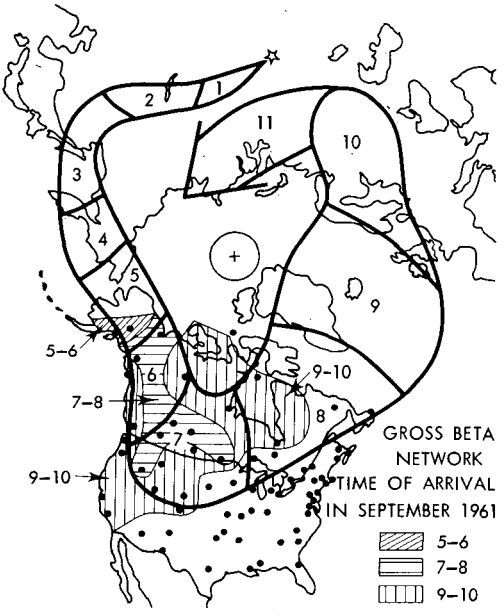

Fig. 2—Estimated upper tropospheric trajectory of debris from the Sept. 1, 1961, U.S.S.R. test. Shading indicates dates of first appearance of debris on surface air filters.

lay of several days between the predicted arrival at 30,000 ft and at ground level. This delay results, in our opinion, from time to mix downward or for particulates to settle out.

The literature contains innumerable examples of trajectories of nuclear clouds obtained by many techniques. Of these methods the application of isentropic analysis is one of the two most valuable improvements over past Weather Bureau procedures. Isentropic analysis permits the tracking of air parcels undergoing adiabatic vertical motions. A dramatic case in which the isentropic trajectories appear to explain better the observations of ground-level air concentrations has been given by Reiter.[4] In the mean, the isentropic surfaces slope downward from north to south in the troposphere; thus trajectories moving southward will be brought closer to the ground or man's environment, whereas those moving northward rise away from the ground.

A second, less important, improvement is the computation of trajectories by an electronic computer rather than by hand. An illustration of a computer forecast currently in operational usage by the Weather Bureau appears in Fig. 3 with starting points at the Nevada Test Site (NTS). In practice, it is felt that the additional wind information and knowledge of local topographic conditions permit meteorologists at NTS to start computation of the trajectories more correctly than can be done by machine. After 6 hr the machine trajectories are used as the basis for continuing the forecasts to 30 hr. Figure 4, taken from the Weather Bureau analysis of trajectories for STROBE (the use of constant-level

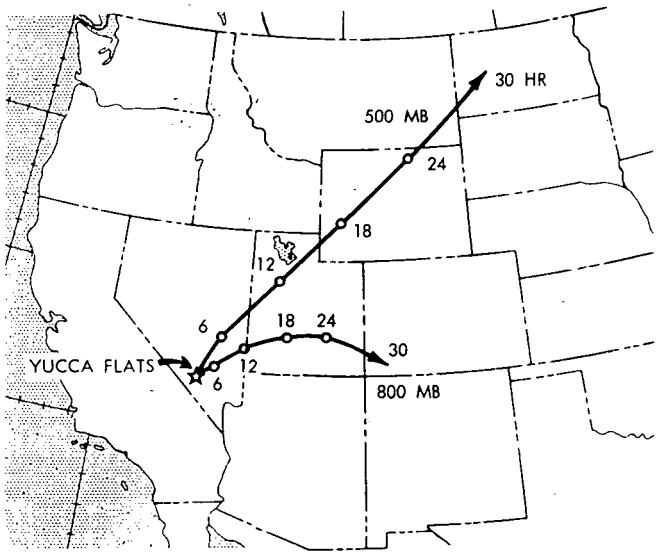

Fig. 3—Example of a 30-hr operational trajectory forecast prepared by computer for the Nevada Test Site.

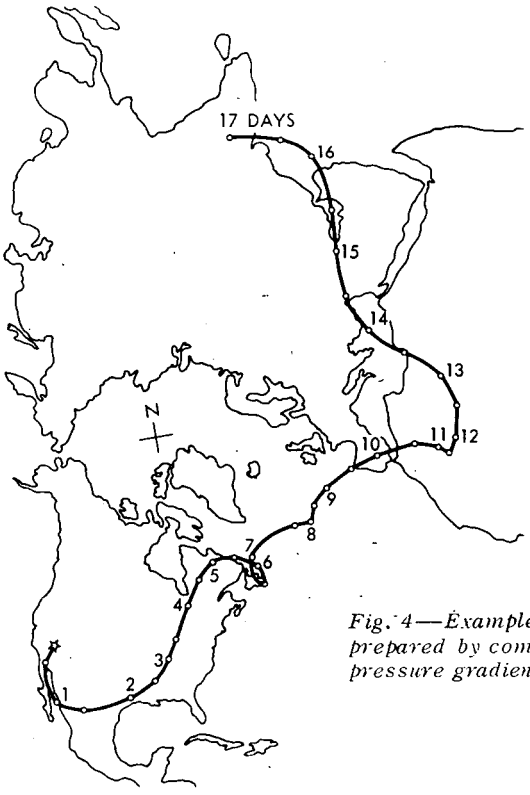

Fig. 4—Example of a 17-day 500-mb trajectory prepared by computer using observed winds and pressure gradients.

balloons to augment weather information), shows a long-period machine trajectory carried for 17 days at 500 mb. In this case, observed winds and pressure gradients, not forecasts, guide the computation of the air trajectory. Analysis of the results of machine forecast and reconstructed trajectories suggests approximate agreement between hand subjective and machine objective procedures.

Finally, it should be noted that techniques to incorporate the benefits of isentropic analysis into machine computations are available.

Atmospheric Dispersion

The prediction of atmospheric dispersion at distances beyond about 100 miles assumes Fickian diffusion; that is, the flux of material is in the direction of and proportional to the gradient of concentration. For simplicity, although the procedure is not necessarily correct, the coordinate axes are chosen in the vertical and the horizontal directions. In its simplest form, the standard deviation of the spread of a pollutant may be written as

$$\sigma_h = \sqrt{2K_h t}$$

and

$$\sigma_v = \sqrt{2K_v t}$$

where σ = standard deviation of the Gaussian distribution of a pollutant around its mean position
K = coefficient of eddy diffusion
t = time
h and v = horizontal and the vertical directions, respectively

In the quasi-empirical application of this law, it becomes necessary to use different values of K (particularly K_h) with different transit times. Figure 5 is a graphical presentation of K_h vs. time as summarized by Heffter.[5]

There are many reasons to expect atmospheric dispersion to depart from a simple Gaussian distribution described by Fickian diffusion. The dominant reason is the vertical wind shear (the change of wind direction and/or speed with altitude) superimposed on vertical diffusion. Figure 6 shows schematically how an initial cylinder of marked air parcels grows by diffusion (the light shading) and by wind shear and vertical mixing (the cross hatching). The latter process results from the stretching of the cylinder by the wind shear and the vertical mixing, which brings material upwards or downwards ahead of or behind the moving cylinder and adds to the growth resulting solely from horizontal mixing.

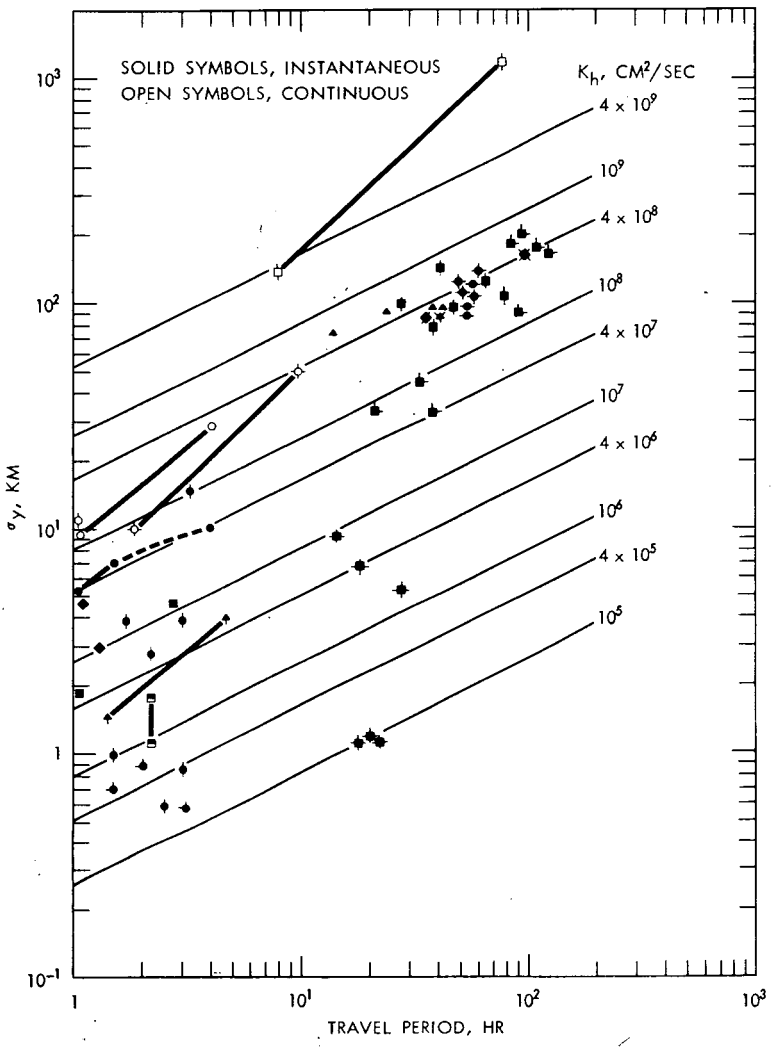

Fig. 5—Values[5] of the coefficients of horizontal eddy diffusion based upon observations for periods of greater than 1 hr.

In practice, it is difficult to distinguish between spread due to horizontal mixing and that due to shear and vertical diffusion. Figure 7 illustrates two cases in which the width of the peak concentration of nuclear debris from Operation Ranger along a line perpendicular to the mean flow appears to be related to the directional shear of the wind.[6] Thus, in the upper part of Fig. 7, all the trajectories from the first nuclear cloud passed the 95°W meridian between 38°N (at 9000 ft) and 39.5°N (at 12,000 ft). Only one filter paper lying in this latitude range located the peak. This is a case of small directional shear. In the lower part of Figure 7, the fifth cloud was intercepted over the Gulf of Mexico at 82°W. At 15,000 ft the trajectory crossed the flight line at about

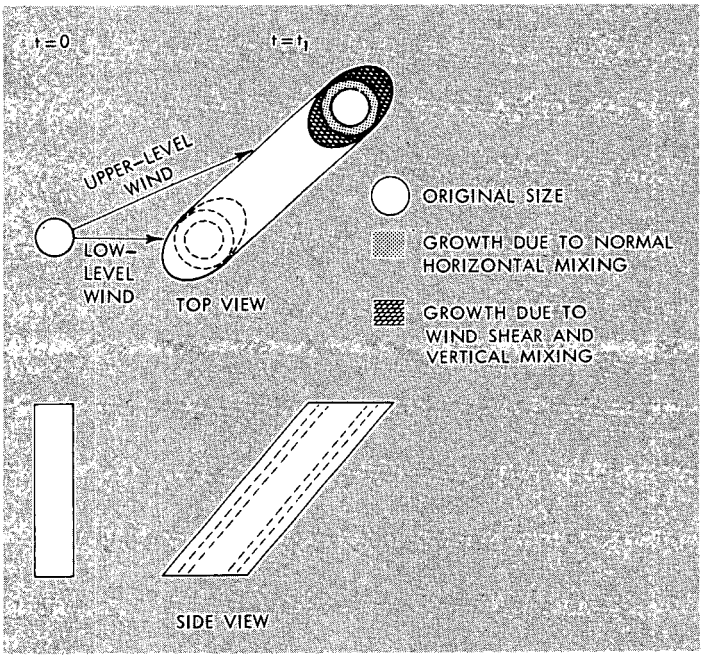

Fig. 6—Schematic representation of cloud growth due to diffusion, wind shear, and vertical mixing.

24°N, whereas at higher altitudes, e.g., 24,000 ft, the trajectory crossed the flight line at about 21.5°N. In this case, the width of the peak concentration samples covers 4 to 5 degrees of latitude. This is a case of moderate directional shear.

STRATOSPHERIC FALLOUT

The greater interest in predictions of stratospheric than of tropospheric fallout arises from several considerations: so far, only stratospheric debris from weapon tests is still available to fall out; the largest fraction by far of long-lived fission products has been injected into the stratosphere by nuclear explosions; and there is at present a livelier scientific interest in stratospheric than in tropospheric transport and diffusion. With two important exceptions, short-lived radioactivity decays in the stratosphere before reaching the ground; thus only long-lived isotopes should be considered. The exceptions are the scavenging of radioactivity by thundershowers penetrating into the stratosphere[7] and the quick exit from the stratosphere postulated by Danielsen,[8] Reiter,[4] and others.

It should also be noted that time of fallout after a test series has been the prime means of distinguishing between tropospheric and

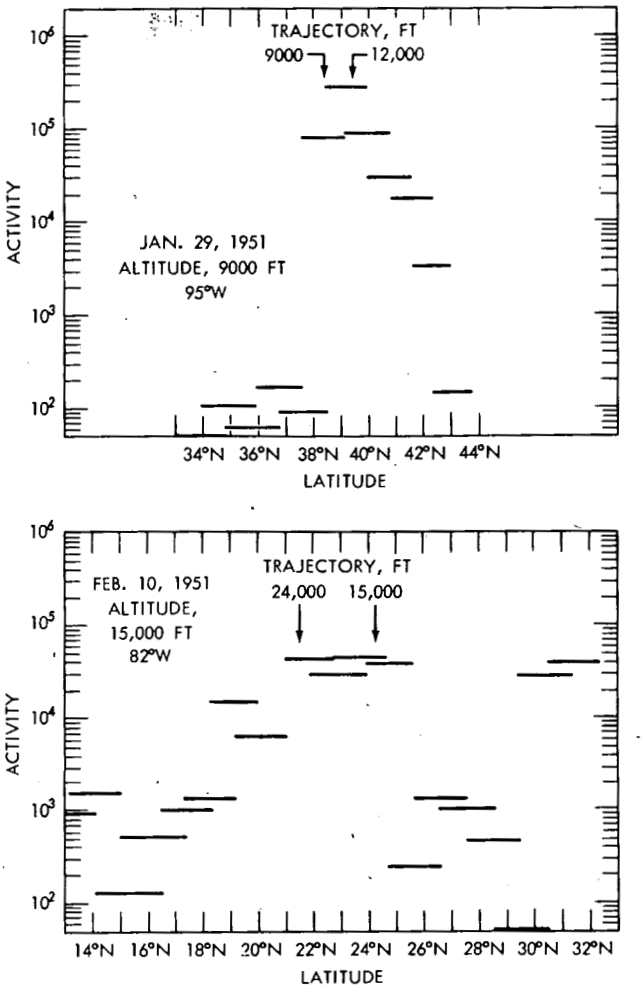

Fig. 7—Aircraft filters obtained in cross-wind flights during Operation Ranger illustrating effect of directional wind shear.

stratospheric fallout. Thus, during and for a month or two following a nuclear test series, the fallout associated with the series is classified as tropospheric fallout; afterwards, the fallout is classified as stratospheric fallout. It has been suggested that shortly after the cessation of a test series, if confusion arises as to the source, the origin of the radioactivity may be obtained from a series of successive ratios of a short-lived to a long-lived isotope. If the decrease with time in the ratio follows the decay of the short-lived isotope, the source is attributed to the stratosphere where scavenging is not present.

Inventory

Any prediction of stratospheric fallout requires quantitative data on the initial distribution of radioactivity in the stratosphere. Sources of data, analytical techniques, and errors in the inventories have been reported elsewhere in detail.[9]

Briefly, between the tropopause and about 70,000 ft, aircraft sampling sponsored by the Defense Atomic Support Agency (DASA) and the U. S. Atomic Energy Commission (AEC) provides the data; between 65,000 and 105,000 ft (occasionally to 120,000 ft) the AEC's balloon sampling program supplies the information. The radionuclides ^{90}Sr and ^{14}C are the two which are adequately measured in the atmosphere to obtain inventories. Results of measurements of these nuclides reported by Machta, List, and Telegadas,[9] together with a few more recent values, are given in Tables 1 and 2. Note that of the items, the oceanic uptake values of ^{14}C and the local fallout of ^{90}Sr have been estimated rather than observed and that the value for the deposited ^{90}Sr has been obtained from the AEC–USDA soil-sampling program and the HASL pot and ion-exchange network. A random error of the total inventory of either the ^{90}Sr or ^{14}C of the order of 40% at the 90% confidence level is quoted. Unfortunately, there is evidence of an unknown systematic error possible due to greater fallout of ^{90}Sr over the oceans than over land.

The tables also list, in the last lines, the amounts of ^{90}Sr and ^{14}C calculated to have been produced from nuclear testing on the basis of the announced fission and fusion yields. Although the conversion from energy yield to amount of ^{90}Sr and, particularly, of ^{14}C may be questionable, it is of interest to note that the observed inventories fall slightly short of those computed. Part of the difference might be due to the presence of ^{90}Sr and ^{14}C above 100,000 ft, and part of the ^{90}Sr discrepancy might be due to the larger oceanic than land fallout. Since the differences between observed and computed inventories are far less than a factor of 2 (indeed, in January 1964 it was only 25%), the two techniques reenforce confidence in the total accountable amount of these nuclides.

History of Forecasting Methods

Soon after Operation Castle at the Pacific Proving Grounds in 1954, it was realized that the continued worldwide fallout could be accounted for best by assuming a stratospheric reservoir of ^{90}Sr with a residence time measured in years. Later, aircraft and balloon measurements confirmed the presence of a large ^{90}Sr and ^{14}C content in the lower stratosphere. Libby[10] was the first to propose a rational forecasting technique for predicting the rate of exit of this debris. Libby considered that a simple exponential removal rate could explain the observed fallout data and be used to predict future fallout. The assumption of a simple ex-

Table 1—GLOBAL ^{90}Sr INVENTORY, MEGACURIES

	May 1960	May 1961	April 1962	January 1963	January 1964
Stratosphere					
Northern hemisphere					
To 21 km	0.25	0.22	1.11	4.51	2.7
21 to 30 km	0.25	0.12	0.13	1.21	0.7
Southern hemisphere					
To 21 km	0.25	0.26	0.21	0.42	0.4
21 to 30 km	0.19	0.12	0.05	0.10	0.2
Troposphere	0.03	0.03	0.16	0.32	0.3
Total in atmosphere					
To 30 km	1.0	0.8	1.7	6.6	4.3
Worldwide deposition	4.3	4.5	5.1	5.8	7.9
Estimated local fallout	2.6	2.5	2.5	2.4	2.4
Total	7.9	7.8	9.3	14.8	14.6
Cumulative production	8.8	8.5	11.1	19.1	18.6

Table 2—GLOBAL EXCESS ^{14}C INVENTORY,* 10^{27} ATOMS

	November 1960	May to June 1961	March to April 1963	July 1963	December to January 1964
Stratosphere					
Northern hemisphere					
To 21 km	2.0	2.4	14.2	14.8	13.4
21 to 30 km	1.2	1.7	6.0	6.5	4.6
Southern hemisphere					
To 21 km	1.7	1.7	2.3	4.1	3.5
21 to 30 km	(0.9)	(1.5)	(1.3)	(1.3)	(1.9)
Troposphere	10.5	11.8	24.5	28.4	28.1
Total in atmosphere					
To 30 km	16.3	19.1	48.3	55.1	51.5
Oceanic uptake	5.1	6.2	12.1	13.4	16.2
Total	21.4	25.3	60.4	68.5	69.4
Cumulative production	24.3	24.3	91.7	91.7	91.7

*Parentheses denote estimates where there were no observations.

ponential fallout rate is equivalent to the assumption of first-order kinetics.

In an exponential formulation, the stratospheric content at time t is given by the simple expression

$$C(t) = C(0)e^{-t/T_m} = C(0)[1 - t/T_m + (2!)^{-1}(t/T_m)^2 - (3!)^{-1}(t/T_m)^3 + \ldots]$$

where C = stratospheric content
T_m = mean residence time
t = time
C(0) = initial content

The mean residence time, the time for the content to reduce to one-half its original content, is related to the half residence time, $T_{1/2}$, by $T_m = T_{1/2}/0.693$. The exponential form is frequently expressed as the fractional removal from the stratosphere per year (or other time interval) when the mean residence time is small so that the square and higher-order terms in the exponential expansion are negligible:

$$\frac{C(t) - C(0)}{C(0)} = \frac{t}{T_m}$$

When t equals one year and the T_m is expressed in years, the ratio t/T_m becomes $1/T_m$ and is the fractional removal per year. Thus a 10-year mean residence time corresponds to a fractional removal rate of 0.1 per year. It should be noted that this approximation breaks down when the mean residence time becomes small, say, less than five years.

The mathematical formulation in which a fixed fraction of the stratospheric content removes to the troposphere per unit of time and vice versa needs no physical rationalization. However, for realistically applying the mathematics, one may argue as follows: Both the stratosphere and troposphere are well mixed layers of the atmosphere, but the interface between the two layers, the tropopause, may be treated as a semipermeable membrane inhibiting the rapid exchange between the two layers. Such a physical model, as in chemical experiments, can be shown to lead to a simple exponential exchange rate.

Unfortunately, the physical attributes of the exponential model do not realistically conform according to meteorological concepts. The troposphere may be well mixed on the time scale of months but the stratosphere is not. Furthermore, the tropopause contains no special inhibiting properties; rather it simply marks the bottom of the stably stratified stratosphere and the top of the more turbulent troposphere. The reason for the longer residence time of debris in the stratosphere than in the troposphere is the lesser vertical mixing (to bring air quickly to the troposphere) and the absence of scavenging mechanisms;

that is, it practically never precipitates from the rare clouds in the stratosphere.

Early estimates of the mean residence time given by Libby ranged from five to ten years based on estimated stratospheric burdens of ^{90}Sr and pitifully incomplete deposition information. In general, most estimates in recent years have been for shorter times than the original values and are based on much more complete information. The simplicity of the method of describing and forecasting stratospheric fallout has led many persons to employ the exponential formulation, even today, despite its limitation.[11]

Problems with the use of a single mean residence time for debris introduced anywhere in the stratosphere arose in the late 1950's. The ^{90}Sr from the autumn 1958 U.S.S.R. tests appeared to return to the troposphere with a mean residence time of one-half year, whereas the experiment with radiotungsten, whose source was the lower equatorial stratosphere, yielded a longer mean residence time. Furthermore, it was felt that virtually no ^{102}Rh from the Orange rocket shot of Aug. 12, 1958, at Johnston Island had reentered the troposphere in the first year after its injection at very high altitudes.

Table 3, modified from a forthcoming report,[11] summarizes some of the observed mean residence times in years. There are three methods by which the mean residence times may be computed. The first and oldest simply compares, say, the annual amount of fallout with the stratospheric content at the beginning of the year. This is the counterpart of the forecasting procedure in which the future annual deposition is derived from the stratospheric content at the beginning of the year. A second procedure compares the stratospheric content at two times, say, the beginning and the end of a year. The decrease readily provides

Table 3—SOME ESTIMATES OF MEAN STRATOSPHERIC RESIDENCE TIMES

Year of measurement	Northern hemisphere		Southern hemisphere		Global	
	^{90}Sr	^{185}W	^{90}Sr	^{185}W	^{90}Sr	^{185}W
1959			3.0*		0.5†	
1960	2.0*		3.8*		2.5*	
1961	1.2*		3.0*		1.8*	
1963	2.1*				2.0*	
1959 and 1960	0.8‡	0.6§	2.9‡	1.8§		0.8§
1960 and 1961	∞‡		∞‡			

*$T_m = 1/\ln [I/(I - F)]$, where I is the stratospheric inventory in January and F the annual deposit.

†Contribution from 1958 U.S.S.R. tests. $T_m = 1/\ln [I/(I - F)]$, where I is the stratospheric inventory in January and F is the annual deposit.

‡$T_m = 1/\ln (F_1/F_2)$, where F_1 and F_2 are the total deposits of one year compared to the next year.

§$T_m = 1/\ln (I_1/I_2)$, where I_1 and I_2 are the stratospheric inventories at the start of one year compared to the start of the next year.

the mean residence time on the assumption that the loss is due to transfer into the troposphere. Finally, a less reliable technique, but one which is independent of stratospheric inventories, compares the observed deposition during two successive years. The decrease in the annual fallout amount suffices to fix both the mean residence time and the stratospheric content with an assumption of an exact exponential decrease in the stratospheric burden with time. This last procedure has provided anomalous results in the period 1960 and 1961 (but before the resumption of tests) when the annual fallout rate during the second year was equal to or greater than the first year. As already noted, the amount of ^{102}Rh increased between the first and second year of fallout, giving rise to a negative mean residence time.

Some of the deficiencies of the simple exponential model may be corrected by several empirical procedures that can incorporate fallout experience and some meteorological thinking. The first attempts to do this were made by Machta,[12] as illustrated in Fig. 8 to 11. In Fig. 8 the stratosphere is subdivided into a series of boxes, each representing a characteristic removal rate. It is argued that empirical knowledge cannot justify further subdivision at this time. The time history of the lower equatorial and the lower northern-hemisphere polar stratosphere appear in Fig. 9. The vertical bars delineate the spring seasons during which the maximum fallout rates are expected. It may be noted that a much greater fraction exits from the stratosphere in the first year

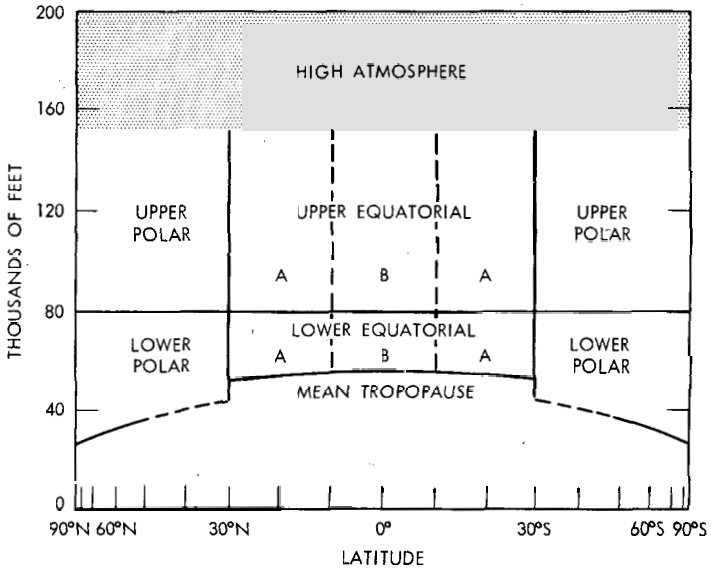

Fig. 8—Schematic subdivision of stratosphere into regions having characteristic removal rates.

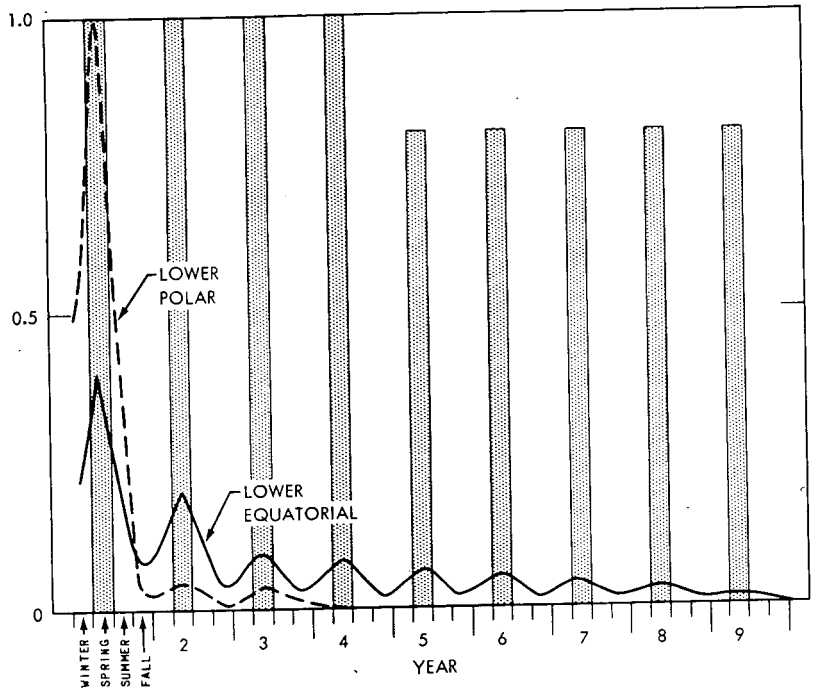

Fig. 9—Expected distribution with time of relative deposition from the lower equatorial stratosphere and from the lower polar stratosphere.

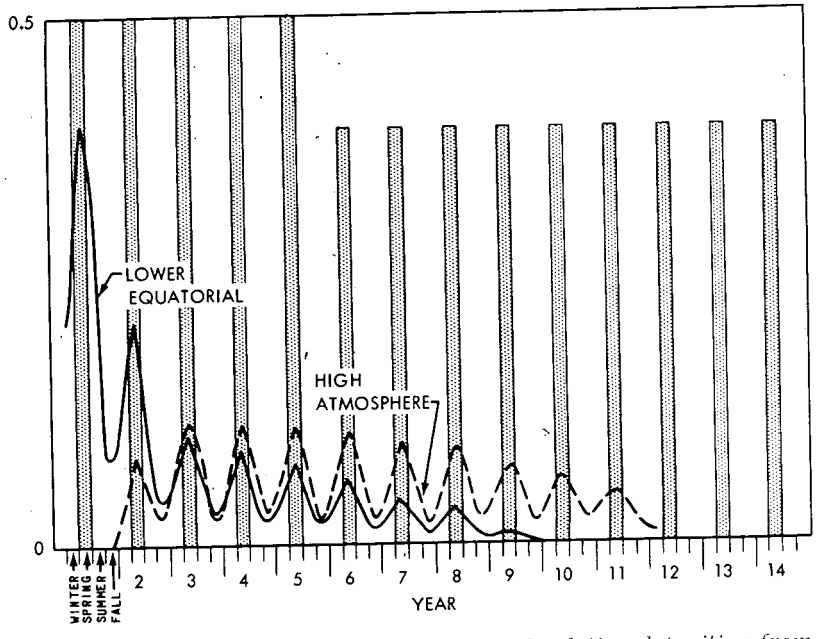

Fig. 10—Expected distribution with time of relative deposition from lower equatorial stratosphere and from the high atmosphere.

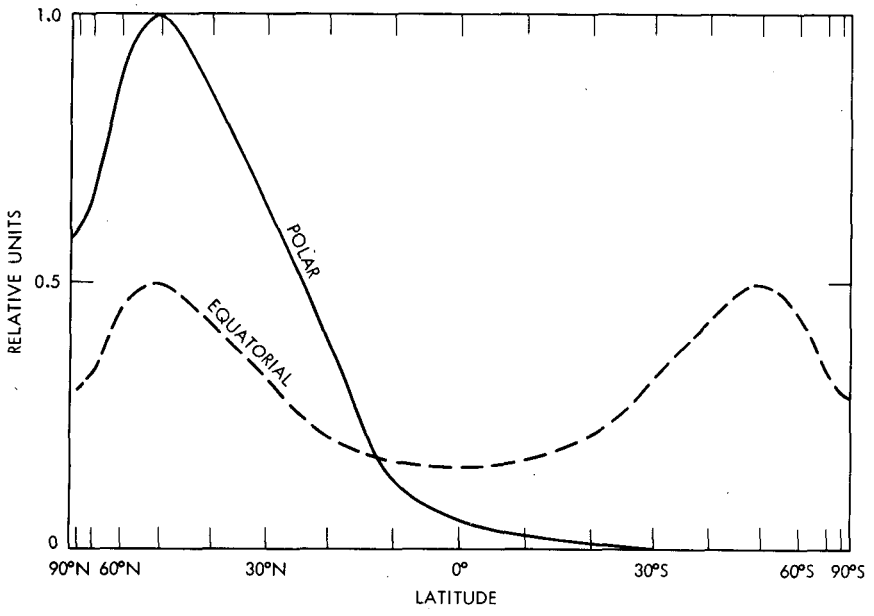

Fig. 11—Comparison of latitudinal distribution of total ^{90}Sr deposition from lower stratospheric injections in equatorial and polar regions.

from a polar period than from an equatorial period. Figure 10 compares the fallout rates for a lower equatorial, high atmospheric source. Although little fallout reaches the earth's surface during the first year from the high-altitude source, the deposition rate remains constant after the second year for an extended period. There is at least one further piece of information necessary to complete the prediction: the knowledge of the geographical distribution of the ^{90}Sr deposition. This distribution is given in Fig. 11. Debris from an equatorial injection partitions equally between hemispheres, but the deposition peaks in temperature latitudes. Strontium-90 introduced into the lower polar stratosphere remains largely in the northern hemisphere. Within each latitude band there are also variations depending on rainfall and other factors.[13]

DASA has produced models similar to that just described in which the atmosphere is subdivided into characteristic boxes. DASA's model is computerized. However, it assumes the exponential model with different residence times in various boxes.

Telegadas and List[14] have suggested a scheme for the prediction of fallout based on the stratospheric content of ^{90}Sr in the lower polar stratosphere. The arguments for the use of this volume of the atmosphere derive both from meteorological considerations and the findings of the Orange rocket ^{102}Rh experiment. Table 4 shows verification of the annual fallout relative to the stratospheric ^{90}Sr content in the volume

Table 4—STRATOSPHERIC ^{90}Sr COMPARED WITH NORTHERN-HEMISPHERE FALLOUT, MEGACURIES

	Stratospheric content below 16.8 km (55,000 ft) at 30 to 90°N	Fallout deposited during following year	
		Predicted	Observed
January 1959	0.7		0.9
May 1960	0.07		0.2
November 1960	0.08		0.2
January 1962	0.9		1.0
January 1963	1.8	2.0	2.1
January 1964	1.1	1.2	

from the tropopause to 55,000 ft and 30 to 90°N. Except for the year following May 1960 or the year following November 1960, the past verification suggests that the northern-hemisphere deposition as measured by the HASL pot and ion-exchange collection network will be slightly more than the ^{90}Sr content of the polar lower stratospheric box. There is no explanation for the failure of the method for the year following May 1960 and the year following November 1960. The last line shows the prediction submitted to the Federal Radiation Council in mid-1964 for the 1964 fallout prediction. The previously mentioned DASA prediction method agrees with this forecast.

Empirical models similar to those just described leave much to be desired in terms of the confidence of the forecast. The models fail to explain why the prediction should be correct; rather they depend on past experience for justification. However, the source configuration rarely duplicates itself, and there is evidence that year to year differences in removal rates exist. It is for these reasons that many groups have been working on realistic models of stratospheric transport.

Theoretical Models

Meteorological models of stratospheric transport may arise from many considerations. First and foremost, they may be started on the basis of certain preconceived rates of vertical and horizontal mixing and organized meridional circulations with the objective of reproducing the patterns of the tracer experiments such as the radiotungsten or the ozone distributions. A second and more fundamental approach is to allow the diffusive and meridional circulation to develop from the heating and cooling of the atmosphere with appropriate boundary conditions in a computer model. Both kinds of considerations are being actively pursued by various investigators.

The Air Resources Laboratory of the Weather Bureau in collaboration with Ben Davidson of New York University and the group at Iso-

topes, Inc., are following one version of the first approach. In it, a preconceived model of mixing and organized circulation (in the meridional plane) is verified by a known tracer experiment. The arbitrary parameters such as the intensities of the horizontal and the vertical eddy-diffusion coefficients and the magnitude of a certain meridional circulation are tested through a time-iterative process. For example, a source at say 56,000 ft and 10°N (simulating the radiotungsten experiment) is inserted at the initial time. Then through an iterative transport process employing Fickian diffusion and a Brewer–Dobson circulation with a certain intensity, an electronic computer determines the concentrations (and some other elements) at all latitudes and heights as a function of time. The computed pattern at a given time may be compared with the observed radiotungsten distribution at the same number of months following the injection. The differences can suggest the way the meteorological parameters should be changed to improve the comparison. An example of the procedure based on a computer model devised by W. B. Ramsay of the Weather Bureau is given as Fig. 12. The source is at the star. After one year of rather rapid circulation, the peak has moved to 45°N latitude. The radiotungsten experiment clearly indicates that this combination of mixing rates and circulation speeds is erroneous.

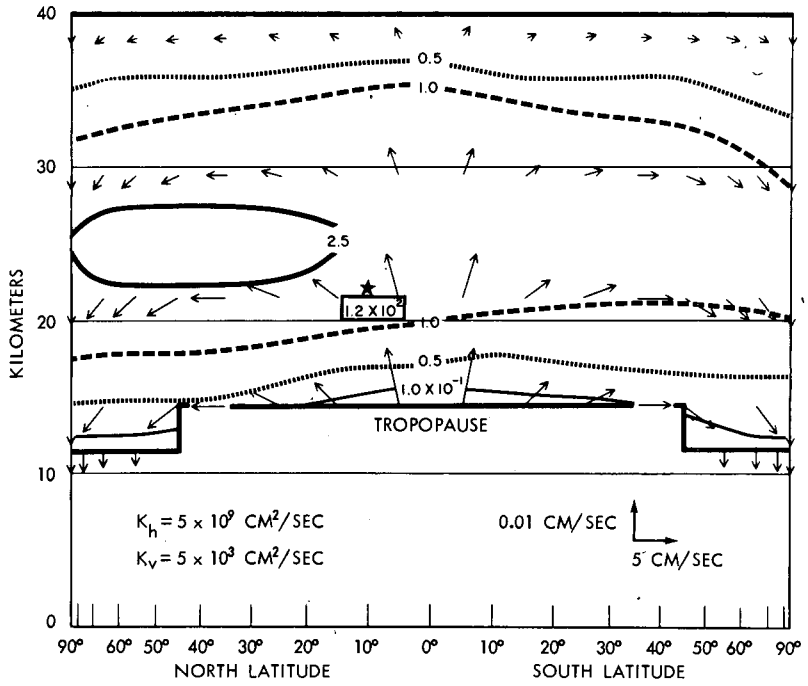

Fig. 12—Stratospheric circulation model showing distribution of contaminant 12 months after an initial injection at 10°N and 22 km.

Sundstrom[15] of Sweden has approached the same problem differently. He assumes that the horizontal and the vertical mixing intensities at a given point are both proportional to the variability of the horizontal component of the wind, an observable quantity. A single proportionality constant converts the wind variability to diffusion constants so that the latter may differ with altitude and latitude. In the first very simplified model, a single meridional circulation cell within each hemisphere was assumed to be present in the stratosphere. By a comparison of the observed ozone distribution in the stratosphere with that expected from an estimate of photochemical production, the two unknowns can be found which yield a best fit between prediction and observation. The first unknown is the factor converting wind variability to diffusion coefficients and the second is the sense and magnitude of the preassigned meridional circulation.

There is one serious defect in the preceding approaches which, if corrected, increases the complexity of either the New York University–Weather Bureau iterative or Sundstrom's statistical methods. This defect may be illustrated in Fig. 13. In this north–south meridional, cross-section isolines of concentration slope downward toward northerly latitudes as radionuclides frequently do in the northern hemisphere. It is assumed that the surface of most intense mixing occurs not along horizontal planes but parallel to sloping lines labeled M. The flux of a tracer substance is directed from north to south along the gradient in the horizontal planes, but the flux along the M surface is from south to north. Since there is no *a priori* reason why the principal mixing ought to be oriented exactly along horizontal surfaces, a mixing model using Fickian diffusion should be capable of allowing the mixing to take place along any arbitrary surface. Davidson's model incorporates this capa-

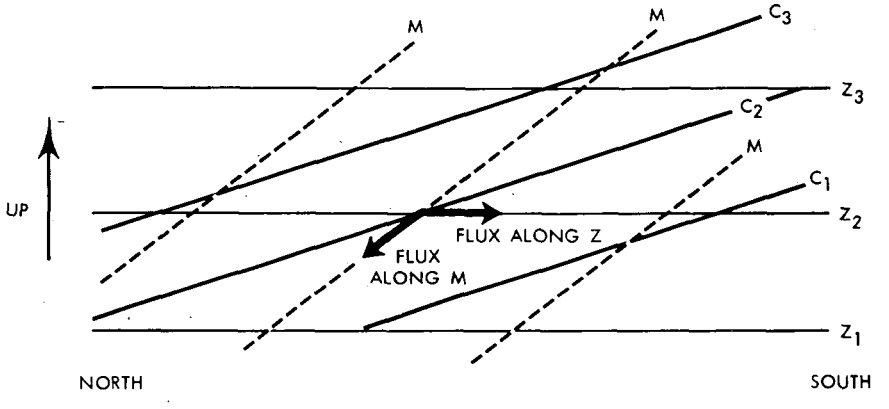

Fig. 13—Schematic diagram of mixing along a sloping surface. Z = height, C = mixing ratio, and M = principal mixing surface.

bility. Now, in addition to the intensity of mixing, the slope of the principal mixing surface also must be specified. This introduces another degree of freedom in specifying the transport processes. Reed[16] has offered a method for determining the slope.

The second approach is to allow a purely meteorological general-circulation model to generate, insofar as possible, the turbulent mixing and organized circulations. The current model of the Geophysical Fluid Dynamics Laboratory of the Weather Bureau is such an example. It is expected that the radiotungsten will be inserted in the stratosphere at its source in this model and then transported by the turbulent and organized circulations. In this way, the likelihood that the air motions generated by the computer approximate reality may be tested. If they do transport the tracer to a realistic distribution and if they subsequently provide good patterns for other substances like ozone, cosmic-ray radionuclides, and ^{14}C, an increasing confidence in the reality of the independently determined transport processes and their magnitudes may be gained.

So far it cannot be said that the prediction of any of the meteorological models is preferred over that obtained from empirical methods. However, it is likely that there will be such a preference in a matter of a few years. If, as is hoped, a single model can reproduce the major features of the distributions of both artificial and natural tracers, the predictions of such a model will undoubtedly be correct in the mean. Only the year to year differences from the mean picture might then present difficulties.

MOST IMPORTANT FALLOUT-FORECASTING NEEDS

Given an injection of contaminants at any arbitrary point in the atmosphere, how well can one predict its subsequent history? This forecast, with reasonable accuracy, is the central need in most pollution problems.

The discussion is made simpler by separating the trajectory from the global aspects. In the former case, most areas will have zero concentrations, but those regions along the path will be finite. Accuracy of prediction of concentration at a given point may be meaningless in the presence of a "yes–no" situation. In global fallout, on the other hand, very large regions contain varying amounts of fallout, and prediction of air concentration or deposition at specific points or limited areas may be described in terms of Gaussian frequency curves.

There have been several studies of the verification of free air trajectories. These, in general, suggest that the true position of an air parcel will lie in a circle around the forecast position with a radius about 20 to 30% of the path length. Unfortunately, there are virtually no verifications of long-range trajectories from ground-level or low-

altitude sources. Although the more abundant weather data in the lower atmosphere should make the low-altitude trajectories more accurate than high-altitude ones (at least after the fact), local topographic irregularities can more than nullify these benefits. Without verification, predicted and after-the-fact reconstructed trajectories are computed in blissful ignorance. It is this gap for which constant-volume balloons, the "tetrons," could potentially provide data. At present, it is likely that most meteorologists feel that the path of a cloud of pollutants at the surface can be as reliably tracked with meteorological data as in the upper troposphere, but detailed proof is virtually nonexistent. Paralleling the absence of trajectory verification data at low altitudes is the lack of experimental data on horizontal and vertical mixing after long travel times.

In the writer's opinion, the long-range transport, diffusion, and removal of contaminants in the lower atmosphere deserve prime attention.

Sources higher in the troposphere also present transport and diffusion problems but, surprisingly, more is known concerning long-range atmospheric behavior, and terrain-induced mesoscale systems may play less havoc with the predictions. One should incorporate, as some investigators have already done, the three-dimensional motion via isentropic analysis and take advantage of high-speed computers. These steps may improve ground-level-contamination predictions during nonprecipitating weather. However, for many, if not most, of the mid- or upper-tropospheric radioactive clouds, the pollutant enters man's environment during precipitation. Although there have been many excellent studies of precipitation scavenging, the fallout forecaster still cannot make a quantitative prediction of deposition in rain; therefore predictions are limited to qualitative statements.

The fate of debris added to the lower stratosphere can be predicted, in a broad way, with more confidence than for debris injected elsewhere in the atmosphere because there has been more experience with such sources. The physical models producing the stratospheric transport have been narrowed to two: one is a version of the Brewer–Dobson circulation and the other is the model for down-the-gradient mixing along sloping surfaces. Both appear to yield similar fallout predictions for injections in most parts of the lower stratosphere. This favorable state of affairs mainly stems from the multitude of nuclear clouds injected into the lower stratosphere and followed by sampling programs of the AEC, the Department of Defense, and the Public Health Service. There is still much to be learned from tracers in the lower stratosphere and much that can be gleamed from meteorological research to improve man's ability to predict stratospheric fallout. However, one has the distinct impression that atmospheric transport and

removal can be predicted better than, for example, the insult of the ionizing radiation to man can be interpreted.

Predicting the fate of injections at higher altitudes in the stratosphere presents a less satisfying picture. Experience from such sources is limited to two man-made injections. Preliminary indications suggest that the arrival times and locations from both are surprisingly similar despite differences in explosion heights. Partitioning between the hemispheres appears to be about equal for injections at 17°N. If the information on source strength is approximately correct, the fallout data suggest that peak ground-level concentrations fall very short of those one would find by diluting the source uniformly into the entire atmosphere. Thus, if a rough calculation, made with the assumption of a uniform distribution throughout the whole atmosphere, suggests no health concern, the use of more sophisticated procedures becomes unnecessary. A major problem in many cases of pollutant transport of a high stratospheric debris is the particulate settling speeds. If there is significant settling out of particulates, extrapolation from past nuclear tests will be incorrect.

REFERENCES

1. L. Machta, Mechanisms for Determining Global Fallout, in Fallout from Nuclear Weapons Tests, Hearings before the Special Subcommittee on Radiation of the Joint Committee on Atomic Energy, Congress of the United States, Vol. 2, pp. 778-806, May 5-8, 1959.
2. L. B. Lockhart, Jr., R. A. Baus, R. J. Patterson, Jr., and A. W. Saunders, Jr., Radiochemical Analyses of Air-Filter Samples Collected During 1958, Report NRL-5390, U. S. Naval Research Laboratory, Aug. 14, 1959.
3. L. Machta, The Nuclear Radiation Program of the International Geophysical Year, Annals of the International Geophysical Year—1964.
4. E. R. Reiter, A Case Study of Radioactive Fallout, *J. Appl. Meteor., 2*(6): 691-705 (1963).
5. J. L. Heffter, The Variation of Horizontal Diffusion Parameters with Time for Travel Periods of One Hour or Longer, *J. Appl. Meteor.*, in press.
6. L. Machta, H. L. Hamilton, Jr., L. F. Hubert, R. J. List, and K. M. Nagler, Airborne Measurement of Atomic Debris, *J. Meteor., 14:* 165-167 (1957).
7. R. J. List, K. Telegadas, and G. J. Ferber, Meteorological Evaluation of the Sources of Iodine-131 Contamination in Pasteurized Milk, *Science, 146:* 59-64 (1964).
8. E. F. Danielsen, The Laminar Structure of the Atmosphere and Its Relation to the Concept of a Tropopause, *Archiv. Meteor. Geophys. Bioklim., A11(3)*: 293-332 (1959).
9. L. Machta, R. J. List, and K. Telegadas, Inventories of Selected Long-Lived Radioisotopes Produced During Nuclear Testing, in Fallout Program Quarterly Summary Report, USAEC Report HASL-142, pp. 243-271, Health and Safety Laboratory, Jan. 1, 1964.
10. W. F. Libby, Radioactive Strontium Fallout, *Proc. Natl. Acad. Sci., 42*(6): 364-390 (1946).
11. United Nations, Report of the United Nations Scientific Committee on the Effects of Atomic Radiation, General Assembly, 19th Session, Suppl. 14 (A/5814), New York, 1964.

12. L. Machta and K. Telegadas, World-wide Fallout since 1959 — Meteorological Aspects, Radiation Standards, Including Fallout, Hearings before the Subcommittee on Research, Development and Radiation, Joint Committee on Atomic Energy, Congress of the United States, Pt. 1, pp. 54-71, June 4-7, 1962.
13. L. T. Alexander, R. H. Jordan, R. J. Dever, E. P. Hardy, Jr., G. H. Hamoda, L. Machta, and R. J. List, Strontium-90 on the Earth's Surface, USAEC Report TID-6567, February 1961.
14. K. Telegadas and R. J. List, Global History of 1958 Nuclear Debris and Its Meteorological Implications, *J. Geophys. Res., 69*(22): 4741-4753 (1964).
15. Sundstrom, unclassified reference not available at this time.
16. R. J. Reed and K. E. German, A Theoretical Note on the Large-Scale Eddy Diffusion of Ozone, to be published in the *Monthly Weather Review*.

SOME ASPECTS OF THE GENERAL CIRCULATION OF THE LOWER STRATOSPHERE

R. E. NEWELL and A. J. MILLER
Massachusetts Institute of Technology, Cambridge, Massachusetts

ABSTRACT

A review is presented of the temperature and wind structure of the lowest 80 km of the atmosphere. The interaction between radiative and dynamic processes to produce the observed temperature distribution is discussed. It is concluded that the lower stratosphere and the mesosphere receive energy from the regions immediately below.

It appears that mass transfer in the lower stratosphere is primarily accomplished by large-scale eddy processes. Forced mean meridional circulations arise from these processes; the possible magnitudes and signs of the mean circulations are examined.

Various terms in the energy budget of the lower stratosphere are presented and discussed for the period of the International Geophysical Year.

INTRODUCTION

The majority of the studies performed by the Planetary Circulations Project with AEC support have been concentrated on the region of the atmosphere between 15 and 30 km. Insofar as many of our findings have indicated that this layer is closely coupled to systems above and below it, it is perhaps appropriate to commence with a brief discussion of some general properties of the circulation below 80 km.

CIRCULATION SYSTEMS BELOW 80 KM

Meridional cross sections of average temperature and zonal wind for winter and summer have been published by several authors (e.g.,

Refs. 1 and 2). In the troposphere temperatures decrease with altitude and latitude in both seasons, and zonal winds have maximum westerly components in middle latitudes at heights of about 12 km. The winter values are the largest. Above the maximums, zonal winds decrease to a transition zone at about 25 km. Temperatures in the 15- to 25-km region vary little with height in middle latitudes but increase polewards to about 60° latitude in winter and 90° in summer. Above 25 km, temperatures increase with altitude to about 50 km and decrease again to 80 km. In winter there is a decrease, and in summer there is an increase polewards in the 25- to 50-km region. The reverse occurs in the 50- to 80-km region. Associated with this temperature structure is another global scale vortex that is westerly in the winter hemisphere and easterly in the summer hemisphere. In addition to these vortexes, there is yet another in the equatorial stratosphere which alternates between westerly and easterly with a 26-month period.

One of the major problems of general-circulation research at the present time is to explain why these particular configurations of temperature and wind occur. The problem has been attacked chiefly by diagnostic studies of the momentum and the energy budgets. Also of particular value have been the concepts of available potential energy as formulated by Lorenz.[4] If we consider the diabatic heating and cooling of the atmosphere by radiative processes, we have the following general picture (based on work by Davis[5] for the upper troposphere, 5 to 15 km; by Kennedy[6] for the 10- to 30-km region; and by Murgatroyd and Goody[7] for the 30- to 80-km region): The low-latitude troposphere is heated by radiation while the higher latitudes are cooled; thus there is a generation of available potential energy. This in turn is converted into kinetic energy by large-scale quasi-horizontal eddy processes that transport heat polewards. Incidental effects are that angular momentum is also systematically accumulated in the upper troposphere in middle latitudes and a westerly jet stream is built up.

The energy-releasing processes are essentially adiabatic motions in which the mean slope of air parcels are about one-half as steep as the mean inclination of potential-temperature surfaces, as pointed out by Eady.[8] In the lower stratosphere, as noted elsewhere,[9–11] the situation is different, with the mean slopes of individual parcels being steeper than the mean isentropic surfaces. Therefore a forced motion, with kinetic energy being converted to potential energy, is implied. As noted at the previous AEC fallout conference,[12] the possibility that poleward-moving parcels are descending and warming adiabatically while equatorward-moving parcels are rising and cooling adiabatically allows one to explain the observations of White,[13] Peixoto,[14] Murakami,[15] and Peng[16] of a countergradient heat flux in the lower stratosphere. It is perhaps worth emphasizing that the concept of these sloping motions in the stratosphere initially was developed from rather

crude measurements of a trace substance, ozone, and was substantiated by ^{185}W measurements.[17]

In the lower stratosphere there is cooling where the air is warm at middle latitudes and heating where it is cold at low latitudes; this leads to a destruction of available potential energy. The loss must be made up from the available potential energy of the eddies, which in turn comes from kinetic energy. The ultimate source of this kinetic energy must be outside the stratosphere. A survey of the energy generated layer by layer indicates that the driving energy for the lower stratosphere must come from the troposphere.

Above 25 km and up to about 50 km, there is cooling in the cold higher latitudes in the winter and maximum warming near the summer pole. This heating configuration obviously again implies a generation of available potential energy, and here the heat-engine region effectively stretches from pole to pole. Above this, as has been discussed elsewhere, there is an additional refrigeration that receives its driving energy from the 25- to 50-km region. For the higher level systems, it appears that in winter large-scale eddies are of most importance in the momentum budget and, by inference, the heat budget of middle and high latitudes, whereas in summer and at low latitudes the observations are not yet sufficient to decide the relative importance of mean and eddy motions.[9,18]

Approximate numerical values of the generation of zonal available potential energy, together with the zonal available potential energy and kinetic energy layer by layer, are shown in Table 1.

A more detailed picture of the conversion of zonal available potential energy to eddy available potential energy is shown in Fig. 1. This is based on our International Geophysical Year (IGY) stratospheric data[16] matched to the wind and temperature data analyzed by Buch[19] and Peixoto.[14] The large negative regions in the troposphere represent

Table 1—DISTRIBUTION OF GENERATION OF ZONAL AVAILABLE POTENTIAL ENERGY, G_z, ZONAL AVAILABLE POTENTIAL ENERGY, A_z, AND KINETIC ENERGY OF ZONAL FLOW, K_z, WITH HEIGHT FOR ZONE FROM 20 TO 60°N, WINTER*

Layer, km	G_z, ergs/cm^2/sec	A_z, ergs/cm^2	K_z, ergs/cm^2
10 to 15	−2.9	11×10^6	460×10^6
15 to 20	−117	60×10^6	120×10^6
20 to 25	1.9	0.3×10^6	6.5×10^6
25 to 30	4.4	0.8×10^6	8.5×10^6
30 to 40	6.9	3.1×10^6	22×10^6
40 to 50	2.7	11×10^5	153×10^5
50 to 60	0.29	0.07×10^5	71×10^5
60 to 70	−0.65	0.9×10^5	24×10^5
70 to 80	−0.15	1.1×10^5	6.1×10^5

*Details of the computational procedure can be found in Ref. 9.

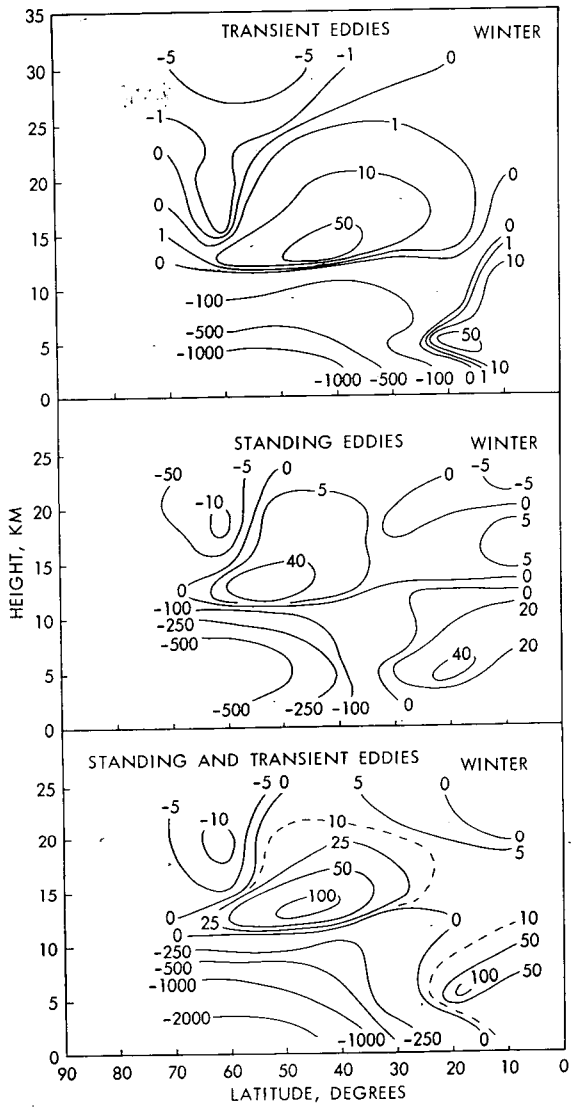

Fig. 1—Distribution of the components contributing to the conversion of zonal potential energy to eddy potential energy, ergs/cm²/sec for a column 2.5 km deep.

a transfer of potential energy from the mean zonal to the eddy state; this is the first step in the atmospheric heat engine after the generation by radiative processes. Additional negative values in the higher latitudes of the stratosphere form a part of the upper-level heat engine. In middle latitudes in the lower stratosphere there is a refrigerated region, and another is evident in the tropics (recently discussed by Starr and Wallace[20]). It is evident from the data that the standing

eddies play a relatively important role in the lower stratosphere, as noted earlier by Murakami.[15] This point will be mentioned again later in the paper. The zone of forced motion in the lower stratosphere has been investigated in detail from IGY data by Barnes[21] and Oort,[10] and both find that zonal available potential energy is created in this region.

MASS TRANSFER

How is mass transported in this system? We may write an equation for the poleward transport in a (hypothetical) meridional plane:[22]

$$[\overline{QV}] = [\overline{Q}][\overline{V}] + [\overline{Q}^*\overline{V}^*] + [\overline{Q'V'}]$$

where Q represents a particular property such as the concentration of a trace substance and V represents the north to south component of the wind. Primes denote deviations from a time average, and asterisks, a deviation from a zonal average; bars denote time averages, and brackets, averages around a latitude circle. The left-hand side of the equation represents the average poleward flux of a property over a given period, say one month. The first term on the right-hand side represents the portion of the total transport due to mean meridional motions, the second is that due to transient eddies, and the third is that due to so-called "standing eddies," which are in reality the quasi-stationary large-scale flow pattern evident on mean maps. A similar equation with the vertical velocity, W, in place of V may also be written, but the terms are difficult to evaluate because of the uncertainties regarding estimates of W.

When Q represents heat or momentum, it has been found that for the lowest 25 km of the atmosphere in extratropical regions the transient and standing eddy terms are sufficient to balance the appropriate budgets. Are they also sufficient to balance the mass budget? The paper presented at the previous AEC fallout conference[12] based upon ozone data suggested that they are in the region of the lower stratosphere.

Prior to 1960 it was generally considered that mean meridional motions were of prime importance in the lower stratosphere. One of the major difficulties of such ideas is that they are not consistent with the findings concerning the momentum and the energy budgets. The equatorward and upward motion of U.S.S.R. debris is also difficult to reconcile with a poleward meridional motion throughout. However, this is not to imply that the meridional motions are unimportant as Barnes[23] emphasized at the previous AEC fallout conference. Since that time three of our colleagues have given thought to the problem. Oort[24] collected all our IGY data (230 stations) on the mean meridional motion and constructed a coherent picture of the results at 100, 50,

and 30 mb. The results indicated a three-cell structure with equatorward drift at middle latitudes, but the values were too large to satisfy the momentum budget. Dickinson[25] has considered the mean meridional motions as being a forced circulation produced by the overall imbalances of other terms in the momentum and the energy budgets. He has estimated the mean meridional motions from the equation for the conservation of momentum alone and finds a three-cell structure similar to that found by Oort. Reproduction of such large values as those observed by Oort required a coefficient of eddy friction in the vertical direction of 10^6 cm^2/sec at 50 mb; this value is certainly too large. It will be recalled that values of 10^4 to 10^3, depending on latitude and season, have been put forward for the lower stratosphere (Friend et al.)[26] based on the spread of ^{185}W. Such values represent the vertical diffusion produced by all scales of motion combined, and it is possible that the large-scale motions produce essentially all the diffusion, in which case the appropriate value remaining to be ascribed to friction is zero.

Another of our colleagues, P. Gilman, has also given much thought to the problems of mean meridional motion[27–29] considered as forced by heat and momentum sources and sinks and has shown theoretically that a three-cell circulation is a necessary consequence of conditions in the lowest 20 km of the atmosphere.

For present purposes let us consider diabatic heating by radiation and by convergence of horizontal-eddy heat fluxes as the only important heat-forcing functions and convergence of horizontal momentum eddy fluxes as the only important momentum-forcing function. Thus friction, vertical flux of heat by eddies, and vertical flux of momentum by eddies are ignored. Clark[30] has demonstrated that the latter is the case for the stratosphere (100 to 30 mb). From our data the heating due to convergence of vertical-eddy heat fluxes is also small compared with the diabatic heating in the lower stratosphere. Estimates of the vertical-eddy heat flux in the troposphere are not very reliable. There are no real observations of friction. Thus the approximations made are partly a matter of expediency. With these assumptions the equations for the mean meridional motion given by Gilman and others simplify to

$$\bar{V} = \frac{H + \dfrac{\Gamma G}{\partial \bar{u}/\partial p}}{\dfrac{1}{a}\dfrac{\partial \bar{T}}{\partial \phi} - \dfrac{\Gamma Z}{\partial \bar{u}/\partial p}}$$

$$H = \frac{\dot{T}}{C_p} - \frac{1}{a \cos \phi}\frac{\partial}{\partial \phi}\left([\overline{V'T'}] + [\bar{V}^*\bar{T}^*]\right)\cos \phi$$

$$G = -\frac{1}{a \cos^2 \phi} \frac{\partial}{\partial \phi} \left([\overline{u'V'}] + [\bar{u}^* \bar{V}^*] \right) \cos^2 \phi$$

$$\Gamma = -T \frac{\partial (\ln \theta)}{\partial p}$$

$$Z = f - \frac{1}{a \cos \phi} \frac{\partial \bar{u}}{\partial \phi} \cos \phi$$

The symbol $\dot{T}$ represents the rate of diabatic heating. The other symbols have their usual meteorological significance. Cross sections of the eddy heat and momentum transports and mean zonal wind and temperature were constructed from the data reported by Buch[19] and Peixoto[14] for the region below 100 mb and from data reported by Murakami[15] and Peng[16] and other, unpublished data for the levels of 100 mb and above. The diabatic heating, $\dot{T}$, was obtained from the work of Davis[5] for the 5- to 10-km region and from the work of Kennedy[6] for the 10- to 30-km region.

The terms in the equation for V were then evaluated at grid points 2.5 km apart in height and 10 degrees apart in latitude. The final results appear in Fig. 2. It is immediately evident that a coherent three-cell structure is present with small equatorward velocities in middle latitudes in both seasons and a larger poleward flow in equatorial regions. The magnitudes in the lower stratosphere are very much lower than those given by Oort.[24] The possible error in the results depends on the accuracy of the cross sections; therefore it is difficult to specify the error quantitatively. Those involving wind velocities are likely to be biased because of the selectivity introduced by the early loss of balloons at high wind speeds (see Ref. 31). In addition, values in the vicinity of the tropics are no doubt dependent on the 26-month oscillation. Latent heat is not included in the diabatic-heating distributions used, but this does not affect the values calculated for the lower stratosphere. In fact, a comparison of the magnitudes of the two terms in the numerator of the equation for V shows that, although the heat-forcing function predominates or is very important in the determination of V at 5 km, its importance decreases with height. In the 12.5- to 17.5-km calculations, the momentum-forcing function is predominant (in numerator and denominator); therefore thermal effects play a secondary role. This pattern perhaps is to be expected since, as we noted earlier, the tropospheric heat engine is driven by the heating effects whereas the lower stratosphere appears to be dynamically coupled to the troposphere.

As far as trace substances are concerned, the preceding findings seem to imply that the mean meridional circulations do not contribute significantly to the mass budget in the middle-latitude lower strato-

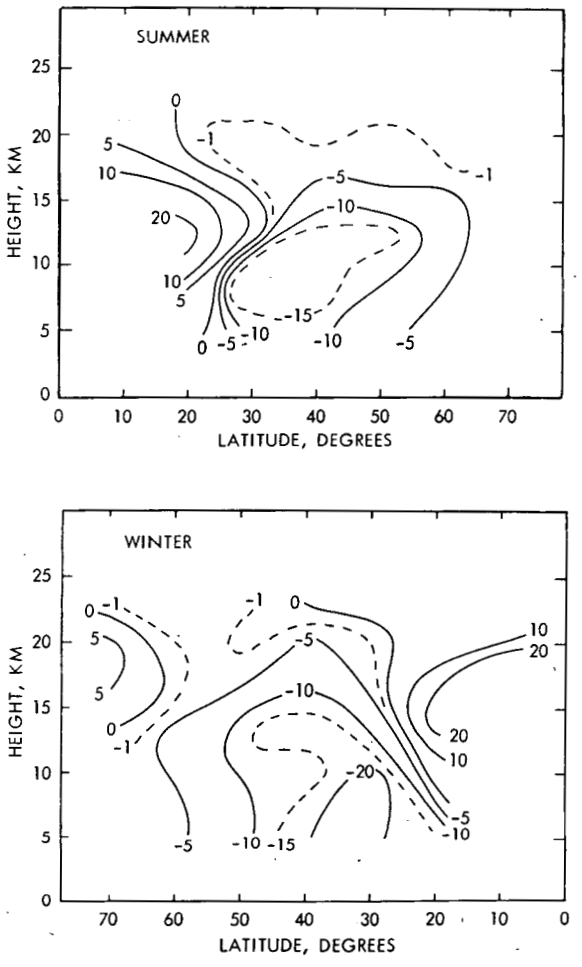

Fig. 2—Mean meridional velocity calculated from approximate heat and momentum-forcing functions, cm/sec.

sphere; it will be recalled that a similar conclusion was reached from considerations of the ozone budget. Hering and Borden[32] have recently reached the same conclusion from a much more comprehensive study of detailed ozone soundings. The role of these mean circulations in the upper tropical troposphere and the stratospheric region immediately above may be quite important. Their effect cannot extend very much into the stratosphere, however, since, as has been noted by many authors in relation to the ^{185}W distributions, the center of gravity of tracer concentrations remains in the vicinity of the equator for two years or more.[33] An altitude limit of about 18 to 19 km seems to be indicated. We may note that similar general findings have been reported over the years by Starr and Peixoto for water vapor in the

lower troposphere. In a recent contribution[34] they find that water-vapor transport in middle latitudes is governed by eddy processes, whereas in the tropics the Hadley cell is dominant in the production of an equatorward flux.

SEASONAL CHANGES IN MASS TRANSFER AND ENERGETICS

At the previous AEC fallout conference, it was demonstrated that the quasi-horizontal eddy processes that carry ozone poleward vary in intensity and accomplish a maximum transport in the early part of the year. The computations have since been extended, and Table 2 shows the combined covariance results for 16 stations in Europe between

Table 2—OZONE–MERIDIONAL WIND COVARIANCE AT THE 100-MB LEVEL WITH THE NUMBER OF CASES IN PARENTHESES

	Centimeters of ozone at S.T.P. × cm/sec			
Year	January–March	April–June	July–September	October–December
1957			3.63 (829)	4.40 (887)
1958	10.29 (908)	−2.49 (1185)	2.60 (1261)	5.12 (1077)
1959	7.63 (424)	2.29 (646)	4.38 (638)	8.81 (519)
Average	9.44	−0.80	3.33	5.63

30 and 60°N. The covariance is between total ozone amounts and 100-mb meridional wind. It has also been demonstrated that the standing-wave contribution to the ozone flux is of comparable size to the transient-eddy contribution in middle latitudes and has a similar seasonal variation.[35]

If these processes also bring more radioactive material down into the troposphere, then one can argue that the spring maximum in fallout is due to an increase in magnitude of the large-scale mixing processes in the lower stratosphere during the early part of the year. Of course, this will be coupled to the seasonal change in large-scale mixing processes which also occurs in the 25- to 30-km region and in layers above.

The extra eddy-mixing of ozone in the lower stratosphere may be brought about by inclined motions that are more steeply inclined in the early part of the year than at other times. Air parcels would thus suffer greater vertical displacements in their passage through the large-scale wave pattern. With this type of mechanism, it can be shown[3] that a potential-energy increase will occur at the expense of kinetic energy; therefore the supply of energy to the region from the troposphere must also increase. Insofar as this vertical flux may depend on the amplitude of the standing waves in the troposphere, ac-

cording to the mechanisms discussed by Eliassen and Palm[36] and Van Mieghem,[37] then there is some circumstantial evidence that it changes with season and has a maximum in the early part of the year.[35]

Let us remember that the preceding paragraph is speculative (it may be useful to guide us in further analysis) and return to the IGY data. From these data various terms in the energy budget of the lower stratosphere (100 to 30 mb) can be estimated. Data from 230 upper air stations have been used. From individual-station data, three-month seasonal averages are calculated for temperature, zonal and meridional wind components, and geopotential in addition to variances and covariances between the various quantities. The three-month means are then plotted on maps, isolines are drawn, and grid-point values are read for the calculation of zonal averages. The entire procedure is carried out for the 00Z and 12Z observations independently. Vertical velocities are calculated by the adiabatic method from the daily station data; observations 24 hr apart are used.[21] Covariances between the vertical velocities and other quantities are calculated and treated as above. Certain of the quantities in the energy budget have already been published[10,21] for portions of the IGY. One of the authors of this paper (A. J. Miller) is presently engaged in a study of the vertical-flux processes in the region for the entire IGY period, and the values of quantities involving vertical velocity presented in Table 3 represent preliminary results from this study. Values for

Table 3—SEASONAL VARIATION OF THE ENERGY BUDGET OF THE LOWER STRATOSPHERE [100 TO 30 MB (16 TO 24 KM)] IN TRANSIENT-EDDY TERMS

	Ergs/cm²/sec					
	July–Sept. 1957	Oct.–Dec. 1957	Jan.–Mar. 1958	Apr.–June 1958	July–Sept. 1958	Oct.–Dec. 1958
Convergence of kinetic energy	−0.23	0.16	−0.40	−0.30	0.18	0.98
Convergence of heat energy	−28.3	−23.9	−35.8	−33.3	1.1	−62.7
Convergence of potential energy	5.3	−1.3	13.4	12.0	9.7	4.2
Conversion of kinetic to potential energy	4.7	7.0	5.2	10.2	3.2	13.3
Generation of zonal available potential energy[6]	−37*		−81†	−77‡		
Conversion of mean zonal available potential energy to eddy potential energy (horizontal part)[10]	−10.4	−13.9	−17.0	−14.5		

*July.
†January.
‡April.

00Z and 12Z are averaged in the table. Convergence terms had to be evaluated from data at 75 and 40 mb; therefore they were, as expected, smaller than the values representing the entire 100- to 30-mb region. It is evident that the convergence of kinetic energy so calculated is much smaller than that of potential energy; caution must be used in interpreting the result as a vertical flux of potential energy. The terms are calculated from adiabatic assumptions, and "vertical" should really be interpreted as "toward lower pressures." The convergence of potential energy supplies energy to the lower stratosphere most of the year. However, it is obviously impossible to make statements about the general case from these results. We shall be in a better position to specify the mean state when a five-year period has been studied. Such a study is presently in progress. In addition, particular case studies such as those pursued by Sekiguchi[38,39] will enable the details of these conversions and flux processes to be examined. The role of standing eddies and the limitations of the observations used for all the vertical flux quantities will be discussed elsewhere.

CONCLUDING REMARKS

The climatological data processed to date have enabled us to construct a broad general outline of the manner in which the lower stratosphere is driven from below. If the ideas presented are correct, then it would appear that the distribution of trace substances in the lower stratosphere is governed by the energy production and vertical flux of energy in the troposphere. We might therefore expect differences between hemispheres, just as there are seasonal effects in each hemisphere. For example, if a good fraction of the driving energy is exported from the troposphere in the form of standing waves, then we would expect smaller vertical fluxes in the southern hemisphere, where these waves are less important, than in the northern hemisphere.[40] Thus one might expect smaller amounts of total ozone to be in the southern hemisphere. Since there is apparently not so much seasonal variation of the standing waves in the southern hemisphere, one might also expect less marked spring maximums in ozone and also, perhaps, in fallout. Part of the long-term plan of the Planetary Circulations Project is to examine circulations of the two hemispheres for similarities and differences.

It should be possible to verify the concepts concerning seasonal changes in slope discussed herein from observational data on trace substances. In particular, the detailed ozone data now available from the ozone sondes will be valuable in this respect; in fact, from the data reported by Hering and Borden,[32] there is a slope change evident with a maximum in the spring; however, the limited longitude coverage must be borne in mind.

ACKNOWLEDGMENTS

We are grateful to Mrs. Dorothy Berry and Mrs. Ann Bracken for their help with the computations.

REFERENCES

1. R. J. Murgatroyd, Winds and Temperatures Between 20 Km and 100 Km — A Review, *Quart. J. Roy. Meteorol. Soc., 83:* 417-458 (1957).
2. R. E. Newell, The Circulation of the Upper Atmosphere, *Sci. American, 210*(3): 62-74 (1964).
3. R. E. Newell, Stratospheric Energetics and Mass Transport, *Pure Appl. Geophys., 58:* 145-156 (1964).
4. E. N. Lorenz, Available Potential Energy and the Maintenance of General Circulation, *Tellus, 7:* 157-167 (1955).
5. P. A. Davis, An Analysis of the Atmospheric Heat Budget, *J. Atmos. Sci., 20:* 5-22 (1963).
6. J. S. Kennedy, Energy Generation Through Radiative Processes in the Lower Stratosphere, S.M. thesis, Report No. 11, Contract No. AT(30-1)2241, Planetary Circulations Project, Massachusetts Institute of Technology, 1964.
7. R. J. Murgatroyd and R. M. Goody, Sources and Sinks of Radiative Energy from 30 to 90 Km, *Quart. J. Roy. Meteorol. Soc., 84:* 225-234 (1958).
8. E. T. Eady, Long Waves and Cyclone Waves, *Tellus, 1:* 33-52 (1949).
9. R. E. Newell, Preliminary Study of Quasi-horizontal Eddy Fluxes from Meteorological Rocket Network Data, *J. Atmos. Sci., 20:* 213-225 (1963).
10. A. H. Oort, On the Energy Cycle in the Lower Stratosphere, Report No. 9, Contract Nos. AT(30-1)2241 and AF19(604)-5223, Planetary Circulations Project, Massachusetts Institute of Technology, 1963.
11. P. A. Sheppard, Atmospheric Tracers and the Study of General Circulation of the Atmosphere, *Repts. Progr. Phys., 26:* 213-267 (1963).
12. R. E. Newell, The Transport of Ozone and Radioactivity in the Atmosphere: Implications of Recent Stratospheric Circulation Findings, in Radioactive Fallout from Nuclear Weapons Tests, USAEC Report TID-7632, pp. 210-222, February 1962.
13. R. M. White, The Counter-gradient Flux of Sensible Heat in the Lower Stratosphere, *Tellus, 6:* 177-179 (1954).
14. J. P. Peixoto, Hemispheric Temperature Conditions During the Year 1950, Sci. Report No. 4, Report AFCRL-63-928, Planetary Circulations Project, Massachusetts Institute of Technology, 1960.
15. T. Murakami, Stratospheric Wind Temperature and Isobaric Height Conditions During the IGY Period, Part I, Report No. 5, Contract Nos. AT(30-1) 2241 and AF19(604)-5223, Planetary Circulations Project, Massachusetts Institute of Technology, 1962.
16. L. Peng, Stratospheric Wind Temperature and Isobaric Height Conditions During the IGY Period, Part II, Report No. 10, Contract Nos. AT(30-1)2241 and AF19(604)-5223, Planetary Circulations Project, Massachusetts Institute of Technology, 1963.
17. R. E. Newell, The Transport of Trace Substances in the Atmosphere and Their Implications for the General Circulation of the Stratosphere, *Geofisica Pura e Appl. (Milano), 49:* 137-158 (1961).
18. C. Leovy, Simple Models of Thermally Driven Mesospheric Circulation, *J. Atmos. Sci., 21:* 327-341 (1964).
19. H. Buch, Hemispheric Wind Conditions During the Year 1950, Final Report, Part II, General Circulations Project, Massachusetts Institute of Technology, 1954.

20. V. P. Starr and J. M. Wallace, Mechanics of Eddy Processes in the Tropical Troposphere, *Pure Appl. Geophys., 58:* 138-144 (1964).
21. A. A. Barnes, Jr., Kinetic and Potential Energy Between 100 and 10 Mb During the First Six Months of the IGY, in Studies of the Stratospheric Circulation, Final Report, Report AFCRL-63-435, pp. 8-31, Planetary Circulations Project, Massachusetts Institute of Technology, 1962.
22. R. E. Newell, The General Circulation of the Atmosphere and Its Effects on the Movement of Trace Substances, *J. Geophys. Res., 68:* 3949-3962 (1963).
23. A. A. Barnes, Jr., General Circulation of the Stratosphere, in Radioactive Fallout from Nuclear Weapons Tests, USAEC Report TID-7632, pp. 204-209, February 1962.
24. A. H. Oort, Direct Measurement of the Meridional Circulation in the Stratosphere During the IGY, Report No. 6, Contract Nos. AT(30-1)2241 and AF19(604)-5223, Planetary Circulations Project, Massachusetts Institute of Technology, 1962.
25. R. E. Dickinson, The Momentum Balance of the Stratosphere During the IGY, in Studies of the Stratospheric General Circulation, Final Report, Report AFCRL-63-435, pp. 132-167, Planetary Circulations Project, Massachusetts Institute of Technology, 1962.
26. J. P. Friend, H. W. Feely, P. W. Krey, J. Spar, and A. Walton, The High-altitude Sampling Program, Final Report, Report DASA-1300, Vol. 3, Defense Atomic Support Agency, 1961.
27. P. A. Gilman, Indirect Measurements of the Mean Meridional Circulation in the Southern Hemisphere, Sci. Report No. 3, Planetary Circulations Project, Massachusetts Institute of Technology, 1963.
28. P. A. Gilman, On the Vertical Transport of Angular Momentum in the Atmosphere, *Pure Appl. Geophys., 57:* 161-166 (1964).
29. P. A. Gilman, On the Mean Meridional Circulation in the Presence of a Steady State, Symmetric, Circumpolar Vortex, *Tellus, 16:* 160-167 (1964).
30. J. R. Clark, Storage and Vertical Transport of Stratospheric Momentum During the IGY, S.M. thesis, Massachusetts Institute of Technology, 1963.
31. C. H. B. Priestley and A. J. Troup, Strong Winds in the Global Transport of Momentum, *J. Atmos. Sci., 21:* 459-460 (1964).
32. W. S. Hering and T. R. Borden, Jr., Ozone Sonde Observations over North America, Environmental Research Paper No. 38, Report AFCRL-64-30(11), Air Force Cambridge Research Laboratories, 1964. (Data were also discussed in paper presented at International Atmospheric Ozone Symposium, Albuquerque, N. Mex., Aug. 31 to Sept. 4, 1964.)
33. R. E. Newell, Transfer Through the Tropopause and Within the Stratosphere, *Quart. J. Roy. Meteorol. Soc., 89:*167-204 (1963).
34. V. P. Starr and J. P. Peixoto, The Hemispheric Eddy Flux of Water Vapor and Its Implications for the Mechanics of the General Circulation, *Arch. Meteorol. Geophys. Bioklimatol., Ser. A, 14:* 111-130 (1964).
35. R. E. Newell, Further Ozone Transport Calculations and the Spring Maximum in Ozone Amount, *Pure Appl. Geophys.*, in press.
36. A. Eliassen and E. Palm, On the Transfer of Energy in Stationary Mountain Waves, *Geofys. Publikasjoner (Oslo), XXII:* 23 pp. (1961).
37. J. Van Mieghem, New Aspects of the General Circulation of the Stratosphere and Mesosphere, *Met. Abh., 36:* 5-62 (1963).
38. Y. Sekiguchi, Energy Variation in the Stratosphere During the Winter Season and Its Relation to Dynamic Stability of the Polar Vortex, Atmospheric Research Laboratory, University of Oklahoma Research Institute, 1963.
39. Y. Sekiguchi, Energy Variation in the Stratosphere During the Winter Season and Its Relation to Dynamic Stability of the Polar Vortex and Ozone Variation, paper presented at the International Atmospheric Ozone Symposium, Albuquerque, N. Mex., Aug. 31 to Sept. 4, 1964.
40. G. O. P. Obasi, Poleward Flux of Atmospheric Angular Momentum in the Southern Hemisphere, *J. Atmos. Sci., 20:* 516-528 (1963).

CADMIUM-109 RESULTS FOR UP TO 20 KM

M. I. KALKSTEIN, A. THOMASIAN, and J. V. NIKULA
Air Force Cambridge Research Laboratories, Bedford, Massachusetts

ABSTRACT

About 0.25 Mc of ^{109}Cd was produced as a unique tracer in the U. S. Starfish test of July 9, 1962, detonated at 400 km above Johnston Island. Subsequent measurements of samples collected up to about 20 km revealed an increase in concentrations at high latitudes in the southern hemisphere in the spring of 1963. This increase was coincident in time with the usual warmings in the southern-hemisphere polar stratosphere. The increase in the northern hemisphere occurred late in the winter of 1963–1964 and did not reach the values measured in the southern hemisphere. Meteorological observations indicate that this winter was quite mild in terms of disturbances in the polar region, with the principal disturbances occurring late in the winter. Stratospheric concentrations measured thus far correspond to roughly one-half of what was expected on the basis of the ^{102}Rh experiment.

INTRODUCTION

About 0.25 Mc of ^{109}Cd was produced as a unique tracer during Operation Dominic I in the U. S. Starfish test of July 9, 1962, detonated at 400 km above Johnston Island.[1] Cadmium-109 (470-day half-life) decays by electron capture to ^{109m}Ag (39 sec), which in turn decays by an 88-kev isomeric transition to the ground state. In addition to the ^{109}Cd, about 0.13 Mc of the long-lived isomer ^{113m}Cd, a 0.58-Mev beta emitter, was calculated as having been produced.[2]

PROCEDURES

Stratospheric filter samples* have been obtained by WU-2 aircraft up to an altitude of 21.3 km. Cadmium is chemically separated by cadmium sulfide precipitations, purified by basic ferric acetate and palladium sulfide scavengings, and finally electroplated from a cyanide solution. Yields generally range between 40 and 80%. Counting of the samples is accomplished by measuring the silver K X rays (about 22 kev energy) with a small, thin scintillation detector and a pulse-height analyzer. Conversion to absolute decay rates is based on an intercalibration performed by several laboratories on a ^{109}Cd source circulated by the AEC Health and Safety Laboratory.

RHODIUM REVIEW

The ^{109}Cd experiment is the second tracer experiment. Its predecessor was the ^{102}Rh tracer associated with the Orange rocket shot of Aug. 12, 1958, detonated during Operation Hardtack I at about 43 km above Johnston Island.[3] In part, the ^{109}Cd tracer experiment was meant to check findings from the ^{102}Rh experiment as well as to provide new information. Briefly, the major findings of the ^{102}Rh experiment were that there were (1) a delay of over a year before the appearance of a sizable fraction of the tracer at about 20 km, (2) an apparent major influx from high altitudes into the lower stratosphere taking place at high latitudes in the winter season, and (3) a predominance of the debris at 20 km at high latitudes (above 30°) in both hemispheres with considerably lower concentrations at low latitudes.

CADIUM RESULTS

The first observations of ^{109}Cd in the stratosphere were reported by Salter.[4] Beginning in December 1962, balloon samples collected at above 30 km in the southern hemisphere showed the presence of the tracer.

Our studies to date have been confined to altitudes of about 20 km and below. The first of our samples that obviously indicated the presence of ^{109}Cd were collected in mid-1963; however, some earlier samples indicated the possible presence of this tracer. The results obtained to date are shown in Fig. 1.

*Samples have been provided through the assistance of Capt. Adrian Polk of the Defense Atomic Support Agency, by H. W. Feely of Isotopes, Inc., and by the 4080th Strategic Wing, U. S. Air Force, Davis-Monthan Air Force Base.

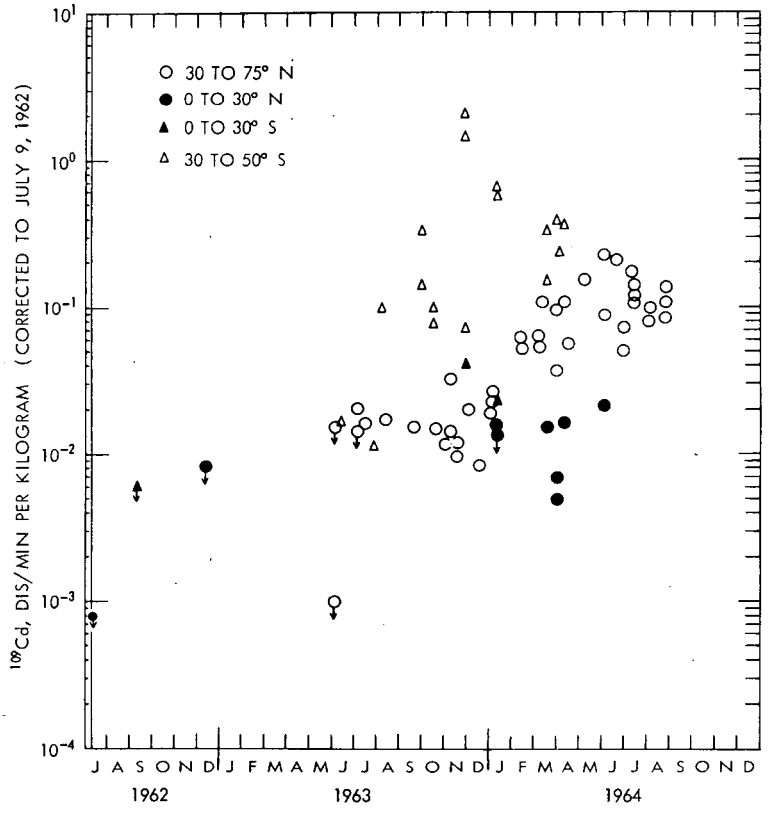

Fig. 1—Cadmium-109 concentrations above 19.2 km.

DISCUSSION

The first appreciable rise in ^{109}Cd concentrations did not occur until the beginning of the southern-hemisphere spring of 1963 with concentrations reaching a maximum value at the end of November at high latitudes in the southern hemisphere. This is approximately three months later than the corresponding observations for the increase of ^{102}Rh in the northern hemisphere during the winter of 1959–1960. This is consistent with the difference in timing between hemispheres for the major winter disturbances in the polar vortex region.[5] Concentrations in the southern hemisphere dropped off markedly after November. This decrease suggests that perhaps the November samples (44 and 48°S) represented a hot spot.

The northern-hemisphere winter of 1963–1964 has been characterized as being quite mild in terms of disturbances in the polar region,

with the principal disturbances occurring late in the winter.[6] This also is reflected in the measurements of the concentrations of ^{109}Cd, with the high-latitude increase in the northern hemisphere first beginning about December or January and reaching high levels in March and April of 1964. In addition, the northern-hemisphere concentrations have been consistently lower than those in the southern hemisphere.

The latest stratospheric concentrations presented here correspond roughly to one-half of what was expected on the basis of the ^{102}Rh experiment. This could be due to less than average transport of the ^{109}Cd tracer to the low stratosphere, escape of some of the tracer from the earth's magnetic and gravitational field, or a lower production of the ^{109}Cd than 0.25 Mc. The last possibility would be consistent with the value of about 0.12 Mc estimated by Cowan.[7]

REFERENCES

1. U. S. Atomic Energy Commission Health and Safety Laboratory Cadmium-109 Conference, Dec. 6, 1963. (A "best" estimate of 0.25 ± 0.15 Mc of Cd^{109} was arbitrarily adopted.)
2. I. J. Russell and R. V. Griffith, The Production of Cd^{109} and Cd^{113m} in a Space Nuclear Explosion, in Fallout Program Quarterly Summary Report, USAEC Report HASL-142, pp. 306-322, Health and Safety Laboratory, Jan. 1, 1964.
3. M. I. Kalkstein, Rhodium-102 High Altitude Tracer Experiment, *Science, 137:* 645 (1962).
4. L. P. Salter, in U. S. Atomic Energy Commission Health and Safety Laboratory Cadmium-109 Conference, Dec. 6, 1963.
5. H. Wexler, Seasonal and Other Temperature Changes in the Antarctic Atmosphere, *Quart. J. Roy. Meteorol. Soc., 85:* 196 (1959).
6. W. S. Hering, Air Force Cambridge Research Laboratories, private communication, July 1964.
7. G. A. Cowan, memorandum to the U. S. Atomic Energy Commission Health and Safety Laboratory Cadmium-109 Conference, Dec. 6, 1963.

STRATOSPHERIC RADIOACTIVITY IN THE SOUTHERN HEMISPHERE FROM 1961 AND 1962 WEAPON TESTS

LEONARD P. SALTER
Health and Safety Laboratory, U. S. Atomic Energy Commission,
New York, New York

ABSTRACT

An evaluation of data from air-filter samples collected between 60,000 and 105,000 ft at 34°S gives some indication of the ^{90}Sr concentrations for nuclear debris attributable to the 1961 U.S.S.R. test series and to Starfish Prime, the U. S. detonation at 400 km on July 9, 1962.

Strontium-90 from the 1961 U.S.S.R. series was present in small amounts below 70,000 ft at 34°S throughout 1962 and may have been a significant component of the relatively large levels observed above 100,000 ft in late 1962 and early 1963. This material probably accounted for a major part of the fivefold increase in ^{90}Sr concentration from April to June 1963 between 70,000 and 90,000 ft. We ascribe the 1961 debris above 70,000 ft to the approximately 25 Mt shot of the series.

As deduced from measurements of ^{109}Cd, Starfish Prime debris first appeared within the range of the sampling program in December 1962 at 105,000 ft at 34°S. By mid-1964 it was present throughout the stratosphere of both hemispheres. The distribution of this material appears similar to that from Orange, the high-altitude rocket shot of August 1958. The following movements broadly describe the dominant features of the distribution pattern: (1) rapid horizontal spreading at high altitudes, (2) subsidence into the polar stratosphere, and (3) movement in the stratosphere toward the equator in the hemispheric spring and summer.

INTRODUCTION

The establishment of a balloon-sampling station at Mildura, Australia, in early 1961 provided an opportunity for studies of nuclear debris in the stratosphere of the southern hemisphere in greater detail than during the period of weapons testing in the 1950's. Some results for such debris from the 1961 and 1962 test series are discussed here. Data will be presented on the fraction of stratospheric ^{90}Sr at 34°S attributable to the 1961 U.S.S.R. series and to Starfish Prime,* the U. S. detonation of July 9, 1962, during Operation Dominic I at 400 km above Johnston Island at 17°N.

The presence of debris from these detonations in the stratosphere of the southern hemisphere and its contribution to the total ^{90}Sr are of considerable interest both for determining the transport mechanisms for radioactive materials injected into the atmosphere from a nuclear detonation or the burnup of a nuclear-powered satellite device and for predicting fallout patterns for such atmospheric contaminants.

Mildura, Australia, at 34°S, is one of the two stations from which high-altitude samples have been collected on a regular basis since 1961 under a program sponsored by the AEC. Balloon-borne filtering devices using IPC 1478 filter paper are operated under contract with the Department of Supply, Commonwealth of Australia. Duplicate samples have been collected monthly at 50,000, 60,000, 70,000, 80,000, and 90,000 ft from 1961 to mid-1962 and at 65,000, 80,000, 90,000, and 105,000 ft since mid-1962. A similar collection schedule has been carried out for the AEC by Detachment 1, 6th Weather Squadron, Goodfellow Air Force Base, San Angelo, Tex., at 31°N. The sampling program now includes sites at 9 and 65°N operated on an alternating basis.

Filters are sent to the Health and Safety Laboratory (HASL) where gamma spectra are obtained. One sample from each pair collected is then radiochemically assayed for several fission products and other radionuclides produced by weapons testing. Most of the analyses on samples collected since early 1962 have been performed by Isotopes, Inc., Westwood, N. J. Results of total gamma activity measurements and radionuclide analyses are reported quarterly.[1–4]

1961 AND 1962 ATMOSPHERIC TESTS

Between the resumption of weapons testing by the U.S.S.R. on Sept. 1, 1961, and the end of 1962, several nuclear test series in the atmosphere took place.[5,6] These are summarized in Table 1. The column headed "mean date for series" in Table 1 is used as the mean formation time for the production of radionuclides for the series.

*Starfish Prime is referred to as Starfish throughout.

Table 1—SUMMARY OF 1961 AND 1962 ATMOSPHERIC TESTS

Detonation	Inclusive dates	Latitude	Mean date for series	Fission yield, Mt
U.S.S.R.	Sept. 1–Nov. 4, 1961	52°N, 75°N	Oct. 15, 1961	17
U.S.S.R.	Oct. 23 (~25 Mt)	75°N	Oct. 15, 1961	8
U.S.S.R.	Oct. 30 (~55 Mt)	75°N		
United States	Apr. 25–July 11, 1962	2°N	July 1, 1962	11
United States	July 9, 1962*	17°N		
United States	Oct. 2–Nov. 4, 1962	17°N	Oct. 15, 1962	
U.S.S.R.	Aug. 5–Nov. 17, 1962	52°N, 75°N	Oct. 15, 1962	60
U.S.S.R.	Dec. 18–Dec. 24, 1962	52°N, 75°N	Dec. 20, 1962	

*Starfish Prime detonation at 400 km.

The 1961 U.S.S.R. test series has been subdivided into three components since data obtained at 31°N in 1962 suggests that each of these components may have followed significantly different distribution patterns. The altitude profiles for long-lived ^{90}Sr concentrations, ^{95}Zr (65-day half-life)/^{90}Sr, and ^{54}Mn (310-day half-life)/^{90}Sr activity ratios are shown in Fig. 1 for February 1962 at 31°N. Manganese-54 is a neutron-activation product rather than a fission product, and one may reasonably presume, therefore, that it was produced in largest quantities in the 55-Mt thermonuclear detonation of Oct. 30, 1961, in which the highest neutron flux was produced. These data show that (1) a considerable fraction of new debris, indicated from high values for the $^{95}Zr/^{90}Sr$ ratio, was present at 60,000, 90,000, and 105,000 ft but only traces at 70,000 and 80,000 ft; (2) the largest quantity of new debris was at 60,000 ft where both $^{95}Zr/^{90}Sr$ and total ^{90}Sr were the greatest; (3) the new debris at 60,000 and 105,000 ft was low in ^{54}Mn, whereas that at 90,000 ft contained relatively large amounts of ^{54}Mn. The following hypotheses may be made to explain these observations: (1) debris from all the 1961 U.S.S.R. tests except the 25- and 55-Mt thermonuclear events stabilized below 70,000 ft; (2) fresh debris at 90,000 ft was due primarily to the 55-Mt device for which the activity ratio of $^{54}Mn/^{90}Sr$ at formation was about 100, a value determined from the observed ^{54}Mn and a calculation for the new ^{90}Sr based on the observed ^{95}Zr and the expected $^{95}Zr/^{90}Sr$ formation ratio; (3) fresh debris above 100,000 ft came from a shot other than the 55-Mt detonation (either from the 25-Mt shot or from one or more unannounced high-altitude detonations). If the 25-Mt device accounted for this new material, a large fraction of the debris from this shot may have been present above the maximum sampling altitude of 105,000 ft.

Neutron-activation products other than ^{54}Mn, such as ^{55}Fe and ^{124}Sb, were also found in the stratosphere after the 1961 U.S.S.R. test series.[3] Additional quantities of these radionuclides, as well as ^{88}Y, were produced in the 1962 atmospheric tests.[4] Their use as tracers for

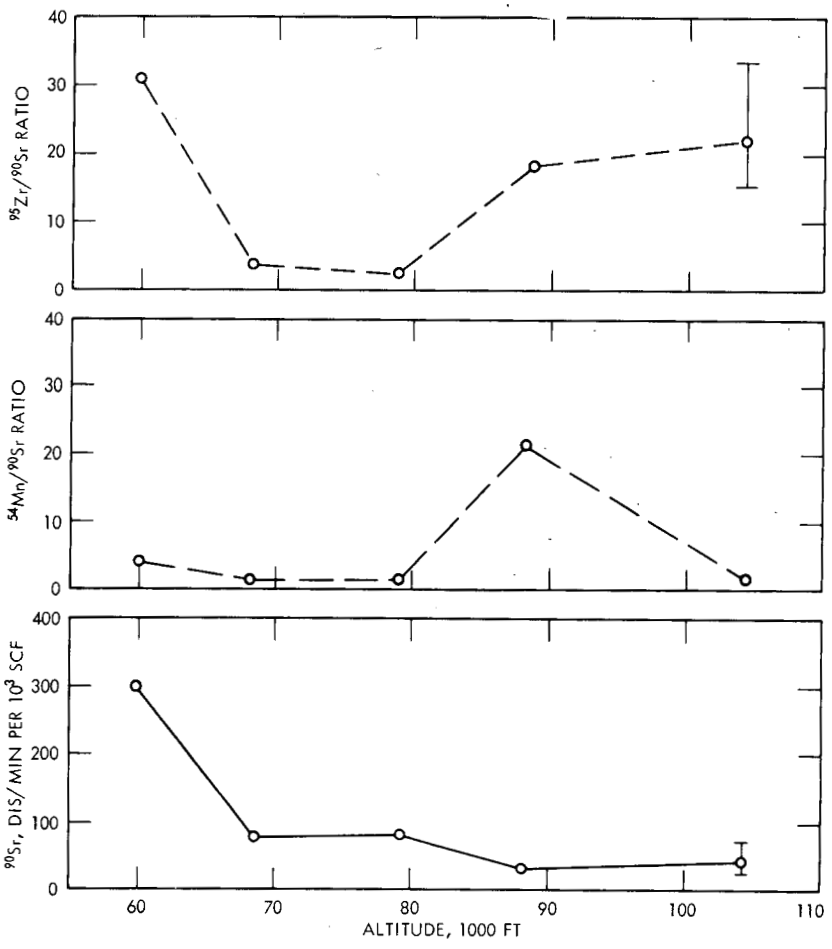

Fig. 1—Activity concentrations of ^{90}Sr and activity ratios for $^{54}Mn/^{90}Sr$ and $^{95}Zr/^{90}Sr$.

1961 debris, therefore, became increasingly difficult as material from the 1961 and 1962 tests mixed.

The only other shot for which published information indicates unique tracers exist is Starfish, detonated July 9, 1962. In this 1.4-Mt detonation, an estimated 250 ± 150 kc of ^{109}Cd (470-day half-life) and about 25% as much ^{113m}Cd (14-year half-life) were produced.[7,8] On the basis of an assumed fission to total yield of 50% and no fractionation, a $^{109}Cd/^{90}Sr$ activity ratio of 3.5 ± 2.0 may be calculated. If escape from the ionosphere occurred for neutron-activation products relative to the highly charged fission products, then the $^{109}Cd/^{90}Sr$ activity ratio would be correspondingly smaller.

1962 AND 1963 STRATOSPHERIC ACTIVITY AT 34°S

To some extent the levels of nuclear debris at 34°S may be followed by measurements of total gamma activity. These are particularly useful in defining incursions of new debris or other changes in the regime of material, especially when the ^{90}Sr concentrations are only slightly affected. Figure 2 shows the gamma activity concentrations at 34°S since 1962. From these data the following increasing activity trends appear to be the most significant at 34°S in 1962 and 1963: 65,000 ft from July to September 1962, 80,000 ft from August to November 1962, 105,000 ft in December 1962, 90,000 ft from December 1962 to June 1963, 80,000 ft from April to June 1963, and 65,000 ft in September 1963.

A study of the fission-product radionuclides ^{140}Ba (12.8-day half-life), ^{95}Zr (65-day half-life), ^{144}Ce (285-day half-life), and ^{90}Sr (27.7-year half-life), as well as the cadmium isotopes and ^{54}Mn, permits some evaluation of the origin of debris that accounts for these increases. Published radiochemical data[3,4] corrected for laboratory bias were used for this study. These were augmented by radiochemical results for ^{109}Cd and ^{113m}Cd obtained at HASL and spectral analysis for ^{140}Ba, ^{95}Zr, and ^{54}Mn.

The fission-product results are used in equations of the following general form to calculate values for A_n, the activity concentration on the sample-collection date of nuclide A produced in the *nth* test series:

$$A_{tot} = \sum A_n$$

$$\frac{B_n}{A_n} = Ze^{-(\lambda_B - \lambda_A)T_n}$$

where A_{tot} = total activity concentration of A on the collection date
Z = formation activity ratio of fission product B to fission product A
λ_B and λ_A = decay constants of fission products B and A, respectively
T_n = time elapsed between the series formation date and the sample collection date

The values of T_n are calculated from the "mean date for series" given in Table 1. The formation-activity-ratio values, Z, are calculated from data on fission yields for a typical thermonuclear device.[9] They are given in Table 2 with the ratio half-lives. In weapons tests, however, fission yields and, therefore, activity ratios vary significantly depending on the energy spectrum of prompt neutrons emitted and the fissionable materials present. The use of a single-valued constant determined from a typical device for the average formation ratio for all series may introduce a considerable error into the evaluation.

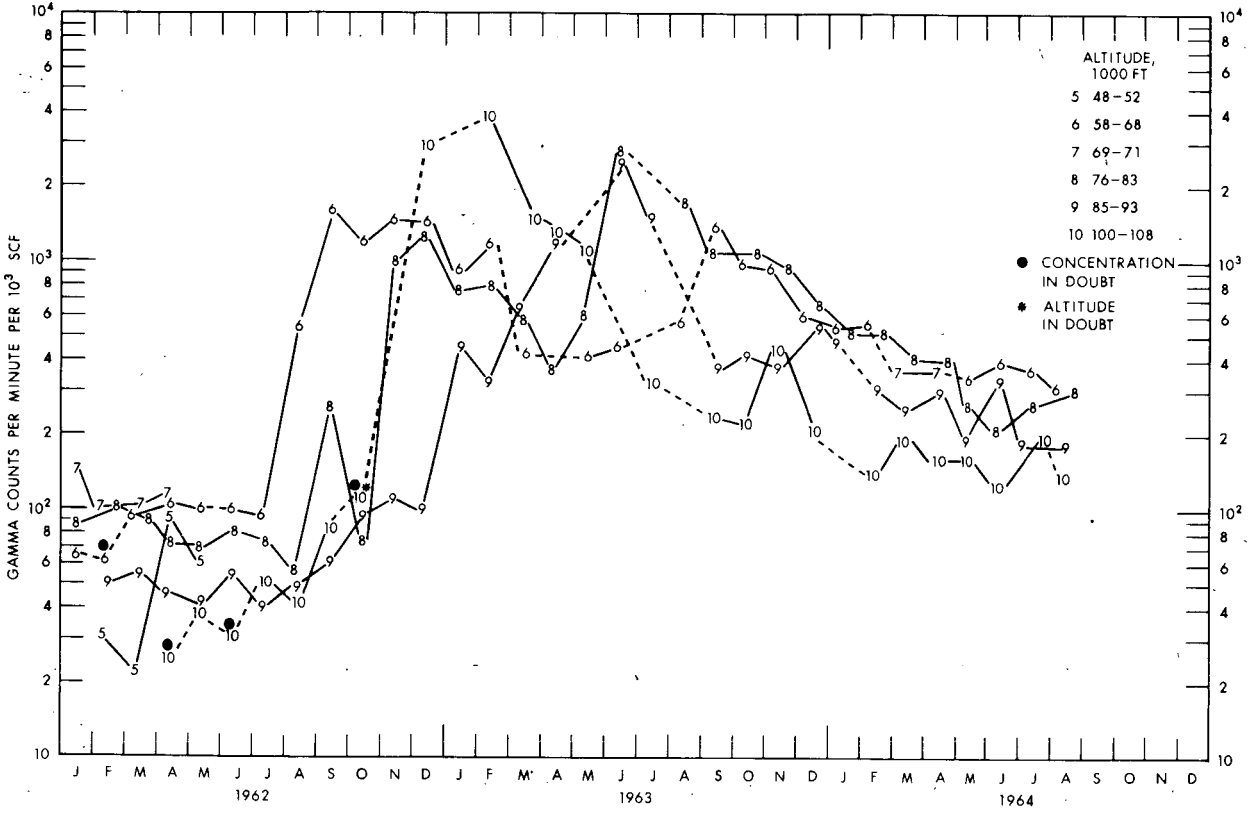

Fig. 2—Gamma activity concentrations at 34°S at Mildura, Australia.

Table 2— FORMATION ACTIVITY RATIOS FOR FISSION PRODUCTS FROM A TYPICAL THERMONUCLEAR DEVICE

Nuclide ratio, B/A	Formation activity ratio, Z	Ratio half-life, days $[\ln 2/(\lambda_B - \lambda_A)]$
$^{140}Ba/^{95}Zr$	5.2	15.9
$^{89}Sr/^{95}Zr$	0.65	227
$^{91}Y/^{95}Zr$	0.82	639
$^{95}Zr/^{144}Ce$	4.7	84
$^{144}Ce/^{90}Sr$	48	293
$^{137}Cs/^{90}Sr$	1.45	$\sim 10^5$

CONTRIBUTIONS FROM THE 1961 U.S.S.R. TESTS

The concentration profiles for total ^{90}Sr at 34°S are given in the second column of Table 3 for several periods in 1962 and 1963. The calculated fractions attributable to the 1961 U.S.S.R. test series are given in the third column.

The results indicate that 1961 debris was present in the lower stratosphere in the first half of 1962, accounting for a few percent of the total ^{90}Sr. It was undetectable above 70,000 ft although a few high, but suspect, $^{144}Ce/^{90}Sr$ values suggest that traces might have been present at 105,000 ft. The fresh debris accounting for increased gamma activity concentrations at 65,000 and 80,000 ft in August and September was due to the Dominic I series, April through July 1962, that increased the ^{90}Sr levels just slightly above that attributable to pre-1961 debris. Only for the latter part of the year at 65,000 and 105,000 ft is it possible to assign more than 10% of the ^{90}Sr to the 1961 tests, as may be seen from the December data. Although the higher gamma activity concentration at 105,000 ft may in part be explained as being attributed to the 1961 debris, the larger fraction of postmoratorium material at this latitude came from 1962 tests.

Additional ^{90}Sr from 1961 tests at the high altitudes sampled is suggested by the April 1963 data. However, it was in June at 77,000 and 86,000 ft, when the gamma activity concentrations were at their peak and the total ^{90}Sr had increased by a factor of 5 over April levels, that the largest amounts of 1961 debris appeared to be present: up to 500 dis/min per 10^3 scf.

Conclusions about these levels of 1961 U.S.S.R. debris must be reserved until evidence that the fission-product formation ratios for a typical device which were used in the calculations approximate the average for weapons detonated in 1961 and 1962. If, for instance, the average $^{144}Ce/^{90}Sr$ ratio for Dominic I was 40 instead of 48, it is pos-

Table 3—STRONTIUM-90 CONCENTRATIONS AT 34°S IN 1962 AND 1963

Altitude, 1000 ft	^{90}Sr concentration, dis/min per 10^3 scf			
	Total	1961 U.S.S.R.	Maximum from 55-Mt test	Starfish
		February–July 1962		
50	10–30	~1	*	
60	60–110	~1	*	
70	60–80	*	*	
80	40–90	*	*	
90	30–40	*	*	
105	10–20	?	*	
		September 1962		
63	110	<10	*	
78	55	*	*	
90	20	*	*	
100	20	?	*	*
		December 1962		
63	130	20	~2	*
78	80	<10	<2	*
89	25	*	<3	*
105	100	30	~2	20
		April 1963		
77	75	~2	~1	*
91	120	10	<3	20
104	130	40	<2	30
		May 1963		
66	115	30	<2	*
104	130	80	10	<1
		June 1963		
67	130	30	10	~1
77	620	450	30	~1
86	600	500	30	<1
		October 1963		
68	380	250	20	2
80	370	250	20	20

*Negligible.

sible to assign a considerable fraction of the ^{90}Sr attributed here to the 1961 series to these later tests; and, if it was 32, all of it.

It is of interest to estimate what the major source of the debris that was assigned to the 1961 tests might have been. The detonations which reached into the lower stratosphere listed in the first line of Table 1 may account for the 1961 debris below 70,000 ft at 34°S, but they are unlikely to be the source of material observed at the higher

altitudes. An upper limit for the amount of ^{90}Sr from the 55-Mt test may be determined by assuming that the total ^{54}Mn found in the sample came from this device and applying the calculated value of 100 for the $^{54}Mn/^{90}Sr$ ratio. These results, given in the fifth column of Table 3, indicate that this detonation can at most account for only a small fraction of the ^{90}Sr attributed to the whole series. If the 1961 debris is indeed present to the extent shown, it is probable that the major source was, therefore, the 25-Mt device. This is consistent with the hypothesis presented earlier that most of the material from this device reached altitudes considerably above 100,000 ft from where it spread laterally across the equator and then mixed downward, appearing in significant amounts at 105,000 ft in late 1962 and at successively lower altitudes in 1963.

CONTRIBUTIONS FROM STARFISH

Cadmium-109 was first observed in samples collected from 105,000 ft at 34°S in December 1962. This marked the initial appearance of debris from Starfish in the balloon sampling-program range about five months after its injection into the ionosphere at 17°N. Concentration profiles for ^{109}Cd through mid-1964 are summarized in Fig. 3. All ^{109}Cd data have been corrected to July 9, 1962. The ^{109}Cd to total observed ^{90}Sr activity ratios are given under the ^{109}Cd concentration values.

The results for ^{109}Cd at 34°S show that Starfish debris had descended as low as 90,000 ft in early 1963 and then apparently shifted completely outside the sampling range in May. It reappeared in July, and, by the end of the year, debris was present at all altitudes sampled at 34°S in significant amounts. By mid-1963, one year after its production, only traces of ^{109}Cd had been detected at 31°N, but a few results in samples collected from 45°N and 65°N at that time indicated ^{109}Cd concentrations comparable to those observed earlier at 34°S.

In March 1964, ^{109}Cd concentrations at 34°S showed a decrease with altitude from 40 dis/min per 10^3 scf at 70,000 ft to 25 dis/min per 10^3 scf at 105,000 ft; at 31°N they ranged from less than 2 dis/min per 10^3 scf at 65,000 ft to 18 dis/min per 10^3 scf at 105,000 ft. In June 1964, ^{109}Cd was present in slightly higher concentrations in the northern polar stratosphere than at 31°N.

The ^{109}Cd data delineating the movement of debris from Starfish are generally consistent with that for ^{102}Rh produced in the Orange rocket shot, the U. S. high altitude test of Aug. 11, 1958, at 17°N during Operation Hardtack I which has been discussed by Kalkstein[10] and Telegadas and List.[11]

Although ^{102}Rh data above 70,000 ft are not available for the first year after the Orange shot, high $^{144}Ce/^{90}Sr$ ratios[11,12] from 90,000 ft at

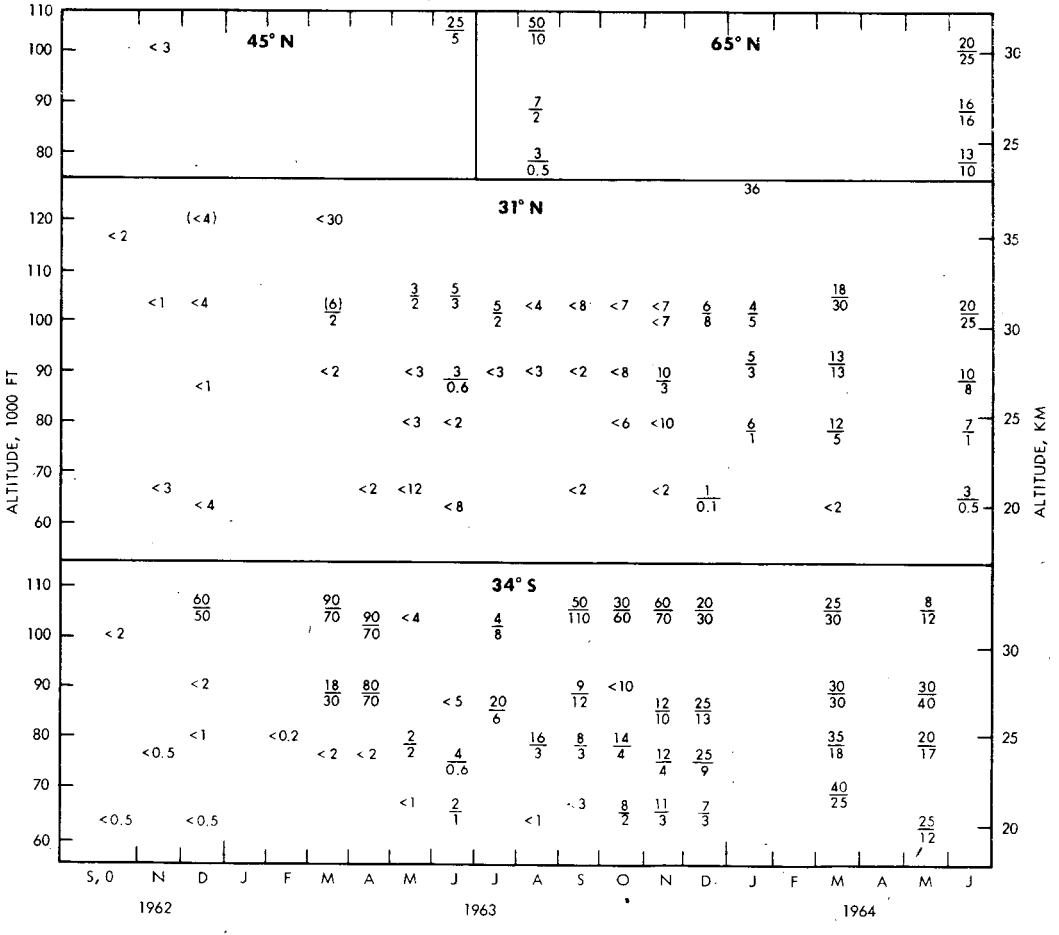

Fig. 3—Cadmium-109 concentration and $^{109}Cd/^{90}Sr$ profiles. Single values or values above line are disintegrations per minute of ^{109}Cd per 10^3 scf as of July 9, 1962. Values below the line are $100 \times {}^{109}Cd/{}^{90}Sr$ activity ratios. Data computed from doubtful volume are shown in parentheses. Counting errors are less than 20% except for data shown as an upper limit. These limits are based on the concentration values (when errors are greater than 20%) plus two standard deviations due to counting.

45°N in the first half of 1959 suggest an appearance of Orange debris in the polar stratosphere of the northern hemisphere about six months after its production. Unfortunately, even fewer data from the southern hemisphere are available for this period. The presence of Starfish debris at 34°S in December 1962 may be explained by the rapid meridional movement of material at very high altitudes followed by subsidence into the polar stratosphere and circulation toward the equator in the southern-hemisphere summer. The scant ^{109}Cd data for mid-1963 at 45°N and 65°N tend to confirm such a distribution pattern. The absence of ^{109}Cd at 31°N in this period probably reflects the relatively slower mixing into low latitudes which occurs in the hemispheric winter.

Data for ^{102}Rh (Ref. 11) and ^{109}Cd concentrations at 31°N in the second spring after the Orange and Starfish shots, respectively, are given in Table 4. The relative concentrations at a given altitude are

Table 4 — RHODIUM-102 AND CADMIUM-109 AT 25 TO 35°N ABOUT 20 MONTHS AFTER PRODUCTION

Altitude, ft	^{102}Rh, dis/min per 10^3 scf*	^{109}Cd, dis/min per 10^3 scf†
105,000		18–21
90,000	130–200	10–13
80,000	50–80	7–12
65,000	20–130	0–3
Estimated production	3 Mc	0.25 Mc

*As of Aug. 11, 1958.
†As of July 9, 1962.

consistent with the estimated production for these tracers: about 3 Mc of ^{102}Rh (Ref. 12) and about 0.25 Mc of ^{109}Cd (Ref. 7).

The levels of ^{90}Sr due to Starfish may be determined from the observed ^{109}Cd levels and the value for ^{109}Cd/^{90}Sr of 3.5 estimated above for this device. Although these ^{90}Sr levels may be relatively consistent, they are subject to bias introduced because of the uncertainties in the ratio.

At 31°N the fraction of ^{90}Sr attributed to Starfish on the basis of this estimated ratio was generally less than a few percent through 1963, increasing to about 10% at 105,000 ft in 1964.

For 34°S Starfish ^{90}Sr concentrations are given in the last column of Table 3 for comparison with those attributable to the 1961 U.S.S.R. tests.

Although debris attributed to both the 25-Mt 1961 U.S.S.R. device and Starfish was present at 105,000 ft in December 1962 and April 1963 at 34°S, significant differences in its distribution in the southern hemi-

sphere are suggested from the data for April 1963 at 90,000 ft and also those for May and June. Although Starfish debris moving northward from the southern polar stratosphere was present at both 90,000 and 105,000 ft at 34°S in equal amounts by April 1963, it is apparent that debris from the 1961 25-Mt test and/or other 1962 shots which stabilized in the high stratosphere moving southward across the equator was present in relatively larger quantities at 105,000 ft than at 90,000 ft. With the beginning of the southern-hemisphere winter season in May 1963, the absence of ^{109}Cd in the May and June samples suggests that not only did the equatorward movement of Starfish debris halt but that this material actually retreated to latitudes higher than 34°S. At the same time, the southward movement of even larger quantities of debris from the other shots continued, as is noted by the high ^{54}Mn levels at 105,000 ft in May. Finally, this latter material subsided to lower altitudes, accounting for the high ^{90}Sr levels at 77,000 and 86,000 ft in June and at 65,000 ft in September and October.

CONCLUSIONS

Fission-product data have been used to trace debris from the 1961 U.S.S.R. weapons tests at 34°S in 1962 and 1963. This material may account, in part, for the high activity levels at 105,000 ft observed at the end of 1962 and at lower altitudes in mid-1963. It is suggested that this may be attributed to the 25-Mt detonation, the debris from which reached into the high stratosphere and then moved across the equator and mixed downward in the southern hemisphere.

Early data on ^{109}Cd indicate that material from Starfish Prime behaved similarly to that from Orange. Rapid lateral mixing at high altitudes followed by subsidence in the polar regions and then movement into lower latitudes in the summer months appear to be dominant factors in the transport of this debris.

Additional data on ^{109}Cd and other activation products produced in the 1961 to 1962 test series and on actual formation ratios of fission products in weapons tests should help in future evaluation of radioactive materials in the stratosphere. The failure of a satellite device earlier this year[13] containing 17 kc of ^{238}Pu may provide yet another tracer for studying movements of stratospheric materials if burnup of this device occurred.

REFERENCES

1. Health and Safety Laboratory, Fallout Program Quarterly Summary Report, USAEC Report HASL-115, p. 70, October 1961.
2. Health and Safety Laboratory, Fallout Program Quarterly Summary Report, USAEC Report HASL-124, p. 151, July 1962.

3. Health and Safety Laboratory, Fallout Program Quarterly Summary Report, USAEC Report HASL-140, p. 166, October 1963.
4. Health and Safety Laboratory, Fallout Program Quarterly Summary Report, USAEC Report HASL-149, p. 54, October 1964.
5. Federal Radiation Council, History of Nuclear Weapons Testing, in Estimates and Evaluations of Fallout in the United States from Nuclear Weapons Testing Conducted Through 1962, Report No. 4, p. 4, May 1963.
6. U. S. Weather Bureau, Announced Nuclear Detonations, in Fallout Program Quarterly Summary Report, USAEC Report HASL-142, p. 219, Health and Safety Laboratory, January 1964.
7. L. P. Salter, Note on the Detectability of Cadmium Isotopes from Starfish in 1964 Ground Level Samples, in Fallout Program Quarterly Summary Report, USAEC Report HASL-142, p. 303, Health and Safety Laboratory, January 1964.
8. I. J. Russell and R. V. Griffith, The Production of Cd-109 and Cd-113^m in a Space Nuclear Explosion, in Fallout Program Quarterly Summary Report, USAEC Report HASL-142, p. 306, Health and Safety Laboratory, January 1964.
9. N. A. Hallden, I. M. Fisenne, L. D. Y. Ong, and J. H. Harley, Radioactive Decay of Weapons Debris, in Fallout Program Quarterly Summary Report, USAEC Report HASL-117, p. 194, Health and Safety Laboratory, December 1961.
10. M. I. Kalkstein, Rhodium-102 High Altitude Trace Experiment, *Science, 137:* 645 (1962).
11. K. Telegadas and R. J. List, Global History of 1958 Nuclear Debris and Its Meteorological Implications, *J. Geophys. Res., 69:* 4741 (1964).
12. R. Frankel and L. P. Salter, On the Ce-144/Sr-90 Ratio in Precipitation, in Fallout Program Quarterly Summary Report, USAEC Report HASL-115, p. 276, Health and Safety Laboratory, October 1961.
13. J. H. Harley, Possible Pu-238 Distribution from a Satellite Failure, in Fallout Program Quarterly Summary Report, USAEC Report HASL-149, p. 138, Health and Safety Laboratory, October 1964.

TROPOSPHERIC ^{14}C VALUES IN THE PACIFIC NORTHWEST AND THE ARCTIC BASIN DURING 1964

JAMES A. YOUNG, NILS E. ERICKSON, and ARTHUR W. FAIRHALL
University of Washington, Seattle, Washington

ABSTRACT

Samples of atmospheric CO_2 were collected by using a molecular sieve and counted for their ^{14}C content. Taking 0.95 of the National Bureau of Standards oxalic acid standard as the pre-1945 level of ^{14}C in the atmosphere, the results are expressed as percent above normal. During the summer of 1963, tropospheric levels reached about 115% above normal, followed by a rapid drop to about 88% above normal in the early fall of 1963, a level which was maintained until May 1964, when a new summer rise was noted. The sudden drop in ^{14}C specific activity is attributed to exchange of atmospheric CO_2 with dissolved CO_2 in the ocean. Increases in the tropospheric ^{14}C concentration is attributable to injection of CO_2 of high specific activity from the stratosphere. Samples of CO_2 taken during the passage of storm fronts give evidence of this injection, as well as evidence of exchange with oceanic CO_2.

INTRODUCTION

Samples of atmospheric CO_2 of from 2 to 8 liters are collected periodically for ^{14}C analysis from several locations in the state of Washington and the Arctic basin. The collection system consists of a Linde type 4-A molecular sieve designed for field use.

The first successful use of a molecular-sieve material for sampling of atmospheric CO_2 for ^{14}C was apparently made by Fergusson.[1] Previous investigators attempting to use this material for similar studies experienced difficulty because the untreated sieve material has

a rather severe memory effect for CO_2. Using ^{14}C-labeled CO_2, we have verified that Fergusson's pretreatment method reduces the memory effect to less than 1%, which is entirely adequate for extended field use of the material.

EXPERIMENTAL PROCEDURES

A photograph of one of the samplers used in this study is shown in Fig. 1. The sieve material is contained in a double-top 1-gal paint can through which air is drawn by means of a suction unit located in the

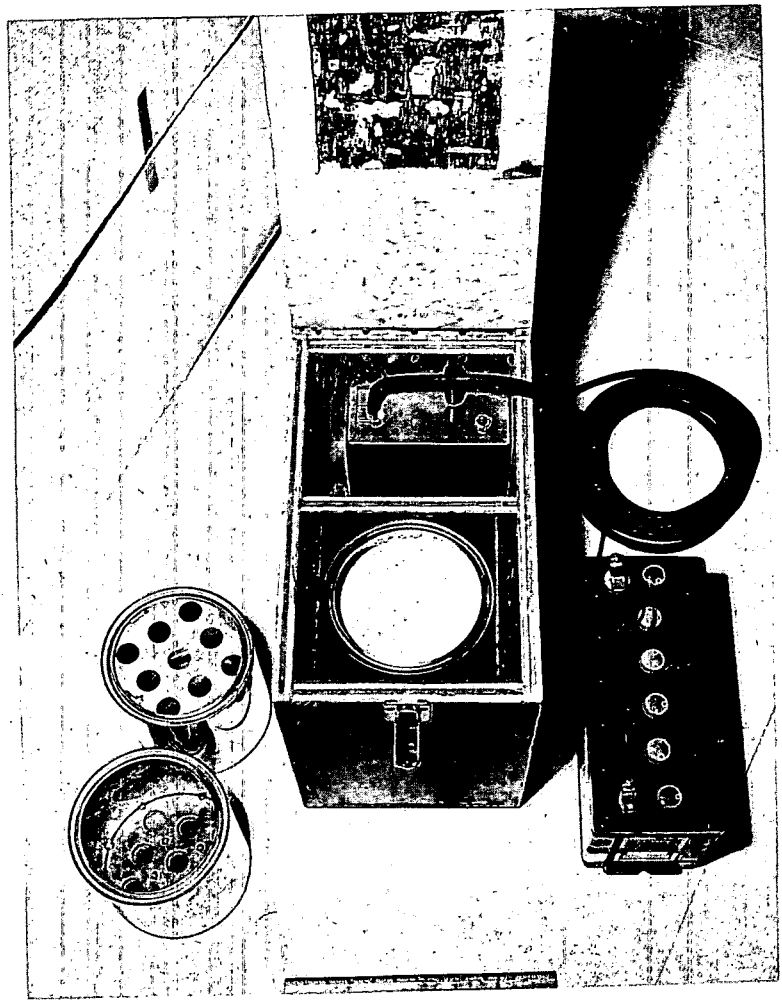

Fig. 1—Air sampler used to collect samples of CO_2 at ground levels.

bottom of the box. The motor in the suction unit operates from a 12-volt automobile battery or, by means of a step-down transformer built into the box, 115-volt alternating current.

Typical sampling times to collect sufficient CO_2 for analysis, about 5 liters, range from 45 to 90 min. The reason for this range in time is that water is preferentially adsorbed by the sieve and displaces CO_2. During times of the year when the total water content of the air is high, collection times have to be reduced to avoid displacing CO_2. This also reduces the total amount of CO_2 collected; however, a sufficient volume is obtained for counting. Studies of various sections of the cans reveal that CO_2 is quantitatively removed from the air, provided the collection time is not too long. This has been checked independently by comparing the amounts of water and CO_2 which outgassed from the exposed sieve material. Atmospheric CO_2 concentrations are known to be about 315 ppm, and the water concentration of the air that is sampled can be calculated from the relative humidity. The calculated ratio of water to CO_2 in the air that was sampled agreed with the amounts of water and CO_2 that were recovered to within about 10%, which is the limit imposed by the memory of the sieve for water.

Since CO_2 is quantitatively removed, it can be used to calculate the quantity of air that was sampled. We have used this technique to calibrate airflow through canisters in connection with our aircraft sampling program of fallout debris in the lower stratosphere.

The molecular sieve produces considerable quantities of radon during outgassing of the sample. Our standard procedure is to outgas the sieve, convert the CO_2 into methane for counting purposes, and then let the radon decay for four to six weeks before counting the methane. The conversion procedure removes any trace gases (e.g., NO_2 and SO_2) that might affect the counting characteristics of the gas.

The double-top paint cans are sufficiently sturdy that they can easily be shipped to remote locations without damage or leakage. The only precaution to be taken is that, when shipments are made by air, the shipping container must provide sufficient pressure to the ends of the cans to keep the reduced external pressure from popping the lids. Likewise, when sampling in extremely cold climates, the cans should be warmed to approximately room temperature before they are tightly sealed. Brief exposure to air in the laboratory during normal handling procedures does not significantly contaminate the sample.

Routine collection of atmospheric CO_2 samples with this type of device has been made in the Puget Sound area (48°30′N, 122°W) on a weekly basis since September 1963. Samples have been collected about every two weeks at several sites in the Arctic basin since January 1964. Two of the Arctic sites are Point Barrow, Alaska (71°20′N, 156°39′W) and floating ice island Arlis II. These samples have been collected through the cooperation of personnel connected with the

Arctic Research Laboratory and Project Husky. It is forecast that Arlis II will enter the North Pacific sometime in the spring of 1965; therefore a sampling site will then be established on floating ice island T-3 to replace it.

The University of Washington oceanographic vessel, the *Brown Bear*, collects samples at irregular intervals at locations roughly 100 miles west of the Washington coast.

In addition to collecting ground-level samples, we collect samples in pod-mounted air samplers carried by jet trainers that operate out of the Whidbey Island Naval Air Station. Flights are made at approximately weekly intervals. Except for the summer months, when the tropopause is above the ceiling of this aircraft, samples are collected in both the upper troposphere and the lower stratosphere.

Part of our studies include determinations of the role of storms in effecting transfer of stratospheric air into the troposphere and in effecting exchange between CO_2 in the atmosphere and CO_2 dissolved in the sea. During the passage of particular storm fronts over the Seattle area in the spring of 1964, samples of CO_2 were taken at intervals of 3 to 4 hr at a location near the summit of Hurricane Ridge on the Olympic Peninsula at an elevation of about 5000 ft.

The ^{14}C specific activity of the samples is determined in one of two low-background radiocarbon counters. The normal, or pre-1945, level of ^{14}C in the atmosphere is taken to be 0.95 times the ^{14}C specific activity of the National Bureau of Standards oxalic acid standard used in radiocarbon dating. The results of the measurements are then expressed in terms of percent above normal.

RESULTS

Figure 2 shows the ground-level ^{14}C specific activities for samples collected between August 1963 and July 1964. The specific activity evidently decreased from a high of about 110% above normal in the summer of 1963 to a low of about 88% above normal in the late winter and early spring of 1964. Prior to the summer high in 1963, the ^{14}C specific activity of atmospheric CO_2 was less than 40% above normal. A new summer rise during the summer of 1964 was also evident. It is interesting to note that the values measured at locations in the Arctic basin do not differ significantly from those measured in the Puget Sound area.

Since the total CO_2 in the atmosphere changes only very slightly with the season of the year, a decrease in the specific activity must be due to exchange with a reservoir of much lower specific activity. We believe this reservoir to be the ocean. Fall and early winter are stormy periods in these latitudes, and high wind velocities favor exchange of gas molecules between the atmosphere and the surface of the ocean.

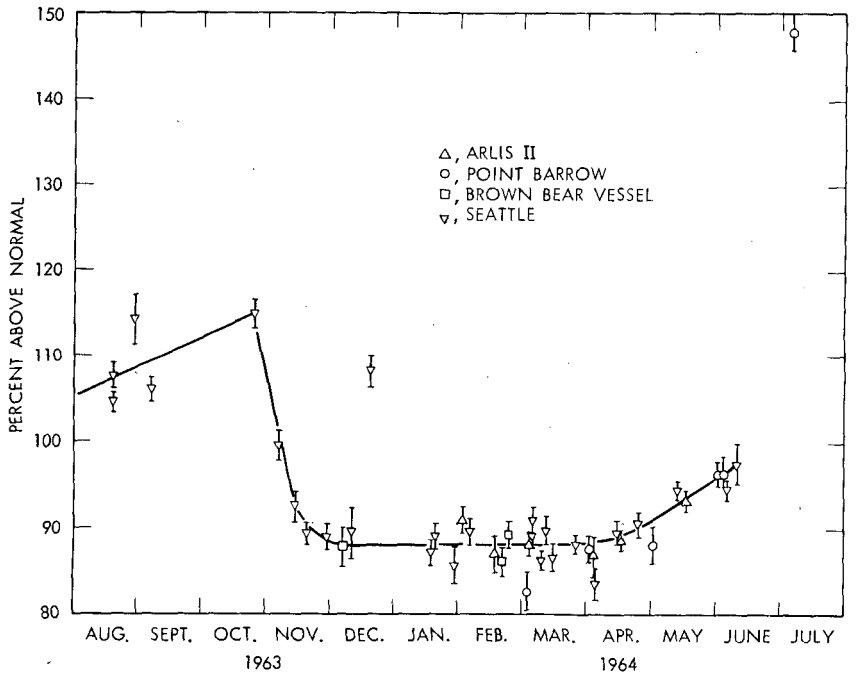

Fig. 2—Specific ^{14}C content of atmospheric CO_2 relative to pre-1945 levels.

An increase in ^{14}C specific activity is associated with injection of CO_2 of high specific activity from the stratosphere. Evidently the rate of injection from the stratosphere predominates over exchange with the ocean during the summer and vice versa during the fall and early winter.

It is of interest to note that the amount of exchange of CO_2 between the atmosphere and the ocean which is necessary to explain the decrease in the ^{14}C specific activity during the fall months amounts to about one-fifth of the tropospheric CO_2, assuming there is no injection of CO_2 of high specific activity from the stratosphere during this period. However, since there probably is an injection of CO_2 of high specific activity, then more than one-fifth of the troposphere must have exchanged with the ocean. This implies a more rapid exchange of CO_2 between the atmosphere and the oceans than has previously been estimated.[2–5]

An experiment to test the role of storms in bringing down stratospheric air into the troposphere is illustrated in Fig. 3. During the period from Apr. 9 to 11, 1964, a particularly well-developed system of three storm fronts passed in rapid succession over the northwest.

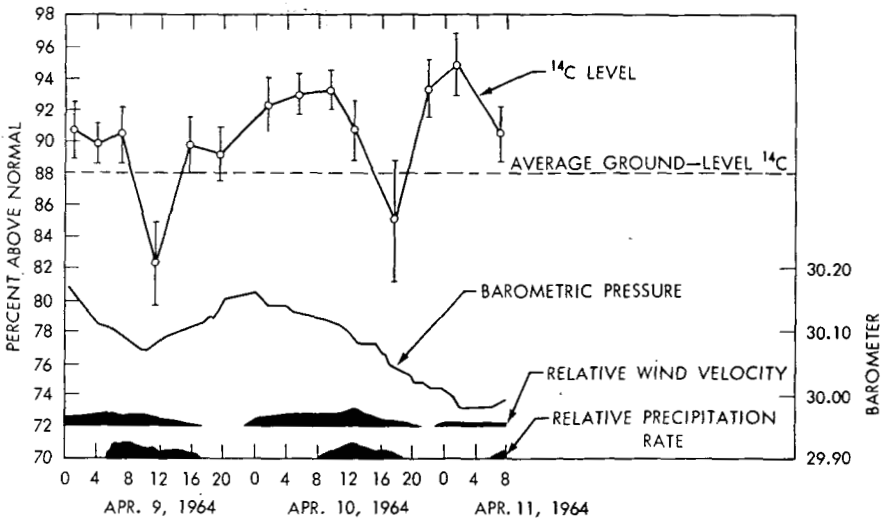

Fig. 3—Specific ^{14}C content of samples of atmospheric CO_2 collected on Hurricane Ridge during the passage of successive storm fronts. Activities of ^{14}C are expressed in percent above pre-1945 levels.

Samples of atmospheric CO_2 collected on Hurricane Ridge at about 4-hr intervals showed ^{14}C specific activities that fluctuate significantly above and below the nearly constant ^{14}C specific activity measured at ground levels during the late winter and early spring. Particularly interesting are the two low values of the specific activity which were measured after most of the precipitation, snow, had fallen. Since the source of this moisture was marine air, the low specific activity probably represented an air mass from over the ocean which had undergone partial exchange and which had not yet mixed with the air masses of higher specific activity which were associated with the storm system.

REFERENCES

1. G. J. Fergusson, Upper Tropospheric Carbon-14 Levels During Spring 1962, *J. Geophys. Res., 68:* 3933-3941 (1963).
2. H. E. Suess, Natural Radiocarbon and the Rate of Exchange of Carbon Dioxide Between the Atmosphere and the Sea, in Proceedings of Conference on Nuclear Processes in Geologic Settings, pp. 52-56, National Academy of Sciences—National Research Council Publication, Washington, D. C., 1953.
3. H. Craig, The Natural Distribution of Radiocarbon and the Exchange Time of Carbon Dioxide Between Atmosphere and Sea, *Tellus, 9:* 1-17 (1957).
4. R. Revelle and H. E. Suess, Carbon Dioxide Exchange Between Atmosphere and Ocean and the Question of an Increase of Atmospheric CO_2 During the Past Decades, *Tellus, 9:* 18-27 (1957).
5. J. R. Arnold and E. C. Anderson, The Distribution of Carbon-14 in Nature, *Tellus, 9:* 28-32 (1957).

FISSION-PRODUCT CONCENTRATIONS IN THE TROPOSPHERE AND LOWER STRATOSPHERE OVER THE PACIFIC NORTHWEST SINCE 1962

P. H. GUDIKSEN, G. L. JONES, W. R. SCHELL, C. A. L. SWANSON, N. ERICKSON, and A. W. FAIRHALL
University of Washington, Seattle, Washington

ABSTRACT

The concentration of fission products, injected into the atmosphere by nuclear-weapons detonations, has been studied by aircraft sampling in the lower stratosphere and upper troposphere over the Pacific Northwest since 1962. The individual activities of ^{54}Mn, $^{95}Zr-^{95}Nb$, ^{137}Cs, $^{106}Ru-^{106}Rh$, ^{125}Sb, and ^{144}Ce were determined by gamma-ray spectrometry and subsequent computer analysis. In general, a direct correlation between stratospheric and tropospheric activity levels at any given time is observed. This correlation indicates that rapid diffusion may be taking place across the tropopause. The $^{95}Zr-^{95}Nb/^{137}Cs$ activity ratios for stratospheric and tropospheric samples at any given time are the same, thus demonstrating that no fractionation processes are operating across the tropopause. The $^{54}Mn/^{137}Cs$ ratios display a maximum during April and May 1963; thereafter the decrease in the ratios is consistent with the 300-day half-life of ^{54}Mn. The maximum is probably due to a nonuniformly mixed stratosphere with respect to ^{54}Mn.

INTRODUCTION

In our fallout studies the atmospheric structure is being studied over a particular geographic area located in the region of the tropopause gap. Samples are collected by using a U. S. Navy TA-3B twin-jet trainer through the cooperation of the Whidbey Island Naval Air Station.

The height of the tropopause over the Washington area is usually low enough to permit sampling of the lower stratosphere also with this aircraft.

EXPERIMENTAL PROCEDURES

The increase in the ^{14}C content of the atmosphere from nuclear tests has made this nuclide an important atmospheric tracer. In an attempt to measure the level of ^{14}C produced during nuclear tests in the atmosphere, a stainless-steel sampler was designed which exposes a maximum surface area of Ascarite (sodium hydroxide on asbestos) to the airstream.

The sampler (see Fig. 1) was machined to fit the celestial-navigation-sextant mount of the aircraft. The sampler was designed to withstand speeds approaching Mach 1 and to penetrate above the boundary layer of the aircraft.

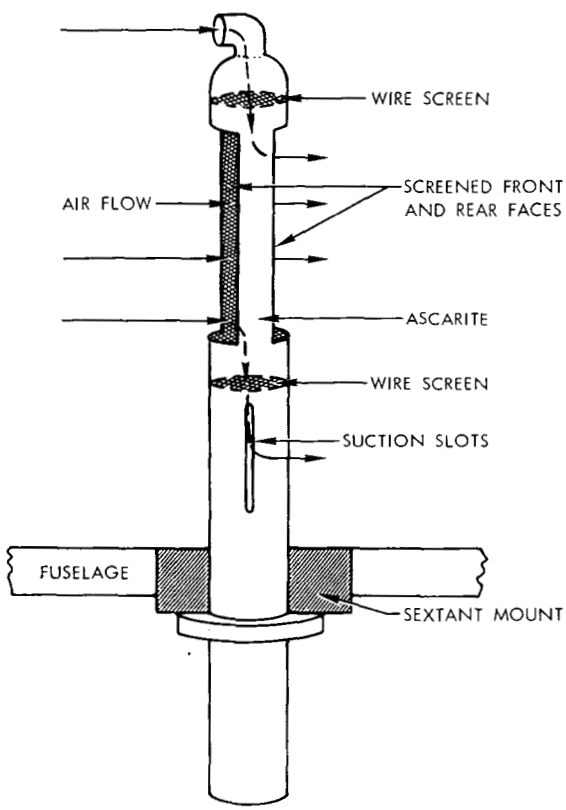

Fig. 1—Stainless-steel air sampler inserted into the sextant mount of a U. S. Navy TA-3B twin-jet trainer.

The samples were taken during routine training flights along the flight tracks shown in Fig. 2. Normally four samples, with a sampling time of 45 min for each, were taken during each flight, two above and two below the tropopause. The outside air temperature was monitored during each flight and utilized whenever possible as an indicator of the tropopause height. In-flight wind speeds were recorded from the aircraft's radar bombing system, and a log of in-flight information was taken.

Unfortunately, we were unable to collect sufficient CO_2 with this sampler to determine the ^{14}C content; however, we found that the Ascarite did serve as a filter medium for nuclear debris.

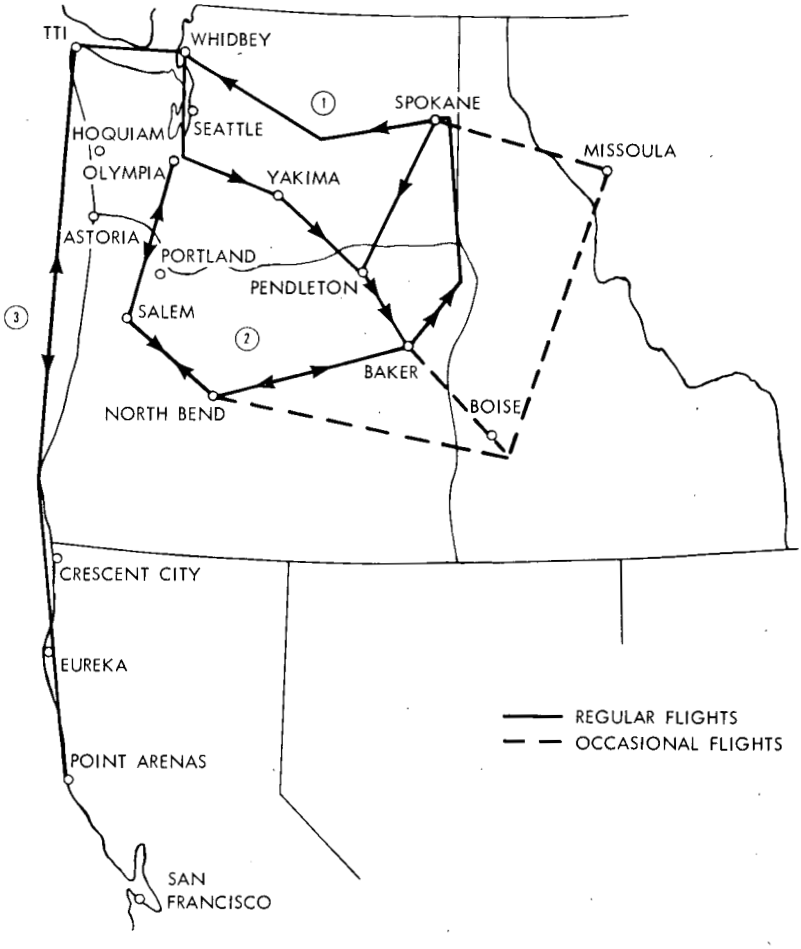

Fig. 2—Air-sampling routes over the Pacific Northwest which are followed in the sampling program.

For collection of sufficient CO_2 for ^{14}C analysis, a new sampler was designed which can be mounted under the wing in the nose section of the Aero 8A-1 bomb simulator. A cross-sectional view of this sampler is shown in Fig. 3. Air is directed through a smoothly contoured 2-in.-diameter tube that is attached to a rotating inlet plate. Rotation

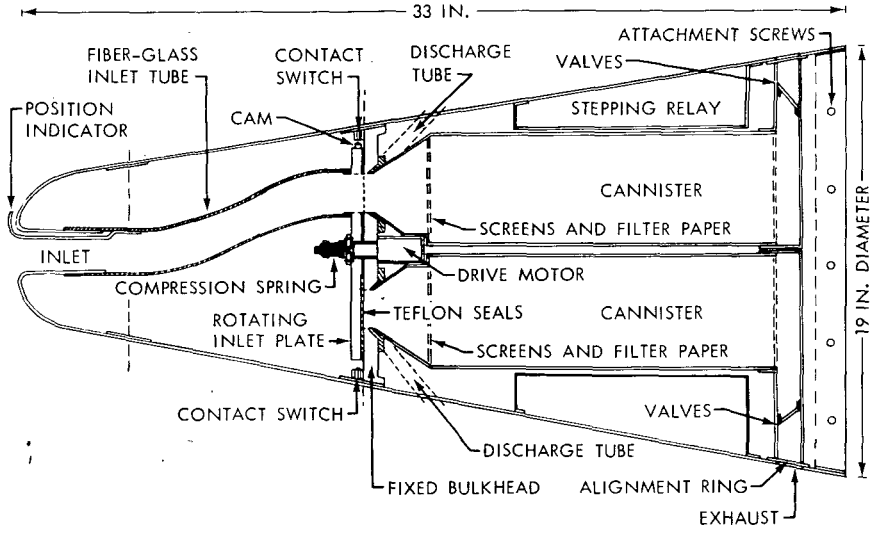

SPECIFICATIONS

MATERIALS: ALL ALUMINUM 5052—H32 (YIELD STRENGTH, 28,000 LB; ULTIMATE, 33,000 LB)
DRIVE MOTOR: 6 TO 24 VOLTS DIRECT CURRENT; GEAR REDUCTION, 1 TO 3 RPM
STEPPING RELAY: 24 VOLTS DIRECT CURRENT
CANNISTER LOAD: INERT MOLECULAR SIEVE AND FILTER PAPER
LOADED OPERATING WEIGHT: ABOUT 60 LB

Fig. 3—Cross-sectional view of wing-mounted air sampler.

of this plate aligns the inlet tube with one of the six ports located in the fixed bulkhead. Three ports connect to direct overboard discharge tubes. Each of the remaining ports is the inlet to one of the three cylindrical cannisters. Individual exhaust from the cannisters is through a spring-loaded flap valve into the ambient airstream. These cannisters are loaded with an IPC 1478 filter sandwiched between two wire screens in the front and with approximately 8 lb of Linde type 4-A molecular sieve material for CO_2 collection behind the screens and filter.

The drive motor, which rotates the inlet plate, is powered through a stepping switch by the aircraft's 28-volt d-c system. For operation of the sampler in flight, the main power switch in the aircraft cockpit is turned on. The drive motor rotates the inlet plate until the inlet tube is aligned with a cannister port. At this time one of the three double-

pole contact switches mounted on the fixed bulkhead is activated by a cam on the rotating inlet plate, thus opening the circuit to the drive motor, which stops the rotation. The main power switch is then turned off.

Airtightness is maintained at the cannister inlet by applying spring pressure on specially designed Teflon seals placed between the rotating plate and the fixed bulkhead. Silicone grease applied to the seals helps to prevent air leakage as well as to lubricate the moving parts.

Leak tests were performed on unexposed cannisters filled with molecular-sieve material. After a 4-hr flight, the CO_2 recovered from the sieve amounted to 0.05 liter-atmosphere of CO_2. Since this amount is comparable to the amount of CO_2 absorbed by the molecular sieve during its handling in the laboratory, leakage during flight is insignificant.

Flow-rate calibrations have begun but have not yet been completed. For a 45-min sampling period, we have obtained about 8 liter-atmospheres of CO_2 at an altitude of 29,000 ft and approximately 5 liter-atmospheres at 39,000 ft. The results seem to be reproducible to within $\pm 10\%$ from flight to flight. In addition, we have tested the CO_2 absorption efficiency by sectioning the cannisters into two parts and analyzing each part separately for absorbed CO_2 content. We found that only about 3% of the total amount of CO_2 was absorbed in the back quarter section, thus demonstrating that virtually all the CO_2 passing through the cannister is absorbed by the molecular sieve.

RESULTS

The gross fission-product gamma-ray spectrum of a typical stratospheric sample collected in April 1964 is shown in Fig. 4. The data were obtained with a 3- by 3-in. NaI crystal and a 512-channel analyzer.

The individual activities of ^{54}Mn, $^{95}Zr-^{95}Nb$, ^{137}Cs, $^{106}Ru-^{106}Rh$, ^{125}Sb, and ^{144}Ce were determined by spectrum stripping with the use of a computer. The $^{95}Zr-^{95}Nb$ activity is plotted vs. the collection date in Fig. 5. The top curve represents the activity of stratospheric samples, and the lower curve represents the activity of tropospheric samples. The activities are expressed in terms of picocuries per 45-min sampling time. Conversion to conventional units based on 1000 scf of air will be made when the calibration of air flow rates are completed. Preliminary results indicate that the volume of air at standard temperature and pressure sampled in the stratosphere is about five-eighths of the volume of air sampled in the troposphere. The numbers indicate the sampling altitude in thousands of feet. The curve at the bottom of Fig. 5 represents the height of the tropopause on the sampling date.

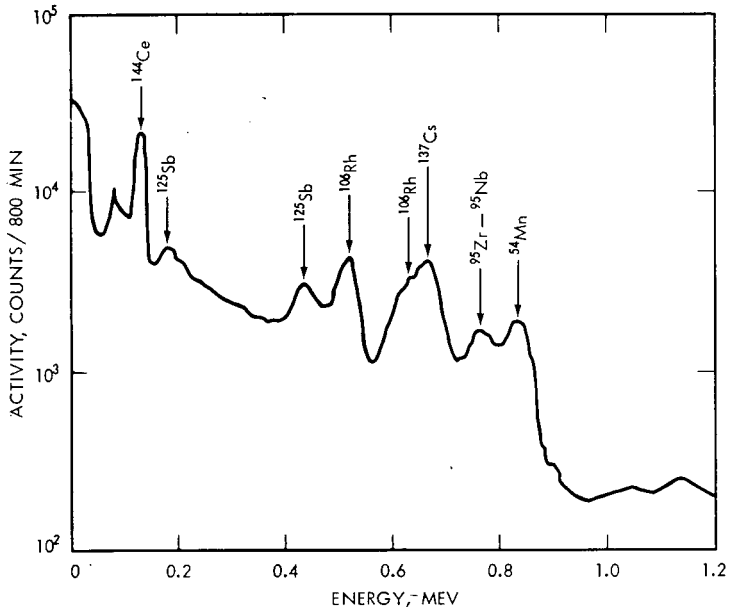

Fig. 4—Gross fission-product gamma-ray spectrum.

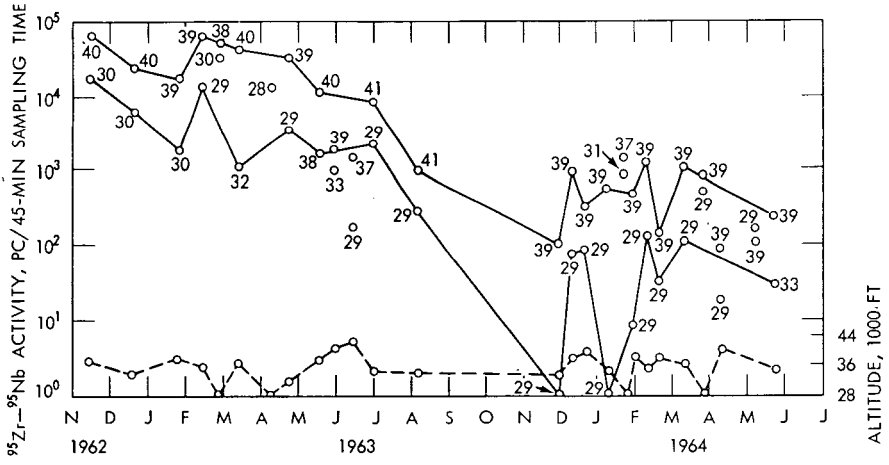

Fig. 5—Variation of $^{95}Zr-^{95}Nb$ activity of stratospheric and tropospheric air samples. No samples were collected between August and November 1963. Data were obtained with sampler shown in Fig. 1.

Since the sampling altitude was generally maintained near 30,000 ft on the outward flight and near 40,000 ft on the return flight and since the height of the tropopause varied from flight to flight, the data show that the distance below the tropopause generally determines the activity levels of the tropospheric samples. Thus there is a concentra-

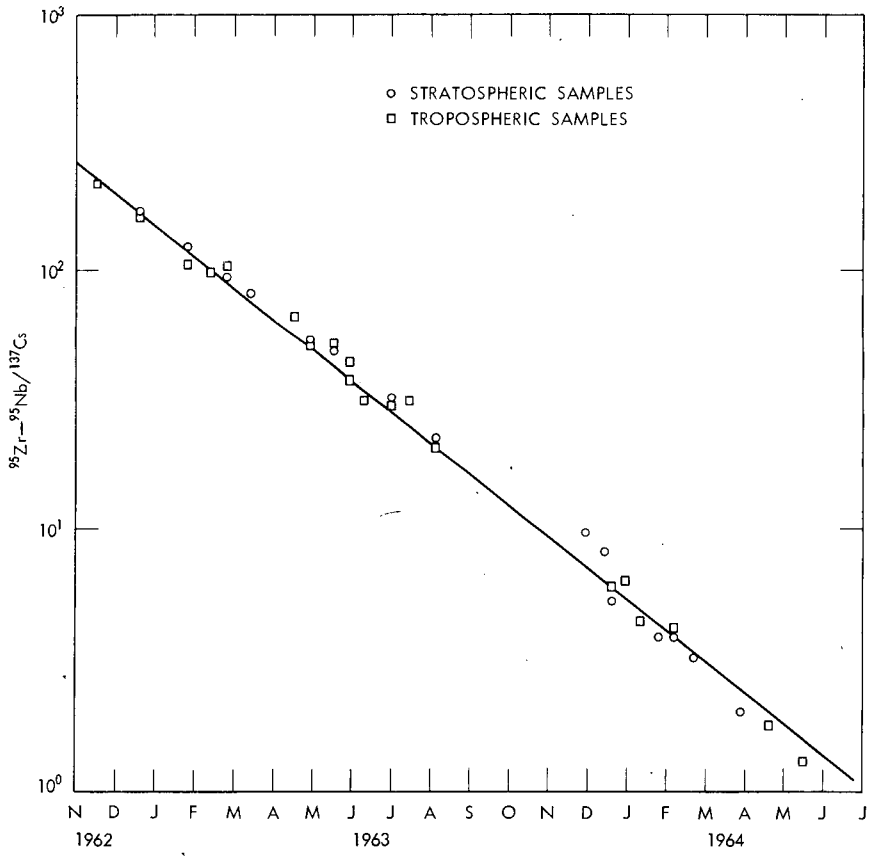

Fig. 6—Ratios of $^{95}Zr-^{95}Nb/^{137}Cs$ activities in stratospheric and tropospheric air samples.

tion gradient of fission-product debris in the upper troposphere. In general, there is also a direct correlation between stratospheric and tropospheric activity levels at any given time. This correlation indicates that rapid diffusion of nuclear debris is probably occurring across the tropopause.

Figure 6 shows the $^{95}Zr-^{95}Nb/^{137}Cs$ activity ratios vs. collection time. The ratios decrease with a 75-day half-life, which is close to the half-life of ^{95}Zr (65 days). The activity ratios for stratospheric samples are the same as for tropospheric samples collected at the same time, thus indicating that no fractionation processes are operating across the tropopause.

The $^{54}Mn/^{137}Cs$ activity ratios are shown in Fig. 7. A maximum occurs during April and May 1963; thereafter the decrease in the ratio is consistent with the 300-day half-life of ^{54}Mn. Manganese-54

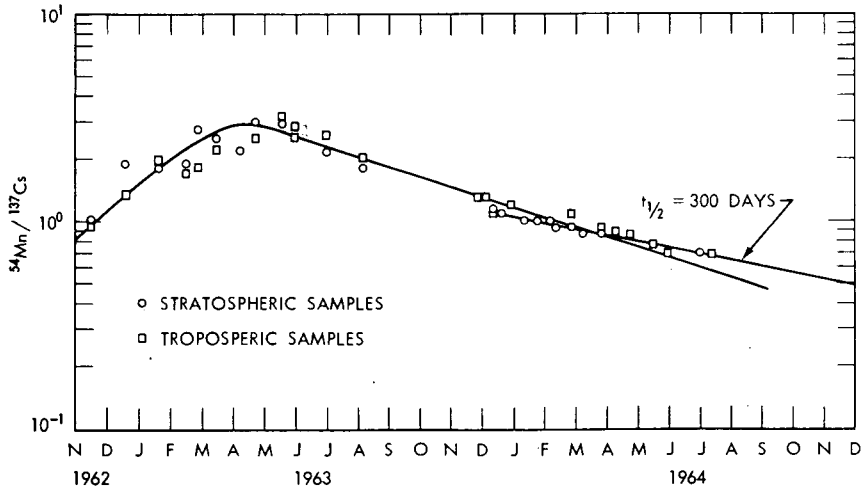

Fig. 7—Ratios of $^{54}Mn/^{137}Cs$ activities in stratospheric and tropospheric air samples.

was produced in relatively large quantities in the 1961 and 1962 tests. The maximum is probably due to the late arrival of this radionuclide from higher altitudes.

RADIOACTIVITY AND POTENTIAL VORTICITY

E. F. DANIELSEN
The Pennsylvania State University, University Park, Pennsylvania

ABSTRACT

Continuous records of radioactivity, wind, and temperature made by WB50 aircraft during Project Springfield substantiate the transfer of radioactivity from the stratosphere to the troposphere by tropopause folding. The continuous records are supported by filter samples of radioactivity taken by both WB50 and RB57 aircraft at critical positions relative to the fold. As expected the radioactivity correlates positively with the potential vorticity; thus the latter can be used as a meteorological tracer of stratospheric air. It can also serve as an indicator of radioactivity concentrations when direct measurements are not available.

INTRODUCTION

Project Springfield was organized to obtain simultaneous measurements of atmospheric radioactivity and significant meteorological variables. Simultaneous measurements were essential for testing the validity of two concepts of fundamental importance to the fallout problem. The first concept, based on a folding of the tropopause, assumes that a nonturbulent transport is the major mode of mass exchange between stratosphere and troposphere. The second concept, based on the conservation of potential vorticity, assumes a positive correlation between the concentration of radioactivity and potential vorticity. These concepts predict a layered distribution of radioactivity and ozone in both the troposphere and stratosphere when the potential vorticity is layered.

POTENTIAL TEMPERATURE AND ENTROPY

Both concepts evolved from studies of atmospheric motions on surfaces of constant entropy. These surfaces, more steeply inclined than pressure surfaces, move with the air parcels when the flow processes are isentropic. They are ideally suited for trajectory analyses because entropy is slowly varying except in certain identifiable regions.

An isentropic surface is also a surface of constant potential temperature. This derived temperature, usually denoted by Θ, corresponds to the temperature a parcel of air would attain if compressed to sea level, or 1000 mb. The compression must be adiabatic, i.e., no gain or loss of heat by conduction or radiation. In this paper the isentropic surfaces shall be referred to and identified by Θ.

TROPOPAUSE FOLDING

The vertical distribution of Θ and some of its implications as a coordinate will be clarified in Fig. 1. It illustrates schematically the first concept: a steepening and a folding of the tropopause with the transport of a layer of stratospheric air into the troposphere. In the upper left diagram, the thin lines sloping upward to the north in the troposphere and downward to the north in the gray-toned stratosphere are isolines of Θ. Proceeding from upper left to upper right and then to lower left, notice how the Θ lines change their slope and spacing as the tropopause folds.

After the tropopause folds the Θ lines in the stratospheric layer have the same slope and horizontal and vertical spacing as in the tropospheric zone extending from the fold. In other words, the layer has the identical characteristics of a tropospheric frontal zone, i.e., a large horizontal temperature gradient and a large hydrostatic stability (small vertical spacing between Θ lines). For these reasons the folded tropopause has been misanalyzed by meteorologists as a tropospheric frontal zone in the manner shown at the lower right of the figure. The difference in analyses is not trivial since the two lower diagrams imply a drastically different spatial distribution of radioactivity and ozone.

POTENTIAL VORTICITY

However, the stratospheric layer can be distinguished from the tropospheric frontal zone if another quasi-conservative property of the atmosphere is utilized. From the equations of motion, continuity, and

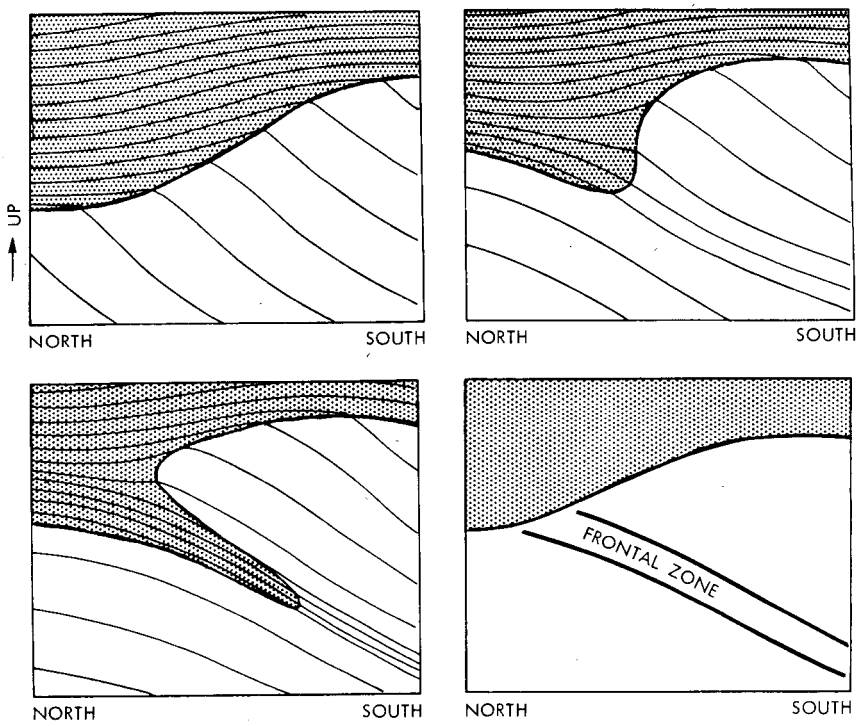

Fig. 1—Schematic illustrations of tropopause folding and tropospheric frontogenesis. Lower right diagram is erroneous conventional analysis of lower left diagram. Thin lines represent potential temperature.

energy, the potential vorticity can be derived. Its exact and approximate mathematical forms are, respectively,

$$P = \alpha \nabla\Theta \cdot (\nabla \times V + 2\Omega)$$

and

$$P_\Theta = -g \frac{\partial\Theta}{\partial p} (\zeta_\Theta + f)$$

where P = potential vorticity
α = specific volume
V = wind velocity
Ω = angular velocity of earth
Θ = potential temperature
p = pressure
g = acceleration of gravity
$\zeta_\Theta = K \cdot \nabla \times V_\Theta$
$f = K \cdot 2\Omega$
K = unit vector in vertical

Excluding vertically oriented Θ surfaces, the approximate form is sufficiently accurate for our purposes and more readily evaluated. In

this form the potential vorticity is the product of the stability and the vertical component of the total vorticity, where the total vorticity is the sum of the relative vorticity (computed from the winds on a Θ surface) and the vertical component of the earth's vorticity.

In the simplest idealized concept of stratosphere and troposphere, the stability and baroclinity change rapidly at the tropopause, as shown in the upper left diagram of Fig. 1. If, also, the tropopause coincides with the maximum wind on each Θ surface, the vorticity also changes rapidly at the tropopause.

The Θ surfaces drawn in Fig. 2 satisfy these conditions. Recognizing that the wind shear or spin is positive in the stratosphere (i.e., $\zeta_\Theta > 0$ and f is positive everywhere), we see that a large stability is multiplied by a large absolute spin in the stratosphere. Conversely, in the troposphere a small stability correlates with a small absolute spin, $\zeta_\Theta < 0$. The positive correlation between stability and spin makes the change in potential vorticity at the tropopause larger in magnitude than the change in stability.

Recalling also that the potential vorticity is conserved for isentropic processes, we can appreciate its importance in both identifying and tracing the movement of stratospheric air. When the stability of tropospheric air is greatly increased as in frontogenesis, the spin is correspondingly decreased. Tropospheric fronts can therefore be recognized by large negative values of ζ_Θ and small values of P_Θ. The stratospheric layers will have positive values of ζ_Θ and large values of P_Θ.

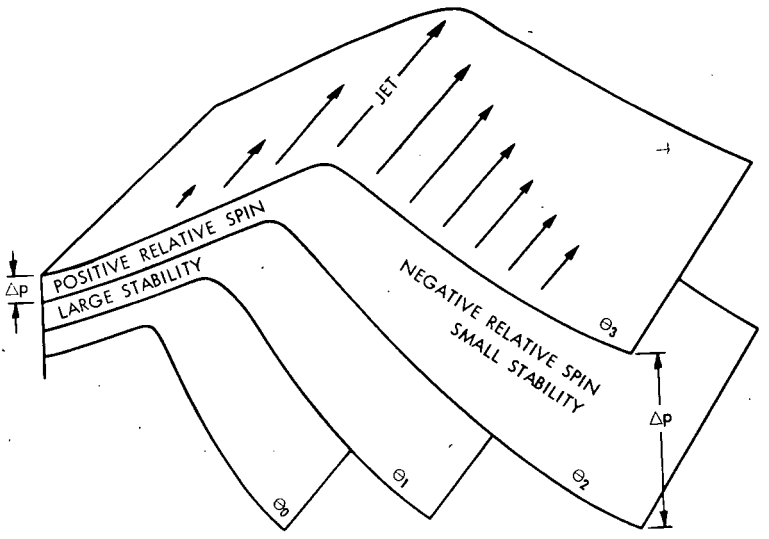

Fig. 2 — Explanation of large potential vorticity in the stratosphere and small potential vorticity in the troposphere.

If the concepts just discussed are valid, we should expect to find layers of stratospheric air in the troposphere and tropospheric air in the stratosphere. We should also expect a positive correlation between the radioactivity and the potential vorticity. In other words, the potential vorticity should tell us about the history or origin of the air. The conventional classification of air as stratospheric or tropospheric tells us only about the moment, because it is based on stability, and stability is not conserved during motion.

MISSION OF APR. 18 AND 19, 1963

Let us now turn to the actual Springfield observations to check the concepts. Figure 3 is a hemispheric analysis of the stream function, ψ, on the 310°K isentropic surface.* It determines the geostrophic winds, not the actual winds. The actual winds are approximately parallel to the ψ lines. The wind speeds are related to their spacing and the curvatures of the air-parcel trajectories. When air speeds up it crosses to lower values of ψ, and when it turns cyclonically the wind speed is less than the speed implied by the gradient of ψ. Figure 3 does not show the actual winds, but they are on the original chart. Both the actual winds and the ψ analyses are necessary to construct the trajectories. Superimposed on the ψ analysis is the area of maximum stability on the 310°K surface. Within the gray area the stabilities are greater than 0.2°Θ/mb; thus the air would be classified as stratospheric. Notice that the gray area correlates with the low centers, or areas of large ζ_Θ. Therefore this area also approximates the region of large P_Θ. We would also expect the gray area to approximate the region of maximum radioactivity on the 310°K surface.

The original chart also includes an analysis of the pressure topograph of the Θ surface. Over most of the gray area the pressures are between 250 and 350 mb. At low latitudes the surface reaches to the 800- to 900-mb level, and over Texas, New Mexico, and Mexico it intersects the ground. The latter area is outlined with a dashed line.

On April 18, two WB50 and two RB57 aircraft were sent to obtain measurements along a northwest to southeast flight track (perpendicular to the flow) south of the low center in Wyoming. The cross section along the flight track is shown in Fig. 4. Isentropic lines are drawn for a 2°K interval; this permits a visual estimate of stability. The dashed lines depict the isotachs, lines of equal wind speed, at intervals of 10 knots. Positive values correspond to southwesterly winds.

*This is the first hemispheric hand analysis prepared from the wind and the temperature observations. A smoothed machine analysis of the stream function has been developed by A. Gustafson.

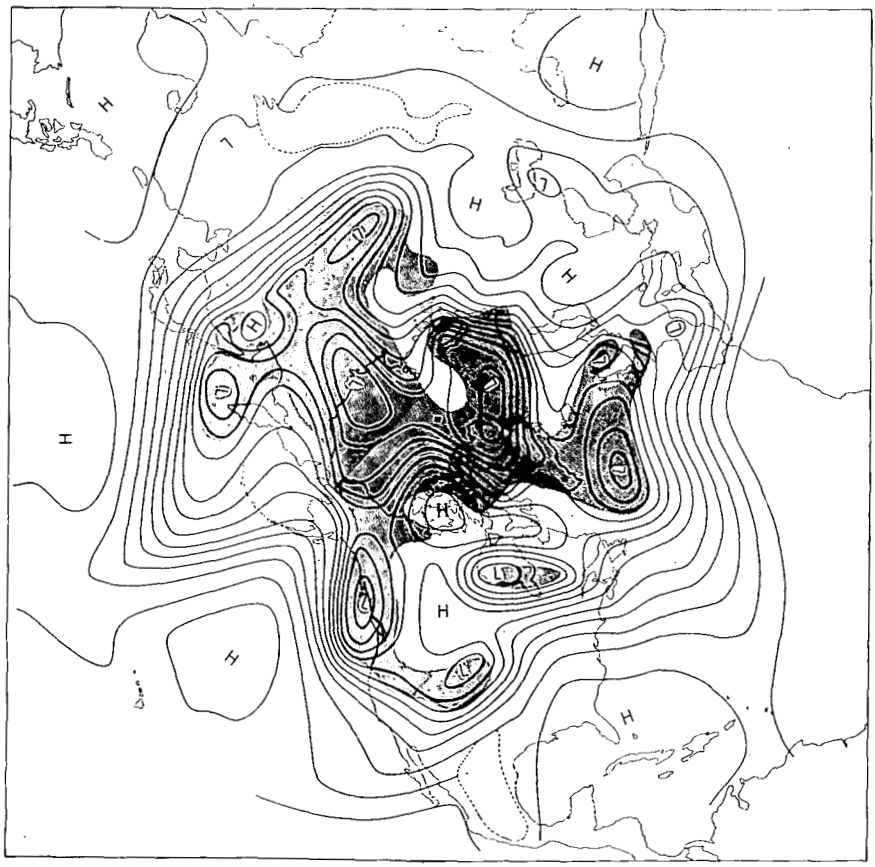

Fig. 3—Northern-hemisphere isentropic chart for 310°K, Apr. 19, 1963, at 00Z. Stream-function isolines are drawn at an interval of 60 × 10^5 ergs/g. Within the gray area, the 310°K surface is in the stratosphere.

When the WB50's arrived over Wyoming, cumulonimbus clouds and snow showers delayed the mission. After an hour's delay permission was granted to cross the airways and to proceed with the mission. The plane assigned the lower altitude flew the prescribed distance along the track but encountered only clouds. The pilot aborted the mission. At the higher altitude the pilot was just about to turn back when his plane broke into the clear. The plane had entered the stratospheric layer. The pilot traversed the layer, flew well beyond it and returned, but because of limited fuel, he could not repeat this pattern at another altitude. Three samples were taken which gave total beta readings of 2 dis/min per standard cubic foot at two points outside the layer and 136 dis/min per standard cubic foot within the layer. These values are plotted in Fig. 4 along with the total beta readings for the RB57 samples. Note the similarity in values north of the jet at Denver, 114, 136,

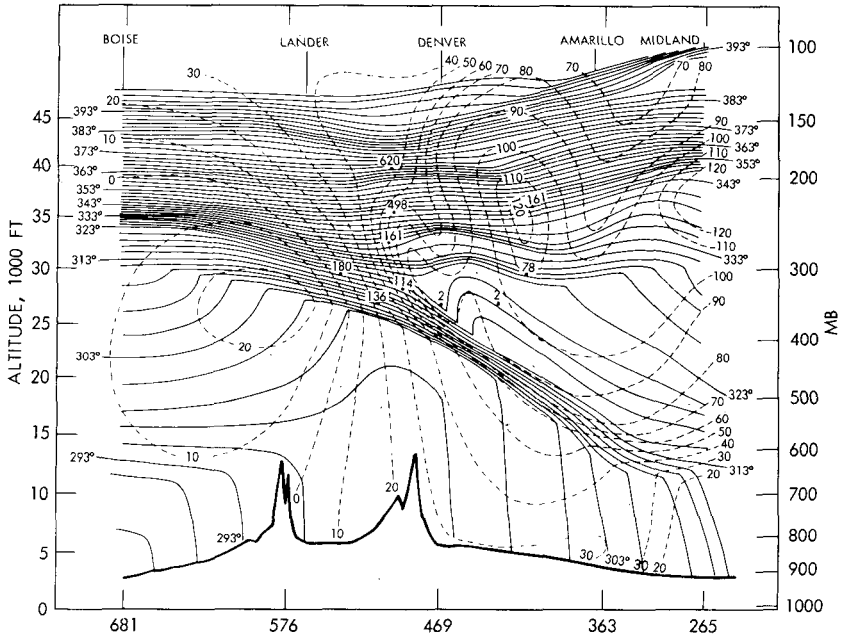

Fig. 4—Vertical cross section for Apr. 19, 1963, at 00Z. Continuous lines are Θ isotherms at 2°K intervals. Dashed lines are isotachs at 10-knot intervals. Total beta activities are plotted at sampling sites in disintegrations per minute per standard cubic foot.

161, and 180 dis/min per standard cubic foot. All these large values were obtained where ζ_Θ is positive. At higher values of Θ, the values increase to 498 and 620 dis/min per standard cubic foot.

In addition to the filter samples, the WB50 obtained a continuous record of accumulated radioactivity. Also, while in flight, a meteorologist recorded the temperature, relative humidity, and wind every 10 min. These recordings are presented in Fig. 5. As the plane entered the stratospheric air at 1920Z, the radioactivity accumulation rate increased. The temperature and wind traces do not show a corresponding increase because a cumulonimbus cloud penetrating the layer forced the plane to ascend to 27,000 ft. The initial temperature and wind changes are therefore due to altitude changes and are not representative of horizontal flight. After 1940Z a constant altitude, 27,000 ft, was maintained.

Note that the rapid increase in temperature, wind speed, and accumulation rate all coincide. The changes of 14°C, 75 knots and 3500 counts/min are all dramatic. After the stratospheric layer was passed, the temperature dropped 4°C, the wind speed dropped 15 knots and the radioactivity accumulated remained essentially constant. On the return flight similar changes in all three variables were recorded.

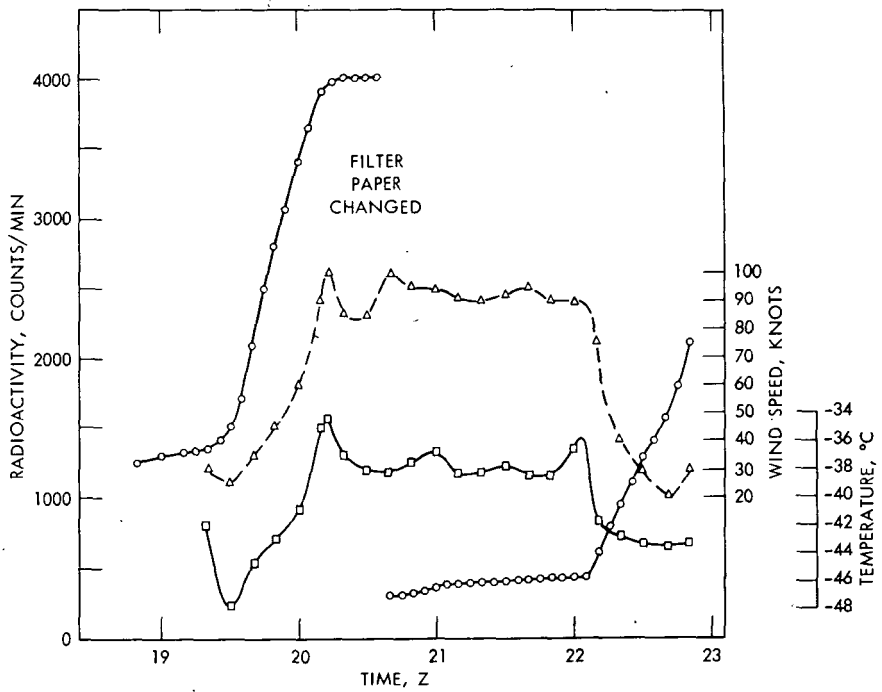

Fig. 5—Wind speed, temperature, and accumulated radioactivity recorded by WB50 aircraft (see Fig. 4). Apr. 18, 1963, at 23,000 to 27,000 ft.

The slope of the accumulated radioactivity was not as steep as during the first transit. It was on the second transit that the filter sample was taken which gave a total beta count of 136 dis/min per standard cubic foot. On the first transit, values of 200 dis/min per standard cubic foot would be expected from the accumulation rate.

In Fig. 6 the ^{90}Sr activity in disintegrations per minute per 1000 scf are plotted against the distribution of potential vorticity. This distribution was tediously calculated by hand from the Θ and isotach analyses of Fig. 4. The distribution is presented as calculated, but no claim is made for accuracy of the details. Maximums and minimums may be shifted by slight changes in the original analyses, but the general pattern cannot be significantly altered.

The numerical correspondence between the ^{90}Sr activity and P_Θ/g is remarkable. It lends support for the assumption of a positive correlation between radioactivity and potential vorticity. It also implies that the radioactive layer in the troposphere extends to the 500-mb, or 18,000-ft, level. Unfortunately, no measurements were made below 27,000 ft to confirm or refute this implication.

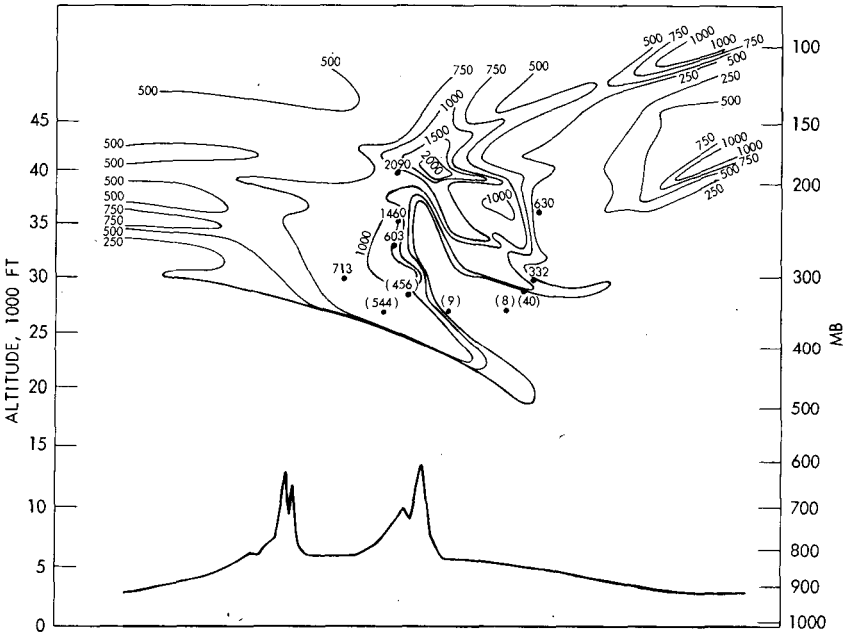

Fig. 6—Distribution of potential vorticity computed from Fig. 4. Lines of constant are drawn at intervals of 250×10^{-6} deg-cm-sec/g. Strontium-90 beta activity at sampling sites in disintegrations per minute per 1000 scf.

MISSION OF APR. 21 AND 22, 1963

The 310°K isentropic chart for April 22 at 00Z is presented in Fig. 7. During the three-day period, the low in Wyoming moved east of Nova Scotia. The low over Hudson Bay moved southward and eastward to southeastern Canada, and the low off the British Columbia coast moved southeastward into Nevada. Low stabilities associated with the eastern Pacific ridge had advected across western Canada and isolated large P_Θ's over the western United States.

As before, the WB50 and the RB57 aircraft were sent on northwest to southeast flight tracks to obtain measurements southeast of the low centered in Nevada. Note that the 310°K surface again intersects the earth's surface, but this time the area is larger and extends into Colorado and western New Mexico.

The cross section along the flight tracks, Fig. 8, extends from Winnemucca, Nev., to Albuquerque, N. Mex. Isentropic lines are drawn for a 4°K interval, and the isotachs are again at intervals of 10 knots. The heavy lines are guide lines to assist the reader in interpreting Fig. 9.

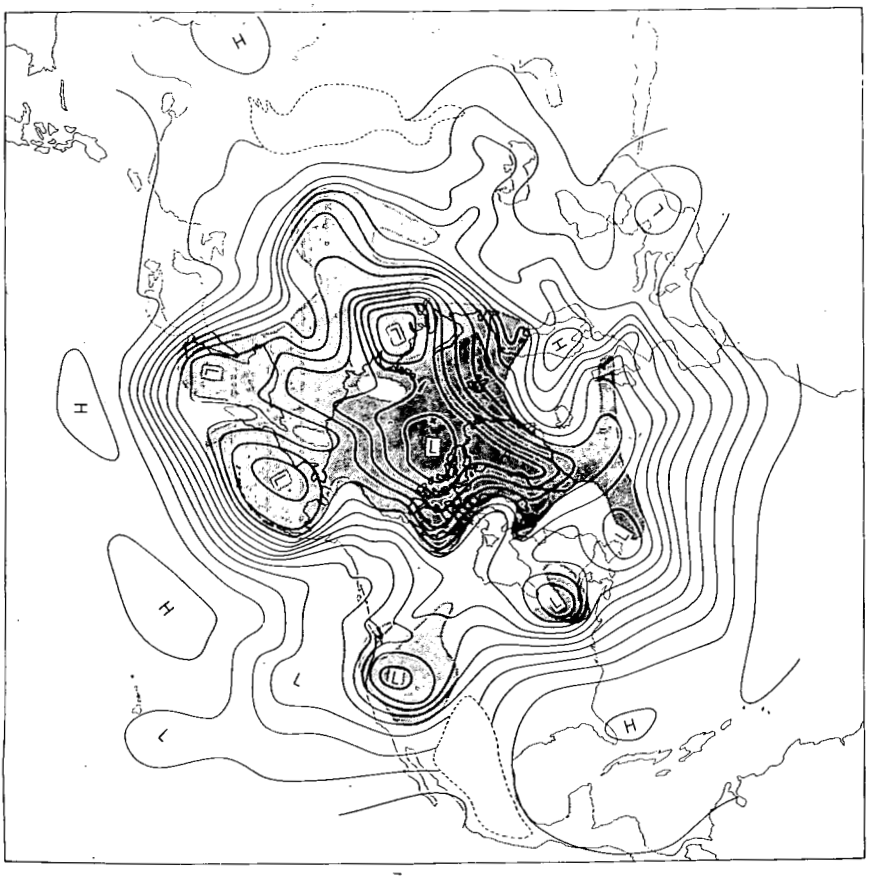

Fig. 7—Northern-hemisphere isentropic chart for 310°K, Apr. 22, 1963, at 00Z (see Fig. 3).

Both WB50 airplanes, following the paths shown in Fig. 9, traversed the stable layer from left to right then retraversed the layer at the same altitudes from right to left. Radioactivity samples were taken on the return flights. Their beta values are plotted in Fig. 9 at 21,000 and 23,000 ft. The aircraft operating at the lower altitude then descended to 19,000 ft, and the aircraft operating at the higher altitude ascended to 26,000 ft. Additional samples were taken at these altitudes.

Outside the layer the beta values are low, between 1 and 3 dis/min per standard cubic foot. These values correspond to those measured in tropospheric air on April 18 and 19. Inside the layer the beta values vary from 20 dis/min per standard cubic foot at 19,000 ft to 87 and 92 dis/min per standard cubic foot at 24,000 and 26,000 ft, respectively.

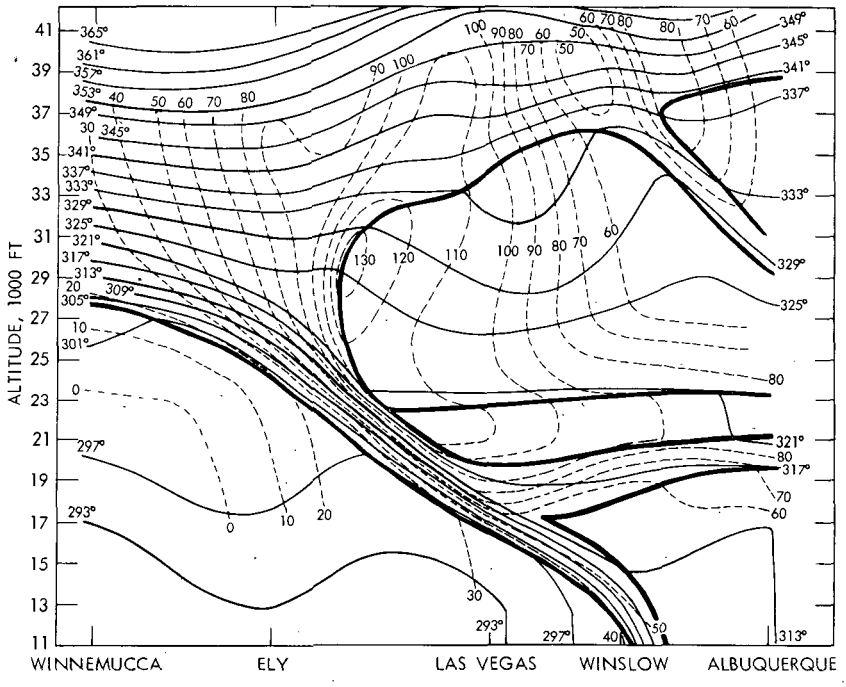

Fig. 8—Vertical cross séction for Apr. 22, 1963, at 00Z. Isolines of Θ at 4°K intervals. Isotachs at 10-knot intervals. Heavy lines are guide lines for Fig. 9.

The RB57 samples taken at 28,000 gave readings of 99 and 163 dis/min per standard cubic foot. Once again these large values correspond to those measured in the layer three days earlier. Three of the four values are lower by about a factor of 2. The RB57 aircraft also monitored the lower latitude jet stream as shown in the upper right of Figs. 8 and 9.

Continuous records are of course more revealing than point samples. In Fig. 10 accumulated radioactivity and recorded temperatures are plotted vs. time for the traverse and retraverse by both aircraft. The similarity in recordings is beautiful. The only discrepancy (aircraft No. 2 at 2230Z) was caused by the aircraft's making a 90° turn while taking a sample. The orientation of the layer was changing with time; therefore the flight track did not remain orthogonal to the flow. Instructed to sample along a heading orthogonal to the track, the pilot turned left after reentering the layer. The plane then reapproached the warm boundary of the layer. This caused an increase in temperature and a temporary decrease in the accumulation rate. Both changes attest to the accuracy of the measurements.

The average slope of the accumulated radioactivity trace during the time of sampling is a measure of the activity per unit volume ob-

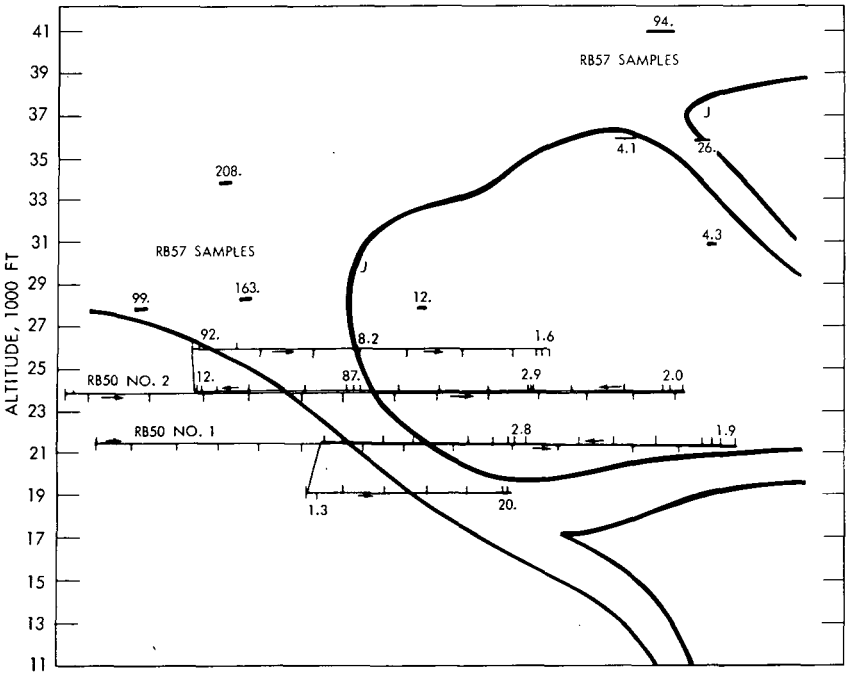

Fig. 9—Flight paths of WB50 aircraft along vertical cross section shown in Fig. 8. Total beta activities in disintegrations per minute per standard cubic foot. April 21 (18Z) to April 22 (01Z), 1963.

tained from the sample. By comparing the average slopes to the activities a conversion factor was calculated. This permits one to estimate the activity directly from the slope of the continuous radioactivity trace at any point on the flight path. It is worth noting that the samples in the layer were taken near the boundaries where the slopes were smaller than those at the center of the layer. Dilution of the activity by mixing with the tropospheric air is implied by these smaller slopes along both boundaries.

Figure 11 illustrates the potential-vorticity distribution and the ^{90}Sr activity as did Fig. 6. It also includes two values at the center of the layer (21,500 and 24,000 ft). These values were calculated from the slope of the accumulation traces. As before, the numerical correspondence is remarkable especially when allowances are made for the flight path during the time of sampling. In this case we have proof that the radioactivity extends to the 19,000-ft level, with the concentrations at 21,000 ft almost as large as at 28,000 and 34,000 ft. This supports the concept of tropopause folding with transport rather than diffusion as the predominant mode of transfer. Furthermore, the split in the potential-vorticity tongue at 20,000 ft is confirmed by the accumulated

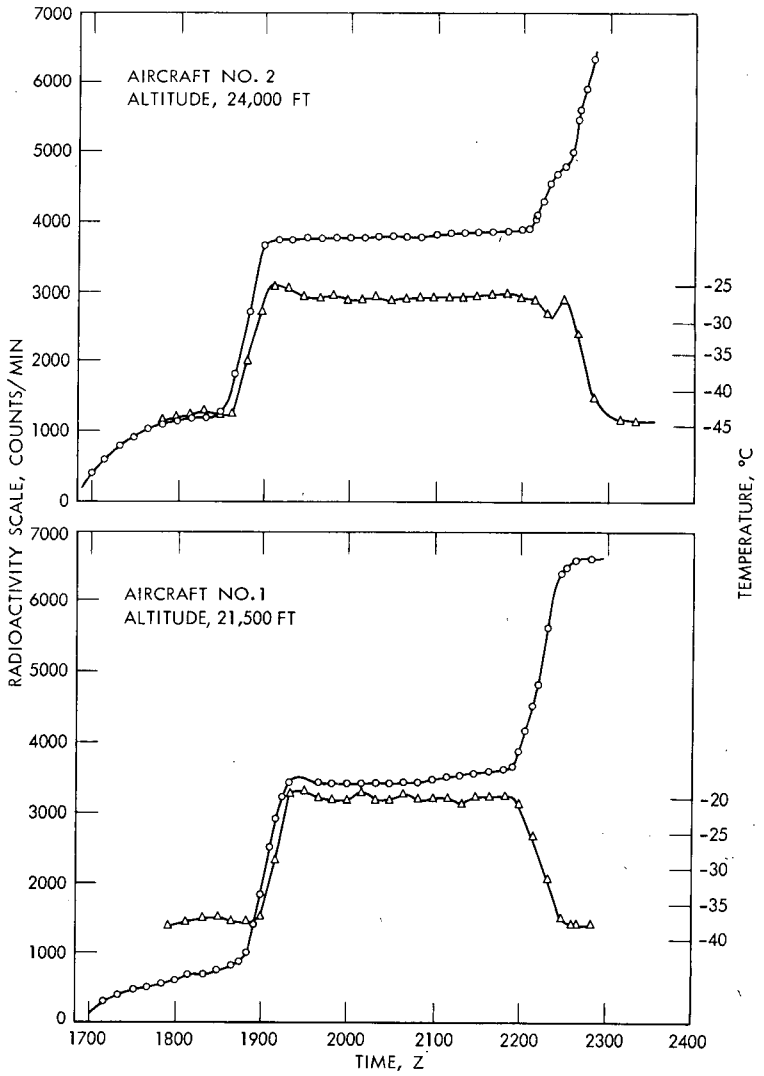

Fig. 10—Temperature and accumulated radioactivity recorded by WB50 aircraft on Apr. 21, 1963. See Figs. 8 and 9.

radioactivity trace, which has two steps, the first of which is the steeper. This suggests that the folding process extends to a smaller scale where it acts as a mixing process.

A more complete exposition is available in a recently published report.[1] This report details many interesting aspects of Project Springfield which have been passed over in this presentation.

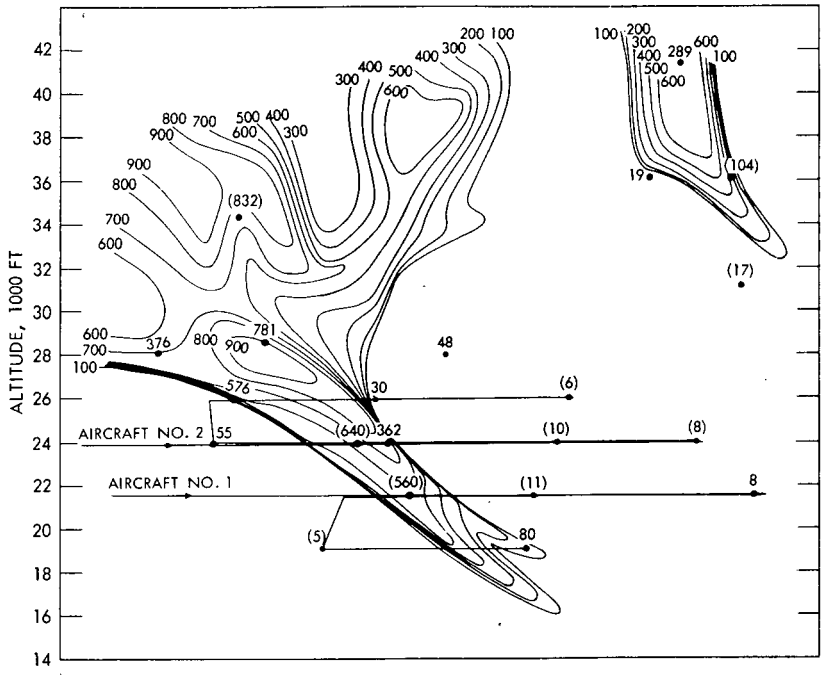

Fig. 11—Distribution of potential vorticity computed from Fig. 8 (see Fig. 6). Apr. 22, 1963 (00Z). Strontium-90 beta activity at sampling sites in disintegrations per minute per 1000 scf.

CONCLUSIONS

Project Springfield provided excellent data to support the concept of tropopause folding and the formation of radioactive layers in the troposphere. The data also confirm the positive correlation between potential vorticity and radioactivity. This correlation provides a physical basis for studying the movement and dispersion of radioactivity and ozone through the atmosphere. The data also confirm the accuracy of the isentropic trajectories and the importance of isentropic surfaces in analyzing atmospheric motions.

REFERENCE

1. E. F. Danielsen, Project Springfield Report, Report DASA-1517, Defense Atomic Support Agency, July 1964.

ATMOSPHERIC TRANSPORT PROCESSES LEADING TO RADIOACTIVE FALLOUT OVER THE UNITED STATES IN NOVEMBER 1962

ELMAR R. REITER and JERRY D. MAHLMAN
Colorado State University, Fort Collins, Colorado

ABSTRACT

Radioactive fallout in excess of 320 pc/m^3 of air was observed over the South Central United States Nov. 24 to 27, 1962. Atmospheric transport processes leading to these abnormally high values of fallout were studied in detail. It was estimated that 0.6×10^{12} metric tons of air were involved in the rapid sinking process that transported air from the tropopause level to the ground in a matter of approximately two days. Wet washout processes also removed some radioactive debris from the atmosphere.

INTRODUCTION

It has been established by a number of case studies[1–8] that atmospheric motions, especially in the jet-stream region, are capable of rapidly transporting downward radioactive debris from the tropopause or the lower stratosphere to the ground.

The purposes of the study reported in this paper were to (1) arrive at quantitative estimates of the efficiency of such transport processes in the removal of stratospheric debris and (2) derive, if possible, forecasting procedures for stratospheric fallout based upon dynamic considerations. These objectives were achieved by a detailed analysis of a case of strong radioactive fallout over the South Central United States which occurred Nov. 24 to 27, 1962 (see Fig. 1). The motion of

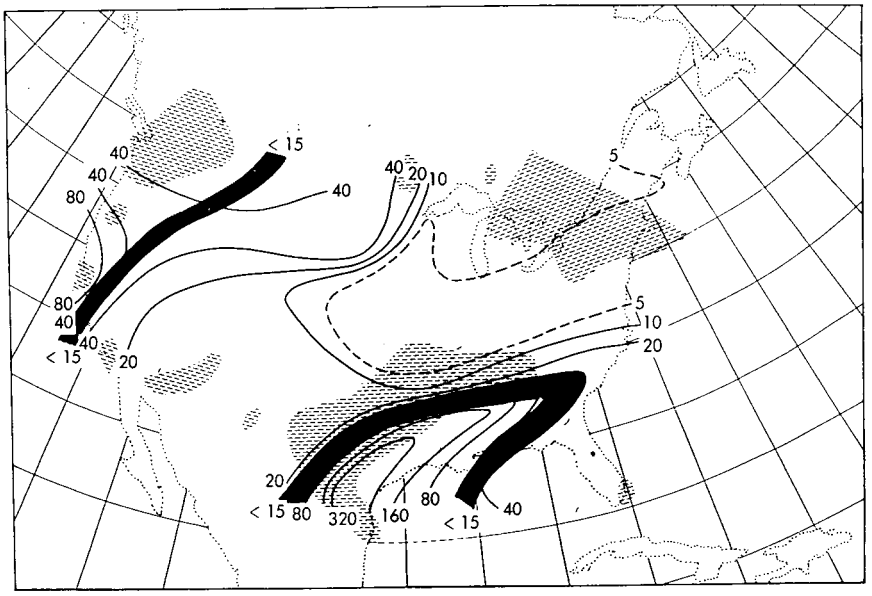

Fig. 1—Pattern of radioactive fallout intensities (pc/m³ of dry air) observed over the United States in a 24-hr sampling period ending at approximately 15 GCT, Nov. 25, 1962. Lightly hatched regions indicate precipitation during the 24-hr period ending at 0600 GCT of the same day, as reported in the "Daily Weather Map" of the U. S. Weather Bureau. The dark belts outline regions in which the reported debris age is less than 15 days.

contaminated air was traced along isentropic surfaces for the period of time for which diabatic effects were assumed to be negligible.

TRANSPORT OF DEBRIS BY LARGE-SCALE ATMOSPHERIC MOTIONS

Mechanism of Downward Transport

For adiabatic flow conditions in a coordinate system with potential temperature, θ, as the vertical coordinate, the vorticity equation

$$Q = -DQ + q_x \frac{\partial w}{\partial x} + q_y \frac{\partial w}{\partial y} \qquad (1)$$

where Q = the vertical component of absolute vorticity
D = the divergence
q_x and q_y = the horizontal components of relative vorticity
w = the vertical displacement

reduces to the simple form

$$\dot{Q} = -DQ \tag{2}$$

The divergence is easily estimated from streamline and isotach analyses on an isentropic surface. Equation 2 indicates that a decrease of the vorticity of an air parcel will be accompanied by divergence.

Since the flow in the vicinity of a jet maximum is characterized by a pronounced vorticity pattern, it is easily seen that in this region we should expect relatively strong fields of divergence and convergence which give rise to large-scale vertical motions. This has been recognized from cross sections (classical examples of which have been given by Palmén and Newton[9]), as well as from isobaric analyses. (For literature references see Ref. 10.)

Jet-stream analyses on isobaric charts, say, of the 300-millibar (mb) surface, indicate a strong vorticity gradient, almost of a zero-order discontinuity, in the jet axis. If absolute vorticity were considered a conservative quantity, it would be difficult to visualize air parcels crossing the jet axis in isobaric motion. The model proposed by Reiter[3,4] and shown in Fig. 2 resolves this difficulty. The model shows air parcels moving along isentropic surfaces; thus they may descend underneath the jet axis, satisfying in good approximation Eq. 2 as well as the theorem of conservation of potential vorticity

$$\dot{P} = \dot{Q}S + Q\dot{S} = 0 \tag{3}$$

where P is the potential vorticity and S is the stability, $\partial\Theta/\partial p$. The symbol Θ is the potential temperature, and p is the pressure. While moving from the cyclonic to the anticyclonic side of the jet stream (defined with respect to the position of the jet core), the air parcels apparently do not even appreciably change their speed.

Since air masses in the vicinity of a jet maximum do not move isobarically, isentropic analyses seem more appropriate than isobaric ones for study of the jet-stream structure. Figure 3 shows winds at the 300°K isentropic surface for Nov. 22, 1962. Figure 2 shows that on the average stronger anticyclonic than cyclonic shears prevail. This is in line with Arakawa's instability criteria

$$\frac{\partial u}{\partial y} = f + \frac{u}{R}\tan\phi \qquad \left(\frac{\partial u}{\partial y} > 0\right) \tag{4}$$

$$\frac{\partial u}{\partial y} = -\frac{f}{2} - \frac{2u}{R}\tan\phi \qquad \left(\frac{\partial u}{\partial y} < 0\right) \tag{5}$$

where f is the Coriolis parameter, R is the earth's radius, and ϕ is the geographic latitude. These criteria give the limiting shear for anti-

cyclonic and cyclonic flow derived for zonal motion. The anticyclonic shears shown in Fig. 3a, measured to the south of the jet maximum, are of the order of 1.4×10^{-4}/sec. This suggests negative values of absolute vorticity and dynamic instability in this area.

According to Eq. 5 limiting shears of 0.643×10^{-4}/sec should prevail at the geographic latitude of the Great Lakes. Thus cyclonic dynamic instability should be expected there.

From Figs. 2, 3a, 3b, and 4 [Fig. 4 shows a cross section through the jet stream from Green Bay, Wis., to Oklahoma City, Okla., at 12 Greenwich civil time (GCT) on Nov. 22], we may conclude that there is a marked difference between wind profiles on an isobaric surface and on an isentropic surface. Isobaric profiles show strong cyclonic and weaker anticyclonic shears. Usually the jet axis is indicated by a sharp peak in wind speeds. Isentropic profiles, when taken along a potential-temperature surface contained within the stable layer underneath the jet core, show a sharp anticyclonic shear, a weaker cyclonic shear, and a "platform" of almost uniform winds inside the stable layer. This is indicated schematically in Fig. 5. Also the locations of jet axes on isentropic charts may be quite different from those on isobaric surfaces, as may be seen from Fig. 4.

Figures 3a and 3b show a splitting of the jet stream. One branch moves toward the northeast with the air contained in the middle and upper troposphere. The other moves toward the south and is characterized by strong decelerations and a sinking motion. It is this branch which carries radioactive debris to the ground.

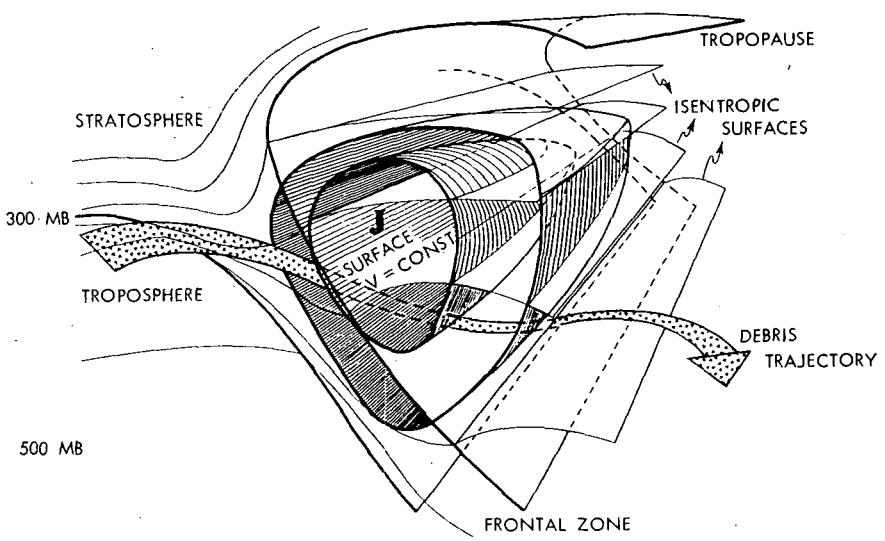

Fig. 2—Schematic section through a jet stream and its associated "jet-stream front."

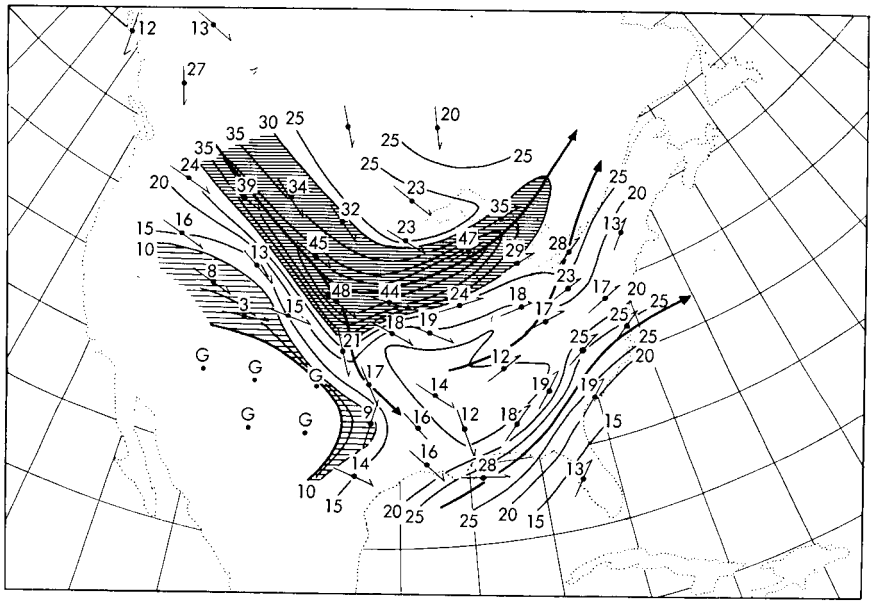

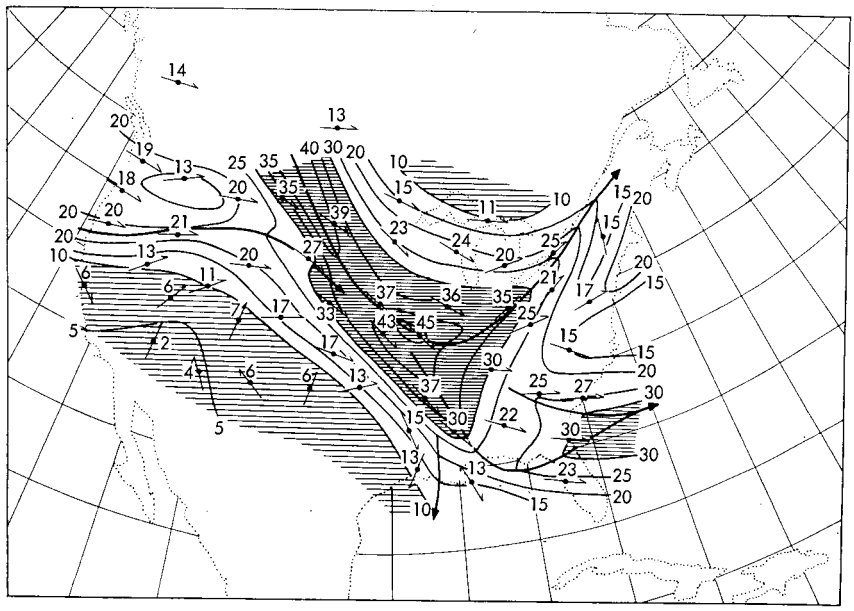

Fig. 3—Isotachs (thin solid lines, mps) on the 300°K isentropic surface at 00 and 12 GCT on Nov. 22, 1962. Numerical values of speeds are plotted next to stations. Heavy solid lines with arrows indicate jet axes. Regions with speeds more than 35 mps and less than 10 mps are shaded differently.

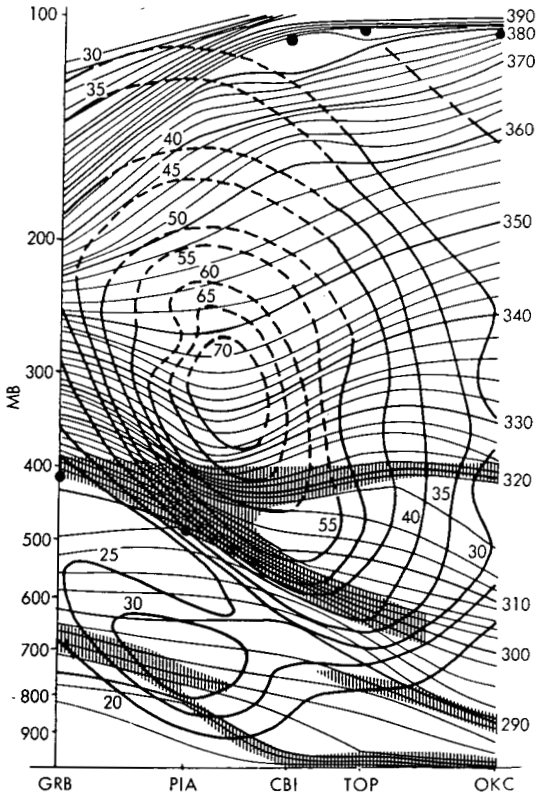

Fig. 4—Cross section through the troposphere and lower stratosphere from Green Bay (GRB), Wis., to Oklahoma City (OKC), Okla., at 00 GCT on Nov. 22, 1962. Thin lines are isotherms of potential temperature (°K). Heavy lines are isotachs (mps); these are dashed in regions with missing data. Stable regions below 400 mb are shaded. Coded tropopauses are indicated by heavy dots.

Splitting of the jet stream was observed in previous case studies of radioactive fallout.[3,4,7] This indicates that part of the upper tropospheric air that moves through the jet stream is caught in the anticyclonic circulation of the lower troposphere. The dynamic causes for this splitting are not yet certain. Conceivably, dynamic instabilities in jet streams on an isentropic surface may play an important role.

Magnitude of Isentropic Transport

It is difficult to estimate the total amount of stratospheric air descending into tropospheric regions in a jet-stream system as shown in Figs. 3a and 3b. The main problem is finding a suitable procedure to

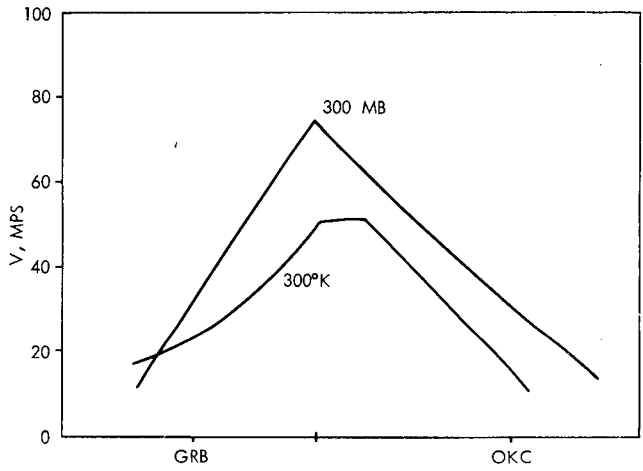

Fig. 5—Schematic wind profiles along the 300-mb isobaric and the 300°K isentropic surfaces approximately corresponding to conditions shown in Fig. 4.

define the boundaries of air traveling in the northern jet branch. The air contained in this branch moves rather rapidly over areas with an insufficiently dense radiosonde network. Thus estimates of transport have been made of the southern jet branches only to avoid the difficulties presented by these phenomena. These are presented in Table 1, which is based on this study and on one undertaken by Mahlman.[7]

It was assumed that the sinking air showed potential vorticities larger than 10×10^{-9} cm-sec-deg/g (see Fig. 6), that it was dry to the point of "motorboating" of the humidity sensor (see Figs. 7a and 7b), and that strong wind shears outlined its boundaries against the surrounding tropospheric air (see Figs. 3a and 3b). With the horizontal extent of the sinking air mass thus established, we can compute the total amount of air involved in the fallout process,

$$M = \frac{\overline{\Delta p}}{g} \int dA \tag{6}$$

where M = mass
Δp = thickness of stable layer
A = area
g = acceleration of gravity

by planimetering the areas dA between isolines of Δp, i.e., the thickness of the stable layer in which the isentropic surface under investigation is contained.

Difficulties were encountered in the estimates made for November 1962 because the stable, upper, contaminated layer, characterized by

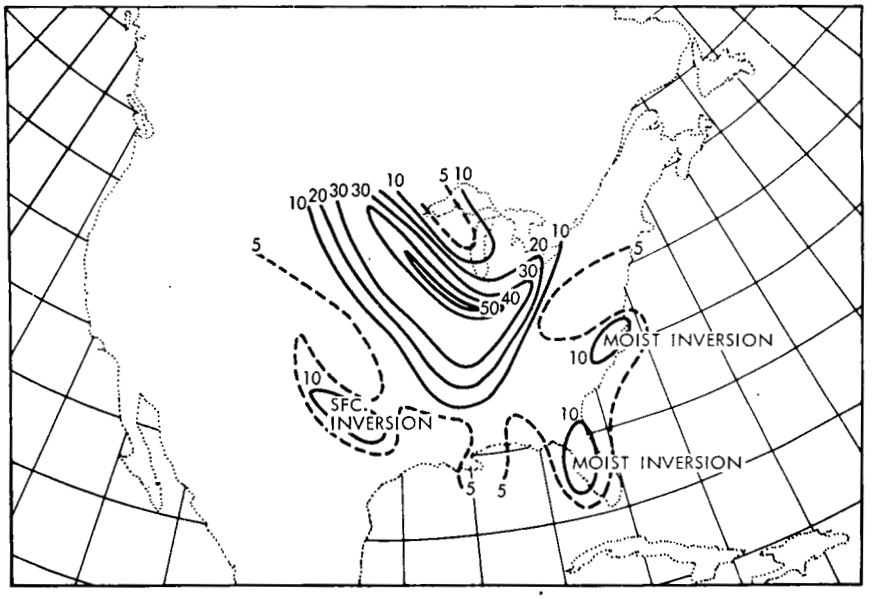

Fig. 6 — Potential vorticities (units, 10^{-9} cm-sec-deg/g) of 300°K isentropic surface, at 12 GCT on Nov. 22, 1962.

295 and 300°K isentropic surfaces, attached itself to a lower stable layer with potential temperatures of about 290°K. This lower layer was too low and too slow to be of stratospheric origin (see Fig. 8 and for comparison see also Fig. 4). Thus original estimates of the amount of air involved in the sinking process were too high (see Table 1). Adjustments were made by subtracting the air mass within the lower stable layer from the total.

From Table 1 it appears that 0.6×10^{12} metric tons is a good order-of-magnitude estimate of the air involved in the transport pro-

Table 1 — AMOUNT OF AIR INVOLVED IN TRANSPORT OF RADIOACTIVITY TO THE GROUND

Date and time	Calculated mass	
	Uncorrected value, 10^{12} metric tons	Corrected value, 10^{12} metric tons
Nov. 23, 1962, 00 GCT	0.87	0.64
Nov. 23, 1962, 12 GCT	0.98	
Nov. 24, 1962, 00 GCT	0.79	
Nov. 24, 1962, 12 GCT	1.0	
Mar. 29, 1963, 12 GCT		0.6
Mar. 30, 1963, 00 GCT		0.4
Mar. 30, 1963, 12 GCT		0.4
Mar. 31, 1963, 00 GCT		0.2

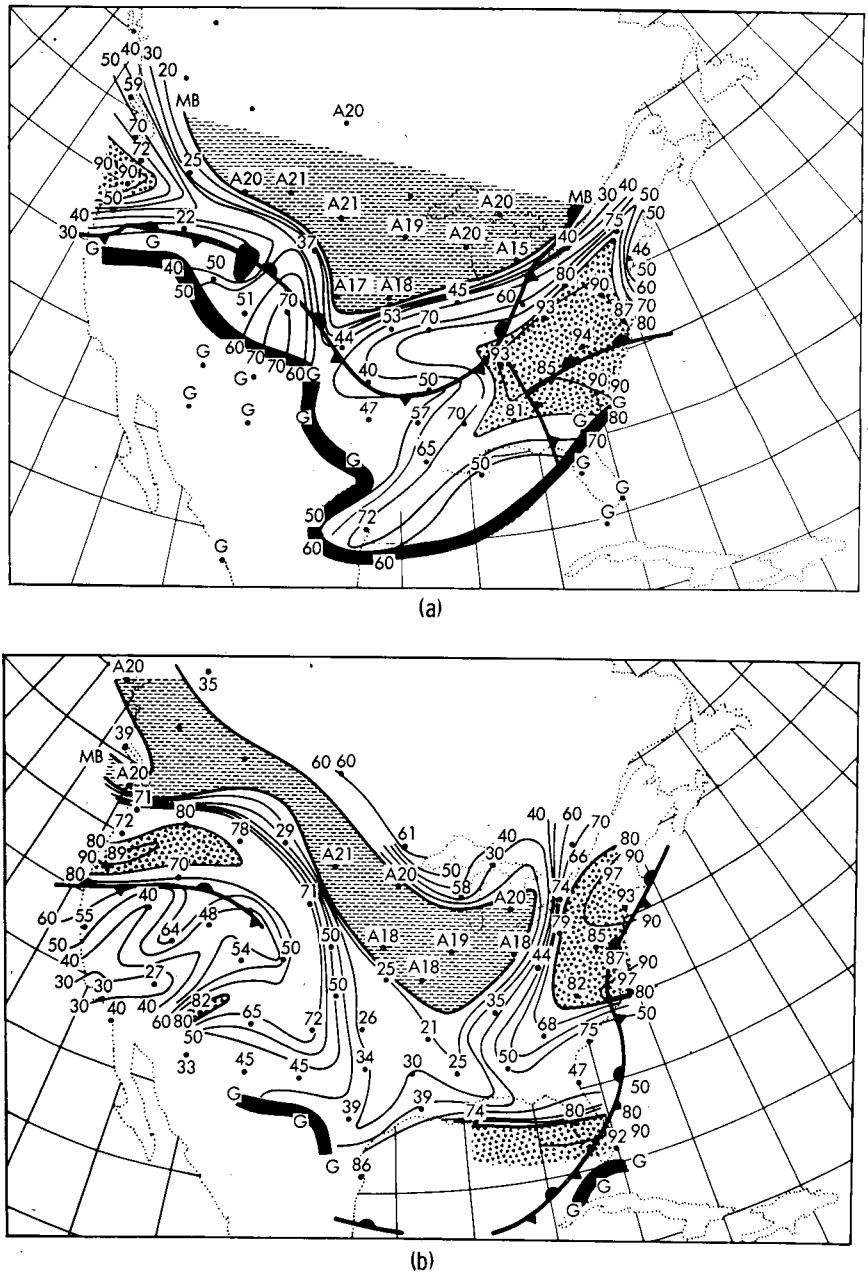

Fig. 7—Relative humidities (%) of 295°K isentropic surface at 00 and 12 GCT on Nov. 22, 1962. Dark belt indicates intersection of this isentropic surface with ground. Areas with humidities larger than 80% and with "motorboating" values are shaded differently. Humidity values are plotted next to stations; maximum humidities possible under "motorboating" conditions are prefixed with the letter "A." Surface frontal systems have been entered into the diagram.

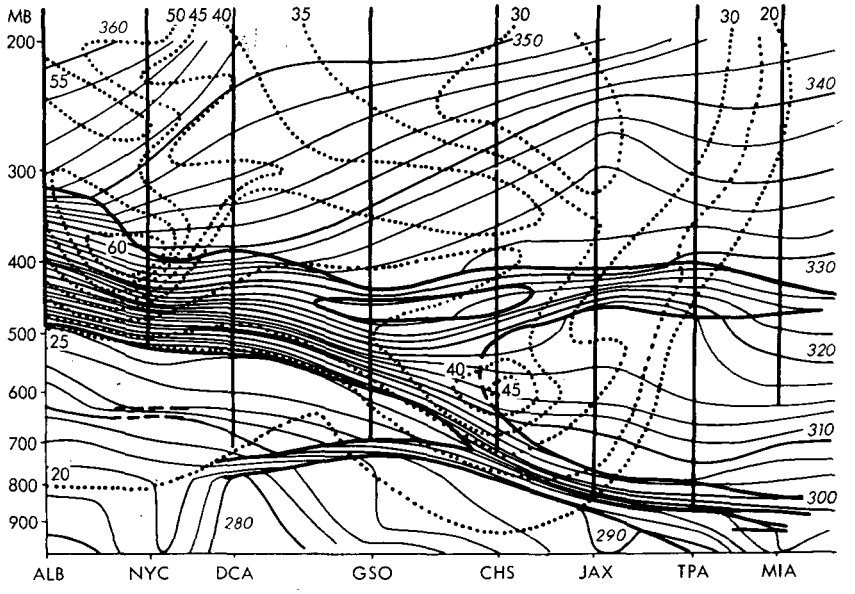

Fig. 8—Cross section through the atmosphere from Albany (ALB), N. Y., to Miami (MIA), Fla., at 00 GCT on Nov. 23, 1962. Thin lines indicate potential temperatures (°K, slanting numbers). Dotted lines indicate isotachs (mps, vertical numbers). Heavy lines outline stable regions. Heavy vertical lines over station location mark the extent of "motorboating" humidity reports.

cesses that carry stratospheric or tropopause air down to the ground in one sweeping motion. According to Fig. 9 the average rate of sinking of this air is approximately 200 mb within 12 hr, or 5.1 cm/sec. This estimate does not include the air in the northern jet-stream branch of Figs. 3a and 3b, which may have come out of the stratosphere but which travels in the middle troposphere. If this air were included in considerations of stratospheric–tropospheric mass exchange, an estimate of approximately 1.5×10^{12} metric tons of air involved in the transport process would be more appropriate.

The total amount of air above the 200-mb level (assumed to be the mean tropopause level) is approximately 1.04×10^{21} g, or 5.2×10^{20} g in one hemisphere. The amount of 1.5×10^{18} g transported down through the tropopause by one jet maximum, therefore, constitutes approximately 0.35% of the stratospheric air of one hemisphere, or approximately 1% of the stratospheric air north of 45° latitude.

So far, we have considered only the effects of one jet maximum. Assume that five planetary waves, each carrying a polar front jet maximum, are active around the hemisphere at the same time and that the subtropical jet stream and the arctic front jet stream have similar

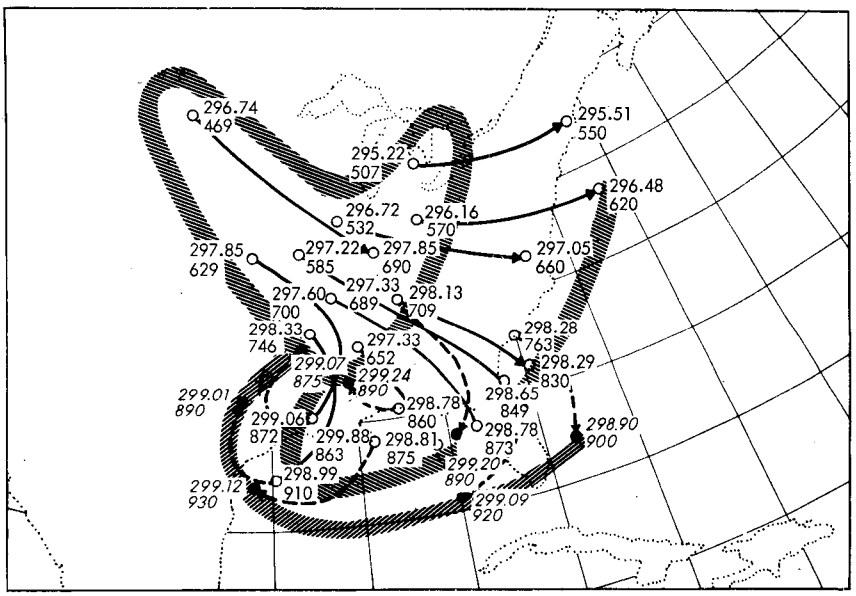

Fig. 9—Trajectories on the 295°K isentropic surface from Nov. 22, 1962, at 12 GCT to Nov. 23, 1962, at 00 GCT (full lines with arrows) and on Nov. 23, 1962, from 00 GCT to 12 GCT (broken lines with arrows). Numerical values of Montgomery stream function (units, 10^7 cm^2/sec^2) and of pressure (mb) are given at starting and terminal points of trajectories (vertical figures are for the first two map times, and slanting figures are for Nov. 22, 1962, at 00 GCT). The centers of the hatched bands indicate the probable boundaries of tropopause air.

effects on stratospheric–tropospheric mass exchange. A rather conservative estimate would be that one hemispheric circulation pattern per month of the nature described suffices to carry the equivalent mass of the stratosphere north of 45° latitude downward through the tropopause level within one year. Jet streams, therefore, have to be considered as very powerful mechanisms for vertical exchange processes in the atmosphere.

Forecasting of Radioactive Fallout

Although no actual forecasts of fallout were attempted in this study, certain facts brought out during this and previous investigations lend themselves to prognostic application. Sharply defined regions of concentrated fallout far away from the site of nuclear explosions should be expected only when high tropospheric or stratospheric air traveling in a jet stream is able to sink through the vertical extent of the troposphere in a matter of a very few days. Only a narrow range of potential temperatures allows a quasi-adiabatic mass flow from the tropo-

Table 2—CHARACTERISTIC POTENTIAL TEMPERATURES OF LAYERS CONTAINING CONCENTRATED RADIOACTIVE FALLOUT REACHING THE GROUND

Date	Location	Isentropic surface followed within contaminated stable layer	Age of debris	Remarks	Reference
Sept. 17 to 21, 1961	Southeastern United States	298 and 303°K	~8 days	Debris layer also encountered by balloon over Flin Flon, Canada, on Sept. 14 and 15, 1961	3, 4, 11
Mar. 30 to Apr. 2, 1963	Western United States	300°K	>100 days	Test ban treaty in effect	7
Nov. 24 to 27, 1962	South Central United States	295 and 300°K	<15 days	Dry fallout combined with local washout	6

pause level to the ground. Table 2 suggests that potential temperatures of 295 to 305°K, when found within the stable layer underneath the jet core, could carry such a rapid downward transport. (In the special case of a warm and low stratosphere or a jet stream in relatively high latitudes, potential temperatures as low as 290°K may produce the same effect.)

Potential temperatures lower than 295°K characterize cold tropospheric air masses. Air masses traveling at higher potential temperatures (especially in the case of the subtropical jet stream) must undergo diabatic cooling before they can reach the ground. Such diabatic processes have a tendency to diffuse radioactive debris over a larger area, thus decreasing the observed concentrations.

Cases of cyclogenesis associated with jet streams with potential temperatures between 295 and 305°K in their stable layer should be viewed as potential fallout-weather situations. The possible implications of dynamic instability in the development of such weather patterns have not yet been studied in detail. However, this is a promising area for future research.

OUTLOOK FOR FUTURE RESEARCH

If jet maximums of moderate intensity are capable of transporting air masses equivalent to the mass of the stratosphere poleward of 45° latitude into the troposphere within one year, a rather powerful mechanism of return flow of tropospheric air into the stratosphere must exist. Such a flow may in part be moist adiabatic and associated with precipitation. Thus computations of air trajectories become difficult since potential vorticity and specific humidity no longer will be conservative quantities.

The geographic distribution and magnitude of return flow will drastically influence the contamination level of stratospheric layers in which originally tropospheric air mixes with stratospheric air. The understanding of these mixing processes, as well as of the exchange mechanisms across the tropopause, would be enhanced greatly by detailed measurements of atmospheric properties at low stratospheric levels. These measurements might be of such characteristics of tropospheric air as ozone and water-vapor concentrations and chemical and radioactive tracers.

REFERENCES

1. D. O. Staley, Evaluation of Potential Vorticity Changes near the Tropopause and the Related Vertical Motions, Vertical Advection of Vorticity and Transport of Radioactive Debris from Stratosphere to Troposphere, *J. Meteorol.*, *17*: 591-620 (1960).

2. D. O. Staley, On the Mechanism of Mass and Radioactivity Transport from Stratosphere to Troposphere, *J. Atmosph. Sci., 19:* 450-457 (1962).
3. E. R. Reiter, *A Case Study of Radioactive Fallout,* Colorado State University Atmospheric Science Technical Paper No. 42, 1963.
4. E. R. Reiter, A Case Study of Radioactive Fallout, *J. Applied Meteorol., 2:* 691-705 (1963).
5. E. R. Reiter, Comments on Paper by S. Penn and E. A. Martell, 'An Analysis of the Radioactive Fallout over North America in Late September 1961,' *J. Geophys. Res., 69:* 786-788 (1964).
6. E. R. Reiter and J. D. Mahlman, *Heavy Radioactive Fallout over the Southern United States, November 1962,* Colorado State University Atmospheric Science Technical Paper No. 58, 1964.
7. J. D. Mahlman, *Relation of Stratospheric–Tropospheric Mass Exchange Mechanisms to Surface Radioactivity Peaks,* Colorado State University Atmospheric Science Technical Paper No. 58, pp. 1-19, 1964.
8. E. F. Danielsen, Radioactivity Transport from Stratosphere to Troposphere, *Mineral Ind. Penna. State Univ., 33(6):* 1-7 (1964).
9. E. Palmén and C. W. Newton, A Study of the Mean Wind and Temperature Distribution in the Vicinity of the Polar Front in Winter, *J. Meteorol., 5(5):* 220-226 (1948).
10. E. R. Reiter, *Jet Stream Meteorology,* University of Chicago Press, Chicago, 1963.
11. K. A. Anderson, *Thin Atmospheric Layers of Radioactive Debris During September 1961,* Cosmic Ray Group, Department of Physics, University of California, Berkeley, Calif., pp. 1-23, 1962.

RELATION OF UPPER AIR HEMISPHERIC INDEX PATTERNS TO SEASONAL FALLOUT FLUCTUATIONS

JERRY D. MAHLMAN
Colorado State University, Fort Collins, Colorado

ABSTRACT

The downward transport of radioactive debris from the stratosphere, in connection with tropopause-level cyclogenesis, is considered as a possible physical explanation for the spring fallout maximum. To examine this possibility, an index designed to measure the relative amount of cyclonic activity in the atmosphere is derived and then compared with seasonal variations in mean fallout intensity. It is established from the analyses that the spring fallout peak cannot be adequately explained by an increase of cyclonic activity at this time of year. It appears, however, that shorter period fallout peaks, superimposed upon the mean seasonal curve, are related to the occurrence of cyclogenesis in the upper troposphere.

INTRODUCTION

In nearly every year since about 1955, a spring maximum of surface radioactivity, resulting from nuclear testing has appeared in the northern hemisphere.[1–3] This spring peak is distinct from the heavy fallout that follows shortly after periods of heavy testing in the atmosphere. The fallout maximums which occur soon after these testing periods are in accordance with the assumption that the mean tropospheric residence time of radioactive debris is of the order of one month. Because the spring peaks often occur many months after the termination of atmospheric nuclear testing, it is necessary to postulate

that the stratosphere provides the debris source for these maximums.[1,4]

As a result of the higher static stabilities and lack of precipitation scavenging in the stratosphere, much longer mean particle residence times would be expected in this region than in the troposphere. At present, a plausible estimate of mean residence time is five years for the tropical stratosphere and one year or less for the polar stratosphere.[5] It is thus reasonable to assume that the stratosphere is the probable debris source for these seasonal oscillations in surface fallout intensity.

With this assumption the problem of explaining the seasonal fallout variations now becomes one of understanding the physical processes that lead to an exchange of mass between the stratosphere and troposphere. It has been suggested by several authors[6–9] that the transport of mass and radioactive debris downward from the stratosphere is associated with extratropical cyclones. Staley[7] demonstrates that this type of mass exchange occurs as a discrete intrusion and hence results in the transport of large amounts of contaminated air into the troposphere. It has been further hypothesized that the sinking is associated with cyclogenetic processes at tropopause level and leads to the occurrence of individual shorter period surface fallout peaks.[10] More-recent research[11] has in part verified this hypothesis and also revealed that this sinking process is characterized by extremely strong vorticity advection and mass convergence.

Because of the apparent dependence of individual fallout maximums upon upper tropospheric cyclones, one may inquire whether the fluctuations in mean seasonal fallout are thus a result of yearly changes in cyclonic activity. A proposed way to partially examine this will be to develop an index parameter that describes the relative amount of tropopause-level cyclonic activity in the middle latitudes and compare the seasonal variations of the index with those of the mean fallout intensity.

DEVELOPMENT OF THE CYCLONE INDEX

Some of the initial attempts toward the development of a simple quantitative description of the state of atmospheric flow at a given level were begun by Rossby[12] and Allen *et al.*[13] These efforts to produce numerical indexes that would reduce the complexities of atmospheric motions resulted in the well-known zonal index. The concept of utilizing this index to describe atmospheric motions on a global basis has proved to be exceedingly valuable in many areas of atmospheric research. However, for more specialized problems, this index fails to provide a sufficiently reliable description of the state of atmospheric motions.[14,15] Also, if hand computation is necessary, the time required to calculate a series of index values may be prohibitive.

In the previous section the desirability of testing the relation between the formation of extratropical cyclones and surface radioactive fallout by using atmospheric indexes was mentioned. It is imperative that the type of index parameter employed provides an adequate description of the relative amount of cyclonic activity in the atmosphere. Because these cyclonic disturbances strongly influence the direction of the upper wind field, it appears feasible that the derived index parameter be determined by the deviation of the mean wind vector from westerly flow. It also will be advantageous to restrict the index to a nondimensional and normalized form. In conformance with this restriction, a purely zonal westerly current will be arbitrarily defined to possess an index of 1.0 and a purely meridional current will be defined to be 0.0. (These index values are now in the same sense as the high and low index concepts derived from the original zonal index.)

To simplify the mathematical approach as much as possible, one may assume a time-independent sinusoidal velocity current at a given height which is everywhere tangent to the isobars and is superimposed upon a plane earth. The normal distance, y, of a given wave from the x-axis in such a system is then given by

$$y = A \sin \frac{2\pi x}{L} \tag{1}$$

where A is the amplitude of the wave and L is the wavelength. The slope of the current at any point in this system is thus

$$\frac{dy}{dx} = \frac{2\pi A}{L} \cos \frac{2\pi x}{L} \tag{2}$$

The mean value of a function $\beta(\xi)$ over the interval a,b is defined to be

$$\overline{\beta} = \frac{1}{b-a} \int_a^b \beta(\xi)\, d\xi \tag{3}$$

By Eq. 3, the mean slope of the sinusoidal current over one-fourth of a wavelength is given by

$$\left(\overline{\frac{dy}{dx}}\right) = \frac{1}{(nL + L/4 - nL)} \frac{2\pi A}{L} \int_{nL}^{nL+L/4} \cos \frac{2\pi x}{L}\, dx \tag{4a}$$

or which reduces to

$$\left(\overline{\frac{dy}{dx}}\right) = \frac{4A}{L} \tag{4b}$$

where $n = 1, 2, 3, \ldots$. Because of the symmetry of the current, by integration over any $nL/4$ wavelengths, the mean absolute value of the slope is thus

$$\left|\overline{\frac{dy}{dx}}\right| = \frac{4A}{L} \tag{5}$$

Also, by definition,

$$\left|\frac{dy}{dx}\right| = \tan |\alpha| \tag{6a}$$

or

$$\left|\overline{\frac{dy}{dx}}\right| = \tan |\overline{\alpha}| \tag{6b}$$

Here $|\overline{\alpha}|$ is defined to be the mean absolute value of the deviation from a pure west wind ($\alpha = \theta - 270°$, where θ is the instantaneous wind direction). By substituting Eq. 6b into Eq. 5 and solving for $|\overline{\alpha}|$, one obtains

$$|\overline{\alpha}| = \text{arc tan} \frac{4A}{L} \tag{7}$$

which is an expression for the mean absolute value of the deviation from westerly flow for a sinusoidal current of arbitrary amplitude and wavelength.

Now, if a cyclone index is defined in terms of the previously specified conditions for zonal ($C = 1.0$) and meridional ($C = 0.0$) flow, one may write

$$C = 1 - \frac{|\overline{\alpha}|}{90°} \qquad (0° \leq |\overline{\alpha}| \leq 90°) \tag{8}$$

If this derived index is to adequately describe the state of the flow of any given current, the value of $|\overline{\alpha}|$ calculated from the given sinusoidal current must compare favorably with the theoretical value obtained from Eq. 7. The calculated value of $|\overline{\alpha}|$ is obtained from this given sinusoidal current by measuring $|\alpha|$ at particular points along a discrete grid interval. This grid distance must necessarily be less than one-half wavelength so that a reliable sample can be obtained. The theoretical value of $|\overline{\alpha}|$ from the given sinusoidal current is then compared with the measured value of $|\overline{\alpha}|$ obtained from the same ideal current. The comparison between the measured and

the theoretical values is then statistically analyzed by employing a Student's "t" test. This analysis reveals that the value of $|\overline{\alpha}|$ measured from the given sinusoidal current is significantly lower (at the 95% probability level) than its comparable theoretical value. This results from the bias introduced by measuring the slope of the current along the latitude circle rather than along the wave itself. This difficulty may be readily circumvented, however, because the statistical analysis also showed that the measured root-mean-square value of $|\overline{\alpha}|$, $(\overline{\alpha^2})^{1/2}$ is an excellent approximation to the theoretical value of $|\overline{\alpha}|$. One thus may replace $|\overline{\alpha}|$ in Eq. 8 by $(\overline{\alpha^2})^{1/2}$ to obtain

$$C = 1 - \frac{(\overline{\alpha^2})^{1/2}}{90^\circ} \tag{9}$$

Recalling that $\alpha = \theta - 270^\circ$, Eq. 9 may be defined in terms directly applicable to atmospheric measurement so that

$$C = 1 - \frac{1}{90^\circ}\left[\frac{\sum_{i=1}^{n}(\theta - 270^\circ)^2}{n}\right]^{1/2} \tag{10}$$

where n is the number of measurements along the chosen latitude circle. The index C is now in a form so that its measured value (computed by measuring α along a discrete grid interval) compares favorably with the theoretical value of the given ideal current. This is advantageous because a value of C can now be calculated from the data for any current, regardless of its complexity.

APPLICATION OF THE DERIVED CYCLONE INDEX TO THE ATMOSPHERE

In this research the possible correlations between the derived cyclone index C as applied to the atmosphere and fluctuations of radioactive fallout at the surface were examined. Because the radioactive debris that results from a recent atmospheric test tends to mask older stratospheric debris, it is imperative that such correlations be tested over a period in which no nuclear testing has taken place. Also, this chosen period must be long enough after the cessation of nuclear testing so that the influence due to tropospheric debris is minimized.

To satisfy these specified restrictions, the period following the last atmospheric test in December 1962 was chosen for the analysis. This was an especially suitable period because the stratospheric-

debris intensity was relatively high as a result of heavy testing prior to the test ban.

Since fallout maximums tend to appear in relation to tropopause-level cyclones,[7,8,10,11] 300 mb was chosen as the most representative level for the calculation. Because the maximum cyclonic intensity generally occurs within the 40 to 60°N latitude band, 50°N was chosen as an appropriate latitude for the calculation of a series of cyclone-index values. Also, since the United States provides the only fallout network that gives values representative over a large area, the index was calculated from 70°W to 110°E longitude instead of around the entire hemisphere.

If Eq. 10 is applied to the atmosphere under the previously specified conditions, a difficulty arises because the flow direction is often nonsymmetrical with respect to a given longitude line. In theory, this could be avoided by driving the cyclone index in terms of a more complicated atmospheric current that incorporates the tilting of troughs.[16,17] This approach, however, increases the complexity of the derivation of C considerably. These problems resulting from the asymmetry of the current were in part avoided by measuring a mean θ over the 10-degree latitude interval of 45 to 55°N instead of taking a point value at 50°N.

By an incorporation of the previous specified conditions, the cyclone index was calculated at 24-hour intervals for the period of January to October 1963. Computational noise and the higher frequency components were filtered from the time series by using a weighted smoothing technique.[18] See Fig. 1. By independent cross-checks the cyclone index was seen to provide a statistically reliable indication of the relative amount of cyclonic activity in the atmosphere. The index was also checked by calculating separate time series with the use of the 00 GMT and the 12 GMT data, respectively. The major fluctuations in the two resultant smoothed time series were identical. The calculated filtered index time series for the indicated period showed a succession of index increases terminated by index drops of equal magnitude.

RELATION OF THE INDEX SERIES TO THE FALLOUT DISTRIBUTION

The time distribution of fallout in air over the United States was determined by computing area-weighted averages of gross beta activity in picocuries per cubic meter of air from the U. S. Public Health Radiation Surveillance Network. Two distinct scales of fallout intensity with respect to time were obtained by calculating five-day and monthly averages of the mean area-weighted fallout intensity (see Fig. 1). This

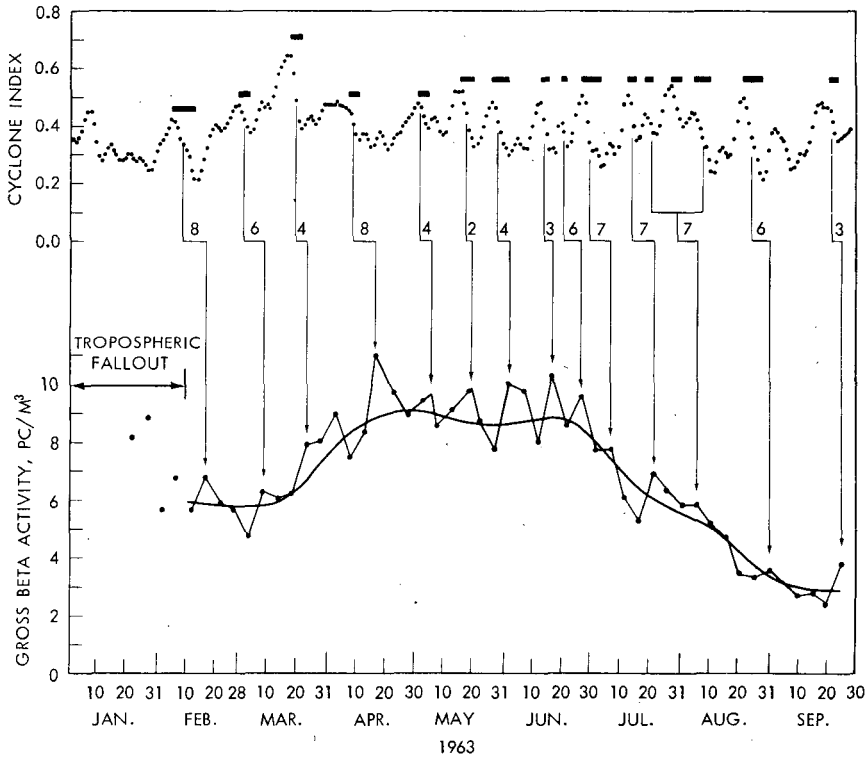

Fig. 1—Time series of comparison between derived cyclone index and shorter period fallout fluctuations. Upper part of diagram is a plot of the smoothed cyclone-index series. In the lower part: the connected lines are five-day mean gross beta activity, and the smooth line is representative of mean monthly fallout values. Vertical arrows show correspondence between rapid cyclone-index drops and fluctuations of surface-fallout intensity upon the mean monthly distribution. Plotted numbers associated with the arrows give the time in days after the center date of the period over which the drop occurred. Solid bars represent time increment over the period of index decrease. Values of $[100(C_1 - C_2)]/\Delta t$ *computed during rapid decreases of cyclone index are given in Table 1.*

figure shows that an irregular fallout fluctuation of short duration is superimposed upon the seasonal oscillation as determined from the monthly averages. Because of the large number of observations that determine these five-day means and the relatively small variance between the individual measurements, even relatively small fluctuations of fallout intensity become statistically significant. Figure 2 shows that a very pronounced increase in mean fallout characterized the spring of 1963 and that a spring peak also occurred in 1964. The 1964 maximum is in agreement with a distinct spring fallout maximum[2]

Table 1 — VALUES OF $[100(C_1 - C_2)]/\Delta t$ COMPUTED PRIOR TO THE FINAL SMOOTHING OF C AS SHOWN IN FIG. 1*

Dates	$[100(C_1 - C_2)]/\Delta t$		$[100(C_1 - C_2)]/\Delta t$ in ascending order	
Feb. 6 to 13	3.6	Fallout	0.7	None
Feb. 19 to 22	0.7	None	1.3	None
Mar. 1 to 4	3.3	Fallout	2.0	None
Mar. 18 to 21	9.7	Fallout	2.4	None
Mar. 25 to 27	2.0	None	3.0	None
Apr. 7 to 10	4.0	Fallout	3.0	None
Apr. 18 to 21	3.0	None	3.3	None
May 2 to 4	6.0	Fallout	3.3	Fallout
May 7 to 10	3.0	None	3.4	None
May 15 to 21	5.0	Fallout	3.5	Fallout
May 26 to 30	4.3	Fallout	3.6	Fallout
June 6 to 9	1.3	None	3.6	Fallout
June 12 to 14	8.0	Fallout	3.8	Fallout
June 19 to 22	4.7	Fallout	4.3	Fallout
June 28 to July 5	5.0	Fallout	4.7	Fallout
July 7 to 10	2.4	None	4.9	Fallout
July 13 to 16	8.3	Fallout	4.9	Fallout
July 20 to 23	3.6	Produced one	5.0	Fallout
July 27 to 31	3.8	fallout	5.0	Fallout
Aug. 6 to 12	3.5	increase	6.0	Fallout
Aug. 15 to 17	3.4	None	8.0	Fallout
Aug. 22 to 29	4.9	Fallout	8.3	Fallout
Sept. 2 to 9	3.3	None	8.4	Fallout
Sept. 17 to 23	8.4	Fallout	9.7	Fallout

*Calculated values are arranged initially by date and then according to ascending order of calculated $[100(C_1 - C_2)]/\Delta t$. The word "fallout" signifies that a fallout maximum was observed shortly after the index decrease, and "none" denotes that no subsequent fallout peak was observed.

in 1960, more than a year after the voluntary test moratorium of late 1958.

Since radioactive debris in the stratosphere decreases with time as a result of natural decay, it appears to be advantageous to express fallout values in terms of intensities adjusted to an arbitrary age. This has the advantage that similar mass-transport processes at different times will produce a more comparable measured radioactive-debris intensity in the troposphere. Also, this adjustment may lead to a more accurate determination of the relative time rate of depletion of the stratospheric-debris inventory as a result of stratospheric-tropospheric exchange mechanisms.

The rate of decay of the 1963 debris was determined by analyzing the time change of the relative contribution of each specific nuclide and taking into account the resultant change in mean half-life of the debris

as time progressed (see Table 2). This was done for each month so that the rate of decay of a given fallout sample could be obtained by computing the mean half-life from the available data (see Fig. 3). The measured fallout intensities were then adjusted to an age of 100 days by taking simple ratios from Fig. 3, thus yielding the age-adjusted fallout intensities of Fig. 2.

Table 2 — PERCENT CONTRIBUTION OF PARTICULAR NUCLIDES IN TOTAL MONTHLY RADIOACTIVE DEBRIS MEASURED IN RAINFALL AT WESTWOOD, N. J.

Nuclide	Half-life,* days	Contribution in 1963, %					
		Jan.	Feb.	Mar.	Apr.	May	June
^{90}Sr	10,120	00.9	01.2	01.6	02.0	02.2	02.8
^{89}Sr	50.5	26.2	23.8	18.0	15.2	11.4	10.1
^{144}Ce	285	21.5	34.2	36.8	49.7	44.8	51.6
^{95}Zr	65.0	44.8	34.2	30.8	25.8	28.2	26.2
^{137}Cs	11,140	01.4	01.6	02.3	02.8	03.2	04.1
^{141}Ce	33.1	05.2	05.0	10.5	04.5	10.2	05.2

*Half-life of each nuclide is given in days.[19]

A comparison of the index time series with that of the mean age-adjusted monthly fallout was then attempted. This analysis revealed that no significant relation appeared to exist between these two quantities. Although there were general index breakdowns preceding the January and April fallout peaks shown in Fig. 2, equally large breakdowns at other times did not produce similar trends in mean fallout distribution. It thus appears that a simple causal relation cannot be established between the seasonal changes of the index and the spring fallout maximum.

On the other hand, a similar comparison between the cyclone index and the mean five-day age-adjusted fallout was constructed (Fig. 1). In this case a very interesting relation between the two time series was noted. The diagram reveals that the shorter period fluctuations superimposed upon the mean monthly fallout curve appear to be related to rapid decreases of the cyclone index. It also was noted that the fallout peaks occurred approximately five days after the center date of the period over which the drop in C took place.

Because a fallout peak did not occur shortly after all the observed drops in the cyclone index, an attempt was made to determine whether or not it was possible to differentiate between the fallout-producing and the non-fallout-producing index decreases. By trial it was empirically determined for the limited sample of data that the parameter $[100(C_1 - C_2)]/\Delta t$ provided a reliable method for separating the fallout-producing index drops from the nonproductive ones (C_1 and C_2 are the

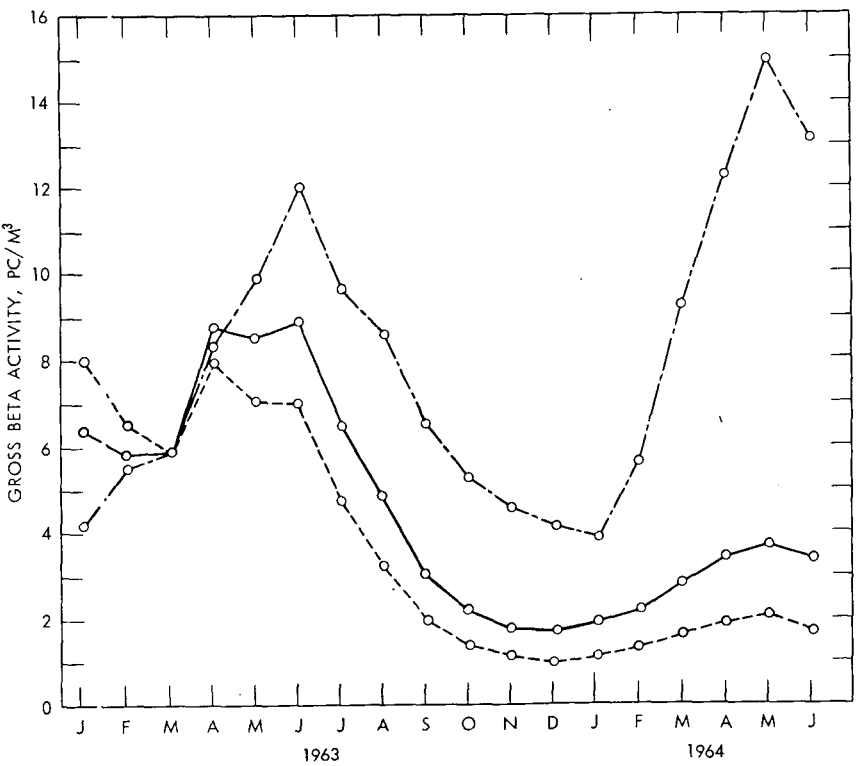

Fig. 2—Mean monthly area-averaged gross beta activity in air over the United States after the test ban of December 1962. Lower curve (- - -) represents actually measured radioactivities and shows a pronounced spring maximum of fallout in 1963 with a lesser peak in the spring of 1964. Middle curve (——) represents the measured fallout adjusted to a common age of 100 days by the decay curve of Fig. 3. Upper curve (— — —) gives the fallout intensity of the lower curve adjusted to age 100 days by the well-known empirical formula $AT^{1.2}$ = constant. From the discrepancy between the two upper curves, it is evident that this formula is invalid for longer-lived fallout samples.

initial and final values of the cyclone index over the period of decrease, and Δt is the time in days over which the decrease occurred) (see Table 2). It was concluded from the data in Table 2 that any value of $[100(C_1 - C_2)]/\Delta t$ measured to be significantly greater than 3.5 would probably produce an increase in surface fallout (over that of the mean seasonal value) a short time later. This increase has interesting implications in that it indicates a possibility of constructing a prediction model for the shorter period fallout fluctuations. However, it must be pointed out that the validity of this inference is not completely certain because of the relatively short time period over which the analysis was performed. Furthermore, no significant relation could be

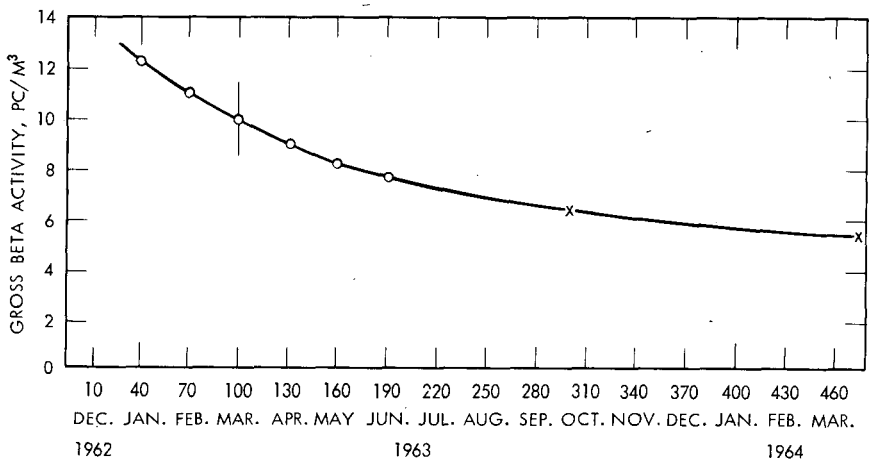

Fig. 3—Natural decay curve for a mixed debris sample computed from Table 2. Source intensity at time 100 days (mid-March 1963) is assumed to be 10 pc per cubic meter of air. Abscissa is in monthly increments along with the approximate time in days. Time 100 days is marked on the curve with a vertical line. The circles represent measured decay relative to the original source for a particular time. Extrapolated values are denoted by an x.

established between the magnitude of this parameter and the relative amount of fallout subsequently observed. This is very probably due to a number of complicating factors not taken into account in the simplified model presented here.

SUMMARY AND FUTURE OUTLOOK

An index designed to measure the relative amount of cyclonic activity in the atmosphere was developed to compare its variations with changes in seasonal-fallout intensity. A definite relation between the index and seasonal-fallout variations was not substantiated. On the other hand, the analysis indicated that an apparent correlation existed between large decreases of the cyclone index and subsequent shorter period increases in surface fallout over that of the mean seasonal curve.

It thus appears that tropopause-level cyclogenesis is the predominate mechanism leading to the intrusion of stratospheric air into the troposphere, as hypothesized earlier.[10,11,20] However, it cannot be stated that these cyclogenetic processes are the primary causes of the spring fallout peaks. It appears that the spring fallout maximum is probably due to a combination of factors that are still poorly understood.

In the future the validity of the apparent relation between the cyclone index and the shorter period fallout fluctuations will have to be more thoroughly tested. Also, the proposed prediction model will have to be refined and tested so that more quantitative estimates of future fallout will be possible. The interaction between seasonal variations in the stratospheric circulation and the tropopause-level cyclogenetic process will have to be examined in far greater detail, especially in connection with the observed rates of depletion of nuclear debris in the stratosphere.

ACKNOWLEDGMENTS

The author wishes to thank Elmar R. Reiter for the extensive encouragement and guidance he gave while the research was being performed. William D. Ehrman provided invaluable technical and computational assistance, and Mrs. Viola Weiland typed the manuscript. The data used in the analysis were provided by the National Weather Records Center in Asheville, N. C.

REFERENCES

1. L. M. Fry, F. A. Jew, and P. K. Kuroda, On the Stratospheric Fallout of Strontium-90: The Spring Peak of 1960, *J. Geophys. Res., 65:* 2061-2066 (1960).
2. P. F. Gustafson, S. S. Brar, and M. A. Kerrigan, Appearance of a Spring Maximum in Nuclear Test Debris in 1960, *Science, 133:* 460-461 (1961).
3. D. H. Peirson, Beryllium-7 in Air and Rain, *J. Geophys. Res., 68:* 3831-3832 (1963).
4. W. F. Libby and C. E. Palmer, Stratospheric Mixing from Radioactive Fallout, *J. Geophys. Res., 65:* 3307-3317 (1960).
5. W. F. Libby, Radioactive Fallout, Particularly from the Russian October Series, *Science, 45:* 151-175 (1959).
6. P. B. Storebø, Orographical and Climatological Influences on Deposition of Nuclear-bomb Debris, *J. Meteorol., 16:* 600-608 (1959).
7. D. O. Staley, Evaluation of Potential-vorticity Changes near the Tropopause and the Related Vertical Motions, Vertical Advection of Vorticity, and the Transfer of Radioactive Debris from Stratosphere to Troposphere, *J. Meteorol., 17:* 591-620 (1960).
8. D. O. Staley, On the Mechanism of Mass and Radioactivity Transport from Stratosphere to Troposphere, *J. Atmos. Sci., 19:* 450-467 (1962).
9. Y. Miyake, K. Sarukashi, Y. Katsurage, and T. Kanazawa, Seasonal Variation of Radioactive Fallout, *J. Geophys. Res., 67:* 189-193 (1962).
10. J. D. Mahlman, Relation of Stratospheric-Tropospheric Mass Exchange Mechanisms to Surface Radioactivity Peaks, *Transport Processes in the Atmosphere Leading to Radioactive Fallout, Progress Report No. 1, Technical Paper No. 58,* Colorado State University, 1964.
11. E. R. Reiter and J. D. Mahlman, Heavy Fallout over the Southern United States in November 1962, *Transport Processes in the Atmosphere Leading to Radioactive Fallout, Progress Report No. 1, Technical Paper No. 58,* Colorado State University, 1964.

12. C.-G. Rossby *et al.*, Relation Between Variations in the Intensity of the Zonal Circulation of the Atmosphere and the Displacements of the Semi-permanent Centers of Action, *J. Marine Res., 2:* 38-55 (1939).
13. R. A. Allen, R. Fletcher, J. Holmboe, J. Namias, and H. C. Willett, Report on an Experiment in Five-day Weather Forecasting, *Papers Phys. Oceano. Meteorol. Mass. Inst. Technol. Woods Hole Oceano. Inst., 8*(3): (1940).
14. J. Namias, The Index Cycle and Its Role in the General Circulation, *J. Meteorol., 7:* 130-139 (1950).
15. H. Riehl, T. C. Yeh, and N. E. LaSeur, A Study of Variations of the General Circulation, *J. Meteorol., 6:* 181-194 (1950).
16. L. Machta, Dynamic Characteristics of a Tilted-trough Model, *J. Meteorol., 6:* 261-265 (1949).
17. H. Arakawa, Tilted-trough Model as an Interaction Between Low- and High-latitude Disturbances, *J. Meteorol., 10:* 64-66 (1953).
18. R. B. Blackman and J. W. Tukey, *Measurement of Power Spectra*, Dover Publications, Inc., New York, 1958.
19. E. P. Hardy, Jr., J. Rivera, and W. R. Collins, Jr., Fallout Program Quarterly Summary Report, USAEC Report HASL-142, Health and Safety Laboratory, Jan. 1, 1964.
20. E. F. Danielsen, Radioactivity Transport from Stratosphere to Troposphere, *Mineral Ind. Penn. State Univ., 33*(6): 1-7 (1964).

ATMOSPHERIC RADIOACTIVITY ALONG THE 80TH MERIDIAN (WEST)

LUTHER B. LOCKHART, JR., ROBERT L. PATTERSON, JR.,
ALLEN W. SAUNDERS, JR., and ROBERT W. BLACK
U. S. Naval Research Laboratory, Washington, D. C.

ABSTRACT

Operation of the Naval Research Laboratory (NRL) 80th Meridian Air Sampling Program, from May 1956 through December 1962, took place during an interesting period in the nuclear age and the development of nuclear weaponry and covered the nearly three-year moratorium on nuclear testing as well as the episodes of intensive testing of high-yield devices both before and after the moratorium. Data collected during this program helped substantiate a number of concepts regarding atmospheric mixing processes and residence times of radioactive particulate matter in the atmosphere.

This paper summarizes measurements of the concentrations of both gross beta activity and ^{90}Sr activity in the air at ground level along the 80th meridian (west) during the period 1957 to 1962. More-detailed results and interpretations are given for collections of radioactivity made in 1962.

INTRODUCTION

At the time of inception of the 80th Meridian Air Sampling Program in 1955, there were even more uncertainties than there are now in the behavior of airborne nuclear-bomb debris. The concept of delayed deposition of stratospheric debris was in its infancy, and the seasonal aspects of this deposition were unsuspected. No information was available on the extent of transequatorial migration of radioactive aerosols

in the troposphere; indeed, there was little information on levels of either fission products or natural radioactivity in the air of the southern hemisphere.

Preliminary discussions were also underway during this period regarding the advisability of including in the forthcoming International Geophysical Year (IGY) program a study of atmospheric nuclear radiation, following the suggestion of The Netherlands. In this regard, it may be of interest to note here that the U. S. Naval Research Laboratory (NRL) had previously, in 1954, recommended that the U. S. National Committee for the IGY propose to the international organization a comprehensive program of measurement of both natural and fission-product activity in the air; this recommendation was not carried out, however.

It was with this background information in mind that representatives of NRL, the Division of Biology and Medicine of the U. S. Atomic Energy Commission (AEC), and the U. S. Weather Bureau met and concluded that a program of measurement of fission-product activity in the air was desirable, regardless of whether or not it later became a part of the proposed nuclear-radiation study of the IGY. Everyone contacted in regard to participation in this program was enthusiastic about it, and excellent cooperation was obtained from all participating groups. This program has been financed jointly by the Office of Naval Research and the Division of Biology and Medicine, AEC.

Actual operation of a portion of the network of stations began in May 1956; air filters were used at a few sites, and standard AEC gummed-film fallout collectors and experimental NRL cheesecloth collectors were employed at others. As they became available, filters and blower units were supplied to all stations. Later, cheesecloth and gummed-film collections were discontinued because of their lack of correlation with air-concentration measurements. By the start of the IGY in July 1957, an effective 80th meridian network was in operation, with daily collections of gross fission-product activity from the air at ground level being taken. The sampling sites and cooperating agencies participating in this program are listed in Table 1.

In December 1962 NRL voluntarily terminated its association with the 80th meridian network and transferred direction to the Health and Safety Laboratory (HASL), AEC. A complete listing of NRL reports and publications resulting from this AEC-sponsored program is included in the reference section (Refs. 1 to 26).

PROCEDURES

Positive-displacement blowers were used to draw air through 8-in.-diameter absolute filters (Navy equivalent of ACC type 6 cellulose–

Table 1—COLLECTING SITES ASSOCIATED WITH NRL IN THE STUDY OF AIRBORNE FISSION PRODUCTS ALONG THE 80TH MERIDIAN

Station	Latitude	Longitude	Elevation, m	Period of operation	Cooperating organizations
Thule, Greenland	76°35′N	68°35′W	259	Apr. 1958 to Dec. 1962*	U. S. Air Force
Coral Harbour, NWT, Canada	64°12′N	83°22′W	59	Mar. 1958 to Dec. 1959	Meteorological Branch, Department of Transport, Canada
Moosonee, Ontario, Canada	51°16′N	80°39′W	10	Nov. 1957 to Dec. 1962*	Meteorological Branch, Department of Transport, Canada
Bedord, Mass.	42°27′N	71°22′W	80	Jan. 1958 to Dec. 1959	USAF Cambridge Research Center
Washington, D. C.*	38°59′N	77°29′W	82	May 1956 to Dec. 1962*	U. S. Weather Bureau
Columbia, S. C.	33°57′N	81°07′W	69	Jan. 1958 to Oct. 1959	U. S. Weather Bureau
Miami, Fla.	25°49′N	80°17′W	4	June 1957 to Dec. 1962*	U. S. Weather Bureau
San Juan, Puerto Rico	18°26′N	66°00′W	10	June 1957 to Dec. 1962*	U. S. Weather Bureau
Miraflores, Panama Canal Zone	9°00′N	79°35′W	10	June 1956 to Dec. 1962*	U. S. Naval Research Laboratory, Canal Zone Corrosion Laboratory
Bogota, Colombia	4°37′N	74°04′W	2640	July 1957 to Dec. 1959	Instituto Geofisico de los Andes Colombianos
Quito, Ecuador	0°08′S	78°26′W	2818	Apr. 1957 to Dec. 1959	Observatorio Astronomico de Quito
Guayaquil, Ecuador	2°10′S	79°52′W	7	May 1956 to Dec. 1962*	Meteorological Office Direccion General de Aviacion Civil
Iquitos, Peru	3°45′S	73°11′W	117	Oct. 1957 to Dec. 1959	Corporacion Peruana de Aeropuertos y Aviacion Comercial (CORPAC)
Lima, Peru	12°01′S	77°07′W	30	May 1956 to Dec. 1962*	Corporacion Peruana de Aeropuertos y Aviacion Comercial (CORPAC)
Huancayo, Peru	12°07′S	75°20′W	3353	Oct. 1957 to Dec. 1959	Instituto Geofisico de Huancayo
Chacaltaya, Bolivia	17°10′S	68°15′W	5220	Sept. 1957 to Dec. 1962*	Universidad Mayor de San Andres, Laboratorio de Fisica Cosmica de Chacaltaya
Antofagasta, Chile	23°37′S	70°16′W	519	Nov. 1957 to Dec. 1962*	NASA Satellite Tracking Station
Porto Alegre, Brazil	30°02′S	51°13′W	24	Dec. 1957 to Oct. 1959	Servico de Meteorologia (Brasil)
Santiago, Chile	33°27′S	70°42′W	520	July 1956 to Dec. 1962*	Oficina Meteorologica de Chile
Puerto Montt, Chile	41°27′S	72°57′W	5	Dec. 1957 to Dec. 1962*	Oficina Meteorologica de Chile
Punta Arenas, Chile	53°08′S	70°53′W	3	Oct. 1956 to Dec. 1962	Oficina Meteorologica de Chile

*Operation continuing as part of HASL 80th meridian network.

asbestos paper) at a constant rate (approximately 1200 m^3/day) with filter changes daily, thrice weekly, or weekly as the situation warranted. Air flow was not measured at the collecting site but was calculated from blower performance as a function of station altitude and pump-rotation rate.

Samples, with pertinent data attached, were returned to NRL via air transportation and measured for gross beta activity two weeks following the end of the collection period. Prior to measurement the samples were ashed at 650°C and compressed to disks of 1 sq in. area, each weighing about 1 g. The radioactivity standard was RaDE (^{210}Pb-^{210}Bi) (1.17 Mev beta) mounted with a similar quantity of ash. The activity was determined on conventional beta-counting equipment equipped for automatic sample changing. The time to reach a preset total of 2000

to 10,000 or more counts was recorded, depending on the sample activity and the time available. No corrections were made for radioactive decay.

These ashed samples were later combined on a monthly or bimonthly basis and subjected to sequential radiochemical analysis for such radionuclides as ^{89}Sr, $^{90}Sr(^{90}Y)$, ^{91}Y, ^{137}Cs, ^{141}Ce, $^{144}Ce(^{144}Pr)$, ^{147}Pm, ^{185}W and $^{210}Pb(RaD)$ by conventional procedures.[3]

Since transfer of this operating network to HASL, some changes have been instituted by that agency, namely, the use of polystyrene filters instead of cellulose–asbestos filters, gamma counting instead of beta counting, and filter changes on a four per month schedule rather than on a weekly schedule.[27] Radiochemical analyses for a selected list of nuclides, including many of the preceding and some additional ones, are also being undertaken; thus there should be reasonable continuity in this program.

GROSS FISSION PRODUCTS IN THE AIR

The monthly average gross fission-product concentrations in the air along the 80th meridian (west) during the period from 1957 through 1962 are reported in Figs. 1 and 2 for representative low-altitude sites in the northern and southern hemispheres. Since no corrections have been made for radioactive decay during the period between collection and measurement, the actual air concentrations existing during periods of active nuclear testing must have been considerably higher (perhaps as much as a factor of 2 in some cases).

Maximums in fission-product levels can be observed at the northern hemisphere sites (Fig. 1) during the spring of each year regardless of the extent of testing during the previous season. The presence of such peaks during the moratorium on testing proved conclusively that there was a seasonal factor involved in the rate of stratospheric deposition of radioactive debris. Other peaks can be associated with direct tropospheric contamination by devices detonated immediately preceding the measurement.

In the southern hemisphere the seasonal variation in radioactivity levels is not at all obvious, and the major peaks of activity may be readily correlated with prior nuclear tests in the tropics (Pacific Proving Grounds or Christmas Island area) or subtropics (Sahara Desert).

These data can also be presented in the form of tropospheric burdens of gross fission-product activity, a method of display that accentuates the major trends taking place in radioactivity levels and gives a rough idea of the total quantity of radioactivity in the air at any one time. The activity burdens calculated for the northern and southern

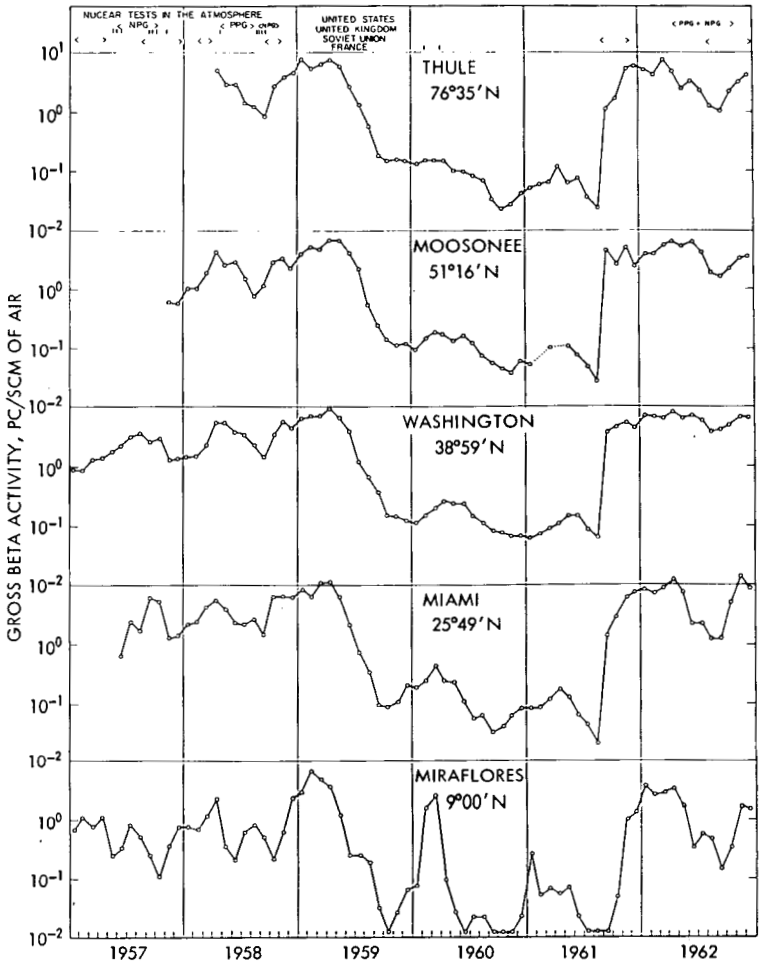

Fig. 1—Fission-product radioactivity in the ground-level air at some sites in the northern hemisphere.

hemispheres, shown in Fig. 3, are based on the naïve assumption that the concentration of radioactive material per unit volume found at ground level at a given site is uniform up to the tropopause and is characteristic of that latitude. It is recognized that there often exist higher concentrations of activity in the upper troposphere and that, particularly during periods of nuclear testing, there is no uniform distribution within latitude bands. Notwithstanding these and other less obvious objections, this method of presentation does represent rather clearly the behavior of fission debris in the atmosphere.

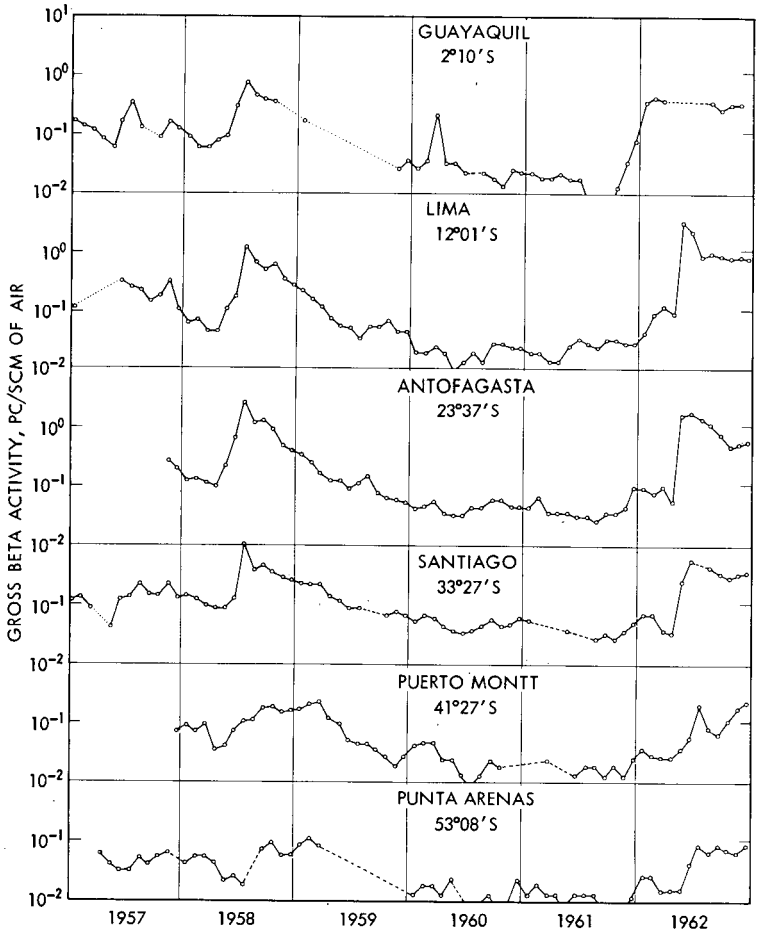

Fig. 2—Fission-product radioactivity in the ground-level air at some sites in the southern hemisphere.

The large spring peaks in the northern hemisphere following intensive periods of testing in the fall of 1958 and the fall of 1961 are obvious. The rapid decrease in activity levels in the months following the peak concentrations and the supposed cessation of stratospheric subsidence indicates that the average residence time for tropospheric debris in the northern hemisphere is something less than 30 days. The smaller spring peaks during 1960 and 1961 during the moratorium on nuclear testing observed by the United States, the Union of Soviet Socialist Republics, and the United Kingdom are also apparent but superimposed on them is activity from French tests held in the Sahara.

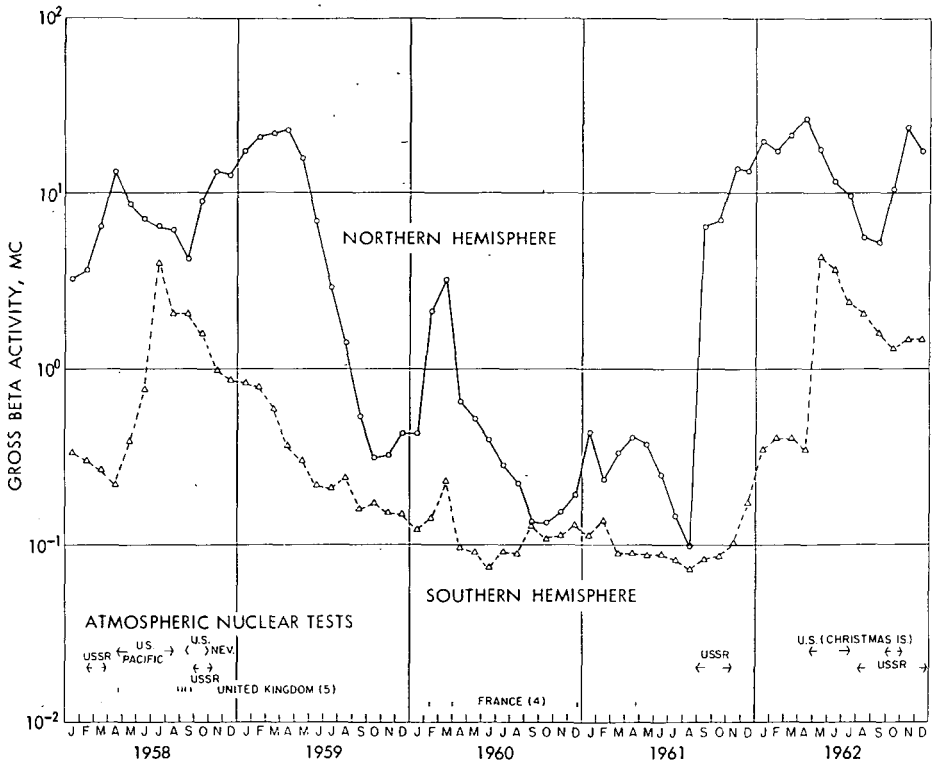

Fig. 3—Tropospheric burdens of gross fission-product radioactivity.

This activity was confined principally to the north temperate zone although sensitive radiochemical analyses did indicate the presence of short-lived fission products from the first French test throughout the northern hemisphere and as far south as Antofagasta, Chile.[14,16] The small peak in the southern-hemisphere burden during March 1960 is also due to French nuclear debris.

The southern-hemisphere burdens do not show any true seasonal trends. This may be variously explained by differences in the meteorology of the two areas, by transequatorial migration of debris during the higher spring peak of the northern hemisphere which serves to cover up the southern-hemisphere fall minimums, or by the different stratospheric distribution of debris in the two hemispheres. The last explanation seems to be the most reasonable one. Activity concentrations in the southern hemisphere during the moratorium were extremely low compared to those north of the equator, with the disparity increasing with increasing latitude; consequently there apparently was less stratospheric debris in a position to be affected by the winter–

spring subsidence or the exchange of stratospheric air, which is primarily a phenomenon of the higher latitudes.

Transequatorial migration of radioactive particulate matter in the troposphere is definitely inhibited, as evidenced by the large disparity in the activity burdens in the two hemispheres which exists for months at a time and by the large gradient in activity that is invariably observed near the equator. The profiles of the gross beta-activity concentrations as a function of latitude during the corresponding periods in the springs of 1959 through 1962, shown in Fig. 4, demonstrate that equatorial crossover is small during the winter–spring season when

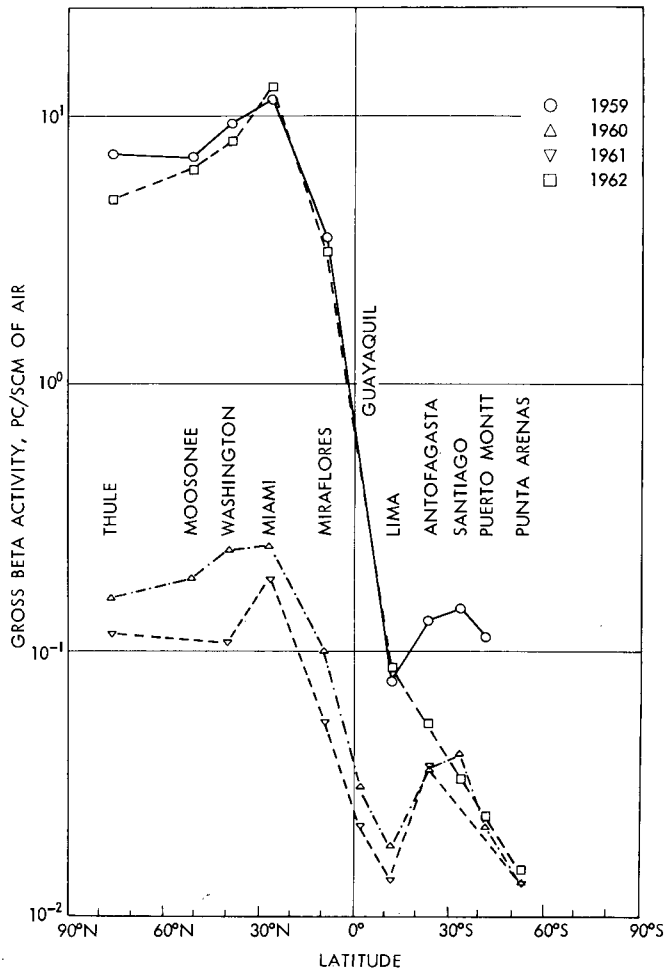

Fig. 4—Profiles of gross beta activity along the 80th meridian during the month of April in successive years.

northern-hemisphere activity levels are highest. Some crossover does occur, as has been observed in the past during the Operations Greenhouse and Hardtack tests and the French Sahara tests and following the renewal of testing of large-yield devices by the U.S.S.R. in September 1961. Several months after the northern-hemisphere air had become heavily contaminated by the U.S.S.R. 1961 tests, short-lived fission products were detected at several sites in South America.

From the relative activity levels in the two hemispheres in early 1962, shown in Fig. 3, it can be estimated that only a few percent of the radioactivity from the northern hemisphere could have migrated south of the equator. Because of the small background there of much older, long-lived radioactivity, the new debris contributed heavily to the gross-activity levels at the lower latitudes but added little to the concentrations of such long-lived fission products as ^{90}Sr and ^{137}Cs.

The Operation Dominic I tests held in the Christmas Island area (2°N) beginning in late April 1962 caused large increases in radioactivity in the lower latitudes of the southern hemisphere during May but contributed surprisingly little activity to the ground-level air in the northern hemisphere. At both Miami and Miraflores, where the major impact of tropospheric debris from these tests was expected, the activity concentrations during the period April through June decreased with a half-period of less than one month, similar to the rate observed in the spring of 1959. Radiochemical analyses confirmed the small influence of these tests on activity levels in the northern hemisphere during 1962; the situation may be similar to that existing following the Operation Hardtack tests of 1958 when ^{185}W results showed the major part of the long-lived radioactive debris to be held in the stratosphere until the next spring.[13,15]

^{90}Sr IN THE AIR

The concentrations of ^{90}Sr in the ground-level air at a number of sites along the 80th meridian are shown in Figs. 5 and 6; calculated tropospheric burdens of ^{90}Sr are shown in Fig. 7. These results are more significant in delineating the magnitude of the seasonal changes in activity levels than are gross-activity measurements since they are less sensitive to radioactive decay.

A definite spring maximum of ^{90}Sr is observed in the northern hemisphere every year regardless of the past history of nuclear testing. The occurrence of maximums each spring during the moratorium on nuclear testing provides direct evidence that there is a seasonal factor involved in the downward mixing of radioactive debris from the stratospheric source. The seasonal cycle has its highest amplitude in the subtropical latitudes; moreover, the time of arrival of the radioac-

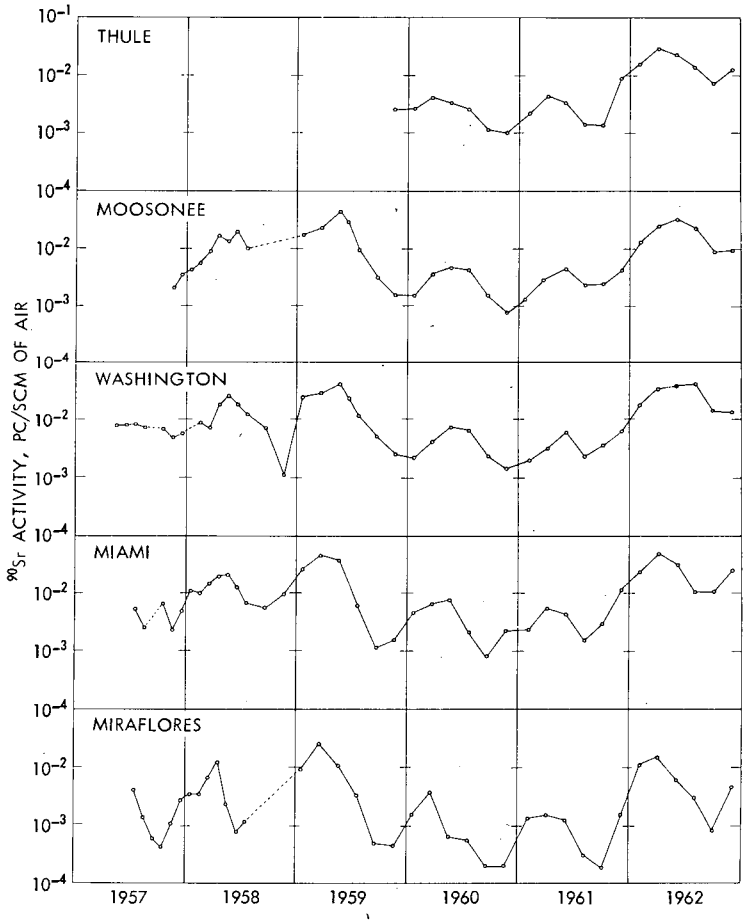

Fig. 5—Concentrations of ^{90}Sr in the air at selected sites in the northern hemisphere.

tivity maximum varies with the latitude, arriving earlier in the more southerly regions.

In the southern hemisphere a similar but less well-defined pattern of behavior appeared to exist; the spring maximum was most obvious at the Antofagasta site and occurred during November and December, at the time of the fall minimum in the northern hemisphere. This out-of-phase relation is to be expected if a purely meteorological process is the controlling factor. Guayaquil, located essentially on the equator, exhibits the seasonal trends characteristic of the northern hemisphere because of the far greater concentrations of radioactivity in air masses from that source.

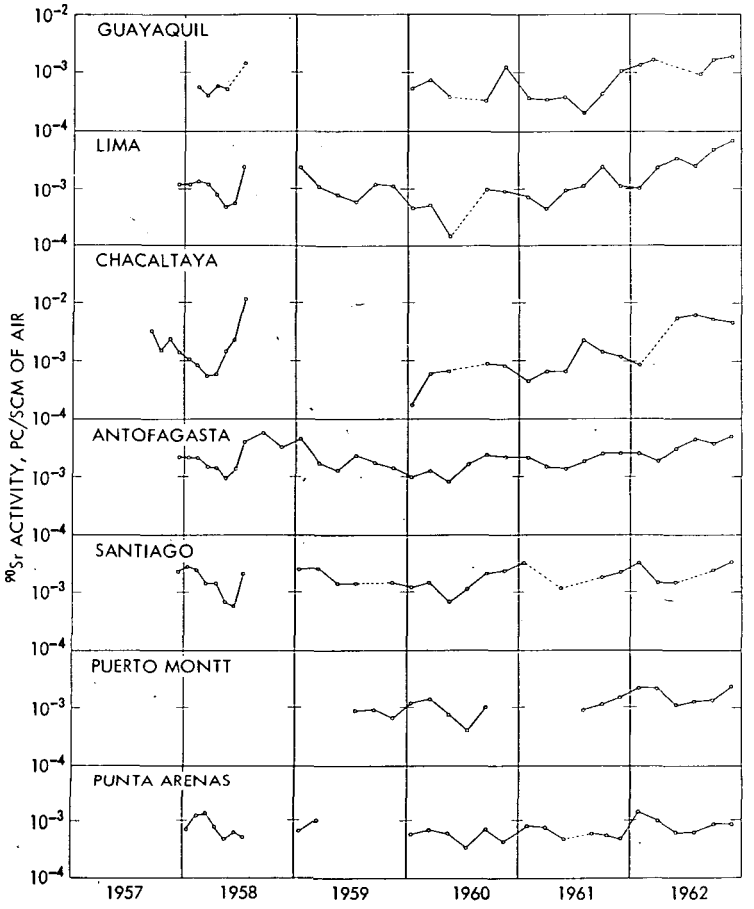

Fig. 6—Concentrations of ^{90}Sr in the air at selected sites in the southern hemisphere.

SOURCES OF AIRBORNE RADIOACTIVITY DURING 1962

The radiochemical analyses of bimonthly composited samples of airborne fission products collected during 1962 have permitted a reasonable identification of the source of the debris in the ground-level air at various sites along the 80th meridian. The relative amounts of ^{89}Sr, ^{91}Y, ^{144}Ce, and ^{90}Sr have been employed to determine both an average shot date and the percentage contribution of the youngest component in the mixture, as described elsewhere.[23] Assumptions were made that all fresh debris in the northern hemisphere originated from U.S.S.R. tests of 1961–1962 and that all in the southern hemisphere

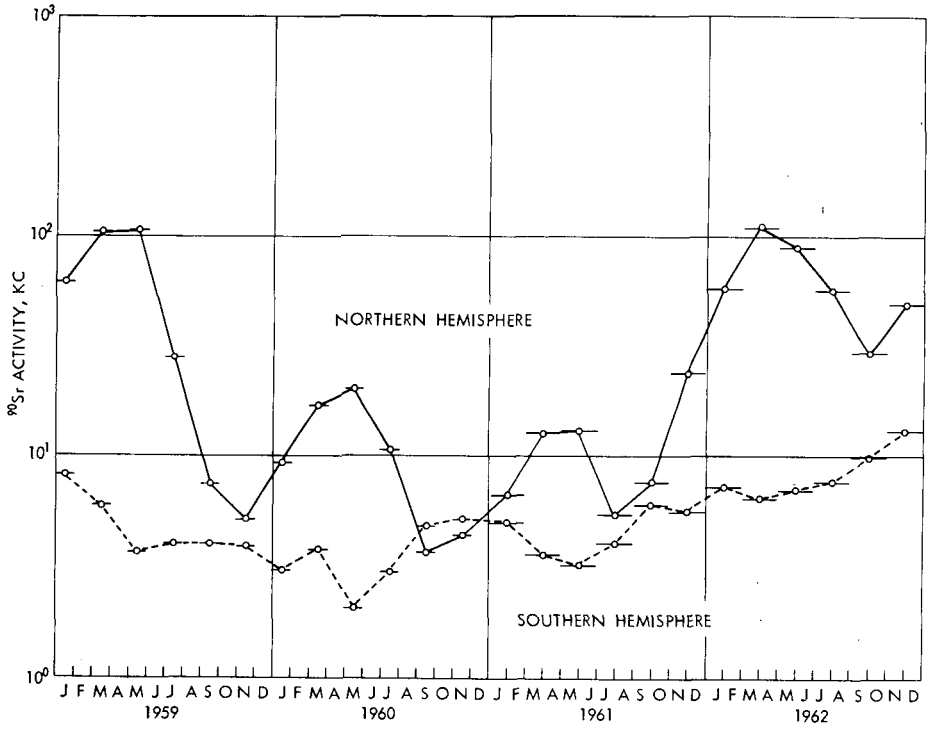

Fig. 7—Tropospheric burdens of ^{90}Sr activity.

after April 1962 resulted from the U. S. Christmas Island tests. The small magnitude of the equatorial crossover of tropospheric debris would not significantly change the conclusions.

The small effect of the U. S. Christmas Island tests on the radioactivity levels in the northern hemisphere is shown in Fig. 8, where ^{89}Sr/^{90}Sr ratios in 80th meridian air samples and in precipitation at Westwood, N. J.[28] and Rijswijk, The Netherlands,[29] are plotted against time. The solid line extrapolating back to a shot date of Oct. 15, 1961, during the U.S.S.R. 1961 series, characterizes very well the decay of the ^{89}Sr/^{90}Sr activity ratio during the spring of 1962. The relatively constant composition at all the northern-hemisphere sites is evidence of the well-mixed condition of the troposphere. A slow, progressive change in the source material is indicated by the gradual increase in the relative amount of the shorter lived component, ^{89}Sr. No appreciable change in this pattern occurred until the July–August collection period. Though some ^{140}Ba was detected in rainwater at Westwood, N. J., in May and June,[30] which must have come from the Operation Dominic I tests, an upper limit of 10 to 15% can be set on the contribu-

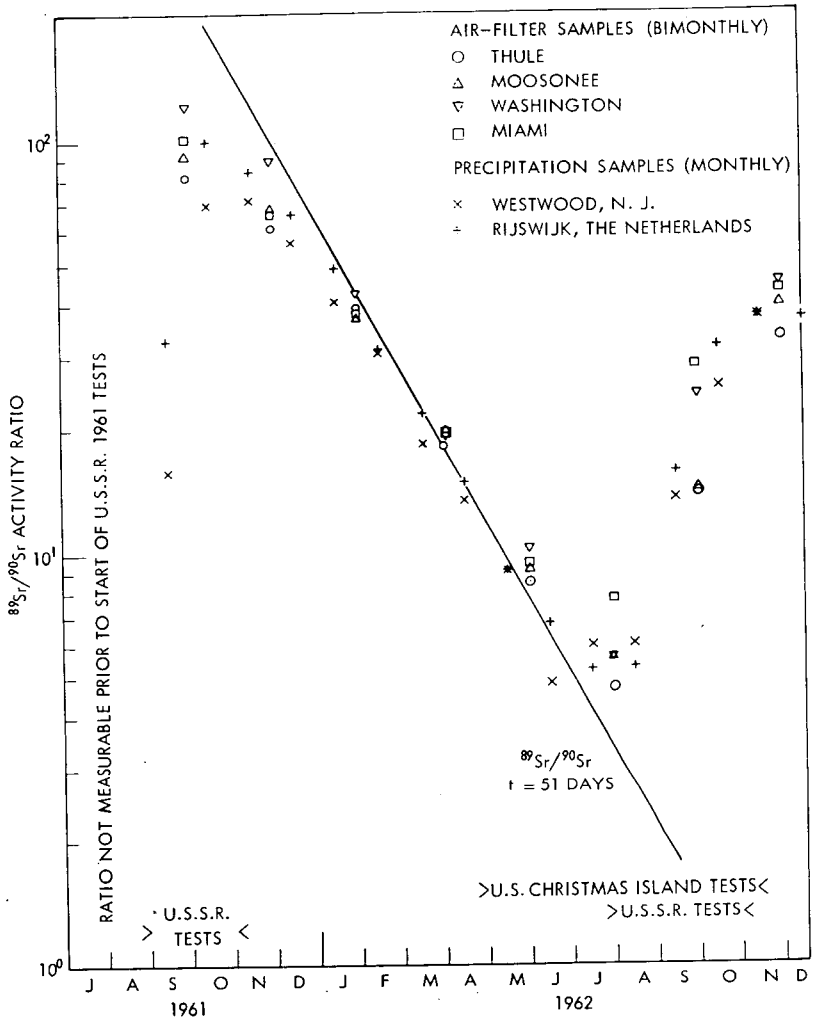

Fig. 8—Ratios of ^{89}Sr to ^{90}Sr activity in the air and in precipitation at various northern-hemisphere sites during 1962. The $^{89}Sr/^{90}Sr$ ratio is 180 at t_0 (Oct. 15, 1961).

tion of U. S. tests to northern-hemisphere ^{89}Sr levels during this period. This increase is equivalent to less than a 1% contribution of the U. S. tests to the ^{90}Sr levels. After July the $^{89}Sr/^{90}Sr$ ratio increased abruptly; the U.S.S.R. 1962 series (August 5 to December 24) was assumed to be the dominant contributor to the ^{89}Sr levels. Similar conclusions can be drawn from $^{89}Sr/^{144}Ce$ and $^{91}Y/^{144}Ce$ activity ratios.

Latitudinal profiles of the ^{90}Sr activity concentrations in the air along the 80th meridian (west) are plotted in Figs. 9 to 11 for the bi-

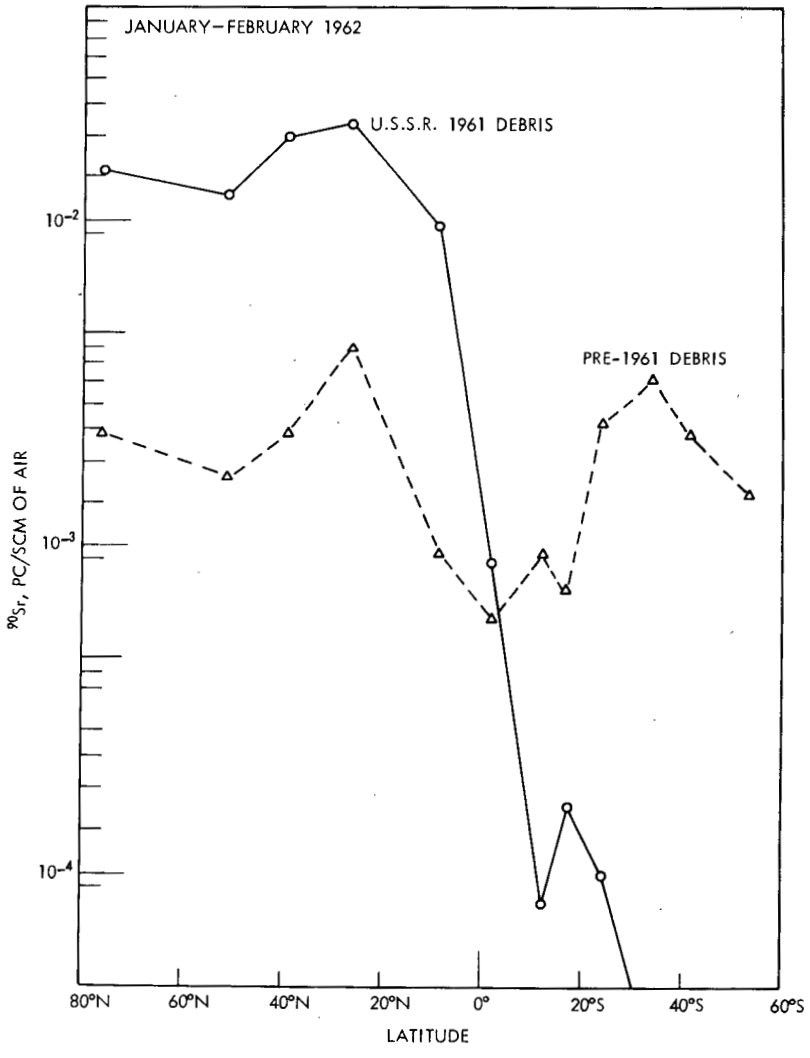

Fig. 9—Profiles of the ^{90}Sr concentrations in January and February 1962 in the air along the 80th meridian (west).

monthly periods January and February, May and June, and November and December as functions of the nuclear-test series serving as the sources.

In the January and February period (Fig. 9), the old pre-1961 debris was of equivalent concentration in the two hemispheres and showed the expected distribution with midlatitudinal maximums and an equatorial minimum. The fresh debris from the U.S.S.R. 1961 tests

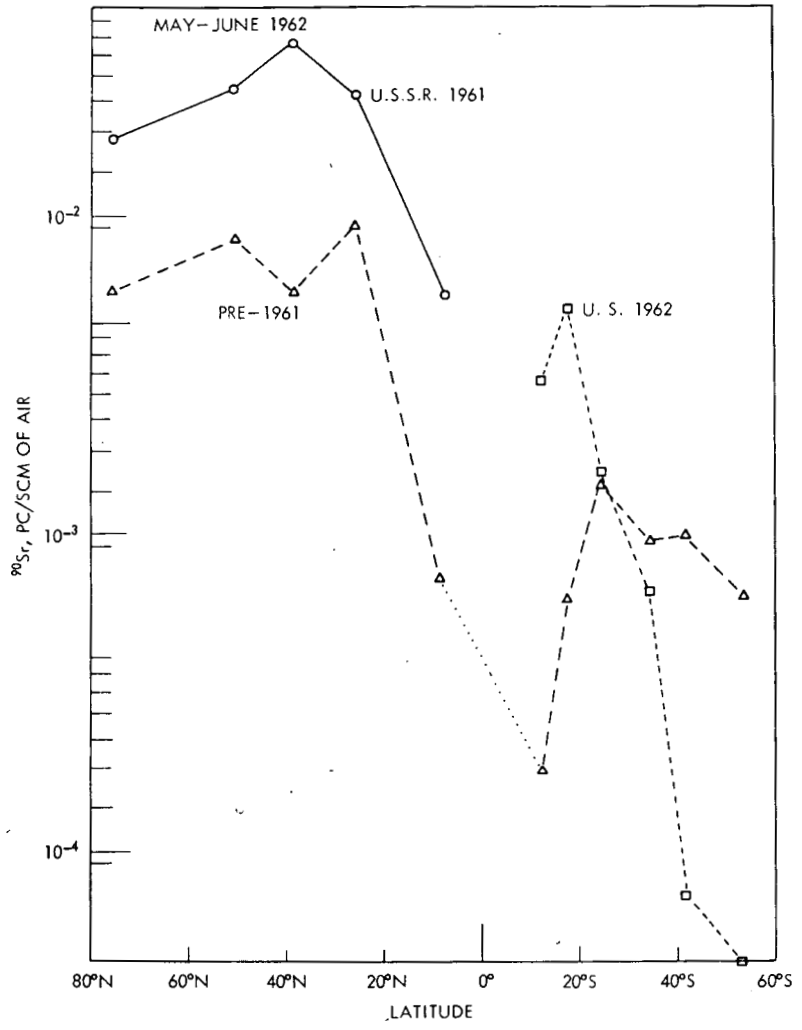

Fig. 10—Profiles of the ^{90}Sr concentrations in May and June 1962 along the 80th meridian (west).

was the dominant source of ^{90}Sr in the air of the northern hemisphere but was of minor importance south of the equator. The shape of the profile for the fresh debris, which is distinctly different from that for the older debris, suggests a limited exchange of tropospheric air across the equator followed by entrainment of the transferred air in a rising cell that descends to ground level in the subtropical region of the southern hemisphere. The highest concentrations of ^{90}Sr in the

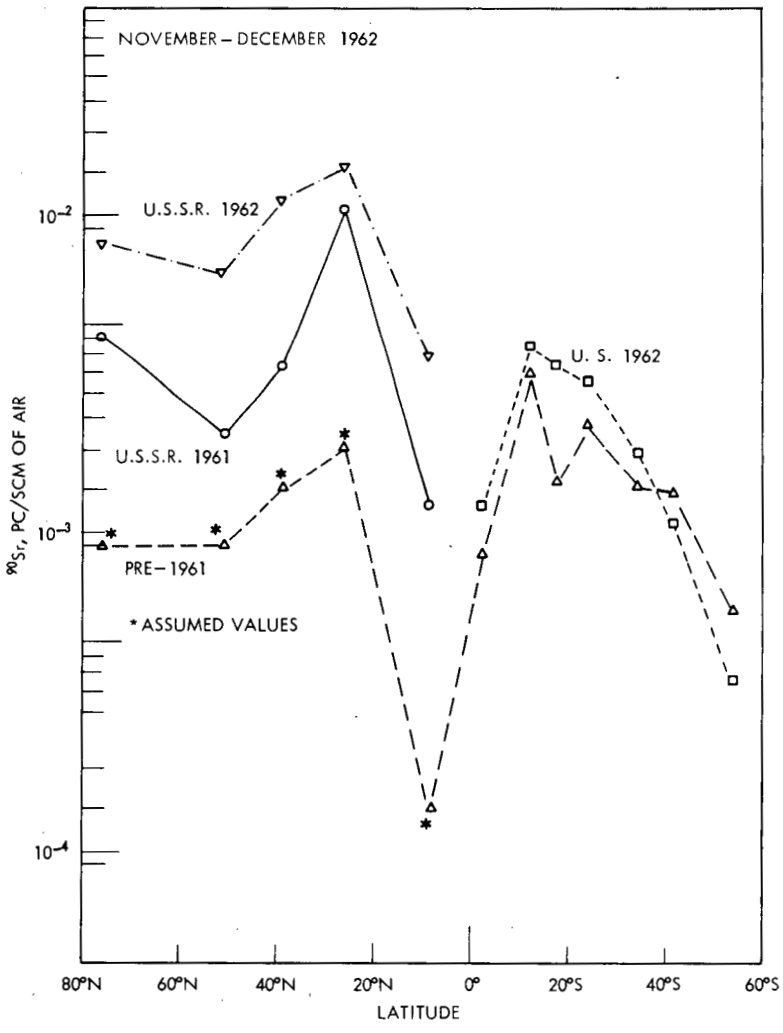

Fig. 11—Profiles of ^{90}Sr concentrations in November and December 1962 along the 80th meridian (west).

southern hemisphere were observed at the high-altitude collecting station at Chacaltaya.

In the March and April collections (profiles not shown) the patterns of distribution of ^{90}Sr in the ground-level air were relatively unchanged from the preceding period. Even at this date negligible penetration of the fresher debris to southern Chile had occurred. An estimated 85% of the ^{90}Sr activity at the three northernmost sites (Thule, Moosonee, and Washington) can be attributed to the U.S.S.R.

1961 tests; this is in agreement with the reports that 85 to 90% of the ^{90}Sr in rainfall at Abingdon and Milford Haven in the United Kingdom[31] and at Westwood, N. J.,[30] during the spring of 1962 could be ascribed to the 1961 U.S.S.R. test series.

In the May and June profile shown in Fig. 10, the pre-1961 debris continued to exhibit the expected shape with higher ^{90}Sr values in the north as a result of the spring maximum there. The northern portion of the 1961 U.S.S.R. ^{90}Sr profile was also relatively unchanged; the curve could not be extended south of the equator because of the influx there of fresh debris from the 1962 Operation Dominic I tests, which started April 25. The activity from the Christmas Island area arrived at its highest concentration at the high-altitude site at Chacaltaya, Bolivia, as had occurred in past tests in the Pacific area.[7,11] It was confined to the relatively low latitudes of the southern hemisphere. As indicated earlier, no significant quantity of this activity appeared at ground level in the northern hemisphere.

During the July and August period, there was only a minor contribution of ^{90}Sr from the U.S.S.R. 1962 tests to the northern-hemisphere air, and, in general, patterns of ^{90}Sr throughout the world were similar to those of the previous period. In later periods it was not possible to make a completely objective assignment of debris to the various sources because of the lack of sufficient analytical data to discriminate between the four possible sources of debris. For these last two periods, values based on past experience were assumed for the pre-1961 ^{90}Sr concentrations in the northern hemisphere. This permitted a resolution of the residual two-component mixture. The resulting profiles for the November and December period are shown in Fig. 11; the September and October profiles, which are not shown, were similar.

At the end of 1962, the profiles of premoratorium ^{90}Sr and ^{90}Sr from the U. S. 1962 tests were nearly identical in the southern hemisphere. Moreover, activity ratios indicated the effective date of formation of new debris at all these sites to be in June 1962. A stratospheric origin for both components thus appears reasonable. In the northern hemisphere, U.S.S.R. 1962 tests were the major contributor to the ^{90}Sr levels, and dates of formation in September and October were obtained. This is apparently a case where the direct tropospheric introduction of ^{90}Sr was of greater significance than deposition from a well-charged stratospheric source. The peak in the U.S.S.R. 1961 ^{90}Sr profile at Miami is due to the earlier arrival there of the start of the 1963 winter–spring subsidence of stratospheric debris.

CONCLUSIONS

This study of the fission-product content of the atmosphere has covered an interesting period of the nuclear age and in the development

of nuclear weaponry. At its initial stage the concept of a stratospheric residence time for radioactive debris was highly speculative, and seasonal variations in the deposition from this reservoir were not apparent, primarily because of the disadvantageous scheduling of nuclear tests. The temporary moratorium on nuclear testing following several extensive series of high-yield nuclear tests permitted the unambiguous verification by many investigators of seasonal changes in the deposition rate of stratospherically stored debris over the entire northern hemisphere. It also permitted determination of the effect of the latitude of injection on the residence time of radioactivity in the stratosphere with shorter residence periods observed for the arctic stratosphere. During this period and also after the renewed testing had begun in the arctic region, the lack of an effective mechanism by which particulate matter could be transferred across the equator in the lower atmosphere was again noted.

With the conduct of full-scale testing of high-yield nuclear devices in both the arctic and tropic regions in 1962, followed by what is presumed will be a more permanent moratorium on testing, the condition of the stratospheric inventory and prospects for observations during the coming years are equivalent to those existing in the period 1959 to 1961. The multiplicity of sources is again causing difficulty in making quantitative interpretations of atmospheric mixing or transport processes, although for a while there should be an ample quantity of radioactivity available for many interesting studies.

REFERENCES

1. L. B. Lockhart, Jr., R. A. Baus, and I. H. Blifford, Jr., Atmospheric Radioactivity Along the 80th Meridian, 1956, Report NRL-4965, U. S. Naval Research Laboratory, July 1957.
2. L. B. Lockhart, Jr., Information on Fallout, in *The Nature of Radioactive Fallout and Its Effects on Man,* Hearings Before the Special Subcommittee on Radiation of the Joint Committee on Atomic Energy, Congress of the United States, 85th Congress, 1st Session, Vol. 1, pp. 650-673, U. S. Government Printing Office, Washington, D. C., 1957.
3. R. A. Baus, P. R. Gustafson, R. L. Patterson, Jr., and A. W. Saunders, Jr., Procedure for the Sequential Radiochemical Analysis of Strontium, Yttrium, Cesium, Cerium, and Bismuth in Air-filter Collections, Report NRL-Memo-758, U. S. Naval Research Laboratory, November 1957.
4. L. B. Lockhart, Jr., R. A. Baus, and I. H. Blifford, Jr., Fission-product Radioactivity in the Air Along the 80th Meridian, January–June 1957, Report NRL-5041, U. S. Naval Research Laboratory, November 1957. See also *Tellus, 11*(1): 83-90 (1959).
5. R. A. Baus, R. L. Patterson, Jr., A. W. Saunders, Jr., and L. B. Lockhart, Jr., Radiochemical Analysis of Air-filter Samples Collected During 1957, Report NRL-5239, U. S. Naval Research Laboratory, December 1958.

6. L. B. Lockhart, Jr., R. A. Baus, P. King, and I. H. Blifford, Jr., Atmospheric Radioactivity Studies at the U. S. Naval Research Laboratory, Report NRL-5249, December 1958. See also *J. Chem. Ed.*, *36*(6): 291-295 (1959).
7. L. B. Lockhart, Jr., R. A. Baus, R. L. Patterson, Jr., and A. W. Saunders, Jr., Contamination of the Air by Radioactivity from the 1958 Nuclear Tests in the Pacific, *Science, 130:* 161-162 (1959).
8. L. B. Lockhart, Jr., R. L. Patterson, Jr., and W. L. Anderson, Measurements of the Air Concentration of Gross Fission-product Radioactivity During the IGY, July 1957–December 1958, Report NRL-5359, U. S. Naval Research Laboratory, September 1959. See also *Tellus, 12*(3): 298-307 (1960).
9. L. B. Lockhart, Jr., and P. King, Speculations on Atmospheric Processes via Fission Product Levels, *Am. Scientist, 47*(3): 386-396 (1959).
10. L. B. Lockhart, Jr., Current Information on the Radioactivity of the Air, in *Fallout from Nuclear Weapons Tests,* Hearings Before the Special Subcommittee on Radiation of the Joint Committee on Atomic Energy, Congress of the United States, 86th Congress, 1st Session, Vol. 1, pp. 483-591, U. S. Government Printing Office, Washington, D. C., 1959.
11. L. B. Lockhart, Jr., R. A. Baus, R. L. Patterson, Jr., and A. W. Saunders, Jr., Radiochemical Analyses of Air-filter Samples Collected During 1958, Report NRL-5390, U. S. Naval Research Laboratory, October 1959. See also *J. Geophys. Res., 65*(6): 1711-1722 (1960).
12. L. B. Lockhart, Jr., and R. L. Patterson, Jr., Critical Analysis of Measurements of the Gross Fission Product Activity in the Air at Ground Level, Report NRL-5440, U. S. Naval Research Laboratory, February 1960.
13. L. B. Lockhart, Jr., R. L. Patterson, Jr., A. W. Saunders, Jr., and R. W. Black, Contribution of Hardtack Debris to Contamination of the Air During 1959, *Science, 132*(3420): 154 (1960).
14. R. L. Patterson, Jr., and L. B. Lockhart, Jr., Long-Range Detection of the French Nuclear Tests of 1960, *Science, 132*(3425): 474 (1960).
15. L. B. Lockhart, Jr., R. L. Patterson, Jr., A. W. Saunders, Jr., and R. W. Black, Fission-product Radioactivity in the Air Along the 80th Meridian (West) During 1959, Report NRL-5528, U. S. Naval Research Laboratory, August 1960. See also *J. Geophys. Res., 65*(12): 3987-3997 (1960).
16. L. B. Lockhart, Jr., R. L. Patterson, Jr., A. W. Saunders, Jr., and R. W. Black, Fission-product Radioactivity in the Air Along the 80th Meridian (West) During 1960, Report NRL-5692, U. S. Naval Research Laboratory, October 1961.
17. L. B. Lockhart, Jr., R. L. Patterson, Jr., A. W. Saunders, Jr., and R. W. Black, Atmospheric Radioactivity Patterns Along the 80th Meridian (West), 1959-1961, in Radioactive Fallout from Nuclear Weapons Tests, A. W. Klement, Jr. (Ed.), USAEC Report TID-7632, Book 1, pp. 188-203, February 1962.
18. L. B. Lockhart, Jr., Atmospheric Radioactivity, in Proceedings of the Sixth Navy Science Symposium on Weapons and Weapons Effects, San Francisco, Calif., May 2-3, 1962, Report ONR-12 Vol. 1, pp. 1-27, Naval Radiological Defense Laboratory, 1962.
19. L. B. Lockhart, Jr., and R. L. Patterson, Jr., Intercalibration of Some Systems Employed in Monitoring Fission Products in the Atmosphere, Report NRL-5850, November 1962. See also *Radiological Health Data, 3*(12): 466-470 (1962).

20. L. B. Lockhart, Jr., R. L. Patterson, Jr., A. W. Saunders, Jr., and R. W. Black, Fission-product Radioactivity in the Air Along the 80th Meridian (West) During 1961, Report NRL-5869, U. S. Naval Research Laboratory, January 1963. See also *Rad. Health Data, 4*(2): 71-78 (1963).
21. L. B. Lockhart, Jr., and R. L. Patterson, Jr., Intercalibration of the Major North American Networks Employed in Monitoring Airborne Fission Products, Report NRL-6025, December 1963. See also *Radiological Health Data, 5*(1): 12-15 (1964).
22. L. B. Lockhart, Jr., R. L. Patterson, Jr., and W. L. Anderson, Characteristics of Air-filter Media Used for Monitoring Airborne Radioactivity, Report NRL-6054, U. S. Naval Research Laboratory, March 1964.
23. L. B. Lockhart, Jr., R. L. Patterson, Jr., A. W. Saunders, Jr., and R. W. Black, Summary Report on Fission-product Radioactivity in the Air Along the 80th Meridian (West), 1957-1962, Report NRL-6104, U. S. Naval Research Laboratory, June 1964. See also *Rad. Health Data, 5*(6): 255-265 (1964).
24. R. L. Patterson, Jr., and L. B. Lockhart, Jr., Geographical Distribution of Lead-210 (RaD) in the Ground-level Air, in *The Natural Radiation Environment,* J. A. S. Adams and W. M. Lowder (Eds.), Chap. 23, pp. 383-392, University of Chicago Press, Chicago, 1964.
25. L. B. Lockhart, Jr., Behavior of Airborne Fission Products. *Am. Scientist, 52*(3): 301-305 (1964).
26. R. L. Patterson, Jr., L. B. Lockhart, Jr., and W. L. Anderson, Performance Characteristics of the FPP-15 Filter Material Used in the U.S.S.R. for Environmental Radioactivity Monitoring, Report NRL-6165, U. S. Naval Research Laboratory, September 1964.
27. W. R. Collins, Jr., The 80th Meridian Network, January 1963, *Rad. Health Data, 4*(7): 342-346 (1963).
28. A. Walton and M. W. M. Leo, Studies of Nuclear Debris in Precipitation, USAEC Report NYO-9534, Isotopes, Inc., March 1963.
29. J. Blok and J. F. Bleichrodt, Summary of Radioactive Fallout Measurements. III. Netherlands Medisch Biologisch Laboratorium, RVO-TNO Report MBL/1963/13, August 1963.
30. A. Walton and M. W. M. Leo, Studies of Nuclear Debris in Precipitation, USAEC Report NYO-9533, Isotopes, Inc., November 1962.
31. R. S. Cambray, E. M. R. Fisher, G. S. Spicer, C. G. Wallace, and T. J. Webber, Radioactive Fallout in Air and Rain—Results to the Middle of 1962, Report AERE-R-4094, United Kingdom Atomic Energy Authority Research Group, November 1962.

VARIATION OF FISSION PRODUCTS AND NATURAL RADIOACTIVITY IN SURFACE AIR

P. F. GUSTAFSON, S. S. BRAR, and S. E. MUNIAK
Division of Biological and Medical Research, Argonne National Laboratory, Argonne, Illinois

ABSTRACT

Collection of particulates in surface air by air filters has been in progress at Argonne, Ill., for a number of years. Measurement of the radioactivity in these filters has been done by gamma-ray spectrometry with the use of large NaI crystals. The concentrations of various fission and activation products as well as ^{7}Be were determined by computer analysis of the complex spectra. Variations in the concentration of various nuclides, particularly of ^{137}Cs and ^{54}Mn, as well as in the ratio between nuclides, are used to determine the sources of debris observed in surface air. The differences in distribution as a function of time are discussed for various sources.

VARIATION OF RADIOACTIVITY IN SURFACE AIR

Airborne particulates were collected on asbestos-base filter paper having an efficiency of approximately 96% for particles of greater than 0.25 μ in diameter exposed on air pumps operated at flow rates of approximately 40 m^3/hr. Three such pumps have been in continuous operation since mid-1961, providing daily samples from some 3000 m^3 of air for these studies. Prior to this date portions of the filters from the Industrial Hygiene and Safety Division onsite and offsite monitoring network were used for analysis. Since September 1961, gross gamma activity in the daily or two-day filter collections was determined by a spectral method discussed in Ref. 1, which takes into account the con-

tribution from natural activity in the air. A known portion of each filter was cut into small pieces and mixed with similar pieces from other filters to form monthly or semimonthly composites. These composites were compressed into a disk and placed in a plastic petri dish. The petri dish was then placed on top of a 4- by 4-in. NaI crystal for gamma-ray analysis. Pulse-height analysis was made with a multichannel analyzer with IBM typewriter or punched-card readout. Both sample and detector were enclosed in 6-in.-thick steel shielding for background reduction and stabilization. Counting times of 100 min were sufficient to accumulate 100,000 or more net counts in the energy region from 0.1 to 2.0 Mev. Both the monthly and the semimonthly composites contained particulates collected from about 10^4 m^3 of air. Sufficient time had elapsed between the collection of the last filter and the time of measurement to ensure that the radon and thoron daughter products had decayed to an insignificant intensity.

The concentration of the various gamma-emitting radionuclides was determined by a computer solution of the requisite number of simultaneous equations.[2] During those times when fresh fission debris was present, ^{141}Ce, ^{144}Ce, ^{125}Sb, ^{103}Ru, ^{106}Ru, ^{137}Cs, $^{95}Zr-^{95}Nb$, and $^{140}Ba-^{140}La$ were determined by this method. Iodine-131 was not readily collected on these filters, and $^{140}Ba-^{140}La$ was used as an indicator of the upper limit of ^{131}I present in surface air at the time.[1] On rare occasions $^{132}Te-^{132}I$ and ^{99}Mo have been observed in surface air; however, analyses of these nuclides were not included in the routine program. In addition, ^{54}Mn and ^{124}Sb have been determined when their presence in the gamma-ray spectrum was suspected. Successive spectra were taken of the same filter composite over a period of several months. This has made it possible to obtain a more exact determination of the shorter-lived components and hence has also improved the estimates of the longer lived nuclides. Beryllium-7 has also been determined from the difference spectra obtained from successive measurements of air filters collected several months after the cessation of testing. In the absence of fresh debris, ^{144}Ce, ^{125}Sb, ^{137}Cs, ^{106}Ru, $^{95}Zr-^{95}Nb$, and ^{54}Mn were determined in the initial spectrum, and ^{7}Be was determined in the difference spectra.

During times of atmospheric testing of nuclear weapons and for some time thereafter, the levels of gross activity in surface air are relatively high. In addition, the gross activity undergoes seasonal variations, with maximum concentrations occurring in the spring and lower values during autumn and winter. This seasonal variation is more pronounced in the case of longer lived radionuclides, such as ^{137}Cs, as illustrated in Fig. 1. Spring maximums were observed in 1960 and 1961; in the absence of current or recently concluded testing, a meteorological origin for these maximums is strongly indicated. From 1954 through 1960 the maximum was observed at Argonne during April and May

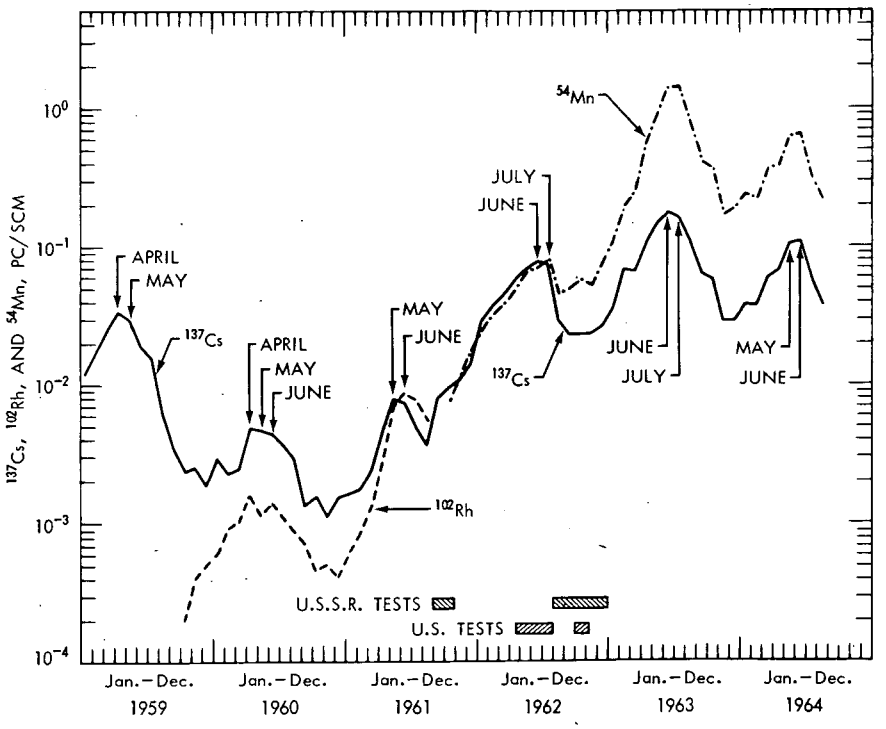

Fig. 1—^{137}Cs, ^{102}Rh, and ^{54}Mn in surface air at Argonne, Ill.

each year. In 1961 the maximum was observed during May and June, and in 1962 and 1963, during June and July. In 1964 the maximum occurred during late May and early June, as indicated in Fig. 1. Similar observations have been made at other locations within the northern hemisphere.[3–5]

During 1961 through mid-1964, an appreciable portion of the total ^{137}Cs present in surface air was of high-altitude origin as inferred from the measured concentrations of ^{102}Rh and ^{54}Mn, which are also illustrated in Fig. 1. The ^{102}Rh was produced for the most part as a tracer in the Orange shot of the Operation Hardtack I test series on Aug. 11, 1958, which had a burst height of about 43 km over Johnston Island.[6] The concentrations of ^{102}Rh have been corrected for radioactive decay to that date. Manganese-54 was produced in high-yield shots during the Soviet 1961 test series, and there are indications from the Ash Can balloon flights made at San Angelo, Tex.,[7,8] that ^{54}Mn was also produced during high-yield and/or high-altitude shots during 1962. The ^{54}Mn values shown in Fig. 1 have been corrected for radioactive decay to mid-October 1961. Thus both ^{102}Rh and ^{54}Mn may be reasonably used as tracers for high-altitude debris. As seen in Fig. 1, ^{102}Rh reached a

maximum concentration during June and July 1961, and the ^{54}Mn spring maximums have coincided in time with those of ^{137}Cs during 1962 through 1964. The $^{137}Cs/^{102}Rh$ activity ratio for Orange debris is not known, although a production figure of 3 Mc of ^{102}Rh has been reported by Kalkstein.[6] Cesium-137 from other shots at high altitude may have become mixed with that from Orange. Aircraft sampling at 50,000 ft during May 1961 indicated a $^{137}Cs/^{102}Rh$ ratio of nearly unity.[9] This value would imply that nearly all the ^{137}Cs seen during the spring of 1961 was of high-altitude origin.

Likewise, it is difficult to determine the actual amount of ^{137}Cs produced along with the ^{54}Mn. The highest concentrations of ^{54}Mn observed in the Ash Can balloon flights were collected[7] during the spring of 1962 and indicated $^{54}Mn/^{137}Cs$ ratios of 30 to 1 to 40 to 1. Sampling conducted at 60,000 to 65,000 ft indicated $^{54}Mn/^{137}Cs$ ratios closer to 10 to 1 during most of 1962 with a decrease to approximately 5 to 1 in 1963 and 1964 as shown in Fig. 2. The $^{54}Mn/^{137}Cs$ ratio observed in surface air at Argonne during this time is also indicated in Fig. 2.

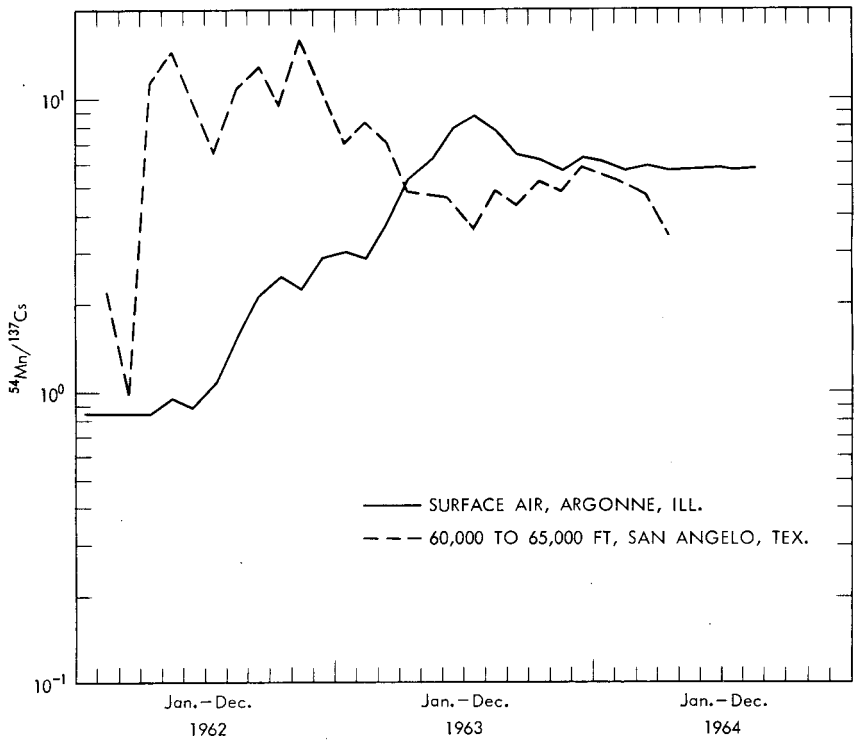

Fig. 2—$^{54}Mn/^{137}Cs$ activity ratio in surface air at Argonne, Ill., and at 60,000 to 65,000 ft at San Angelo, Tex.

Through mid-1962 the surface-air measurements indicated that 10% or less of the total ^{137}Cs present was of high-altitude origin, as shown by a $^{54}Mn/^{137}Cs$ ratio of essentially unity. From July 1962 until July 1963, the ratio in surface air rose steadily, reaching a peak value of 8 to 1. The ratio then dropped during late summer to a value of 6 to 1, which has been maintained through mid-1964. Taken at face value, this would imply that the bulk of the ^{137}Cs present in surface air during 1963 and into 1964 was associated with ^{54}Mn and may have originated at considerable altitude. The peak value of the ratio seen during July 1963 may have resulted from the downward movement of debris during the preceding winter and spring months. A second decrease in ratio seen in the Ash Can results during early 1964 does not seem to have caused a similar decrease in the ratio in surface air during the spring and the summer of 1964. This may indicate that somewhat different sources or mixtures of debris were sampled at Argonne and at San Angelo. There did appear to have been an appreciable component of ^{137}Cs in surface air during 1961–1964 that was of high-altitude origin. The delay in descent might have been due to particle size, or the length of the pathway traversed may in itself have been sufficient to delay the occurrence of spring maximums in surface air relative to past observations. The concentration of airborne radioactivity in surface air is influenced by the precipitation history of the air mass in which it is contained. A change in the amount of precipitation as well as in its time of occurrence would affect the concentration of activity found in tropospheric air, particularly at the surface. Thus a decrease in precipitation over a wide area during the spring would lead to a spring maximum of increased magnitude and, conceivably, of longer duration.

The concentration of ^{137}Cs in surface air measured at Argonne and at Chilton, England,[3,10] is shown in Fig. 3 for the period 1959 through mid-1964 and for Washington, D. C.,[4,5] for the period 1959 through mid-1962. The times at which the spring maximums occurred at each location were almost the same. However, the amplitudes differed between the three sites during any given year. In 1959, 1960, and 1961, the concentrations seen at Washington and Chilton were quite comparable, whereas the concentrations observed at Argonne were lower by essentially a factor of 2. In 1962 the situation was partially reversed, with comparable values at Washington and Argonne but with only about one-half of these concentrations at Chilton. The reversal between Argonne and Chilton was maintained through mid-1964. This reversal in relative amplitude could be due to differences in the source of debris, changes in circulation, changes in precipitation, or a combination of the three. The source of debris seen at both Chilton and Argonne appears to be the same as judged from the $^{95}Zr/^{137}Cs$ activity ratio plotted as a function of time as shown in Fig. 4. The ratio observed month by month is almost identical during 1962 to mid-1964. The values of the

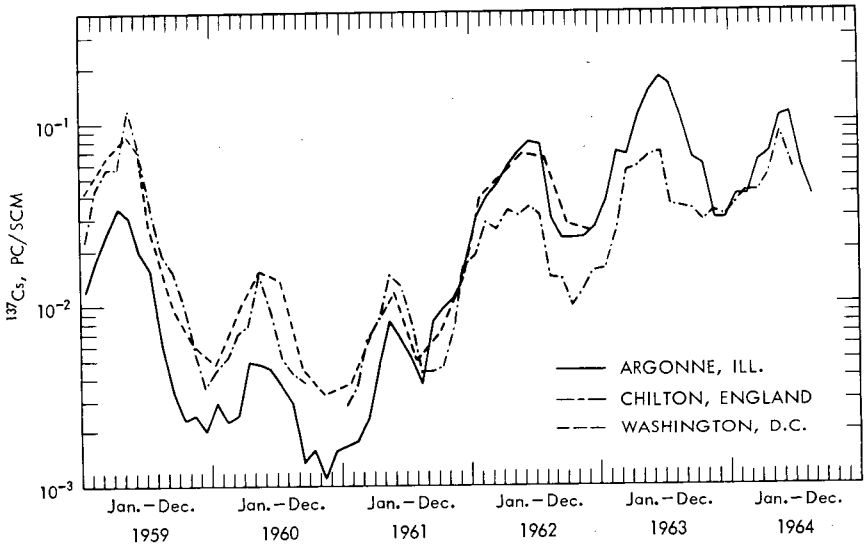

Fig. 3—^{137}Cs concentration in surface air at Argonne, Ill., Washington, D. C., and Chilton, England.

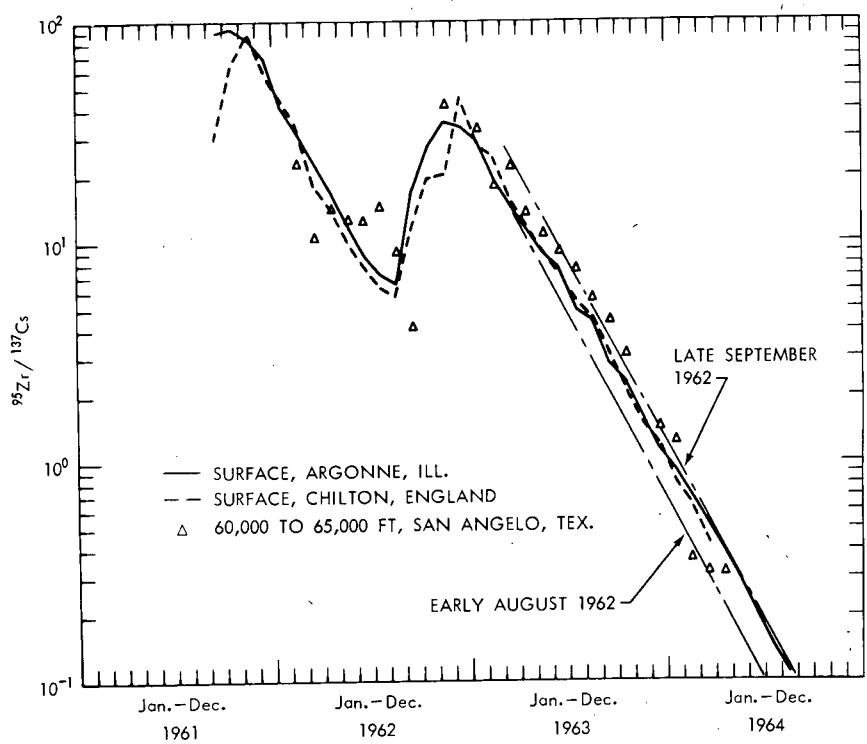

Fig. 4—^{95}Zr/^{137}Cs activity ratio in surface air at Argonne, Ill., and Chilton, England, and at 60,000 to 65,000 ft at San Angelo, Tex.

$^{95}Zr/^{137}Cs$ ratio observed in samples taken at 65,000 ft by the Ash Can balloon flights[7,8] are also shown in Fig. 4. These latter data indicate a somewhat more recent time of production for debris collected at 65,000 ft during 1963–1964 than is observed in surface air. The similarity between the $^{95}Zr/^{137}Cs$ ratios at Chilton and Argonne, as well as the constancy of the $^{54}Mn/^{137}Cs$ ratio in surface air at Argonne for the past year or more, point to a well-mixed stratospheric source for the bulk of surface activity.

Further information regarding the cause of the change in the relative magnitude of the activity levels seen at Chilton and Argonne may be obtained from ^{7}Be measurements in surface air, the results of which are shown in Fig. 5. Reliable ^{7}Be concentration values were not obtained from October 1961 through mid-1963. The concentrations observed in late 1963 and into 1964 are some two to three times greater than those seen during 1959 through mid-1961. This might be due in part to decreased precipitation over the area in question. (Lower than average annual rainfall has been observed in the North Central United States for the past two or three years.) However, the major cause appears to be a difference in circulation resulting in a more rapid transport of stratospheric air to the surface. The apparent production of ^{7}Be calculated according to the method of Cruikshank *et al.*[11] in 1963–1964 was some three times greater than that during 1959–1961. With the use of the equilibrium ^{7}Be production rates in a stationary atmosphere presented by Murayama,[12] the apparent age of ^{7}Be in surface air was approximately 65 days in 1963–1964 compared with the 170 days seen previously. Hence it appears that meteorological processes have caused a more rapid transport of stratospheric debris to ground level over the North Central United States during the last few years than has previously been the case.

The $^{54}Mn/^{137}Cs$ ratio and activity ratios between various fission products have been used to partition the total ^{137}Cs observed in surface

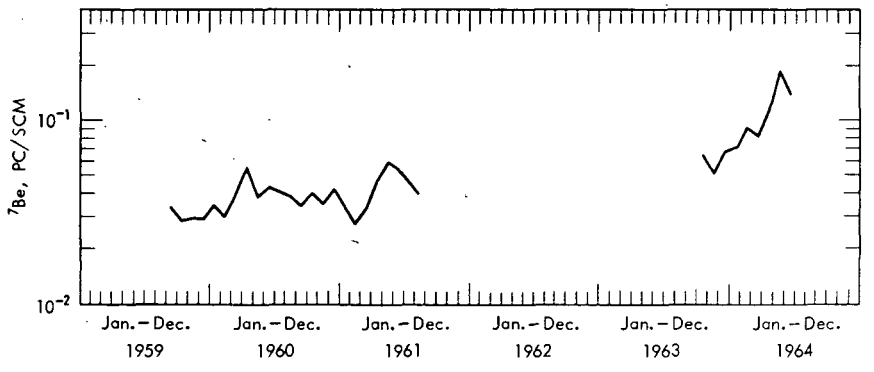

Fig. 5—^{7}Be concentration in surface air at Argonne, Ill.

air into that due to various test series as illustrated in Fig. 6. The contribution of pre-1961 tests has been removed by taking the averages of the ^{137}Cs observed in like months in 1960 and 1961 and subtracting them from the 1962 values. In 1963 the pre-1961 ^{137}Cs levels were reduced by 10%, and reduction by another 10% was used for 1964.

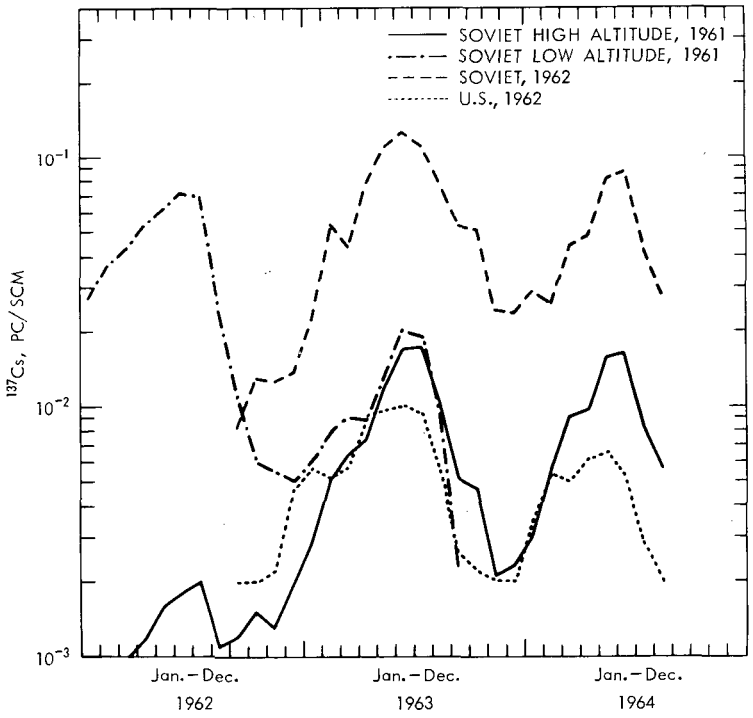

Fig. 6—Partition of ^{137}Cs in surface air at Argonne, Ill.

An initial $^{54}Mn/^{137}Cs$ activity ratio of 40 to 1 was used to obtain the 1961 high-altitude component in 1962–1963, and during 1963–1964 a ratio of 20 to 1 was used. The amount of debris from the Operation Dominic I series was estimated by a comparison with the observations of $^{181}W/^{137}Cs$ made in air collected during 1958–1960. The Soviet 1963 contribution was derived from the best fit of the $^{95}Zr/^{137}Cs$ ratio curve, which indicated a mean time of production of Oct. 15, 1962, during the interval January to July 1963 and of Nov. 15, 1962, during the remainder of 1963 and into 1964. This attempt at partitioning may be somewhat in error, particularly regarding the high-altitude 1961 component in 1963–1964, as well as the evaluation of Dominic I debris. During the spring of 1962, less than 10% of the total ^{137}Cs present in surface air was of pre-1961 origin, and in 1963 and 1964 this source accounted for

less than 5%. Soviet testing in 1961 accounted for more than 90% of the ^{137}Cs in the spring of 1962, 25 to 30% in 1963, and less than 20% in 1964. Of the 1961 debris present in the spring of 1964, all is presumed to be due to high-altitude shots. The Operation Dominic I series appeared to account for 5% or less of the total debris in both 1963 and 1964. Approximately 70% of the debris in 1963 and 75% in 1964 is attributed to the Soviet 1962 tests. The slow decrease in the concentration of ^{137}Cs in surface air from the Soviet 1962 tests in going from the spring of 1963 to the spring of 1964 supports the contention that this debris is contained well up in the stratosphere and will continue to be the source of relatively high ^{137}Cs levels for the next few years.

In summary, a change in the time of the occurrence of th spring maximum during 1961 through 1964 has been accompanied by changes in the relative intensity of the maximums observed at Argonne and at Chilton, England. The source of debris appears to be the same at both locations, and the change in amplitude is attributed to a change in general atmospheric circulation patterns. The rather slow decrease in intensity of the spring maximum between 1963 and 1964 points to a large stratospheric source, one which may lead to substantial maximums for the next few years.

REFERENCES

1. P. F. Gustafson, S. S. Brar, and U. C. Mishra, Determination of Airborne Fission Product Radioactivity Using Gamma-Ray Spectrometry, *Nature, 195:* 557-559 (1962).
2. P. F. Gustafson, S. S. Brar, and M. A. Kerrigan, Airborne Radioactivity Due to Nuclear Weapons Tests, *J. Geophys. Res., 67:* 4641-4651 (1962).
3. R. S. Cambray, E. M. R. Fisher, G. S. Spicer, C. G. Wallace, and T. J. Webber, Radioactive Fall-Out in Air and Rain Results to the Middle of 1963, British Report AERE-R-4392, 1963.
4. L. B. Lockhart, Jr., R. L. Patterson, Jr., A. W. Saunders, Jr., and R. W. Black, Fission Product Radioactivity in the Air Along the 80th Meridian (West) During 1959, Report NRL-5528, Naval Research Laboratory, Aug. 15, 1960.
5. L. B. Lockhart, Jr., R. L. Patterson, Jr., A. W. Saunders, Jr., and R. W. Black, Summary Report on Fission Product Radioactivity in the Air Along the 80th Meridian (West)—1957-1962, Report NRL-6104, Naval Research Laboratory, Apr. 2, 1964.
6. M. I. Kalkstein, Rhodium-102 High-Altitude Tracer Experiment, *Science, 137:* 645-652 (1962).
7. L. P. Salter, High Altitude Balloon Sampling Program, in Fallout Program Quarterly Summary Report, USAEC Report HASL-140, pp. 166-214, Health and Safety Laboratory, Oct. 1, 1963.
8. L. P. Salter, High Altitude Balloon Sampling Program, in Fallout Program Quarterly Summary Report, USAEC Report HASL-149, pp. 54-99, Health and Safety Laboratory, Oct. 1, 1964.
9. E. P. Hardy, Jr., J. Rivera, and R. Frankel, Global Atmospheric Radioactivity, May-June 1961, in Fallout Quarterly Summary Report, USAEC Report HASL-117, pp. 225-229, Health and Safety Laboratory, Dec. 30, 1961.

10. D. H. Peirson, United Kingdom Atomic Energy Research Establishment, Harwell, private communication, September 1964.
11. A. J. Cruikshank, G. Cowper, and W. E. Grummitt, Production of Be^7 in the Atmosphere, *Can. J. Chem., 34:* 214-219 (1956).
12. N. Murayama, Meteorological Features of Cosmic Ray Produced Beryllium-7, *J. Meteorol. Soc. Japan, Ser. II, 42:* 43-52 (1964).

RADIOACTIVE RAINOUT RELATIONS ON DENSELY GAUGED SAMPLING NETWORKS

FLOYD A. HUFF
Illinois State Water Survey, Urbana, Illinois

ABSTRACT

Studies have been made of the relation between the rainout of radioactivity in convective storms and the three rainfall factors of volume, intensity, and duration. Data were used from four densely gauged sampling networks operated during the 1962 and 1963 spring and summer seasons in central Illinois. The network areas ranged from 10 to 6000 square miles and provided data on both microscale and mesoscale relations. Analyses of spatial variability showed a trend for the relative variability of radioactive rainout to (1) exceed the storm-rainfall variability, (2) decrease with increasing rainfall volume and storm duration, and (3) increase with increasing network size. Investigation of the point representativeness of single measurements of radioactive rainout in a 15-storm sample indicated that an average error of 20 to 25% is introduced when a single observation is assumed to represent the mean rainout over areas of 10 to 12 square miles. Correlation analyses indicated that at a given point the rainfall is not strongly related to the radioactive rainout. However, when areal patterns of rainfall and rainout are compared and allowance is made for displacement of high and low centers due to various meteorological influences, a strong association is indicated between the major features of the patterns in most storms.

INTRODUCTION

During the 1962 and 1963 spring and summer seasons, several networks of rainwater samplers were operated in central Illinois in con-

junction with a research program on the rainout of radioactivity in convective rainstorms. This research was performed to determine the time and the space distributions of storm rainout and the relation of these distributions to various meteorological factors. This paper is restricted to discussions of space distributions.

Two major purposes of the Illinois research were to determine quantitative relations for the spatial variability of radioactive rainout in convective storms and to ascertain the accuracy with which a point radioactivity measurement represents the mean storm rainout for areas of various sizes. Such knowledge has important applications in investigations aimed toward defining the atmospheric processes and the hydrometeors controlling the radioactive rainout in rainstorms and in the design of sampling networks for health-hazard monitoring. The sampling-network problem will become increasingly important if large increases in fallout occur in the future. Another problem that has not been satisfactorily solved to date is the relation between radioactive rainout and rainfall parameters; that is, how well can the rainout be estimated from a knowledge of the volume, the intensity, and the duration of the associated precipitation and how similar are the areal patterns of radioactive rainout and rainfall.

Through use of data collected on densely gauged networks in Illinois, considerable information on the mesoscale features of radioactive rainout has now been compiled and is presented in this paper for the use of persons and organizations involved in radioactive-fallout projects. It is not implied that the Illinois study provides complete answers to the several problems that exist, but the results do supply considerable quantitative information not available previously. Furthermore, the results clearly illustrate how erroneous conclusions may be reached when the characteristics of radioactive rainout are based upon data assembled from widely spaced observation points.

MEASUREMENT PROCEDURES

During 1962 storm-rainwater samples were collected for radiochemical analyses in the three concentrated rain-gauge networks shown in Fig. 1. The East Central Illinois network consists of 49 recording rain gauges in 400 square miles, the Kaskaskia network has five recording rain gauges in 12 square miles, and the Boneyard network consists of 11 recording and nine nonrecording rain gauges in 10 square miles. These concentrated rain-gauge networks provided a detailed pattern of the time and the space distribution of the amount, the intensity, and the duration of rainfall within the area.

On the East Central Illinois network, rainwater samples were obtained from weighing-bucket rain gauges, most of which had 12.6-in.-

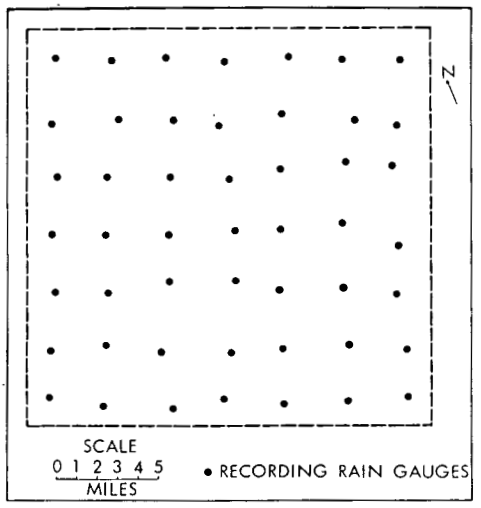

(a)

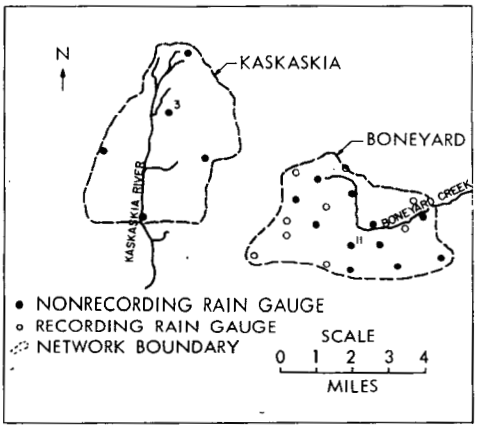

(b)

Fig. 1—Sampling networks in 1962. (a) East Central Illinois network and (b) Kaskaskia and Boneyard networks.

diameter orifices. The galvanized buckets were coated with a plastic paint to reduce possible contamination. The buckets were washed with water from a pressure sprayer twice weekly on a routine basis and, occasionally, more frequently during periods of sample collection. On the Kaskaskia and the Boneyard networks, polyethylene containers with a catch area of approximately 300 sq in. were placed by each rain gauge to collect rainwater samples since the rain gauges had 8-in. instead of 12.6-in. orifices. On these small networks the rainwater samplers were thoroughly cleaned shortly before each storm.

The 1963 sampling networks are shown in Fig. 2. The outer border encompasses an area of 6000 square miles containing 16 auto-

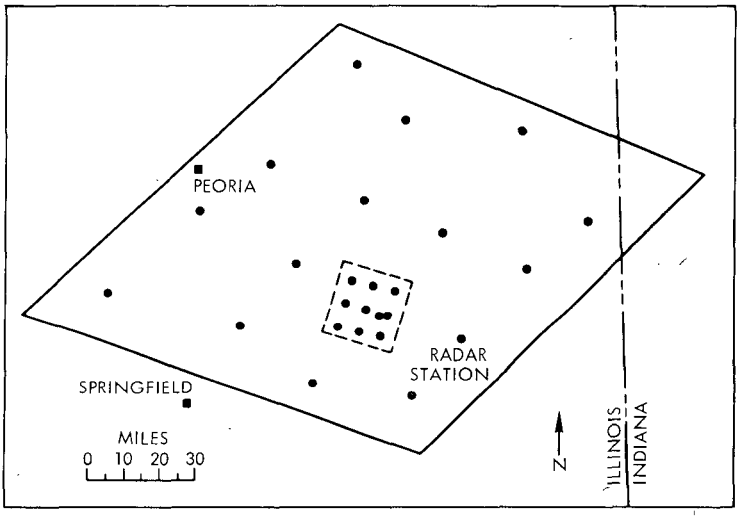

Fig. 2—Sampling networks in 1963.

matic rainwater samplers used in conjunction with a special sampling program,[1] and the inner region is the East Central Illinois network. Also, at each of the stations shown in Fig. 2, polyethylene collectors were used to obtain samples of the total storm rainfall for the studies discussed in this paper. A recording rain gauge was located at each of the rainwater sampling stations. Through use of the networks shown in Figs. 1 and 2, data were collected on areas of 10 to 6000 square miles in the two-year sampling period, 1962 and 1963. Data collection was continued on the East Central Illinois network in 1964.

Measurements of gross beta radioactivity were made with proportional counters. These instruments employ 2π geometry and are provided with lead shielding such that the beta background does not exceed 50 counts/min. Preparation of the samples for counting radioactivity was done by using the method described by Weatherford,[2] in which the water sample is divided into suspended and dissolved solids and eventually reduced to dryness on planchets. Repetitive counts were made with each sample until consecutive concentrations agreed within one Poisson standard deviation of the counting error for the sample. This error was usually less than 5% for the 1962 and 1963 data. All samples were allowed to sit for 10 days or longer before counting to minimize the effects of natural surface radionuclides such as radon, and counts for a specific storm on a specific network were made on the same day or on consecutive days to minimize uncertainty in the calculations that might arise from the progressive decay of the beta samples.

Measurements of ^{89}Sr and ^{90}Sr were made by Isotopes, Inc., utilizing techniques developed in their laboratories.[3] Walton et al.[4] indicate that the overall error of the routine radiochemical analysis was ± 7 and ± 9% for ^{90}Sr and ^{89}Sr, respectively.

SPATIAL VARIABILITY OF RAINWATER RADIOACTIVITY

An investigation was made of the spatial variability of the concentration and deposition of gross beta rainout and ^{89}Sr and ^{90}Sr rainout on the sampling networks. This investigation was made to obtain quantitative data on the probable variability of radioactivity on a mesoscale in convective storms and to determine the relation between the relative variability of radioactivity and rainfall. The relative variability was obtained by the simple method of Conrad and Pollak[5] in which it is defined by

$$V = 100 \frac{AD}{M}$$

where V is the relative variability in percent, M is the mean of the sample, and AD is the average deviation from the mean. The relative variability was chosen as the variability parameter so that factors measured in dissimilar units, such as concentration and deposition, could be compared. The Conrad and Pollak method was selected because of the simplicity of calculation and because the average dispersion about the mean was considered a desirable statistic for this study.

The relative variability of beta concentration, beta deposition, and storm rainfall was calculated for eight storms on the Boneyard network and seven storms on the Kaskaskia network in 1962. Five samples were obtained in each of the Kaskaskia storms and five or six samples in each of the Boneyard storms. Since the two networks are nearly equal in area, the data were combined to obtain a larger sample upon which to establish trends or relations. The rainfall variability was based upon observations at the same points at which the rainwater samples were taken.

The relative variability of gross beta radioactivity and storm rainfall for each storm is presented in Table 1, along with data on storm mean rainfall. In Table 1 beta concentration refers to the quantity of radioactive material per unit volume of rainwater. Beta deposition is the quantity of radioactive material deposited per unit area. This is determined by the product of the concentration of radioactive material and the rainfall depth. On the average, the relative variability of gross beta radioactivity was nearly twice that of storm

Table 1—RELATIVE VARIABILITY OF GROSS BETA RADIOACTIVITY AND STORM RAINFALL ON KASKASKIA AND BONEYARD NETWORKS

Date, 1962	Network	Relative variability, %			Mean rainfall depth, in.
		Storm rainfall	Beta concentration	Beta deposition	
May 10	Boneyard	7	22	20	0.68
May 10	Kaskaskia	4	13	14	0.72
May 26	Boneyard	9	38	30	0.51
May 26	Kaskaskia	24	25	20	0.46
May 27	Boneyard	8	10	16	0.55
May 27	Kaskaskia	20	44	58	0.43
June 8	Boneyard	23	15	27	0.53
June 9–10	Boneyard	6	20	20	1.08
June 9–10	Kaskaskia	6	11	14	1.18
July 2	Boneyard	12	29	24	1.00
July 2	Kaskaskia	44	23	20	0.41
July 2–3	Boneyard	6	24	26	3.84
July 2–3	Kaskaskia	17	10	10	3.59
July 14–15	Kaskaskia	13	39	28	1.95
August 24	Boneyard	18	52	54	0.27
Average		14	25	25	

rainfall in the 15-storm sample of Table 1. In 12 of the 15 storms, the beta variability exceeded the storm-rainfall variability.

A slight trend was found for the gross beta variability to decrease with increasing mean rainfall and storm duration. The same slight trends were found with storm-rainfall variability. Studies by the Illinois State Water Survey[6] and the U. S. Weather Bureau[7] have shown that the relative variability of storm rainfall varies inversely with mean rainfall and storm duration. This is in agreement with the trends observed in the 15-storm sample. Thus it appears that the relative variability of both the rainwater radioactivity and the storm rainfall tends to decrease with increasing storm duration and mean rainfall, which is not surprising since rainfall is the carrier of the radioactivity.

Correlation coefficients were calculated between the variables of Table 1 to evaluate further the trends previously discussed. The correlation coefficients were calculated from the logarithms of the numbers since graphical plots of the data indicated exponential relations. These coefficients, which indicate relatively low correlations, are presented in Table 2. Although they are weak, the correlations support the slight trends discussed earlier.

The relative variability discussed in the preceding paragraphs provides a measure of the average dispersion about the mean. Table 3 provides a measure of the maximum variation of gross beta and storm rainfall within the Boneyard and the Kaskaskia networks. This table

Table 2—CORRELATION BETWEEN GROSS BETA RELATIVE VARIABILITY AND RAINFALL FACTORS ON KASKASKIA AND BONEYARD NETWORKS

	Correlation factor
Beta-concentration variability vs. mean storm rainfall	−0.32
Beta-deposition variability vs. mean storm rainfall	−0.45
Beta-concentration variability vs. storm-rainfall duration	−0.20
Beta-deposition variability vs. storm-rainfall duration	−0.33
Storm-rainfall variability vs. mean storm rainfall	−0.25
Storm-rainfall variability vs. storm-rainfall duration	−0.30

Table 3—RATIO OF MAXIMUM TO MINIMUM VALUES OF GROSS BETA ACTIVITY AND STORM RAINFALL

	Fifteen-storm ratios			
	Mean	Median	Maximum	Minimum
Beta concentration	2.7	2.3	9.5	1.4
Beta deposition	2.5	2.0	6.8	1.3
Storm rainfall	1.8	1.5	4.0	1.1

indicates that gross beta activity has more extreme variation in storms on the average than does storm rainfall. This is in agreement with the average relative variability data of Table 1. Gross beta deposition was found to vary slightly less areally than did concentration. The beta-concentration ratio equaled or exceeded the rainfall ratio in 12 of the 15 cases, and the beta-deposition ratio was greater than the rainfall ratio in 11 of the 15 cases. The average relative variability of both beta concentration and beta deposition exceeded average storm-rainfall variability in 12 out of 15 cases (Table 1). Thus the foregoing statistics indicate a strong tendency for greater areal variability in gross beta activity than is exhibited by storm rainfall. In turn, this suggests partial control of rainout of radioactivity by other atmospheric factors with relatively large spatial variability. It seems logical to expect the surface rainout to be related to the drop size distribution in the storm clouds in which the rainfall developed; this distribution should be highly variable in the convective storms that make up the 15 samples used in the variability study. Regardless of the cause, however, the study indicates that great variability in rainout of radioactivity may occur within small areas of 10 to 15 square miles and within distances of 1 to 2 miles in midwestern convective storms. If this degree of varia-

bility should occur under heavy fallout conditions, it could be a factor of great importance.

For comparison purposes, the mean relative variability of ^{89}Sr and ^{90}Sr rainout in five storms on the Boneyard and the Kaskaskia networks and in five storms on the East Central Illinois network was determined. Results are summarized in Table 4, in which five-storm

Table 4—MEAN RELATIVE VARIABILITY OF ^{89}Sr AND ^{90}Sr RAINOUT IN 1962 STORMS

	Network	
	Boneyard–Kaskaskia	East Central Illinois
^{89}Sr, %		
Concentration	15	20
Deposition	20	24
^{90}Sr, %		
Concentration	15	19
Deposition	20	20
Storm rainfall, %	12	16

averages are shown. This table shows that, on the average, the relative variability of both the concentration and the deposition of ^{89}Sr and ^{90}Sr was greater than storm-rainfall variability. Comparison of Tables 1 and 4 indicates that, in general, the relative variability of gross beta is somewhat greater than that of ^{89}Sr and ^{90}Sr. Although the statistics are based on a relatively small sample of storms and may be altered as more data become available, the differences are in the expected direction since the beta variability reflects the combined variability of a large number of fission products. Table 4 shows the expected trend for the relative variability to be greater on the East Central Illinois network of 400 square miles than on the small networks of 10 and 12 square miles.

POINT RAINFALL REPRESENTATIVENESS

Gross beta and strontium data collected on the Boneyard and the Kaskaskia networks have been used in this study, which was confined to convective storms. The radioactivity at a central gauge in each network was compared with the average radioactivity determined from all samples on the network. It was assumed that the network averages represented accurate estimates of the true areal average, and the central gauge differences were treated as sampling errors. Because of

observational and analytical errors involved in the calculations of radioactivity at a point, the above assumptions are not completely correct in some cases. These errors could result in differences that are greater or less than the true difference in a specific case, but, after a large number of cases are combined, the resulting average difference should closely approximate the true relation. The 15-storm averages used in the Illinois study are considered adequate to provide an approximation of the general magnitude of the point vs. areal differences, but a large number of storms must be analyzed before a highly accurate measurement of these differences can be assured. Also, it should be realized that the magnitude of the differences between point and areal measurements would be expected to be larger, on the average, if a central sampling gauge were not used for the point measurement. The decrease in reliability of a point estimate of the areal mean as the distance of the single sampling point increases from the center of the area has been clearly demonstrated by Linsley and Kohler[8] with the use of rainfall data from a concentrated network of gauges.

Gauge 3, located near the center of the network, was used as the central gauge on the Kaskaskia network (Fig. 1), and areal means were based on the samples collected at each of the five gauges in the network. This network provides a nearly uniform sampling network, at least within practical limitations dictated by the existing road systems. Gauge 11 (Fig. 1) was used as the single point sample on the Boneyard network, and the areal means were based on five or six samples collected in each storm on the network. The sampling stations were not situated as uniformly as on the Kaskaskia network.

The data from the Kaskaskia and the Boneyard networks were combined to obtain a larger sample in this initial study, and average sampling errors were calculated. The sampling error was obtained by dividing the difference between the central gauge and the network average by the network average and multiplying by 100. An average error of 23% was obtained for gross beta concentration in the 15-storm sample, compared with 22% for deposition and 9% for storm rainfall. Standard deviations from these mean percentages were 12, 15, and 3%, respectively, for beta concentration, beta deposition, and storm rainfall. From this limited sample, indications are that a single sampling point in areas of 10 to 12 square miles will indicate the average gross beta rainout over the area in convective rainstorms with an average accuracy of 20 to 25%; however, in approximately one-third of the storms, the sampling error may equal or exceed 35%. Of course, as pointed out earlier, a much larger sample must be analyzed before the size of the sampling errors can be established with a high degree of accuracy.

POINT RELATIONS BETWEEN RADIOACTIVE RAINOUT AND RAINFALL FACTORS

Data from the 1962 and 1963 networks were used to investigate the relation between the concentration and the deposition of rainout of radioactivity and the intensity, the duration, and the volume of rainfall between network stations in convective storms. This point-to-point study was then extended to compare areal patterns of rainout and rainfall. Gross beta data were used in the study.

Correlation analyses between rainout of gross beta and rainfall factors are summarized in Table 5. These analyses indicate a general trend for gross beta concentration to decrease with increasing rainfall volume, duration, and intensity. Gross beta deposition shows a general trend to increase with the three rainfall factors. The strongest correlation was found with storm-rainfall volume, as expected, since it incorporates the influences of both duration and rate. Results similar to those presented in Table 5 were obtained also from five 1962 storms in which rainout of ^{89}Sr and ^{90}Sr was determined.

The correlation coefficients in Table 5 are not outstanding. For example, the highest median coefficient of 0.70 between rainfall volume and deposition indicates that only about 49% of the variance in beta deposition is explained by the variation in storm-rainfall amounts. Furthermore, in most of the various categories presented in Table 5, the correlation coefficient had a wide range from positive to negative values among the storms. For example, the correlation coefficient between beta concentration and rainfall volume varied from 0.58 through zero to −0.77 on the East Central Illinois network. However, the deposition trend was much more stable since only one negative coefficient resulted from the correlations between rainfall volume and beta deposition on the East Central Illinois network, and all coefficients

Table 5 — MEDIAN CORRELATION COEFFICIENTS BETWEEN GROSS BETA ACTIVITY AND RAINFALL FACTORS

Network	Rainfall volume	Rainfall duration	Rainfall rate	Number of storms
	Correlation with Beta Concentration			
6000 Square miles	−0.39	−0.24	−0.29	9
East Central Illinois	−0.63	−0.40	−0.24	9
Boneyard–Kaskaskia	−0.36	−0.36		15
	Correlation with Beta Deposition			
6000 Square miles	0.70	0.31	0.28	9
East Central Illinois	0.64	0.41	0.48	9
Boneyard–Kaskaskia	0.56	0.38		15

were positive on the larger 6000 square mile network. With duration and rate considerable fluctuation from negative to positive coefficients occurred with both concentration and deposition.

All available data from the rainwater sampling network were used in the plots shown in Fig. 3. However, only the East Central Illinois network of 400 square miles was in operation during the August storms. The eight storms described in Fig. 3 were selected to illustrate typical correlations between radioactive rainout and rainfall volume at a group of points in a relatively small area in the same convective storm. In some storms, such as those of June 10, July 1, and August 28, there was a pronounced trend for the beta concentration to vary inversely with the rainfall amount. Correlation coefficients of -0.82, -0.76, and -0.77, respectively, were obtained in these three storms. In other storms described in Fig. 3, however, the inverse trend was relatively weak, and, in the storm of August 6, the trend was reversed to produce a correlation coefficient of 0.58. Several investigators, employing storm-to-storm data at a single point, have noted an inverse correlation between radioactivity per unit volume and rainfall amount. The results of the Illinois study, in which multiple sampling points within the same storm were employed, lead to the conclusion that an inverse correlation usually prevails from point to point in convective storms, but the correlation is often weak. Occasionally, it is positive rather than negative.

An effort was made to determine whether the correlation between radioactivity and rainfall would improve if the storm rainfall were divided into several parts instead of using total storm data. Convective storms usually consist of several rain bursts, and it is possible that combining all the storm rainfall into a single sample masks the true radioactivity–rainfall relation to some extent. Automatic rainwater samplers used at 16 stations in 1963 provided consecutive samples containing 0.04 to 0.06 in., and up to 12 samples were obtained in each storm at stations in the automatic-sampler network.[9]

For each of 20 storms in which a large number of these samples were obtained within the network, graphical plots were made in which gross beta concentration was related to rainfall rate. The scatter of points in most storms was relatively great and indicated a low degree of correlation. For example, in the storm of June 10, a total of 60 samples was obtained from 12 stations, which showed a correlation coefficient of -0.35 between beta concentration and rainfall rate. Since the graphical plots indicated that this storm provided one of the better relations among the 20 storms investigated, no further mathematical calculations were made. In the 20 storms the trend found most frequently was for the beta concentration to decrease with rainfall rate, but the opposite tendency occurred in several storms.

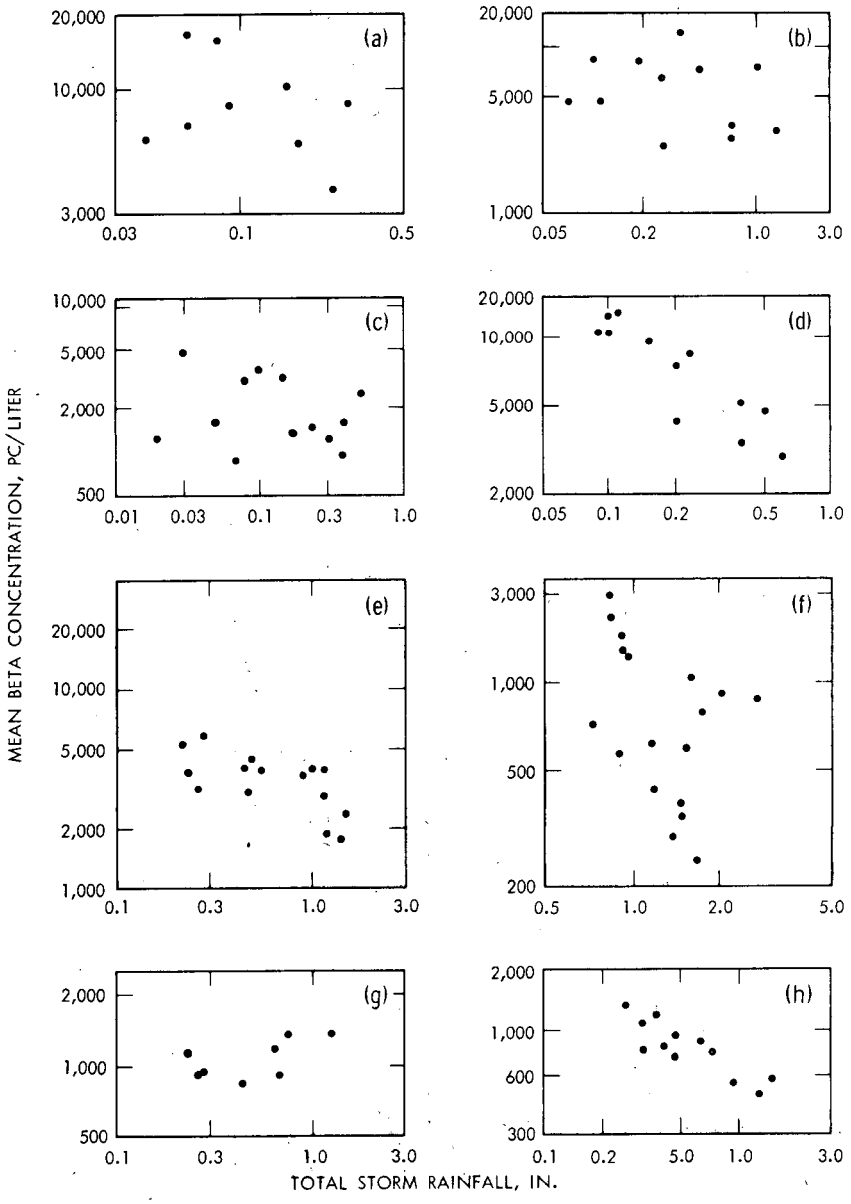

Fig. 3—Relation between gross beta concentration and storm rainfall in selected 1963 storms. (a) Pre-cold frontal rainfall on April 17; (b) low center passage on April 22; (c) post-cold frontal rainfall on May 28; (d) pre-cold frontal squall line on June 10; (e) air-mass showers on July 1; (f) stationary-front rainfall on July 6; (g) warm frontal rainfall on August 6; and (h) warm frontal rainfall on August 28.

AREAL-PATTERN RELATIONS

Comparisons were made between the areal patterns of rainout of radioactivity and rainfall on the networks in 1962 and 1963 storms. It is quite possible for point-to-point correlations to be poor, whereas areal patterns may show considerable similarity. For example, high and low regions in the rainfall and radioactivity patterns would be displaced from each other if the greatest concentration of radioactivity tended to occur near the edge of convective rain cells rather than near the cell center. Other factors, such as storm movement and raindrop fall velocity, may also cause displacement of high and low centers of radioactive rainout and rainfall from each other. With such conditions correlation coefficients from point data might be relatively low, although a definite physical relation was apparent in the areal patterns.

Comparison of the areal patterns of beta rainout and total storm rainfall on the East Central Illinois network in 1963 revealed a relatively strong association between the patterns of beta deposition and storm rainfall, with respect to the location of highs and lows in the patterns, in seven of nine storms in which data were available to define the patterns accurately. In no case was the spatial displacement of centers greater than six miles when the pattern association was rated strong. In all cases regions of heavy beta deposition tended to be associated with regions of relatively heavy rainfall, and light rainfall was associated with light deposition. The areal patterns of beta concentration and storm rainfall did not compare as favorably as the patterns of deposition and rainfall. The association of patterns was relatively strong in six of the nine storms, but the high and low association was not consistent. High beta concentrations occurred in low rainfall regions in five of the six cases, whereas, in the other case, the association was strong but high beta concentrations were associated with high rainfall values. Huff[1] has indicated that the occasional reversal from a direct to an inverse relation between beta concentration and rainfall is dependent upon the maturity of the storm system and its degree of vertical development.

An example of pattern associations is illustrated in Fig. 4 for the storm of July 1 on the East Central Illinois network. Relatively high beta concentrations in the northern and the southeastern parts of the network correspond with relatively light rainfall in these regions. A region of relatively light beta concentration extends from the eastern to the southern part of the network, but it is displaced about three miles east of the corresponding rainfall high in the south-central part of the network. Similarly, generally close association is indicated between regions of highs and lows in the beta deposition and the rainfall patterns, although the high centers are displaced from each other by several miles.

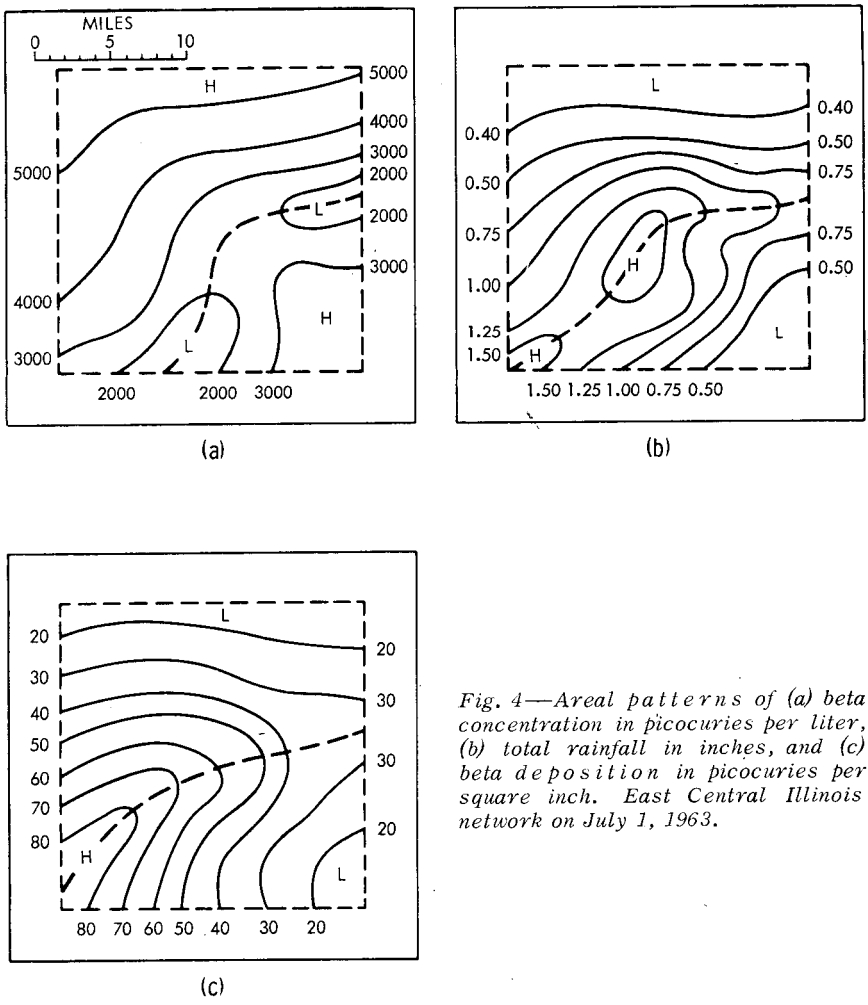

Fig. 4—Areal patterns of (a) beta concentration in picocuries per liter, (b) total rainfall in inches, and (c) beta deposition in picocuries per square inch. East Central Illinois network on July 1, 1963.

The results of the 1963 beta-pattern comparisons on the East Central Illinois network compare favorably with those obtained for nine storms in 1962 on the small Kaskaskia and Boneyard networks, in which six of the nine storms showed a relatively strong association between beta concentrations and storm-rainfall patterns.[9] Also, results compare favorably with those obtained with 1962 strontium patterns.[1]

During 1964 the rainwater sampling network on the East Central Illinois network (Fig. 2) was increased from 10 to 30 total storm samplers to verify further the results of the 1962 and 1963 pattern comparisons. Analyses of beta concentration and deposition were

made for eight storms. These included cases of (1) thunderstorms, rainshowers, and steady rain and (2) storms of various rainfall volume, intensity, and duration. Results were similar to those obtained in 1963. In all storms a relatively strong association was indicated between the patterns of beta deposition and storm rainfall with high and low centers of deposition lying near corresponding high and low centers of rainfall. The association between patterns of beta concentration and storm rainfall was relatively strong in six of the eight storms but was similar to the association observed in 1963; the association between high and low centers was not consistent. Generally, high beta concentrations corresponded with light rainfall amounts, but exceptions were even more frequent than in 1963; that is, it was not uncommon to find high beta concentrations located near areas of high rainfall amounts.

In summary, pattern comparisons among beta concentration, beta deposition, and storm rainfall on several networks in 1962–1964 indicate a generally strong association between patterns of deposition and rainfall if allowance is made for small displacement in the location of corresponding high and low centers. The causes of these displacements can be only hypothesized at this time. The correspondence between beta concentration and rainfall patterns is better than correlation of these two factors at a given point indicates, but the relation is not strong enough to permit the use of storm rainfall as a single predictor of beta-concentration patterns. Close association was found frequently enough, however, to indicate that rainfall volume has a strong influence on the beta-concentration pattern and that it should be studied further in conjunction with other meteorological factors that may help define the rainout patterns.

REFERENCES

1. F. A. Huff, Study of Rainout of Radioactivity in Illinois, Second Progress Report to Atomic Energy Commission, Contract AT(11-1)-1199, Illinois State Water Survey, January 1964.
2. R. L. Weatherford, Preparation of Samples for Radioactivity Counting, in Proceedings of the Second Sanitary Engineering Conference, Radiological Aspects of Water Supplies, University of Illinois Engineering Experiment Station Circular No. 69, January 1960.
3. A. Walton and Ralph E. Fried, Studies of Nuclear Debris in Precipitation, Seventh Progress Report to Atomic Energy Commission, Contract AT(30-1)-2415, Isotopes, Inc., August 1961.
4. A. Walton, Micah W. M. Leo, and Colin Sanderson, Study of Rainout of Radioactivity in Illinois, Annual Report to Illinois State Water Survey, Contract AT(11-1)-1199, Isotopes, Inc., February 1963.
5. V. Conrad and L. W. Pollak, *Methods in Climatology*, pp. 54-55, Harvard University Press, Cambridge, Mass., 1950.
6. F. A. Huff and J. C. Neill, Rainfall Relations on Small Areas in Illinois, *Illinois State Water Surv. Bull., 44*, 1957.
7. U. S. Weather Bureau, Thunderstorm Rainfall, Hydrometeorological Report No. 5, Washington, D. C., 1947.

8. R. K. Linsley and M. A. Kohler, Variations in Storm Rainfall over Small Areas, *Trans. Am. Geophys. Union, 32*(2): 245-250, 1951.
9. F. A. Huff, Study of Rainout of Radioactivity in Illinois, First Progress Report to Atomic Energy Commission, Contract AT(11-1)-1199, Illinois State Water Survey, January 1963.

UNIVERSITY OF OKLAHOMA PROGRAM FOR STUDIES OF CONVECTIVE STORMS AND SCAVENGING OF RADIOACTIVE PARTICLES

WALTER J. SAUCIER, SAMUEL J. HALL, and ROBERT Y. NELSON
University of Oklahoma, Norman, Oklahoma

ABSTRACT

A description is presented of the objectives, the facilities, and the operations of the University of Oklahoma program for studying the role of convective storms in the scavenging and the washout of radioactive particles from the atmosphere.

INTRODUCTION

The broad objectives of the University of Oklahoma program are (1) to examine thunderstorm convection as a mechanism for fallout of nonaqueous particulates, especially radioactive particles, and (2) to add to the knowledge of the physics of cloud growth and precipitation of such storms by the use of identifiable particulates such as radionuclides as tracers. The second objective is really a by-product of the first. At present we wish to determine the radioactive fallout and the variations in this fallout in thunderstorm rainfall, to determine the distributions of radioactivity in the thunderstorm environments, and to observe and measure the thunderstorm convection by means of rainfall records, ground meteorological records, weather radar surveillance, and routine meteorological data.

METEOROLOGICAL SETTING

The stratosphere acts as a reservoir for radioactive debris injected there during nuclear weapons tests. Owing to stratification,

the residence half-time of the stratosphere for aerosol-size particles is measured in years, depending on particle size and varying with altitude, season, and geographic position. In comparison, the corresponding residence half-time in the troposphere, where the medium is subjected to greater mixing, is of the order of just a few weeks. Consequently one is led to surmise that, several months or years after injection of the debris into the atmosphere, the vertical distribution of radioactivity should be characterized by relatively low concentrations of radioactive particles and relatively small vertical gradients of their concentration in the troposphere and by a rapid upward increase in concentration through the tropopause and lower stratosphere. In a broad sense such a distribution undoubtedly exists, as has been verified by long periods of sampling at various levels of the atmosphere. In initiating this work, we placed faith in this view, believing that if we could separate those storms which were entirely tropospheric from the more convective ones which penetrated into the stratosphere, a major part of the problem in this research would be solved. Storm height can be determined by means of ground-based radar, by observations from aircraft, and indirectly with less precision from routine meteorological data. It would then be a relatively simple task to relate storm height to tropopause height, to radioactive concentrations in the precipitation samples collected, and to atmospheric radioactivity being determined by other agencies to assess the mechanism of thunderstorm collection and washout of radioactive particles.

However, things are not so simple. A factor to be taken into account is that the air from which most of the water is condensed comes from the lower troposphere. Low-level air converges horizontally and rises; the air at the top diverges horizontally as the air from below rises into those levels. The storm is so dominated by the low-level air that the washout mechanism applies largely to particles that entered the storm in the lower troposphere. There will be particles aloft which enter into the precipitate because of entrainment of air into the vertical storm circulation in middle and high levels, injection of water masses upward into the air above the storm during its process of upward development, and some horizontal motion of air through the upper part of the storm where those winds are significantly greater than the horizontal displacement of the storm.

Perhaps an even greater difficulty arises from the large variations in radioactive concentration in the atmosphere, the troposphere, the lower stratosphere, and the tropopause region, as found by others in their careful sampling and analyzing of content. Beyond molecular- and eddy-diffusion processes, there are organized differential movements of air that produce sharp vertical and horizontal gradients in atmospheric composition. Also, the tropopause cannot be treated as a substantial air surface in this scale. The tropopause may displace it-

self relative to air in response to certain dynamical, as well as radiative, controls. It is also known that a break in the tropopause occurs near the polar-front jet stream and that with large amplitude of the thermal pattern of the troposphere the geographic position of this break has larger amplitude than do the streamlines, and winds there are stronger than the horizontal displacement of the pattern, producing some systematic horizontal movement of below-tropopause air to above the tropopause and conversely. All these differential and relative movements present some added difficulties in establishing the pattern of composition which enters into and which is modified by the storm circulation. An answer to this is to acquire more samples of atmospheric radioactivity in the air affecting the storm. We obtained samplings by aircraft this season and would like to see such sampling expanded.

It is pertinent to provide a background for the work at the University of Oklahoma before proceeding to describe the facilities for performing this research and to discuss the results obtained so far.

Thunderstorms occur everywhere in the contiguous United States, though very infrequently along the west coast. They are more common in the southern than in the northern states. Annual maximum frequencies occur in Florida and in the southern Rocky Mountains, but the large central area of the United States experiences an annual average of 40 or more thunderstorm days. The severe thunderstorms which are attended by hail or tornadoes and have great vertical depth are most common in the Central Plains area, as suggested by Fig. 1, a Weather Bureau Chart which shows the 40-year total of tornadoes observed in two-degree squares of latitude and longitude. "Tornado Alley" extends from north-central Texas through central Oklahoma, eastern Kansas, and into Iowa. The peak of activity in Oklahoma is in the spring season. Norman and Oklahoma City are located in central Oklahoma. It is evident why the public in that area is conscious of severe thunderstorms and why university meteorologists there are interested in the whole thunderstorm mechanism. There is good reason for the U. S. Weather Bureau locating its National Severe Storms Laboratory (NSSL) in Norman to carry on research in all phases of these storms. The area of stippled overlay in Oklahoma in Fig. 1 denotes an attempt to depict the Beta Surface Network of observation stations maintained by NSSL. It should be corrected by removing approximately the northern half.

The spring season in Oklahoma includes both the nonconvective rainfall systems, which are of entirely tropospheric character and attend the usual extratropical cyclones, and the thunderstorm rain systems, most of which are tropospheric but the most violent of which penetrate through the tropopause. The rainfall maximum in May and early June reflects the peak of convective activity. Consequently, in

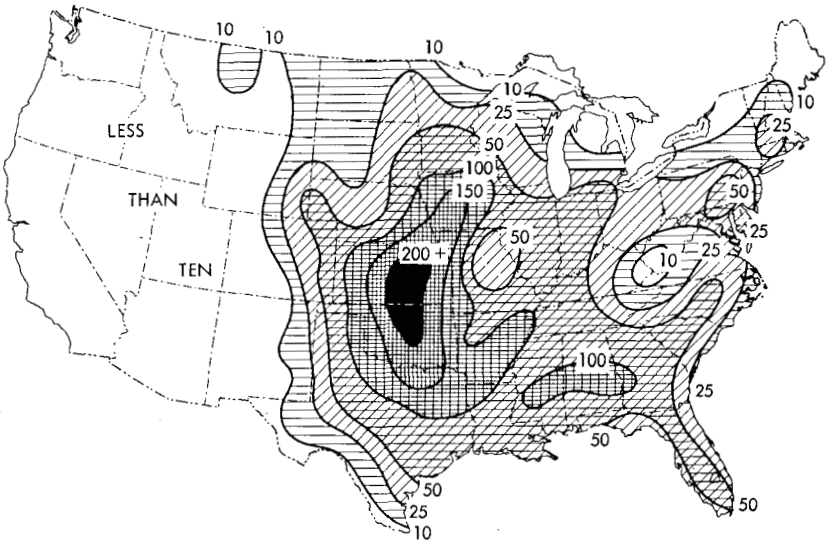

Fig. 1—Tornadoes observed during the 40-year period of 1916 to 1955. Isopleths are based on total number by two-degree squares, counting the first point of contact with ground of 7206 tornadoes. (U. S. Weather Bureau Chart, revised April 1960).

the three-month period from mid-March to mid-June, we are able to observe all the types of rainfall systems with which we need be concerned. Figure 2 is an example of a weather situation that produces intense squall-line thunderstorm activity in the general geographical region in which Oklahoma is located. The squall line is located some distance ahead of the cold front in the warm moist air characterized by some convective instability.

FACILITY AND PROCEDURE

Figure 3 shows the Beta Surface Network of stations over south-central Oklahoma. On the average, they are about 12 by 18 miles apart. The network was expanded westward from the original 36 stations to 47 stations in the last two years to include most of the Agricultural Research Service (ARS) network of recording rain gauges. The ARS network is outlined by an irregular dashed line marking a watershed boundary. In this figure Oklahoma City is located slightly to the north of the Beta Surface Network, and Norman is at station No. 4. Each station in the network produces continuous records of rainfall, wind direction and speed, barometric pressure, temperature, and relative

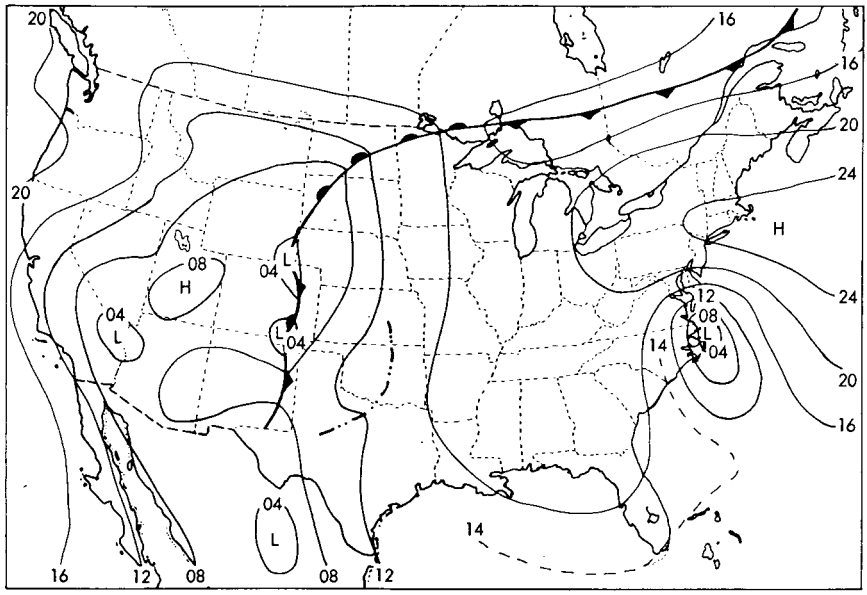

Fig. 2—Example of a weather situation that produces intense squall-line thunderstorm activity.

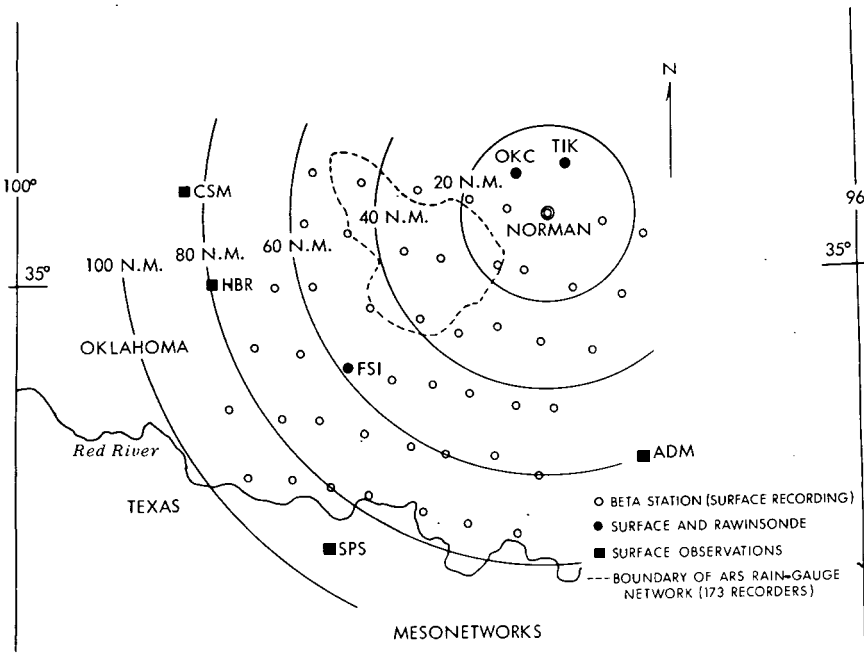

Fig. 3—Beta Surface Network stations in south-central Oklahoma.

humidity during the spring season. Weather radars are operated at the Oklahoma City airport, Tinker Air Force Base southeast of Oklahoma City, NSSL in Norman, Wichita Falls, and Fort Worth. At most of these, photographic scope records are made for later research use. An M-33 radar system at Norman is also employed by this project for current storm surveillance and for obtaining wind soundings in the thunderstorm surroundings.

During the 1963 storm season, we maintained rainfall collectors situated over the northwest one-third of the network. These were pans of 25 sq ft area which emptied into 10-liter plastic jugs. With this surface area of the pan, a rainfall of 0.15 in. gave a 10-liter sample, which was believed to be more than sufficient for the radiochemical analyses planned. Under each pan, a dry filter paper, which was exposed to the air but sheltered from the rain, was placed horizontally to collect a sample of the dry fallout. This was to serve as an index to the dry fallout collected by the pan which would contaminate the subsequent rain sample. Each time the pan was washed, by either hand or rainfall, the filter paper was changed. The radioactivity of the filter paper was found to be below threshold in each case. Therefore the procedure for observing dry fallout was discontinued in 1964.

Analysis of the 1963 data revealed that the radioactivity, as well as the rainfall, varied considerably from one collector to the next, even though the sample collected by any pan was a composite of the entire storm over that location. This was attributed to the existence of significant horizontal gradients in radioactivity within the storm produced by variations in the storm circulation of dimensions equal to or smaller than the collector network. Also, propagation of the storm would produce local time variations in the amount of radioactivity collected. To obtain meaningful results required a sampling technique that would measure the time variations at each station. These time variations measured at each in a network of collectors, compared with the intensive meteorological records for the storms, would lead to a more complete picture of the circulation, propagation, and development of the storm. The rain-sample collector pans were modified so that each would obtain as many as ten 1-gal sequential samples of rainfall per storm. A 1-gal sample represents about 0.05 in. of rain. The tenth sample at each collector integrated all rainfall from the storm beyond about 0.50 in. Some loss occurred between samples due to strong winds.

The automatic sample collector was designed by S. J. Hall from the pattern devised earlier by the Illinois State Water Survey group. Figure 4 is a photograph of the original collector pan on the left and of the automatic sequential sample collector on the right. As each jug in sequence is filled to the desired level, it drops by its weight, and the next jug is driven into position by torque on the axial drum supplied by a pulley and weight system. The weights are common build-

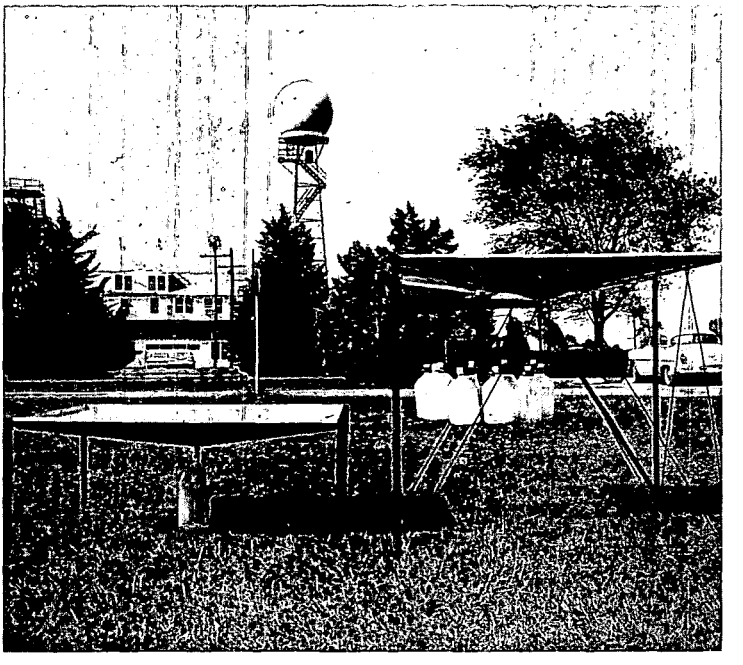

Fig. 4—Sample collectors.

ing bricks. In the background of this photograph is part of the radar facility of NSSL.

For the 1964 season, automatic rain-sample collectors were operated in the network of recording rain gauges. Figure 5 shows in detail the ARS network and the locations of our collectors. The collectors were located between 25 and 50 miles from the recording radars in an area where radar resolution is best. On the average the collectors were 8 to 10 miles apart as a compromise between sampling several thunderstorms of the season and sampling an invididual thunderstorm by more than one collector. Since the collectors make no record of time, each collector was located adjacent to a recording rain gauge maintained by either ARS or NSSL so that the time and duration of any rain sample could be resolved by reference to the record of the rain gauge. Other factors figuring in the location of the collectors are logistical. They must be accessible by automobile after the rain for retrieval of the samples, their sum distances from the laboratory should be minimized for easier maintenance accessibility, and they must be protected as much as possible from pranksters, vandals, and animals.

Radiochemical analyses of the rain samples were made by the Department of Sanitary Science and Public Health, University of Oklahoma, under the direction of R. Y. Nelson. For the 1963 season the work in-

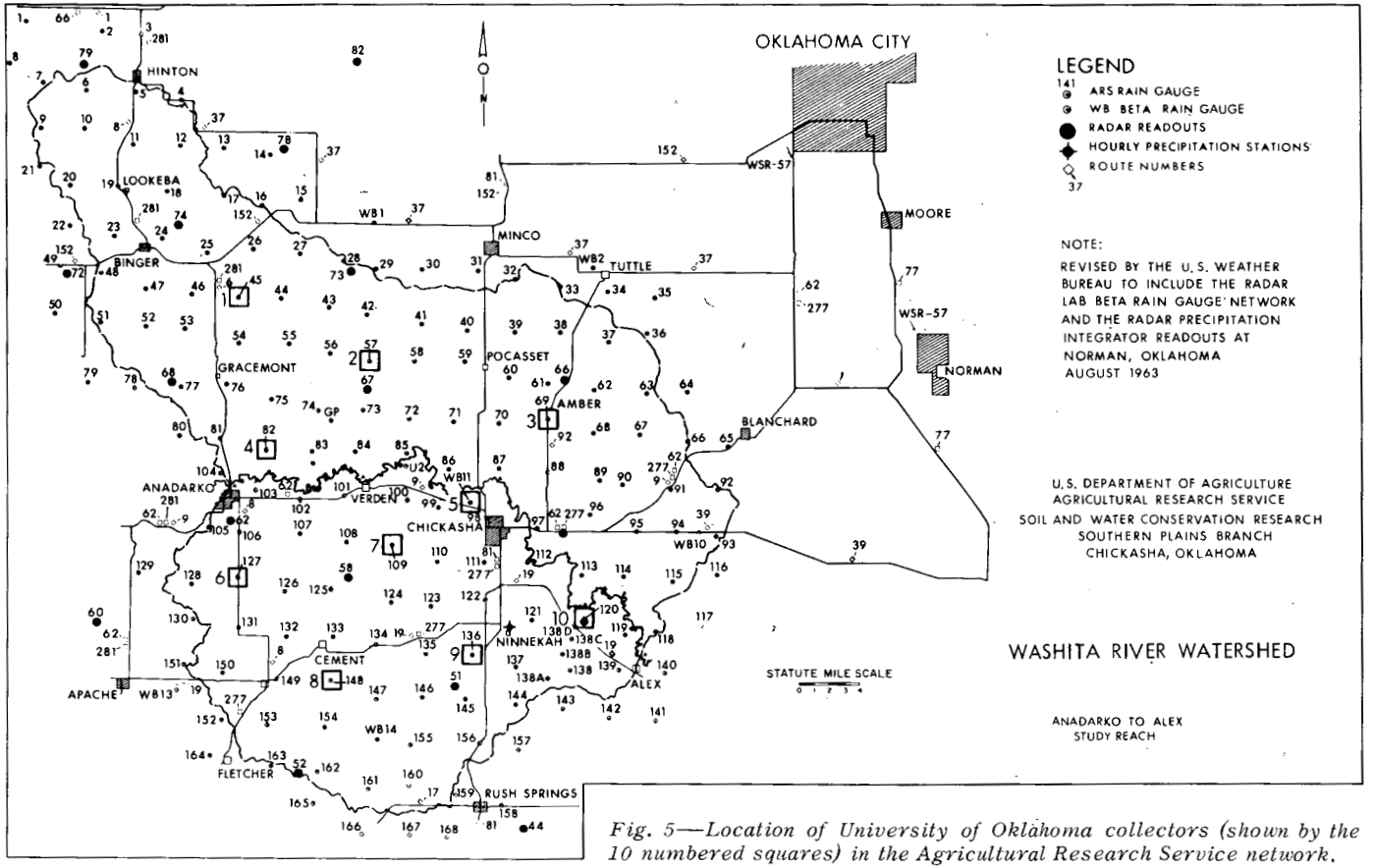

Fig. 5—Location of University of Oklahoma collectors (shown by the 10 numbered squares) in the Agricultural Research Service network.

volved the following: determinations in rain samples of total dissolved and total suspended beta activity and of ^{89}Sr and ^{90}Sr; a feasibility study on hailstones from the May 26, 1963, Midwest City storm; development of beta scintillation spectroscopy techniques; and evaluation of the effect of dust on the rain collectors on the radioactivity levels found in the rain samples. Modifications were made for the 1964 season. Measurements of the radioactivity of dust were discontinued, and there were no hail collections. The decreased level of atmospheric ^{89}Sr activity led us to discontinue that analysis in view of the greatly increased number of rain samples obtained by the sequential collectors. Emphasis in the 1964 analyses was in determining the beta activity in the rain samples. Strontium-90 analyses were made on most of the rain samples but not all because of the time and the cost involved. Gamma-activity determinations were made as time allowed in the course of the other analyses.

Preliminary results of the 1964 operational season are presented in the paper by Hall.* Analyses are still in process; therefore conclusions drawn from the 1964 data are merely tentative.

*See paper by Samuel J. Hall, this volume.

RADIOACTIVITY IN PRECIPITATION: CASE STUDIES FROM THE 1964 SPRING SEASON

SAMUEL J. HALL
University of Oklahoma, Norman, Oklahoma

ABSTRACT

Four case studies are presented of convective storms in which time samples of rainfall were collected. The profiles obtained from these collections are analyzed showing time variations of total beta-radioactivity content, rainfall rate, and ratio of particulate to dissolved beta activity. These data, with their respective radar data analyses, indicate the temporal changes of beta concentration as well as areal distributions in convective storms. For mature storms a minimum of beta concentration is associated with maximum rainfall rates. For dissipating storms a maximum of beta concentration is associated with maximum rainfall rates.

INTRODUCTION

During the springtime maximum of severe convective storms in Oklahoma, data were collected for storms of varying nature and intensity. Case studies of four storm situations of differing natures and stages of development are presented. One case, occurring on April 23, 1964, was an isolated cell, whereas the other three cases, on April 17, May 9, and May 10, were squall lines. The squall-line storms of May 9 and May 10 were parts of the same synoptic situation; therefore they are investigated and compared accordingly.

The observation and rainfall-collection program is discussed elsewhere,* but I will mention here that data were taken for storms

*See paper by Walter J. Saucier, Samuel J. Hall, and Robert Y. Nelson, this volume.

passing over the rain-gauge network of the Agricultural Research Service of the U. S. Department of Agriculture. This network is located in central Oklahoma within the "beta" network of the Weather Bureau's National Severe Storms Laboratory (NSSL) and under surveillance by the NSSL WSR-57 radar. Time-rainfall collections were made for all storms investigated over the network shown in Fig. 1.

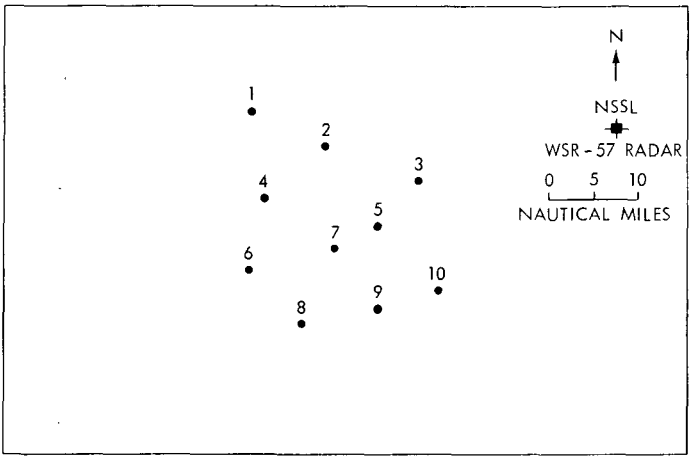

Fig. 1—Network of automatic rainfall collectors.

ANALYSIS OF STORM OF APRIL 17

The surface synoptic chart for 0000Z, Fig. 2, shows a strong cyclone system over Minnesota, with a cold front extending southwestward through South Dakota, Wyoming, Utah, and Nevada. At this time and during the storm period, Oklahoma was influenced by generally southwesterly flow through the troposphere. The convective cells that developed into a short squall line were well ahead of the surface front.

The squall line, oriented northeast–southwest and moving eastward at 20 knots, was about 40 nautical miles long and 20 nautical miles wide when the southernmost cell appeared over station 1. Figure 3 shows the position and intensity of the cell at this time. The maximum intensity, 48 db, was maintained as the storm continued eastward over the network. A time sequence of the positions of the area of maximum intensity of the cell, Fig. 4, shows that the maximum-intensity area increases from 0020 to 0033 CST and then decreases to 0046 CST. This cycle is repeated from 0046 to 0125 CST. During these cycles station 1 was beneath a portion of the storm-cell cloud mass.

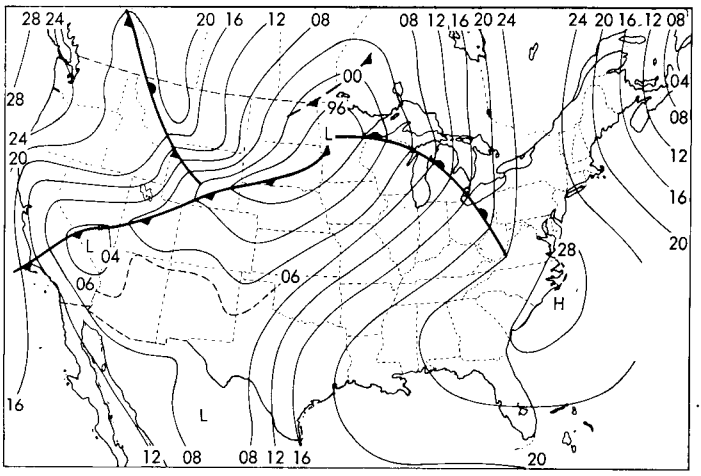

Fig. 2—Surface synoptic chart for 0000Z on Apr. 17, 1964.

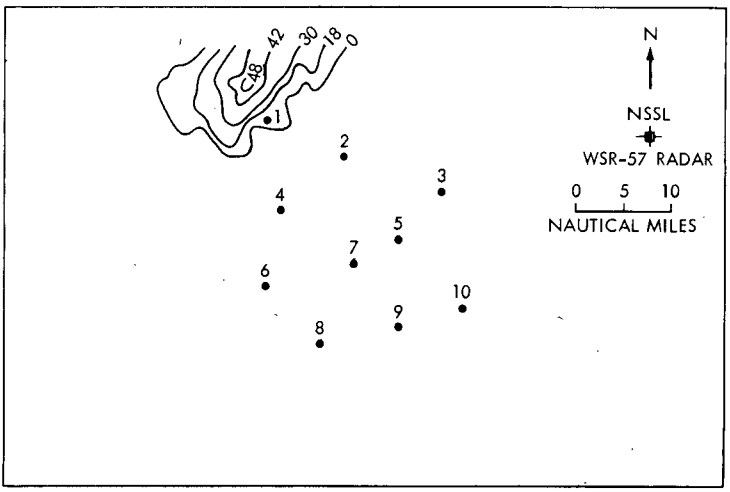

Fig. 3—Storm position with radar-echo-intensity contours (db) for 0020 CST on Apr. 17, 1964.

The rainfall-sample cross sections and time cross sections of total beta-activity concentration, rainfall rates, and ratios of particulate to dissolved beta activity for rain samples collected are shown in Fig. 5 for station 1. The initial total beta concentration was 334.5 pc/liter with a strong rainfall rate of 1.80 in./hr. After the initial burst of strong rainfall, the intensity decreased as did the beta con-

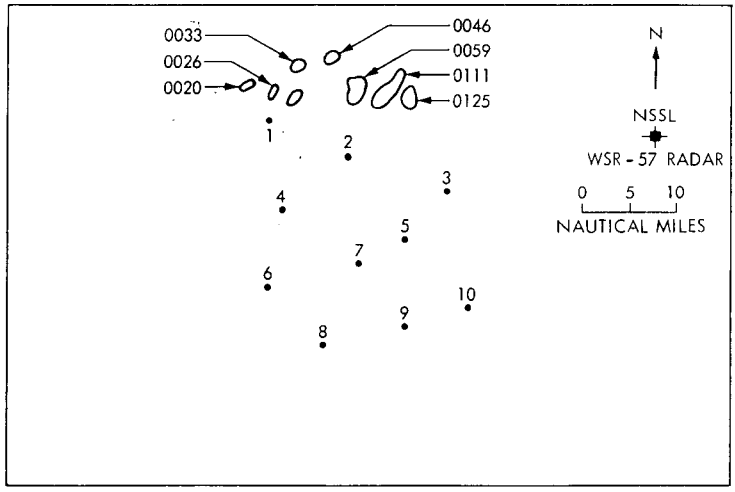

Fig. 4—Time sequence of radar-echo intensity of 48 db for storm on Apr. 17, 1964, from 0020 to 0125 CST.

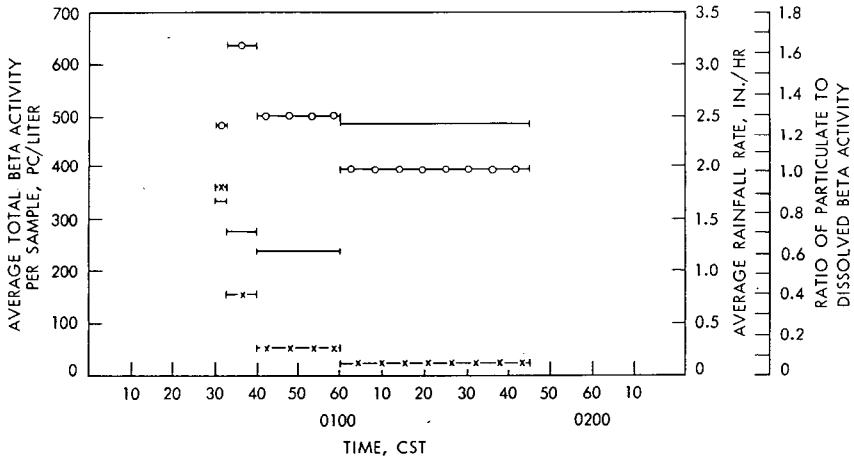

Fig. 5—Time cross sections of total beta concentration (solid lines), rainfall rate (lines with x's), and ratios of particulate to dissolved beta activity (lines with zeros) for station 1 for storm of Apr. 17, 1964.

centration, but, when the rainfall rate became very weak, the beta activity in the rain samples was at a maximum for that station. A comparison of the Fig. 5 with the Fig. 6 time cross sections of radar-echo intensity and storm height shows that rainfall did not occur until the radar-echo intensity and storm height over the station were at

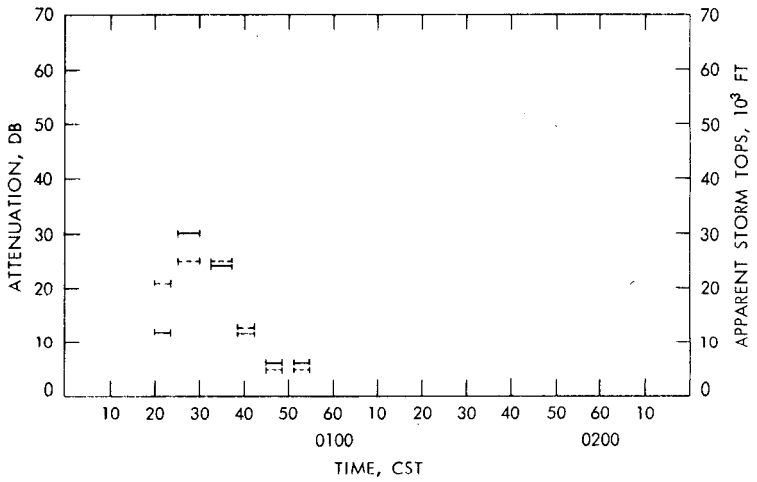

Fig. 6—Time cross sections of radar-echo intensity (solid lines) and radar storm tops (dashed lines) over station 1 for storm of Apr. 17, 1964.

maximum values. This occurred when the radar-echo intensity maximum was in its closest proximity to the station and was increasing in area. When the radar storm top was a maximum of 25,000 ft over the collector, the radar top of the echo-intensity center was 25,000 ft and increased to a maximum of 36,000 ft. Since the tropopause height in the vicinity was 41,200 ft, the entire storm cell was confined to the troposphere.

The ratio of particulate to dissolved material (see Fig. 5) increased from the first to the second sample. Table 1 shows that this occurrence was due to differential decreases in the beta concentration of both the particulate and the dissolved materials. Table 1 also shows that an increase in the particulate and the dissolved beta concentration was quite marked during the period of very light rainfall, apparently because of evaporation of peripheral rainfall.

This storm was a strong, but small, cell that was confined to the troposphere. The rainfall collections made were not from the region of maximum intensity, but rather from a region about halfway between the maximum and the boundary of the rain area. During the sampling period the storm was in the mature stage. Later, after having moved out of the network, it began to dissipate at around 0200 CST.

ANALYSIS OF STORM OF APRIL 23

A quasi-stationary front, extending westward from a low-pressure center over Virginia, crossed southern Kansas as is illustrated in

Fig. 7. Low-level wind flow over Oklahoma was southerly, veering to southwesterly up to the tropopause. A single, late-afternoon storm crossed the collection network. This storm was not associated with a squall line, although squall-line activity occurred about 18 hr later 200 miles southeast of the collection network.

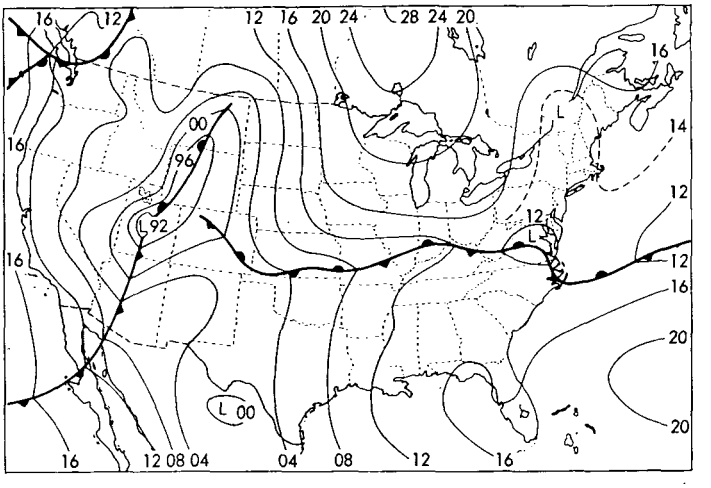

Fig. 7—Surface synoptic chart for 0000Z on Apr. 24, 1964.

The storm approached the network from the south–southwest with an apparent speed of 35 knots. Figure 8 shows radar-echo intensity contours as the storm entered the network at 1709 CST. The radar top of the 48-db intensity maximum was 56,000 ft and, as can be seen from Table 2, had penetrated more than 15,000 ft into the stratosphere. It is from this region of the storm that multiple samples were obtained. Smaller cells continued to develop in the western portion of the storm but were of little consequence in this complex storm.

Figures 9 and 10, the rainfall-sample cross sections and echo-intensity and radar storm-top cross sections, respectively, for station 8 show that the beta activity in samples varied inversely with the storm height, the intensity, and the rainfall rate. The cell that deposited the rainfall was weakening as it crossed station 8. The radar top had decreased to 42,000 ft, which was its height over station 8 when the rainfall was a maximum. Figure 11 illustrates the radar-intensity contours at this time. The arrow indicates the axis of maximum rainfall from the cell with the head marking the northern extent of the strong rainfall for this dissipating cell.

The ratio of particulate to dissolved beta activity increased after the initial sample and was generally in phase with the rainfall inten-

Table 1—RESULTS OF TOTAL-BETA-ACTIVITY ANALYSES AND CORRESPONDING RAINFALL RATES

Date	Sample	Particulate, pc/liter	Dissolved, pc/liter	Particulate + dissolved, pc/liter	Particulate/ dissolved	Rainfall rate, in./hr
April 17	101	169.0	165.5	334.5	1.21	1.80
	102	167.0	105.3	272.3	1.59	0.77
	103	133.0	105.5	238.5	1.26	0.27
	104	242.0	246.0	488.0	0.98	0.12
Average		192.3	155.6	347.9	1.24	0.74
April 23	201	833	327	1160	2.55	0.12
	501	235	230	465	1.02	1.20
	502	117	382	559	0.47	1.20
	601	79	272	351	0.29	0.21
	701	790	145	935	5.45	1.04
	801	318	236	554	1.35	1.92
	802	329	153	482	2.15	1.92
	803	250	126	376	1.98	3.20
	804	246	189	435	1.30	0.56
	901	158	183	341	0.86	0.47
Average		341.5	224.3	565	1.52	1.18
May 9	101*	91.0	152.0	243.0	0.60	0.009
	102*	112.1	164.5	276.6	0.68	0.16
	201	438.0	162.0	600.0	2.70	0.10
	401*	325.0	88.9	413.9	3.66	0.27
	402*	200.0	125.5	325.5	1.59	0.07
	501	54.0	201.0	255.0	0.27	0.33
	502	48.7	99.4	148.1	0.49	1.50
	503	44.3	43.7	88.0	1.01	0.86
	504	42.7	85.6	128.3	0.50	1.20
	505	80.7	95.1	175.8	0.85	1.50
	506	30.4	36.5	66.9	0.83	2.00
	507	32.3	41.2	73.5	0.78	0.67
	508*	37.6	21.2	58.8	1.77	0.15
	509*	27.1	31.1	58.2	0.87	1.00
	510*	32.5	94.6	127.1	0.34	1.20
	601	152.2	124.0	276.2	1.23	0.37
	602	130.5	132.5	263.0	0.98	1.68
	603	28.4	41.7	70.1	0.68	3.36
	604	12.9	30.6	43.5	0.42	3.36
	605	34.5	42.1	76.6	0.82	1.68
	606	46.4	79.5	125.9	0.58	0.13
	701	69.3	142.5	211.8	0.49	0.47
	702	121.8	120.0	241.8	1.02	1.95
	703*	21.5	75.2	96.7	0.29	0.11
	801	67.8	149.0	216.8	0.46	1.32
	802	85.1	103.5	188.6	0.82	4.40
	803	56.2	75.5	133.7	0.74	3.77
	804	95.6	149.0	244.6	0.64	1.32
	805*	33.7	67.2	100.9	0.50	0.33
	901	33.1	60.3	93.4	0.55	0.52
	902	50.1	61.7	111.8	0.81	1.04
	903	46.1	47.7	93.8	0.97	1.04
	904	32.7	48.5	81.2	0.67	1.56
	905	22.4	33.8	56.2	0.66	1.04
	906	10.2	15.8	26.0	0.65	1.56
	907*	34.7	69.7	104.4	0.50	0.22
	1001	252.5	189.5	442.0	1.33	0.33
	1002	39.6	94.3	133.9	0.42	1.05
	1003	89.5	134.5	224.0	0.67	1.80
	1004	204.5	173.0	377.5	1.18	3.15
	1005	50.5	172.0	222.5	0.29	1.40
	1006*	38.2	96.7	134.9	0.40	0.09
Average		82.3	91.6	176.9	0.85	1.19

*Samples containing rainfall from more than one cell.

Table 1 — (Continued)

Date	Sample	Particulate, pc/liter	Dissolved, pc/liter	Particulate + dissolved, pc/liter	Particulate/ dissolved	Rainfall rate, in./hr
May 10	101	102.2	144.5	246.7	0.71	2.16
	102	278.0	265.0	543.0	1.05	2.16
	103	131.5	238.5	370.0	0.55	0.36
	104	77.7	50.0	127.7	1.55	0.54
	105	171.0	70.7	241.7	2.42	0.54
	106*	142.0	88.3	230.3	1.61	0.72
	201*	285.0	162.0	447.0	1.76	0.78
	202	49.6	64.9	114.5	0.76	1.65
	203	43.7	64.8	108.5	0.67	0.94
	204	88.2	71.8	160.0	1.23	4.40
	205	107.3	97.3	204.6	1.10	1.32
	206*	47.5	77.1	124.6	0.62	0.83
	207*	401.5	269.5	671.0	1.49	0.60
	301	123.0	234.5	357.5	0.52	0.68
	302	54.3	87.6	141.9	0.88	5.40
	303	96.6	72.5	169.1	1.33	5.40
	304	54.8	61.8	116.6	0.89	5.40
	305	31.3	70.1	101.4	0.45	5.40
	306*	87.7	106.0	193.7	0.83	0.77
	307*	769.5	204.5	974.0	3.76	0.68
	401	91.5	338.5	430.0	0.27	2.70
	402	44.1	212.5	256.6	0.21	5.40
	403	43.0	153.5	196.5	0.28	3.38
	404*	89.0	143.0	232.0	0.62	0.75
	501*	45.8	123.5	169.3	0.37	0.02
	502*	67.6	42.5	110.1	1.59	0.03
	503	24.3	45.8	70.1	0.53	2.00
	504	31.4	37.9	69.3	0.83	6.00
	505	24.9	44.3	69.2	0.56	4.80
	506	73.8	74.0	147.8	1.00	4.80
	507					1.20
	508	104.7	94.7	199.4	1.11	0.43
	509					0.08
	601*	89.0	131.0	220.0	0.68	0.16
	602*	26.0	59.5	85.5	0.44	0.25
	603	21.7	40.2	61.9	0.54	2.28
	604	64.9	84.8	149.7	0.77	2.85
	605	63.0	94.0	157.0	0.67	3.80
	606	105.0	91.2	196.2	1.15	3.80
	607*	87.1	119.0	206.1	0.73	0.19
	701*	93.3	182.5	275.8	0.51	0.80
	702	86.8	97.8	184.6	0.89	1.92
	703	50.4	61.8	112.2	0.82	3.20
	704	71.4	107.5	178.9	0.66	3.20
	705	124.5	106.1	230.6	1.17	1.60
	706	132.0	110.5	242.5	1.19	0.87
	707	149.5	101.2	250.7	1.48	0.38
	801*	74.8	94.3	169.1	0.79	0.90
	802	60.9	58.8	119.7	1.04	3.00
	803	67.5	80.7	148.2	0.84	5.40
	804	89.7	93.3	183.0	0.96	2.70
	805	102.9	125.6	228.5	0.82	1.80
	901*	69.9	123.0	192.9	0.57	0.06
	902	157.5	93.2	250.7	1.69	0.90
	903	163.1	57.3	220.4	2.85	0.90
	904	125.5	49.0	174.5	2.56	0.90
	905	172.5	58.6	231.1	2.94	1.80
	906	74.1	52.5	126.6	1.41	2.28
	907	89.4	58.8	157.2	1.52	2.28
	908	24.8	69.0	93.8	0.36	2.28
	909	32.5	81.9	114.4	0.40	2.28
	1001*	83.7	174.5	258.2	0.48	0.99
	1002	38.8	80.2	119.0	0.48	1.25
	1003	225.5	64.5	290.0	3.50	1.95
	1004	42.4	56.6	99.0	0.75	3.45
	1005					4.60
	1006	86.1	71.2	157.3	1.21	2.76
Average		105.1	105.3	219.2	1.07	2.09

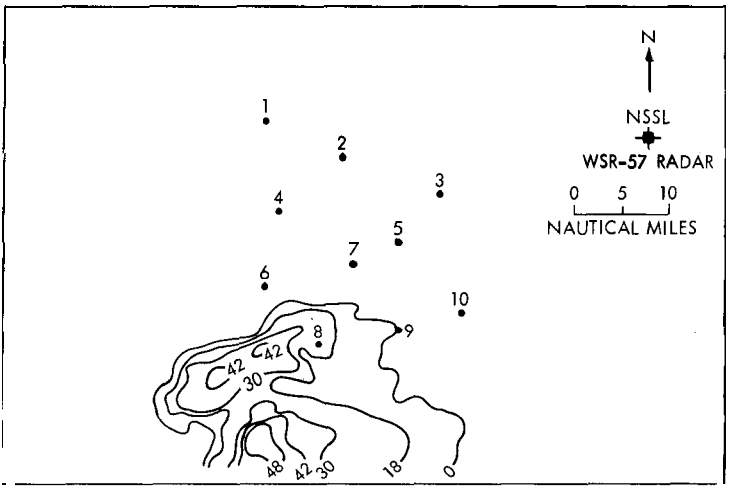

Fig. 8—Storm position with radar-echo-intensity contours (db) for 1709 CST on Apr. 23, 1964.

Table 2—TROPOPAUSE HEIGHTS OVER CENTRAL OKLAHOMA

Date	Time, CST	Tropopause height, ft
April 17	0600	41,197
April 23	1800	40,672
May 9	1800	41,328
May 10	1800	43,296

sity. There was little apparent peripheral evaporation at station 8 since, as can be noted from Fig. 9, the rainfall rate during the final sample collection was of moderate intensity.

With the exception of station 5, at which two samples were collected, station 8 was the only one at which multiple samples were taken. Between-station comparisons from Table 1, radiochemical-analysis results, and the precipitation and total-beta-activity patterns of Fig. 12 show that activity maximums occurred at stations 2 and 7, where the particulate beta concentrations were considerably higher than those at the other stations. The rainfall at station 2 was of the weak peripheral type, but 0.26 in. fell at station 7, which apparently had a collector malfunction since only one collecting jug was filled to overflowing. The 0.26 in. of rainfall should have yielded more than one sample. This, however, does not account for the high particulate beta concentrations. An overfilling malfunction also occurred at station 9,

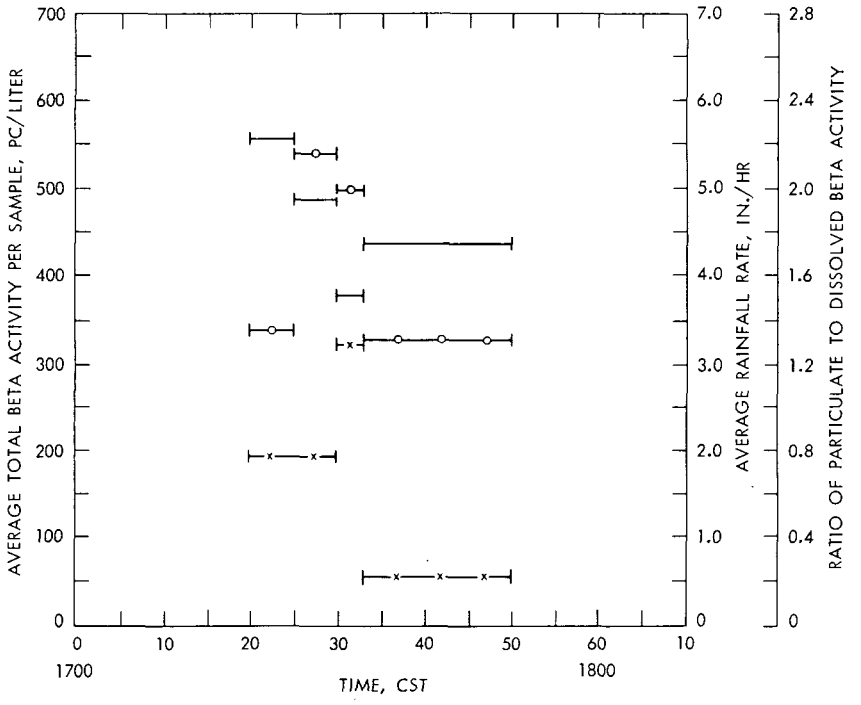

Fig. 9—Time cross sections of total beta concentration (solid lines), rainfall rate (lines with x's), and ratios of particulate to dissolved beta activity (lines with zeros) for station 8 for storm of Apr. 23, 1964.

but the total beta concentration was not out of line with the values obtained at station 8.

Analysis of radar data indicated that the collections at stations 5 and 7 were from the same rain area that passed over station 8. The first collections were being taken from the leading edge of the storm at station 5 at the same time the final sample was being taken from the trailing edge at station 8. The rainfall center of the dissipating cell passed four miles west of station 5. The radar storm top at this time was at 34,000 ft and no longer penetrated into the stratosphere. Comparisons of the collection data from the leading edge at station 5, given in Table 1, with those from the leading edge at station 8 show that the total beta concentration at station 5 increased with time whereas the ratio of particulate to dissolved beta activity decreased with time. These occurrences are the inverses of the initial events at station 8, but the magnitudes are in line. Table 1, which compares collections between the leading edge and the trailing edge, shows that the beta-activity concentrations of the leading edge were slightly higher, 465 and 559 pc/liter, than the concentration at the trailing edge, 435 pc/liter.

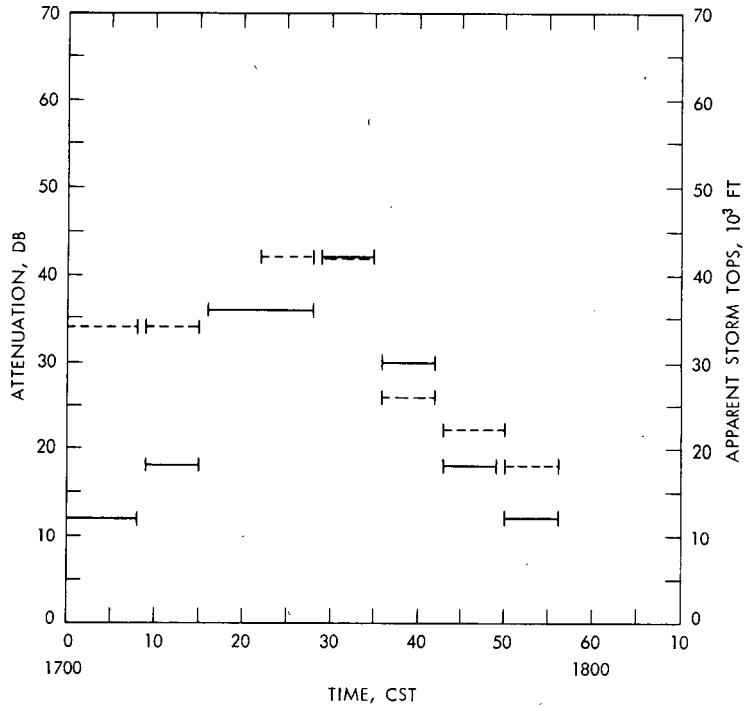

Fig. 10—Time cross sections of radar-echo intensity (solid lines) and radar storm tops (dashed lines) over station 8 for storm of Apr. 23, 1964.

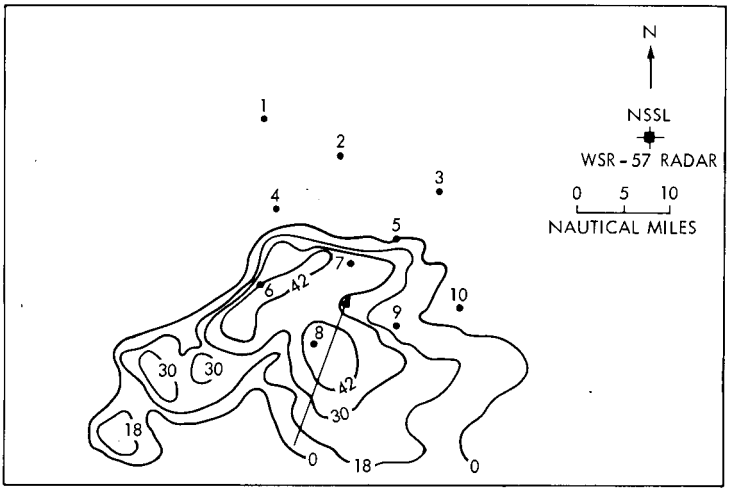

Fig. 11—Storm position with radar-echo-intensity contours for 1729 CST on Apr. 23, 1964. Arrow indicates axis and northern extent of rainfall maximum.

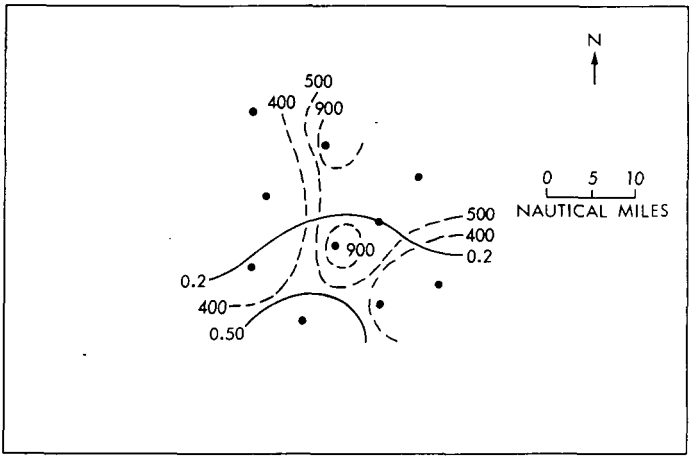

Fig. 12—Precipitation pattern (solid lines) and total-beta-concentration pattern (dashed lines) for Apr. 23, 1964. Precipitation is in tenths of inches of rainfall, and total beta concentration is in picocuries per liter.

The ratio of particulate to dissolved beta activity at the leading edge decreased with time, and the observed minimum occurred at the leading edge. This could have been due to fewer dust particles being carried aloft by the diminishing low-level convergence in advance of the dissipating cell.

ANALYSIS OF STORM OF MAY 9

At 1800Z on May 9, a quasi-stationary surface front was positioned as shown in Fig. 13. Winds were southeasterly at the surface over Oklahoma, veering west–southwesterly up to the tropopause. Afternoon squall-line activity began about 100 nautical miles west of the collection network and moved eastward at about 20 knots. By 1900 CST the squall line entered the collection network. At this time the line was oriented northeast–southwest and was about 100 miles long and about 30 miles wide. The southern portion crossed the collection network at about 20 knots. The individual cells had an eastward movement.

The storm structure that passed over the network was quite complex. Figure 14 shows the storm position and intensities of the major cells. Most of the collectors had multiple sample collections (see Table 1; samples containing rainfall from more than one cell are indicated by an asterisk). Samples from the northwest portion of the network, where the rainfall was generally light, contained peripheral rains from several small cells.

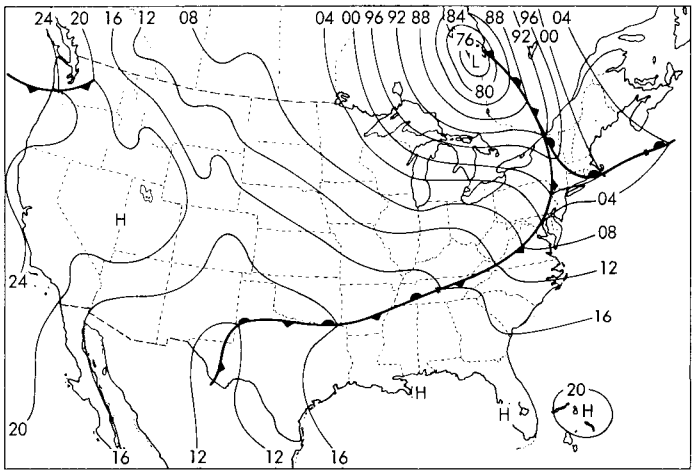

Fig. 13—Surface synoptic chart for 1800Z on May 9, 1964.

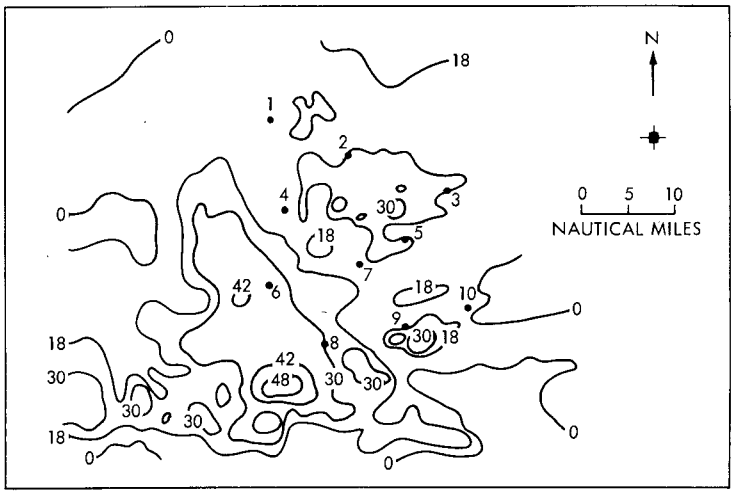

Fig. 14—Storm position with radar-echo-intensity contours (db) for 2029 CST on May 9, 1964.

Figures 15 to 20 are the rainfall-sample cross sections for stations 5 through 10, respectively. These, along with Figs. 21 to 26, the time cross sections of echo intensity and radar storm tops over stations 5 through 10, respectively, show the general nature of the beta-concentration profiles. The figures show that with the exception

(Text continues on page 551.)

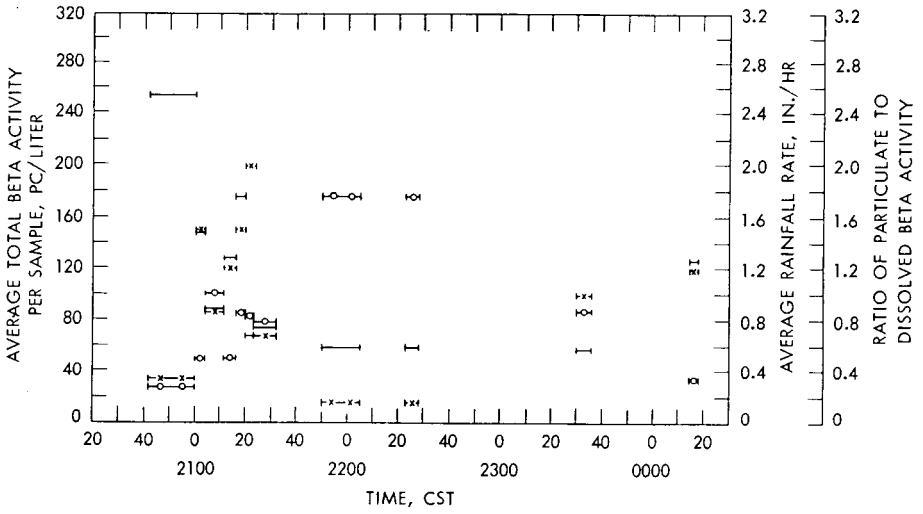

Fig. 15—Time cross section of total beta concentration (solid lines), rainfall rate (lines with x's), and ratios of particulate to dissolved beta activity (lines with zeros) for station 5 for storm of May 9, 1964.

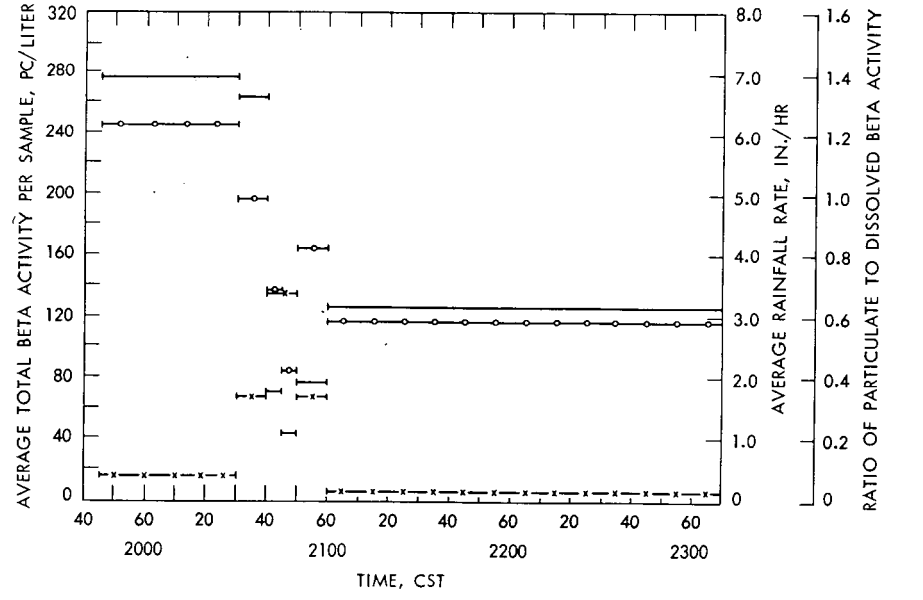

Fig. 16—Time cross section of total beta concentration (solid lines), rainfall rate (lines with x's), and ratios of particulate to dissolved beta activity (lines with zeros) for station 6 for storm of May 9, 1964.

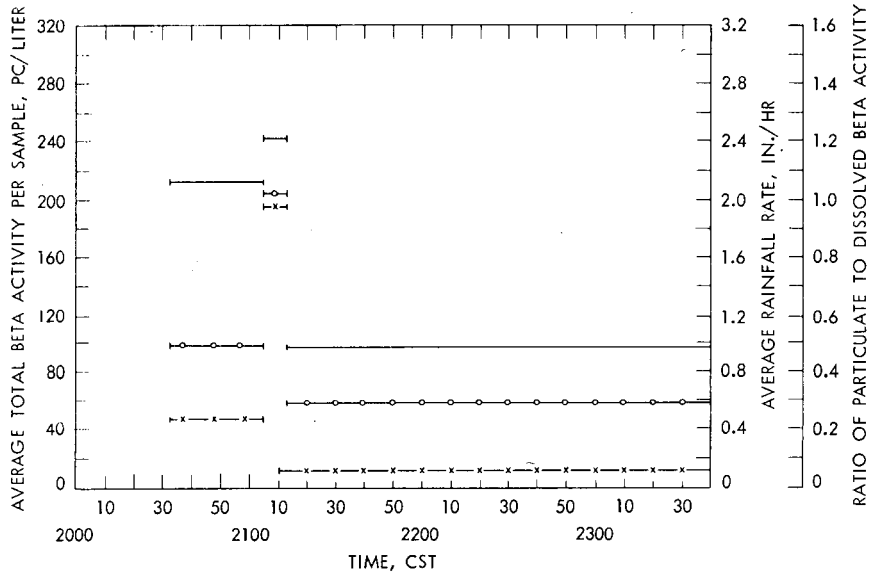

Fig. 17—Time cross section of total beta concentration (solid lines), rainfall rate (lines with x's), and ratios of particulate to dissolved beta activity (lines with zeros) for station 7 for storm of May 9, 1964.

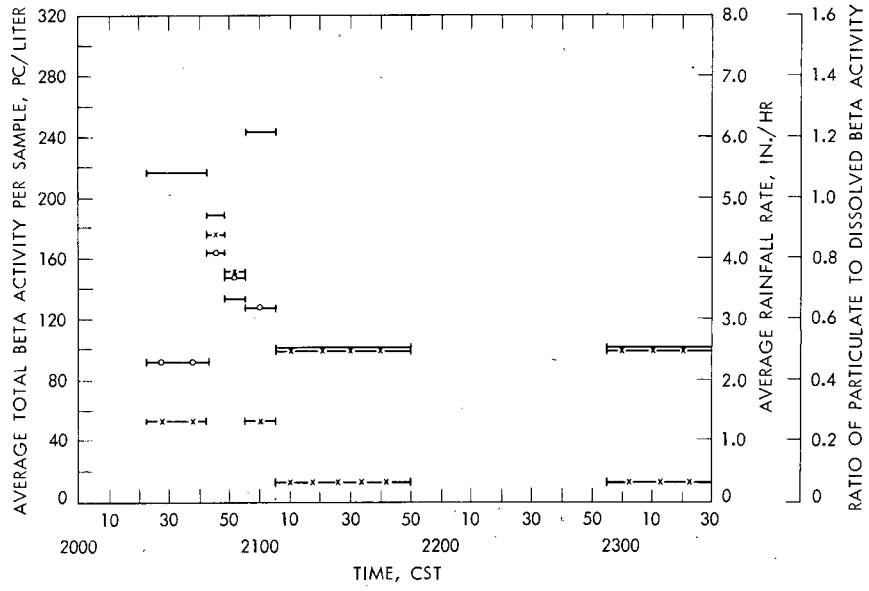

Fig. 18—Time cross section of total beta concentration (solid lines), rainfall rate (lines with x's), and ratios of particulate to dissolved beta activity (lines with zeros) for station 8 for storm of May 9, 1964.

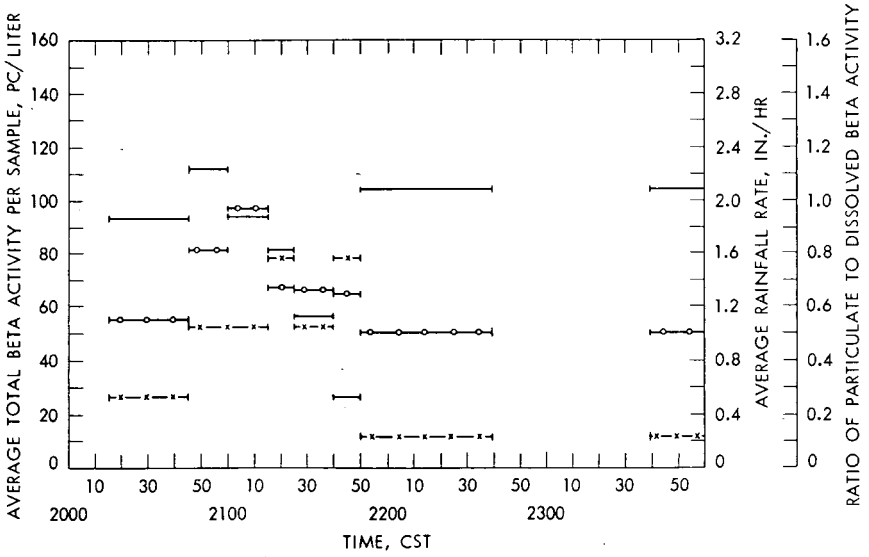

Fig. 19—Time cross section of total beta concentration (solid lines), rainfall rate (lines with x's), and ratios of particulate to dissolved beta activity (lines with zeros) for station 9 for storm of May 9, 1964.

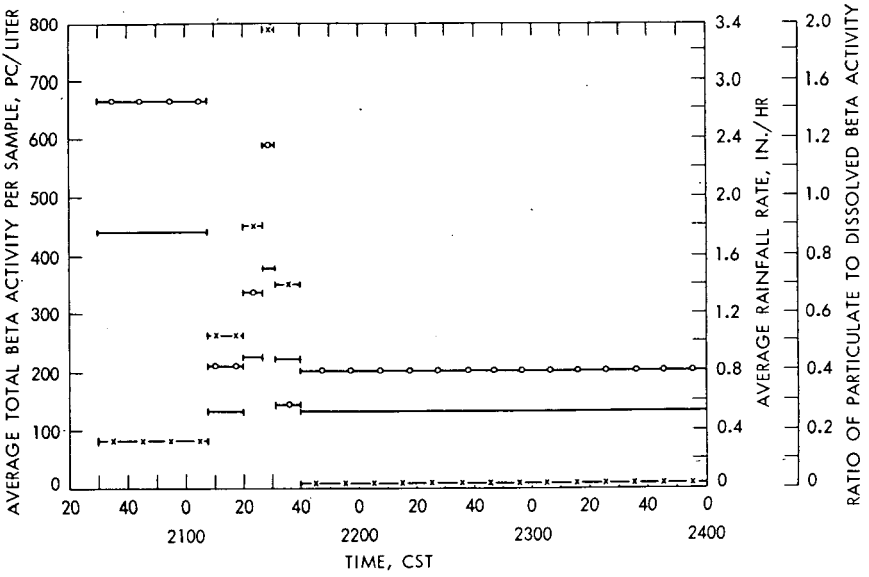

Fig. 20—Time cross section of total beta concentration (solid lines), rainfall rate (lines with x's), and ratios of particulate to dissolved beta activity (lines with zeros) for station 10 for storm of May 9, 1964.

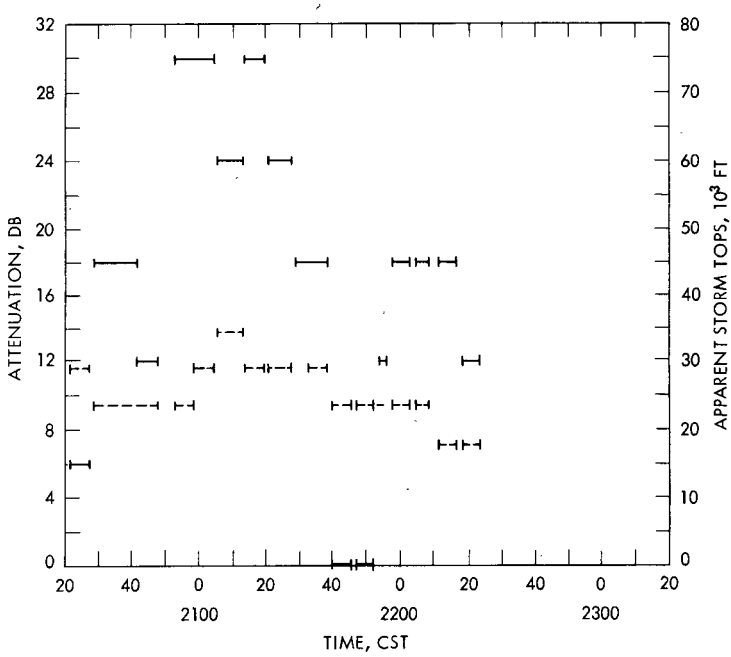

Fig. 21—Time cross section of radar-echo intensity (solid lines) and radar storm tops (dashed lines) over station 5 for storm of May 9, 1964.

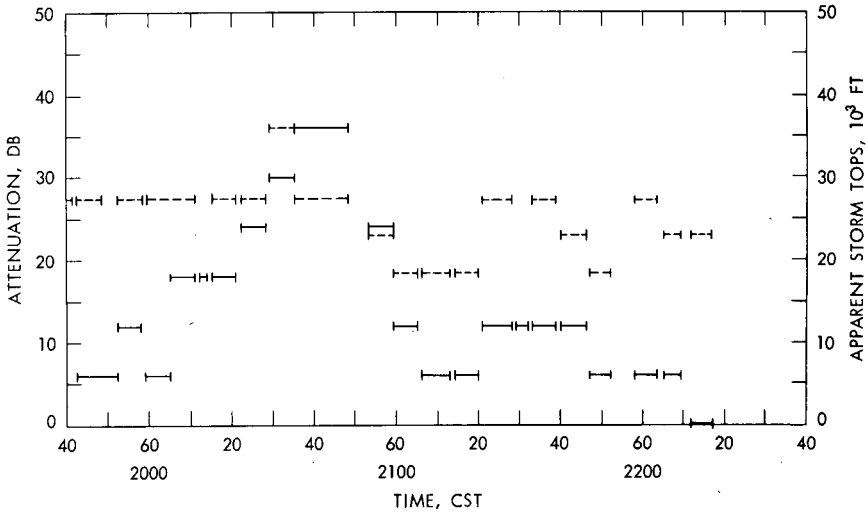

Fig. 22—Time cross section of radar-echo intensity (solid lines) and radar storm tops (dashed lines) over station 6 for storm of May 9, 1964.

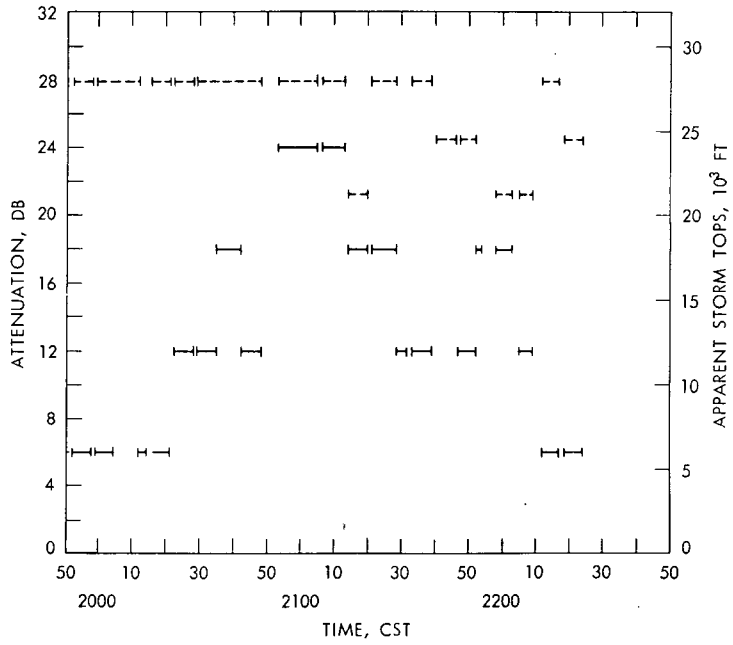

Fig. 23—Time cross section of radar-echo intensity (solid lines) and radar storm tops (dashed lines) over station 7 for storm of May 9, 1964.

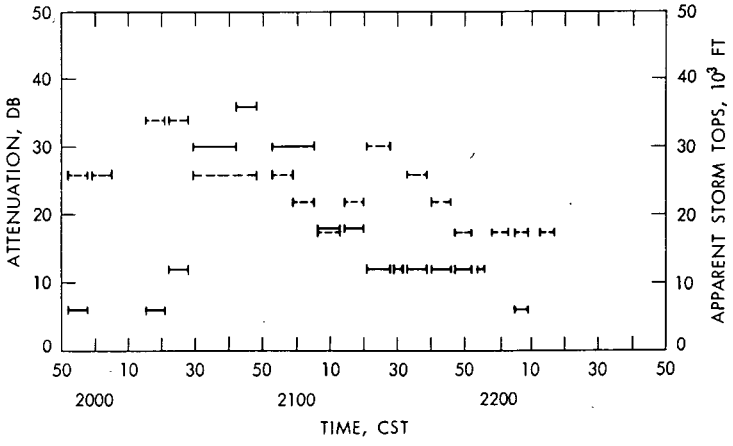

Fig. 24—Time cross section of radar-echo intensity (solid lines) and radar storm tops (dashed lines) over station 8 for storm of May 9, 1964.

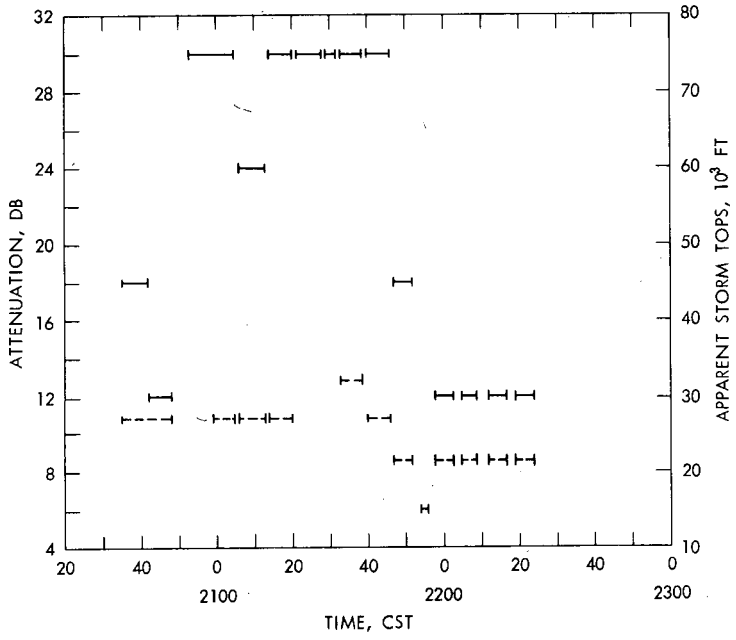

Fig. 25—Time cross section of radar-echo intensity (solid lines) and radar storm tops (dashed lines) over station 9 for storm of May 9, 1964.

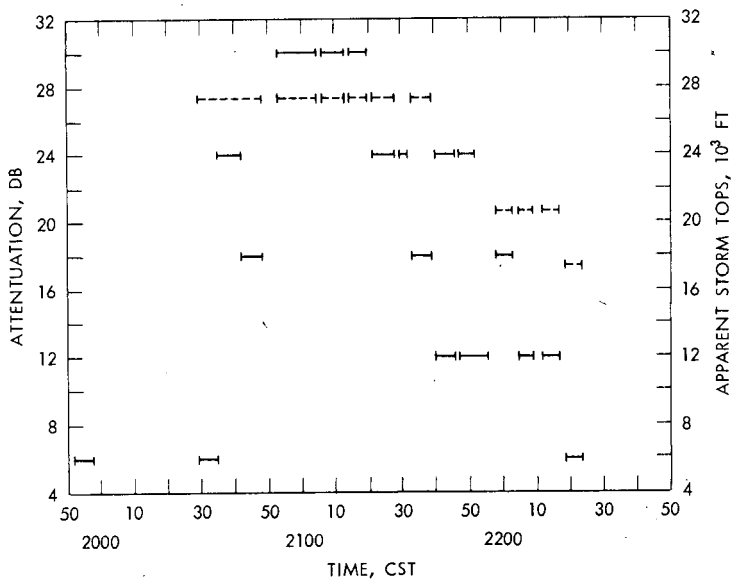

Fig. 26—Time cross section of radar-echo intensity (solid lines) and radar storm tops (dashed lines) over station 10 for storm of May 9, 1964.

of station 8, which had an initial strong rainfall rate of 1.32 in./hr, the initial rainfall rates were moderate, generally less than 0.5 in./hr. At all the stations the rainfall rates increased after the initial burst. At stations 5, 6, and 10, the initial samples had the maximum beta concentration, whereas at station 8 the concentration decreased from an initial secondary maximum then increased to a maximum. The beta-concentration profiles at stations 7 and 9 were similar in that the beta activity at these stations increased to a maximum in the second samples taken at these stations and then decreased to a minimum. Aside from the general inverse relation between rainfall rate and beta concentration, three of the six stations (stations 6, 8, and 9) showed such an inverse relation at the time of later maximums or minimums in beta concentration, but two of the three cases (stations 8 and 9) are not well defined.

The ratios of particulate to dissolved beta activity were maximums in the initial samples at stations 6 and 10. These values were 1.23 and 1.33, respectively. The ratios at the other stations were quite low, around 0.5. Table 1 shows that, with few notable exceptions, the particulate beta concentration is considerably low at most stations, with the average of all samples for this storm being 82.3 pc/liter and the ratio of particulate to dissolved beta activity being 0.85.

The major cells that crossed the network are shown in time sequence in Fig. 27. The area of maximum intensity, 48 db, passed between three to eight miles south of station 8 and at this time had radar tops at about 52,000 ft. This shows stratospheric penetration of more than 10,000 ft since the tropopause height was around 41,000 ft (see Table 2). The time cross sections of radar tops show that there was no tropopause penetration over the collectors.

By a relation of the data of Fig. 27 to the rainfall collections, it is seen that at station 6 the beta concentration was at a minimum as the echo-intensity maximum crossed the station. This was the only station that appeared to be crossed by an intensity center in the storm, and the corresponding beta concentration was the minimum for that station and for that cell. This area of the storm was dissipating as it progressed eastward over station 7, and the rainfall-rate maximum had decreased but was still of a relatively strong intensity. Instead of a minimum in the beta concentration, there was a maximum associated with the rainfall-rate maximum.

The cell structure that crossed station 8 was rather complex. Figure 27 shows that as the intense echoes were approaching from the west development was occurring east of and over the station. Figure 18 shows that the beta concentration was not at a minimum when the rainfall rate was at a maximum, but that the minimum concentration occurred when the maximum echo intensity was in its closest proximity to station 8 and the rainfall rate was still strong. The absolute maxi-

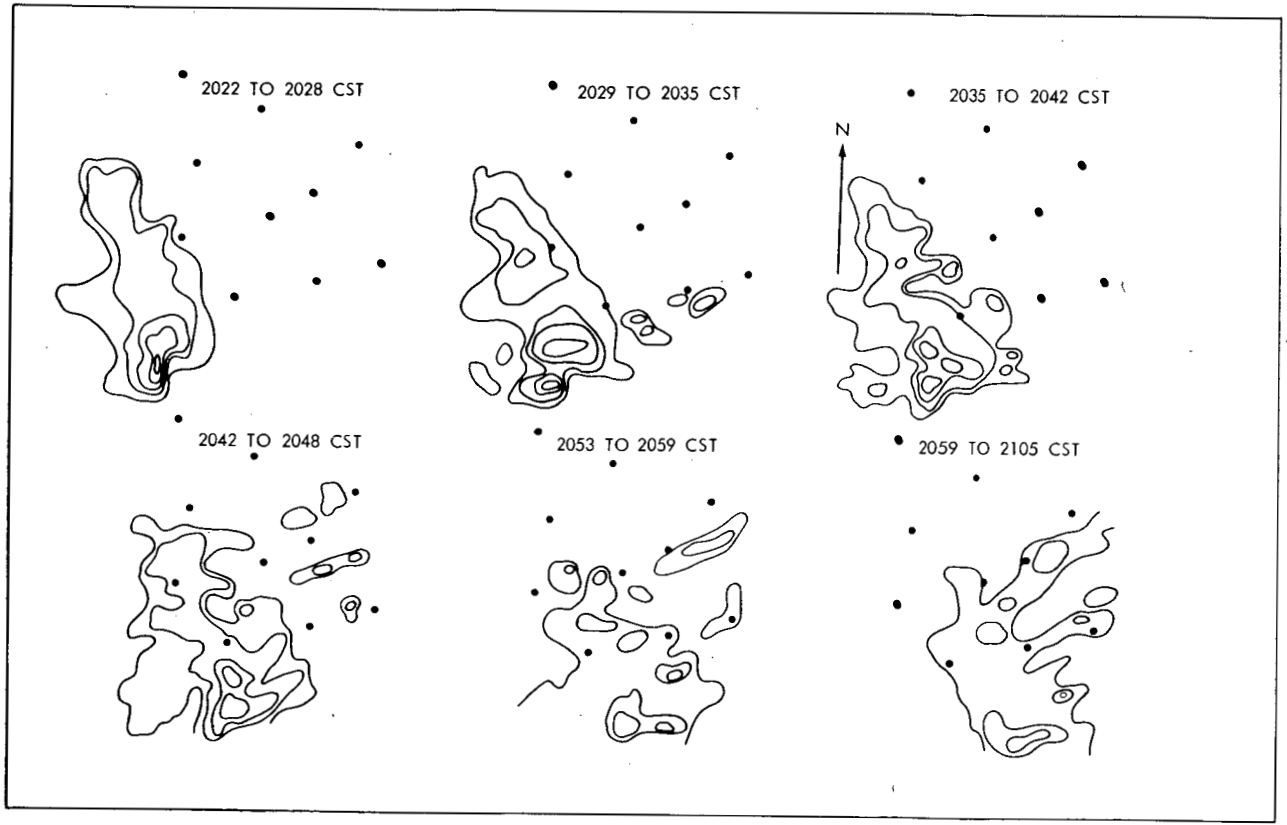
2022 TO 2028 CST
2029 TO 2035 CST
2035 TO 2042 CST
N
2042 TO 2048 CST
2053 TO 2059 CST
2059 TO 2105 CST

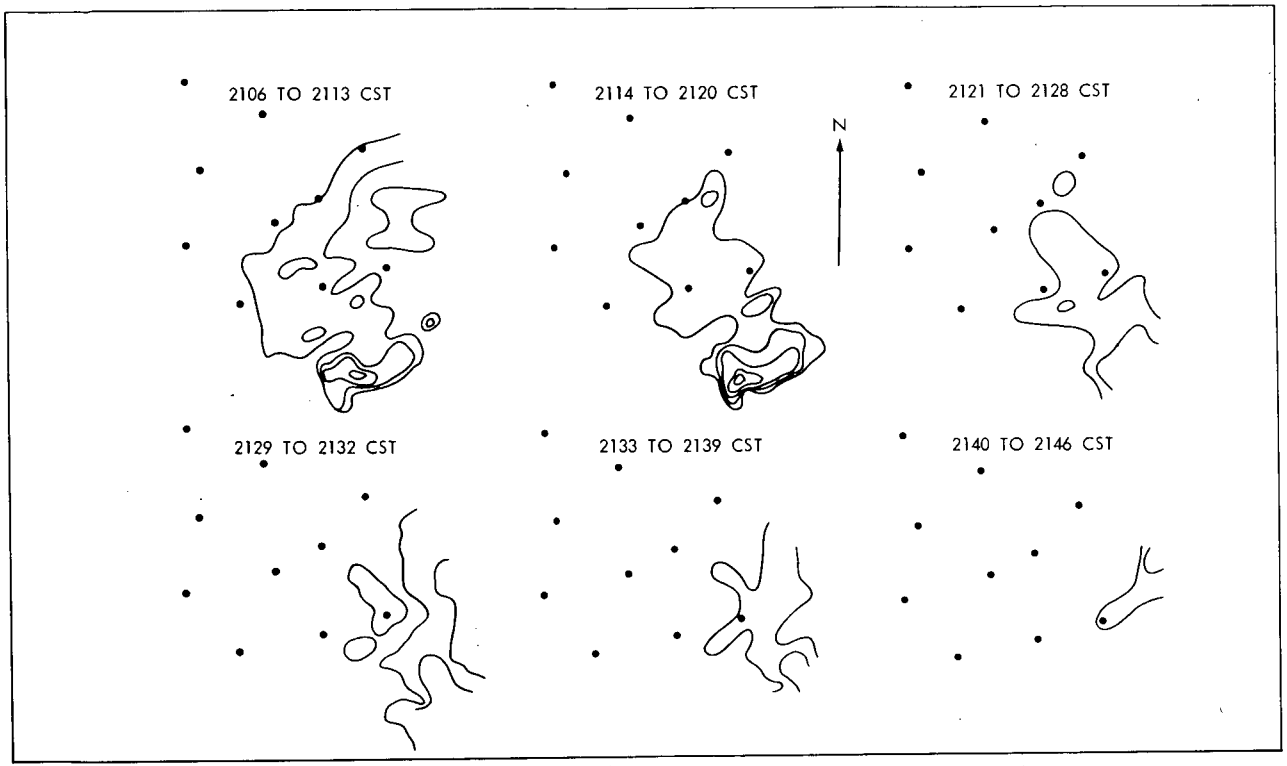

Fig. 27—Time sequence of radar-echo intensities for storm of May 9, 1964. Outer contours are 30 db increasing inward in 6-db intervals. See Fig. 1 for station numbers.

mum in the beta concentration was found in the sample which was taken just after the echo-intensity maximum at the station had passed and the cell was dissipating. The final collection was from weak peripheral rainfall.

A similar occurrence regarding cell dissipation existed between stations 8 and 9 as had occurred between stations 6 and 7, i.e., a direct relation between the beta concentration and the rainfall rate. Minor development occurred near station 9, resulting in an inverse relation between rainfall rate and beta concentration as shown in Fig. 19.

At station 10 the initial rainfall rate was moderate, and the absolute maximum of beta concentration at this station was found in the first sample taken. From Fig. 27 it can be seen that general stratification took place in the vicinity of station 10 after about 2121 CST. It was after this time that, as seen in Fig. 20, the rainfall-rate maximum occurred, accompanied by a peak in the beta concentration. A similar occurrence took place at station 5 (see Fig. 15) during cell dissipation in that area.

ANALYSIS OF STORM OF MAY 10

The synoptic situation had changed little from the previous day. The incipient wave on the quasi-stationary front over the Texas–New Mexico border (Fig. 13) had developed. Figure 28 shows the related cyclone better developed. Winds over the network were southeasterly at the surface veering to southwesterly up to the tropopause. Convective activity occurred over the state during the morning and after-

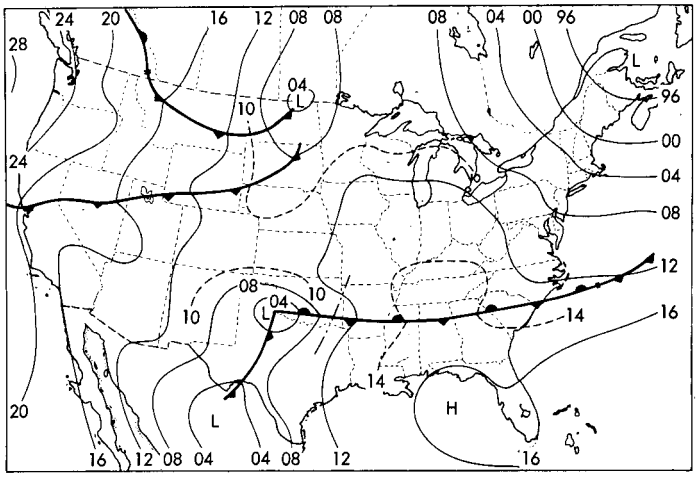

Fig. 28—Surface synoptic chart for 0000Z of May 11, 1964.

noon, with small weak cells moving through the network. A line of storms developed about 30 miles east of Norman and moved eastward.

Around 1545 CST convective activity west of the network increased. By 1600 CST a definite line was taking shape, and at 1700 CST it was about 20 nautical miles across, oriented southwest–northeast with range limits at 250 degrees azimuth and 100 nautical miles range and 300 degrees azimuth and 40 nautical miles range, respectively. The line was moving eastward at about 30 knots with the southern end passing through the network.

The time sequence of echo intensities for the storm is given in Fig. 29. It can be seen as the eastern-moving storm entered the network there were two large major cells that were developing. The northernmost cell moved out of the network before dissipating, but the southernmost cell was already decreasing in intensity before leaving the network. There was minor cell development behind the squall line.

During the period 1801–1807 CST, the radar top of the northern cell was at 46,000 ft. Table 2 shows the tropopause at 43,296 ft; thus this cell had penetrated into the stratosphere. The southern cell had radar tops of 44,000 ft and was intensifying as it approached station 8. The time cross sections of radar tops over the stations (Figs. 30 to 33) show storm tops near tropopause height over collectors 1, 4, 8, and 9. Figs. 34 to 37 are the rainfall-sample cross sections for the 10 collectors, all of which obtained multiple samples. The beta-concentration profiles for all the collectors except those at station 1 show a decrease in total beta concentration from the initial to the second sample with a corresponding increase in rainfall rate. At station 1 the rainfall rate is 2.16 in. per hour for the first two samples with the total beta concentration increasing from the first sample to the second.

The beta concentration was at a maximum in the initial sample at four stations (2, 3, 4, and 9) and at a maximum in the final sample at four stations (5, 6, 7, and 8). Of these eight stations, 3, 4, 5, 7, and 9 have their minimum beta concentrations associated with their maximum rainfall rates. The rainfall-rate maximums at six of the stations (1, 2, 3, 5, 6, and 8) correspond to maximums in ratios of particulate to dissolved beta activity. Generally, the ratios of the initial samples were low; these low values possibly were due to little dust blowing as a result of the previous day's rains.

The time sequence of radar-intensity centers (see Fig. 29) shows that one of the centers crossed the upper two-thirds of the network whereas the other crossed the most southern row of stations. The collection at station 1 was multicellular with the rainfall-rate maximum being from the cell (see Fig. 29) whose center passed north of the collection network. The collections at this station from the cell that crossed the network show that the rainfall rate from that portion of the cell was weak, with radar storm tops around 34,000 ft. The area

(Text continues on page 561.)

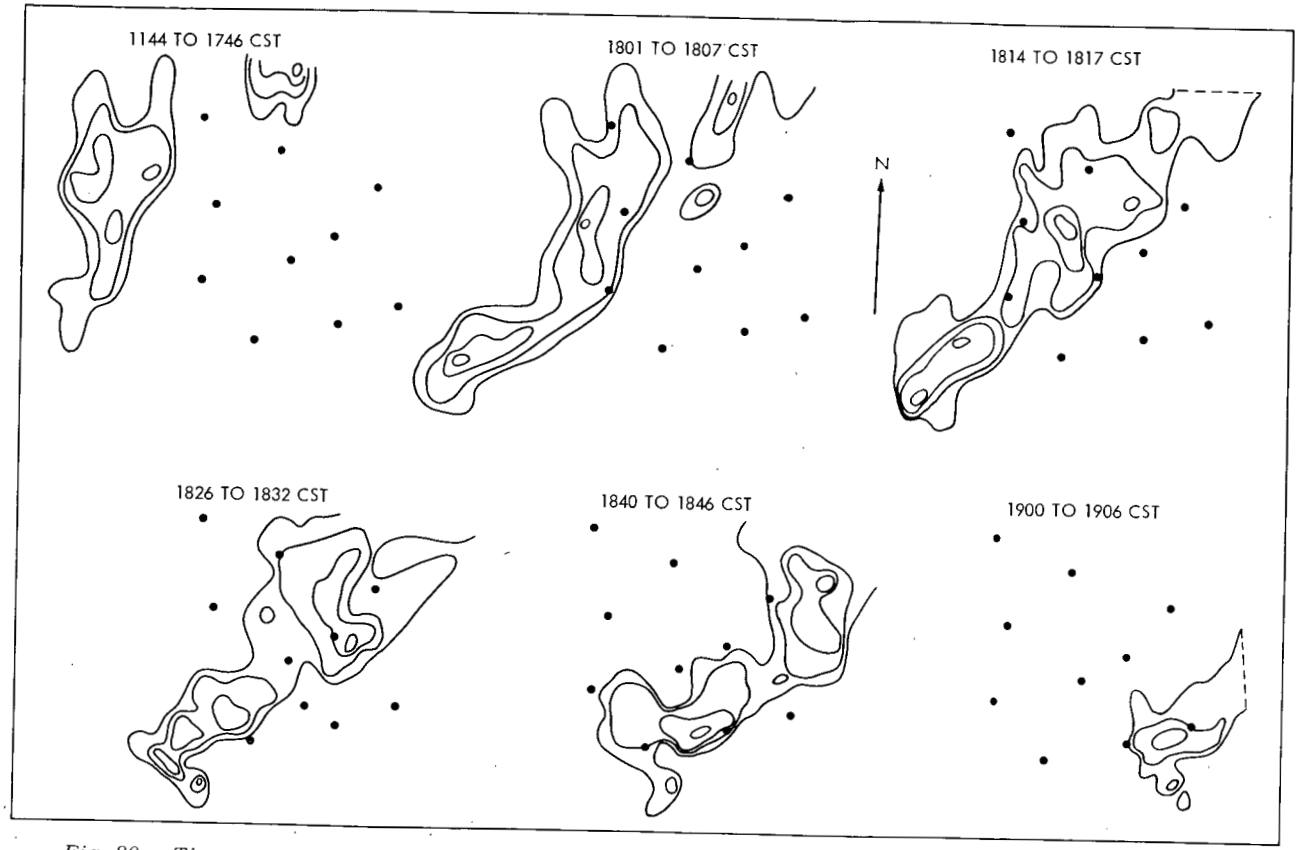

Fig. 29—Time sequence of radar-echo intensities for storm of May 10, 1964. Outer contours are 30 db increasing inward in 6-db intervals. See Fig. 1 for station numbers.

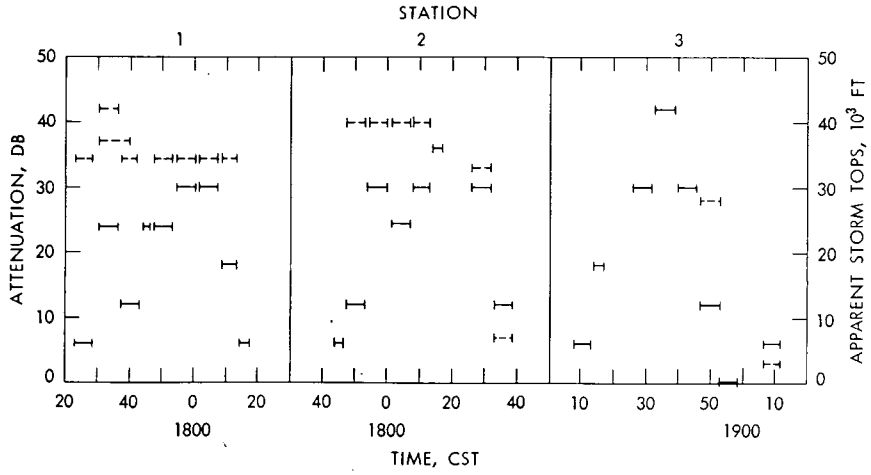

Fig. 30—Time cross sections of radar-echo intensity (solid lines) and radar storm tops (dashed lines) over stations 1 to 3 for storm of May 10, 1964.

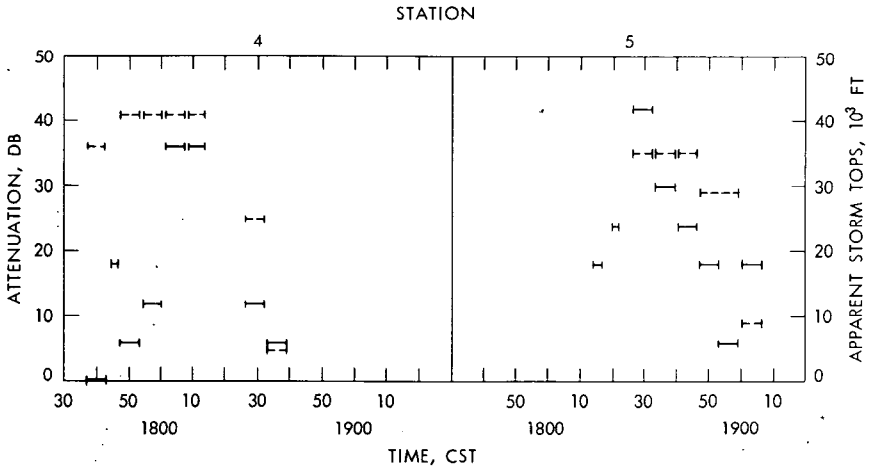

Fig. 31—Time cross sections of radar-echo intensity (solid lines) and radar storm tops (dashed lines) over stations 4 and 5 for storm of May 10, 1964.

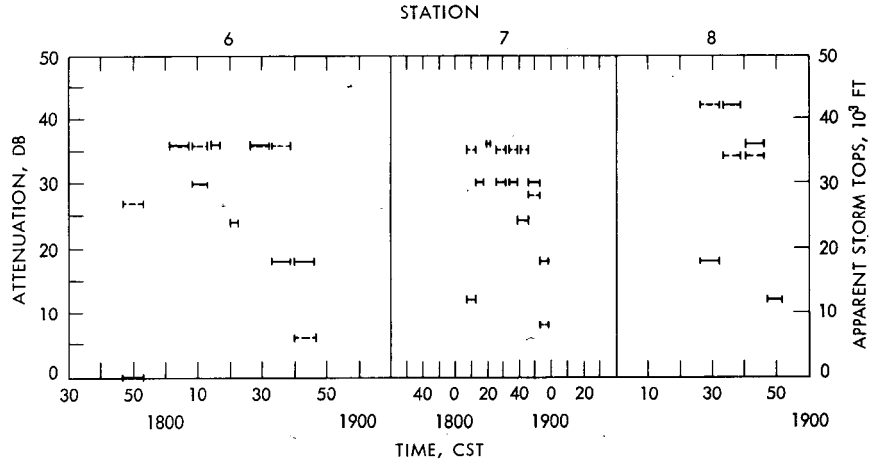

Fig. 32—Time cross sections of radar-echo intensity (solid lines) and radar storm tops (dashed lines) over stations 6 to 8 for storm of May 10, 1964.

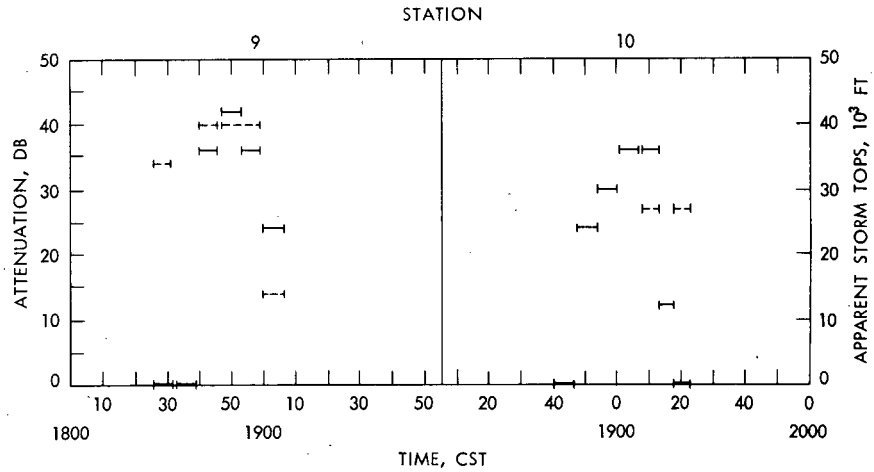

Fig. 33—Time cross sections of radar-echo intensity (solid lines) and radar storm tops (dashed lines) over stations 9 and 10 for storm of May 10, 1964.

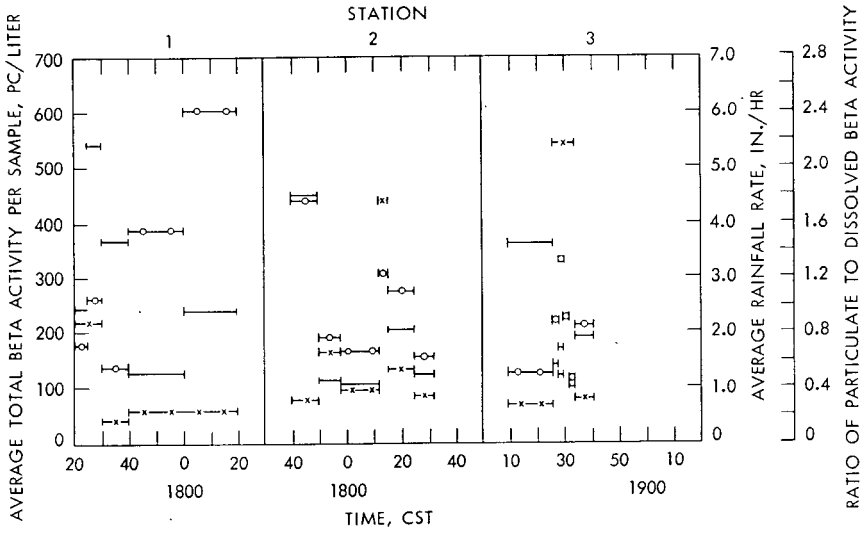

Fig. 34—Time cross sections of total beta concentration (solid lines), rainfall rate (lines with x's), and ratios of particulate to dissolved beta activity (lines with zeros) for stations 1 to 3 for storm of May 10, 1964.

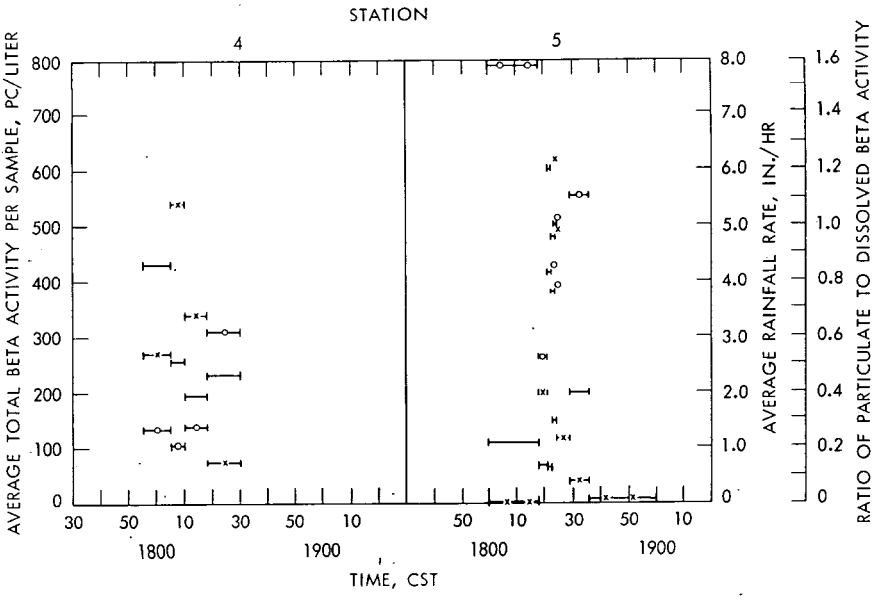

Fig. 35—Time cross sections of total beta concentration (solid lines), rainfall rate (lines with x's), and ratios of particulate to dissolved beta activity (lines with zeros) for stations 4 and 5 for storm of May 10, 1964.

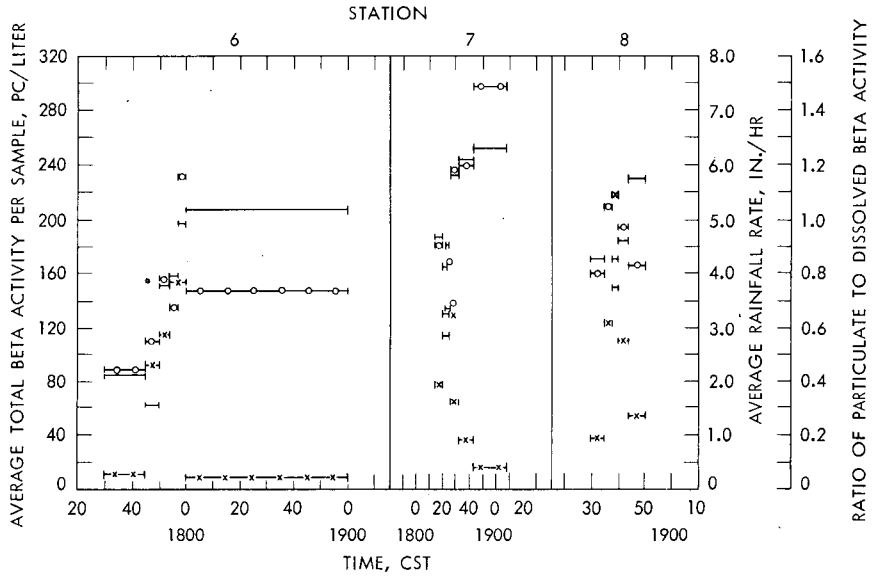

Fig. 36—Time cross sections of total beta concentration (solid lines), rainfall rate (lines with x's), and ratios of particulate to dissolved beta activity (lines with zeros) for stations 6 to 8 for storm of May 10, 1964.

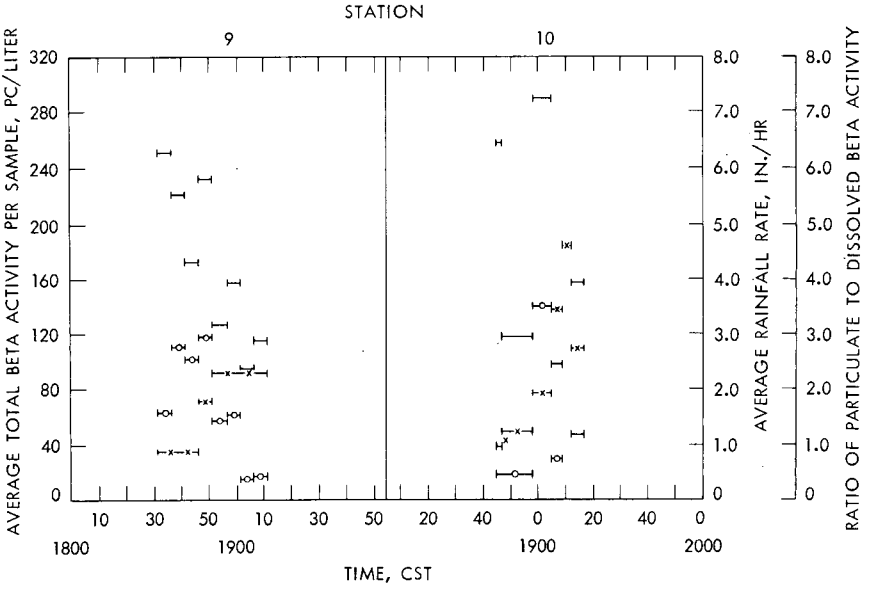

Fig. 37—Time cross sections of total beta concentration (solid lines), rainfall rate (lines with x's), and ratios of particulate to dissolved beta activity (lines with zeros) for stations 9 and 10 for storm of May 10, 1964.

that crossed station 6 was becoming less intense, and, even though the storm itself was not dissipating, the total-beta concentration and rainfall-rate profiles show the characteristic of a beta-concentration maximum and a rainfall-rate maximum occurring together, similar to those profiles of dissipating cells of the previous day. The intensity center crossed station 4, and, even though it was decreasing, the inverse relation of beta-concentration minimum and rainfall-rate maximum was in evidence. In a comparison of the beta at stations 1, 4, and 6 during the times of rainfall-rate maximums, Figs. 34 to 36 show that the values at the three stations are quite close to each other despite the differing relations of the beta concentrations to the rainfall-rate maximums at stations 4 and 6.

The cell intensified again after it had passed station 4. The orientation of the leading edge of the storm was such that precipitation began almost concurrently at stations 5 and 7. The resulting rainfall-sample cross sections and echo-intensity and radar-storm-top profiles in Figs. 31, 32, 35, and 36 are quite similar. The intensity center crossed station 5, where the maximum in rainfall rate was greater and the beta-concentration minimum was less than values at station 7. The radar storm tops over both stations were at 35,000 ft. Thus at this time the cell was confined to the troposphere, although it had maximized before crossing the stations. That the more intense area crossed station 5 is reflected in the rainfall-rate cross section. The rainfall rate at this station was almost twice that of station 7.

The northern portion of this cell crossed station 3, and, even though the rainfall rate was inversely related to the total beta concentration, Fig. 34 shows that the intense rainfall persisted for 8 min, during which time four samples were collected. These samples were possibly related to storm development that took place south of station 3, but the rainfall-sample profiles of this station were similar to those at stations 5 and 7 for this cell.

The section of the cell which crossed station 2 was north of the echo-intensity maximum; Fig. 34 indicates the minimum beta concentration not associated with rainfall maximum. At this time the entire cell was intensifying and the structure in the area of station 2 was complex in that the echo-intensity and rainfall-rate maximums coincided with an increase in beta concentration from the previous sample, with the maximum in the beta concentration occurring with a sharp decline in the rainfall rate.

The cell that crossed the southern portion of the network had attained maximum radar tops of 44,000 ft before entering the network, which decreased and then intensified again over the network. The cell moved from the network still with its maximum intensity of 48 db. Figure 29 shows that the maximum echo intensity passed two miles north of station 8, directly over stations 9 and 10. The resulting

rainfall-sample cross sections are similar in that at these stations the beta-concentration minimums were not coincident with the rainfall-rate maximums. At station 9 the cell crossed during a minimum in the maximum intensity. Figure 37 shows that with the relatively moderate rainfall at that station, four samples were collected during the sustained 20-min maximum. These four samples indicate a beta-concentration profile similar to that shown in Fig. 34 for station 3 during its stronger sustained maximum. At both stations the concentration associated with the minimums for the stations, along with the ratio of particulate to dissolved beta activity, was at a peak in the second of the four samples.

RESULTS

Comparison of Tables 1 and 3 with the radiochemical analysis results obtained[1] during the storms in the spring of 1963 show that the beta concentration in the precipitation samples had decreased by a power of 10. Such a decrease is expected because of decay and fallout in the interim, although we are not sure that the degree of decrease is consistent with other observations. The results discussed here of storms of different sizes and intensities show that the ones of April 17 and April 23 had the higher values of average total-beta concentration, with the highest concentrations occurring at the stations that collected peripheral rainfall. In the storms of May 9 and May 10, which were larger storms and from which more samples per station were obtained, the maximum concentration occurred at the station that had the least total rainfall.

Of the 18 rainfall-sample cross sections presented, 15 had a decrease in beta concentration from the first to the second sample with 14 of these inversely related to the rainfall rate. Only six of the sample cross sections had the ratios of particulate to dissolved beta activity of the initial and second samples in phase and decreasing with those of the total beta concentration. The decreases in the ratios corresponded to decreases in particulate beta concentrations. In 12 of the 18 cross sections, there was a peak in the ratios associated with the rainfall-rate maximums.

The beta concentration and the rainfall-rate profiles fit the classifications as discussed by Huff.[2] Of the 18 beta-concentration profiles, eight had beta maximums associated with the leading edge of the storm, with five having a secondary maximum associated with the rainfall-rate maximum. There were two profiles that had their maximum beta concentrations near the rainfall-rate maximums with the secondary maximum associated with the leading edge of the storm. In five profiles the beta concentration decreased from the initial sample to a minimum, which in three of the cases was associated with

Table 3—AVERAGE BETA ACTIVITY AND TOTAL RAINFALL FOR EACH STATION

Date	Station	Average beta activity, pc/liter		Total rainfall, in.
April 17	1	347.9		0.36
			Average	0.36
April 23	2	1160.0		0.06
	5	512.0		0.20
	6	351.0		0.21
	7	935.0		0.26
	8	461.7		0.64
	9	341.0		0.35
			Average	0.29
May 9	1	259.8		0.30
	2	600.0		0.05
	3			0.67
	4	396.7		0.56
	5	118.0		0.95
	6	142.6		1.68
	7	183.4		0.78
	8	176.9		1.98
	9	81.0		1.82
	10	255.8		1.26
			Average	1.01
May 10	1	293.3		0.96
	2	261.5		1.54
	3	293.5		1.17
	4	278.8		1.80
	5	119.3		0.84
	6	153.8		1.33
	7	210.8		1.04
	8	169.7		0.78
	9	173.5		1.45
	10	184.7		1.38
			Average	1.23

the maximum rainfall rate, and then increased to a maximum in the rainfall from the rear of the storm. In four of these five cases, the maximums occurred in weak peripheral rainfall. The remaining three profiles increased to a maximum of beta concentration associated with the rainfall-rate maximum at the stations.

The effects of light peripheral rainfall are shown in the smoothed total-rainfall and average-beta-concentration patterns for April 23 and May 9, Figs. 12 and 38, respectively. The patterns for May 10 show that the values of total rainfall and average beta concentration were

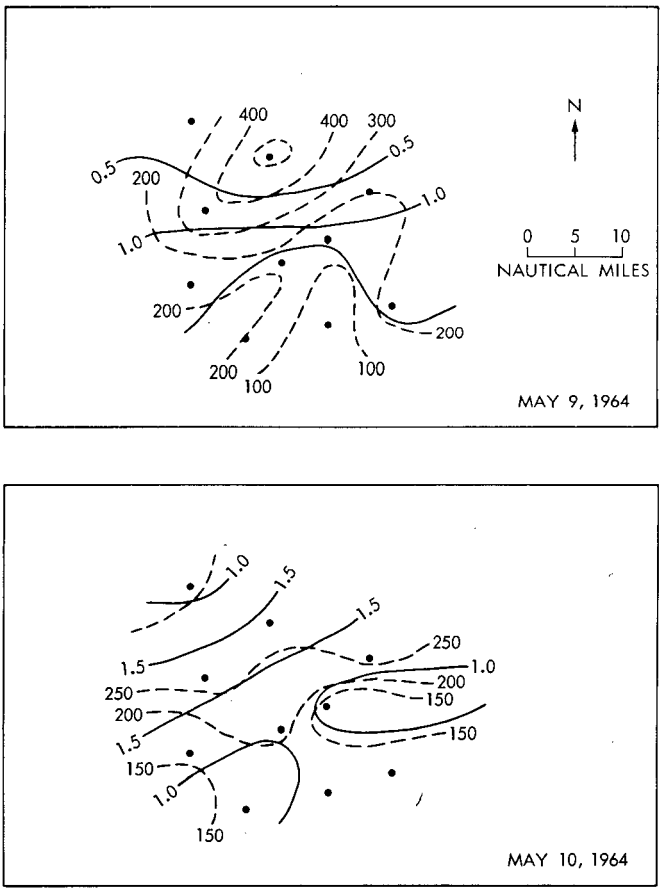

Fig. 38—Precipitation patterns (solid lines) and total-beta-concentration patterns (dashed lines) for May 9 and May 10, 1964.

greater over the northern two-thirds portion of the network crossed by the larger of the two cells.

The relation of the beta-concentration cross sections to position with respect to the intensity centers of the cells, the relation between rainfall rates and total beta concentration appears to vary, not only with the stage of development of a storm but with the changes that occur while the storm is in a certain stage, in the mature stage in particular. The profiles obtained from these few cases indicate that the minimum beta concentration occurs with the rainfall-rate maximum for cells that do not penetrate into the stratosphere (station 6 in the storm of May 9 and stations 5 and 7 in the storm of May 10). The cell that penetrated the stratosphere over station 8 in the storm of April 23

had a similar profile but had greater beta-concentration values. For dissipating cells, the beta-activity maximums occur with the rainfall-rate maximums (stations 5, 7, and 10 in the storm of May 9 and stations 9 and 10 in the storm of May 10) along with a peak in the ratios of particulate to dissolved beta activity, possibly because of entrainment aloft on the back sides of the storms. The profiles of beta concentration collected at stations to the right and left of intensity centers are similar to those at the center for both the mature cells and the dissipating cells, but, because the rainfall rates are less intense, the evaporation effect is more pronounced in the initial and the final collections.

REFERENCES

1. S. J. Hall and E. H. Klehr, *Severe Convective Storms and the Stratospheric Scavenging of Radioactive Particles,* First Progress Report (Contract Number AT-(40-1)-3083), University of Oklahoma, 1963.
2. R. A. Huff, *Study of Rainout of Radioactivity in Illinois,* Second Progress Report (Contract Number AT(11-1)-1199), Illinois State Water Survey, 1964.

AIR CLEANSING BY CONVECTIVE STORMS

DONALD F. GATZ and A. NELSON DINGLE
The University of Michigan,
Ann Arbor, Michigan

ABSTRACT

Data relating to rain cleansing of the atmosphere have been gathered throughout five convective rain-producing weather systems and analyzed with respect to the concentrations of radioactivity in sequential samples of rain. For some of the rains, analyses of the pollen content of sequential samples were also made. A consistent pattern of temporal variation of concentration of both contaminants was observed in the three rains of highest rainfall rate. This pattern, a rapid decrease of concentration with time during the first portions of the rain, was absent in the two rains of lowest rainfall rate. The fact that rapid decreases in concentration occurred simultaneously for both radioactivity and pollens is taken as evidence that both contaminants were removed from the same air. Since pollens have their source at the earth's surface, it is concluded that both radioactivity and pollens entered the convective system from low levels via the convective updraft. It seems possible that the absence of the rapid temporal decrease of concentration in the rains of low intensity may be due to the lack of a persistent, organized updraft in these systems.

INTRODUCTION

Radiochemical analyses of samples of rainwater collected at fixed ground stations from rain systems of all types have shown substantial time variation of the concentration of radioactive substances in the rain. These variations are present when one rainfall is compared with another (e.g., by Walton, Fisher, and Krey[1]) as well as from sample to sample

within a single rainfall. Variations within rains have been reported by others;[2,3] variations also occurred in the five rains discussed in this paper. Because the variability within a system is pertinent to the understanding of that between systems, this paper is especially concerned with the study of the variations within individual rainfalls. The principal focus concerns variations within convective rains.

OBSERVATIONAL PROGRAM

A basic premise of our research has been that any information bearing on rain scavenging, whether of radioactive or of other material, is pertinent to the problem and probably useful in its solution. Therefore we have paid specific attention to the rain scavenging of airborne pollens whose source, distribution, and physical properties can be defined very well.

Sampling Pans

Rain was collected in two large pans, which together total 5.2 m^2 in area. The sampling pans were located on the flat roof of the structure shown in Fig. 1, in which sample bottling operations were carried out. The pans were tilted slightly to provide drainage. The rainwater was conveyed from the pans to the bottling station directly below by flexible plastic tubing. It is emphasized that the sampling operations were carried out at a single manned station.

Sampling Procedure

Before each rain the pans were scrubbed to remove all dry deposition. This technique was found sufficient to remove nearly all the radioactive fallout from the pans, and it can be assumed to have removed pollen grains. For rains in which both radionuclides and pollens were determined, the usual procedure was to take alternate samples for radiochemical and pollen analysis, at least during the early and middle parts of each rain. In most cases, 1-gal samples were taken for radiochemical analysis and 1-qt samples were taken for pollen analysis. When radionuclides alone were to be determined, successive 1-gal samples were taken.

Complementary Data

In addition to data obtained from the radiochemical analyses of rain samples, supporting data on the nature of the precipitation system that produced the rain were taken at the collection station and acquired elsewhere. These additional data include conventional synoptic weather

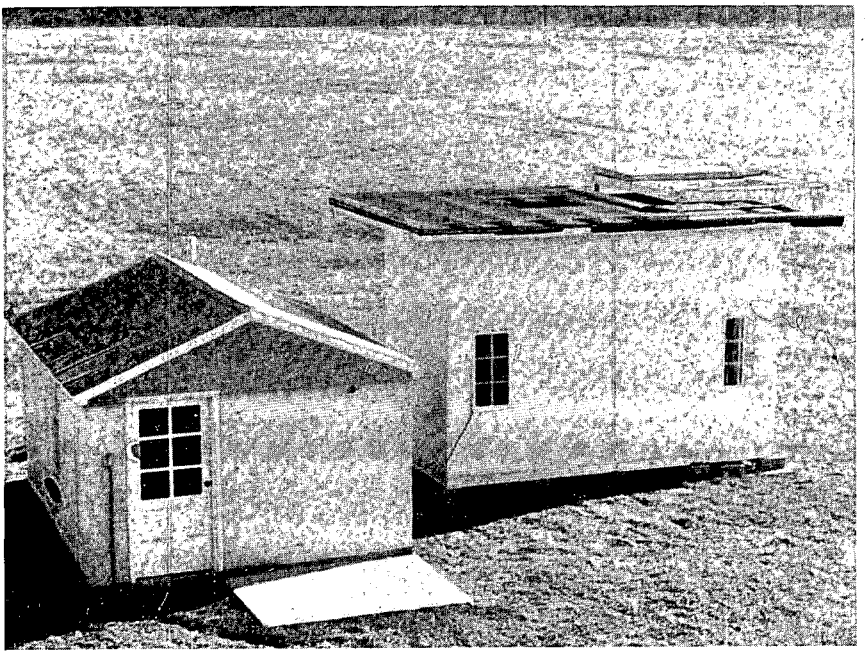

Fig. 1—View showing location of rain-sampling pans.

data and radar observations of movement of precipitation areas and height of echo tops.

Rainfall-rate data were obtained by a tipping-bucket recording rain gauge. This instrument records an event mark on a strip-chart recorder after every 0.01 in. of rain. The data were used to provide the detailed time record of rainfall rate. The variations observed in these records indicate the basic character of the rain and help to resolve the fine structure of the rain system.

Maximum heights of radar echoes were obtained from the hourly reports of the operator of the WSR-57 radar at the U. S. Weather Bureau Station at the Detroit Metropolitan Airport, which is located about 8 nautical miles east of the sampling station. It was found that the Weather Bureau radar observations were best suited to a qualitative classification of the precipitation system (i.e., squall line, stratiform area, etc.); this information has been incorporated into the description of each rain.

SAMPLE ANALYSES

Radiochemical Analysis

The radiochemical analysis procedure consisted of the following steps: The sample was pumped through a graduated series of filters to

remove insoluble particles. The filtrate was reduced by evaporation and the residue ultimately transferred to a stainless-steel planchet and counted for radioactivity. The filters were dried, placed into identical planchets, and similarly counted. Early in the program the samples were counted only for gross beta activity by using a low-background (1 count/min) beta counter. After the resumption of atmospheric testing by the U.S.S.R. in September 1961, radioactivity levels rose sufficiently to permit determination of individual radionuclides by gamma spectrometry.

In each rainwater sample fission-product radionuclides were determined in three groups: (1) ^{141}Ce, $^{144}Ce-^{144}Pr$; (2) ^{103}Ru, $^{106}Ru-^{106}Rh$; and (3) $^{95}Zr-^{95}Nb$. In addition, $^{140}Ba-^{140}La$ were determined when fallout was fresh. The necessity for grouping the radionuclides as indicated arises from the method of analysis.

In the investigation of the mechanisms whereby fission products are brought to earth by rain, the changes of radioactivity levels with time provide the best clues. Thus the precision of the analysis procedure is more important than its accuracy. The precision of sample preparation and counting is estimated to be approximately 15 to 20%. This is entirely acceptable in view of the magnitude of observed sample-to-sample variations.

It will be seen later that time variations of the several radionuclide groups are largely parallel. Nevertheless, it was felt that random errors would be minimized by computing the total of the measured radionuclides. Therefore, unless specified to the contrary, only the variations of the total are considered in the discussion. For convenience, the concentration of total measured radionuclides is sometimes referred to as the "concentration."

Pollen Analysis*

Insoluble material was separated from each sample by centrifugation. A known amount of a readily identifiable tracer pollen, which would not normally be found in rain and a small amount of glycerine jelly were thoroughly mixed with the insoluble residue. Several microscope slides were prepared from each sample. Each slide was made by placing a single drop of the jellied mixture on a slide and covering it with a glass cover slip. The number of grains of each pollen species of interest and the tracer pollen were counted under a microscope for one or more slides from each sample. Under the assumption that equal fractions of the total number of tracer and natural pollens were present on the slides counted, it was possible to compute the total number of

*An alternate procedure to the one described here was used for the rain of Sept. 1, 1961, and has been described by Gatz and Dingle.[4]

pollens of each species in the whole sample. These figures were converted to concentration units by dividing by the volume of the sample. A standard deviation of less than 10% is estimated for most samples.

RESULTS

Of the rain-producing events that are discussed, a broad categorization into two types appears to be reasonable. We shall therefore consider three of these events as having involved relatively well-organized convective systems in contrast to the relatively poorly organized, or diffuse, convective activity of the other two. The descriptive characteristics and quantitative criteria which pertain to each category and which indicate the distinctions between them are presented in detail and are summarized in Table 1.

Table 1 — SUMMARY OF CHARACTERISTICS THAT TEND TO DISTINGUISH WELL-ORGANIZED CONVECTIVE RAIN-PRODUCING SYSTEMS FROM DIFFUSE ONES

Characteristic	Well organized	Diffuse
Total rainfall	>15 mm	<15 mm
Duration	1 hr or less	2 hr or more
Overall average intensity	15 mm/hr or higher	7.5 mm/hr or less
High intensity portions	Considerable above 25 mm/hr	Little or none above 25 mm/hr
Electric activity	Usual	Not usual
Cleansing effect	Prominent at beginning	Obscured

Well-organized Systems

Three of the observed convective rain-producing events are considered to fall into this category. In broad terms these three events are distinguished by a rainfall yield of 15 mm or more within a period of 1 hr or less. The events that fit these criteria are those of Sept. 1 and 23, 1961, and June 25, 1962.

Synoptic Conditions It is appropriate to examine the weather maps to note superficial indications of similarity and difference among the three events discussed. U. S. Weather Bureau Daily Series analyses for the nearest appropriate synoptic times for the 500-mb and the surface levels are shown in Fig. 2.

The rain of September 1 was associated with a nonfrontal convergence zone that had migrated northward from the Gulf of Mexico; the other two rains were associated with cold frontal passages.

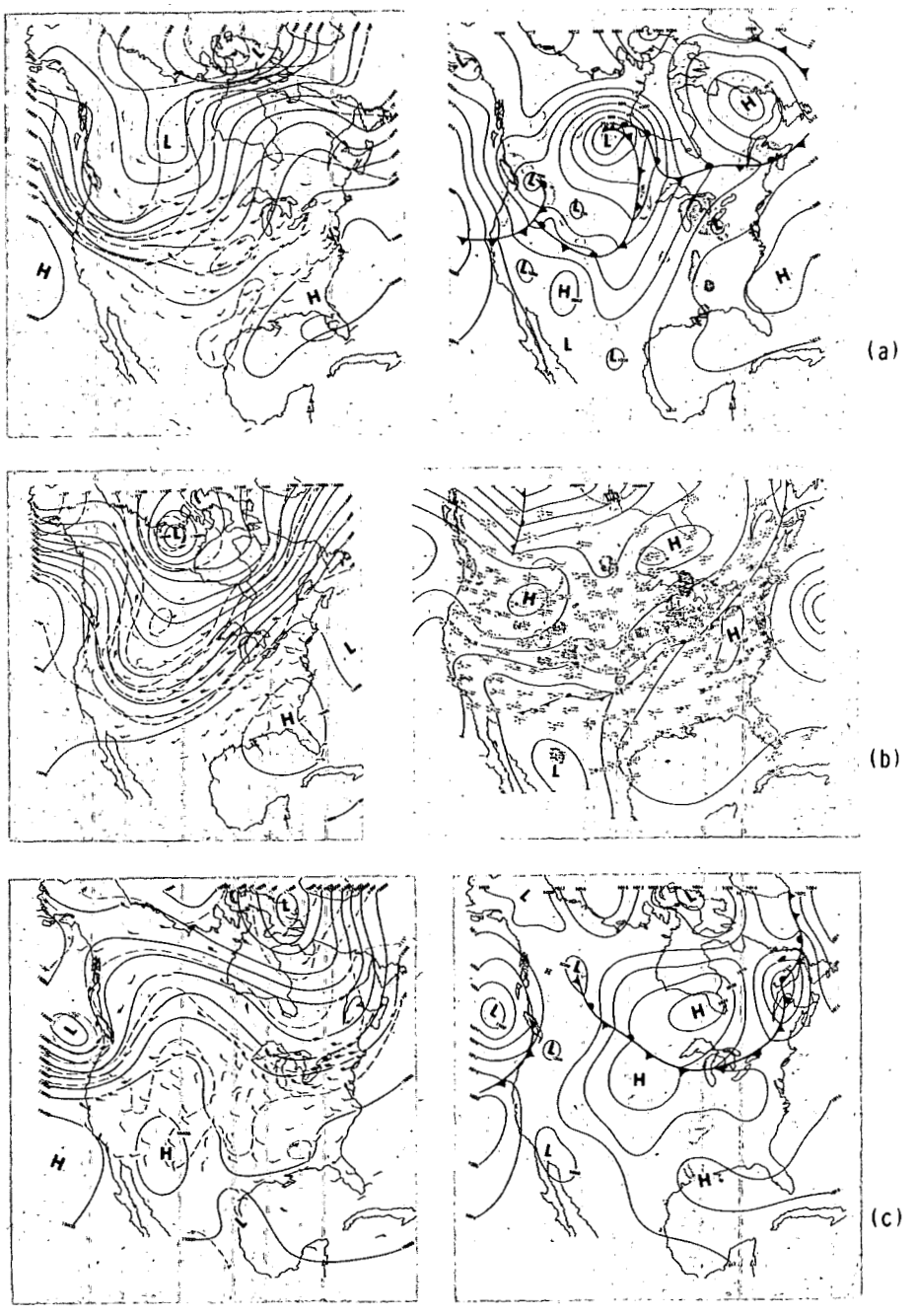

Fig. 2—Synoptic weather data for well-organized systems. (a) Data for rain of Sept. 1, 1961; 500-mb data at 1900 EST; surface data at 1300 EST. (b) Data for rain of Sept. 23, 1961; 500-mb data at 1900 EST; surface data at 0100 EST on September 24; (c) Data for rain of June 25, 1962; 500-mb data at 1900 EST; surface data at 1300 EST.

In the case of the June 25 rain, the flux of Gulf air into the system over southern Michigan appeared to be very poor, that of September 1 was excellent throughout the lower half of the atmosphere, and that of September 23 was much less vigorous. This last case was dependent mainly on a very weak divergent flow from the anticyclone just west of the Appalachian chain.

Rainfall Intensity The rainfall-intensity graphs were formed by detailed reduction of the tipping-bucket rain-gauge record. The results are shown in Figs. 3 to 5. Here the September 1 rain is distinguished from the other two in the persistence of rainfall rates of 20 mm/hr and above. The two initial showers, which averaged about 70 and 60 mm/hr, respectively, lasted for about 10 min each. This feature is quite similar to the 12-min showers of 60 to 70 mm/hr average intensity which initiated both the September 23 rain and the June 25 rain. As a result of the sustained moderate intensity of the September 1 rainfall, it yielded a total of 1.86 in., whereas the yield of the September 23 rain was 0.70 in. and that of the June 25 rain was 0.64 in. Maximum intensities observed were 95, 114, and 133 mm/hr, respectively, showing an inverse correlation of this characteristic with the total yield. Both cold frontal rains exhibited suppressed showery activity toward the end of the rainfall, that on June 25 reaching nearly 50 mm/hr and that on September 23 nearly 20 mm/hr. Lightning and thunder were associated with all the showers, but data on the duration and intensity of the electrical activity are lacking.

Interpretation of the rain-intensity graphs and data on rates of motion of the respective weather systems suggests that the basic major shower units have a dimension of the order of 4 to 5 nautical miles along the direction of motion. Those of the June 25 system appear to be smaller. The fact that the initial shower in this case developed very rapidly just prior to the onset of rain at the station suggests that at a more mature state of development the basic elements would have joined and produced a structure more nearly comparable to the other systems.

Finer structure, of the order of 1 min or less in duration and 0.5 nautical mile or less in extent, is indicative of the the shaft-like character of heavy rain which is seen in radar range–height–indicator (RHI) presentations. The relation of these two scales of rain structure to the cleansing action of the rain and to the entrainment of contaminated air is discussed.

Contaminant Concentrations Graphs of the concentrations of pollen and of radioactive materials are given in the upper part of Figs. 3 to 5. The periods during which the samples of rainwater were collected are shown in the middle of the figures. The samples whose number designations are modified by "P" were analyzed for their pollen content only.

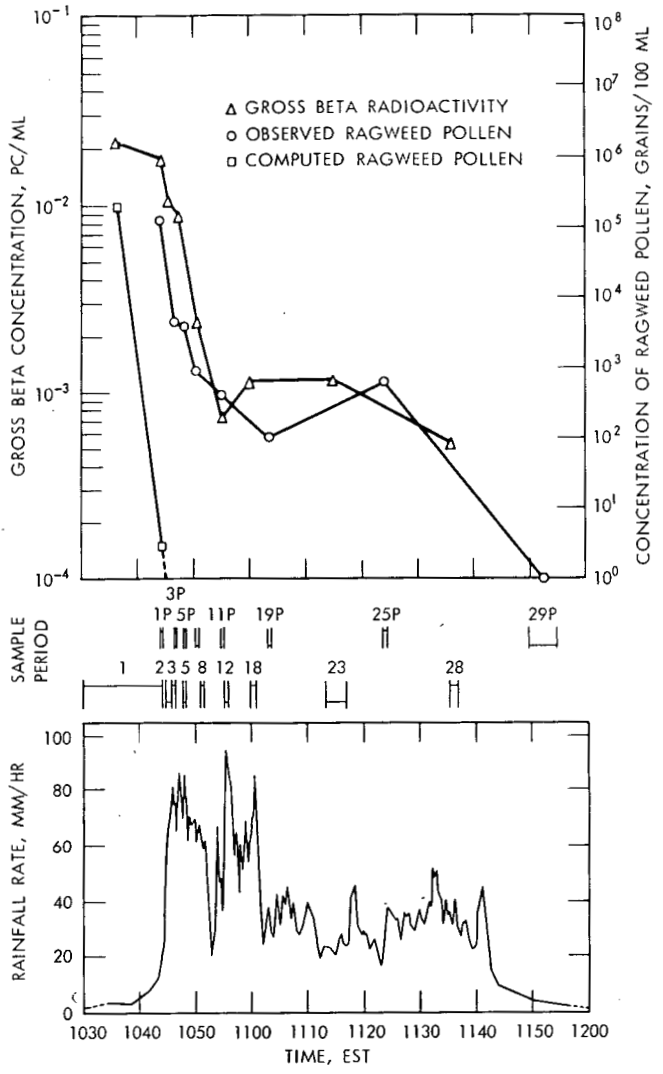

Fig. 3—Results of rainwater analyses and rainfall-rate data for Sept. 1, 1961. The curve of computed ragweed-pollen concentration is explained in the text.

Since the natural pollination seasons ended before September 23, no pollen analysis was made for this rain.

In each of the three cases and for both classes of contamination, an early sharp decrease of concentration is observed in the initial heavy shower. Subsequent increases and decreases also demand interpretation. Although, unfortunately, the complete continuum of samples was not analyzed for any of these three rains, the results indicate

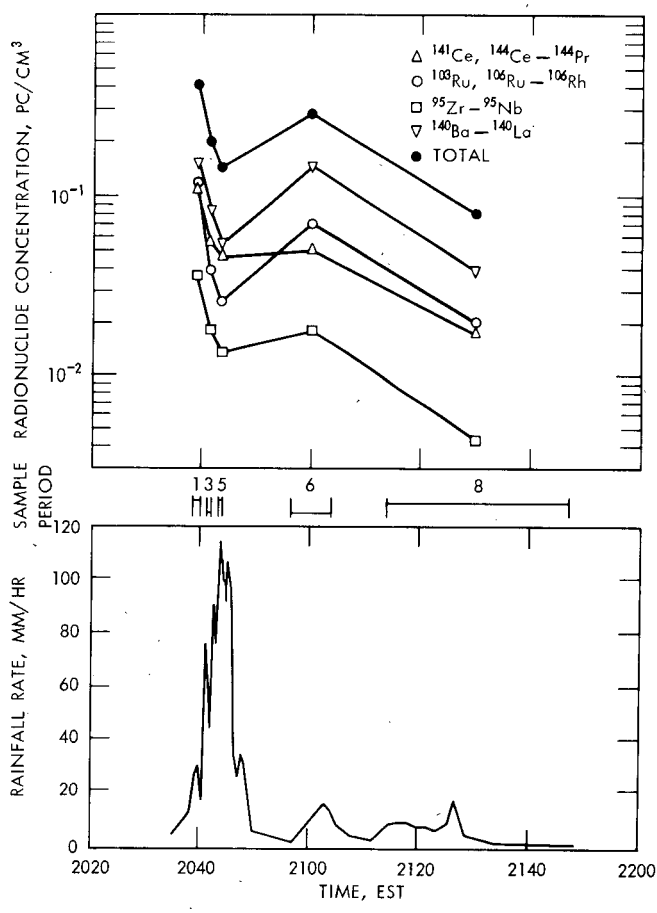

Fig. 4—Results of rainwater analyses and rainfall-rate data for Sept. 23, 1961.

that such an analysis would be sufficiently interesting that a complete continuum will be analyzed in future work.

Diffuse Systems

Two rain-producing events among those reported here are considered to fit the category of diffuse convective activity as previously described. These are the events of Sept. 30, 1961, and May 19, 1962.

Synoptic Conditions The nearest appropriate U. S. Weather Bureau maps, for the 500-mb and surface levels, are shown in Fig. 6. The rain collections on September 30 were obtained from two prefrontal squall lines, the first of which preceded the cold front by about 90 nautical

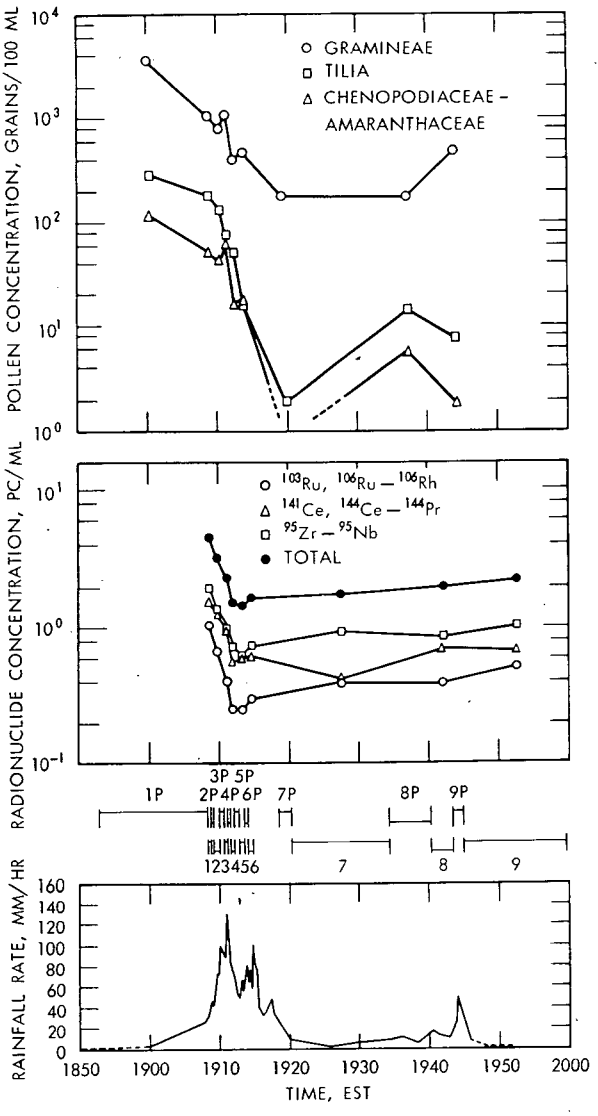

Fig. 5—Results of rainwater analyses and rainfall-rate data for June 25, 1962. The common names and diameters of the several pollens are given in the appendix to this paper.

miles. No thunder was heard, and the structure in general was a loose composite of relatively weak convective cells.

The rain of May 19 took place in an apparently convergent flow in warm air without being directly associated with identifiable frontal or squall passages. Radar observations showed no well-developed cells of strong convection, all echo tops occurring below about 36,000 ft.

Rainfall Intensity The rainfall-intensity graphs for these two events are shown in Figs. 7 and 8. Transit of the station by rain-producing cells is

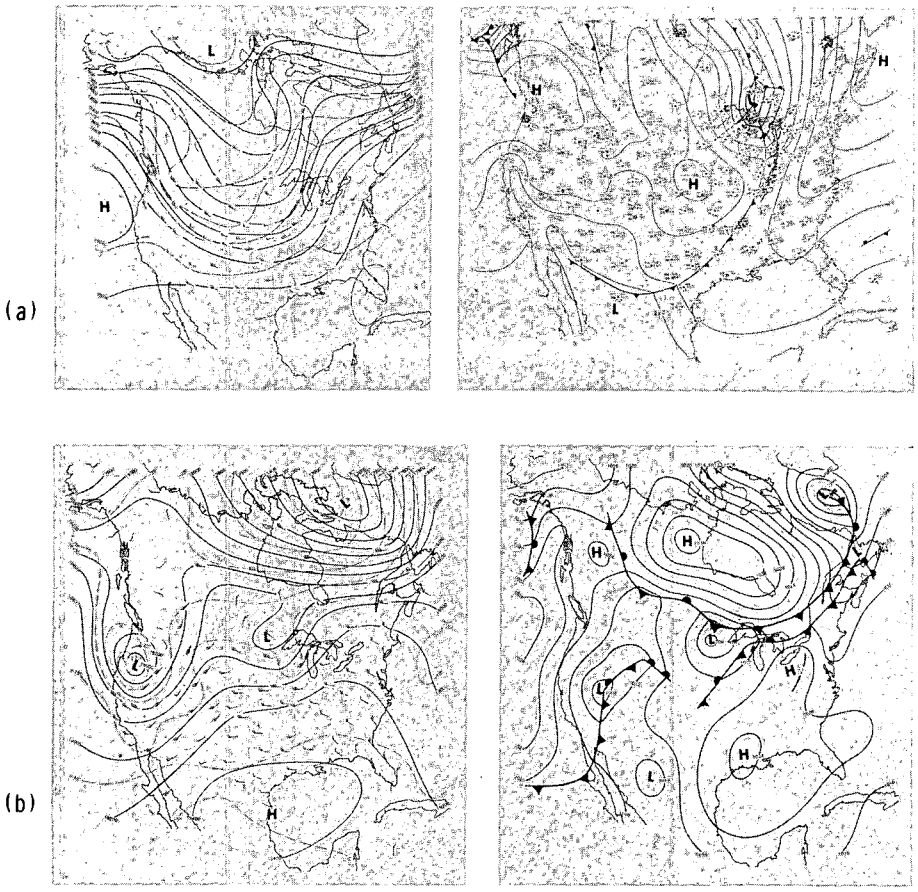

Fig. 6—Synoptic weather data for diffuse systems. (a) Data for rain of Sept. 30, 1961; 500-mb data at 1900 EST; surface data at 0100 EST on October 1. (b) Data for rain of May 19, 1962; 500-mb data at 1900 EST; surface data at 1300 EST.

clearly indicated. The precise position of the station with respect to the central or most intense rain shaft is not known, but a near-diametric transit is probably indicated by the maximum intensity spikes of 38 mm/hr on September 30 and 14 mm/hr on May 19. The low-intensity portions were apparently composed of stable rain and spray between active cells. The total rainfall amounts from these systems were 0.37 and 0.27 in., respectively.

Contaminant Concentrations In both cases, the changes of the contamination levels of the rain samples are considerably different from those considered above (well-organized systems). Again, pollens were not present in sufficient number for a meaningful pollen analysis of the

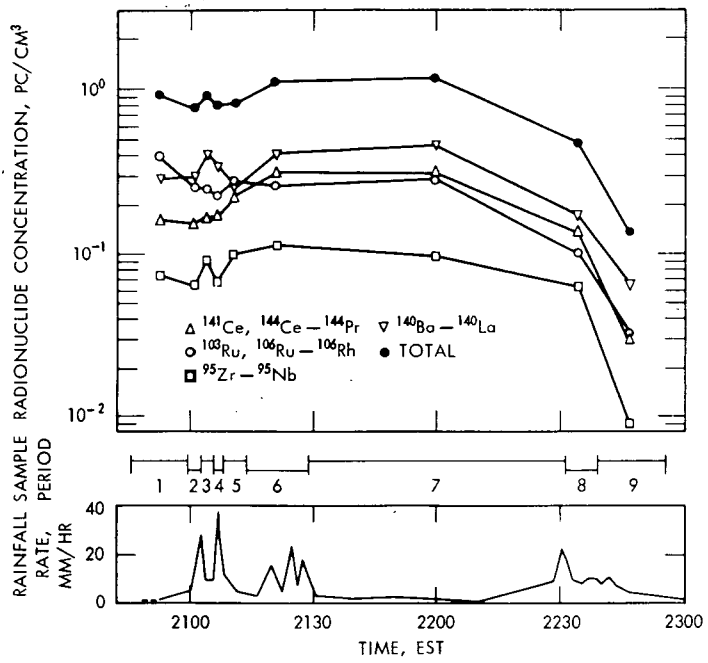

Fig. 7—Results of rainwater analyses and rainfall-rate data for Sept. 30, 1961.

September 30 rain samples. In the May 19 rain, the pollens appear to have been progressively washed out except for the upward tendencies of samples 4P and 6P. The radioactive materials, on the other hand, show peculiar tendencies in both cases. More detailed discussion of these peculiarities is presented later, but it should be noted here that there is a strong likelihood that tropospheric (intermediate) radioactive debris was present in both cases. Necessarily, a low frequency of sampling is associated with low-intensity rainfall; however, in both of these situations, samples were taken continuously throughout the rains.

Summary

The two classes of convective rain-producing situations that we have distinguished have a number of contrasting characteristics. Although the sample size is extremely small (because of this, it will probably be necessary to revise the classification criteria as more data become available), the distinctive characteristics are brought together in Table 1.

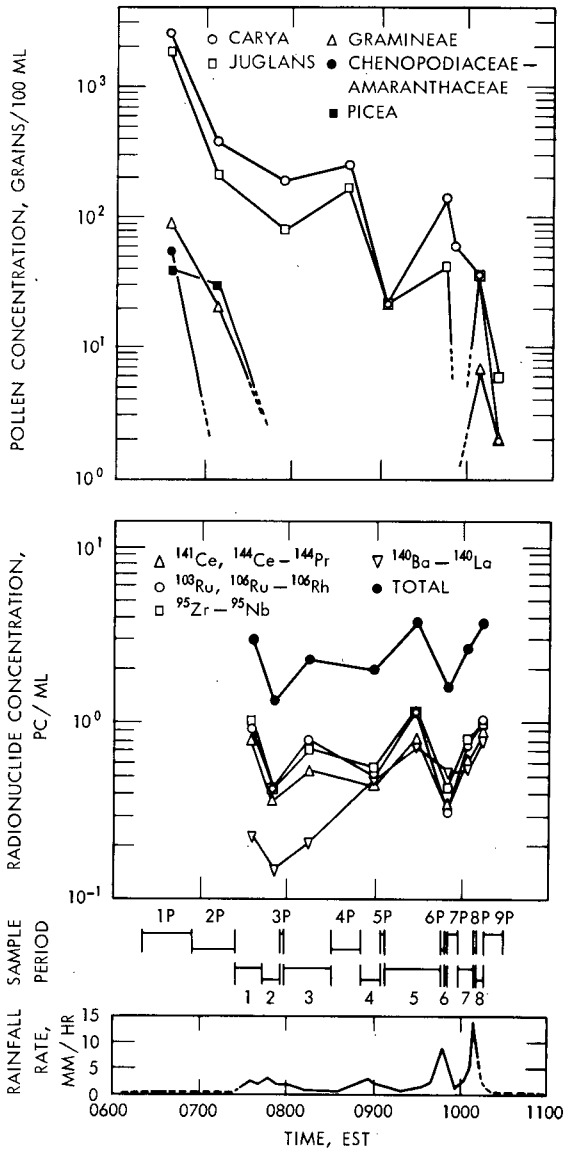

Fig. 8—Results of rainwater analyses and rainfall-rate data for May 19, 1962. The common names and diameters of the several pollens are given in the appendix to this paper.

DISCUSSION OF RESULTS

A consistent pattern was observed in the time variation of the concentration of atmospheric contaminants in rain during the early portions of the well-organized storms. Concentrations of plant pollens were determined in two of these storms; fallout radioactivity was determined in all three. In the cases for which data are available on both contaminants, concentrations of radioactivity and pollens exhibit similar patterns of temporal change during the early parts of the rain, both showing a rapid decrease in concentration.

The similar trends of two contaminants that are known to be highly dissimilar in physical properties and behavior suggest that both were removed from the same air. Since the pollens are low-level air tracers, one infers from this that low-level air is the carrier of the radioactivity and pollens that are found at the beginning of the heavy rains.

It is of interest to consider the possible modes and locations of input of contaminants to the convective system. With regard to the pollens, the bulk of which are contained in the lowest few thousand feet of the atmosphere, it is pertinent to refer to a previous study[4] of ragweed-pollen concentrations in the rain of Sept. 1, 1961. Computations of washout which were made in that study and which were based upon the hypothesis of a stagnant atmosphere beneath the rain-generating level are plotted in Fig. 3. Comparison of the curves of computed and observed pollen concentrations led to the conclusion that a more or less continuous flux of contamination into the storm was necessary for pollen to be found in rain that fell more than a few minutes after the beginning of rainfall. This requirement is fulfilled as long as low-level pollen-bearing air can be entrained into the storm. Most such input must be associated with the convective updraft that also supplies the water vapor.

Circulation models for persistent convective storms (e.g., Newton[5]) usually show a strong updraft to be located at the leading edge of the storm. Thus the first rain to fall at a station is expected to fall partially through the updraft or in close proximity to it. It therefore has good opportunity to mix with contaminated updraft air and to become highly contaminated itself. The rapid decrease in the contamination level occurs as the system moves across the station. The rain that falls from the interior of the storm has little chance of contact with the contaminated updraft.

In contrast to that of the pollens, the vertical distribution of artificial radioactivity is such that the highest concentrations are found in the upper troposphere and especially in the stratosphere. This is true except for those cases where stable laminae of highly radioactive stratospheric air are present at low levels of the troposphere.* Suppose

*See paper by E. F. Danielsen, this volume.

that the debris enters from the top of the cloud as it penetrates to the high troposphere or the stratosphere. It has been suggested[6] that the peak concentration of radionuclides in precipitation will occur as the cloud tops reach a maximum height. If the rainfall-rate peak is assumed to be directly associated with the cloud-top maximum, the rate peak would be expected to contain high concentrations of debris. The concentration of radioactivity at the rate peak is expected to be decreased somewhat by dilution of the particulate matter in high concentrations of liquid water. Nevertheless, moderate concentrations at the rate peak would be expected rather than minimum concentrations, as were observed in the three well-organized rains.

These considerations and the fact that both classes of contaminants decrease rapidly at the same time suggest that the low-level input is the source of both the radioactivity and the pollens found at the beginning of the heavy rain.

In the diffuse rains of September 30 and May 19, peculiar trends of contaminant concentrations were noted. The absence of a consistent temporal pattern of concentration changes in these cases might be expected from a consideration of the likely circulations of weak convective systems. As Weickmann[7] has pointed out, heavy storms with high rainfall rates are associated with circulations of a high degree of organization and persistent updrafts. Weak storms lack such organized circulation; their updrafts are more transient. It is consistent with these observations that an organized pattern of concentration changes, such as that observed during the early portions of the heavy rains, should be associated with an organized and persistent updraft whereas the absence of an organized pattern should be associated with weak and disorganized convection.

In view of the high concentration of contaminants found in the first rain arriving at the station, it is clear that this rain must be associated with a large value of the product of the volume of the air column it sweeps out and the mass (or activity) of contaminants in that volume. This criterion may be met by various combinations of drop trajectory, distribution of contaminants, and storm-circulation patterns. The present data do not permit a definite specification of any of these parameters.

CONCLUSIONS

The observation of simultaneous rapid temporal decreases in concentrations of both radioactivity and plant pollens in rain from the early portions of three well-organized convective rain systems is interpreted as evidence that both classes of contaminants were removed from the same air. Because plant pollens are released into the atmosphere at the earth's surface, it is concluded that both radioactivity and pollens were removed from an updraft of warm, moist air originating at low levels of the atmosphere.

Insofar as the patterns of convection in the two observed cases of diffuse convective rains are such that pockets of contaminated low-level air are left between the relatively weak and isolated precipitation cells, the irregular trends of contaminant concentrations observed in these cases are entirely consistent with the previously stated hypothesis.

ACKNOWLEDGMENTS

This research was conducted under Public Health Service grants E-1379 and AP-1, U. S. Atomic Energy Commission contract AT(11-1)-739, and Michigan–Memorial Phoenix project 245.

APPENDIX

For convenience, the following table has been prepared, giving the common names and approximate diameters reported of all of the pollens determined in rainwater. The diameters reported are the mean of a small number of measurements made on the pollens found in rainwater.

Pollen	Common name	Approximate diameter, μ
Carya	Hickory	47
Chenopodiaceae–Amaranthaceae	Goosefoots–Pigweeds	25
Gramineae	Grasses	29
Juglans	Walnut	42
Picea	Spruce	75
Tilia	Linden	42

REFERENCES

1. A. Walton, E. L. Fisher, and P. W. Krey, Studies of Nuclear Debris in Precipitation, 8th Progress Report (Contract AT(30-1)-2415), USAEC Report NYO-9531, Isotopes, Inc., 1962.
2. A. N. Dingle, Rain Scavenging Studies, in Radioactive Fallout from Nuclear Weapons Tests, A. W. Klement, Jr. (Ed.), USAEC Report TID-7632, pp. 74-79, February 1962.
3. L. P. Salter, R. Kruger, and C. L. Hosler, Sr^{90} Concentration in Precipitation Resulting from Large-scale Uplift, *J. Appl. Meteorol.*, *1*(3): 357-365 (1962).
4. D. F. Gatz and A. N. Dingle, Washout of Ragweed Pollen by Rainfall, *J. Geophys. Res.*, *68*(12): 3641-3648 (1963).
5. C. W. Newton, Structure and Mechanism of the Prefrontal Squall Line, *J. Meteorol.*, *7:* 210-222 (1950).
6. P. Kruger and C. L. Holser, Sr^{90} Concentration in Rain from Convective Showers, *J. Appl. Meteorol.*, *2:* 379-389 (1963).
7. H. Weickmann, Cloud Physics, U. S. National Report 1960–1963, IUGG, *Trans. Am. Geophys. Union*, *44*(2): 382 (1963).

METEOROLOGICAL INFLUENCES UPON ^{90}Sr FALLOUT CONCENTRATION IN PRECIPITATION: PART 2. CONVECTIVE ACTIVITY AND EXTRATROPICAL CYCLONES*

PAUL KRUGER,† CHARLES L. HOSLER,‡ and ALBERT MILLER§
Hazelton-Nuclear Science Corporation, Palo Alto, California

ABSTRACT

The meteorological effects upon ^{90}Sr fallout deposition from convective activity and from extratropical cyclones were examined in several locations. Data from 14 convective shower storms in Pennsylvania showed that the changes in ^{90}Sr concentration in the precipitation were in accord with the life cycle of convective cells; the time of peak concentration coincided with the time of maximum radar-echo cloud-top heights. For the large-scale uplift associated with extratropical cyclones, the slower changing ^{90}Sr concentrations were associated with evaporation effects upon the rainfall, the precipitation-growth mechanism, the passage of fronts and trough lines, and the stratification of nuclear debris in the atmosphere.

INTRODUCTION

Our presentation at the previous AEC fallout conference covered the first part of our program, the role of large-scale uplift[1] on ^{90}Sr

*Part 1, Large-scale Uplift, was presented at the previous AEC fallout conference.[1]

†Also at Stanford University, Stanford, Calif.

‡Also at Pennsylvania State University, University Park, Pa.

§Also at San Jose State College, San Jose, Calif.

deposition by precipitation. Since then, study has been made of other precipitation-producing systems. For evaluation of the relative importance of the several meteorological parameters involved in the rainout removal of radioactive debris from the atmosphere, examination has been made of several different types of weather systems, each of which is characterized by its own precipitation-causing processes. The parameters important in determining the nuclear-debris concentration vary for each of these weather systems. For example, rapidly changing cloud tops and entrainment from the surroundings are important parameters for convective cells, whereas the vast volumes of the atmosphere involved in extratropical cyclones suggest that trajectories in complex circulation may be the controlling parameter in determining nuclear-debris concentrations at a given location.

Precipitation-formation processes, such as all water or water–ice, affect the concentration of nuclear debris in ground-level precipitation through the different processes of nucleation and raindrop growth. Evaporation below cloud bases is also important. Finally, the availability of nuclear debris in the atmosphere for rainout processes is time and location dependent.

The following meteorological parameters that we believe to be important in the determination of nuclear-debris deposition in precipitation were studied:

Maximums along troughs and fronts
Precipitation growth mechanisms
Height of rain-generation levels
Proximity of jet streams and tropopause
Stratification of debris across inversions
Evaporation of raindrops

The weather systems studied and their respective collection sites were as follows:

Weather system	Collection site
Extratropical cyclones	Central Pennsylvania and the west coast of the United States
Showers and thunderstorms	Oklahoma and central Pennsylvania
Orographic lifting	Hawaii
Fog and stratus	California

A study of orographic lifting is being made in conjunction with an analysis of the effect of the trade-wind inversion on the vertical transport of nuclear debris. The ^{90}Sr concentration in samples of air and precipitation taken during two short periods in 1963 indicated a dependence of concentration upon the inversion strength. A more extensive collection and atmospheric-analysis program was completed during August 1964; the preparation of the data from this program is underway. Some sampling of drizzle and fog has been made along the

coast near Stanford, Calif. Final evaluations of these studies will be reported as each is completed.

Collections were made during two severe storms in May 1963 in Oklahoma. These collections were originally made as part of our study of convective activity and in conjunction with objectives of Project Springfield.* Preliminary analysis of the radiochemical and meteorological data shows surprising results with respect to convective activity. These storms will be the subject of a separate report.

Two extratropical cyclonic storms were sampled at State College, Pa., during November 1962 and March 1963. These storms occurred after the cessation of atmospheric nuclear-weapons detonations. They are also being studied separately because of the unusual interest aroused by their having debris age changes that occurred during the storm periods.

The report presented here discusses the studies of precipitation from extratropical cyclones and from showers and thunderstorms.

CONVECTIVE ACTIVITY

Introduction

Initial studies[2] of large-scale-uplift systems showed that ^{90}Sr concentration in precipitation where drop sizes are small was dependent upon the experience of the precipitation in falling from the base of the clouds to the ground. For large-scale-uplift systems, the height of the generating level and the nucleation process may be relatively constant over periods of several hours. With lateral uniformity of water content and ^{90}Sr-bearing nucleating particles throughout a given air mass, the extent of growth of raindrops by accretion in the cloud and evaporation below the cloud thus is determined primarily by the height of the ceiling.

For convective activity, vertical motions within individual cells are greatly enhanced relative to large-scale uplift, and several parameters simultaneously affect the ground-level ^{90}Sr concentration. Precipitation originates from rapidly varying heights during the life cycle of an individual convective cell. Variations may also occur in the precipitation-generating process, in the drop sizes, in the ^{90}Sr-bearing particulate air concentrations, and in the water content of the cloud.

*Project Springfield is the code name for a special atmospheric-sciences research project funded by the Defense Atomic Support Agency and the U. S. Atomic Energy Commission in cooperation with the U. S. Weather Bureau and several universities and industrial groups. This project has as its goal the documentation of the spring-fallout maximum by use of aircraft sampling and intensive measurements and radioanalysis of rainfall.

It is postulated[3] that the ^{90}Sr concentration from a simple convective cell moving directly over a collector is related to the life cycle of the cell and reaches a maximum value during the mature stage. Therefore the maximum value should be related to the height of the convective cell and the concentration of ^{90}Sr-bearing particles in the environment.

Air is incorporated into convective cloud systems not only through the warm–moist updraft at the base of the cloud but also by entrainment of drier air by mixing processes with the environment[4] at all levels. Dry particulate debris containing higher ^{90}Sr concentration of stratospheric origin thus may be used as condensation nuclei at these higher levels. Amplification of ^{90}Sr availability to the precipitation also may result by the penetration of the tropopause by the cloud tops[5] or by mixing of the clouds in the middle troposphere with parcels of dry air of recent stratospheric residence. This last phenomenon has been described by Danielsen[6] and Staley.[7]

Furthermore, the moisture content of the air supporting the precipitation varies during the life cycle of the cell. During the downdraft period of the mature stage, some of the water moving downward must evaporate to maintain the saturation of the air. The extent of the downdraft evaporation is related to the height of the storm and the intensity of the downdraft. This evaporation and the subsequent evaporation of the resulting smaller drops below the cloud base enhance the already increasing ^{90}Sr concentration with increasing height of the cloud tops.

The postulation that the ^{90}Sr concentration in precipitation from the cumulus stage of a cell increases as the height of the cloud develops[8] also requires the condition that the ^{90}Sr-bearing particulates be involved in the condensation and accretion process and that scavenging of particulate matter below the cloud by the falling raindrops is of small consequence. This requirement is supported by several observations. For example, Greenfield,[9] Langmuir,[10] and Vaughan and Perkins[11] have each shown that for aerosols smaller than a few microns the collection efficiency of falling drops is extremely low. Furthermore, Landsberg[12] has pointed out that the number of condensation nuclei decreases rapidly with height. More recently, Durbin and Murgatroyd[13] have shown that at cloud levels the number of nuclei is less than the concentrations of cloud particles ordinarily observed. In addition, the work of Junge[14] indicates that the layer of sulfates in the atmosphere is likely to collect radionuclides such as ^{90}Sr. Since $(NH_4)_2SO_4$ is hygroscopic, it may serve as a source of excellent condensation nuclei. Thus each of the smaller number of particles in the higher levels of the cloud has a higher probability of being utilized as a condensation nucleus. Since the ^{90}Sr-bearing particles are known to be of stratospheric origin after a month or so following nuclear detonation, it is believed that removal of ^{90}Sr-bearing debris results primarily from condensation processes

within the cloud and that direct capture below the cloud is relatively unimportant.[8]

Experiments

During the period from 1961 through 1963, a total of 14 convective shower systems has been studied. In each case time aliquots of the showers were obtained of the minimum sample size consistent with adequate sensitivity for radiochemical analysis. The use of radar analysis of the cloud systems was increased each year. Maximum radar-echo cloud tops were measured[3] for the seven showers sampled in 1961. Radar-echo cloud-top profiles were obtained[15] for the three 1962 showers. Time–height–intensity (THI) cross sections were prepared[16] for the four 1963 showers. These cross sections, showing the radar reflectivity structure with altitude in the clouds, have proved invaluable in conjunction with general meteorological data in evaluating the fallout concentrations. The methods of collection and radiochemical analysis of the precipitation have been given in our earlier reports.[1]

Summary

The collection, radiochemical, and meteorological data for the individual 14 convective showers studied to date are given in Refs. 3, 15, and 16. A summary of these data is given in Table 1. The peak ^{90}Sr concentration in each shower was compared to the average concentration for the shower as a whole. The maximum radar-echo tops are given for each shower corrected to mean sea level. For the 1962 and 1963 showers, the time of the peak cell top from the radar cross section was compared to the time of the peak ^{90}Sr concentration. The distance of the shower's position with respect to the jet-stream location and the height of the tropopause was also determined for each event.

As illustrations of the data previously reported, one of the radar-top cross-section analyses of the 1962 convective showers is shown in Fig. 1, and one of the THI reflectivity-cross-section analyses of the 1963 showers is shown in Fig. 2. In all the 1962 and 1963 showers, the average precipitation rate and the age of the strontium fission products (given by the $^{89}Sr/^{90}Sr$ ratio) were also calculated. These data are shown in the respective cross-section analyses.

Discussion

The convective-activity showers studied in the period from 1961 through 1963 involved nuclear-weapon debris of differing time origin each season. The 1961 showers contained ^{90}Sr debris at least three years old, originating from nuclear-weapon tests prior to the moratorium of 1958. The average ^{90}Sr concentration was low, usually less than 1 dis/min per liter. The debris in these storms came from well-

Table 1—SUMMARY OF RADIOCHEMICAL AND METEOROLOGICAL DATA FOR CONVECTIVE SHOWERS, 1961–1963

Date	Average ^{90}Sr concentration, dis/min per liter	Peak ^{90}Sr concentration		Maximum radar-echo tops		Jet-stream position, miles	Tropopause height, ft	Tropopause height relative to maximum tops, ft
		Dis/min per liter	Time, EST	Height, ft	Time, EST			
1961								
Mar. 8	8.8	51.0		29,000		75 N	{23,500 / 44,400}	+5,500
May 8	0.09	0.4		20,000		400 S	41,800	−21,800
May 8	6.1	6.7		41,000		400 S	41,800	−800
May 9	5.6	9.9		40,000		150 S	38,900	+1,100
July 24	0.05	1.1		40,000		300 S	44,500	−4,500
Aug. 28	0.35	0.8		38,000		190 S	42,000	−4,000
Sept. 14	0.21	1.6		36,500		450 S	48,000	−11,500
1962*								
June 24	38.2	45.5	1300	41,000	1255	200 NW	43,000	−2,000
Aug. 20	15.6	38.8	1740	46,000	1735	160 N	47,000	−1,000
Sept. 10	4.8	12.0	1245	30,000	1240	250 NW	49,300	−19,300
1963†								
Apr. 19	65	155	2100	26,000	2040	180 S	39,600	−13,600
Apr. 22	205	420	2310	36,000	2320	180 N	40,000	−4,000
May 10	165	250	1930	40,000	1940	200 N	45,000	−5,000
May 21	85	125	2040	17,000	2040	80 NW	39,500	−12,500

*From radar-top cross-section analyses.
†From showers isolated by cell from THI cross-section analyses.

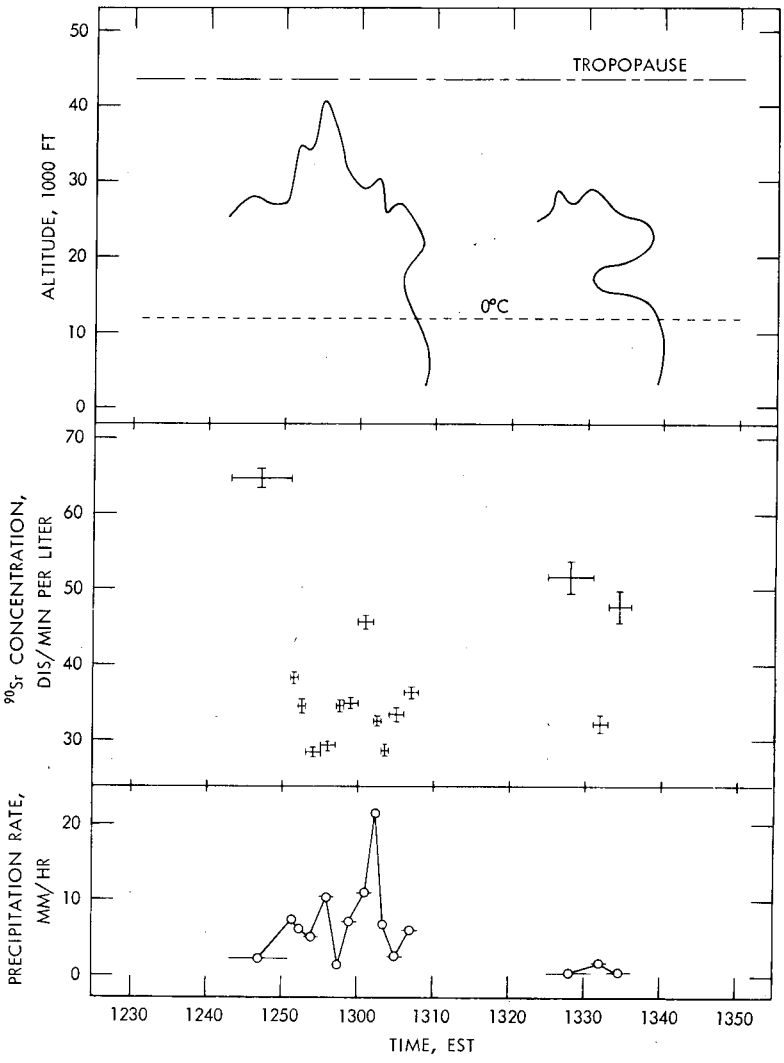

Fig. 1—Time cross sections for the storm of June 24, 1962.

mixed stratospheric air, and the ^{89}Sr of this debris had decayed to below detectable levels. The showers sampled in 1962 involved air with ^{90}Sr debris of recent origin. The ^{89}Sr/^{90}Sr ratios indicated an age consistent with that of fission products from the late 1961 U.S.S.R. detonations until the Sept. 10, 1962, showers, which also contained newer debris, likely from the U. S. Dominic I detonations in the Pacific in the spring of 1962. The peak ^{90}Sr concentrations were about 40 times greater than those in the 1961 showers. The four 1963 storms of April and May oc-

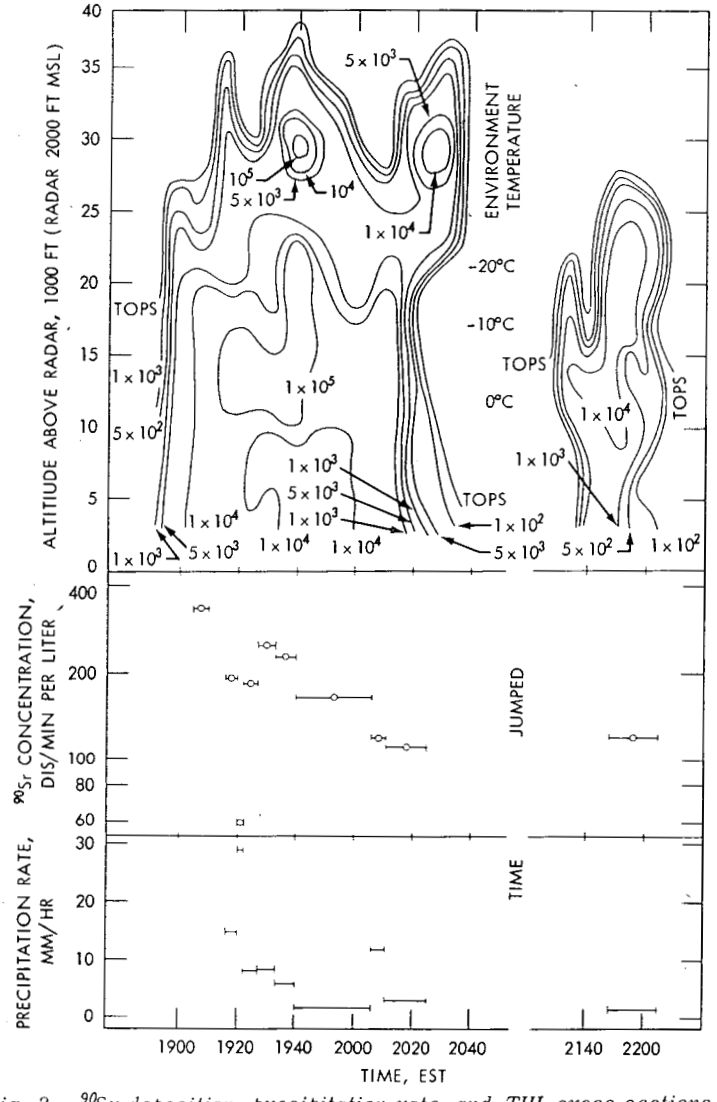

Fig. 2—^{90}Sr deposition, precipitation rate, and THI cross sections for the storm of May 10, 1963. Contours of reflectivity are given in units of mm^6/m^3.

curred about four to five months after the last recorded atmospheric test.[17] in December 1962. The $^{89}Sr/^{90}Sr$ ratios for these four storms were plotted together with the ratios obtained for the other storms sampled as part of this project in Pennsylvania, Oklahoma, Hawaii, and California. These ratios are shown in Fig. 3 with the many total storm ratios obtained by Kuroda[18] in Arkansas rains. The apparent 50.5-day

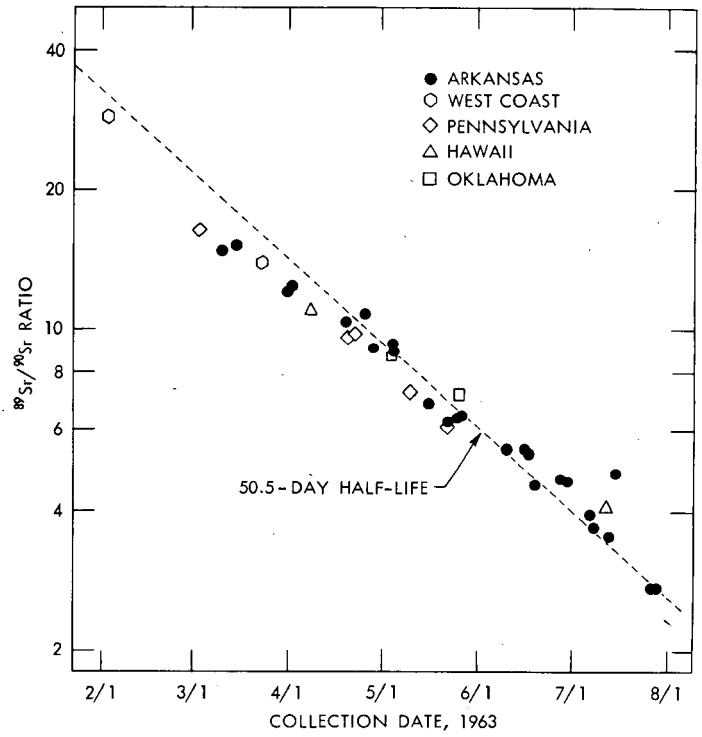

Fig. 3—$^{89}Sr/^{90}Sr$ ratios averaged for storms sampled in several locations in the United States during 1963 and shown in comparison to the values of Kuroda[18] for Arkansas (solid points).

half-life of the ratio indicates a well-mixed atmosphere at the precipitation-generating levels with respect to fission-product age, and the intercept at 167 for weapon fission yields[19] corresponds to an "apparent detonation date" of Oct. 5, 1962, falling within the latest period of testing.

The peak concentrations of the four storms discussed in this report were about 10 times greater than those of 1962; thus they were about 400 times greater than those of 1961.

Several features distinguish ^{90}Sr deposition in precipitation from convective activity. The first is the relatively large concentration changes over short time periods in conjunction with the cell structural features of the clouds, such as maximum reflectivity values and altitude, presence of high- and/or low-level precipitation, cell boundaries, etc. Another is the proportional dependence of the ^{90}Sr concentration upon rainfall intensity. This is the reverse of the ^{90}Sr dependence observed in large-scale uplift systems, where the concentration generally is inversely proportional to the rainfall intensity when the ceiling remains

low. This observed reversal may be considered one predominantly distinguishing feature between convective activity and large-scale uplift.

A major feature has been the peak-concentration dependence upon the location of the cloud system with respect to the jet stream and the tropopause; this dependence upon the location of the cloud system with respect to the tropopause was especially noticeable during the 1961 period. During the three-year period of relatively minor new input of ^{90}Sr into the stratosphere by atmospheric weapons testing following the 1958 testing moratorium, the air concentration of nuclear debris may have been at a maximum uniform value over large air masses.

Figure 4 shows the peak concentrations in the seven 1961 showers related to the top of the cumulus cloud with respect to the tropopause height and the horizontal distance to the jet stream.[20] This dependence is consistent with the supposition that the nuclear-debris concentration in air at the tropopause and near the jet stream is greater at any given time than at lower levels in the troposphere. The observations, however, may also be consistent with the supposition that layers of dry air of recent stratospheric origin may be present in the middle troposphere at times, resulting in layers of large nuclear-debris concentration between large volumes of air at low nuclear-debris concentration. The growth of a cumulus cloud through such layers and the extent of entrainment of the debris as new nucleation particles would, of course, also be dependent upon the maximum growth of the cumulus clouds. The

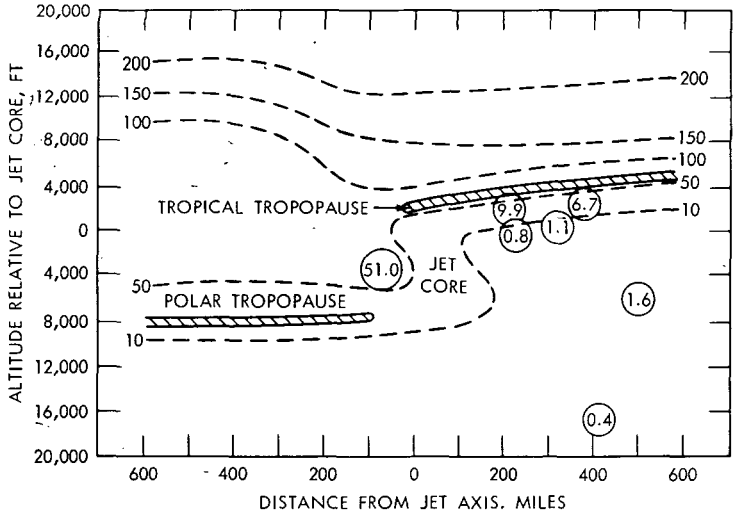

Fig. 4—Peak ^{90}Sr concentration in disintegrations per minute per liter in convective-shower precipitation plotted at relative positions of maximum cloud tops and distances from jet core and superimposed on air-concentration plot in disintegrations per minute per 1000 scf from Giles.[20]

time period of growth and evaporation history during descent to the ground compared to the time period of maximum growth of the clouds from the middle troposphere would likely obscure resolution of the two mechanisms. The use of THI cross sections in 1963 showing the radar reflectivity allowed more detailed observations of ground-level ^{90}Sr concentrations with respect to individual bursts of precipitation observed at given altitudes in the cloud structure. The THI cross-section analysis of the showers of May 10, 1963, Fig. 2, shows the relation between the height at which the precipitation originated and the observed ^{90}Sr concentration in ground-level rain. The ^{90}Sr concentration curve from 1920 to 2025 EST follows the maximum radar-tops curve during this period, and the sharp rise from 60 to 249 dis/min per liter follows the growth of the closed isopleth of 10^5 mm^6/m^3 reflectivity from an altitude between 11,000 and 17,000 ft above the radar site to an altitude between 10,000 and 23,000 ft, with a high cell of similar reflectivity at 29,500 ft.

A final observation of convective activity has been made with respect to the spring peak of nuclear-debris deposition.[8] It is suggested that the greater occurrence of thunderstorms during the spring months may be responsible in part for the observed spring peak. It is likely that convective activity acts in concert with one or more stratospheric–tropospheric debris transfer processes in incorporating the nuclear debris into precipitation that transports it to the ground or the lower layers of the atmosphere through virga, where it can deposit through subsequent low-level precipitation processes. This aspect was examined in two giant thunderstorm systems in Oklahoma during May 1963. Although the data are not yet ready for publication, an interesting feature of these severe storms has been the lack of convective-activity ^{90}Sr deposition features. The radioactivity data appear to be more indicative of steady-state precipitation and will be the subject of a separate report when the evaluation is completed.

EXTRATROPICAL CYCLONES

Much of the precipitation falling over the mid-latitudes of the northern and southern hemispheres is associated with extratropical cyclones. These large vortexes extend to great heights covering large areas and are probably responsible for a large fraction of the nuclear-debris deposition from the troposphere to the ground. The general large-scale uplift of such cyclones may be augmented with smaller-scale convective activity or orographic lifting or both, leading to precipitation caused by one or more mechanisms acting simultaneously. Elliott and Hovind[21] have recently analyzed such complex storms entering the West Coast from the Pacific. When the concurrent effects of convective activity or orographic lifting are small, the time variations observed

in the precipitation from such storms may be expected to be dependent upon the slower changing meteorological features of large-scale uplift. The effects of frontal zones and changes in generating mechanisms should be observable as perturbations on the steady state of the large-scale uplifting. For precipitation from large air masses, the ground-level concentration of nuclear debris was believed[2] to be dependent upon the following parameters:

1. The height of the precipitation-generating level.
2. The precipitation generation and growth mechanisms in the cloud.
3. The amount and the characteristics of the radioactive aerosols initially in the air masses participating in the precipitation process.
4. The specific humidity at the generating level.
5. The previous precipitation experience of the air at the generating level.
6. The descent experience of the precipitation from the cloud in which the precipitation originates to the ground.

Summary of Part 1 (Reported in Ref. 1)

Our initial studies of three wave cyclones in the winter of 1960 at Pittsburgh, Pa., were concentrated upon storms in which the stability of the air led to layer clouds with limited imbedded convective activity. In each storm, the precipitation elements were generated in the ice phase at approximately 18,000 ft. Thus the first two variables given above were considered constant. By an additional limitation of observations to precipitation involving only one air mass with an expected conservation of debris to water ratio, the second two variables were considered constant for the period of precipitation. Even with these approximations, the changes of ^{90}Sr concentration in the rain were observed to be strongly dependent upon descent experience as expressed in terms of ceiling height. The ceiling may be considered an index of the humidity profile and the depth of the lower layers of air. These parameters affect the rate of evaporation or the growth of the raindrops falling from the cloud and thus the final ground-level concentration.

Newer Experiments

Subsequent continental cyclonic storms were sampled at State College, Pa., at the site of the Pennsylvania State University 3-cm M33 radar system, with which data time cross sections of the clouds and precipitation were prepared. Ceiling balloons were released to measure ceiling heights. Since 1962 a detailed radiochemical study of a complex Pacific Ocean wave cyclone has been made[22] in addition to an analysis of the nuclear-debris deposition in California from wave cyclones during the winter 1961–1962 following resumption of nuclear

testing by the U.S.S.R.[23] From these studies, some of the parameters significant in determining nuclear-debris-deposition mechanisms by cyclone precipitation have been examined. The collection, radiochemical, and meteorological methods for these studies have been the same as those reported in Ref. 1.

Concurrent studies under another program are being made by aliquoted collections along the entire length of the 1500-mile west coast of the United States. Examination is being made of the meteorological parameters on the synoptic scale encompassing an entire wave cyclone, including the effects of wave history, air-mass trajectories, storm intensities, variation in the height of the tropopause, location and intensity of the jet stream, etc. One such cyclone[24] was sampled in March 1962.

Discussion

The data for the several wave-cyclone studies are given in Refs. 2 and 22. These data are summarized, with pertinent illustrations given, in the discussion of the parameters observed to be important in determining ground-level ^{90}Sr deposition rate from the wave cyclones examined.

Evaporation This effect has been discussed.[1] It has already been pointed out by Bleichrodt *et al.*[25] that evaporation of raindrops falling through unsaturated layers of air should lead to increased concentration of radioactivity in rainfall. This effect should be especially pronounced for steady precipitation of relatively small drops that often accompany large-scale disturbance. For example, data taken from Mason[26] indicate that evaporation would reduce the volume of a drizzle-size drop falling from a cloud base 2000 ft above ground through air of 80% relative humidity by a factor of 16. The onset of rain from large cyclonic storms is frequently from middle clouds; thus the effect of evaporation on ground-level nuclear-debris concentration should be especially strong during the first few hours of rain.

Studies of the cyclones in central Pennsylvania were made to isolate the collection periods during which precipitation fell from stable single air-mass systems with no observable change in cloud tops or storm structure. Analyses of changes in ^{90}Sr concentration were made in terms of changes in ceiling height. Figure 5 shows the fractional change in ^{90}Sr concentration, $\overline{\Delta C}$, as a function of the fractional change in ceiling, $\overline{\Delta H}$. A line drawn through the origin indicates a relation expressed by

$$\ln C = \ln H^{1.25 \pm 0.65}$$

When the assumptions of steady-state precipitation conditions, the variability in temperature and humidity profiles below the clouds,

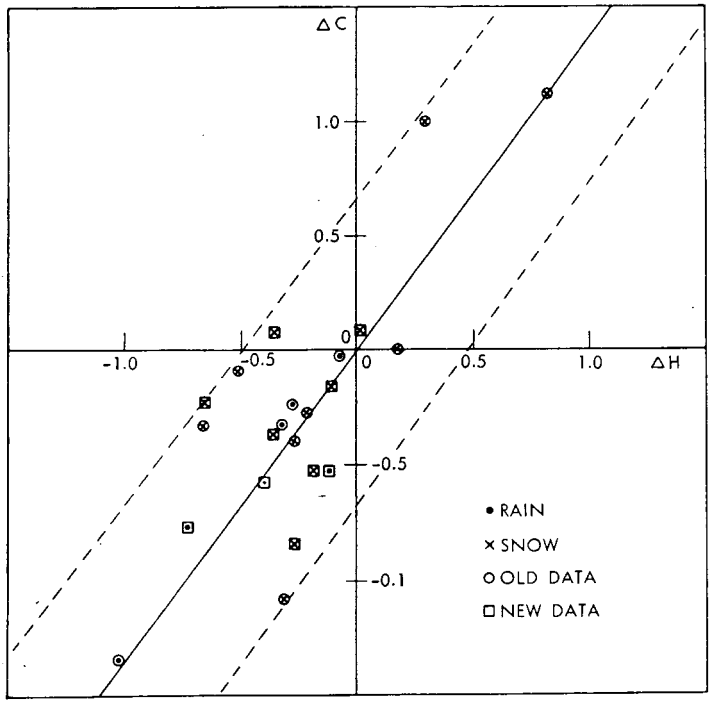

Fig. 5—Fractional change in ^{90}Sr concentration, $\overline{\Delta C}$, as a function of fractional change in ceiling, $\overline{\Delta H}$. ($\overline{\Delta C} = 1.25\ \overline{\Delta H} \pm 0.65$.)

the variability in drop size distributions, and the errors associated with low frequency of ceiling measurement and long sample times are considered, it is indeed surprising to see an uncertainty in the exponent of only 50%.

The effect of evaporation has also been observed in Pacific cyclones. In many cases very dry air overrides the shallow marine layer, and the first rain falling from the middle clouds accompanying an approaching wave falls through about 6000 ft of air with a relative humidity of 30% or less. The Santa Barbara collection of Feb. 7, 1962, shows this effect markedly.[22] A cross section of this storm is shown in Fig. 6, and the vertical distribution of temperature and humidity before and after saturation of the marine layer is shown in Fig. 7. During the first few hours after rain began, the dry air between 2000 and 7500 ft gradually reached saturation. The first rainfall reaching the ground contained a high ^{90}Sr concentration, which decreased to one-third of its initial value 2 hr later.

Precipitation-growth Mechanisms The role of this mechanism in determining ground-level nuclear-debris concentrations has been given earlier.

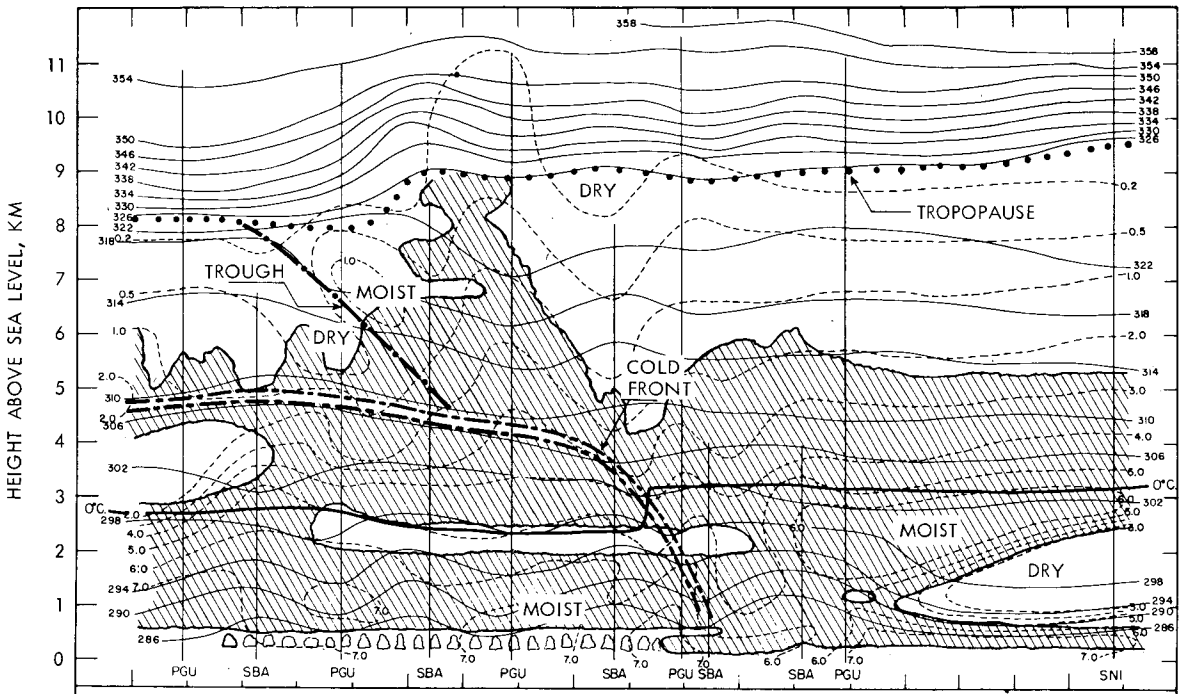
HEIGHT ABOVE SEA LEVEL, KM
DRY
TROPOPAUSE
TROUGH
MOIST
DRY
COLD FRONT
MOIST
DRY
MOIST
0°C
PGU SBA PGU SBA PGU SBA PGU SBA PGU SBA PGU SNI
2200 2100 2000 1900 1800 1700 1600 1500 1400 1300 1200 1100 1000 0900 0800 0700 0600 0500 0400
VERTICAL TIME SECTION
Solid lines: Potential Temperature, °K; Dashed lines: Mixing Ratio, g/kg;
Stations: PGU-Point Arguello, SBA-Santa Barbara, SNI-San Nicolas Island
EVENTS:
Trough Passage, 500 mb
Frontal Passage
Overturning of Marine Layer
Rain at Ground level
Rain Began
Surface Weather Reports, Santa Barbara Airport:

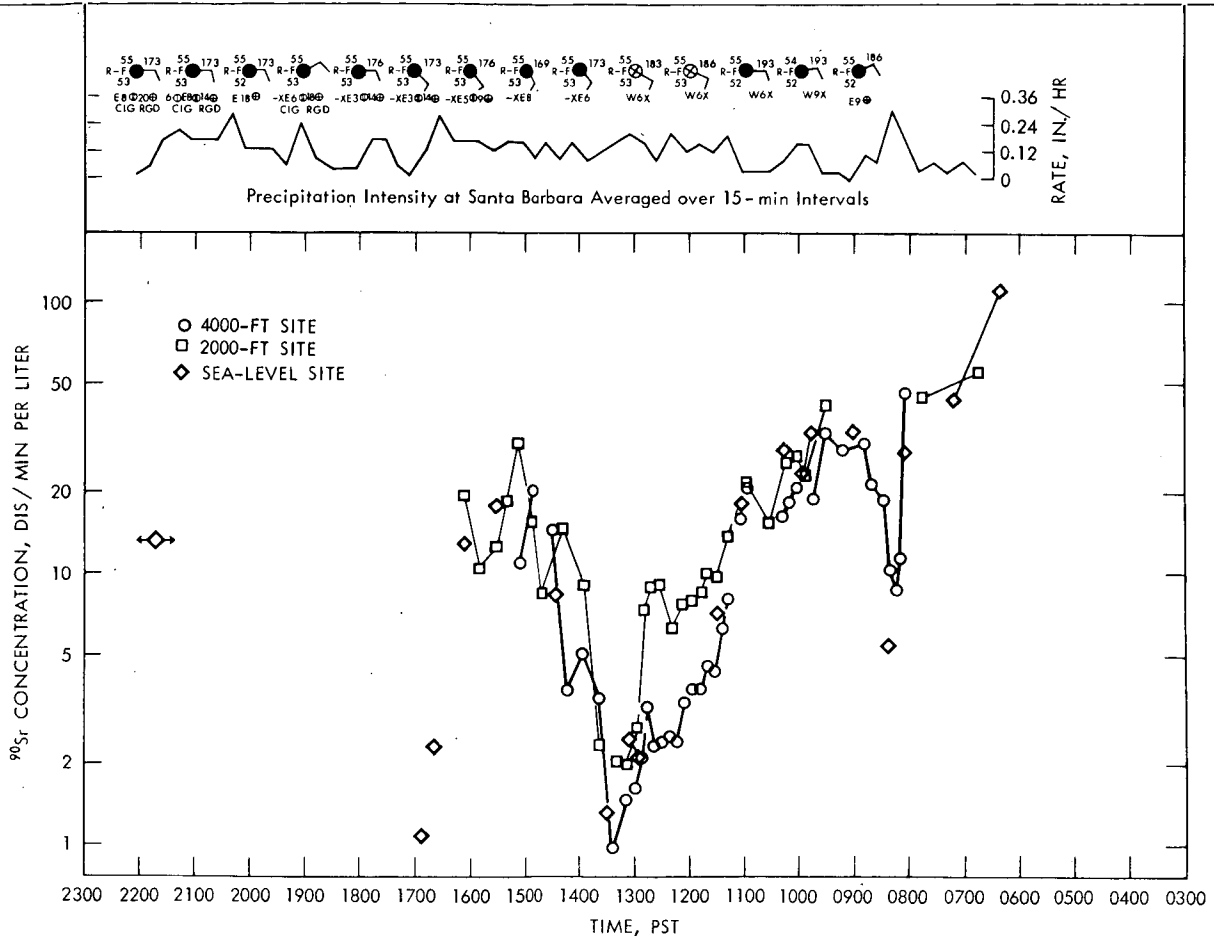

Fig. 6—Meteorological and ^{90}Sr radiochemical analyses of storm at Santa Barbara, Calif., on Feb. 7, 1962.

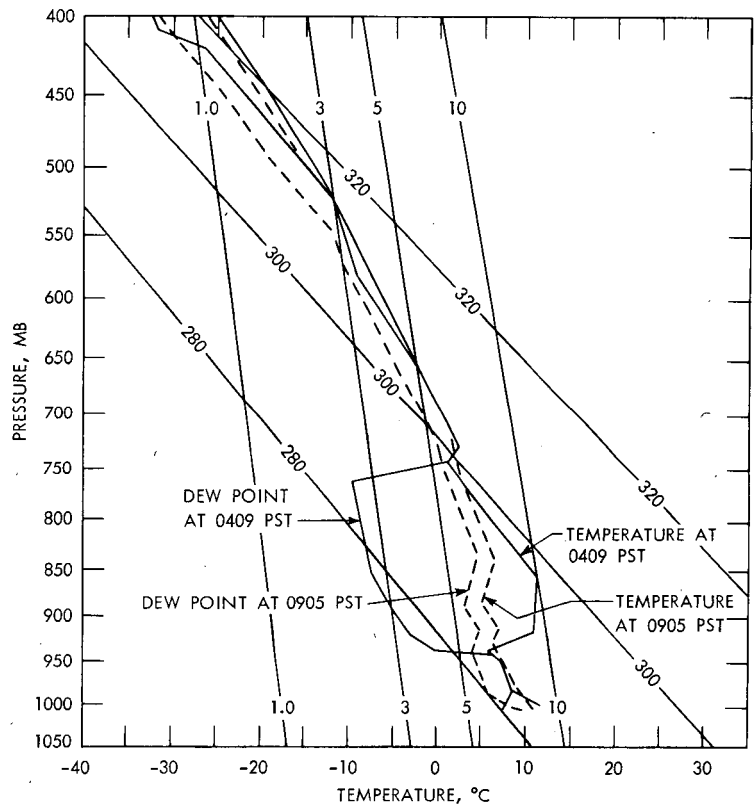

Fig. 7—Vertical distribution of temperature and humidity at 0409 PST at San Nicolas and at 0905 PST at Point Arguello on Feb. 7, 1962.

The concentration of debris in rain formed by the coalescent growth of tiny droplets should be greater than that in rain formed by diffusional growth of ice crystals since many more nucleation particles per drop of rain are involved in the former process. However, coalescent growth occurs mostly in the lower levels of the atmosphere where there are greater amounts of condensation nuclei from terrestrial origin. Since ^{90}Sr-bearing particles are of stratospheric origin, the expected increase in all water-growth raindrops may not be very large. In five storms that occurred during our studies of large-scale uplift in central Pennsylvania, the precipitation growth changed from an ice–water mechanism to an all-water mechanism. Such changes occurred in periods of precipitation from single air masses, with other cloud parameters such as tops and ceilings relatively constant. The data are shown in Table 2. The ^{90}Sr concentration changed by a factor of about 3.5 in going from an ice to an all-water mechanism. The factor was about the same for the periods of pre- and post-U.S.S.R. testing in the fall of 1961.

Table 2—INFLUENCES OF PRECIPITATION MECHANISM AND FRONTAL PASSAGE ON ^{90}Sr CONCENTRATION

Storm	Increase factor due to mechanism change	Increase factor due to frontal passage
Jan. 12 and 13, 1960	2.5	3.5
Nov. 28 and 29, 1960		13.3
Feb. 28 and Mar. 1, 1961	3.5	
Mar. 8 and 9, 1961		12.5
Average, pre-U.S.S.R. testing Sept. 1, 1961	3.0 ± 0.5	9.8 ± 4.2
Dec. 9 and 10, 1961	5.4	
Dec. 11 and 12, 1961	2.6	3.6
Jan. 6 and 7, 1962	3.5	2.9
Average, post-U.S.S.R. testing Sept. 1, 1961	3.8 ● 1.0	3.3 ± 0.4
Overall average	3.5 ± 1.3	7.2 ± 4.6

Fronts and Trough Lines Several observations have been made of greater nuclear-debris concentrations in air near frontal zones and trough lines. For example, Miyake *et al.*[27] noted that the concentration of ^{90}Sr increases in the frontal zone of extratropical cyclones. This phenomenon has been observed in both our Pennsylvania and Pacific Coast cyclone studies. In five storms examined in the eastern United States, the ^{90}Sr concentration following frontal passage increased by a factor of between 3 and 13. These data are shown in Table 2. In the Santa Barbara, Calif., cyclone study, an increase by a factor of more than 10 was noted (see Fig. 6) just prior to the passage of the trough line at 500 mb.

The concentration change may also be related to the distance from the collection site to the trough line aloft. Evidence for this relation was seen in simultaneous collections[23] made at Palo Alto and Santa Barbara during January 1962 when a trough line oriented east–west moved slowly southward. The ^{90}Sr concentration increased at Santa Barbara and simultaneously decreased at Palo Alto as the trough line at 500 mb traveled south.

This increase in ^{90}Sr concentration in frontal zones may be due to any of several changing cloud parameters. For example, the vertical extent of the clouds usually increases in the frontal zone, and the freezing level may change abruptly. In addition, the existence of dry layers of recent stratospheric air, as suggested by Danielsen[6] and Staley,[7] may be responsible for the observed ^{90}Sr-concentration increase.

Stratification of Nuclear Debris In a given air mass, the vertical distribution of reactive materials should be a function of the vertical distribution of stability. Thus in regions where the vertical distribution of eddy mixing

varies considerably from day to day, the ^{90}Sr concentration should be a continuous function with height. In areas where temperature inversions persist at approximately the same height for weeks or months, such as along the west coast of the United States or in the Tradewind Belt, stratification of nuclear debris may be expected. Our first observation of this effect was noted in the Santa Barbara cyclone study.[22] From Figs. 6 and 7 it is deduced that the rain falling from the upper altostratus layer evaporated in the dry air below, producing strong cooling that led to the removal of the inversion above the surface marine layer. The sudden infusion of the marine layer into the precipitating system appears to be responsible for the brief but sharp decrease in the ^{90}Sr concentration and the corresponding increase in the rainfall rate. The dilution of the upper-layer rainwater may be linked to an initial difference in air concentration below and above the temperature inversion. This effect is currently being studied in greater detail as part of the orographic rain study underway along the slopes of the Mauna Loa Volcano on the Island of Hawaii.

REFERENCES

1. P. Kruger, L. P. Salter, and C. L. Hosler, Meteorological Influences on Sr^{90} Fallout Concentrations in Precipitation: Part 1, Large-scale Uplift, in Radioactive Fallout from Nuclear Weapons Tests, A. W. Klement, Jr. (Ed.), USAEC Report TID-7632, pp. 242-255, February 1962.
2. L. P. Salter, P. Kruger, and C. L. Hosler, Sr^{90} Concentration in Precipitation from Large-Scale Uplift, *J. Appl. Meteorol., 1:* 357-365 (1962).
3. P. Kruger and C. L. Hosler, Meteorological Evaluation of Radioactive Fallout, USAEC Report NSEC-62, Nuclear Science and Engineering Corp., Mar. 31, 1962.
4. P. Squires, Penetrative Downdrafts in Cumuli, *Tellus, 10:* 381 (1958).
5. H. R. Byers, *General Meteorology,* 3rd Ed., McGraw-Hill Book Company, Inc., New York, 1959.
6. E. F. Danielsen, The Laminar Structure of the Atmosphere and its Relation to the Concept of a Tropopause, *Arch. Meteorol. Geophys. Bioklimatol., Ser. A, 11*(H.3): 293 (1959).
7. D. O. Staley, On the Mechanism of Mass and Radioactivity Transport from Stratosphere to Troposphere, *J. Atmos. Sci., 19:* 450 (1962).
8. P. Kruger and C. L. Hosler, Sr^{90} Concentration in Precipitation from Convective Showers, *J. Appl. Meteorol., 2:* 379-389 (1963).
9. S. M. Greenfield, Rain Scavenging of Radioactive Particulate Matter from the Atmosphere, *J. Meteorol., 14:* 115 (1957).
10. I. Langmuir, The Production of Rain by Chain-reaction in Cumulus Clouds at Temperatures above Freezing, *J. Meteorol., 5:* 175 (1948).
11. L. M. Vaughan and W. A. Perkins, The Washout of Aerosol Particles and Gases by Rain, Technical Report No. 88, Aerosol Laboratory, Stanford University, 1961.
12. H. Landsberg, Atmospheric Condensation Nuclei, *Gerlands Beitr. Geophys. Suppl. Bd. III, Erg. d Kosm. Phys., 155,* (1938).
13. W. G. Durbin and R. J. Murgatroyd, A Series of Measurements from Aircraft of Freezing and Condensation and Salt Nuclei over Southern England, *Nubila, 6*(1): 55-73 (1964).

14. C. F. Junge and J. E. Manson, Stratospheric Aerosol Studies, *J. Geophys. Res., 66:* 2163-2182 (1961).
15. P. Kruger, D. R. Booker, L. G. Davis, and C. L. Hosler, Radioactive Fallout in Convective Shower Precipitation, USAEC Report HNS-24, Hazelton-Nuclear Science Corp., June 1963.
16. P. Kruger, L. G. Davis, and C. L. Hosler, Sr^{90} Concentration in Convective Shower Precipitation, Spring 1963, USAEC Report HNS-50, Hazelton-Nuclear Science Corp., June 1964.
17. U. S. Public Health Service, Reported Nuclear Detonations, December 1962, *Radiological Health Data, 4:* 60 (1963).
18. P. Kuroda, Radioactive Fallout, Annual Progress Report, AEC Contract AT (40-1)-2529, University of Arkansas, Dec. 31, 1963.
19. J. Z. Holland, Stratospheric Radioactivity Data Obtained by Balloon Sampling, USAEC Report TID-5555, May 1959.
20. K. C. Giles, Distribution of Radioactivity with Respect to Tropopauses and Jet Streams, in Fallout Program Quarterly Summary Report, USAEC Report HASL-115, pp. 184-257, Health and Safety Laboratory, 1964.
21. R. D. Elliott and E. L. Hovind, On Convective Bands Within Pacific Coast Storms and Their Relation to Storm Structure, *J. Appl. Meteorol., 3:* 143-154 (1964).
22. P. Kruger and A. Miller, Radiochemical Fallout Study of a Pacific Cyclonic Storm, *J. Geophys. Res., 69:* 1469-1480 (1964).
23. P. Kruger, G. Hamada, and A. Miller, Radioactive Fallout in California During the Winter, 1961-2, *J. Appl. Meteorol., 2:* 608-613 (1963).
24. P. Kruger, Synoptic-Scale Fallout Patterns in Precipitation along the Pacific Coast of the United States, Technical Report No. 31, Civil Engineering Department, Stanford University, February 1964.
25. J. F. Bleichrodt, J. Bloh, R. H. Dekker, and C. J. H. Lock, The Dependence of Artificial Radioactivity in Rain on Rainfall Rate, *Tellus, 11:* 404-407 (1959).
26. B. J. Mason, *The Physics of Clouds,* p. 234, Oxford Press, London, 1957.
27. Y. Miyake, K. Saruhashi, Y. Katsuragi, and T. Kanazawa, Seasonal Variation of Radioactive Fallout, *J. Geophys. Res., 67:* 189-193 (1962).

FISSION PRODUCTS IN THE ATMOSPHERE AND IN RAIN

P. K. KURODA, PENTTI KAURANEN,* B. D. PALMER,
K. K. MENON, and L. M. FRY
University of Arkansas, Fayetteville, Arkansas

ABSTRACT

The concentrations of ^{89}Sr, ^{90}Sr, ^{140}Ba, ^{141}Ce, and ^{144}Ce in individual samples of rain and snow have been measured radiochemically at Fayetteville, Ark., for the past several years. Certain features of the isotopic ratio data may be explained as being due to atmospheric fractionation of nuclear debris taking place on a global scale. High concentrations of ^{54}Mn, ^{124}Sb, and ^{125}Sb were observed in the air-filter samples collected in connection with Project Star Dust in 1962 and 1963. The $^{125}Sb/^{90}Sr$ ratio in 1963 samples was found to correspond to values reported for the production ratio in thermonuclear explosions, but some samples collected at high northern altitudes in 1962 showed an excess of ^{125}Sb. It appears that ^{125}Sb was partly produced through second-order neutron capture in ^{123}Sb. A sudden increase of ^{54}Mn concentration was observed in April 1963 at an altitude range of 30,000 to 35,000 ft.

INTRODUCTION

Levels of ^{89}Sr, ^{90}Sr, ^{140}Ba, ^{141}Ce, and ^{144}Ce in individual samples of rain and snow have been measured radiochemically at Fayetteville, Ark., during the past several years. A set of Project Star Dust high-altitude air-filter samples was received by the University of Arkansas in the fall of 1963, and a study on the distribution of fission products and a number of nonfissiogenic nuclides such as ^{54}Mn and ^{124}Sb has recently been undertaken.

*Present address: Department of Physics, University of Helsinki, Helsinki, Finland.

Samples of rain and snow were collected by means of a sampling system installed on the roof of the Chemistry Building of the University of Arkansas. This paper reviews some of the results obtained so far.

RADIOCHEMICAL PROCEDURES

^{89}Sr, ^{90}Sr, and ^{140}Ba

Radiochemical procedures used for the determination of ^{89}Sr, ^{90}Sr, and ^{140}Ba were essentially the same as those described by Kuroda.[1] Further studies on the radiochemical procedures have recently been carried out by Hodges,[2] and the details will be published elsewhere.

^{141}Ce and ^{144}Ce

A radiochemical procedure which has recently been developed at the University of Arkansas[3] was used for the determination of radiocerium. The method depends on the oxidation–reduction and liquid–liquid extraction cycle with the use of a tri-*n*-butyl phosphate (TBP)–carbon tetrachloride mixture (20% TBP by volume) as the organic solvent.

^{124}Sb and ^{125}Sb

Radiochemical procedures that were used for ^{124}Sb and ^{125}Sb have been recently described by Kauranen.[4]

^{54}Mn

After the antimony fraction was removed, sulfides of iron, manganese, ruthenium, cobalt, etc., were precipitated by the addition of NH_3 and $(NH_4)_2S$. The precipitate was leached with 1% HCL. The HCL solution was then boiled to expel H_2S. Ammonium hydroxide was added to precipitate iron etc., and manganese was precipitated again as the sulfide. The precipitate was leached with 0.5*N* HNO_3, the solution was made 2*N* in HNO_3, and saturated $NaBrO_3$ solution was added. The precipitate of MnO_2 was filtered on a glass-fiber filter paper, washed with water and acetone, dried, weighed, and counted with a 3- by 3-in. NaI(Tl) crystal and a multichannel analyzer.

The chemical yield was determined after counting. The precipitate of MnO_2 was dissolved in H_2O_2, diluted, and filtered, and 6*N* HNO_3 was added to the filtrate. A slight excess amount of solid $NaBiO_3$ was added, and the solution was filtered through a fritted glass filter. A known excess of standard $FeSO_4$ solution was added, in excess, to the filtrate.

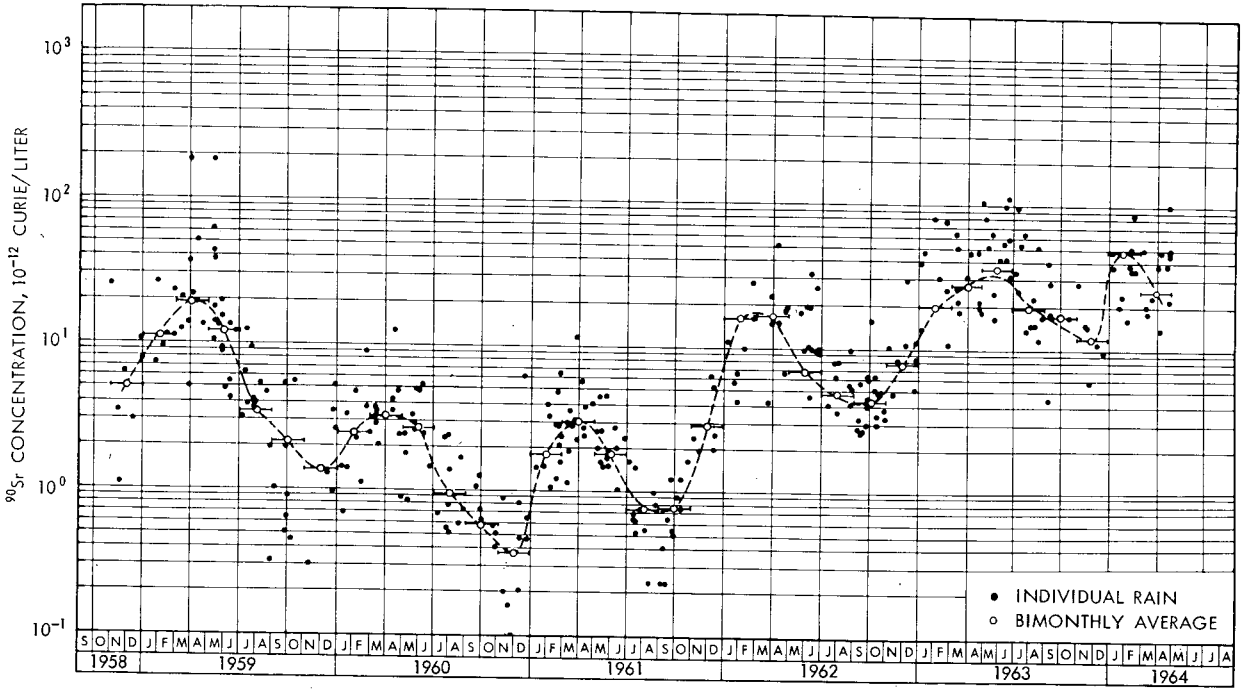

Fig. 1—^{90}Sr concentrations in rain at Fayetteville, Ark., during the period Oct. 31, 1958, through Apr. 26, 1964.

This excess was then determined by titrating with a standard $KMnO_4$ solution. A blank experiment was also performed. The chemical yield of manganese was usually between 25 and 50%.

RESULTS AND DISCUSSIONS

Isotopic Ratios in Rain

Figure 1 shows the variation of the concentration of ^{90}Sr in individual rains as well as in the bimonthly average concentrations. The data show a marked seasonal variation.

Figure 2 shows the variation of the $^{140}Ba/^{90}Sr$ and $^{140}Ba/^{89}Sr$ ratios in rain since November 1961. Owing to the short half-life of ^{140}Ba, these ratios are sensitive to the injection of fresh nuclear debris. During a test moratorium period, the isotope ratios decay linearly on a semilog scale, as can be seen in the figure. The response of the $^{140}Ba/^{90}Sr$ ratio to the late December nuclear explosions appears to have been delayed almost two months, and the $^{140}Ba/^{90}Sr$ ratios in rain reached the straight line ab in Fig. 2 only after March 1964. A very similar trend is seen in the $^{140}Ba/^{89}Sr$ ratio data. The straight line cd has a slope corresponding to the difference between the decay of ^{140}Ba and ^{89}Sr.

The observed data may be explained as being due to the fact that some of the nuclear explosions that occurred in the late fall of 1962 were high-altitude shots, and hence the debris did not reach the lower atmosphere immediately.

Figure 3 shows the $^{89}Sr/^{90}Sr$ ratios in rain. Data obtained at Lemont, Ill.,[5] and at Milford Haven, England,[6] are also plotted. Accurate measurement of the $^{89}Sr/^{90}Sr$ in nuclear debris is tedious and difficult. The radiochemical techniques involved in the determination of the $^{89}Sr/^{90}Sr$ ratio in nuclear debris have recently been thoroughly reinvestigated by Hodges,[2] and, as a result of improvement in technique, the recent data are probably more accurate than old data. A rather large scatter of the experimental points seen in the data prior to 1962 might be at least partly due to experimental errors.

The straight line ab in Fig. 3 has a slope corresponding to the 50.4-day half-life of ^{89}Sr. The $^{89}Sr/^{90}Sr$ ratios in rain after the December 1962 nuclear explosions approached the straight line ab asymptotically and joined it at the end of April. By a comparison of this trend with those observed in the cases of the $^{140}Ba/^{90}Sr$ and the $^{140}Ba/^{89}Sr$ ratio data, shown in Fig. 2, an impression is obtained that the response of the $^{89}Sr/^{90}Sr$ ratios to the late December 1962 nuclear explosions were somewhat slower than those of the $^{140}Ba/^{90}Sr$ and the $^{140}Ba/^{89}Sr$ ratios.

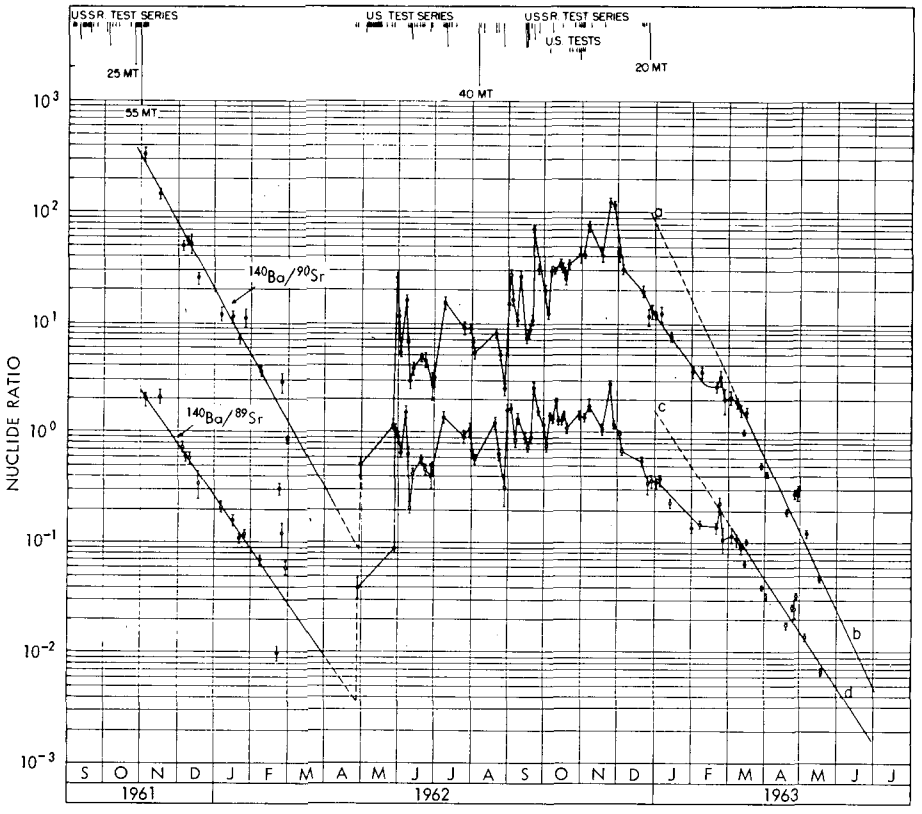

Fig. 2—$^{140}Ba/^{90}Sr$ and $^{140}Ba/^{89}Sr$ in individual rain samples at Fayetteville, Ark.

This difference might be an indication of nonuniform mixing of these fission products due to fractionation. Let us compare the mass chains 89, 90, and 140:

$$^{89}_{36}Kr \xrightarrow{\beta^-} {}^{89}_{37}Rb \xrightarrow{\beta^-} {}^{89}_{38}Sr \xrightarrow{\beta^-}$$
3.2 min 15 min 50.4 days

$$^{90}_{36}Kr \xrightarrow{\beta^-} {}^{90}_{37}Rb \xrightarrow{\beta^-} {}^{90}_{38}Sr \xrightarrow{\beta^-}$$
33 sec 2.9 min 28 years

$$^{140}_{54}Xe \xrightarrow{\beta^-} {}^{140}_{55}Cs \xrightarrow{\beta^-} {}^{140}_{56}Ba \xrightarrow{\beta^-}$$
16 sec 66 sec 12.8 days

In the case of the mass chains 89 and 90, the most probable fragment charge lies near Z = 36, which corresponds to the gaseous element krypton; hence the fission products would exist predominantly as the gaseous precursors ^{89}Kr and ^{90}Kr shortly after a nuclear explosion.

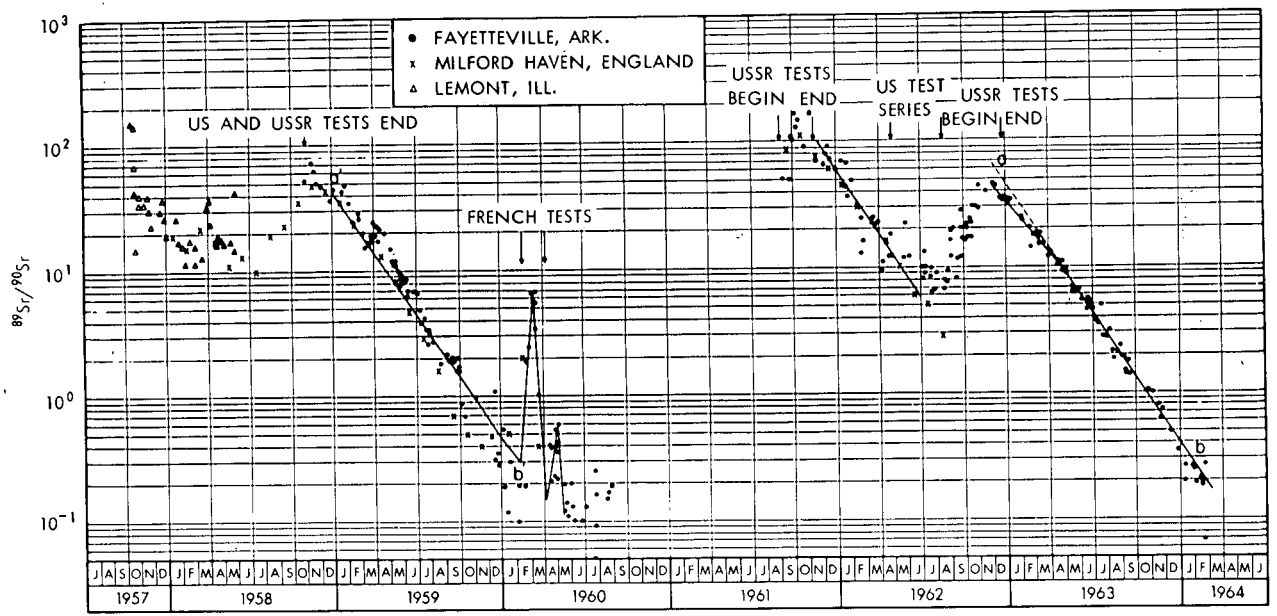

Fig. 3—$^{89}Sr/^{90}Sr$ in individual rain samples at Fayetteville, Ark., Milford Haven, England, and Lemont, Ill.

Similarly, in the case of the mass chain 140, the most probable fragment charge lies near Z = 54; hence the gaseous nuclide ^{140}Xe plays an important role.

According to Edvarson et al.,[7] particle formation occurs about 15 to 20 sec after the explosion of a thermonuclear device of the order of magnitude of 1 Mt. The half-life of ^{140}Xe is shorter than that of ^{90}Kr, whereas the half-life of ^{89}Kr is much longer. Thus the fission products belonging to the mass chain 140 will have a much better probability of being incorporated into particles that start growing immediately after a nuclear explosion than those belonging to the mass chain 89. This would tend to enrich ^{140}Ba in larger particles and ^{89}Sr in smaller particles.

Figure 4 compares the $^{141}Ce/^{144}Ce$ ratio data with the $^{89}Sr/^{90}Sr$ and the $^{140}Ba/^{89}Sr$ ratio data. Here again, an impression is obtained that the

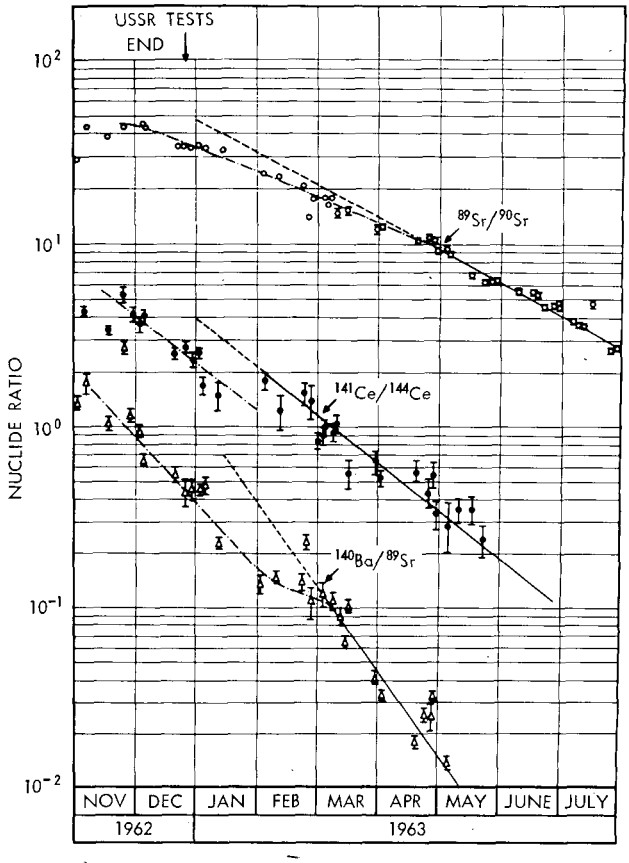

Fig. 4—$^{141}Ce/^{144}Ce$, $^{89}Sr/^{90}Sr$, and $^{140}Ba/^{89}Sr$ ratios in rain after the cessation of nuclear tests in December 1962.

response of the $^{89}Sr/^{90}Sr$ ratio data to the late December 1962 nuclear explosions were slower than that of the $^{141}Ce/^{144}Ce$ ratio data.

^{54}Mn, ^{124}Sb, and ^{125}Sb in the Stratosphere

A few weeks after a nuclear explosion, the antimony fraction of fission debris consists predominantly of 2.7-year ^{125}Sb. This nuclide has previously been determined in ground air by Anderson et al. [8] and by Edvarson and Löw.[9] Crooks et al.[10] determined ^{125}Sb in air and rainwater, and Fry and Karras[11] observed it in rain. Antimony-125 data from balloon samples collected from the upper stratosphere (above 60,000 ft) have been reported by Salter[12] from Project Ashcan.

Also 60-day ^{124}Sb, a shielded nucleus with a very low primary fission yield, has recently been observed in the atmosphere; its concentration in some cases was extremely high. This nuclide was most probably produced through the (n,γ) reaction from ^{123}Sb. In 1962, ^{124}Sb was detected by Gustafson et al.[13] between 60,000 and 100,000 ft above Thule, Greenland, with a balloon-borne gamma spectrometer. Later, high ^{124}Sb concentrations in the upper stratosphere were reported by Salter.[12] His report also indicates that the U.S.S.R. tests in late 1961 and again in late 1962 are the sources of the observed ^{124}Sb. Because of its short half-life, the large amounts of ^{124}Sb that were observed in 1963 were assumed to have been produced by tests only in the year 1962.

Samples from high latitudes and altitudes collected in July and September 1962 show an unusual composition (Fig. 5). The main gamma peak is due to ^{54}Mn that, according to Holland,[14] was produced predominantly in one single 55- to 60-Mt U.S.S.R. detonation in October 1961. The same samples also contain an exceptionally high amount of ^{125}Sb, which deserves some discussion.

The thermal fission yield of mass chain 125 is very low (0.021% according to Katcoff[15]), but for fast neutrons it is considerably higher. For thermonuclear explosions, Hallden et al.[16] report a cumulative yield of 0.29% for ^{125}Sb, based on a half-life of 2.0 years. We have used the somewhat longer half-life of 2.7 years, which has been recently confirmed by two investigations: Klehr and Voigt[17] and Wyatt et al.[18] This value changes the yield of ^{125}Sb to 0.394%. Hallden's yield for ^{90}Sr is 3.50%, which gives the activity ratio $^{125}Sb/^{90}Sr = 1.16$ for fresh thermonuclear debris (allowing for the decay of 9.4-day ^{125}Sn). Tables 1 and 2 give the experimental values for this activity ratio (the data for 1963 have been corrected for decay to Jan. 1, 1963). In most cases, the experimental data are very close to the calculated ratio. However, the samples from the high northern atmosphere in July and September 1962 show $^{125}Sb/^{90}Sr$ activity ratios between 3 and 5 (Table 2). Salter[12] reports $^{125}Sb/^{90}Sr$ ratios of up to about 8 for some balloon samples collected at San Angelo, Tex., in July and August 1962.

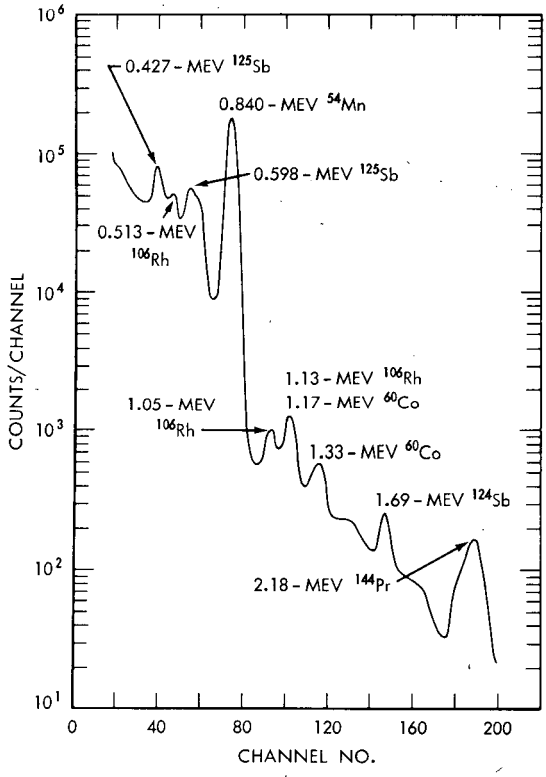

Fig. 5—Gamma spectrum of Star Dust sample high in activation products. Sample collected between 60 to 70°N and 00 to 07°W on Sept. 7, 1962. The 800-min spectrum was taken 13.5 months after collection.

These numbers are even higher than the $^{125}Sb/^{90}Sr$ ratio from the 14-Mev neutron fission of ^{238}U. For example, Broom[19] reported a value of 2.5 for this ratio. These data indicate a nonfission origin for most of the ^{125}Sb in the previously mentioned exceptional samples.

Antimony-125 can be produced by activation through the following three reactions:

$$^{124}Sn(n,\gamma)^{125}Sn \xrightarrow{\beta^-} {}^{125}Sb$$

$$^{125}Te(n,p)^{125}Sb$$

$$^{123}Sb(n,\gamma)^{124}Sb(n,\gamma)^{125}Sb$$

If tin is activated, ^{113}Sn should also be produced. The tin fraction was isolated from several samples and counted, but no ^{113}Sn could be detected (activity was less than 3 to 4 dis/min, whereas that of ^{125}Sb in the same samples was between 100 and 10,000 dis/min). No ^{121}Te could be detected in the same way.

Table 1 — ^{125}Sb AND ^{90}Sr IN THE NORTHERN ATMOSPHERE, JULY–SEPTEMBER 1962

Sampling dates	Latitude	Altitude, 10^3 ft	^{125}Sb, dis/min per 10^3 scf	^{90}Sr, dis/min per 10^3 scf	$^{125}Sb/^{90}Sr$, curie/curie
July 13	15 to 21°N	65.5 to 66.5	339	447	0.76
July 26	61 to 64°N	45	346	336	1.03
July 26	61 to 64°N	66.5	1820	430	4.2
July 27	31 to 35°N	67.3 to 67.7	1870	595	3.1
Sept. 7	67 to 73°N	64 to 60	1750	407	4.3
Sept. 7	61°N to 67°N	62.5 to 63.6	2100	447	4.7
August*	31°N	60	752	454	1.7
August*	31°N	71	5900	735	8.0
August*	31°N	88	163	59	2.8

*Balloon sample, from report by Salter.[12]

Table 2 — CONCENTRATIONS* OF ^{124}Sb, ^{125}Sb, AND ^{90}Sr IN THE NORTHERN ATMOSPHERE BETWEEN 60 AND 72°N IN 1963

Sampling dates	Altitude, 10^3 ft	^{124}Sb, dis/min per 10^3 scf	^{125}Sb, dis/min per 10^3 scf	^{90}Sr, dis/min per 10^3 scf	$^{124}Sb/^{90}Sr$, curie/curie†	$^{125}Sb/^{90}Sr$, curie/curie†
Jan. 22	65	(<1,000)	2,560	4,360	(<0.30)	0.56
Jan. 24	45	(<150)	450	420	(<0.30)	0.96
Apr. 16	25		53	46		1.22
Apr. 16	30	(35)	516	495	(0.23)	1.12
Apr. 16	35	(86)	1,000	1,010	(0.28)	1.06
Apr. 16	45	496	2,750	2,400	0.60	1.23
Apr. 16	55	18,400	4,870	5,330	10.3	0.98
Apr. 16	65	15,600	2,440	2,380	21.5	1.11
July 16	40	49	562	597	0.75	1.07
July 16	50	764	1,470	1,700	4.0	0.98
July 16	60	5,720	3,055	3,320	15.7	1.04
Sept. 3	55	690	1,600	1,570	6.4	1.24
Sept. 3	65	2,240	1,780	1,705	21.0	1.22
Sept. 5	30	(<1)	22	23	(<0.4)	1.22
Sept. 22‡	43	(13)	117	135	(2.0)	1.03

*For values in parentheses, the standard deviation for counting exceeds 20%.
†*Corrected for decay to Jan. 1, 1963.*
‡Latitude, 41 to 44°N.

Thus the most likely source for the excess ^{125}Sb seems to be second-order neutron capture in ^{123}Sb. More than one year after collection, the samples with high ^{125}Sb still contained a measurable quantity of ^{124}Sb, which indicates that originally very large amounts of ^{124}Sb were produced. The high ^{54}Mn content shows that structural or other materials of the nuclear device were exposed to very high neutron fluxes. Calculations on the neutron flux in a thermonuclear explosion

have been carried out by Dorn[20] and by Hoff and Dorn[21] on the basis of transuranium-element production. The results indicate an exposure of material to the order of several times 10^{24} neutrons/cm^2 with neutron energies ranging from thermal (< 10 kev in the bomb) to more than 14 Mev. Up to 17 successive neutron captures have been found to take place in exposed uranium. It is easy to show that an exposure of this magnitude will provide for a large amount of multiple neutron capture in antimony, even if a fast-neutron-capture cross section of only 0.1 barn is used for the antimony isotopes.[22]

It may be also pointed out in this connection that the samples collected in 1963 which are high in ^{124}Sb content do not show exceptional ^{125}Sb content. This indicates that the ^{124}Sb produced in late 1962 originated in a lower neutron flux.

Figure 6 shows the distribution of ^{124}Sb in April and July 1963. High ^{124}Sb concentrations occurred also in the middle and tropical latitudes during the spring and summer of 1963, generally at somewhat higher altitudes than in the polar samples. The concentration isolines have an upward slope from the polar to the tropical stratosphere, and a clear increase of the ^{124}Sb content in the tropical stratosphere can be observed between April and July. If nuclear tests in the polar stratosphere were the only sources of ^{124}Sb, these findings would give strong support to the theory of eddy diffusion for the horizontal transport of material in the stratosphere, as described by Newell[23] and Friend et al.[24] It would apparently be difficult to explain the southward move-

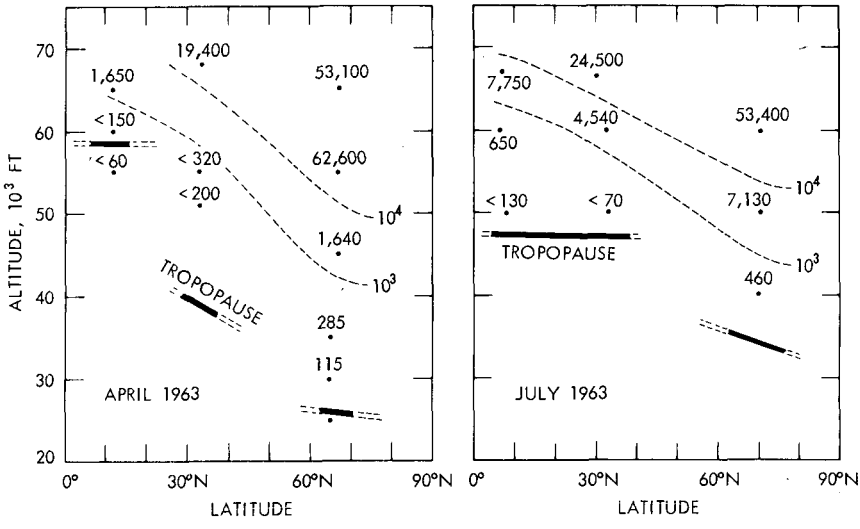

Fig. 6 — ^{124}Sb concentrations in the atmosphere in April and July 1963 in disintegrations per minute per 10^3 scf. Tropical (~10°N) and middle (~30°N) latitude values are estimated from gross gamma-ray spectra.

ment of ^{124}Sb in terms of the Brewer–Dobson model,[25] which implies a meridional northward movement of stratospheric air. However, since definite information on the ^{124}Sb production sites and times is not available at present, this reasoning is, of course, inconclusive.

Table 3 shows the distribution of ^{54}Mn in the northern stratosphere. High concentrations of ^{54}Mn were observed in April 1963 at

Table 3—CONCENTRATIONS OF ^{54}Mn AND ^{90}Sr IN THE NORTHERN ATMOSPHERE BETWEEN 60 AND 73°N

Sampling dates	Altitude, 10^3 ft	^{54}Mn, dis/min per 10^3 scf	^{90}Sr, dis/min per 10^3 scf	$^{54}Mn/^{90}Sr$*
July 26, 1962	45	706	336	2.2
July 26, 1962	67	17,734	430	4.4
Sept. 7, 1962	60–64	10,012	407	2.9
Sept. 7, 1962	63–64	13,036	447	3.5
Jan. 22, 1963	65	6,950	4,360	2.7
Jan. 24, 1963	45	870	420	3.3
Apr. 16, 1963	25	95	46	3.2
Apr. 16, 1963	30	3,140	495	10.0
Apr. 16, 1963	35	8,400	1,010	13.1
Apr. 16, 1963	45	4,750	2,400	3.1
Apr. 16, 1963	55	3,060	5,330	0.9
Apr. 16, 1963	65	5,330	2,380	3.5
July 16, 1963	40	1,030	597	2.7
July 16, 1963	50	2,010	1,700	1.9
July 16, 1963	60	3,550	3,320	1.7
Sept. 3, 1963	55	1,870	1,570	1.9
Sept. 3, 1963	65	1,530	1,705	1.4
Sept. 5, 1963	30	31	23	2.1
Sept. 22, 1963	43	210	135	2.5

*As of July 1, 1962.

an altitude range of 30,000 to 35,000 ft, but no sudden change of the ^{124}Sb and ^{125}Sb concentrations relative to ^{90}Sr was observed at this altitude. Thus it appears that the ^{54}Mn was produced independently in one of the nuclear devices detonated during the fall of 1962. It is interesting to note that the ^{54}Mn concentration at this altitude became extremely low by September 1963.

Concentration of fission products from the nuclear detonation by Communist China on Oct. 16, 1964, are given in Fig. 7. Determinations were made from rain collected at Fayetteville, Ark., on Oct. 26, 1964.

ACKNOWLEDGMENTS

The Project Star Dust filter samples were made available by the U. S. Defense Atomic Support Agency. Flight data supplied by H. W. Feely, Isotopes, Inc., Westwood, N. J., are gratefully acknowledged.

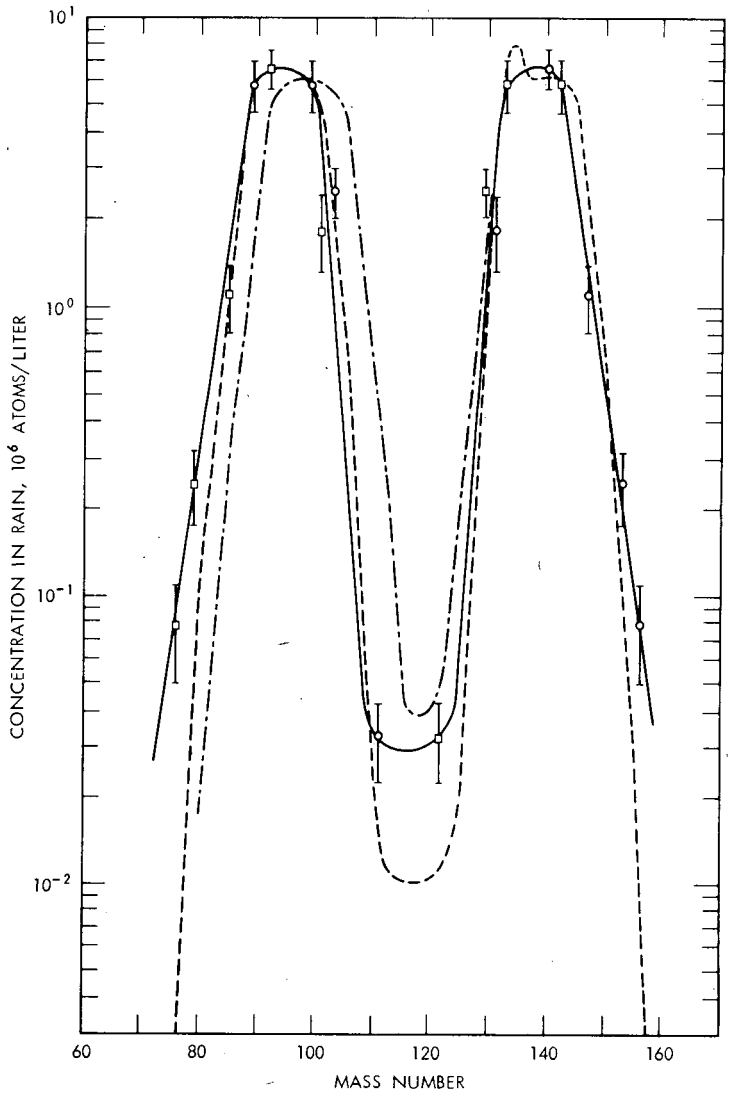

Fig. 7—Fission products in the Oct. 26, 1964, rain collected at Fayetteville, Ark. The concentrations in rain are expressed in terms of 10^6 atoms per liter of rain as of Oct. 16, 1964 (the date of the nuclear explosion). The vertical bars indicate the magnitude of decay of the longer lived nuclides since December 1962.

REFERENCES

1. P. K. Kuroda, Radiostrontium in Rain Water, in Radiological Physics Division Semiannual Report, July through December 1957, USAEC Report ANL-5829, p. 167, Argonne National Laboratory, February 1958.
2. H. L. Hodges, Radiochemical Determination of ^{90}Sr, ^{89}Sr, and ^{140}Ba in Nuclear Debris, Ph. D. Dissertation, University of Arkansas, January 1964.

3. M. P. Menon, K. K. Menon, and P. K. Kuroda, On the Stratospheric Fallout of Bomb-produced Cerium Isotopes, *J. Geophys. Res., 68:* 4495-4499 (1963).
4. Pentti Kauranen, Radioactive Antimony Isotopes in the Atmosphere, *J. Geophys. Res., 69*(23): 5075-5080 (1964).
5. P. K. Kuroda, On the Stratospheric ^{90}Sr Fallout, USAEC Report ANL-5920, pp. 1-40, Argonne National Laboratory, 1958.
6. R. S. Cambray, E. M. R. Fisher, T. P. Spicer, C. G. Wallace, and T. J. Webber, Radioactive Fall-out in Air and Rain; Results to the Middle of 1962, Report AERE-R-4094, United Kingdom Atomic Energy Authority, November 1962.
7. K. Edvarson, K. Löw, and J. Sisefsky, Fractionation Phenomena in Nuclear Weapons Debris, *Nature, 184:* 1771-1774 (1959).
8. W. Anderson, R. E. Bentley, R. P. Parker, J. O. Crookall, and L. K. Burton, Comparison of Fission Product and Beryllium-7 Concentrations in the Atmosphere, *Nature, 187:* 550 (1960).
9. K. Edvarson and Kersten Löw, Concentration of Some Fission Product Nuclides in Ground-level Air, *Nature, 188:* 125 (1960).
10. R. N. Crooks, T. W. Ewett, E. M. R. Fisher, M. B. Lovett, and R. G. Osmond, Radioactive Fallout in Air and Rain; Results to the Middle of 1961, Report AERE-R-3766, United Kingdom Atomic Energy Authority, October 1961.
11. L. M. Fry and M. Karras, unpublished data.
12. L. P. Salter, High Altitude Balloon Sampling Program, in Fallout Program Quarterly Summary Report, USAEC Report HASL-140, p. 166, Health and Safety Laboratory, Oct. 1, 1963.
13. D. F. Gustafson, R. B. Keener, G. A. McGinnis, and R. A. Soller, Fission Product Radioactivity in the North Polar Stratosphere, *Science, 138:* 434 (1962).
14. J. Z. Holland, Problems Arising in the Study of Radioactive Contamination of the Upper Atmosphere, in Proceedings of the International Conference on Radioactive Pollution of Gaseous Media, Saclay, France, November 1963, in press.
15. S. Katcoff, Fission-product Yields in Neutron Induced Fission, *Nucleonics, 18*(11): 201 (1960).
16. N. A. Hallden, I. M. Fisenne, L. D. Y. Ong, and J. H. Harley, Radioactive Decay of Weapons Debris, in Fallout Program Quarterly Summary Report, USAEC Report HASL-117, p. 194, Health and Safety Laboratory, Dec. 30, 1961.
17. E. H. Klehr and A. F. Voigt, The Half-life of Antimony-125, *J. Inorg. Nucl. Chem., 16:* 8 (1960).
18. E. I. Wyatt, S. A. Reynolds, T. H. Handley, W. S. Lyon, and H. A. Parker, Half-lives of Radionuclides—II, *Nucl. Sci. Eng., 11:* 74 (1961).
19. K. M. Broom, 14.7 Mev Neutron Induced Fission of ^{238}U, *Phys. Rev., 126:* 627 (1962).
20. D. W. Dorn, Mike Results—Implications for Spontaneous Fission, *Phys. Rev., 126:* 693 (1962).
21. R. W. Hoff and D. W. Dorn, Production of Transuranium Elements in a Thermonuclear Explosion—Anacostia, *Nucl. Sci. Eng., 18:* 110 (1964).
22. D. J. Hughes, Fast Neutron Cross Sections and Nuclear Level Density, *Phys. Rev., 91:* 1423 (1953).
23. R. E. Newell, The General Circulation of the Atmosphere and Its Effects on the Movement of Trace Substances, *J. Geophys. Res., 68:* 3949 (1960).
24. J. P. Friend, H. W. Feely, P. W. Krey, J. Spar, and A. Walton, The High Altitude Sampling Program, Report DASA-1300, Vol. 1, p. 93, Isotopes, Inc., Aug. 31, 1961.
25. G. M. B. Dobson, Origin and Distribution of the Polyatomic Molecules in the Atmosphere, *Proc. Roy. Soc. (London), A236:* 187 (1956).

CHARACTERISTICS OF RELATIVE ^{90}Sr CONCENTRATIONS IN SURFACE AIR

HERBERT L. VOLCHOK
Health and Safety Laboratory, U. S. Atomic Energy Commission,
New York, New York

ABSTRACT

Since taking over the 80th Meridian (West) Air Sampling Program at the beginning of 1963, the Health and Safety Laboratory has slightly enlarged the scope of the program by the addition of a number of sites and has effected some minor operational changes. The 1963 data of air concentration of ^{90}Sr at ground level along the 80th Meridian are presented along with the Naval Research Laboratory data covering the period 1957 and 1962. Almost all sites in 1963 exhibited higher concentrations in 1963 than at any previous time. The $^{89}Sr/^{90}Sr$ ratio indicated that the nuclear debris in the northern hemisphere was relatively well mixed compared to that in the southern hemisphere which showed older debris. When the 1962 and 1963 data are normalized and averaged, very systematic seasonal changes, largely unaffected by the testing program, are observed. Symmetry between the hemispheres is very clearly shown when a four-month offset in time is assumed; thus peak values in the north occur in March and April and in the south, in November and December. A qualitative relation between concentration of ^{90}Sr in air and concentration of ^{90}Sr in precipitation is described.

INTRODUCTION

At the end of 1962, the Health and Safety Laboratory (HASL) assumed responsibility for the 80th Meridian (West) Air Sampling Program, which was formerly conducted by the Naval Research Labora-

tory (NRL). Up until that time, the program, under the direction of Luther B. Lockhart, Jr., had provided one of the most consistent and useful studies of the concentrations and relations of fission products and natural radionuclides in ground-level air.[1] Since taking over the program, HASL has broadened the geographical coverage somewhat by the addition of a number of sampling stations. Figure 1 shows the locations of all the current sites in the ground-level-air program. On the 80th meridian we have added New York City, Westwood, N. J., and Pedro Aguerre Cerda in Antarctica. Other U. S. sites that have been added are Palo Alto, Calif., Seattle, Wash., Appleton, Wisc., Oklahoma City, Okla., and Chattanooga, Tenn.

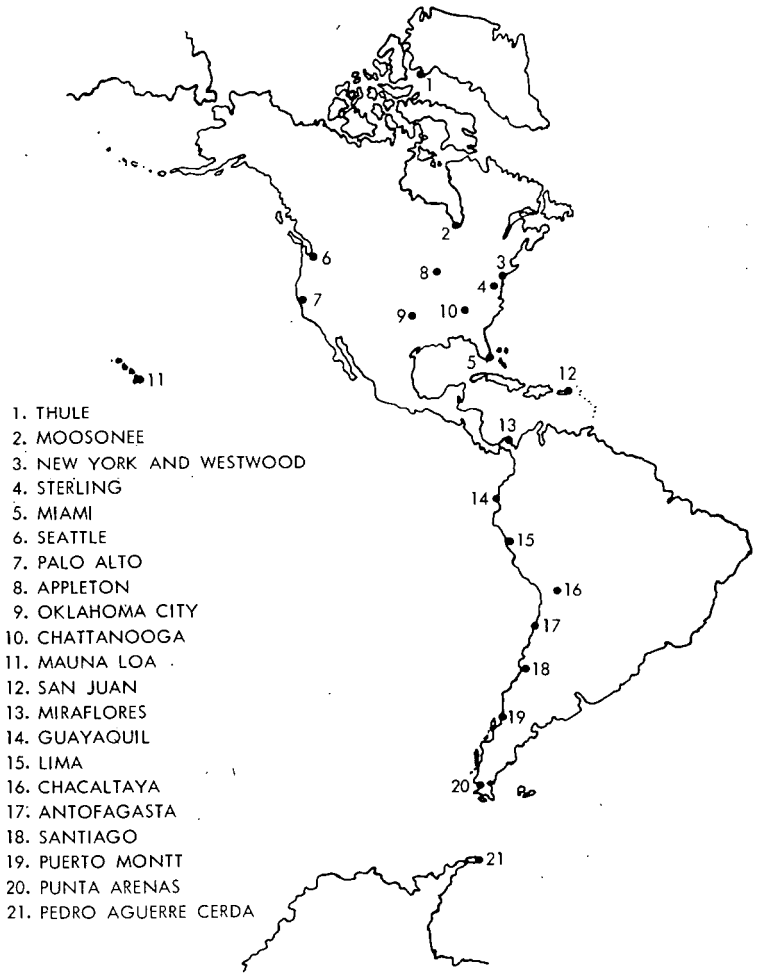

Fig. 1—Ground-level air-sampling sites.

The only other changes of note that have been made in the program are that a different type of filter paper is used, gamma instead of beta counting is used for measuring gross-fission-product radioactivity, and some additional nuclide analyses for special situations are made.

^{90}Sr LEVELS IN 1963

In Fig. 2 we have copied NRL's presentation of ^{90}Sr concentrations in ground-level air of the northern hemisphere along the 80th meridian (west) and have added HASL's 1963 data. It is quite clear that the concentrations at all sites were higher in 1963 than in any previous year. The peak values in 1963 are clearly the highest of all years reported. Generally, the spring peaks in 1963 are quite broad, especially in the

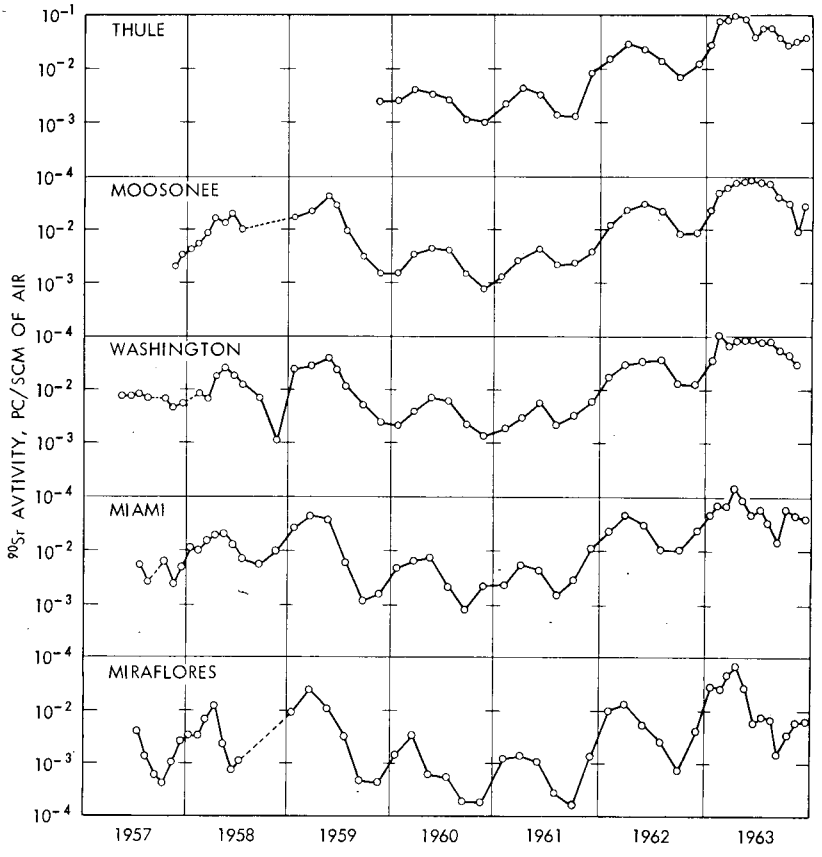

Fig. 2—Concentrations of ^{90}Sr in the air at selected sites in the northern hemisphere along the 80th meridian (west). 1957–1962, NRL data; 1963, HASL data.

higher latitudes. This makes it difficult to delineate arrival time as a function of latitude. The peaks seem to occur in the months of April, May, and June, as in previous years, with no particular trend along the meridian. The high ^{90}Sr concentrations in air for 1963 are in agreement with the high levels of ^{90}Sr deposition,[2] but it is interesting to note that the peak in fallout deposition in the northern hemisphere seems to have occurred a month or two later than the peak observed in the ground-level air.[3]

Figure 3 is a copy of NRL's ^{90}Sr concentration graph for the 80th meridian sites in the southern hemisphere with HASL's 1963 data added. As in the north, the ^{90}Sr air concentrations were generally higher than in previous years; however, they were not as sharply defined as those in the northern hemisphere. No generalized seasonal peak is shown in

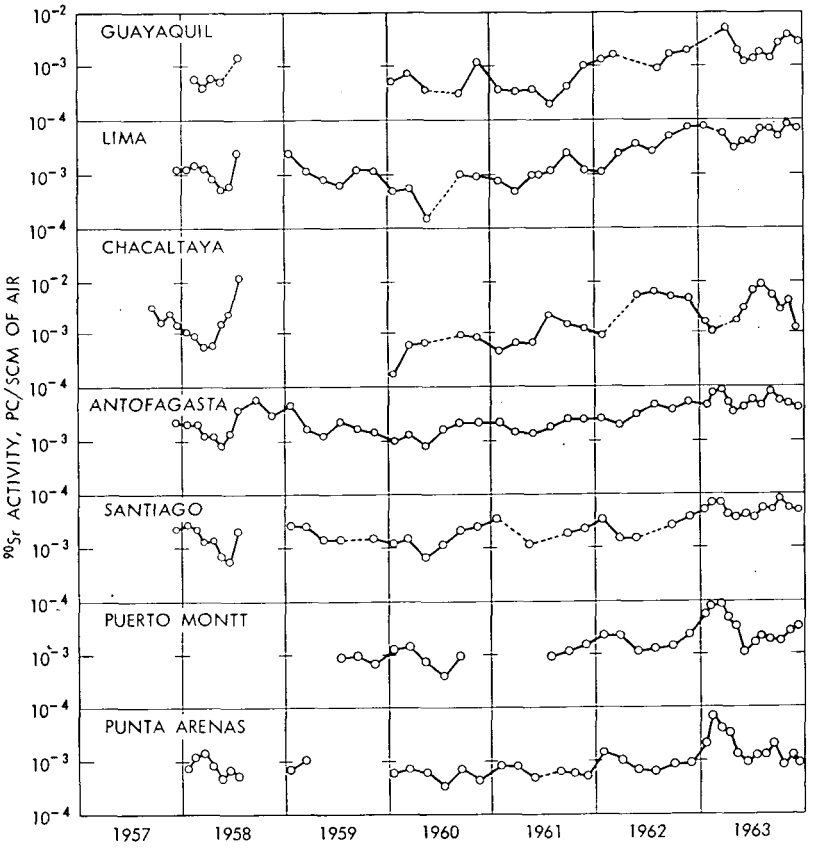

Fig. 3—Concentrations of ^{90}Sr in the air at selected sites in the southern hemisphere along the 80th meridian (west). 1957–1962, NRL data; 1963, HASL data.

these data, although some specific oscillations should be mentioned. For instance, at Chacaltaya a peak in July or August seems to appear quite regularly, whereas at the three southernmost sites, Santiago, Puerto Montt, and Punta Arenas, a peak in the early part of each year seems to appear. These variations are believed to be quite significant and will be referred to again in a later section.

$^{89}Sr/^{90}Sr$ RATIO IN GROUND-LEVEL AIR

A broad impression of the homogeneity of the ground-level air in 1963 can be gained by study of the $^{89}Sr/^{90}Sr$ ratio measured in 80th meridian samples. Figure 4 is a plot of this ratio for sites in the northern hemisphere. Also included on the graph are data from a few

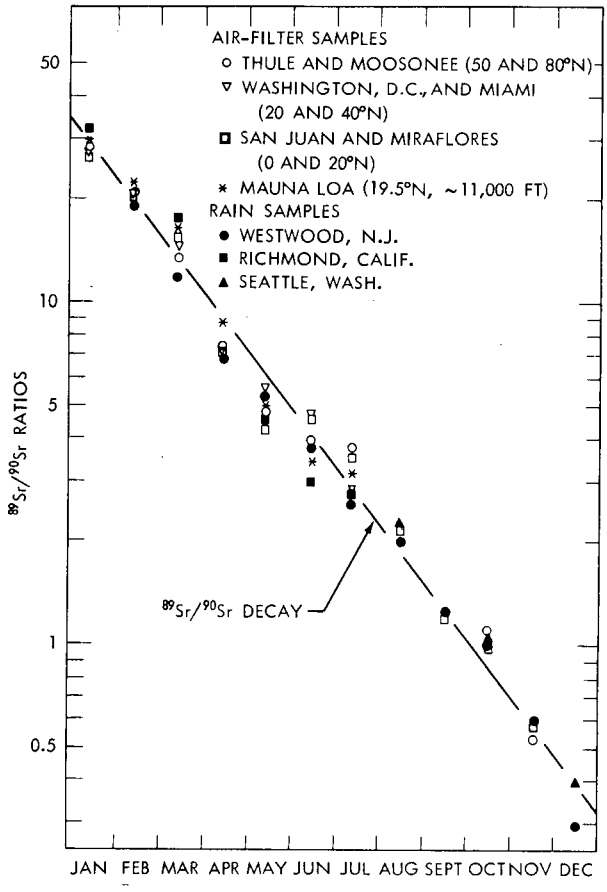

Fig. 4—$^{89}Sr/^{90}Sr$ in air and precipitation in the northern hemisphere in 1963.

of the HASL pot and column deposition stations to allow comparison of rain samples with ground-level-air values. The air-sampling stations have been grouped and averaged by rough latitude bands to facilitate plotting the data on the graph. It is evident that the agreement between stations and between sample types is very good in spite of the fact that the analyses were carried out by a number of different laboratories. Broadly, the data seem to follow the predicted slope of the ratio's decay as indicated by the dashed line in the figure. It is not thought that the slight deviations in April, May, and October are indicative of the addition of older debris since the geographical spread of these sites is so great. For instance, in May the grouping of data, which falls below the line, consists of points from the entire network (9 to 76°N) and includes the Mauna Loa site at 155°W. From this spread it is not likely that the deviation is significant.

By late summer of 1963, the concentration of ^{89}Sr in ground-level air had decayed to levels where the measurement techniques were inadequate. Thus, in the absence of any significant new injections of fission debris into the atmosphere, effective use of the ratio had ended by the end of 1963.

Figure 5 illustrates the $^{89}Sr/^{90}Sr$ ratio for the data from the southern hemisphere in 1963. The dashed line is the slope of the decay of the ratio as defined by the data from the northern hemisphere, copied directly from Fig. 4. The fact that the ratios observed are lower than the decay line through almost the entire year indicates that the debris in the southern-hemisphere ground-level air was generally older than that in the north. Qualitatively, as one would expect, values at all the sites seem to be approaching the northern-hemisphere ratio later in the year.

Two interesting relations can be pointed out in Fig. 5. The first relates to ground-level transfer of debris across the equator. It can be seen that the Guayaquil, Equador (about 2°S), point for April lies very close to the northern-hemisphere value. The same situation was noted in 1962 at Guayaquil and in 1959 for the sample from Quito, a site almost on the equator. In all these instances, the next site south, Lima, Peru, at about 12°S, had a much lower value of $^{89}Sr/^{90}Sr$. These data suggest that in the northern-hemisphere spring, when air concentrations generally reach their maximum, some measurable transfer of air occurs at ground level across the equator. Measurements of the $^{89}Sr/^{90}Sr$ ratio in precipitation have shown similar relations in the near-equatorial regions.[4]

The other interesting point that is suggested by the $^{89}Sr/^{90}Sr$ ratios of the southern-hemisphere air concerns the data from Chacaltaya, Bolivia. This site located at about 17°S is of special interest because of its unusual elevation, about 17,000 ft above mean sea level. In Fig. 5 the data from Chacaltaya are connected by a heavy line. Here it can be

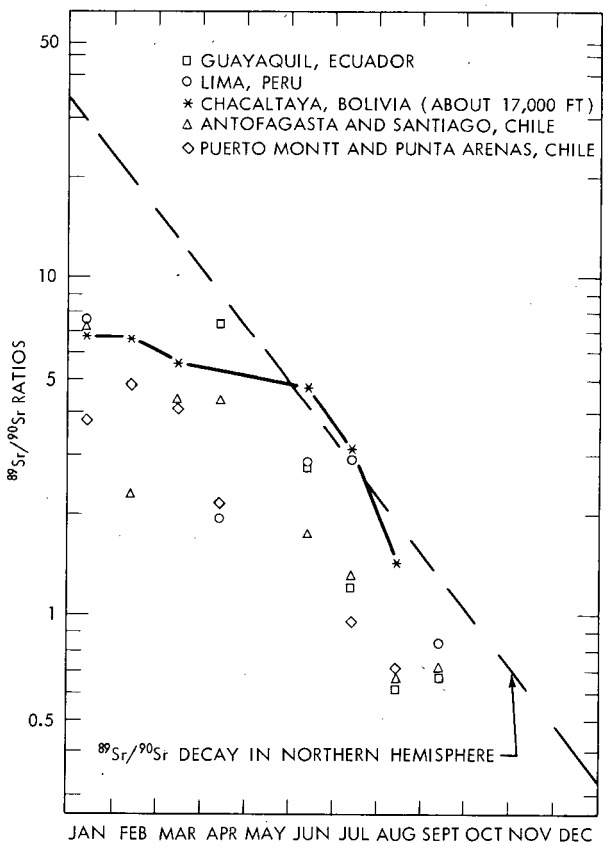

Fig. 5—$^{89}Sr/^{90}Sr$ in air-filter samples in the southern hemisphere in 1963.

seen that the airborne debris at Chacaltaya achieved approximately the average $^{89}Sr/^{90}Sr$ ratio of the northern hemisphere in June 1963 and maintained this composition through the next three months. This corresponds roughly with the annual peak at this site, which was noted earlier in the discussion of Fig. 3. Whether this material is of southern stratospheric origin or has moved in from the northern troposphere cannot yet be clearly determined. The timing of this event, however, suggests that it is probably the very earliest transfer of debris from the southern stratosphere and is the onset of the southern-hemisphere spring peak.

On that basis it then becomes quite clear that the timing of the annual peaks in fallout deposition is dependent not only upon latitude and rainfall but also upon the elevation of the sampling site.

REPRODUCIBILITY AND SYMMETRY OF ANNUAL OSCILLATIONS

In the study of the seasonal variations of ^{90}Sr concentrations in ground-level air, as in the precipitation studies, it has been seen that the absolute activity levels are so variable between samples from site to site and between the hemispheres as to obscure possibly the very relations sought. In an attempt to better focus the data on these problems, the absolute ^{90}Sr air concentrations were normalized in the following way: (1) the average bimonthly concentration at each site was computed by adding all the values for each year and dividing by six, and (2) each bimonthly concentration value was then divided by the average computed. By this method, each piece of data is relative to all other data regardless of latitude, year, or absolute concentration. All the values then become fractions of the annual average and thus tend to distribute about unity. Use of this normalizing procedure tends to point up the systematic fluctuations while damping the short-term effects.

Figure 6 illustrates the method. Here, all the data were reduced as previously described and plotted against latitude for each bimonthly period. It can be seen from this figure that the maximum spread of values is from about two-tenths to three times the average.

It is quite clear that the two curves in each of the six bimonthly periods follow similar trends. If the extensive atmospheric testing during 1962 compared to the complete absence of such testing in 1963 is considered, these curves clearly illustrate the strong and reproducible

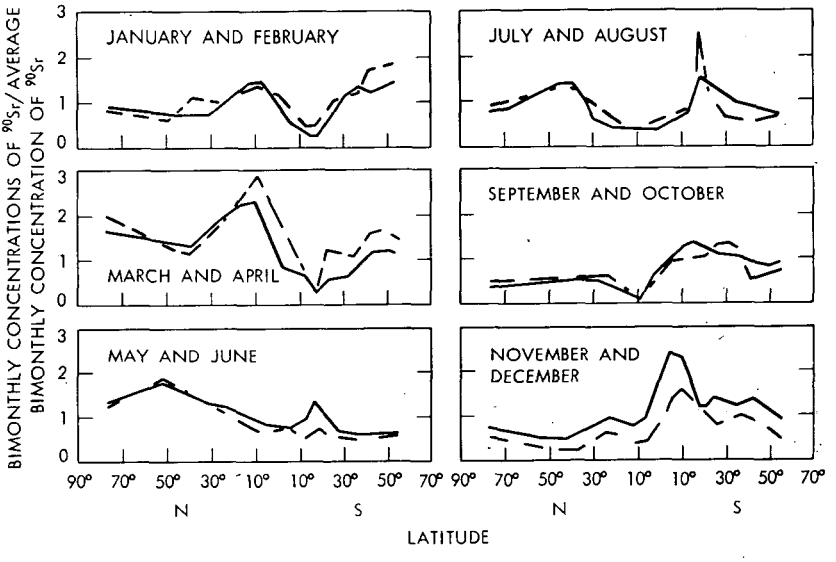

Fig. 6—Relative ^{90}Sr concentrations in tropospheric air along the 80th meridian. ——, 1962 NRL data; – – –, 1963 HASL data.

effect that the meteorological factors have on the relative air concentrations. It is suggested that,whether or not atmospheric testing is being carried out, the main peaks and valleys of relative air concentrations will occur. We hope to substantiate this conclusion by looking at data from past years and at future collections.

To simplify examination of these results for annual oscillations, Figs. 7 and 8 were prepared. In these the relative values for the two years were averaged; all areas under the curves that had values greater than unity were shaded. In Fig. 7 no obvious symmetry can be seen between the hemispheres. It was found by trial and error that by offsetting the hemispheres by four months the best symmetry (under the limitations of these data) is achieved. This is illustrated in Fig. 8. The first appearance of substantially higher than average air concentrations is in January or February in the northern hemisphere and in September or October in the south. The southern hemisphere seems to exhibit a geographically broader but lower intensity peaking in this initial period. In this and also in the next period, it is interesting to note that the highest values are at fairly low latitudes, probably between the equator and 20°. In the final two periods shown in the lower third of the figure, the hemispheres are remarkably symmetrical, with high relative activities at latitudes above 20°.

Since this method of analysis eliminates the effects of the absolute differences of the source concentrations, it would appear that the particular hemispheric characteristics represent true meteorological differences. Both hemispheres exhibit annual fluctuations with higher than average relative concentrations at some latitudes for two-thirds of the year. The initial appearance of the high is at low latitudes followed by increased values and a poleward shift. The asymmetry between the hemispheres occurs mostly in the first half of the season, whereas the southern hemisphere values do not vary to as great a degree as do those of the northern hemisphere.

DEPENDENCE OF AIR CONCENTRATIONS UPON RAINFALL

It has been suggested that precipitation characteristics may play an important role in determining air concentrations of ^{90}Sr. We attempted to study this by utilizing the rain data from the worldwide HASL pot and column network. These data were averaged over 10° latitudes bands and normalized in the same manner as the ^{90}Sr values, i.e., bimonthly rainfall amounts are expressed as fractions of the annual bimonthly average.

The best fit with the relative ^{90}Sr data was found by offsetting the precipitation one month, i.e., by comparing August and September rain concentrations with September and October air concentrations. The result of this comparison for the northern hemisphere is shown in Fig. 9.

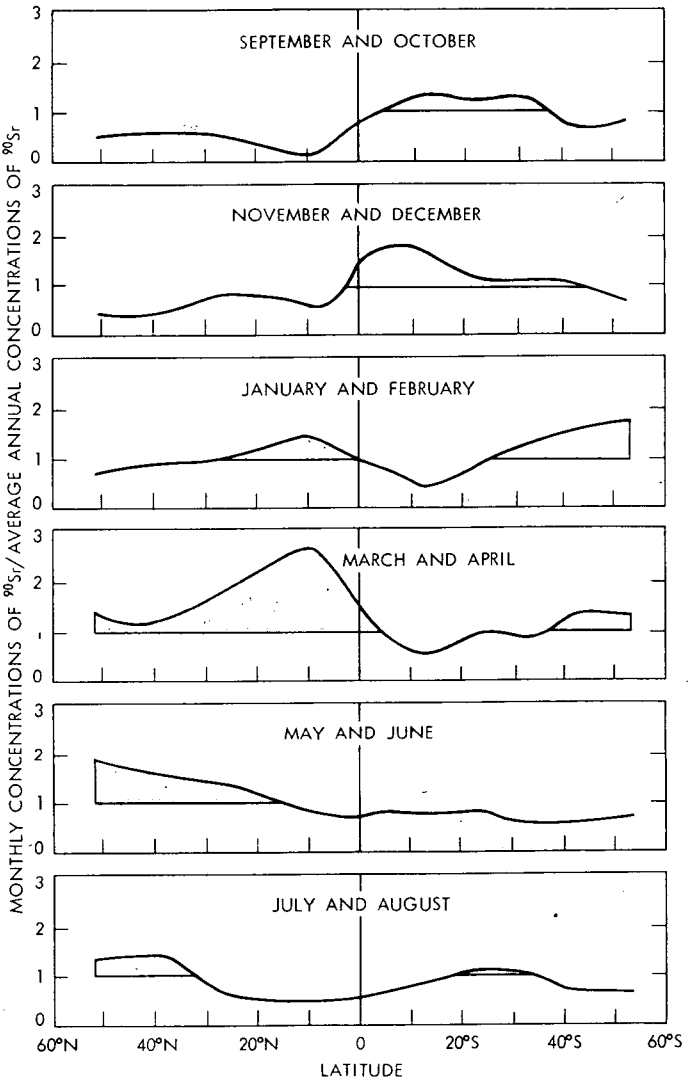

Fig. 7—Relative ^{90}Sr concentrations in tropospheric air along the 80th meridian (1962 and 1963 averages). The shaded areas represent excess concentrations.

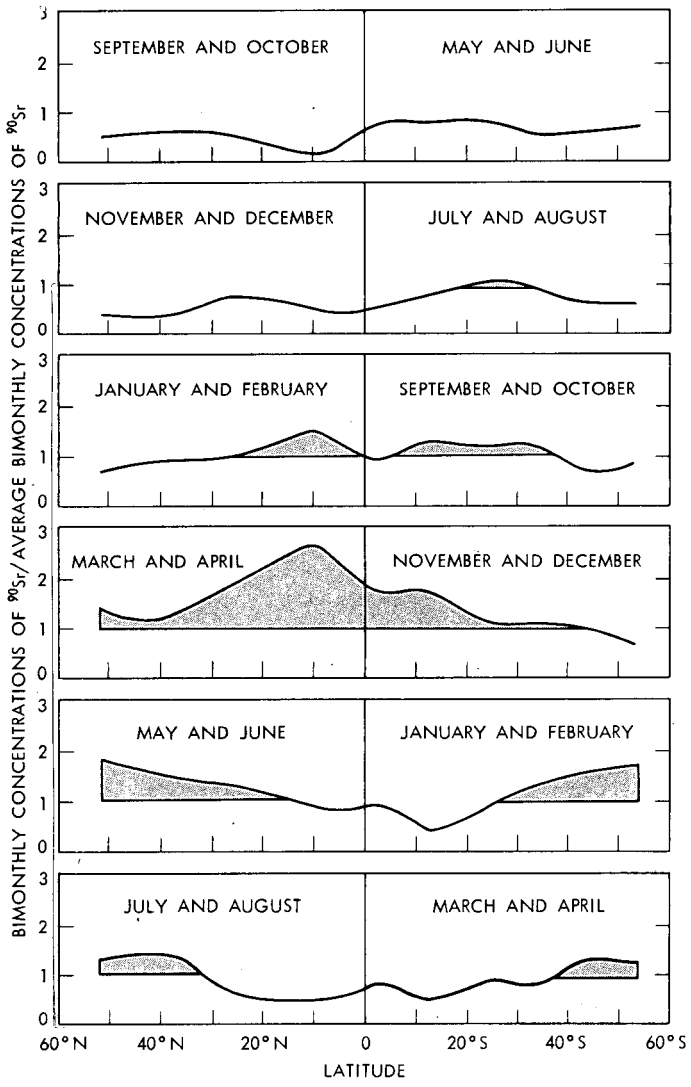

Fig. 8—Relative ^{90}Sr concentrations in tropospheric air along the 80th meridian (1962 and 1963 averages). The shaded areas represent excess concentrations.

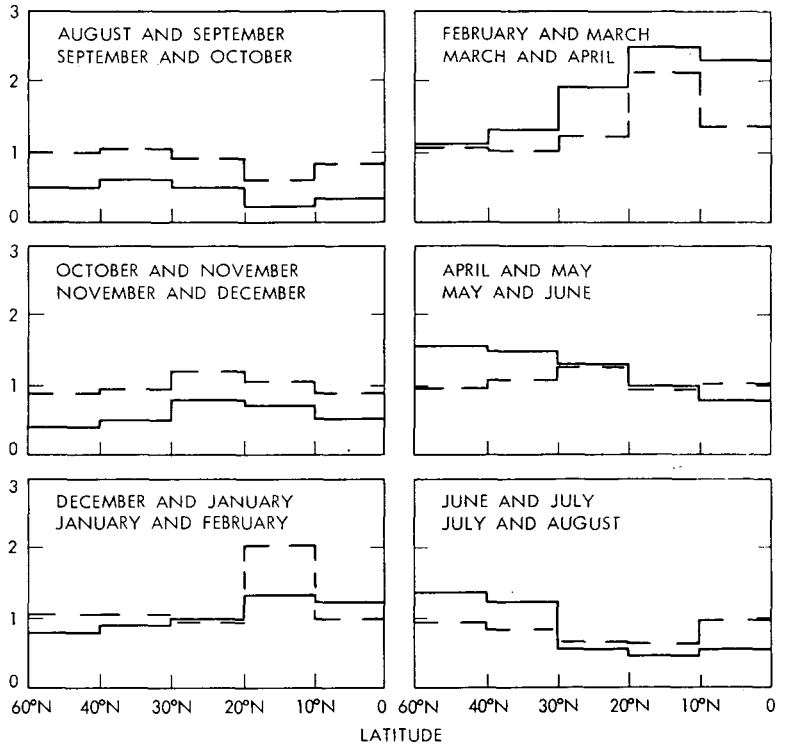

Fig. 9—Relative ^{90}Sr concentrations in precipitation and tropospheric air in the northern hemisphere. – – –, average bimonthly precipitation vs. bimonthly precipitation (1962–1963 HASL pot and column network); ——, average bimonthly ^{90}Sr concentration vs. bimonthly ^{90}Sr concentration [1962–1963 80th meridian (west) network].

The relative rainfall values were plotted as the reciprocal in this graph to make the correlation easier to see.

It is certainly very clear that in the first two periods when no highs in air concentration occurred an inverse proportional relation exists. In the subsequent periods, although the relation is not quite as simple, a general dependence of air concentration upon precipitation is exhibited. For example, at the highest northern-hemisphere peak time (March and April), it would appear that the relative high at low latitudes must be due in part to the relatively low rainfall in the immediately preceding time period. Conversely, in the middle latitudes at that time, the much lower relative ^{90}Sr values correlate with higher precipitation.

Undoubtedly, this effect cannot completely explain the bimonthly profiles of air concentrations, but it does appear to influence the data to a measurable degree. It is felt that major meteorological air-transport mechanisms determine the broad patterns and timing of

these seasonal fluctuations and that the fluctuations are broadly reproducible from year to year. Superimposed on these fluctuations are the individual yearly rainfall patterns, which to a degree control the buildup of air concentrations, as qualitatively outlined previously.

REFERENCES

1. L. B. Lockhart, Jr., R. L. Patterson, Jr., A. W. Saunders, Jr., and R. W. Black, Summary Report on Fission Product Radioactivity in Air Along the 80th Meridian (West), 1957–1962, Report NRL-6104, U. S. Naval Research Laboratory, June 15, 1964.
2. E. P. Hardy, Jr., and J. Rivera, Fallout Program Quarterly Summary Report, USAEC Report HASL-149, Health and Safety Laboratory, Oct. 1, 1964.
3. Federal Radiation Council, Revised Fallout Estimates for 1964–1965 and Verification of the 1963 Predictions, October 1964.
4. E. P. Hardy, Jr., J. Rivera, and W. R. Collins, Jr., Fallout Program Quarterly Summary Report, USAEC Report HASL-146, Health and Safety Laboratory, June 1, 1964.

DISTRIBUTION OF RADIOACTIVITY WITH HEIGHT IN NUCLEAR CLOUDS

GILBERT J. FERBER
U. S. Weather Bureau, Washington, D. C.

ABSTRACT

During Operation Dominic I at Christmas Island in 1962, aircraft sampling of nuclear clouds was done soon after cloud stabilization to investigate the amount of radioactive debris that stabilizes in the troposphere and its distribution with height. The detonations studied were all air bursts over water. Some data for surface bursts obtained during Operation Redwing in 1956 are used for comparison. Results indicate that for air bursts less than 1% of the total radioactivity is present in the stem of the nuclear cloud. It is estimated that about one-third of the total debris from the Christmas Island clouds initially stabilized in the troposphere.

Project Stemwinder has shown that in-cloud dose-rate monitoring by aircraft is a relatively simple and economical way to obtain information on the distribution of radioactive debris in a nuclear cloud. Used in conjunction with limited radiochemical analysis of samples, this type of monitoring could produce a reliable inventory of the debris in a nuclear cloud.

INTRODUCTION

The objective of Project Stemwinder was to probe and sample nuclear clouds as soon as possible after cloud stabilization to investigate the amount of radioactive debris that stabilizes in the troposphere and its distribution with height. Sampling was done with RB-57 aircraft of the 1211th Test Squadron under the scientific direction of the Atmospheric Radioactivity Research Branch, U. S. Weather Bureau.

The detonations investigated were all air bursts over water during Operation Dominic I at Christmas Island in 1962. Some data for surface detonations obtained by aircraft sampling during Operation Redwing in 1956 are used to compare with the Project Stemwinder data.

The project was conceived as an attempt to utilize available sampling aircraft to narrow the area of uncertainty involved in two related problems. The first problem was concerned with the operational need for prediction of the possible local hazards due to rainout of radioactive debris from a portion of a nuclear cloud that might pass over Christmas Island shortly after an air burst. Since the tops of rain clouds in the Christmas Island area were generally below 20,000 ft. and often below 10,000 ft, the amount and distribution of activity in the stem of the mushroom cloud was of primary concern. The second problem was concerned with the partitioning of nuclear debris between the stratosphere and the troposphere as a function of nuclear yield, tropopause height, burst height, and, possibly, other factors. Such partitioning has been an important consideration in estimating the long-range fallout from nuclear tests since nuclear debris has a mean residence time of several weeks in the troposphere (intermediate fallout) as opposed to many months or years in the stratosphere (worldwide fallout), depending on the latitude and altitude of injection. The fraction of the debris which remains in the troposphere may be particularly important in considering the possible hazards from relatively short-lived nuclides such as ^{131}I since the stratospheric portion usually decays to insignificant amounts before it can return to the surface of the earth.

It is emphasized that the preceding remarks apply only to the very small particles that contribute to the intermediate and the worldwide fallout. In the case of surface detonations, much of the radioactivity is associated with relatively large particles that comprise the local fallout. These large particles are not affected by the tropopause and appear in the local fallout regardless of whether they are initially injected into the troposphere or into the stratosphere.

CLOUD HEIGHTS OF AIR BURSTS IN A TROPICAL ATMOSPHERE

Operation Dominic I shot data (including those for yield, burst height, and cloud-top, base, and tropopause heights) are given in the Project Stemwinder final report.[1] Since there was no scientific program to document cloud heights, a "best guess" was made for each cloud by evaluating estimates made by observers on the ground and in the sampling aircraft and by using the dose rates reported at the various sampling altitudes to verify, where possible, the visual observations. Variations in the burst heights did not appear to have any

consistent effect on the cloud heights. Evidently, the effect of the burst height was masked by the influence of meteorological factors and/or the errors in the cloud-height estimates.

Selected data[2] were added from other Pacific test series to aid in drawing the mean curve and the curves for the estimated range of cloud heights (see Fig. 1). Almost all the detonations in previous U. S.

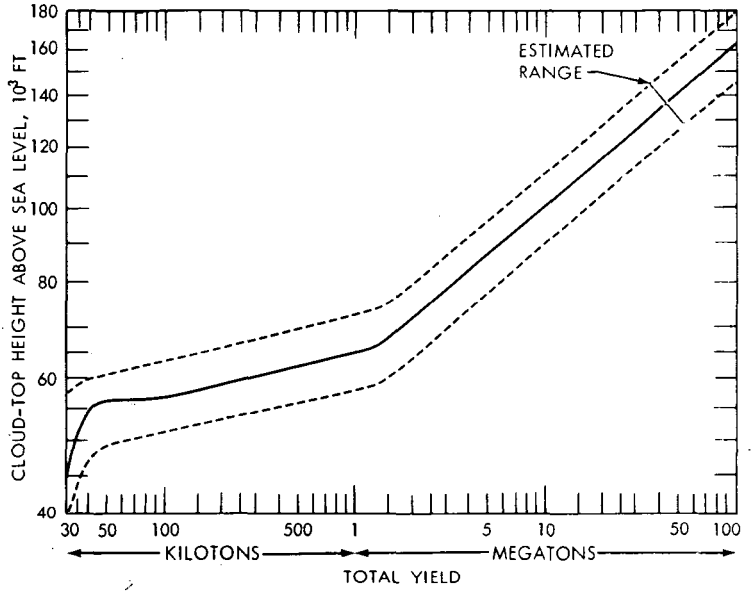

Fig. 1—Cloud-top heights and estimated range for air bursts ($180Y^{0.4}$ < burst height < $0.15\ H_T$) in a tropical atmosphere.

tests in the Pacific had been surface bursts, and the documentation of nuclear cloud dimensions had been generally poor. The curves shown in Fig. 1 are intended to be valid only for air bursts in a tropical atmosphere and for burst heights less than about 15% of the expected cloud-top heights. For this purpose, an air burst may be defined as a detonation at an altitude equal to or greater than $180Y^{0.4}$, where Y is the total yield in kilotons. It is emphasized that there are no reliable cloud-top data for yields greater than about 5 Mt, and the extrapolation of the curves beyond this point represents little more than an educated guess. Indeed, over the entire range of yields shown in Fig. 1, the dashed curves indicate only the expected range of cloud heights for the stated conditions and should not be interpreted as representing absolute limits.

STEM-CLOUD PENETRATIONS

An RB-57 aircraft was available for stem-penetration missions immediately following seven of the Dominic I detonations. The navigator was provided with a dose rate meter with a range from 0.01 to 2000 mr/hr and was instructed to record the dose rate as the aircraft penetrated the stem cloud at specified altitudes. The dose rates measured in the cockpit were then used to estimate the amount of activity in the cloud.

The relation between cloud concentration and dose rate in a uniform infinite cloud[3] is given by

$$C = \frac{D\rho}{\rho_0} \frac{84\rho_0}{(3.7 \times 10^4)(1.6 \times 10^{-6})E} \tag{1}$$

where C = cloud concentration, $\mu c/cm^3$
D = dose rate, r/sec
ρ_0 = standard density of air at sea level = 1.293×10^{-3} g/cm^3
ρ = density of air at sampling altitude, g/cm^3
E = average gamma energy, Mev
84 = energy absorbed per roentgen, ergs per gram of air
1.6×10^{-6} = ergs/Mev
3.7×10^4 = dis/sec per microcurie

If the unit of dose rate is converted to roentgens per hour and the concentration to megacuries per cubic mile,

$$C = 2.1 \frac{\rho}{\rho_0} \frac{D}{E} \tag{2}$$

For stem penetrations within an hour after the burst, E was assumed to be 1 Mev. For the sampling missions between 2 and 5 hr after the burst, a value of 0.86 Mev was used.[4] Figure 2 gives the value of ρ/ρ_0 as a function of altitude for a typical tropical atmosphere.[5] With the use of appropriate values for E and ρ/ρ_0 in Eq. 2, the dose rates recorded during stem penetration were converted to cloud concentrations. An estimate of the stem diameter was then used to estimate the total volume of cloud in a 1000-ft-thick layer. The total amount of activity in the layer and the fraction of the bomb represented by that activity was then determined by multiplying the concentration by the volume. The results are shown in Fig. 3 as a plot of the fraction of the bomb present in a 1000-ft-thick layer of the stem cloud vs. height (indicated as percent of the total stem height). The three highest Dominic I data points are derived from the extended sampling missions described later in this paper. The Redwing data used for the figure

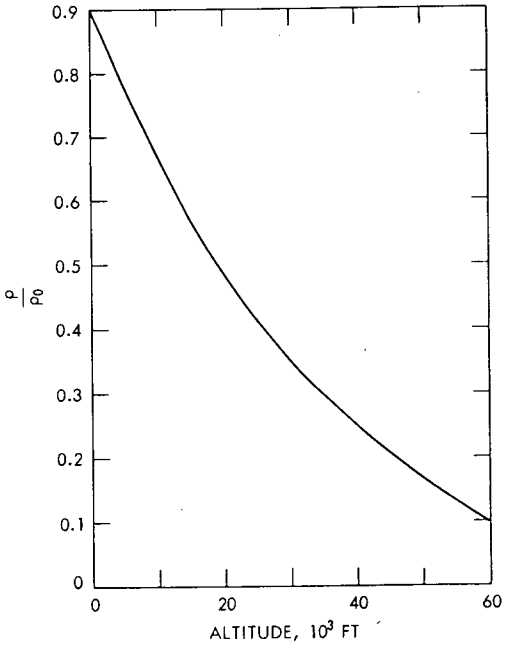

Fig. 2—Ratio of air density (ρ) to standard sea-level air density ($\rho_0 = 1.293 \times 10^{-3}$ g/cm³) as a function of altitude.

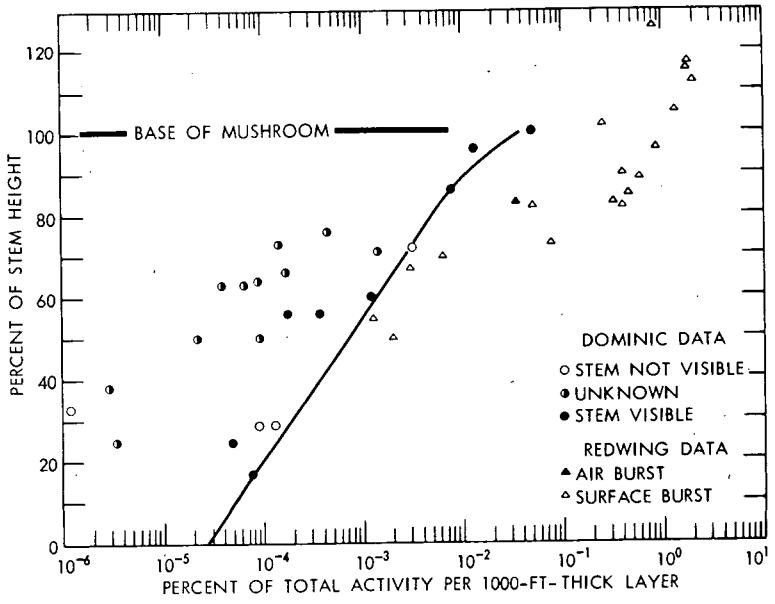

Fig. 3—Variation with height of the percent of the total activity residing in a 1000-ft-thick horizontal layer of the cloud.

also are discussed later. The curve is intended to represent a conservative estimate (for safety considerations) of the stem activity as a function of height for air bursts.

The rather large scatter in the data may be attributed to several factors. It appears that stem visibility may be the most important of these. Most of the higher activity readings occurred during penetrations when the stem cloud was visible to the pilot. The relatively low readings were obtained when the cloud was not visible or when it was not known whether the cloud was visible. It is quite possible that the aircraft did not actually penetrate the stem on these occasions. The dose rates measured inside the aircraft may have been due to "shine" from the stem cloud or to activity from diffuse material outside of the stem core. In those cases where the stem was not visible and where several passes were made at the same altitude, only the highest reading has been used.

Unfortunately, for the lower 80% of the stem, virtually all the data for the larger detonations are questionable because of the stem-visibility problem. Therefore it is impossible to say whether or not the low stem activity found for these shots indicates a real decrease in the fraction of activity in the lower part of the stem with increasing nuclear yield.

The following factors also contribute to the uncertainty in the results:

1. Stem-volume estimates. For the determination of the total activity present in a 1000-ft-thick layer, the stem diameter at the penetration altitude was estimated. The values used were based on visual estimates made by observers on the ground and in the sampling aircraft or, where necessary, on estimates for other detonations in the same yield range. The estimated diameter could be in error by as much as a factor of 2 in some cases.

2. Stem-height estimates. The stem was considered to extend from sea-level to the base of the cloud regardless of the burst height. The cloud bases used were based on visual observations from the ground and from the sampling aircraft and verified, where possible, by radiation readings taken in the sampling aircraft. The uncertainty in the height of the cloud-base (stem height) is about 10%.

3. Representativeness of dose-rate readings. The measured dose rates are assumed to represent those in a uniform, infinite cloud. The assumption appears to be reasonably valid for those penetrations where the stem was visible. The aircraft required 20 sec or more to traverse the cloud at a speed of about 7 miles/min while the mean free path of gamma radiation in air is on the order of a few hundred feet. The navigator reported that the dose rate usually rose sharply on entering the cloud, remained fairly steady (within a factor of 2) during

penetration, and then dropped sharply. (It would be advantageous to use automatic time–intensity recorders in future operations.)

The effect of aircraft shielding on the dose rate in the cockpit is also uncertain. Tests made at the ground, using a point source outside the aircraft, indicated that there was no appreciable shielding effect on gamma radiation by the aircraft. Equation 2 assumes that the receptor is completely surrounded by a uniform radiation field. Actually, of course, the receptor was surrounded by a "blank space" equivalent to the volume of the aircraft. No attempt has been made to correct for this. However, the effect should be small, probably less than a factor of 2, since the mean free path of the gamma radiation is large compared to the dimensions of the aircraft. Experimental determination of the correction factor should be planned in connection with any future operation of this type.

AIRCRAFT SAMPLING IN THE VICINITY OF THE CLOUD BASE

Aircraft equipped with Los Alamos Scientific Laboratory air-filter tanks were used for sampling after five Dominic I detonations. Approximately 1-hr sampling missions were flown at altitudes from 35,000 to 48,000 ft at 2 to 5 hr after detonation. The two sampling tanks were opened simultaneously when contact with the cloud was made and remained open for the entire sampling period. As the sampling patterns were flown, readings in the cockpit were made at 1-min intervals with a hand-held AN/PDR-27J Radiacmeter capable of measuring activity in a range from 0.01 to 500 mr/hr. Sampling missions were successful after four of the five detonations. The radiochemical analyses of the samples are reported elsewhere.[6]

The dose-rate readings obtained during three extended sampling missions were sufficient for estimations of the distribution and the amount of activity in the clouds at the sampling altitudes. Similar analyses were done for all three missions. The results are included in Fig. 3.

One of the clouds was sampled at an altitude of 45,000 ft at approximately 3 to 4 hr after detonation. The base of the cloud was reported to be at about 45,000 ft. Both the shot-time wind data and the position of the cloud indicate east-southeast cloud travel at about 15 knots. For correction for the movement of the cloud during the sampling period, the reported aircraft positions were adjusted to the sampling midtime of $3\frac{1}{3}$ hr after detonation. The corrected radiation field and the actual unadjusted sampling track are shown in Fig. 4. If a decay exponent of -1.2 is assumed, integration of the pattern yields 520 r/hr-cu mi at 1 hr in a 1000-ft-thick layer. From Eq. 2 this is equivalent to 270 Mc, or 4.9×10^{-4} of the total fission products produced by the detona-

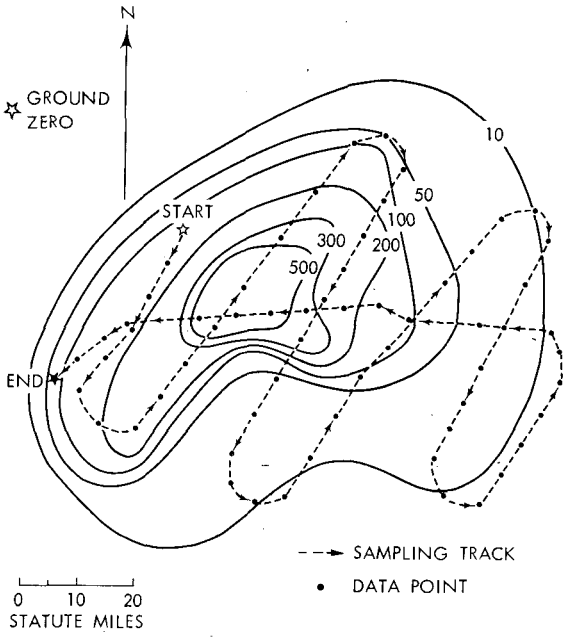

Fig. 4—Sampling track and radiation pattern in a nuclear cloud at 45,000 ft. Values given are in milliroentgens per hour at H + 3⅓ hr.

tion. The cloud covered an area of 5200 square miles at the 45,000-ft altitude.

The sampling track appears to have covered the cloud very well. However, the pilot reported shine from higher portions of the cloud during the last few minutes of sampling when the aircraft was outside the visible cloud. The readings due to shine were about 100 mr/hr. It is possible that a significant fraction of the in-cloud readings may also have been due to shine from the upper portions of the cloud; therefore the estimate of the amount of activity at 45,000 ft may be high.

COMPARISON WITH RADIOCHEMICAL RESULTS

The radiochemical analyses of the samples obtained on the three extended sampling missions provide a check on the method of calculating the amount of debris present from the dose-rate readings in the cloud. The total number of fissions collected in each sample has been determined,[7] based on the number of atoms of ^{99}Mo present corrected for the fission yield of ^{99}Mo for thermal fission of ^{235}U. If the total volume of air passing through the sampling tank and the average dose rate along the sampling path are known, the fissions per sample can be estimated by the same method that was used to estimate the fraction of

the bomb in a 1000-ft-thick layer. The volume sampled is determined from the altitude, the air temperature, the aircraft speed, the sampling time, and the sampling-tank and filter-paper characteristics.[8] The average dose rate is determined from the readings taken in the cockpit at 1-min intervals during the sampling period. From Eq. 2 the gamma megacuries in the sample can be calculated. If it is assumed that 1 kt of fission (1.4×10^{23} fissions) is equivalent to 550 gamma megacuries at 1 hr, the following conversion factor can be used: 1 Mc (H + 1) = 2.64×10^{20} fissions. Table 1 gives the pertinent data and the fissions

Table 1 — COMPARISON OF CALCULATED AND ANALYZED FISSIONS PER SAMPLE

Mission	Altitude, ft	Sample volume, cu ft	Average dose rate, mr/hr at H + 1	Calculated fissions per sample	Fissions per sample (radiochemical analyses)
A	43,000	1.06×10^6	190	1.9×10^{14}	3.3×10^{14}
B	48,000	1.11×10^6	270	2.3×10^{14}	4.9×10^{14}
C	45,000	1.10×10^6	560	5.6×10^{14}	5.8×10^{14}

per sample as calculated from dose-rate readings and as determined from radiochemical analyses of the samples.

The agreement between the calculated values and the results of the sample analyses is remarkably good, considering the uncertainties due to the possibility of shine from other portions of the cloud, aircraft shielding, and aircraft contamination. The calculated values for the samples from missions A and B are low by about a factor of 2, possibly because of the effect of the blank space previously mentioned. The calculated value for the sample from mission C is in almost perfect agreement with the result of the sample analysis. Mission C is the one depicted in Fig. 4 and for which there was reason to suspect a shine contribution to the dose rates which may have compensated for the blank-space effect.

Additional experimental data are needed to evaluate all the factors involved, but the results indicate that the method employed on these missions is a practical and promising way to obtain the distribution of activity in a nuclear cloud.

REDWING IN-CLOUD DOSE-RATE DATA

The doses and dose rates at various altitudes in several nuclear clouds (all but one from surface bursts) were investigated by aircraft penetrations[9] during Operation Redwing in 1956. Some of these penetrations were complete traverses through the cloud. Since the altitude,

the mean speed of the aircraft, the time in the cloud, and the average dose rate are reported, these data can be utilized in the same manner as the Dominic I stem penetrations to compute the device fraction contained in the cloud at the penetration altitudes. The computed device fractions are plotted in Fig. 3 for comparison with the Dominic I data.

Several interesting features may be noted. It appears that the activity in the upper half of the stem is greater for surface bursts than for air bursts and that the difference increases with altitude. The largest gradient of activity with altitude appears at about 70 to 80% of the stem height; this implies that for surface bursts the "radiological base" lies below the visual cloud base. However, this inference may not be warranted since the high activities encountered below the base may be due to the descent of fallout particles.

The values computed for the lower portion of the mushroom indicate about 1 to 2% of the total fission products per 1000 ft. Since the mushroom portion of the clouds investigated averaged about 30,000 ft in vertical extent, the average activity in the mushroom must have been about 3% per 1000 ft. Thus we have some basis for believing that this admittedly crude method can give at least the right order of magnitude for the activity at a given altitude, even when the average dose rate recorded during a single pass through the cloud is used.

We note that the one Redwing data point for an air burst gives about five times the activity indicated by the curve estimated from the Dominic I data. This greater activity might be attributed to the fact that the detonation took place at a lower scaled height than any of the Dominic I air bursts. The burst height was somewhat below the minimum altitude for a true air burst according to our definition (burst height > $180Y^{0.4}$); therefore the activity distribution might be expected to be intermediate between those for air bursts and surface bursts. Although the close-in fallout measured after this detonation was very light, it was considerably more than that found after any Dominic I shot, where shipboard dose rates never exceeded 0.1 mr/hr. However, since only one surface vessel was available for fallout measurements during the Dominic I tests, the very limited number of measurements obtained does not permit the drawing of firm conclusions.

RESULTS AND CONCLUSIONS

Activity in the Stem Cloud for Air Bursts

Although the Dominic I stem-penetration data leave a good deal to be desired for defining the distribution of activity in the stem, the curve in Fig. 3 represents a best estimate based on our interpretation of these data. A major uncertainty lies in the assumption that the distribution in the stem does not vary with yield. As indicated previously,

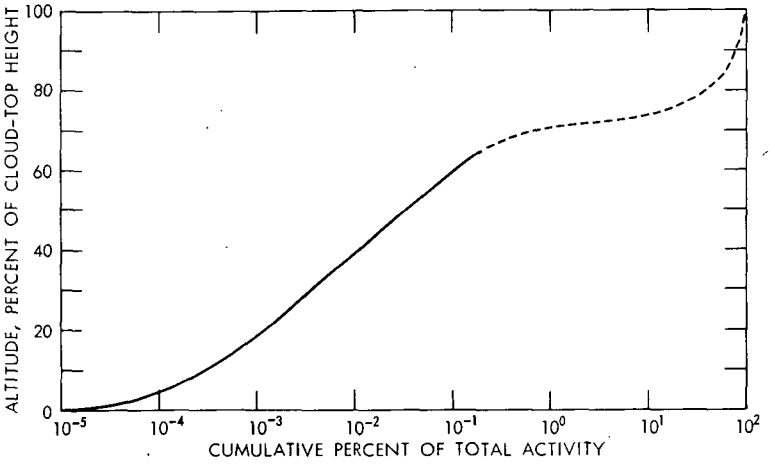

Fig. 5—Cumulative activity as a function of height in the nuclear cloud for air bursts.

this curve may represent an overestimation of the activity in the lower part of the stem for the larger yields (above about 200 kt).

Cumulative Activity with Height in the Nuclear Cloud for Air Bursts

With the use of the stem-activity curve in Fig. 3, an estimate of the cumulative activity with height in the nuclear cloud was derived. The solid portion of the curve in Fig. 5 was obtained from the stem-activity curve by using an average stem height of 40,000 ft and by assuming the stem-top height (or visual cloud base) to be 63% of the cloud-top height (the average for the Dominic I series). Since the entire stem appears to contain less than 1% of the total activity, it is obvious that the activity must increase rapidly with height at or above the base of the cloud. The dashed portion of the curve represents a subjective estimate (based, in part, on the Redwing data for surface detonations) of the distribution of activity in the mushroom portion of the cloud. The activity in the mushroom is assumed to be distributed as follows:

Layer, % of cloud-top height	Fraction of total activity, %
65 to 70	0.6
70 to 75	14
75 to 80	25
80 to 85	25
85 to 90	15
90 to 95	15
95 to 100	5

For air bursts it appears reasonably certain that less than 1% of the total activity is present in the stem and that less than 0.1% stabilizes between the surface of the earth and one-half of the cloud-top altitude. The fraction of activity per unit altitude increases with height throughout the stem, and the region of maximum vertical gradient, which might be termed "the radiological base of the cloud," probably occurs somewhat above the visual cloud base. The peak activity per unit altitude is assumed to occur between 75 and 85% of the distance from the surface to the cloud top. It is also assumed that for air bursts the distribution of activity relative to the cloud-top height does not vary with nuclear yield, burst height, or atmospheric conditions.

Actually, the interaction of these factors must exert some influence on the activity distribution. The estimated top and base heights of the Dominic I clouds indicate that the ratio of base height to top height has a tendency to decrease with increasing yield. However, it is uncertain to what extent these indications are valid since the variation among detonations of about the same yield is almost as great as that for the range of yields from 40 kt to several megatons. The mean ratio is 63%, with individual clouds varying from 53 to 73%. Some of the variation may be attributed to errors in the estimates of the base and top heights, but part of it is undoubtedly real. There is a similar uncertainty concerning the height of the radiological base.

Partition of Activity Between Stratosphere and Troposphere

The height of the tropopause varies with latitude, season, and daily atmospheric changes. The daily and seasonal variations are less in tropical latitudes than elsewhere. The tropopause heights averaged about 54,000 ft above sea level for the Dominic I tests, varying between 50,000 and 58,000 ft on individual shot days. This variation is representative of the tropical tropopause.

With the use of the activity distribution in Fig. 5, a mean tropopause height of 54,000 ft, and the mean cloud-height curve in Fig. 1, a typical curve of the percent of total debris in the troposphere as a function of yield has been calculated. The curve, shown in Fig. 6, is intended to be valid at the time of cloud stabilization for air bursts in a tropical atmosphere. Another curve has been drawn to indicate the likely maximum tropospheric fraction, based on a high tropopause (58,000 ft) and low cloud heights (from the lower curve in Fig. 1). These extremes do not represent absolute maximums since higher tropopauses and lower clouds may occur occasionally. In addition, the uncertainties in the activity–height curve (Fig. 5) make it impossible to define a meaningful and useful absolute maximum tropospheric fraction. No attempt has been made to estimate the minimum tropospheric fraction, but, in the megaton-yield range, it could be several orders of magnitude below the typical fraction.

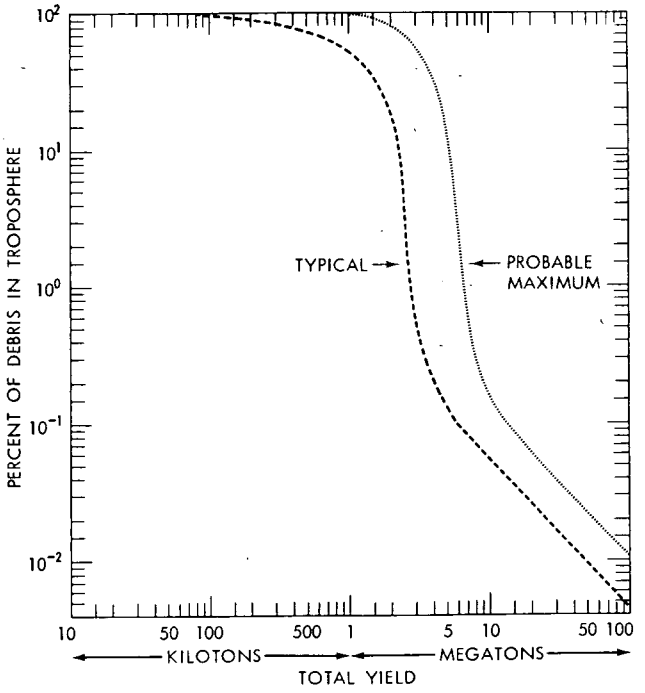

Fig. 6—Percent of total activity initially injected in the troposphere as a function of total yield for air bursts in a tropical atmosphere.

The most critical uncertainty in the estimates is for the range of yields from about 700 kt to about 5 Mt, where the radiological cloud base may lie in the vicinity of the tropopause. For yields less than 700 kt, the tropospheric fraction (at cloud stabilization) can be estimated to within a factor of 2 or less. For yields above about 5 Mt, the fraction in the troposphere becomes very small, although precisely how small it may be has not yet been determined.

An estimate of the kiloton equivalent of fission products stabilized in the troposphere as a function of total yield for air bursts is shown in Fig. 7. The typical and maximum curves are derived from the curves in Fig. 6, based on the assumption that the yield is entirely due to fission. Several interesting features may be noted. The maximum tropospheric contamination is produced by bursts in the low megaton range (assuming 100% fission yield). With typical cloud heights and an average tropopause height of 54,000 ft, the maximum tropospheric contamination is about 500 kt for yields between about 800 kt and 2 Mt. As the yield increases, the tropospheric debris decreases rapidly and then levels off at about 5 kt of fission equivalent for yields from 10 to 100 Mt. The maximum curve, based on a high tropopause and low cloud heights,

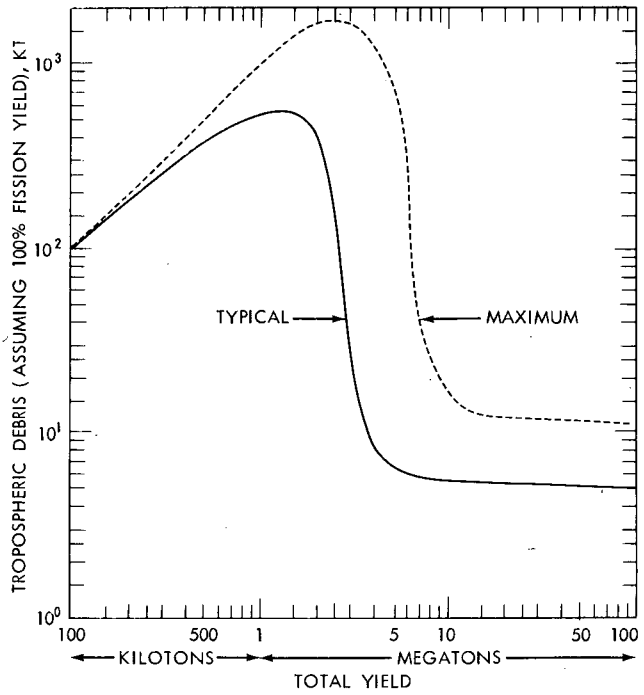

Fig. 7—Amount of debris (kilotons equivalent) initially injected in the troposphere as a function of total yield for air bursts in a tropical atmosphere.

is quite similar with a maximum tropospheric contamination of about 1.5 Mt for yields between 2 and 3 Mt, all fission. This curve also decreases rapidly and then levels off at about 12 kt of tropospheric debris for yields between 15 and 100 Mt. It should be recalled here that these curves are based on the activity–height curve given in Fig. 5 and are subject to the same uncertainties. For thermonuclear devices the amount in the troposphere should be multiplied by the fission fraction of the device.

Dominic I Debris in the Troposphere

With the use of the estimated tropospheric fraction and the fission yield for the individual Christmas Island detonations, it is estimated that about one-third of the total radioactivity initially stabilized in the troposphere. Since a half-residence time of one month is generally accepted for tropospheric debris,[10] about one-sixth of the total activity might be expected to be deposited at the surface, mostly in tropical latitudes, within a month after the conclusion of this test series. A rough integration[11] of the activity found in the AEC Health and Safety Laboratory monthly fallout-deposition collections indicated that only about half this amount was deposited in the latitude band from 30°N to 30°S

through August 1962. The difference between the expected and the measured amounts may be due to the uncertainties in the estimates of the tropospheric fraction and the deposition. However, there are several reasons for believing that the amount deposited in the latitude band was actually less than that estimated from the tropospheric fraction at time of cloud stabilization.

First, some of the debris which initially stabilized below the tropopause may have ascended into the stratosphere in convective cells or as a result of thermally induced direct circulation. Second, some debris was transported to mid-latitudes at altitudes below the tropical tropopause. Since there is a polar tropopause in mid-latitudes, generally between 30,000 and 40,000 ft, the debris which was transported away from the equatorial region at altitudes from about 40,000 to 55,000 ft would have become incorporated into the mid-latitude stratosphere. An interesting example of such transport was provided by the interception of one of the Dominic I clouds by sampling aircraft over the western United States.[12] In addition, sampling of the lower stratosphere over the United States indicates that it contained fresh debris from the Dominic I tests during most of the month of May 1962. Finally, the evidence for a half-residence time of one month for tropospheric debris may actually apply only to debris below the polar tropopause. The residence time for debris in the troposphere, above 40,000 ft, in tropical latitudes has not been established. Only a very small fraction of the debris from the Dominic I tests stabilized below 40,000 ft. The fraction was much smaller than that for previous Pacific test series, which consisted primarily of surface bursts.

In any case, it has become increasingly evident that the potential hazard due to short-lived fission products is not attributable solely to the portion initially injected in the troposphere since there is an exchange of air between the stratosphere and troposphere. Therefore the three-dimensional trajectory of the debris-laden air would have to be considered in determining the fate of a particular debris cloud.

It has also been shown[12] that severe thunderstorms that penetrate the lower stratosphere provide an effective mechanism for bringing stratospheric debris directly to the ground. It appears that thunderstorm scavenging of stratospheric debris from the Dominic I tests accounted for most of the ^{131}I found in milk in the midwestern United States in May 1962.

RECOMMENDATIONS FOR FUTURE WORK

Project Stemwinder has shown in-cloud dose-rate monitoring by aircraft to be a relatively simple and economical way to obtain information on the distribution of radioactive debris in nuclear clouds.

Through the use of this technique, it may be possible to greatly reduce the amount of radiochemical analyses which would be required to obtain a reliable inventory of radioactivity in a nuclear cloud. This type of monitoring might be particularly well suited to clouds from large nuclear cratering detonations such as those contemplated for the Plowshare program. Such clouds should be visible for at least several hours and would probably be confined to the troposphere.

Tentative answers have been found for the questions that led to Project Stemwinder, but large uncertainties still exist. The experience gained in the project indicates that for air bursts the lower stem should be monitored soon after cloud stabilization while it is still visible and that several penetrations should be made at each altitude to ensure that representative readings are obtained. Additional data are particularly needed for yields in the megaton range.

An obvious limitation of Project Stemwinder was the aircraft ceiling of 50,000 ft. A determination of the amount of debris initially stabilized in the troposphere requires sampling to an altitude of 60,000 ft. Aircraft with the capability of operating at this altitude have been used for cloud sampling, but they were not available for Project Stemwinder.

The following recommendations are offered for any future operations:

1. A continuous-recording gamma-intensity instrument package with a range from 1 mr/hr to 1000 r/hr should be used for aircraft cloud penetrations.

2. Experimental determination of the dose-rate reduction due to the aircraft should be attempted.

3. An attempt should be made to monitor the entire cloud from a low- or an intermediate-yield detonation. Thus the distribution of activity throughout the cloud can be ascertained, and the total computed activity can be compared with the fission yield of the device as a check on the method.

ACKNOWLEDGMENTS

Project Stemwinder was originally conceived and coordinated by Joshua Holland, Chief, Fallout Studies Branch, Division of Biology and Medicine, U. S. Atomic Energy Commission, whose vigorous efforts brought the project into being in the space of a few weeks prior to the start of Operation Dominic I. The ideas and efforts of the late A. Vay Shelton, Lawrence Radiation Laboratory (Chief, Hazards Evaluation Branch for Dominic I, Joint Task Force 8) and of Robert J. List, Kosta Telegadas, and Jerome L. Heffter, Atmospheric Radioactivity Research Branch, U. S. Weather Bureau, were instrumental in planning and carrying out the project. The excellent cooperation and high skill of Paul Guthals, Los Alamos Scientific Laboratory, and Harry Hicks

and Edward Fleming, Lawrence Radiation Laboratory, in directing and controlling the sampling aircraft contributed much to the success of the project. Our thanks are also due to Col. Templeton Walker, Commander, 9th Weather Reconnaissance Wing, and to all the members of the 1211th Test Squadron who displayed great enthusiasm and a high degree of professional competence in carrying out the sampling missions.

REFERENCES

1. G. J. Ferber, Operation Dominic I — Project Stemwinder, Operation Dominic Report, WT-2060, U. S. Weather Bureau, May 1964. (Classified)
2. L. Fussel, Jr., Cloud Photography, Operation Redwing Report, ITR-1343, Edgerton, Germeshausen and Grier, Inc., March 1957. (Classified)
3. J. Healy, Radioactive Cloud Dose Calculations, in *Meteorology and Atomic Energy*, D. Slade (Ed.), Chap. 6, U. S. Weather Bureau, Washington, D. C., in preparation.
4. G. Higgins, Calculation of Radiation Fields from Fallout, USAEC Report UCID-4539, Lawrence Radiation Laboratory, University of California. Jan. 25, 1963.
5. E. G. Reid, Average Atmospheric Characteristics at the Eniwetok Proving Ground (April–June 1956), Stanford University, private communication, July 1958.
6. P. A. Benson, The Analysis of Particulate Debris from Pacific Air Shots, Quarterly Progress Reports, 1962–1964, various pages, Tracerlab, Division of Laboratory for Electronics, Inc.
7. P. A. Benson, Total Fissions Collected in Dominic Samples, Tracerlab, Division of Laboratory for Electronics, Inc., private communication, November 1963.
8. K. Telegadas and R. J. List, B-57 Air Sampling Program (1960), USAEC Report HASL-105, Health and Safety Laboratory, Jan. 9, 1961.
9. E. A. Pinson et al., Operation Redwing — Project 2.66a, Early Cloud Penetrations, Report WT-1320, Air Force Special Weapons Center, Kirtland AFB, February 1960. (Classified)
10. United Nations, Report of the Scientific Committee on the Effects of Atomic Radiation, Supplement No. 16, General Assembly, 17th Session, p.248, New York, 1962.
11. R. J. List, U. S. Weather Bureau, private communication, January 1964.
12. R. J. List, K. Telegadas, and G. J. Ferber, Meteorological Evaluation of the Sources of Iodine-131 Contamination in Milk, *Science*, *146:* 59(1964).

TRENDS IN THE GLOBAL DISTRIBUTION OF TRITIUM SINCE 1961

L. L. THATCHER, B. R. PAYNE, and J. F. CAMERON
International Atomic Energy Agency, Vienna, Austria

ABSTRACT

A tritium project was organized in 1961 by the International Atomic Energy Agency and the World Meteorological Organization. The latter group is responsible for precipitation-sample collection in their world-wide network of 102 stations. Several conclusions from this project have been reached.

Tritium levels rose from an average base of 80 tritium units (T.U.) for continental sites in the northern hemisphere to average peaks of 2000 T.U. in 1962 and 4000 to 5000 T.U. in 1963. Individual peaks were higher, reaching 10,000 T.U. in northern Canada. Levels in precipitation were lower in 1964. The peak year appears to have been 1963. The rate of decrease from 1963 to 1964 is less than the comparable period 1959 to 1961, possibly reflecting the higher altitudes involved in the last testing.

Tritium and ^{90}Sr deposition values over the globe show interesting consistencies that may permit the estimation of tritium concentration for unsampled areas. The HTO/^{90}Sr ratio increases toward the high mid-latitudes in the northern hemisphere.

The southern-hemisphere precipitation averaged only 15 T.U. in 1963 compared to several thousand tritium units for the northern hemisphere.

It is estimated that in 1962 and 1963 the deposition of tritium had been approximately 44 or 96 kg, depending on whether or not oceanic exchange was included in the calculation. This would leave either 124 or 72 kg in the stratosphere based on the assumption of a 168-kg production in 1961 and 1962.

DESCRIPTION OF PROJECT

The International Atomic Energy Agency (IAEA) and the World Meteorological Organization (WMO) have been jointly conducting a worldwide survey of tritium in precipitation since 1961. The objectives of the project are to compile data on the ground-level global distribution of tritium in precipitation, to analyze its migration patterns, and to provide an accurate inventory in both area and time. Sample collection began in early 1961 at numerous sites, and thus it has been possible to establish the base level for tritium prior to the resumption of weapons testing in late 1961, to follow the rise of the tritium levels through 1962 and 1963, and to detect the incipient decay in 1964.

The global sampling network is provided by WMO. It includes 102 stations distributed strategically over land and ocean areas in both hemispheres. Collections of precipitation for one sample are made over a period of one month in a standard rain gauge (usually 8 in.). All collections are made at ground level. Samples of oceanic precipitation are taken at island stations and aboard weather ships.

The samples are sent from the collection stations to IAEA and other cooperating tritium laboratories for measurement of their tritium concentration. The organizations that contribute to tritium measurements and their identifying code letters used in this paper are given as follows:

International Atomic Energy Agency	IA
International Meteorological Institute, Stockholm	S
Chalk River, Environmental Studies Group	CR
Scripps Institute of Oceanography	LJ
Weizman Institute	W
New Zealand Institute of Nuclear Studies	NZ
Tata Institute of Fundamental Research, Bombay	T

Additional data for North America provided by the U. S. Geological Survey have been used in this report. The identifying code for these data is GS.

The IAEA laboratory is now responsible for measurements from approximately one-half of the stations in the network. In addition to this, IAEA has the responsibility for the routine operation of the sample transmission system, conducts periodic laboratory intercomparisons to ensure the reliability of the data, assembles data from laboratories outside the network which voluntarily contribute, and publishes network and contributed data in Tritium Water Lists. Five of these lists have been issued so far.

Measurement Technique

The tritium measurements are made according to the procedure of Bainbridge et al.[1] by direct counting for "hot" samples and after

electrolytic enrichment for samples of lower concentration such as from the southern hemisphere. Occasionally, liquid scintillation counting is used for some very hot samples.

The procedure for the preparation of water samples is vaporization of 5 ml of water through a vacuum furnace containing hot magnesium turnings and reaction of the resultant hydrogen with ethylene to produce ethane (platinum–palladium catalyst). Ethylene is used to produce the ethane rather than acetylene, which has a higher tritium reaction capacity, because acetylene with the necessary low background has not yet been found in Europe. The ethane is then counted under proportional conditions in a low-background counter (anticoincidence and mass shielding). Two counting systems are used to provide intercomparison and cross-checking of results.

Electrolytic enrichment is usually 10-fold. This is achieved by electrolysis from 250 to 15 ml under the conditions outlined in Ref. 1. Recently it has been shown[2] that both the reproducibility and the percent of tritium recovery can be improved by the use of steel cathodes treated with phosphoric acid. The phosphoric acid forms a protective coating on the steel that apparently provides a superior surface for the tritium–protium fractionation. The treatment produces a gray-brown surface that becomes covered with a fine, adherent black deposit on electrolysis. The black deposit (presumably finely divided iron) is never disturbed. It reaches a maximum thickness after a few electrolyses and then apparently does not change. The enrichment of tritium becomes constant to within an average of ±4% after the black deposit has stabilized.

Tritium Production

Figure 1, which is an extension of a figure given by Martell,[3] reviews the tritium production and its effect on the hydrosphere since 1953. Tritium production history is shown in the upper graph, and the response of the hydrosphere is illustrated in the lower graph by the Ottawa tritium precipitation record as given by R. M. Brown of Chalk River. The plot represents quarterly averages obtained from the Ottawa data for individual rains in the Tritium Water Lists.[4] Tritium production has been calculated on the basis of Leipunsky's estimate of 0.7 kg of tritium per megaton of fusion. World tritium inventory in the summer of 1961 was estimated to be approximately 40 kg. The 1961 testing is estimated to have increased the level by approximately 68 kg, and the 1962 testing, by approximately 100 kg. Thus by the end of 1962 the world tritium inventory is estimated[5] to have reached approximately 200 kg.

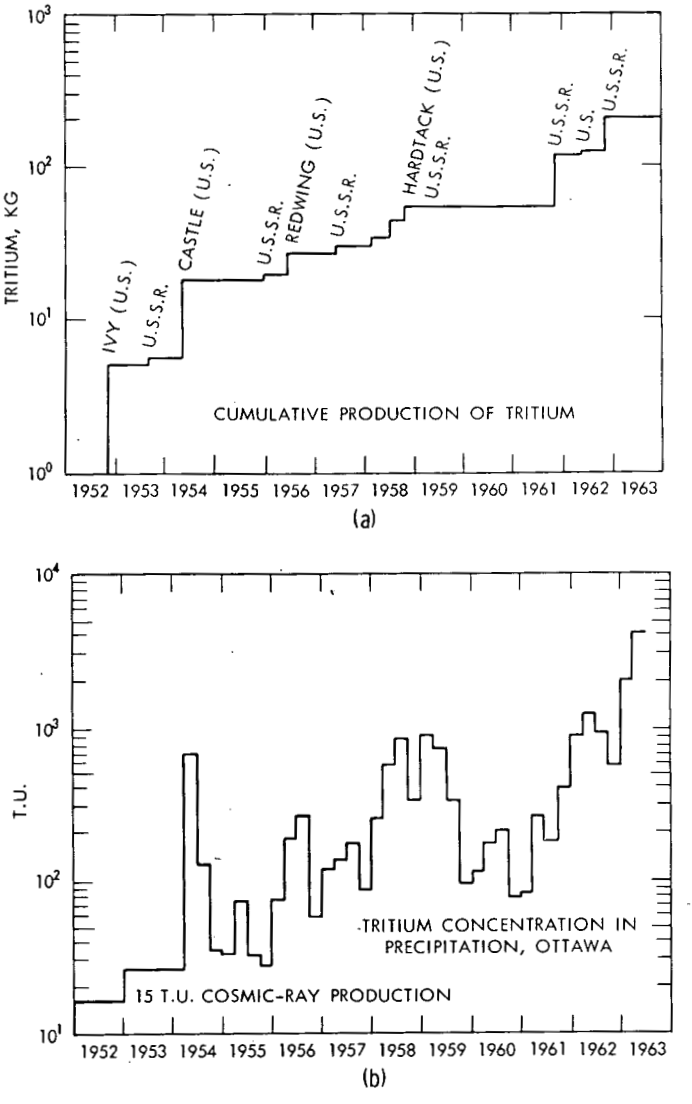

Fig. 1—The cumulative production of tritium and the response in Ottawa precipitation.

GENERAL OBSERVATIONS ON GLOBAL TRITIUM DISTRIBUTION

Global tritium information is presented in Tables 1 to 5 and in Figs. 2 to 9. The tables provide organized data from five regions of the

globe: Europe and the Mediterranean, Africa and surrounding ocean areas, South Continental Asia and the Indian Ocean, Eastern Asia and the Pacific, and the Americas.

The data cover 1961 through early 1964. It is generally arranged in the five tables on a north to south basis with a few exceptions. Approximately one-half of the network stations are represented. The other stations are not represented for various reasons: failure to receive the samples, contamination of samples making them unfit for measurement, or insufficient measurements.

The figures plot the concentration–time trends for key stations in each of the five global subdivisions and provide a basis for intercomparisons between individual stations and regions.

The most striking observation is the general similarity of trends in tritium concentration throughout the northern hemisphere. While the absolute concentrations vary from site to site, the same relative concentration changes in precipitation are observed at almost all sites in the northern hemisphere. The exceptions to the overall pattern are found in sites where the seasonal climatological pattern is affected by extraordinarily powerful influences, as in the monsoon region of India.

The consistency of the overall pattern strongly suggests that the major control on tritium fallout is stratospheric rather than tropospheric. The stratospheric control regulates the major phases of the tritium cycle, and the tropospheric controls affect only the relative variations between sites.

Tritium at all stations rose sharply in November and December 1961 following the release of 95 Mt of fusion by the U.S.S.R. in late October 1961. The base in September and October 1961 was approximately 80 T.U. for continental sites in the mid-latitudes and 20 to 40 T.U. for sites influenced by oceanic air. In November and December the tritium concentration of precipitation rose to an average of approximately 200 T.U. for continental sites as a result of tropospheric fallout.

The tritium rise continued in early 1962 to attain a peak of approximately 1000 T.U. at continental mid-latitude sites by March. Further rise continued to approximately 2000 T.U. at several sites and remained at this level through July or August. Decline was apparent in September, and minimum levels were generally reached in October or November. The minimum for 1962 was approximately 400 to 500 T.U.

In 1963 the pattern established in 1962 was repeated with a general rise in January which continued to peak levels in May which were sustained through July or August. The peak was higher than in 1962, averaging 4000 to 5000 T.U. for continental sites. At some northern sites concentrations of 8000 to 10,000 T.U. were observed. For tritium, 1963 appears to have been the peak fallout year. The October or November minimum was in the range of 1000 T.U.

(Text continues on page 659.)

Table 1—EUROPEAN AND MEDITERRANEAN TRITIUM CONCENTRATIONS, T.U.

Station	Location	Laboratory	Jan.	Feb.	Mar.	Apr.	May	June	July	Aug.	Sept.	Oct.	Nov.	Dec.
1961														
Isfjord Rad, Spitzbergen	78°04′N 13°38′E	S							172	90	39	51	1880	1210
Reykjavik, Iceland	64°08′N 21°56′W	S	25	45	40	60	74	107	104	78	43	34	92	301
Lista, Norway	58°06′N 06°34′E	S		33	36	61	91	116	138	73	42	61	86	124
Valentia, Ireland	51°56′N 10°15′W	S and IA	21	27	23	51	47	82	72	33	18	22	89	108
Stuttgart, Germany	48°46′N 09°11′E	S		48	46	117	106	65	90	91	47	68	124	
Vienna, Austria	48°07′N 16°34′E	IA		39	43	123	174	125	140	104	62	56	131	136
Genoa, Italy	44°24′N 08°58′E	IA											132	98
Tel Aviv, Israel*	31°57′N 34°54′E	W and IA	24	44			110						235	
Alexandria, UAR	31°12′N 29°57′E	IA												216
1962														
Nord, Greenland	81°36′N 16°40′W	IA	2580	1540	4620			2270	1790	1910		1200	1060	1330
Isfjord Rad, Spitzbergen	78°04′N 13°38′E	S		294		628			1250	673	355	365	201	334
Reykjavik, Iceland	64°08′N 21°56′W	S	272	262	189	392	431	626	491	531	207	200	166	260
Lista, Norway	58°06′N 06°34′E	S	289				596	414	861	408	266	166		
Valentia, Ireland	51°56′N 10°15′W	S and IA	173	121	288	339	441	354	406	230	172	92	179	172
Stuttgart, Germany	48°46′N 09°11′E	S	245	932	683	791	1040	1200	849	498	309	379	494	633
Vienna, Austria	48°07′N 16°34′E	IA		1230	1080	1030	1210	990	1230	880	550	520	650	650
Genoa, Italy	44°24′E 08°58′E	IA	161		459	592	762	845			449	312	514	530
Alexandria, UAR	31°12′N 29°57′E	IA	254	231								187		253
1963														
Nord, Greenland	81°36′N 16°40′W	IA				7200	5550		9850	7770		2460	2980	4830
Isfjord Rad, Spitzbergen	78°04′N 13°38′E	S	409	565	887	1280	2180	3650	1920	3970	2260	1410		
Reykjavik, Iceland	64°08′N 21°56′W	S	303	475	529	1680	2320	3930	3710	2010	916	729	386	
Lista, Norway	58°06′N 06°34′E	S	204	763	1090	1500	2840	2510			1060	510	716	
Valentia, Ireland	51°56′N 10°15′W	S and IA	524	535	835	1090	1020	2000	2090	1600	637	502		
Stuttgart, Germany	48°46′N 09°11′E	S	933	1660	1790	3800	3350	5860	5440	2940	4240	1340	893	
Vienna, Austria	48°07′N 16°34′E	IA	1260	1900	2900		5930	4970	5950	3010	2200		790	1330
Genoa, Italy	44°24′N 08°58′E	IA	412	1150	625	2020		2700		2040	1140	1090	397	563
Ankara, Turkey	40°07′N 33°00′E	W						6020	5400		2510	1350		810
Tel Aviv, Israel*	31°57′N 34°54′E	W and IA	330	445	1250	1950	4700						590	705
Alexandria, UAR	31°12′N 29°57′E	IA	310	742	1240	1760						471	516	440
1964														
Nord, Greenland	81°36′N 16°40′W	IA	6280	6510										
Vienna, Austria	48°07′N 16°34′E	IA	1660	1170	2740	2970	2690	2360	2600					
Genoa, Italy	44°24′N 08°58′E	IA	400	552	1080	700	1380		1090					
Ankara, Turkey	40°07′N 33°00′E	W	1710											
Tel Aviv, Israel*	31°57′N 34°54′E	W and IA	510	390	545	650			787					
Alexandria, UAR	31°12′N 29°57′E	IA	559	648	751									

*Data from nearby locations used in part.

Table 2—AFRICAN AND SURROUNDING OCEAN AREA TRITIUM CONCENTRATIONS, T.U.

Station	Location	Laboratory	Jan.	Feb.	Mar.	Apr.	May	June	July	Aug.	Sept.	Oct.	Nov.	Dec.
1961														
Khartoum, Sudan	15°36′N 32°33′E	IA									71			
Entebbe, Uganda	00°03′N 32°27′E	S	8.8	21	11	13	8.9	12	7.1	12	12	7.8	5.2	34
Leopoldville, Congo	04°19′S 15°19′E	S		23	14	32	14					7.6	21	
Make, Seychelles	04°37′S 55°27′E	S				3.4			4.7	3.9	0.8	3.5	5.4	
Dar es Salaam, Tanganyika	06°52′S 39°16′E	S	38	3.3			2.8	6.2	4.5	2.9	43	3.0	5.6	9.7
Windhoek, South Africa	22°34′S 17°06′E	S				15	24	16					23	19
Pretoria, South Africa	25°45′S 28°14′E	S												
Malan, South Africa	34°21′S 18°30′E	S				16	8.8	10	8.2	5.4	12	14		16
Gough Island, South Atlantic	40°19′S 09°54′W	S				3.4	4.5	6.7	4.9	7.2	8.7	6.9	8.0	6.8
Marion Island, South Atlantic	46°53′S 37°52′E	S				4.0	5.6	4.6	4.0	16	14	9.0	8.4	7.4
1962														
Khartoum, Sudan	15°36′N 32°33′E	IA						694	437	475	401	365		
Entebbe, Uganda	00°03′N 32°27′E	S									7.4			
Leopoldville, Congo	04°19′S 15°19′E	S					38							
Make, Seychelles	04°37′S 55°27′E	S									5.6	5.7	8.1	
Dar es Salaam Tanganyika	06°52′S 39°16′E	S	23	14	13	6.0	6.1	21		10	23	5.5		
Windhoek, South Africa	22°34′S 17°06′E	S		25								38	47	65
Pretoria, South Africa	25°45′S 28°14′E	S	16	15	16	15						43	45	63
Malan, South Africa	34°21′S 18°30′E	S	14	26	4.2	8.8	9.9	5.1	9.1	15	8.2	11	11	14
Gough Island, South Atlantic	40°19′S 09°54′W	S	7.5	6.6	4.3	4.2	7.3	7.7	11	16	15		12	14
Marion Island, South Atlantic	46°53′S 37°52′E	S	11	7.5	7.6			8.7	18	12	21	18	20	17
1963														
Khartoum, Sudan	15°36′N 32°33′E	IA					727		1550	2170	1070			
Entebbe, Uganda	00°03′N 32°27′E	S	74	108	148	34	94	292						
Leopoldville, Congo	04°19′S 15°19′E	S					64							
Make, Seychelles	04°37′S 55°27′E	S	21.6	16.6										
Dar es Salaam, Tanganyika	06°52′S 39°16′E	S	21	33	23	14	11	18	16	4.4				
Windhoek, South Africa	22°34′S 17°06′E	S	46	67	48									
Pretoria, South Africa	25°45′S 28°14′E	S	37	48										
Malan, South Africa	34°21′S 18°30′E	S	27	19	9.2									
Gough Island, South Atlantic	40°19′S 09°54′W	S	31	12	8.6									
Marion Island, South Atlantic	46°53′S 37°52′E	S	19	20										
1964														
Khartoum, Sudan	15°36′N 32°33′E	IA							1000					

Table 3 — SOUTH CONTINENTAL ASIA AND INDIAN OCEAN TRITIUM CONCENTRATIONS, T.U.

Station	Location	Laboratory	Jan.	Feb.	Mar.	Apr.	May	June	July	Aug.	Sept.	Oct.	Nov.	Dec.
1961														
Teheran, Iran	35°41′N 51°19′E	IA		86		141								354
New Delhi, India	28°35′N 77°12′E	T							65	88	33	29	37	
Luang-Prabang, Laos	19°53′N 102°23′E	IA							60	57	75			
Bombay, India	18°54′N 72°49′E	T						44	19	14		18		
Rangoon, Burma	16°46′N 96°10′E	IA							17	17	15	21		
1962														
Teheran, Iran	35°41′N 51°19′E	IA	690	592		2040					1740	449	586	649
New Delhi, India	28°35′N 77°12′E	T	479	900	748			←		188	→			
Luang-Prabang, Laos	19°53′N 102°23′E	IA			226			157						
Bombay, India	18°54′N 72°49′E	T						←		58	→			
Rangoon, Burma	16°46′N 96°10E	IA					157	116		54				
1963														
Teheran, Iran	35°41′N 51°19′E	IA	874	1360	342	4450	4770	4880		4200	4370	1820	4450	1740
New Delhi, India	28°35′N 77°12′E	T						←		246	→			
Luang-Prabang, Laos	19°53′N 102°23′E	IA												
Bombay, India	18°54′N 72°49′E	T						←		436	→			
Rangoon, Burma	16°46′N 96°10′E	IA					400	331	433	300	185	135	88	
1964														
Teheran, Iran	35°41′N 51°19′E	IA	2730	1400	1150	3020								

Table 4—EASTERN ASIAN AND PACIFIC TRITIUM CONCENTRATIONS, T.U.

Station	Location	Laboratory	Jan.	Feb.	Mar.	Apr.	May	June	July	Aug.	Sept.	Oct.	Nov.	Dec.
1961														
Pohang, Korea	36°03′N 129°23′E	IA							29	18	56	56	46	
Tokyo, Japan*	35°41′N 139°46′E	UC and IA			70	30	120	40		30	30	50	80	100
Manila, Philippines	14°31′N 121°00′E	IA		18		14	12					23	35	
Kaitoke, New Zealand†	41°S 175°E	NZ	11	11	8.9	5.1		7.7	7.7	10.6	16.9		10.7	9.6
1962														
Adak, Alaska	51°53′N 176°39′W	CR			273	569	587	489	477	271	196	181	228	329
Pohang, Korea	36°03′N 129°23′E	IA								236	224	205		
Tokyo, Japan*	35°41′N 139°46′E	UC and IA	330	690	220	190			130	70		220	380	160
Midway Island, Pacific	28°13′N 177°22′E	LJ								43	32	25	44	26
Hilo, Hawaii	19°44′N 155°04′W	LJ		53	78	103	70	75	77	33	21	27	27	42
Wake Island, Pacific	19°17′N 166°39′E	LJ								39	22	23	19	27
Johnston Island	16°44′N 169°31′W	LJ							46	19	9.9	29	26	13
Christmas Island	02°00′N 157°24′W	LJ					17	14	10	6.6	5.5	4.2		
Canton Island	02°46′S 171°43′W	LJ							6.0		8.6		13	26
Kaitaia, New Zealand	35°09′S 173°17′E	NZ										15	18	
Melbourne, Australia	37°49′S 144°58′E	NZ	18		8.5			25		27			30	
Kaitoke, New Zealand†	41°S 175°E	NZ	9.8	9.5	6.8	11.6	16		13.6	193	18.4	24		21
1963														
Adak, Alaska	51°53′N 176°39′W	CR	562	830	869	1770	2650	3900	3420	2580	1510	549		
Pohang, Korea	36°03′N 129°23′E	IA			1120	1410	1700	1940	952	806	871	766		883
Tokyo, Japan*	35°41′N 139°46′E	UC and IA		700	1680	950	990	980	970	790	920		450	
Midway Island, Pacific	28°13′N 177°22′E	LJ	60	95	187	658	730	321	412	255	147	159		82
Hilo, Hawaii	19°44′N 155°04′W	LJ	64	90	154	224	250	373	232	178	102	88	81	
Wake Island, Pacific	19°17′N 166°39′E	LJ		32	134	225	253	242	281					
Johnston Island	16°44′N 169°31′W	LJ	78	55	164	191	189	180						
Guam, Mariana	13°29′N 144°48′E	IA		54	74		128		183		88			
Canton Island	02°46′S 171°43′W	LJ	14	10	3.5	11	5.6	8.6	15	12	6.6	12	5.5	10
Kaitaia, New Zealand	35°09′S 173°17′E	NZ	11											
Kaitoke, New Zealand†	41°S 175°E	NZ	10.6	10.6	16	13	11.2		26	55	34	44	21	
1964														
Pohang, Korea	36°03′N 129°23′E	IA	960	715	1270	868	1230							
Tokyo, Japan*	35°41′N 139°46′E	UC and IA	955			666	811							

*University of California at Los Angles data (1961–1963) adjusted for evaporation and counter calibration.
†Original data not by month; data adjusted to monthly schedule.

Table 5— NORTH AND SOUTH AMERICAN TRITIUM CONCENTRATIONS, T.U.

Station	Location	Laboratory	Jan.	Feb.	Mar.	Apr.	May	June	July	Aug.	Sept.	Oct.	Nov.	Dec.
1961														
Goose Bay, Labrador	53°19′N 60°23′W	CR	195	269			195	269	228	214	90	64	169	177
Palmer, Alaska*	61°35′N 149°10′W	GS									89		182	263
Whitehorse, Yukon	60°43′N 135°04′W	CR					317	275	223	120				499
Fort Smith, Northwest Territory	60°01′N 111°58′W	CR								184				
Edmonton, Alberta	53°34′N 113°31′W	CR					364	338	260	73	85			
Ocala, Fla.*	29°11′N 82°09′W	GS									43		38	66
Lincoln, Nebr.*	40°49′N 96°41′W	GS									79		237	634
Menlo Park, Calif.*	37°27′N 122°11′W	GS									29	55	145	115
Flagstaff, Ariz.	35°12′N 111°40′W	IA												448
Waco, Texas	31°37′N 97°13′W	IA												400
Stanley, Falkland Islands	51°42′S 57°52′W	IA											21	20
1962														
Groennedal, Greenland	61°13′N 48°07′W	IA					1240	1580	1600		456	498	568	593
Goose Bay, Labrador	53°19′N 60°23′W	CR	1680	915	905	1090	1130	1700	1490	1060	528	314	482	476
Bethel, Alaska	60°47′N 161°43′W	CR		658	562	508	1140	1190	421	561	452	314	378	739
Palmer, Alaska*	61°35′N 149°10′W	GS	394	336	762	595	1180		911	556	536	341	848	435
Whitehorse, Yukon	60°43′N 135°04′W	CR	1010	1498	1030	1280	2120	2430	2040	1140	747	634	556	378
Fort Smith, Northwest Territory	60°01′N 111°58′W	CR					2570	1900	1810	1260	731	736	636	790
Edmonton, Alberta	53°34′N 113°31′W	CR				1560	1940	2240	2000	1480	904	795	614	1140
Albany, N. Y.*	42°40′N 73°49′W	GS							1200	924	527	254	374	732
Washington, D. C.	38°55′N 77°00′W	GS							1150					
Hatteras, N. C.	35°15′N 75°40′W	IA	150		256		723		680		166	218	228	
Ocala, Fla.*	29°11′N 82°09′W	GS		104	195	198	399		400	156	88	93	124	
Chicago, Ill.	41°47′N 87°44′W	IA	736	819	1250	1420	1060	1010	1390	663	1760		521	1070
Lincoln, Nebr.*	40°49′N 96°41′W	GS	683	840	1480	1200	930		1350	411	376	396	590	989
Menlo Park, Calif.*	37°27′N 122°11′W	GS	133	252	90	198						82	186	163
Albuquerque, N. Mex.*	35°05′N 106°38′W	GS							570	560	185	303	387	532
Flagstaff, Ariz.	35°12′N 111°40′W	IA	655	647	1272	2040	2040	1340	523		428	408	723	872
Waco, Texas	31°37′N 97°13′W	IA	601	378	970	690	467	400		535	257	217	351	340
Stanley, Falkland Islands	51°42′S 57°52′W	IA	25	30	25	55	25	35	43					

(Table 5 continues on page 656)

Table 5 — (Continued)

Station	Location	Laboratory	Jan.	Feb.	Mar.	Apr.	May	June	July	Aug.	Sept.	Oct.	Nov.	Dec.
1963														
Goose Bay, Labrador	53°19′N 60°23′W	CR	1230	1420	2420	3660	4300	6800	5260	4910		2165	854	1050
Bethel, Alaska	60°47′N 161°43′W	CR		941	1400	2000	3714	4280	3500	1955	1440	927	1475	1115
Whitehorse, Yukon	60°43′N 135°04′W	CR	2900	2240	3265	10000	6790	7270	8900	4660	2010	2315	1515	2100
Fort Smith, Northwest Territory	60°01′N 111°58′W	CR	2150	2480	4200	6400	3390	7140	6960	5120	3100	1780	1740	1572
Edmonton, Alberta	53°34′N 113°31′W	CR	1740	2530	3080	4580	3730	7450	8510	6330	3100	2930	2030	2265
Hatteras, N. C.	35°15′N 75°40′W	IA				683				1380		456		249
Chicago, Ill.	41°47′N 87°44′W	IA	1460	1910	1830	2790	3750	3440	3180	3570	2220	1140	563	2090
Flagstaff, Ariz.	35°12′N 111°40′W	IA	954	1380	1720	2510	2320		1980	1160	1035	1090	941	
Waco, Texas	31°37′N 97°13′W	IA	477		499	1270	2000	1230		637	708	290	416	509
Cayenne, French Guiana	04°50′N 52°22′W	IA	101	99	122	130	97	166		119	59		91	
Stanley, Falkland Islands	51°42′S 57°52′W	IA				55	25	35	43	98				
1964														
Chicago, Ill.	41°47′N 87°44′W	IA	1760	2470	2160		3890	2070						
Flagstaff, Ariz.	35°12′N 111°40′W	IA	770											
Waco, Texas	31°37′N 97°13′W	IA	615	806	673	398	447	404						
Stanley, Falkland Islands	51°42′S 57°52′W	IA	43	33	47	21								

*Samples may not correspond precisely with beginning of month.

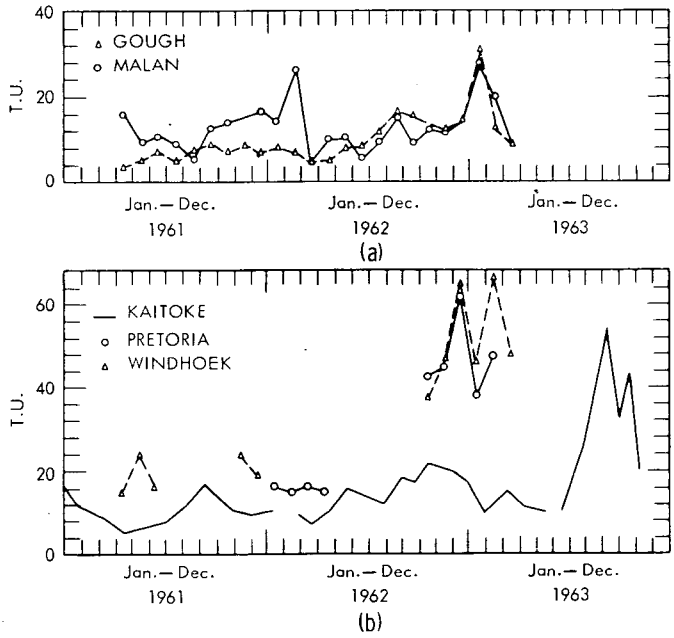

Fig. 2—Tritium in the southern hemisphere.

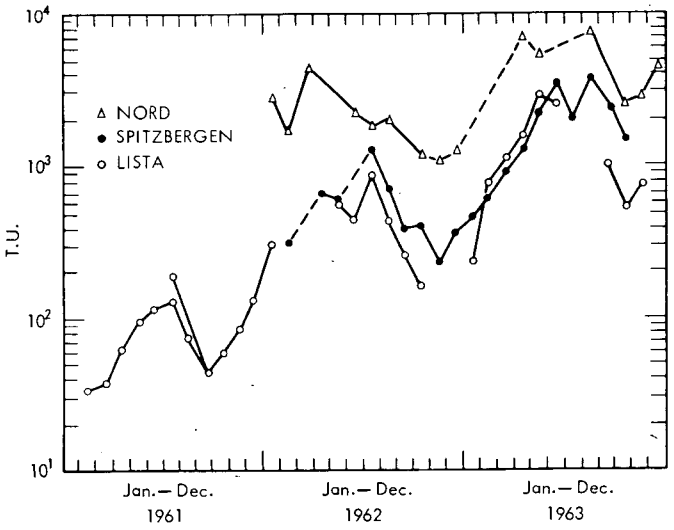

Fig. 3—Tritium fallout in northern Europe.

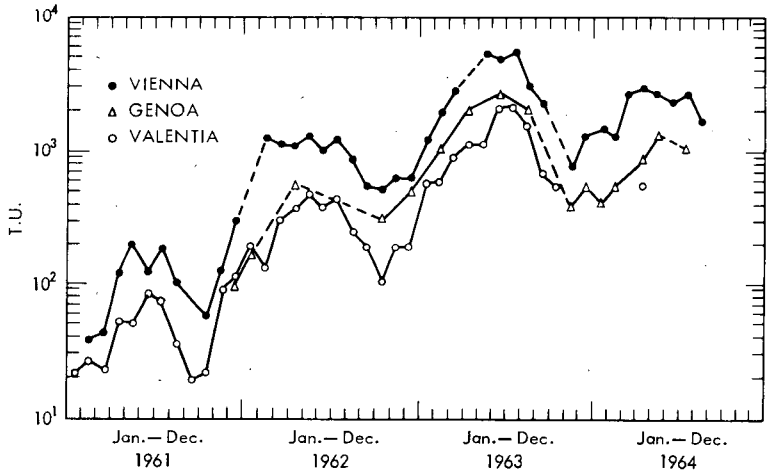

Fig. 4—Tritium fallout in the mid-latitudes of Europe.

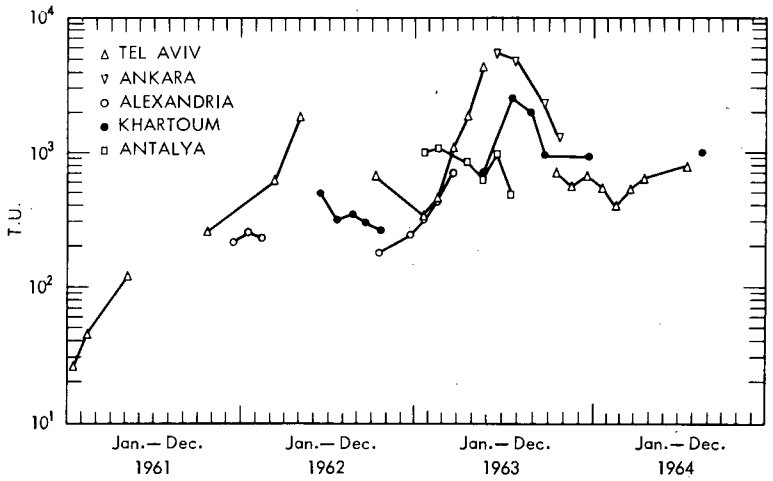

Fig. 5—Tritium fallout in the Mediterranean region.

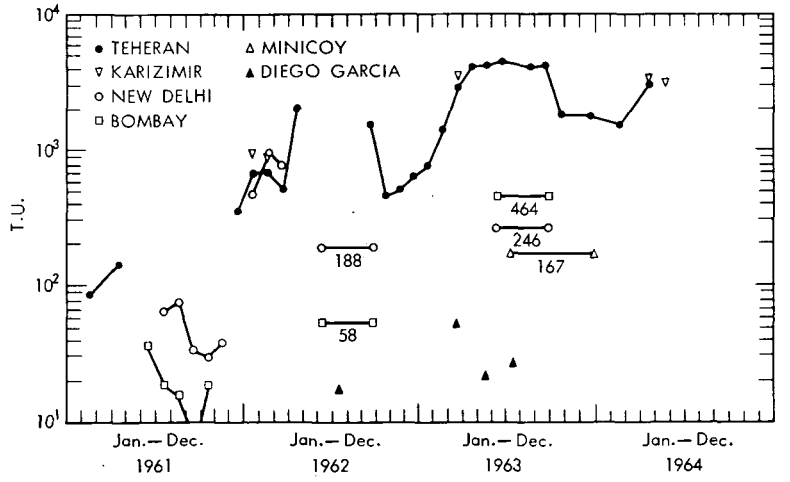

Fig. 6—Tritium fallout in South Continental Asia.

In 1964 the usual spring peak appeared but at a lower level than in 1963. Comparative mean peak values are given below for several continental mid-latitude sites:

Station	1963	1964
Vienna, Austria	4837 (March through July)	2674 (March through July)
Chicago, Ill.	2955 (March through June)	2648 (March through June)
Flagstaff, Ariz.	1332 (January and March)	965 (January and March)
Teheran, Iran	4450 (April)	3020 (April)

It is apparent that tritium concentration in precipitation began trending downward in 1964. The rate of decrease of tritium in the interval 1963–1964 is seen to be less than the rate of decrease in the corresponding interval 1959–1960. It appears to be comparable to the decrease in the interval 1960–1961. This is illustrated in Fig. 10, which presents the respective decay slopes. The difference is thought to be due to the respective altitudes of injection involved in the 1958 and the 1961–1962 test series.

Throughout the development and the apparent decay of the 1963 tritium peak, the concentrations of tritium in precipitation at sites influenced by oceanic air have been consistently below the concentrations observed at continental locations in the same latitude belt. This is, of course, due to the diluting effect of the low tritium water vapor from the surface ocean water. The results of this factor is to create nonuniformities in the average tritium fallout concentrations for individual sites within a given latitude belt. Annual tritium deposition values for different sites within a given latitude belt are more uniform

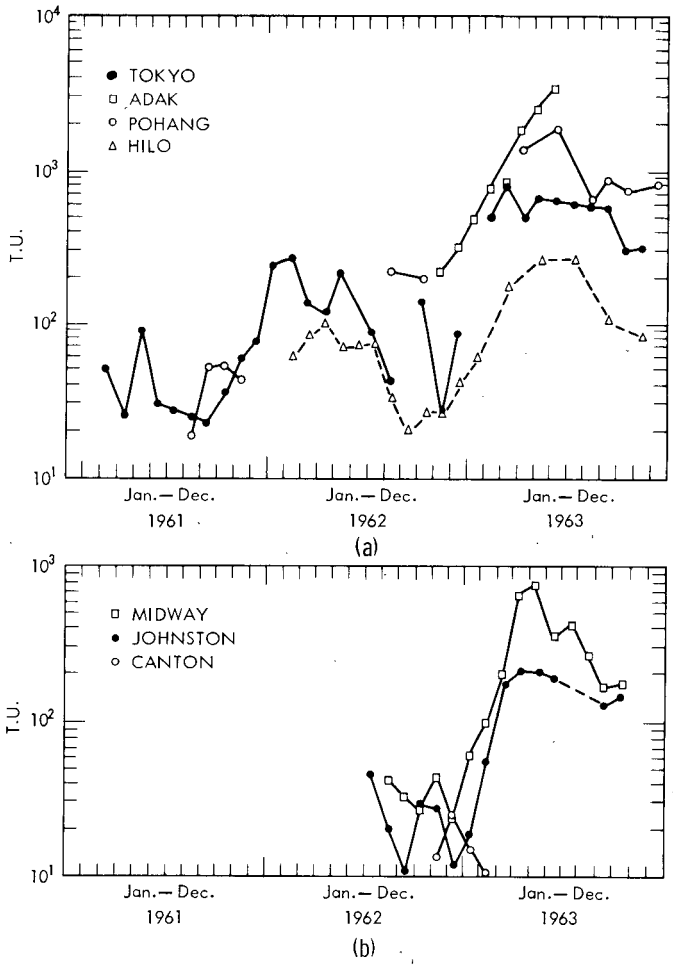

Fig. 7—Tritium fallout in the Pacific.

than the concentration values. This indicates that the amount of precipitation at a given site affects the concentration to some extent.

The effect of altitude is observed at several locations. Generally, the tritium concentration in precipitation increases with altitude. An example is provided by Srinagar, India (at an altitude of 5250 ft), which reports the highest average tritium values measured in India by the Tata Institute. The level for the spring of 1963 at Srinagar averaged 3660 T.U., which was higher than that at Chicago. Amritsar in the same region of North India but at a lower elevation (about 600 ft) has shown lower tritium concentrations. For example, in the last half of 1962, Srinagar averaged 479 T.U. whereas Amritsar averaged 202 T.U.

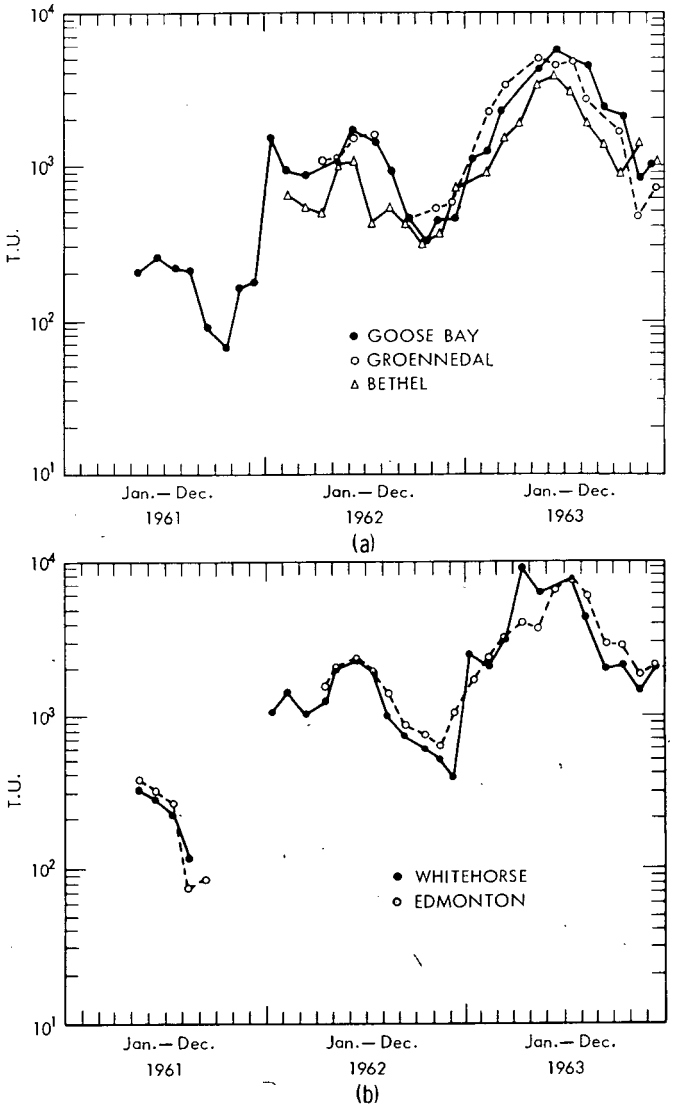

Fig. 8—Tritium fallout in northern Canada.

Similarly, Pretoria (at about 5000 ft) has shown relatively higher tritium peaks than other South African sites, according to data of the International Meteorological Institute. The New Zealand Institute of Nuclear Science has provided data from Mount Cook that shows a strong altitude effect. Snow at 6800 ft measured 40 T.U. in 1961, a value much higher than values found in measurements at sea-level

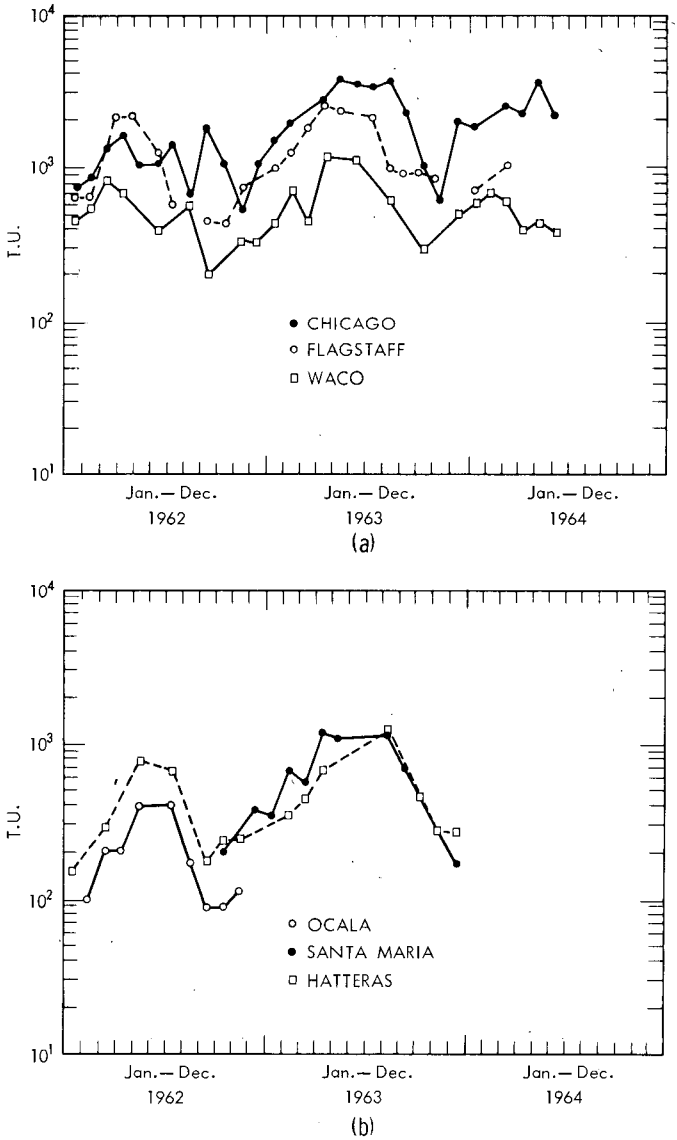

Fig. 9—Tritium fallout in the United States.

locations. In the southern hemisphere the preponderance of ocean over land makes a clear-cut identification of an altitude effect uncertain.

Tritium data from the southern hemisphere (Fig. 2) are very limited as compared to those from the northern hemisphere. Sustained records are available only for two or three stations in South Africa (S)

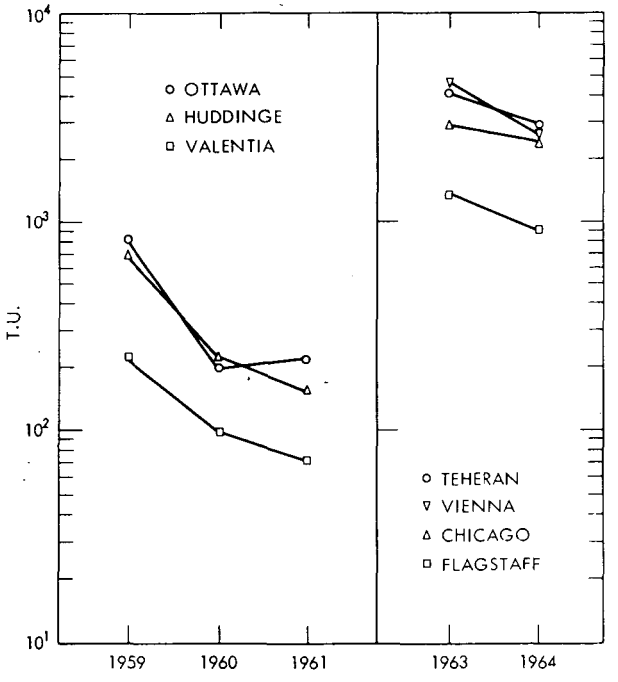

Fig. 10—Comparative rates of tritium decline after cessation of tests in 1959 and 1963.

and a few stations in New Zealand and Australia (NZ). Shorter records for South Pacific island locations (LJ) are also available.

The information clearly shows that the tritium pulse in the southern hemisphere in 1962 to 1963 remained far below that in the northern hemisphere. The mean tritium level for precipitation in the southern hemisphere appears to be about 15 T.U., somewhat higher on the continents and somewhat lower on the ocean islands.

The northern hemisphere is remarkable for the general conformity of the tritium peaks at widely separated sites. The same degree of uniformity is not found in the southern-hemisphere sites. Malan, South Africa, shows two peaks (S), both in the southern summers of 1961–1962 and 1962–1963. The peak in 1962–1963 is very certain, inasmuch as it is reproduced at four stations: Gough Island, Malan, Pretoria, and Windhoek (S). Tritium peaks at Kaitoke, New Zealand (NZ), in 1961 and 1962 are less distinct, but the 1963 peak is very pronounced. The Kaitoke peaks appear to be two to three months in advance of the South African peaks, appearing in the southern spring rather than in the summer. Similar time displacement is observed with the ^{90}Sr fallout peaks between Pretoria and Wellington, New Zealand. Explanation of the

significance of the displacement between the South African and the New Zealand fallout awaits further study.

At northern-hemisphere stations where both tritium and ^{90}Sr data are available, it has been rather consistently observed that the tritium fallout peaks are delayed behind the ^{90}Sr peaks by one or two months. The ^{90}Sr fallout peak is reached around April or May, whereas the tritium peak is reached around June or July. The tritium peak extends further into the late summer because of reevaporation effects. No explanation for the phase displacement of the rising limb of the curve (spring) is available at present.

OBSERVATIONS RELATED TO GLOBAL SUBDIVISIONS

Europe and the Mediterranean

Figure 3 shows tritium relations among several northern European sites. Concentrations in precipitation at the northern Canadian and European sites showed the most immediate and highest response to the late October (23–30) weapons tests in 1961. The January 1962 level for Nord was 2580 T.U., the highest measured in that month anywhere in the world network. Nord has consistently reported the highest concentrations, probably partly attributable to the low precipitation. Other European stations showed relatively sharp rises modified principally by the contribution of maritime air. This is illustrated by the persistently high level of Vienna as compared to Valentia (Fig. 4). The decrease in 1964 is illustrated by the Vienna and the Genoa levels.

The Mediterranean-region data are less complete than the continental data (Fig. 5). Still, the same general trends are shown. Concentrations of about 200 T.U. were measured in November at Tel Aviv (W) and in December at Alexandria (IA). The rise of the spring peak in 1962 appears to be delayed slightly with respect to the European peak, but apparently the peak reached levels fully as high. This is based on one measurement of 1755 T.U. (W) for Tirat Yael, Israel (recorded as Tel Aviv).

In 1963 the beginning of the spring rise for Tel Aviv is two months behind Vienna, but again the peak value in June is nearly the same. In 1964 the Tel Aviv peak is much lower than the Vienna peak.

The departures from the standard European mid-latitude pattern for the Tel Aviv data indicate that the Mediterranean has a measurable influence on the tritium fallout pattern. Additional evidence is obtained by the consideration of results from Antalya (W) and Ankara (W), Turkey. Antalya is a coastal site, whereas Ankara is situated approximately 200 miles north at an altitude of 3000 ft. In January and

February 1963, Antalya concentrations exceeded Tel Aviv concentrations by a factor of 3, but after March Antalya concentrations were lower by approximately the same factor. Concentrations at Antalya were lower than those at Ankara by a factor of 5 for the comparable months (June and July). The Ankara curve superimposes on the curve for Vienna almost precisely, indicating that it is controlled essentially by the same continental climatic factors. The tritium records for Antalya and Ankara are too limited for conclusions, but the fact that Ankara is sheltered from Mediterranean air and receives most of its precipitation from the north is clearly evident. On the Mediterranean coast the local climatology dominates over the stratospheric input, and hence the variations of the local tritium record may be useful for the analysis of water-vapor transport in this region.

Africa

The main features of tritium variations in Southern Africa have been discussed under the general consideration of the southern hemisphere.

Equatorial Africa illustrates the relatively sharp division of air masses that prevails at the equator. Data from Entebbe, Uganda (S), at 00°03'N and from Dar es Salaam (S) at 06°52'S clearly illustrate the comparative isolation of the hemispheres. Throughout 1963 Entebbe levels were much higher than those at Dar es Salaam, averaging 125 T.U. compared with 17 T.U. Apparently surges of northern-hemisphere air may reach Dar es Salaam at times, as indicated by two monthly measurements of 38 and 43 T.U. in January and September 1961 compared to an average of approximately 5 T.U. for the other months.

South Continental Asia and the Indian Ocean

In this region there is a sharp division between the sites dominated by continental air and the sites that are seasonally subject to overwhelming air masses from the Arabian and Bengal seas. The highest tritium levels were measured at Teheran, Iran (IA), and Karizimir, Afghanistan (IA), both continental sites (Fig. 6). In 1962 the peak summer tritium levels at Teheran appear to exceed the Vienna level by almost 1000 T.U. In 1963 and 1964 the Teheran peaks equal those at Vienna.

These sustained high levels are strongly contrasted with New Delhi and Bombay (T), where the monsoon rains arrive in June and continue through September. The January, February, and March measurements in 1962 for New Delhi average as high as those for Teheran and indicate that New Delhi is dominated by continental air at this time

of year. With the onset of the monsoon in June, the tritium level dropped sharply to average 188 T.U. for the four months of the monsoon season. This is approximately one-tenth of the level at Teheran during these months. In 1963 the same pattern is repeated at the somewhat higher tritium level of 246 T.U.

Bombay shows the same pattern as New Delhi but with more pronounced oceanic influence. Minicoy, an island off the southwest coast, had an average level of 167 T.U. in the 1963 monsoon season. This is only 79 T.U. lower than New Delhi and shows the complete dominance of the oceanic air masses deep into the continent in the monsoon season. In 1963 New Delhi (246 T.U.) had a lower level than Bombay (464 T.U.) during the monsoon. This is the reverse of expectations. The situation is attributed to the 1963 monsoon coming predominantly from the Bengal Sea, whereas in 1962 it came predominantly from the Arabian Sea.

Tritium levels at Diego Garcia (IA), an island in the Indian Ocean at 06°34′S, show the typical low values of the southern hemisphere. The average for 1963 was 34 T.U.

The Pacific Ocean

In the Pacific, tritium data have been obtained at a series of stations ranging from 51°35′N, Adak, Alaska, to 41°S, Kaitoke, New Zealand. Here the sampling sites are clearly dominated by an oceanic environment; and, consequently, as a group the tritium concentrations at the northern-hemisphere sites are substantially lower than in the other four northern-hemisphere areas considered in this report.

The highest concentrations are found at Adak (CR) and Pohang (IA), at Adak because of the high latitude and at Pohang because of the nearby Asian continent, which provides a continental air-mass effect. Tokyo, at approximately the same latitude as Pohang, shows consistently lower concentrations.

Comparison of the 1963 tritium data at the Pacific islands, Midway (LJ) (28°N), Hawaii (LJ) (19°44′N), Johnston (LJ) (16°44′N), indicates a significant latitude trend. All three sites are completely oceanic-dominated, and therefore the latitude effect can be revealed without ambiguity. The mean values for the February through September 1963 data are given below. Data for Tokyo and for Adak (based on an assumed 1500 T.U. for August and September) are also given.

Station	Latitude	T.U.
Adak	51°53′N	2030
Tokyo	35°41′N	876
Midway	28°13′N	351
Hilo	19°44′N	204
Johnston	16°44′N	155

The increase of tritium concentration toward the northern mid-latitudes is clear.

Southern-hemisphere tritium data for the Pacific is represented by Canton Island (LJ) and Kaitoke, New Zealand (NZ) (Figs. 2 and 7). Canton at 02°46′S shows typical southern-hemisphere values for 1963, averaging 9.4 T.U. At Kaitoke the mean tritium concentration for the same period is 24.2 T.U. There is no evidence of a peak at Canton, but a spring peak is clearly defined at Kaitoke. Although Kaitoke may be influenced by the land mass of New Zealand to some extent, this effect would not appear to be very significant because of the overwhelming ratio of water over land area. Kaitoke is a coastal location (near Wellington). Thus it appears that the higher mean concentrations at Kaitoke may represent a true latitude effect. This would suggest the entry of the annual tritium fallout pulse at the higher southern latitudes and gradual migration of the pulse northward.

The Americas

The highest tritium concentrations in the entire survey with the single exception of Nord, Greenland, are found in northern Canada (Fig. 8). Although the 1961–1962 record for Canada is not complete, it seems fairly certain that these northern sites showed the same immediate response to the Oct. 23 to 30, 1961, testing that was observed in the Arctic regions of Europe. In January 1962, for example, the tritium measurement at Whitehorse, Yukon (CR), was 1010 T.U., and at Goose Bay, Labrador (CR), it was 1680 T.U.

The single highest monthly tritium measurement found throughout the entire survey was the 10,000 T.U. value for April 1963 at Whitehorse.

The effect of the prevailing cross-continent direction of air circulation may be observed in Canada where west and east stations are located at approximately the same latitude. The difference is most marked in 1961 when the influx of spring tritium was minimum (compared to later years) and reevaporated tritium showed its maximum effect. Between Edmonton (53°34′N, 113°31′W) and Goose Bay (53°19′N, 60°25 W), an apparent time difference of approximately one month existed between the fall tritium decay curves, with the summer peak persisting longer at Goose Bay. This was as expected.

The same effect is not observed in 1963 for Edmonton and Goose Bay, but it is suggested for Whitehorse and Goose Bay. Presumably, as the proportionate input of stratospheric tritium decreases and the reevaporation component increases, in 1964 and 1965 the delay of the annual tritium decline in the east as compared to the west should reappear.

The North American continent provides the opportunity to study a meridional traverse over an essentially continental environment, just as the Pacific provided the same traverse for an oceanic environment. Data for Fort Smith (CR), Edmonton (CR), Chicago (IA), and Flagstaff (IA) are averaged for the full year of 1963.

Station	Location	Mean T.U.
Fort Smith	60°01′N, 111°58′W	3836
Edmonton	53°34′N, 113°31′W	4193
Chicago	41°47′N, 87°44′W	2333
Flagstaff	35°12′N, 111°40′W	1471

The tritium concentrations increase toward the north. However, it is not certain that this is solely a latitude effect.

The difference between the Canadian and U. S. sites must be attributed in part, at least, to the effect of oceanic air from the Gulf of Mexico; therefore it is not entirely a latitude effect. In other parts of the world, sites south of Chicago have shown higher tritium averages. Teheran (35°41′N) averaged 3150 T.U. for the first half of 1963, compared to 2333 T.U. for Chicago. Presumably, Teheran is less affected by oceanic air masses than is Chicago and is therefore more truly representative of a continental site at this latitude. Data for eastern North America (IA, GS) are given in Fig. 9, showing an increasing oceanic component from Hatteras, N. C., to Ocala, Fla.

Data from South America are incomplete, partly because of the poor cooperation of national authorities. Large parts of Brazil remain unsampled. Data from Buenos Aires indicate that higher tritium concentrations may be developing in South America, possibly because of high-altitude interception by the Andes. The March 1964 measurement of Buenos Aires rain (IA) was 110 T.U., and the April measurement was 86 T.U. In the Falkland Islands relatively high concentrations were measured in 1964 as follows (IA): January, 42 T.U.; February, 29 T.U.; March, 43 T.U.; and April, 18 T.U.

RATIO OF TRITIUM TO ^{90}Sr IN PRECIPITATION

The fractionation of tritium from particulate fallout in the course of global circulation may be observed by comparing tritium and ^{90}Sr deposition at selected sites. As a gaseous molecule, the transport phenomena for tritium are not identical with the transport phenomena for ^{90}Sr, and the investigation of these differences should lead to a better understanding of the transport mechanisms. The relation between HTO and ^{90}Sr deposition may be observed in Figs. 11 and 12 for typical northern-hemisphere and southern-hemisphere sites, respectively.

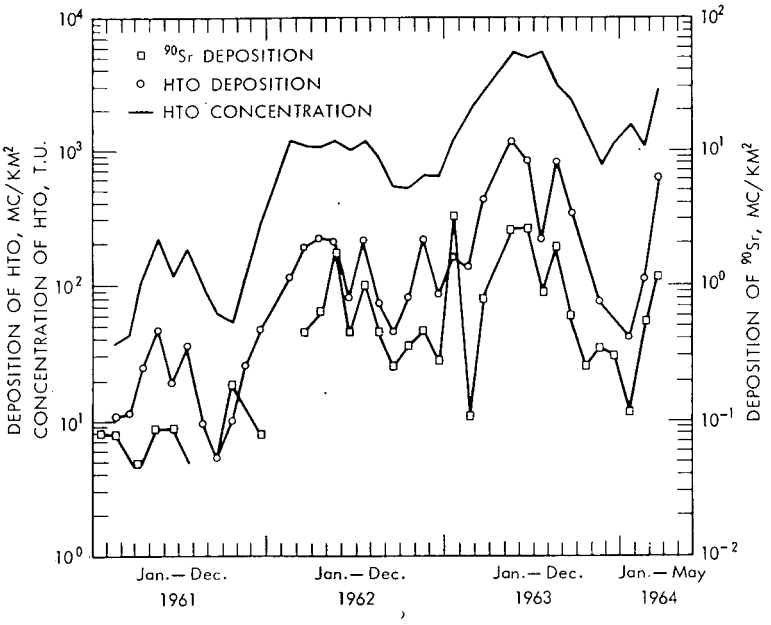

Fig. 11—Comparison of tritium deposition and ^{90}Sr deposition at Vienna, Austria.

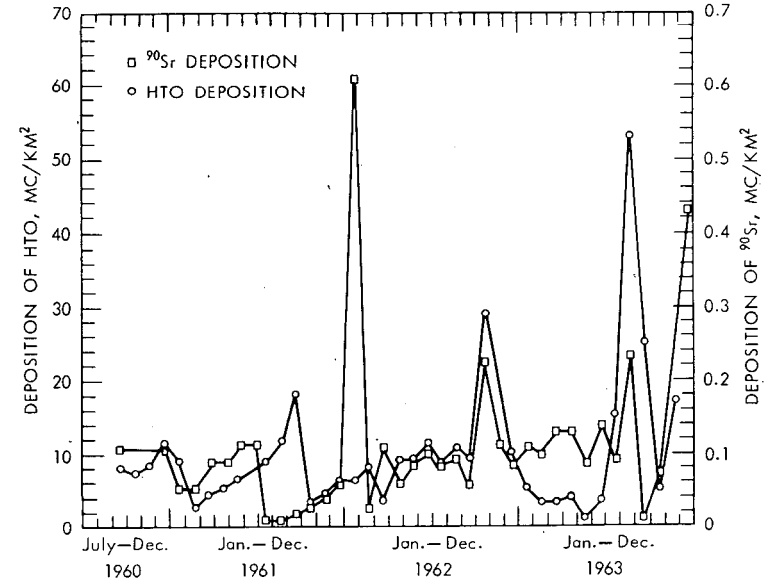

Fig. 12—Comparison of tritium deposition and ^{90}Sr deposition at Kaitoke (Wellington), New Zealand.

Such a comparison has been undertaken by using the IAEA tritium data and the Health and Safety Laboratory (HASL) ^{90}Sr data. It is generally observed that tritium fallout and ^{90}Sr fallout give the same general pattern with time at any given site. This is shown for Vienna in Fig. 11, where millicuries of fallout per square kilometer are plotted. The similarities for tritium and ^{90}Sr are obvious. However, important differences exist, and the examination of these should give significant information.

It is found that the ratio of tritium to ^{90}Sr has varied over the years. This reflects the variation in proportions of tropospheric and stratospheric fallout in the air masses. Immediately following a weapons-test series that involves both kiloton and megaton bursts, the ^{90}Sr component is relatively higher because of the contribution of the kiloton bursts whose products remain in the troposphere. These fall out quickly, and after a few months the stratospheric fallout predominates. This contains a higher proportion of tritium from the fusion weapons. Data for Vienna (IA), which are given in Table 6, clearly show these effects.

Table 6—VIENNA FALLOUT, MC/KM^2

Month	December 1961 through February 1963		March 1963 through December 1963	
	^{90}Sr	HTO	^{90}Sr	HTO
December	0.07	49		
March	0.44	186	0.80	435
April	0.69	210		
May	1.71	199	2.60	1330
June	0.46	80	2.60	850
July	1.00	205	0.86	208
August	0.46	74	1.92	820
September	0.24	45	0.60	342
October	0.35	83		
November	0.47	208	0.35	77
December	0.27	86	0.30	54
January	3.20	160		
February	0.10	134		
Total	6.16	1424	10.27	4116
Ratio HTO/^{90}Sr = 232			Ratio HTO/^{90}Sr = 406	

It is seen from the monthly data that ratios are more variable shortly following a test series. For example, in the first half of 1963, the minimum ratio was 50 in January, and the maximum was 1340 in February. In the last half of 1963, the range had narrowed to 180 for the minimum in December and to 570 for the maximum in September.

The ratio for 1961 before October, which should reflect a purely stratospheric input, was 316. This reflects the lower fusion to fission ratio for the 1958 tests as compared to the 1961 and 1962 tests.

In Table 7 the ratio of the deposition rate for tritium to the deposition rate for ^{90}Sr is given for 1963 at several sites in the northern and southern hemispheres. A single site did not always provide both the tritium and ^{90}Sr fallout data. In this situation the two nearest neighboring sites were taken to give the data on both nuclides. In the north the ratio increases toward the high latitudes, and in the south the ratio is substantially lower and remarkably uniform. These distribution patterns indicate significant differences between the atmospheric transport mechanisms in the two hemispheres. The significance is being investigated.

Table 7—RATIO OF RATE OF DEPOSITION FOR TRITIUM AND ^{90}Sr IN 1963, MC/KM^2 PER CENTIMETER OF PRECIPITATION

Site			
Tritium	^{90}Sr	Latitude	Ratio
Reykjavik	Keflavik	64°N	336
Goose Bay	Goose Bay	61°N	654
Stuttgart (four months)	Frankfurt	48°N	475
Vienna	Vienna	48°N	420
Chicago	Argonne	42°N	365
Teheran	Teheran	35°N	214
Waco	Dallas	31°N	231
Hong Kong	Hong Kong	22°N	199
Hilo	Hilo	19°N	75
Entebbe	Nairobi	0°N	65
Brisbane	Brisbane	27°S	60
Perth	Perth	32°S	63
Kaitoke	Wellington	41°S	53
Port Stanley (Falkland Islands)	Punta Arenas	51°S	61

The mean ratio for the five sites in the southern hemisphere is 60, and the individual departures from this ratio are small. This suggests the interesting possibility of calculating tritium-fallout concentrations for the many sites in the southern hemisphere for which tritium measurements are not available. The equation is

$$T.U. = \frac{1.9 \times 10^2}{n} \sum_1^n \frac{D_1}{P_1} + \frac{D_2}{P_2} + \ldots + \frac{D_n}{P_n}$$

where D is the monthly deposition of ^{90}Sr in millicuries per square kilometer (obtained from HASL lists), P is the monthly precipitation in centimeters, and n is the number of months included.

At present this method of calculating tritium fallout may be checked only against one measurement series, that for Rio de Janeiro in 1962. The calculated tritium-concentration average for 1962 is 25 T.U. Measurements (average of six months) gave 36 T.U. Further study is being given to the calculation of tritium-fallout concentrations from data on particulate fallout.

COMPUTATION OF TRITIUM INVENTORY

Deposition of tritium over land and ocean was computed for 1963. This with the data for 1962 and previous years permits estimation of the remaining stratospheric inventory as of Jan. 1, 1964. Such a computation requires accurate values for the tritium concentration by latitude bands in 1963 and similarly accurate values for the precipitation within the bands. The tritium distribution with latitude was obtained by averaging data from oceanic stations and plotting the tritium-concentration curves as shown in Fig. 13. Oceanic stations were used

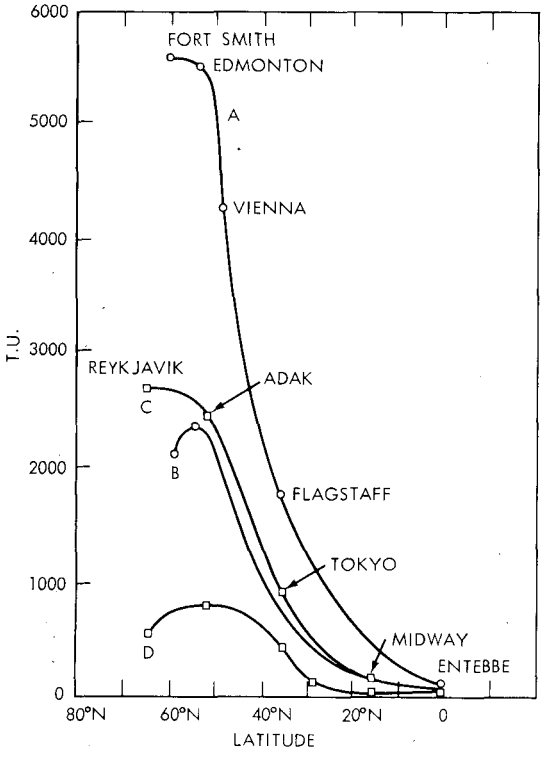

Fig. 13—Northern-hemisphere tritium-concentration curves used to establish total deposition. Continental sites: A, spring; B, fall. Oceanic sites: C, spring; D, fall.

because the land stations are affected by return of tritium to the atmosphere through evapotranspiration. Two curves were prepared, one to represent the high fallout season (March through August) and the other to represent the low fallout season (September through February). The precipitation data of Brooks and Hunt[6] were used for precipitation over the continents and those of Wüst[7] for precipitation over the oceans. Precipitation over the continents and the oceans within a given latitude band may be significantly different. Hence it is not satisfactory to take an average value for precipitation within a given latitude band.

The results of the computation are given in Table 8.

Table 8— PRECIPITATION OF TRITIUM IN 1963

Latitude band	Land		Ocean	
	Mc	Kg	Mc	Kg
90° to 70°N	4.0*	0.4*	4.0*	0.4*
70° to 60°N	21.0*	2.1*	14.0*	1.4*
60° to 50°N	37.2	3.8	46.5	4.7
50° to 40°N	35.8	3.6	62.6	6.3
40° to 30°N	20.5	2.1	35.7	3.6
30° to 20°N	10.2	1.0	12.6	1.3
20° to 10°N	4.6	0.5	11.4	1.2
10° to 0°N	2.9	0.3	10.8	1.1
0° to 90°S	2.0	0.2	10.0	1.0
Totals	138.2	14.0	201.6	21.0

*Estimated values. In the 90 to 70°N latitude band, one-half the area is considered "land" because of permanent ice.

The computation indicates that 14 kg of tritium were brought down by rain or snow over the continents in 1963 and that 21 kg was brought down over the oceans. This corresponds to a total activity of approximately 340 Mc of tritium.

The computation considers only the direct precipitation of tritium by rain or snow and does not introduce the factor of vapor exchange of tritium with the oceans. Bolin[8] and Eriksson[9] have shown that this may be a major effect and may increase the tritium deposition over the oceans by a factor with a possible maximum value of 3. When this factor is applied to the data in Table 8, the total tritium deposition for 1963 is increased to 77 kg.

On the basis of these values for deposition, the tritium inventory in the stratosphere at the beginning of 1964 may be computed. In the computation it is assumed that the tritium deposition in 1962 was 25% of that in 1963. This factor was obtained from the continuous fallout record for several stations which indicate approximately a 1 to 4 ratio for the two years. Hence tritium direct precipitation for the two years is 9 and 35 kg, respectively, which totals 44 kg. This would

leave a stratospheric inventory of 124 kg. When tritium deposition by oceanic exchange is also considered, the possible deposition becomes 19 and 77 kg to give a total of 96 kg. This would leave a stratospheric inventory of 72 kg.

Continued observations of tritium fallout in 1964 and 1965 should permit a more accurate analysis of the vapor-exchange effect. The rate of fallout is presumed to be approximately a first-order function of the stratospheric concentration. Therefore the tritium fallout concentration in 1964 should have average values that reflect a stratospheric inventory between the two extreme values of 124 and 77 kg. The IAEA is continuing the record of tritium in precipitation and is applying the information to the analysis of vapor exchange and other significant aspects of environmental tritium.

ACKNOWLEDGMENTS

The IAEA and the WMO are indebted to the International Meteorological Institute; the Environmental Group, AECL, Chalk River; the Scripps Institute of Oceanography; the Weizman Institute; the Tata Institute of Fundamental Research; and the New Zealand Institute of Nuclear Science for tritium measurements over the years. Their continued cooperation has made the project discussed in this paper possible. Appreciation is expressed to the U. S. Geological Survey and to the many other groups who have contributed data from national projects.

REFERENCES

1. A. E. Bainbridge, P. Sandoval, and H. E. Suess, Natural Tritium Measurements by Ethane Counting, *Science, 134:* 552 (1961).
2. P. Zutchi and J. Sas-Hubicki, Electrolytic Enrichment of Tritium Using Phosphate Treated Mild Steel Cathodes, Report presented at the IAEA-WMO panel on World-Wide Survey of Hydrogen and Oxygen Isotopes in Precipitation, Vienna, October 1964.
3. E. A. Martell, On the Inventory of Artificial Tritium and Its Occurrence in Atmospheric Methane, *J. Geophys. Res., 68*(13): 3759 (1963).
4. Tritium Water Lists Issued by the International Atomic Energy Agency, February 1962, October 1962, November 1963, September 1964, and January 1965.
5. Federal Radiation Council, Estimates and Evaluation of Fallout in the United States from Nuclear Weapons Testing Conducted through 1962, Report, May 1963.
6. C. E. P. Brooks and Th. Hunt, *Mem. Roy. Meteorol. Soc. (London), 3*(28), (1932).
7. G. Wüst, *Arch. Meteorol. Geophys. Bioklimatol., Ser. A, 7:* 305 (1954).
8. B. Bolin, On the Use of Tritium as a Tracer for Water in Nature, in *Second United Nations International Conference on the Peaceful Uses of Atomic Energy, Geneva, 1958,* Vol. 18, pp. 336-346, United Nations, New York, 1959.
9. E. Eriksson, An Account of the Major Pulses of Tritium and Their Effects in the Atmosphere, *Tellus, 17*(1): 118 (1965).

OXYGEN-18, DEUTERIUM, AND TRITIUM IN NATURAL WATERS AND THEIR RELATIONS TO THE GLOBAL CIRCULATION OF WATER

ERIK ERIKSSON and BERT BOLIN
International Meteorological Institute, University of Stockholm, Stockholm, Sweden

ABSTRACT

The occurrence of the nuclides ^{18}O, deuterium, and tritium in natural waters is discussed on the basis of the general circulation of water derived from standard meteorological observations of humidity, precipitation, and evaporation. If the establishment of a characteristic vertical distribution of moisture, deuterium, and ^{18}O is rapid (a few days) in comparison with the large-scale horizontal transfer rates of moisture over the oceans, one can relate the vertical distribution of deuterium and ^{18}O in air moisture and the content of these nuclides in precipitation to the humidity distribution, the isotopic composition of sea water, and the characteristic fractionation factor for condensation–evaporation. Observed isotopic composition of rainwater and recent measurements of tritium in atmospheric moisture over equatorial regions are discussed in view of theoretical results. Furthermore, the meridional transports of moisture, deuterium, and ^{18}O which have the ocean surface as the source are compared with the transfer of tritium which has a stratospheric source. Finally, an estimate of the total inventory of tritium is given and related to the global fallout of tritium.

INTRODUCTION

Extensive investigations into the transfer of moisture in the atmosphere have been conducted during the last decade, e.g., Ref. 1. We

therefore know rather well the meridional transfer of water vapor associated with a large-scale motion of the atmosphere and have an approximate idea about the importance of the meridional circulation cells found in tropical latitudes and the large-scale eddy exchange that is predominant in middle and high latitudes for bringing about this transfer. Investigations into the moisture exchange between oceans and continents are less complete. The occurrence of various nuclides in water, such as ^{18}O, deuterium, and tritium, has given us another tool for studies of the circulation of water in nature. Even though a considerable increase of the number of observations of these nuclides has occurred during the last few years, particularly through the worldwide network organized by the International Atomic Energy Agency it should be emphasized that it is the combination of ordinary meteorological observations of water vapor in the atmosphere and the distribution of these nuclides that will give us a better understanding of the water cycle in nature. In this paper we shall therefore attempt to relate the distribution of these nuclides and their transfer to the distribution and transfer of ordinary water. It will be clear from the analysis to be given that data are still insufficient to improve greatly on our present knowledge of the water budget of the atmosphere. However, some interesting results are presented, and a clearer picture of which observations are of particular interest in this connection is obtained. More details are given in Refs. 2 and 3.

BASIC FEATURES OF WATER CIRCULATION

The main source for atmospheric water is the sea, which also receives most of the precipitation. Of the yearly evaporation from the sea, about 90% is precipitated over it, whereas only 10% is brought back to the sea in rivers from the continents. Precipitation over land is about $2\frac{1}{2}$ times greater than the runoff; thus nearly 60% of the precipitation evaporates. This evaporation, which is also called evapotransportation, is largely due to water consumption by vegetation. It is of importance for a discussion of the occurrence of various nuclides in natural waters to realize that most of the evaporation from land areas takes place by evaporation from capillary systems. Such evaporation will initially cause fractionation of the isotopes, but this raises the concentration of the heavy isotopes in the evaporating parts whereby the rate of evaporation of these parts increases. An equilibrium is reached when the flow through capillaries to the evaporating surface equals the rate at which evaporation of the isotope takes place. Fractionation therefore essentially depends on possible fractionation in the capillary systems. Provided no such fractionation occurs, the groundwater acquires the average isotopic composition of precipitation.

The main sources of water vapor over ocean areas are the subtropics and the trade-wind belts between latitudes 10 and 25°N and 10 and 25°S. Except for a belt around the equator, evaporation exceeds precipitation between 40°N and 40°S. Polewards of latitude 40°, the evaporation is less than precipitation. The net evaporation from the sea can be estimated approximately from the distribution of salinity in the surface layers of the ocean.[4] It can also be computed from the water transfer in the atmosphere computed from meteorological observations.[1] On the whole, these two methods yield results that are in satisfactory agreement with each other. Figure 1 shows the meridional distribution of the total water transport in the atmosphere across latitude circles for summer, winter, and year. In Fig. 2 the corresponding

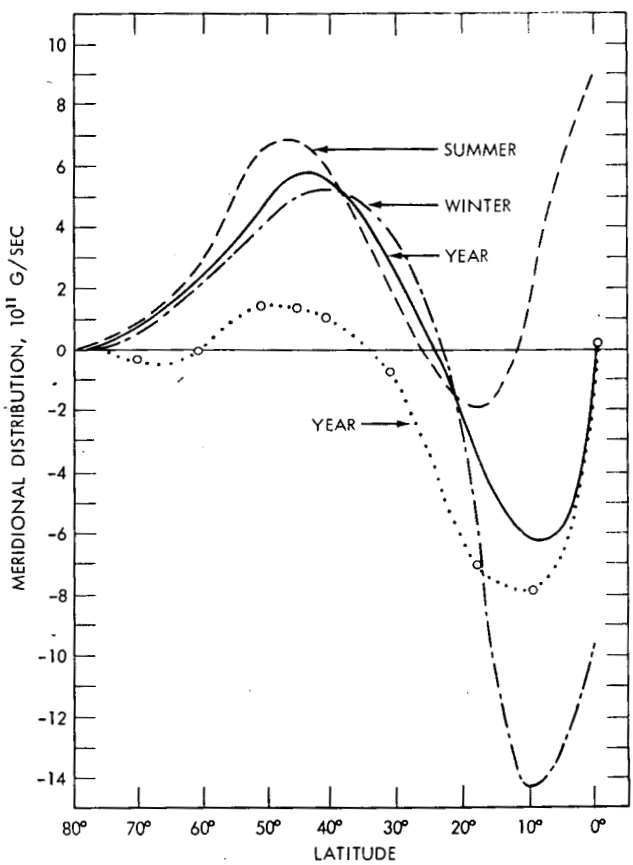

Fig. 1—Meridional moisture transfer. The dotted curve denotes the part of the total yearly transfer due to a mean meridional circulation. [From V. Starr and J. P. Peixoto, Arch. Meteorol. Geophys. u Bioklimatol., Ser. A, 14: *111-130 (1964).]*

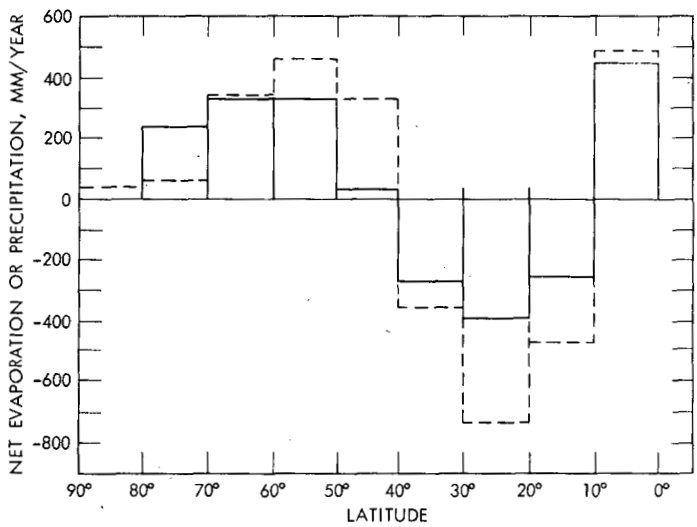

Fig. 2—Convergence of meridional moisture transfer (solid lines) as computed from the transfer depicted in Fig. 1 expressed in net precipitation (evaporation in case of negative values). The dashed lines give the corresponding values deduced from ocean salinity. [G. Wüst, Arch. Meterol. Geophys. u Bioklimatol., Ser. A, *7: 305-328 (1954).]*

net evaporation or precipitation is shown. It has been computed as the divergence or convergence of the meridional water-vapor flux. We therefore know the net transfer between the atmosphere and the sea rather well, but our knowledge of the gross exchange is considerably less accurate.

The water-vapor content of the air decreases quite rapidly with elevation owing to the decreasing temperature and thus decreasing saturation vapor pressure. Most of the water in the atmosphere and therefore also the transfer of water vapor in the atmosphere occurs in layers below about 5 km. The lower branch of the meridional circulation cells (see Fig. 3) in the tropics brings moist air from subtropical latitudes to equatorial regions in the lower part of the atmosphere, but their return branches in the upper troposphere above 10 km are very dry. This obviously means a net transport of water vapor towards the equator, and Fig. 1 shows that actually the major part of the horizontal transfer in the tropics is due to these meridional circulation cells. The upward air motions in the intertropical convergence zone related to the mean meridional circulation cells carry moist air to higher levels whereby it is cooled and condensed with the water being brought to the surface of the earth as precipitation. Water

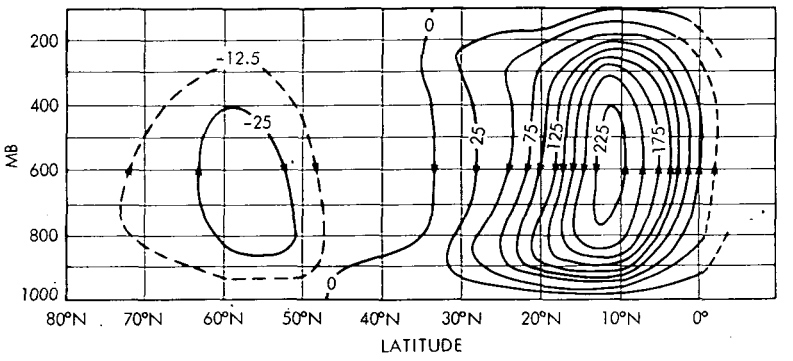

Fig. 3—Mean meridional circulation during the winter. The tubes between the streamlines transport 25 × 10^6 tons/sec. [From E. Palmén and L. Vuorela, Quart. J. Roy. Meteorol. Soc., 89: *134 (1963).]*

vapor is also constantly transferred upwards owing to turbulent motions of the atmosphere. This latter transfer is likely considerably more intense than that due to the meridional circulation cells. The transfer upwards of water vapor due to a meridional circulation cell equals the net horizontal convergence and amounts to a few hundred millimeters of precipitation per year. According to Jacobs,[6] the annual precipitation in tropical latitudes in the neighborhood of the tropical convergence zone is between 1000 and 2000 mm. Thus most of the water that falls as precipitation must have evaporated in the same latitudes. The lifetimes of water in the atmosphere is rather short. Considering removal of water vapor from the atmosphere by precipitation only, neglecting the direct molecular exchange at the sea surface, and adopting 5 g/cm^2 as a characteristic value for the total water content of an air column in tropical latitudes, we find that 1500 mm of precipitation implies a mean residence time for water in the atmosphere of about 12 days. This is obviously an upper limit since direct molecular exchange may be appreciable.

With this general picture of the water transfer in the atmosphere in mind, we may ask ourselves what variations of the isotopic composition of water results from the series of physical processes involved. We shall next give a few simple deductions, on the basis of which we shall be able to interpret some of the general features of the distribution of various nuclides in precipitation and atmospheric moisture as depending upon evaporation, condensation, and turbulent transfer. We shall also be able to indicate some measurements of special interest for a better understanding of the transfer mechanisms in the atmosphere.

VARIATIONS OF ISOTOPIC COMPOSITION

It is useful to consider a few idealized cases to obtain an insight into how the different physical processes interplay with each other. For a more detailed treatment, see Ref. 2.

The fractionation that occurs when water vapor condenses in an air parcel that moves upward and is cooled by an adiabatic expansion has been discussed thoroughly by Dansgaard.[7] We distinguish between the reversible moist adiabatic process in which all condensed water vapor remains in the air as cloud droplets and the pseudo-adiabatic process in which all condensed water falls out as precipitation. The latter process usually best describes reality since the water content of a cloud in the form of small droplets in suspension seldom is very great (the mixing ratio is usually less than 0.5×10^{-3}). In a precipitating cloud, droplets from above fall through any given air parcel and are in exchange with the environments; the speed of the exchange depends on the fall velocity and thus on the size of the droplets.[8] This fall and exchange is approximately what takes place in an individual convection cell. Since they are involved in the large-scale vertical transfer of moisture, such convection cells represent the turbulent eddies that are responsible for part of this transfer. In addition, advection by the mean meridional circulation cell takes place.

To clarify some simple aspects of this vertical transfer, we neglect horizontal transfer and consider a steady state. We also assume a pseudo-adiabatic condensation process and neglect for a moment the exchange between the droplets and their environments after they have formed and fallen through the atmosphere.

A bar denotes a time average, and a prime denotes a departure from this average; for example,

$$q = \bar{q} + q' \tag{1}$$

The maintenance of a constant vertical distribution of water vapor implies

$$\frac{d}{dZ}\left[\overline{\rho w}\,\bar{q} + \overline{(\rho w)'q'}\right] = -P \tag{2}$$

where Z = vertical distance
ρ = air density
w = vertical velocity
P = rate of condensation per unit volume and unit time

Equation 2 expresses a balance between vertical advection, vertical turbulent transfer, and condensation (equals precipitation). Similarly, we obtain for any isotope considered

$$\frac{d}{dZ}\left[\overline{\rho w}\ \overline{qR} + \overline{(\rho w)'(qR)'}\right] = -\overline{\alpha R P} \tag{3}$$

where R is the concentration of the isotope considered in grams per gram of H_2O and α is the fractionation coefficient for condensation or evaporation.

For the following approximate treatment, we shall introduce an eddy exchange coefficient A defined by

$$\overline{(\rho w)'q'} = -A\frac{d\bar{q}}{dZ}$$

and

$$\overline{(\rho w)'(qR)'} = -A\ \frac{d(\overline{qR})}{dZ} = -A\ \frac{d(\bar{q}\bar{R})}{dZ} \tag{4}$$

In the last part of Eq. 4, we have for simplicity introduced one further approximation in replacing $\overline{qR}$ by $\bar{q}\bar{R}$, thus assuming that there is no correlation between the isotopic composition and the humidity content of an air parcel. This approximation is somewhat questionable in view of the likeliness that the descending and comparatively dry air has experienced more condensation and therefore might have fewer heavy isotopes (see Ref. 3). Assuming similarly $\overline{RP} = \bar{R}\bar{P}$, our two basic transfer equations become

$$\frac{d}{dZ}\left(\overline{\rho w}\ \bar{q} - A\frac{d\bar{q}}{dZ}\right) = -\bar{P}$$

and

$$\frac{d}{dZ}\left[\overline{\rho w}\ \bar{q}\ \bar{R} - A\frac{d(\bar{q}\bar{R})}{dZ}\right] = -\alpha\bar{R}\bar{P} \tag{5}$$

Let us consider two special cases.

CASE 1: Vertical advection (A = 0). From the two equations given as Eq. 5, we derive

$$\frac{1}{\bar{R}}\frac{d\bar{R}}{dZ} = (\alpha - 1)\frac{1}{\overline{\rho w}\ \bar{q}}\ \frac{d(\overline{\rho w}\ \bar{q})}{dZ} = \frac{(\alpha - 1)\bar{P}}{\overline{\rho w}\ \bar{q}} \tag{6}$$

This relation is equivalent to Rayleigh's distillation formula

$$\frac{\delta R}{R} = (\alpha - 1)\ \frac{\delta q}{q} \tag{7}$$

Introducing a characteristic vertical distribution of water vapor given by

$$\bar{q} = \bar{q}_0 \, e^{-\lambda Z} \tag{8}$$

we obtain in such a steady state

$$\bar{R} = \bar{R}_0 \exp\left[-(\alpha - 1)\lambda Z\right] \tag{9}$$

implying a balance between the advection of water vapor upwards and removal by precipitation. With a characteristic value of $\lambda = (4\ \text{km})^{-1}$, we would expect a change of R by approximately 90 $^{0}/_{00}$ and 10 $^{0}/_{00}$ over 4 km for deuterium and ^{18}O, respectively (assuming an ambient temperature of about +10°C).

CASE 2: Vertical transfer of water vapor by turbulence ($\overline{\rho w} = 0$). Assuming for simplicity that A is a constant, we derive the equation

$$\frac{d^2\bar{R}}{dZ^2} + 2\,\frac{1}{\bar{q}}\,\frac{d\bar{q}}{dZ}\,\frac{d\bar{R}}{dZ} - (\alpha - 1)\,\frac{1}{\bar{q}}\,\frac{d^2\bar{q}}{dZ^2}\,\bar{R} = 0 \tag{10}$$

We note that this equation is independent of A.

Adopting the vertical moisture distribution given by Eq. 8, we obtain the following expression for the vertical variation of the isotopic composition of the water vapor:

$$\bar{R} = \bar{R}_0 \exp\left[-(\pm\sqrt{\alpha} - 1)\lambda Z\right] \tag{11}$$

The plus sign in Eq. 11 corresponds to the case in which a convergence of the turbulent transfer upwards balances the removal by precipitation, whereas the minus sign implies a corresponding balance between convergence of a downward transfer by turbulence and removal by precipitation. The vertical distribution of the convergence has been prescribed by the assumptions of a constant value of A and the vertical moisture distribution (Eq. 8). The general character of the result does not change for other reasonable assumptions in this respect.

In the cases of deuterium and ^{18}O, only the plus sign is of interest since the ocean surface is the source for the turbulent transfer. Comparing the results of these cases with Eq. 9, we find a vertical decrease that is only one-half of what was obtained in the advective case. This is of course an expression of the fact that mixing, in addition to bringing about an upward transfer, also tends to decrease the vertical gradient of the isotopic composition brought about by fractionation. We can also qualitatively get an idea about the effect of isotopic exchange between falling droplets and the environment. Large droplets (diameter >0.2 cm) equilibrate slowly and fall rapidly; therefore the theory above is applicable. Small droplets, however, adjust to the environment rapidly, and, in the limit of an infinitely rapid adjustment, there is no net effect of the fractionation. Thus no vertical gradient in the isotopic

composition of the atmospheric moisture is to be expected. Very few data on the isotopic composition of atmospheric moisture are available, but they are clearly of interest in view of the deductions above.

In the present context, we may consider that sea water contains no tritium. On the other hand, a considerable amount of tritium has been introduced into the stratosphere by the explosion of thermonuclear devices, and nuclear industry produces an increasing amount of tritium that is released into the lower troposphere. Recent measurements (March 1964) in the atmospheric moisture in tropical latitudes (over the Congo, see Fig. 4) show a marked increase of tritium with elevation, indicating a downward transfer of tritium due to vertical mixing. The mere fact that tritium is found at upper levels in the tropics supports the idea that eddy motion is of greater importance for the vertical transfer than the meridional circulation cell. Considering now the simple example evaluated above, we see that with a source aloft the isotope increase with elevation is twice as rapid as the decrease of the moisture content, i.e., with $\lambda = (4\ \text{km})^{-1}$, we obtain an increase by a factor of 2 over a vertical interval of about 1.4 km. Of course, this treatment is not directly applicable to the case of tritium since horizontal transfer processes, also of importance for tritium distribution, become of importance in the upper troposphere and lower stratosphere. The simple example indicates, however, the possible role of turbulence for the vertical transfer of tritium in the lowest part of the troposphere also. Qualitatively, we note that the isotopic exchange between falling droplets and environment decreases the amount of tritium brought to

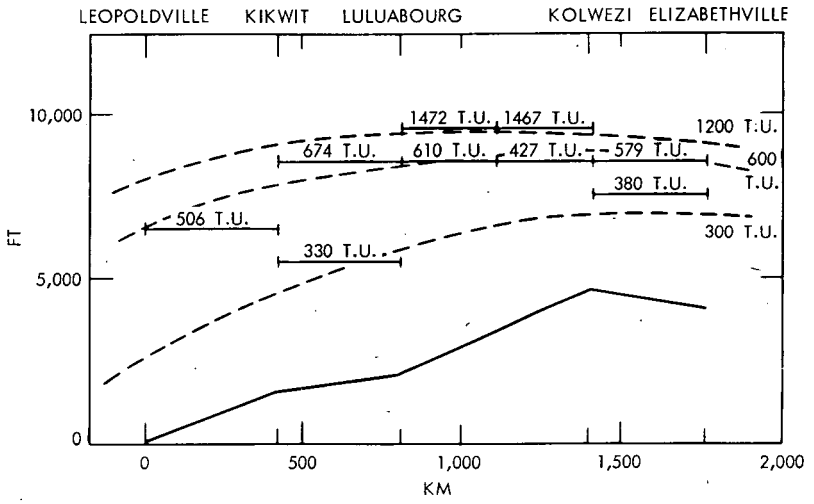

Fig. 4—Tritium concentration in atmospheric water vapor.

the surface of the earth by precipitation since the tritium concentration in atmospheric moisture decreases downward. The importance of turbulence for the vertical transfer thereby is increased.

A few remarks should be given here on the difference in vertical transfer of a radioactive gas such as tritiated water and radioactivity in the form of particles such as ^{90}Sr. In the case of ^{90}Sr, evaporation from and condensation onto falling droplets has no direct effect on the transfer of radioactivity by precipitation, which indicates that turbulent transfer and deposition may be more important for tritium than for ^{90}Sr. Furthermore, the transfer to a smooth ocean surface (more than 95% of the ocean surface is smooth) is due to molecular diffusion in the boundary layer next to the water surface. Also in this respect there is a marked difference between transfer of a gas and transfer of particles. Very small particles behave like air molecules and large particles (>1 μ) settle through the thin molecular boundary layer rather quickly, whereas the transfer of intermediate particles (0.01 to 1 μ) is considerably reduced. It is well known that a considerable part of the radioactivity found in particles is in those of submicron size.

We have so far restricted the discussion to vertical moisture transfer only and have disregarded the importance of horizontal flux. This may be justified as a first rough approximation over areas where local evaporation and vertical transfer exceed the large-scale horizontal convergence of moisture. For any study of the circulation of water in nature, the horizontal transfer processes are fundamental; and in this context it is of interest to study the geographical variations of the isotopic composition of precipitation. Dansgaard[7] has shown how the ^{18}O-content of precipitation systematically decreases toward the poles and inland over the large continents. He has deduced a close relation between the ^{18}O content of precipitation and the mean air temperature. In a Rayleigh process the ^{18}O content of the condensate depends on the isotopic composition of the vapor when it is evaporating from the sea surface and the fraction of the vapor that remains at the instant of precipitation.[7] Since the amount of water remaining in the atmosphere at condensation depends on the condensation temperature and since this temperature on the average may be some fixed number of degrees lower than the mean temperature at the earth's surface, such a relation between ^{18}O content and temperature may be expected. We note, however, that this is valid only poleward from about 55°N, where less than 10% of all oceans are found and where evaporation is rather limited owing to low temperatures. Only in these parts of the world can the successive removal of water vapor, as we approach the excessively cold arctic and antarctic regions, be approximately considered as a Rayleigh process; elsewhere the exchange between the atmosphere and the sea is of dominating importance, constantly maintaining the ^{18}O content rather close to that of sea water. As was shown

previously when the vertical transfer was considered, the turbulent exchange processes tend to reduce the differences in ^{18}O content from one place to another, and the same presumably holds for horizontal turbulent exchange. Dansgaard's measurements also show that the mean ^{18}O concentrations vary only about 10 per mille within the latitude belt 55°N to 55°S (excluding only some continental stations for which other processes might be of importance) in spite of the fact that the total water content of an air column may vary from an average of about 6.5 g/cm^2 in the tropics to about 1 g/cm^2 close to the polar regions. A much more careful study of the variations of the isotopic composition of rainwater must be conducted in conjunction with measurements of the isotopic composition of atmospheric moisture to arrive at more conclusive results about the flux of water vapor through the atmosphere.

The preceding discussion is, of course, very tentative in many respects. It shows, however, that we may expect considerable differences in the distribution of various isotopes as a result of the relative importance of different physical processes contributing to the transfer processes. Data are still inadequate for a more quantitative evaluation of these differences. Obviously systematic measurements of the isotopic composition of atmospheric water vapor as a function of elevation and latitude seem very desirable, and simultaneous measurements of particles and artificial radioactivity would provide additional important information. Studies of the isotopic composition of precipitation as conducted at present are of course also of value, although they are insufficient since such measurements represent an integration over the condensation and evaporation processes, the result of which may be difficult to interpret by itself.

It should be added that some simple studies of the tritium budget of the atmosphere as compared with that of ^{90}Sr give some further support to the general picture of the vertical transfer affecting tritiated water vapor and particular matter differently as previously indicated. Machta[9] has shown that the sum of the total deposition of ^{90}Sr over land and by rain over the oceans added to the amount remaining in the atmosphere is about 80% of the total injected (summer 1963). A corresponding inventory of tritium[2] shows quite a different result. In this inventory it is estimated that the direct air–sea transfer of tritium must be about twice that due to precipitation to obtain an approximate balance. This probably is a lower limit since only bomb-produced tritium was considered in the computation.

REFERENCES

1. V. Starr and J. P. Peixoto, The Hemispheric Eddy Flux of Water Vapor and Its Implications for the Mechanics of the General Circulation, *Arch. Meteorol. Geophys. Bioklimatol., Ser. A, 14:* 111-130 (1964).

2. E. Eriksson, An Account of the Major Pulses of Tritium and Their Effects in the Atmosphere, *Tellus, 17:* 1 (1965).
3. E. Eriksson, Deuterium and Oxygen-18 in Precipitation and Other Natural Waters; Some Theoretical Considerations; to be published in *Tellus.*
4. G. Wüst, Gesetzmassige Wechselbeziehungen zwischen Ozean und Atmosphäre in der zonalen Verteilung von Oberflächensalzgehalt, Verdunstung und Niederschlag, *Arch. Meteorol. Geophys. Bioklimatol., Ser. A, 7:* 305-328 (1954).
5. E. Palmén and L. Vuorela, On the Mean Meridional Circulation in the Northern Hemisphere During the Winter Season. *Quart. J. Roy. Meteorol. Soc., 89:* 131 (1963).
6. W. C. Jacobs, The Energy Exchange Between Sea and Atmosphere and Some of Its Consequences, *Bull. Scripps Inst. Oceanog. Univ. Calif., 6*(2): 122 pp. (1951).
7. W. Dansgaard, Stable Isotopes in Precipitation, *Tellus, 16:* 436-468 (1964).
8. B. Bolin, On the Use of Tritium as a Tracer for Water in Nature, in *Proceedings of the Second United Nations International Conference on the Peaceful Uses of Atomic Energy, Geneva, 1958,* Vol. 18, pp. 336-343, United Nations, New York, 1959.
9. L. Machta, paper presented to the U. N. Scientific Committee on the Effects of Atomic Radiation, to be published by the World Meteorological Organization.

INDIVIDUAL PAPER DISCUSSION

Discussions that took place following the presentation of individual papers are given in this section. These discussions preceded the scheduled general discussions for the session.

KRUGER: Mr. List, your values for annual fallout concentration over the United States seem quite reasonable. In trying to compare the East Coast value to the Midwest value, have you tried to separate the East Coast concentration into two components: that part which originates from polar sources, which is comparable to the Midwest data, and that part from tropical sources, which is not comparable ?

LIST: No.

REITER: Dr. Newell, are there any meteorological data that would substantiate your claims concerning the difference between hemispheres?

NEWELL: There are the data by Lamb and Obasi which suggest that standing eddies in the troposphere play a smaller role in the southern than in the northern hemisphere. Sudden warmings in the stratosphere are more gradual in the southern hemisphere according to Godson's work. Ozone data summarized by Ramanathan at the Arosa Ozone Symposium suggest smaller total amounts in the southern hemisphere; however the number of collecting stations in this hemisphere is very small.

SAUCIER: Mr. Gudiksen, concerning your closing remarks, do you imply conservation of mass in the jet-stream core for a week or

more and that a jet-stream core can be traced from Washington back across the sparse-data areas of the Pacific and Asia to a test site over Russia?

GUDIKSEN: I am not stating that mass is conserved for this time length but that at least some of the debris that is injected into the jet stream at one point will be carried for long distances; however, a large part of this debris will be lost along the way. About the second part of your question, the Weather Bureau was able to produce rough trajectories for a jet stream from Washington back across the Pacific.

MACHTA: Dr. Volchok, did you study the seasonal variations during the year 1960?

VOLCHOK: No.

MACHTA: This year is of special consequence because the seasonal variation was more evident in the southern hemisphere than in other years. Furthermore, both the tropospheric and stratospheric concentrations of the two hemispheres were about equal.

WALLACE: Dr. Volchok, do you have any explanation for the fact that the spring maximums of radioactivity in tropospheric air in the two hemispheres occur four months apart instead of six months apart?

VOLCHOK: Not right off. I think it is very interesting.

HERDE: I would like to hear again, I believe I have heard at one time, the explanation of the origin of ^{7}Be, manganese, and some of the other nonfission products. I think it very appropriate to identify the origin of those that are relatively new.

REITER: Dr. Gustafson, would you like to comment on that?

GUSTAFSON: Beryllium-7 is actually produced by fissioning or spallation of oxygen and nitrogen by energetic cosmic rays by both primary protons and secondary mesons. The amount of ^{7}Be produced per gram of air increases with altitude up to at least 70,000 ft and also with increasing geomagnetic latitude. There is a modest production of this radionuclide in the troposphere, but its primary source is in the low or middle stratosphere. [Editor's note: There was further discussion on this subject during the general discussion.]

JONES (Illinois State Water Survey): Mr. Hall, how did you measure the duration of each sample?

HALL: By relating the rainfall traces on the rain-gauge charts, the total amount of rainfall, and the number of samples, we were able to estimate quite closely the time and the duration of each rain sample.

REITER: I have some doubts whether convective systems penetrating into the stratosphere, such as the ones you mentioned penetrat-

ing up to 50,000 ft, are as effective in incorporating stratospheric air as they would be, for instance, in washing away some tropospheric contaminated inversions when penetrating them. It seems to me that the entrainment rate at these lower levels actually is larger. Am I correct in assuming that from the cloud tops diffusion of tropospheric air and evaporation of moisture are directed into the stratosphere? Do we have any indication of the properties of the convective systems? How effectively are they entraining the contaminated air?

HALL: We don't have enough cases yet to really determine the stratospheric penetration. We are not able to make any statement on it yet.

REITER: Well, it seems to me that maybe we could talk the AEC into making some measurements of this kind since it would be quite interesting from various points of view.

TORREY: Mr. Pelletier, during your work around the Fermi reactor, you found that all the gross beta activity couldn't be recovered from the rain because of activity sticking in the polyethylene containers. Were you able to solve this problem?

PELLETIER: I think so. We use tracer material in the rain jug before we put it out for exposure and use several acid rinses to clean the jug after it has been exposed. We have scraped out the inside of one of these jugs after an exposure but found insignificant radioactivity in the scrapings.

ZIEMER: In reporting gross beta activity, what is your standard of reference, and do other laboratories use the same reference standard?

PELLETIER: We use ^{204}Tl. I don't know what standards other laboratories use.

ZIEMER: Do you think this would account for some of the differences in the values you reported?

PELLETIER: Well, remember we are plotting a ratio. Since both air and rain are presumably calibrated on the same basis, the counting efficiency, regardless of the standard used, will cancel out. I don't think the use of different standards could account for the differences in values. Mr. Huff, have you measured total deposition over a time and then compared it with that from the convective storms only?

HUFF: No. Our work has been entirely concerned with convective type rainfall. We have done very little with the stable, winter type precipitation.

VAN MIDDLESWORTH: When measuring the total beta concentration, what is the contribution from the natural radioactivity in the soil, i.e., soil swept up by the winds as dust. Has there been any evaluation of the radium content of this dust? Would the contribution from this source be large or small?

HUFF: You are touching on a point that I mentioned that the relatively large concentration at the beginning of the storm period may very well be related to entrainment of low-level or surface particulates into the storm. As I said, we have some indirect evidence that is discussed in one of our progress reports. We cannot quantitatively state that 10 or 20 or 50% of the beta concentration on the leading edge of the storm is coming from this source. I wish we had measurements that would allow us to do this. In relation to the radon problem, we store the samples for several days before we use them to try to reduce the radioactivity from this source in our analyses. I would be glad to discuss this with you in more detail later.

STOUT: Mr. Gatz, do you have cases where there were two consecutive rain showers with little or no break in the rain and you still found a high pollen content during the second shower period?

GATZ: We have such a case but not in any of the rains reported here. The rain of May 9, 1964, which we sampled near Chickasha, Okla., had two rather intense rainfall-rate peaks. The peaks occurred 13 min apart and were separated by a short period of relatively light rain. The data on pollen concentrations are not yet available, but the radionuclides showed the usual temporal variations in both bursts. That is, the concentration was high at the beginning of the rain burst and then fell rapidly. It will be extremely interesting to see if a similar pattern occurred with the pollen concentrations.

REITER: It seems to me that not only the pollen is "sticky" but the whole problem is because now we have three points of view here. Your impression seems to be that the low-level air carries most of the radioactivity because of the agreement with pollen concentrations early in the storm. There also seems to be some evidence that quite a number of storms may have high concentrations of contaminants due to the tapping of the stratosphere by cloud tops. From the one case which we analyzed, we are convinced that some low tropospheric intrusion of stratospheric air got tapped by precipitation.

SHLEIEN: Have you considered the possibility of material originally deposited on the ground being whipped up by winds and redeposited in rainfall?

GATZ: We haven't made any calculations, but this may very well be the source of a part of the contaminants in the low-level air.

SHLEIEN: The reason I mention this is that we have found ^{226}Ra concentrations in precipitation which very likely originated from a ground source.

GATZ: The occurrence of ^{226}Ra in rain is very strong evidence that resuspended particulate matter from the earth's surface gets into the rain. If we were able to obtain the temporal variation of ^{226}Ra in rain, we would have additional evidence pertaining to the question of where the scavenged material enters the storm.

HUFF: Dr. Kruger, I'm surprised by your finding that there is a direct relation between the rainout concentration and the rainfall intensity. Did you have a large number of cases, and did this relation hold for all storms?

KRUGER: The ^{90}Sr concentration as a function of rainfall intensity is a difficult relation to establish for convective showers in that, instead of just gross measurements, the relation should be examined in detail under the same storm conditions. On a gross basis, for our 14 convective showers, increased ^{90}Sr concentrations occurred with decreasing precipitation rates in about 50% of the cases. Many of these increased concentrations occurred in the first cells passing over the site, and the increase could be ascribed to evaporation effects below the clouds. For later cells with more humid lower layers, most of the ^{90}Sr concentration curves followed the precipitation-rate curve quite well. Thus in a single storm we could observe an inverse relation during the initial and the final period and a direct relation in between where two or more radar tops could be identified.

SAUCIER: You presented rather great detail for the radar storm analyses. Do you have similar detail for radioactivity measurements? For instance, what is the time duration of your rain samples?

KRUGER: In general, we do. The time duration of rain samples are generally taken as the minimum time to collect sufficient volume of water such that ^{90}Sr concentrations can be determined with a precision of better than $\pm 5\%$. The time, therefore, varies not only with the precipitation rate but also with the general levels of nuclear debris in the atmosphere. In 1962 and 1963, when the nuclear-debris levels were reasonably high, we were able to measure ^{90}Sr in samples of less than 0.1 liter. Thus, generally, we could limit our time span to meteorologically interesting time periods of half hours or less for large-scale systems and to minutes for convective showers. For some convective showers, we were able to obtain half-minute samples during intense periods. Our radar cross sections usually show the ^{90}Sr concentration and the precipitation-rate data sample by sample.

POLAN: Mr. Ferber, does your curve showing the amount of debris in the troposphere apply only to pure air bursts or does it apply to contact surface bursts as well?

FERBER: It is for air bursts only. If there is contact with the surface there will be local fallout and therefore perhaps a different distribution of debris with height. The few data we have indicate that there is more activity in the stem for surface bursts than for air bursts.

SETTER: Dr. Thatcher, please explain what is meant by "the overwhelming effect of oceanic air" in causing the low concentrations of tritium in precipitation collected from oceanic stations.

THATCHER: I think this expression is actually used in connection with continental stations that are annually affected by "overwhelming" oceanic air masses. These are the stations in the monsoon belt. Here the stations show the typical pattern of continental tritium fallout in approximately the first half of the year; i.e., they show relatively high tritium concentrations and a pronounced spring peak. At the onset of the monsoon, at about midyear, the tritium concentrations at these stations drop dramatically because of the rush of moisture-laden air from the ocean (principally the Indian Ocean). Surface ocean water has a low tritium concentration because of downwind mixing. Reevaporated water from the land, on the other hand, has a high tritium concentration because of very limited mixing with old soil water. In the first half of the year, much of the limited rain that occurs derives from reevaporated water.

GENERAL DISCUSSION

REITER: I am faced with the difficult task of trying to condense into a few words what has taken $1\frac{1}{2}$ days to explain. Of course I can only present a very brief outline of some of the questions that were raised during this session. In presenting a few points here, I am not choosing them with any particular reference or preference but rather to stimulate a discussion.

This session covered a very wide range of topics on the atmospheric relations to radioactive fallout. We listened to many speakers, whose topics ranged from meteorology to nuclear chemistry. A bridging of the gaps between the diverging fields discussed would help to promote understanding, particularly in the usage of rather specific terminology. I would not be in the least surprised if some chemist should ask the question: "What is potential vorticity, and what is it supposed to be good for?"

Let us make an attempt to arrange the topics covered in this session into four groups: One group dealt with the very large-scale

transport processes in the higher atmosphere, pointing out differences between the more disturbed northern-hemisphere flow patterns and the more zonal southern ones. The second group was concerned with an attempt to explain seasonal changes in radioactive fallout, especially the rather conspicuous spring maximum, etc. The third group concentrated on various aspects of dry transport processes of radioactive debris. The fourth group, dealt with the rather complex wet transport processes and washout phenomena.

One area that was covered in this session concerns the chemistry and origin of some of the radioactive tracers that are carried about in the atmosphere. One question has already been asked about beryllium and other nonfission products, and I wonder if this question has been answered in full. Is there someone in the audience who might be able to contribute something to this?

SALTER: There was a question earlier on the origin of several nonfission products. The answer at that time was specifically in relation to ^{7}Be. I think it would be helpful to summarize these radionuclides and their origins as far as we can tell from the data from high-altitude sampling.

From the 1961 U.S.S.R. series, ^{54}Mn, ^{55}Fe, ^{57}Co, ^{58}Co, ^{124}Sb, and ^{204}Tl have been observed. The major fractions of these neutron-activation products were most likely formed in the high-yield (55- and/or 25-Mt) shots of the series. Dr. Kuroda pointed out that ^{125}Sb levels appeared in his tropospheric air and precipitation samples. On looking back over our high-altitude data, I concur with his suggestion that an excess of ^{125}Sb over that expected from fission was produced in a high-yield device and that the ratio of excess ^{125}Sb to ^{90}Sr in the device was about 10 to 1.

In addition to the data for $^{54}Mn/^{90}Sr$ that I showed yesterday for 31°N in February 1962, we have some data from samples collected at 70,000 ft in the summer of 1962 in which almost all the debris appears to have originated in the high-yield 1961 U.S.S.R. tests. In these samples the $^{54}Mn/^{90}Sr$ ratio, corrected for decay to October 1961, is about 100 to 1, and the excess $^{125}Sb/^{90}Sr$ ratio is about 10 to 1.

From all the 1962 U. S. and U.S.S.R. atmospheric tests taken as a group, we have observed ^{88}Y and additional quantities of ^{54}Mn and ^{124}Sb. Iron-55 and other neutron-activation products probably were produced also in some of these detonations. Unfortunately, the relatively high frequency of testing after April 1962 limits our ability to assign the specific production of radionuclides to a given device except for the ^{124}Sb, which appears to have been formed predominantly in the December 1962 U.S.S.R. series.

Cadmium-109 (470-day half-life) was produced in the 1962 Starfish detonation by neutron activation of cadmium that was added to the

device. Cadmium-113m (14-year half-life), which is a beta emitter, was produced also in this shot. Because of this nuclide's longer half-life and more easily detected radiation, it may turn out to be of great value in tracing Starfish debris. The ^{113m}Cd data must be corrected, however, for the amount of this isotope of cadmium present as a fission product. From the branching ratio* and the unclassified data on yields for ^{113m}Cd†, we have estimated a $^{113m}Cd/^{90}Sr$ activity ratio in thermonuclear fission of 0.003 to 1. This ratio is in good agreement with data from a few samples measured from the northern hemisphere which have no ^{109}Cd. In our samples we have found a $^{113m}Cd/^{109}Cd$ ratio due to Starfish of about 0.2 to 1.

REITER: I should like to ask Dr. Newell how far up in the atmosphere he thinks hemispheric differences in circulation patterns can be traced. He has mentioned that explosive warmings are less dramatic in the southern than in the northern hemisphere. It has been my understanding that the antarctic stratosphere warms very quickly around the equinoxes, whereas the arctic stratosphere may warm at various dates. Data from the IGY suggest that the troposphere of the southern hemisphere possesses a more zonal character of flow than that of the northern hemisphere. How far up in the stratosphere are the same differences in flow characteristics expected to be present? For the northern hemisphere we have some rather interesting meteorological-rocket-network data. Such data still are lacking for the southern hemisphere. Do the transport observations of radioactive debris give any significant indication of hemispheric differences at higher stratospheric levels?

NEWELL: From the conventional radiosonde network in the northern hemisphere, we can compute standing- and transient-eddy transports up to about 25 mb (25 km) and can obtain approximate estimates of the transient-eddy transports up to 10 mb (31 km). Although the work reported to date refers to the IGY only, the Planetary Circulations Project is presently concerned with a study of the transports which covers a five-year period. One of our former colleagues, Dr. Obasi of the Nigerian Meteorological Service, has made a study of momentum transports over the southern hemisphere for the IGY. His work indicates that the data above 100 mb (16 km) are not adequate for reliably defining the transports or for making comparisons between northern and southern hemispheres.

The meteorological-rocket-network data span the height range of 30 to 60 km. With 12 stations in the northern hemisphere, we can

*From G. R. Crocker, Estimates of Fission Product Yields of a Thermonuclear Explosion, Report USNRDL-TR-642, U. S. Naval Radiological Defense Laboratory, Apr. 4, 1963.

†From A. C. Wahl, 14-Year ^{113m}Cd, *J. Inorg. Nucl. Chem., 10:* 1–3 (1959).

obtain approximate estimates of the transient-eddy momentum transports over North America to 60 km; with only two stations in the southern hemisphere, we can make no comparison between hemispheres.

Ozone transports over North America to about 30 km are available from Hering's work. Since most of the seasonal ozone change occurs in the height interval of 10 to 25 km, one does not need to know the circulation changes above 25 km to account for the spring maximum in ozone.

In the case of fallout, events are a little more complicated. We argued at the conference here in 1961 that the spring maximum was due to extra mixing in the lower stratosphere in late winter which brought debris down to the region above the middle-latitude tropopause from where it could excape into the troposphere by the processes discussed by Danielsen and Reiter. We felt that seasonal changes in the lower stratosphere rather than seasonal changes in these processes accounted for the spring maximum.

An additional item that is involved when one considers the magnitude of the fallout maximum rather than ozone is the availability of material at about 25 km to be mixed downwards. This availability obviously depends on the testing pattern and on mixing above 25 km. Thus eventually we would like to compare meteorological observations above 25 km in both hemispheres.

REITER: Dr. Newell mentioned the upper stratospheric circulation in winter, and this leads into another question I wanted to ask Dr. Danielsen about the transport processes induced by the jet stream. It is quite possible, in my opinion, that the polar night jet stream might have a similar dynamic effect on vertical debris transport in the stratosphere as has the tropopause jet stream for transport processes from stratosphere to troposphere. Unfortunately, at this time I don't think there is sufficient data on the polar night jet stream to allow a sophisticated treatment of its dynamics. It should be very worthwhile, however, to tackle this interesting problem.

DANIELSEN: I agree with Dr. Reiter on the need for studying the polar jet. I cannot contribute anything on that subject, but I would like to hazard an interpretation of the data Dr. Volchok presented today. He showed that the values of surface-air radioactivity first exceeded the normal during January and February at low-latitude stations (10°N) in the northern hemisphere, i.e., midwinter in the northern hemisphere. In contrast, the corresponding increase in the southern hemisphere was in September and October, i.e., spring in the southern hemisphere. The bimonthly profiles of excess concentrations of ^{90}Sr for the two hemispheres matched with an eight-month lag (northern to southern) rather than with a six-month lag.

I would like to suggest that the eight-month lag is produced by the asymmetry in the northern- and southern-hemisphere land masses. If the transport of radioactivity from the stratosphere to troposphere is predominately due to folding of the tropopause, which can be shown to be related to cyclogenesis, then a difference between the hemispheres might be expected. Cyclogenesis over a rotating globe depends on the vertical component of the earth's vorticity, which is a function of latitude, baroclinity, and hydrostatic stability. Fleagles' results, I think, are most applicable here. He showed that when the baroclinity (north–south temperature gradient) was at a maximum at 45° latitude, the most probable latitude for cyclogenesis was close to 60° and cyclogenesis was prohibited from 30° to the equator. Cyclogenesis between 45° and 25° would require a larger baroclinity or a lower hydrostatic stability. Cylconic development and tropopause folding in this latitude range is probably responsible for the maximum deposition of radioactivity at the surface between the equator and 30° latitude.

The temperature gradients are primarily produced by cooling at high latitudes during fall and winter. Cyclones develop at high latitudes and transport the cold air equatorward. This transport increases the baroclinity at lower latitudes. Thus an equatorward shift of the zone of maximum baroclinity, and therefore the zone of maximum cyclogenesis, occurs during winter in both hemispheres.

However, in the southern hemisphere when the cold air spreads northward, it travels over water that is warmer than land (there is very little land between 70 and 30°S). The resulting heating of the air acts to reduce the equatorward shift of the baroclinity. In the northern hemisphere the large land masses at high latitudes accelerate the cooling trend. Even when they become snow covered, the land masses at mid-latitudes can contribute to the cooling. Certainly, they do not heat the air as does the warmer water. Therefore we might expect more frequent and vigorous cyclogenesis between latitudes 25 and 45° to develop earlier in the northern-hemisphere winter than in the southern-hemisphere winter.

The asymmetry in the land masses might also affect the concentration of radioactivity in the extruded stratospheric air. Since the radioactivity in the stratosphere must descend to the lower cyclonic stratosphere before it is transported into the troposphere, a diabatic cooling process is required. I think radiative cooling plays an important part in the stratospheric descent of the air that brings down the radioactivity to the level of the tropopause folding.

I suggest that both the asymmetric lag and the asymmetry in the magnitude of the deviation from the bimonthly averages might be a direct consequence of the asymmetry in the land masses of the two hemispheres.

HAWLEY: Dr. Libby has suggested that there may be a selective plant-uptake mechanism involved in the transpiration of tritiated water over normal water. This, if true, may help explain such things as the greater concentrations of ^{3}H over continents than over oceans and over large forested areas than over semiarid areas and also seasonal variations. Dr. Thatcher, has your group been considering this?

THATCHER: By analogy with deuterium, one might expect that a selective plant-uptake mechanism with respect to tritium might exist. The plant would reject tritium as it usually does deuterium in the metabolic process, and this would increase the evaporation of tritiated water leading to a higher air concentration. The IAEA data do not appear to support this mechanism, however, since the concentrations found in semiarid regions, such as at Teheran, are generally just as high as those in regions that support an abundant vegetation, such as at Vienna. The more humid regions are more greatly influenced by oceanic air, however, which would counteract the proposed effect for vegetation. The data should be carefully scanned in an attempt to identify this effect.

BOLIN: There is, of course, fractionation when evapotranspiration takes place from vegetation. It is important to realize, however, that, for estimating this, the effect of water transfer through the capillary systems in the plants must be considered. We do not know precisely what the final effect is, but changes in the composition of water due to fractionation insofar as tritium is concerned is small compared to the variations that have been observed in precipitation.

REITER: Dr. Bolin, did you imply that from tritium measurements at the ground, together with knowledge of the observed tritium gradient in the atmosphere, you could make inferences on the precipitation physics in the atmosphere?

BOLIN: The vertical transfer of tritium, deuterium, ^{18}O, and particulate matter takes place through the same mechanism of turbulence. Since the sources and sinks of these tracers are different but partially related, observations of the vertical distribution of all of them would yield some information on the turbulent processes and the intensity of the transfer. Considering the vertical distribution in the trade-wind belt to be in an approximate steady state might yield information on the turbulent transfer of water vapor and have a bearing on our estimates of evaporation from the ocean surface. I am not sure how such data would be precisely interpreted, but in any case the simultaneous use of several tracers for studies of the vertical transfer should be advantageous.

REITER: If I understand correctly, you are proposing a tool for investigating, say, the much thought-about question of water-vapor transport from the ocean to the atmosphere.

BOLIN: Yes.

DINGLE: Dr. Reiter, I surmised from your report* that your studies indicate that perhaps a large bulk of the stratospheric debris that is brought into the troposphere in stable lamina tends to circulate downward anticyclonically and then into a following cyclonic system where it may be rained out. Is this a little different from what has been expressed at other times and places, derived from Danielsen's model, that the cyclonic branch of the extruded lamina carries important amounts of radioactive debris into the leading cyclonic system to be rained out there? What is your opinion of relative values of contribution of the two branches of the extruded lamina to the rainout.

REITER: In answering these questions, I should like to emphasize that the precipitation observed in our case study which you are referring to is more or less incidental. The case as such should still be treated as being characteristic for dry fallout. I don't think there is any disagreement with your impression that dry fallout should occur from the anticyclonic branch of the jet stream that moves within the observed stable layer.

The fact that we did have some precipitation in this case was due to a small disturbance that moved in. However, it was completely dry at the locations of some of the stations collecting fallout, as you may see from the cross-sections presented in the report. Convection from underneath eventually penetrated this dry contaminated layer. When the dry layer was tapped from underneath it had already moved to as low as 900-mb. Thus moist processes helped in the removal of radioactive debris, but they should not be considered, in this case, the primary cause of fallout.

As far as rainout processes are concerned, I agree with you that the branch of the stable layer which continues to move cyclonically in the middle troposphere probably is more significant than the anticyclonic branch. The cyclonic branch of the jet stream overrides the warm front, and the contaminated air masses therefore could be tapped to a significant degree by moist and precipitating air masses from underneath. This, however, is something that we have not yet studied in detail. Usually moist cases are somewhat neglected because they are too complicated to be treated by trajectory analysis. Dr. Danielsen, do you have any comments on this discussion.

*E. R. Reiter, Transport Processes in the Atmosphere Leading to Radioactive Fallout Progress Report No. 1, Colorado State University, Department of Atmospheric Science, Technical Paper No. 58, September 1964.

DANIELSEN: I agree with what was said.

DINGLE: I have the impression the process in connection with this extrusion is very important in the generation of some of the radiation "hot spots" that we see in the central part of the country.

REITER: I would tend to agree with you on that point, but I think that, if a very crude division into dry fallout and rainout cases is made, I would classify the generation of the hot spots as dry fallout cases simply because the air moved in in a matter of two days, as a matter of fact, from the tropopause to the surface, and then got caught in a disturbance, creating some wet "hot spots." Some of these cases probably could be explained that way, but I would, as far as the debris transport then goes, rather classify them as dry fallout cases that got sprinkled down through a series of coincidences.

DANIELSEN: I would like to add a comment. I have studied the trajectories associated with a cyclonic development over the central United States in the spring of 1956. As the vortex moved northeastward over the Great Lakes, dry air entered the northeast section of the vortex. Trajectory analyses indicated that air moving rapidly eastward across central Canada in the upper troposphere subsided rapidly, turning anticyclonically until at low elevations its momentum was reversed. Although the dry air ascended again after entering the vortex, its relative humidity remained low and precipitation was cut off. Therefore in the northeast quadrant of the low, where maximum precipitation might be expected, only very light rain or drizzle was reported. This rain may have been loaded with radioactivity, however, caused by evaporation during its fall through the dry air. Definitely, the anticyclonic branch of the descending flow can link into another cyclonic flow, and, in general, both must be considered.

REITER: There is still one rather interesting point which Mr. List made to me which I hope he will repeat.

LIST: It concerns rainfall scavenging. Since it usually occurs in the very lowest levels of the storm, why do we propose that towering cumulus clouds will bring debris down from the stratosphere? I believe the reason is that, although the efficiency of the entrainment mechanism may be very much less in the stratosphere, the concentrations of radioactivity are several orders of magnitude higher; therefore, even if the entrainment mechanism is an order of magnitude less efficient, considerable amounts of radioactivity from the large reservoir in the stratosphere would be brought down.

While I have the floor, I want to make some philosophical comments, i.e., that in previous years at meetings like this we were concerned with gross features of fallout and considered ourselves successful if we could tell what the fallout was going to be, given the

amount that was injected. But now I see, and I am glad to see, that we are much more concerned with the actual physical mechanisms that are involved in fallout. After all, these are the things that will lead to meteorologists' understanding a little more about what is going on. I think that as far as the AEC health problem goes, it is under reasonable control. I believe the difficulties are internal in the meteorological profession rather than in not being able to predict what will come out, given a certain injection into the atmosphere.

NEWELL: I would like to make a comment on what Mr. List said. Does anyone really know whether the tops of these clouds that are supposedly penetrating the stratosphere are water or ice? It seems to me that the majority of the radar echoes from high clouds that we see in New England, which rarely penetrate the stratosphere, are from ice, and the ice blows away from the cloud more or less like the smoke at the top of a chimney. Thus stratospheric debris, even if it were collected with high efficiency, would be carried away from the cloud and lost to it as the ice evaporated downstream.

Do we know from actual aircraft flights whether these clouds were water or ice and whether they were really 15,000 ft above the tropopause? The temperatures at that altitude suggest that they may be ice. There is a big question in my mind as to the actual heights of these showers, particularly those reported by radar at great ranges where beam-width exaggeration effects can be large.

LIST: The sightings are visual. We do not know the composition.

NEWELL: At the previous fallout conference in 1961, Dr. Kruger suggested that there were more high-level penetrations of the stratosphere in the spring. I just wanted to report that after the conference I collected 10 years of data from the Massachusetts Institute of Technology Weather Radar Research group and went through it tabulating maximum echo tops for each day. I then averaged these values by months and found that the peak radar echoes in New England occurred in July. Is this different in other parts of the country? Dr. Kruger, where were your measurements made?

KRUGER: Our convective-activity collections, until recently, have taken place in central Pennsylvania. I do not have any data of the kind you described, although undoubtedly they could be obtained from Pennsylvania State University records. We have been collecting from convective storms for the past three years, and most of them have occurred during the spring months.

SESSION IV

Distribution and Cycling of Radionuclides

F. W. Lengemann, Chairman

CESIUM-137 PASSAGE FROM PRECIPITATION TO MILK

GERALD M. WARD, JAMES E. JOHNSON, and HAROLD F. STEWART*
Colorado State University, Fort Collins, Colorado

ABSTRACT

One of the principal objectives of this ^{137}Cs study at Colorado State University was to establish useful ratios for the passage of ^{137}Cs through the steps of the food chain to man. This paper presents coefficients that have been calculated for the transfer of ^{137}Cs from precipitation to forage plants and from forage plants and other feeds to milk.

METHODS

Three fiber-glass funnels, each with a catch area of 47.2 sq ft, were located 5 ft aboveground and were used as precipitation collectors in a pasture area. An 80-cm^3 ion-exchange column of Dowex 50-W-X12 was connected to each funnel. At the top of the column a glass-wool filter was placed to collect the sediment invariably contained in each sample. The columns were selectively eluted for ^{137}Cs in the laboratory with 1 liter of 0.5*M* NH_4NO_3.

Forage samples were collected by cutting known areas of randomly selected sites in the pasture. Hay samples were taken with a core sampler from bales of hay. The forage and hay samples were dried and ground to a constant density before counting. Grain was counted in a pelleted form.

Milk was collected from cows on pasture and composited. For studies involving feed comparisons, milk from each cow and a sample

*U. S. Public Health Service Officer.

of the feed were collected daily. The total feed intake and the total milk production were recorded for each cow.

All samples were analyzed for ^{137}Cs by gamma-ray spectrometry. The detector used was a 4-in.-thick by 8-in.-diameter NaI(Tl) crystal shielded from background radiation by a 5-in.-thick steel-wall chamber. It was connected to a 400-channel pulse-height analyzer. Rain elution was counted in 1-liter bottles, and sediment was counted on a 4-in.-diameter filter pad; both were placed directly on the crystal.

Hay and forage samples were counted in $2\frac{1}{2}$-gal cardboard containers standardized by weight and density to a constant geometry. Milk samples were counted in a 5.47-liter beaker. Empirically determined spectrum-stripping equations were used to determine the ^{137}Cs activity. Crude-fiber determinations were made according to the standard Association of Official Agricultural Chemists method.

RESULTS

Precipitation-Forage Transfer of ^{137}Cs

It is generally assumed that most of the ^{137}Cs found in forage plants arises from direct foliar absorption and that soil uptake is minor.[1] We have attempted to show soil uptake of fallout ^{137}Cs by growing corn plants in a greenhouse. These plants showed no evidence of ^{137}Cs uptake; however, the quantity of forage which could be grown was limited, resulting in small samples.

Calculations from our data on pasture soil and forage indicated that soil uptake was small compared to direct foliar absorption. The mean value of pasture-forage activity during 1964 was about 400 pc/m^2. The cumulative soil activity was about 80,000 pc/m^2. Therefore uptake of 0.5% would account for all of the pasture activity, or 0.1% uptake would account for all the activity in third-cutting 1964 hay (Table 1). Relations between rainfall and forage activity suggested that soil uptake is probably of the order of 0.01% and therefore negligible, for example, in the case of first-cutting hay (Table 1).

Deposition coefficients between rainfall and plants were calculated from the ratio of ^{137}Cs precipitation deposition per square meter to the activity found in forage per square meter. Considerable variation was expected in the coefficients because of the uncertainties involved in comparing rainfall and plant activities. When relatively long intervals occurred between rains, plant growth tended to dilute the activity already present in plants; this was particularly true when the pastures were irrigated. Significant deposition of ^{137}Cs from air or dust is a possibility, but we have been unable to clarify this point with our data.

Table 1 presents the deposition coefficients found by comparing cumulative fallout during the growing period with activity per square

Table 1—FORAGE AND RAINFALL ACTIVITIES DURING 1963 AND 1964 AND CORRESPONDING DEPOSITION COEFFICIENTS FOR ^{137}Cs

Feed	Harvest date	Yield, g/m^2	Rainfall, in.	Mean forage ^{137}Cs activity, pc/kg	Forage ^{137}Cs, pc/m^2	Rainfall* deposition, pc/m^2	Forage–rainfall deposition coefficient
Alfalfa hay	June 15, 1963	340	4.38	4825	1642	3424	0.48
Alfalfa hay	July 20, 1963	225	0.21	2357	530	754	0.70
Alfalfa hay	Aug. 30, 1963	210	0.46	1092	229	1079	0.21
Corn silage	Sept. 15, 1963	1013	4.71	1670	1690	5239	0.32
Alfalfa hay	June 15, 1964	340	4.12	4070	1384	4174	0.33
Alfalfa hay	July 20, 1964	225	0.38	680	153	1147	0.13
Alfalfa hay	Sept. 10, 1964	210	0.66	380	80	889	0.09

*Integrated values for growth period.

meter of first, second, and third cuttings of alfalfa hay in 1963–1964 and also of corn silage for 1963. First-cutting hay was harvested about June 15, 1963, during or after the period of heaviest fallout. This cutting showed the maximum ^{137}Cs activities of the cumulative deposition during the growing period. The deposition coefficient for first-cutting hay was much higher than for second- and third-cutting hay, except for the second cutting in 1963. A possible explanation is related to the type and amount of rainfall during the three growing periods. During the first-cutting growing period, during the spring, there were heavy, frequent rains. During the second-cutting growing period, the rainfall consisted of many rains of low total rainfall. It is reasonable to assume that the uptake of ^{137}Cs is greater for this type of rain than that for heavy rains, which can wash off ^{137}Cs initially deposited. During the corresponding period of 1964, when the total rainfall was greater but fell in fewer rains, there was a significant decrease in the deposition coefficient.

Measurement of activity in pastures is, in general, an undesirable way by which to quantify fallout deposition. Grazing animals selectively remove some fraction of the vegetation daily while the remainder continues to grow until it reaches maturity, at which time it is preferentially not eaten. Pastures change rapidly in growth rate and to some extent in botanical composition, depending upon available moisture and environmental temperature. All these factors contribute to the difficulty of calculating a precise and useful deposition coefficient.

However, although the deposition coefficient of ^{137}Cs for precipitation to forage is a difficult parameter to determine for growing forage, approximate results may be obtained by the averaging procedure applied to the data of Table 1.

It is also possible to determine a deposition coefficient characteristic of daily rains when the pasture ^{137}Cs levels and the immediate deposition by rainfall are known. Such a coefficient was determined for certain rains in the 1964 pasture season. By an empirical determination of a half-time for pasture activity which combines losses due to grazing, wash-off, and dilution by new pasture growth, the pasture activity on the day following a rain can be determined by extrapolating the measured values after the rain. Similarly, the residual contribution from previous rains can be determined and subtracted from this value. This method has been applied to six rain days for the 1964 forage growing period (Table 2) and can be expressed in a general equation:

$$kR = P_1 - P_t e^{-\alpha t}$$

where k = deposition coefficient
R = rain deposition to the pasture, pc/m^2
P_1 = pasture activity on the day following the rain, pc/m^2
P_t = measured value of pasture activity on t days preceding the rain, pc/m^2
$\alpha = 0.693/T_{1/2}$ where $T_{1/2}$ is the pasture-activity half-time

The deposition coefficients determined in this manner were far from constant; however, the variability could be qualitatively linked to a dependence on the volume of precipitation in each rain. The deposition coefficients of Table 2 were generally found to vary inversely with the amount of rainfall. These coefficients are probably also dependent on other factors, such as the intensity and the duration of

Table 2—CALCULATION OF DEPOSITION COEFFICIENT FROM INDIVIDUAL RAINS AND PASTURE-FORAGE CONCENTRATIONS

Date, 1964	Rainfall, in.	^{137}Cs deposition, pc/m^2	Extrapolated ^{137}Cs pasture activity, pc/m^2	Deposition coefficient (k)
May 7	0.21	640	532	0.83
May 26	0.33	480	330	0.69
May 28	1.91	1017	570	0.56
June 8	0.15	280	185	0.67
June 21	0.11	700	180	0.26
June 30	0.09	182	275	1.79
			Mean	0.80

individual rains and accompanying wind and ground dust storms. The degree to which forage covers the ground also represents a large factor in determining the efficiency of deposition.

Comparison between the ^{137}Cs concentration of milk and rainfall activity (Fig. 1) indicated that milk produced by cows on pasture

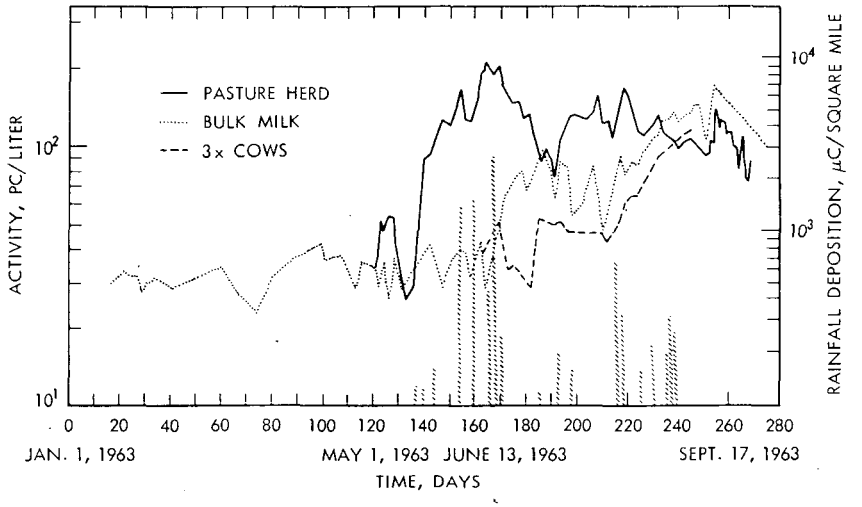

Fig. 1—Concentrations of ^{137}Cs in milk produced by cows on pasture, cows fed in a dry lot (bulk milk), and high-milk-producing cows milked three times a day and fed in a dry lot (3x) related to corresponding rainfall activity, 1963.

responded almost immediately to increases in forage activity, except for the period around day 240, at which time the herd was largely dependent upon hay for feed rather than on pasture. This response does not agree with the statement that "peak concentrations of cesium-137 in milk have appeared about one month after peak fallout rates."[2]

Feed-Milk Transfer of ^{137}Cs

Dairy cattle normally are fed large amounts of hay and/or pasture, both of which may contain much higher levels of fallout ^{137}Cs than those found in grains, which are the other major components of the diet. It is much easier to obtain reliable estimates of the transfer coefficient between feeds and milk than between precipitation and feeds because experiments to test the latter can be designed at will whereas, for the former, experiments are dependent upon the vagaries of the weather.

An average value for the ratio of ^{137}Cs contained in feed which would be found in milk would be most useful for prediction of the activity in milk expected from cows that had grazed on contaminated

Table 3— SECRETION OF ^{137}Cs AND POTASSIUM IN MILK FROM HOLSTEIN COWS* IN RELATION TO STAGE OF LACTATION, PREGNANCY, AGE, AND LEVEL OF PRODUCTION

Cow No.	Stage of lactation, days	Stage of pregnancy, days	Age, years	Level of production, liters/day	Milk/feed ratios		
					^{137}Cs, % of intake	Transfer coefficient†	Potassium, % of intake
507	29	0	5.6	28.4	14.8	0.0052	16.1
509	35	0	5.4	33.3	14.2	0.0043	21.0
505	49	0	5.6	32.5	13.1	0.0040	19.1
572	61	0		19.8	8.1	0.0041	9.1
509	72	0	5.5	34.0	11.0	0.0032	17.1
521	75	0	5.4	26.2	7.2	0.0027	14.2
1	93	0	5.1	31.1	14.5	0.0047	14.8
509	98	20	5.6	31.4	7.6	0.0024	14.7
532	98	0	5.4	34.6	16.4	0.0047	23.8
50	108	41	4.4	27.1	7.6	0.0028	11.0
521	110	6	5.5	20.8	8.5	0.0041	13.3
532	134	8	5.5	25.4	9.4	0.0037	16.2
521	138	33	5.6	23.2	9.8	0.0042	12.9
532	161	35	5.6	29.6	9.2	0.0031	15.6
572	167	80	7.9	14.1	5.8	0.0041	7.8
572	203	116	8.0	11.2	4.3	0.0038	5.2
572	230	142	8.0	9.4	3.8	0.0041	4.2
86	232	0	8.3	8.4	2.8	0.0033	4.4
532	248	161	5.4	7.5	2.7	0.0036	3.0
599	328	97	8.0	5.7	2.1	0.0037	2.5
					Mean	0.0038	

*The ration for all cows consisted of approximately 10 kg of alfalfa hay and 5 kg of mixed grains.

†As defined in text.

fields. A mean value for this transfer coefficient* was found to be 0.0038 with a standard deviation of 0.0008 for a group of 10 Holstein cows that were fed what is considered an average diet for dairy cattle (Table 3). In this group of cows, the amount of milk produced per day varied widely as did the percentage of total ^{137}Cs secreted per day in the milk. However, when the results were expressed as a transfer coefficient, the variation was greatly reduced, although the range in values still varied by a factor of 2 (0.0024 to 0.0052). The percentage per liter thus appears to be relatively constant and in an average diet amounts to about 0.33% of the total ^{137}Cs intake. Limited data from our laboratory indicate that low-milk-producing cows excreted a proportionately higher percentage of ^{137}Cs in the urine than did high-milk-producing cows. These data mean that the level of production for the dairy herds supplying a milk shed would be of little importance in explaining variations in the ^{137}Cs level in milk.

*Transfer coefficients were calculated by dividing the ^{137}Cs content of milk in picocuries per liter by the total daily intake of ^{137}Cs in feed in picocuries.

The age of cows, the stage of lactation, or the stage of pregnancy did not appear to have significant effects on the percentage of ^{137}Cs secreted into milk. On the other hand, the type of feed did have a significant effect. This effect was noted when comparisons were made between rations containing large amounts and those containing small amounts of grain with proportionate decreases or increases in the amount of hay. The transfer coefficient was always lower for those animals fed small amounts of grain and large amounts of hay. One explanation for the difference is that ^{137}Cs is bound by fibrous residues in the feed as suggested by the experiments of Mraz and Patrick.[3] They found increased ^{137}Cs excretion by rats fed fibrous feeds. Comparisons were made between the crude-fiber content of the diet and the transfer coefficient. These comparisons showed that the coefficient decreased rather consistently as the fiber content of the ration increased.

In the Colorado State University study, thirty-three observations were available from individual Holstein cows whose diet included from about 10 to 40% crude fiber. The regression coefficient calculated from these data was

$$Y = 0.785 - 0.11 \times \text{crude-fiber intake (kg/day)}$$

where Y is the transfer coefficient (^{137}Cs secreted per liter of milk daily as a percentage of the total daily intake of ^{137}Cs in the feed).

Our results indicate that it is very important to consider the crude-fiber content of the diet if comparisons are to be made between herds which vary in their intake of this constituent.

There are, of course, numerous differences between high-grain and high-hay rations besides the difference in crude-fiber content. One difference is that hay contains four to five times the concentration of potassium found in grain. An increased potassium intake in high-hay diets, according to the Observed Ratio concept, would decrease the amount of ^{137}Cs found in milk. However, in one feeding trial rice hulls were added to the ration. Thus this feed had a fiber content similar to that of hay but a potassium content similar to that of grain. The transfer coefficient was 0.0030 as compared to 0.0063 for a diet where mixed grain replaced rice hulls. The experiences of other investigators have indicated only a minor influence on ^{137}Cs retention by the addition of extra potassium to the diet.[4] Additional experiments are contemplated for the study of the quantitative relation between the fiber content of the ration and the levels of ^{137}Cs found in milk and in urine as well as the effect of supplemental potassium.

The mean transfer coefficient of 0.0038 (Table 3) is similar to the average amount secreted in 66 hr reported by Cragle[5] but lower than the 0.01 suggested by Garner.[6]

SUMMARY

The ^{137}Cs deposited on forage from rainfall varied from about 80% on pasture plants collected shortly after a rain to a low of about 10% for alfalfa hay harvested late in the summer. Rainfall intensity appears to be an important factor in the deposition coefficient.

About 0.33% of the ^{137}Cs intake in feed is secreted per liter of milk by cows fed a common ration. However, this percentage is related to the crude-fiber content of the ration and increases by a factor of 2 if the diet is low in crude fiber as in the case where cows are fed large amounts of grain.

REFERENCES

1. J. Z. Holland, Distribution and Physical–Chemical Nature of Fallout, *Federation Proc., 22*: 1390 (1963).
2. Federal Radiation Council, Estimates and Evaluation of Fallout in the United States from Nuclear Weapons Testing Conducted Through 1962, Report No. 4, May 1963.
3. F. Mraz and H. Patrick, Organic Factors Controlling the Excretory Pattern of Potassium-42 and Cesium-134 in Rats, *J. Nutrition, 61*: 535 (1957).
4. R. H. Wasserman, C. L. Comar, and D. N. Tapper, Influence of Dietary Potassium and Sodium on Cesium-134 Retention in Rats, *Proc. Soc. Exptl. Biol. Med., 113*: 305 (1963).
5. R. G. Cragle, Uptake and Excretion of Cesium-134 and Potassium-42 in Lactating Dairy Cows, *J. Dairy Sci., 44:* 352 (1961).
6. R. J. Garner, Environmental Contamination and Grazing Animals, *Health Phys., 9:* 507 (1963).

FISSION-PRODUCT CYCLES IN AN AGRICULTURAL SYSTEM. I. SAMPLE HETEROGENEITY

HOWARD A. HAWTHORNE
Laboratory of Nuclear Medicine and Radiation Biology,
University of California at Los Angeles, Los Angeles, California

ABSTRACT

The dispersion of ^{90}Sr and ^{137}Cs within the components of a dairy farm were examined as a preliminary step in developing mathematical models of the system. The high variability in mass of the matrixes and in the concentrations of ^{90}Sr and ^{137}Cs nullified any assumption of general homogeneity within the system. Variations in matrix mass of fission-product vectors were consistently smaller than variations in ^{90}Sr and ^{137}Cs concentrations within the matrixes, soil, plants, and milk. Models representing the movements of fission products among the components of a food chain must account for fission-product dispersion within matrixes and for variations in matrix mass.

SAMPLE HETEROGENEITY

An exploratory study was conducted to assess variability in the different components of a small dairy farm through which ^{90}Sr and ^{137}Cs pass before entering milk. The variations examined were those of radionuclide concentrations in soil, plants, and milk and variation in the mass of these matrixes. The soil matrix was examined in three-dimensional space. Variations in the isotopic burdens of plants and in crop production were evaluated in two dimensions of space and the dimension of time, and variations in the consumption of feed by cows and its contamination levels were studied in the dimension of time, as were the ^{90}Sr and ^{137}Cs content of milk and its production. Heterogeneity

among representative samples collected in 1962 and 1963 is the subject of this preliminary report.

The study was made on a privately owned dairy farm located near St. George, Utah. Thirty-three acres of cultivated land support a milking herd of 17 to 24 cows in a dry-lot operation. Alfalfa is the principal crop and feed, with small acreages of barley and sorghum grown for silage to use as feed supplements. The sizes and brief cropping histories of the fields used in this report were: field 4, 5.8 acres, plowed in July 1961 for sorghum and in November for barley with alfalfa; field 5, 8.0 acres, last plowed in 1960 and in alfalfa thereafter; field 6, 6.6 acres, in continuous alfalfa for 11 years. An annual mean precipitation of 12 in. is augmented by irrigation water from the Virgin River.

Small samples, consisting of 6 to 8 specimens from each material of interest, were analyzed for ^{90}Sr and ^{137}Cs according to the methods for wet chemistry[1] given in USAEC Report NYO-4700(Rev.).

The vertical distributions of ^{90}Sr and ^{137}Cs were determined for soil in the cultivated fields from samples taken in November of 1962. The distribution of radionuclides is shown in Fig. 1 as mean millicuries per square mile per inch depth of the profiles of fields 4 to 6. In field 4 ^{90}Sr and ^{137}Cs were at a maximum in the surface inch with a gradual decrease through the plowed layer. In field 5, ^{90}Sr decreased with depth whereas ^{137}Cs peaked in the lowest part of the plowed layer. Both ^{90}Sr and ^{137}Cs were more uniform in the profile of field 6 than in the other fields, but the ^{137}Cs in the surface inch exceeded that in fields 4 and 5. The mean summation of nuclides with depth in these fields was 160 and 460 mc/square mile for ^{90}Sr and ^{137}Cs, respectively. The radioactivity in specimens taken from below 18 in. was beneath the detection limit of the chemical processes used.

Characterizations of radioactivity may be given in various dimensional units. The collection unit for specimens is often a mass unit that is combined with its radioactivity and then extrapolated into suitable dimensions. In Fig. 1 the millicuries per square mile were derived from the mass of soil per unit area in kilograms per square meter and the radioactivity per unit mass in picocuries per kilogram. The equation is

$$\text{Kg of soil/m}^2 \times \text{pc/kg of soil} \times \text{constant} = \text{mc/square mile}$$

There are uncertainties concerning the precision and the reliability with which a mean value can describe several specimens collectively. These uncertainties, or variances, in a sample of specimens may be extremely difficult to partition successfully among the factors contributing to it.

In the equation given, the independent variables are the kilograms of soil per square meter and the millicuries per square mile. The

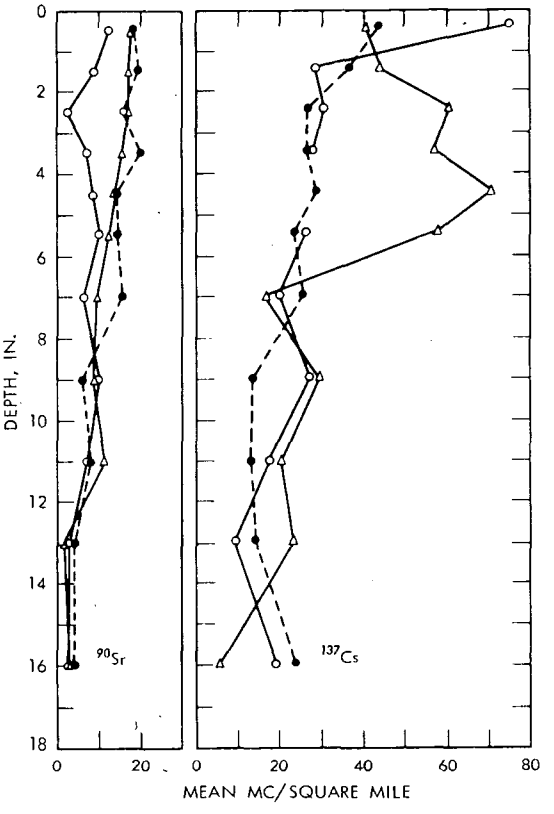

Fig. 1 — Variations in the vertical distribution of ^{90}Sr and ^{137}Cs in soil from the profiles of three fields, November 1962. ●, field 4; Δ, field 5; ○, field 6.

picocuries per kilogram of soil are directly proportional to the millicuries per square mile and inversely proportional to the kilograms of soil per square meter. Variation in the radioactivity of a sample of several soil specimens is a complex function of the variation of the two independent variables plus variation introduced among specimens by the sampling and nuclide-extraction procedures. It is unfortunate that the sampling method requires that the millicuries per square mile be computed from the picocuries per kilogram of soil. Soil samples were taken to find the amount and variability in fission-product deposition from site to site, but the real variability in the field was confounded with other variations among the specimens analyzed.

Equipment for weighing and for linear measurements was quite accurate. Figure 2, a scatter diagram, shows the variability among weights of soil specimens taken from field 4. Measurements of soil mass per unit area tended to diverge for specimens taken above and below the plow pan.

Dispersion in picocuries of ^{90}Sr per kilogram of soil is shown in Fig. 3. The variation was greatest within the plowed layer and de-

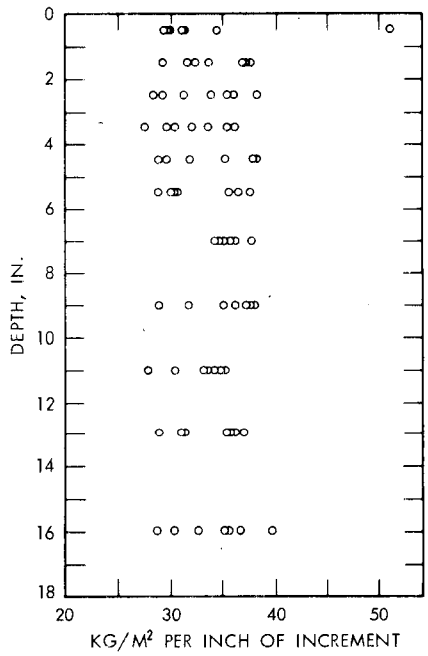

Fig. 2—Dispersion among the weights of solid specimens taken in samples from different depths in the profile of field 4.

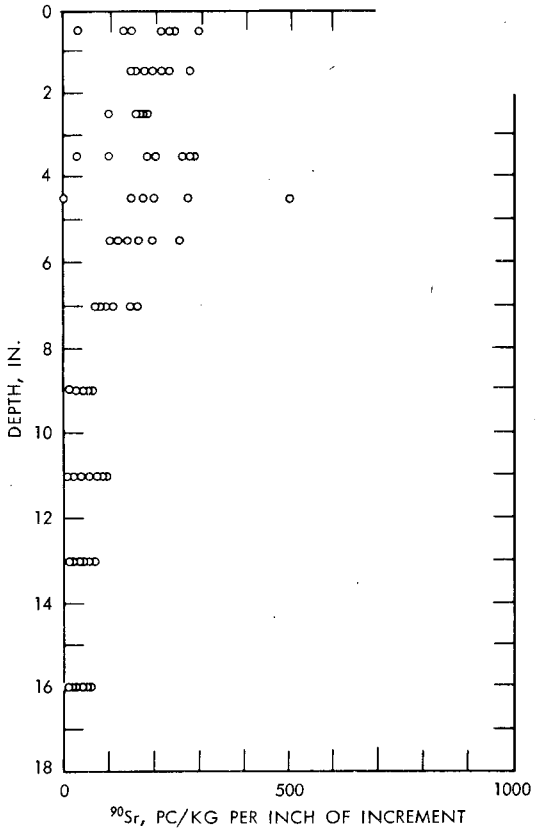

Fig. 3—Variability in the concentration of ^{90}Sr in specimens from samples taken at different depths in the soil profile of field 4, November 1962.

creased below the plowed zone. Figure 4 is a similar diagram for picocuries of ^{137}Cs per kilogram of soil in the same soil specimens that were analyzed for the ^{90}Sr of Fig. 3, and the variability, though greater than that of ^{90}Sr, was distributed similarly. The variation in fission-product concentrations shown in the figures includes that introduced (1) during sampling of the soil profile in the field, (2) in the selecting of representative subsamples for chemical analyses, (3) from chemical treatment to extract radionuclides, (4) from the uncertainties in counting the isotopes extracted, and (5) by the actual variation in radioactivity among the specimens in the field (evaluation of this factor was the reason for collecting the specimens).

The ^{90}Sr and ^{137}Cs computed from the data illustrated in the preceding figures are given in nanocuries per square meter for different depths in the soil profile in Figs. 5 and 6. These figures illustrate the uncertainty that is associated with mean values that purport to describe the fission products of a relatively small field. The components of the variances in these computed values were discussed earlier. In the first

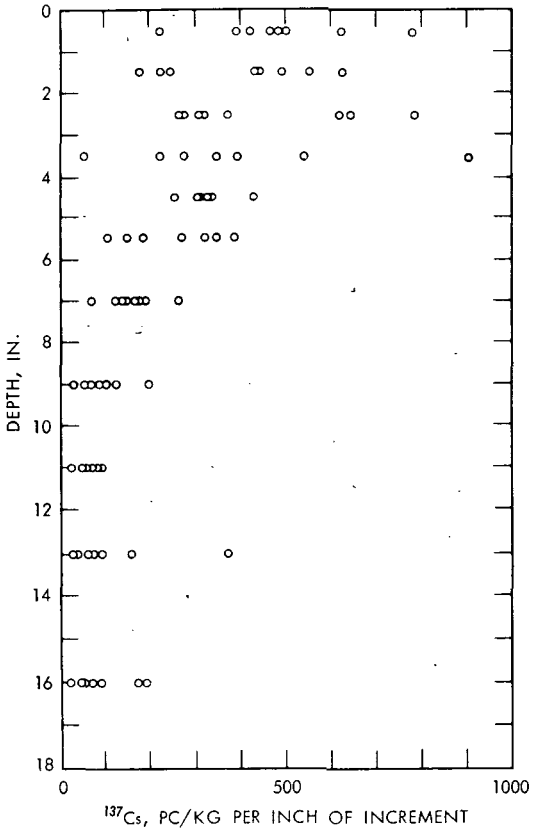

Fig. 4—Deviations in the concentration of ^{137}Cs among specimens from soil samples collected at different positions in the profile of field 4, November 1962.

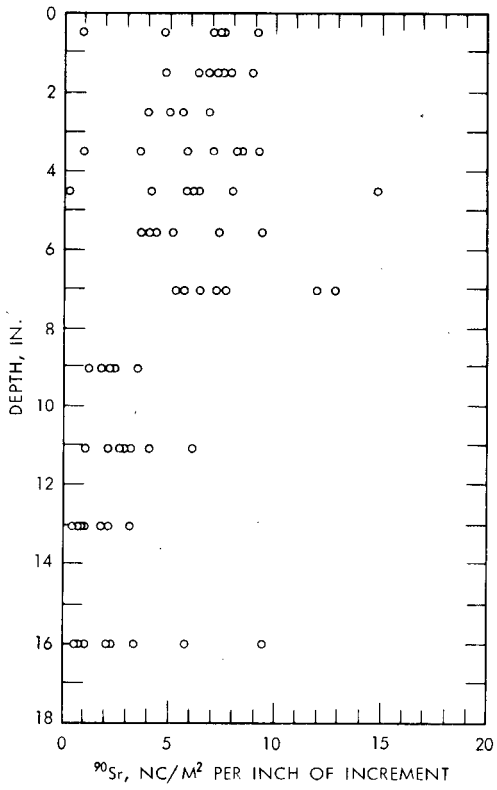

Fig. 5 — Variation in the ^{90}Sr computed from random specimens of samples removed in a vertical sequence from the soil profile of field 4, November 1962.

30 soil samples analyzed, the composite variance for nanocuries per square meter exceeded the variance for picocuries per kilogram of soil 19 times. The converse occurred 10 times, and the variances were equal once. Predictions of compensatory combinations of deviations in the data, i.e., low kilograms of soil per square meter associated with high picocuries per kilogram of soil, were unreliable.

Taken together, Figs. 2 to 6 showed the variation that existed among the factors from which the ^{90}Sr and the ^{137}Cs per unit area of soil were derived. They were concerned with variability in specimen mass per unit volume and the variation in fission-product concentration per unit mass. They demonstrated variation in three-dimensional space.

Another kind of variability encountered in the study is illustrated in Fig. 7, which shows differences in the rate of production of mass of alfalfa per unit area. The graph represents the mean production of alfalfa in three fields on the indicated harvest dates. Variances in the weights of alfalfa for all harvests, in grams per square meter, were tested for homogeneity by a modified Bartlett's test.[2] The variances among fields were equal for each month; but the variances of individual

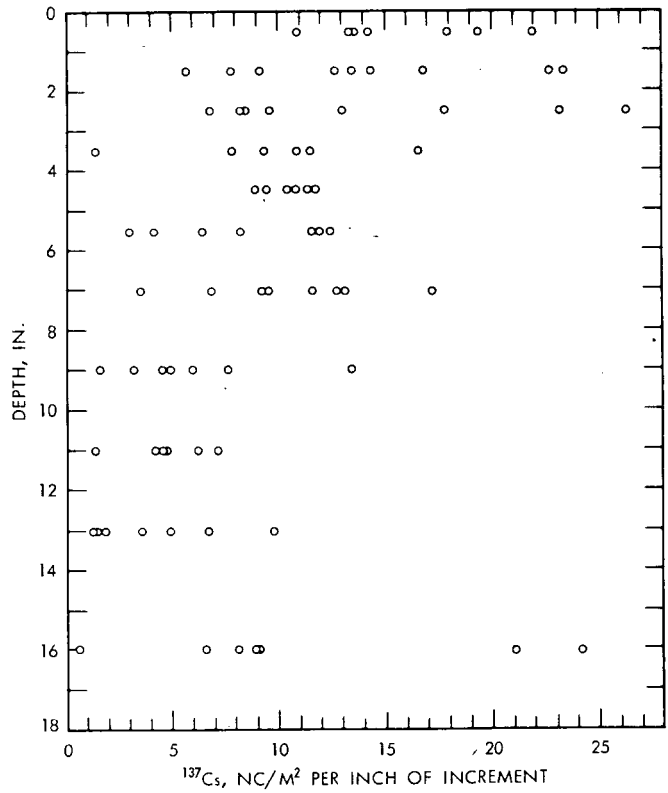

Fig. 6—Variation in the ^{137}Cs computed from random specimens of samples taken in a vertical sequence from the soil profile of field 4, November 1962.

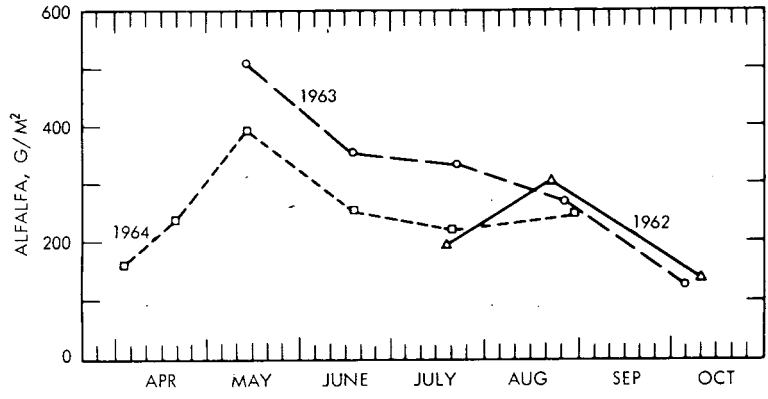

Fig. 7—Mean weights of alfalfa harvested from three fields during three growing seasons.

fields were unequal, both among years and harvests. This finding nullified predicting alfalfa production from intermittent harvests during a growing season. Measurements of production are required for all harvests in a study period.

The amounts of ^{90}Sr and of ^{137}Cs associated with alfalfa in each field were computed with the same equation used for computing soil fission products. The same uncertainties apply to the mean value as a description of the amounts of ^{90}Sr and of ^{137}Cs with a crop as were given earlier for the radionuclide content of the soils of the fields. Components of variances are as intricately intertwined between the dependent variable and the independent variables as they were for soils. Again, there is a confounding of the real variation in fission-product distribution in space with variation introduced by sampling and analytical procedures.

Measures of the variability of a material may be expressed in several forms. In Fig. 8 the mean production of alfalfa is indicated for one field with the dispersion among square-meter specimens illustrated as plus or minus one standard deviation. As expected, the weight of alfalfa varies with the season of the year and from year to year. In addition, the reliability with which the means can be defined also varies among the harvests.

The points of greatest interest in studies of a dairy farm are those where man becomes a consumer of the farm products. Figure 9 illustrates the variation of ^{137}Cs and ^{90}Sr per unit volume of milk over a

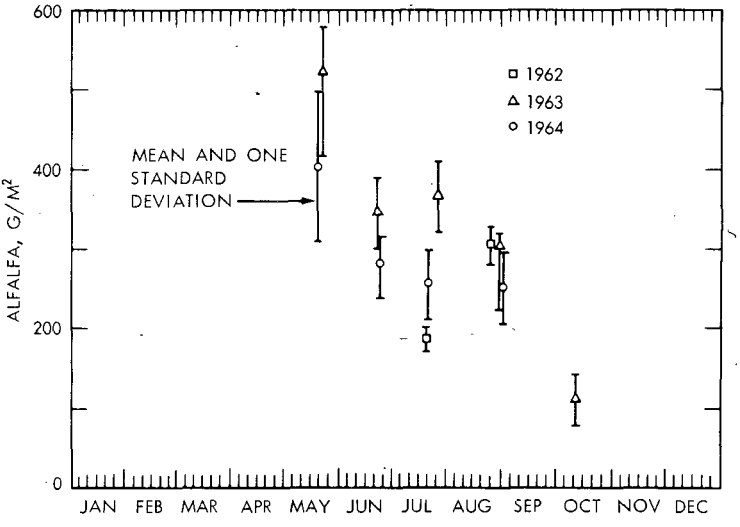

Fig. 8—Mean weight of alfalfa samples, with dispersion among specimen weights characterized by one standard deviation, in harvests from one field during three growing seasons.

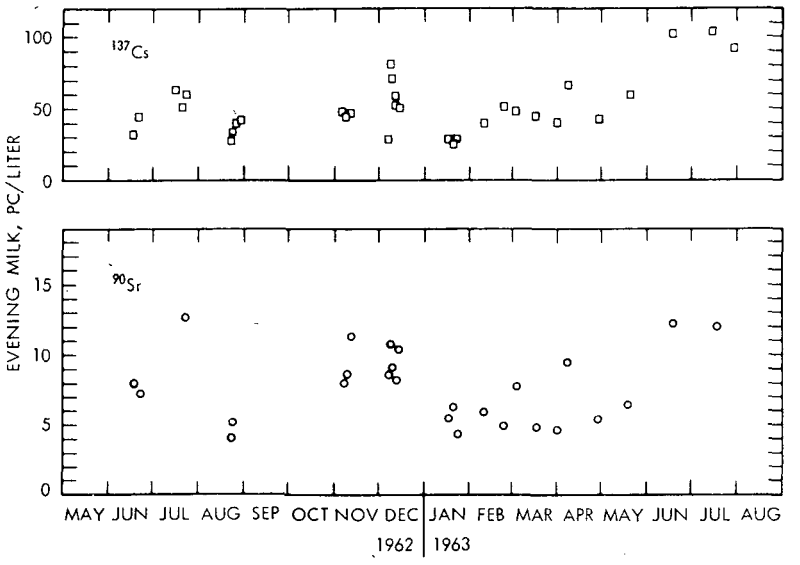

Fig. 9—Distribution of the mean concentrations of ^{137}Cs and ^{90}Sr in evening milk. Composite samples from a herd of 17 to 24 cows.

period of one year. In this interval the diet of the cattle changed six times because of the feeding of hay grown in different seasons of the year. The deposition of fallout changed while each cutting of alfalfa was growing, and the rates of growth varied simultaneously, as shown in Figs. 7 and 8. Individual cows began and terminated lactation periods, thereby varying the volume of milk produced daily. Differences in the metabolic efficiency among cows in extracting ^{90}Sr and ^{137}Cs from feeds also contributed to daily variability.

The high cost of radiochemical determinations precludes dissipating analytical resources on objectives that cannot be achieved with precision. Ascertaining whether a particular objective should be attempted necessitates that estimates be made of the size of sample required to obtain the precision desired within a specified confidence interval. Therefore, since this was an exploratory study, only small samples of six to eight specimens were analyzed for ^{90}Sr and ^{137}Cs. Their means and standard deviations were used to estimate sample requirements for defining fission-product concentrations in different materials on the farm. The weights of the specimens in a sample were used to estimate the size of the sample needed to determine the quantities of the different materials.

The population parameter needed for reliable estimates of sample size is the population standard deviation.[3] This parameter was not available. However, the sample standard deviations can be used with

Students' t distribution to estimate the population standard deviations.[4] Estimates of sample size made in this way cannot take advantage of the continuous flow of new information arriving as more specimens are analyzed.

Blocks of 100 specimens were assembled, each containing related materials: soil, plants, or milk. Each specimen was assigned a random number to separate replicate specimens of a sample. The specimens were analyzed in numerical sequence; thus the radiochemical determinations for replicates from any given sample were acquired at spaced intervals in time. Sequential-analysis statistical techniques become feasible when information on replicate specimens is obtained in this manner. Uncompleted analyses can be terminated when standards of precision and reliability are met.

On the average, use of sequential analysis results in a 50% reduction in sample size as compared to the use of single fixed-sample-size estimates.[5] However, the number of specimens in a sample are not known until the hypothesis under test is accepted or rejected. The procedure is not appropriate for estimating sample sizes. It does, however, require fewer specimens in a sample than are estimated when Students' t distribution is used.

Two estimates of sample size were made by using the sample statistics of means and standard deviations: assuming a normal distribution in one case and using the Students' t distribution in the other. The ratios of the two sample-size estimates (t/normal) fell in the range of 1.5 to 1.7 for coefficients of variation from 0.05 to 0.40. Therefore the procedure has been to make an estimate of sample size from statistics that are assumed to be normally distributed. In the following tables the numbers of specimens shown for samples of soil, alfalfa, and milk apply only to this farm and are fewer than those which were estimated with statistical rigor. They do, however, take into account the reductions in analytical burden which ensue from applying sequential analysis.

A formula is given in Table 1 for calculation of the number of specimens required to state the mean at some desired precision. At the same time the investigator may specify what risk he is willing to take that the sample mean may actually fall outside the precision limits he has chosen. It is apparent from Table 1 that, even though the absolute radioactivity varied in the soil profile (Fig. 1), the required number of specimens does not differ greatly through the plowed zone and that the required precision can be attained. Table 2 shows how the required number of specimens changed for the same month from year to year and also from month to month in the same year. These changing sample sizes reflect the changing variability in alfalfa growth rates.

The data of Table 3 show that there was less variability in ^{137}Cs in the milk than there was in the alfalfa consumed to produce the milk

Table 1—NUMBER OF SPECIMENS* REQUIRED TO ASSESS PICOCURIES PER SQUARE METER OF ^{90}Sr IN THE SOIL OF ONE FIELD WITH STATED PRECISION†

Depth, in.	Confidence level 0.90	0.95	0.99
0 to 1	10	14	24
1 to 2	9	13	23
2 to 3	8	10	18
3 to 4	8	11	19
4 to 5	9	13	22
5 to 6	43	60	105
6 to 8	20	28	49

*Size of sample = $(ZC/P)^2$, where Z is the confidence-level constant, C is the standard deviation/mean, and P is the precision level.

†Precision level used was ±10% of the mean.

Table 2—NUMBER OF SPECIMENS* REQUIRED TO DEFINE ALFALFA PRODUCTIVITY IN ONE FIELD WITH STATED PRECISION†

Alfalfa, g/m^2	Confidence level 0.90	0.95	0.99
July			
1962	5	7	11
1963	7	10	17
1964	7	9	16
1963			
May	2	3	4
June	5	7	12
July	7	10	17
August	13	19	33
October	8	11	19

*Size of sample = $(ZC/P)^2$, where Z is the confidence-level constant, C is the standard deviation/mean, and P is the precision level.

†Precision level used was ±10% of the mean.

and less than there was in the soil in which the alfalfa grew. The concentration of ^{137}Cs in each of these materials varied more than the mass of material or the absolute amount of ^{137}Cs in the material. We see again that the variation in the product of two factors is not predictable. Partitioning the variances among each of the factors involved in finding the absolute amount of radioactivity and that introduced in specimen collection, preparation, chemical analysis, and counting of nuclides can be very troublesome.

Study of arrays of similar tables showed that there was a high degree of variation within each of the different radionuclide matrixes and

Table 3 — NUMBER OF SPECIMENS* REQUIRED FOR STATED PRECISION† IN ASSESSMENT OF ^{137}Cs

	Confidence level		
	0.90	0.95	0.99
Soil, 0 to 1 in. deep			
Kg/m^2	2	2	4
Pc/kg	33	46	79
Pc/m^2	11	15	26
Alfalfa			
Kg/m^2	3	4	6
Pc/kg	50	70	121
Pc/m^2	43	60	103
Milk			
Kg/milking	2	3	4
Pc/kg	8	12	20
Pc/milking	9	13	22

*Size of sample = $(ZC/P)^2$, where Z is the confidence-level constant, C is the standard deviation/mean, and P is the precision level.

†Precision level used was ±10% of the mean.

that assumptions of general homogeneity were unwarranted. Since the ultimate objective of the study is to construct mathematical models of the cycles of ^{90}Sr and ^{137}Cs, measurements of the amounts of ^{90}Sr and ^{137}Cs present are required. The point to be made here is that definition of the amounts of fission products in the system is subject to an uncertainty that varies in time and three-dimensional space. The system is dynamic. Mathematical models of the system must take these variations into account. A stochastic model is required. It must be constructed from actual observations upon the system over some time interval instead of upon assumptions if it is to be realistically definitive.

REFERENCES

1. Health and Safety Laboratory, Manual of Standard Procedures, USAEC Report NYO-4700(Rev.), August 1962.
2. W. J. Dixon and F. J. Massey, Jr., *Introduction to Statistical Analysis*, McGraw-Hill Book Company, Inc., New York, 1957.
3. G. W. Snedecor and W. G. Cochrane, *Statistical Methods Applied to Experiments in Agriculture and Biology*, 5th ed., Iowa State University Press, Ames, Iowa, 1956.
4. W. G. Cochrane and G. M. Cox, *Experimental Designs*, John Wiley & Sons, Inc., New York, 1950.
5. A. Wald, *Sequential Analysis*, John Wiley & Sons, Inc., New York, 1947.

USE OF SURFACE-AIR CONCENTRATION AND RAINFALL MEASUREMENTS TO PREDICT DEPOSITION OF FALLOUT RADIONUCLIDES

CHARLES A. PELLETIER, G. HOYT WHIPPLE, and HAROLD L. WEDLICK
The University of Michigan, Ann Arbor, Michigan

ABSTRACT

An empirical model relating deposition and air concentration of gross beta radioactivity is presented. The model is based on measurements in the western Lake Erie area between January 1963 and June 1964 and has the form

$$\frac{D}{C_A} = H\,(a - e^{-br})$$

where D = deposition, pc/m^2
C_A = air concentration, pc/m^3
H = constant, m
a = factor to account for dry fallout onto precipitation collector, dimensionless units
b = elimination constant, $(\text{inches of rain})^{-1}$
r = rainfall amount, in.

The meaning and the applicability of the model are discussed. The model is used to predict the deposition of gross beta radioactivity at a single location in southeastern Michigan.

INTRODUCTION

The overall objective of our research program is to develop a mathematical model to describe the cycling of fallout radionuclides

through the milk food chain. We are concentrating our efforts on a single farm in Tecumseh, Mich. We have divided the program into two parts. The first part is a routine sampling program in which we measure the radioactivity in every medium that might enter into the milk food chain. The second part of the program is the development of a mathematical model. In developing the model, we are relying heavily on theoretical considerations and on the experimental results of other investigators. In certain cases, however, we have designed special experiments for the sole purpose of providing information for the model. The results of the routine sampling program will be used to check and refine the model.

In our climate a greater proportion of radioactive contamination is deposited by precipitation than by dry processes. Therefore the first exchange of radioactivity in the milk food chain is between air and precipitation. To keep the development of the model separate from the data collected on the farm, we have used data from an environmental survey around the Enrico Fermi Atomic Power Plant* to develop the model.

BACKGROUND

Chamberlain[1] has used the term washout factor, W_g, to equate the radioactivity in rain to the radioactivity in air. He defines the term as the ratio of the rain concentration to the air concentration measured at 1200 m, both concentrations being computed on a weight basis. Peirson and Keane[2] have also used the washout factor but have used the air concentration at ground level rather than at 1200 m.

Table 1 shows the washout factors measured by various investigators. As far as this paper is concerned, the important thing to note is that the washout factors can vary considerably when computed over periods of less than a few months.

One cannot discuss the deposition from rain without mentioning the deposition from dry fallout. This is because, unless they are covered when there is no precipitation, all precipitation collectors will collect some dry fallout. A useful term in measuring dry fallout[2] is the deposition velocity, V_g, which is defined as the ratio of the deposition rate onto a surface to the air concentration measured above that surface.

Surface characteristics are important in dry-fallout measurements. Megaw and Chadwick[5] have reported a fivefold increase in deposition velocity measured on real grass relative to that measured on horizontal sheets of filter paper. The aerosol used in this case was

*This survey was made by the National Sanitation Foundation, Ann Arbor, Mich., under contract with the Power Reactor Development Company, Detroit, Mich.

Table 1—WASHOUT FACTORS, W_g, AND DRY-DEPOSITION VELOCITIES, V_g, FOR FALLOUT RADIOACTIVITY FOR DIFFERENT LOCATIONS AND DATES*

W_g†[3]	Time of W_g	V_g, ‡[2] cm/sec	Time of V_g
	England		
230 (^{137}Cs)§ 130 (^{95}Zr)§ 560 (^{137}Cs) 520 (^{144}Ce) 480 (^{140}Ba) 500 (^{95}Zr) 420 (^{131}I)	July 1958–June 1959 (yearly average)[1] Sept.–Nov. 1960 (three-month average)[2] Sept.–Nov. 1961 (three-month average)[2]	0.07 (gross beta)	1956–1957 (average)[4]
	Norway		
645–6450 (gross beta)	Sept. 1956–Sept. 1959 (range of monthly averages)[3]	0.70 (gross beta)	Sept. 1956–Sept. 1959 (average)[3]
	Holland		
516–3220 (gross beta)	Sept. 1955–Apr. 1957 (range of monthly averages)[3]		
	Germany		
430 (gross beta)	July–Dec. 1957 (six-month average)[3]		
	United States (Tecumseh, Mich.)		
475–2100 (gross beta)	Jan. 1963–June 1964 (range of four-week averages)	0.29 (gross beta)	Sept. 1961–Jan. 1962 Av. 1962–Jan. 1963 (average)
		0.20 (gross beta)	Feb. 1962–July 1962 Feb. 1963–June 1964 (average)

*Unless otherwise specified, washout factors were computed using surface-air concentrations.

†W_g is the radioactivity concentration in rain in picocuries per kilogram divided by the radioactivity concentration in air in picocuries per kilogram.

‡V_g is the rate of deposition in picocuries per square centimeter per second divided by the concentration in air in picocuries per cubic centimeter.

§Computed using air concentrations at 1200 m.

artificially generated; particle sizes were reported to be in the submicron range. For purposes of this paper, we are concerned only with the dry fallout onto precipitation collectors.

Table 1 also shows some measured deposition velocities of gross beta radioactivity onto precipitation collectors. It appears that the dry-deposition velocity can vary widely from place to place and from time to time. The important thing to note here is that, despite these different deposition velocities, the total deposition of dry fallout onto the

collectors was only a small fraction of the total activity collected. For the sampling sites in England where the deposition velocity was 0.07 cm/sec, only 7% of the total deposition was associated with dry fallout. At the sampling site in Norway where the deposition velocity was 0.7 cm/sec, only 14% of the total deposition was associated with dry fallout.

SAMPLING AND ANALYTICAL PROCEDURES

Environmental Survey Around the Enrico Fermi Atomic Power Plant

There were ten rain-sampling and nine air-sampling locations used in the environmental survey around the Fermi Reactor. Figure 1 shows the locations of these sampling sites. The area included in this survey is roughly 500 square miles. The terrain is relatively flat, and the wind blows predominantly from the southwest. The Enrico Fermi Reactor was either not operating during the period covered by these mea-

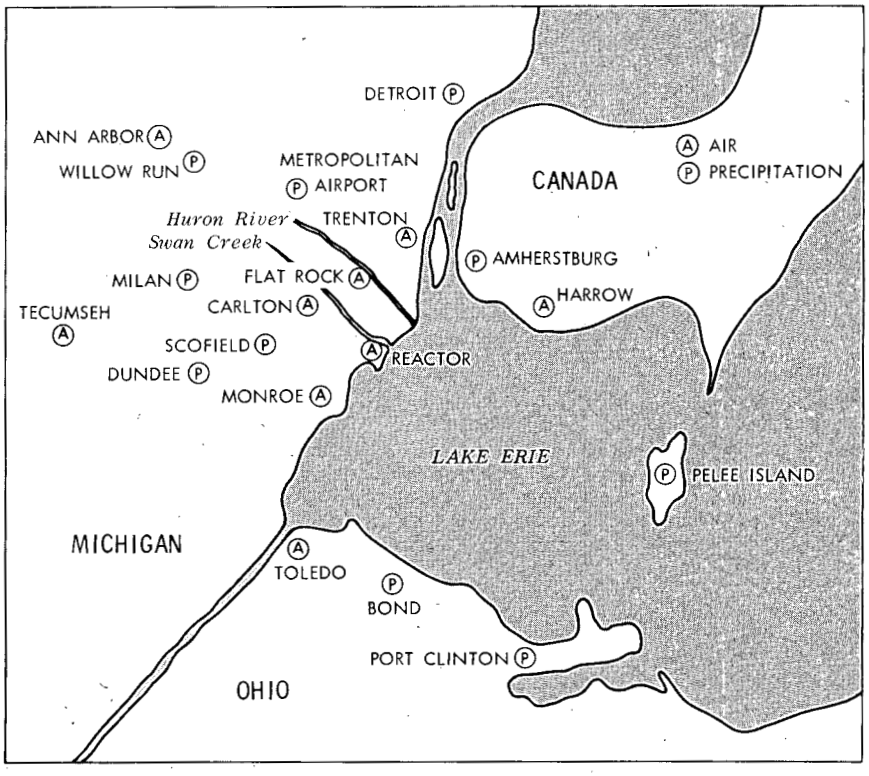

Fig. 1—Sampling sites for the environmental survey around the Enrico Fermi Atomic Power Plant.

surements or operating at an extremely low power level. Therefore the activity measured at the sampling locations was entirely from nuclear testing.

During a four-week period, precipitation was collected through a 10.5-in.-diameter polyethylene funnel into a rain jug. Zirconium carrier was added to the collection jug prior to each sampling period. At the end of the sampling period, the funnel was washed with $3N$ HNO_3, and the wash was measured and added to the contents of the rain jug. The rain jug was returned to the laboratory, its contents were measured, and then the jug was washed thoroughly with HNO_3 and HCl. The contents and the wash solutions were transferred to a beaker and evaporated to dryness, the residue finally being transferred to a 2-in.-diameter stainless-steel planchet for beta counting. The beta counter used was a low-background thin-window flow Geiger counter that was calibrated with the beta radiation from ^{204}Tl.

Air samples were collected by drawing air through high-efficiency membrane filters during a period of two weeks. The air volume was measured with a gas meter and subsequently corrected for the pressure drop across the filter. At the end of the two-week period, the air filter was brought back to the laboratory, allowed to decay for seven days, and then counted.

The rainfall was measured from the volume of rain collected during the four-week period. We have noted that, on the average, the 10.5-in.-diameter funnel collected more rain for its diameter than the standard rain gauge. However this effect was at least partially offset by the effect of evaporation during the four-week sampling time.

Measurements at the Study Farm at Tecumseh

The deposition and precipitation measurements on the Tecumseh farm were made on a weekly basis. Collections were made through an 8-in.-diameter polyethylene funnel.

Stewart et al.[6] have reported that an 8-in.-diameter polyethylene funnel will collect more rain than the 8-in.-diameter standard rain gauge. Therefore, as in the case of the 10.5-in.-diameter funnel, we expect the rainfall measurement to be higher than would be measured by the standard rain gauge. However, because the four-week evaporation period was not available for the Tecumseh measurements, the rainfall measurements at Tecumseh and those from the environmental survey around the Fermi Reactor may really not be comparable. As will be shown later on, this is probably the reason for only fair agreement between the predicted and the measured depositions at the Tecumseh farm.

Air samples were collected at the Tecumseh farm in the same manner as the air samples that were collected for the environmental

survey around the Fermi Reactor, except that the collection time was only one week.

RESULTS

Table 2 shows the results of the measurements for both the Fermi Reactor survey and the Tecumseh farm. For the purposes of analysis of the data from the Fermi Reactor environmental survey, all nine air concentrations, all ten deposition measurements, and all ten rainfall measurements were averaged for each four-week collection period. Each value in Table 1 therefore represents a four-week average over an area of about 500 square miles.

When the ratios of deposition to air concentration were plotted against rainfall, the points were scattered, but they showed an upward trend with increasing rainfall. However, when the data were divided into groups according to date, the scattering was almost eliminated, and the data were found to follow three distinct curves as shown in

Table 2—RESULTS OF GROSS BETA MEASUREMENTS OF PRECIPITATION AND AIRBORNE DUST COLLECTED IN THE NETWORK OF STATIONS FOR THE ENVIRONMENTAL SURVEY OF THE ENRICO FERMI ATOMIC POWER PLANT AND AT THE TECUMSEH STUDY FARM

End of sampling interval	Fermi environmental survey			Tecumseh study farm		
	Deposition, pc/m^2	Rainfall, in.	Air concentration, pc/m^3	Deposition, pc/m^2	Rainfall, in.	Air concentration, pc/m^3
1963						
Jan. 24	7.05×10^4	0.216	7.57	8.5×10^4	0.316	6.28
Feb. 21	4.61×10^4	0.226	5.57	7.9×10^4	0.498	7.70
Mar. 21	15.5×10^4	2.08	5.67	17.8×10^4	1.54	6.83
Apr. 18	17.1×10^4	1.52	7.29	20.6×10^4	1.30	8.38
May 16	33.0×10^4	3.53	9.10	30.2×10^4	2.84	9.38
June 13	31.0×10^4	3.96	7.30	16.5×10^4	1.64	8.48
July 11	3.1×10^4	0.03	8.85	10.9×10^4	1.10	9.48
Aug. 8	10.2×10^4	1.81	6.10	10.7×10^4	2.59	9.88
Sept. 5	5.76×10^4	1.39	4.0	5.05×10^4	1.16	4.78
Oct. 3	3.50×10^4	1.27	2.20	2.96×10^4	1.06	3.25
Oct. 31	1.37×10^4	0.57	1.68	2.37×10^4	1.07	2.00
Nov. 27	3.04×10^4	1.85	1.09	2.20×10^4	1.43	1.07
Dec. 26	1.18×10^4	0.61	0.81	1.09×10^4	0.511	0.92
1964						
Jan. 23	1.55×10^4	1.08	0.94	1.68×10^4	0.925	0.83
Feb. 20	1.69×10^4	1.01	1.12	1.12×10^4	0.555	1.15
Mar. 19	2.73×10^4	1.42	1.22	3.40×10^4	1.550	1.24
Apr. 16	8.55×10^4	3.94	1.45	7.16×10^4	3.140	1.65
May 14	9.30×10^4	4.50	1.50	6.20×10^4	3.120	1.81
June 11	7.60×10^4	2.28	1.78	5.95×10^4	2.89	1.98

Fig. 2. The curves shown in this figure could be fitted to the general equation

$$\frac{D}{C_A} = H\,(a - e^{-br}) \qquad (1)$$

where D = four-week deposition, pc/m^2
C_A = average four-week air concentration, pc/m^2
H = constant, m
a = factor to account for dry fallout onto the precipitation collector, dimensionless units
b = elimination constant, (inches of rain)$^{-1}$
r = four-week rainfall, in.

Actually, from the point of view of curve fitting, there was little choice between a linear model and the exponential model shown by Eq. 1. When the term "b" in Eq. 1 becomes small, the equation tends to become linear, especially in the region of the measurements. This is also true when the term "H" becomes very large. The main reason for choosing the exponential model was that it conforms to what little theory there is concerning the washout of particles from the atmosphere.[7,8]

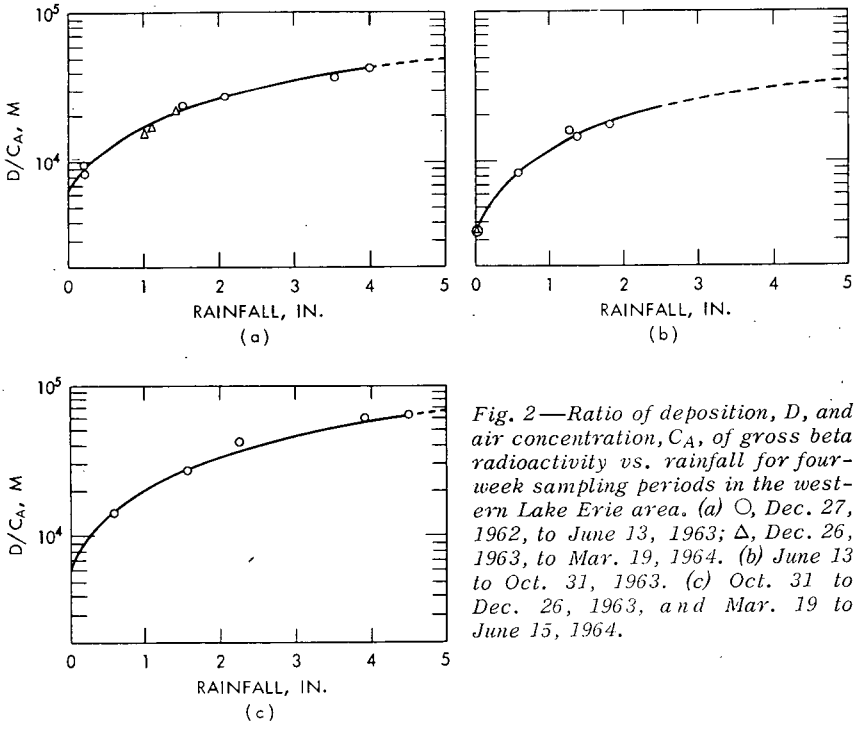

Fig. 2—Ratio of deposition, D, and air concentration, C_A, of gross beta radioactivity vs. rainfall for four-week sampling periods in the western Lake Erie area. (a) ○, Dec. 27, 1962, to June 13, 1963; △, Dec. 26, 1963, to Mar. 19, 1964. (b) June 13 to Oct. 31, 1963. (c) Oct. 31 to Dec. 26, 1963, and Mar. 19 to June 15, 1964.

Another reason was that the exponential model has three terms to manipulate whereas the linear model has only two. For a process as complicated as the deposition of airborne radioactivity, this additional term seemed to be an advantage.

The specific equations for the points in Fig. 2 are shown in Table 3.

Table 3 — EQUATIONS OF THE FORM OF EQ. 1 DETERMINED BY CURVE FITTING TO THE DATA SHOWN IN FIG. 2

Dates	Equation
Dec. 27, 1962, to June 13, 1963 Dec. 26, 1963, to Mar. 19, 1964	$1.0 \times 10^5 (1.065 - e^{-0.11r})$ (part a, Fig. 2)
June 13, 1963, to Oct. 31, 1963	$0.8 \times 10^5 (1.04 - e^{-0.11r})$ (part b, Fig. 2)
Oct. 31, 1963, to Dec. 26, 1963 Mar. 19, 1964, to June 15, 1964	$1.4 \times 10^5 (1.04 - e^{-0.11r})$ (part c, Fig. 2)

The values of the parameters H, a, and b do not necessarily have any physical significance. The best fit to the points for the first six four-week periods (part a, Fig. 2) was made with b equal to 0.11. Except for the one for the daily rainfall data, all subsequent curves could also be fitted with b equal to 0.11. However, these curves could have been fit equally as well with smaller values of b and correspondingly higher values of H. It appears that with values of b in the range of 0.11 we are at the threshold of being able to distinguish an exponential function from a linear one.

APPLICATION OF THE MODEL

The model used to predict the deposition of gross beta radioactivity at Tecumseh had the values of H and a for the time periods shown in Table 3. The results are shown in Fig. 3. The model overestimated the measured deposition 14 times with an average overestimation of 27.8%. The model underestimated the measured deposition only 5 times with an average underestimation of 19.2%. The computed total deposition for the entire 76-week period was 12% higher than the measured total deposition. It appears that there is a systematic difference between the computed and the measured depositions. The most likely explanation for this discrepancy lies in the measurement of rainfall, which has already been mentioned. Plans have been made to compare the collection efficiency of the 10.5-in.-diameter funnel during a four-week collection period and of the 8-in.-diameter funnel during a weekly collection period to the efficiency of the standard rain gauge during a weekly collection period.

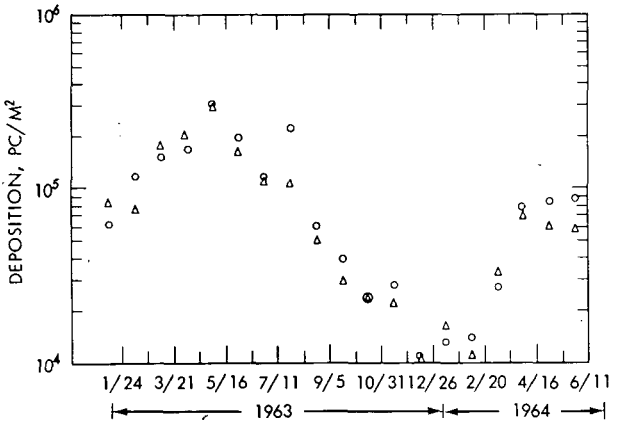

Fig. 3—Comparison between the predicted (○) and the measured (△) depositions of gross beta radioactivity for four-week sampling periods at Tecumseh, Mich.

DISCUSSION

Admittedly, the model was used in an arbitrary fashion to predict the deposition on the Tecumseh farm. It certainly is undesirable to have to keep the model current with an extensive program of measurements just to be able to predict the deposition at one location. In the following discussion an attempt is made to show that the model in its general form may be widely applicable. On the other hand, it will be shown that its applicability to specific situations is limited because at the present time the behavior of certain terms in the model cannot be predicted.

Applicability

First of all, with the model selected it was assumed that radioactivity is washed from the atmosphere exponentially with rainfall. Since the rainfall collected during a four-week period is the sum of individual rainfalls, one might expect to find an exponential relation between the deposition and the amount of rainfall on, say, a daily basis. In the literature on this subject, the relation that is repeated again and again is the apparently logarithmic one between the radioactivity concentration in rain and the amount of daily rainfall. This relation has been reported in Norway[3] from 1956 to 1959, in Great Britain[4] in 1956 and 1957, and in Russia.[9] The period during which the relation was found in Russia was not reported, but it probably was in 1960 and/or 1961. Figure 4 shows the relation plotted logarithmically. The points in Fig. 4 were determined by dividing the daily rain concentrations by their respective monthly concentration, averaging the data over several months

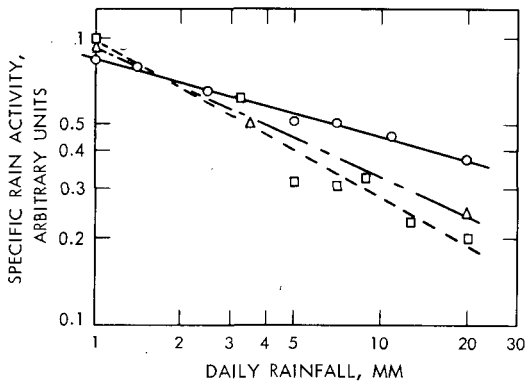

Fig. 4—Specific activity of daily rainfall vs. rainfall amounts for Leningrad, U.S.S.R. (□, dates unknown), England (○, 1956 and 1957), and Kjeller, Norway (△, 1956 to 1959).

according to daily rainfall, and then plotting the averages on an arbitrary scale. That these data show exponential cleansing of radioactivity from the atmosphere is shown in Fig. 5. The product of the radioactivity concentration and the amount of rainfall is the total deposition. These products were computed from the data in Fig. 4, and they were plotted against rainfall in Fig. 5. The data from England and Norway could be fitted with the model having values of b equal to 0.76 and 1.27, respectively. The fit was unambiguous. The data from Russia were too scattered for a quantitative measurement of b.

Figures 6 and 7 show more-direct evidence that the model might be applied to other locations and times. Figure 6 shows a plot of the ratio of deposition to the air concentration as a function of rainfall for two sites in Great Britain[10] during the period August 1962 through April 1963. The points can be joined by a curve having the form of the model with b equal to 0.11. It should be pointed out that from August to February fresh fallout predominated in this area. Figure 7 shows similar data for Kjeller, Norway, from January through September 1959. These points can also be fitted with the model having a value of b equal to 0.11. Furthermore, these data from Norway permit evaluation of the term "a," which is included in the model to account for dry fallout onto

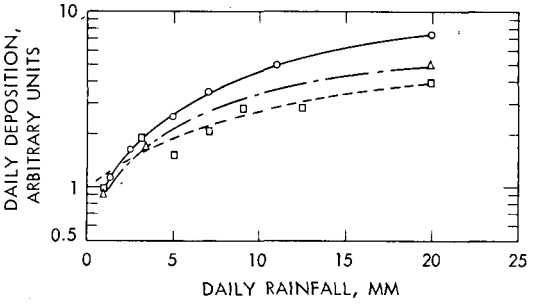

Fig. 5—Daily deposition vs. daily rainfall amounts for Leningrad, U.S.S.R. (□, dates unknown), England (○, 1956 and 1957), and Kjeller, Norway (△, 1956 to 1959).

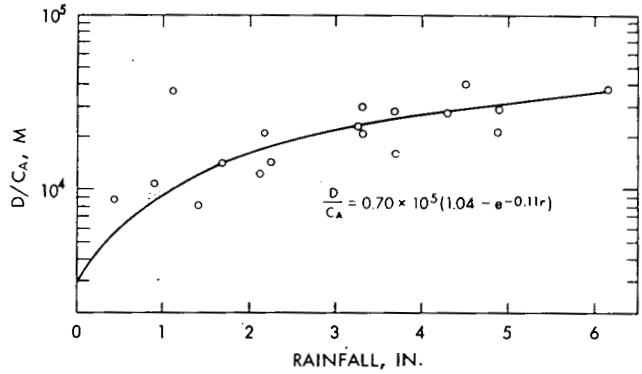

Fig. 6—Ratio of deposition, D, and air concentration, C_A, of gross beta radioactivity vs. rainfall for monthly samples at Chilton and Milford Haven, England, from August 1962 to April 1963.

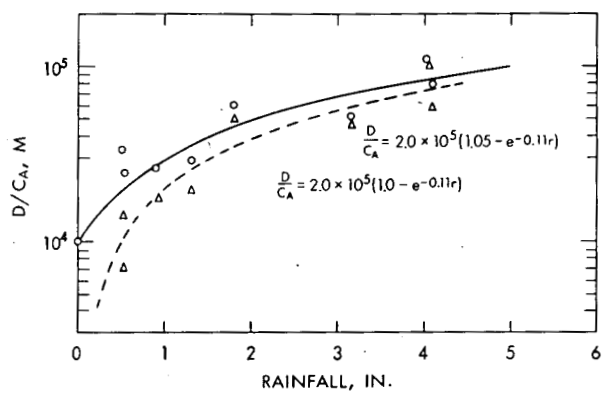

Fig. 7—Ratio of deposition, D, and air concentration, C_A, of gross beta radioactivity vs. rainfall for average monthly collections from January 1959 through September 1959 at Kjeller, Norway. ○, dry plus wet deposition; △, wet deposition.

the collector. Separate measurements of dry and wet fallout were made during this period. The best fit to the points representing total deposition was made with a value for a of 1.05. If a is set equal to 1.0, the contribution of dry fallout, in effect, is eliminated. Figure 7 also shows a fairly good fit of the wet-deposition data to the curve with a equal to 1.0.

Limitations

Two parameters in the model stayed fairly constant over the time periods and at the locations covered in this paper. All the data could be fitted with the model having a value for b of 0.11. The dry-fallout factor, a, varied only from 1.04 to 1.065. On the other hand, the parameter

H varied from 0.7×10^5 m for the Norwegian data of 1959 to 2.0×10^5 m for the British data of 1962 and 1963. Differences in sampling techniques could easily cause a difference of a factor of 3 between two locations. However, the measurements in the western Lake Erie area were made by the same group using the same sampling techniques, and the value of H changed from 0.8×10^5 to 1.4×10^5 m. It seems certain that, for the western Lake Erie measurements at least, the changes in H are real and will have to be explained.

At the present time the authors think the most likely explanation for the sudden changes in H lies in the distribution of radioactivity with height in the atmosphere. Obviously an air sample taken at ground level does not necessarily represent the air concentration at the rain-generating level. However, if the distribution of radioactivity with depth, whatever it may be, remains fairly constant for a period of time, then the ground-level air concentration will be proportional to the air concentration aloft over this same period of time. Now, if the radioactivity in rain is a function of the air concentration at the rain-generating level, it would also be a function of the surface-air concentration. If then the depth distribution changed to some other distribution, the relation between the surface-air concentration and the rain concentration would also change. In Fig. 8 we have plotted the air concentration in the western Lake Erie area as a function of time. The first change in H occurred at a time when the air concentration began an exponential decrease. This probably coincides with the time when mixing between the stratosphere and the troposphere decreased or stopped altogether. The next change in H occurred near the bottom of the exponential decrease, one month before the activity began to increase again. Since the only source of radioactivity during this period was the stratosphere, this change indicates that there was an increase in the exchange between the stratosphere and the troposphere. The next change in H occurred after 8 weeks and continued for 12 weeks. There were no changes in the air concentration that would set this period apart from the others. It may have been that there was a change in the rate of mixing between the stratosphere and the troposphere that could not be seen at the ground level during this 12-week period.

In the final analysis the model will have limited use in the predicting of deposition until we can find the reason for and predict the changes in H or until enough data have been accumulated to allow derivation of some empirical relation for H.

There is one more point that should be brought out. It was not possible with our data to show a correlation between the surface-air concentration and the amount of rainfall. When 143 weeks of air-concentration measurements taken at Tecumseh were plotted against weekly amounts of rain during the period from November 1961 to July 1964, a slightly negative slope was found by linear regression analysis,

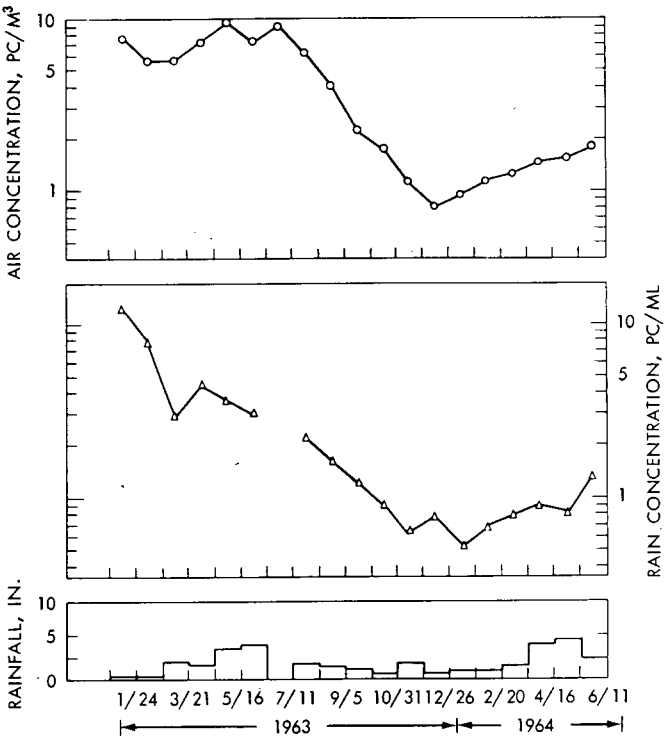

Fig. 8—Average air and rain concentrations of gross beta radioactivity for four-week sampling periods between Dec. 27, 1962, and June 15, 1964, in the western Lake Erie area.

but the correlation coefficient was less than 0.2 and not significant at any reasonable level of confidence. The samples were divided into periods of fresh and older fallout, but still no significant correlation could be found between air concentration and rainfall. It was concluded from these observations that in the climate studied at least the air concentrations of radioactivity at a given location are less dependent on the amount of local rainfall than they are on some more widespread phenomena. However, this may not be true in other climates.[11]

CONCLUSIONS

There appears to be a correlation between the radioactivity in surface air and the radioactivity in rain. The measurements reported here and those of others indicate that this relation can be described by an exponential model. However, the use of such a model to predict deposition will be limited until the behavior of certain terms in the model

can be predicted. The model selected was able to predict depositions only fairly well, considering that the location used to test the model was within the network of the samplers used to develop the model. Also the time period during which the model was tested was the same as the period during which the model was developed. On the other hand, a systematic sampling error seems to have entered into the comparison. The fact that the model could be used to fit data at other times and at other locations indicates that the model may be more widely applicable than for the conditions for which it had been developed.

REFERENCES

1. A. C. Chamberlain, Aspects of the Deposition of Radioactive and Other Gases and Particles, in *Aerodynamic Capture of Particles, Proceedings of a Conference Held at B.C.U.R.A., Leatherhead, Surrey, 1960,* edited by E. G. Richardson, Pergamon Press, Inc., New York, 1960.
2. D. H. Peirson and J. R. Keane, Characteristics of Early Fall-out from the Russian Nuclear Explosions of 1961, *Nature, 196:* 801 (1962).
3. S. H. Small, Wet and Dry Deposition of Fallout Materials at Kjeller, *Tellus, 12:* 309 (1960).
4. N. O. Stewart, R. G. D. Osmond, R. N. Crooks, and E. M. Fisher, The Worldwide Deposition of Long-lived Fission Products from Nuclear Test Explosions, British Report AERE-HP/R-2354, October 1957.
5. W. J. Megaw and R. C. Chadwick, Some Field Experiments on the Release and Deposition of Fission Products and Thoria, British Report AERE-HP/M-114, December 1956.
6. N. G. Stewart, R. N. Crooks, and E. M. R. Fisher, The Radiological Dose to Persons in the United Kingdom Due to Debris from Nuclear Test Explosions Prior to January 1956, British Report AERE-HP/R-2017, September 1956.
7. A. C. Chamberlain, Aspects of Travel and Deposition of Aerosol and Vapor Clouds, British Report AERE-HP/R-1261, Sept. 17, 1953.
8. P. B. Størebo, Orographical and Climatological Influences on Deposition of Nuclear Bomb Debris, *J. Meterol., 16:* 600 (1959).
9. V. P. Shvedov and S. I. Shirokov (Eds.), Radioactive Contamination of the External Environment, State Publishing House of Literature in the Field of Atomic Science, Moscow, 1962 (USAEC Report AEC-tr-6049, 1963).
10. R. S. Cambray and E. M. R. Fisher, Radioactive Fallout: Short-lived Fission Products in Air and Rain, August 1962–April 1963, British Report AERE-R-4384, July 1963.
11. L. B. Lockhart, Jr., R. A. Baus, and I. H. Blifford, Jr., Fission Product Radioactivity in Air Along the 80th Meridian, January–June 1957, *Tellus, 11:* 83 (1959).

RADIATION TO BONE FROM ^{90}Sr IN NEW YORK CITY RESIDENTS

JOSEPH RIVERA
Health and Safety Laboratory, U. S. Atomic Energy Commission,
New York, New York

ABSTRACT

From measurements of the ^{90}Sr content of the diet in New York City, Chicago, and San Francisco made every three months since 1960 and measurements of the ^{90}Sr content of the vertebrae of accident victims obtained at the three cities since 1961, parameters describing the bone metabolism of ^{90}Sr by individuals of ages from birth to 20 years have been inferred. The radiation dose to New York City residents from ^{90}Sr received to date has been calculated.

LEVELS IN BONE

One of the main problems with which fallout investigators have been concerned is the establishment of what radiation doses have been delivered to bone from ^{90}Sr produced in nuclear weapon tests and what doses will be delivered to bone as a result of past and possible future tests.

This problem can be divided into two parts. The first is to reconstruct the past ^{90}Sr/calcium ratios in diets. This reconstruction can be done as information is gained on the relation between fallout rates, cumulative deposition of ^{90}Sr, and ^{90}Sr/calcium levels in foods. As our understanding of the meteorological processes governing the transport and depostion of nuclear debris advances, we should be able to establish retrospectively what the ^{90}Sr/calcium levels were likely to have been in the past, where actual data do not exist, and we should also be able to predict better what these levels will be in the future. The sec-

ond part of the problem is to relate ^{90}Sr/calcium levels in the diet to ^{90}Sr/calcium levels in bone. This paper is concerned principally with this second part.

A relatively simple model relating diet and bone ^{90}Sr/calcium ratios is described by the equation

$$Ca_nX_n = Ca_{n-1}X_{n-1} - f_nCa_{n-1}X_{n-1} + f_nCa_{n-1}K_nZ_n + (Ca_n - Ca_{n-1})K_nZ_n$$

where Ca_n = skeletal calcium of an individual at the end of year n
X_n = ^{90}Sr/calcium ratio of the skeleton at the end of year n
f_n = fraction of skeletal calcium exchanged during the year
K_n = bone/diet observed ratio
Z_n = ^{90}Sr/calcium ratio of the diet

This model assumes that the ^{90}Sr content of the skeleton at the end of a year is equal to that of the previous year minus that lost by resorption plus that gained by replacement and that gained by accretion during the year. The metabolic parameters that must be known to apply the model are therefore the net calcium accretion rate, the bone/diet ^{90}Sr/calcium discrimination factor, and the bone turnover rate.

Mitchell et al.[1] have estimated the net calcium accretion rate for every age from birth to 20 years, after which skeletal growth ceases and the net calcium accretion rate becomes zero. These estimates are the best available for the net calcium accretion rate. An attempt to estimate the bone/diet ^{90}Sr/calcium discrimination factor and the bone turnover rate was made by considering the results of diet measurements[2] and bone-survey results in New York, Chicago, and San Francisco for the last two years.[3] The method used was to apply Eq. 1 to relate yearly changes in the ^{90}Sr concentrations in bone at specific ages to observed changes in the diet ^{90}Sr/calcium levels with different values of discrimination factors and turnover rates.

Where a sufficient number of bone samples were available, the ranges of values for the discrimination factor and the turnover rate which gave good fits to the data were small. For adults the best discrimination factor was 0.25, which is in agreement with other studies, and the best turnover rate was about 3½% per year. For infants (0 to 1 year of age) the discrimination factor calculated was about 0.35, and the average turnover rate was about 75% per year. These estimates are in rough agreement with those of Bryant and Loutit[4] and Beninson et al.[5]

For individuals between 2 and 20 years of age, however, there were relatively few bone samples, and the estimated discrimination factors and turnover rates were therefore more uncertain. From the

data available it appeared that strontium/calcium discrimination increases somewhat between the ages of 2 and 10, when calcium accretion rates are low and then decreases during puberty when calcium accretion rates increase. Bone turnover rates seem to be directly proportional to net calcium accretion rates.

Based on these general observations of strontium/calcium discrimination factors and bone turnover rates as functions of age and on estimates of the diet ^{90}Sr/calcium ratio in New York City from 1956 to 1963 (diet levels before 1956 were assumed to be negligible), the ^{90}Sr/calcium ratios of the skeletons of individuals from 1 year to 30 years of age in 1962 and in 1963 were calculated. The factors used that gave the best fits to the data and the estimates based on observed diet levels are listed in Tables 1 and 2, respectively. A comparison of the calculated and the observed levels shown in Fig. 1 indicates the reasonable validity of the factors chosen. There was very good agreement between calculated and observed levels in adult bone. As more data become available, adjustments in the factors may result in better agreement between predictions and observations. With the use of the

Table 1 — METABOLIC PARAMETERS USED TO PREDICT ^{90}Sr CONCENTRATIONS IN HUMAN BONE

Age	Bone/diet discrimination factor (K)	Annual bone turnover rate (f)	Net calcium accretion rate, g/year
0	0.10*		28
1	0.35	0.75	72
2	0.25	0.25	47
3	0.19	0.10	32
4	0.18	0.05	22
5	0.17	0.04	18
6	0.16	0.04	20
7	0.15	0.04	25
8	0.13	0.04	33
9	0.13	0.04	44
10	0.13	0.07	55
11	0.14	0.08	67
12	0.15	0.08	76
13	0.16	0.09	85
14	0.17	0.09	91
15	0.18	0.08	91
16	0.19	0.08	88
17	0.20	0.07	79
18	0.21	0.06	62
19	0.23	0.05	38
20	0.25	0.035	5
21	0.25†	0.035†	0†

*Fetal bone/mother's diet.
†These values are assumed to persist.

Table 2 — ESTIMATED ^{90}Sr/CALCIUM RATIOS IN DIETS OF NEW YORK CITY RESIDENTS*

Year	Picocuries per gram of calcium	Year	Picocuries per gram of calcium
1956	6	1960	10
1957	6	1961	10
1958	10	1962	14
1959	13	1963	32

*Diet levels prior to 1956 are assumed to have been negligible.

past ^{90}Sr/calcium ratios in bone due to exposure to varying ^{90}Sr levels in the diet since 1956, as calculated with Eq. 1 and the factors listed in Table 1, the doses received so far by New York City residents of different ages were calculated (if a factor of 2.7 mrad per year to bone per picocurie of ^{90}Sr per gram of calcium in bone is assumed.[6]) These dose estimates are shown in Fig. 2. The doses accumulated so far are very low compared to the dose delivered to bone from natural radioactivity, i.e., approximately 130 mr/year (page 21 of Ref. 6). The doses from ^{90}Sr that will ultimately be delivered to New York City

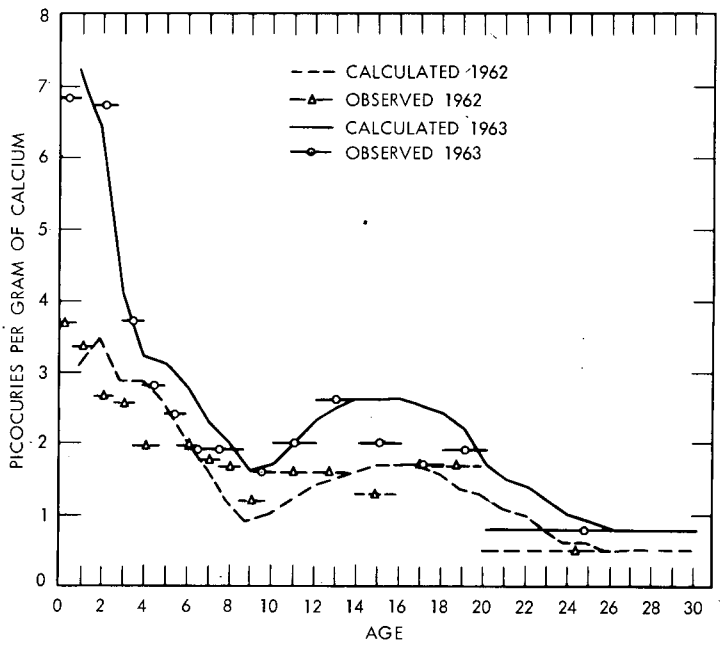

Fig. 1—Strontium-90 in bone in New York City residents.

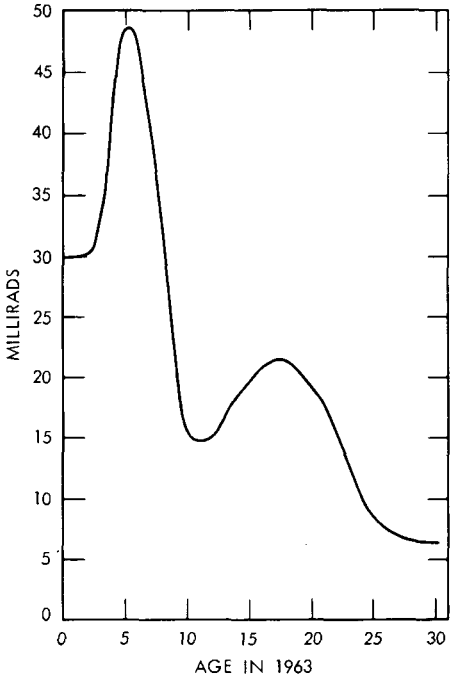

Fig. 2—Bone dose received by New York City residents by the end of 1963.

residents if there is no further testing probably will not be too different from the average value of 174 mrad estimated by the United Nations Scientific Committee on the Effects of Atomic Radiation (UNSCEAR) for the worldwide average per capita dose commitment.[7]

Much more data will have to be obtained before the problem of relating diet and bone ^{90}Sr levels is completely solved. Efforts are being made to obtain measurements of stable strontium levels in bone and diet as well as ^{90}Sr so that comparisons of changes in true specific activity in bone can be related to changes in the diet. Such data will lead to estimates of the turnover rate which are independent of the strontium/calcium discrimination considerations.

A more precise knowledge of strontium metabolism in man will be necessary before the risks incurred as a result of exposure to ^{90}Sr in the diet can be quantitatively evaluated. Such an evaluation must be made, for example, when a decision has to be reached as to whether or not remedial action to reduce risk under given circumstances is warranted. It is also necessary if more precise estimates of dose commitments as defined by UNSCEAR are to be made.

REFERENCES

1. H. H. Mitchell, F. R. Steggerda, and H. W. Bean, *J. Biol. Chem., 158:* 625 (1945).

2. J. Rivera and J. H. Harley, HASL Contributions to the Study of Fallout in Food Chains, USAEC Report HASL-147, Health and Safety Laboratory, July 1, 1964.
3. J. Rivera, Strontium-90 in Human Vertebrae, in Fallout Program Quarterly Summary Report, USAEC Report HASL-146, pp. 236-238, Health and Safety Laboratory, July 1, 1964.
4. F. J. Bryant and J. F. Loutit, Human Bone Metabolism Deduced from Strontium Assays, British Report AERE-R-3718, April 1961.
5. D. Beninson, E. Ramos, and R. Touzet, Strontium-90 Levels in the Diets and Bones of Children—Progress Report—1964, in Fallout Program Quarterly Summary Report, USAEC Report HASL-149, pp. 119-129, Health and Safety Laboratory, Oct. 1, 1964.
6. United Nations, *Report of the Scientific Committee on the Effects of Atomic Radiation*, Supplement No. 16 (A/5216), New York, 1962.
7. United Nations, *Report of the Scientific Committee on the Effects of Atomic Radiation*, Supplement No. 14 (A/5814), New York, 1962.

CESIUM-137 AND STRONTIUM-90 RETENTION FOLLOWING AN ACUTE INGESTION OF RONGELAP FOOD

EDWARD P. HARDY, Jr.,* JOSEPH RIVERA,* and ROBERT A. CONARD†
*Health and Safety Laboratory, U. S. Atomic Energy Commission, New York, New York, and †Brookhaven National Laboratory, Upton, New York.

ABSTRACT

Marine and plant foods used by natives living on Rongelap in the Marshall Islands contain higher levels of long-lived fission-product radionuclides than do diets of people living in the United States due to residual contamination from fallout in 1954. During the 1963 medical survey of the Rongelap population, three food items indigenous to the Rongelap diet were brought back to the United States and consumed over a seven-day period by a member of the medical team. The ingestion of these foods introduced levels of ^{90}Sr and ^{137}Cs which were 20 and 60 times higher, respectively, than in the normal diet and was therefore considered in terms of an acute intake of two fission-product radionuclides that are important from a radiological standpoint. Urinary and fecal collections were analyzed separately, and whole-body ^{137}Cs measurements were made with a whole-body counter. The urine was the principal excretory route for the ^{137}Cs, whereas the feces was the main removal means for the ^{90}Sr. The retention of ^{90}Sr could be represented by a series of exponentials, whereas the retention of cesium as determined by whole-body counting indicated that a single long-term component with a biological half-life of 74 days describes the removal process. Reasonably good agreement was obtained between retention as determined by whole-body counting and by excretion measurements. It is estimated that about 25% of the ^{90}Sr from the Rongelap food was retained by the body at the end of 190 days. The

average urinary to fecal excretion ratio was 3.5 for ^{137}Cs and 0.06 for ^{90}Sr. These findings are in agreement with other studies during which ^{90}Sr and ^{137}Cs were ingested under a variety of experimental and accidental conditions.

INTRODUCTION

Natives of Rongelap in the Marshall Islands consume indigenous plant and sea foods that contain long-lived fission-product radionuclides from fallout that occurred in 1954 during Operation Castle. The body burdens of these people, particularly with regard to ^{90}Sr and ^{137}Cs, are higher than those of U. S. inhabitants. Although estimates of total-body concentrations of these two radionuclides have been made directly for ^{137}Cs with a portable whole-body counter and indirectly for ^{90}Sr from urine analyses, the amount of foods consumed varies at different times of the year, and therefore information on the assimilation and excretion of specific nuclides as related to body burden has been difficult to evaluate. It was felt that a controlled intake and excretion study with the use of the ^{90}Sr and ^{137}Cs naturally present in Rongelap food would provide valuable data. Since controlled intake and excretion studies on Rongelap natives was not feasible in the field, it was decided by one of the authors (Robert A. Conard) that useful information in this regard might be obtained from an intake and excretion study carried out on himself using Rongelap foods brought back to Brookhaven National Laboratory (BNL), where a whole-body counting facility would be available for the study, and consumed under controlled conditions. Although these foods did not represent a typical native diet, it was felt that the relatively high levels of ^{90}Sr and ^{137}Cs present in them would make it possible to study quantitatively the excretion rates of these nuclides after an acute ingestion.

BACKGROUND

As part of the annual medical examinations of Rongelap natives who have been exposed to fallout radiation following the detonation of a high-yield thermonuclear device at Bikini Atoll in March 1954, 24-hr urine specimens are collected. These samples have been analyzed for ^{90}Sr at the Health and Safety Laboratory (HASL) during the past several years. The purpose of these analyses has been to attempt to relate excretion to total-body burden of ^{90}Sr resulting from the long-term chronic exposure of the natives to this radionuclide through ingestion. A portable whole-body counter was used during the 1961 survey, as in previous surveys, to measure the ^{137}Cs body burdens of the natives directly, but this instrument has not been available for

subsequent surveys. Therefore HASL was requested to analyze the urine specimens collected in 1963 and 1964 for ^{137}Cs as well as for ^{90}Sr.

In 1962, the year of the last reported survey,[1] the mean urinary ^{90}Sr level for individual adult 24-hr specimens was about 12 pc/liter, from which the body burden was estimated[1,2] to be 12 nc. In comparison adults in a metabolic ward at Hines Hospital in Chicago, Ill., in 1962 were excreting an average of 0.5 pc of ^{90}Sr per liter of urine and, based on bone ^{90}Sr levels,[3] probably had body burdens of around 0.5 nc. In 1961 the average ^{137}Cs body burden of the Rongelapese was 14.7 nc per kilogram of body weight compared to 0.048 nc per kilogram of body weight measured in U. S. medical-team personnel.[2,4] The ^{90}Sr and ^{137}Cs body burdens of Rongelapese in 1961 and 1962 were therefore about 24 and 300 times higher, respectively, than those of individuals living in the United States. The average ^{137}Cs body burden of Rongelap natives in 1961 was as high as or higher than the burdens of Lapps and Eskimos, who have unusually high body burdens. Assuming that 50 kg is the average weight of a Rongelap native, one can calculate, based on the reported data, an average body burden in 1961 of 735 nc of ^{137}Cs. This value may be compared to the measurements[5] made on Finnish Lapps in May 1962 which showed an average body burden of 508 nc of ^{137}Cs. Whole-body counts[6] of Alaskans at Anaktuvuk Pass showed an average of 421 nc of ^{137}Cs during the summer of 1962. It is now clear that the high Rongelapese body burdens are the result of consuming the various types of contaminated food which come from the sea or are produced on Rongelap.[2] This is reasonable since the 1961 whole-body-count data showed that the mean ^{137}Cs levels of Rongelapese who were exposed to the heavy fallout in 1954 were not significantly different from the body burdens of those who were not exposed.[4]

During a single 24-hr period in September 1959, nine Rongelap total-diet samples were collected by the University of Washington Laboratory of Radiation Biology and subsequently analyzed for ^{137}Cs and ^{90}Sr as well as for other nuclides.[7] The ^{137}Cs and the ^{90}Sr daily intakes averaged 2.4 and 0.084 nc, respectively. Although individual foods were not analyzed in this study, it was reported that pandanus was one of the highest contributors of these radionuclides to total diet.

MATERIALS AND METHODS

During the 1963 Rongelap medical survey, several kilograms each of pandanus pulp, coconut meat, and coconut milk were collected, frozen, and brought back to the United States. Over the seven-day period from July 2 to 8, 1963, one of the authors consumed 4.85, 1.75, and 3.20 kg of the pandanus, coconut meat, and coconut milk, respectively, in addition to a normal diet. Total fecal and urinary samples were collected for two consecutive three-day periods prior to the

consumption of the Rongelap food, for three- and four-day periods while the food was being consumed, and for two consecutive three-day periods after the last day on which the Rongelap food was consumed. Thereafter, for the next 184 days, 24-hr excreta samples were collected on Friday of each week. Whole-body counts were done at regular intervals.

Food aliquots and excreta specimens were sent to HASL for ^{90}Sr and ^{137}Cs analyses. The food was dry-ashed in a muffle furnace at approximately 450°C and solubilized by fusing with sodium carbonate and dissolving the pulverized melt in hot water and finally mineral acid. Cesium-137 was separated by the hot-water leach and then extracted from solution with ammonium phosphomolybdate. The cesium was purified by sorption on the selective elution from a cation-exchange resin and then precipitated as the tetraphenylborate for counting. A complete description of this procedure is given in the HASL procedural manual.[8] The mineral-acid portion of the dissolved melt was evaporated to dryness in dilute acid. The dehydrated silica was filtered, and a carbonate-collection precipitation was carried out on the solution. After filtration the carbonate precipitate was dissolved in nitric acid, and the solution was evaporated to dryness. Successive fuming nitric acid separations were used to separate strontium from calcium and other interfering ions. Radium and lead were removed by scavenging with barium precipitated as the chromate. Traces of other fission products were scavenged with yttrium hydroxide. After equilibration of the ^{90}Sr with its daughter, ^{90}Y was precipitated as the hydroxide and converted to the oxalate for counting. This procedure is also described in the HASL manual.[8] All counting was done with low-level beta scintillation counters designed at HASL.[9] The urinary and the fecal samples were wet-ashed with nitric acid, and the residues were fused to effect complete dissolution. From this point, identical procedures to those previously described were used to separate ^{90}Sr and ^{137}Cs.

Cesium-137 body burdens were measured with the BNL whole-body counter. Measurements were taken at convenient intervals during and after the consumption of the Rongelap food. These ^{137}Cs values were corrected for contributions of ^{137}Cs present in the normal diet. This correction was made with the assumption that the subject's normal diet during the experimental period was similar to that of non-milk-drinking BNL personnel during the same period. The normal body burden was assumed to have increased linearly[10] from 6.35 nc in July to 10.8 nc at the end of December 1963.

RESULTS

The amount of ^{90}Sr and ^{137}Cs ingested via the Rongelap food over the seven-day period is shown in Table 1. Pandanus contributed the

Table 1—INTAKE DATA FOR ^{90}Sr AND ^{137}Cs IN RONGELAP FOOD, JULY 2 TO 8, 1963

Food item	Intake for seven-day period		
	^{90}Sr, pc	^{137}Cs, pc	Calcium, g
Pandanus	4,379	57,327	0.992
Coconut milk	56	5,656	0.329
Coconut meat	48	2,824	0.460
Total intake	4,483	65,807	1.781
Average intake per day	640	9,401	0.254
Picocuries of ^{90}Sr per gram of calcium	2,517		

major portion of the activity of both radionuclides. The average ^{90}Sr and ^{137}Cs intake per day from these Rongelap foods was about 20 and 60 times higher, respectively, than from a normal New York City area diet during this time.[11] Initially, the activity from the Rongelap food essentially masked the contribution from the normal diet, but later in the study the effect of the normal diet on the excretion rates became increasingly important. In retrospect, it was unfortunate that the normal diet of the subject was not measured because the ^{90}Sr and ^{137}Cs levels in foods were increasing during this period.

The ^{90}Sr and the ^{137}Cs levels found in the urinary and the fecal collections are given in Table 2 and are plotted as a function of time in Figs. 1 and 2. Calcium measurements were made on the food and excreta samples, but, since the calcium intake from the normal diet was not known, the urinary and fecal calcium excretion data are difficult to interpret quantitatively. The average urinary calcium was 170 ± 40 mg/day, and the average fecal calcium was 360 ± 150 mg/day. These values do not indicate a metabolic abnormality, although the low fecal calcium reflects a very high absorption.

In Fig. 1 the ^{137}Cs excretion via the urine and the feces is plotted. The smoothed curves through the data points were drawn by eye. As has been observed in other studies,[12–17] the main means of ^{137}Cs excretion is urine. Fecal excretion fell off very rapidly, indicating that only a relatively small amount of the ^{137}Cs ingested was not absorbed. Neither the urinary nor the fecal excretion rate fell to preexperiment levels at the end of 190 days. This was probably due to the increase in the normal diet ^{137}Cs which took place during this period.

The excretion pattern of ^{90}Sr as shown in Fig. 2 contrasts markedly with that of ^{137}Cs. The fact that the majority of the ingested ^{90}Sr was not absorbed by the body is evidenced by the high fecal excretion levels that were observed almost immediately following the consumption of

Table 2 — ^{90}Sr, ^{137}Cs, AND CALCIUM IN EXCRETA

Sampling period, 1963	Series	Urine, ml	Feces, g	^{90}Sr, pc		Ca, g		^{137}Cs, pc		^{90}Sr, pc/day		Ca, g/day		^{137}Cs, pc/day		Pc of ^{90}Sr per g of Ca	
				Liter of urine	Kg of feces	Liter of urine	Kg of feces	Liter of urine	Kg of feces	Urine	Feces	Urine	Feces	Urine	Feces	Urine	Feces
June 26–28	Pre	2520	645	3.1	48	0.25	0.84	58	50	2.6	10.2	0.21	0.18	49	11	12	57
June 29–July 1	Pre	3430	573	2.6	110	0.19	1.88	43	73	3.0	21.0	0.21	0.35	49	14	14	58
July 2–4	Rongelap food	4240	1081	10.8	991	0.11	1.53	431	707	15.3	357	0.15	0.55	609	255	98	648
July 5–8	Rongelap food	4420	809	8.6	1406	0.06	1.97	617	1835	9.5	284	0.06	0.39	682	371	143	714
July 9–11	Post	3610	482	10.8	264	0.13	1.28	439	1102	13.0	42.4	0.15	0.20	528	177	83	206
July 12–14	Post	3900	544	*	153	*	2.49	*	709	*	27.8	*	0.45	*	128	*	61
July 19	Post	1150	327	4.7	*	0.14	0.57	508	306	5.4	*	0.16	0.18	584	100	34	*
July 26	Post	609	211	5.9	166	0.17	1.48	710	514	4.1	35.0	0.12	0.31	490	108	35	112
Aug. 8	Post	905	186	4.7	138	0.17	1.31	513	581	4.2	25.7	0.15	0.24	464	108	28	105
Aug. 9	Post	1900	156	1.7	121	0.09	2.12	218	594	3.3	18.9	0.17	0.33	414	93	19	57
Aug. 16	Post	1350	297	3.0	104	0.15	2.22	341	*	4.0	31.9	0.20	0.66	460	*	20	47
Aug. 23	Post	1280	270	2.4	131	0.11	2.66	273	350	3.1	35.4	0.14	0.72	349	95	22	49
Aug. 30	Post	770	221	3.6	75	0.16	1.15	297	357	2.8	16.5	0.12	0.25	229	79	23	65
Sept. 6	Post	660	441	3.9	46	0.19	0.79	*	135	2.6	20.2	0.12	0.35	*	60	20	58
Sept. 13	Post	†	176	†	97	†	2.22	†	557	†	17.0	†	0.39	†	98	†	44
Sept. 20	Post	678	†	3.7	†	0.29	†	295	†	2.5	†	0.20	†	200	†	13	†
Sept. 21	Post	1040	†	2.9	†	0.19	†	282	†	3.0	†	0.20	†	293	†	15	†
Oct. 4	Post	920	160	3.0	105	0.26	2.30	236	386	2.7	16.7	0.24	0.37	217	62	11	46
Oct. 21	Post	1180	230	2.6	109	0.19	2.30	219	274	3.0	25.1	0.22	0.53	258	63	13	47
Nov. 5	Post	680	320	4.7	‡	0.24	1.22	217	299	3.2	‡	0.16	0.39	148	96	20	*
Dec. 6	Post	1100	60	2.5	172	0.21	3.33	128	417	2.7	10.3	0.23	0.20	141	25	12	52
Jan. 7‡	Post	780	94	3.2	149	0.18	2.76	196	356	2.5	14.0	0.14	0.26	152	34	18	54

*Sample lost.
†No sample received.
‡This sampling date was in 1964.

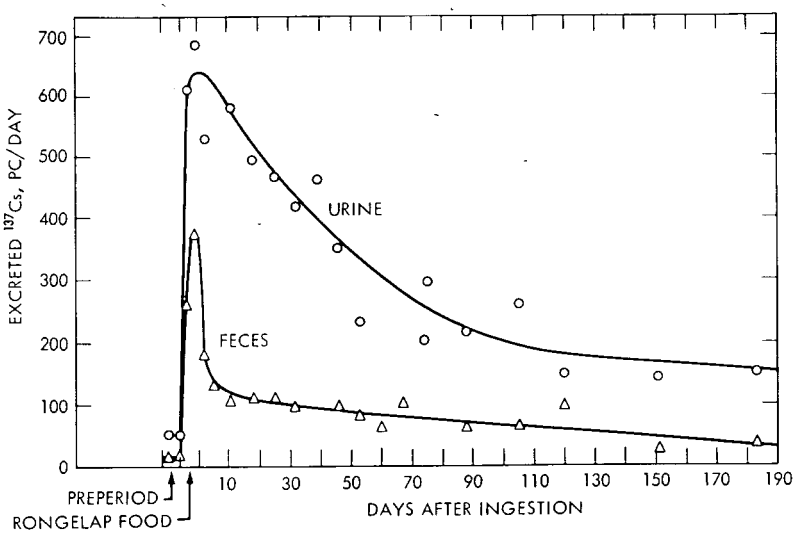

Fig. 1—Excretion of ^{137}Cs following ingestion of Rongelap food.

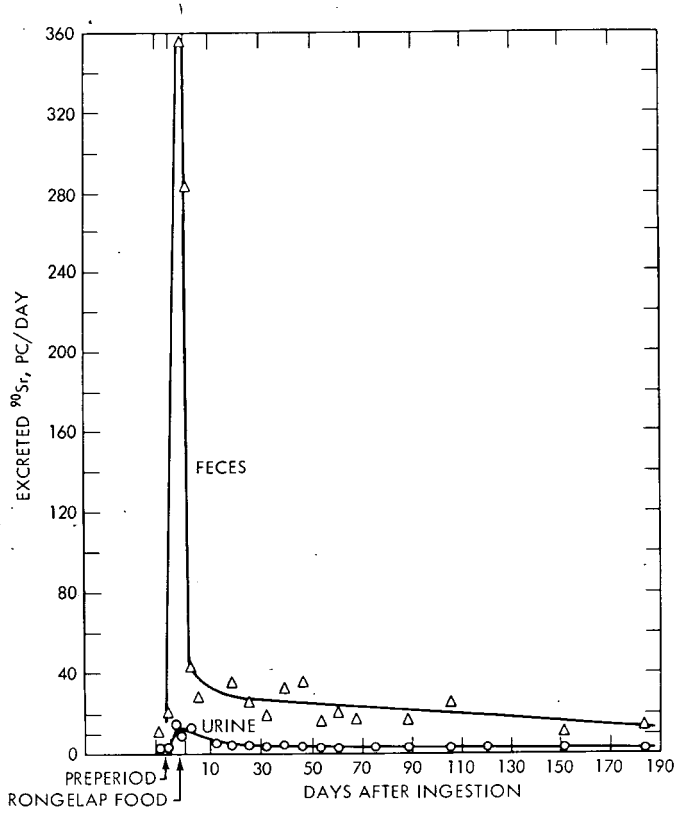

Fig. 2—Excretion of ^{90}Sr following ingestion of Rongelap food.

the high-activity food. Only a small increase in urinary ^{90}Sr excretion was observed, and both fecal and urinary elimination rates fell off sharply within 10 days after the acute-ingestion period. By 180 days both urinary and fecal excretion of ^{90}Sr had dropped to pre–high-intake levels.

Through integration of the smoothed excretion-rate curves, the amounts of ^{137}Cs and ^{90}Sr excreted per 10-day interval were determined. Excretions during the 7-day acute-ingestion period and the first 10 days after the high-activity-food consumption terminated were summed over the entire 17-day period. With the assumption that the increase in the ^{137}Cs excretion rate of the subject was proportional to the increase in the normal body burdens of laboratory personnel, a background correction was determined and applied to each 10-day excretion value. Since the ^{90}Sr excretion rate returned to preexperiment levels toward the end of the study, it was assumed that any increase in the excretion rate due to an increase in the normal ^{90}Sr diet level was not measurable. Therefore only the preexperiment ^{90}Sr level was subtracted.

The background-corrected cumulative excretions expressed as percent of intake are plotted against time in Figs. 3 and 4. Fifty percent of the ^{137}Cs ingested via the Rongelap food had been excreted in urine after 85 days, whereas only 14% had been excreted in feces during the same time. In contrast, almost 50% of the ^{90}Sr dose had been excreted in feces at 10 days, whereas only 2.5% had been eliminated in urine.

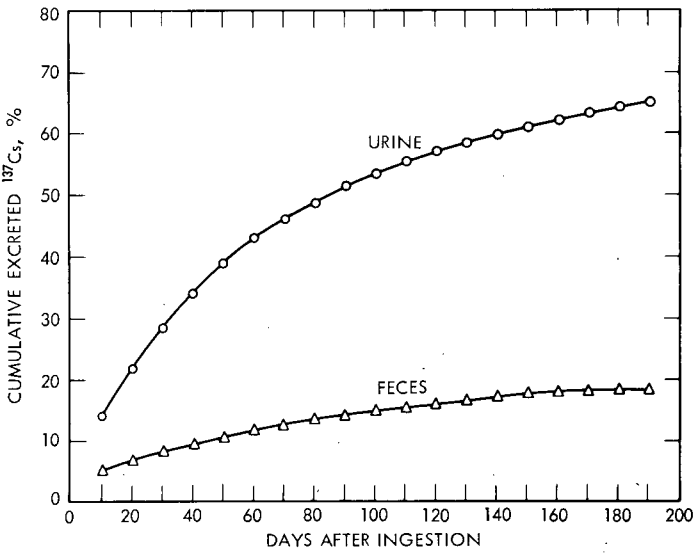

Fig. 3—Cumulative urinary and fecal excretions of ^{137}Cs following ingestion of Rongelap food.

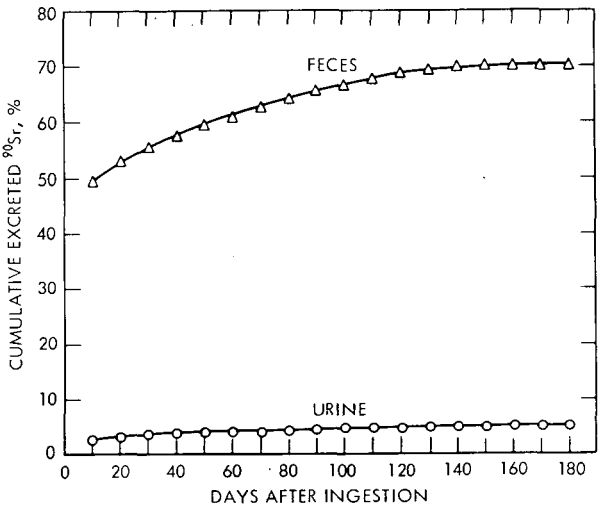

Fig. 4—Cumulative urinary and fecal excretions of ^{90}Sr following ingestion of Rongelap food.

Since the integration limits were relatively large initially compared to the rate of change of excretion level, the cumulative curves were not extrapolated beyond the point at 10 days after termination of the high-activity-food consumption. The urinary to fecal ^{137}Cs excretion ratio averaged 3.5, ranging between 2.8 and 3.8, and the ^{90}Sr excretion ratio averaged 0.06, ranging between 0.05 and 0.07.

The cumulative excretion data were substracted from the total intake to obtain the amount of each radionuclide retained. These results along with the BNL whole-body ^{137}Cs measurements are given in Table 3. When the two sets of ^{137}Cs data are compared, they appear to be in reasonably good agreement with each other. The fact that the whole-body measurements are the more accurate, however, is seen from the semilog plot in Fig. 5. The expected single exponential fit demonstrates that the ^{137}Cs from Rongelap food behaves in a similar metabolic manner to that observed under other intake conditions.[12–17] The deviations from a single exponential function of the retention data as derived from excretion measurements may be attributed to inaccuracies in the estimation of the contributions from the normal dietary intake and the accumulation of errors inherent in the procedure. The biological half-life as measured by the whole-body counter is 74 days, whereas the apparent half-life as measured on the initial straight-line portion of the excretion-data curve is 64 days. When it is considered that the excretion data underestimate the retention slightly in the early stages of measurement, the agreement is not unreasonable. It should be pointed out that the short-lived (one to two days) component that has

Table 3— THE RETENTION OF ^{137}Cs IN RONGELAP FOOD (MEASURED BY WHOLE-BODY COUNTER AND FROM EXCRETION) AND THE RETENTION OF ^{90}Sr (MEASURED FROM EXCRETION)

Days after ingestion of Rongelap food	^{137}Cs retention, nc		^{90}Sr retention, nc
	Whole-body counter	Excretion	
1	57.90		
2	57.10		
3	55.71		
4	55.64		
7	53.21		
10		53.34	2.17
11	51.00		
18	46.83		
20		47.22	1.98
25	45.38		
30		42.10	1.86
32	42.56		
39	38.88		
40		37.71	1.76
46	36.80		
50		33.73	1.66
53	36.16		
60	32.88	30.42	1.60
70		27.53	1.52
74	27.73		
80		24.97	1.44
88	25.68		
90		22.96	1.37
100		21.02	1.32
105	22.11		
110		19.38	1.28
120	19.19	17.91	1.21
120		16.56	1.20
140		15.26	1.17
150	14.34	14.22	1.16
160		13.22	1.14
170		12.33	1.14
180		11.50	1.14
184	9.37		
190		10.81	

been observed by other investigators[14,16,17] was not measured in this study since the acute-ingestion period was longer than the expected half-life of the short-term component.

The ^{90}Sr retention curve as determined from excretion data (Fig. 6) does not describe a single exponential function as is the case with ^{137}Cs. The whole-body retention of ^{90}Sr is more closely represented by a sum of exponentials[18,19] or a power function.[19,20] In this

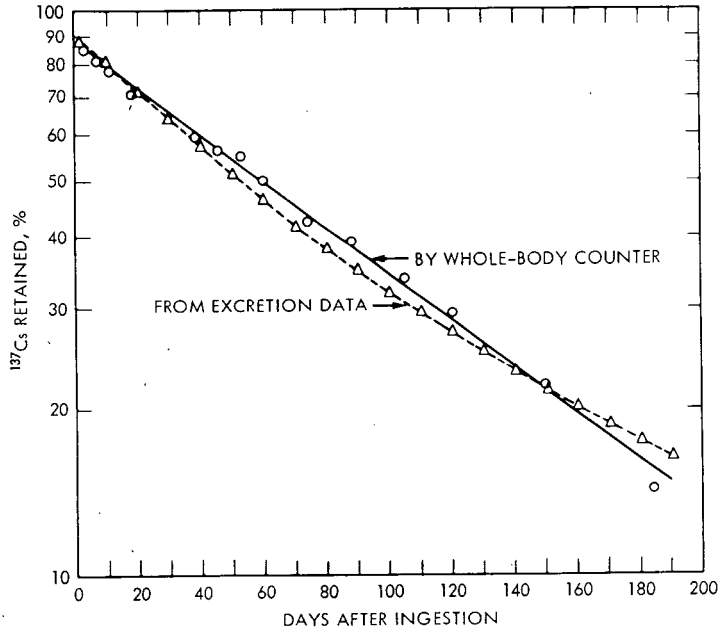

Fig. 5 — Percent retention of ^{137}Cs from Rongelap food.

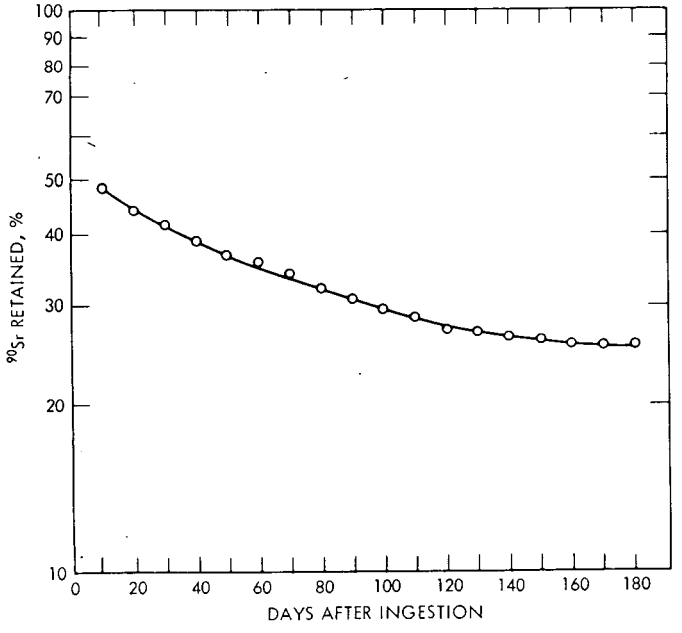

Fig. 6 — Percent retention of ^{90}Sr from Rongelap food as measured from excretion.

study the retention curve is best described as a series of exponentials that level off after 140 days and approach a value of 25%. This is a somewhat higher retention value than that reported in other studies.[21]

DISCUSSION

A number of investigators have shown that the whole-body retention for a single administration of ^{137}Cs can be expressed by a two-component exponential function of time:[14,16,17]

$$R_t = (1 - a)\, e^{-(0.693/T_1)t} + a e^{-(0.693/T_2)t}$$

where R_t is the fractional retention at t days, a is a constant, and T_1 and T_2 are biological half-lives in days. The short-term component has a half-life, T_1, of about one day,[14,16,17] and the principle component has a half-life, T_2, that varies from study to study, ranging from 50 to 150 days (Refs. 12 to 16 and 22 to 25). The comparison of biological half-lives under conditions of both acute and chronic exposures is justified based on the work of Rundo.[26] The short-term component was not calculated in this study since the acute ingestion took place over a seven-day period and the initial excretion collection periods were over three-day intervals. The long-term component as determined by both whole-body counting and excretion data (74 and 64 days, respectively) was within the range of biological half-life values found by other investigators. Rundo[14] has pointed out that a large part of the variations in body burden can be attributed to the variability in biological half-life rather than to differences in dietary habits. The low excretion of ^{137}Cs in feces relative to urine showed that the ^{137}Cs in the Rongelap food was rapidly and almost completely absorbed. Since the finding that a single long-term component describes the excretion from the whole body is in agreement with other studies, it can be said that the ^{137}Cs in Rongelap food is not in a unique chemical form with respect to the various accidental and experimental intake conditions under which the behavior of ^{137}Cs in man has been studied.

The urinary to fecal ratio was found to be reasonably constant and was within the range of 3 to 10 found by others.[12–16] Rundo[16] has used the urinary to fecal ratio to estimate the uptake of ^{137}Cs ingested in food. The fraction of ^{137}Cs ingested in food which is transferred from the gastrointestinal tract to blood was at least 0.9. The data obtained in this study do not indicate that the ^{137}Cs in Rongelap food behaves in a significantly different manner.

The excretion pattern of the ^{90}Sr from the Rongelap food was markedly different from that of ^{137}Cs. Most of the ^{90}Sr was not absorbed, as evidenced by the much higher fecal than urinary excretion.

The net absorption (intake–fecal excretion expressed as percent of intake) was 30%, a factor of 2 higher than the average for 10 normal adults on a high-calcium diet reported by Spencer et al.[21] The low fecal calcium excretion found in the present study was indicative of a high ^{90}Sr absorption.

Although the retention curve for ^{90}Sr shows that the biological half-life varies with time after exposure, the data do not fit a power function as found by others.[18–20] If it had been possible to measure excreta over a longer period of time, a power function may have been described.

SUMMARY

The ^{137}Cs and the ^{90}Sr body burdens of people living on Rongelap Island are high compared to most other populations of the world. The reason for this is that the natives consume foods that are contaminated with long-lived fission-product radioactivity resulting from a fallout incursion in 1954. Their ^{137}Cs body burdens are comparable to those of people living in other limited areas such as Lapland and northern Alaska where unique ecological conditions are conducive to high ^{137}Cs concentrations in indigenous foods. The metabolism of ^{137}Cs and ^{90}Sr has been studied in the Lapland and Alaskan groups but not in the Rongelap natives.

Since facilities for a metabolic-balance study were not available on Rongelap Island, several native food items were brought back to BNL and consumed by one of the authors under controlled conditions. Urinary and fecal specimens were collected and whole-body counting measurements were made over a period of 180 days. The intake of ^{90}Sr over a seven-day period was 20 times higher than normal and that of ^{137}Cs was 60 times higher than normal.

Fifty percent of the ingested ^{137}Cs in the Rongelap food had been excreted in urine after 85 days, whereas 14% had been eliminated in feces during the same time. In contrast, most of the ^{90}Sr was unabsorbed. Fifty percent had been excreted in feces at 10 days, whereas only 2½% had been excreted in urine. The retention of ^{137}Cs as determined by both whole-body counting and excretion measurements showed a biological half-life of 74 days. Strontium-90 retention as a function of time was best described as a series of exponentials and approached a value of 25% after 140 days.

These findings fall within the range of results of many other studies conducted under a wide variety of natural, accidental, and experimental conditions.

ACKNOWLEDGMENTS

The authors are grateful to John Ankain of Rongelap Island for collecting and preparing the native foods. We wish to thank Stanton

Cohn, Ernest Gusmano, and Michael Stravino of BNL for making the whole-body counting measurements and Joseph Catania, Melvin Feiner, John Kelly, and Richard Neff of HASL for performing the radiochemical analyses on the excreta samples.

REFERENCES

1. R. A. Conard, L. M. Meyer, W. W. Sutow, W. C. Moloney, A. Lowrey, A. Hicking, and E. Riklon, Medical Survey of Rongelap People Eight Years After Exposure to Fallout, USAEC Report BNL-780 (T-296), Brookhaven National Laboratory, January 1963.
2. S. H. Cohn, Metabolism of Fission Products in Man: Marshallese Experience, in *Diagnosis and Treatment of Radioactive Poisoning,* Meeting Proceedings, Vienna, 1962, pp. 235-251, International Atomic Energy Agency, Vienna, 1963 (STI/PUB/65).
3. J. Rivera, Strontium-90 in Human Vertebrae, in Fallout Program Quarterly Summary Report, USAEC Report HASL-146, p. 240, Health and Safety Laboratory, July 1, 1964.
4. R. A. Conard, H. E. MacDonald, L. M. Meyer, S. Cohn, W. W. Sutow, D. Karnefsky, A. A. Jaffe, and E. Riklon, Medical Survey of Rongelap People Seven Years After Exposure to Fallout, USAEC Report BNL-727 (T-260), Brookhaven National Laboratory, May 1962.
5. J. K. Miettinen, Measurements of Caesium-137 in Finnish Lapps in 1962–1963 by a Mobile Whole-body Counter, in *Assessment of Radioactivity in Man,* Symposium Proceedings, Heidelberg, 1964, Vol. II, pp. 193-207, International Atomic Energy Agency, Vienna, 1964 (STI/PUB/84).
6. H. E. Palmer, W. C. Hanson, B. I. Griffin, and W. C. Roesch, Cesium-137 in Alaskan Eskimos, *Science, 142*(3588): 64-65 (1963).
7. D. Chakravarti and E. E. Held, Chemical and Radiochemical Composition of the Rongelapese Diet, *J. Food Sci., 28*(2): 221-228 (1963).
8. Health and Safety Laboratory, Manual of Standard Procedures, USAEC Report NYO-4700(Rev.), Sec. E-55-02 for ^{137}Cs and Sec. E-38-01 for ^{90}Sr, August 1962.
9. J. H. Harley, N. A. Hallden, and I. M. Fisenne, Beta Scintillation Counting with Thin Plastic Phosphors, *Nucleonics, 20*(1): 59-61 (1962).
10. S. H. Cohn, E. A. Gusmano, and R. A. Love, Recent Trends in the Level of Fallout Cesium-137 in Man, *Nature, 205*(4971): 537 (1965).
11. J. Rivera and J. H. Harley, HASL Contributions to the Study of Fallout in Food Chains, USAEC Report HASL-147, Health and Safety Laboratory, July 1, 1964. (See page 41 for ^{137}Cs reference and page 54 for ^{90}Sr reference.)
12. S. E. Hammond, F. O. Bold, and N. F. MacDonald, Cesium-137 Excretion and Retention Following Single Exposure, *Health Phys., 9*(5): 523-528 (1963).
13. R. Hesp, The Retention and Excretion of Cesium-137 by Two Male Subjects, in *Assessment of Radioactivity in Man,* Symposium Proceedings, Heidelberg, 1964, Vol. II, pp. 61-74, International Atomic Energy Agency, Vienna, 1964 (STI/PUB/84).
14. C. R. Richmond, J. E. Furchner, and W. Langham, Long Term Retention of Radiocesium in Man, *Health Phys., 8*(13): 201-205 (1962).
15. B. Rosoff, S. H. Cohn, and H. Spencer, 1. Cesium-137 Metabolism in Man, *Radiation Res., 19*(4): 643-654 (1963).
16. J. Rundo, VI. A Survey of the Metabolism of Caesium in Man, *Brit. J. Radiol., 37*(434): 108-114 (1964).
17. J. Rundo and B. T. Taylor, The Assessment of Radioactive Caesium in Man, in *Assessment of Radioactivity in Man,* Symposium Proceedings, Heidelberg,

1964, Vol. II, pp. 3-20, International Atomic Energy Agency, Vienna, 1964 (STI/PUB/84).

18. M. Fujita, Body Burden and Excretion of Strontium Following Ingestion, in *Assessment of Radioactivity in Man,* Symposium Proceedings, Heidelberg, 1964, Vol. II, pp. 385-399, International Atomic Energy Agency, Vienna, October 1964 (STI/PUB/84).
19. S. H. Cohn, H. Spencer, J. Samachson, and J. S. Robertson, The Turnover of Strontium-85 in Man as Determined by Whole Body Counting, *Radiation Res., 17*(2): 173-185 (1962).
20. G. E. Harrison, Uptake, Retention and Excretion of Strontium in Man, in *Diagnosis and Treatment of Radioactive Poisoning,* Meeting Proceedings, Vienna, 1962, pp. 119-129, International Atomic Energy Agency, Vienna, 1963.
21. H. Spencer-Laszlo, J. Samachson, E. P. Hardy, Jr., and J. Rivera, Strontium-90 Balances in Man, *Clin. Sci., 24*(3): 405-412 (1963).
22. E. Häsänen and J. K. Miettinen, The Body Burden of Cs-137 in People of Southern Finland, 1961–1963, in *Assessment of Radioactivity in Man,* Symposium Proceedings, Heidelberg, 1964, Vol. II, pp. 183-192, International Atomic Energy Agency, Vienna, 1964 (STI/PUB/84).
23. M. Izawa and H. Tsubota, Cesium-137 Concentration in Human Urine and Estimation of Cesium-137 Body Burden Due to World-Wide Fallout, *J. Radiation Res., 3*(2): 120-129 (1962).
24. K. Lidén and Y. Naversten, The Enhanced Radiocaesium Levels of People in Northern Sweden, in *Assessment of Radioactivity in Man,* Symposium Proceedings, Heidelberg, 1964, Vol. II, pp. 169-182, International Atomic Energy Agency, Vienna, 1964 (STI/PUB/84).
25. Y. Naversten and K. Lidén, Half-Life Studies of Radiocaesium in Humans, in *Assessment of Radioactivity in Man,* Symposium Proceedings, Heidelberg, 1964, Vol. II, pp. 79-87, International Atomic Energy Agency, Vienna, 1964 (STI/PUB/84).
26. J. Rundo, J. I. Mason, D. Newton, and B. T. Taylor, Biological Half-life of Caesium in Man in Acute and Chronic Exposure, *Nature, 200*(4902): 188-189 (1963).

EARLY FOOD-CHAIN KINETICS OF RADIONUCLIDES FOLLOWING CLOSE-IN FALLOUT FROM A SINGLE NUCLEAR DETONATION

WILLIAM E. MARTIN
University of California at Los Angeles, Los Angeles, California

ABSTRACT

Plant samples and rabbits were collected from representative locations in the Sedan fallout field before and at various times after the detonation. Radiochemical and statistical analyses indicated highly significant correlations between estimates of gamma dose rates and maximum concentrations of ^{89}Sr or ^{131}I in plant samples and in the stomach contents, bone ash, or thyroids of rabbits collected between 15 and 110 miles from ground zero.

The effective half-lives of ^{89}Sr and ^{131}I on fallout-contaminated plants were approximately 18 and 5.0 to 5.5 days, respectively. Maximum concentrations of ^{89}Sr in rabbit bone ash occurred about 30 days after the detonation and remained high for at least 60 days; but maximum concentrations of ^{131}I in rabbit thyroids occurred by or before five days and then declined to pre-Sedan levels in less than 60 days after the detonation.

Deterministic exponential models were formulated and found to function satisfactorily, with parameter values derived from the data, in providing a partial explanation of the quantitative kinetic relations between initial concentrations of ^{89}Sr and ^{131}I on plants and subsequent concentrations in the bone ash or thyroids of rabbits collected in the Sedan fallout field. Major sources of error in the estimation of input-parameter values and in the use of such models to make predictions are described and discussed.

Similar models were proposed for the study of radionuclide kinetics in human food chains (i.e., pasture plants, cow milk, and human

tissues or organs) following environmental contamination by a single fallout event. The results of hypothetical calculations were compared with the Radiation Protection Guides recommended by the Federal Radiation Council.

INTRODUCTION

To explain the kinetics of radionuclide transfers in a given food chain, it is first necessary to describe the routes and rates of transfer affecting specific food-chain compartments. The major route and some of the minor routes of radionuclide transfer and exchange in a terrestrial ecosystem are shown in Fig. 1.

Some of the fallout particles initially deposited on soil surfaces may be redeposited by wind or rain on plants,[1] but most of them are mechanically trapped and not susceptible to redeposition.[2] Material deposited on soil may enter food chains by stem-base absorption,[3] by downward leaching in the soil profile and subsequent root uptake,[4,5] or by accidental ingestion, especially by burrowing animals.[6] Most of the fallout deposited directly on soil can be regarded as unavailable for rapid entry into major food chains.

Some of the radioactivity contained in the fallout particles, mostly $< 44\ \mu$ in diameter,[1,7] retained on foliage may be assimilated by foliar absorption,[8,9] but a much larger fraction is subject to fairly rapid removal by wind or rain.[10,11] While it remains on plant surfaces, this material may be ingested by herbivores.

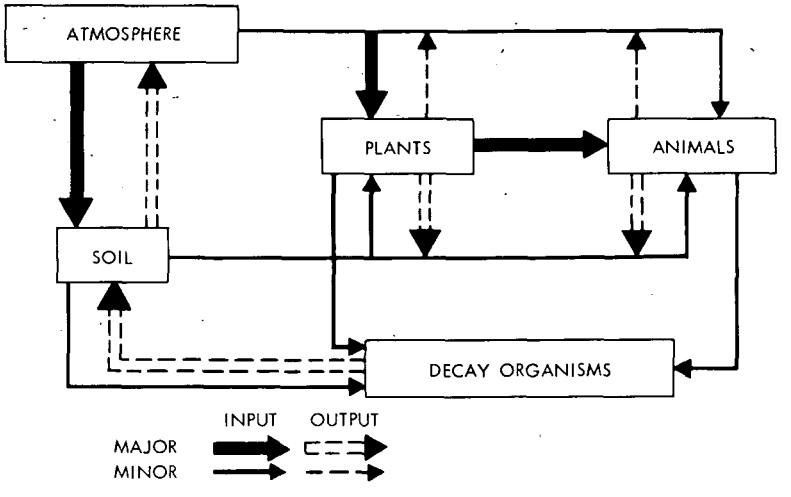

Fig. 1—Major and minor routes of radionuclide transfer and exchange in a terrestrial ecosystem contaminated by radioactive fallout.

Herbivorous mammals may be externally contaminated by direct exposure to fallout or by contact with contaminated plants or soils. Radionuclides may accumulate in animal tissues via inhalation, which, in many cases, is relatively unimportant or via ingestion of contaminated materials. Although inhalation, ingestion of contaminated soil or water, and ingestion of fallout particles while the animal is preening cannot be dismissed entirely, it is probably reasonable to assume that externally contaminated plants are the major sources of radionuclides for assimilation by herbivorous mammals (e.g., jackrabbits or dairy cattle) feeding in a fallout-contaminated environment during the first 30 to 90 days after close-in fallout.

The summer of 1962 provided an excellent opportunity to study the food-chain kinetics of ^{89}Sr and ^{131}I in relation to desert shrubs and rabbits in the Sedan fallout field. These studies included the formulation and testing of mathematical models that can be shown to provide at least a partial explanation of the kinetic relations between initial concentrations of ^{89}Sr and ^{131}I on fallout-contaminated plants and subsequent concentrations of ^{89}Sr in the bone ash or of ^{131}I in the thyroids of rabbits collected in the Sedan fallout field. Although the results of these studies[11–17] are not conclusive, partly because the causes of variation are imperfectly understood, they do provide evidence that mathematical models similar to those used by radiochemists to explain decay-chain kinetics,[18] by physiologists to explain tracer kinetics,[19] and by the International Commission on Radiological Protection (ICRP) to establish maximum permissible concentrations[20] can also be used to study food-chain kinetics under field conditions.

The objectives of this paper are (1) to summarize some of the data related to ^{89}Sr and ^{131}I on desert shrubs and in rabbit tissues following fallout from Project Sedan, (2) to present the deterministic models that provide a partial explanation of these results, and (3) to illustrate the potential value of similar models in studying the food-chain kinetics of radionuclides on pasture plants, in cow milk, and in human tissues following a single fallout event.

METHODS

Project Sedan, a peaceful nuclear-explosives test, involved the detonation of a 100 ± 15 kt thermonuclear device at a depth of 635 ft in alluvium and tuff at the north end of the Nevada Test Site on July 6, 1962. As predicted, the early fallout was relatively light and occurred primarily within a 150-mile sector, N60°W to N60°E, from ground zero in Yucca Flat.

Before and at various times after the detonation, plant samples and rabbits were collected from representative locations in the Sedan fallout field (see Fig. 2). Each sampling station was marked by a metal

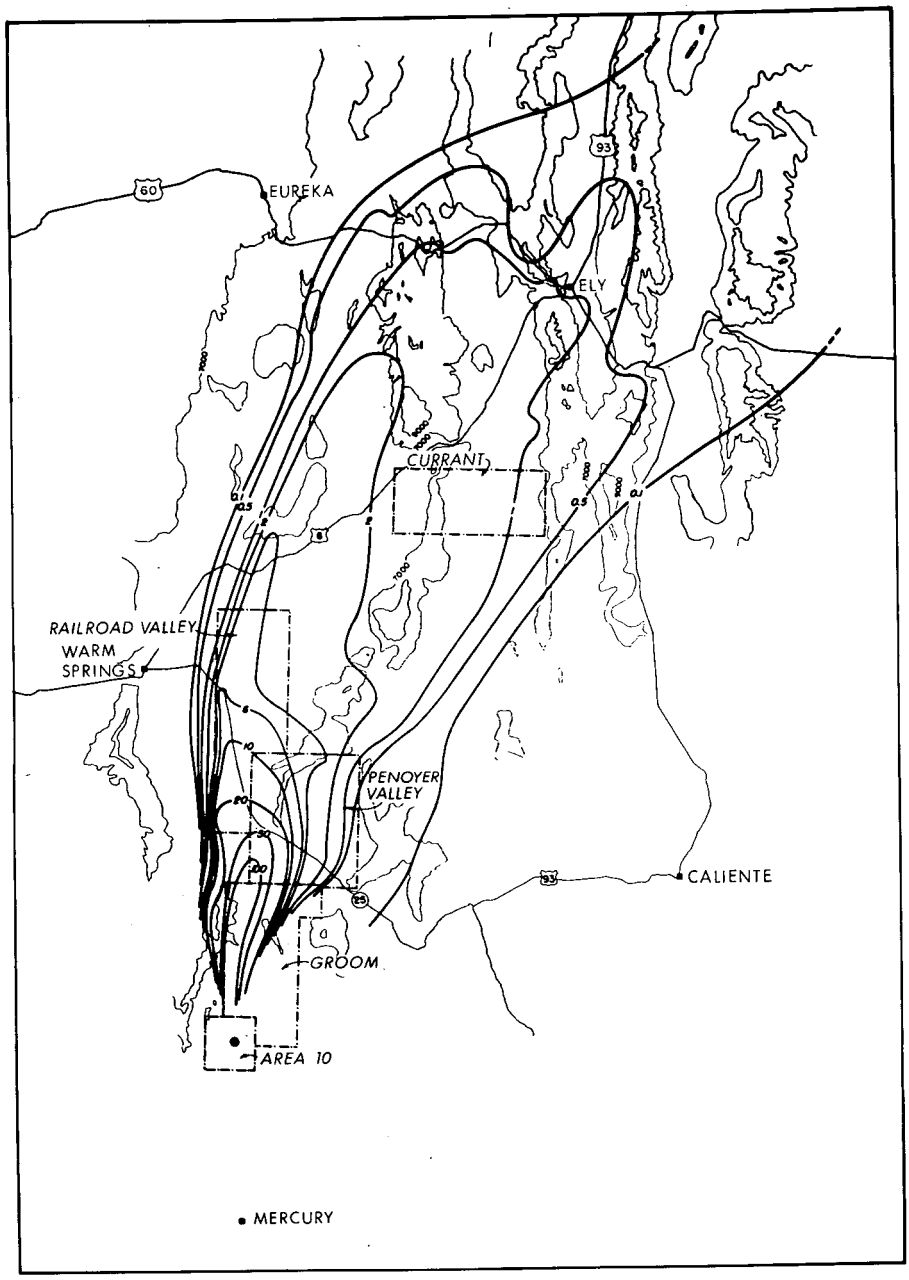

Fig. 2—Approximate locations of study areas and sampling stations in the Sedan fallout field. Dose-rate contours (mr/hr at H + 24) are based on aerial surveys.[22]

post to facilitate its relocation and positive identification. Plant samples were collected by clipping twigs and foliage from the crowns of desert shrubs growing within a radius of 150 ft from each station marker. *Artemisia tridentata* (sagebrush) was the species collected at all stations in Groom Valley and the Currant Area, and *Atriplex confertifolia* (shadscale) was collected at all but three of the stations in Penoyer and Railroad valleys. Most of the rabbits representing a given location were shot within a few hundred yards of a station marker, but rabbits taken within a 1-mile radius were accepted as representatives of the general location. Most of the rabbits collected were blacktailed jackrabbits (*Lepus californicus*), but a few cottontail rabbits (*Sylvilagus auduboni*) were taken in mountainous areas where jackrabbits were not always available.

Radiochemical analyses were made to determine the ^{89}Sr and ^{131}I contents of plant samples, the ^{89}Sr content of rabbit bone ash, and the ^{131}I content of rabbit thyroids. The stomach contents of rabbits were analyzed for ^{131}I, but the samples remaining after aliquots were removed for this purpose were too small to be used in making analyses for ^{89}Sr. Following each determination, a decay correction was made to indicate the ^{89}Sr or ^{131}I concentration at the time the sample was collected. The procedures followed in making these analyses are described elsewhere[11,16,21] in considerable detail.

For simplicity, the only samples considered in this paper are those collected at the 20 representative locations indicated in Fig. 2. Additional data are given in other publications.[13,16] Estimates of the initial gamma dose rates (R_0 = mr/hr at 3 ft aboveground at H + 24) were obtained from a tracing of Guillou's[22] original large-scale map prepared from aerial surveys made before and after the detonation.

Correlation and regression analyses were made to examine the relation between initial gamma dose rates, R_0, and initial concentrations of ^{89}Sr or ^{131}I on plants, P_0; between P_0 and maximum concentrations of ^{89}Sr in rabbit bone ash, B_{30}; and between P_0 and maximum concentrations of ^{131}I in rabbit thyroids, A_5. Similar analyses were also made to determine the relations between S_0 and R_0, A_5, and S_0, where S_0 represents the initial concentration of ^{131}I in rabbit-stomach contents.

Estimates of ^{89}Sr and ^{131}I retention by plants in relation to theoretical deposition rates, different parts of the fallout field, and different plant species were based on Eq. 1:

$$f_p = \frac{a_p}{a_s} \tag{1}$$

where f_p = retention index of N_i deposited on plants, sq ft/g [N.B. This index multiplied by G = g (dry weight) of plants per square foot would give the fraction of N_i deposited on plants]

a_p = pc N_i/g (dry)/R_0 deposited on plants

a_s = pc N_i/sq ft/R_0 deposited on uniform plane
N_i = a given radionuclide (e.g., ^{89}Sr or ^{131}I)

Estimates of a_p were based on the results of radiochemical analyses, P_t, and estimates of a_s (theoretical values) were based on Eq. 2:

$$a_s = \frac{0.693 F_k Y}{T_r D_d C R_k} \tag{2}$$

where $F_k = 1.43 \times 10^{23}$ fissions (^{235}U)/kt (Ref. 23)
Y = percent fission yield (atoms/fission) of N_i (4.79% ^{89}Sr, 3.1% ^{131}I) (Ref. 24)
T_r = radioactive half-life of N_i in days (50.5-day ^{89}Sr, 8.04-day ^{131}I)
$D_d = 3.2 \times 10^3$ dis/pc/day
$C = 2.79 \times 10^7$ sq ft/sq mile
$R_k = 4.5 \times 10^4$ mr/hr/kt/sq mile at 3 ft aboveground at H ± 24 (Ref. 25)

The relations between initial gamma dose rates, R_0, and initial concentrations of ^{89}Sr or ^{131}I on fallout-contaminated plants, P_0, were tentatively defined by linear regression formulas. For example, where $\overline{P}_0$ and $\overline{R}_0$ are the means of P_0 and R_0 and b_{xy} is the coefficient of regression of P_0 on R_0,

$$P_0 = \overline{P}_0 \pm b_{xy} (R_0 - \overline{R}_0) \tag{3}$$

The deterministic exponential models used to describe and explain the time-specific relation between ^{89}Sr or ^{131}I concentrations on plants, P_t, and of ^{89}Sr in bone ash, B_t, or of ^{131}I in thyroids, A_t, are given (if at $t = 0$, $P = P_0$, $B = 0$, and $A = 0$) by Eqs. 4 to 6:

$$P_t = P_0 e^{-\lambda_p t} \tag{4}$$

$$B_t = P_0 \frac{W_p f_b}{W_b} \left(\frac{e^{-\lambda_p t}}{\lambda_b - \lambda_p} + \frac{e^{-\lambda_b t}}{\lambda_p - \lambda_b} \right) \tag{5}$$

$$A_t = P_0 W_p f_a \left(\frac{e^{-\lambda_p t}}{\lambda_a - \lambda_p} + \frac{e^{-\lambda_a t}}{\lambda_p - \lambda_a} \right) \tag{6}$$

where t = days after fallout deposition
P_t = pc ^{89}Sr/g (dry) or pc ^{131}I/g (dry) on plants at $t > 0$
B_t = pc ^{89}Sr/g of rabbit bone ash at $t > 0$
A_t = pc ^{131}I (total) in rabbit thyroid at $t > 0$
W_p = g (dry) of contaminated plant material consumed per rabbit per day
W_b = g (dry) of bone ash per rabbit

f_b = fraction of ingested ^{89}Sr deposited in the rabbit's skeleton
f_a = fraction of ingested ^{131}I deposited in the rabbit's thyroid
$\lambda_p = 0.693/T_p$ where T_p = effective half-life of ^{89}Sr or ^{131}I on plants
$\lambda_b = 0.693/T_b$ where T_b = effective half-life of ^{89}Sr in rabbit's skeleton
$\lambda_a = 0.693/T_a$ where T_a = effective half-life of ^{131}I in rabbit's thyroid

RESULTS

Estimates of average gamma dose rates, of ^{89}Sr concentrations in plant samples and in the bone ash of rabbits, and of ^{131}I concentrations in plant samples, in the stomach contents of rabbits, and in rabbit thyroids are given in Tables 1 and 2. The approximate locations at which these samples were collected are shown in Fig. 2.

The wide range of values and the relatively large standard errors of the means given in Tables 1 and 2 indicate a high degree of apparently inherent variability.* The wide range of ^{89}Sr and ^{131}I concentrations in plant samples and in rabbit tissues or stomach contents is partly a reflection of the wide range of initial contamination levels as indicated by estimated gamma dose rates; but much of the inherent variability is undoubtedly related to the probabilistic nature of the environmental and biological processes that influence the external contamination of plants and the accumulation of radionuclides in animal tissues. The probabilistic approach to the study of food-chain kinetics and the use of stochastic models to simulate these processes are considered in this symposium by Turner.†

The results of correlation and regression analyses given in Table 3 show that the quantitative interrelations of initial dose-rate estimates and estimates of maximum ^{89}Sr or ^{131}I concentrations in plants and animal tissues are highly significant in spite of their inherent variability. As might be expected, the correlation between initial gamma dose rates, R_0, and initial concentrations of ^{89}Sr or ^{131}I on plants, P_0, are highly significant. The correlations and regressions of plant contamination on maximum concentrations of ^{89}Sr in bone ash, B_{30}, and of ^{131}I in thyroids, A_5, are also highly significant. The somewhat higher correlation between ^{131}I concentrations in stomach contents, S_0, and in thyroids, A_5, suggests some difference between the plants collected for radiochemical analyses and those actually eaten by the rabbits in the Sedan fallout field.

*Since the standard deviations (= sx $\sqrt{n}$) are large in relation to the means, the frequency distributions of these variates are sharply skewed. Preliminary investigations indicate that they may be lognormal rather than normal.

†See paper by Frederick B. Turner, this volume.[15]

Table 1—AVERAGE GAMMA DOSE RATES, R_0, AND AVERAGE CONCENTRATIONS OF ^{90}Sr IN PLANT SAMPLES AND IN THE BONE ASH OF RABBITS COLLECTED FROM DIFFERENT PARTS OF THE SEDAN FALLOUT FIELD AT VARIOUS TIMES AFTER THE DETONATION*

Study areas	Initial gamma dose rates†			Days after detonation	Plant samples, pc ^{89}Sr/g (dry)			Rabbit bone ash, pc ^{89}Sr/g (dry)		
	$\bar{x}$	$s\bar{x}$	n		$\bar{x}$	$s\bar{x}$	n	$\bar{x}$	$s\bar{x}$	n
Groom Valley	45.0	±30%	5	5	4059	±30%	5	1459	±42%	5
				15	2716	±38%	5	3648	±62%	5
				30	1544	±50%	5	3667	±41%	5
				60	788	±38%	5	3581	±74%	5
Penoyer Valley	16.8	±45%	5	5	948	±37%	5	1363	±51%	5
				15	470	±30%	5	2024	±37%	5
				30	332	±39%	5	2283	±61%	5
				60	283	±44%	5	552	±34%	5
Railroad Valley	6.8	±32%	5	5	397	±14%	5	334	±30%	5
				15	269	±13%	5	620	±68%	5
				30	164	±19%	5	783	±33%	5
				60	127	±30%	5	462	±33%	5
Currant Area	1.5	±33%	5	5	318	±20%	5	295	±54%	5
				15	183	±23%	5	323	±31%	5
				30	136	±18%	5	427	±26%	5
				60	55	±15%	5	280	±31%	5
All areas	17.5	±30%	20	5	1436	±32%	20	863	±29%	20
				15	909	±37%	20	1680	±38%	20
				30	544	±40%	20	2097	±30%	20
				60	313	±32%	20	1389	±34%	20
Pre-Sedan concentrations					30	±17%	14	56	±30%	16

*$\bar{x}$ = mean, $s\bar{x}$ = standard error expressed as a percentage of the mean, and n = number of samples. (Based on data given by Martin and Turner.[13])
†R_0 = mr/hr at 3 ft aboveground at H + 24.

When P_0 or S_0, B_t, and A_t are given, the parameter values required to solve Eqs. 4 to 6 are W_p, W_b, T_p, T_b, T_a, f_b, and f_a. Some of these parameter values can be obtained from experimental results reported in the literature, and others can be obtained from the data given in Tables 1 and 2. For our purposes those obtained from the field data may be more accurate.

Various studies[26,27] have indicated that adult jackrabbits consume approximately 100 g of dry plant material per day; therefore W_p = 100 g. Unpublished data collected during this and previous studies[1,2,28] indicate that the average adult jackrabbit in Nevada weighs about 2000 g and has a skeleton weighing 200 g (fresh). Since the ratio of fresh bone weight to bone-ash weight is approximately 4 to 1, W_b = 50 g. The ratio, W_p/W_b = 100/50, indicates a feeding rate of approximately 2.0 g of dry plant material per gram of bone ash per rabbit per day. The feeding

Table 2— AVERAGE CONCENTRATIONS OF ^{131}I IN PLANT SAMPLES AND IN THE STOMACH CONTENTS AND THE THYROIDS OF RABBITS COLLECTED FROM DIFFERENT PARTS OF THE SEDAN FALLOUT FIELD AT VARIOUS TIMES AFTER THE DETONATION*

Study areas	Days after detonation	Plant samples, pc ^{131}I/g (dry)			Rabbit stomach contents, pc ^{131}I/g (dry)			Rabbit thyroids, nc ^{131}I per thyroid		
		$\bar{x}$	$s\bar{x}$	n	$\bar{x}$	$s\bar{x}$	n	$\bar{x}$	$s\bar{x}$	n
Groom Valley	5	11966	±33%	5	5194	±29%	5	467	±34%	5
	10	6671	±39%	5	1283	±32%	4	386	±43%	4
	15	3192	±34%	5	1018	±47%	5	139	±52%	5
	20	1224	±49%	5	424	±28%	5	83	±35%	5
	25	526	±36%	5	161	±50%	5	61	±31%	5
	30	273	±30%	5	149	±32%	5	16	±31%	5
Penoyer Valley	5	1244	±33%	5	1853	±31%	5	257	±34%	5
	10	659	±30%	5	1212	±20%	4	141	±14%	4
	15	412	±36%	5	638	±17%	4	88	±34%	5
	20	227	±46%	5	311	±40%	5	40	±48%	5
	25	192	±64%	5	115	±44%	5	29	±52%	5
	30	81	±41%	5	81	±52%	4	1.5	±70%	5
Railroad Valley	5	713	±11%	5	693	±41%	2	111	±65%	4
	10	376	±10%	5	604	±34%	4	85	±36%	5
	15	211	±11%	5	348	±39%	3	61	±34%	5
	20	119	±17%	5	148	±31%	5	22	±45%	5
	25	96	±14%	5	75	±19%	5	29	±52%	5
	30	48	±25%	5	33	±24%	4	11	±27%	5
Currant Area	5	501	±15%	5	322	±37%	3	26	±27%	5
	10	200	±20%	5	57	±12%	3	7	±23%	5
	15	121	±57%	5	46	±28%	4	6	±50%	5
	20	56	±27%	5	42	±36%	5	6	±30%	5
	25	35	±26%	5	28	±50%	4	1.6	±10%	5
	30	26	±15%	5	7	±43%	5	1.1	±34%	5
All areas	5	3606	±40%	20	2506	±29%	15	221	±28%	19
	10	1977	±44%	20	838	±21%	15	143	±34%	18
	15	984	±40%	20	554	±31%	16	74	±36%	20
	20	406	±43%	20	231	±23%	20	38	±26%	20
	25	212	±32%	20	96	±27%	19	30	±27%	20
	30	113	±27%	20	69	±29%	18	12	±50%	20
Pre-Sedan concentrations		312	±57%	14	207	±51%	17	5.4	±61%	15

*$\bar{x}$ = mean, $s\bar{x}$ = standard error expressed as a percentage of the mean, and n = number of samples. (Based on data given by Turner and Martin.[16])

rate applicable to the accumulation of ^{131}I in the thyroid was taken as 100 g of dry plant material per whole thyroid per rabbit per day.

As shown in Table 1 and Fig. 3, the apparent rate of ^{89}Sr loss from fallout-contaminated plants tended to decrease with increasing time after the detonation, but the average effective half-life, T_p, from D + 5 to D + 30 (5 to 30 days after the detonation) was approximately 18 days. The average concentration of ^{89}Sr in bone ash, B_t, increased rapidly from D + 5 to D + 15 and then more slowly to a maximum (apparent

Table 3—RESULTS OF CORRELATION AND REGRESSION ANALYSES BASED ON ESTIMATES OF INITIAL GAMMA DOSE RATES AT 20 REPRESENTATIVE LOCATIONS IN THE SEDAN FALLOUT FIELD AND ON THE CONCENTRATIONS OF ^{89}Sr AND ^{131}I IN PLANT SAMPLES OR IN THE STOMACH CONTENTS, BONE ASH, OR THYROIDS OF RABBITS COLLECTED AT THE SAME LOCATIONS

Variables* [x(y)]	Correlation coefficients	Regression coefficients	Regression formulas [$x = \bar{x} + b_{xy}(y - \bar{y})$]
^{89}Sr			
$P_0(R_0)$	0.755†	83.75 ± 16.65†	$P_0 = 83.75\ R_0 + 335$
$B_{30}(P_0)$	0.698†	0.742 ● 0.250†	$B_{30} = 0.742\ P_0 + 761$
^{131}I			
$P_0(R_0)$	0.738†	0.405 ± 0.187†	$P_0 = 0.405\ R_0 + 0.147$
$S_0(R_0)$	0.835†	0.184 ± 0.029†	$S_0 = 0.184\ R_0 + 0.817$
$A_5(P_0)$	0.626†	12.76 ± 3.72†	$A_5 = 12.76\ P_0 + 122$
$A_5(S_0)$	0.769†	38.82 ± 7.59†	$A_5 = 38.82\ S_0 + 57$

*R_0 = mr/hr at 3 ft aboveground at H + 24; $P_0(^{89}Sr) = 1.26\ P_5$ (pc/g on plants at t = 0); $P_0(^{131}I) = 2.00\ P_5$ (nc/g on plants at t = 0); $S_0(^{131}I) = 2.00\ S_5$ (nc/g in stomachs at t = 0); $B_{30}(^{89}Sr)$ = observed values (pc/g in bone ash at t = 30 days); and $A_5(^{131}I)$ = observed values [nc(total) in thyroids at t = 5 days].

†Statistically significant at the 1% level of probability.

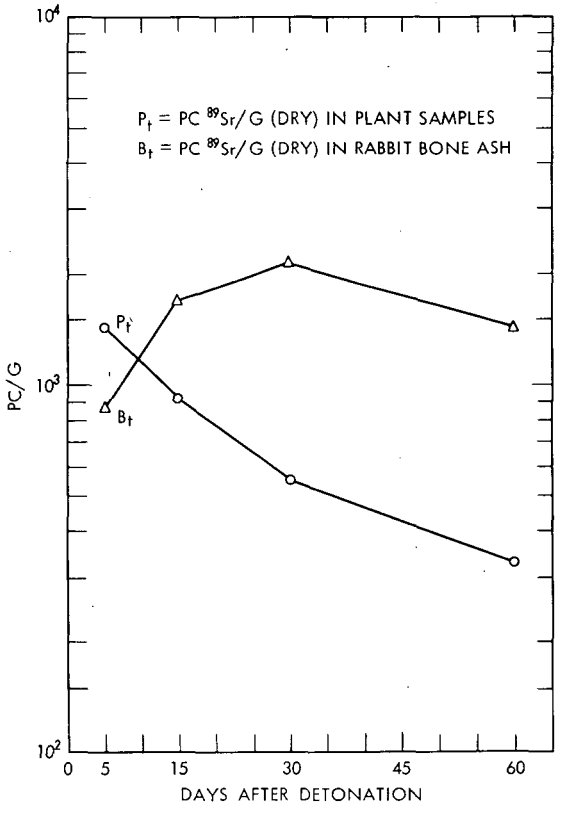

Fig. 3—Average concentrations of ^{89}Sr in plant samples, P_t, and in the bone ash of rabbits, B_t, collected from representative locations (see Fig. 2) in the Sedan fallout field at various times after the detonation.

equilibrium) about D + 30. The rate of decline from D + 30 to D + 60 approximated the radioactive half-life of ^{89}Sr. Estimates of the effective half-life of ^{89}Sr in rabbit bone (T_b = 20 days) were based on the average rates of loss from plants and the average rates of accumulation in bone ash. After estimates of the other required parameter values were obtained, these and the observed values for B_t were used to solve Eq. 5 for f_b. The average value thus obtained was $f_b = 0.0575$.

As shown in Table 2, the average concentrations of ^{131}I in plant samples (sagebrush) from Groom Valley and the Currant Area were higher than the average concentrations in the stomach contents of rabbits from the same locations. In the Penoyer and Railroad valleys, ^{131}I concentrations in the stomach contents of rabbits were somewhat higher than those in plant samples (mostly shadscale) from the same locations. Apparently the rabbits in these areas were feeding on plants other than sagebrush and shadscale.

This supposition is supported by the estimates of f_p given in Table 4. The average f_p values based on the plant samples from all locations are approximately the same for ^{89}Sr and ^{131}I. However, the average f_p value for ^{131}I based on concentrations in plant samples is higher than the average based on concentrations in the stomach contents of rabbits. For both ^{89}Sr and ^{131}I, the f_p values for sagebrush are higher than those for shadscale. The differences between f_p values for ^{89}Sr and ^{131}I in the different study areas are probably due to disparities between actual and theoretical, a_s, deposition rates, i.e., to fractionation or to errors in the estimation of average gamma dose rates. In general, these results indicate that the plants (probably grasses and broad-leaved-herbs) representing the average rabbit's diet were less efficient than sagebrush but somewhat more efficient than shadscale in regard to the interception of fallout particles.

As shown in Table 2 and Fig. 4, the average concentrations of ^{131}I in plant samples from all stations were higher than the average ^{131}I concentrations in the stomach contents of rabbits from the same areas;

Table 4 — ESTIMATES OF f_p BASED ON EQS. 1 AND 2 AND OF INITIAL CONCENTRATIONS OF ^{89}Sr AND ^{131}I IN PLANT SAMPLES, P_0, AND OF ^{131}I IN THE STOMACH CONTENTS OF RABBITS, S_0*

Study areas†	Plant species	^{89}Sr	P_0	^{131}I	P_0	^{131}I	S_0
Groom Valley	Sagebrush	4.86	$\times 10^{-3}$	5.61	$\times 10^{-3}$	2.42	$\times 10^{-3}$
Penoyer Valley	Shadscale‡	3.03	$\times 10^{-3}$	1.56	$\times 10^{-3}$	2.32	$\times 10^{-3}$
Railroad Valley	Shadscale	3.14	$\times 10^{-3}$	2.21	$\times 10^{-3}$	2.24	$\times 10^{-3}$
Currant Area	Sagebrush	11.9	$\times 10^{-3}$	7.02	$\times 10^{-3}$	4.51	$\times 10^{-3}$
Average for all locations		4.40	$\times 10^{-3}$	4.34	$\times 10^{-3}$	3.02	$\times 10^{-3}$

*$P_0(^{89}Sr) = 1.26\ P_5$, $P_0(^{131}I) = 2.00\ P_5$, and $S_0(^{131}I) = 2.00\ S_5$.
†Locations of study areas are shown in Fig. 2.
‡Some of the plant samples from this area were *Grayia spinosa*.

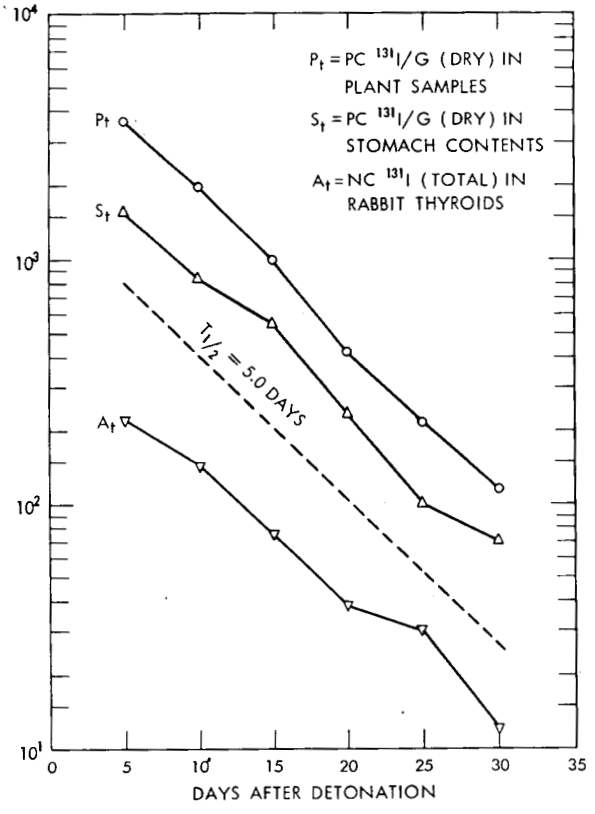

Fig. 4—Average concentrations of ^{131}I in plant samples, P_t, in the stomach contents, S_t, and in thyroids, A_t, of rabbits collected from representative locations (see Fig. 2) in the Sedan fallout field at various times after the detonation.

but the apparent rates of loss, indicating an effective half-life, T_p, of 5.0 to 5.5 days, were about the same. The average concentrations of ^{131}I in rabbit thyroids attained a maximum by or before D + 5 and declined at a half-time rate of 5 to 6 days.

French[27] and French and Van Middlesworth[29] did some experimental work with jackrabbits near the National Reactor Testing Station in Idaho. Their reports give estimates of T_a ranging from 1.5 to 2.5 days and of f_a ranging from 0.29 ± 0.09 to 0.158 ± 0.086. A more recent report by McBride[30] gives estimates of T_a = 2.0 days and f_a = 0.29. By trial and error we have found that estimates of T_p = 5.0 days and T_a = 2.0 days are reasonable approximations in relation to the data given in Table 2 and Fig. 4. With the use of these parameter values and the observed average values of A_t, Eq. 6 was solved for f_a. The results based on plant data, $\bar{P}_0$, indicate f_a = 0.18, and the results based on stomach-

contents data, $\bar{S}_0$, indicate $f_a = 0.26$. (N.B. If stomach-contents data were available for ^{89}Sr, one might expect to find a similar difference in estimates of f_b required to fit the observed data points.)

Figures 5 and 6 show the relatively close agreement between observed average concentrations of ^{89}Sr in rabbit bone ash and of ^{131}I in rabbit thyroids and the hypothetical values obtained through solution of Eqs. 5 and 6. Because of variations within and between the different study areas (Groom, Penoyer, Railroad, and Currant), the parameter values that apply to the Sedan fallout field as a whole may or may not apply with equal accuracy to different areas within the fallout field. For example, if they were based on initial ^{131}I concentrations in plant samples, estimates of ^{131}I concentrations in thyroids, A_t, would be higher than those observed in the Groom and Currant study areas but lower than those observed in the Penoyer and Railroad valleys. However, the disparities between hypothetical and observed ^{89}Sr concentrations in the bone ash of rabbits from different parts of the Sedan fallout field, based on R_0 rather than physiography, are generally less than the standard errors of the observed means.[13]

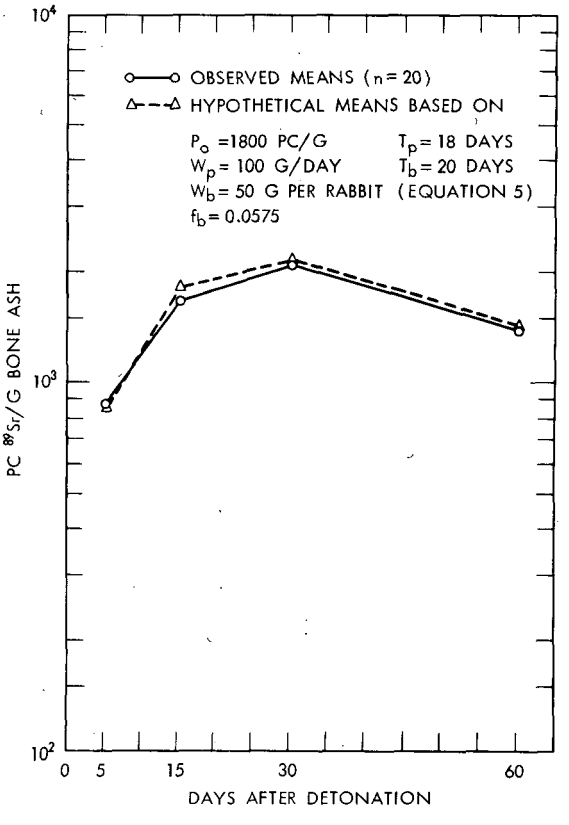

Fig. 5—Observed and hypothetical average concentrations of ^{89}Sr in the bone ash of rabbits collected from representative locations (see Fig. 2) in the Sedan fallout field at various times after the detonation.

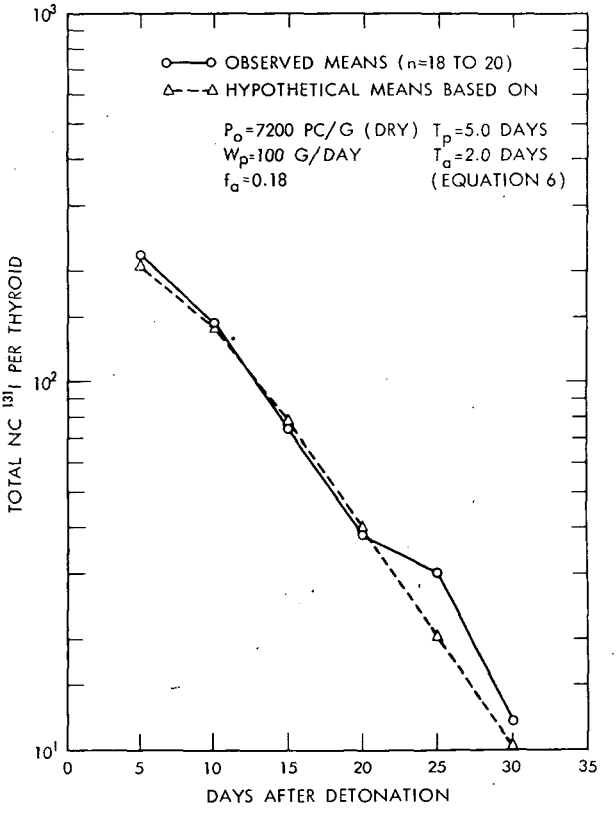

Fig. 6—Observed and hypothetical average concentrations of ^{131}I in the thyroids of rabbits collected from representative locations (see Fig. 2) in the Sedan fallout field at various times after the detonation.

DISCUSSION

These results seem to indicate that Eqs. 4 to 6 function satisfactorily, with estimated parameter values based on observed means, in explaining the early food-chain kinetics of ^{89}Sr and ^{131}I on plants and in the skeletons or thyroids of rabbits collected from 20 representative locations in the Sedan fallout field at between 5 and 60 days after the detonation. The input parameters for Eqs. 4 to 6 (W_p, W_b, f_b, f_a, T_p, T_b, and T_a) are known to vary; but the means of these values can be used, with fair success, as though they were constants. This deterministic approach to the problem permits us to describe and explain certain aspects of food-chain kinetics in relatively simple mathematical terms. It may also permit us to make errors in estimating parameter values; these errors are difficult to detect because the several parameters are

interdependent. The variations within and between different study areas and the twofold difference between estimates of f_a based on ^{131}I concentrations in plant samples and in the stomach contents of rabbits are good examples of the kinds of disparities to be anticipated.

Although it is quite tempting to use such models to predict the biological consequences of close-in fallout, there are many good reasons for proceeding with caution. Some of the uncertainties, possible sources of error, and other obstacles to the achievement of this goal are described and discussed below.

From our analyses, the relation between initial gamma dose rates, R_0, and initial concentrations of radionuclides on fallout-contaminated plants, P_0, appears to take the form of a linear regression formula. There are several reasons for viewing this apparently simple relation with suspicion. For example, Guillou[22] has noted that the probable accuracy of R_0 estimates based on aerial-survey data is no greater than $\pm 50\%$. Consequently the regression coefficients given in Table 3 could be in error by $\pm 50\%$, and errors associated with extrapolations beyond the standard regression formula limits could be even greater.

Because of nuclide fractionation and downwind variations in the particle-size composition of fallout, one might not expect to find significant correlations between gross gamma dose rates and concentrations of specific radionuclides on plants or soils in fallout fields resulting from surface or low-altitude nuclear detonations. Previous studies[1,7,28] along the hot lines of fallout from balloon- and tower-supported detonations have shown correlations between plant and animal contamination and the distribution of fallout particles $< 44\ \mu$ in diameter.* In several cases, the highest percentages of fallout $< 44\ \mu$ in diameter and the highest levels of plant and animal contamination were found at intermediate distances from ground zero and hence at intermediate levels of gross gamma dose rate. Under these conditions, it would not be possible to predict plant contamination levels by means of linear regression formulas involving R_0 as the independent variable.

As shown in Table 4, it is also necessary to consider those factors which influence a plant's ability to intercept and retain the fallout particles deposited on it. Other things being equal, it may be assumed that plants with dense foliage composed of oily, resinous, or pubescent leaves should have higher f_p values than plants with sparse foliage composed of smooth or waxy leaves; but more data are needed to determine f_p values for a variety of wild and cultivated plant species in relation to specific morphological features, the particle-size composition of fallout, and various deposition rates.

*Autoradiographs and microscopic examinations have shown that virtually all the radioactive particles on plant foliage in the Sedan fallout field were $< 50\ \mu$ in diameter and that about half of those measured were $< 20\ \mu$ in diameter.

Also needed are data to indicate the effects on f_p of plant density (e.g., g/sq ft) and other phytosociological characteristics of vegetation such as species composition, community structure, and phenology. In desert-shrub communities, for example, shrubs are widely spaced, and it is probably safe to assume that the f_p value for plants in a given area is independent of plant density. In pasture or forest, where plants are more crowded and where some may grow in the shade of others, f_p may decrease as density increases. Some evidence of this relation in regard to ^{131}I has been cited recently by Straub and Fooks.[31]

Many of these factors (fractionation, particle-size composition and distribution, and retention factors, $a_L = f_p$) are considered in the fallout model proposed by Miller.[32] If suitable plant data were available for a given situation, Miller's model would surely provide a theoretically sounder basis than unqualified linear regression formulas for the prediction of the initial concentrations of radionuclides on plants at different locations in a close-in fallout field. If one wanted to use the food-chain model described earlier (Eqs. 3 to 6) to make predictions of P_0, P_t, B_t, and A_t, a fallout model such as Miller's should be substituted for Eq. 3.

After the deposition of fallout, the concentration of a given radionuclide on fallout-contaminated plants can be expected to decline at a rate significantly faster than would be predicted on the basis of its radioactive half-life. Our estimates of effective half-lives on plants in the Sedan fallout field, 18 days for ^{89}Sr and 5.0 to 5.5 days for ^{131}I, indicate environmental half-lives (i.e., half-time rates of loss due to all causes other than radioactive decay) of approximately 28 days for ^{89}Sr and 15 days for ^{131}I. Since there was little or no rain in the area of the Sedan fallout field during the period of this study, the environmental half-life of ^{89}Sr on plants can be attributed primarily to wind action that removed particles from foliage or foliage from plants. The shorter environmental half-life of ^{131}I on plants may reflect the combined effects of wind action and sublimation.[11,12]

Other studies have indicated that our estimates of environmental and effective half-lives may not be applicable to other situations. For example, Bartlett et al.[10] sprayed solutions of different fission products on grass that was then exposed to both wind and rain for periods up to 60 days. Their results indicated an average environmental half-life of about 14 days for each of the radionuclides used. The difference between their results and ours is probably due to the effects of rain in removing soluble materials, but rain should have similar effects on particulate materials.

Considering the large number of variables involved (e.g., plant species, local weather conditions, the particle-size composition of material deposited on plants, the developmental stage of foliage, etc.), one should expect to find a wide range of apparent effective half-lives

of different radionuclides on fallout-contaminated plants. In the absence of pertinent measurements, it is reasonable to assume an environmental half-life of 14 days or less for ^{131}I and for other radionuclides on fallout-contaminated plants in humid regions. Except for ^{131}I, an environmental half-life of 28 days should be more accurate for arid regions. In general, the effective half-life of a given radionuclide on plants, T_p, could be estimated, where T_e is the environmental half-life and T_r is the radioactive half-life, by

$$T_p = \frac{T_r \times T_e}{T_r + T_e} \tag{7}$$

Our method[13] of estimating the effective half-life of ^{89}Sr in rabbit bone (T_b = 20 days) was made necessary by the absence of pertinent experimental data, and our only confidence in the accuracy of our estimate is based on the results obtained (Fig. 5) when we used it to solve Eq. 5. Our estimate of the effective half-life of ^{131}I in rabbit thyroids (T_a = 2.0 to 2.5 days) was well within the range of experimental results reported by French[27] (T_a = 1.5 to 2.5 days). Whenever possible, the effective half-lives of radionuclides in animal tissues or organs should be determined by experimental as well as by empirical methods. One can then judge which of several possible values should be applied to a given set of circumstances.

Animal retention factors, e.g., f_b and f_a, are especially difficult to evaluate; and, as shown in Eqs. 5 and 6, errors in the estimation of these parameter values would result in proportional errors in the prediction of tissue burdens. Our estimates of retention factors for ^{89}Sr (f_b = 5.75%) and for ^{131}I (f_a = 18% if based on P_0 or f_a = 26% if based on S_0) represent mathematically arbitrary numbers calculated to obtain reasonably good fits between hypothetical and observed average tissue burdens. Because of the methods used in the estimation of these values, their physiological significance is doubtful; but these values may be just as useful as those obtained from feeding experiments. For example, French's experimental results indicated f_a values ranging from < 10 to >30% for jackrabbits, whereas the averages obtained for Dutch rabbits under laboratory conditions were only half as high. We collected samples of sagebrush and shadscale from the Sedan fallout field and fed them to Dutch rabbits in the laboratory. The results reported by Turner[14] indicated f_a values ranging from 2.0 ± 0.6% (based on samples from the Currant Area) to 12.0 ± 8.0% (based on samples from Groom Valley). Because of the difference in animal species (Dutch rabbits vs. jackrabbits) and because our field data indicate that jackrabbits in the Sedan fallout field were feeding on plants other than sagebrush and shadscale, these results are of dubious value in relation to the food-chain model.

DETERMINISTIC MODELS FOR HUMAN-FOOD-CHAIN KINETICS

The data summarized and discussed in the preceding pages have served to illustrate the usefulness of deterministic exponential models in providing at least a partial explanation of the early food-chain kinetics of radionuclides following a single fallout event. Although the results of these studies are not conclusive, they are promising and provide a basis for the supposition that similar models should be useful in the study of radionuclide transfers in food chains leading to man.

For example, suppose that an ordinary pasture is contaminated by fallout from a single nuclear detonation or from a reactor accident and that the milk produced by dairy cattle grazing in the contaminated pasture is consumed by people living on the farm or in a nearby village. If an estimate of the initial concentration of a given radionuclide, N_i, on pasture plants, P_0, can be obtained from direct measurement or predicted by a suitable fallout model, the subsequent concentration of N_i on pasture plants, P_t, in cow milk, M_t, and in the human tissue or organ of reference, H_t, can be estimated, with the assumptions that $P = P_0$, $M = 0$, and $H = 0$ at $t = 0$, by Eqs. 8 to 10:

$$P_t = P_0 e^{-\lambda_p t} \tag{8}$$

$$M_t = P_0 K_m f_m \left(\frac{e^{-\lambda_p t}}{\lambda_m - \lambda_p} + \frac{e^{-\lambda_m t}}{\lambda_p - \lambda_m} \right) \tag{9}$$

$$H_t = P_0 K_m f_m K_h f_h \left[\frac{e^{-\lambda_p t}}{(\lambda_m - \lambda_p)(\lambda_h - \lambda_p)} + \frac{e^{-\lambda_m t}}{(\lambda_p - \lambda_m)(\lambda_h - \lambda_m)} + \frac{e^{-\lambda_h t}}{(\lambda_p - \lambda_h)(\lambda_m - \lambda_h)} \right] \tag{10}$$

where t = days after fallout

N_i = a given radionuclide (e.g., ^{89}Sr or ^{131}I)

P_0 = pc N_i/g (dry) on pasture plants at $t = 0$

P_t = pc N_i/g (dry) on pasture plants at $t > 0$

M_t = pc N_i/ml (fresh) in milk produced at $t > 0$

H_t = pc N_i/g (fresh) in the human tissue or organ of reference at $t > 0$

K_m = dry weight (g) of plants consumed/volume (ml) of milk produced per day

K_h = volume (ml) of milk consumed per day/weight (g) of human organ or tissue

f_m = fraction of ingested N_i secreted in cow milk

f_h = fraction of ingested N_i deposited in human tissue or organ of reference

$\lambda = 0.693/T$

T_p = effective half-life of N_i on pasture plants

T_m = effective half-life of N_i in cow milk production

T_h = effective half-life of N_i in human tissue or organ of reference

To illustrate the potential value of the model formulated above, we have adopted the parameter values listed in Table 5. Most of these values are based on experimental data reported in the literature; but, when two or more estimates of a given parameter value were found, we usually selected the one resulting in higher concentrations in milk or

Table 5—PARAMETER VALUES USED WITH EQS. 8 TO 10 TO CALCULATE HYPOTHETICAL CONCENTRATIONS OF ^{89}Sr AND ^{131}I ON PASTURE PLANTS, IN COW MILK, AND IN HUMAN TISSUES FOLLOWING A SINGLE FALLOUT EVENT*

Parameter†	^{89}Sr	^{131}I	References
P_0	100 pc/g	400 pc/g	Arbitrary values
K_m	1.4 g/ml/day	1.4 g/ml/day	33
f_m	0.02	0.06	34, 35
K_h (adult)	1/7 ml/day/g	50 ml/day/g	20
K_h (infant)	10/7 ml/day/g	500 ml/day/g	20
f_h	0.21	0.30	20
K_r‡	1.43×10^{-4}	1.17×10^{-5}	20
T_p	18.0 days	5.5 days	13, 16
T_m	2.5 days	2.0 days	34
T_h	50.4 days	7.5 days	20

*Results are shown in Figs. 7 and 8.
†Parameters are defined in the text.
‡Used with Eq. 11 to calculate tissue doses.

human tissues. The results of calculations based on Eqs. 8 to 10 and the parameter values listed in Table 5 are shown in Figs. 7 and 8. Obviously, for different values of P_0, the corresponding values of M_t and H_t would be proportionally larger or smaller than shown in Figs. 7 and 8. Using the same effective half-lives but different estimates of K_m, f_m, K_h, or f_h would also result in proportionally higher or lower estimates of M_t and H_t.

The total dose, D_t, delivered by N_i to the human tissue or organ of reference is given, for $t = 0$ to $t = \infty$, by

$$D_t = P_0 K_m f_m K_h f_h K_r \left[\frac{1 - e^{-\lambda_p t}}{\lambda_p(\lambda_m - \lambda_p)(\lambda_h - \lambda_p)} + \frac{1 - e^{-\lambda_m t}}{\lambda_m(\lambda_p - \lambda_m)(\lambda_h - \lambda_m)} + \frac{1 - e^{-\lambda_h t}}{\lambda_h(\lambda_p - \lambda_h)(\lambda_m - \lambda_h)} \right] \quad (11)$$

where D_t = total dose (rem) delivered by N_i, from $t = 0$ to $t > 0$, to the human organ or tissue of reference

$K_r = [(3.20 \times 10^3 \text{ dis/pc/day}) (E)/(6.24 \times 10^7 \text{ Mev/100 ergs/g})]$

E = effective absorbed energy (Mev) per disintegration of N_i [Mev absorbed/disintegrations of N_i × relative biological effectiveness (RBE)]

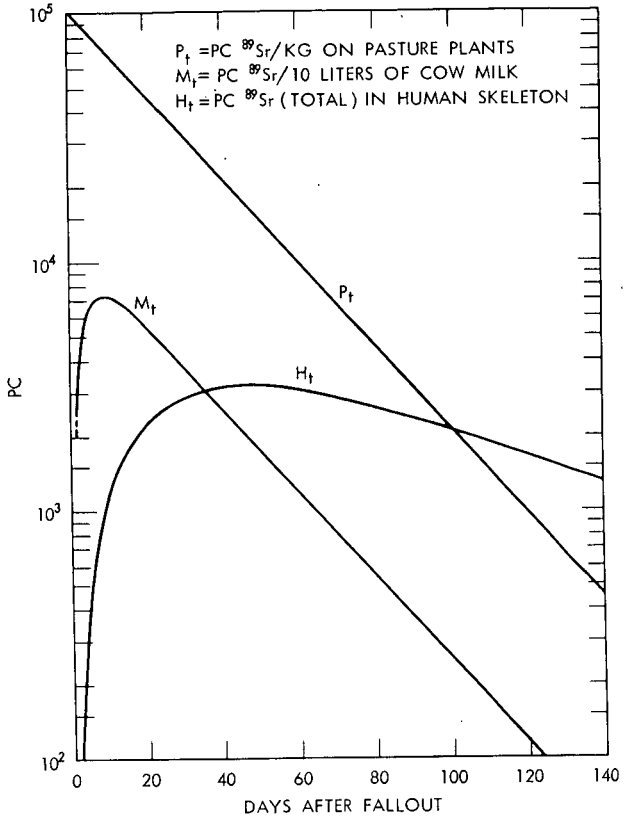

Fig. 7—Hypothetical concentrations of ^{89}Sr on pasture plants, in cow milk, and in human skeletons following environmental contamination by a single fallout event.

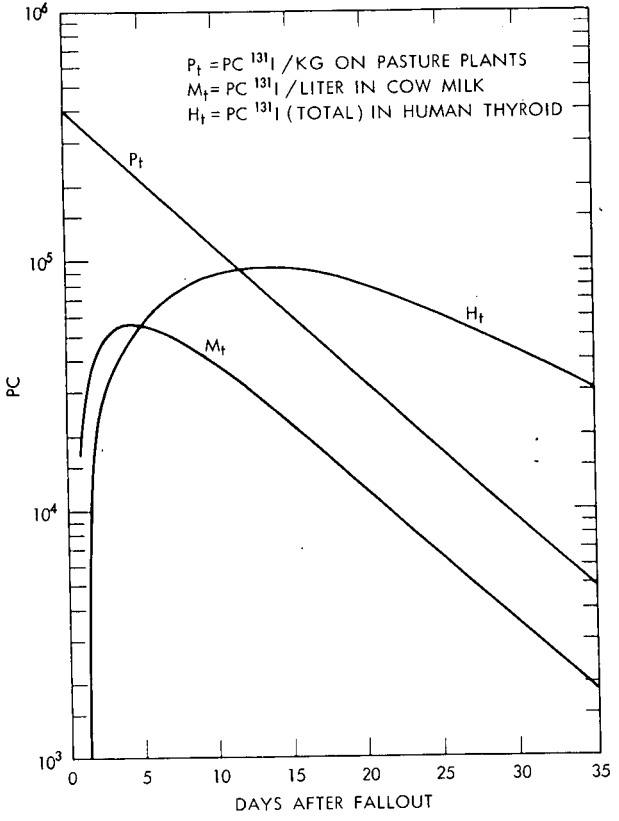

Fig. 8—Hypothetical concentrations of ^{131}I on pasture plants, in cow milk, and in human thyroids following environmental contamination by a single fallout event.

If the concentration of N_i on pasture plants is not known, estimates of doses to human tissue can be based on concentrations in milk (M_t = pc N_i/ml). If the time of fallout is known and M_t is given for a specified time of milking, Eq. 9 can be simplified, as shown in Eq. 12, to obtain an integration constant, I_0, that can then be substituted for the expression $P_0K_mf_m$ in Eqs. 10 and 11 to obtain estimates of concentrations in, H_t, and doses to, D_t, the human tissue or organ of reference:

$$M_t = I_0 \frac{e^{\lambda_p t} - e^{\lambda_m t}}{\lambda_m - \lambda_p} \tag{12}$$

James[36] recently used a similar method to estimate human thyroid doses resulting from a single fallout event, but many of his parameter values (i.e., $f_h = 0.25$, $K_r = 1.0 \times 10^{-5}$, $T_p = 5.0$ days, and $T_m = 1.9$ days) were not as pessimistic as those given in Table 5. James concluded from his investigation that a maximum concentration of 2800 pc of ^{131}I per liter of milk resulting from a single fallout event would, if a milk consumption of 1 liter/day were assumed, result in a total dose of 0.5 rad to a 2.0-g thyroid. Our results (Table 6) indicate that a maximum concentration of only 1850 pc of ^{131}I per liter of milk would be required for a potential dose of 0.5 rem to a 2.0-g human thyroid. (N.B. In this case 1 rem = 1 rad × RBE, and RBE = 1.0; therefore 1 rem = 1 rad.)

Pendelton et al.[37] based their estimates of thyroid doses on estimates of total ^{131}I intake, I_t, by people consuming 1 liter of milk per day in various parts of Utah during the summer of 1962. According to our hypothesis, the value of I_t would be given by

$$I_t = I_0 V_h \left[\frac{1 - e^{-\lambda_p t}}{\lambda_p(\lambda_m - \lambda_p)} + \frac{1 - e^{-\lambda_m t}}{\lambda_m(\lambda_p - \lambda_m)} \right] \tag{13}$$

where I_0 is an integration constant obtained from Eq. 12 and V_h is the volume of milk in milliliters consumed per person per day.

With the use of I_t from Eq. 13, the total thyroid dose would be given, where W_h is the thyroid weight (fresh) in grams, by

$$D_t = \frac{I_t K_r f_h}{\lambda_h W_h} \tag{14}$$

The Radiation Protection Guides (RPG's) recommended by the Federal Radiation Council (FRC)[38] are said to represent "... a reasonable balance between biological risk and benefit to be derived from useful applications of radiation and atomic energy." The RPG's for human bone and thyroid are based on average rates of radiostrontium and radioiodine intakes which, in the opinion of the FRC, should result in doses no greater than 1.5 rem/year to "... individuals in the gen-

Table 6—SUMMARY OF HYPOTHETICAL VALUES THAT, IF INDICATED BY MEASUREMENTS MADE AFTER ENVIRONMENTAL CONTAMINATION BY A SINGLE FALLOUT EVENT, WOULD IMPLY TOTAL DOSES OF 0.5 REM TO THE SKELETONS OR THYROIDS OF INFANTS CONSUMING 1 LITER OF MILK PER DAY

Hypothetical values*	^{89}Sr	^{131}I
Initial concentrations on pasture plants, P_0	61.0 pc/g	13.7 pc/g
Maximum concentrations in milk, M_t	4500 pc/liter	1850 pc/liter
Time after fallout, t_{max}	8 days	4 days
Total intake (to $t = \infty$)	1.60×10^5 pc	2.63×10^4 pc
Maximum concentration in human tissue, H_t	27 pc/g†	1580 pc/g†
Time after fallout, t_{max}	50 days	15 days
Total dose (at $t = \infty$)	0.5 rem†	0.5 rem†

*Calculations were based on Eqs. 8 to 14 and the parameter values listed in Table 5.

†Based on a 700-g skeleton or a 2.0-g thyroid.

eral population..." or an average of 0.5 rem/year "... to be applied to suitable samples of an exposed population group." Average annual intakes of >2000 pc ^{89}Sr/day or >100 pc ^{131}I/day "... would be presumed to result in exposures exceeding the RPG..."

With the assumptions of a skeleton weight of 700 g and a thyroid weight of 2.0 g, Eq. 14 and the parameter values listed in Table 5 indicate that total annual intakes of 160,000 pc of ^{89}Sr or of 26,300 pc of ^{131}I could result in doses of 0.5 rem/year to the bones and the thyroids of infants. These values are lower than those indicated by the FRC (i.e., 720,000 pc ^{89}Sr/year and 36,500 pc ^{131}I/year) because the parameter values in Table 5 are more pessimistic than those adopted by the FRC.

For further comparison with the FRC's recommendations, we have estimated the hypothetical values of various measurements which, if obtained following a single fallout event, could result in doses of 0.5 rem to the bones and thyroids of infants. These hypothetical values are given in Table 6.

Tables 1 and 2 show that initial concentrations of ^{131}I on plants in various parts of the Sedan fallout field were about four times higher than the initial concentrations of ^{89}Sr. The estimates given in Table 6 indicate that initial concentrations of ^{89}Sr about 4.5 times higher than those of ^{131}I are required to deliver comparable doses to human tissues. We might therefore suppose that ^{131}I is considerably more hazardous than ^{89}Sr in an area contaminated by close-in fallout.

The data given in Table 2 indicate that the initial concentration of ^{131}I on plants in the vicinity of Currant, Nev., was approximately 1000 ± 150 pc/g. Similar plant samples collected in a hot spot (centered near Fruitland, Utah), which was discovered after the Small Boy detonation

on July 14, 1962, indicated an initial ^{131}I concentration (on July 15) of approximately 800 ± 200 pc (n = 6). If we assume an f_p value of about 3.0×10^{-3} for pasture plants compared to approximately 7.5×10^{-3} for desert shrubs, the initial concentrations of ^{131}I on pasture plants in the vicinity of Currant, Nev., and Fruitland, Utah, could have been 400 and 320 pc/g, respectively.

If our hypothetical pastures, dairy herds, and human populations had been located in these areas, the total ^{131}I intakes by people drinking 1 liter of milk per day could have ranged from 670,000 to 825,000 pc, and the doses to the thyroids of children could have been 11.4 to 14.6 rem. With the use of the more optimistic parameters adopted by the FRC, the estimated doses based on these intakes would be 9.2 and 11.3 rem. (N.B. These estimates are comparable to the highest estimates reported by Pendelton et al.[37] for stations located in other parts of Utah).

Actually, there are very few milk cattle in the area of the Sedan fallout field, and, since we collected no milk samples, our treatment of the problem is strictly hypothetical. However, one sample collected near Ely, Nev., and analyzed by the U. S. Public Health Service[39] contained 2800 pc ^{131}I/liter on July 24, 18 days after the detonation. If this value represents the concentration at the time of milking, it could indicate a possible thyroid dose of 2.6 rems.

Solutions to Eq. 13 indicate that ^{131}I intakes during periods of 7, 14, or 21 days following environmental contamination by a single fallout event should account for 42, 85, or 97%, respectively, of the total potential intakes from $t = 0$ to $t = \infty$. Therefore the simplest countermeasures to avoid 85% or more of the potential biological hazard related to ^{131}I would be (1) to feed cattle on stored feed for a period of two or more weeks after a detonation or (2) to use the milk produced during that period for making cheese or other dairy products that would not be consumed for a period of three or more weeks after milk production.

REFERENCES

1. R. L. Lindberg, E. M. Romney, J. H. Olafson, and K. H. Larson, Factors Influencing the Biological Fate and Persistence of Fallout, Operation Teapot, Report WT-1177, University of California at Los Angeles, January 1959.
2. K. H. Larson, H. A. Hawthorne, and J. H. Olafson, Nevada Test Site Fallout: Some Characteristics, Its Apparent Environmental Equilibrium and Biological Availability, in Radioactive Fallout from Nuclear Weapons Tests, A. W. Klement, Jr. (Ed.), USAEC Report TID-7632, pp. 4-24, February 1962.
3. R. S. Russell, Deposition of Sr^{90} and Its Content in Vegetation and in Human Diet in the United Kingdom, *Nature, 182:* 834-839 (1958).
4. National Academy of Sciences, the Behavior of Radioactive Fallout in Soils and Plants, *Natl. Acad. Sci.—Natl. Res. Council Publ. No. 1092*, 37 pp., 1963.

5. H. Nishita, E. M. Romney, and K. H. Larson, Uptake of Radioactive Fission Products by Crop Plants, *Agri. Food Chem., 9:* 101-106 (1961).
6. N. R. French and K. H. Larson, Environmental Pathways of Radioactive Iodine from Nuclear Tests in Arid Regions, USAEC Report UCLA-499, University of California at Los Angeles, December 1961.
7. E. M. Romney, R. G. Lindberg, H. A. Hawthorne, B. G. Bostrom, and K. H. Larson, Contamination of Plant Foliage with Radioactive Fallout, *Ecology, 44:* 343-349 (1963).
8. L. J. Middleton, Absorption and Translocation of Strontium and Cesium by Plants from Foliar Sprays, *Nature, 181:* 1300-1303 (1958).
9. A. A. Selders and F. P. Hungate, the Foliar Sorption of Iodine by Plants, USAEC Report HW-44890, Hanford Atomic Products Operation, Sept. 1, 1956.
10. B. O. Bartlett, L. J. Middleton, G. M. Milbourn, and H. M. Squire, the Removal of Fission Products from Grass by Rain, United Kingdom Agricultural Research Council Report ARCRL-5, pp. 52-54, 1961.
11. W. E. Martin, Losses of Sr^{90}, Sr^{89}, and I^{131} from Fallout Contaminated Plants, *Radiation Botany,* in press.
12. W. E. Martin, Loss of I^{131} from Fallout-contaminated Vegetation, *Health Phys., 9:* 1141-1148 (1963).
13. W. E. Martin and F. B. Turner, Food-chain Relationships of Radiostrontium in the Sedan Fallout Field, USAEC Report PNE-237F, University of California at Los Angeles, March 1965.
14. F. B. Turner, Quantitative Relationships Between Fallout Radioiodine on Native Vegetation and in the Thyroids of Herbivores, *Health Phys., 9:* 1241-1247 (1963).
15. F. B. Turner, the Uptake of Fallout Radioisotopes by Mammals and a Stochastic Simulation of the Process, this volume.
16. F. B. Turner and W. E. Martin, Food-chain Relationships of Radioiodine Following Two Nuclear Tests in Nevada, USAEC Report PNE-236P, University of California at Los Angeles, May 10, 1963.
17. F. B. Turner and W. E. Martin, Food-chain Relationships of I^{131} in Nevada Following the Sedan Test of July 1962, USAEC Report PNE-236F, University of California at Los Angeles, July 24, 1964.
18. G. Friedlander and J. W. Kennedy, *Nuclear and Radiochemistry,* Chap. 5, pp. 127-144, John Wiley & Sons, Inc., New York, 1955.
19. W. E. Siri, *Isotopic Tracers and Nuclear Radiation,* Chap. 15, pp. 388-402, McGraw-Hill Book Company, Inc., New York, 1949.
20. International Committee on Radiation Protection, Report of Committee II on Permissible Dose for Internal Radiation, *Health Phys., 3:* 1 (1960).
21. Health and Safety Laboratory, Manual of Standard Procedures, USAEC Report NYO-4700(Rev.), August 1962.
22. R. B. Guillou, Part II, Aerial Radiometric Survey, Project Sedan, USAEC Report PNE-225P, pp. 36-64, University of California at Los Angeles, August 1962.
23. S. Glasstone (Ed.), *The Effects of Nuclear Weapons,* U. S. Government Printing Office, Washington, D. C., 1962.
24. S. Katcoff, Fission-product Yields from Neutron-induced Fission, *Nucleonics, 18*(11): 201-208 (1960).
25. G. Higgins, Calculation of Radiation Fields from Fallout, USAEC Report UCID-4539, University of California Lawrence Radiation Laboratory, Jan. 25, 1963.
26. A. D. Arnold, Forage Consumption and Preferences of Experimentally Fed Arizona and Antelope Jack Rabbits, *Univ. Ariz. Agri. Expt. Sta. Tech. Bull., 95:* 51-86 (1961).
27. N. R. French, Iodine Metabolism in Wild Jack Rabbits, in Oklahoma Conference—Radioisotopes in Agriculture, Held April 2 and 3 at Oklahoma State University, Stillwater, Oklahoma, USAEC Report TID-7578, pp. 113-121,

Associated Midwest Universities and Argonne National Laboratory, Apr. 13, 1960.
28. K. H. Larson and J. W. Neel, Summary Statement of Findings Related to the Distribution, Characteristics, and Biological Availability of Fallout Debris Originating from Testing Programs at the Nevada Test Site, USAEC Report UCLA-438, University of California at Los Angeles, Sept. 14, 1960.
29. N. R. French and L. Van Middlesworth, Biological Monitoring of Recent Airborne Fission Products, in *Proceedings of the Second International Conference on the Peaceful Uses of Atomic Energy, Geneva, 1958*, Vol. 18, pp. 516-518, United Nations, New York, 1958.
30. R. McBride, Radioiodine Uptake at the NRTS and Environs, *Health Phys., 9:* 1127-1230 (1963).
31. C. P. Straub and J. H. Fooks, Cooperative Field Studies on Environmental Factors Influencing I^{131} Levels in Milk, *Health Phys., 9:* 1195-1204 (1963).
32. C. F. Miller, *Fallout and Radiological Countermeasures* (2 volumes), Stanford Research Institute, Menlo Park, Calif., 1963.
33. A. C. Chamberlain, J. F. Loutit, R. P. Martin, and R. S. Russell, The Behaviour of I^{131}, Sr^{89}, and Sr^{90} in Certain Agricultural Food Chains, in *Proceedings of the International Conference on the Peaceful Uses of Atomic Energy, Geneva, 1955,* Vol. 13, pp. 360-363, United Nations, New York, 1956.
34. C. L. Comar and R. H. Wasserman, Radioisotopes in the Study of Mineral Metabolism, in *Progress in Nuclear Energy, Biological Sciences*, Series IV, Vol. 1, pp. 153-196, Pergamon Press, Inc., New York, 1956.
35. F. W. Lengemann and E. W. Swanson, Secretion of Iodine in Milk of Dairy Cows Using Oral Doses of I^{131}, *J. Dairy Sci., 40:* 216-224 (1957).
36. R. A. James, Calculation of Radioactive Iodine Concentrations in Milk and Human Thyroid as a Result of Nuclear Explosions, USAEC Report UCRL-7716, University of California Lawrence Radiation Laboratory, Feb. 14, 1964.
37. R. C. Pendelton, C. W. Mays, R. D. Lloyd, and A. L. Brooks, Differential Accumulation of I^{131} from Local Fallout in People and Milk, *Health Phys., 9:* 1261-1270 (1963).
38. Federal Radiation Council, Background Material for the Development of Radiation Protection Standards, Report No. 2, U. S. Government Printing Office, Washington, D. C., 1961.
39. U. S. Atomic Energy Commission, Off-site Environmental Contamination from Nuclear Explosives at the Nevada Test Site, September 15, 1961–September 15, 1962, USAEC Report TID-18892.

FISSION-PRODUCT DEPOSITION AND DIETARY LEVELS IN THE CHICAGO AREA

P. F. GUSTAFSON, S. S. BRAR, and S. E. MUNIAK
Argonne National Laboratory, Argonne, Illinois

ABSTRACT

Measurements of gamma-emitting fission products in soil core samples have been made by gamma-ray spectrometry since 1957. These provide a running inventory of ground deposition and accumulation of a number of radionuclides. Concurrent measurements of fission products in air and in precipitation have made it possible to relate airborne activity to deposition. The only gamma-emitting fission product present in soil which is of biological importance is ^{137}Cs. The other gamma emitters constitute a source of external radiation of varying magnitude but are not metabolically active. Quarterly food sampling in the Chicago area has been conducted in conjunction with the Health and Safety Laboratory Tri-City Sampling Program since April 1961. These samples have been analyzed for ^{137}Cs and have shown traces of other gamma-emitting fission or activation products from time to time, notably ^{54}Mn. Changes in the ^{137}Cs level in the diet with time have been compared with whole-body measurements of ^{137}Cs in Chicago residents. The concentration of ^{137}Cs in human rib bone was determined in 1961 prior to the resumption of nuclear testing and in specimens collected in 1962–1963.

ANALYSES

Soil core samples have been collected from the Argonne, Ill., site and analyzed for gamma-emitting radioactivity since 1957. Two cores 4 in. in diameter and 6 in. deep were taken from two locations on the site at each sample collection. The cores were air-dried in the laboratory, pulverized, and homogenized, and approximately 2 kg was placed

in a reentrant stainless-steel container for gamma-ray analysis. The container fits over a 5-in.-diameter 4-in.-thick NaI crystal. Pulse-height analysis was done with a multichannel analyzer. The amounts of the various gamma emitters present were determined by a computer program and the use of appropriate standards according to a method previously described.[1] The concentrations of the following fission products have been determined: $^{141}Ce-^{144}Ce$, $^{103}Ru-^{106}Ru$, ^{125}Sb, ^{137}Cs, $^{95}Zr-^{95}Nb$, and $^{140}Ba-^{140}La$ when appropriate. In addition, the concentration of ^{54}Mn in soil has been measured by this method. The concentration of natural radioactivity is also obtained in the course of analysis, and the dose rate due to the various radioactive species has been calculated.[2]

Gamma-ray spectral analyses have been carried out on surface-air samples collected on appropriate filters as well as on precipitation samples. Monthly soil sampling during times of relatively high deposition of fission products coupled with air and precipitation measurements have led to the following empirical relation among airborne radioactivity, precipitation, and deposition:

$$\text{Deposition (mc/square mile)} = \text{rainfall (in.)} \times \text{activity concentration (pc/scm)} \times 28.3 \quad (1)$$

These measurements were made during a time when nuclear testing was in progress and the concentration of debris in surface air was quite variable from day to day. As a result the factor 28.3 was subject to a rather large uncertainty, 28.3 ± 14.1. Even so, when Eq. 1 is applied over a considerable time interval, the deposition calculated agrees well with direct soil measurements. The monthly deposition of ^{137}Cs calculated according to Eq. 1 for the year 1963 is illustrated in Fig. 1. The calculated ^{137}Cs deposition for the year was 78 mc/square mile compared with 70 mc/square mile from soil core measurements. Measurements of ^{137}Cs in surface air at the site extend back to 1953, as do measurements of local precipitation. The annual deposition has been calculated for each year since 1953, and the values are shown in Fig. 2. The accumulation of ^{137}Cs is plotted in Fig. 2, account being taken of the radioactive decay of ^{137}Cs according to a half-life of 30 years. The total calculated accumulation of 310 mc/square mile as of August 1964 is in agreement with the value of 330 mc/square mile measured in July 1964. The annual deposition correlates with the time distribution and intensity of nuclear testing that has occurred prior to the year of measurement. As expected, the highest deposition occurred during 1963, and the second highest level occurred during 1959. The years 1960 and 1961, during the test moratorium, showed low deposition values.

A considerable fraction of the total ^{137}Cs uptake by plants is due to freshly deposited debris, i.e., ^{137}Cs deposited during the growing season

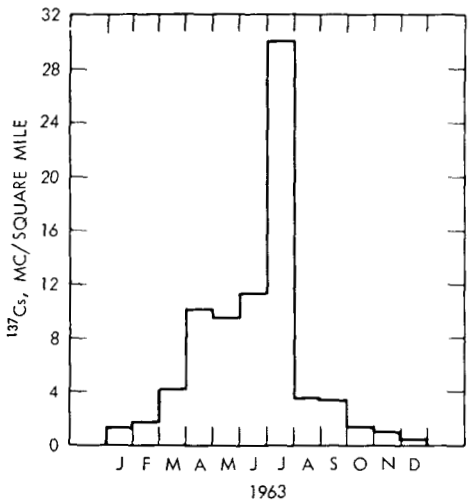

Fig. 1—Monthly deposition of ^{137}Cs during 1963 at Argonne. Totals: from air and precipitation data, 78 mc/square mile; from soil measurements, 70 mc/square mile.

of the plant in question. This is illustrated[3] in Fig. 3 by the ^{137}Cs content of wheat grown at Chillicothe, Tex., during 1957 through 1960. Although the total ^{137}Cs deposition on the ground was greater in 1960 than in 1959, the ^{137}Cs in the grain was lower by almost an order of magnitude in 1960 relative to 1959. The high level present in the 1957 crop is attributable to nuclear weapons testing at the Nevada Test Site during the spring and summer of that year. Thus it is apparent that years of heavy fallout result in corresponding elevation in the ^{137}Cs level in wheat and, presumably, in other plant material and, by inference, in animals feeding on such plant material.

It is not surprising therefore that the levels of ^{137}Cs in the diet shown in Fig. 4 increased rapidly after the resumption of nuclear testing in September 1961. Foods were purchased quarterly in two supermarkets in the Chicago area according to a list supplied by the Health and Safety Laboratory for the Tri-City Food Sampling Program.[4] The ^{137}Cs content of each food on the list was determined by a gamma-ray spectrometric method analogous to that used for the soil cores.[5] The foods were counted in bulk amounts of 1 to 2 kg without ashing or chemical processing prior to analysis. The results from April 1961 through July 1964 expressed in picocuries of ^{137}Cs per day are shown in Fig. 4. The sudden increase in October 1961 is probably a transient effect due to the heavy fallout that occurred in late September 1961, much of which was dry deposition. In 1962 the highest level in the diet was observed in the July sampling and was largely due to the concentration of

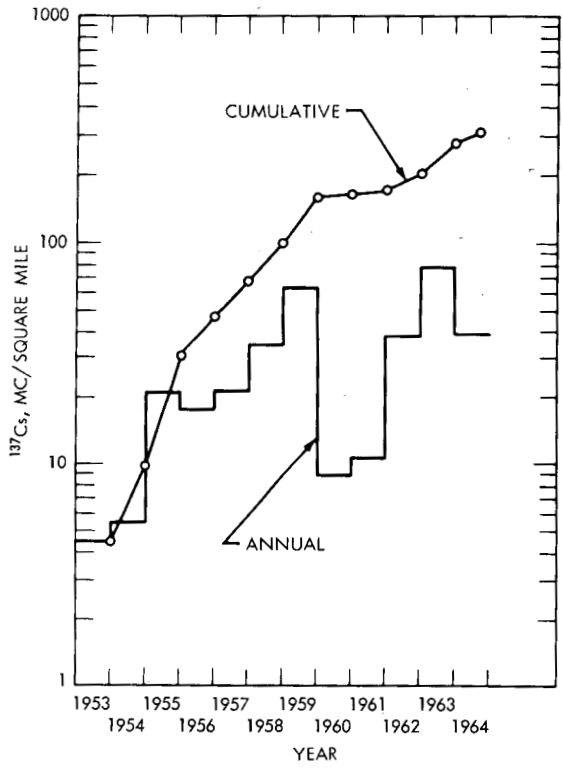

Fig. 2—Annual deposition and accumulation of ^{137}Cs at Argonne.

^{137}Cs in milk. In 1963 the highest level was not reached until the November sampling and was due to a general elevation of the ^{137}Cs levels in all foodstuffs sampled. The sampling in 1964 has shown a gradual general decrease in ^{137}Cs activity through July, and preliminary results from the October sampling indicates a continuation of the trend. The highest ^{137}Cs level in the Chicago diet was reached in January 1964, amounting to 240 pc/day, an increase of approximately 5 over the values of 55 and 53 pc/day for April and July 1961, respectively.

The average ^{137}Cs body burden in 8 to 10 adult Chicago residents is also plotted in Fig. 4. These measurements were made by C. E. Miller in the Argonne National Laboratory whole-body counter.[6,7] The body burdens are expressed in picocuries of ^{137}Cs per gram of potassium. The biological half-life of ^{137}Cs in the human body (approximately 100 days in adults) causes a lag between body burden and dietary level. Hence the lowest body burden actually occurred after the resumption of nuclear testing in 1961. Likewise the body burden is still increasing into 1964, although the dietary level has begun to decrease. The whole-

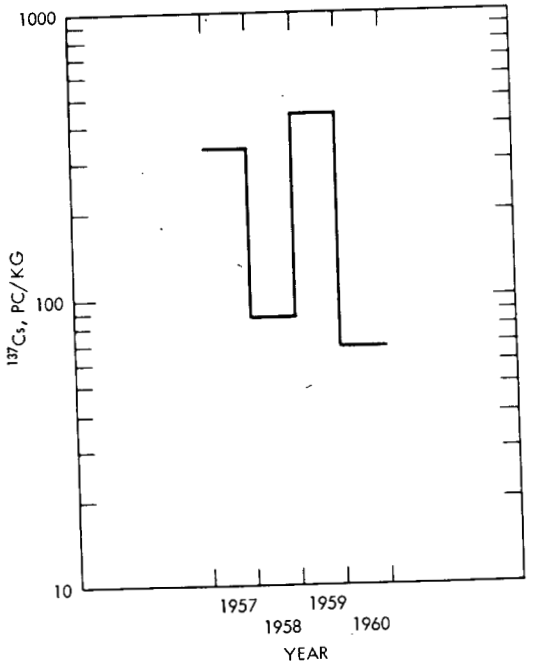

Fig. 3—Content of ^{137}Cs in wheat grown at Chillicothe, Tex.

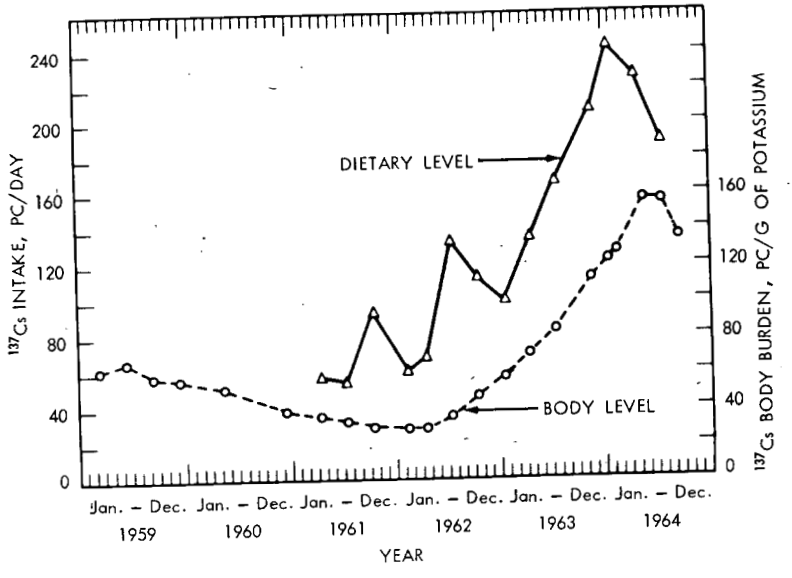

Fig. 4—Levels of ^{137}Cs in diet and human subjects in Chicago, Ill.

body measurements[8] made in September 1964 indicate that the body burden has reached its maximum level, some fivefold greater than the minimal levels during late 1961. If it is assumed that a human weighs 70 kg and contains 135 g of potassium, the whole-body burden is equivalent to a 70-day intake of food at a given ^{137}Cs level or to 130 kg of food according to the standard diet considered. The relative contribution of various foodstuffs to the total ^{137}Cs level has changed somewhat during the period of observation in that milk assumes greater importance during and for some time after nuclear testing. The partition of ^{137}Cs among the various foodstuffs shown in Fig. 5 for the November 1963 sampling is fairly representative.

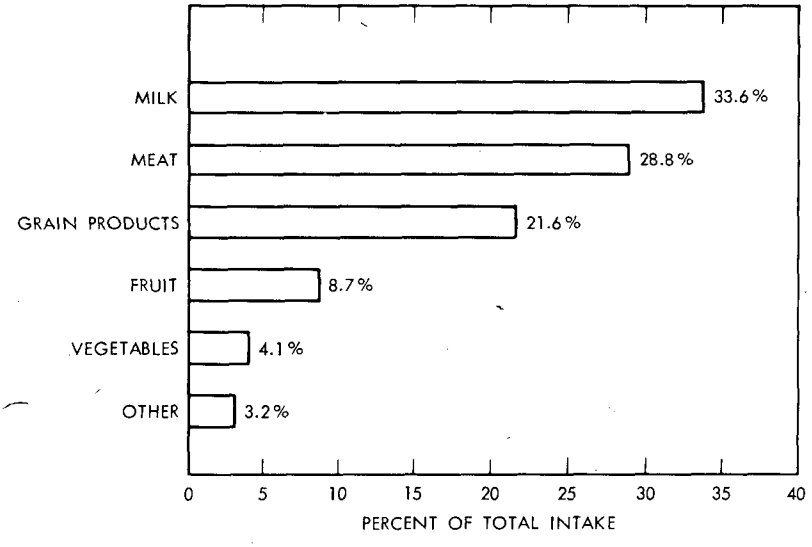

Fig. 5—Distribution of ^{137}Cs in the diets of Chicago residents in November 1963.

Although cesium, being chemically similar to potassium, is primarily distributed in soft tissues, there is evidence that some of this element does become incorporated in bone. A number of samples of human rib bone were collected in 1961 prior to the resumption of testing.[9] These were selected from various age groups ranging from infants to persons over 60 years. A second collection was made from mid-1962 to late 1963. The results of both samplings are shown in Fig. 6. The specimens have had the marrow removed by cracking the bone, scraping the marrow cavity, and washing with distilled water. The marrow and the wash water were saved, and the ^{137}Cs was measured. The intact bone was then ashed at 400°C, and the ash from various subjects within a specified age group were grouped and counted by

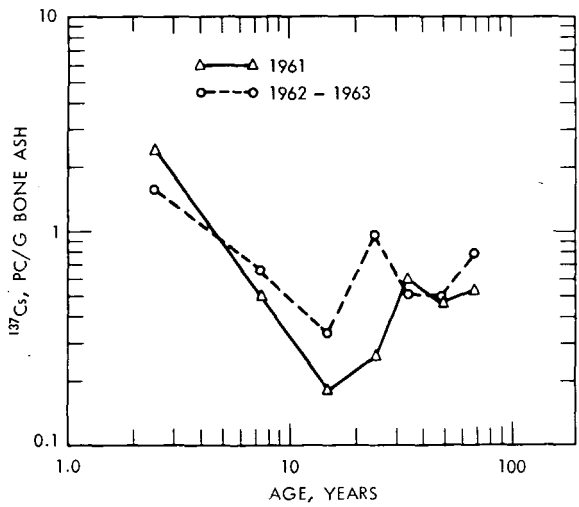

Fig. 6—Concentration of ^{137}Cs in human rib bone in Chicago, Ill.

gamma-ray spectrometry. The same general distribution pattern as a function of age was shown for the two samplings, namely, higher concentrations in the 0- to 5-year age group followed by a decrease to minimum values in the 10- to 20-year age group, after which the concentration gradually increased with age. The high concentrations in the very young are thought to be due to the highly cartilagenous quality of the bone involved, and the decrease in concentration with age up to 20 years follows the pattern of ossification of cartilage. The increase with age, also seen by Yamagata and Yamagata,[10] has not as yet been explained. Yamagata and Yamagata found rib bone to be somewhat higher in ^{137}Cs than other bone, and the recent findings of Rivera[11] bear this out. The same general pattern is seen in the 1962–1963 sampling, with some increase noted in all but the 0- to 5-year age group. This may have been due to the larger proportion of bone from 0 to 2 year olds in the 1961 sampling than were present in the later collection. The average increase in the 1962–1963 sampling was approximately 50% compared with an increase in whole-body burden during 1963 by a factor of 3 to 4 over that present in 1961. If the ^{137}Cs in rib is actually incorporated in bone, its biological half-time should be considerably longer than that for soft tissue, being on the order of years. Hence increase in bone content due to higher dietary levels will proceed much more slowly. Rivera[11] has estimated that less than 5% of the whole-body ^{137}Cs was present in bone during 1961. In light of the marked increase in whole-body ^{137}Cs and the 50% increase in bone content, the skeleton may be presumed to contain currently 1% or less of the total. Only after many

years of decreased ^{137}Cs intake would the ^{137}Cs in bone begin to amount to an appreciable portion of the whole-body content.

SUMMARY

In summary, an empirical relation between airborne radioactivity and deposition has been found which has been verified by direct soil measurements. The influence of fallout rate rather than fallout accumulation on plant and animal uptake is apparent. Milk was found to be the most important single dietary contributor of ^{137}Cs after the resumption of nuclear testing in 1961. The fivefold increase in dietary level between 1961 and late 1963 has been matched by a similar increase in whole-body burden with a time lag of some six to nine months. Some ^{137}Cs has been shown to be incorporated in bone, but its relative radiobiological importance is minimal at this time.

REFERENCES

1. P. F. Gustafson and S. S. Brar, Measurements of γ-Emitting Radionuclides in Soil and Calculation of the Dose Arising Therefrom, in *The Natural Radiation Environment,* J. A. S. Adams and W. M. Lowder (Eds.), pp. 499-512, University of Chicago Press, Chicago, 1964.
2. P. F. Gustafson, J. Kastner, and J. Luetzelschwab, Environmental Radiation: Measurement of Dose Rates, *Science, 145:* 44-47 (1964).
3. P. F. Gustafson, Radioactivity in Grains, in Proceedings of the North Central Experiment Stations Workshop on Radionuclides in Foods and Agricultural Products, F. Haghiri and R. R. Johnson (Eds.), pp. 41-48, Special Report Series, No. 1, Ohio Agricultural Experiment Station, 1963.
4. J. Rivera and J. H. Harley, HASL Contributions to the Study of Fallout in Food Chains, USAEC Report HASL-147, pp. 31-32, Health and Safety Laboratory, July 1, 1964.
5. S. S. Brar, P. F. Gustafson, and S. E. Muniak, Cs^{137} in Various Chicago Foods, in Fallout Program Quarterly Summary Report, USAEC Report HASL-146, pp. 225-232, Health and Safety Laboratory, July 2, 1964.
6. C. E. Miller and J. B. Corcoran, *In Vivo* Measurement of Cs^{137}: Summary of Observations up to June 1961, in Radiological Physics Division Semiannual Report, USAEC Report ANL-6398, pp. 41-42, Argonne National Laboratory, September 1961.
7. C. E. Miller, Cs^{137} Trends in Humans from 1955 to 1964, in Health Division Gamma-ray Spectroscopy Group Semiannual Report, USAEC Report ANL-6839, pp. 79-84 Argonne National Laboratory, January 1965.
8. C. E. Miller, Argonne National Laboratory, personal communication.
9. R. W. Anderson and P. F. Gustafson, Concentration of Cesium-137 in Human Rib Bone, *Science, 137:* 668 (1962).
10. N. Yamagata and T. Yamagata, The Concentration of Cesium-137 in Human Tissues and Organs, *Bull. Inst. Health (Japan), 1960* (United Nations Document A/AC.82/G/L.396).
11. J. Rivera, Cesium-137, Stable Strontium and Radium-226 in Two Human Skeletons, in Fallout Program Quarterly Summary Report, USAEC Report HASL-149, pp. 134-136, Health and Safety Laboratory, Oct. 1, 1964.

SOME ASPECTS OF FALLOUT IN BRAZIL

FRANCISCO X. ROSER and THOMAS L. CULLEN*
Pontifícia Universidade Católica, Rio de Janeiro, Brazil

ABSTRACT

The Brazilian network of fallout stations ranges from the equator to approximately 30°S and is composed of 10 ion-exchange column and pot collection stations. At Rio de Janeiro the surface-air contamination is measured with filters. Three effects are discussed in this paper: the spring maximum, the ocean–continent effect, and the correlation between filter and ion-exchange column data.

The spring maximum does not occur at equatorial stations where there are only wet and dry seasons. It emerges slowly with increasing latitude and is well marked in southern Brazil, but the effect is less pronounced than in the northern hemisphere. Data from ocean, coastal, and interior stations do not support the ocean–continent effect hypothesis. Comparison of column and filter data for Rio de Janeiro shows a positive correlation, but definite conclusions can be drawn only from a study of many stations.

FALLOUT IN BRAZIL

The program of radioactivity measurements in Brazil was begun in 1956 at the suggestion of the United Nations Committee on the Effects of Atomic Radiation. One branch of the work has centered on fallout, with rainfall collection samples processed at the AEC Health and Safety Laboratory (HASL) in New York and with Staplex and Naval Research Laboratory (NRL) filters processed at Pontifícia Universidade Católica (Catholic University), Rio de Janeiro. The second branch of the program concerns itself with the study of the Brazilian areas of high natural radioactivity. This paper is concerned with three ques-

*Loyola Seminary, Shrub Oak, N. Y.

tions discussed in the literature in the past year: the spring maximum, the ocean–continent effect, and the correlation between filter and column data.

Brazil with its wide latitude spread offers an excellent opportunity to observe the emerging but weak spring-maximum effect in the southern hemisphere. The 10 stations at which measurements were made in this study encompass a range from the equator to approximately 30°S; they are given in Table 1.

Table 1 — BRAZILIAN FALLOUT-COLLECTION STATIONS

Station	Latitude	Longitude	Altitude, ft	Method of collection
Belém	1°27′W	48°29′W	25	Column
Manaus	3°02′S	60°01′W	95	Pot
Recife	8°06′S	34°58′W	10	Pot
Brasilia	15°52′S	47°56′W	3450	Column
Trindade Island	20°31′S	29°20′W	120	Pot
Nova Friburgo	22°17′S	42°32′W	2800	Column
Rio de Janeiro	22°54′S	43°13′W	100	Pot
Itaici	23°06′S	47°11′W	2190	Pot
São José dos Campos	23°13′S	45°51′W	2109	Pot
São Leopoldo	29°45′S	51°11′W	115	Pot

The average deposition rates of ^{90}Sr at the stations are given in Fig. 1 in histogram form, and precipitation data are also presented where the data are reliable. No graph is given for the Recife station since service from there has been irregular.

The equatorial stations of Belém and Manaus do not have a four-season cycle but a rainy and a relatively dry season. Here the spring maximum would have no meaning. The fallout curve simply follows the precipitation curve. These stations are sensitive to trophospheric fallout from the Sahara tests. In an irregular way they also show data more typical of northern stations after northern tests, as, for example, the Belém results for April 1962 (5.64 mc/square mile) and February 1964 (2.43 mc/square mile). The interhemispheric equatorial front moves southward during the northern summer; therefore these stations are essentially in the northern troposphere for five months of the year. The front shift, however, would probably not be an efficient transport mechanism in view of the general minimal conditions near the equator.

Sufficient precipitation data for Trindade and Brasilia are not at hand; therefore a meaningful average curve cannot be presented. The available data do indicate, however, that no spring maximum exists and that precipitation is the strongest influencing factor. (See Fig. 2.) Fallout for Nova Friburgo follows the rainfall curve. In Rio de Janeiro,

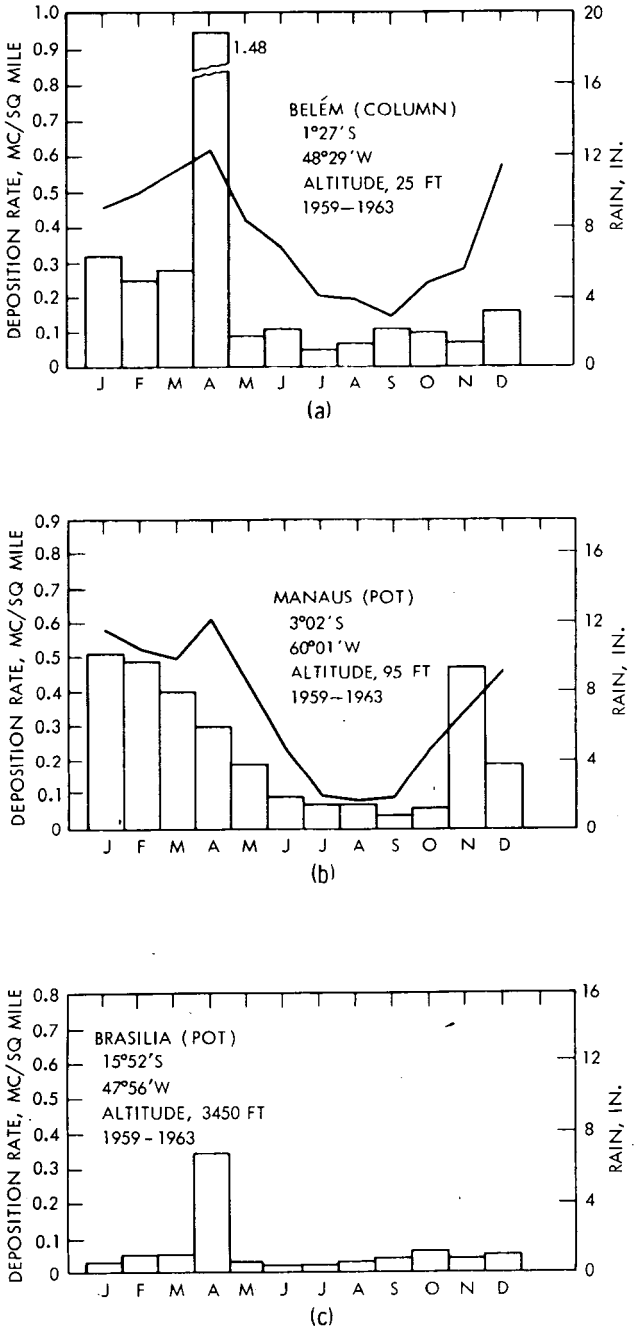

Fig. 1—Monthly average of ^{90}Sr deposition and precipitation.

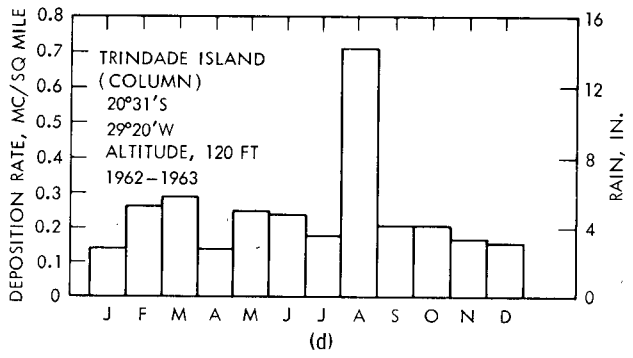

(d)

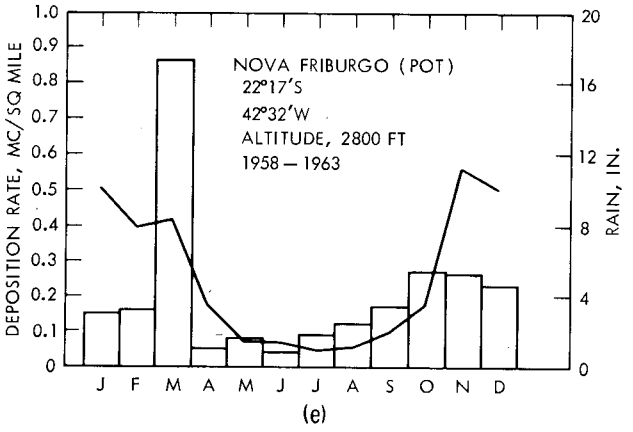

(e)

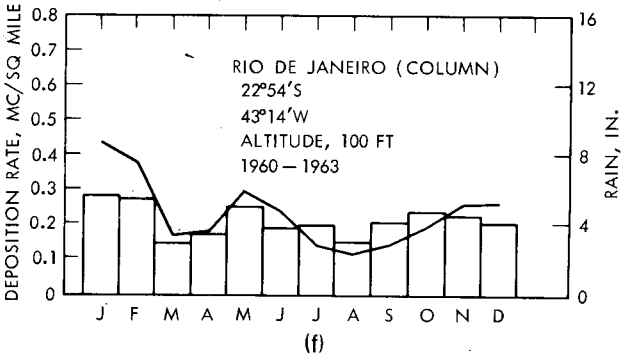

(f)

Fig. 1—(Continued)

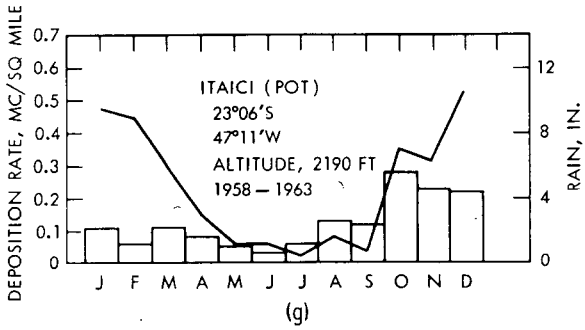

(g)

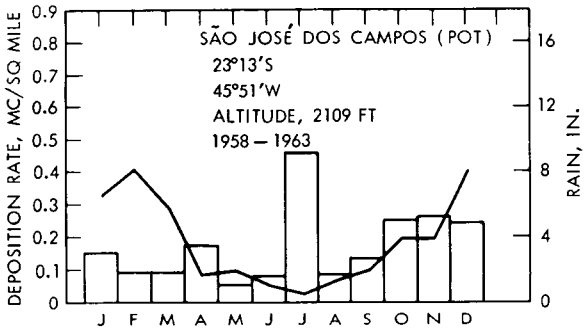

(h)

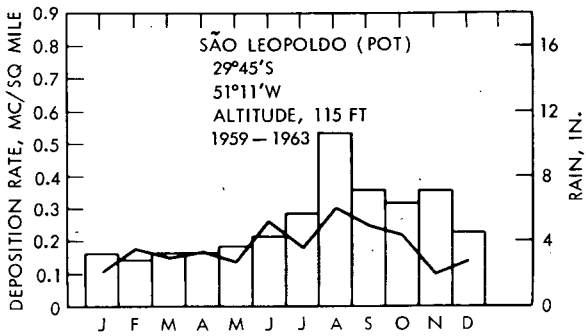

(i)

Fig. 1—(Continued)

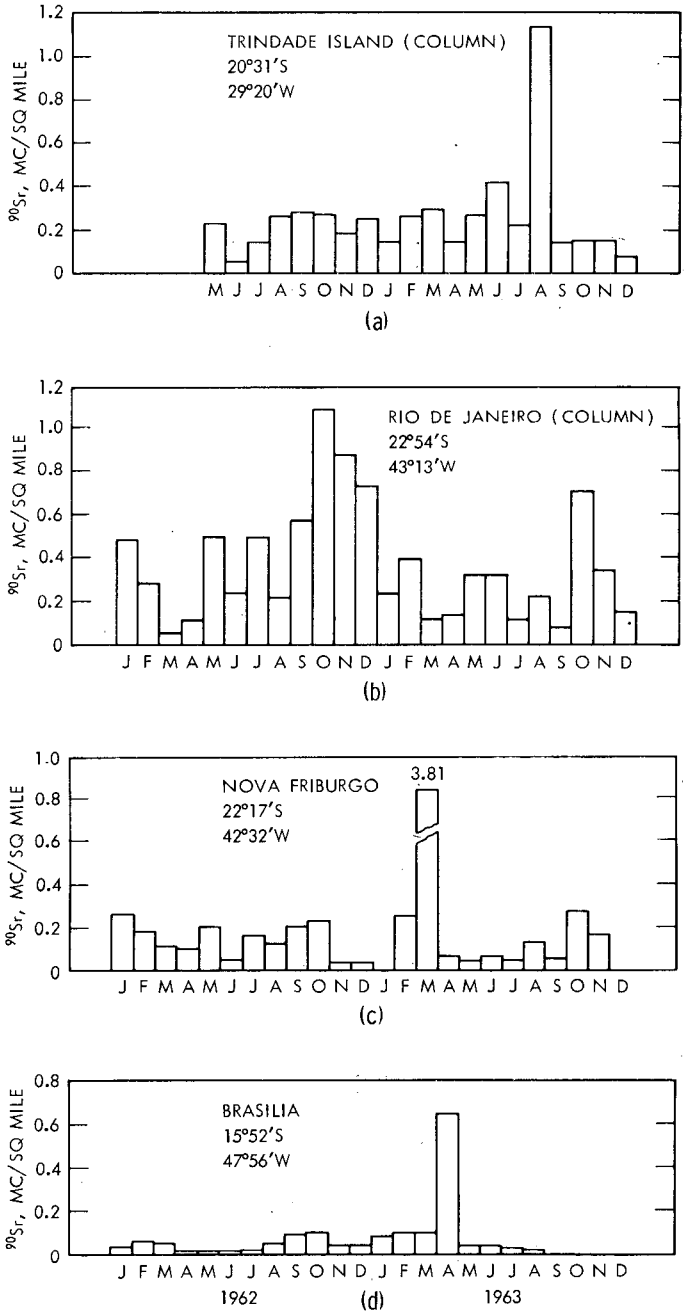

Fig. 2—Fallout in 1962 and 1963 for four stations showing possible island–continent effect.

where the rainfall rises to a maximum twice a year, the fallout curve parallels the rainfall curve.

In the two stations at Itaici (to the northwest of São Paulo) and São José dos Campos (to the northeast of São Paulo), the curves can be interpreted as showing the first faint indications of a spring maximum. The fallout does not reach a maximum in the summer months as does the rainfall, but in October and November.

The spring maximum is more definitely noticed in São Leopoldo, close to 30°S, although it is much less pronounced than in the northern hemisphere.

A large percentage of the land mass of the southern hemisphere lies between 0 and 35°S, with relatively small land masses between 35 and 70°S. The different black-body characteristics of land masses and oceans introduce a great cooling-factor difference between the northern and southern hemispheres, particularly in the 35 to 70° zone. We should therefore expect a quite different set of effects in the thermodynamic systems of the northern and southern atmospheres.

The station on Trindade Island was begun in 1962 to study the possible ocean–continent effect. The monthly data for this station, together with that of the coastal station of Rio de Janeiro, the mountain station of Nova Friburgo, and the inner plateau station of Brasilia, are given in Fig. 2. The island and coastal stations show higher levels than the inland stations at higher altitude. The ratio between the two sets of stations, however, is not as great as was predicted by the hypothesis. No definite conclusions can be drawn, moreover, from only four stations.

The monthly averages for ground-air contamination, as measured by Staplex filters, for Rio de Janeiro are given in Fig. 3. The most prominent effect is that observed during the seasons in which nuclear tests were conducted, as can be seen in the years of 1956, 1957, 1958, and 1962. What might first appear as winter–early spring maximums for the months of August, September, and October are really seasonal variations due to the testing periods.

One might expect that during the nontesting years of 1960 and 1961 a slow increase in ground contamination would be observed as the northern and southern stratospheres came into equilibrium. This was not observed in the Staplex-filter data because of low counting rates. The effect was noticed, however, on the NRL filter data taken at the same location.

A comparison between the filter and column data for Rio de Janeiro is given in Fig. 4. Although a positive correlation can be noted in these curves, no conclusion can be suggested from the data of a single station. The data that are given here should be combined with the HASL studies from many stations on the subject.

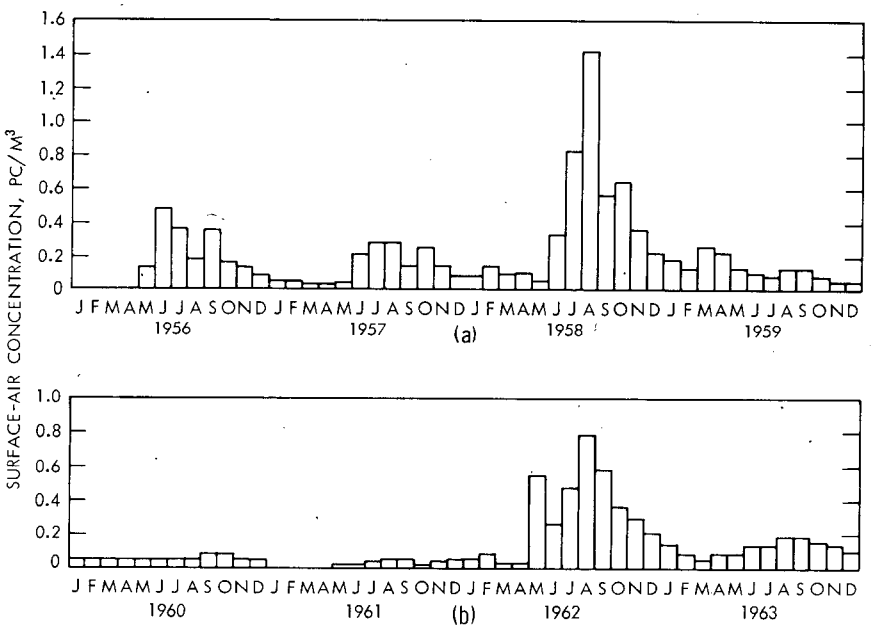

Fig. 3—Surface-air concentration at Rio de Janeiro based on Staplex-filter data, 1956–1963.

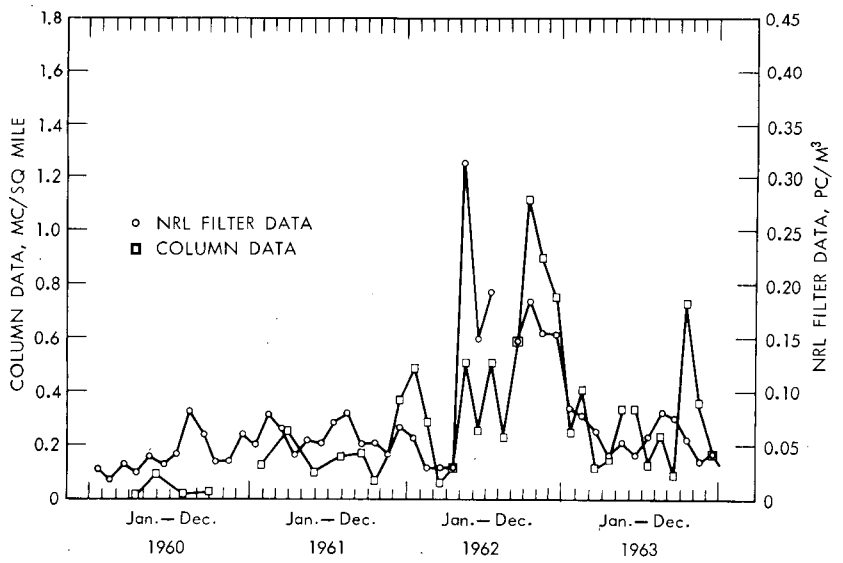

Fig. 4—A comparison of filter and column measurements at Rio de Janeiro, 1960–1963.

A concluding suggestion for such synoptic types of study of the many stations of South America may not be out of place. The vast difference between precipitation on the east and west coasts must be kept in mind. Studies can be made relating air contamination or fallout to precipitation, and the monthly rainfall at a station can be taken as a practical index of precipitation. Ideally, what is wanted is the precipitation history of an air mass. In the United States the practical index can be substituted for the ideal without much prejudice. In South America, however, where precipitation can differ from place to place by orders of magnitude and where the most important precipitation history of an air mass takes place east of the Andes, use of such an index can lead to wrong conclusions.

UPTAKE OF FALLOUT RADIONUCLIDES BY MAMMALS AND A STOCHASTIC SIMULATION OF THE PROCESS

FREDERICK B. TURNER
University of California at Los Angeles, Los Angeles, California

ABSTRACT

A deterministic model, designed to predict time-specific levels of ^{131}I in the thyroids of herbivores as a function of ^{131}I on vegetation, was revised as a probabilistic simulation of the experience of a consumer in a fallout field. The stochastic model was used to generate synthetic populations of up to 1000 individuals. The frequency distributions of thyroidal ^{131}I in 24 of these hypothetical populations were analyzed in terms of the recommended assumption of the Federal Radiation Council, namely, that the majority of individuals in a population does not vary from the average by a factor greater than 3. In only two of the distributions did more than 2% of the population exceed three times the mean.

The frequency distributions predicted by the model were all skewed to the high side and approximated lognormal distributions. A number of frequency distributions of radionuclides recorded in the literature were reviewed, and X^2 tests indicated that most of them were not normal. All the non-Gaussian distributions were skewed to the high side, and some of them were apparently lognormal. It is concluded that the general form of the synthetic distributions produced by the model is in agreement with most past observations. It is further suggested that such asymmetrical distributions may be more likely than normal ones. The implications of this possibility, in terms of health physics, is discussed.

Consideration is also given to the possible relation between the frequency distribution of a radionuclide in diets and the frequency

distribution of the substance in the tissues of animals consuming these diets.

INTRODUCTION

An important aspect of the general problem of radioactive fallout is the time-specific relation between fallout radionuclides on vegetation and the amounts of such material assimilated by herbivores and ultimately consumed by man. One should be able to represent such relations by mathematical models so that, if the amount of a radionuclide in one compartment of a food chain is measured, inferences may be drawn as to how much is or will be present in other compartments.

Such models should take into consideration the considerable variability that occurs in natural systems, as evidenced by the British work[1] in Australia in 1956 and investigations at the Laboratory of Nuclear Medicine and Radiation Biology, University of California at Los Angeles,[2,3] during the test series of 1953 and 1955. Consumers occupying apparently homogeneous environments and presumably exposed to similar diets show tissue burdens of radionuclides which differ greatly. From the standpoint of health physics, it is important to understand this variability because the high extremes are more important than modal values. This problem has been discussed previously by Libby[4] with regard to worldwide fallout of ^{90}Sr, by Eisenbud et al.[5] with reference to fallout ^{131}I in New York City, and, more generally, by Neuman[6] and Ellett and Brownell.[7] The point has also been recognized by the Federal Radiation Council,[8] which has recommended the arbitrary assumption that the majority of individuals in a population does not vary from the average by a factor greater than 3.

Although several radionuclides need to be considered in food-chain transfers, recently there has been particular interest in environmental problems involving ^{131}I (e.g., Pendleton,[9] Reiss,[10] Knapp,[11] Martin,[12] Turner,[13] and the summary analysis of the 1962 Congressional Hearings[14]).

In a consideration of the quantitative relations between ^{131}I in fallout and in human foods, it is possible to seek some simple empirical relation, e.g., the ratio of ^{131}I per liter of milk to the gross gamma activity on the ground. This approach has been adopted by Knapp,[11] who indicates that, for a number of past events involving the release of ^{131}I to the environment, the ratio of the maximum amount of ^{131}I, I_{max}, in milk (pc/liter) to the gross gamma activity (mr/hr) on the ground at H + 24, r_0, varied from about 18,000 to 220,000. Such an approach certainly avoids any difficulties in attempting to evaluate intermediate steps in this relation and may have merit in emergency situations where no other estimates of potential hazards are available.

From a theoretical standpoint it is more fruitful to consider the contamination of milk by ^{131}I as the last link in a chain of related events and to attempt to develop a step-by-step representation of the process by means of a compartment model. Such a model could be arranged in three compartments: iodine on cattle forage, iodine in cattle, and iodine in milk (a fourth compartment, the ground surface, could also be added if desired). But would such a model perform adequately when applied to a real environmental situation? The general idea might be evaluated with the use of a more simple model, e.g., one involving only two compartments.

PROCEDURE

Following the Sedan shot of July 1962, the model approach was tested in terms of the time-specific relation of ^{131}I on desert vegetation to that in the thyroids of jackrabbits consuming this vegetation.[13,15] The deterministic model used has been discussed previously by French[16] and French and Van Middlesworth[17] and is repeated here in slightly modified form for convenience:

$$A = \frac{IDF}{\lambda_E - \lambda_p} (e^{-\lambda_p t} - e^{-\lambda_E t})$$

where A = amount of ^{131}I in thyroid of consumer
I = amount of ^{131}I per gram of vegetation on day of contamination
D = number of grams of vegetation consumed per day
F = fraction of ingested ^{131}I reaching thyroid of consumer
λ_p = physical decay constant of ^{131}I, 0.0865 (ln 2/half-life in days)
λ_E = effective decay constant of ^{131}I in thyroid of consumer
t = time in days after the contamination event

When t is defined as the number of days following the introduction of ^{131}I into the environment, the model predicts the amount of ^{131}I in the thyroid of a consumer at time t in terms of a specified initial level of contamination of food, I.

The values of the other parameters involved were either measured directly during the month following the Sedan shot or based on existing experimental results. The rate of disappearance of ^{131}I from vegetation is not accurately expressed by λ_p as shown in the preceding equation but is more rapid because of loss from plants by means other than radioactive decay. The effective half-life of ^{131}I on plants was estimated to be 5.5 days on the basis of periodic analyses of vegetation samples.

The initial amount of this nuclide per gram of vegetation, I, was also estimated from measurements of plant material. Bulk samples collected in the field and the air-dried stomach contents of jack-

rabbits were analyzed.[12,13] The amount of food ingested daily, D, was taken as 100 g/day on the basis of work by Currie[18] in Utah and by Arnold[19] in Arizona. The absorption and thyroidal uptake of ingested ^{131}I, F, was taken as 0.16 on the basis of research by French[15] with jackrabbits during the summer in Idaho. The effective half-life of ^{131}I in the jackrabbit thyroid was estimated to be 2.5 days according to French's findings.

The function of the model, as a deterministic expression of what is really a probabilistic process, has already been analyzed.[13] It is now instructive to consider the variability of the parameters influencing the relation between ^{131}I on vegetation and in the thyroids of herbivores. From such a consideration we may develop a hypothesis regarding the nature of the frequency distribution of ^{131}I in consumer populations. The importance of such understanding has already been discussed.

If the possible variation of a prediction for any time t is to be considered, the variability of each input parameter and the type of frequency distribution generated by the interaction of these parameters must be known. Although the variation of the inputs was known approximately, it was not possible to predict the interaction of the variables theoretically. Hence the deterministic model was revised as a probabilistic simulation of the experience of an herbivore in an area contaminated by ^{131}I, and the simulation was programmed for IBM-7094 computer solution.

The revision is a discrete version of the deterministic model, with an interval of one day between meals. When the interval is zero, as if feeding were continuous, the discrete version is identical with the continuous. The advantage of the discrete version is that it facilitates the simulation of the feeding experience of a group of individuals over a period of time. The purpose of designing the stochastic version of the model is to permit the variables to take on different values and to examine the influence of chance variation in the inputs on the predictions of the model.

It is easier to visualize the stochastic model if one considers what occurs when an herbivore occupying a fallout field consumes a series of meals, each containing a varying amount of ^{131}I. Ultimately one wishes to estimate the amount of ^{131}I, A, in the thyroid of the consumer at the end of some arbitrarily defined period of time. For example, the amount of thyroid ^{131}I after 30 days is the sum of 30 terms. Each term represents the ^{131}I remaining in the thyroid from one of 30 meals. From a given meal containing ^{131}I, some fraction, F, is absorbed and reaches the thyroid. The 30-day thyroidal uptake of the nuclide may be given as follows:

$$F(D_1C_1 + D_2C_2 \ldots + D_{30}C_{30}) \qquad (1)$$

where D_i is the number of grams of food consumed and C_i is the amount of ^{131}I per gram of food. This series does not represent the amount in the thyroid after 30 days. The ^{131}I that reaches the thyroid is lost by both secretion and radioactive decay; therefore it declines exponentially with an effective half-life reflecting these two processes. Hence the amount that reaches the thyroid on the first day is reduced by the end of 30 days to

$$FD_1C_1E^{30} \tag{2}$$

where E equals $(1/2)^{1/b}$ and b, the effective half-life of ^{131}I in the thyroid in days, equals $0.693/\lambda_E$. The term $e^{\lambda_E t}$ equals E^t. The amount ingested on the *ith* day after fallout and remaining 30 days afterward is

$$FD_iC_iE^{30+1-i} \tag{3}$$

The required series for 30 days is thus

$$A = FD_1C_1E^{30} + FD_2C_2E^{29} \ldots + FD_{30}C_{30}E \tag{4}$$

So far C_i has been taken as the amount of ^{131}I per gram of food at the time of consumption. Yet we wish to derive C_i from the amount deposited on vegetation on the first day. The loss of ^{131}I from vegetation is approximately exponential, but the effective half-life, v_i, varies from day to day. The relation between the amount of ^{131}I on vegetation consumed on the second day and the original amount on vegetation may be expressed as

$$C_2 = x_2V_1 \tag{5}$$

where x_2 is the original amount of ^{131}I on the vegetation making up the meal consumed on the second day and

$$V_1 = (1/2)^{1/v_1} \tag{6}$$

On the *ith* day, the relation would be

$$C_i = x_iV_1V_2V_3 \ldots V_{i-1} \tag{7}$$

or

$$C_i = x_i \prod_{j=1}^{i-1} V_j \tag{8}$$

The expression for A given in Eq. 4 can now be rewritten

$$A = F\left(D_1x_1E^{30} + D_2x_2V_1E^{29} + D_3x_3V_1V_2E^{28} \ldots + D_{30}x_{30}E \prod_{j=1}^{29} V_j\right) \tag{9}$$

It is now necessary to assign distributions to the variables, which are assumed to be probabilistically independent. Thyroidal uptake of ingested ^{131}I, F, and the effective half-life of this ^{131}I in the thyroid, b, are considered constant for any individual, but they differ among individuals. The term F was chosen randomly from 114 values ranging from 0.05 to 0.35 (see Table 1). The nature of the distribution was inferred from the work of French.[15] The value of b (days) was chosen randomly from the following distribution: 1.5, 2.0, 2.0, 2.5, 2.5, 2.5, 3.0, 3.0, and 3.5. The values of D_i and v_i change from day to day. The value of D_i (grams) was chosen at random from the following distribution: 80, 90, 90, 100, 100, 100, 100, 110, 110, and 120. The value of v_i (days) was similarly selected from the following distribution: 5.0, 5.33, 5.33, 5.5, 5.5, 5.5, 5.75, 5.87, 6.0.

Table 1—FREQUENCY DISTRIBUTION ASSIGNED TO F IN THE OPERATION OF THE PROBABILISTIC MODEL

Number of cases	Value assigned to F	Number of cases	Value assigned to F
2	0.05	6	0.19
3	0.06	5	0.20
3	0.07	4	0.21
3	0.08	3	0.22
4	0.09	3	0.23
5	0.10	2	0.24
5	0.11	2	0.25
7	0.12	2	0.26
7	0.13	1	0.27
8	0.14	1	0.28
9	0.15	1	0.29
10	0.16	1	0.31
8	0.17	1	0.32
7	0.18	1	0.35

In the preceding discussion the successive amounts of ^{131}I per gram of vegetation consumed have been expressed as functions of $x_1 \ldots x_{30}$. So we must now consider the nature of the distribution of ^{131}I per gram on the first day. Let this distribution be represented by values of x. A typical distribution of x (based on 41 values from Penoyer Valley, about 40 miles from ground zero) and the distribution of X (equals log x) are portrayed in Fig. 1. Because of its shape, the distribution of X was assumed to be normal, with mean and variance equal to the mean and variance of the sample values of X. The means and variances of four such distributions of X are given in Table 2 (see Fig. 2 for locations of sampling areas with regard to the Nevada Test Site).

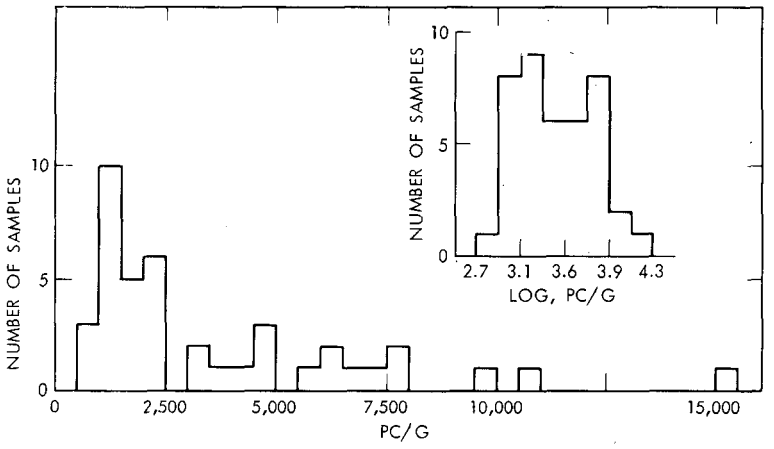

Fig. 1—Estimated distribution of ^{131}I on vegetation in Penoyer Valley on July 6, 1962.

Because x is equal to 10^X, 30 values of $X_1 \ldots X_{30}$ were selected at random from normal distributions (as defined in Table 2), and the antilogarithms of these numbers defined the values of x_i (with i = 1 to 30).

The simulation was programmed in the following form:

$$A = F \sum_{i=1}^{n} E^{n+1-i} D_i 10^{X_i} \prod_{j=1}^{i-1} V_j$$

where E is equal to $(\frac{1}{2})^{1/b}$ and V_j is equal to $(\frac{1}{2})^{1/v_j}$. After four days this expression (in expanded form) would be

$$A = F[E^4 D_1\ 10^{X_1} + E^3 D_2 10^{X_2} V_1 + E^2 D_3 10^{X_3}(V_1 V_2) + E D_4 10^{X_4}(V_1 V_2 V_3)]$$

Thus the daily decline in ^{131}I on vegetation is simulated and day to day variations in the rate of loss are permitted to occur by chance. Most important, the initial amount per gram of food is permitted to vary. An herbivore feeding at random in a fallout field will consume heavily contaminated foliage on some days and lightly contaminated food on others. The 30-day experience of a single hypothetical consumer was simulated in the manner described. Only the cumulative totals of thyroid ^{131}I at 5, 10, 15, 20, 25, and 30 days were printed out. Through repetition of this procedure, distributions representing synthetic populations of consumers were built up by the computer.

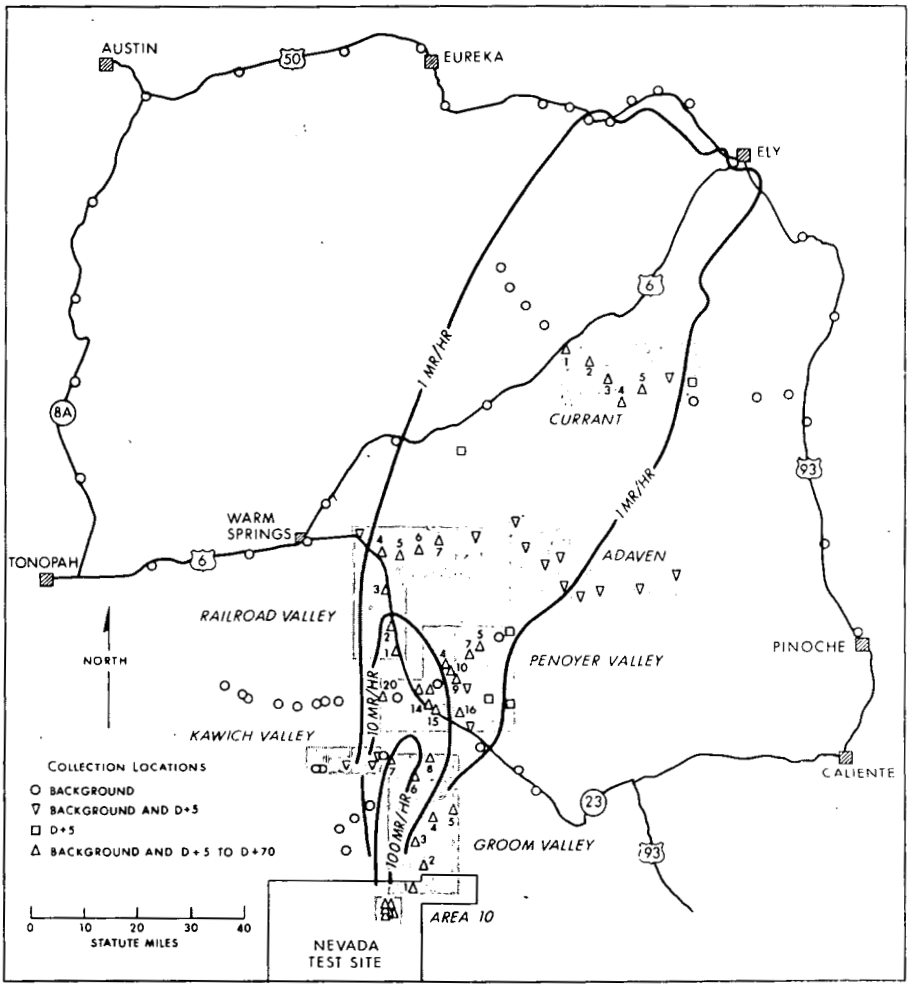

Fig. 2—Location of sampling stations in Nevada within the Sedan fallout pattern, July to September 1962.

RESULTS

Figure 3 shows four representative frequency distributions of 100 individuals based on measurements of ^{131}I in bulk samples of vegetation (see Table 2). Each distribution constitutes a prediction for specific time and locality. All the distributions are asymmetrical and skewed to the high side. Figure 4 shows four distributions of 1000 individuals predicated on the same data. These distributions are not as irregular as those shown in Fig. 3, but they still show an evident skewing. Over

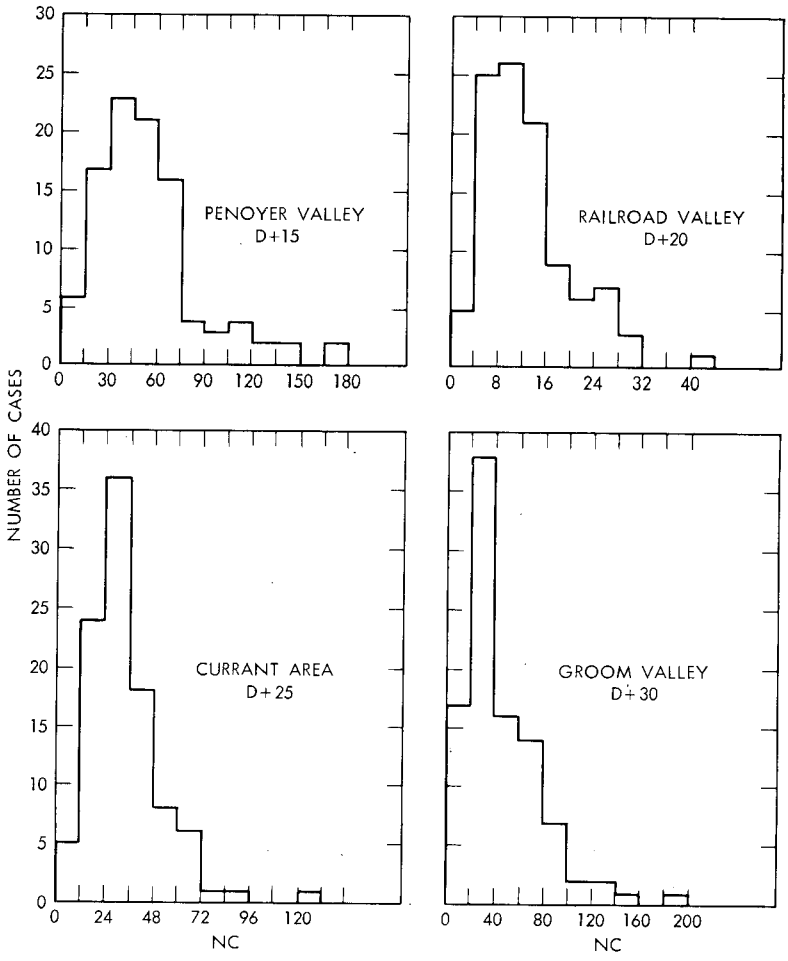

Fig. 3—Four synthetic distributions of 100 cases based on measurements of ^{131}I in vegetation samples from four areas in southern Nevada.

70 distributions were generated by the computer—some based on ^{131}I measurements of stomach contents and others on measurements of ^{131}I in bulk samples of plants—and all were skewed. When the logarithms of the values were plotted, the curves tended to be symmetrical. Figure 5 shows the frequency distribution of the logarithms of the numbers tabulated in Fig. 3 as Groom Valley D + 30. When this distribution is compared to a normal distribution with the same mean and variance, the total X^2, with seven degrees of freedom, is 5.30 ($X^2_{0.05}$ = 14.07).

Statistical attributes of 24 synthetic distributions are shown in Table 3. As may be seen, the fractions of these populations exceeding

Table 2 — ESTIMATED ^{131}I ON VEGETATION IN FOUR AREAS IN SOUTHERN NEVADA AS OF JULY 6, 1962*

	Mean of logs	Variance	Arithmetic mean of distribution, pc/g	Size of sample
Groom Valley				
Vegetation	4.075	0.228	17,481	30
Stomach contents	3.611	0.272	6,533	27
Penoyer Valley				
Vegetation	3.428	0.120	3,695	41
Stomach contents	3.488	0.100	3,930	36
Railroad Valley				
Vegetation	3.184	0.017	1,656	29
Stomach contents	3.218	0.058	1,980	25
Currant Area				
Vegetation	2.825	0.110	890	31
Stomach contents	2.494	0.100	414	25

*Estimates are based on decay corrections of bulk samples of vegetation and of stomach contents of jackrabbits ($\lambda = 0.126$). The antilogarithm of the mean of the logs is the geometric mean of the distribution and is not the same as the arithmetic mean.

three times the mean are invariably small, usually less than 2%. An analysis of actual observations gave similar results. In only 2 of 133 jackrabbits (in 24 samples of 5 to 9 individuals) did the thyroid ^{131}I level of an individual exceed three times the sample mean.

There is no doubt that, when the model is used in the manner defined, it predicts skewed frequency distributions of ^{131}I in populations of consumers. But how well do the predicted distributions agree with observed frequency distributions? Unfortunately, our 1962 data simply are not sufficient to make such comparisons. From a given locality (for a specific time) few animals were taken, and no convincing comparisons involving theoretical distributions of 100 or 1000 individuals and observations of less than 10 can be made.

However, most of the observed distributions suggested asymmetry, with a few very high values, as compared with the median. For example, two samples are indicated in Table 4. Figure 6 shows these observations, as well as normal and lognormal distributions based on the mean and variances of the two samples. The high values observed in both samples are more probable if the distribution is lognormal than if it is normal.

DISCUSSION

Although it is difficult to support some of the theoretical predictions of the model from observations during 1962, other work on frequency

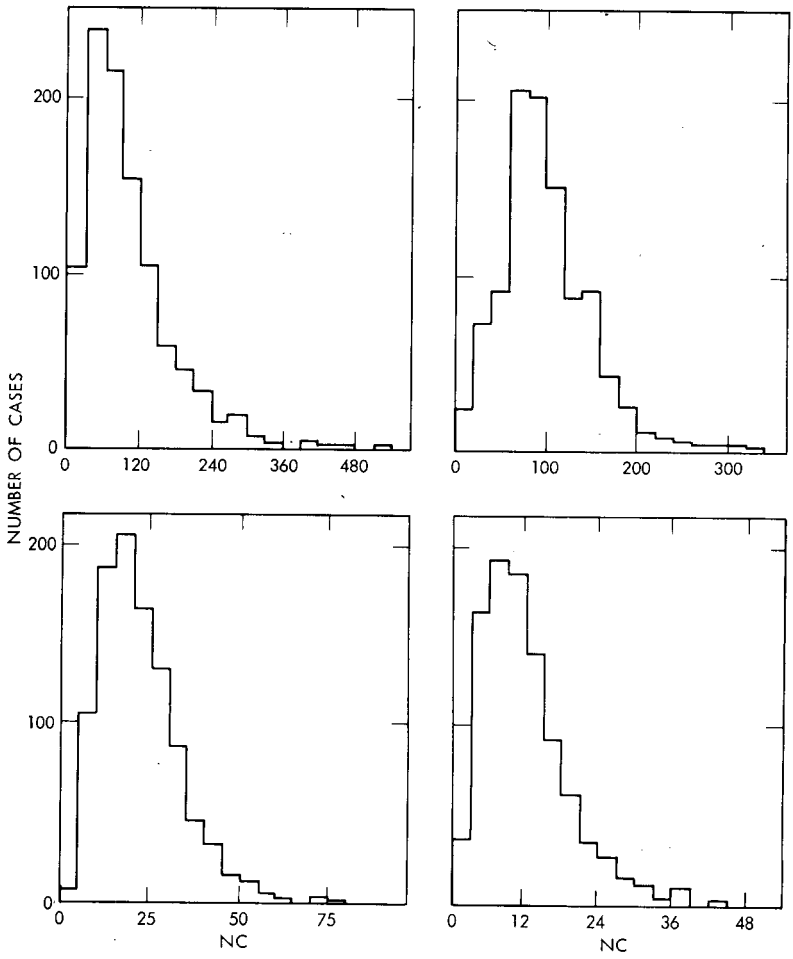

Fig. 4—Four synthetic distributions of 1000 cases based on measurements of ^{131}I in vegetation samples.

distributions of radionuclides in consumers is pertinent to this problem. Of particular interest is the shape of such distributions. If these distributions are skewed to the high side, or lognormal, then both statistical analyses and predictions based on such data need to be developed with this fact in mind.

In 1956 Turekian and Kulp[20] discussed the frequency distribution of stable strontium in human bone. They concluded that the strontium/calcium ratio approximated a normal distribution, even though there was evident skewing to the high side. Anderson et al.[21] have indicated that ^{40}K and ^{137}Cs in human populations are normally distributed. Both of the histograms appear symmetrical, although the distribution of

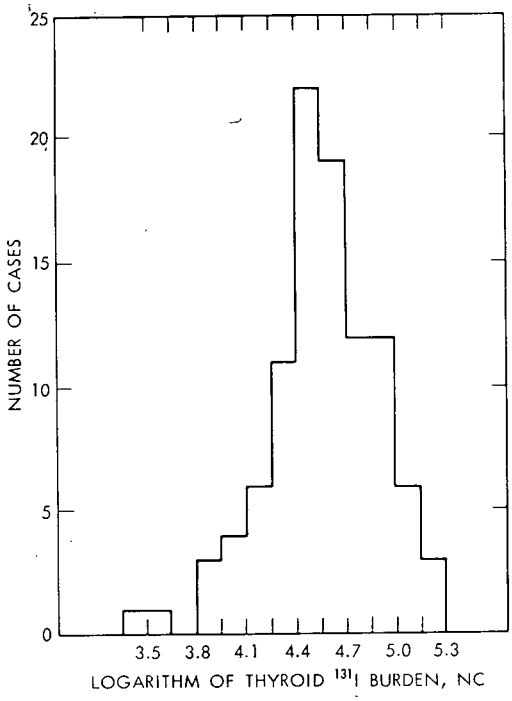

Fig. 5—Distribution of the logarithms of the values portrayed in Fig. 3 as Groom Valley D + 30.

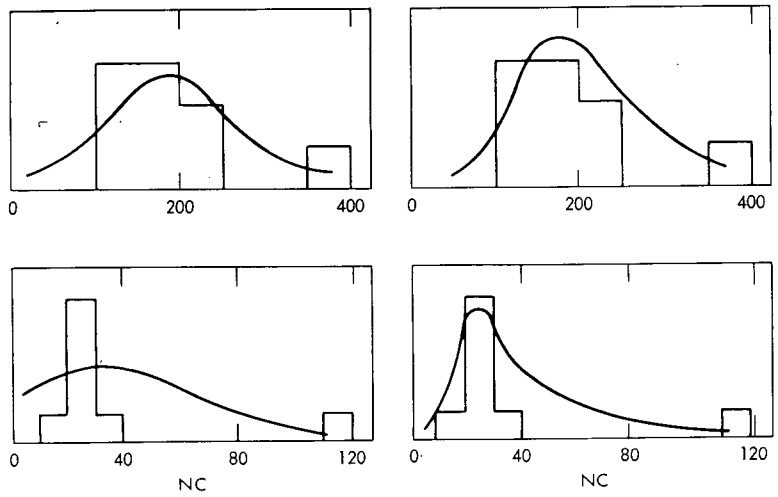

Fig. 6—Normal (left) and lognormal (right) distributions fitted to observations of ^{131}I in thyroids of jackrabbits from Penoyer Valley during July 1962.

Table 3—SOME STATISTICAL ATTRIBUTES OF SYNTHETIC POPULATIONS OF 1000 INDIVIDUALS GENERATED BY A PROBABILISTIC MODEL OF ^{131}I FOOD-CHAIN TRANSFER (MEAN, MAXIMUM, AND MINIMUM INDICATE NANOCURIES OF ^{131}I IN THYROIDS OF HERBIVORES)

Area	D + days	Mean	Standard deviation	Standard error of mean	Maximum	Minimum	Range	Population exceeding three times the mean, %
Groom	5	585.4	487.3	15.4	4611.4	52.1	4559.3	1.2
Valley	10	479.1	364.4	11.5	3785.7	31.6	3754.1	2.6
	15	295.7	205.8	6.5	1359.2	23.5	1335.7	1.9
	20	174.1	124.5	3.9	1238.6	5.3	1233.3	1.4
	25	99.6	71.5	2.3	511.3	5.6	505.7	2.1
	30	54.2	39.4	1.2	330.0	3.5	326.5	2.0
Penoyer	5	99.7	62.6	2.0	413.3	13.5	399.8	1.5
Valley	10	79.6	46.5	1.5	319.7	7.8	311.9	0.7
	15	50.1	31.1	1.0	240.8	2.8	238.0	1.3
	20	29.0	18.4	0.6	111.8	2.2	109.6	1.5
	25	16.1	10.4	0.3	74.1	1.4	72.7	1.4
	30	8.8	5.9	0.2	58.7	0.9	57.8	1.0
Railroad	5	43.9	19.1	0.6	136.4	7.2	129.2	0.1
Valley	10	35.0	16.9	0.5	121.0	5.7	115.3	0.2
	15	21.9	11.3	0.4	79.9	3.0	76.9	0.4
	20	12.7	7.0	0.2	51.1	2.0	49.1	0.7
	25	7.1	4.1	0.1	28.4	0.9	27.5	1.2
	30	3.9	2.3	0.08	15.9	0.5	15.4	1.3
Currant	5	25.0	16.1	0.5	117.0	1.5	115.5	1.5
Area	10	19.3	11.7	0.4	77.5	2.3	75.2	1.3
	15	12.1	7.4	0.2	47.7	1.1	46.6	1.0
	20	7.0	4.3	0.1	29.0	1.0	28.0	1.2
	25	3.9	2.5	0.08	16.8	0.3	16.5	1.3
	30	2.1	1.4	0.04	10.0	0.2	9.8	1.3

^{40}K is slightly skewed. Libby[4] cited these last two papers, as well as work by Palmer and Queen[22] with ^{226}Ra in human bone, and data pertaining to ^{90}Sr in bones of stillborn children in Chicago. Libby stated: "All these data show a normal frequency distribution...," and "It is completely clear...that the distributions agree with one another in general shape...." Langham[23] repeated these contentions in considering worldwide hazards from ^{90}Sr in fallout.

From four of the distributions discussed above, normal distributions with means and variance equal to those of the samples considered have been constructed (the ^{226}Ra data were taken from a later paper by Palmer and Queen[24]). The observed distributions have been compared with the theoretical ones, and the results of X^2 tests are shown in Table 5.

The data of Turekian and Kulp have already been reviewed by both Dahl[26] and Neuman.[6] Dahl compared the observed distributions with appropriate normal and lognormal distributions and showed that the observations were in much better accord with the latter. The X^2 test shown in Table 5 confirms that the observed distribution is not normal. About one-third of the total X^2 for the ^{40}K distribution was due to a few unusually high values, reported to have been caused by surface contamination during periods of tropospheric fallout.[21] Hence the nature of this distribution is unclear. There is no reason to conclude

Table 4 — ANALYSES OF THYROID ^{131}I IN TWO SAMPLES OF JACKRABBITS TAKEN IN PENOYER VALLEY DURING JULY 1962

	July 16	July 26
Observations, nc ^{131}I per thyroid	388, 209, 205, 195, 172, 170, 130, 115, 106	117, 37.1, 29.2, 28.6, 26.1, 20.9, 20.7, 12.6
Number	9	8
Arithmetic mean	187.7	32.4
Variance	7097	1103
Geometric mean	174.5	29.1
Variance of logarithms of observations	0.0287	0.0789

Table 5 — COMPARISON OF FOUR OBSERVED FREQUENCY DISTRIBUTIONS WITH NORMAL DISTRIBUTIONS OF THE SAME MEAN AND VARIANCE

Reference	Size of sample	Radio-nuclide	Total X^2	Degrees of freedom*	$X^2_{0.05}$	P
Turekian and Kulp[20]	227	^{90}Sr	56.23	10	18.31	<0.001
Anderson et al.[21]	254	^{40}K	27.31	9	16.92	0.001
Libby[4]	53	^{90}Sr	7.86	8	15.51	0.4 to 0.5
Palmer and Queen[24]	50	^{226}Ra	7.53	3	7.81	0.06

*Taken as n − 3, where n is equal to the number of intervals in the frequency distribution.[25]

that the other two distributions tested are not normal, although data of Bryant et al.[27] indicated a non-Gaussian distribution of strontium/calcium ratios in British stillborn.

More recently, other evidence has accumulated indicating that frequency distributions of radionuclides in consumers are not normal. Walton et al.[28] and Muth et al.[29] have studied the concentration of ^{226}Ra in human skeletons. In both investigations the observed frequency distributions were non-Gaussian, and Walton et al. stated that the distribution they observed was lognormal (see also Kulp and Schulert[30]). Onstead et al.[31] have determined the amount of ^{137}Cs in 751 men and 259 women. A comparison of these distributions with appropriate normal distributions implies that the observations are not distributed normally (Table 6). However, when a logarithmic probability plot of the cumulative frequency distribution of ^{137}Cs in all 1010 subjects is made, a straight line results (see Fig. 7). This indicates that the distribution is lognormal. Similarly, Yamagata[32] has stated that the frequency distribution of natural ^{133}Cs in 78 samples of human muscle is lognormal.

Table 6—COMPARISONS OF THREE OBSERVED FREQUENCY DISTRIBUTIONS OF ^{137}Cs IN HUMANS WITH APPROPRIATE NORMAL DISTRIBUTIONS*

Subjects	Size of sample	Total X^2	Degrees of freedom	$X^2_{0.05}$	P
Men	751	79.62	18	28.87	<0.001
Women	259	25.63	12	21.03	0.01 to 0.02
Combined	1010	66.98	19	30.14	<0.001

*Based on Onstead et al.[31]

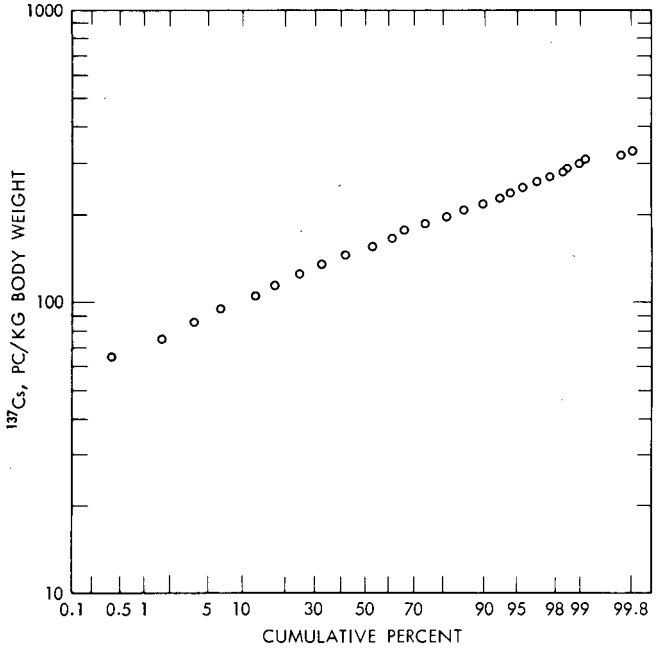

Fig. 7—Cumulative frequency distribution of ^{137}Cs in 1010 humans (based on Onstead et al.[31]).

Unpublished data from our laboratory suggest that non-Gaussian distribution of radionuclides in populations of wild animals exposed to local fallout are more common than symmetrical ones. Figure 8 shows the evidently skewed distribution of ^{90}Sr in 55 jackrabbits (*Lepus californicus*) collected from Jackass Flats, Nev., in 1959. When the distribution is compared with a normal distribution of the same mean and variance, the total X^2, with four degrees of freedom, is 17.05 ($X^2_{0.05} = 9.49$). However, the logarithms of these observations

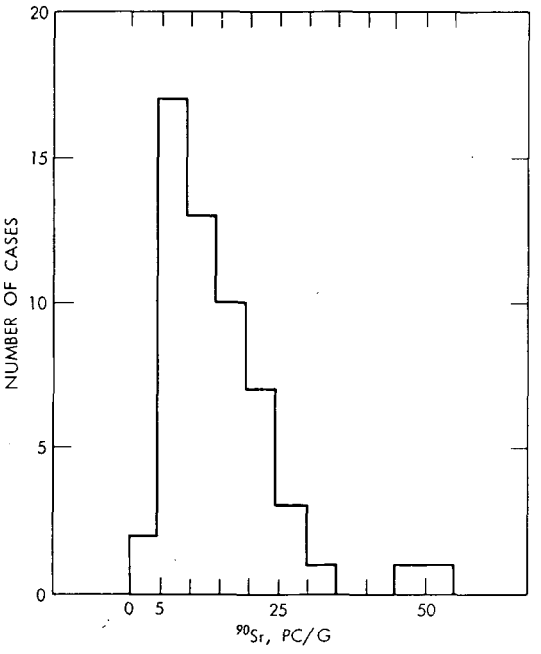

Fig. 8—Frequency distribution of bone ^{90}Sr in 55 jackrabbits from Jackass Flats, Nev.

are normally distributed. The total X^2, with seven degrees of freedom, is 2.57 ($X^2_{0.05} = 14.07$).

It may also be noted that Snyder and Cook[33,34] have analyzed the frequency distributions of a number of stable trace elements in human tissues (e.g., cadmium, copper, zinc, aluminum, and iron) and concluded that all distributions are skewed to the right, with the sample means exceeding the sample medians.

It is clear then that radioelements and trace elements in the tissues of the individuals constituting a population do not always exhibit normal distributions. In fact, normal distributions may prove to be unusual. It is suggested here that a more likely expectation is a non-Gaussian distribution skewed to the high side and often normal following a log transformation. Another possibility is given by Ellett and Brownell,[7] who analyzed measurements of ^{137}Cs in 878 samples of human muscle collected between 1959 and 1963. By normalizing the data to eliminate the time variation, they were able to construct a probability histogram based on 670 samples. This histogram was clearly asymmetrical and skewed to the high side. Although a X^2 test indicated a probability of less than 1% that the distribution was log-normal, Ellett and Brownell found that their observations could be well fitted to a gamma distribution.

For certain statistical treatments involving such distributions, a data transformation may be desirable. However, the most important feature of distributions skewed to the high side is that the number of individuals exceeding the mean is greater than expected in a normal distribution of the same mean and variance. For example, it has been pointed out that, with the data of Turekian and Kulp to fix the standard deviation and with the assumption of a mean ^{90}Sr level of 10 pc ^{90}Sr/g Ca for the population, the percentage of the population exceeding twice the mean is 0.6 for a normal distribution and 5 for a lognormal distribution.[35] Table 7 shows a similar comparison taken from Neuman.[6]

Table 7—NUMBER OF PEOPLE EXPECTED TO HAVE ^{90}Sr BONE BURDENS EXCEEDING 100 PC ^{90}Sr/G Ca, ASSUMING NORMAL AND LOGNORMAL DISTRIBUTIONS OF ^{90}Sr IN THE WORLD POPULATION*

Average ^{90}Sr in world population, pc ^{90}Sr/g Ca	Number of people	
	Normal distribution	Lognormal distribution
50	3,000,000	100,000,000
35	1,000	8,000,000
25		100,000

*From W. F. Neuman, *Bull. Atomic Scient.*, *14:* 31-34 (1958).

The observations and theoretical predictions regarding ^{131}I which are set forth in this paper are consistent with the recommendation of the Federal Radiation Council. Snyder and Cook[33,34] have also adduced support for this assumption. However, the probability of individuals exceeding three times the population mean is apparently by no means as remote as stated by Libby: "...at steady state among people living in a given locality only one person in about 700 will have more than twice the average Sr^{90} burden, and the chances of anyone having as much as three times the normal burden will be about one in twenty million."[4]

Why do non-Gaussian distributions arise? Are they simply a reflection of diet? Clearly, levels of radionuclides in consumers must be generally correlated with intake. We do not expect to find high levels of ^{90}Sr in areas where foods are known to be low in ^{90}Sr, or vice versa. However, to say that high levels of dietary ^{90}Sr are associated with high levels of bone ^{90}Sr implies nothing about the influence, if any, of the frequency distribution of ^{90}Sr in a large number of individual diets on the frequency distribution of ^{90}Sr in the bones of the consumers of these diets.

This problem has been approached theoretically by means of the probabilistic model described above. It will be recalled that the dis-

tribution of ^{131}I from local fallout on plants was prescribed as lognormal. (Whether lognormal distributions are characteristic of materials deposited in stratospheric fallout is not known, but Osburn[36] has pointed out that gross beta activity from stratospheric fallout in Colorado alpine environments is lognormally distributed). Did the use of lognormal distributions of ^{131}I on plants give rise to the asymmetrical distributions predicted in consumer populations, or is the frequency distribution of a radioisotope in a population largely independent of the distribution of the substance in the diets of the consumers? As of now, these questions cannot be resolved. If the first of the alternatives is true, then non-Gaussian distributions of radionuclides in consumer populations may simply reflect the distribution of such substances in the environment.

Ahrens[37] has maintained that trace elements (e.g., thorium) are lognormally distributed in granitic rocks. Rogers and Adams[38] have confirmed these observations and have developed a model that predicts lognormal distributions of rock materials present in low concentrations. Thus there is a theoretical basis for expecting naturally occurring radioelements (such as thorium and ^{226}Ra) to be lognormally distributed within homogeneous geological bodies. However, there is no obvious relation between the Rogers–Adams model, developed in terms of the fractional crystallization or diffusion of elements in rock, and the deposition of fallout radionuclides.

Regardless of whether skewed frequency distributions of radioelements in consumers arise because of the distribution of these substances in their diets or in spite of it, there is one point pertinent to both arguments. The Rogers–Adams model applies to distributions of elements within homogeneous bodies. Thorium is lognormally distributed in samples from the Conway granite of New Hampshire, but if samples are included from adjoining granites the new distribution is no longer lognormal. In biology, the population is analogous to the homogeneous body of the geologists. Hence, if different populations are combined to create a large composite distribution, there is no way to predict its nature. The distribution may be of almost any form. Kulp et al. give such a distribution (Ref. 39, Fig. 4D, p. 1253); and, as pointed out by the authors, it "...is clearly not normal, nor does it correspond closely to a lognormal pattern." The distribution of ^{90}Sr in the world population may be useful in some endeavors, but it is much easier to attach ecological significance to distributions of radionuclides in consumers from a localized area. For example, the distribution of ^{90}Sr in skeletons from New York City (Ref. 39, Fig. 4A, p. 1253) appears approximately lognormal.

A final problem is whether or not the form of some of the observed distributions is a technical artifact. If values at the low end of a distribution are particularly susceptible to error or are rejected

because of poor counting statistics, the resulting bias could influence the form of reported distributions. No effort has been made in this paper to evaluate the possible role of errors in determining the shape of frequency distributions.

ACKNOWLEDGMENTS

It is a pleasure to acknowledge the generous assistance of Robert I. Jennrich, Department of Preventive Medicine and Public Health, University of California at Los Angeles, in the preparation of this paper. Thanks are also due to Evelyn Read, who programmed the probabilistic model for computer solution. Appreciation is expressed for the excellent assistance of Richard H. Rowland and Bruce W. Kowalewsky in data reduction and analysis. Finally, the helpful comments and criticisms of Thomas G. Hennessy, William A. Rhoads, Norman S. MacDonald, William E. Martin, and Lee L. Eberhardt are gratefully acknowledged.

REFERENCES

1. J. F. Loutit and R. S. Russell (Eds.), The Entry of Fission Products into Food Chains, in *Progress in Nuclear Energy, Biological Sciences,* Series VI, Vol. 3, Pergamon Press, Inc., New York, 1961.
2. R. G. Lindberg, J. T. Scanlon, J. C. Watson, W. A. Rhoads, and K. H. Larson, Environmental and Biological Fate of Fallout from Nuclear Detonations in Areas Adjacent to the Nevada Proving Grounds, Operation Upshot-Knothole, Report WT-812, University of California at Los Angeles, February 1954.
3. R. G. Lindberg, E. M. Romney, J. H. Olafson, and K. H. Larson, Factors Influencing the Biological Fate and Persistence of Radioactive Fallout, Operation Teapot, Report WT-1177, University of California at Los Angeles, January 1959.
4. W. F. Libby, Radioactive Fallout, *Proc. Natl. Acad. Sci. U. S., 43:* 758-775 (1957).
5. M. Eisenbud, B. Pasternack, G. Laurer, Y. Mochizuki, M. E. Wrenn, L. Block, and R. Mowafy, Estimation of the Distribution of Thyroid Doses in a Population Exposed to I^{131} from Weapons Tests, *Health Phys., 9:* 1281-1289 (1963).
6. W. F. Neuman, Uncertainties in Evaluating the Effects of Fallout from Weapons Tests, *Bull. Atomic Scient., 14:* 31-34 (1958).
7. W. H. Ellett and G. L. Brownell, Caesium-137 Fall-out Body Burdens, Time Variation and Frequency Distribution, *Nature, 203:* 53-55 (1964).
8. Federal Radiation Council, Background Material for the Development of Radiation Protection Standards, Report No. 2, September 1961.
9. R. C. Pendleton, R. D. Lloyd, and C. W. Mays, Iodine-131 in Utah During July and August 1962, *Science, 141:* 640-642 (1963).
10. E. Reiss, H. T. Blumenthal, B. Commoner, M. W. Friedlander, J. Klarmann et al., Local Fallout: Hazard from Nevada Tests, *Nucl. Inform., 5:* 1-12 (1963).
11. H. A. Knapp, Iodine-131 in Fresh Milk and Human Thyroids Following a Single Deposition of Nuclear Test Fallout, USAEC Report TID-19266, 1963.

12. W. E. Martin, Loss of I^{131} from Fallout-contaminated Vegetation, *Health Phys., 9:* 1141-1148 (1963).
13. F. B. Turner, Quantitative Relationships Between Fallout Radioiodine on Native Vegetation and in the Thyroids of Herbivores, *Health Phys., 9*(12): 1241-1246 (1963).
14. Joint Committee on Atomic Energy, Eighty-seventh Congress, Radiation Standards, Including Fallout. Summary Analysis, Hearings Before the Subcommittee on Research, Development, and Radiation, June 4-7, 1962.
15. N. R. French, Iodine Metabolism in Wild Jackrabbits, Oklahoma Conference—Radioisotopes in Agriculture, Held April 2 and 3, 1959, Oklahoma State University, USAEC Report TID-7578, pp. 113-121, Associated Midwest Universities, 1959.
16. F. B. Turner and W. E. Martin, Food-chain Relationships of Iodine-131 Following Two Nuclear Tests in Nevada, USAEC Report PNE-236P, University of California at Los Angeles, May 10, 1963.
17. N. R. French and L. Van Middlesworth, Biological Monitoring of Recent Air-borne Fission Products, in *Proceedings of the Second United Nations International Conference on the Peaceful Uses of Atomic Energy, Geneva 1958,* Vol. 18, pp. 516-517, United Nations, New York, 1958.
18. P. O. Currie, U. S. Department of Agriculture, Forest Service Office, Colorado State University, personal communication, Feb. 5, 1963.
19. J. F. Arnold, Forage Consumption and Preferences of Experimentally Fed Arizona and Antelope Jackrabbits, *Ariz. Univ. Agri. Expt. Sta. Tech. Bull., 98:* 51-86 (1942).
20. K. K. Turekian and J. L. Kulp, Strontium Content of Human Bones, *Science, 124:* 405-407 (1956).
21. E. C. Anderson, R. L. Schuch, W. R. Fisher, and W. Langham, Radioactivity of People and Foods, *Science, 125:* 1273-1278 (1957).
22. R. F. Palmer and F. B. Queen, Normal Abundance of Radium in Cadavers from the Pacific Northwest, USAEC Report HW-31242, Hanford Atomic Products Operation and University of Oregon, July 6, 1956.
23. W. H. Langham, Potential Hazard of World-wide Sr^{90} Fallout from Nuclear Weapons Testing, *Health Phys., 1:* 105-124 (1958).
24. R. F. Palmer and F. B. Queen, Normal Abundance of Radium in Cadavers from the Pacific Northwest, *Am. J. Roentgenol., 79:* 521-529 (1958).
25. P. G. Hoel, *Introduction to Mathematical Statistics,* p. 250, John Wiley & Sons, Inc., New York, 1962.
26. E. Dahl, The Dangers from Fall-out Strontium-90 After Atomic Bomb Explosions, English Translation from *Teknisk Ukeblad,* July 4, 1957.
27. F. J. Bryant, E. J. Henderson, G. S. Spicer, M. S. W. Webb, and T. J. Webber, Radioactive and Natural Strontium in Human Bone, United Kingdom Results for 1957, British Report AERE-C/R-2583, May 1958.
28. A. Walton, R. Kologrivov, and J. L. Kulp, The Concentration and Distribution of Radium in the Normal Human Skeleton, *Health Phys., 1:* 409-416 (1959).
29. H. Muth, B. Rajewsky, H.-J. Hantke, and K. Aurand, The Normal Radium Content and the Ra^{226}/Ca Ratio of Various Foods, Drinking Water and Different Organs and Tissues of the Human Body, *Health Phys., 2:* 239-245 (1960).
30. J. L. Kulp and A. R. Schulert, Strontium-90 in Man and His Environment, Vol. II, Analytical Data, USAEC Report NYO-9934, Columbia University, September 1961.
31. C. O. Onstead, E. Oberhausen, and F. V. Keary, Messungen des Kalium- und Cäsium-137-Gehaltes der deutschen Bevölkerung, *Atompraxis, 9:* 337-341 (1960).
32. N. Yamagata, The Concentration of Common Cesium and Rubidium in Human Body, *J. Radiation Res. (Japan), 3:* 9-30 (1962).

33. W. S. Snyder and M. J. Cook, Variability of Relative Organ Concentration of Trace Elements in Human Tissue, *Health Phys.*, *9:* 57-62 (1963).
34. W. S. Snyder and M. J. Cook, The Distribution of Dose Resulting from a Constant Level of Contamination of the Environment by Sr^{90} and various Other Radionuclides, *Health Phys.*, *9:* 417-423 (1963).
35. Government of India, *Nuclear Explosions and Their Effects*, p. 197, The Publication Division, Ministry of Information and Broadcasting, Delhi, India, 1958.
36. W. S. Osburn, Jr., The Dynamics of Fallout Distribution in a Colorado Alpine Tundra Snow Accumulation System, in *Radioecology*, V. Schultz and A. W. Klement, Jr. (Eds.), pp. 51-71, Reinhold Publishing Corporation, New York, 1963.
37. L. H. Ahrens, The Lognormal Distribution of the Elements (A Fundamental Law of Geochemistry and Its Subsidiary), *Geochim. Cosmochim. Acta, 5:* 49-73 (1954).
38. J. J. W. Rogers and J. A. S. Adams, Lognormality of Thorium Concentrations in the Conway Granite, *Geochim. Cosmochim. Acta, 27:* 775-783 (1963).
39. J. L. Kulp, A. R. Schulert, and E. J. Hodges, Strontium-90 in Man III, *Science, 129:* 1249-1255 (1959).

CONTROLLED ENVIRONMENTAL RADIOIODINE TESTS

CLYDE A. HAWLEY, JR.,* and EARL H. MARKEE, JR.†
*Idaho Operations Office, U. S. Atomic Energy Commission, Idaho Falls, Idaho
†U. S. Weather Bureau, National Reactor Testing Station, Idaho Falls, Idaho

ABSTRACT

The Controlled Environmental Radioiodine Tests project consists in a series of planned atmospheric releases of ^{131}I under varying meteorological conditions and in varying chemical forms. The primary objective of the project is to determine the quantitative behavior of ^{131}I as it passes through the air–vegetation–cow–milk–human chain. So far, two releases have been made, a preliminary one over a natural-grass open-range area and the other over an established irrigated pasture. Measurements included deposition velocities, milk to grass activity ratios, half-lives on grass, half-lives in milk, portable-instrument readings relative to contamination levels, and human-thyroid-uptake fractions. This paper compares some of the results of the two releases. Details of the preliminary test have been published;[1] details of the second test have not yet been published.

INTRODUCTION

The Controlled Environmental Radioiodine Tests (CERT) project consists in a series of planned atmospheric releases of radioiodine under varying meteorological conditions and in varying chemical forms. The CERT project is directed toward furnishing radioiodine-behavior information directly applicable to the National Reactor Testing Station (NRTS) and its environs (Fig. 1) in practical ways. These include establishing a basis upon which rapid, accurate decisions can be made during and after an accident situation as an aid to developing realistic NRTS reactor-siting criteria and in the preparation and the

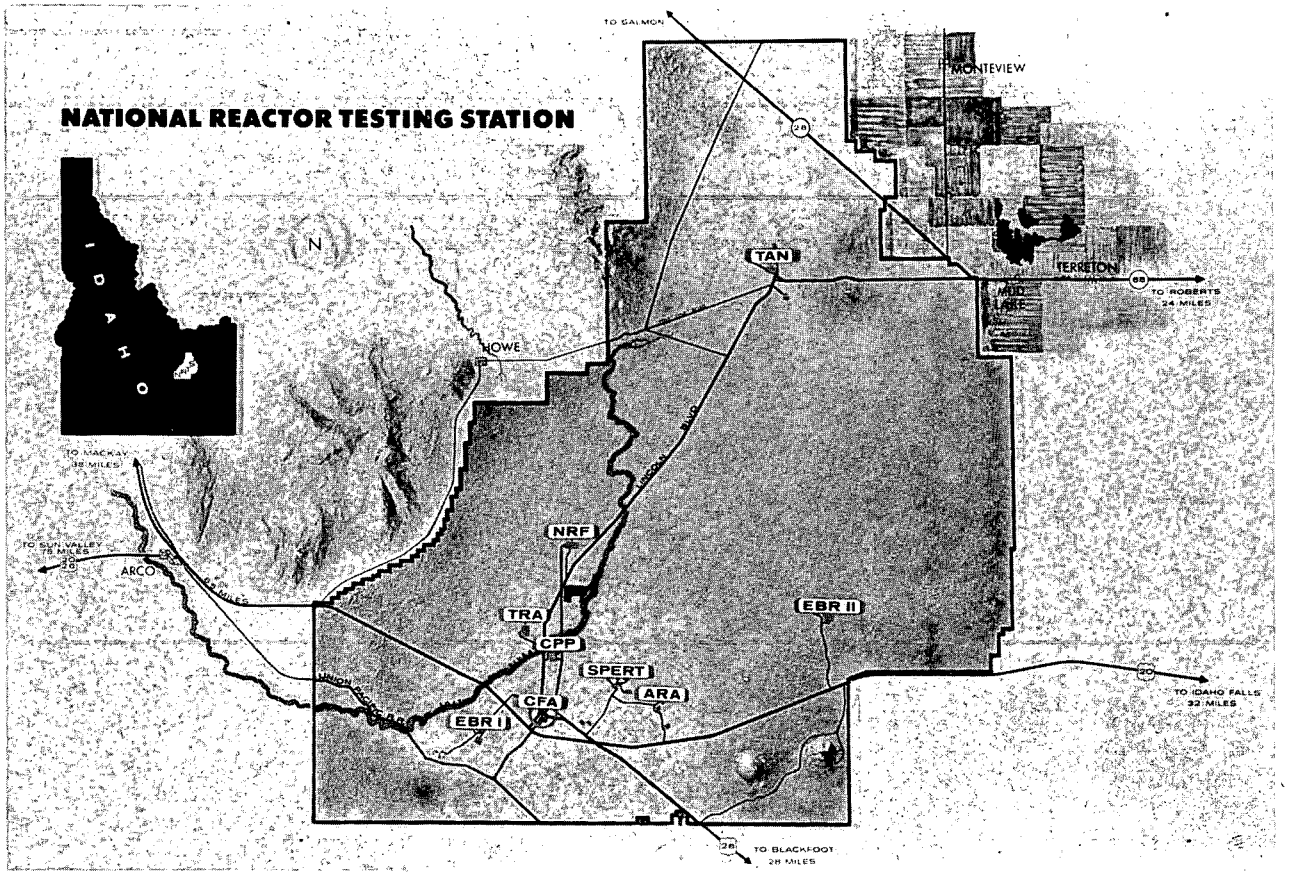

Fig. 1—National Reactor Testing Station and environs. Experimental dairy farm location denoted by cow silhouette between the labels TRA and NRF.

review of safety-analysis reports. The series of experiments will provide some insight into the behavior of radioiodine in general. This paper compares some of the results of the first two releases.*

GENERAL DESCRIPTION OF TESTS AND COMPARISON OF RESULTS

So far, two releases of gaseous molecular ^{131}I have been made. The first, which was made in the spring of 1963, was over a rolling open-range natural-grass terrain (Figs. 2 and 3). The first test was preliminary in the sense that it was necessary to know if the desired information could be gained from the basic experimental design prior to the expenditure of time and money to establish an actual dairy setup in the semiarid desert at the NRTS. The results of the preliminary experiment were encouraging, and therefore the project proceeded. The second test, which was made in September 1964, utilized the same quantities, the same release mechanism, and the same form of ^{131}I; the only major difference was that the iodine was released over an established irrigated pasture (Figs. 4 and 5). This paper is primarily a comparison of the data that were gained as a result of the two releases. Measurements made included deposition velocities, half-lives on the grass, milk to grass activity ratios, milk activities, portable-instrument readings relative to contamination levels, and human-thyroid-uptake fractions. Attempts were also made to measure the mechanisms involved in the differences observed between the physical half-life of the ^{131}I and the observed half-life on the grass. The radioiodine release mechanism was identical in both cases (Figs. 3 and 6). In each case, 1 curie of $Na^{131}I$ was separated into 200-mc aliquots and added to each of five flasks. At release time 10% sodium nitrite was added through the outlets in the suction flasks. This oxidized the iodide into molecular iodine gas. Nitrogen sparging was started, and the flow rates of the nitrogen were adjusted so that the iodine was released over a period of about 30 min. The release rate was monitored through the use of precalibrated Cutie Pie type portable ionization chambers. Final readings indicated that in both cases about 95% of the total radioiodine was released.

Meteorological Conditions

Both tests were made during moderately unstable conditions. The wind speeds were stronger during test 2; the anemometers at the 4-m

*Data resulting from the second release were still being collected at the time of submission of this manuscript. Therefore detailed data, methods of calculation, references to and comparison with other work, and acknowledgments have been intentionally deleted. Full details will be published in an IDO report.

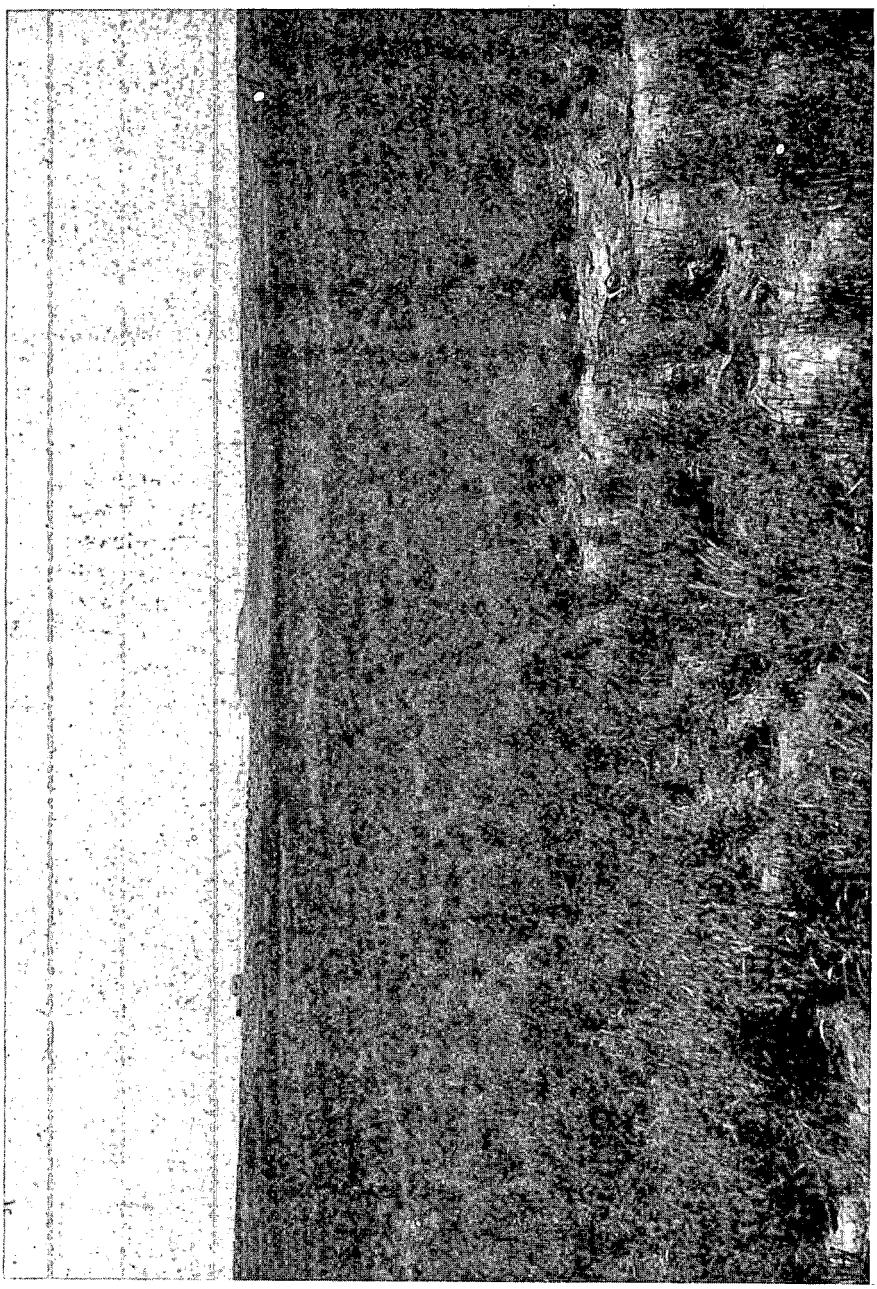

Fig. 2—Crosswind view of first release site showing grass type and density.

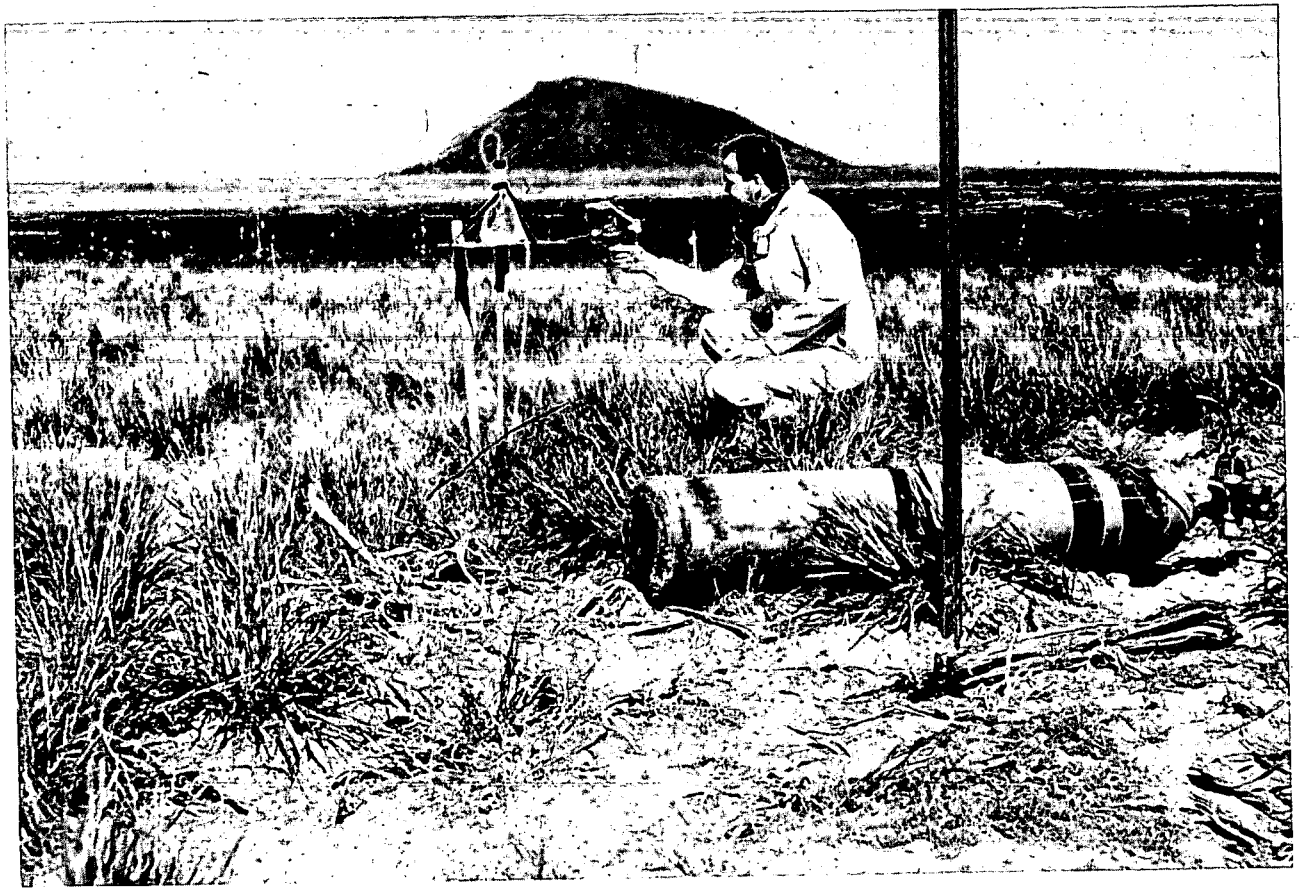

Fig. 3—View of first release site showing release mechanism and terrain features.

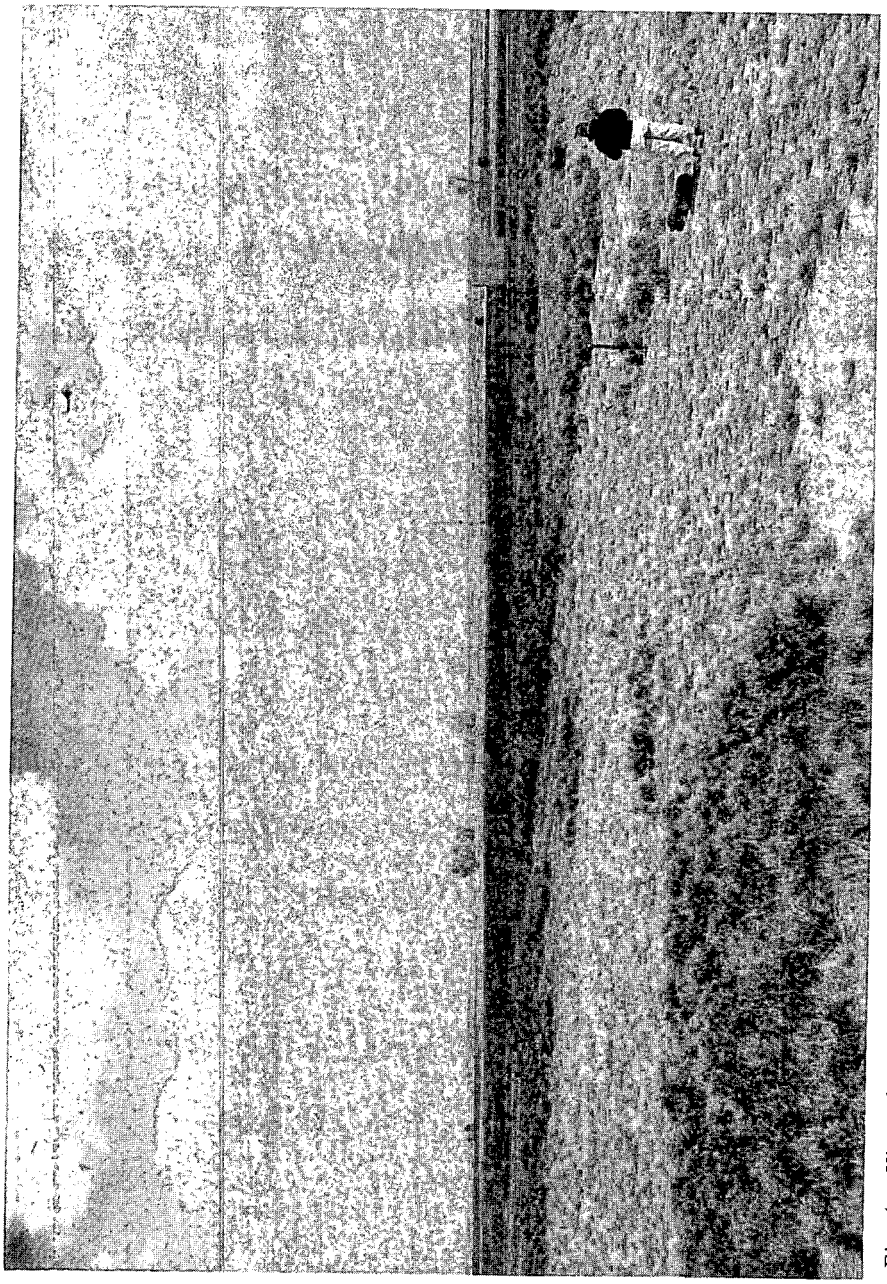

Fig. 4—View of second release site (experimental dairy farm) showing pasture, sampling grid, one release station, and aerial-monitoring airplane.

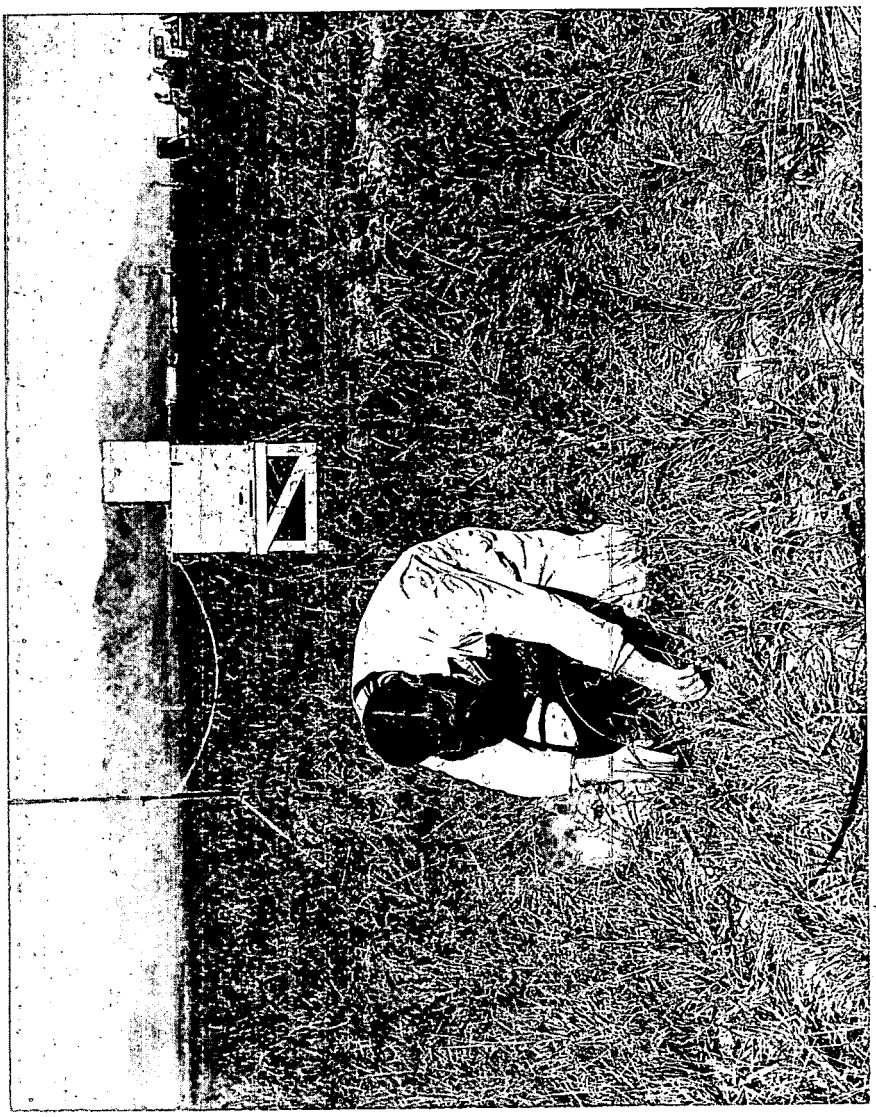

Fig. 5 — View of irrigated pasture showing grass type and density and grass sampling technique. Barn and corrals in background.

Fig. 6—Close-up view of release mechanism.

level indicated average speeds of 7.1 and 9.3 m/sec during tests 1 and 2, respectively. The values of turbulence parameters measured during both tests in terms of horizontal and vertical wind fluctuations were almost identical.

Deposition Velocities

Figures 7 and 8 show the initial distributions of radioiodine deposited on the pastures. The deposition velocities, V_g, on various mediums for both tests are summarized in Table 1.

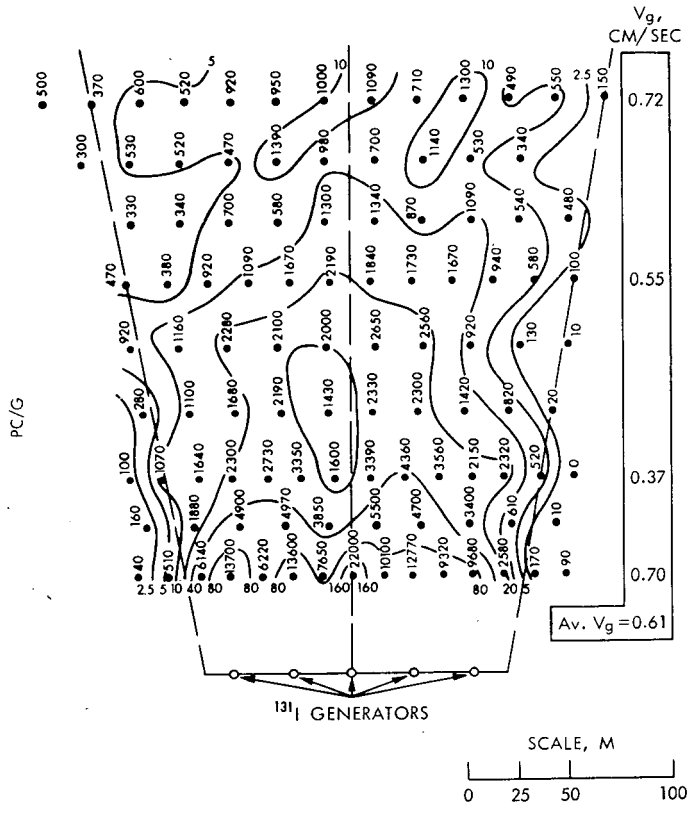

Fig. 7—Diagram of initial deposition of ^{131}I on grass and deposition velocities in first test.

The deposition velocities are generally higher for test 2 except on soil. It is interesting to note that if the grass deposition velocities are divided by their particular average grass densities, 153 and 246 g/m^2 in tests 1 and 2, respectively, the deposition is practically the same

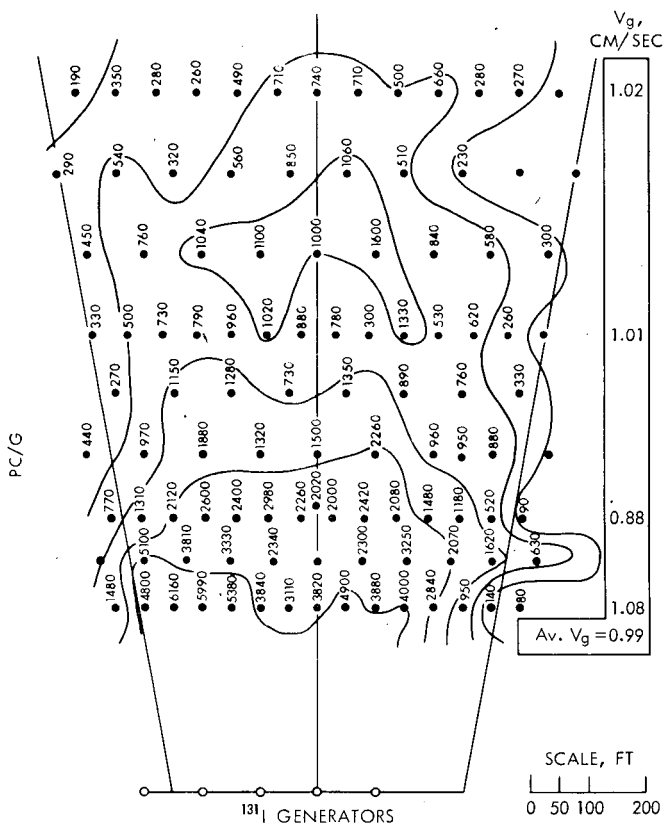

Fig. 8—Diagram of initial deposition of ^{131}I on grass and deposition velocities in second test.

Table 1—SUMMARY OF DEPOSITION DATA

Deposition medium	Deposition velocity, cm/sec	
	Test 1	Test 2
Grass	0.61	0.98
Soil	0.68	0.38
Carbon	0.57	0.73
Sticky paper	0.14	0.41

during both tests. This indicates the strong influence of grass density on the amount of radioiodine deposited per unit area. The soil contamination indicates the same influence, which manifests itself in an inverse relation with grass density. The deposition velocities on carbon plates and sticky paper, which are standard deposition mediums, were

significantly higher for test 2. This suggests that the meteorological factors were different enough between the two tests to influence deposition rates. However, at present, no definite relations to the friction velocity and the mean wind speed have been found.

Half-life on Grass

In the first test no specific area was used to measure the half-life on the grass. The daily samples that were taken to measure the activity consumed by cows were used to develop a half-life figure. This turned out to be between three and four days, whereas in the second test a plot was established which showed the half-life to be between five and six days. This range agrees better with the literature. The method used during the first test was used as a check during the second test. With this system the half-life was between four and five days. Figure 9 shows all three results. The reasons for the disagreements have not been determined.

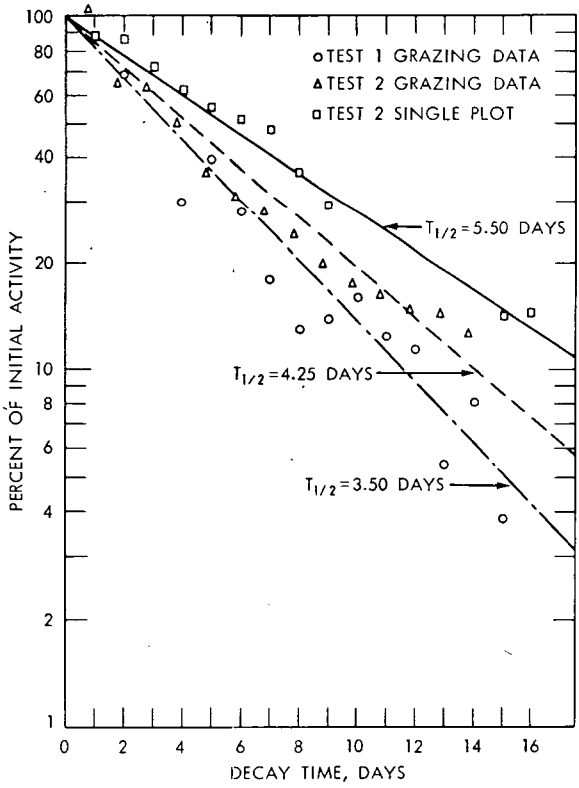

Fig. 9—Half-life of ^{131}I on grass.

Milk Activities

In both tests peak activity in the milk from cows was reached in about two days. During the first test the highest and the lowest activity levels in the milk produced by individual cows were within a factor of 2. In the second test the difference between the highest and the lowest levels was about a factor of 5 (see Fig. 10). The reason for this spread, which is consistent, has not yet been examined.

In the second test all six cows were placed under controlled grazing on hot pasture for two weeks. After this time three of the cows were removed to corrals and fed stored feed. The other three were allowed to graze the entire pasture without control. After five more days all cows were placed on cold pasture. Table 2 shows the half-lives of activity in the milk.

Table 2—HALF-LIVES OF ACTIVITY IN MILK

Period	Cow No.	$T_{½}$, days
Sept. 17 to 20	6	1.03
	28	1.15
	29	0.99
Sept. 22 to 26	8	0.64
	52	0.88
	53	0.74
Sept. 29 to Oct. 2	6	4.8
	8	22.7
	28	2.2
	29	7.9
	52	5.8
	53	8.2

As can be seen from Table 2, milk activity decreases with a half-life of about one day until some time has elapsed (probably about four or five days). The decay scheme then becomes a good deal more complex and may vary widely among individual cows.

Milk to Grass Ratio

One of the objectives of the CERT project is to determine a ratio of consumed activity in terms of curies per gram of ingested forage to the resultant milk activity in terms of curies per liter of milk. If a meaningful comparison is to be reached, the half-life or turnover time in the cow as well as the sampling time increments must be considered.

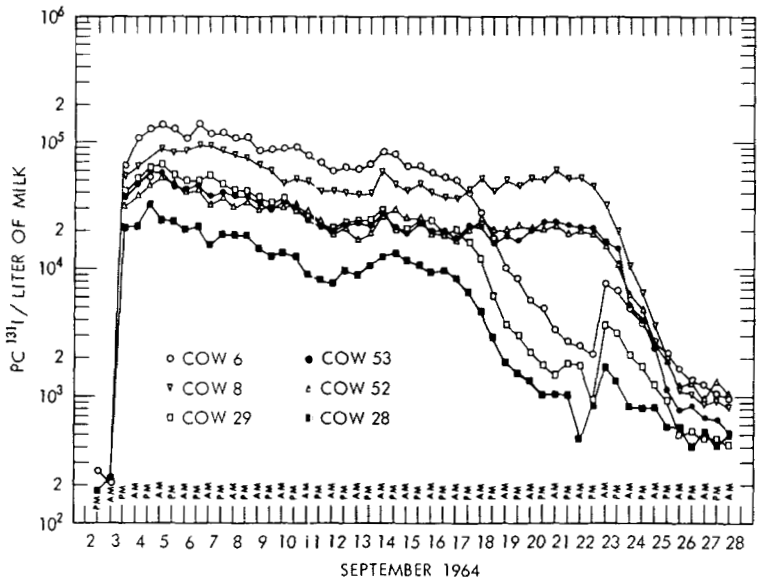

Fig. 10—Milk activities in second test.

For the first four to five days, the half-life in the cow is about one day. The ratios reported here are based on an "effective" number of curies consumed. That is, the grass activity per gram is multiplied by the amount consumed in grams by the average cow. These numbers are then corrected in time. One-half of the first day's activity was used because the sampling period encompassed one whole day, during which time only one-half of the activity ingested by the cow on that day would influence the milk activity levels. Added to this were one-half of the preceding day's activity, one-fourth of the day's before that, etc. The net result is a composite of all the ingested activity that influences the milk activity levels. These ratios should hold true as long as the cow's intake of radioiodine is sustained. The ratio resulting from the wet-weight data from the first test was 240 ± 35, whereas the second test yielded a ratio of 135 ± 20. The reasons for this change of ratio are being investigated.

Portable-instrument Readings

Scintillator readings were taken across the contaminated pasture immediately following the deposition of the radioiodine. Figure 11 shows an apparent linear relation between grass activity and scintillator readings.

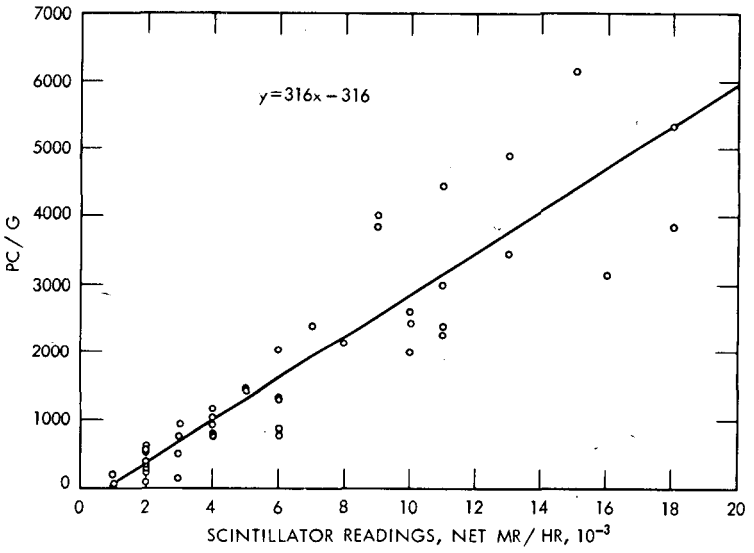

Fig. 11—Portable-scintillator readings vs. grass activity levels.

Human-thyroid-uptake Data

In the first test one cow was selected to furnish milk for human-volunteer consumption. The data from the counting of the human thyroid after ingestion of the milk showed the uptake fraction to be 0.19. In the second test inhalation-thyroid-dose measurements were made on three people who were on the test grid during the time of cloud passage. The infinity thyroid-dose measurements were 14, 7, and 6 mrads, averaging 9 mrads. Based on the thyroid uptake factor of 0.19 observed in the first test, the dose to be expected from ingestion of 1 liter of milk per day from the second test is roughly a factor of 100 greater than the inhalation dose.

FUTURE RELEASES

Later in 1964 a release over dead dry grass is planned. In the spring of 1965, a release is planned in which the behavior of radioiodine under inversion conditions will be investigated. During the summer of 1965, at least two more releases will be made involving different chemical forms of radioiodine.

REFERENCE

1. C. A. Hawley, Jr., C. W. Sill, G. L. Voelz, and N. F. Islitzer, Controlled Environmental Radioiodine Tests at the National Reactor Testing Station, USAEC Report IDO-12035, Idaho Operations Office and U. S. Weather Bureau, June 1964.

INFORMATION INTEGRATION PROJECT OF THE LAWRENCE RADIATION LABORATORY–LIVERMORE PROGRAM ON MAN-MADE RADIATION IN THE BIOSPHERE

ARTHUR R. TAMPLIN and JASON L. MINKLER
Lawrence Radiation Laboratory, University of California,
Livermore, California

ABSTRACT

The mission of the Lawrence Radiation Laboratory–Livermore program is to develop a comprehensive understanding of the implication of radionuclide releases into the biosphere. The Information Integration Project was established as an integral part of this program. In essence, the purpose of this project is to collect, collate, and analyze the existing worldwide literature on fallout and its transfer through the biosphere into man.

Thus this effort can be described as an attempt to facilitate the solution of the mission problems in the shortest period of time with optimum utilization of personnel. It is intended that the project will accomplish this goal by allowing us to complement rather than duplicate current and past research pertinent to the overall problem.

To proceed as expeditiously as possible with the literature survey and analysis, we developed an information-retrieval system as a part of the Information Integration Project. The scientific-literature explosion is a most important national problem. In this respect our experience indicates that information systems are a problem for the scientist and not just for the librarian and that these systems should be manned by scientists who are actively working on the various problems with which the system is concerned. Unless this is so, the system will most likely not be properly problem oriented (classification will

be ambiguous). More important is the consideration that reading and abstracting the literature is a valuable training aid and that this training is lost unless it is applied to the problems of science. Knowledge gained should be knowledge used; we need sources of knowledge, not information cesspools.

INTRODUCTION

Lawrence Radiation Laboratory–Livermore program objectives include (1) more-adequate predictive models to allow prediction of the distribution of radionuclides within the biosphere subsequent to their release under any credible circumstance regardless of the location and (2) countermeasures that will prevent either their access to man or their accumulation or retention in the vital organs and tissues of the body.

To accomplish the objectives of the overall mission, three separate, yet necessarily closely integrated, projects have been established within the Lawrence Radiation Laboratory–Livermore (LRL–L) program: Experimental, Theoretical, and Information Integration. Since this paper is concerned with the Information Integration Project, we will not discuss the other two here except to state that in nature and purpose they are experimental and theoretical approaches to the problems.

INFORMATION INTEGRATION PROJECT

General Aspects

The purpose of this effort can realistically be described as the development of a research tool to facilitate the solution of problems in the shortest period of time with optimum utilization of personnel. It is intended that the Information Integration Project will accomplish the goal by allowing us to complement rather than duplicate current and past research both within and outside U. S. Atomic Energy Commission (AEC) installations. A vast amount of work remains to be done on all aspects of the overall problem of entry into and interaction with the biosphere of radionuclides from whatever source. At the same time a vast amount of work has already been done in various areas; unfortunately the data have never been assembled so that the whole could be analyzed and integrated. Although in some limited cases it may be expedient to do an experiment without consulting the literature, such an approach is unrealistic for a problem of the magnitude contemplated in the LRL–L program. A thorough search, abstraction, and analysis of the past and, on a continuing basis, the current worldwide literature are essential to the program for several reasons:

1. They will assure that no important aspect of the overall problem is overlooked.

2. The integration of data generated in diverse research projects may lead to the solution of problems without lengthy experimentation through the development of theoretical models concerning fallout and related problems. The collection and critical evaluation of worldwide input data and the integration of such data into theoretical models will reveal crucial gaps in our knowledge.

3. The experimental programs can thus be directed toward filling gaps rather than repeating previously recorded efforts. At the same time the existing literature will furnish important guidelines in assuring appropriate experimental design. Some of the gaps will become fruitful areas of investigation for our Bio-Medical Research Group, and others may more appropriately be left to other laboratories within the AEC or elsewhere.

4. Our scientists will not pursue programs that are being adequately investigated by others.

The overall problem of radionuclides in the biosphere can be broken down into three major categories: (1) the source of the nuclide, (2) the transport of the nuclide from the source, and (3) the interaction of the nuclide with the biosphere. The information-retrieval and -integration system will be directed to problems within each of these categories.

Figure 1 is a flow chart of the overall mission problem beginning with the source, proceeding through the transport and interaction phases, and ending with the burden in man. Figure 2 is a further breakdown of the physiology and biochemistry of the interaction phase of the problem.

Source The basis for concern over radionuclides in the biosphere is that they are produced in large quantities in nuclear detonations and reactors. It is therefore essential that we obtain, evaluate, and integrate all data pertinent to concentration, chemical state, or physical state of radionuclides that are produced and could be released to the biosphere. In other words, it is desirable to have an inventory of fission products and induced nuclides that could be produced in any of a variety of situations. Thus all the pertinent literature from past tests must be collected and evaluated along with the literature on laboratory research in this problem area. In addition, a great deal of theoretical study has been applied to this problem area, and the techniques and results of these efforts must be evaluated.

Transport Transport implies conduction of radionuclides away from the source by natural phenomena and includes atmospheric (tropospheric and stratospheric) and water–soil transport. Another very

large and important area in which all pertinent data should be rapidly collected and collated concerns the inventory and mass balance between material injected into the troposphere and its subsequent fallout. This is particularly important with respect to the radionuclides with short and intermediate half-lives.

Interaction with the Biosphere . This aspect of the overall problem undoubtedly contains by far the greatest volume of literature. At the same time it is also the area that will benefit the most from collation and integration of the data. This portion of the problem begins with the scavenging or the collecting of particulate or gaseous materials from the atmosphere by plants and proceeds via the passage of the radionuclides through food chains to man. Since prediction of the effects of radionuclides introduced into ecosystems is eventually desired, it is essential to determine the localization and biological half-lives of the radionuclides within the substructures of organisms. The pertinent data will come both from experiments designed specifically for the problems and from experiments designed for other purposes. Integration of bits and pieces of data from a number of articles will, in many cases, allow the solution of some of the more general problems or point the way to definitive experiments. In this area the approach will be to keep abreast of the current literature on a continuing basis and to pick up the past literature on an element-priority basis. Priority will be established on the basis of half-life, production abundance, and biological significance.

General Description

A scientist approaching the literature with a specific problem in mind is looking for specific kinds of information that result from specific types of experiments. Often his search for such information will be unsuccessful. His second approach to the literature will then involve a search for specific kinds of collateral information that will allow him to arrive at the solution of his problem by analytical means. In each case it is important to note that the scientist is seeking specific pieces of information.

For example, to predict the ^{131}I burden in man, the scientist will need to predict the ^{131}I concentration in cow milk as a function of time after contamination of a pasture by fallout. The first question he will ask the literature is: "Have experiments been done that simultaneously measured the ^{131}I concentration on forage and in cow milk?" As it turns out, the literature is not too productive in this respect; the pertinent papers are mostly concerned with reactor effluent. They do, however, allow the development of a first-order predictive equation. The scientist must, however, search the literature for collateral information to ensure the adequacy of this equation for weapons-test

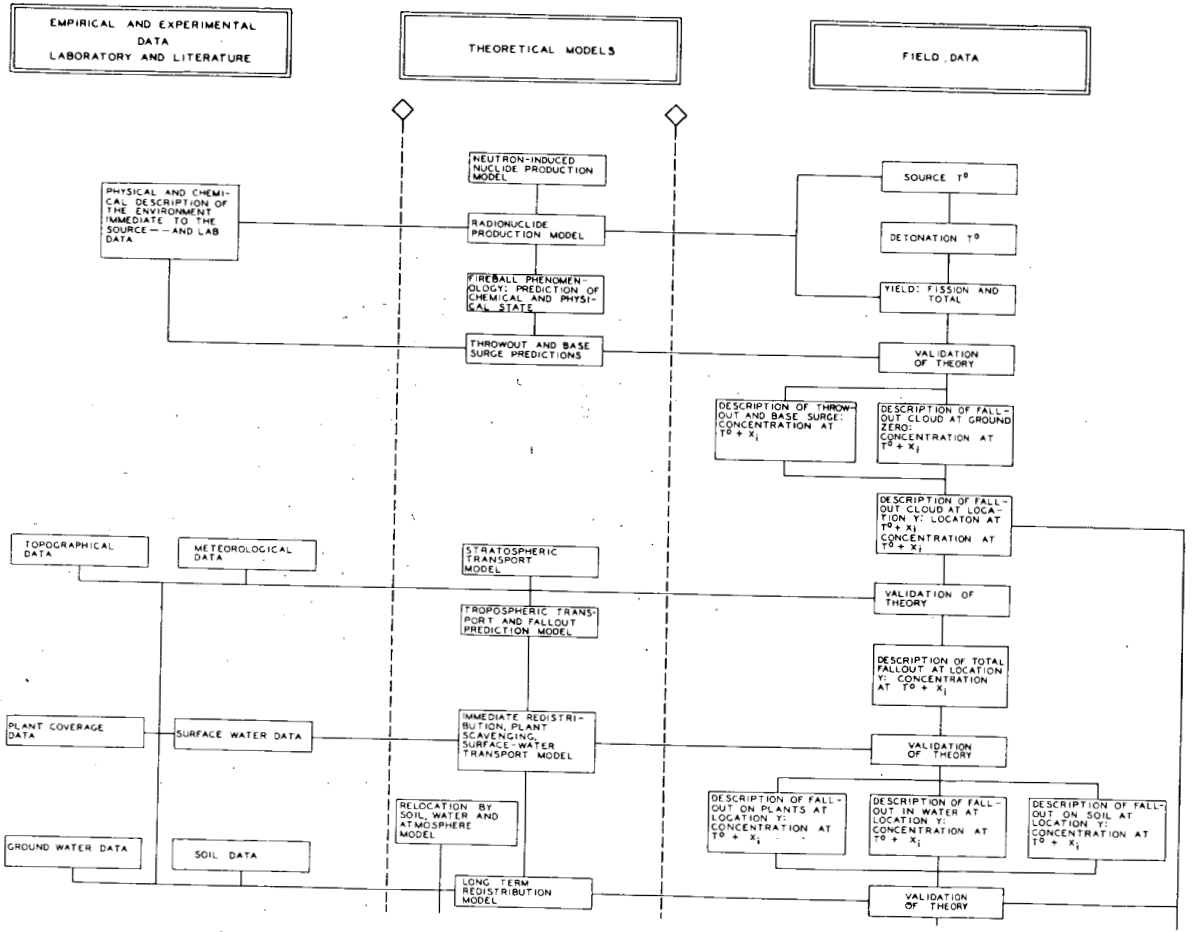
EMPIRICAL AND EXPERIMENTAL DATA LABORATORY AND LITERATURE
THEORETICAL MODELS
FIELD DATA
PHYSICAL AND CHEMICAL DESCRIPTION OF THE ENVIRONMENT IMMEDIATE TO THE SOURCE — AND LAB DATA
NEUTRON-INDUCED NUCLIDE PRODUCTION MODEL
RADIONUCLIDE PRODUCTION MODEL
FIREBALL PHENOMENOLOGY: PREDICTION OF CHEMICAL AND PHYSICAL STATE
THROWOUT AND BASE SURGE PREDICTIONS
SOURCE T⁰
DETONATION T⁰
YIELD: FISSION AND TOTAL
VALIDATION OF THEORY
DESCRIPTION OF THROWOUT AND BASE SURGE: CONCENTRATION AT T⁰ + Xi
DESCRIPTION OF FALLOUT CLOUD AT GROUND ZERO: CONCENTRATION AT T⁰ + Xi
DESCRIPTION OF FALLOUT CLOUD AT LOCATION Y: LOCATON AT T⁰ + Xi CONCENTRATION AT T⁰ + Xi
TOPOGRAPHICAL DATA
METEOROLOGICAL DATA
STRATOSPHERIC TRANSPORT MODEL
TROPOSPHERIC TRANSPORT AND FALLOUT PREDICTION MODEL
VALIDATION OF THEORY
DESCRIPTION OF TOTAL FALLOUT AT LOCATION Y: CONCENTRATION AT T⁰ + Xi
PLANT COVERAGE DATA
SURFACE WATER DATA
IMMEDIATE REDISTRIBUTION, PLANT SCAVENGING, SURFACE-WATER TRANSPORT MODEL
VALIDATION OF THEORY
RELOCATION BY SOIL, WATER AND ATMOSPHERE MODEL
DESCRIPTION OF FALLOUT ON PLANTS AT LOCATION Y: CONCENTRATION AT T⁰ + Xi
DESCRIPTION OF FALLOUT IN WATER AT LOCATION Y: CONCENTRATION AT T⁰ + Xi
DESCRIPTION OF FALLOUT ON SOIL AT LOCATION Y: CONCENTRATION AT T⁰ + Xi
GROUND WATER DATA
SOIL DATA
LONG TERM REDISTRIBUTION MODEL
VALIDATION OF THEORY

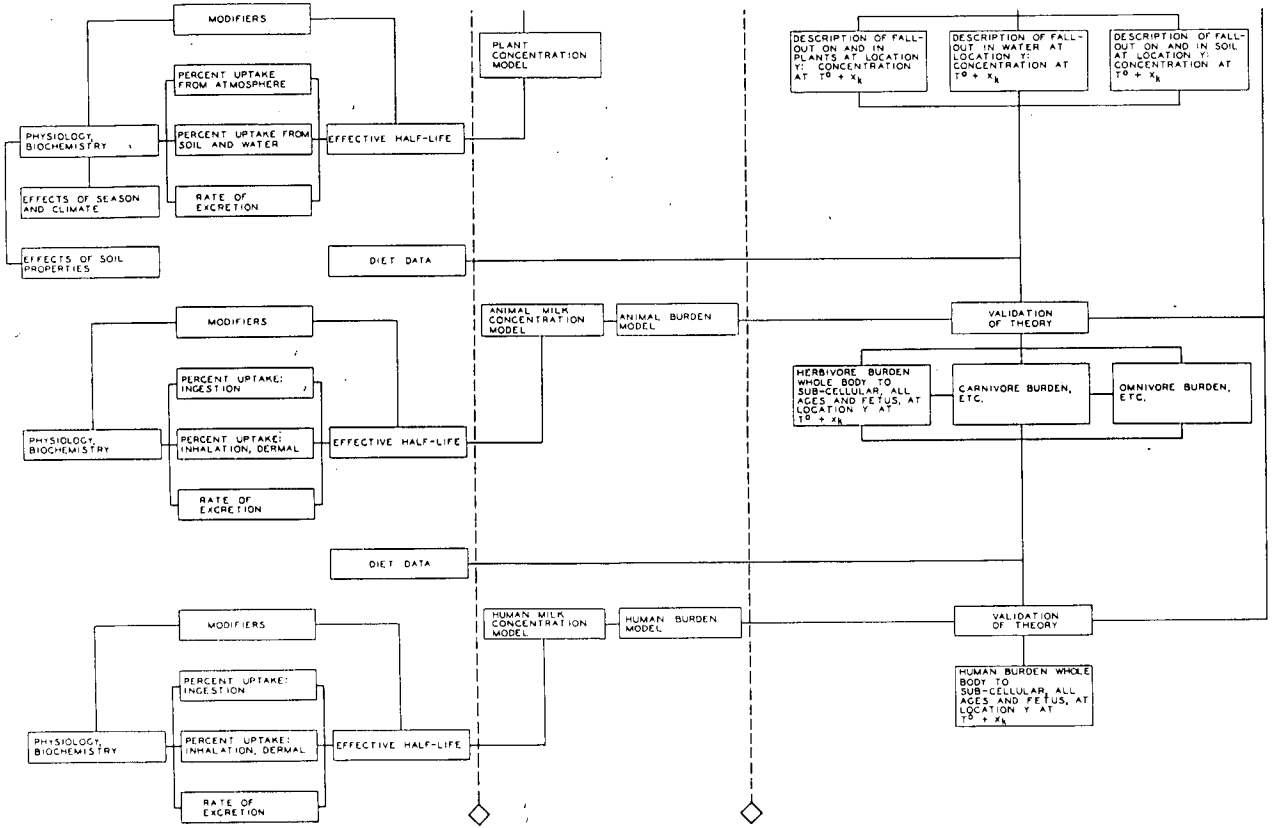

Fig. 1—Flow chart of LRL–L program in terms of the relations between different areas of study pertinent to the overall problem.

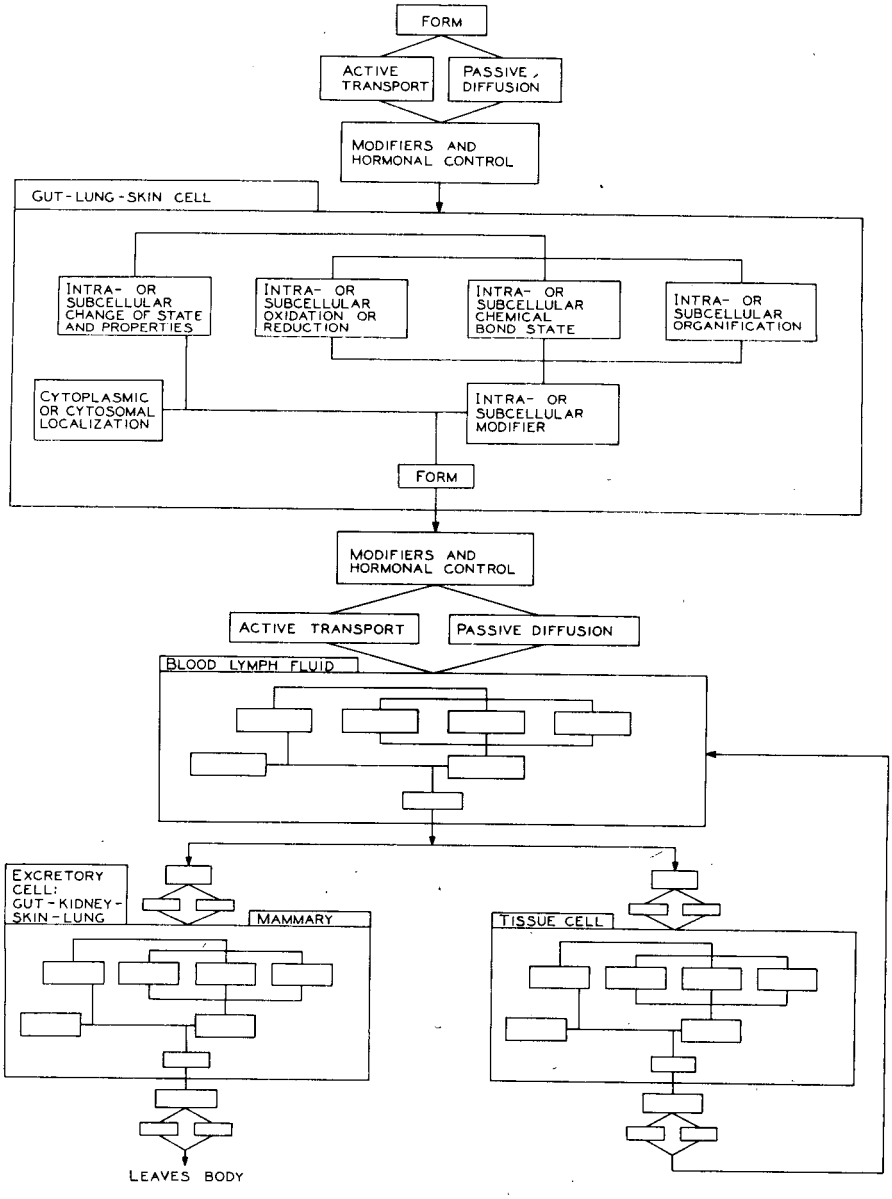

Fig. 2—Physiology–biochemistry phase of the LRL–L program. Unlabeled boxes are identical with their corresponding labeled box.

fallout. Among the specific questions he must then ask the literature are:

1. Is there a group of papers that reports ^{131}I concentration in milk in various areas and another group that reports ^{131}I in fallout in the same areas?

2. Are there papers that report the effective half-life of fallout ^{131}I on forage?

3. To go with question 2, are there papers that report the biological availability of fallout ^{131}I?

4. Are there papers that report the fraction of ingested ^{131}I excreted in cow milk?

Depending upon the availability of information on the preceding questions, each question could be permuted into several specific questions for additional collateral information. For example, the data for question 1 could be inconsistent unless the fraction of ^{131}I that is retained by plants is similar for dry fallout and fallout brought down by rain. This would be another specific question for the literature. Lacking specific information on ^{131}I with respect to this question, the scientist may ask for data concerning another soluble nuclide, e.g., ^{137}Cs. Obviously, any of these lines of questioning which proves unsuccessful will point out crucial gaps that need to be filled by experimental efforts.

In searching the literature for these specific kinds of information, the scientist must use various bibliographies and abstracting journals. By the very nature of these literature aids, he must read numerous articles to obtain the few that are pertinent to his specific question. Furthermore, in asking a series of questions such as the preceding ones, he may request the same (and at times useless) reference several times.

On the other hand, with a problem as broad as this overall mission problem, practically any specific kind of information in a piece of literature may eventually apply to some segment of the problem. This is particularly true when one considers that many of the problems will have to be solved in an analytical manner with the use of collateral data. To proceed as expeditiously as possible with our mission problems in the areas concerned with nuclear explosives, we developed an information-retrieval system as part of the Information Integration Project. The first time a member of the group reads a piece of literature, he codes into the system the specific kind(s) of information contained in the document. As a result the various pieces of literature will be recalled in the future (by the original reader or any other individual) only when a need arises for these specific kinds of information.

Consequently the Information Integration Project will service three major functions:

1. Literature retrieval. This implies simply that the system will be able to supply a bibliography of the literature pertinent to any particular aspect of the overall problem. To a large extent this purpose will be fulfilled as a natural consequence of meeting the other two objectives of the system. However, literature retrieval will be the sole objective for theoretical or conceptual discussions of the various facets of the overall problem, e.g., mathematical models of atmospheric transport of radionuclides.

2. Data retrieval. This necessarily implies literature retrieval, i.e., retrieval of literature that contains data pertinent to some aspect of the problem. The requirement for data retrieval is twofold: for data against which to test predictive or theoretical models and for data to be used to develop critical values or relations that are parts of predictive or theoretical models.

3. Critical-value determination. This is the prime function of the Information Integration Project. The other two are simply means to this end. This function implies both literature and data retrieval. A critical value is meant to imply a value that has been accepted on a critical basis. For example, it could represent the mean and variance for a group of determinations, each of which has been carefully analyzed and accepted.

One could consider the overall mission objective to be the development of a series of equations that trace the fate of radionuclides from the source to the burden in humans. Within this concept the critical values would then represent the combination of the various equations and the coefficients and exponents of the equations. In other words, the object here is to develop and maintain a handbook of critical constants and relations pertinent to all aspects of the mission problem, ranging from the nuclear-explosive source to the radionuclide burden in man.

Figure 3 presents a flow chart for the overall project operation. The literature-retrieval aspect of the system is essentially a normal library function. However, one step has been added, namely, a check against the author's other publications. Its purpose is to prevent multiple entries of identical data into the data file. Multiple entries could occur for two major reasons. First, although reference citations of articles published in journals have become relatively well standardized, the citation of government or company reports is in a state of chaos. Second, the same data appear frequently in several publications; quite commonly an author's work appears in both a company report and a journal. Many times the same article has been found in several journals.

The data-retrieval aspect, i.e., the mechanism for coding data and concepts, is discussed later. The details of the determination of critical values will be discussed in subsequent reports in connection with specific areas of the problem. The first of these reports will

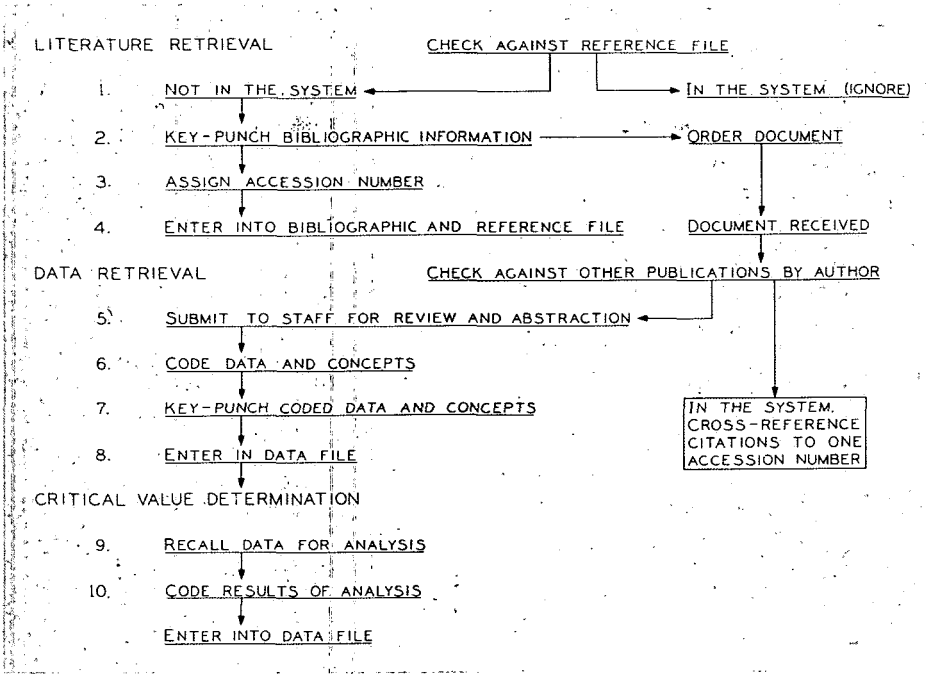

Fig. 3—Flow chart of system operation of LRL–L program.

cover the critical relations involved in predicting the course of the various radioactive isotopes of iodine from source to human burden.

Information-retrieval System

Information systems are a problem for the scientist and not just for the librarian. Information systems should be manned by scientists who are actively working on the various problems with which the system is concerned. Unless this is so, the system will most likely not be properly problem oriented. More important is the consideration that reading and abstracting the literature is a valuable training aid and that this training is lost unless it is applied to the problems of science. In other words, information retrieval is no end unto itself; it must be intimately tied to ongoing theoretical and experimental programs. Knowledge gained should be knowledge used; we need sources of knowledge, not information cesspools.

The human brain is the world's finest information storage and retrieval system, and also it is able to analyze and integrate information. It is a complete information system. Thus a person who is reading and coding the literature for a machine system is simultaneously storing this information in his own brain; he is absorbing and learning.

Electronic computers are not oracles, and it is only from human brains that the analytical approaches will come. The coder will most likely become one of the experts who can best analyze and integrate the data that have been stored for retrieval. He must be a working scientist.

Furthermore, it is important to reemphasize that information retrieval is not the prime purpose of the Information Integration Project. Rather, the project has been developed to expedite the future retrieval of literature read by members of the group. Thus our objective is not to read, catalog, and create an encyclopedia of the existing literature. Rather, the literature is to be examined only to the extent that we may be able to adequately define the state-of-the-art knowledge concerning the release of radionuclides to the biosphere from nuclear explosives and to point out the crucial gaps in this knowledge that require experimental efforts. Therefore our selection of the literature to be examined will always be dictated by our analysis of the overall mission problem. The selection of literature on collateral information will not be made on the basis of interesting problems but only upon the requirements of the mission problems.

Within our present concept the system will consist of four separate files, each serving a special function:

1. Bibliographic file. This file will contain the bibliographic information for each article entered into the system, i.e., authors, title, journal or report number, volume, pagination, and date. As an article is entered into the system, it will be assigned an accession number. This file will be ordered on accession number, and the accession number will be carried on entries into all other files.

2. Reference file. This file will contain the accession number and the bibliographic citation (journal or report number, volume, pages, and date). The journals will be assigned a numerical code; each report will be entered by its own alphanumeric code. The file will be ordered according to source. Before a new article or report is requested or assigned an accession number, the file will be searched to determine whether or not the same data are already in the system.

3. Data file. This file will contain the alphabetic and the numeric information abstracted from the documents which is coded into a three-dimensional matrix. It is expected that in the X,Y plane there will be 100 rows and 100 columns. The 100 columns are intended to represent disciplines or problem segments, whereas the rows will be logical breakdowns for respective columns. Thus the system is planned to contain 10^4 primary index points. We plan that the system be open-ended in the Z direction, but we expect that no index point will have more than 100 subcategories. This means that we plan to have about 10^6 coded storage slots.

4. Table file. This file will contain the tabular data from the documents. Tables will be assigned consecutive numbers, and note of the

existence of each table will be made in the data file. The precise nature of the table file is yet to be determined; a number of approaches are being considered, some of which are still in the equipment-development stage. Until the most versatile file system is selected, the original documents will be used as the storage means for the tables.

Procedure for Coding Information

If an information-retrieval system is to fulfill objectives of the sort listed in the subsection on general aspects discussed earlier, one guiding principle must be applied: The system must be designed to respond to requests for specific information from the various scientists. For example, when a scientist requests all the data on the ^{90}Sr concentration in rainfall in California, he does not want all the literature on fallout or on ^{90}Sr, nor does he want all the literature on ^{90}Sr in rainfall. He has made a specific request. In addition, he has made a predictable request because he is approaching his problem in a manner consistent with its logical and orderly solution.

There are, in addition to this guiding principle, two important guidelines with respect to the mechanics of the system:

1. Each specific kind of information should be stored in a single unique location. This obviously requires an unambiguous, detailed classification of information.

2. Closely related to item 1, the transcription of the information from the literature to the system must be simple and rapid since transcription from the literature to the system will have to be done by the hand of man at least in the foreseeable future. Simplicity helps to guarantee accuracy as well as speed, and speed is required in the handling of a large volume of literature.

To meet the preceding requirements, we adopted a coding matrix wherein the flow through the columns of the matrix corresponds to the flow through the problem from source to human burden as set forth in Figs. 1 and 2. Each column of the matrix (see Table 1) represents a separate and unique segment of the mission problem as it flows from radionuclide source to human burden. Since it is expected that there will be in excess of 10^4 specific kinds of information pertinent to the overall problem, this matrix will fulfill the need for both rapid and unambiguous classification. It is necessary only to recognize where a specific kind of information fits into the problem to determine how to code it into the system. This, of course, also emphasizes the earlier statement that information-retrieval systems are a problem for the working scientist.

To a considerable extent the columns also separate the problem into the various scientific disciplines involved in the overall problem.

Table 1 — COLUMN HEADINGS FOR CODING MATRIX

Column	Column description
1	Source and data-station data
2	Source to cloud relations
3	Cloud properties
4	Source to fallout and cloud to fallout relations
5	Fallout properties, including throwout, base surge, and reactor effluent
6	Fallout and precipitation
7	Material balance and future predictions
8	Redistribution relations
9	Translocation into and/or within plants
10	Plant to animal and fallout to animal relations
11	Translocation in animals
12	Animal burden
13	Plant to man, animal to man, and fallout to man relations
14	Translocation in man
15	Human-dosage relations
16	Effects
17	Countermeasures
18	Properties of biological materials

As a result the system will serve as a communication link at the interfaces between disciplines required for solution of the overall mission problems. For example, it will serve to direct a physicist or a meteorologist to focus on a problem in such a manner that his results are pertinent to a biological problem.

Columns 1, 3, 5, 6, 8, 12, and 15 (see Table 1) will contain the field data shown in the right-hand column of Fig. 1. Columns 9, 11, and 14 will contain data on controlled laboratory experiments. Columns 2, 4, 7, 10, and 13 will contain those relations requiring determination of critical values through the use of the data in the other columns.

Each column contains a number of boxes that designate general categories of information within the column, and each box in turn contains a listing of specific kinds of information within the particular category. Thus each specific kind of information will be identified by a six-digit code: two digits for the column, two for the box, and two for the listing. It is important to point out that this matrix is dynamic in that it is changed almost daily (and it is important that this flexibility be preserved) by the addition of a column, a box, or a new item in a listing. For example, in column 2 there is a box designated "Fireball Phenomenology"; it is expected that this box will eventually become a column.

A complete description of the system and the coding procedures has been reported[1] and will not be discussed here except to indicate that, along with a specific entry, considerable additional information

is recorded. Thus we can determine those papers, and only those papers, which, for example:

1. Record as a function of time the concentration of a particular isotope in the blood of sheep that have been given an intravenous injection of the isotope.

2. Record the concentration of a particular isotope in rainfall at some particular geographic location over some particular period of time.

3. Record the data in item 2 and also in cow milk at the same place and time. The data on milk, of course, could appear in different references.

REFERENCE

1. A. R. Tamplin and J. L. Minkler, Information Integration System for LRL–L Program on Man-made Radiation in the Biosphere, USAEC Report UCRL-7945-T, University of California Lawrence Radiation Laboratory, July 15, 1964.

STUDIES OF ^{90}Sr AND STABLE STRONTIUM IN DIET AND BONE IN ARGENTINA

D. BENINSON, E. RAMOS, and R. TOUZET
Argentine Comisión Nacional de Energía Atómica, Buenos Aires, Argentina

ABSTRACT

Results of ^{90}Sr and stable-strontium measurements in bone samples from children and in foods of the corresponding diets are presented and discussed. The data show that ^{90}Sr/calcium ratios in total diet are very close to those of the milk level for children during the first year of life. Typical intakes for very young children in the past three years in Argentina are on the order of a few picocuries of ^{90}Sr and about 1 mg of natural strontium per day.

Strontium-90 levels in bone of different age groups are presented from samples for which a detailed diet history has been assembled. Typical levels in children's bones are in the order of 1 pc per gram of calcium. Natural strontium in bone seems to increase slowly with age from about 0.23 mg per gram of calcium, reaching the adult value of about 0.4 mg per gram of calcium between the second and third year of life.

With the use of a rough model and bone and diet data, discrimination factors for different age periods have been estimated. Estimates from ^{90}Sr and stable-strontium data agree adequately and suggest that strontium is less discriminated against in very young infants than in older children or adults. This, however, could be of little relevance for risk estimations if skeletal turnover is rapid in the first years of life.

INTRODUCTION

Among the fission products, ^{90}Sr is most relevant as a long-term potential risk because of its long half-life and metabolic pattern lead-

ing to bone deposition. The highest bone levels have been observed in children since their skeletons tend to follow readily the changes of ^{90}Sr in the diet. Evaluation of diet to bone transfer parameters in children is of importance in predicting the body burdens resulting from different environmental conditions. This evaluation presents several difficulties, including the fact that the diets of infants include specially processed food items based on milk and several additives that cannot be correlated a priori with adult aliments usually surveyed in most fallout programs.

This paper summarizes the studies carried out in Argentina on ^{90}Sr and stable strontium in the diets and the bones of children. The work has two aims: (1) the determination of ^{90}Sr levels in bones of children whose diet history could be established with reasonable reliability and (2) the estimation of representative levels in children's aliments, included in the corresponding progress reports.[1,2]

SAMPLING AND ANALYTICAL PROCEDURES

Five samples per month per brand of special baby foods were sampled at the consumption point. Other food items were sampled in connection with the regular Argentine Comisión Nacional de Energía Atómica (CNEA) fallout survey. Samples of each type were pooled monthly and processed.

Bone samples were obtained mainly from pediatric hospitals. These samples were selected to exclude those cases where the causes of death might have influenced substantially the mineral composition of bone. Information was obtained from the hospitals on the alimentation in each case; the family and the intervening practitioner were also interviewed on the subject.

The samples were processed by the Health and Safety Laboratory (HASL) using radiochemical procedures[3] and counted in low-background equipment for ^{90}Sr determinations. Natural strontium was determined by an X-ray fluorescence technique described elsewhere.[2]

^{90}Sr AND STABLE STRONTIUM IN FOOD

^{90}Sr

Table 1 summarizes the mean results of ^{90}Sr determinations in food, excluding milk, in the period 1961–1963. Standard errors of each entry, which correspond to 10 to 50 samples, are of the order of 5 to 15%. The values shown in Table 1 under the heading "Special Baby Foods" are representative of the country. The other food levels refer strictly to the Argentine litoral area and the Buenos Aires Province;

Table 1 — PICOCURIES OF ^{90}Sr PER GRAM OF CALCIUM IN BABY FOODS

	1961	1962	1963
Special Baby Foods			
Baberlac compuesto	1.05	1.47	2.32
Eledón con fécula	0.85	2.65	2.37
Eledón con fécula y glúcido	4.02	2.37	2.41
Baberlac simple	3.52	3.48	3.72
Nestógeno	3.19	3.68	3.00
Casenolín	1.85	0.49	1.51
Secalbum	0.82	0.51	0.26
Yogalmina	2.96	2.98	2.23
Leche Nido	2.17	1.88	2.37
Leche Kasdorf	5.03	4.61	5.20
Leche S.M.A.	3.14	3.13	2.82
Leche Cundor	2.60	2.60	2.83
Osteolact	3.03	3.79	3.32
Other Foods			
Flour	15.58	19.91	18.20
Semolina	17.93	22.41	20.11
Farex	0.83	0.95	0.64
Maizena	3.85	2.75	
Quaker	8.18	8.18	10.26
Potato	14.85	18.47	18.24
Calabash	3.15	8.44	5.31
Onion	12.80	16.07	14.63
Tomato	23.95	28.94	25.95
Pool of vegetables	6.45	8.06	8.60
Banana	5.90	6.42	6.04
Apple	6.26	7.77	7.40
Eggs	5.24	6.55	7.01

but, owing to the scope of production[3] and to wide food distribution, they are believed to be applicable to other areas.

Table 2 shows the milk levels, representative of the litoral area, grouped by six-month periods together with pertinent fallout information. Milk levels are believed to be related to fallout rate and cumulative deposition by the expression[4]

$$C = aD + bd$$

where C = average milk level, in pc per gram of calcium
D = cumulative deposition at the middle of the period, in millicuries per square kilometer
d = average fallout rate in the period, in millicuries per square kilometer per year
a and b = proportionality factors

Table 2 — FALLOUT AND ^{90}Sr IN MILK

Period	Cumulative deposition, mc/km^2	Average fallout rate, mc/km^2 per year	Average level in milk, pc/g of Ca
First semester 1960	6.8	0.60	1.63
Second semester 1960	7.1	1.02	2.14
First semester 1961	7.7	0.96	1.85
Second semester 1961	8.0	1.40	3.22
First semester 1962	8.8	0.70	3.05
Second semester 1962	9.4	2.68	3.54
First semester 1963	10.6	1.15	3.31
Second semester 1963	11.5	2.21	4.17

Multiple regression with the use of data from Table 2 gives a = 0.27 and b = 0.42.

With the use of the expression, milk levels can be predicted with a standard deviation of the estimate of ±0.37 pc per gram of calcium. Prediction of levels in other baby foods based on milk is difficult since some of the brands are fortified with animal or mineral calcium and include variable amounts of cereals.

Stable Strontium

Natural strontium determinations in food items are less comprehensive and are based on a sampling period of 1½ years (Table 3). Results show that milk-based baby food and milk have about 1 mg of strontium per gram of calcium. Only scanty results are available for other individual foods not covered by Table 3. This table, however, includes values for several samples of composite diets which have been analyzed. The composition of these samples was based on dietary information discussed later in this paper.

Mean Daily Intakes

Estimation of daily intakes for children of different age groups requires qualitative information on diet composition which is not available for most regions in Argentina. This information could be obtained with a reasonable degree of reliability only for Buenos Aires Province.[5–7] Breast feeding introduced some uncertainty, particularly in the age group of 0 to 6 months. Best available estimates for contribution to daily calcium intake from breast feeding in Buenos Aires Province are 47 and 17% for age groups of 0 to 3 and 3 to 6 months, respectively.

A compilation on diet composition and contribution of different foods to calcium intake has been published elsewhere.[1,8] Daily-intake estimates of natural strontium and ^{90}Sr have been computed from that

Table 3 — MEAN STABLE STRONTIUM IN FOODS

Food	Number of samples	Calcium, % in ash	Strontium, ppm in ash	Mg of Sr/ g of Ca
Milk	24	15.0	140	0.95 ± 0.08
Baberlac compuesto	10	11.8	123	0.85 ± 0.09
Milk Nido	10	11.3	140	1.26 ± 0.21
Eledón con fécula y glúcidos	10	15.6	116	0.92 ± 0.06
Baberlac simple	10	11.3	171	1.50 ± 0.20
Biberol	9	14.2	70	0.48 ± 0.08
Yogalmina	10	15.2	90	0.59 ± 0.09
Levulosa	10	17.4	200	1.15 ± 0.05
Osteolact	10	15.3	110	0.72 ± 0.06
Secalbum	10	25.2	551	2.28 ± 0.38
Nestógeno	10	13.7	140	1.02 ± 0.15
Nestún	10	6.4	170	2.65 ± 0.40
Eledón con fécula	10	14.6	100	0.69 ± 0.05
Quaker	7	3.13	310	9.91 ± 1.10
Farex	10	25.0	200	0.80 ± 0.06
	Composite Diets			
Age group, months				
6 to 9	10			1.21 ± 0.20
9 to 12	9			1.24 ± 0.17
12 to 24	10			1.31 ± 0.26
24 to 36	10			1.35 ± 0.21
Adults	10			1.75 ± 0.22

information and the mean levels given in Tables 1 to 3; the results are summarized in Table 4. Strontium-90 intakes are means of the period 1961–1963; annual values show an increase of about 40% in these three years. Table 4 shows that for young children the strontium/calcium and the ^{90}Sr/calcium ratios in total diet are very close to those in milk. In particular, the ^{90}Sr/calcium ratio in total diet averaged over the first year of life can be taken to be the same as that of milk. Typical intakes are on the order of a few picocuries of ^{90}Sr and about 1 mg of natural strontium per day.

^{90}Sr AND NATURAL STRONTIUM IN BONES OF CHILDREN

^{90}Sr

Samples of bone were limited at most to a few bones per child. Skeletal-burden estimations must, therefore, rely on some knowledge of the distribution of values within the body. There is some evidence of a very high turnover in the skeleton in the first two years of life,[9] and therefore it will be assumed that bones are uniformly labeled.

Table 4 — MEAN DAILY INTAKES OF CALCIUM, STABLE STRONTIUM, AND ^{90}Sr

Age group, months	Calcium, g/day	Stable strontium, mg/day	^{90}Sr, pc/day
0 to 3*	1.00	0.69	1.95
3 to 6*	0.99	0.96	2.64
6 to 9	0.84	1.02	2.85
9 to 12	0.86	1.07	3.05
12 to 24	0.72	0.94	2.70
24 to 36	0.68	0.92	2.65
Adults	0.70	1.22	4.50

*Calculations assume breast feeding in the proportion mentioned in the text and an observed ratio (mother's diet/milk) of 0.12.

Table 5 — ^{90}Sr IN BONE AND DIET HISTORY

Age group, months	No.	Average age, months	Average bone-level $^{90}Sr/Ca$, pc/g	0- to 6-month diet level $^{90}Sr/Ca$, pc/g	6- to 12-month diet level $^{90}Sr/Ca$, pc/g	12- to 24-month diet level $^{90}Sr/Ca$, pc/g	24- to 36-month diet level $^{90}Sr/Ca$, pc/g	Mothers'* diet level $^{90}Sr/Ca$, pc/g
Stillbirths	38		0.97					6.90
0 to 6	34	2.1	1.16	2.56				5.84
6 to 12	20	9.5	1.12	1.98	3.49			4.15
12 to 24	20	18.7	0.95	1.60	2.73	3.94		3.80
24 to 36	11	33.6	0.87	1.31	2.59	3.41	4.02	3.40

*During pregnancy.

Table 5 summarizes the results from bone samples for which a detailed dietary history could be assembled. Table 6 gives estimates of the corresponding calcium increments in skeleton between consecutive average ages of age groups. These values have been computed with the following information. The calcium content of a newborn child is esti-

Table 6— CALCIUM INCREMENTS IN SKELETON CORRESPONDING TO ^{90}Sr IN BONE AND DIET HISTORY

Age group, months	Calcium content, g	Age group, months	Calcium content, g
Fetal	24	12 to 24	39.6
0 to 2.1	12.3	6 to 9.5	17.7
0 to 6	30.4	12 to 18.7	22.1
6 to 12	30.4	24 to 33.6	21.5

mated to be about 24 g in the Argentine litoral area.[10] In addition, published calculations[11,12] show that the calcium increase in the child fits reasonably well the expression

$$\frac{\text{Calcium retained}}{(\text{Calcium ingested}) \times (\text{weight of child})} = \text{constant}$$

A not readily assessed uncertainty is introduced by the calculation procedure.

The whole question of averaging is debatable. It is felt, however, that the near constancy of daily intakes and skeletal calcium increase supports averaging, assuming linearity. Detailed tables for the calcium level in bone for this area are published elsewhere.[1,2,8]

The ^{90}Sr/calcium ratios in children's bone in the Argentine litoral area are a little lower than those observed in Australia and less than one-half of most values found in the northern hemisphere. Dose rates incurred in bone from this contamination is of the order of 3 mrad per year.

Stable Strontium

Analysis of stable strontium in bone was made of materials obtained during 1963, including samples for which no diet history could be satisfactorily assembled. Means and standard errors are compiled in Table 7. It should be noted that determinations of different bones from the same child show no significant variations within the skeleton. Results suggest that stable-strontium/calcium ratios increase slowly with age, from 0.23 mg/g in fetal bone to about 0.4 mg/g in the third year of life, the value which is also observed in adults.

Table 7—STABLE STRONTIUM IN BONE

Age group, months	No.	Age mean, days	Ca, % in ash	Sr, ppm in ash	Mg of Sr/ g of Ca
Stillbirths	17		30.5	67	0.23 ± 0.02
0 to 3	19	30	28.5	77	0.25 ± 0.02
3 to 6	16	114	30.0	87	0.29 ± 0.04
6 to 9	12	243	35.7	85	0.24 ± 0.02
9 to 12	15	349	31.9	71	0.31 ± 0.02
12 to 24	3	540	36.0	110	0.32 ± 0.05
24 to 36	5	1020	34.7	142	0.41 ± 0.07
Adults	26		33.0	117	0.37 ± 0.02

DISCRIMINATION BETWEEN STRONTIUM AND CALCIUM

Diet to bone discrimination factors could, in principle, be estimated from ^{90}Sr or stable-strontium levels in bones and diet history. Stable-strontium calculations are to be preferred in equal conditions because equilibrium is ensured.

The strontium/calcium ratio in bone is related to those of diets by the following expression, which defines a crude model:

$$\text{Strontium/calcium in bone} = \frac{Ca_f L_M F_M + \Sigma \Delta Ca_i L_i F_i}{Ca_f + \Sigma \Delta Ca_i}$$

where Ca = amount of calcium from placental origin
L_M = strontium/calcium ratio in the total diet of the mother
F_M = fetal bone/diet of the mother
Ca_i = calcium increment during period i
L_i = strontium/calcium ratio in the diet during period i
F_i = average observed ratio of bone/diet of the child during period i

With the data on bone and diets presented in this paper, the expression allows calculation of the corresponding discrimination pileup for the older age groups; but not too much value should be attributed to them.

The calculations shown below are based on the ^{90}Sr bone values with corresponding diet history and on stable-strontium values and representative diets for the region studied.

Age group	Observed ratio estimated from stable strontium	Observed ratio estimated from ^{90}Sr
Stillbirths	0.13	0.14
0 to 3 months	0.81	0.80
3 to 6 months	0.49	
6 to 9 months	0.50	0.33
9 to 12 months	0.28	
12 to 24 months	0.30	0.27
24 to 36 months	0.22	0.26

The stillbirths' entries are, of course, the total discrimination factors between the mothers' diets and the fetal bones. The agreement between the two sets of estimates is fairly good. In spite of all uncertainties involved, the values suggest that in young infants there is little discrimination against strontium and that discrimination builds up reaching the "agreed" adult value of 0.25 during the second year of life.

The importance of such small discrimination in young infants should not be overestimated. If bone turnover is rapid, the skeleton burden of ^{90}Sr would depend strongly on intakes at later ages, and the 0.25 value would be relevant in any long-term-risk evaluation. Turnover rates could likely be estimated from ^{90}Sr/stable-strontium specific-activity measurements, but this would require more data than those obtained in the study presented in this paper.

REFERENCES

1. D. Beninson, A. Migliori, and E. Ramos, Strontium-90 in the Diets and Bones of Children. Progress Report 1962–1963, in Fallout Program Quarterly Summary Report, USAEC Report HASL-149, pp. 105-118, Health and Safety Laboratory, January 1965.
2. D. Beninson, E. Ramos, and R. Touzet, Strontium-90 in the Diets and Bones of Children. Progress Report 1964, in Fallout Program Quarterly Summary Report, USAEC Report HASL-149, pp. 119-129, Health and Safety Laboratory, January 1965.
3. Health and Safety Laboratory, Manual of Standard Procedures, USAEC Report NYO-4700(Rev.), August 1962.
4. United Nations Scientific Committee on the Effects of Atomic Radiation, Report of the Scientific Committee on the Effects of Atomic Radiation, United Nations Document A/5216, p. 303, New York, 1962.
5. Instituto Nacional de la Nutrición, Buenos Aires, Argentina, private communication.
6. Cátedra de Pediatría, University of Buenos Aires, private communication.
7. Instituto Nacional de la Nutrición, *Contenido en Calcio y Potasio de los Alimentos de la Republica Argentina,* Buenos Aires, 1957.
8. D. Beninson, R. Touzet, and E. Ramos, Radioestroncio y Estroncio Estable en la Dieta y el Hueso Humano, Comisión Nacional de Energía Atómica Report, in press.
9. F. Bryant and J. Loutit, The Entry of ^{90}Sr into Human Bone, *Proc. Royal Soc., B159:* 449 (1964).
10. Cátedra de Pediatría, University of Buenos Aires, private communication.
11. H. H. Mitchell, T. F. Hamilton, F. R. Steggerda, and H. W. Bean, The Chemical Composition of the Adult Human Body and Its Bearing on the Biochemistry of Growth, *J. Biol. Chem., 158:* 625-637 (1945).
12. H. Sherman, *Calcium and Phosphorus in Foods and Nutrition,* Columbia University Press, New York, 1947.

CESIUM-137 BODY BURDENS AND THEIR VARIATIONS IN NORWEGIAN SCHOOL BOYS

AKSEL STRØMME
State Institute for Radiation Hygiene and the Norwegian Radium Hospital, Oslo, Norway

ABSTRACT

The global distribution of fallout of radionuclides from nuclear-weapon tests has not been uniform. It has been especially high in Norway; therefore determinations of the level of fallout have been of particular interest. As a part of the investigations reported, ^{137}Cs body burdens and potassium levels were studied in 22 school boys from one school in Oslo with a whole-body counter at the Norsk Hydros Institute for Cancer Research. Examinations of the boys were made in March 1963, October 1963, March 1964, and October 1964.

BODY BURDENS AND THEIR VARIATIONS

As shown in Table 1, most of the boys (17) were born in 1946. The case numbers were assigned on the basis of their ^{137}Cs body burden at the first examination. Number 1 was assigned to the boy with the lowest body burden; number 22 was assigned to the boy with the highest. These numbers are maintained throughout this paper.

Figure 1 shows the height and the weight of the boys in March 1963 and October 1964.

Table 2 shows the height and weight of the boys also. The numbers in parentheses are the case numbers. Note that the average height in centimeters increased only 1 cm, from 179 to 180 cm. The weight has, on the average, increased from 67.5 kg to 69 kg. Some of the boys increased in weight only slightly, whereas some gained several kilograms; on the other hand, there are also some who decreased in weight.

Table 1—AGE OF SCHOOL BOYS AT TIME OF FIRST MEASUREMENT

Number of cases	Year of birth	Age in 1963, years	Case No.
4	1945	18	5, 7, 9, and 12
17	1946	17	1 to 4, 6, 8, 10, 11, and 13 to 21
1	1947	16	22

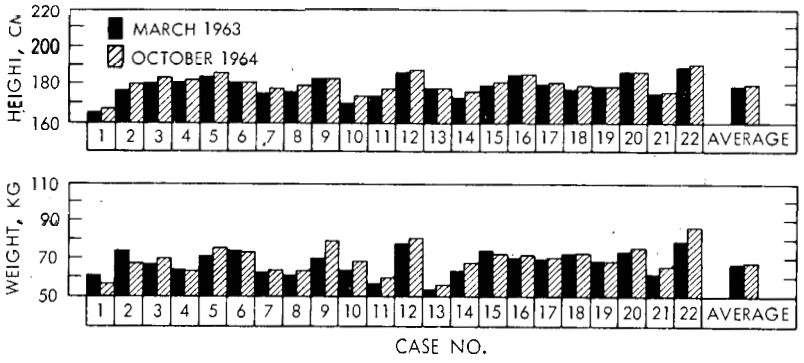

Fig. 1—Height and weight of boys.

Table 2—HEIGHT AND WEIGHT OF SCHOOL BOYS*

Date	Height, cm			Weight, kg		
	Average	Lowest	Highest	Average	Lowest	Highest
March 1963	179	166 (1)	190 (22)	67.5	53 (13)	79 (22)
March 1964	180	167 (1)	191 (22)	70	56 (13)	85 (22)
October 1964	180	167 (1)	191 (22)	69	55 (13)	86 (22)

*Numbers in parentheses are case numbers.

Figure 2 shows the body burden of ^{137}Cs in nanocuries. This figure shows that the body burdens of all the boys increased from March to October 1963. The body burdens increased in 11 from October 1963 to March 1964, whereas they decreased also in 11 during this period. During the period March to October 1964, body burdens increased in 15 and decreased in 7.

Table 3 shows the body burdens in nanocuries at the times of the examinations. Note that the average body burden rose from 23.2 nc in

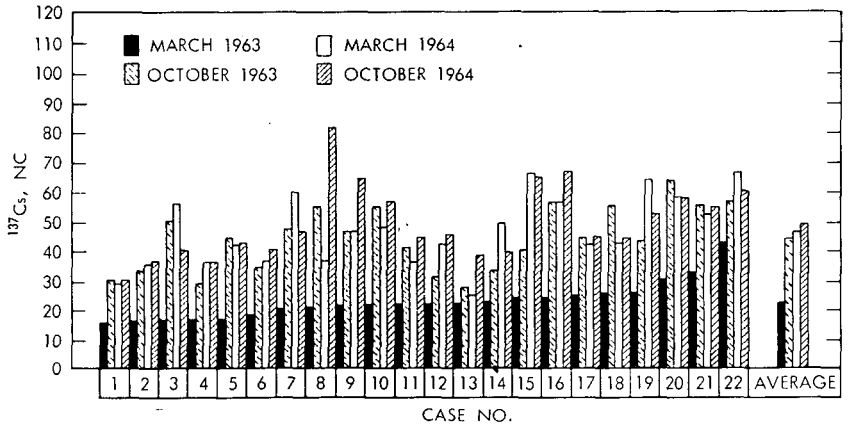

Fig. 2—^{137}Cs body burdens.

Table 3—^{137}Cs BODY BURDENS*

Date	Body burden, nc		
	Average	Lowest	Highest
March 1963	23.2	16.0 (1)	43.5 (22)
October 1963	44.9	27.9 (13)	64.5 (20)
March 1964	47.2	24.8 (13)	67.5 (22)
October 1964	49.9	30.7 (1)	80.9 (8)

*Numbers in parentheses are case numbers.

March 1963 to 44.9 nc in October 1963 and then to 47.2 nc in March 1964. In October 1964 the average body burden was 49.9 nc.

The ratio between ^{137}Cs and potassium, where ^{137}Cs is given in picocuries and potassium is given in grams, is often preferred to express the body burden of ^{137}Cs; however, the most recent method of expressing body burdens of radioactive materials is to give the amount of the radioactive material per kilogram of body weight.

In Fig. 3 the body burdens are expressed as the ratio of picocuries of ^{137}Cs per gram of potassium. If this figure is compared with Fig. 2, it can be seen that there is good agreement between them. The ^{137}Cs/potassium ratio increased in all the cases from March to October 1963. During the period October 1963 to March 1964, the ^{137}Cs/potassium ratio increased in the same boys in whom the total ^{137}Cs body burden increased.

During the period March to October 1964, the situation remained the same except for two cases, Nos. 15 and 20, which showed a decreased ^{137}Cs body burden and a slightly increased ^{137}Cs/potassium

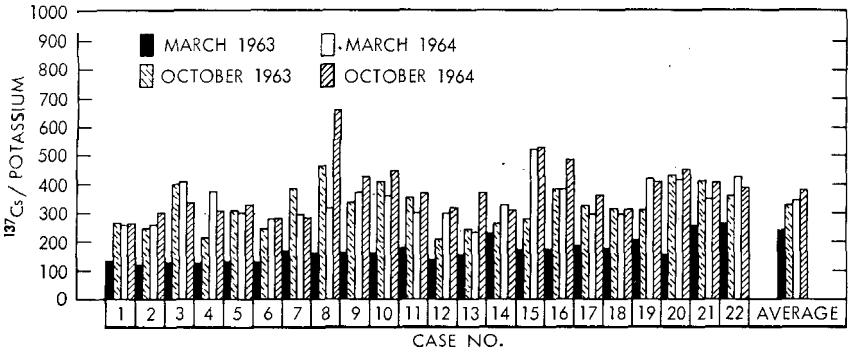

Fig. 3—Body burdens expressed in picocuries of ^{137}Cs per gram of potassium.

ratio. This means that the amount of potassium decreased proportionally more than the amount of ^{137}Cs.

It must be pointed out, however, that the increase or the decrease in several cases is only slight. This is at least partly explained by the fact that the boys are of an age when metabolism is rapid and liable to marked individual variations.

Table 4 shows the changes in the ^{137}Cs/potassium ratio. Note that the average ratio rose from 169 in March 1963 to 328 in October 1963, to 344 in March 1964, and then to 385 in October 1964.

Figure 4 shows the ^{137}Cs changes per kilogram of body weight in the time of observation. Note that the three ways of illustrating the ^{137}Cs body burden do not give substantially different results in this figure.

Table 5 shows the variation in the average value in picocuries of ^{137}Cs per kilogram of body weight. This value rose from 344 in March 1963 to 653 in October 1963, to 674 in March 1964, and to 723 in October 1964.

Table 6 shows the change in ^{137}Cs body burden expressed in percent. The table shows the average change in each period in the total

Table 4 — VARIATION OF ^{137}Cs/POTASSIUM RATIO*

	^{137}Cs/potassium ratio		
Date	Average	Lowest	Highest
March 1963	169	121 (2)	267 (23)
October 1963	328	209 (12)	467 (8)
March 1964	344	229 (13)	520 (15)
October 1964	385	266 (1)	658 (8)

*Numbers in parentheses are case numbers.

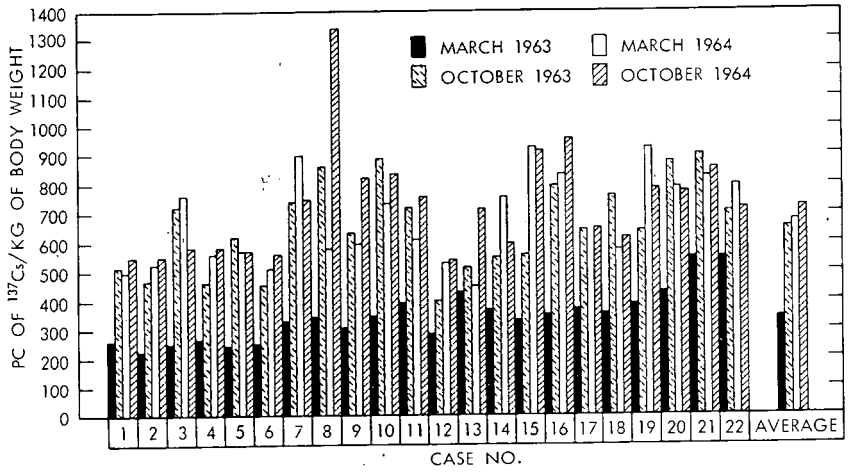

Fig. 4—Variation in the amount of ^{137}Cs per kilogram of body weight.

Table 5—VARIATION OF PICOCURIES OF ^{137}Cs PER KILOGRAM OF BODY WEIGHT RATIO*

Date	Picocuries of ^{137}Cs/kilogram of body weight		
	Average	Lowest	Highest
March 1963	344	222 (2)	551 (22)
October 1963	653	394 (12)	901 (21)
March 1964	674	443 (13)	924 (19)
October 1964	723	540 (12)	1284 (8)

*Numbers in parentheses are case numbers.

Table 6—CHANGES IN ^{137}Cs BODY BURDEN IN PERCENT

Change	March to October 1963	October 1963 to March 1964	March to October 1964
Increase of the average ^{137}Cs body burden since last examination	94	5	6
Increase of the average ratio of picocuries of ^{137}Cs per gram of potassium since last examination	94	5	12
Increase of the average ratio of picocuries of ^{137}Cs per kilogram of body weight since last examination	90	3	7

^{137}Cs body burden, in the ^{137}Cs/potassium ratio, and in the ^{137}Cs per kilogram of body weight ratio. There is good agreement among the three ways of illustrating the ^{137}Cs body burden.

Figure 5 illustrates the increase of ^{137}Cs when the values obtained at the first examination in March 1963 are set equal to 100.

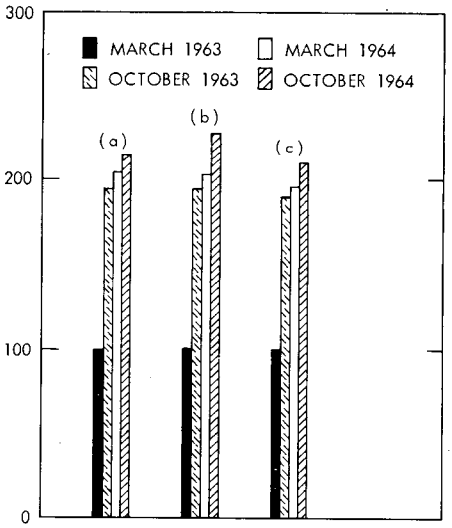

Fig. 5—Increase in ^{137}Cs body burden if values obtained in March 1963 are set equal to 100. (a) Total ^{137}Cs body burdens; (b) picocuries of ^{137}Cs per gram of potassium; and (c) ^{137}Cs per kilogram of body weight.

CORRELATION BETWEEN PRECIPITATION AND AMOUNT OF ^{137}Cs IN MILK IN NORWAY

KJELL MADSHUS* and AKSEL STRØMME†
*Norsk Hydros Institute for Cancer Research, Oslo, Norway
†The Norwegian Radium Hospital, Oslo, Norway

INTRODUCTION

The distribution of radioactive fallout has been nonuniform in different parts of the world. Because of atmospheric movements, turbulence and diffusion in the stratosphere, and prevailing west to east winds in the troposphere, most of the fallout from a nuclear explosion descends on the hemisphere in which the explosion occurred. The northern hemisphere therefore is the most contaminated since most nuclear tests have been made in it. Some radioactive particles come down as dry debris,[1] but mostly they are brought down by rain or snow. The regional climate, precipitation type and rate, and topographical peculiarities, to a high degree, determine the amount of fallout.

The main routes of radioactive particles from the atmosphere and the soil to man are through plants and animal products. Among the various radioactive nuclides present in fallout, ^{137}Cs is one of the most important from a medical point of view. About half of the body burden of this nuclide in man is often considered to come from milk intake, although it has been shown[2,3] that this is not always the case. In Western Europe, however, a considerable part of the body burden of ^{137}Cs in man does come from this source.

The minimum concentration of radioactive nuclides in milk is in spring, when cows are kept in sheds and partly fed uncontaminated fodder. The biological half-life of ^{137}Cs in cows is only about 20 days;[4] therefore the body burden of this nuclide in cows is rapidly reduced when they are partly fed uncontaminated fodder.

Table 1—TOTAL NUMBER OF DAIRIES IN NORWAY AND NUMBER OF DAIRIES FROM WHICH SAMPLES WERE TAKEN

Year	Dairies	Dairies supplying samples
1962	342	272
1963	342	297
1964	327	292

From November 1958 until September 1961, there were no atmospheric nuclear tests. Therefore it seemed reasonable to assume that in the spring of 1962 we would find a smaller ^{137}Cs body burden in cows and consequently a decreasing concentration of this nuclide in milk for the next few years if no more nuclear weapons were detonated in the atmosphere. At that time the cows were fed supplementary fodder and grass gathered before the bomb tests were resumed in the autumn of 1961.

A systematical analysis of ^{137}Cs in milk was started, and these analyses were repeated on the same scale during the springs of 1963 and 1964. (Spring means, in this connection, primarily the months of March and April; however, a few of the milk samples were gathered in February and May.)

The total number of dairies and the number of dairies from which milk was sampled each year are given in Table 1. Practically all the dairies in Norway were included in the investigation. Milk from 30 of these dairies has been examined regularly every month since the spring of 1963. Figure 1 shows their locations. Figure 2 shows that at least in the period from March 1963 to March 1964 the lowest concentration of ^{137}Cs in milk occurred during spring.

Figure 3 is a map of Norway. Counties are outlined and numbered 1 to 18. Heavier lines have been drawn on the map dividing the country into three zones. These lines follow the borders of the counties except in Sør-Trøndelag (14) and Nord-Trøndelag (15), which are divided into two parts each—a western part near to the coast, included in zone 2, and an eastern part, included in zone 1. The country was divided into these three zones because of varying meteorological conditions, which will be described later. Except in counties 14 and 15, no dairies are situated near the zone lines since these lines run through very mountainous regions.

CORRELATIONS

Figure 4 shows the average concentration of ^{137}Cs in the milk for each county in the three zones in the springs of 1962, 1963, and 1964. It can be seen from this figure that concentrations of ^{137}Cs in zone 1 are different from those in zone 2; usually they are much higher in

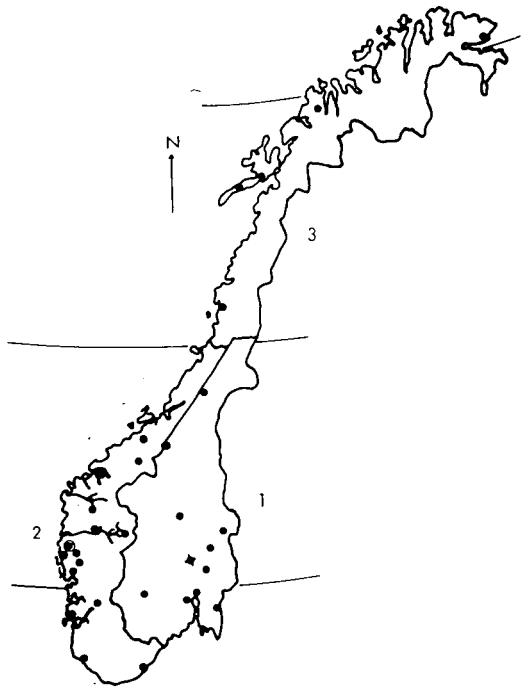

Fig. 1—Location of 30 dairies from which milk was given monthly examination. The numbers 1, 2, and 3 indicate zones (see Fig. 3).

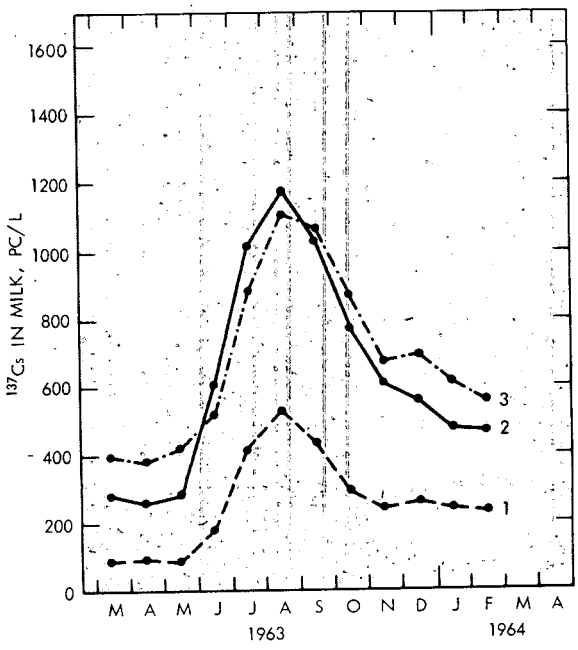

Fig. 2—Average concentration of ^{137}Cs in milk from March 1963 to February 1964. The numbers 1, 2, and 3 indicate zones (see Fig. 3).

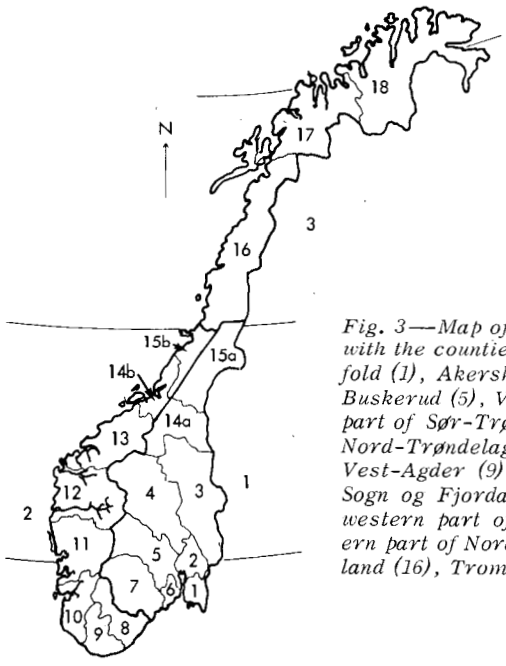

Fig. 3—Map of Norway divided into three zones, with the counties numbered 1 to 18. Zone 1: Østfold (1), Akershus (2), Hedmark (3), Oppland (4), Buskerud (5), Vestfold (6), Telemark (7), eastern part of Sør-Trøndelag (14a), and eastern part of Nord-Trøndelag (15a). Zone 2: Aust-Agder (8), Vest-Agder (9), Rogaland (10), Hordaland (11), Sogn og Fjordane (12), Møre og Romsdal, (13), western part of Sør-Trøndelag (14b), and western part of Nord-Trøndelag (15b). Zone 3: Nordland (16), Troms (17), and Finnmark (18).

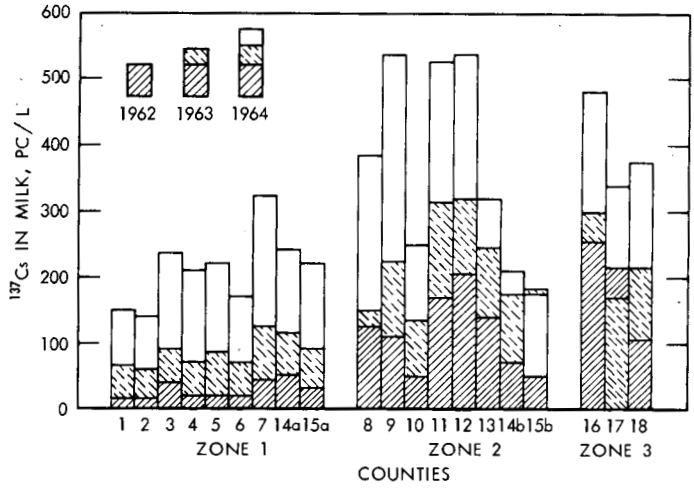

Fig. 4—Average concentration of ^{137}Cs in milk from each county in the springs of 1962, 1963, and 1964.

zone 2. Figure 5 shows the average concentrations of ^{137}Cs in the milk for the three zones in each spring.

The precipitation rate and form vary widely in the three zones. The primary purpose of our studies was to investigate whether or not there was any correlation between the precipitation and the concentration of ^{137}Cs in milk.

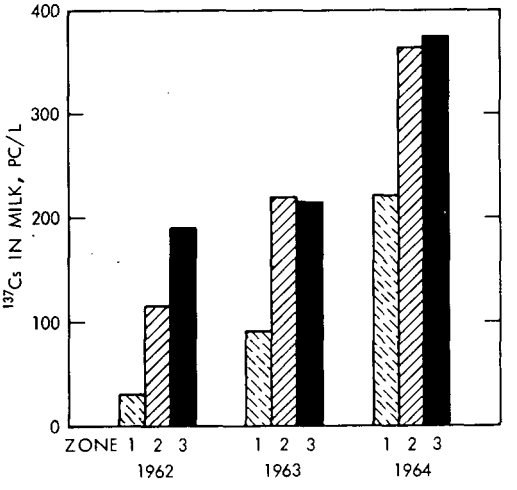

Fig. 5—Average concentration of ^{137}Cs in milk in the three zones in the springs of 1962, 1963, and 1964.

From gamma spectroscopic measurement performed in our laboratory, we knew the amount of ^{137}Cs in the milk from the same dairies at the same time of the year for three consecutive years. It was presumed that the ^{137}Cs deposited in the soil before the new nuclear-weapon test series in the autumn of 1961 would give the same contribution to the milk's content in 1962, 1963, and 1964 because of the long half-life of ^{137}Cs (30 years) compared to the time of observation (3 years). Cesium-137 is strongly bound in the soil and diminishes very slowly.[5] Besides, most of the ^{137}Cs ingested by cows originates from ^{137}Cs deposited directly from the air to the leaves and, to a far lesser degree, from the soil through the roots of plants.[6] Any increase of the ^{137}Cs content of milk therefore should be exclusively due to increased fallout from the new test series.

The year 1961 is used as the basic year for the studies, but, to minimize local variations in the precipitation for that year, we used the average precipitation for 1959, 1960, and 1961 instead of the precipitation in 1961 only.

Several facts are important when one considers the precipitation in the various districts from which the dairies receive their milk supplies. The precipitation rate in Norway varies considerably from one county to another and is measured by a large number of stations.

Apart from exceptional occurrences such as local squalls, stations situated near each other in a small but not too mountainous area record only slight differences in the amount of precipitation. Stations situated on the leeside of mountains or mountain ranges, however, commonly record considerably less precipitation than stations situated where the geological formations force moist air upward. Where moist air is forced upward because of topographical conditions, the precipitation usually increases with the height above the sea. These conditions very often occur in regions in Western and Northern Norway where stations are situated rather close to each other but have very different precipitation rates. Observations from single stations are therefore not representative for their districts, and in these studies the average precipitation rates from several stations in and around the district in question were used. The precipitation rate in the district from which the dairy receives its milk was therefore estimated as the average probable precipitation rate measured by meteorological stations in and around the district. (If any error is made by this method of calculation, the same error will be made the following years. Other differences from the true precipitation will also be reduced.)

Figures 6 to 8 show the specific concentration of ^{137}Cs in spring milk vs. the precipitation in the preceding year. In Fig. 6 the average precipitation for 1959, 1960, and 1961 has been used, whereas in Figs. 7 and 8 the precipitation in 1962 and 1963, respectively, has been used.

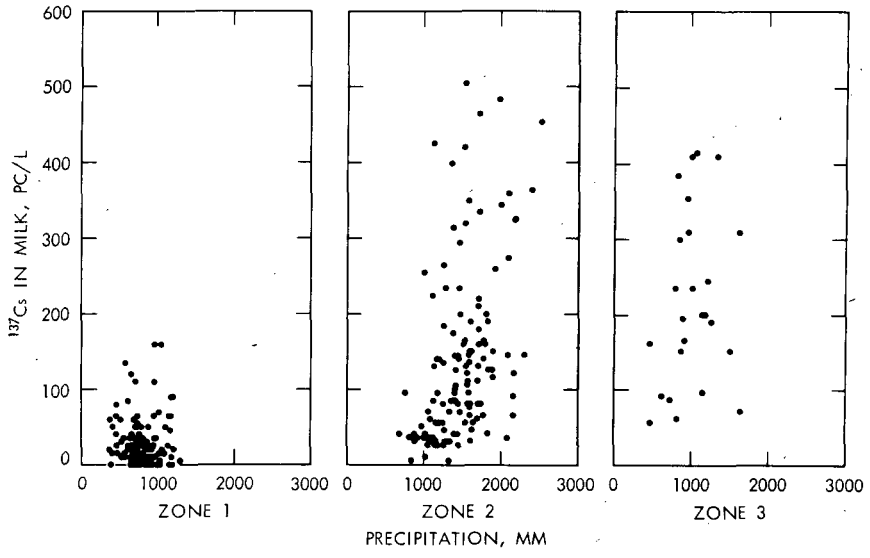

Fig. 6—Cesium-137 in milk in the spring of 1962 vs. the average precipitation for 1959, 1960, and 1961.

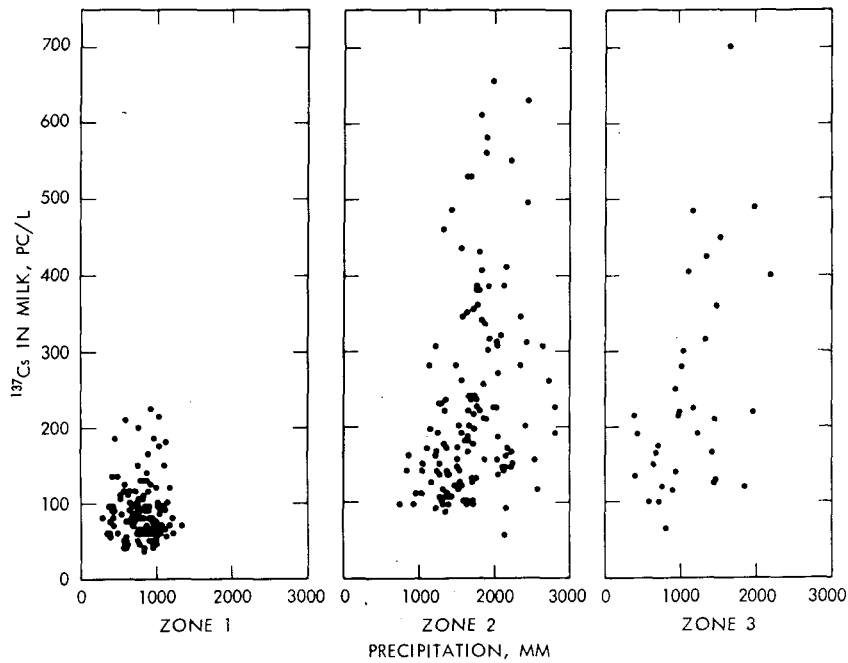

Fig. 7—Cesium-137 in milk in the spring of 1963 vs. the precipitation in 1962.

In Norway the grass that is to be cut for hay is usually grown during May, June, and July. Besides finding the correlation between the yearly precipitation and the ^{137}Cs concentration in milk, it was of interest to correlate the amount of precipitation in this period with the ^{137}Cs concentration in the milk the next spring. Statistical analyses showed no such correlation in any of the three zones. However, in zones 2 and 3 there is a statistically significant correlation between the yearly precipitation and the concentration of ^{137}Cs in milk the following spring. This correlation is valid for zone 2 for all three years and for zone 3 for precipitation in 1962 and 1963 and milk in the springs of 1963 and 1964, respectively. In zone 1 no such correlation was found.

The coefficients of correlation are shown in Table 2. Several of these amount to statistically significant correlations, but only those which are consecutive (underlined in the table) were used. In Fig. 9, with respect to zone 2, and in Fig. 10, with respect to zone 3, the correlations between precipitation and ^{137}Cs are drawn as lines of regression together with their curves of 95% confidence. (In every calculation we tried equations of both first and second degree, but the

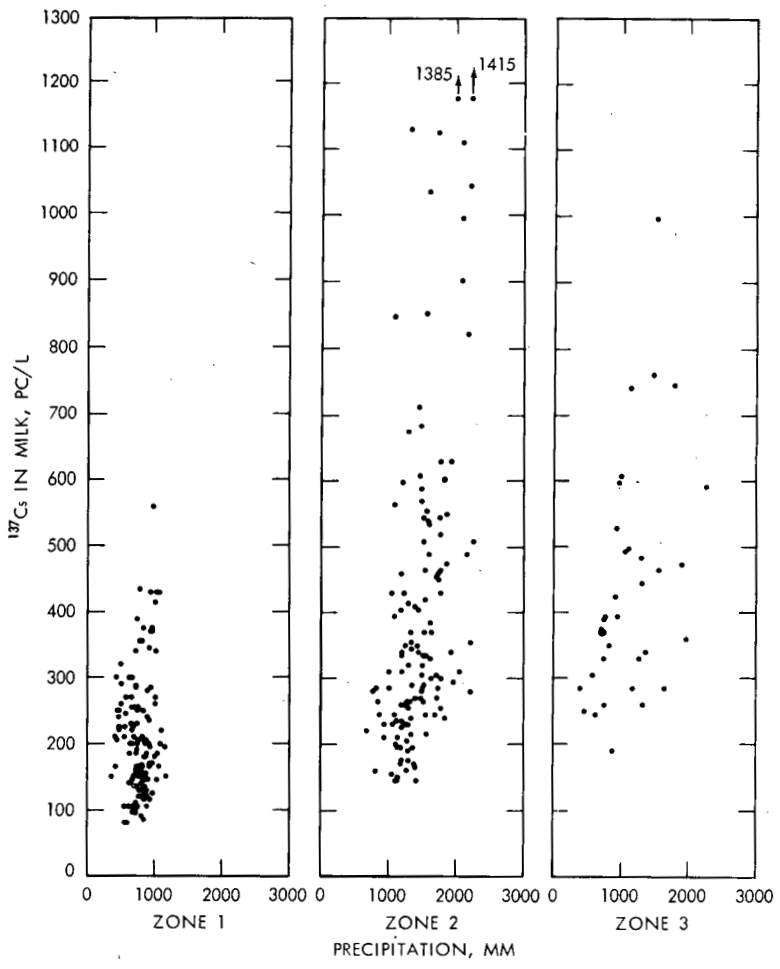

Fig. 8—Cesium-137 in milk in the spring of 1964 vs. the precipitation in 1963.

Table 2— COEFFICIENTS OF CORRELATION* BETWEEN ^{137}Cs CONCENTRATIONS IN MILK AND AMOUNTS OF PRECIPITATION

	^{137}Cs vs. precipitation in May, June, and July			^{137}Cs vs. precipitation per year		
Zone	1962	1963	1964	1962	1963	1964
1	0.310	0.008	0.360	0.009	0.11	−0.002
2	0.312	0.182	0.373	0.413	0.395	0.500
3	0.011	0.466	0.273	0.299	0.496	0.436

*Underlined values are consecutive.

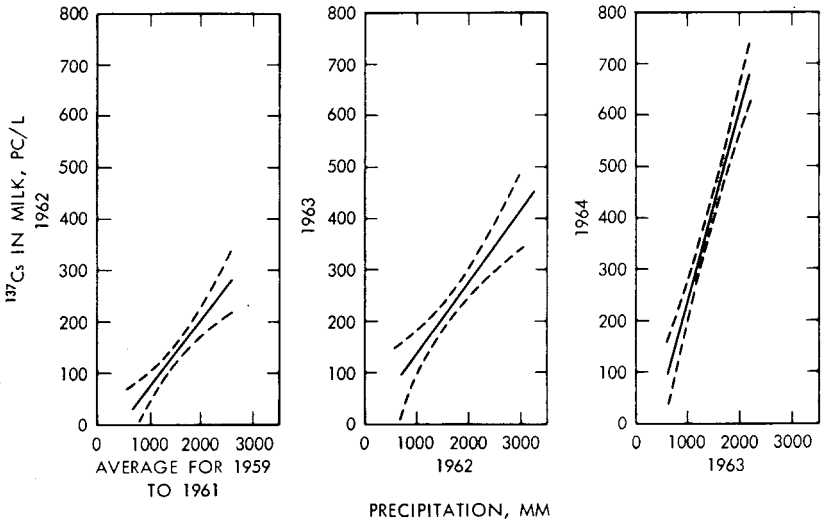

Fig. 9—Data for zone 2 showing lines of regression and corresponding curves of 95% confidence for the years indicated.

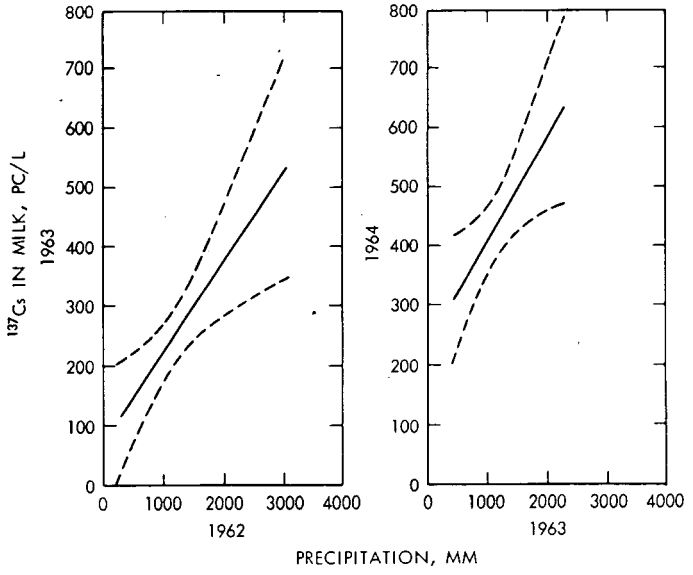

Fig. 10—Data for zone 3 showing lines of regression and corresponding curves of 95% confidence for the years indicated.

Fig. 11 — Total yearly precipitation in Norway averaged over a 30-year period. Contours are drawn for every 200 m of precipitation.

curves turned out to be so similar that only equations of first degree were used.)

DISCUSSION

The prevailing winds in Norway blow from west to east. At some distance from the coast, mountains force masses of moist air upward where the temperature is lower, causing moisture to condense and fall as rain or snow. This condition favors an increase in radioactive fallout. Figure 11 shows the total yearly precipitation in Norway averaged over a 30-year period. In zone 1 a greater part of the precipitation falls in summer as rain. A considerable part of the remaining precipitation that falls in this zone comes down as snow, bringing fallout with it. Part of this snow melts and together with its content of radioactive particles flows away while the earth is still frozen without contaminating the soil. In this way some of the radioactive particles are carried to the rivers and therefore do not contribute to the contamination of milk. In zone 2 most of the precipitation falls in winter as rain. In the counties Aust-Agder (8), Vest-Agder (9), and the southern part of Rogaland (10), the precipitation is more evenly distributed over summer and winter. In zone 3 by far the greater part of the dairies and also the districts where the milk is collected are situated along the coast. Here, too, most of the precipitation falls in winter, but a greater percentage than that in zone 2 falls as snow instead of rain. The precipitation continually decreases northward. In the interior of Finnmark (18) the climate is rather dry. Here most of the precipitation falls in summer as rain. The precipitation in zone 2 and partly in zone 3 is greater than that in zone 1 and therefore presumably washes out larger amounts of fallout from the atmosphere.

SUMMARY

The prevailing winds in Norway blow from west to east. Along the west coast the peculiar topographical conditions favor a greater precipitation and thus a greater deposition of radioactive fallout than in the eastern part of the country. The precipitation in several districts in Norway was estimated for three consecutive years (1961, 1962, and 1963), and the concentration of ^{137}Cs in milk from about 90% of the dairies in Norway was measured during the following spring of each year. Along the coast a statistically significant correlation between the precipitation one year and the amount of ^{137}Cs in the milk the following spring was demonstrated for three consecutive years. In the eastern part of Norway, no such systematic correlation was found.

Neither was any such correlation found between the precipitation during the months when grass for storage is grown (May, June, and July) and the amount of ^{137}Cs in the milk the following spring.

ACKNOWLEDGMENTS

The authors wish to acknowledge the assistance of P. Ogland, Norwegian Meteorological Institute, and D. Wøien, Computing Center, Oslo, Norway, for their contributions to these studies and also for support provided by the authors' organizations in addition to that by the U. S. Atomic Energy Commission.

REFERENCES

1. I. H. Blifford, L. B. Lockhart, and R. A. Baus, Relationship Between the Air Concentration of Radioactive Fission Products and Fallout, Report NRL-4607, U. S. Naval Research Laboratory, November 1955.
2. K. Lidén, Cesium-137 Burdens in Swedish Laplanders and Reindeer, *Acta Radiologica, 56:* 237 (1961).
3. K. Madshus, A. Strømme, and K. Koren, Caesium-137 Body Burden in Persons Chosen at Random from Selected Areas of Norway, *Nature, 200*(4903): (1963).
4. K. G. Vohra, V. S. Bhatnagar, U. C. Mishra, and S. Ragupathy, Measurement of Caesium-137 in Milk, *Health Physics, 6*(3/4): 142-148(1961).
5. M. Eisenbud, *Environmental Radioactivity,* pp. 104-105, McGraw-Hill Book Company, Inc., New York, 1963.
6. W. M. Myers, Differential Ion Uptake by Plants, *Symposium on Radioisotopes in the Biosphere,* pp. 210-211. R. S. Caldecott and L. A. Snyder (Eds.), University of Minnesota, Minneapolis, 1960.

DIETARY INTAKE OF RADIONUCLIDES: EFFECT OF CONSUMPTION PATTERNS AND EVALUATION BY USE OF INTEGRATING SAMPLES

J. C. THOMPSON, JR., and F. W. LENGEMANN
New York State Veterinary College, Cornell University,
Ithaca, New York

ABSTRACT

Most of the methods being utilized to estimate annual radionuclide-intake levels must use food-consumption data in the estimating process. However, estimates of food consumption have not matched the precision of laboratory radionuclide determinations. Thus much of the accuracy in estimating radionuclide intake may be lost because of the inadequacy, unrepresentativeness, or unavailability of accurate food-consumption data for much of the United States. Existing consumption data give gross indications of radionuclide intake, but these estimates may vary by more than 75% simply by the use of one estimate of food consumption instead of another. The errors of intake estimates may be even greater for specific population groups, but the lack of consumption data prevents their determination.

In an attempt to circumvent the difficulties of estimating dietary radionuclide intake, the use of an indicator product has been advanced. In some instances this product has been a component of the diet, but the inherent variations in consumption along with other unknown variables make this procedure unreliable. Experimental evidence has shown that it may be possible to use urine as an indicator for dietary levels of ^{90}Sr. This would be a self-compensating process for the changes in diet structure and would not require precise knowledge of food consumption. Studies have shown that the Observed Ratio based on urine/diet levels, or ^{90}Sr per gram of calcium in the urine/^{90}Sr per gram of

calcium in the diet, averaged 0.97 ± 0.08 for a group of normal subjects on normal diets for a 17-day period.

The determination of accurate estimates of radionuclide-intake levels is of vital importance if we are to determine the hazard from such radionuclides. The lack of this information can lead to uncertainty and hesitation during accidental releases of radioactivity or during accelerated nuclear-testing programs.

INTRODUCTION

The shortcomings of our procedures for estimating radionuclide intake were emphasized by the events following the 1961–1962 nuclear-test series. Although most of the confusion was centered around the estimates of ^{131}I intake, it was the inadequacy of certain basic data needed to properly interpret ^{131}I analyses which caused many of the problems. The basic data were missing because there were no networks biologically oriented to investigate the relations among air concentrations, ground deposition, pasture contamination, uptake processes, and milk distribution and processing operations and the ultimate consumption levels by various components of the population. The lack of this information made estimation of ^{131}I intake extremely difficult and the results controversial. In addition, there were uncertainties because of differences in uptake associated with age as well as the possibility that certain groups of people obtained measurable quantities of ^{131}I from nonmilk sources.

These uncertainties are similarly important in regard to the other radionuclides of concern in the human diet. Little is known of the differences in food intake and how its pattern may vary geographically or economically. No monitoring networks have been developed to follow radionuclides completely through the food chain to examine the interrelations that influence the uptake of these radionuclides. During the present moratorium it seems appropriate to develop such techniques and to quantify the relations in a manner that will provide accuracy both now and in the future should the need arise. Such action would alleviate the confusion experienced in the past in initiating plans designed to cope with levels of radionuclides thought to be too high for continued ingestion of the foods concerned.

In an attempt to show the nature of the variations in radionuclide intake, the emphasis of this paper is directed toward changes in food consumption and the resultant effect on radionuclide-intake levels. Strontium-90 will be used as the radionuclide in these comparisons, but many of the same principles apply to ^{137}Cs and to the shorter-lived radionuclides if consideration is given to the shorter half-lives.

TOTAL-DIET ^{90}Sr-INTAKE VARIATIONS

The methods used to estimate the level of ^{90}Sr in the diet can be classified under several categories:

1. Analysis of the total diet as consumed.
2. Analysis of a diet composite made up of individual foods that were selected and weighted by average per capita consumption data.
3. Analysis of individual foods weighted by consumption data and summarized for total-diet estimates.
4. Ratio analysis, which is the practice of relating another nuclide, preferably a gamma emitter, or the ^{90}Sr content of biological substances such as urine, feces, etc., to the dietary ^{90}Sr level (^{137}Cs/^{90}Sr, urine/diet, etc.).

The first two categories represent the most common methods in use and must contain accurate estimates of (1) radionuclide concentrations, (2) food consumption, and (3) diet composition to provide good estimates of intake levels. Seldom are these requirements met in full. Most of the emphasis has been directed toward the refinement and standardization of radiochemical procedures and the improvement of counting facilities. This effort has produced results that can generally be considered as dependable and representative for most fallout situations. However, no similar effort has been directed toward the development of food-consumption data. For estimation of radionuclide intake, it is necessary to blend the data from radionuclide networks with food-consumption statistics. If the food data are inaccurate, outdated, or inadequate in coverage, then the estimate of radionuclide intake is of questionable value.

Many of the food data in use are based on survey results[1] of 6000 households taken by the U. S. Department of Agriculture in 1955. This survey utilized a "recall-list" technique where respondents were asked about the foods consumed during the previous seven days. The sampling was conducted during the months of April, May, and June. The difficulty of extrapolating a week's recall data of this type to reflect a year's consumption is immediately obvious, but this is the standard practice utilized in nearly all estimates of annual radionuclide intake. Other problems such as the season of the year in which the survey was taken would result in variations of equal or greater magnitude. As an example of the complexities associated with expanding a week's results to a year, a comparison of similar recall-list techniques used during the Pilot Food Stamp Plan[2] in 1961 can be given (see Table 1). This survey is particularly appropriate because it shows consumption during a similar period of the year (April and May) in contrast with a later period (September and October) when the effects of season and the stamp program are evident. Two of the more seasonal vegetables,

Table 1—COMPARISON OF APPARENT ANNUAL CONSUMPTION* OF VARIOUS FOODS WHEN A ONE-WEEK SURVEY IS EXPANDED TO AN ANNUAL ESTIMATE, 1961 (PILOT FOOD STAMP PROGRAM)

Foods	Rural low income		Urban low income		Balance-sheet-analysis average (U. S.)
	Apr.–May	Sept.–Oct.	Apr.–May	Sept.–Oct.	
Fresh sweet corn	1.6	62.9	1.6	58.2	7.9
Fresh tomatoes	12.5	101.4	4.2	35.9	12.7
All vegetables	146.1	275.1	177.8	325.0	170.5
All fruits	126.9	150.8	121.7	176.8	153.8
Meat, fish, and eggs	163.1	172.1	214.8	291.2	208.9
Grain products	268.1	251.5	212.2	277.5	146.3
Dairy products	517.6	427.5	383.3	386.8	493.1

*Annual consumption rate in pounds.

sweet corn and tomatoes, give examples of the extremes of annual consumption patterns that can result from expanding a week's survey results. Major-category groupings show the nature of variations in the complete diet structure. These can be compared with balance-sheet data that are actually computed on a year's disappearance of food in the United States.[3] Grouping foods in this manner minimizes much of the variation found in individual foods, but it is indicative of the changes that occur when estimating procedures vary so widely.

Other estimates of food consumption may be obtained from consumer panels or nutrition studies, but such sources are usually lacking in area coverage or are confined to very restricted numbers and situations. It is obvious that the uses made of most food-consumption data leave much to be desired in terms of accurately estimating radionuclide intake.

The typical variations experienced in radionuclide intake from 1960–1963 are shown in Figs. 1 to 3, where various consumption estimates for three geographic areas of the United States are combined with radionuclide data from the Health and Safety Laboratory Tri-City Diet Studies.[4] The estimates for 1963 show the Northeast ranging from 8400 to 16,500 pc of ^{90}Sr, the North Central area from 5500 to 10,900 pc, and the West from 3800 to 7400 pc. The general trend of increased ^{90}Sr intake which followed the nuclear tests is well defined in each estimate.

In these figures the same ^{90}Sr data are used for each estimate of intake, but the food-consumption values are taken from various studies (Refs. 1 to 3, 5, and 6). The range of variations is restricted by the limited number of population groups for which there are estimates of food consumption. However, it is obvious that the teen-age diet had the

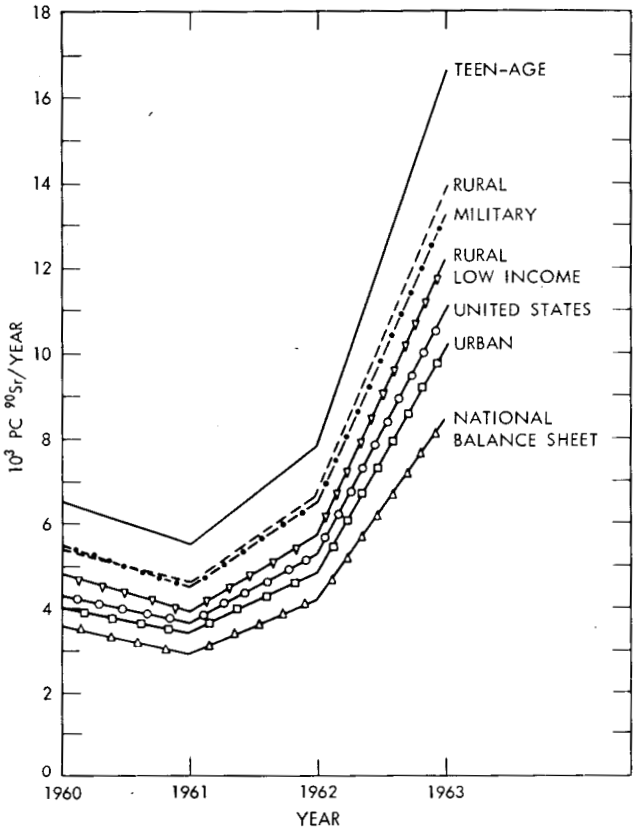

Fig. 1—Annual ^{90}Sr-intake estimates calculated from various food-consumption data for the northeastern United States for 1960–1963.

largest ^{90}Sr intake in each area, followed by the rural-household diet and the standard military diet. The diet of the teen-age group was constructed for the segment of the population considered to have the largest food intake, the 19-year-old male. Therefore it would be expected that the highest estimate of ^{90}Sr intake would be for this group.

Graphically, the intake estimates may seem to be within reasonable bounds, but if we consider that only one of these consumption estimates is used in the standard method of assessing ^{90}Sr intake, then it is desirable to investigate the nature of the variation around such an estimate. Figures 4 to 6 show this variation if average U. S. per capita food-consumption data are used in conjunction with radionuclide data to estimate ^{90}Sr intake. Variations about this estimate range from a 20% underestimate to a 55% overestimate, or a potential 75% error.

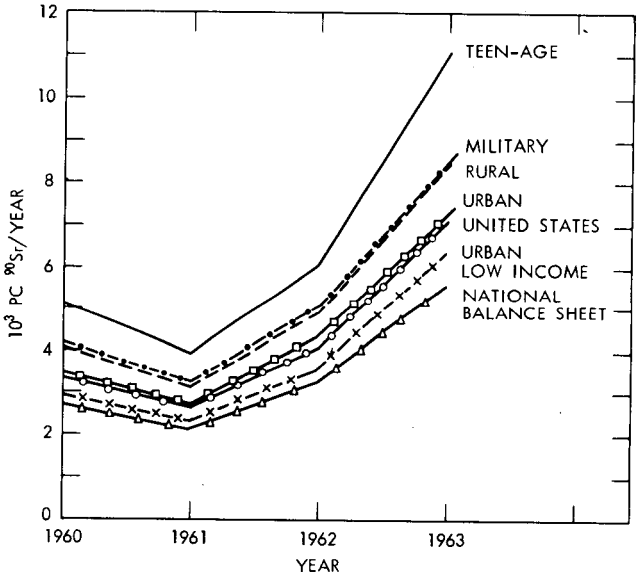

Fig. 2—Annual ^{90}Sr-intake estimates calculated from various food-consumption data for the north-central United States for 1960–1963.

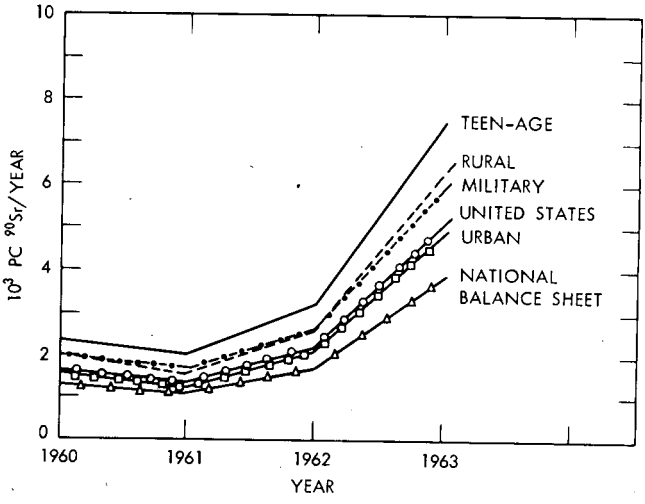

Fig. 3—Annual ^{90}Sr-intake estimates calculated from various food-consumption data for the western United States for 1960–1963.

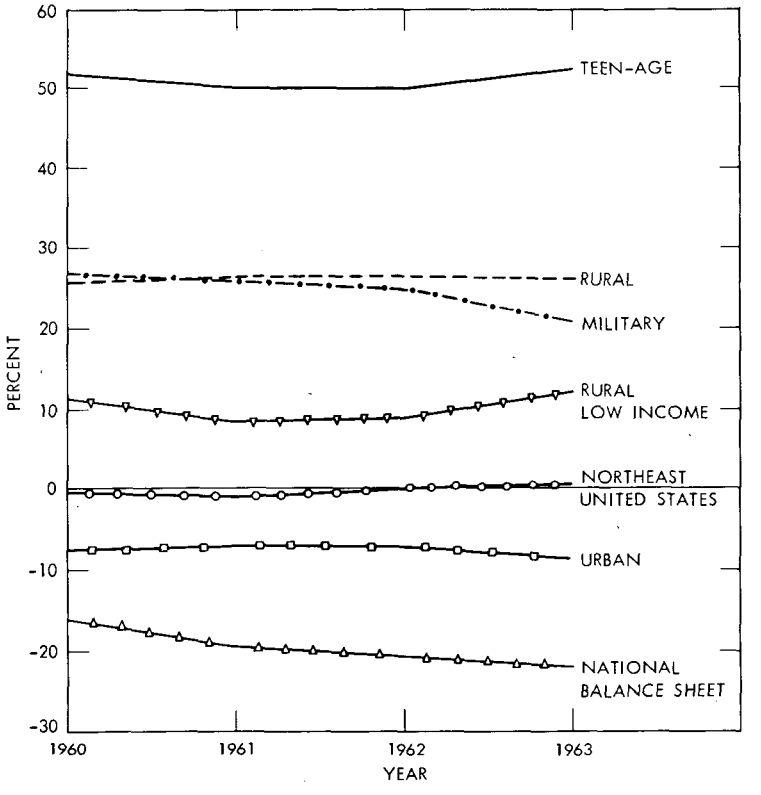

Fig. 4—Influence of using various consumption estimates on annual ^{90}Sr-intake levels for the northeastern United States for 1960–1963.

This error can be attributed to the misuse, unrepresentativeness, or unavailability of accurate food-consumption data. To operate within the bounds of such an error leaves many unanswered questions about the actual radionuclide intake. The potential variations in excess of these examples are many since we have very little information on diet structures for many groups of our population. Some data on "high" food consumers indicate a rate of consumption for certain food groups that is twice the average rates used in these computations.[7]

When these possible variations are coupled with the geographic differences in fallout deposition, it becomes, not a question of how close to actual intake our estimates are, but a question of how far our estimates may be from true intake values. The ranges of ^{90}Sr in milk provide a corollary to this concept since it is not uncommon to experience a 15-fold difference in reported concentrations within the United States. When these differences are coupled with variations in

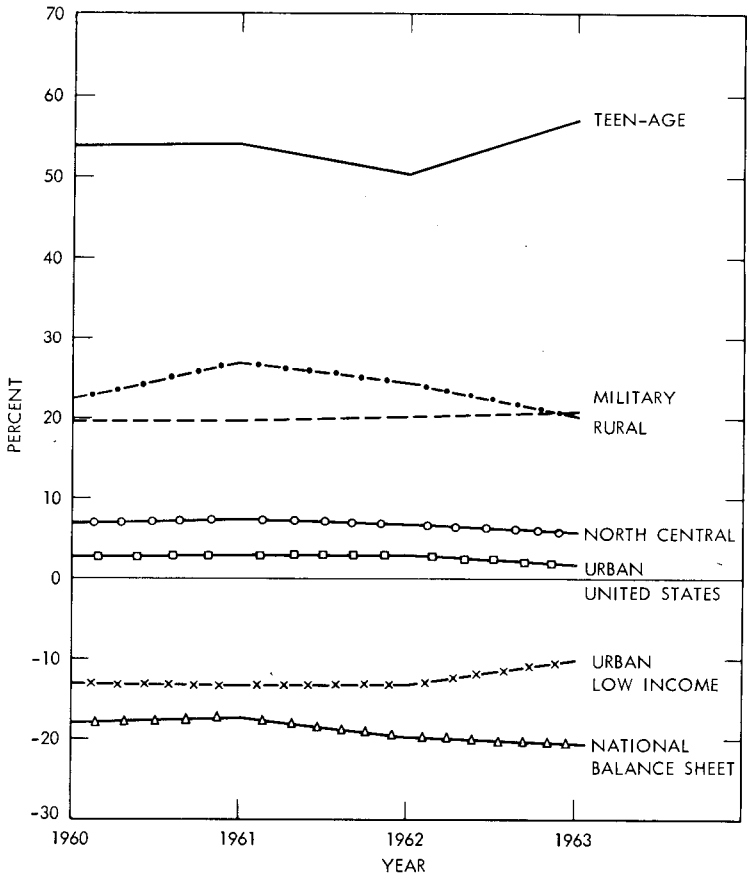

Fig. 5—Influence of using various consumption estimates on annual ^{90}Sr-intake levels for the north-central United States for 1960–1963.

milk consumption, the resulting estimates of radionuclide intake from milk equal or exceed the dispersion found in total-diet estimates.

VARIATIONS IN ^{90}Sr INTAKE FROM FLUID MILK BY GEOGRAPHIC AREA AND SEASON

Fluid milk can be used as a more definitive illustration of the radionuclide-intake problem since it has been possible to develop average monthly consumption data for many of the major market areas.[8] Forty of the markets correspond to the U. S. Public Health Service pasteurized-milk network and can therefore be used in conjunction with radionuclide data[9] as reported by this network (see Fig. 7).

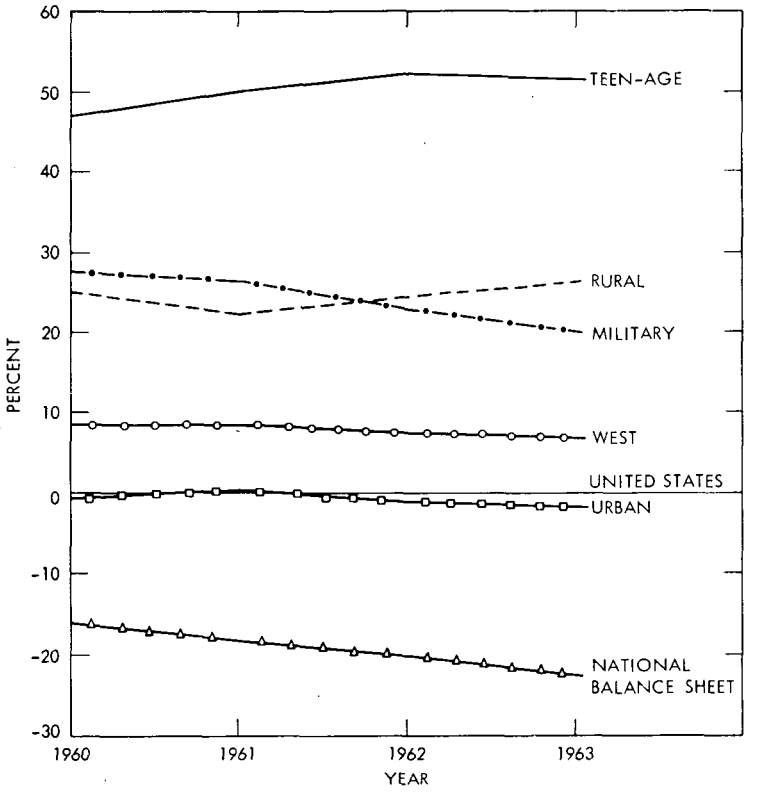

Fig. 6—Influence of using various consumption estimates on annual ^{90}Sr-intake levels for the western United States for 1960–1963.

With ^{90}Sr as an example, the annual intake from fluid milk varied from 400 to 4400 pc during 1963, or better than tenfold. The inadequacy of the use of one value as an estimate of ^{90}Sr intake from milk is quite obvious. However, it is possible to subdivide the areas by geographical features and reduce the range in values from tenfold to fivefold or less. When the data were grouped in this manner, it was clear that even further subdividing might be desirable (see Table 2). The existence of such widespread values in a product such as milk for which there is less variation annually, seasonally, and between various social, economic, and ethnic groups than many other foods indicates the need for more-precise estimating procedures. When the potential variations in total-diet estimates are considered (Figs. 4 to 6) and when these are coupled with variations of equal or greater magnitude in nearly every food product or food category, then it becomes highly questionable if our estimates of radionuclide intake are accurate for many groups of the population.

Table 2—COMPARISON OF ^{90}Sr INTAKE FROM MILK BY GEOGRAPHIC AREAS OF THE UNITED STATES, 1961–1963, PICOCURIES OF ^{90}Sr PER YEAR

Area	1961		1962		1963	
	Average	Range	Average	Range	Average	Range
Northeast	1220	900–1500	1662	1300–2200	3283	2500–4400
North Central	1058	800–1600	1433	900–2100	2676	1900–4300
South	917	300–1400	1757	700–2800	2623	1000–4000
West	771	600–1300	902	300–1700	1654	400–2500
United States	986	300–1600	1500	300–2800	2626	400–4400

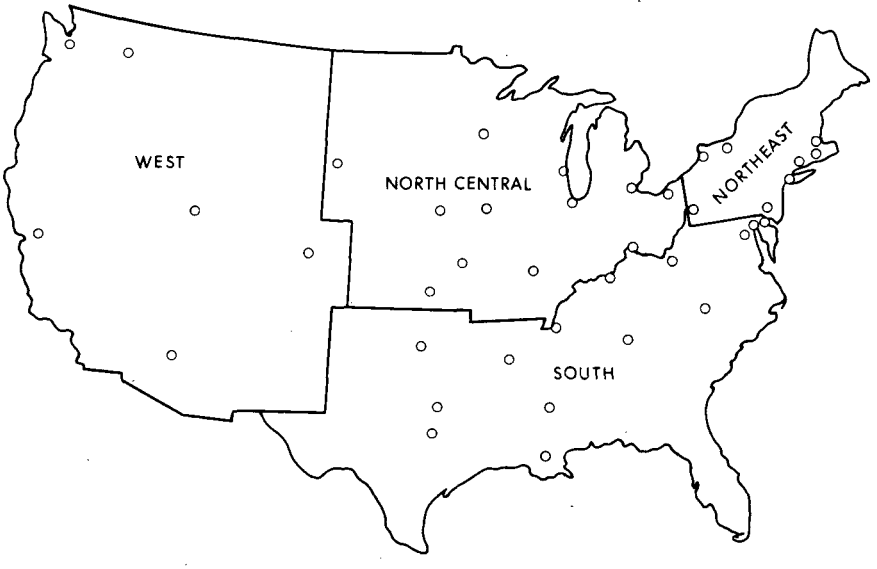

Fig. 7—Geographic location of markets included in the monthly milk-consumption network.

The range of values given for ^{90}Sr intake from milk are based on average consumption data for the total population in each area. Thus they do not indicate the variations arising from age or other variables that may influence the relative rate of consumption. Variations in milk consumption by age can be obtained from the Public Health Service–Bureau of the Census study[10] conducted during July 1962 (see Table 3). The range in values, which is from three- to fourfold, illustrates another consideration in the estimating of dietary ^{90}Sr intake. Since most milk is consumed by children and since this is the group of the population considered most susceptible to ^{90}Sr deposition, the age factor must be critically examined.[12]

Table 3—AVERAGE CONSUMPTION OF MILK BY VARIOUS AGE GROUPS IN THE UNITED STATES, JULY 1962, LITERS PER DAY

Age	Male	Female
Under 1	0.527	0.479
1 to 4	0.530	0.503
5 to 9*	0.479	0.447
10 to 14*	0.510	0.382
15 to 19*	0.510	0.293
20 to 24	0.352	0.213
25 to 29	0.293	0.192
30 to 34	0.263	0.166
35 to 44	0.243	0.160
45 to 54	0.228	0.154
55 to 64	0.240	0.169
Over 65	0.246	0.192
All ages	0.346	0.251

*Consumption in this table refers to quantities consumed at home. Since the school lunch program is in effect most of the year in many areas, it would be appropriate to add 0.237 liter (1 pint) per day to school groups.[11]

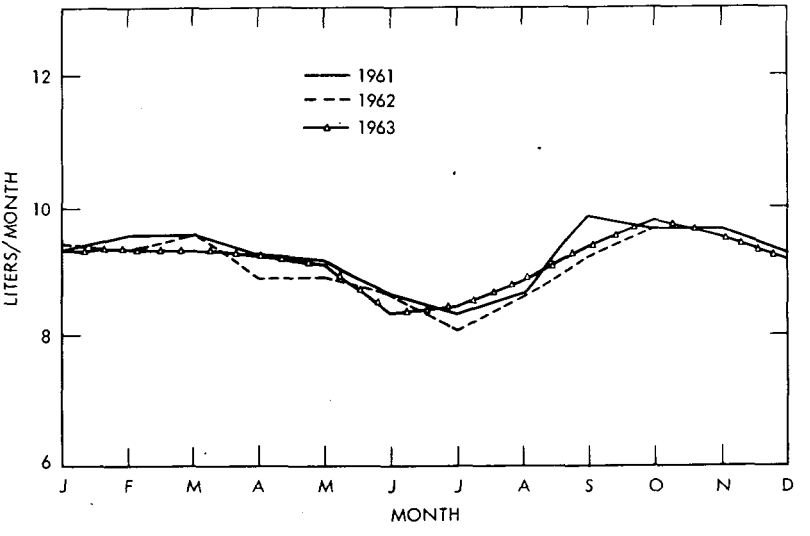

Fig. 8—Seasonal variation in monthly per capita milk consumption for 40 major U. S. markets for 1961–1963.

Another consideration is the seasonality of milk-consumption patterns as shown in Fig. 8. The typical summer decline can be associated with several factors such as school vacation and temperature. This decline is similar to the December-holiday decline that also occurs. The influence of a seasonal pattern of consumption on radionuclide intake may be an important consideration if large re-

leases of radioactivity were to occur (in which ^{131}I would be particularly significant). The pattern of seasonal ^{90}Sr intake from milk is shown in Fig. 9 for the 1961–1963 period. It is evident that the summer declines in milk consumption have not been of sufficient

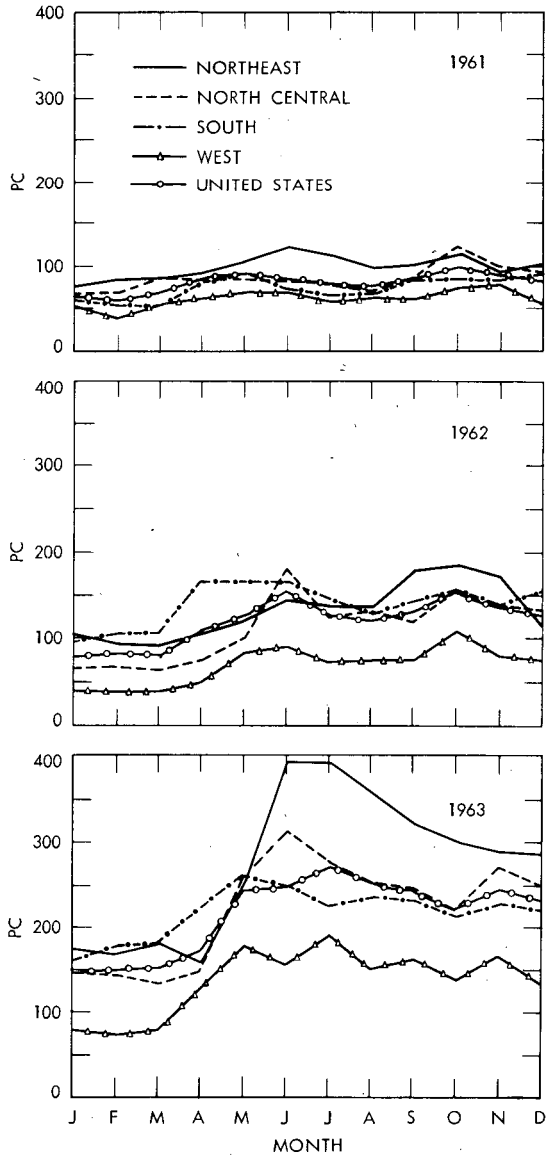

Fig. 9—Seasonal variation in ^{90}Sr intake from milk by geographic area of the United States for 1961–1963.

magnitude to offset the higher ^{90}Sr levels experienced during these months. The highest intake levels generally occur in the Northeast, followed by the North Central, South, and Western areas. However, in 1962 the South had the highest ^{90}Sr intake from milk.

In a consideration of some of the variables influencing radionuclide intake (from the various food-consumption estimates to the differences in milk consumption arising from geographic area, age, and seasonal influences), it is obvious that much of the information needed to assess radionuclide intake accurately is lacking. Thus our current estimates of radionuclide intake may only be considered as conditionally acceptable on a general population basis. We have no real indication of the range of values actually encountered, and it is this range, particularly the upper portion of it, which is of major importance. This is especially true since there is a general concensus that we are not currently at dangerous levels on a population-wide basis. If this follows, then we should know just how close the upper range of actual intake approaches a level of concern or, conversely, how much above our present evaluation of contamination are some groups of the population. It may not be critical at this time to know the bounds of our estimate for some radionuclides, but, if nuclear testing should resume or accidents should occur, we would need this information.

ALTERNATIVE METHODS OF ESTIMATING ^{90}Sr-INTAKE LEVELS

In an attempt to refine the process of estimating ^{90}Sr intake without accurate and up-to-date food-consumption data, an Observed Ratio (OR) study based on urine/diet levels has been proposed. Such a study would investigate the relation between the ^{90}Sr/calcium ratio in the urine to the ^{90}Sr/calcium ratio in the diet. Among the advantages of such a study are the following:

1. Urinary samples reflect total ^{90}Sr and calcium that enters the body. Thus there would be no need to estimate the contributions of various foods, and no food-consumption data would be needed.
2. Sudden changes would be quickly detected.
3. Sampling and bulking would be relatively simple.
4. Results could be classified in many different ways.
5. Time patterns of accumulation and dose estimations could be obtained.

Several studies in this area have already been conducted in conjunction with field nutrition studies[13] or in metabolic wards.[14,15] However, in each of these investigations, the pooling of urine has precluded an examination of individual variations that may influence the sampling

techniques and general applicability of such work. In addition, the representativeness of the samples from the field studies is questionable, and the conditions inherent in metabolic-ward studies do not reflect normal behavior for most individuals.

In an attempt to examine the nature of individual variations as well as to determine the feasibility of this approach under normal conditions, a urine/diet study was conducted during March 1964. Fourteen volunteers (7 males and 7 females) ranging in age from 21 to 33 years were placed on balanced diets for 17 days. The content of each day's diet was the same throughout the entire 17-day period. All diets were made up in advance from the same coded batches of raw products. They were prepared in frozen-dinner form and distributed to the volunteers on a prescribed schedule. The volunteers followed their normal daily work or recreational patterns, consuming the meals on their normal schedules. Daily urinary collections were started after six days and were subdivided to permit comparison of first morning specimens with "rest-of-day" or total 24-hr samples. Alternate-day samples were analyzed for each person to measure variations over time and between subjects. All volunteers completed the study and adhered strictly to the schedule.

The average ^{90}Sr level in the diet was 24.8 pc per gram of calcium for the male diet and 22.3 pc per gram of calcium for the female diet. Diet-calcium intakes were approximately 1.0 g in each instance.

Results of the analyses indicated an overall $OR_{urine/diet}$ of 0.97 ± 0.08 (1.07 for females and 0.87 for males). This compares with the $OR_{urine/diet}$ of 0.82 for young adults determined in the Samachson study.[15] The similarity of results would seem to indicate that urinary ^{90}Sr/calcium values can be used to predict dietary levels. However,

Table 4 — RELATIVE DISTRIBUTION OF $OR_{urine/diet}$ VALUES, DIETARY STUDY, 1964

$OR_{urine/diet}$	Percent of observations	$OR_{urine/diet}$	Percent of observations
< 0.50	1.9	1.25 to 1.49	3.8
0.50 to 0.74	23.1	1.50 to 1.74	1.9
0.75 to 0.99	44.2	1.74 to 1.99	3.8
1.00 to 1.24	17.3	> 2.00	3.8

this would not apply to estimates of individual persons since the range of daily $OR_{urine/diet}$ values observed in this study extended from 0.49 to 2.95. Although the difference between high and low values seems rather large, the OR values were concentrated in the range between 0.50 and 1.24 (see Table 4). Since 85% of the OR values were observed within this range, this procedure would seem to be suitable for esti-

mating ^{90}Sr dietary levels of representative samples of the population. It may be necessary to derive adjusted values for certain population groups that differ in consumption characteristics from the average levels, but such adjustment factors could be experimentally determined to provide estimating capabilities for most of the population.

Other results of the study indicated no statistically significant differences of $OR_{urine/diet}$ levels among individuals or within the same individuals over the time period of the study. This would indicate a capability for bulking samples among individuals over a given time span to obtain estimates of dietary ^{90}Sr levels. This procedure has already been used to estimate dietary ^{90}Sr levels in Poland[16] during a five-month period in 1962. Urinary samples were collected at random from persons undergoing periodic medical examinations. Diet estimates were based on the preliminary $OR_{urine/diet}$ values obtained in the work of Comar and Georgi[14] and Shulert.[13] Diet levels of 20 to 30 pc ^{90}Sr per gram of calcium were estimated on this basis, whereas observed dietary levels in surrounding countries were closer to a range of 10 to 20 pc ^{90}Sr per gram of calcium during that period. Use of more recently derived $OR_{urine/diet}$ values from this study and those of Samachson[15] would have placed the estimate within a range of 14 to 17 pc ^{90}Sr per gram of calcium.

Analyses of the urinary subsamples revealed that statistically significant differences were observed between the $OR_{urine/diet}$ of first morning urine specimens and total daily specimens (first morning averaged 1.62, compared to 1.13 for the daily average). This indicates that urinary samples should be representative of the total day's excretion for more accurate estimations of dietary ^{90}Sr levels.

Another study has been conducted to determine the feasibility of using the urinary $^{137}Cs/^{90}Sr$ ratio as an effective estimator of ^{90}Sr levels. The ease of measuring a gamma emitter such as ^{137}Cs in comparison to the time-consuming radiochemical procedures required for ^{90}Sr makes this approach most attractive. The experiment was set up so that 24 young rats received radiocesium and radiostrontium in the drinking water for a period of 67 days. After this period the rats were changed to nonradioactive water. Urinary collections were maintained throughout both phases. During the first 20 days, the urinary cesium/strontium ratio climbed rapidly to an equilibration ratio that was then maintained until the shift to nonradioactive water was made at 67 days (see Fig. 10). After the shift to nonradioactive water, the urinary cesium/strontium ratio climbed rapidly for four days to a value three times greater than the equilibrium value. It then began a steep decline that persisted during the next 45 days of observation. Interpreting these results for the human population indicates the possibility of using the ^{137}Cs content of the urine as an estimator of ^{90}Sr during periods of rather stable environmental levels

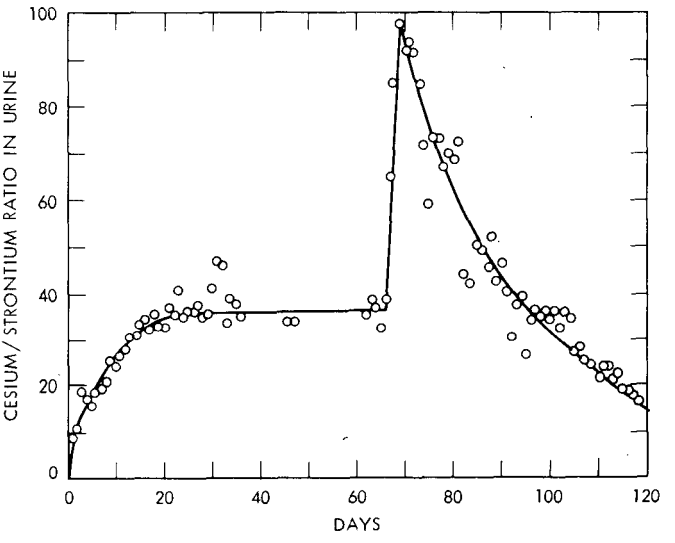

Fig. 10—Urinary cesium/strontium ratio in rats showing time pattern of increase, equilibration, and decline.

of these two nuclides. If the levels of the radionuclides fluctuated independently or if the dietary intake were altered significantly, the shift in the cesium/strontium ratio would make its use questionable for such estimating procedures. Thus the real advantage of using radiocesium would be to quickly estimate urinary ^{90}Sr for an ultimate estimate of dietary radiostrontium levels. This speed would be lost during an emergency situation when radionuclide levels are changed suddenly. The use of ^{137}Cs would require a period for equilibration to the new levels before estimates could be made.

SUMMARY

Variations in radionuclide intake resulting from changes or differences in food consumption can be significant, but the actual range of intake levels may be unknown because of lack of appropriate food-consumption data. Much added or updated information on food consumption is needed if we are to be capable of assessing the real hazard of radionuclide intake for many segments of the population. It appears that the estimates for the population at large may be usable in a gross sense, but they do not provide methods of estimating the extremes. It is these extreme areas which are of primary importance in any accidental release or sudden concentration of radioactivity.

In an attempt to compensate for the inadequacy of radionuclide estimates derived from food-consumption data, several approaches have been proposed:

1. Development of improved food-consumption estimates for many segments of the population.
2. Determination and use of appropriate $OR_{urine/diet}$ values for the various population groups. Food-consumption information would not be necessary to obtain this information.
3. Use of the urinary $^{137}Cs/^{90}Sr$ ratio as a ^{90}Sr indicator when environmental levels of fallout are relatively stable.

None of the preceding techniques will completely solve the problem, but each may aid in defining the population groups requiring further study.

With the continued nuclear moratorium, the need is to refine our techniques of estimation so that in the future we will not suddenly be faced with a problem of high radionuclide intake from a specified area or group of people. Our current methods in this program leave much to be desired. If there is a definite need to determine accurate radionuclide-intake data, then much improvement is needed.

ACKNOWLEDGMENT

Special thanks are given to C. L. Comar for his comments and assistance in preparing this paper.

REFERENCES

1. Agricultural Research Service, U. S. Department of Agriculture, Household Food Consumption Survey—1955, Reports 1 to 5, December 1956.
2. R. B. Reese and S. F. Adelson, Food Consumption and Dietary Levels Under the Pilot Food Stamp Program, Agricultural Economic Report No. 9, June 1962.
3. Economic Research Service, U. S. Department of Agriculture, National Food Situation—Food Consumption Per Capita, Report NSF-109, August 1964.
4. E. P. Hardy, Jr., et al., Fallout Program Quarterly Summary Reports, USAEC Reports HASL-105 (January 1961) to HASL-146 (July 1964), Health and Safety Laboratory.
5. M. H. Stein and E. I. Childs, A Total Diet Composite, Report No. 18-60, Quartermaster Food and Container Institute for the Armed Forces, May 1960.
6. Division of Pharmacology, Food and Drug Administration, Teen-Ager Diet Survey, *Radiol. Health Data, 4:* 18 (1963).
7. Agricultural Research Service, U. S. Department of Agriculture, High Consumption of Foods, Report HHE(Adm)-200, 1960.
8. Agricultural Marketing Service, U. S. Department of Agriculture, Federal Milk Order Market Statistics, Report Nos. FMOS-10 to -49, 1961 to 1964.

9. U. S. Public Health Service, Pasteurized Milk Network, *Radiol. Health Data, 2*(6) (1961) to 5(4) (1964).
10. U. S. Public Health Service—Bureau of the Census, Consumption of Selected Food Items in U. S. Households, *Radiol. Health Data, 4:* 124 (1963).
11. R. E. Moffett, L. Lundquist, and S. Johnson, The School Milk Program, Northeast Regional Research Publication Bulletin 368, November 1961.
12. Federal Radiation Council, Implications to Man of Irradiation by Internally Deposited Sr^{89}, Sr^{90} and Cs^{137}, December 1964.
13. A. R. Schulert, Assessment of Dietary Sr^{90} Through Urine Assay, *Nature, 189:* 933 (1961).
14. C. L. Comar and J. R. Georgi, Assessment of Chronic Exposure to Radiostrontium by Urinary Assay, *Nature, 191:* 390 (1961).
15. J. Samachson and H. Spencer-Lazlo, Sr^{90} Plasma Levels and Excretions in Young Adults, *Nature, 195:* 113 (1962).
16. W. Czosnowska, The Sr^{90} Level in Urine of Population in Poland in 1962, *Nukleonika, 8:* 779-782 (1963).

SESSION IV
DISCUSSION

INDIVIDUAL-PAPER DISCUSSION

Discussions that took place following the presentation of individual papers are given in this section. These discussions preceded the scheduled general discussions for the session.

HERDE: Dr. Martin, in your slide showing theoretical buildup of ^{131}I in milk and in human thyroids, you also showed an extrapolated value for the ^{131}I in the environs, i.e., in the atmosphere and on the foliage being eaten by animals. That line went straight to the zero-time ordinate. I wonder if you should have taken into consideration the buildup of ^{131}I that is not present immediately, which results from decay of ^{131}Sn, ^{131}Sb, and ^{131}Te in this case. I am not sure that it would change the model or the formula, but certainly the slide could show the buildup of ^{131}I in fallout as well as in the thyroid and in the milk.

MARTIN: No data were obtained to show the theoretical buildup of ^{131}I on plants. Instead, an arbitrary value for the concentration on plants at time zero was obtained by extrapolation from determinations made on D + 5 and D + 10. In this case time zero is approximately H + 12 hr, which would correspond roughly to the real levels of ^{131}I buildup from fission-product precursors.

HERDE: In 1955 I made thyroid measurements of native rabbits killed during the first evening after detonations and found four or five times as much ^{133}I as ^{131}I. I wondered whether you thought it worthwhile to assay for these shorter-lived nuclides. The challenge is enhanced by evidence of the presence also of ^{135}I. I have hoped that someone would start where my 1955 work for UCLA left off and extend it to demonstrate the significance of those shorter-lived isotopes of

iodine, although I realize they are not usually as important to man. Under certain conditions ^{133}I may be of health significance. It was very significant in the thyroid uptake by those men exploring a contaminated tunnel following an underground detonation in 1963. Obtaining better knowledge of ^{133}I cannot always be ignored from a health-hazard standpoint.

MARTIN: I agree with that. However, no data were collected to indicate thyroidal uptake of ^{133}I or ^{135}I by rabbits in the Sedan fallout field. The objective was to study ^{131}I. Since the half-lives of ^{133}I (20.8 hr) and ^{135}I (6.7 hr) are much shorter than the half-life of ^{131}I (8.04 days), we did not expect to find significant quantities of those isotopes in samples collected five days or more after the detonation.

FROM THE FLOOR: Dr. Tamplin, what is the number of the UCRL report you mentioned?

TAMPLIN: UCRL-7945-T.

BOYETT: Dr. Tamplin, you mentioned that a vital part of the program at LRL concerned the deposition rate of radionuclides on forage plants and animals, I believe. Are you gathering literature or has some information been obtained, as a part of this program, on the deposition of small particles on human skin?

TAMPLIN: We haven't been gathering information on that. However, with respect to iodine, for example, we have worried about the entrance of iodine in humans through the skin. This is probably the only kind of data we have looked at that deals with deposition on the skin. We have run across some reports that deal with the collection of fallout on the fur of animals, and this, as Dr. Martin mentioned, leads to a route of entry through preening for jackrabbits. I think we also have reports about fallout on the fur of some rats that were housed in cages, but, so far as the deposition of small particles on human skin, we haven't considered that.

GENERAL DISCUSSION

LENGEMANN: Dr. Ward, in all our experiments with cesium, we have noted that when milk cows are given radiocesium daily for a period of about 30 days, the milk radiocesium approaches 1.5% of the daily radiocesium intake per liter of milk. In your studies your animals only attained a value of 0.3% of the daily intake per liter of milk. How do you account for such a discrepancy between laboratory and field studies?

WARD: This is a thing that we have been interested in and have investigated to some extent. I believe it is related to the cellulose in

the feed. Originally, we thought it was due to availability, or what we called availability (and I suppose it really is); i.e., the cesium in natural feeds was less available to the animal, and, as I pointed out rather briefly in the talk, we do find large differences between high-concentrate, or high-grain, rations and those which contain predominantly hay or forage. We feel that cesium in forage is less available and in grain is more so. The cesium chloride isotope solution should be even more available.

Our work, the little we have done, seems to indicate it is a matter more of adsorption in the digestive tract, the undigested fibrous material adsorbs cesium and carries it out in the feces. This seems to agree fairly well with the observations of Patrick and others at Oak Ridge some years ago in working with rabbits and rats where they found that, if they fed the animals fibrous feed, a much higher percentage of the material was excreted in the feces. It also agrees with the well-established fact that there is a higher percentage excreted in the feces and a smaller percentage in the urine of ruminants as compared to nonruminants. The major difference between the species is that ruminants depend on a highly fibrous feed.

LENGEMANN: What would the radiocesium content of the milk be if the milk cows were consuming a high grain diet?

WARD: The figure I gave, 0.3% per liter, referred to a diet containing about 20 lb of hay and 10 lb of grain, which is about the average diet for milk cows in the United States. When we fed the minimum of hay, about 5 lb, and 20 to 30 lb of grain, the figures were 0.6 to 0.7% per liter. If one wanted to feed a straight grain ration, which introduces a lot of complications, the percentage presumably would go somewhat higher.

VAN MIDDLESWORTH: Dr. Ward, if the adsorption in the gut is partly responsible for this cesium loss, could your data suggest that added carrier cesium in the diet would increase the absorption rather than decrease it? That is, saturating the adsorption capacity with carrier perhaps would cause an increased absorption of fallout material rather than a decreased absorption. The body burden would be increased by giving carrier. Such a result is the opposite of the usual and expected result of addition of carriers.

WARD: I suppose that is right. I think, in the case of the ^{137}Cs, we are talking about such small numbers of atoms of material that if it were saturated this could well be the case.

LENGEMANN: Mr. Rivera, in some of your calculations, you used 0.35 for the discrimination factor for the infant from zero to one year of age. On the basis of the data reported by Dr. Beninson, it is difficult to see how such a value could arise.

RIVERA: This 0.35 was sort of a value for the whole year. It took into account not only Dr. Beninson's data but also our data and those of Loutit. We also took into account turnover during this time; therefore this was sort of an average effective discrimination factor for the year.

BENINSON: The values I presented did not assume any turnover. If 50% turnover for the first year were used, as Mr. Rivera has done, my data would give a value of about 0.4 for the discrimination factor.

RIVERA: There is the most interesting question when we get sufficient data that we want to investigate; i.e., will this discrimination of 0.35 also obtain during adolescence? The few data I have seem to indicate that discrimination may diminish at adolescence and reach this value. If we could find some animals that had an adolescence, maybe we could do some experiments with them to see if they have diminished discrimination during this second burst of skeletal growth rate.

TAMPLIN: Mr. Hardy, in the Rongelap study the ^{90}Sr was estimated from urine levels as 12 nc. How was this done?

HARDY: Do you mean how was the body burden estimated from the urine data?

TAMPLIN: Yes.

HARDY: This calculation was made by Dr. Cohn at Brookhaven,* using assumptions described in a report by K. T. Woodward et al.† I do not have these references with me and am not prepared to describe the calculation.

LENGEMANN: Mr. Hardy, in your study using the Rongelap diet, your data showed no return to the control level of radiocesium in the urine and feces when the individual was shifted back to his usual diet. Yet for radiostrontium there was a return to normal. You attributed the failure of the cesium level to return to the control level to a rise in the cesium content of the usual diet of the subject. Wouldn't you expect an increase also in the radiostrontium in the normal diet, leading to a failure of the urinary and fecal strontium to return to the control level?

---

*S. H. Cohn, Metabolism of Fission Products in Man: Marshallese Experience, in *Diagnosis and Treatment of Radioactive Poisoning, Symposium Proceedings, Vienna, 1962,* pp. 235-251, International Atomic Energy Agency, Vienna, 1963.

†K. T. Woodward, A. G. Schrodt, J. E. Anderson, H. A. Claypool, and J. B. Hartgering, The Determination of Internally Deposited Radioactive Isotopes in the Marshallese People by Excretion Analysis, USAEC Report DASA-1180, Walter Reed Army Medical Center, Institute of Research, 1959.

HARDY: We know that the ^{90}Sr level in the diet was also increasing, but ^{137}Cs was increasing at a faster rate and was more clearly reflected in the excretion values than was ^{90}Sr.

VAN MIDDLESWORTH: I would like to ask Dr. Strømme about something he had in a reprint he showed me but did not include in his paper regarding the different muscles of the body containing widely varying concentrations of cesium. Can you comment on this large difference? I wonder if the muscle cesium/potassium ratio was different. How do you account for these phenomena?

STRØMME: We have studied only one man so far for the paper I showed you. However, I know that reindeer have been studied very well in Norway, and it seems that the active muscles contain much more cesium than the inactive muscles. I don't know if this is true for potassium. The material was too scarce for potassium studies.

HARDY: Mr. Brar, can you or Dr. Gustafson give any reason for the increase in the ^{137}Cs bone levels after 20 years of age?

BRAR: No, I don't think we can. We are just trying to find what is in the bone. We don't know why it is there. People have not suspected there would be any cesium in the bone at all, but rather that all of it would be in tissue. However, Japanese investigators have found some, and we also have found some.

One of the speakers this morning mentioned that ^{137}Cs uptake from the soil was quite small, but still one finds quite a bit of this nuclide in grains, especially in those which are contained in pods, such as soybeans. Is there any possibility that cesium is absorbed through the leaves or stalks? Could someone answer that?

WARD: I am not a plant physiologist, but the answer is that cesium is very mobile in the plant once it has been absorbed. Presumably absorption occurs largely through foliar absorption. The cesium gets into the plant system and then could be transferred to the seeds quite readily.

BENINSON: On the same problem, I think that most of the data show that cesium levels depend mainly on the current rate of fallout. However, Dr. Frederickson and others claim that for some soils the soil-uptake component is important. Probably a good relation can be found which takes into account both the current year's fallout and the average of the fallout for the past two years. With this sort of equation it seems possible to fit the actual measured milk data. However, from experimental work on contaminated soil and in connection with waste disposal, it would seem that no cesium or, at most, a very small fraction would be taken up from soil.

RIVERA: In regard to cesium coming up from the soil, I think Wright Langham pointed out that it very critically depends on the soil. We know, for example, that in Rongelap a lot of foods are highly contaminated with cesium. It is not due to current fallout; therefore it must be getting into the food from the soil.

WARD: It should be pointed out that the soil is also quite different from the agricultural soils in this country as I understand it.

RIVERA: One of the earlier speakers showed a soil depth of penetration profile, and there was a little bump for cesium at 18 in., I think. I wonder what the explanation for this is.

HAWTHORNE: I think you will have to treat that as an experimental fact. I don't really have an explanation for it. I will speculate here and say that it may be concerned with the previous cultivation regime and represent where the top layer of soil was turned upside down and then sampled before it was returned.

FROM THE FLOOR: Is it difficult to control the influence on the assimilation of these various nuclides in the diet by the vitamin balance in the feed, e.g., tying vitamin D and calcium together? Is this difficult to do or is it, in fact, considered?

BENINSON: I don't know. My data were just on people under normal conditions. I don't know of any experimental work. Dr. Comar may wish to comment on this.

COMAR: One can produce small changes in the absorption and retention of various radionuclides by dietary changes. For example, vitamin D or lactose will increase absorption of alkaline earths, but not much can be done and a normal diet still be maintained. By use of an abnormal diet, it may be possible to change absorption by a factor of as much as 2, 3, or even 4, but with normal diets it is very difficult to do so.

RIVERA: I wonder if Dr. Thompson considers any of the diets, any of the variances he calculated, abnormal?

THOMPSON: No, I would not say that any of the diets used in the calculations were abnormal.

LENGEMANN: Several times during the presentations, we were given residence times of nuclides on plant foliage. We have had values, depending upon half-life, or 3 to 18 days and so on, but the statement has been made that when only the residence time is considered, i.e., when the radioactive half-life of the nuclide considered is eliminated, that there is relatively little difference between the isotopes of strontium, cesium, and iodine. I wonder whether we should observe differences between these materials as far as residence time on pasture

plants is concerned, or are they to be considered the same? Dr. Ward, you made one computation.

WARD: Mine was only on cesium. I would also like to know the answer. I suppose that it would have to do with the availability and mobility of the different ions. I really don't know. Dr. Hawley has some data.

HAWLEY: So far, our experience has been limited to iodine. We have certainly studied this question. On the surface at least, the statement that was made this morning was new to us, certainly to me. I would agree with Dr. Ward that it would depend upon the mobility of the ions or the particles being dealt with. When we were talking about iodine earlier, I did not mention a lot of things. One of them was that we set up intentionally to sample and try to determine the rate from airborne concentrations at which the iodine was coming back off the grass. Also, we set the experiment up with a kind of pseudoparticle sizing arrangement. This was so that we could get some information about the physical status of the material that would float around. It looks as though it is very nearly gaseous within the limits of what we are talking about, down to 1 μ anyway. It is coming off appreciably, but I can't give you any numbers yet. We have the data, and we intend to analyze and publish them.

Someone has asked me if we did any sizing in this iodine study. My answer was that we did but probably in too simple a manner. Our experimental farm in Idaho is located on the same grid that the Convair or General Dynamics people used during some fuel-element meltdown tests, which produced mixed fission elements. They tried to sample the whole spectrum of things. Their data indicate that there is a marked change in iodine behavior at about 1000 m from the ground, or surface, release point. With the fairly rough instruments we are using, it looks as if we might have about the same thing. For example, we found a change in ratio between a fibrous filter and the backup carbon. The ratio of activity between the two was very nearly 2 to 1, carbon to paper, across this grid close to the release point; but at about 1000 m or so, 1500 m in our last experiment, there was a marked change where the ratio of collection, or efficiency of collection, was almost unity, which indicated that somewhere in this range the iodine was behaving more like a particulate. We are planning to watch these things in plant-growth rooms and environmental chambers, and we are hoping to simulate them somewhat along the line of Chamberlain.

I think that it is an oversimplification to state that a particle, no matter what it adheres to, is going to have about the same residence time as another.

SOLDAT: I recently read a British document* which discussed ingestion hazards from fission-product contamination on vegetation. In this document it was assumed that all fission products would be removed from vegetation with a half-residence time of 14 days. This time would be that superimposed upon the radioactive half-life. For ^{131}I this turns out to be about a five-day total combined (effective) half-life. I assume that only particulate material is concerned here. Some of you may be familiar with this document. Since hazards mostly from fallout were evaluated, I would expect that the material is particulate. This is an indication that, at least for purposes of first approximation, some people have assumed that there is a uniform residence time regardless of nuclide.

There is one other comment I would like to add in view of the CERT tests that were discussed by Dr. Hawley. We had a small test at Hanford in July 1963 in which we had some human volunteers stationed some 200 m downwind; the uptake of ^{131}I from inhalation was about 25%. The breathing rate of these individuals was calibrated before the release and was about 0.5 cm^3/hr, or about half of the working value used by the International Commission on Radiological Protection as a standard for man. However, these people were at rest at the time. They were sitting in the expected path of the cloud.

WARD: Dr. Thompson, with regard to cesium, would you recommend urine analysis to predict cesium intake? This is of particular interest to me because we are planning such an experiment. Do you think this would be an adequate way of judging the intake?

THOMPSON: I think it is quite obvious from our graph that urine analysis has extreme limitations. Maybe Dr. Lengemann would like to comment on this.

LENGEMANN: We have data on intake and urinary excretion of radiocesium by both cows and rats. We, however, have not yet attempted to analyze the data for the correlation. This is to be done in the near future. A preliminary look at the data suggests that the correlation should be quite good.

WARD: I was thinking about a human diet.

LENGEMANN: Although we have no data for such an inference, I feel that it should also be a good correlation for the human.

BENINSON: I have a point of a general nature. It is on the relevance of the average and of the scatter in contamination of the diet. Is it really important to identify the extreme values at the levels we are

*Home Office, Science Advisors Branch, Basic Assumptions for Use in Assessment of the Radiological Hazard to Food from Fallout, British Report SA/PR-40(Rev.), May 1962.

talking about? If these values are used later on for estimation of radiation risks, we must keep in mind that in all these estimations, in one way or another, a linear relation between dose and probability of effect is assumed. If this is so, we are almost bound to use average values and not extreme ones. If we go to high doses, of course, this breaks down; but, at the low doses we are talking about, I think that it is only meaningful to use mean concentrations for the evaluation of risks.

LIST OF ATTENDEES

ALEXANDER, Lyle T., Agricultural Research Service, U. S. Department of Agriculture, Room 327, Soils Building, Plant Industry Station, Beltsville, Md. 20705

ALLEN, James S., Agricultural Research Service, U. S. Department of Agriculture, Room 327, Soils Building, Plant Industry Station, Beltsville, Md. 20705

ALLEN, Robert E., Weapons Effects Specialist, Nuclear Explosives Environmental Safety Branch, Division of Operational Safety, U. S. Atomic Energy Commission, Washington, D. C. 20545

ANDERSON, Maj. Donald L., Biology Branch, Division of Biology and Medicine, U. S. Atomic Energy Commission, Washington, D. C. 20545

ANDERSON, Wendell L., Chemistry Division, Code 6140, U. S. Naval Research Laboratory, Washington, D. C. 20390

ANTON, George T., SNPO-N, P. O. Box 1676, Las Vegas, Nev. 89101

ARTMAN, Capt. Joseph T., Division of Reactor Development, U. S. Atomic Energy Commission, Washington, D. C. 20545

ASHENFELTER, Thomas E., Atmospheric Radioactivity Research Branch, U. S. Weather Bureau, Washington, D. C. 20235

AUERBACH, Stanley I., Radiation Ecology Section, Building 2001, Oak Ridge National Laboratory, Oak Ridge, Tenn. 37831

AUTH, Maj. William J., Headquarters, U. S. Air Force Technical Applications Center, 2525 Telegraph Road, Alexandria, Va.

BAKER, Clara Mae, Fallout Studies Branch, Division of Biology and Medicine, U. S. Atomic Energy Commission, Washington, D. C. 20545

BAKER, Richard C., Union Carbide Corporation, Nuclear Division, P. O. Box 1410, Paducah, Ky. 42002

BALES, Ronald E., Division of Radiological Health, Radiological Health Laboratory, U. S. Public Health Service, 1901 Chapman Avenue, Rockville, Md. 20852

BARCHERS, Lydia M., Administrative Branch, Division of Biology and Medicine, U. S. Atomic Energy Commission, Washington, D. C. 20545

BARRER, Lester A., 11411 Fair Oak Drive, Silver Spring, Md. 20902

BARRETT, Paul A., Division of Headquarters Services, U. S. Atomic Energy Commission, Washington, D. C. 20545

BARTH, Delbert S., Southwestern Radiological Health Laboratory, U. S. Public Health Service, P. O. Box 684, Las Vegas, Nev. 89101

BATZEL, Roger E., University of California, Lawrence Radiation Laboratory, P. O. Box 808, Livermore, Calif. 94551

BAZAN, Fernando, Isotopes, Inc., 123 Woodland Avenue, Westwood, N. J. 07675

BEADLE, Robert W., Atmospheric Sampling Engineer, Fallout Studies Branch, Division of Biology and Medicine, U. S. Atomic Energy Commission, Washington, D. C. 20545

BECKER, Johann, National Museum, Quinta da Boa Vista, Rio de Janeiro, GB, Brazil
BELL, Marvin C., UT-AEC Agricultural Research Laboratory, 1299 Bethel Valley Road, Oak Ridge, Tenn. 37832
BELTER, Walter G., Division of Reactor Development, U. S. Atomic Energy Commission, Washington, D. C. 20545
BENINSON, Dan J., Comisión Nacional de Energía Atómica, Departamento de Proyectos Especiales, Avenida Libertador 8250, Buenos Aires, Argentina
BENSON, Philip A., Tracerlab Inc., 2030 Wright Avenue, Richmond, Calif. 94804
BERNARD, Harold, Environmental and Sanitary Engineering Branch, Division of Reactor Development, U. S. Atomic Energy Commission, Washington, D. C. 20545
BIERLY, Eugene W., Fallout Studies Branch, Division of Biology and Medicine, U. S. Atomic Energy Commission, Washington, D. C. 20545
BLIFFORD, Irving H., National Center for Atmospheric Research, Boulder, Colo. 80301
BLOORE, Ernest W., U. S. Army Nuclear Defense Laboratory, Building 5695, Edgewood Arsenal, Md. 21010
BOLIN, Bert, Institute of Meteorology, University of Stockholm, Tulegatan 41, Stockholm VA, Sweden
BOSTROM, Robert G., Division of Radiological Health, U. S. Public Health Service, 1901 Chapman Avenue, Rockville, Md. 20852
BOUTON, E. H., U. S. Army Nuclear Defense Laboratory, Edgewood Arsenal, Md. 21010
BOYETT, Ray H., Health Physics Technology, Health Physics Division, Oak Ridge National Laboratory, P. O. Box X, Oak Ridge, Tenn. 37831
BRAR, Sarmukh S., Argonne National Laboratory, 9700 South Cass Avenue D-202, Argonne, Ill. 60440
BRESLIN, Alfred J., Health and Safety Laboratory, U. S. Atomic Energy Commission, New York Operations Office, 376 Hudson Street, New York, N. Y. 10014
BRUNER, Harry D., M.D., Assistant Director for Medical and Health Research, Division of Biology and Medicine, U. S. Atomic Energy Commission, Washington, D. C. 20545
BUNTING, Mary I., Commissioner, U. S. Atomic Energy Commission, Washington, D. C. 20545
CABLE, Capt. John, Technical Analysis Branch, Division of Biology and Medicine, U. S. Atomic Energy Commission, Washington, D. C. 20545
CARROLL, Charles W., Editorial Branch, Division of Technical Information Extension, U. S. Atomic Energy Commission, P. O. Box 62, Oak Ridge, Tenn. 37831
CHANDLER, Robert P., Radiation Surveillance Center, U. S. Public Health Service, Room 2501, Temporary R Building, Washington, D. C. 20201
CHRISTIAN, John E., Bionucleonics Department, Purdue University, Lafayette, Ind. 47907
CHURA, Nicholas J., Patuxent Wildlife Research Center, Laurel, Md.
CLAFLIN, Capt. Alan B., U. S. Army Nuclear Defense Laboratory, Edgewood Arsenal, Md. 21010
CLAUS, Walter D., Special Assistant to the Director, Division of Biology and Medicine, U. S. Atomic Energy Commission, Washington, D. C. 20545
CLUFF, Frank D., U. S. Weather Bureau Research Station, P. O. Box 2136, Las Vegas, Nev. 89101
COHN, Stanton H., Medical Research Center, Brookhaven National Laboratory, Upton, L. I., N. Y. 11973
COMAR, Cyril L., Department of Physical Biology, New York State Veterinary College, Cornell University, Ithaca, N. Y. 14850
COOGAN, John S., Southwestern Radiological Health Laboratory, U. S. Public Health Service, P. O. Box 684, Las Vegas, Nev. 89101

COSTELLO, David C., Jr., Environmental and Sanitary Engineering Branch, Division of Reactor Development, U. S. Atomic Energy Commission, Washington, D. C. 20545

COWAN, George A., University of California, Los Alamos Scientific Laboratory, P. O. Box 1663, Los Alamos, N. Mex.

COWING, Russell F., Cancer Research Institute, New England Deaconess Hospital, 194 Pilgrim Road, Boston, Mass. 02215

CROCKER, Glenn R., Physical Chemistry Branch, Code 935, U. S. Naval Radiological Defense Laboratory, San Francisco, Calif. 94135

CROSSLEY, D. A., Jr., Radiation Ecology Section, Health Physics Division, Building 2001, Oak Ridge National Laboratory, Oak Ridge, Tenn. 37831

CULLEN, Thomas L., S.J., Loyola Seminary, Shrub Oak, N. Y.

DAHL, Adrian H., Department of Radiology and Radiation Biology, Colorado State University, Fort Collins, Colo. 80521

DANIELSON, Edwin F., Department of Meteorology, College of Mineral Industries, Pennsylvania State University, University Park, Penn. 16802

DARNEAL, Robert L., Radiological Physics and Instrumentation Branch, Division of Biology and Medicine, U. S. Atomic Energy Commission, Washington, D. C. 20545

DAVIS, James H., Defense Intelligence Agency, Department of Defense, Washington, D. C. 20301, ATTN: DIAAP-IK2

DAVIS, Jared J., Environmental Sciences Branch, Division of Biology and Medicine, U. S. Atomic Energy Commission, Washington, D. C. 20545

DAY, Walter C., U. S. Army Corps of Engineers, Nuclear Cratering Group, Lawrence Radiation Laboratory, P. O. Box 808, Livermore, Calif. 94551

DELAWARE, Cdr. Joseph L., Office of Tests, Division of Military Application, U. S. Atomic Energy Commission, Washington, D. C. 20545

DENHAM, Dale H., University of California, Lawrence Radiation Laboratory, P. O. Box 808, Livermore, Calif. 94451

DEVER, Robert F., Agricultural Research Service, U. S. Department of Agriculture, Room 327, Soils Building, Plant Industry Station, Beltsville, Md. 20705

DICKINSON, Maj. Hillmann, Nuclear Test Detection Office, Advanced Research Projects Agency, Department of Defense, Washington, D. C.

DIEFFENBACH, Emery M., Agricultural Research Service, U. S. Department of Agriculture, Room 318, North Building, Plant Industry Station, Beltsville, Md. 20705

DINGLE, A. Nelson, Department of Meteorology and Oceanography, The University of Michigan, Ann Arbor, Mich. 48104

DOMBECK, Norman J., U. S. Army Nuclear Defense Laboratory, Edgewood Arsenal, Md. 21010

DOUTHIT, Robert C., U. S. Army Nuclear Defense Laboratory, Edgewood Arsenal, Md. 21010

DREVINSKY, Peter J., Air Force Cambridge Research Laboratories (CRHU-1), L. G. Hanscom Field, Bedford, Mass. 01731

DROBINSKI, Joseph C., Jr., Northeastern Radiological Health Laboratory, U. S. Public Health Service, 109 Holton Street, Winchester, Mass. 01890

DUKE, Thomas W., Bureau of Commercial Fisheries, Radiobiological Laboratory, Beaufort, N. C.

DUNHAM, Charles L., M.D., Director, Division of Biology and Medicine, U. S. Atomic Energy Commission, Washington, D. C. 20545

DUNNING, Gordon M., Deputy Director, Division of Operational Safety, U. S. Atomic Energy Commission, Washington, D. C. 20545

DURUM, Walton H., Water Resources Division, U. S. Geological Survey, 2212 GSA Building, Washington, D. C.

EASTON, Earlene P., Fallout Studies Branch, Division of Biology and Medicine, U. S. Atomic Energy Commission, Washington, D. C. 20545

EDWARDS, Mary A., Building T-112, University of California, Lawrence Radiation Laboratory, P. O. Box 808, Livermore, Calif. 94551

EISENBUD, Merril, New York University, Institute of Environmental Medicine, Long Meadow Road, Tuxedo, N. Y. 10987
EISTER, Warren, Division of Isotopes Development, U. S. Atomic Energy Commission, Washington, D. C. 20545
ELLIOTT, R. B., Los Alamos Scientific Laboratory, University of California, Los Alamos, N. Mex.
EPPLE, Robert P., Division of Research, U. S. Atomic Energy Commission, Washington, D. C. 20545
ERICKSON, Carl A., 5518 S. Morgan Street, Seattle, Wash. 98108
FAIRHALL, A. W., Department of Chemistry, University of Washington, Seattle, Wash. 98105
FARRIS, Gerald C., Department of Radiology and Radiation Biology, Colorado State University, Fort Collins, Colo. 80521
FEELY, Herbert W., Isotopes, Inc., 123 Woodland Avenue, Westwood, N. J. 07675
FERBER, Gilbert J., Atmospheric Radioactivity Research Branch, U. S. Weather Bureau, Washington, D. C. 20235
FETERIS, Pieter J., The Illinois State Water Survey, P. O. Box 232, Urbana, Ill. 61802
FISHER, Henry L., Radiological Health Laboratory, U. S. Public Health Service, 1901 Chapman Avenue, Rockville, Md. 20852
FLEMING, Edward H., University of California, Lawrence Radiation Laboratory, P. O. Box 808, Livermore, Calif. 94551
FOOKS, Jack H., Research Branch, Division of Radiological Health, U. S. Public Health Service, 1901 Chapman Ave., Rockville, Md. 20852
FOOTE, Robert S., Science Services Division, Texas Instruments, Inc., P. O. Box 5621, Dallas, Tex.
FRANCE, Maj. Germanus J., Ninth Weather Reconnaissance Group, McClellan Air Force Base, Calif.
FREILING, Edward C., Head, Physical Chemistry Branch, Code 935, U. S. Naval Radiological Defense Laboratory, San Francisco, Calif. 94135
FREUDENTHAL, Peter C., New York University Medical Center, Institute of Environmental Medicine, Longmeadow Road, Tuxedo, N. Y. 10987
FRIEDLANDER, Sheldon K., W. M. Keck Engineering Laboratory, California Institute of Technology, Pasadena, Calif.
FRIEND, James P., Isotopes, Inc., 123 Woodland Avenue, Westwood, N. J. 07675
FUQUAY, James J., 2704 W Building, 200 W Area, Hanford Laboratories, General Electric Company, Richland, Wash. 99352
GADE, Cdr. Robert L., Defense Atomic Support Agency, The Pentagon, Room 1B685, Washington, D. C. 20301
GAMERTSFELDER, Carl C., Missile and Space Division, General Electric Company, P. O. Box 8555, Philadelphia, Pa. 19101
GARCIA, Lt. Arnoldo G., U. S. Army Nuclear Defense Laboratory, Edgewood Arsenal, Md. 21010
GARNER, Joseph M., Monsanto Research Corporation, Mound Laboratory, Mound Road, Miamisburg, Ohio
GAST, Robert G., UT–AEC Agricultural Research Laboratory, 1299 Bethel Valley Road, Oak Ridge, Tenn. 37832
GATZ, Donald F., Department of Meteorology and Oceanography, The University of Michigan, Ann Arbor, Mich. 48104
GIBSON, Thomas A., Jr., Plowshare Division, Lawrence Radiation Laboratory, P. O. Box 808 (L-43), Livermore, Calif. 94551
GLEIT, Chester E., Department of Chemistry, North Carolina State University, P. O. Box 5247, Raleigh, N. C. 27607
GOEKE, Roscoe H., Division of Radiological Health, U. S. Public Health Service, Room 1433, Temporary R Building, Washington, D. C. 20201
GOLDMAN, Morton I., Nuclear Utility Services, Inc., 1730 M Street, N.W., Washington, D. C.

GRAHAM, James B., Joint Committee on Atomic Energy, Room H-403, U. S. Capitol, Washington, D. C.

GREENE, Capt. Douglas R., Climatic Center, U. S. Air Force, Building 159, Navy Yard Annex, Washington, D. C. 20333

GREENE, Jack C., Office of Civil Defense, Department of the Army, The Pentagon, Washington, D. C. 20301

GUDIKSON, P. H., Department of Chemistry, University of Washington, Seattle, Wash. 98105

GUSTAFERRO, Capt. Joseph F., USN, Naval Analysis Group, Office of Naval Research, Department of the Navy, Washington, D. C. 20360

GUSTAFSON, Philip F., Argonne National Laboratory, 9700 South Cass Avenue, Argonne, Ill. 60440

HALL, Samuel J., Department of Meteorology, University of Oklahoma Research Institute, Norman, Okla. 73069

HAMADA, Gerald H., Hazleton-Nuclear Science Corporation, 4062 Fabian Way, Palo Alto, Calif. 94303

HAMMOND, Robert R., U. S. Naval Radiological Defense Laboratory, Code 934, San Francisco, Calif. 94135

HARDY, Edward P., Jr., Environmental Studies Division, Health and Safety Laboratory, U. S. Atomic Energy Commission, New York Operations Office, 376 Hudson Street, New York, N. Y. 10014

HARLEY, John H., Director, Health and Safety Laboratory, U. S. Atomic Energy Commission, New York Operations Office, 376 Hudson Street, New York, N. Y. 10014

HAWLEY, Clyde A., Jr., Health and Safety Division, U. S. Atomic Energy Commission, Idaho Operations Office, P. O. Box 2108, Idaho Falls, Idaho.

HAWTHORNE, Howard A., Laboratory of Nuclear Medicine and Radiation Biology, University of California at Los Angeles, School of Medicine, 900 Veteran Avenue, Los Angeles, Calif. 90024

HEALD, Walter R., Agricultural Research Service, U. S. Department of Agriculture, Room 331, Soils Building, Plant Industry Station, Beltsville, Md. 20705

HEFFTER, Jerome L., Atmospheric Radioactivity Research Branch, U. S. Weather Bureau, Washington, D. C. 20235

HEFT, Robert E., Biomedical Department, Lawrence Radiation Laboratory, P. O. Box 808, Livermore, Calif. 94551

HENNESSY, Thomas G., Laboratory of Nuclear Medicine and Radiation Biology, University of California, 900 Veteran Avenue, Los Angeles, Calif. 90024

HERDE, Karl E., U. S. Atomic Energy Commission, Savannah River Operations Office, P. O. Box A, Aiken, S. C. 29802

HERING, Wayne S., Air Force Cambridge Research Laboratories (CRHU-1), L. G. Hanscom Field, Bedford, Mass. 01731

HICKS, H. Gerald, Health and Safety Division, RL, U. S. Atomic Energy Commission, Richland Operations Office, P. O. Box 550, Richland, Wash. 99352

HIGHTOWER, Lt. Col. Dan, Department of Biophysics, Walter Reed Army Institute of Research, WRAMC, Washington, D. C. 20012

HILCKEN, Lt. Col. John A., 037417, U. S. Army Environmental Hygiene Agency, Edgewood Arsenal, Md. 21010

HILL, Jerald E., Physics Department, The Rand Corporation, 1700 Main Street, Santa Monica, Calif.

HILL, Maj. John P., Nuclear Test Detection Office, Advanced Research Projects Agency, Department of Defense, Washington, D. C.

HILSMEIER, William F., U. S. Weather Bureau, Atomspheric Turbulence and Diffusion Laboratory, P. O. Box E, Oak Ridge, Tenn. 37831

HINES, Neal O., Committee on Governmental Relations, 1785 Massachusetts Avenue, N.W., Washington, D. C. 20036

HODGES, Harold L., Sandia Cooperation, P. O. Box 5800, Albuquerque, N. Mex. 87115

HOLLAND, Joshua Z., 2035 E. Newton Street, Seattle, Wash. 98102

HOLLISTER, Hal L., Technical Analysis Branch, Division of Biology and Medicine, U. S. Atomic Energy Commission, Washington, D. C. 20545
HOLMES, A. Wendell, Health and Safety Division, U. S. Atomic Energy Commission, Chicago Operations Office, 9800 South Cass Avenue, Argonne, Ill. 60439
HOWER, Elizabeth A., Program Coordination Branch, Division of Biology and Medicine, U. S. Atomic Energy Commission, Washington, D. C. 20545
HUFF, Floyd A., Illinois State Water Survey, Box 232, Urbana, Ill. 61802
HULL, Andrew P., Health Physics Division, Brookhaven National Laboratory, Upton, L. I., N. Y. 11973
HUMERICK, Eveyln R., Program Coordination Branch, Division of Biology and Medicine, U. S. Atomic Energy Commission, Washington, D. C. 20545
JAMES, Paul E., Agricultural Engineering Laboratory, Agricultural Research Center, U. S. Department of Agriculture, Beltsville, Md. 20705
JOHNSON, James E., Animal Science Department (Dairy), Colorado State University, Fort Collins, Colo. 80521
JONES, Douglas M. A., Illinois State Water Survey, Box 232, Urbana, Ill. 61802
JONES, Sam P., Applied Science Division, Litton Systems, Inc., 2295 Walnut Street, St. Paul 13, Minn.
JORDAN, Harry S., Los Alamos Scientific Laboratory, P. O. Box 1663, Los Alamos, N. Mex.
JOSEPH, Arnold B., Environmental Sciences Branch, Division of Biology and Medicine, U. S. Atomic Energy Commission, Washington, D. C. 20545
KAHN, Bernd, Acting Chief, Radiological Health Research Activities, Robert A. Taft Sanitary Engineering Center, U. S. Public Health Service, 4676 Columbia Parkway, Cincinnati, Ohio 45226
KAHN, James S., University of California, Lawrence Radiation Laboratory, P. O. Box 808, Livermore, Calif. 94551
KALKSTEIN, Marvin I., Air Force Cambridge Research Laboratories (CRHU-1), L. G. Hanscom Field, Bedford, Mass. 01731
KANE, Maj. Ronald D., Headquarters, U. S. Air Force Technical Applications Center, 2525 Telegraph Road, Alexandria, Va.
KARCHES, Gerald J., Acting Assistant Chief, Radiological Health Research Activities, Robert A. Taft Sanitary Engineering Center, U. S. Public Health Service, 4676 Columbia Parkway, Cincinnati, Ohio 45226
KEITH, James E., Division 5414, Sandia Corporation, P. O. Box 5800, Albuquerque, N. Mex. 87115
KELLER, Harry B., University of California, Lawrence Radiation Laboratory (L-43), P. O. Box 808, Livermore, Calif. 94551
KENNEKE, Albert P., Division of Safety Standards, U. S. Atomic Energy Commission, Washington, D. C. 20545
KESSLER, Wayne V., Bionucleonics Department, Purdue University, Lafayette, Ind. 47907
KIRBY-SMITH, John S., Biology Branch, Division of Biology and Medicine, U. S. Atomic Energy Commission, Washington, D. C. 20545
KLEIN, Ralph, U. S. National Bureau of Standards, Washington, D. C.
KLEMENT, Alfred W., Jr., Acting Chief, Fallout Studies Branch, Division of Biology and Medicine, U. S. Atomic Energy Commission, Washington, D. C. 20545
KLEMENT, Frances B., 9903 Cedar Lane, Bethesda, Md.
KLINE, Jerry R., Division of Biology and Medicine, Argonne National Laboratory, Argonne, Ill. 60440
KNIPP, Maj. Arthur L., Jr., Hqs. Joint Task Force Eight, Barton Hall, Washington, D. C. 20305
KNOX, Joseph B., K Division, University of California, Lawrence Radiation Laboratory, Livermore, Calif. 94551
KORANDA, John J., Building T-112, University of California, Lawrence Radiation Laboratory, P. O. Box 808, Livermore, Calif. 94551
KREY, Philip W., Isotopes, Inc., 123 Woodland Avenue, Westwood, N. J. 07675

KRIEGSMAN, William E., Division of Inspection, U. S. Atomic Energy Commission, Washington, D. C. 20545

KRUGER, Paul, Hazleton-Nuclear Science Corporation, 4062 Fabian Way, Palo Alto, Calif. 94303

KUNISHI, Harry M., Agricultural Research Service, U. S. Department of Agriculture, Room 313, Soils Building, Plant Industry Station, Beltsville, Md. 20705

KURODA, Paul K., Department of Chemistry, University of Arkansas, Fayetteville, Ark. 72701

LACY, William J., Civil Defense Research, Office of the Secretary of the Army, Department of Defense, The Pentagon, Washington, D. C. 20301

LAGOMARSINO, Raymond J., Isotopes, Inc., 123 Woodland Avenue, Westwood, N. J. 07675

LANGER, Gerhard, National Center for Atmospheric Research, P. O. Box 1470, Boulder, Colo. 80301

LARSON, Kermit H., Laboratory of Nuclear Medicine and Radiation Biology, University of California, 900 Veteran Avenue, Los Angeles, Calif. 90024

LAUG, Edwin P., Special Investigations Branch, Division of Pharmacology, U. S. Food and Drug Administration, Washington, D. C.

LEE, Hong, Stanford Research Institute, Menlo Park, Calif.

LEITNAKER, Maj. Frank C., MC, Department of Isotope Metabolism, Division of Nuclear Medicine, Walter Reed Army Institute of Research, WRAMC, Washington, D. C. 20012

LENGEMANN, Frederick W., Department of Physical Biology, New York State Veterinary College, Cornell University, Ithaca, N. Y. 14850

LEVENTHAL, Leon, Tracerlab, Inc., 2030 Wright Avenue, Richmond, Calif. 94804

LEWIS, Col. Converse R., Jr., Office of the Surgeon General, Department of the Army, Main Navy Building, Room 1601, Washington, D. C. 20315

LEWIS, Gary B., Reynolds Electrical & Engineering Company (RAD SAFE), Mercury, Nev.

LILIENFELD, Pedro, Del Electronics Corporation, 250 E. Sandford Boulevard, Mount Vernon, N. Y. 10550

LIST, Robert J., Atmospheric Radioactivity Research Branch, U. S. Weather Bureau, Washington, D. C. 20235

LIU, Benjamin Y. H., Department of Mechanical Engineering, University of Minnesota, Minneapolis, Minn. 55455

LOCKHART, Luther B., Jr., U. S. Naval Research Laboratory, Code 6110, Washington, D. C. 20390

LOUGH, S. Allan, Assistant Director for Radiological Physics, Division of Biology and Medicine, U. S. Atomic Energy Commission, Washington, D. C. 20545

LOWDER, Wayne M., Radiation Physics Division, Health and Safety Laboratory, U. S. Atomic Energy Commission, New York Operations Office, 376 Hudson Street, New York, N. Y. 10014

LOYSEN, Peter, Health and Safety Laboratory, U. S. Atomic Energy Commission, New York Operations Office, 376 Hudson Street, New York, N. Y. 10014

LUBOMIRSKI, Ralph S., Nuclear Utility Services, 1730 M Street, N.W., Washington, D. C.

McBIRNEY, Stanley W., Agricultural Research Service, U. S. Department of Agriculture, Room 318, North Building, Plant Industry Station, Beltsville, Md. 20705

McCABE, Lt. Col. John T., 1210th Weather Squadron, Building 159, Navy Yard Annex, Washington, D. C. 20333

McCARVILL, Thomas J., Division of Peaceful Nuclear Explosives, U. S. Atomic Energy Commission, Washington, D. C. 20545

McCRAW, Tommy F., Nuclear Explosives Environmental Safety Branch, Division of Operational Safety, U. S. Atomic Energy Commission, Washington, D. C. 20545

McCUTCHEN, John H., Milk and Food Branch, Division of Environmental Engineering and Food Protection, Bureau of State Services, U. S. Public Health Service, Washington 25, D. C.

MACHTA, Lester, U. S. Weather Bureau, Air Resources Laboratory, Washington, D. C. 20235

MAGIN, George B., Jr., Division of Isotopes Development, U. S. Atomic Energy Commission, Washington, D. C. 20545

MAHLMAN, Jerry D., Department of Atmospheric Science, Colorado State University, Fort Collins, Colo. 80521

MARKARIAN, Carnick A., Radiological Health Laboratory, U. S. Public Health Service, 1901 Chapman Avenue, Rockville, Md. 20852,

MARLOW, William F., Fallout Studies Branch, Division of Biology and Medicine, U. S. Atomic Energy Commission, Washington, D. C. 20545

MARTELL, Edward A., National Center for Atmospheric Research, 1420 30th Street, Boulder, Colo. 80301

MARTER, Walter L., Health Physics Section, E. I. du Pont de Nemours & Co., Inc., Savannah River Plant, Aiken, S. C.

MARTIN, Robert H., Office of Naval Weather Service, Building 200, Navy Yard Annex, Washington, D. C. 20390

MARTIN, Whitfield A., Hqs. U. S. Air Force Technical Applications Center/TD4, Washington, D. C. 20333

MARTIN, William E., Laboratory of Nuclear Medicine and Radiation Biology, University of California, Los Angeles, Calif. 90024

MAXWELL, Roy D., Nuclear Explosives Environmental Safety Branch, Division of Operational Safety, U. S. Atomic Energy Commission, Washington, D. C. 20545

MAYBERRY, Bennie D., Dean, School of Agriculture, Tuskegee Institute, Ala. 36088

MENON, K. K., Department of Chemistry, University of Arkansas, Fayetteville, Ark. 72701

MENZEL, Ronald G., Agricultural Research Service, U. S. Department of Agriculture, Room 335, Soils Building, Plant Industry Station, Beltsville, Md. 20705

MEYER, Eric L., General Hydrology Branch, Water Resources Division, U. S. Geological Survey, Room 1242-A, General Services Building, Washington, D. C. 20242

MEYER, Milton W., Agricultural Research Service, U. S. Department of Agriculture, Room 327, Soils Building, Plant Industry Station, Beltsville, Md. 20705

MILLER, A. James, 54-1522, Department of Meteorology, Massachusetts Institute of Technology, Cambridge, Mass. 02139

MILLER, Carl F., Stanford Research Institute, 333 Ravenswood Avenue, Menlo Park, Calif.

MILLER, Charles E., Jr., Oak Ridge National Laboratory, P. O. Box X, Oak Ridge, Tenn. 37831

MILLER, James E., Fallout Studies Branch, Division of Biology and Medicine, U. S. Atomic Energy Commission, Washington, D. C. 20545

MILLER, Robert, Applied Science Division, Litton Systems, Inc., 2295 Walnut Street, St. Paul 13, Minn.

MISKEL, John A., University of California, Lawrence Radiation Laboratory, P. O. Box 808, Livermore, Calif. 94551

MITCHELL, Harold H., M.D., Rand Corporation, 1700 Main Street, Santa Monica, Calif.

MORGAN, Col. MacPherson, USAF, Deputy Assistant Director for Tests, Division of Military Application, U. S. Atomic Energy Commission, Washington, D. C. 20545

MORRIS, Capt. George A., U. S. Army Corps of Engineers, Nuclear Cratering Group, Lawrence Radiation Laboratory, P. O. Box 808, Livermore, Calif. 94551

MORTON, William B., U. S. Forest Service, Electronics Center, Agricultural Research Center, Beltsville, Md. 20705

MULLER, Ragnwald, Office of the Commissioners, U. S. Atomic Energy Commission, Washington, D. C. 20545

MURRAY, James L., Medical Research Branch, Division of Biology and Medicine, U. S. Atomic Energy Commission, Washington, D. C. 20545

MURTHY, Gopala K., Milk and Food Research, Robert A. Taft Sanitary Engineering Center, U. S. Public Health Service, 4676 Columbia Parkway, Cincinnati, Ohio 45226

MUSGRAVE, Burdon C., Department of Chemistry, University of Arkansas, Fayetteville, Ark. 72701

NATHAN, Marcel, Tracerlab, Laboratory for Electronics, Inc., 2030 Wright Avenue, Richmond, Calif. 94804

NELSON, Daniel J., Radiation Ecology Section, Oak Ridge National Laboratory, Oak Ridge, Tenn. 37831

NERVIK, Walter E., University of California, Lawrence Radiation Laboratory, P. O. Box 808, Livermore, Calif. 94551

NEWELL, Reginald E., 54-1522, Department of Meteorology, Massachusetts Institute of Technology, Cambridge, Mass. 02139

NG, Yook C., Building T-112, University of California, Lawrence Radiation Laboratory, P. O. Box 808, Livermore, Calif. 94551

NICHOLSON, Kenneth J., Technical Analysis Branch, Division of Biology and Medicine, U. S. Atomic Energy Commission, Washington, D. C. 20545

NIELSEN, Julian M., 300 Area, 329 Building, Hanford Laboratories, General Electric Company, Richland, Wash. 99352

NIKULA, John, Air Force Cambridge Research Laboratory, Office of Aerospace Research, L. G. Hanscom Field, Bedford, Mass. 01731

ODUM, Howard Thomas, Puerto Rico Nuclear Center, Caparra Heights Station, San Juan, Puerto Rico 00935

O'FARRELL, Edward, Defense Intelligence Agency, Department of Defense, Washington, D. C. 20301, ATTN: DIAAP-IK2

O'LEARY, Thomas F., Division of Special Projects, U. S. Atomic Energy Commission, Washington, D. C. 20545

OLSON, Jerry S., Radiation Ecology Section, Building 2001, Oak Ridge National Laboratory, Oak Ridge, Tenn. 37831

OSBURN, William S., Institute of Arctic and Alpine Research, University of Colorado, Boulder, Colo. 80301

ÖSTLUND, Göte H., University of Miami, Institute of Marine Science, 1 Rickenbacker Causeway, Virginia Key, Miami, Fla. 33149

OSTROM, Lt. Col. Thomas B., Life Sciences Division, Office of the Chief, Research and Development, Headquarters, Department of the Army, Washington, D. C.

OWE BERG, T. G., 14361 Deanann Place, Garden Grove, Calif.

PACK, Donald H., Air Resources Laboratory, Office of Meteorological Research, U. S. Weather Bureau, Washington, D. C. 20235

PALES, Jack C., U. S. Weather Bureau Research Station, P. O. Box 2136, Las Vegas, Nev. 89101

PALMER, H. E., Hanford Laboratories, General Electric Company, Richland, Wash. 99352

PALMITER, Claire C., Room 1101, Federal Radiation Council, 1815 H Street, N.W., Washington, D. C. 20449

PALUMBO, Ralph F. (Deceased), Laboratory of Radiation Biology, Fisheries Center, University of Washington, Seattle, Wash. 98105

PARK, Archibald B., Agricultural Research Service, U. S. Department of Agriculture, Federal Center Building, Hyattsville, Md. 20781

PATTERSON, Robert L., Jr., U. S. Naval Research Laboratory, Code 6110, Washington, D. C. 20390

PECCI, Joseph, Air Force Cambridge Research Laboratories (CRHU-1), L. G. Hanscom Field, Bedford, Mass. 01731
PECSOK, Donald A., Division of Radiological Health, U. S. Public Health Service, Washington, D. C.
PELLETIER, Charles A., Environmental Health Department, School of Public Health, The University of Michigan, Ann Arbor, Mich. 48104
PETERSEN, Allen H., Building T-112, University of California, Lawrence Radiation Laboratory, P. O. Box 808, Livermore, Calif. 94551
PETERSON, Kendall R., Atmospheric Radioactivity Research Branch, U. S. Weather Bureau, Washington, D. C. 20235
PETERSON, Lt. Cdr. Richard E., Defense Atomic Support Agency, Washington, D. C. 20301
POLAN, Marvin, Ford Instrument Company, Division of Sperry Rand Corp., 31-10 Thomson Avenue, Long Island City, L. I., N. Y. 11101
POLK, Capt. Adrian V., Defense Atomic Support Agency, Washington, D. C. 20301
PORTER, Sydney W., Jr., Armed Forces Radiobiology Research Institute, National Naval Medical Center, Bethesda, Md. 20014
PROUTY, Richard M., Chemistry Section, Patuxent Wildlife Research Center, Laurel, Md. 20810
RABSON, Robert, Biology Branch, Division of Biology and Medicine, U. S. Atomic Energy Commission, Washington, D. C. 20545
RAPP, R. Robert, The Rand Corporation, 1700 Main Street, Santa Monica, Calif.
RAYNOR, Gilbert S., Brookhaven National Laboratory, Upton, L. I., N. Y. 11973
REED, Jack W., Division 5414, Sandia Corporation, Sandia Base, Albuquerque, N. Mex. 87115
REID, Roger D., Director, Biological Sciences Division, Code 440, Office of Naval Research, Washington, D. C. 20360
REITEMEIER, Robert F., Environmental Sciences Branch, Division of Biology and Medicine, U. S. Atomic Energy Commission, Washington, D. C. 20545
REITER, Elmar R., Department of Atmospheric Science, Colorado State University, Fort Collins, Colo. 80521
RHOADS, William A., Laboratory of Nuclear Medicine and Radiation Biology, University of California, 900 Veteran Avenue, Los Angeles, Calif. 90024
RICHARDSON, Raymond M., U. S. Geological Survey, P. O. Box 1065, Oak Ridge, Tenn. 37831
RIVERA, Joseph, Environmental Studies Division, Health and Safety Laboratory, U. S. Atomic Energy Commission, New York Operations Office, 376 Hudson Street, New York, N. Y. 10014
ROBINSON, Capt. Kelly E., U. S. Army Nuclear Defense Laboratory, Edgewood Arsenal, Md. 21010
ROBINSON, Richard A., Oak Ridge National Laboratory, Building 3047, P. O. Box X, Oak Ridge, Tenn. 37831
ROSS, Joseph F., M.D., Laboratory of Nuclear Medicine and Radiation Biology, University of California, 900 Veteran Avenue, Los Angeles 24, Calif. 90024
RUST, John H., Head, Section of Nuclear Medicine, University of Chicago, 947 E. 58th Street, Chicago 37, Ill.
SALTER, Leonard P. (Deceased), Radiochemistry Division, Health and Safety Laboratory, U. S. Atomic Energy Commission, New York Operations Office, 376 Hudson Street, New York, N. Y. 10014
SAUCIER, Walter J., Department of Meteorology, University of Oklahoma, Norman, Okla. 73069
SAUNDERS, Allen W., Jr., U. S. Naval Research Laboratory, Code 6110, Washington, D. C. 20390
SCHELL, William R., Hazleton-Nuclear Science Corporation, 4062 Fabian Street, Palo Alto, Calif. 94303
SCHELSKE, Claire L., Bureau of Commercial Fisheries, Radiobiological Laboratory, Beaufort, N. C.

SCHROEBEL, Wilmer W., Civil Effects Branch, Division of Biology and Medicine, U. S. Atomic Energy Commission, Washington, D. C. 20545

SCHULMAN, Murray, Biology Branch, Division of Biology and Medicine, U. S. Atomic Energy Commission, Washington, D. C. 20545

SCHULTZ, Vincent, Environmental Sciences Branch, Division of Biology and Medicine, U. S. Atomic Energy Commission, Washington, D. C. 20545

SCHULZ, Robert K., Department of Soils and Plant Science, University of California, Berkeley, Calif.

SEITZ, Harold, Isotopes, Inc., 123 Woodland Avenue, Westwood, N. J. 07675

SETTER, Lloyd R., Radiological Health Laboratory, U. S. Public Health Service, 1901 Chapman Avenue, Rockville, Md., 20852

SHIRASAWA, Takeo H., U. S. Naval Radiological Defense Laboratory, San Francisco, Calif. 94135

SHLEIEN, Bernard, Northeastern Radiological Health Laboratory, U. S. Public Health Service, 109 Holton Street, Winchester, Mass. 01890

SKAUEN, Donald M., The University of Connecticut, School of Pharmacy, Storrs, Conn. 06268

SLAZAK, Col. Walter, Director, Nuclear Cratering Group, U. S. Army Corps of Engineers, Lawrence Radiation Laboratory, P. O. Box 808, Livermore, Calif. 94551

SNAVELY, David R., Radiation Surveillance Center, Division of Radiological Health, U. S. Public Health Service, Washington, D. C.

SNOOTS, Jacqueline H., Program Coordination Branch, Division of Biology and Medicine, U. S. Atomic Energy Commission, Washington, D. C. 20545

SNOW, Donald L., Radiation Surveillance Center, Division of Radiological Health, U. S. Public Health Service, Washington 25, D. C.

SOLDAT, Joseph K., Radiological Sciences, Hanford Laboratories, General Electric Company, Richland, Wash. 99352

SOLON, Leonard R., Del Electronics Corp., 250 E Sandford Boulevard, Mount Vernon, N. Y. 10550

SPANGLER, Margaret R., Medical Research Branch, Division of Biology and Medicine, U. S. Atomic Energy Commission, Washington, D. C. 20545

STANWOOD, Herbert A., Jr., Assistant Director for Administration, Division of Biology and Medicine, U. S. Atomic Energy Commission, Washington, D. C. 20545

STEVENSON, Heber J. R., Robert A. Taft Sanitary Engineering Center, U. S. Public Health Service, 4676 Columbia Parkway, Cincinnati, Ohio 45226

STEWART, Gordon L., Tritium Laboratory, U. S. Geological Survey, Room 117, Old Post Office Bldg., 12th and Pennsylvania Avenue, Washington, D. C.

STIEFF, Lorin R., Hqs. U. S. Air Force Technical Applications Center, Washington, D. C. 20333

STOUT, Glenn E., Illinois State Water Survey, P. O. Box 232, Urbana, Ill. 61802

STRAUB, Conrad P., Deputy Director, Robert A. Taft Sanitary Engineering Center, U. S. Public Health Service, 4676 Columbia Parkway, Cincinnati, Ohio 45226

STRØMME, Aksel, The Norwegian Radium Hospital, Montebello-Oslo 3, Norway

STROPE, Walmer E., Assistant Director of Civil Defense (Research), Office of the Secretary of the Army, Department of the Army, Washington, D. C.

SWAN, Raymond H., Mobilization Planning Branch, Division of Construction, U. S. Atomic Energy Commission, Washington, D. C. 20545

TAMPLIN, Arthur R., Building T-112, University of California, Lawrence Radiation Laboratory, P. O. Box 808, Livermore, Calif. 94551

TAMURA, Tsuneo, Health Physics Division, X-10 Site, Oak Ridge National Laboratory, Oak Ridge, Tenn. 37831

TELEGADAS, Kosta, Atmospheric Radioactivity Research Branch, U. S. Weather Bureau, Washington, D. C. 20235

TERRY, Maj. John L., Defense Atomic Support Agency, Room 1B685, The Pentagon, Washington, D. C. 20301

TETER, Norman C., U. S. Department of Agriculture, North Building, Plant Industry Station, Beltsville, Md. 20705

THATCHER, Leland L., Division of Research and Laboratories, International Atomic Energy Agency, Kaerntnerring II, Vienna 1, Austria

THOMASIAN, Anahid, Air Force Cambridge Research Laboratories (CRHU-1), L. G. Hanscom Field, Bedford, Mass. 01731

THOMPSON, John C., Jr., Department of Physical Biology, New York State Veterinary College, Cornell University, Ithaca, N. Y. 14850

THOMPSON, Stanley E., Building T-112, University of California, Lawrence Radiation Laboratory, P. O. Box 808, Livermore, Calif. 94551

TOBEY, Franklin J., Division of Public Information, U. S. Atomic Energy Commission, Washington, D. C. 20545

TODD, Frank A., Assistant to the Administrator, Agricultural Research Service, U. S. Department of Agriculture, Washington, D. C.

TOMPKINS, Paul C., Room 1101, Federal Radiation Council, 1815 H Street, N.W., Washington, D. C. 20449

TORREY, Jack D., Division of Radiological Health, U. S. Public Health Service, 1901 Chapman Avenue, Rockville, Md. 20852

TOTTER, John R., Associate Director for Research, Division of Biology and Medicine, U. S. Atomic Energy Commission, Washington, D. C. 20545

TRUM, Bernard F., Harvard Medical School, Boston, Mass.

TUKEY, H. B., Jr., Department of Floriculture and Ornamental Horticulture, Cornell University, Ithaca, N. Y. 14850

TURNER, Frederick B., Laboratory of Nuclear Medicine and Radiation Biology, University of California, 900 Veteran Avenue, Los Angeles, Calif. 90024

TWARDOCK, A. Robert, College of Veterinary Medicine, University of Illinois, Urbana, Ill.

VALASSIS, Vlassios T., Agricultural Research Service, U. S. Department of Agriculture, Room 327, Soils Building, Plant Industry Station, Beltsville, Md. 20705

VAN DER HOVEN, Isaac, U. S. Weather Bureau, Division of Reactor Development, U. S. Atomic Energy Commission, Washington, D. C. 20545

VAN DYNE, George M., Radiation Ecology Station, Health Physics Division, Oak Ridge National Laboratory, Oak Ridge, Tenn. 37831

VAN MIDDLESWORTH, Lester, Department of Physiology and Biophysics, University of Tennessee, 894 Union Avenue, Memphis, Tenn.

VOCCOLA, Sp-4 Harry W., Defense Atomic Support Agency, Washington, D. C. 20301

VOGELE, William A., Mail No. 817, Martin Company, P. O. Box 988, Baltimore, Md. 21203

VOLCHOK, Herbert L., Environmental Studies Division, Health and Safety Laboratory, U. S. Atomic Energy Commission, New York Operations Office, 376 Hudson Street, New York, N. Y. 10014

VON BRETZEL, Leona C., Fallout Studies Branch, Division of Biology and Medicine, U. S. Atomic Energy Commission, Washington, D. C. 20545

WALLACE, John M., 54-1522, Department of Meteorology, Massachusetts Institute of Technology, Cambridge, Mass. 02139

WARD, Gerald M., Animal Science Department (Dairy), Colorado State University, Fort Collins, Colo. 80521

WATSON, D. G., Biology Laboratory, Hanford Laboratories, General Electric Company, Richland, Wash. 99352

WEAVER, Charles L., Radiological Health Laboratory, U. S. Public Health Service, 1901 Chapman Avenue, Rockville, Md. 20852

WEBSTER, Walter M., Central Intelligence Agency, 2430 E Street, N.W., Washington 25, D. C.

WEDLICK, Harold L., Environmental Health Department, School of Public Health, The University of Michigan, Ann Arbor, Mich. 48104

WEICHOLD, Kathryn E., Administrative Branch, Division of Biology and Medicine, U. S. Atomic Energy Commission, Washington, D. C. 20545

WHEDON, Frances L., Office of the Chief of Research and Development, Department of the Army, The Pentagon, Washington, D. C. 20310

WHICKER, Floyd W., Department of Radiology and Radiation Biology, Colorado State University, Fort Collins, Colo. 80521

WHITBY, Kenneth T., Mechanical Engineering Department, University of Minnesota, Minneapolis, Minn. 55455

WHITMAN, Arthur J., U. S. Atomic Energy Commission, Nevada Operations Office, P. O. Box 1676, Las Vegas, Nev. 89101

WHITNAH, John C., Program Coordination Branch, Division of Biology and Medicine, U. S. Atomic Energy Commission, Washington, D. C. 20545

WILDMAN, Robert D., Radiation Sciences Branch, Research and Development Division, U. S. Atomic Energy Commission, Richland Operations Office, P. O. Box 550, Richland, Wash. 99352

WILKINS, Dale E., Agricultural Engineering Laboratory, Agricultural Research Center, U. S. Department of Agriculture, Beltsville, Md. 20705

WILLIS, Eric H., Isotopes, Inc., 123 Woodland Avenue, Westwood, N. J. 07675

WILSEY, Edward F., U. S. Army Nuclear Defense Laboratory, Edgewood Arsenal, Md. 21010

WOLFF, Arthur H., Division of Radiological Health, Radiological Health Laboratory, U. S. Public Health Service, 1901 Chapman Avenue, Rockville, Md. 20852

WOOD, Rex C., Applied Science Division, Litton Systems, Inc., 2295 Walnut Street, St. Paul, Minn.

WORF, Douglas L., Kaman Nuclear, Garden of the Gods Road, Colorado Springs, Colo.

WRENN, McDonald E., Department of Environmental Medicine, New York University Medical Center, Long Meadow Road, Tuxedo, N. Y. 10987

YEAGER, Lt. Kurt, Hqs. U. S. Air Force Technical Applications Center (TD-6), Washington, D. C. 20333

ZIEMER, Paul L., Bionucleonics Department, Purdue University, Lafayette, Ind. 47907

ZIGMAN, Paul E., U. S. Naval Radiological Defense Laboratory, San Francisco, Calif. 94135

INDEX

B

E

T

U

USAEC Division of Technical Information Extension, Oak Ridge, Tennessee

1 PROGRESS IN MEDICAL RADIOISOTOPE SCANNING $3.50

2 REACTOR KINETICS AND CONTROL $4.25

3 DYNAMIC CLINICAL STUDIES WITH RADIOISOTOPES $4.50

4 NOISE ANALYSIS IN NUCLEAR SYSTEMS $3.75

5 RADIOACTIVE FALLOUT FROM NUCLEAR WEAPONS TESTS $6.50

AVAILABLE FROM
CLEARINGHOUSE FOR FEDERAL SCIENTIFIC AND TECHNICAL INFORMATION
NATIONAL BUREAU OF STANDARDS, U. S. DEPARTMENT OF COMMERCE
SPRINGFIELD, VIRGINIA 22151